This is a reproduction of a library book that was digitized by Google as part of an ongoing effort to preserve the information in books and make it universally accessible.

Google™ books

https://books.google.com

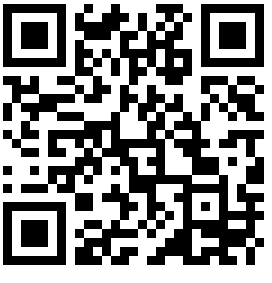

Eng.
TK
9202
.G4
V.8 9
1964/65-1966
ENGINEERING
NOV 17 '65
LIBRARY

POWER REACTOR TECHNOLOGY

A Quarterly Technical Progress Review

Prepared for DIVISION OF TECHNICAL INFORMATION, USAEC, by
W. H. ZINN and J. R. DIETRICH, GENERAL NUCLEAR ENGINEERING CORPORATION

Winter 1964-1965

Progress on Specific Reactor Types:
A Review of Third Geneva Conference Papers

● VOLUME 8
● NUMBER 1

UNIVERSITY OF VIRGINIA LIBRARY
Digitized by Google

TECHNICAL PROGRESS REVIEWS

To meet the needs of industry for concise summaries of current atomic developments, the Atomic Energy Commission is publishing this series, Technical Progress Reviews. Issued quarterly, each of the reviews digests and evaluates the latest findings in a specific area of nuclear technology and science.

The five journals published in this series are:

Isotopes and Radiation Technology, P. S. Baker, A. F. Rupp, and associates, Oak Ridge National Laboratory

Nuclear Safety, Wm. B. Cottrell, W. H. Jordan, and associates, Oak Ridge National Laboratory

Power Reactor Technology, W. H. Zinn and J. R. Dietrich, Combustion Engineering, Inc., Nuclear Division

Reactor Fuel Processing, Stephen Lawroski and associates, Chemical Engineering Division, Argonne National Laboratory

Reactor Materials, R. W. Dayton, E. M. Simons, and associates, Battelle Memorial Institute

Each journal may be purchased from the Superintendent of Documents, U. S. Government Printing Office, Washington, D. C., 20402. *Isotopes and Radiation Technology* at $2.00 per year for subscription or $0.55 for individual issues; the other four journals at $2.50 per year and $0.70 per issue. See back cover for remittance instructions and foreign postage requirements.

The views expressed in this publication do not necessarily represent those of the United States Atomic Energy Commission, its divisions or offices, or of any Commission advisory committee or contractor.

Availability of Reports Cited in This Review

Unclassified AEC reports are available for inspection at AEC depository libraries and are sold by the Clearinghouse for Federal Scientific and Technical Information, National Bureau of Standards, U. S. Department of Commerce, 5285 Port Royal Road, Springfield, Va., 22151. Some of the reports cited are not available owing to their preliminary nature; however, the information contained in them will eventually be made available in formal progress or topical reports.

Unclassified reports issued by other Government agencies or private organizations should be requested from the originator.

Unclassified British and Canadian reports may be inspected at AEC depository libraries. British reports are sold by the British Information Service, 45 Rockefeller Plaza, New York, N. Y.; Canadian reports (AECL series) are sold by the Scientific Document Distribution Office, Atomic Energy of Canada, Ltd., Chalk River, Ontario, Canada.

Classified U. S. and foreign reports identified in this journal as Classified may be purchased by properly cleared Access Permit Holders from the Division of Technical Information Extension, U. S. Atomic Energy Commission, P. O. Box 1001, Oak Ridge, Tenn., 37831. Such reports may be inspected at classified AEC depository libraries.

Digitized by Google

POWER REACTOR TECHNOLOGY

A REVIEW OF RECENT DEVELOPMENTS

Prepared for DIVISION OF TECHNICAL INFORMATION, USAEC,
by W. H. ZINN and J. R. DIETRICH,
COMBUSTION ENGINEERING, INC., NUCLEAR DIVISION

WINTER 1964–1965

VOLUME 8

NUMBER 1

Digitized by Google

Foreword

This quarterly review of reactor development has been prepared at the request of the Division of Technical Information of the U. S. Atomic Energy Commission. Its purpose is to assist interested organizations in the task of keeping abreast of new results in reactor technology for civilian application.

Power Reactor Technology contains reviews of selected recently published reports that are judged noteworthy in the fields of power-reactor research and development, power-reactor applications, design practice, and operating experience. It is not meant to be a comprehensive abstract of all material published during the quarter, nor is it meant to be a treatise on any part of the subject. However, related reports from different sources are often treated together to yield reviews having some breadth of scope, and background material may be added to place recent developments in perspective. Occasionally the reviews are written by guest authors. Reviews having unusual breadth or significance are placed at the front of the issue as Feature Articles.

The intention is to cover the various areas of reactor development from the general viewpoint of the reactor designer rather than from the more detailed points of view of specialists in the individual areas. To whatever extent the coverage of *Power Reactor Technology* may occasionally overlap the fields of the other Technical Progress Reviews, the overlaps will be motivated by this objective of viewing current progress through the eyes of the reactor designer.

A degree of critical appraisal and some interpretation of results are often necessary to define the significance of reported work. Any such appraisal or interpretation represents only the opinion of the reviewer and (in the usual case, when the review is written by Combustion Engineering, Inc., Nuclear Division staff) the Editor. When the review is predominantly interpretive the reviewer is named; unless identified as a guest author, he is a member of the Combustion Engineering, Inc., Nuclear Division staff. Readers are urged to consult the original references to obtain all the background of the work reported and to obtain the interpretation of the results given by the original authors.

For timely coverage, *Power Reactor Technology* must often review fragmentary material. The fixed subject headings listed below have been adopted in the hope of maintaining some continuity and order in the material from one issue to another: all reviews except Feature Articles will be arranged under these headings. A particular issue will not necessarily contain all the headings but only those under which material is reviewed.

Economics, Applications, Programs
Resources and Fuel Cycles
Physics
Fluid and Thermal Technology
Fuel Elements
Materials
Control and Dynamics
Containment, Radiation Control, and Siting
Systems Technology
Components
Design and Construction Practice
Operating Experience
Specific Reactor Types
Specific Applications
Unconventional Approaches

W. H. Zinn, Vice-President
J. R. Dietrich, Editor
Combustion Engineering, Inc.

Digitized by Google

Contents

Progress on Specific Reactor Types

A Review of Papers Presented at the Third Geneva Conference

I Introduction 1
References 2

II Boiling and Pressurized Light-Water Reactors 3
Operating Experience 3
Significant Developments 3
Directions of Future Developments . . . 17
References 20

III Vessel Type Superheating Reactors . 22
Status and Design Features 22
Directions of Future Developments . . . 26
References 27

IV Graphite-Moderated Superheating Reactors 28
References 34

V Heavy-Water-Moderated Pressure-Tube Reactors 35
Operating Experience 35
Significant Features 37
Directions of Future Developments . . . 45
References 45

VI Heavy-Water-Moderated Pressure-Vessel Reactors 47
General Status 47
Operating Experience 50
Significant Developments 51
Directions of Future Developments . . . 54
Czechoslovak Nuclear Power Station . . . 56
References 56

VII Gas-Cooled Clad-Fuel Reactors . . . 58
General Status 58
Fuel Elements 61
Pressure Vessels 66
Refueling Machines 68
Control and Instrumentation 68
Advanced Concepts and Future Directions 69
References 71

VIII Gas-Cooled Unclad-Fuel Reactors . . 72
References 74

IX Sodium-Cooled Reactors 75
Technology of Sodium Systems 75
Sodium Graphite Reactors 80
Fast-Breeder Reactors 84
References 95

X Maritime Reactors 97
References 101

XI Other Reactors 103
Portable Power Plants 103
Direct-Conversion Power Plants 105
Advanced Concepts 106
References 106

Issued quarterly by the U. S. Atomic Energy Commission. Use of funds for printing this publication approved by the Director of the Bureau of the Budget on October 14, 1963.

Digitized by Google

Digitized by Google

Availability of Third Geneva Conference Papers

1. Copies of all papers may be purchased from the European Office of the United Nations for two Swiss francs (46 cents) per paper plus postage. Address: European Office of the United Nations, Palais des Nations, Geneva, Switzerland, Attention: R. Furstenberg, Chief, Distribution Service Documents Division. When UN stocks are exhausted, reproduced copies of all papers may be purchased from the IAEA in Vienna at a price of $1.50 per paper. Address: International Atomic Energy Agency, Kaerntnerring 11, Vienna I, Austria.

2. Reproduced copies of all U. S. papers (no foreign) may be purchased at a price of $1.00 per paper from the Clearinghouse for Federal Scientific and Technical Information (formerly OTS). Address: National Bureau of Standards, U. S. Department of Commerce, 5285 Port Royal Road, Springfield, Va. 22151.

3. The American Nuclear Society will provide Xerox copies of all papers at 25 cents per page. Address: American Nuclear Society, 244 East Ogden Ave., Hinsdale, Ill. 60521.

4. The U. S. Atomic Energy Commission, Division of Technical Information Extension, Oak Ridge, Tenn. 37831, has produced micronegatives of all Geneva papers. Complete sets of duplicate negatives were distributed to the AEC, other government agencies, and their contractors; sets of U. S. papers only were distributed to AEC depository libraries.

(All U. S. papers were abstracted and indexed in Vol. 18, No. 18, of *Nuclear Science Abstracts*. All foreign papers will be similarly abstracted and indexed in Vol. 18, No. 21.)

Digitized by Google

Digitized by Google

Section

1

Power Reactor Technology

Introduction

Of the massive information collection produced by the Third United Nations International Conference on the Peaceful Uses of Atomic Energy, an important fraction deals with specific power-reactor types, with the progress made in their development, and with the experience gained in building and operating individual reactors of the various types. This entire issue of *Power Reactor Technology* is devoted to a review of that information.* More general reviews of the conference have been published elsewhere, notably in *Nucleonics*[1] and *Nuclear News*.[2]

Because of the special nature of this issue, the usual section headings as given in the Foreword do not appear. Instead, each of the following sections is on a particular reactor type.

Of the reactor types under serious development, two can be said to have achieved commercial acceptance: the "water" reactors (pressurized and boiling H_2O) and the "Magnox" gas-cooled reactors. The heaviest building commitments have been made in the latter type, amounting, through 1968, to over 5000 Mw(e) in the United Kingdom and some 1300 Mw(e) in France. The application of the prestressed concrete pressure vessel to this reactor type has done much to improve its potentialities, with respect to both size and operating pressure. Nevertheless, it appears that other types will replace it in future building plans, at least in the United Kingdom. Whether the replacement type will be its direct descendant, the advanced gas-cooled reactor, is not clear at this time.

The water reactors are still in a state of vigorous development, and it appears that, in the economic climate of the United States, it will be difficult for another reactor type to replace them so long as the basic costs of partially enriched nuclear fuels do not rise much above current levels. In the economic competition between the boiling- and pressurized-water types, it is difficult to detect a clear basic advantage of one over the other at the moment, although the rapid trend to plants of very high output may favor the pressurized-water type in the long run.

Another group of reactor types, each of which is represented by one or two bona fide power-generating plants, mostly in the lower capacity ranges, might be said to be in the "demonstration" stage. The most advanced of these are the Russian graphite-moderated superheat reactor (Beloyarsk) and the pressure-tube D_2O reactor [for each of which commitments have been made for a follow-on reactor in the 200-Mw(e) range] and the sodium-graphite reactor. The advanced gas-cooled reactor and the organic-moderated reactor also fall in this group. However, in regard to the latter, indications are that the future of organic liquids in central-station reactors lies in their use as coolants for D_2O-moderated reactors. The interesting variation on the organic-moderated concept represented by the Russian ARBUS reactor appears to be directed specifically to remote-station applications.

The remaining rather large group of reactor types under serious development cannot be said to be "demonstrated" in terms of prototypes of commercial versions. Some are very close to that stage, however. The integral nuclear superheat concept awaits only the full-scale operation of the BONUS and Pathfinder plants to enter the "demonstration" stage: both of these plants are currently in the process of startup. The heavy-water reactor of the pressure-vessel type is represented by two

*The Conference papers are to be published in bound form. Meanwhile, the papers are available and can be obtained from the sources listed on the preceding page.

Digitized by Google

operating plants: the Halden Boiling Water Reactor that produces process steam, and the Agesta plant, a pressurized heavy-water plant that produces 10 Mw of electricity along with hot water for space heating. It would be stretching a point, however, to call these demonstration plants in the sense of the word used here; for the proposed characteristics of the commercial version, as exemplified by the Marviken plant, involve substantial extrapolations in several areas. The high-temperature gas-cooled type has been critical (the Dragon reactor), and the Peach Bottom plant is under construction; the latter is intended as a prototype. At least three versions of D_2O-moderated pressure-tube reactors utilizing coolants other than D_2O are under serious development; the coolants used are H_2O (boiling liquid, fog, or steam), organic, and gas. Experimental reactors having the latter two coolants are being built.

The position of the fast-breeder reactor is a little hard to classify, but it can hardly be said to have reached the demonstration stage despite the facts that it was first used to produce electric power in 1951, that a plant of moderately large output (Dounreay) has been in operation for some time, and that a large commercial plant (the EFFBR) is in process of startup. This is primarily because a fuel acceptable for commercial operation has not yet been demonstrated. Nevertheless, of all the reactor types, the fast breeder is probably the one of most universal interest, and continuing strong development efforts are foreseen for the future.

In the following sections the preceding rather brief remarks are expanded, and the status of each of the reactor types is reviewed on the basis of the information presented at Geneva.

References

1. *Nucleonics*, 22(10): (October 1964).
2. *Nucl. News*, 7(10): (October 1964).

Digitized by Google

Section

II

Power Reactor Technology

Boiling and Pressurized Light-Water Reactors

By John S. Wiley

The nonmilitary land-based boiling and pressurized light-water-moderated reactors of the world, other than the purely experimental ones, are listed in Table II-1. The table includes the more important reactors under construction as well as the reactors in operation. These reactor types are the ones of most interest, and the best known, in the United States; indeed, with the exception of the Russian reactor at Voronezh, all the reactors in Table II-1 were designed either by U. S. firms or with their assistance. Because these types have been covered most thoroughly by *Power Reactor Technology* in the past, this review of the many Geneva papers on light-water reactors is abbreviated in favor of greater coverage for the reactor types less well known in the United States. The major past reviews in *Power Reactor Technology*, of design and operating experience for specific water-moderated reactors, may be located by means of Table II-2.

Operating Experience

The operating experience with Yankee, the CETR, Saxton, and Shippingport is detailed in Ref. 1, and Ref. 2 covers operating experience with the Dresden, Big Rock Point, and Humboldt Bay reactors. References 3 and 4 discuss preliminary operating experience with the Russian pressurized-water reactor, WWER. Operating experience with Shippingport, Yankee, the CETR, and Dresden has been reviewed in past issues of *Power Reactor Technology*, as indicated in Table II-2. Much of the information contained in Refs. 1 and 2 on Shippingport, Yankee, Dresden, and the CETR has been covered in these reviews, but Ref. 2 also contains significant information on the Big Rock Point and Humboldt Bay reactors. Both of these reactors went into commercial operation in late 1963 and have had availability factors of about 95% through the end of the year, a period which did not involve refueling. Both reactors experienced leakage past the inner O-ring seal of the pressure-vessel head. In the case of the Big Rock Point reactor, this was attributed to a number of thermal cycles plus the use of three different operating pressures, and the leakage was stopped by replacement of the O-ring. The vessel-head flange-sealing surface of the Humboldt Bay reactor was modified by grinding to prevent further leakage.

An interesting repair technique was employed on the Big Rock Point reactor. Flow-induced vibration was found to be responsible for the loosening of a cap screw from one of the Zircaloy fuel channels; this vibration was caused by direct impingement of the recirculating flow on a portion of the core support, and the core-support plate had to be removed for installation of a new flow distributor. This work was performed inside the water-filled reactor vessel by four divers with a significantly low resultant radiation exposure.

References 3 and 4 discuss physics studies and preliminary experience with the Russian WWER. As of the date of the references (May 1964), the WWER had not produced nuclear electricity, although the turbines had been rolled on steam from auxiliary boilers. Critical experiments had been done, and the primary coolant system had been debugged.

Significant Developments

Fuel Elements, Fuel Materials, and Cladding

As indicated in Table II-1, the water-moderated reactors typically employ fuel in the oxide form (UO_2, or a UO_2-ThO_2 mixture as in the CETR and the ERR), usually as pressed and

Digitized by Google

Table II-1 BOILING- AND PRESSURIZED-WATER REACTOR-DESIGN DATA

Installation	Power, Mw(e)	Startup	Reactor pressure, psi	Steam conditions, psia/°F	Fuel/cladding	Reactor control	Remarks
Boiling-Water Reactors							
Dresden Nuclear Power Station, Morris, Ill.	200	1959	1015	Primary: 975/452 Secondary: 500/467	UO_2/S.S./Zircaloy-2	Control rods	
Rheinisch-Westfalisches Elektrizitatswerk (RWE), Kahl, West Germany	15.6	1960	1000	750/550	UO_2/Zr	Rods and solid shims	
Elk River Reactor (ERR), Elk River, Minn.	20.0	1962	937	865/900	UO_2ThO_2/S.S.	Rods and fixed (solid) shims	Indirect cycle
Big Rock Point Nuclear Plant, Charlevoix, Mich.	47.8	1962	1050	Direct cycle	UO_2/S.S.	Rods and fixed (solid) shims	Steam drum
Humboldt Bay Power Plant, Unit No. 3, Humboldt Bay, Calif.	50	1963	1035	Direct cycle	UO_2/S.S.	Rods and poison curtains	Pressure suppression
Japan Atomic Energy Research Institute Reactor (JPDR), Tokai-Mura, Japan	11.7	1963	905	495/530	UO_2/Zr	Rods and poison curtains	
Società Elettronucleare Nazionale Reactor (SENN), Punta Fiume, Italy	150	1963	1000	1000/(sat.)	UO_2/S.S. and Zr	Control rods and solid shims	Dual cycle, steam drum
La Crosse Boiling Water Reactor (LACBWR), La Crosse, Wis.	50	1965	1300	1300/577	UO_2/S.S.		
Kernkraftwerk-RWE-Bayernwerk Reactor (KRB), Gundremmingen, West Germany	237	1966	1015	500/467	UO_2/S.S.		
Indian Department of Atomic Energy BWR, Tarapur, India	380 (two reactors)	1968	1015	1015 primary/(sat.) 500 secondary/(sat.)	UO_2/Zircaloy-2	Control rods	Dual cycle forced circulation, internal steam separation, pressure suppression
Oyster Creek Nuclear Electric Generating Station, Oyster Creek, N. J.	540	1967	1000	Direct cycle	UO_2/Zr		
Pacific Gas & Electric Bodega Bay Reactor, Bodega Bay, Calif.	313	1968	1075	Direct cycle	UO_2/S.S.		Pressure suppression
Nine Mile Point Nuclear Power Station, N. Y.	525	1968	1000	Direct cycle	UO_2/Zr	Rods and recirculation pumps	Pressure suppression
N. V. Samenwerkende, Electriciteits Productibedrijven (SEP), Netherlands	50	1968					

Digitized by Google

Pressurized-Water Reactors

Shippingport PWR, Shippingport, Pa.	60	1957	2000	600/486	U-Zr plates and UO_2/Zircaloy-2 rods	Rods and burnable poison	
Centre d'Études de l'Énergie Nucléaire Reactor (BR-3), Mol, Belgium	10.7	1962	2000	520/471	UO_2/S.S.	Rods and chemical shim	
Yankee Atomic Electric Co. Reactor, Rowe, Mass.	160	1960	2300 (max.)	465/460	UO_2/S.S.	Rods and solid shims	
Consolidated Edison Thorium Reactor (CETR), Indian Point, N. Y.	255	1962	1500	370/1000	UO_2/ThO_2/S.S.	Control rods and solid shims	Oil-fired superheater
Novo-Voronezh Atomic Power Station (WWER), Russia	210	1964	1422	455/(sat.)	UO_2/Zr-Nb	Movable fuel and flux trap, safety rods	
Saxton Nuclear Experimental Corporation Reactor, Saxton, Pa.	5	1962	2000	475/462	UO_2/S.S.	Rods and chemical shim	
Società Elettronucleare Italiana (SELNI), Trino, Italy	240	1964	2015	500/467	UO_2/S.S.		
Southern California Edison Co. San Onofre Reactor, Camp Pendleton, Calif.	375	1966	2065	650/495	UO_2/S.S.		
Connecticut Yankee Atomic Power Co. Reactor, Haddam Neck, Conn.	463	1967	2065	690/502	UO_2/S.S.		
Malibu Nuclear Power Station (Malibu-1), Corral Beach, Calif.	462	1968	2065	690/410	UO_2/S.S. or Zr		
Société d'Energie Nucléaire Franco-Belge des Ardennes (SENA), Chooz, France	242	1966	2100	465/460	UO_2/S.S.	Control rods and chemical shim	Underground containment, in-core instrumentation
Kernkraft Baden-Wurttemberg Planungegesellschaft mbH. (KBWP), Obrigheim on the Neckar, West Germany	283	1968	2062	711/(sat.)	UO_2/Zr	Control rods and chemical shim	Double containment
Union Electrica Madrilena Reactor, Zorita de los Canes, Spain	140	1968					

Digitized by Google

Table II-2 LOCATIONS OF PREVIOUS REVIEWS OF DESIGN AND OPERATING EXPERIENCE FOR WATER-MODERATED REACTORS IN *POWER REACTOR TECHNOLOGY*

Reactor	Item	Vol.	Issue	Pages
Shippingport	First refueling	4	2	52-58
	Power-generation history, fuel-element examination, experience with major equipment, radiation control, second core	5	4	61-72
	Instrumentation, second refueling	6	2	64-67
	FEDAL system, loss-of-flow experiments, radiation, hydraulics experiments, fuel failure	6	3	49-55
	Operating history, pressure-vessel irradiation, fuel examinations	7	2	193-196
Yankee	Design	4	3	47-55
	Head closure, containment experience, turbine vibration	4	4	69-70
	Control-rod examination	6	3	55-56
	In-core instrumentation, radioactivity problems, reactivity characteristics	6	4	82-91
Dresden	Design	4	4	56-68
	Control rods, grid-plate cracks, load following	5	2	56-59
	Water chemistry, load schedules, transient experiments	6	2	60-64
CETR	Design	6	3	28-40
	Fuel pool experience, control-system operation, performance	7	3	313-315
Elk River	Design	5	2	33-47
Humboldt Bay and Big Rock Point	Design	7	1	70-84

sintered cylindrical pellets in jackets of Zircaloy or stainless steel. An early exception was the Experimental Boiling Water Reactor, which used plates of uranium metal alloyed with small percentages of zirconium and niobium, clad with Zircaloy. The Shippingport reactor used Zircaloy-clad plates of uranium–zirconium alloy for the seed loadings installed in core 1; since the seed fuel is highly enriched, this alloy was rich in zirconium.

In Ref. 5 the results of the U. S. program on oxide fuels are summarized as follows:

> During the past five years in the United States there has been a systematic approach to design formulation, fabrication development, and performance testing of uranium oxide type fuels. Sufficient data are available to allow a quantitative evaluation of oxide fuels for use in economic central-station power applications. The extensive scope of this program includes:
>
> a. Over 130,000 Zircaloy and stainless steel clad UO_2 fuel rods have been irradiated in operating water and steam cooled (260°-316°C) power reactors. Maximum exposure attained is about 28,000 MWD/TU; maximum heat fluxes are about 350,000 Btu/hr-ft^2 for Zircaloy clad fuel and 450,000 for stainless clad fuel. . . .
>
> b. Over 4000 developmental fuel rods representing 37 different fabrication processes have been irradiated in water and steam cooled test reactors and loops. Maximum exposure attained was 16,000 MWD/TU and 1,435,000 Btu/hr-ft^2 peak heat flux. Plate UO_2 fuel has been irradiated in test loops to 127,000 MWD/TU exposure.
>
> c. More recently, oxide fuel elements have been irradiated to 3600 MWD/TU maximum at 445,000 Btu/hr-ft^2 heat flux in superheat steam (510°C) test reactor loops.

The reference continues with a discussion of fuel-fabrication techniques and the behavior of fuel elements clad in zirconium alloys and stainless-steel alloys. Table II-3 gives additional details on oxide cores clad with Zircaloy-2 and stainless steel, which reflect U. S. design practice.

In general, the in-reactor behavior of the Zircaloy-clad elements has been "outstanding,"[5] with but few failures. Purposely defected elements have operated relatively successfully, with little loss of UO_2 to the coolant and little reaction between the fuel and the available oxygen in the water; washout from powder-filled fuel elements has been slight. Hydrogen pickup by the zirconium-base alloys has generally proved acceptable, with in-pile pickup well correlated with autoclave corrosion data (Fig. II-1).

The outstanding example of in-pile experience with stainless-steel-clad fuel elements is

Digitized by Google

Table II-3 DETAILS OF POWER-REACTOR CORES FABRICATED WITH ZIRCALOY-2 AND STAINLESS STEEL[5]

	Power, Mw(e)	No. of rods	Rod outside diameter, in.	Cladding thickness, in.	Peak heat flux × 10^{-6}, Btu/(hr)(sq ft)	Average exposure,* Mwd/ton of U
Zircaloy-Clad Fuel Elements						
Boiling-water reactors						
Dresden	220	15,500	0.570	0.030	3.46	9,000
Dresden†		192	0.470	0.025	3.46	7,000
Japan	12	3,460	0.564	0.033	2.96	1,000
Kahl	16	3,200	0.571	0.033	3.38	4,500
SENN	150	17,000				
Pressurized-water reactors						
Shippingport core‡	68	16,400	0.411	0.023	3.43	10,000
Shippingport core§	150	Flat plates	Flat plate, 0.100 in. thick	0.020	6.50	
Carolinas-Virginia¶	17	1,230	0.490	0.022	4.69	1,000
Stainless-Steel-Clad Fuel Elements						
Boiling-water reactors						
Dresden	220	4,900	0.440	0.019 (304 S.S.)	2.76	4,000
Elk River	20		0.452	0.020 (304 S.S.)	3.13	500
Humboldt Bay	65	8,428	0.463	0.019 (304 S.S.)	3.65	3,000
Big Rock Point	50	7,392	0.388	0.019 (304 S.S.)	3.50	3,000
Pressurized-water reactors						
Yankee	185	23,142	0.340	0.021 (348 S.S.)	4.46	8,000
Saxton	20 (thermal)	1,512	0.391	0.015 (304 S.S.)	4.44	3,000
Indian Point**	151	23,400	0.304	0.021 (304 S.S.)	5.40	3,000
N.S. *Savannah*	70 (thermal)	5,248	0.500	0.035 (304 S.S.)	2.77	1,500
SELNI	270	24,960	0.385	0.015 (304 S.S.)		Under construction

*Editor's Note: This is the exposure attained as of the writing of Ref. 5 and is not necessarily the maximum attainable.

†Straight-through 9-ft-long rods.

‡Rod fuel only in blanket region.

§Flat plates in entire core. Seed is 0.040-in.-thick plates with ZrO_2-UO_2.

¶Zircaloy-4 cladding; this reactor is cooled and moderated by D_2O.

**Net power is 255 Mw(e), of which 104 Mw(e) is from fossil superheaters.

probably the Yankee reactor. The second core of this power reactor contained two assemblies from the first core, and these two assemblies operated satisfactorily to a maximum burnup of 27,000 Mwd per ton of uranium. Detailed examination of the first core showed that the cladding exhibited no microstructural changes, an increase in burst strength, "limited" amount of crud, and no significant structural changes.[5] Thin-walled cladding, relying on the fuel for support, has been tested in Dresden and in the Vallecitos Boiling Water Reactor (VBWR) with less success; the VBWR results were reviewed in detail in the Winter 1963–1964 issue of *Power Reactor Technology*, 7(1): 27-50, and are summarized in Fig. II-2.

Pertinent conclusions from Ref. 5 are as follows:

> Zircaloy-2 clad rod fuel has been operated satisfactorily to maximum burnup of 16,000 MWD/TU at peak heat fluxes of 510,000 Btu/hr-ft^2, and tests are continuing.
>
> Heavy walled "free standing" fully annealed stainless steel rods have operated satisfactorily to 27,000 MWD/TU maximum and peak heat fluxes of 446,000 Btu/hr-ft^2.
>
> Thin clad "nonfree standing" stainless has shown inter-granular stress induced corrosion at average burnups less than 10,000 MWD/TU and high heat fluxes. Exact cause of the failure mechanism is still under investigation.

It should be noted, however, that more than one variable was changed between the freestanding- and nonfreestanding-cladding experiments. For example, the heavy-walled freestanding fuel elements were irradiated in a pressurized-water-reactor (PWR) environment and were fabricated of type 348 stainless steel. The thin nonfreestanding claddings were irradiated in Dresden and VBWR in a boiling-water-reactor (BWR) environment and were fabricated of type 304 stainless steel.

The irradiation behavior of ceramic fuels is discussed in Ref. 6. The paper presents engineering type information on a number of fuel

Digitized by Google

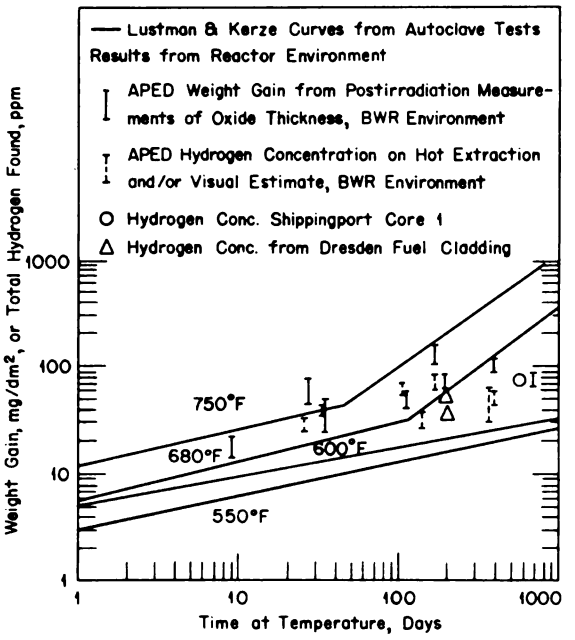

Fig. II-1 Corrosion behavior and hydrogen pickup of Zircaloy-2. Comparison of autoclave and reactor exposures.[5]

materials, including UO_2, ThO_2-UO_2, PuO_2-UO_2, ZrO_2 base–UO_2, UO_2-BeO, UO_2-Al_2O_3, MgO-PuO_2, ZrO_2-PuO_2, UC, PuC, UC-PuC, UN, US, and U_3Si. Of these materials the oxides are of primary importance to water reactors and, naturally, have been investigated most extensively. For example, the thermal conductivity of UO_2, illustrated in Fig. II-3, appears to be reasonably well determined. Increases in k_{UO_2} at high temperatures, where it has been postulated that radiative-energy-transport mechanisms become important, have not been observed in polycrystalline UO_2 even after columnar grain growth. Fission-gas release, although not well understood, is amenable to engineering calculations, at least to the accuracy required for the practical design of fuel elements for the H_2O reactors.* Structural changes in UO_2 have been quantitatively related to fuel operating temperature, temperature gradient, exposure, density, and irradiation history. Reference 6 suggests that future reactor designs may employ lower density UO_2 to encourage fission-gas release and reduce swelling during irradiation. This may be of importance in the design of oxide fuels for long-term irradiation in fast reactors or for those reactors where the provision of a fission-gas plenum results in an unacceptable performance penalty. Reference 7 reports preliminary results for fabrication and irradiation of UO_2-PuO_2 fuel elements in the BR-3 reactor.

References 8 and 9 report on various experiments designed to study the corrosion resistance of zirconium alloys. Reference 8, which is primarily of interest to the specialist, is on metallurgical techniques in which radioactive tracers are used for the study of zirconium alloy corrosion; it also presents some results. Reference 9 is devoted to the zirco-

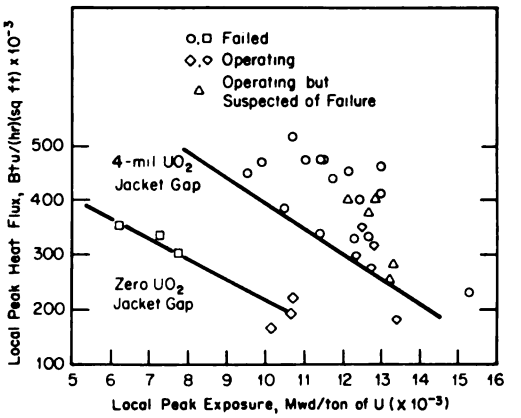

Fig. II-2 Local peak heat flux (within 500 to 1000 hr of failure) vs. local peak exposure for 304 stainless-steel-clad UO_2 fuel.[5]

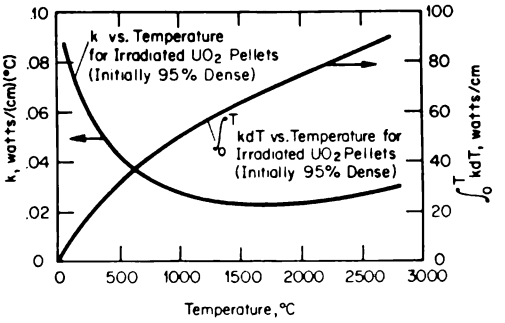

Fig. II-3 UO_2 thermal conductivity and $\int_0^T kdT$ vs. temperature.[6]

*An extensive discussion of the engineering and performance of UO_2 fuel assemblies was presented by the Canadians in Refs. 30 to 32. Their special interest in fission-gas release presumably comes from the fact that they cannot design NPD type fuel rods with large fission-gas spaces to allow for imperfections in gas-release calculations without introducing additional difficulties related to end-cap peaking, fuel shuffling, etc.

Digitized by Google

nium-niobium alloy hydriding problem in water-cooled reactors. This class of alloys is an interesting one since the Russians have traditionally used the zirconium-niobium alloys in their water-cooled power reactors, whereas the Zircaloys have been used almost exclusively in the United States. The reference discusses the effect of stress upon the distribution, or arrangement, of the zirconium hydride corrosion product. The hydride is in the form of platelets, and, if these are oriented parallel to the axis of the tube, their effect on tensile properties is minimized. On the other hand, if the platelets are radially oriented, serious reductions in tensile strength occur. According to Ref. 9:

> ...formation of radially oriented hydrides is a function of values of the tensile stress and does not depend upon the methods of hydriding. Even at the hydrogen content of 0.01% with radially oriented hydrides the pipe properties are sharply impaired; that proves the paramount importance of the values of tensile stress when using zirconium alloys in water-moderated water-cooled power reactors. On all other conditions being equal, preference should be given to the zirconium alloys possessing high yield point as in this case the value of the allowable hydriding stress will be higher and reliability of operation will correspondingly increase.
>
> The allowable hydriding stress of the alloy is the maximum tensile stress at which radial orientation of the hydrides under the specified service conditions does not yet occur. Evidently, it is to be taken into account along with other parameters in designing zirconium alloy claddings for fuel elements or zirconium alloy pipes for service under pressure.

Values of the allowable hydriding stress for two of the zirconium-niobium alloys are given in the reference. For zirconium–1 wt.% niobium, radial orientation of the hydrides occurred at 4.4 kg/mm^2; and, for zirconium–2 wt.% niobium, radially oriented hydrides were formed at a stress of 8.8 kg/mm^2 and over. These values are about half of the yield strength of each alloy at the test temperature of 400°C. Although the stronger zirconium-niobium alloys have not excited much interest in the United States as cladding materials, their use in pressure-tube type reactors and for in-core structural components of pressure-vessel type reactors may increase.

Reference 10 summarizes a considerable amount of U. S. experience on corrosion in aqueous systems. The generally successful use of Zircaloy and stainless steel in power reactors is confirmed, and the superiority of beta-quenched Zircaloy-4 over Zircaloy-2 in high-temperature water is discussed. With regard to stainless steel, the authors note that "...highly stressed thin wall cladding, representing advanced fuel concepts, has failed in VBWR after exposures considerably shorter than required for economic performance...."[10] Although this is true, failures have also been noted in VBWR irradiation of types H and I elements in the Fuel-Cycle Program; these elements were designed to be freestanding [see reviews in *Power Reactor Technology*, 7(1): 27-50 and 7(4): 354-355].

In summary, there is little doubt that metal-jacketed oxide fuel elements can be made to have attractively long service lifetimes in water-cooled reactors. The quantitative principles of optimum design are not completely understood, however, and caution is in order in making substantial departures from the designs which have been proved out by reactor experience. It follows also that, in quoting and using the experience obtained to date, one must be particular and comprehensive in considering the conditions under which the experience was obtained. Some departure from this principle was evident in the informal discussion in the Geneva sessions, where the Shippingport experience with exposure lifetime of the blanket elements appeared to be regarded as typical for oxide fuel elements, even though the thermal demands on the oxide in these elements are relatively quite mild [see the review of Shippingport Operating Experience in *Power Reactor Technology*, 7(2): 193].

Water Chemistry: Use of Mild Steels in Aqueous Systems

The use of mild steels in portions of power-reactor primary circuit piping has been common practice for some time; Dresden, for example, uses low-alloy and carbon steels for the primary and secondary steam piping and the feedwater system. A full-flow condensate demineralizer is provided, however. In Ref. 10 the use of boiler steel is considered for unclad pressure vessels, and the conclusion reached is that the question is "unresolved." The problem is of more than academic interest, however, since at least one power reactor under construction (the second unit of the WWER) is said[29] to utilize an unclad pressure vessel. Accordingly, the discussion presented in Ref.

Digitized by Google

11 serves to illuminate some of the problems associated with the use of mild steel in power-reactor primary circuits.

The water and steam of a typical boiling-water reactor will contain about 0.1 and 20 ppm oxygen, respectively.[11] Experiments done at the Kjeller Research Establishment in Norway, and summarized in Ref. 11, indicate that the initial corrosion-product release rate under these conditions is "high" but, under continued high-temperature operation, decreases to a release rate as low as 2 mg/(dm^2)(month). This is comparable to values for stainless steel. The situation has additional complications in the case of reactor operation since the system may from time to time be kept at lower temperatures for relatively long periods (as during refueling); rather high corrosion rates have been reported in neutral water at low temperatures. The paper[11] suggests that during shutdown the oxygen content of the water should be monitored and reduced to the point that harmful corrosion will be prevented. Under low-oxygen conditions the corrosion film formed at high temperatures is apparently stable, although for long periods of downtime it may be necessary to scavenge the oxygen.

As a further consequence of the corrosion in neutral water at low temperature, low-temperature portions of the primary system may present difficulties in the absence of condensate cleanup systems. The corrosion products introduced into the reactor may precipitate on fuel elements, and Ref. 11 mentions that "rust generators" are to be installed in the Halden Boiling Water Reactor (HBWR) to study the problem.

Control: Soluble and Burnable Poisons

The use of soluble poisons to control reactivity in pressurized-water reactors was reviewed in detail in Sec. IX of *Power Reactor Technology*, 7(4). References 12 to 14 are on aspects of soluble-poison control, and the information reviewed here will be supplementary to the material presented in the 7(4) issue.

The dynamic performance of a chemical-shim system is the subject in Ref. 12. The reactor that was used as a neutron source was a swimming-pool type, and the boric acid was contained in a pipe introduced within the core. The control system (feed and bleed) and associated piping and electronics probably are representative of what could be used for power-reactor control, but the range of dynamic variables was much greater than that encompassed by the chemical-shim application currently considered in power reactors. The response of the control system to various reactivity steps and ramps was investigated with the following results:[12]

> ...the control system examined here seems to have satisfactory dynamic characteristics as regards the fine control of the neutron flux level. There are no particular operation and maintenance problems. The whole system appears to be quite reliable, rugged and easy to handle.

The flow diagram of the poison loop is shown in Fig. II-4.

Operation of the Belgian BR-3 plant with boron in the coolant is described in Ref. 13. The steps performed to prepare the system for operation with the chemical shim, and subsequent transient tests, are detailed in Table II-4. The physical, chemical, and radiochemical characteristics of the reactor coolant were monitored during the course of operations in the chemical-shim experiment, which lasted about a month. In general, the results of the experiment were good. Small, unexplained, reactivity variations occurred (Fig. II-5), but they happened over relatively long times and, in fact, were noticed in normal operations without boron. Water chemistry showed no unusual or unexpected trends, and the reactor coolant activity remained below design limits, although the demineralizer has been bypassed for more than six weeks.

Reference 13 concludes with an interesting discussion of the application of chemical shim to a large [250 Mw(e)] reactor. Depending upon the operational program, from 2 to 10 tons of boric acid per year will have to be disposed of. If the core has contained failed fuel elements, this material will be contaminated by fission products to a varying degree, depending on the number of failed fuel rods. Distillation, electrodialysis, and ion exchange are considered as concentration processes, but no specific recommendations are given. It may be that the success of the soluble-poison concept relies on keeping the number of routinely failed fuel elements within some limit, and the value 1% is mentioned. Fortunately, the experience with the reactor type has illustrated that this limit is probably not an unrealistically difficult one.

Digitized by Google

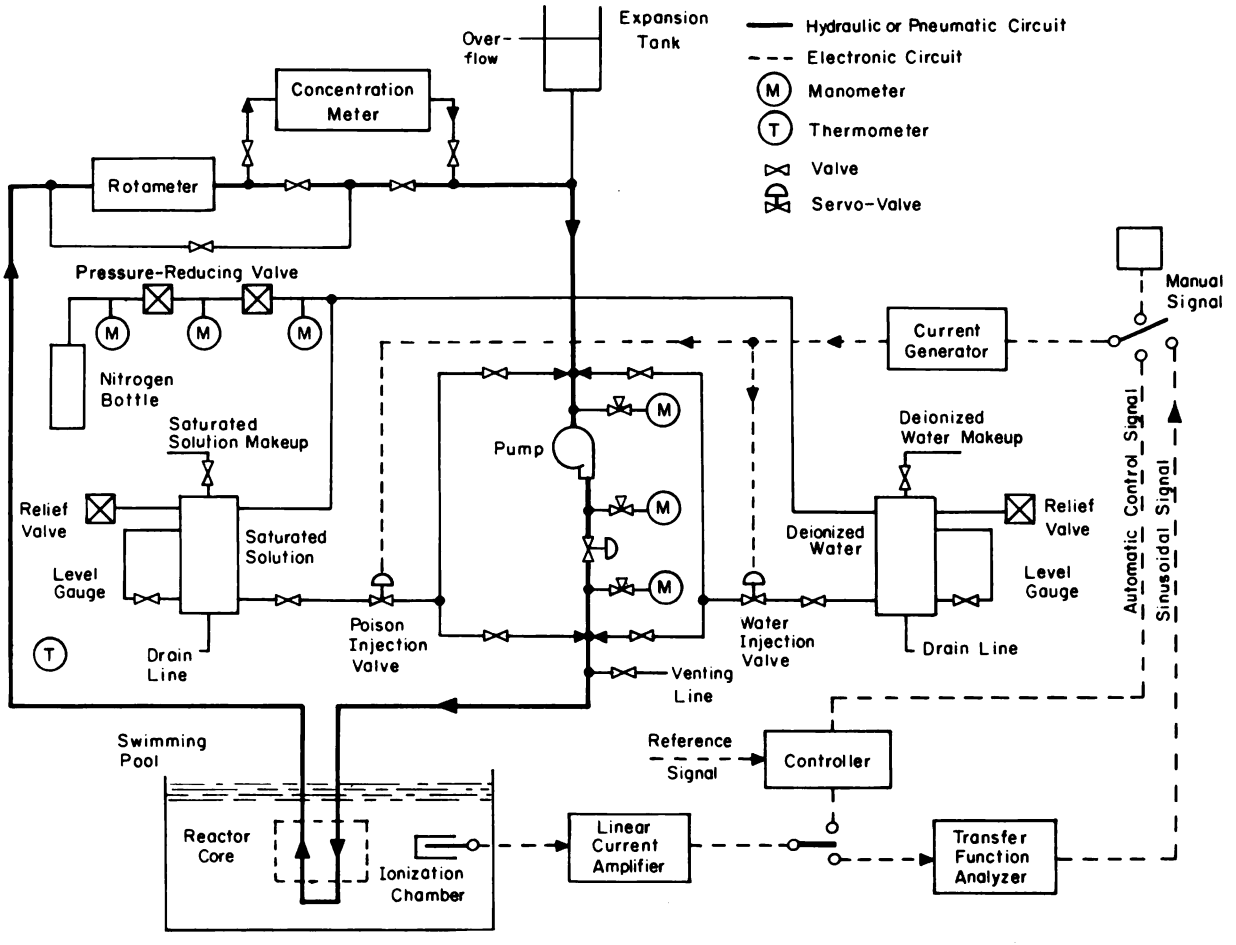

Fig. II-4 Simplified flow diagram of soluble-poison control system.[12]

Table II-4 OPERATIONS WITH THE BR-3 REACTOR: CHEMICAL-SHIM EXPERIMENT[13]

1. Preliminary operation at normal power level, without the mixed-bed demineralizer; the ion beds are not saturated in BO_3^{3-} ions and therefore cannot be used during the boron test.
2. Preliminary operation at normal power level, without demineralizer, the *p*H being reduced from 9.5 to approximately 7.

During these two preliminary tests, the increase of the reactor coolant activity (very predictable) was, however, far from the permissible limits.* Also the air contamination remained, everywhere, far under the maximum permissible concentrations.

3. Power operation with 125 ppm boron present in the primary coolant. This first step in the study of chemical control made it possible to determine the overall effect of bypassing the demineralizer and of the presence of boron in the reactor coolant. It gave information (*a*) on the evolution of chemical characteristics of the water, the boron concentration, and the core reactivity and (*b*) on the possibility of compensating the xenon poisoning.
4. Power operation with a higher boron concentration in the reactor coolant water (350 ppm). This last step, performed after a core shuffling, made possible a more extensive study:

—Startup of the plant, and load pickup with boron present
—Overall compensation of the xenon effect by reduction of the boron concentration
—Power operation with all rods extracted from the core, except two rods for fine control
—Compensation of samarium poisoning and fuel burnup by boron removal. Furthermore, various load rejections and fast load pickups made it possible to test the dynamic behavior of the reactor.

*The activity of the primary coolant increased about a factor of 3 when the resin-bed purification system was not operational. The new value[13] was about 0.24 μc/ml.

Digitized by Google

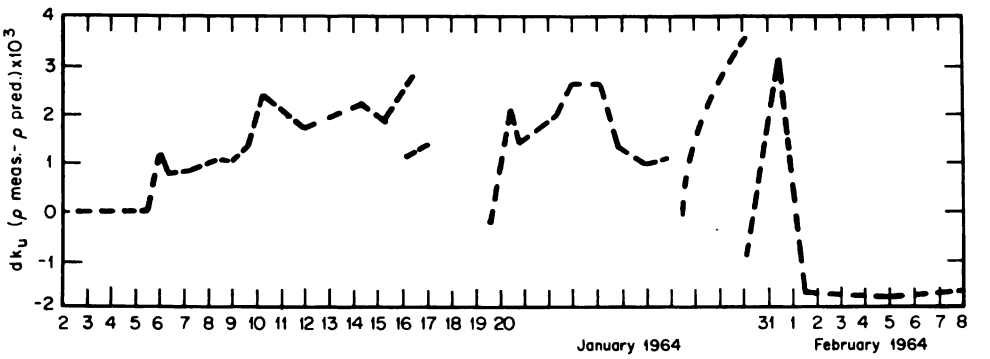

Fig. II-5 Unaccounted reactivity disappearance, dk_u, vs. time. Results of power operation of the BR-3 reactor in the presence of 400 ppm boron.[13]

Operational experience with Yankee, Saxton, and the BR-3 is briefly discussed in Ref. 14. An interesting result of the experiments with Yankee and Saxton has been the discovery of the "*p*H effect" — an increase in reactivity has been observed with increase of the coolant *p*H. The effect has been observed both with and without significant boron levels in the coolant and has not been correlated with the poison content or corrosion-product concentration in the coolant. The increase in reactivity is only a few tenths of a percent, but, as of the time of writing of Ref. 14, no satisfactory explanation had been offered. Hot-laboratory examination of core components of Saxton after nine months of operation with dissolved poison showed "trivial quantities of residual poison on the core."[14]

Reference 14 also discusses recent advances in burnable-poison control. Some of the discussion centers around core 2 of the Shippingport PWR, which utilizes boron–stainless-steel strips as a burnable poison (Fig. II-6). This type of reactor appears to be particularly suited to burnable-poison control since (1) the burnable poison need be incorporated only in the seed elements, (2) only a relatively few burnable-poison sites need be employed, and (3) there is no complication due to the shuffling of fuel assemblies. Also, in the seed-blanket reactor, the control rods are placed in the seed, and hence the burnable poison can be located so as to reduce local peaking due to rod channels. This approach is evident in Fig. II-6.

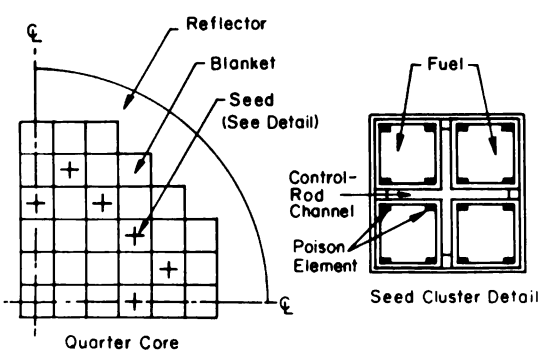

Fig. II-6 Schematic arrangement of burnable poison in the Shippingport core geometry.[14]

Although most of the burnable-poison applications have specified boron as the poison, a number of other materials offer possibilities for use. These are members of the rare-earth family (samarium, dysprosium, erbium, and gadolinium), and each may offer an advantage relative to boron in a particular situation.

Pressure Vessels

Three papers on reactor pressure-vessel design and fabrication[15–17] are from three different countries and present dissimilar views on many aspects of pressure-vessel technology. For example, the "standard" material used for large pressure vessels in the United States is SA-302 grade B steel, the material used for the SEP and SENA pressure vessels is a steel designated "1,2 MD07," and the material of the WWER vessel is a high-strength Cr-Mo-V steel. The exact composition of the latter was not specified, but the compositions of the other two are given in Table II-5. The selection of a pressure-vessel material usually involves a pressure-vessel code, and Ref. 15 contains a discussion of the effects of pressure-vessel codes of various countries.

Digitized by Google

Table II-5 COMPOSITIONS OF VARIOUS PRESSURE-VESSEL STEELS

Country	Designation	Nominal composition, wt.%
United States	SA-302 grade B	<0.25 C, 1.15–1.50 Mn, 0.45–0.60 Mo
Netherlands	1,2 MD07	<0.18 C, 1.0–1.5 Mn, <0.2 Cr, 0.3–0.7 Ni, 0.35–0.55 Mo

In the fabrication of the Russian- and Netherlands-built pressure vessels for the WWER, SENN, SENA, and the KRB reactors, forged rings were used to form the pressure-vessel bodies.[15,17] In contrast, the cylindrical portions of vessels fabricated in the United States are usually rolled, and, if the vessel wall is thin enough, the cladding is roll bonded. The advantages of the forged-ring fabrication technique are discussed in Ref. 15, although, as pointed out in that paper, the resulting vessel is higher in price than a similar one built of sheet material.

Pressure-vessel design and fabrication in the United States are discussed in Ref. 16. The reference opens with a discussion of the recent amendments to the *ASME Pressure Vessel Code* which have resulted in the approval of Sec. III of the *ASME Power Boiler and Unfired Pressure Vessel Codes*, "Rule for Construction of Nuclear Vessels." Older vessels were fabricated in conformity with either Sec. I or Sec. VIII. Although much of the discussion is primarily of interest to the pressure-vessel specialist, Fig. II-7, which illustrates typical BWR and PWR pressure vessels fabricated by either of the ASME codes, Sec. III or Sec. VIII, is a graphic summary of some important effects of the changes. In the particular cases shown, the design by Sec. III results in significant changes in wall thicknesses for the cylindrical sections of the vessel; Table II-6 gives an estimate of the effect on fabrication time for BWR and PWR vessels of various sizes. At first consideration it is surprising that the fabrication times for vessels for both PWR and BWR ap-

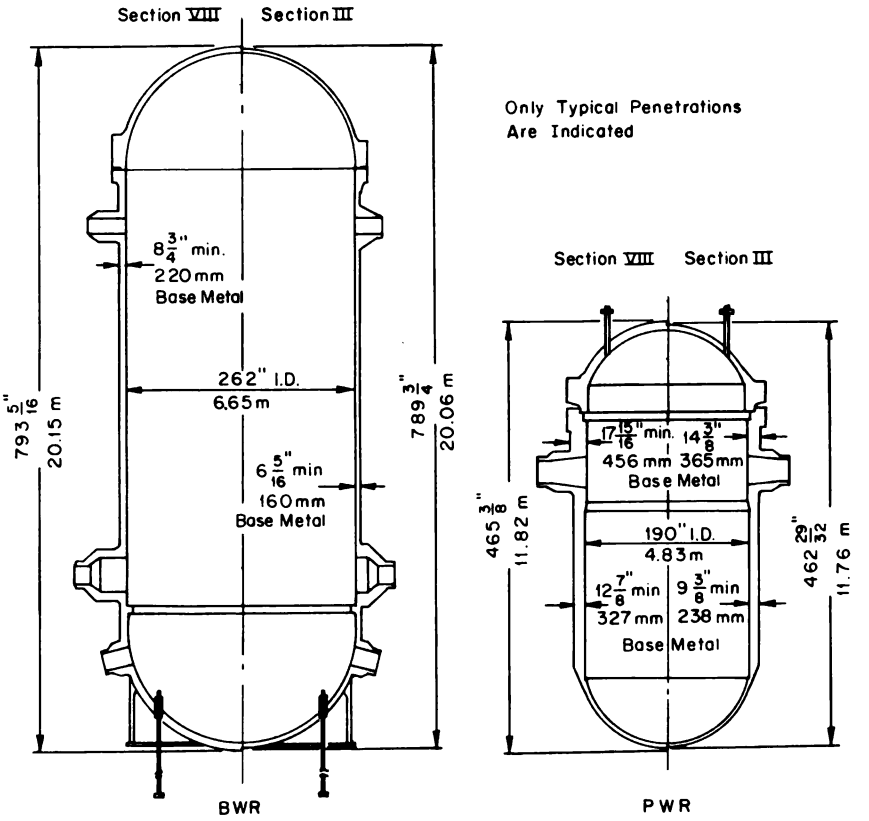

Fig. II-7 Reactor vessel designs for 1000-Mw(e)-capacity plants comparing ASME Code Secs. III and VIII.[16]

Digitized by Google

Table II-6 FABRICATION TIME FOR REACTOR VESSELS OF VARIOUS SIZES[16]

Plant capacity, Mw(e) net	Fabrication time, weeks	
	Sec. III design	Sec. VIII design
250	95	100
500	120	125
750	145	155
1000	165	175
1500	205	220

plication are approximately equal. The reference explains that this is true because the combination of vessel-diameter and vessel-design-pressure requirements offset each other. This, of course, may not always be the case. The relative size difference between BWR and PWR vessels, as indicated in Fig. II-7, is striking. Figure II-8, from the same paper, presents the data in slightly different form. The vessel-size requirements are, of course, determined by reactor design, rather than by vessel-design considerations. Yet the plotted points, although they are not identified in the paper, presumably represent vessels specified for actual plant designs. Hence the lower section of the curve, at least, has authority as a representation of the current state of the art for BWR and PWR design.

The WWER pressure vessel described in Ref. 17 is an unusual one and, for purposes of description, is divided into lower, middle, and upper zones (Fig. II-9). The lower zone consists of three ring portions, each forged as a single piece. The middle zone contains 24 nozzles, which are welded in place as shown in Fig. II-9. The upper zone consists of a one-piece forged flange and a strengthening ring, fitted by means of a shrink-fit technique. The vessel cover is a forged flat plate with 55 penetrations. The internal surface of the vessel is covered with weld-deposited austenitic stainless steel having a thickness of about 20 mm—quite thick in terms of practice in the United States. The vessel-to-cover seal is accomplished by a wedge-shaped nickel gasket compressed between the cover and vessel by means of a thrust ring held in place by studs. The reference describes an alternative seal involving the welding of a flexible collar to both the vessel and the head.

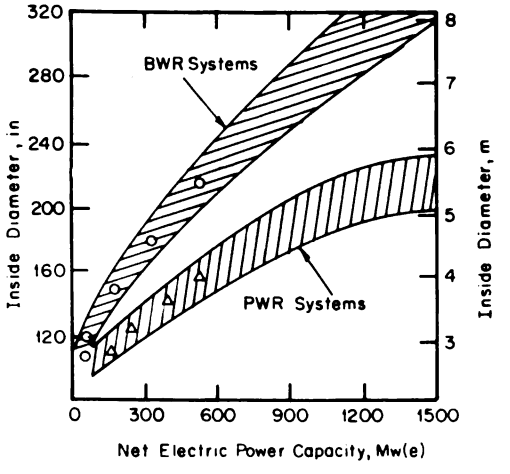

Fig. II-8 Reactor vessel diameter vs. plant power rating.[16]

Thermal and Hydraulic Design

The relatively large number of papers devoted to thermal and hydraulic considerations of water-cooled reactors were all concerned with boiling phenomena and could be grouped into three categories:

—Basic studies of bubble dynamics, velocity profiles, etc.
—Interpretations of experimental data
—Survey papers

The basic studies[18–20] of boiling phenomena were concerned primarily with bubble dynamics, active sites, nucleation, and other variables of interest in two-phase flow. The authors initiated their discussion with a consideration of pool boiling, and, although the detailed results are of primary interest to the specialist, they do indicate that continued progress is being made in gaining an understanding of two-phase behavior.

Of the papers concerned with experimental and analytical results, two presented information on the critical heat flux during unstable burnout in two-phase flow,[21,22] and two were concerned with predicting ϕ_{BO} during stable burnout.[23,24] The test loops used in the experiments reported in Refs. 21 and 22 both employed natural circulation and were instrumented to measure appropriate pressures, powers, flow rates, etc. Typical flow-power curves are illustrated in Fig. II-10. As shown, the flow initially increased, reached a maximum, and then decreased. As power was increased

Digitized by Google

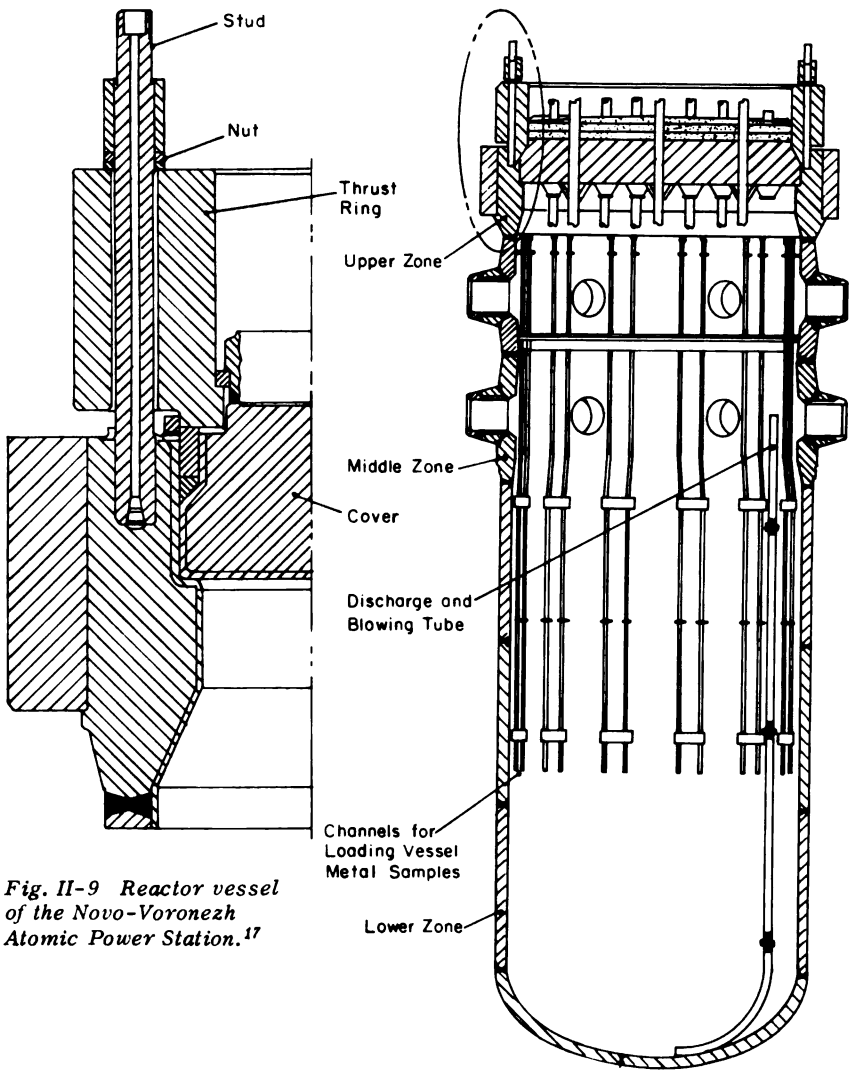

Fig. II-9 Reactor vessel of the Novo-Voronezh Atomic Power Station.[17]

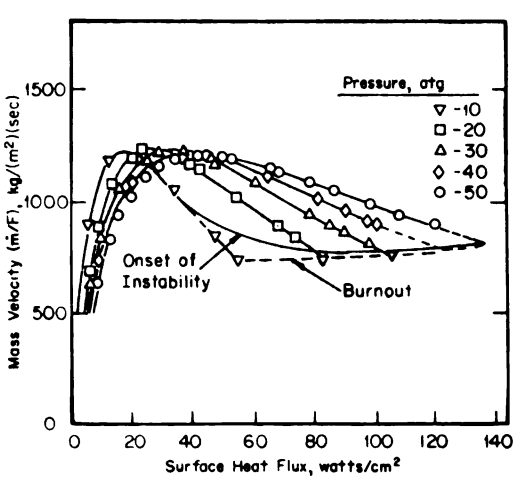

Fig. II-10 Effect of pressure on mass velocity for varying heat flux. Data taken in a natural-circulation loop with test-section diameter of 36 mm and length of 4890 mm. Inlet subcooling, ΔT_{sub}, = 8 ± 0.3°C.

in steps, oscillation usually commenced; three cases are reported:

—Diverging oscillations causing burnout
—Stable oscillations
—Burnout without oscillations

The experimental results were compared against predictions of a theoretical flow model. The predictions were obtained by numerically solving equations of continuity, energy, and momentum; the stability limit was analytically determined as the power input where the oscillations in inlet velocity became divergent upon a step increase of 1% in channel power. Although no general stability criteria are given in the reference, it would appear that the method is generally applicable for specific cases of uni-

Digitized by Google

formly heated test sections of simple geometry. Reference 21 also discusses the effects of inlet subcooling and inlet throttling on burnout heat flux and compares operation with natural and forced convection; these data are shown in Figs. II-11 to II-13.

Reference 23 presents several correlations of burnout heat flux for flow of subcooled water in tubes, steam-water mixture in tubes, and flow in an annular gap. The correlations are empirical, and their interpretation is complicated by the fact that the units are of the "mks" system. Pressure is measured in newtons per square centimeter and latent heat in joules per kilogram; the correlation gives the burnout heat flux in units of watts per square meter, however. The units for pressure should be carefully noted since at least one English translation of a recent Russian heat-transfer article has

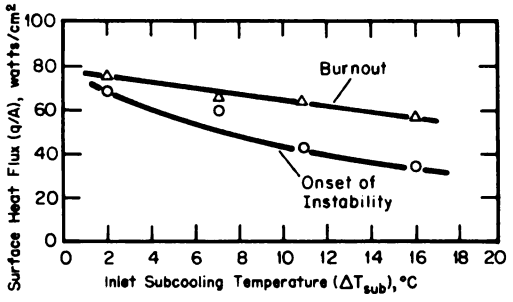

Fig. II-11 Effect of inlet subcooling on critical and burnout heat fluxes.[21] Data taken in a natural-circulation loop with test-section diameter of 20 mm and length of 4890 mm. Pressure = 50 atg.

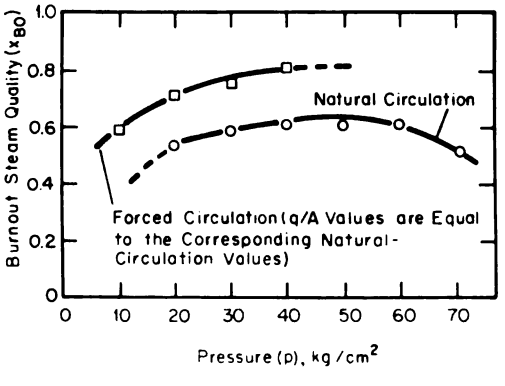

Fig. II-12 Comparison between natural- and forced-circulation burnout data.[21] Test-section diameter, 20 mm; length, 4890 mm. Forced-circulation data were taken with "heavy" inlet throttling.

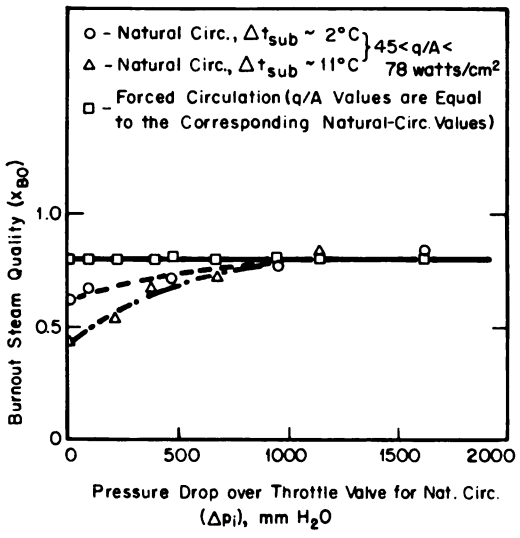
o - Natural Circ., Δt_sub ~ 2°C
Δ - Natural Circ., Δt_sub ~ 11°C
} 45<q/A< 78 watts/cm²
□ - Forced Circulation (q/A Values are Equal to the Corresponding Natural-Circ. Values)
Burnout Steam Quality (x_BO)
1.0
0.5
0
0 500 1000 1500 2000
Pressure Drop over Throttle Valve for Nat. Circ. (ΔP_i), mm H₂O

Fig. II-13 Effect of inlet throttling on burnout.[21] Test-section diameter, 20 mm; length, 4890 mm. Pressure = 50 atg.

translated pressure in newtons per square centimeter as "neuts/cm^2." The correlation for ϕ_{BO} for steam-water mixture in tubes is as follows:

$$\phi_{BO} = [1.46 \times 10^{-4}\, r^{1.72}(1-x)^m - 0.116\, W_g] \frac{2.71}{d_{in}\, 0.48} \quad (1)$$

where ϕ_{BO} = burnout heat flux, watts/m^2
r = latent heat, joules/kg
x = quality
W_g = mass flow rate, kg/(hr)(m^2)
d_{in} = internal tube diameter, mm
$m = 3.48 - 0.54\,(r/4.18 \times 10^6)$

The range of applicability of Eq. 1 is stated to be as follows:

Pressure:	392–981 newtons/cm^2 (568 to 1422 psi)
Mass flow:	$2-18 \times 10^6$ kg/(hr)(m^2)
Quality:	0–0.40
d_{in}:	4–12 mm
Length:	≥200 mm

Equation 1 is plotted in Fig. II-14 for a pipe diameter of 0.18 in., a pressure of 1000 psia, and two different values of W_g. This figure compares the correlation with data appearing in Fig. III-12 of *Power Reactor Technology*, 7(1). The correlation does not predict the experimentally determined "best-fit" curve very

Digitized by Google

well, although the range of experimental data falls within the range of applicability of Eq. 1.

Reference 23 also presents the results of burnout experiments utilizing nonuniformly heated test sections, and these are given in Fig. II-15. The ordinate on the curves is believed by the reviewer to be the weighted mean heat flux, and the heat-flux nonuniformity is believed to be a radial one, although the reference is not particularly clear in these two quite important aspects. The experiments were carried out "... with round tubes of d_{in} = 10 mm, tube length is 400 mm and with the eccentricity between external surfaces and internal ones (three values)...."[23] These three values are probably the ones corresponding to curves 2, 3, and 4 in Fig. II-15.

Reference 24 presents burnout data taken at General Electric—San Jose, Hanford, and Columbia. Since the results of many of these programs have been reviewed in previous issues of *Power Reactor Technology*, additional details will not be discussed here.

References 25 and 26 are in themselves reviews. Reference 25 reviews highlights of two-phase-flow research relative to boiling reactors in the United States, and Ref. 26 describes the experimental work on heat transfer and hydrodynamics with steam-water and two-component mixtures done at the Centro Informazioni Studi Esperienze (CISE), Milan, Italy.

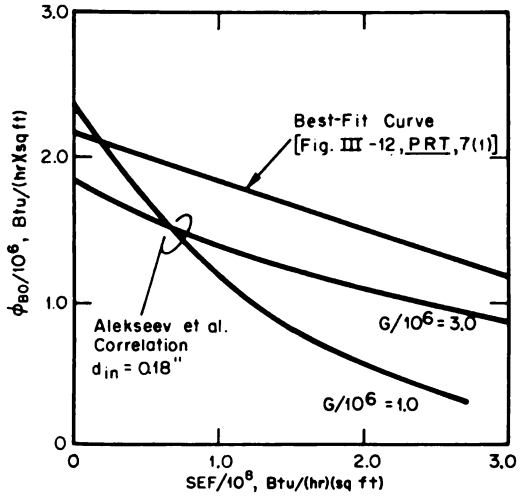

Fig. II-14 Comparison of burnout correlation of Alekseev et al.[23] with burnout data previously published in Power Reactor Technology. *Pressure = 1000 psia.*

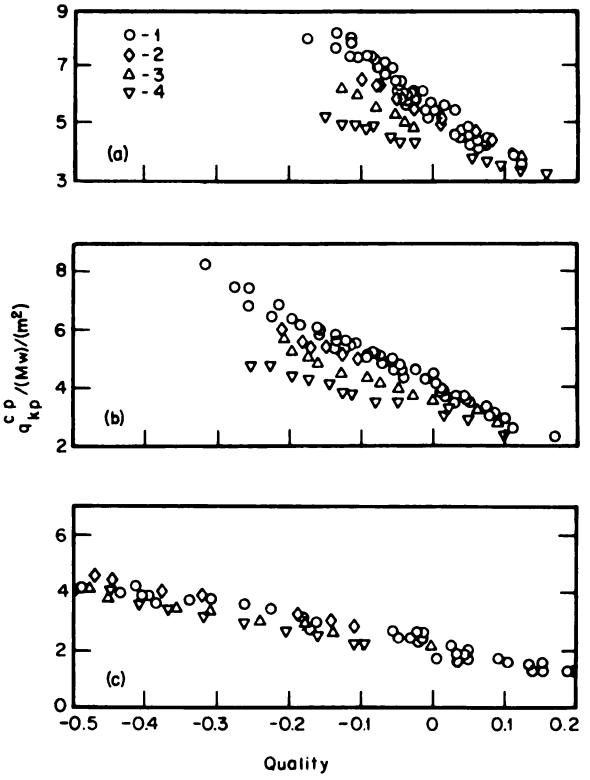

Fig. II-15 Heat-flux concentration nonuniformity influence on q_{BO} in round tubes. Curves 1, 2, 3, and 4 correspond to values $q_{BO}^{max.}/q_{BO}^{av.}$ of 1, 1.12, 1.28, and 1.50. Parts a, b, and c correspond to pressures[23] of 588, 981, and 1765.8 neutrons/cm^2.

Directions of Future Developments

To some extent the future developments in water-reactor technology are tied into the design features of the advanced plants of each type; these are listed last under the appropriate headings in Table II-1. References 27 and 28 present views of two water-reactor manufacturers on developments of their particular type, and Ref. 29 discusses advanced Russian water reactors.

The boiling-water reactors designed by the General Electric Company are tied quite closely to the concept of pressure suppression. On the other hand, the recent Westinghouse-designed reactors utilize a variety of containments from an unshielded steel containment vessel to the double-barrier concept, employing a sandwich of porous concrete between two layers of steel and reinforced concrete. Both the pressure-

Digitized by Google

suppression and double-barrier concepts, however, require that the capability be present in the plant to process potentially contaminated air from within the containment or reactor building during routine operation before release from a plant stack.

Early designs of both the BWR and the PWR stations, as exemplified by Dresden and Yankee, used canned pumps in the primary circuit. This practice seems to be declining, however, since the Big Rock Point BWR uses pumps of the shaft-seal type and the San Onofre PWR is scheduled to use them. This change has come about for several reasons. Possibly in the pressurized-water reactors the most important was the desire to utilize pumps of capacities in excess of 50,000 gal/min. In the boiling-water reactors, the change is probably due primarily to confidence that has been built up in the handling of radioactivity: since the direct-cycle boiling-water reactors must, in any case, provide for the handling of radioactive off-gases, there is less incentive to reduce the leakage of primary water to a bare minimum. Reference 27, in addition, mentions that work is being done to develop a jet pump for use inside the reactor vessel of the boiling-water reactor to "substantially" reduce the flow external to the vessel. For other primary system components, Ref. 28 states that PWR plants currently under design and construction do not provide for primary-coolant-loop stop valves and check valves, since safety and operational studies indicated these valves were not needed.

Fuel-element experience has been relatively good for both the pressurized-water and boiling-water reactors, with the exception of the failures of the stainless-steel-clad elements in the VBWR mentioned previously. As a result, Ref. 27 states that Zircaloy is the "favored" cladding material for current boiling-water reactors, with Incoloy and Inconel slated for testing. On the other hand, the pressurized-water reactors have shown no difficulties when utilizing either stainless-steel cladding or Zircaloy, although large-scale experience with rod elements of the UO_2-Zircaloy type has been limited to the rather mild conditions in the Shippingport blanket. Until the VBWR failures can be tied to a cause not connected with the reactor type, the PWR designer may have additional freedom in the choice of cladding materials because of the ability of the pressurized-water reactor to operate with close control of coolant chemistry. Both references mention that spring type spacers will be considered for present and future fuel-assembly fabrication techniques. This eliminates welding and brazing operations on fuel-cladding surfaces and allows cold-worked cladding to be utilized, if desired.

Control and refueling are two areas of interest for future developments. The chemical-shim control of the pressurized-water reactor has been mentioned previously. In addition, Ref. 28 mentions a so-called "rod-cluster-control" scheme for advanced pressurized-water reactors, to be used in conjunction with chemical shim. This utilizes hollow tubes that replace some of the fuel rods within a fuel assembly; inside each hollow tube is a cylindrical, unfollowed, absorber rod. The several rods within the confines of a single fuel assembly are mechanically connected and are operated, as a cluster, by a single drive unit. No cruciform type control rods are employed. The application of soluble-poison control to the boiling-water reactor is less straightforward and has not been proposed in any commercial design. The use of bottom-entering control rods to assist in axial power flattening will no doubt be continued, and further flattening and reactivity compensation may be obtained with fixed shims of boron stainless steel. Both Refs. 27 and 28 mention "scatter loading," in which exposed fuel assemblies and new assemblies are distributed more or less uniformly over the core volume rather than in zones. Upon refueling, the most highly exposed assemblies are replaced by new assemblies, but there is no shuffling of the remaining assemblies.

The refueling of both reactor types is complicated by above-core structure and mechanism. The boiling-water reactor of the future most likely will have internal steam separators, and these will probably have to be removed before refueling. The pressurized-water reactor, on the other hand, while not requiring steam-separation equipment within the pressure vessel, may have control-rod-drive guide structures above the core which must be moved. This structure becomes more complex when "cluster" rods are used. The efficient removal of the above-core components will probably continue to be an important consideration for both reactor types in order to minimize downtime for refueling purposes. In-core instrumentation, mentioned in both references, will probably continue to follow the control-rod-drive posi-

Digitized by Google

tion, being inserted into the BWR core from the bottom and into the PWR core from the top. Thus the BWR in-core instrumentation need not be removed during fuel handling, whereas Ref. 28 mentions that the PWR in-core instrumentation probably will be removed as a unit, being attached to a common support plate presumably located above the core. One of the criticisms of the water reactors, heard rather frequently in the informal discussions at Geneva, was the long shutdown time required for refueling. No doubt this problem will receive increasing emphasis in coming years.

assembly consists of a guide tube mounted permanently in the core; its shape is hexahedral outside and cylindrical inside. The safety rod is fabricated of a cylindrical absorber 125 mm in diameter, which is followed by a zirconium alloy scatterer without fuel in the WWER-1 and by a fueled follower in the WWER-2.

Some of the differences between the two reactors—for example, the change to electric pressurization and the adoption of ion-exchange water treatment—involve changing to design techniques that have been used in the United

Table II-7 COMPARISON OF WWER-1 AND WWER-2

Parameter	WWER-1	WWER-2
Power, Mw(e)	210	365
Status	Operating	Under construction
No. of stationary fuel assemblies	312	276
Length, m	2.5	2.5
Shape, cross sectional	Hexagonal	Hexagonal
Distance across flats, mm	144	144
Pitch	147	
Fuel-pin geometry	Rods	Rods
Cladding material	Zr-Nb	Zr-Nb or S.S.
Cladding outside diameter, mm	10.2	8.8
No. of pins/assembly	90	127
Fuel material	UO_2 pellets	UO_2 pellets
Fuel-pellet outside diameter, mm	8.7	7.7
No. of movable fuel assemblies		
Compensating	31	60
Safety	6	13
Coolant purification	Evaporation	Ion exchange
No. of primary loops	6	8
Pressurizer type	Gas	Electric
Coolant pressure, atm abs.	100	120
No. of turbines	3	5

Reference 29 is interesting partly because the Voronezh reactors (WWER) are quite different in design from the pressurized-water reactors constructed in the United States. The reference discusses the changes between the first unit of the plant (WWER-1) and the second (WWER-2). A comparison of the two reactors is given in Table II-7. Both reactors employ hexagonal fuel assemblies, but there is a difference in the number of fuel pins per assembly. The movable fuel assemblies of the "compensating" type are for slow changes in reactivity. These consist of a flux-trap type of control rod, hexagonal in shape, mounted on top of a movable fuel assembly very similar in design to the stationary assemblies. The safety

States for a number of years. Other features of the WWER-2, notably the elimination of the cladding in the pressure vessel,[29] represent departures from practice in the United States.

The reference concludes with a discussion of future improvements in the reactor type not specifically tied to the WWER plant. One of the most significant areas for improvement is the method of refueling. Although WWER-1 had not been refueled at the time of the writing of Ref. 29, the authors were aware that, in general, refueling operations "...require a lot of time...." A number of possible solutions are discussed, and the most attractive one is a reactor design employing soluble poison since this application allows the removal of most, if

Digitized by Google

not all, of the control-rod-drive structure from above the core. The resulting reactor is shown in Fig. II-16. The "honeycomb" core design is not well explained in the reference, but the interesting application to refueling is the provision for storage of fuel elements within the pressure vessel. The fuel-element handling

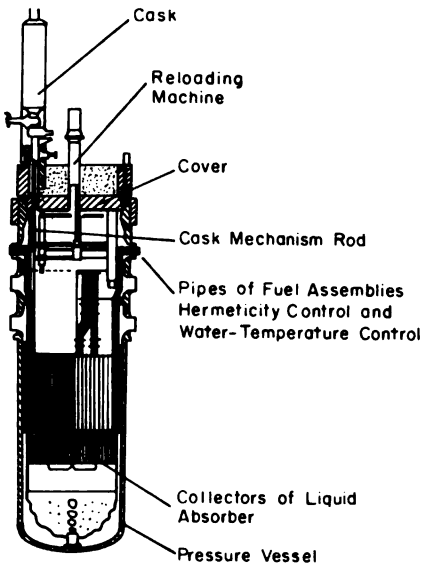

Fig. II-16 Reactor scheme with honeycomb core and with the change of liquid-absorber concentration in the channel system.[29]

would be done after the reactor had been shut down but not depressurized. The centrally located reloading machine would handle the fuel elements, taking new elements from their racks within the vessel and replacing spent elements. After the fuel movement into and out of the core had been accomplished, the reactor would be brought to power, and the spent elements would be transferred through a vessel lock. The latter step need not be done rapidly since reactor operation would not be affected.

Several of the recommendations for advancement in the WWER technology are peculiar to the reactor as designed. In the WWER-1 the clearance between adjacent fuel bundles is only a few millimeters, and the requirement for the movement of the relatively large flux-trap control rods to a position above the core apparently makes the design of the upper grid plate somewhat difficult. If the fuel assemblies are locked in place at their lower end, the lack of open space within the core makes it difficult to get at the locking devices with fuel-handling tools. Accordingly, Ref. 29 suggests that the fuel elements be hydraulically locked in place by a piston located at the bottom of the bundle but connected to the space above the core. The control rods would be bottom driven to facilitate refueling, and the reference illustrates a possible hydraulic-drive mechanism. The upward direction of the flow in the WWER reactor gives rise to what appear to be formidable hydraulics problems, other than the one of merely holding the fuel elements in place. The large fueled followers move against the coolant flow when they move in the direction of reducing reactivity, and they must be adequately cooled during any movement. Downflow is discussed in Ref. 29, but the designers appear reluctant to take the step due to problems connected with flow reversal during main pump coastdown.

References

These references are papers presented at the Third United Nations International Conference on the Peaceful Uses of Atomic Energy, Geneva, September 1964.

1. R. J. Coe and W. C. Beattie, Operational Experience with Pressurized Water Systems, A/Conf. 28/P/202.
2. V. L. Stone, Operating Experience with Boiling Water Reactors, A/Conf.28/P/204.
3. L. V. Komissarov, G. L. L. Lunin, A. N. Novikov, V. A. Sidorenko, and V. D. Sidorenko, Physical Studies of Novo-Voronezh Atomic Power Station Reactor (WWER), A/Conf.28/P/585.
4. G. L. Dunin, V. A. Sidorenko, S. A. Skvortsov, M. A. Borisev, F. Y. Ovchinnikov, V. P. Denisov, V. V. Stekelnikov, A. A. Khokhlachov, and B. S. Yasvenko, Start-Up and Adjustment of Reactor WNER of Novo-Voronezh Atomic Power Station, A/Conf.28/P/305.
5. S. Naymark and C. N. Spalaris, Oxide Fuel Fabrication and Performance, A/Conf.28/P/233.
6. T. J. Pashos, D. R. deHalas, D. L. Keller, and L. A. Neimark, Irradiation Behavior of Ceramic Fuels, A/Conf.28/P/240.
7. J. M. Leblanc, Irradiation of Plutonium Enriched Ceramic Fuel Rods in the BR-3 Power Reactor, A/Conf.28/P/443.
8. V. S. Emelyanov, A. I. Evstyukhin, G. B. Fedorov, G. G. Ryabove, N. V. Borkov, I. I. Korobkov, and P. L. Gruzin, Corrosion Resistance of Zirconium and Its Alloys in Water and Steam at High Temperatures, A/Conf.28/P/341.
9. A. D. Amaev, R. S. Ambartsumyan, A. A. Kiselev, S. T. Konobeevskiy, I. A. Anisimova, A. M. Glukhov, L. M. Lebedev, V. A. Myshkin, V. V. Goncharov, E. G. Ivanov, M. S. Orlov, P. F. Pravdyuk, E. P. Ryazantsev, and V. V. Skvortsov, Influence of Some Factors Upon Hydriding and Variation of Properties of Zirconium Alloy with

Digitized by Google

1% Nb Used for Fuel Element Cladding in Water-Moderated Water-Cooled Power Reactors, A/Conf.28/P/342.
10. J. E. Draley, J. A. Ayres, W. E. Berry, E. Hillner, and S. P. Rideout, Corrosion in Aqueous Systems, A/Conf.28/P/243.
11. K. Videm, Mild Steel in Primary Circuits of Water Cooled Power Reactors, A/Conf.28/P/592.
12. G. C. Ambrosini, T. Bozzoni, G. Cipollina, E. Colussi, and R. Garroni, Stability Analysis and Dynamic Performance of a Chemical System Operated for the Automatic Fine Control of a Nuclear Reactor, A/Conf.28/P/629.
13. M. Plumier, P. Stacquez, P. Dozinel, R. Muyllie, M. Preat, G. Beuken, M. Gueben, and L. Maesen, Practical Results and Prospects of the Use of Soluble Poison in the Pressurized Water Reactors, A/Conf.28/P/518.
14. A. Radkowsky and R. J. Creagan, Poison Control of Thermal Reactors, A/Conf.28/P/274.
15. K. J. de Jong, C. de Peter, and M. C. van Veen, Experiences on the Design, Calculation and the Manufacture for Power Reactor Components, A/Conf.28/P/728.
16. A. L. Gaines and L. Porse, Problems in the Design and Construction of Large Reactor Vessels, A/Conf.28/P/227.
17. V. V. Stekolnikov, A. A. Khokhlatchev, V. P. Denisov, J. V. Vikhorev, N. I. Prigorovskiy, N. A. Lugov, B. I. Kovalenko, and V. B. Dobronravov, High Pressure Vessels of Light-Water Cooled and -Moderated Power Reactors, A/Conf.28/P/331.
18. C. J. Rallis and H. H. Jawurek, The Mechanism of Nuclear Boiling, A/Conf.28/P/600.
19. K. Torikai, M. Nori, M. Akiyama, T. Kobori, and H. Adachi, Boiling Heat Transfer and Burnout Mechanism in Boiling-Water Cooled Reactor, A/Conf.28/P/580.
20. H. Mondin, P. Lavigne, and R. Semeria, Some Fundamental Aspects of Boiling in Nuclear Reactors, A/Conf.28/P/55.
21. K. M. Becker, S. Jahnberg, I. Haga, P. T. Hansson, and R. P. Mathisen, Hydrodynamic Instability and Dynamic Burnout in Natural Circulation Two-Phase Flow. An Experimental and Theoretical Study, A/Conf.28/P/607.
22. M. Bogaardt, C. L. Spigt, F. J. M. Dijkman, and N. Madsen, Heat Transfer and Hydraulic Stability in Boiling Water Reactors, A/Conf.28/P/589.
23. G. V. Alekseev, B. A. Zenkevitch, O. L. Peskov, N. D. Sergeev, and V. I. Subbotin, Burn-Out Heat Fluxes Under Forced Water Flow, A/Conf.28/P/327a.
24. S. Levy, J. Batch, and J. Casterline, Critical Heat Flux Considerations in the Thermal and Hydraulic Design of Water-Cooled Nuclear Reactors, A/Conf.28/P/224.
25. P. A. Lottes, W. H. Cook, K. F. Neusen, R. W. Wright, S. M. Zivi, and N. Zuber, Fluid Dynamics, Stability, and Vapor-Liquid Slip in Boiling Reactor Systems, A/Conf.28/P/230.
26. N. Adorni, S. Bertoletti, I. Casagrande, L. Cravarolo, G. P. Gaspari, A. Hassid, C. Lombardi, E. Pedrocchi, and G. Peterlongo, Basic Heat Transfer and Hydrodynamics Studies in Two-Phase Flow, A/Conf.28/P/867.
27. G. White, Developments in Boiling Water Reactors, A/Conf.28/P/205.
28. J. C. Rengel and W. E. Johnson, Developments in Pressurized Water Reactors, A/Conf.28/P/203.
29. A. Y. Kramerov, Y. V. Markov, S. A. Skvortsov, V. A. Sidorenko, B. P. Denisov, E. V. Kulikov, Y. P. Sorokin, V. V. Stekolnikov, A. A. Hoblachev, and V. P. Tatarnikov, Some Ways of Water-Water Power Reactor Development, A/Conf.28/P/304.
30. W. B. Lewis, J. R. MacEwan, W. H. Stevens, and R. G. Hart, Fission-Gas Behaviour in UO_2 Fuel, A/Conf.28/P/19.
31. R. D. Page, D. G. Hardy, A. J. Mooradian, J. Howieson, G. R. Fanjoy, and D. B. Nazzer, Engineering and Performance of UO_2 Fuel Assemblies, A/Conf.28/P/18.
32. J. A. L. Robertson, A. S. Bain, J. R. MacEwan, and M. J. F. Notley, UO_2 Performance — The Importance of Temperature Distribution, A/Conf.28/P/17.

Digitized by Google

Section

III

Power Reactor Technology

Vessel Type Superheating Reactors

Status and Design Features

The status of the various nuclear superheat projects in the United States has been covered in several previous issues of *Power Reactor Technology*. In particular, Vol. 7, No. 3, presented the designs of the BONUS and Pathfinder integral boiling-superheating power reactors. Both these reactors are currently in the process of startup. Two experimental superheating reactors, BORAX-V and EVESR, have had some operating experience. The present state of the art of the U. S. superheat program is summarized in Ref. 1.

Table III-1 lists pertinent data for three integral boiling-superheating plants. The EVESR (Fig. III-1) is a separate superheat reactor in that it superheats steam from an outside source rather than evaporating and superheating within the same vessel. At present the saturated steam is being supplied by a fossil-fired boiler. The fuel is of annular geometry, as shown in Fig. III-2. Steam flows down the annular flow passage to the bottom plenum of the element, reverses flow direction, and flows up the central hole. Other details of the reactor are given in Table III-2.

Superheating reactors are being studied not only in the United States but also in Germany[2] and the Soviet Union.[3] Reference 2 is a description of a prototype integral superheat reactor that was scheduled to be started in Germany in late 1964. The plant is to be 100 Mw(t) and is to produce steam with a temperature of 500°C at a pressure of 60 ata. The plant site is at Kahl, and the prototype reactor will power an existing turbine-generator set. The reactor core is composed of 45 fuel assemblies, arranged in a 7 by 7 lattice with the corners missing (Fig. III-3). Each assembly is composed of 64 fuel elements of a hollow, annular design (Fig. III-4). The interesting coolant-flow path within the vessel starts with the liquid water undergoing heating and boiling on the exterior of the annular fuel elements, under natural-circulation flow. The saturated steam flows to the upper portion of the pressure vessel and enters the superheating passages of the center 25 fuel assemblies via appropriate piping. Each fuel assembly is two-pass in design, with steam flowing down the center hole of the outer 32 fuel elements and up the center hole of the remaining 32 elements. The partially superheated steam then flows to the outer 20 assemblies, shown shaded in Fig. III-3. The same two-pass flow within the assemblies takes place, producing steam of the final desired temperature. The entire reactor is thus essentially a four-pass superheater.

The combination boiling-superheating fuel element is an advanced concept and must be designed carefully with respect to thermal stresses. In the fuel element shown in Fig. III-4, a rather large temperature difference will exist between the walls in contact with the superheated steam and those in contact with the boiling water. In addition, the superheater wall temperature in the second-pass elements will be greater than the corresponding wall temperature in the first-pass elements. The latter problem is to be solved by bellows, and the other thermal stress is to be taken up by the use of proper material combinations to withstand the stresses. Elements of this general type have been constructed and irradiated in the United States; this program was reviewed in the March 1963 issue of *Power Reactor Technology*, 6(2): 75-80. Superheat tests have also been run in the Kahl boiling-water reactor and are briefly reviewed in Ref. 2. The

Digitized by Google

Kahl facility apparently is an in-pile loop capable of testing fuel elements, but not necessarily elements of full length. In February 1964, two fuel tubes were removed from the loop after a burnup of about 1150 Mwd/ton. These combination elements were clad with Inconel X and Hastelloy C, and both were "undamaged"; the maximum cladding temperature reached was relatively low — about 770°F. These tubes were fabricated from UO_2 pellets of annular geometry, although vibratory compaction is also being studied as a fabrication method.

Details of the Russian superheating reactor are given in Ref. 3. This plant is currently being completed in the Ulyanovsk region of the Soviet Union and will be an extremely flexible test facility. Two cores are presently contemplated for the facility — a small core (for initial use) that will produce saturated steam at a pressure of 100 atm and a large core that will generate 90 atm of superheated steam at a temperature of about 500°C. The reactor as a whole is being designed to generate steam at pressures between 30 and 100 atm. Figure III-5 shows the plant flow diagram. The turbine is designed to operate with saturated steam at a pressure of 29 atm, and the high-pressure steam separator shown in Fig. III-5 provides for throttling of the steam, which will be generated at higher pressures. Superheated steam, when produced, can be delivered to a separate turbine or to a special cooler. The plant also provides for dual-cycle operation by the inclusion of steam generators in which 30 atm of saturated steam can be generated. Data on the reactor are given in Table III-3. Figure III-6 is a view of the reactor as arranged for super-

Table III-1 BOILING-WATER REACTOR PLANTS WITH INTEGRAL SUPERHEAT DESIGN DATA[1]

	BONUS		BORAX-V		Pathfinder	
Site	Puerto Rico		NRTS, Idaho		Sioux Falls, S. Dak.	
Owner*	USAEC		USAEC		NSP	
Reactor designer*	GNEC		ANL		A-C	
Operating contractor*	PRWRA		ANL		NSP	
Electric power, Mw(e) gross	17.5		3.5		66	
Electric power, Mw(t) net	16.5		3.5		62.5	
Thermal output, Mw(t)	50		20		200	
Plant steam cycle	Direct		Direct		Direct	
Position of superheater region	Peripheral		Central or peripheral		Central	
Nominal operating pressure, psig	975		600		600	
Turbine throttle steam pressure, psig	850		350 (587 available)		535	
Saturated steam temp., °F	543		489		489	
Superheated steam temp., °F	900		850		825	
Thermal power to boiling, Mw	37		16.6		157	
Thermal power to superheating, Mw	13		3.4		43	
Gross cycle efficiency, %	35				33	
Net cycle efficiency, %	33				31	
Maximum superheat fuel-cladding temp., °F	1175		1110		1250	
	Boiling	Superheater	Boiling	Superheater	Boiling	Superheater
Effective outside core dia., ft	3.34	4.83	3.25	1.0	5.75	2.5
Core height, ft	4.55	4.55	2.0	2.0	6.0	6.0
Structural material (core)	Zircaloy-2	S.S. 348	Al(X8001)	S.S.	Zircaloy-2	S.S.
Fuel type	Rod	Rod	Rod	Plate	Rod	Double tubular
Fuel material	UO_2	UO_2	UO_2	UO_2–S.S. cermet	UO_2	UO_2–S.S. cermet
Fuel enrichment, %	2.40	3.25	4.95	93	2.2	93
Cladding material	Zircaloy-2	Inconel	S.S. 304	S.S. 304L	Zircaloy-2	S.S. 316L
Control-rod shape	Cruciform	Slab	Cruciform and "T"	Cruciform and "T"	Cruciform	Round rod
Control-rod material	1.0 wt.% B^{10} in S.S.	1.0 wt.% B^{10} in S.S.	Boral	Boral	2 wt.% boron in S.S.	2 wt.% boron in S.S.
No. of steam passes		4		2		1
Average power density, kw(t)/liter	33.6	11.5	42.5	40.5	45.2	46.5

*GNEC = General Nuclear Engineering Corporation.
PRWRA = Puerto Rico Water Resources Authority.
ANL = Argonne National Laboratory.
NSP = Northern States Power.
A-C = Allis-Chalmers.

Digitized by Google

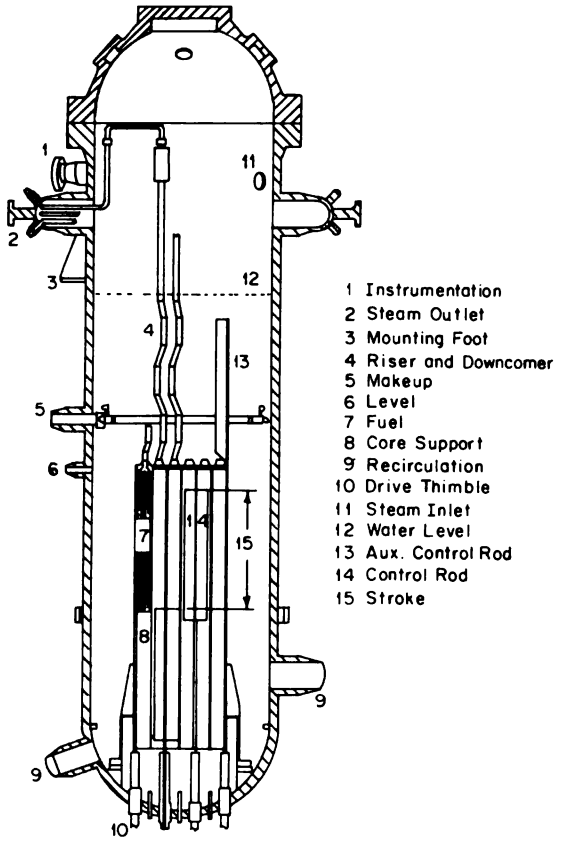

Fig. III-1 EVESR reactor.[1]

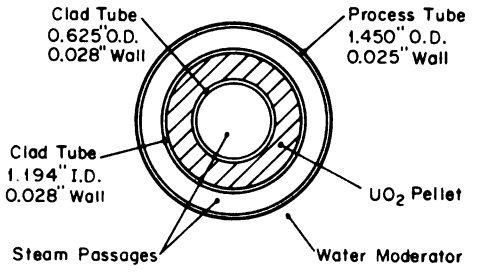

Fig. III-2 EVESR fuel-element cross section.

Table III-2 DESIGN PARAMETERS OF THE EVESR REACTOR

Type	Heterogeneous, light-water-moderated, thermal-neutron, steam-cooled
Power, Mw(t)	12.5 (initial)
No. of fuel elements	32
Process tubes/fuel element	9 (3 by 3 array)
Cladding	Incoloy, Inconel, S.S. 304 (commercial), S.S. 304VM, S.S. 310VM
Maximum cladding-surface temp., °F	1250

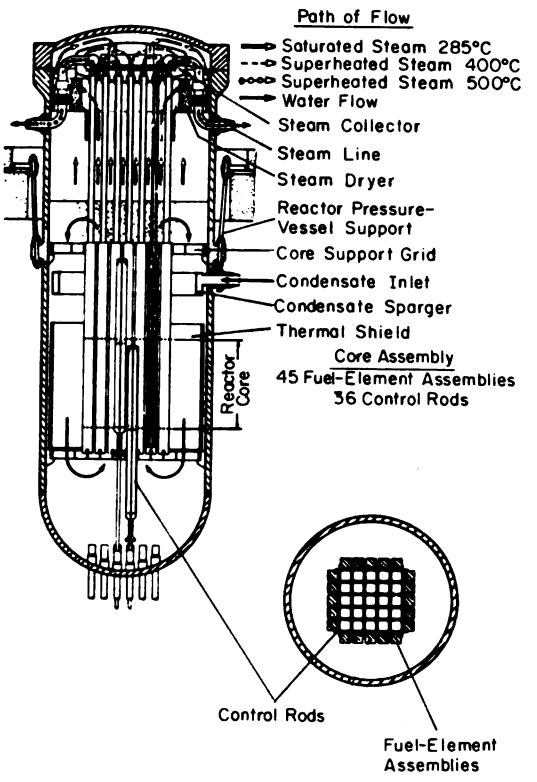

Fig. III-3 Schematic of the Kahl superheating reactor.[2]

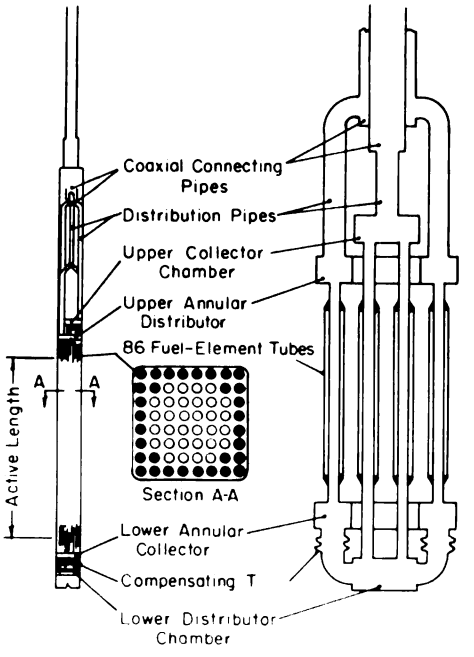

Fig. III-4 Schematic of the Kahl superheating-reactor fuel element.[2] ○, *up pass.* ●, *down pass.*

Digitized by Google

heating, and Fig. III-7 shows the cross section of the "large" core. The reactor is controlled by 31 movable assemblies for reactivity compensation and 6 safety assemblies. These appear to be similar in design and operation to those employed in the WWER, and their positions are illustrated in Fig. III-7. The follower employed in the safety assemblies is a zirconium scatterer, however, and is not fueled.

Table III-3 CHARACTERISTICS OF THE RUSSIAN INTEGRAL SUPERHEATING REACTOR

Pressure-vessel size		
Outside diameter, m	3.8	
Height, m	11.0	
Boiler fuel-assembly details		
Fuel	UO_2	
Cladding	Zr alloy	
Cladding outside diameter, mm	10.2	
Cladding thickness, mm	0.6	
Fuel-element geometry	Hexagonal	
Distance across flats, mm	176	
No. of fuel pins/assembly	127	
Fuel-pin pitch, mm	15.1	
Superheater fuel-assembly details		
Fuel	UO_2	
Cladding	S.S.	
Cladding outside diameter, mm	~10.2	
Cladding thickness, mm	0.5	
Fuel-element geometry	Hexagonal	
Distance across flats, mm	176	
No. of fuel pins/assembly	61	
Steam-flow-channel width, mm	1	
Insulating material	Stagnant steam	
	Large core	Small core
Power, Mw(t)	250	150
Core dimensions		
Diameter, m	2.6	1.8
Height, m	2.0	2.0
No. of fuel assemblies in the core	181	85
Boiling zone	109	
Superheater zone	72	
UO_2 loading in the core, tons	19.3	11.4
Boiling zone	14.6	
Superheater zone	4.7	
Water-to-uranium ratio		2.0
Boiling zone	1.5 to 2.0	
Superheater zone	3.0 to 3.5	
Balance of reactivity, % k_{eff}		
Temperature effect (to 309°C)	2.4	3.5
Steam generation (for average steam fraction)	2.0	Up to 3.5
Doppler effect	1.6	2.0
Xenon and samarium poisoning (in equilibrium state)	4.2	4.7
Fuel burnup	5.7	5.3
Structural elements	1.0	2.5
Total reactivity excess in a cold clean reactor	17.0	21.5
Worth of control devices in a cold reactor, % k_{eff} including:		
Absorbers with mechanical drives	19.0	24.0
Liquid poison	20.0	20.0
Maximum fuel-element heat flux, kcal/(m²)(hr)	1.2×10^6	1.2×10^6

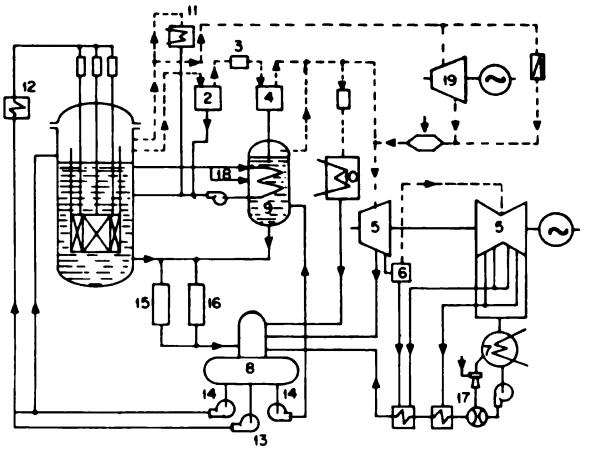

1 Reactor
2 High-Pressure Separator
3 Throttle Valve
4 Mean Pressure Separator
5 Saturated-Steam Turbine
6 Moisture Separator
7 Turbine Condenser
8 Deaerator
9 Steam Generator
10 Auxiliary Condenser
11 Shutdown Cooling Condenser
12 Heat Exchanger
13 Plunger Pump
14 Feedwater Pumps
15 Water-Purifier Evaporating Unit
16 Ion-Exchange Filter
17 Turbine Jet
18 Steam-Generator Feed Line with Step Evaporation
19 Superheated-Steam Turbine

Fig. III-5 Principal flow diagram of the Ulyanovsk plant.[3]

The two-pass superheating fuel element is illustrated in Ref. 3, but the print is of poor quality, at least in the copy seen by this reviewer. Figure III-8 approximates the fuel-pin design, however. The reactor is designed to utilize natural circulation. Construction apparently was well under way when downcomer entrainment was discovered to be a serious design consideration for boiling-water reactors, and according to Ref. 3 the downcomer entrainment will be 10 to 20%.

Consideration of Fig. III-6 indicates that the high downcomer velocity comes about primarily because of the placement of the reactor chimney around the entire core. The BONUS reactor, which is similar in a number of respects to the Russian design, has the core cage around the boiling zone only, and the downcomer velocities are low in the zone of steam-water separation.

Digitized by Google

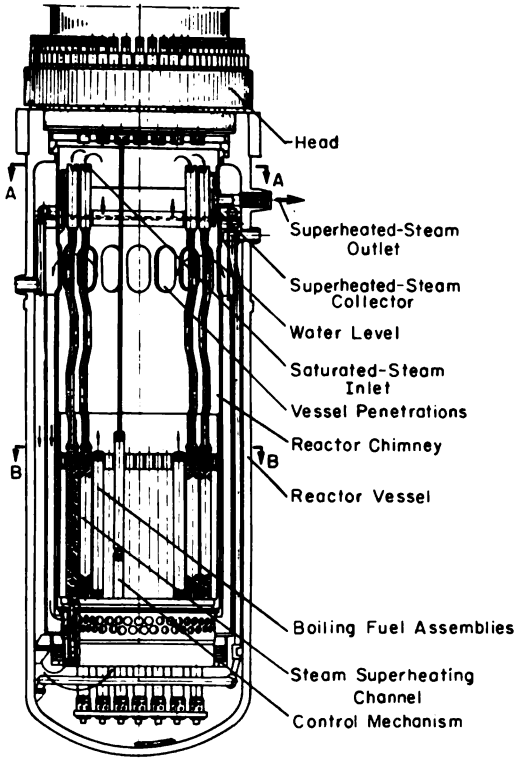

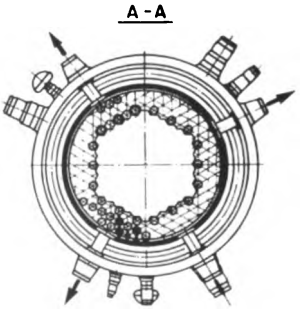

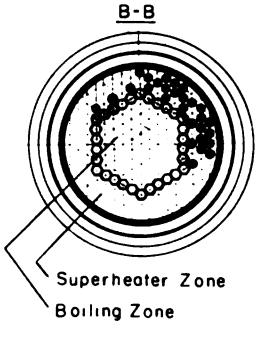

Fig. III-6 General view of the Ulyanovsk steam superheating reactor.[3]

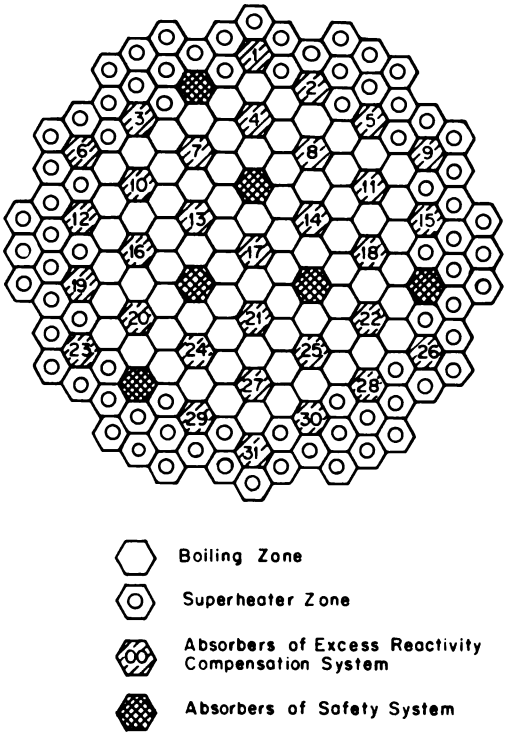

Fig. III-7 Fuel-assembly arrangement in the core of the Ulyanovsk superheating reactor.[3]

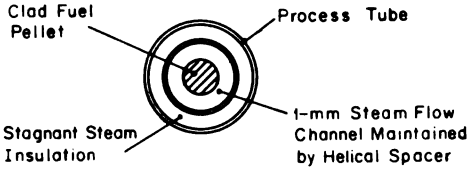

Fig. III-8 Cross section of superheater fuel element in the Ulyanovsk reactor.

Directions of Future Developments

Since no extensive operating experience has yet been gained with a pressure-vessel superheating reactor, it is difficult to comment on the performance of the concept as a whole, much less to predict future trends. In the United States a very considerable effort has been committed to the development of the reactor type, and both integral and separate designs have been constructed. The attention of the reader is directed to the superheat

Digitized by Google

write-up in the Summer 1964 issue of *Power Reactor Technology*, 7(3): 310-312, for a discussion of some of the pertinent problems pertaining to nuclear superheat with integral reactors. With the exception of the nuclear coupling of the boiling-superheating portions of the core, the separate superheat concept exhibits qualitatively the same problems as the integral designs, although the steam-water separation problem may be somewhat different, and presumably more control can be exercised over the conditions of the steam fed to the superheating elements.

The combination boiling-superheating fuel used by the German designers has been discussed previously. A similar principle is being used for the second core of the BONUS reactor,[4] and a typical fuel element is shown in Fig. III-9. The figure shows a design utilizing pelletized fuel, but vibratory compaction is also being considered.

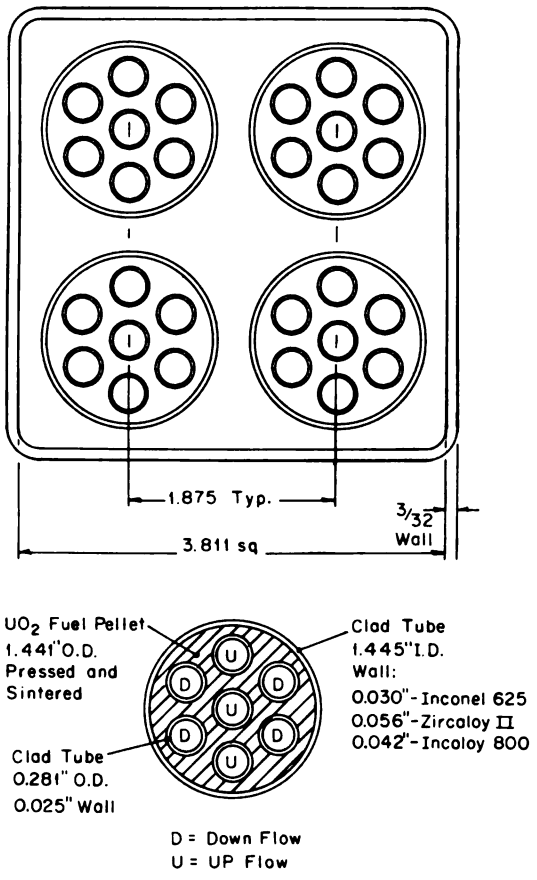

Fig. III-9 Typical fuel-assembly cross section for pelletized fuel in the second core of the BONUS reactor.[4]

References

The references that contain A/Conf. numbers are papers that were presented at the Third United Nations International Conference on the Peaceful Uses of Atomic Energy, Geneva, September 1964.

1. M. Novick, R. E. Rice, C. B. Graham, D. H. Imhoff, and J. M. West, Developments in Nuclear Superheat, A/Conf.28/P/215.
2. H. Kornbichler, Superheat Reactor Development in the Federal Republic of Germany, A/Conf.28/P/535.
3. I. N. Sokolov, V. I. Gritskov, P. N. Bogdanovich, E. V. Kulikov, S. A. Skvortsov, V. P. Spasskov, V. I. Plutinsky, I. A. Philateyev, and A. A. Hohlachev, Experimental Pressure Vessel Reactor for Studies in Boiling and Steam Superheating, A/Conf.28/P/306.
4. J. F. Gibbons, Objectives and Mechanical Design Features of the Advanced BONUS Fuel, in Proceedings of the Ninth Nuclear Superheat Meeting, April 21, 22, and 23, 1964, San Jose, California, USAEC Report SAN-8003, San Francisco Operations Office, June 30, 1964.

Digitized by Google

Section

IV

Power Reactor Technology

Graphite-Moderated Superheating Reactors

The existing reactor of the graphite-moderated superheating type is located at the Beloyarsk power station of the USSR. The reactor (called hereafter Bel-1) has been in operation since May 1964, generating electricity at reduced power. A second reactor of this type (called Bel-2) is currently being built at the same site. For the future outlook and the status of the graphite-moderated reactor to be understood, it is necessary to examine the early history of the Bel-1 plant.

The basic design of the Bel-1 type fuel element was established with the First Atomic Power Station (FAPS).[1] The fuel element for the FAPS reactor is shown in Fig. IV-1. In FAPS the coolant was pressurized water, although this same type of element was also operated under boiling conditions and was used in a test loop to superheat steam.[2] The FAPS element was fueled with 5% enriched uranium alloy. The center tube was unfueled, and the uranium was canned as shown. All the tubes in the fuel channel were made of the Russian steel "1X18H9T," which is similar to the AISI 321 stainless steel.[3] Dimensions of the various tubes are given in Table IV-1. The tubular spirals at the upper end of the FAPS element allow for relative movement between the central tube and the assembly of peripheral tubes. This would be particularly important if the element were used for superheating since the central tube wall would run at a temperature somewhat above saturation and the peripheral tube would operate at a temperature approximating the superheated-steam outlet temperature. The peripheral tubes, the fuel, and the outer cladding can operate as a unit; i.e., when the peripheral tubes expand, the fuel and the outer tube can move relative to the graphite surrounding the fuel tubes.

Table IV-1 DIMENSIONS OF THE FAPS FUEL-ELEMENT COMPONENTS

Item	Diameter, mm	Thickness, mm
Central tube	15	0.6
Peripheral tube	9	0.4
Outer cladding	14	0.2

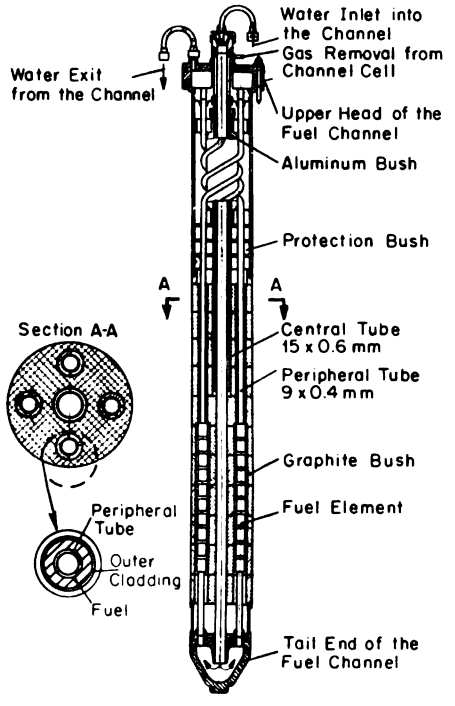

Fig. IV-1 Vertical section of the fuel channel in Russia's First Atomic Power Station.

The fuel element used in Bel-1 is similar to the FAPS design (Fig. IV-1) except that the temperature-compensating coils are located at the bottom of the element.[4,5] Reference 4 is the Second Geneva Conference paper on the design of Bel-1, and Ref. 5 is the Third Geneva Con-

Digitized by Google

ference paper on the development of both Bel-1 and Bel-2. In addition, the peripheral steam tube in Bel-1 was changed in size with respect to FAPS, so that it had a diameter of 9.4 mm and a thickness of 0.6 mm with an outer cladding diameter of 20 mm. The change in location of the expansion coils is not explained, and, in fact, they are placed back at the top of the element in the Bel-2 fuel-element design. The Bel-2 design will be discussed shortly. Instead of four peripherally located fuel elements, the Bel-1 fuel has six, all fed by a central tube. The same size and type of element is used for both boiling and superheating in Bel-1, but the materials may be different in the two applications.

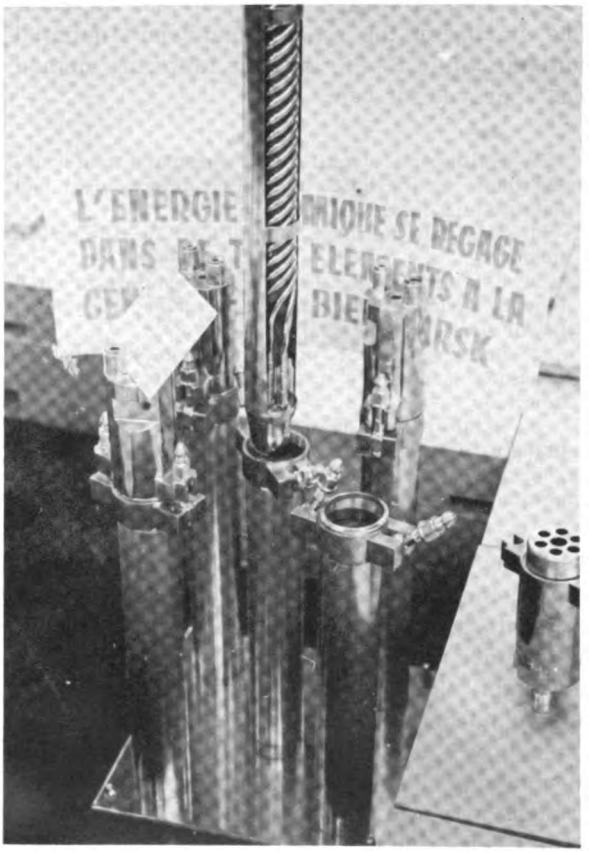

Fig. IV-2a The Bel-1 fuel element on display at the Russian Geneva exhibit. The photograph shows the lower end of a fuel element positioned over a process tube. The mockup shows adjacent process tubes, although for some reason they do not match, positionwise, the holes in the graphite logs. The light-colored blocks shown surrounding the assembly probably simulate the loading face of the reactor, although in the actual plant they are positioned above the location shown in the photograph.

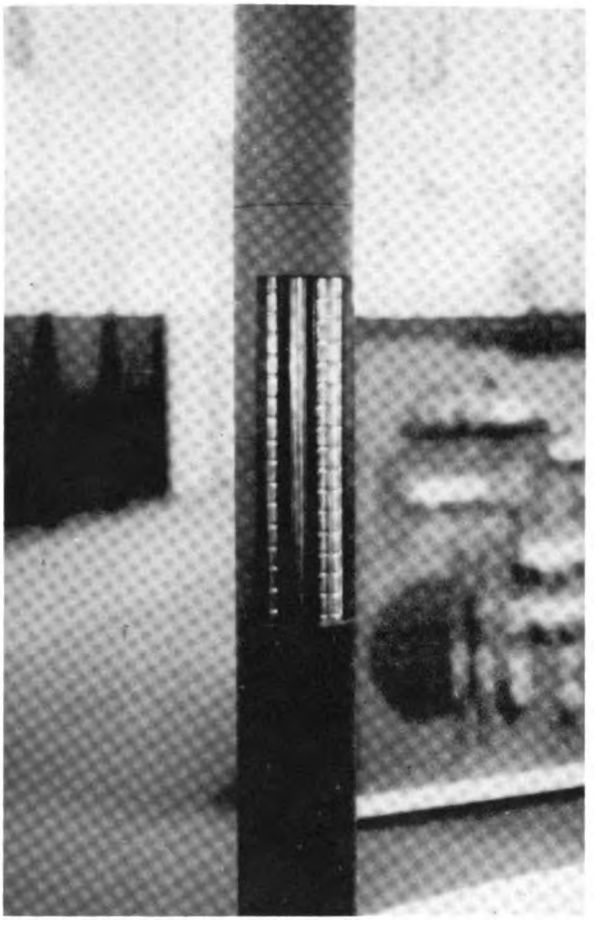

Fig. IV-2b The Bel-1 fuel element showing the upper portion of the compensating coils. The horizontal spacer shown is the same one located at the top of Fig. IV-2a.

Figures IV-2*a*, IV-2*b*, and IV-3 are photographs, taken by the reviewer, of the Bel-1 fuel element on display at the Russian exhibit in Geneva. The compensating coils are shown in Fig. IV-2*b*, and Fig. IV-3 is a cutaway of the fuel element in the uranium-bearing region. Figure IV-3 shows that the outer cladding is dimpled with circular indentations. Although the reasons for these indentations are not given in the references, it is presumed that they assist in giving axial support to the fuel and also act as bellows. There is a thermal-stress design problem arising from a difference in temperature between the inner and outer cladding tubes of the fuel annulus, which are welded together at their ends to contain fission gas. The inner cladding tube is steam cooled, whereas the outer cladding presumably is not. The

Digitized by Google

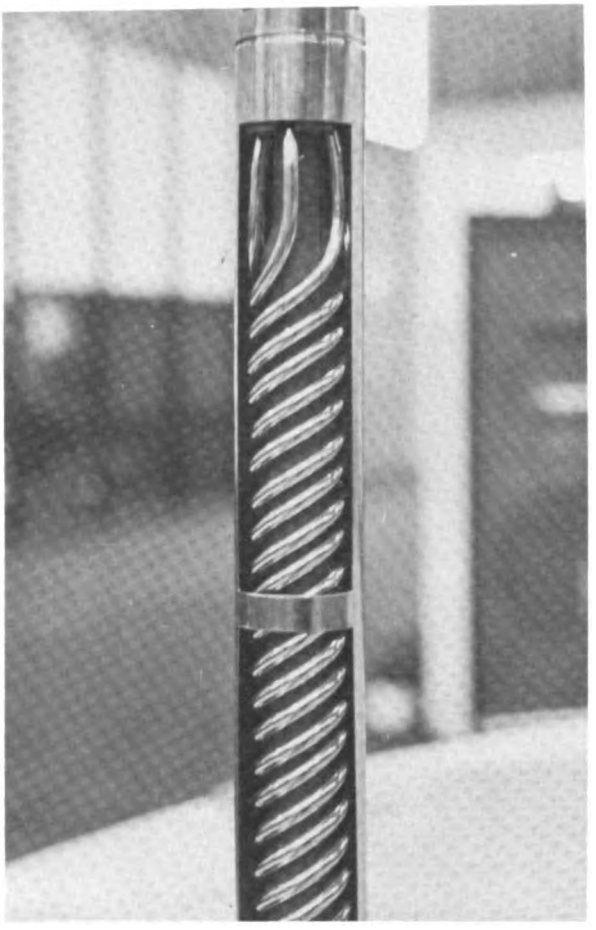

Fig. IV-3 The Bel-1 fuel element illustrating a cutaway view of the fueled region. Three peripheral superheating subelements are shown with the center one being sectioned to illustrate the fuel (dark, vertical portions) and internal cladding surface (shiny, vertical portion). The tubes at the left and right show circumferential indentations, probably for expansion.

fuel is a dispersion of uranium-molybdenum alloy in a magnesium matrix. The evaporating-channel characteristics for Bel-1 and FAPS are listed in Table IV-2, and Table IV-3 lists the superheating-channel characteristics.

An interesting feature of Bel-1 is that the steam to be superheated is not generated directly in the reactor but in a separate steam generator using the indirect-cycle principle. Details are shown in Fig. IV-4.

The permanent structure of the reactor consists of a graphite stack that has a diameter of 9.6 m and a height of 9.0 m. The basic building block is a 200- by 200-mm graphite log penetrated by an axial hole. The core contains 730 boiling assemblies, 268 superheating assemblies, 78 compensating control rods, 16 safety rods, 6 automatic control rods, 2 counting-chamber assemblies, 4 starting-chamber assemblies, and 30 ionization-chamber assemblies, for a total of 1134 core positions.[4] Coolant conditions are given in Table IV-4.

Bel-1 achieved criticality in September 1963, and initial loadings were with boiler-only fuel both flooded and voided. A full core was loaded for critical experiments. This consisted of 500 evaporating elements enriched to 2%, 230 evaporating elements enriched to 1.5%, and 268 superheating elements enriched to 1.5%. According to Ref. 6, only 64 boron-steel compensating rods were used, however. A number of physics experiments were conducted with Bel-1, and these included power distributions, rod worths, power split, and void coefficients. The startup of the reactor had been simulated with the aid of FAPS,[2] and the following method was approved for use:

1. Filling the circuits with water and then heating them up to 180°C at 5–10% power level and establishing the level in the bubbler.
2. The plant heating up to 230°C at 10–15% power level.
3. Establishing the level in the evaporators and blowing through the superheating channels at 2–3% power level.
4. Raising reactor power level to 20% and increasing secondary circuit pressure up to the nominal.
5. Establishing the level in separators, i.e., bringing primary coolant to boiling.
6. Feeding steam to the turbine and further power rising.

To study this process with the Bel-1 reactor, the Russians removed all but two superheater elements and the startup procedure previously determined with FAPS was checked and found adequate. Voiding the superheating elements was found to take about 6 min and to proceed "smoothly." A total of 192 superheating elements were loaded, and the reactor was then brought to power to study voiding of this relatively large number. These results are indicated in Fig. IV-5. The "scavenging" operation mentioned in the figure apparently refers to the injection of a solution of hydrazine hydrate into the secondary circuit to control oxygen concentration. On Apr. 26, 1964, steam was fed to the turbine, but, since less than the normal number of superheating elements were still being used (192), the superheat temperature reached only 390°C (734°F). Future plans called

Digitized by Google

Table IV-2 EVAPORATING-CHANNEL CHARACTERISTICS[5]

	FAPS reactor	Bel-1 reactor	Bel-2 reactor				
			Zone I	Zone II	Zone III	Zone IV	Zone V
Channel power, kw	300	405	771	634	617	545	517
Coolant flow rate through the channel, kg/hr	2500	2400	5500	4700	4150	3550	3250
Steam void at channel outlet, %		33.6	27.6	29.3	30.5	32.1	34.2
Pressure at channel inlet, atm	100	155			155		
Pressure at channel outlet, atm	98	150			145		
Coolant temperature at channel inlet, °C	200	300			300		
Coolant temperature at channel outlet, °C	290	335			338		
Maximum thermal load, kcal/(m²)(hr) (× 10^{-6})	1.8	0.5	0.8	0.7	0.6	0.5	0.5
Circulation rate, m/sec	4	3.5	4.6	4.0	3.5	3.0	2.7
Maximum temperature, °C							
Tube inner wall	324	355			365		
Fuel	382	400			415		
Ratio of burnout heat flux to maximum heat flux		2	1.85	1.9	1.9	2.0	1.95

Table IV-3 SUPERHEATING-CHANNEL CHARACTERISTICS[5]

	Bel-1 reactor	Bel-2 reactor	
Maximum channel power, kw	368	767	
Minimum channel power, kw	202	548	
Steam flow rate through maximum power channel, kg/hr	1900	3600	
Steam flow rate through minimum power channel, kg/hr	1040	2570	
		Bel-2 downstream fuel elements*	Bel-2 upstream fuel elements*
Channel inlet pressure, atm	110	132	124
Channel outlet pressure, atm	100	125	110
Channel inlet steam temperature, °C	316	328	397
Channel outlet steam temperature, °C	510	399	508
Maximum thermal load, kcal/(m²)(hr) (× 10^{-6})	0.48	0.83	0.68
Maximum steam velocity, m/sec	57	76	112
Maximum temperature, °C			
Tube inner wall	530	426	531
Fuel	550	482	565
Graphite	725	735	

*The terms "downstream" and "upstream" apparently should have been translated "downflow" and "upflow," respectively. Obviously the downstream element is the first-pass element, and the upstream element is the second-pass element.

for the addition of more superheat elements to increase the steam temperature to about 500°C.

The future plans for the reactor type introduce the reader to the second Beloyarsk reactor, Bel-2. The graphite stack for this reactor is similar to Bel-1 with respect to size and number of channels, but the second reactor should produce 200 Mw(e). This factor of 2 increase in power is startling at first consideration, but its explanation is reasonably straightforward. The coolant cycle has been changed from indirect boiling to direct boiling, as shown in Fig. IV-6. Two possible arrangements are being considered and are shown as parts *a* and *b* in the figure. The difference between the two cycles is the presence (see part *a* of Fig. IV-6) of a bypass line that allows some of the feedwater to be injected into the steam sepa-

Digitized by Google

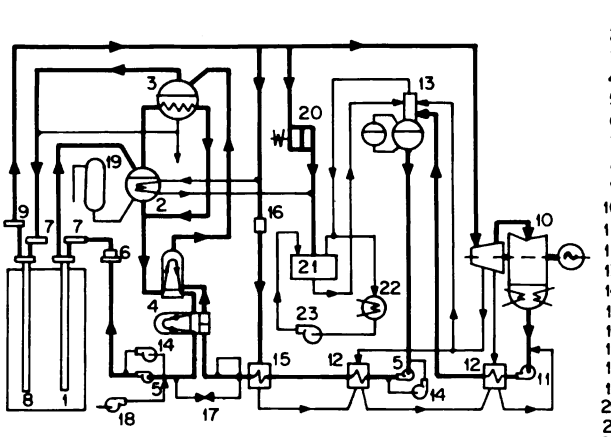

1 Evaporating Channel
2 Steam Drum
3 Evaporator
4 Preheaters
5 Circulating and Feed Pumps
6 Distributing Collector
7 Group Collectors
8 Steam Superheating Channel
9 Superheated-Steam Collector
10 Turbogenerator
11 Condensate Pump
12 Regenerative Preheaters
13 Deaerator
14 Emergency Circ. and Feed Pumps
15 SH Steam Temperature Regulator
16 Fast Oper. Reducing-Cooling Plant
17 Feed Valve
18 Makeup Pump
19 Pressure Compensator
20 Unit of Reducing and Safety Valves
21 Bubbler
22 Process Condenser
23 Process Condenser Pump

Fig. IV-4 Flow sheet of the first unit of the Beloyarsk Nuclear Power Station.[6]

rator after it has passed through the regenerative heater designated as the "steam-generator heater." This is said to be used for "steam washing," but its significance is not readily apparent. Besides the cycle change between Bel-1 and Bel-2, the elements of the latter are to be constructed with slightly larger coolant channels. These details are shown in Table IV-5.

Probably the most significant change between the two reactors is the superheater fuel for Bel-2. Just how the UO_2 is to be used in the Bel-2 superheater elements is not clear; the single mention of UO_2 in Ref. 5 is an offhand one, as follows:

> Upstream superheating elements design and dioxide uranium-based fuel ensure steam superheating up to 500°C; this is confirmed by loop-tests on the first power plant reactor.

On the basis of Table IV-3, we assume that the intent is to substitute UO_2 for the uranium-molybdenum alloy in the dispersion type element, for the maximum fuel temperature listed is far lower than that which would characterize a solid oxide fuel body. It is disappointing that the information on the details of the Beloyarsk elements is so limited, for it is this aspect of the reactor which is probably of greatest interest to designers outside the USSR.

The mechanical design of the Bel-2 superheater elements has also been changed from that of Bel-1. The central, unfueled tube feeding steam to the peripheral channels in the Bel-1 element has been removed and the element converted to two-pass design. These details are shown in Fig. IV-7. As a result the steam velocity is greatly increased, from 57 to 112 m/sec (Table IV-3), and the improved heat-transfer coefficient allows an increase in power. In place of the central tube, an absorber pin is included in the Bel-2 element. These absorbers, which probably are manually manipulated, make possible a reduction of the radial power-peaking factor for the core to 1.3, compared to a value of 1.4 in Bel-1 (see Ref. 5). The evaporating elements for Bel-2 retain the center tube for coolant flow. The increase in power from the boiling portion of the core appears to be the result of rather careful zoning

Table IV-4 MAIN CHARACTERISTICS OF THE REACTOR COOLANT IN THE BELOYARSK NUCLEAR POWER STATION

Characteristics		
Reactor thermal output, Mw	286	
Electrical output, Mw	100	
Ratio of superheating- to evaporating-channel output, %	30.0	
	First circuit	Second circuit
Coolant flow rate, tons/hr	1200	405
Coolant pressure, atm		
At reactor inlet	155	110
At reactor outlet	150	95
Before the turbine	150	90
Coolant temperature, °C		
At reactor inlet	300	316
At reactor outlet	340	510
Before the turbine	340	500
Average steam quality at channel outlet, wt.%	33.6	

Digitized by Google

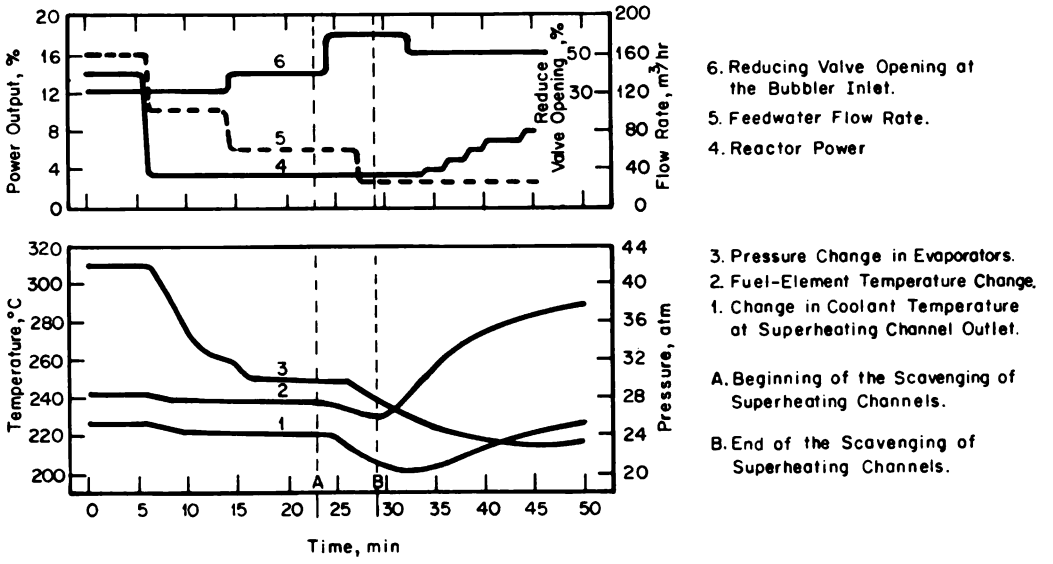
Power Output, %
Reduce Valve Opening, %
Flow Rate, m³/hr
Temperature, °C
Pressure, atm
Time, min
A
B
6. Reducing Valve Opening at the Bubbler Inlet.
5. Feedwater Flow Rate.
4. Reactor Power
3. Pressure Change in Evaporators.
2. Fuel-Element Temperature Change.
1. Change in Coolant Temperature at Superheating Channel Outlet.
A. Beginning of the Scavenging of Superheating Channels.
B. End of the Scavenging of Superheating Channels.

Fig. IV-5 Curves of changes in the main parameters of the plant during transition to steam superheating conditions.[6]

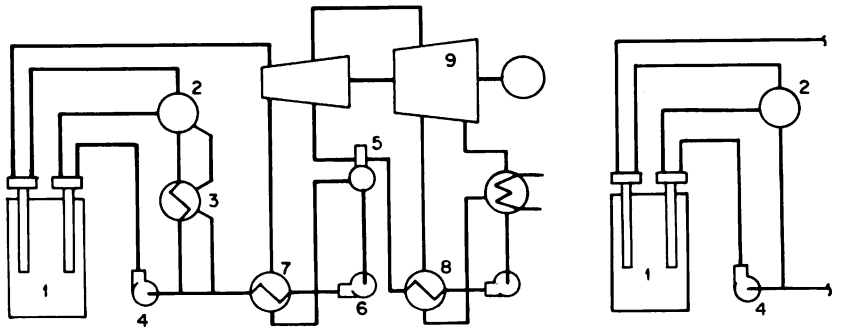

Fig. IV-6 Possible flow sheets for uranium-graphite tube type nuclear superheat reactors.[5]

Table IV-5 COMPARISON OF BEL-1 AND BEL-2 BOILING AND SUPERHEATING FUEL ELEMENTS

	Bel-1	Bel-2
Boiler and superheater fuel-element peripheral-tube diameter/thickness, mm	9.4/0.6	12/0.6
Fuel material		
Boiler element	U-Mo-Mg	U-Mo-Mg
Superheater element	U-Mo-Mg	UO_2

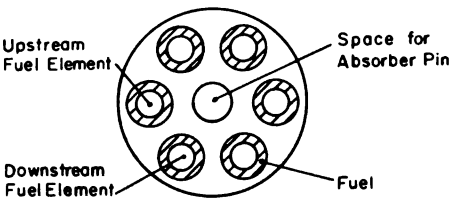

Fig. IV-7 U-shaped superheating channel cross section.[5]

Digitized by Google

of the reactor to match flow and power of the boiling assemblies. The results are indicated in Table IV-2.

The step beyond Bel-2 is stated to be supercritical operation. The tube type Beloyarsk reactors are suited to this type of operation because the pressure-bearing portions of the reactor are of small diameter. Even so, the cladding begins to get quite thick for supercritical-pressure operation, with attendant thermal-stress problems during transients. It is estimated in Ref. 5 that the Bel-1 and Bel-2 reactor size could be made to produce 800 to 1000 Mw(e) if a supercritical, once-through design were possible. It is also suggested that an advanced reactor be operated with partially unclad fuel to remove fission gas and reduce the amount of steel in the core. This would be accomplished by removing the outer cladding tube, although relative movement of the coolant tube with respect to the graphite would have to be provided for.

References

The references that contain A/Conf. numbers are papers that were presented at the Third United Nations International Conference on the Peaceful Uses of Atomic Energy, Geneva, September 1964.

1. N. A. Dollezhal, A. I. Krasin, N. A. Nikolayev, A. N. Grigoryants, and G. N. Ushakov, Operating Experience with the First Atomic Power Station in the USSR and Its Use Under Boiling Conditions, *Proceedings of the Second United Nations International Conference on the Peaceful Uses of Atomic Energy, Geneva, 1958,* Vol. 8, pp. 86-99, United Nations, Geneva, 1958.
2. G. N. Ushakov, L. A. Kochetkov, V. G. Konochkin, V. S. Severjanov, V. Y. Kozlov, O. A. Sudnitsin, N. T. Belinskaja, P. N. Slusarev, and V. A. Ivanov, Operational Experience of the First Atomic Power Station As An Experimental Set-Up, A/Conf.28/P/314.
3. General Electric Company, Hanford Works, Steam Cooled Power Reactor Evaluation — Beloyarsk (URAL) Reactor, USAEC Report HW-67573, April 1961.
4. N. A. Dollezhal, A. K. Krasin, P. I. Aleshchenkov, A. N. Galanin, A. N. Grigoryants, I. Ya. Emelyanov, N. M. Kugushev, M. E. Minashin, U. I. Mityaev, B. V. Florinsky, and B. N. Sharapov, Uranium-Graphite Reactor with Superheated High Pressure Steam, *Proceedings of the Second United Nations International Conference on the Peaceful Uses of Atomic Energy, Geneva, 1958,* Vol. 8, pp. 398-414, United Nations, Geneva, 1958.
5. N. A. Dollezhal, I. Ya. Emelyanov, P. I. Aleshchenkov, A. D. Zhirnov, G. A. Zvereva, N. G. Morgunov, U. I. Mityaev, G. D. Knywseva, K. A. Kryukov, V. N. Smolin, L. I. Lunina, V. I. Kononov, and V. A. Petrov, Development of Superheating Power Reactors of Beloyarsk Nuclear Power Station Type, A/Conf.28/P/309.
6. A. N. Grigoryants, V. P. Nevskii, L. A. Kochetkov, B. G. Ivanov, P. I. Aleshchenkov, A. G. Phylippov, B. G. Dubovskii, M. E. Minashin, M. A. Altshuller, and L. V. Konstantinov, Start-Up and Pilot Operation of the First Unit of the Beloyarsk Nuclear Power Station After I. V. Kurchatov, A/Conf.28/P/308.

Digitized by Google

Section

V

Power Reactor Technology

Heavy-Water-Moderated Pressure-Tube Reactors

The effort on heavy-water-moderated pressure-tube reactors throughout the world is indicated in Table V-1. The Canadian effort is by far the largest and the farthest advanced. The two Canadian power reactors, NPD and CANDU, are both cooled and moderated by D_2O, are fueled with natural UO_2 clad with Zircaloy-2, and employ calandria tanks to contain the moderator. The calandria tubes of NPD are aluminum, whereas those of CANDU are nickel-free Zircaloy-2. Design features of NPD are given in Ref. 1, and those of CANDU, in Refs. 2 and 3.

Until the recent announcement[4] of a program directed toward the development of a 300-Mw(e) organic-cooled plant, there had been no definite plans for a large-scale heavy-water reactor in the United States. Nevertheless, the U. S. effort has been considerable and has resulted in the construction of a 17-Mw(e) prototype (the Carolinas-Virginia plant, CVTR), as well as a reactor that operates at comparable temperatures and thermal-power levels for plutonium-recycle development (the Plutonium Recycle Test Reactor) and a reactor for developing fuel elements for D_2O power reactors (the Heavy Water Components Test Reactor). All these reactors are cooled and moderated by heavy water. The Carolinas-Virginia reactor was described in *Power Reactor Technology*, 6(4): 63-81; the most recent general review of heavy-water reactors was in 7(1): 85-98.

Interest in heavy-water-moderated reactors is also high in other countries, but there is considerable diversity in the choice of coolant. The Steam Generating Heavy Water Reactor (SGHWR)[5–8] utilizes boiling light water, the DON reactor uses organic coolant,[9–11] whereas EL-4 (Refs. 12 to 15) and the Lucens reactors[16–18] are cooled with CO_2. Of the reactors under study or development, the DOR,[19,20] the R-1 and R-2, (Ref. 21), and the U. S. project[22] are all designed to be organic cooled. The German reactor study involved gas cooling.[23] In addition to these power reactors, at least two test reactors are being constructed to study the problems arising from organic cooling. These are the Canadian WR-1, reviewed in the Summer 1964 issue of *Power Reactor Technology*, 7(3): 324-327, and the ESSOR.[24]

Operating Experience

Extensive operational experience has been reported[25,26] for the NPD reactor. Reference 25 contains information on reactor physics aspects of the startup. Various reactivity coefficients were determined, including the moderator-level coefficient of reactivity, reflector reactivity worths, and temperature coefficients of reactivity. The reactivity balances at two different points in the lifetime are shown in Table V-2.

As is indicated in Table V-2, the sources of reactivity adjustment, other than fuel management, are quite limited, consisting only of changes in moderator level and moderator temperature. The normal NPD fueling operation consists of inserting a bundle in one end of a pressure tube, thereby shifting all the bundles within the tube by one bundle length and expelling the last bundle. This bundle may then be either discharged or recycled in a channel fueled in the opposite direction. This operation was studied by means of a computer code simulating the reactor, STOKE, which calculated the burnup of all fuel bundles by increments, taking fuel shifts into account. The code was designed to select the best shift for the current state of the reactor, consistent with the particular refueling scheme being studied. The original NPD loading consisted of natural and depleted UO_2. The fuel-management principle consisted of shifting fuel in the channel containing the bundle with the highest burnup and recycling an expelled bundle

Digitized by Google

Table V-1 D_2O-MODERATED PRESSURE-TUBE REACTORS

Reactor	Country	Status*	Mw(e)	Coolant	Fuel and geometry	Cladding	Core type	Pressure tube	Core orientation	No. of refueling machines	Refueling method	Pressure-tube joints
NPD	Canada	Operational	19.5	D_2O (l)	UO_2, rod cluster	Zircaloy-2	Calandria	Zircaloy-2	Horizontal	2	On-power	Expanded
CANDU	Canada	Being built (1965)	203	D_2O (l)	UO_2, rod cluster	Zircaloy-2	Calandria	Zircaloy-2	Horizontal	2	On-power	Expanded
CVTR	U. S.	Operational	17	D_2O (l)	UO_2, rod cluster	Zircaloy-4	Cold U tubes	Zircaloy-4	Vertical	1	Shutdown, depressurized	Conoseal gasket
SGHWR	England	Being built (1967)	100.0	H_2O (boil)	UO_2 rod cluster	Zircaloy-2 (boiler), S.S. (superheater)	Calandria	Zircaloy-2	Vertical	1	On-power	Expanded
EL-4	France	Being built (1967)	70	CO_2	UO_2	S.S. or Be	Cold tube	Zircaloy-2	Horizontal	2	On-power	Threaded and brazed
DON	Spain	Planned	30	Organic	UC, rod cluster	Finned SAP	Calandria	SAP	Vertical	1		Hot rolled and/or diffusion bonded
Lucens	Switzerland	Being built (1966)	13	CO_2	U–1% Cr	Mg–0.5% Zr	Calandria	Zircaloy-2	Vertical	1 plus a locking machine	Shutdown, depressurized	
DOR	Denmark	Study	235	Organic	UO_2 or UC	SAP	Calandria	SAP	Vertical	1		
R-1	Russia	Study	500	Organic	Beta-U	Mg-Be	Calandria	SAP	Vertical	Probably 1		
R-2	Russia	Study	500	Organic	UO_2		Calandria	SAP	Vertical	Probably 1		
OCHWMPR	U. S.	Study	512	Organic	UO_2	SAP	Cold tube	SAP-lined Zircaloy-2	Vertical	1		
AKB	Germany	Study	100	CO_2	UO_2 or UC	Steel, Zr or Be alloys	Cold tube	Zr-Cu-Mo-lined	Vertical	1		

*The year in parentheses is the probable completion date.

Table V-2 CHANGES IN REACTIVITY BALANCE WITH IRRADIATION[25]

	Reactivity effect in unirradiated core, mk	Reactivity effect in irradiated core (230 full-power days), mk
Leakage at full tank	−71	−69
Control margin*	−2.8	−0.3
Depleted fuel†	−23	0.0
H_2O in D_2O (relative to 100% D_2O)	−10	−27.0
Xenon	−23.9	−24.1
Samarium	0.0	−8.1
Moderator temp. (21–60°C)	−2.8	+0.4
Coolant temp. (21–254°C)	−7.4	−2.6
Power (fuel temp.)	−3.1	−1.4
Total reactivity load	144	132
Fuel burnup		12

*Operating moderator level is below full tank by amounts shown.

†Depleted fuel removed prematurely.

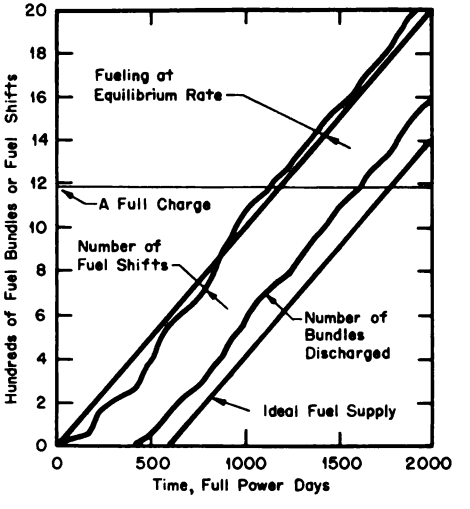

Fig. V-1 Simulation of NPD fueling, assuming that the fuel is recycled if the exit burnup is less than half the equilibrium burnup.[25]

Digitized by Google

if it contained natural uranium and had a burnup less than a specified fraction of the burnup of the discharged fuel at equilibrium. The simulation of the NPD fueling, assuming recycle if the exit burnup was less than half the equilibrium burnup, resulted in the data shown in Fig. V-1. This figure predicts the number of fuel shifts and number of bundles discharged (and fed), assuming the NPD starts from its initial arrangement of partially depleted fuel. In practice, however, the NPD ran with depleted uranium fuel from its initial criticality in April 1962 to December. At that time the moderator and coolant became contaminated with light water, as will shortly be discussed, and the depleted fuel was removed to compensate for the resulting reactivity loss.

The degrading of the D_2O was caused by a major leak at the seal between the fueling machine and the pressure tube the first time on-power fueling was attempted. The spilled heavy water was downgraded from 99.7 to 99.1% D_2O and was contaminated by oil and grout. An upgrading program was initiated, and the purity was about 99.6% as of the writing of Ref. 26. The reference also states that loss and downgrading of the moderator have been negligible and that practically all D_2O losses and downgrading have come from the heat-transport system. The following quotation summarizes the D_2O loss experience on NPD:[26]

(a) Low escape rates depend a great deal on quality of the original design and construction.
(b) Quite high chronic escape rates are acceptable if recovery is efficient i.e. if the "dry-room principle" is followed.
(c) At a large station, it is not economical to sacrifice capacity factor in order to repair leaks. Consequently, if leaks are bad, recovery is essential.
(d) There is no valid experience to show that escape rates can be held to extremely low values over long periods of time, without serious loss of capacity factor.
(e) With efficient recovery, loss rates are virtually independent of escape rates, and can be very low.
(f) NPD experience has shown that use of vapour-recovery equipment is both feasible and sensible.
(g) With efficient recovery, the loss rate can be virtually unaffected by station size.
(h) The "dry-room principle" not only is valuable for the everyday situation, but would have reduced the cost of the acute escape on 3 Dec. 1962 by an order of magnitude.
(i) D_2O losses can be maintained acceptably low in any station whose design is based on NPD experience, and D_2O escape rates can be significantly reduced.

Fuel and pressure-tube performance have been good. Other than the major failure that occurred during the first refueling attempt—the refueling machines have been subsequently modified to prevent a future occurrence—the fueling-machine experience has been "highly successful."

Significant Features

Fuel and Cladding Materials

In support of NPD, CANDU, and various heavy-water-moderated power-reactor studies, the Canadians presented several important papers on the behavior of fuel and cladding materials.[27–30] Some of the details pertain explicitly to NPD and CANDU type reactors, but others are of general interest to reactor designers. A rather interesting conclusion[27] was that high UO_2 density may not be an important goal for operating fuel elements, since low-density material (less than 10.3 g/cm^3) provides for the retrapping of escaped fission gas. The elimination of the need for a plenum or other space within a fuel element to accommodate fission gases may be an important design consideration for certain fuel elements—particularly for the typical short Canadian elements, since plenums at the ends of the elements tend to cause power peaks in the fuel adjacent to the plenums. Reference 28 details the performance of the NPD and CANDU fuel elements and contains some interesting cost data. On the basis of production experience with the NPD and CANDU fuel elements, it is estimated[28] that the average cost of fuel for a 1000-Mw(e) CANDU type reactor would be $50 per kilogram of uranium ±10%. This results in a fuel cost of about 0.8 mill/kw-hr if the fuel is discarded without reprocessing.

Reference 30 discusses in-pile results for test fuel elements cooled by organics. Test elements were manufactured with sintered-aluminum-product (SAP) cladding containing 7 and 10% oxide (SAP 930 and 895, respectively) and a material apparently from another producer also containing 7% oxide, M 257 or M 583. The rods were designed to be freestanding under coolant pressure (300 psi) and with sufficient diametral fuel-jacket clearance to theoretically produce no diametral sheath strain at operating conditions. This was done because of the inability of SAP to deform plastically. The results of the irradiations are given in Table V-3.

Digitized by Google

Table V-3 RESULTS OF IRRADIATIONS IN TERPHENYL MIXTURE IN NRX TEST LOOP[30]

	Test 704-I	Test 704-II	Test 709-I	Test 709-II	Test 712	Test 713	Test 714-I	Test 714-II	Test 719	Test 720
Sheath material	M 583	M 583	M 583	M 583	M 257	M 257	SAP 930	SAP 930	Zircaloy-2, Zr–2½% Nb	SAP 895
Element length, cm	30.5	30.5	61	61	122	122	244	244	50	22
Diametral clearance, cm	0.009 to 0.019	0.019	0.013	0.013	0.015 to 0.018	0.015	0.016	0.016	0.008 and 0.015	0.0025, 0.0050, 0.0075, and 0.0125
Irradiation, full-power days	<1	31.5	63.7	<1	59.3	29	44.6	45.6	82	4
Maximum $\int k\, d\theta$, watts/cm	~38	45.5	37.8	45	36.5	36.5	37.5*	39.9	39	40
Average $\int k\, d\theta$ at flux center, watts/cm		39	35		33.4	34	33.9	38.5	35	40
Average sheath temp., °C	420†	~430†	450	420	470	440	470	470	475	462
Maximum sheath temp., °C	†	†	465	470	496	484	497	525	500‡	462‡
Maximum diameter change, %	§	§	0.3	0.8	0.4	¶	1.5	0.5	1.2	0
Average diameter change, %	§	§	~0	0.3	<0.2	¶	0.5	~0	0.7	0
Average length change, %	§	§	0.03	0.05	0.04	0.04	¶	~0	0.3	0
Burnup at flux center, Mwd/metric ton		1100	2400		2100	1000	1500	1500	2600	130
Fuel-sheath heat-transfer coefficient, watts/(cm)(°C)	¶	¶	~0.4	¶	~0.4	¶	~0.6	¶	¶	¶
Fission-gas release, %	¶	¶	~3	¶	~9	¶	¶	¶	¶	¶
Fouling-film thickness, μm	10 to 500	10 to 1400	40 to 80	<5	<1	¶	<1	<1	<1	<1
Ridge height, μm	**	**	**	**	**	**	40 max.	40 max.	30 av., 60 max.	0
Performance	Failed††	Good	Good	Failed‡‡	Good	Good	Failed§§	Failed§§	Good	Good¶¶

*A transient peak in excess of 40 watts/cm may have existed at the time of failure.
†No sheath thermocouples; temperatures listed are from calculation.
‡Estimated.
§Elements were stored under water and corroded before measurements were made.
¶Not measured.
**Circumferential ridges were observed but not measured in these tests.
††Failure was due to burnout. One element did not have ribs or wire wrap and bowed out and touched the pressure tube. This error was corrected in 704-II.
‡‡709-II contained poor-quality sheathing rejected for use in 709-I. This and the gross overpower are suspected to have led to failure.
§§Failure appeared as stress cracks at the axial center of the elements. The cause of these stress cracks is unknown.
¶¶Diametral-clearance experiment.

Digitized by Google

Although the causes of the stress cracks (tests 714-I and 714-II) were unknown, the reference notes that sheath strain probably did exist, due to migration of cracks within the fuel until the diametral clearance was eventually transferred to a central void. Evidence of a reaction between UO_2 and SAP was observed, and this was also noted in Ref. 31. The good performance of the zirconium-niobium clad UO_2, illustrated in Table V-3, shows promise for the material, but further experiments were planned to test the hydriding behavior.

Table V-4 COMPOSITION OF MAGNESIUM-BASED ALLOYS SUITABLE FOR CLADDING OF GAS-COOLED REACTORS[33]

Type of alloy	Composition of alloys, wt.% (balance Mg)										
	Be	Si	Al	Th	Fe	Mn	Ni	Cu	MgO	Ca	Zr
PMB	From 0.5 to 32		0.01		0.04		0.001	0.005	0.2		
MB-3	0.04	0.5			0.01	0.001	0.001	0.005			
MB-4	0.08 to 0.15	0.7			0.01	0.001	0.001	0.005			
Mg-Al-Be	0.04		0.5		0.01	0.001	0.001	0.005			
Mg-Th-Be	0.04			3	0.01	0.001	0.001	0.005			
Mg-Ca-Zr-Be	0.04				0.01	0.001	0.001	0.005		0.5	0.5

References 32 through 34 are concerned with metallurgical problems of other cladding materials. The FeAl40, which is an iron-aluminum alloy containing 40 at.% aluminum, is a possible cladding for EL-4, the French gas-cooled reactor. The material offers possibilities as a substitute for beryllium, although it apparently has low ductility.[32] The reference gives mechanical-property data and discusses welding and corrosion resistance. The magnesium-beryllium alloy described in Ref. 33 probably is the alloy mentioned for the Russian organic-cooled reactor R-1 (Ref. 21), although in Ref. 33 it is presented as a possible cladding for a gas-cooled reactor. Several alloys were considered (Table V-4), in composition ranges similar to the British Magnox alloys.

Water Chemistry—Experience with D_2O

A key consideration in the heavy-water-moderated reactor is the technology of the moderator itself, and three papers were devoted to this subject.[35–37] Figure V-2 summarizes French experience with a number of low-temperature D_2O-moderated reactors with respect to moderator degradation. The figure apparently pertains to the situation in which no on-stream upgrading was attempted, with the exception of that shown for EL-3. Soluble poisons dissolved in the D_2O were studied, namely boric acid and the sulfates of cadmium, lithium, and gadolinium. Although the concept appeared feasible, the use of a so-called "gaseous" control rod, composed of ^3He, is discussed for application to EL-4.

Canadian experience with the decomposition of D_2O in various reactors is summarized in Table V-5. The NRU and NPD results shown in the table illustrate that increasing acidity and temperature both decrease the equilibrium concentrations of dissolved radiolytic gas. The problem of maintaining a nonexplosive atmosphere in spaces adjacent to the moderator water is not a trivial one and must be considered during reactor design. The NPD reactor moderator chemistry is also complicated by irradiation-formation of nitric acid from nitrogen introduced in air leakage.

Canadian experience in upgrading D_2O is contained in Ref. 37. The various Canadian reactors contain about 200 metric tons of D_2O altogether, and a number of incidents over the years have resulted in the reprocessing of many metric tons of degraded D_2O. The various methods discussed include electrolysis and distillation; distillation is the favored method for on-stream upgrading of reactor moderator because of its flexibility. A significant hazard in handling irradiated heavy water is tritium, the product of neutron capture by deuterium. In the NPD reactor the tritium concentration has reached 1.7 curies/liter and is expected to reach at least 10 curies/liter within a few years. Although the problem can be controlled by design and administrative procedures, it is one which is peculiar to the reactor type. A review of the economics of heavy-water production in the United States is given in Ref. 38.

Digitized by Google

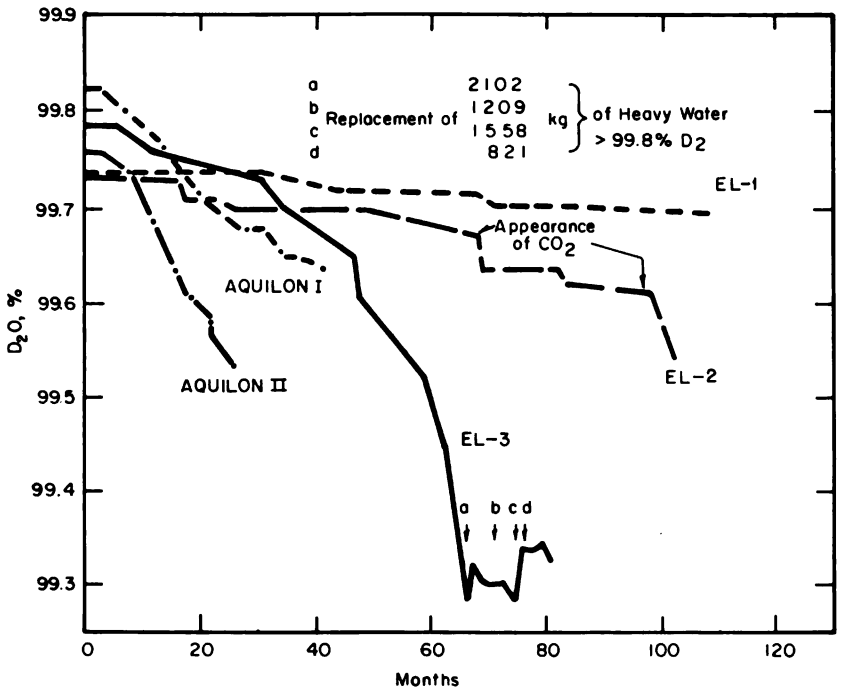

Fig. V-2 Evolution of the isotope content of heavy water in the C.E.A. reactors.[35]

Table V-5 RADIOLYTIC DECOMPOSITION OF HEAVY-WATER MODERATORS[36]

Reactor	Moderator temp., °C	*p*D*	D_2 content of D_2O in core, cm^3/kg	Total gas to recombiner, liters (STP)/min	Water decomposition	
					Liters of D_2 (STP)/min	Grams of D_2O/Mw-hr†
NRX	45	~7	1.6	370	0.15	0.2
NRU						
1960-61	50	~7	5	230	6	1.6
1962-63	50	~7	2	230	3	0.8
1963	50	5.7	1	200	1.6	0.4
NPD	80	~6	1.2	280	8.5	5.1
	40	5.5	3.3	700	27	16

*In NRX and NRU *p*D of 7 corresponds to a conductivity of 0.2 megohm/cm (25°C); acidic conditions were due to DNO_3 added to NRU for a two-month experiment and formed in NPD from air in the helium.

†Megawatt-hours of total reactor thermal power; average power densities are 2.6, 5.0, and 1.7 watts/g for NRX, NRU, and NPD, respectively.

Pressure Tubes

Most of the reactors listed in Table V-1 utilize Zircaloy-2 as the pressure-tube material. Two papers were presented dealing with Zircaloy-2 as applied to pressure-tube construction,[39,40] and two papers were concerned with the zirconium-niobium alloy.[41,42]

The pressure tubes in NPD are seamless Zircaloy-2 tubing, fabricated by hot extrusion and cold drawing.[39] Dimensional gauging and borescope examinations were performed on one of the tubes after a year's service in the reactor, and no significant changes were noted. The NPD design stress was chosen as 9.5 kg/mm^2 at 280°C, whereas the CANDU design stress was selected as 11.2 kg/mm^2 at 300°C. Tensile tests on portions of the NPD pressure-tube materials have given the results shown in Table V-6. In the reactor, however, the tubes are biaxially stressed by the combination of transverse and longitudinal loads produced by the pressurized coolant, with the result that the burst strength of the tube is considerably higher than would be predicted from simple tensile-test data; this is an important design consideration.

Digitized by Google

Table V-6 TENSILE-TEST RESULTS—NPD PRESSURE-TUBE MATERIAL[39]

(Temperature = 280°C)

	Longitudinal properties	Transverse properties
Ultimate strength, kg/mm²	37.3	35
0.2% yield strength, kg/mm²	31.6	33
Elongation, %	22.5	21
Reduction in area, %	45	60

The effects of hydrogen pickup by Zircaloy are complicated; they are also important, since the operating lifetime of a pressure tube is expected to be determined by the amount of hydrogen pickup experienced during corrosion. Hydrogen concentrations up to 250 ppm had little effect on mechanical properties of irradiated and unirradiated Zircaloy-2 so long as the hydrides were randomly arranged. These data are shown in Table V-7. It was established that prior strain, fabrication history, and stress were important in determining hydride orientation:[39]

> ... It was found that hydrides precipitated while Zircaloy was under stress, aligned themselves perpendicular to tensile stresses and parallel to compressive stresses and that directional hydrides significantly decreased the mechanical properties of Zircaloy-2 ...

The use of zirconium-niobium alloys as pressure tubes is receiving study in both Canada[41] and the United Kingdom.[42] The advantage of the niobium alloy is in increased strength; properly heat-treated zirconium–2.5 wt.% niobium attains a strength about 50% higher than Zircaloy-2. These data are illustrated in Fig. V-3. The corrosion and hydriding resistance of zirconium-niobium alloys and Zircaloy-2 are similar, as indicated in Fig. V-4, although the impact strength of the niobium-bearing alloy is higher than that of Zircaloy-2. It appears that the zirconium-niobium alloy may become the preferred material for pressure tubes in cases where zirconium-base alloys are applicable.

The ternary alloy zirconium–2.5 wt.% niobium–0.5 wt.% curium is being developed because of its good corrosion resistance in moist CO_2 and is used in CANDU as a pressure-tube spacer. This spacer maintains clearance between the pressure tube and the calandria, and in CANDU this space is filled with the moist CO_2.

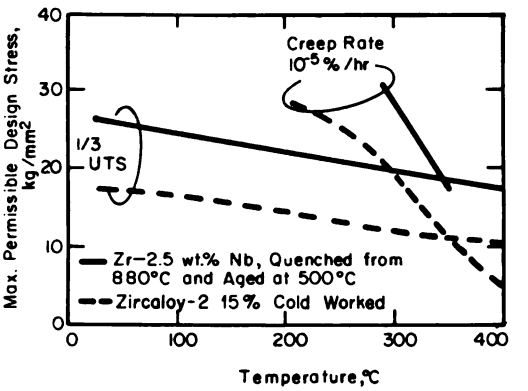

Fig. V-3 Design stresses for zirconium alloys.[41]

Table V-7 EFFECT OF NEUTRON IRRADIATION AND HYDROGEN CONCENTRATION ON THE PROPERTIES OF ZIRCALOY-2 (REF. 39)

(Each Result Is An Average for Three Specimens)

Testing temperature	Hydrogen content, ppm	0.2% proof stress		Ultimate tensile strength		Elongation	
		Unirradiated, kg/mm²	Irradiated, kg/mm²	Unirradiated, kg/mm²	Irradiated, kg/mm²	Unirradiated, %	Irradiated, %
Room temperature	0	56.6	77.3	66.1	78.7	12.4	5.3
	20	62.0	85.8	70.0	85.8	18.5	6.8
	100	61.8	83.4	70.3	83.7	15.2	7.3
	250	60.5	84.4	70.7	84.4	14.1	6.2
300°C	0	29.7	45.0	33.5	45.0	12.8	5.8
	20	30.1	47.1	33.1	47.1	17.9	7.4
	100	29.7	45.7	33.60	45.7	21.8	8.5
	250	32.2	46.4	36.34	46.4	19.0	8.8
400°C	0	27.5	37.3	29.0	37.3	11.1	6.8
	20	26.5	37.3	28.1	37.3	8.7	10.5
	100	25.9	36.6	27.5	36.6	18.0	9.9
	250	27.2	36.6	28.4	36.6	17.4	10.7

Digitized by Google

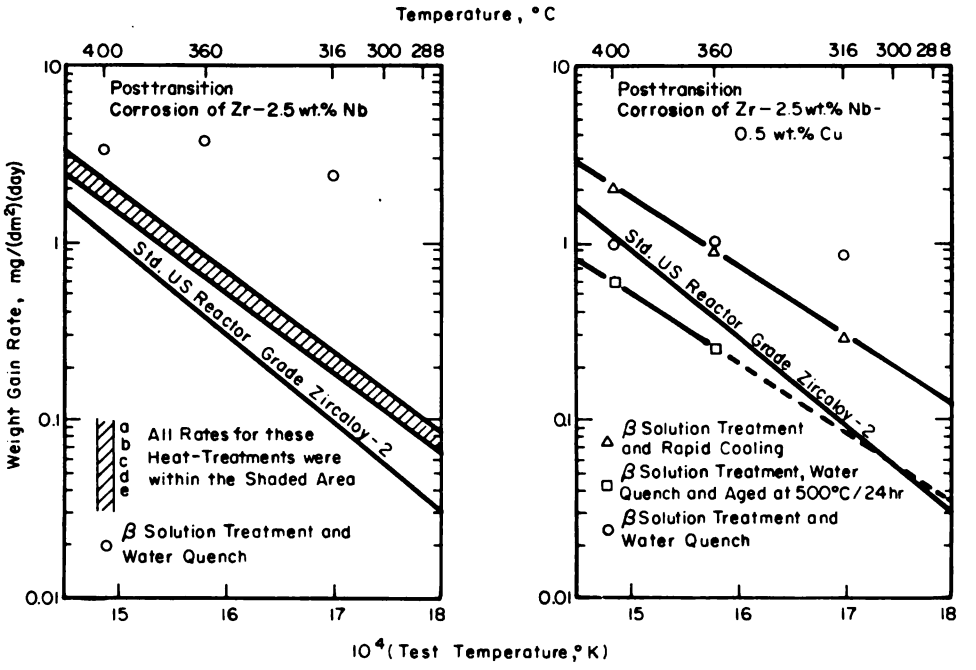
Temperature, °C
400 360 316 300 288
Posttransition
Corrosion of Zr-2.5 wt.% Nb
Std. US Reactor Grade Zircaloy-2
a b c d e All Rates for these Heat-Treatments were within the Shaded Area
β Solution Treatment and Water Quench
Weight Gain Rate, mg/(dm²)(day)
Posttransition
Corrosion of Zr-2.5 wt.% Nb-0.5 wt.% Cu
β Solution Treatment and Rapid Cooling
β Solution Treatment, Water Quench and Aged at 500°C/24 hr
β Solution Treatment and Water Quench
10⁴(Test Temperature, °K)

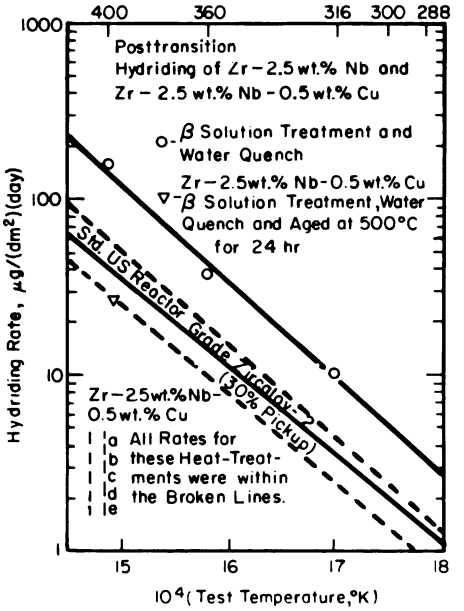
400 360 316 300 288
Posttransition
Hydriding of Zr-2.5 wt.% Nb and Zr-2.5 wt.% Nb-0.5 wt.% Cu
β Solution Treatment and Water Quench
Zr-2.5 wt.% Nb-0.5 wt.% Cu
β Solution Treatment, Water Quench and Aged at 500°C for 24 hr
Std. US Reactor Grade Zircaloy-2 (30% Pickup)
Zr-2.5 wt.% Nb-0.5 wt.% Cu
a b c d e All Rates for these Heat-Treatments were within the Broken Lines.
Hydriding Rate, μg/(dm²)(day)
10⁴(Test Temperature, °K)

Heat-Treatments Received by Zr-2.5 wt.% Nb:

- a Slow Cooled after 2 hr at 650°C
- b Air Cooled after 6 hr at 700°C
- c Air Cooled after ½ hr at 800°C
- d Rapidly Cooled after 10 min at 960°C
- e Quenched from Temperatures in the Range 880-960°C and Aged 24 hr at 500°C

Fig. V-4 The effect of heat-treatment on corrosion and hydriding of zirconium-niobium alloys in pure water and steam.[41]

Thermal and Hydraulic Studies

The performance of fuel elements cooled with a steam-water mixture is discussed in Ref. 43. Experiments were conducted in an in-pile loop in the NRX reactor and also in an ex-pile loop, termed FLARE. The in-pile tests were done primarily to provide corrosion and hydriding data for Zircaloy-2 and zirconium-2.5 wt.% niobium clad fuel elements operating under various conditions typical of the fog-cooled reactor; results are quoted as follows:[43]

> ... corrosion and hydrogen pick-up rates in both Zircaloy-2 and Zr-2½% Nb fuel sheaths are acceptably low when cooled by fog at the conditions of interest for fog-cooled or once-through reactors for periods up to 1600 h, provided the sheath surface remains wet ...

Operation of FLARE yielded interesting data on the "dry-out" heat flux. Dry-out is the

Digitized by Google

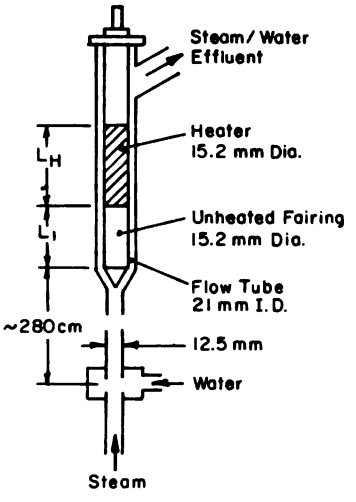

Fig. V-5 Test section.[43]

are noted (incipient dry-out). The power is then adjusted to allow a small temperature oscillation (~5 deg C) and a set of readings taken. At the end of this period a slight increase in the test-element power (~2%) resulted in a sharp increase in surface temperature (~100 deg C)—the dry-out point. Continued operation here gave very large temperature oscillations, despite no recorded changes in the steady-state value of the heat flux, quality or flow. It would appear that there is an alternate wetting and drying out of the surface. A further increase in power (~7%) gives a further rise in surface temperature (up to 512°C). However, in this case there are no oscillations and the surface now appears to be "dry." ...

Figure V-7 illustrates the effect of the unheated fairing length, L_1 (see Fig. V-5), on $\phi_{\text{dry-out}}$.

References 44 through 48 pertain to organic-coolant technology and originated in a number of different countries. Reference 44 is particularly interesting in that it traces the

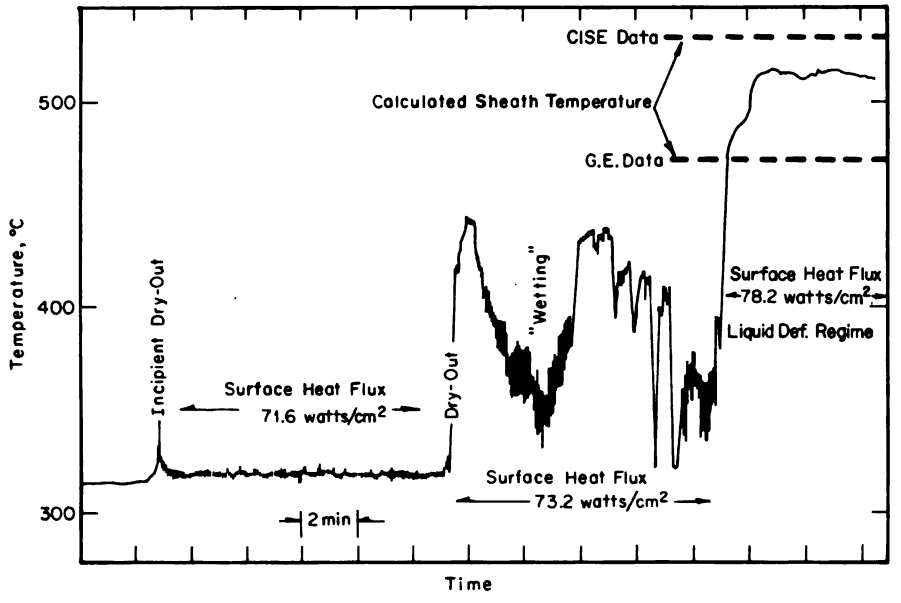

Fig. V-6 Typical sheath-temperature plot obtained from FLARE in dry-out test.[43]

designation of the phenomena that result after the complete evaporation of the protective water film on the heat-transfer surface.[43] Figure V-5 illustrates the test section used in FLARE. Determination of the dry-out heat flux was made for a variety of conditions, and Fig. V-6 illustrates typical wall temperatures for one of the tests. This test was described as follows:

... At the start the test-element power (and heat flux) is being increased until indications of dry-out

evolution in thinking on the use of zirconium alloys in organic-cooled systems. In the late 1950's, preliminary experience had indicated that zirconium alloys were unacceptable for use in organic-cooled reactors due to hydriding. This led to increased study of sintered aluminum (SAP), and the work with zirconium was deemphasized. More recent information, however, has indicated that zirconium alloys may be usable in organic systems provided the

Digitized by Google

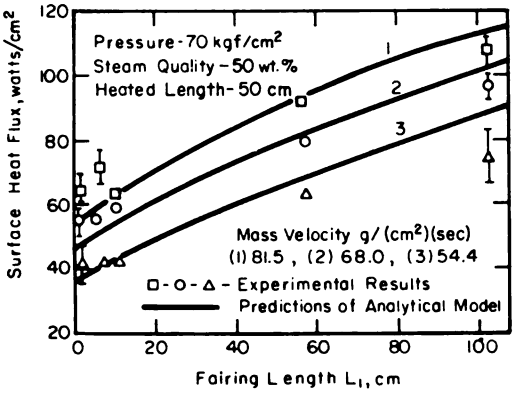

Fig. V-7 The effect of unheated length on the dry-out heat flux.[43]

coolant impurities are carefully controlled. According to the reference:[44]

> The work to date in Canada has shown very clearly that the control of coolant purity is absolutely essential for an organic-cooled reactor. It has been shown further that coolant purity must never be allowed to get out of control since otherwise the subsequent clean-up will be long and difficult. Several years of operating in-reactor and out-reactor loops has proved that the control of coolant purity is no more difficult than in a water-cooled reactor. Provided the proper conditions are observed fouling will not be a problem, at least up to surface temperatures of 500°C, and zirconium alloys such as Zr–2.5% Nb show real promise for fuel sheathing and pressure tubes.

The important variables seem to be water, hydrogen, and chlorine. Water dissolved in the organic seems to have a beneficial effect in reducing hydriding in certain concentration ranges, as may be seen in Table V-8. Increased hydrogen concentrations increase the rate of hydriding at water concentrations less than 40 ppm, but, at "higher" water concentrations, the effect of hydrogen is said to be negligible.[44] Chlorine is thought to be the most important promoter of zirconium hydriding, and Table V-9 illustrates the effect. Surface preparation has been shown to be important, and the effect of temperature appears minor in the temperature range 365 to 425°C.

Table V-9 EFFECT OF CHLORINE ON HYDRIDING OF ZIRCALOY-2 (REF. 44)

	No chlorine added	50 ppm C_2HCl_3 added initially
Temp., °C	375	370
Chloride in coolant at 370°C, ppm		
At start	0.8	8.2
At end (after 67 hr)	0.5	1.6
Hydrogen absorbed, μg/(cm²)(hr)		
Pickled surface	0.39	9.4
Oxidized surface	0.01	2.1

The same importance of coolant purification was noted in the French studies.[46] These experimenters studied the effect of various impurities on fouling in terphenyl mixtures. A heated, stainless-steel test section was utilized, but portions of the loop were fabricated of mild steel. The study was directed toward the elimination, or control, of fouling and concluded that fouling could be avoided if the terphenyl used contained "few impurities and no oxygen."[46] Heat-transfer coefficients were determined during some of the experiments, and a correlation is given in the reference. At wall temperatures in excess of 500°C, a decrease in the heat-transfer coefficient was observed, and this was attributed to localized pyrolysis of the coolant at the surface.

References 47 and 48 discuss burnout heat fluxes for organic coolants. The former is on terphenyl mixtures, terphenyl-benzene, and terphenyl-diphenyl mixtures, whereas the latter is on a biphenyl-diphenyl methane eutectic, a biphenyl-diphenylozid mixture, and Dowtherm A.

Table V-8 EFFECT OF WATER ON HYDRIDING IN AUTOCLAVES[44]
(400°C; Dissolved H_2, 100 ml/kg)

Water content of organic, ppm	Hydriding rate, μg/(cm²)(hr)					
	Zircaloy-2		Ni-free Zircaloy-2		Zr–2.5% Nb	
	As pickled	Preoxidized	As pickled	Preoxidized	As pickled	Preoxidized
40	0.5	0.032 ±0.007	0.5	0.010 ±0.005	1.0	0.12 ±0.012
40 to 60	0.4 ±0.1	0.011 ±0.002	0.280 ±0.020	0.001 ±0.001		0.001 ±0.001
60 to 1000	0.045 ±0.02	0.010 ±0.01	0.025 ±0.015	0.002 ±0.002	0.025 ±0.005	0.001 ±0.001

Digitized by Google

Both references employ correlations of the form $\phi_{BO} = a + bG^c + d\ \Delta T G^e$ for their results, where ϕ_{BO} is the burnout heat flux, G is the mass flow rate, and ΔT is the subcooling. The remaining symbols are constants for a particular fluid.

Directions of Future Developments

The direction of development of the heavy-water-moderated power-reactor program in Canada is covered in Refs. 49 to 51. The near-future plans envision the construction of a 1000-Mw(e) station composed of two 500-Mw(e) plants of the CANDU type. This reactor would evolve from CANDU by means of the following improvements:[50]

—Use of cold-worked zirconium–2½% niobium pressure tubes

—Increase of outlet temperature from 294 to 301.7°C

—Increase of fuel rating from a conductivity integral of 40 to 48 watts/cm

Other changes involve an increase in the pressure-tube diameter, a corresponding decrease in the number of pressure tubes, and, possibly, venting the containment pressure-relief system to a separate gas holder and heat absorber. Interestingly, the large reactor will be controlled by absorbers composed of liquid or gas arranged in vertical through tubes distributed throughout the reactor core, and by soluble poison dissolved in the moderator. The vertical through tubes will be subdivided into a number of separate chambers for flexibility. It thus appears that moderator-level control will not be used for the large reactors, probably for the reasons discussed in Sec. VIII of *Power Reactor Technology*, 7(3).

The longer term direction of the Canadian program is summarized as follows:[51]

For the water-cooled line itself, the following evolution appears reasonable:

Step 1—(Present Stage)—Pressurized D_2O with CANDU Type UO_2 Fuel Bundles Operating at a Rating of $\int kd\theta$ = 40 W/cm.
For the same reactor, a cheaper fuel can be developed by using larger fuel elements operating at $\int kd\theta$ = 48 W/cm.

Step 2—Boiling D_2O—Indirect Cycle—UO_2 Fuel. From 10% to 20% outlet quality, little change is expected in fuel geometry. From 15% to 30% quality, fuel and/or pressure tube geometry may have to change to keep coolant distribution optimum.

Step 3—Boiling H_2O—Direct Cycle—UO_2 Fuel. When outlet qualities between 20% and 30% are shown to be practical, this reactor will be a strong contender.

Elsewhere, as in Canada, the key question in the future development of the heavy-water pressure-tube reactor is which coolant to use. Although the D_2O-cooled version of the reactor has been developed in Canada, its disadvantages with respect to steam-temperature limits, D_2O leakage, and D_2O inventory considerations are appreciated there, as is attested by the Canadian work on the H_2O-cooled and organic-cooled versions. Considering the work throughout the world, one concludes that the three alternate coolants, gas (CO_2), organic liquids, and H_2O in some form, will receive serious developmental tryouts. Of the coolant systems that have been considered seriously in the past, only sodium and direct-cycle boiling D_2O appear to have been eliminated.

References

The references that contain A/Conf. numbers are papers that were presented at the Third United Nations International Conference on the Peaceful Uses of Atomic Energy, Geneva, September 1964.

1. Nuclear Power Demonstration Reactor, reprinted from *Nucl. Eng.*, 7(77): 398 (October 1962).
2. CANDU Douglas Point Nuclear Power Station, reprinted from *Nucl. Eng.*, 9(99): 289 (August 1964).
3. L. J. Ingolfsrud, P. H. G. Spray, and J. H. Jackson, Manufacturing and Construction for the Douglas Point Nuclear Power Project, A/Conf.28/P/7.
4. AEC Announces Plans for Advanced Converter Reactor Development, AEC Press Release, Sept. 24, 1964.
5. S. Fawcett, A. Firth, and J. E. R. Holmes, General Design of the Steam Generating Heavy Water Reactor, A/Conf.28/P/129.
6. N. Bradley, P. J. Cameron, and N. G. Worley, Some Engineering Problems of the S.G.H.W. 100 MW(e) Prototype Reactor, A/Conf.28/P/143.
7. F. Accinni, R. Bonalumi, C. Bruschi, F. Palazzi, S. Rubbia, and G. B. Zorzoli, The Physics of a Steam-Water Mixture Cooled Heavy Water Power Reactor, A/Conf.28/P/625.
8. C. G. Campbell, D. Hicks, I. Johnstone, and D. C. Leslie, Reactor Physics Studies for Steam Generating Heavy Water Reactors, A/Conf.28/P/174.
9. F. Pascual, L. Palacios, and M. K. Sanders, The DON Project, A/Conf.28/P/601.
10. A. Alonso and B. L. Hoffman, Safety Features of the DON Reactor Concept, A/Conf.28/P/495.
11. E. R. Mayquez, J. L. De Francisco, and F. J. Olarte, Experimental Studies of Uranium Carbide–Heavy Water Lattices, A/Conf.28/P/743.

Digitized by Google

12. R. Carle, P. Schulhoff, P. Sevin, and J. Buttin, EL4 Features and Construction Problems, A/Conf.29/P/40.
13. B. B. Du Bois, J. L. Bernard, R. Naudet, and R. Roche, Heavy-Water-Moderated Gas-Cooled Reactors, A/Conf.28/P/39.
14. Y. Girard, P. Lourme, and R. Naudet, Heavy Water Reactor Physics, A/Conf.28/P/76.
15. J. L. Bernard, H. Foulquier, and P. Thome, Core Structures of the Heavy Water–Gas Reactor EL4, A/Conf.28/P/69.
16. P. Krafft, The Lucens Experimental Nuclear Power Station, A/Conf.28/P/692.
17. E. Binggeli, P. Verstraete, and A. Sutter, The Underground Containment of the Lucens Experimental Nuclear Power Plant, A/Conf.28/P/459.
18. H. R. Lutz, R. W. Meier, and J. P. Schneeberger, Natural and Slightly Enriched Uranium Lattice Studies of Voided Metal Rod Clusters in D_2O, A/Conf.28/P/691.
19. M. Moller-Madsen, F. List, and J. Elming, Design Problems in the D_2O-Moderated, Organic-Cooled Reactor Concept DOR, A/Conf.28/P/777.
20. C. F. Hojerup, O. Kalnaes, H. Neltrup, and P. L. Olgaard, Heavy-Water-Moderated, Organic-Cooled Lattices Investigations. Experimental Results and Comparison with Theory, A/Conf.28/P/711.
21. A. I. Alichanov, P. P. Blagovolin, B. I. Ilyiechev, G. N. Karavaev, N. N. Kondaritzky, B. A. Medzibovsky, D. M. Mukhamedov, N. N. Nikolaev, V. V. Stekolnikov, V. F. Titov, B. Z. Torlin, and A. A. Khokhlachev, Natural Uranium Heavy-Water Moderated Organic-Cooled Power Converter Reactor, A/Conf.28/P/877.
22. W. H. Zinn and C. A. Trilling, Heavy Water Power Reactors and Organic Cooled Power Reactors, A/Conf.28/P/209.
23. W. Keller, Potentialities of Heavy-Water Moderated Gas Cooled Pressure Tube Reactors, A/Conf.28/P/778.
24. J. C. Leny, A. Ertaud, C. D'Ayguesvives, J. P. Crette, and J. Panossian, ESSOR, Specific Test Reactor for Heavy Water Reactor Concepts Developed by Euratom, A/Conf.28/P/78.
25. J. W. Hilborn, W. M. Barss, M. F. Duret, J. R. Dickinson, A. C. Whittier, and E. Horton, NPD Start-Up, Reactivity Balance and Fuel Management, A/Conf.28/P/9.
26. L. W. Woodhead and W. M. Brown, Performance and Problems of NPD, A/Conf.28/P/8.
27. W. B. Lewis, J. R. MacEwan, W. H. Stevens, and R. G. Hart, Fission-Gas Behaviour in UO_2 Fuel, A/Conf.28/P/19.
28. R. D. Page, D. G. Hardy, A. J. Mooradian, J. Howieson, G. R. Fanjoy, and D. B. Nazzer, Engineering and Performance of UO_2 Fuel Assemblies, A/Conf.28/P/18.
29. J. A. L. Robertson, A. S. Bain, J. R. MacEwan, and J. F. Notley, UO_2 Performance—The Importance of Temperature Distribution, A/Conf.28/P/17.
30. D. G. Boxall, W. M. Brown, D. B. Nazzer, J. T. Rogers, R. G. Hart, and K. L. Smith, Development of Fuel and Coolant Tubes for a Reactor Cooled by Organic Liquid, A/Conf.28/P/23.
31. N. Hansen, P. Knudsen, A. C. Winther, and E. Adolph, Sintered Aluminum Products for Organic-Reactor Applications, A/Conf.28/P/421.
32. G. Sainfort, G. Cabane, and M. Salesse, FeAl 40, A New Canning Material for Reactors, A/Conf.28/P/71.
33. V. E. Ivanov, V. F. Zelensky, S. I. Feifer, I. A. Petelguxov, and V. K. Khorenko, Development of Heat-Resistant Mg-Be Alloys As a Cladding Material for Fuel Elements, A/Conf.28/P/340.
34. V. Kraus, Diffusion Bonding of Uranium with Magnesium by Means of Intermediate Layers, A/Conf.28/P/526.
35. L. Dolle, D. Conan, and G. Dirian, Behaviour of Water and Heavy Water in Nuclear Reactors and Problems of Power Regulation by Physico-Chemical Methods, A/Conf.28/P/70.
36. H. K. Rae, G. M. Allison, A. R. Bancroft, W. D. Mackintosh, J. F. Palmer, E. E. Winter, J. E. LeSurf, and S. R. Hatcher, Experience with the Chemistry of Water in Moderator and Coolant Systems, A/Conf.28/P/20.
37. J. A. Morrison, M. H. Thomas, L. C. Watson, and L. W. Woodhead, The Management of Heavy Water for Research and Power Reactors, A/Conf.28/P/29.
38. W. P. Beddington, J. F. Proctor, W. C. Scotten, and V. R. Thayer, Production of Heavy Water in the U.S.A., A/Conf.28/P/290.
39. W. R. Thomas, S. B. Dalgaard, W. Evans, V. Fidleris, G. W. Parry, and P. A. Ross-Ross, Irradiation Experience with Zircaloy-2, A/Conf.28/P/21.
40. F. Barbesino, E. Brutto, R. Di Pietro, G. Masini, G. Perona, and R. Sesini, Zircaloy-2 Pressure Tubes Corrosion, A/Conf.28/P/574.
41. C. E. Ells, S. B. Dalgaard, W. Evans, and W. R. Thomas, Development of Zirconium-Niobium Alloys, A/Conf.28/P/22.
42. J. K. Dawson, R. C. Asher, J. Boulton, B. Watkins, and J. N. Wanklyn, The Properties of Zirconium Alloys for Use in Water-Cooled Reactors, A/Conf.28/P/158.
43. A. D. Lane and J. G. Collier, Thermal and Irradiation Performance of Experimental Fuels Operating in Steam-Water Mixtures, A/Conf.28/P/16.
44. W. M. Campbell, A. W. Boyd, D. H. Charlesworth, R. F. S. Robertson, and A. Sawatzky, Development of Organic-Liquid Coolants, A/Conf.28/P/15.
45. P. Leveque, F. Franzetti, P. Van der Veene, and M. Giulani, Technological Studies on Organic Cooling Fluids, A/Conf.28/P/53.
46. F. Lanza, R. Ricque, and J. Villeneuve, Heat Transfer by Organic Liquids, A/Conf.28/P/93.
47. D. A. van Meel, Burn-Out in Subcooled Forced Convection Boiling of Polyphenyls, A/Conf.28/P/590.
48. I. Kiss and F. Szabo, Radiolytical and Heat Transfer Properties of Some Organic Coolant-Moderators, A/Conf.28/P/449.
49. I. L. Wilson, C. E. Beynon, W. G. Morrison, and N. L. Williams, Studies of CANDU-Type Reactors in the 500-MW(e) Range, A/Conf.28/P/6.
50. G. A. Pon, W. B. Lewis, L. R. Haywood, D. B. Primeau, G. J. Phillips, and E. E. Merlo, Prospective D_2O-Moderated Power Reactors, A/Conf.28/P/10.
51. A. J. Mooradian, Future Targets for Canadian Power Reactors, *Can. Nucl. Technol.*, 3(3): 49-53 (Summer 1964).

Digitized by Google

Section

VI

Power Reactor Technology

Heavy-Water-Moderated Pressure-Vessel Reactors

General Status

The heavy-water-moderated pressure-vessel reactors have had their most extensive development in Sweden, where the Agesta reactor was built, and in Norway, where the Halden Boiling Heavy Water Reactor (HBWR) is located. The Agesta Nuclear Power Plant (R3/Adam) was started in 1958, completed in 1962, and reached full power in March 1964. The HBWR has been operating since 1959. Further characteristics of both of these reactors are given in Table VI-1.

Heavy-water systems and fuel-handling equipment for the Agesta reactor are discussed in Refs. 1 and 2. Many of the details exemplify straightforward engineering practice, although some are peculiar to the reactor type. Among the latter is the careful preservation of cleanliness of the primary system:

> Before the final assembly of the components at the production workshops, a very comprehensive and stringent cleaning ... was carried out, for the most part in specially arranged clean rooms where the personnel worked under special clean conditions. Cleaning was mostly effected by washing ... in alkaline water and by washing or wiping with acetone.
>
> Pipes and components of carbon-steel were also used, to a limited extent in the heavy-water systems. After cleaning, these parts were rust-protected by a final rinsing in a bath of VPI dissolved in methanol.
>
> After the final assembly, pipe connections and other access openings were carefully sealed with, for example, plastic covers. Large carbon-steel tanks were not rust-protected by means of VPI but kept filled with a controlled over-pressure of dry nitrogen.

A number of basic designs for components in the Agesta heavy-water system are shown in Fig. VI-1. The centrifugal pumps were all canned pumps, whereas the D_2O piston type, feedback pumps were constructed with double seals around the piston shaft with provision for intermediate drainage. The latter principle, of double seals with D_2O recovery through leak-off pipes, is used generally for the nonhermetic closures.

A unique design feature of the Agesta fuel-handling equipment is the provision for transfer of fuel elements from the reactor D_2O to the storage pool, which contains H_2O. Under normal operation the transferred fuel element is gas cooled after its removal from the reactor and prior to its placement in the storage pool. Clean nitrogen is used as a coolant, and the evaporated D_2O is condensed by means of a Freon refrigeration system. In the event of failure of the gas cooling system, a backup spray of either D_2O or H_2O is provided. This spray system also provides cooling when the gas system is not being utilized. A simplified scheme of the cooling and drying circuit is shown in Fig. VI-2.

The second Swedish heavy-water reactor, the Marviken[3] plant, is also of the pressure-vessel type but is cooled by boiling D_2O in natural circulation. The plant is now under construction near Stockholm and should be operational in 1968. Details of the design are given in Table VI-2. The flow path of the primary coolant,

Table VI-1 CHARACTERISTICS OF THE AGESTA AND THE HBWR

Reactor	Power	Coolant	Coolant pressure, psi	Fuel/cladding (first core)
Agesta	10 Mw(e); 55 Mw, space heating	Pressurized D_2O	500	UO_2/Zircaloy-2
HBWR	10 Mw, process steam	Boiling D_2O	400	Uranium/aluminum

Digitized by Google

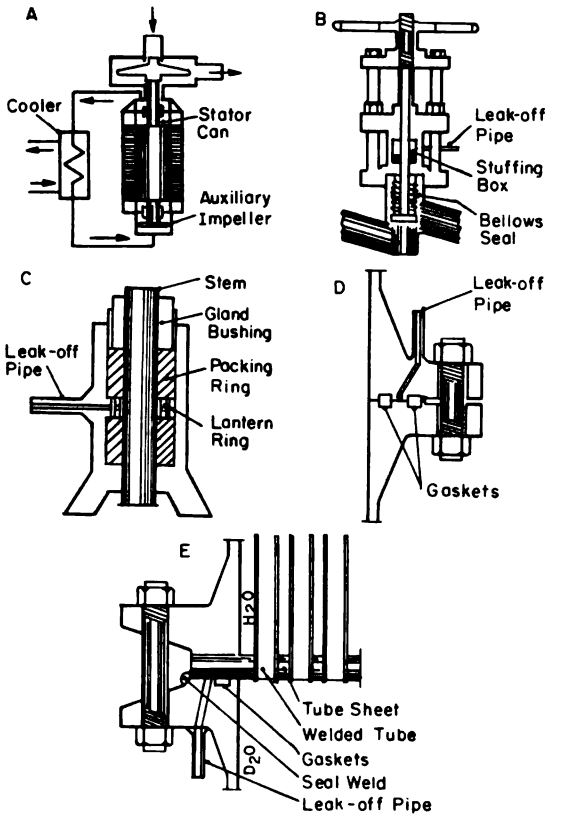

A, Glandless Centrifugal Pump
B, Globe Valve with Bellows Seal
C, Stem with Double Gaskets and Leak-off Pipe
D, Flange Connection with Double Gaskets and Leak-off Pipe.
E, Heat Exchanger D_2O / H_2O

Fig. VI-1 Basic designs for components in the Agesta heavy-water system.[1]

Table VI-2 DESIGN DATA FOR THE MARVIKEN BHWR[4]

Reactor type	
General	BHWR
Cycle	Direct
Circulation	Natural
Superheating	Internal, when provided
Fuel	UO_2
Fuel changing	Onload, continuous
Data	
Net electrical output, Mw(e)	200
Net thermal efficiency, %	34.0
Mean moderator temperature, °C	163
Core volume	
Unreflected, m^3	64.1
Reflected, m^3	94.6
Inner diameter of pressure vessel, m	5.22
Design pressure, bar	57.5
Working pressure, bar	49.5
Pressure-vessel steel	Low alloy (A-302B)
Wall thickness (excluding S.S. lining), mm	76
Outlet steam temp., °C	470
Average enrichment, %	~1.35
Average burnup, Mwd/ton of U	13,000
Fuel for boiling channels	
No. of channels	147
No. of rods per cluster	31
Rod diameter (UO_2), mm	12.5
Can material	Zircaloy-2
Can thickness, mm	0.55
Superheater elements* (2nd charge)	
No. of channels	32
No. of rods per cluster	48
Rod diameter (UO_2), mm	~11.5
Currently assumed can material	20 Cr–35 Ni
Currently assumed wall thickness, mm	0.4–0.25†
Approx. fin height, mm	0.1
Max. surface temp. (hot spot), °C	524

*Current assumption.
†Future changes.

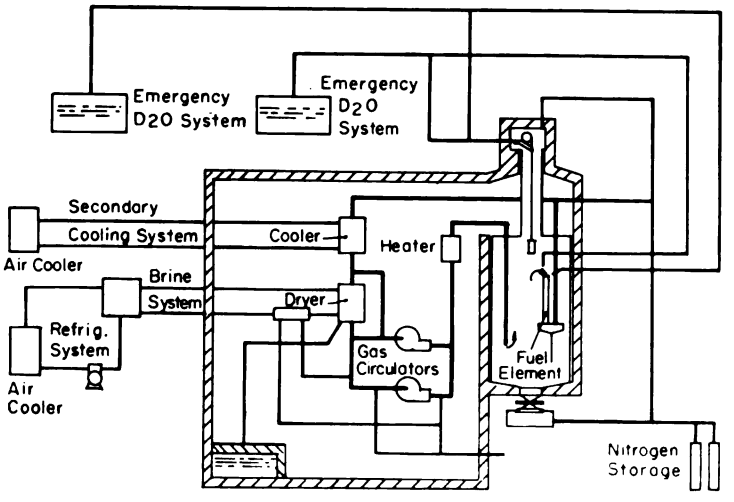

Fig. VI-2 Simplified scheme of the Agesta cooling and drying circuit.[2]

Digitized by Google

which is quite unusual, is shown in Fig. VI-3. Water from the feedwater heaters is pumped into the moderator space at a temperature of about 250°F. The core is constructed of 179 Zircaloy-2 shroud tubes hydraulically isolating the moderator region of the core from the fuel elements. The moderator water therefore flows to the top of the moderator space and exits at a temperature of about 430°F. At the top of the core, the moderator mixes with the liquid portion of the two-phase mixture that cools the fuel elements, and the resulting coolant flows to the downcomer and thence to the fuel elements. The initial operation of Marviken will be with saturated steam.[3] Thirty-two of the shroud tubes will be left empty to serve as flow channels for the saturated steam; the remainder will contain fuel elements. The turbine contains an inlet blading system suitable for saturated-steam operation and interstage moisture separation, but the inlet blading can be modified for operation with superheated steam. When operating on the saturated-steam cycle, Marviken generates 140 Mw(e). The rated power of 200 Mw(e) is attained only through incorporating superheating fuel elements in the 32 empty shroud tubes.

Operation with the relatively cool moderator is done to improve burnup for a given enrichment.[3] High-pressure tests in a mockup of the reactor was 0.5% for steam carry-under and negligible carry-over of water. Figure VI-4 shows an overall arrangement of the reactor plant. The containment is based on the pressure-suppression principle.

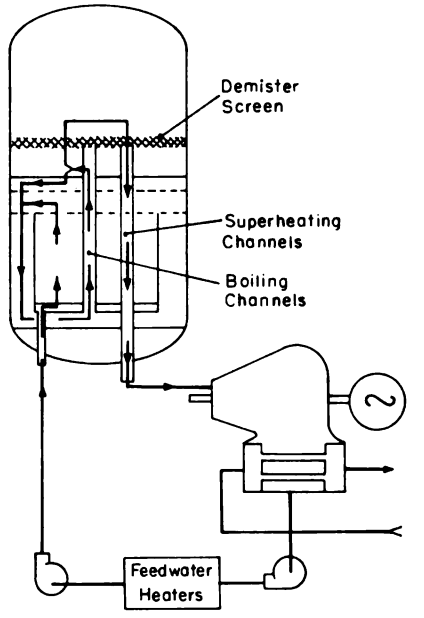

Fig. VI-3 Flow schematic for the Marviken reactor.[4]

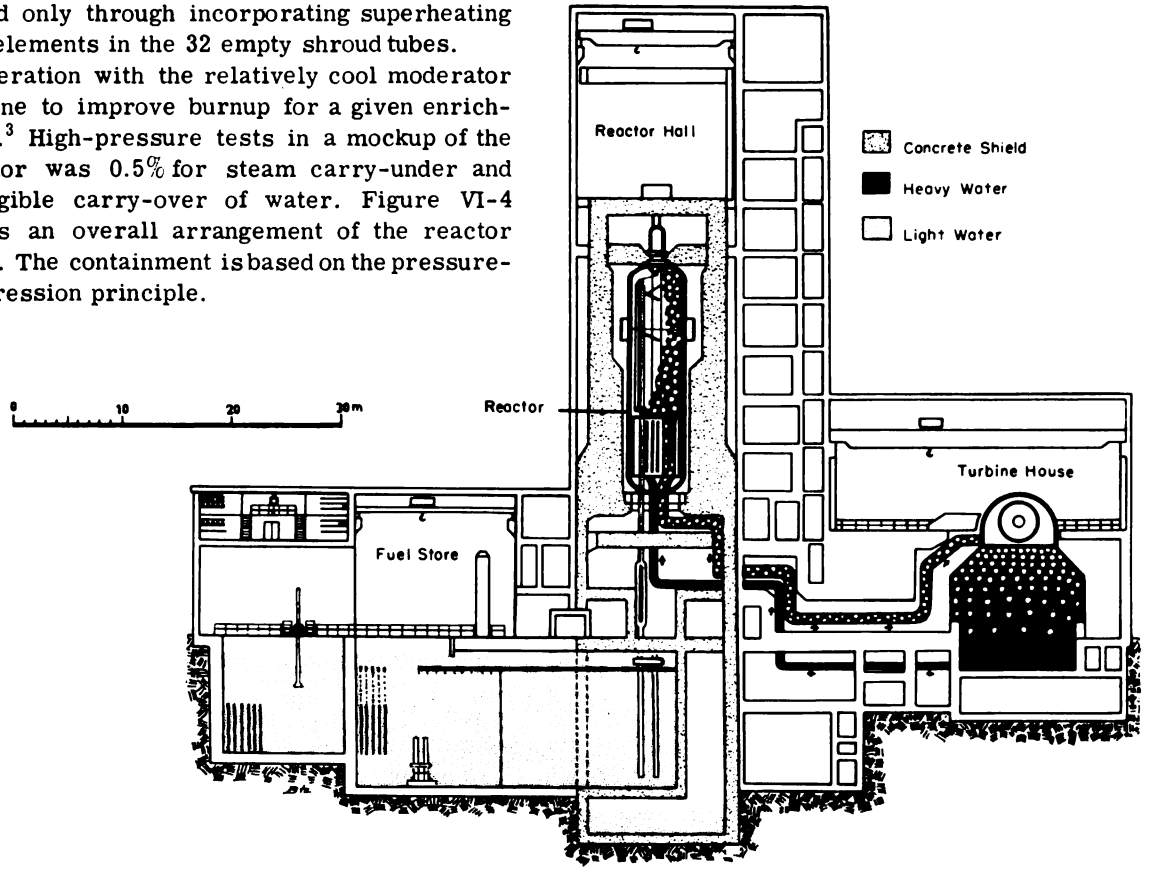

Fig. VI-4 Schematic of the Marviken reactor.

Digitized by Google

Operating Experience

Some operating experience, partly of a preliminary nature, has been reported for the Agesta reactor.[5,6] Reference 6 was issued in May 1964, and the turbine was commissioned in late April 1964. Space heating occurred a month earlier in the town of Farsta. Only one shutdown at power had been experienced, and this was due to a disturbance in the instrumentation power-supply system. The primary circuit was rinsed with light water prior to filling with D_2O. The light water was then drained, and the system was vacuum dried after a nitrogen flush. A second vacuum drying resulted in a pressure decrease to 1.2 mm Hg, and at that point nitrogen was admitted to the system followed by a few liters of D_2O. The vapor-nitrogen mixture was circulated through the system with the fans in the blanket-gas drying circuit, and the liquid was then condensed. Analyses of the condensate indicated that only a few hundred grams of H_2O were present in the system. The system was then filled with D_2O. The plant has not been in operation long enough to produce a significant tritium content in the heavy water.

The Halden reactor operated from June 1959 to April 1961 on its first core. Modifications were made to the plant during the refueling shutdown, and the second core was loaded in March 1962. The second core utilizes 100 fuel assemblies with UO_2 as fuel and Zircaloy-2 as cladding. Each assembly consists of seven fueled pins having a length of 1600 mm (5.25 ft). Although the HBWR is not a power reactor in the usual sense, it does operate at high pressure and temperature, and much of the operating experience is pertinent to power-reactor operation. For example, Ref. 7 contains much information on loss and degradation of D_2O.

Table VI-3 SUMMARY OF HBWR FLANGE AND SEAL STATISTICS

No. of 8-in. flanges	10
No. of smaller flanges	50
No. of reactor-lid mechanical seals	335
Integrated "gasket-length" high-pressure system, m	100

The HBWR flow diagram is shown in Fig. VI-5. The system contains a number of flanges and seals that are not backed up with seal welding or leakage collection, and these are summarized in Table VI-3. The D_2O leakage was studied by various means, but the most useful method was found to be monitoring of the outgoing air for tritium. The tritium content of the reactor heavy water was known. The leakage rate could be calculated by measuring the ven-

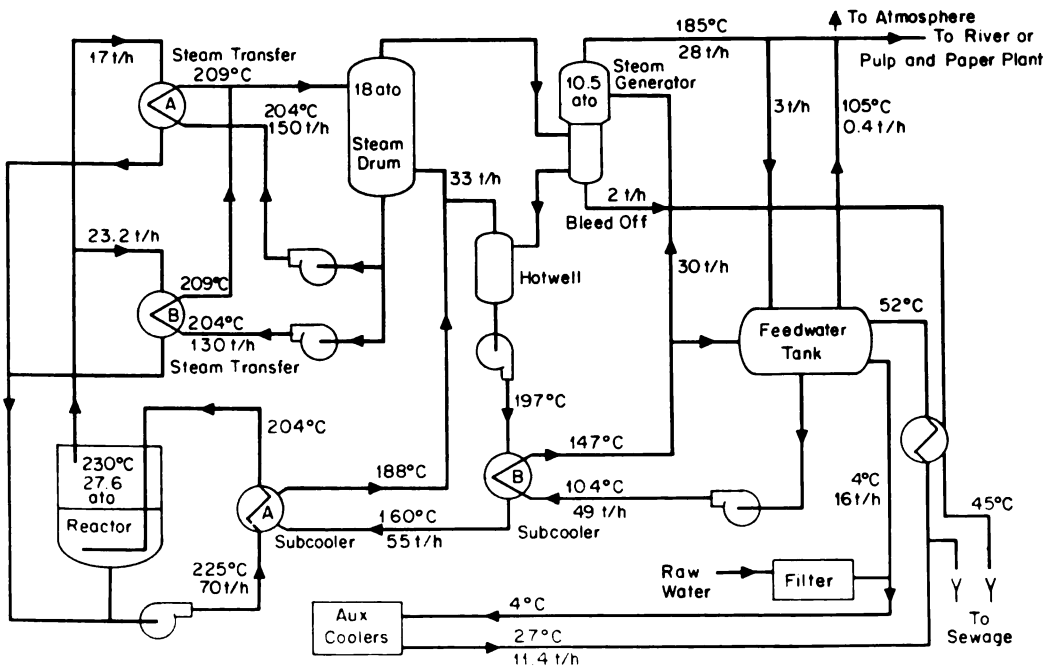

Fig. VI-5 The HBWR simplified flow sheet and 20-Mw operating data.[7]

Digitized by Google

tilation air flow rate and absolute humidity. Inventory measurements were also made, and they corresponded "reasonably well" with the tracer results. The loss of heavy water and the reactor pressure history for the HBWR are shown in Fig. VI-6. The heavy-water inventory for this reactor is 14.5 tons.[7] The loss of 2500 kg of D_2O over a 20-month period (Fig. VI-6) represents a leakage rate of about 10% per year.

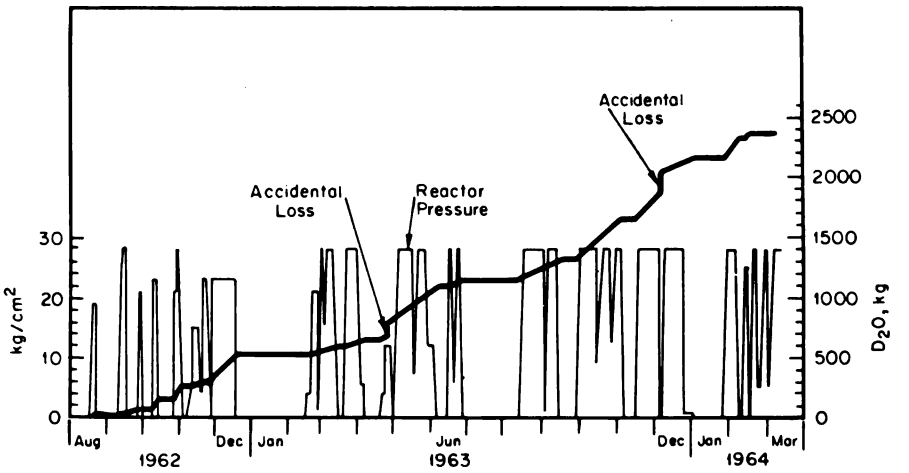

Fig. VI-6 Loss of heavy water in the HBWR and reactor pressure history.[7]

At the start of operation with the second core, the isotopic purity of the D_2O was 99.75%. By the end of 1963 it had fallen to 99.68%. This represents an inleakage of about 10 kg of H_2O to the system.

Significant Developments

Fuel Elements, Fuel Materials, and Cladding

The Swedish experience with fuel and cladding materials is contained in Refs. 8 and 9. Reference 10 is a Norwegian contribution on aluminum alloys as cladding materials. Table VI-4 gives fuel data for the Agesta and Marviken reactors and the pressurized heavy-water reactor (PHWR). The PHWR is a design study and will be discussed shortly.

The Agesta fuel bundle is relatively open, in the sense of having a large rod-to-rod spacing. This is to ensure adequate coolant velocity in natural circulation and also to provide a slightly negative void coefficient. It is said[8] that the helical wire wrap is not applicable to this type of design because of the 3- to 5-mm spacing between rods. The Agesta design provides for spacing and intermediate support points by subdividing the 3-m fuel rod into four subelements and using spring-loaded flexible plate spacers located at the fuel-element junctions.

The Marviken boiling fuel elements are composed of rods built up of two half-length subrods. A midbundle spacer positions the subrods, and the reference mentions that the tendency for steam bubbles to anchor on the spacer grids has been a problem with respect to localized corrosion and overheating. The rod-to-rod spacing in the Marviken is about 9 mm. This is maintained by the spring type spacers. For rigidity the spacers are anchored to a central, supporting Zircaloy tube that apparently is unfueled. In-pile test elements of Swedish design were run in the Canadian NRX reactor and in the VBWR. The highest oxide temperatures were determined by postirradiation examinations to be in the pellet immediately downstream of the spacer, and this is attributed to steam-bubble anchoring.[8]

The corrosion and hydriding results of Swedish experiments on Zircaloy are typical of those observed in other countries. The shroud in the Marviken reactor is a fixed piece of core hardware; thus the requirement of a long in-core lifetime does exist, although the consequences of a failure are not as serious as the failure of a pressure tube in a pressure-tube reactor.

Digitized by Google

Table VI-4 FUEL DATA FOR SWEDISH POWER-REACTOR FUEL ELEMENTS[8]

	Agesta, 55 Mw(t) + 10 Mw(e)	PHWR, 360 Mw(e)	Marviken	
			Boiling element, 140 Mw(e)	Superheating element, 200 Mw(e)
Total heat release in fuel, Mw	60	1134	471	122
Reactor pressure, bars	33.3	74	49.5	49.5
Fuel form	UO_2 (sint.)	UO_2 (sint.)	UO_2 (sint.)	UO_2 (sint.)
Enrichment, %	Natural	1.5	1.3	1.6
Active fuel-element height, mm	3047	4455	4420	4220
Free space in rod, mm	10	65	100	150
Fuel rods per assembly	4 × 19	2 × 49	2 × 30	2 × 48
No. of assemblies	140	177	147	32
Total UO_2 weight, tons	18.5	33.7	25.6	7.0
Can	Zircaloy-2	Zircaloy-2	Zircaloy-2	S.S.
Canning-tube inside diameter, nominal, mm	17.2	10.5	12.6	11.6
Can wall thickness, mm	0.7	0.51	0.6	0.4
UO_2 pellet diameter, nominal, mm	17.0	10.4	12.5	11.5
Mean heat loading, watts/cm	78.5	300	227	180.6
Hot-channel factor (including transient)	4	2	2.99	2.72
Max. transient heat loading, watts/cm	314	600	680	491
Max. heat flux on can surface, watts/cm	54	164	156	126
Mean temperature of the fuel, °C	500	900	800	1200
Max. center temperature (including transient), °C	1325	2450	2760	2670
Coolant/UO_2 area ratio	1.13	16.4	3.52	1.92
Coolant inlet temperature, °C	205	254	255	263
Coolant outlet temperature, °C	220	274	263	470
Mean burnup, Mwd/ton	3600	16,000	13,000	13,000

The use of aluminum as a cladding is being studied primarily as an in-pile experiment.[10] Prototype elements were scheduled to be irradiated in the HBWR in late 1964.

Water Chemistry

Reference 11 is a report on the water-chemistry research at the HBWR. The report covers reactor experiments that were designed to study conditions under which corrosion can be reduced to the point where operation is possible without full-flow condensate purification. This involves a search for conditions under which steam will be produced with a low oxygen content and the alkalinity of the recirculating water will be preserved. Reducing the in-core dissociation of D_2O should also reduce the recombiner load. However, this particular point was not mentioned in the reference.

Figure VI-7 shows the oxygen concentration in the HBWR steam as a function of power, with no additions to the coolant. The D_2 was found in stoichiometric amounts. When D_2 was added to the subcooled feedwater, the net decomposition of D_2O was considerably lessened, as is shown in Fig. VI-8. This figure shows the effect of D_2 addition at various pressures, various locations, and several different powers. Ammonia (as ND_3) was added to the coolant, and it was shown that the radiolysis of ammonia into nitric acid could be prevented by maintaining the D_2 concentrations at or above 0.3 to 0.4 ml per kilogram of heavy water. The radiolysis of ammonia into nitrogen and deuterium did increase the ^{16}N content of the steam, however.

Control and Instrumentation

The Agesta reactor is equipped with top-mounted, hydraulically actuated control-rod drives.[12] A stepping action is accomplished by

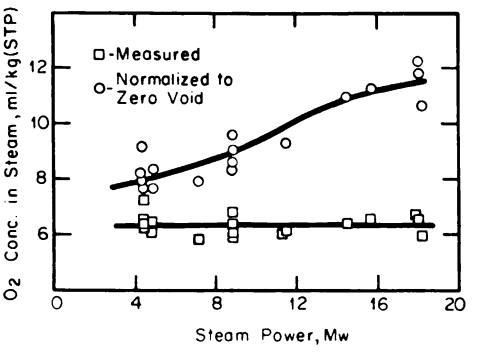

Fig. VI-7 Oxygen concentration in steam vs. steam power at 28 ata.[11]

Digitized by Google

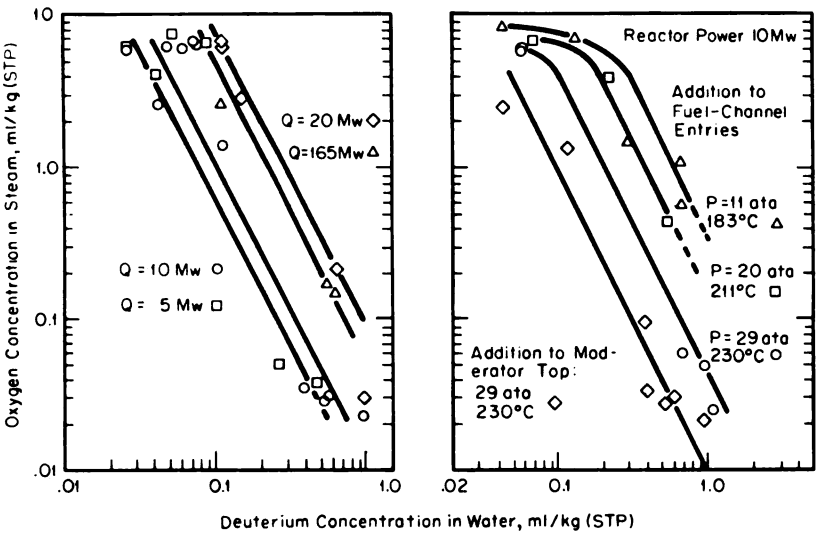

Fig. VI-8 Oxygen concentration in steam vs. deuterium concentration in water entering the fuel channels.[11]

means of two chucks. One chuck normally holds the rod in a given position, and the other grasps the control rod and moves a small distance up or down (10 mm) in response to hydraulic pressure. The Agesta control rods are of silver-indium-cadmium alloy clad with type 304L stainless steel and are tubular in shape.

The Marviken reactor will be equipped with rather unusual control-rod drives. The reactor (Fig. VI-4) is designed for on-power refueling. The entire control-rod drive is to be located within the pressure vessel, immediately above the core, and will be hydraulically actuated. The drive will be positioned by means of the fuel-handling machine and held in place only by the weight of the drive itself. The water, which serves as the hydraulic fluid, is fed through pipes penetrating the pressure-vessel wall and is introduced into the drive by means of piston-ring type seals. The drives are located in the steam atmosphere above the core, but the drive mechanism will be filled with water to control the drop speed upon scram. The position-indicating system is based on ultrasonic location of a reflector plate at the lower end of a control rod. A transducer, at the bottom of the control-rod channel, emits ultrasonic pulses, and the time interval between their transmission, reflection, and absorption back at the transducer gives the location of the control rod.

The in-core instrumentation for the HBWR is detailed in Ref. 13. Most of the information has been presented in *Nucleonics*[14] and will not be repeated here.

Pressure Vessels

The design and fabrication of the Agesta and Marviken pressure vessels are discussed in Ref. 15. The design details of these vessels, and that of a larger reactor to be discussed shortly (BASHFUL-600), are given in Table VI-5. The Agesta vessel has a cylindrical shape with an ellipsoidal bottom dome and a flat lid. The cylindrical portion is roll clad with stainless steel and has an upper flange fabricated of forged parts welded together and clad with weld-deposited stainless steel. The Marviken vessel is quite different from that of the Agesta and is shown in outline form in Fig. VI-4. The

Table VI-5 SURVEY OF REACTOR VESSEL DATA[15]

	Agesta PHWR	Marviken BHWR	BASHFUL-600
Design pressure, bars	40	57.5	80
Design temperature, °C	251	272	293
Vessel inside diameter, m	4.5	5.22	6.6
Cylindrical wall thickness, m	65	76	120
Bottom dome-wall thickness, mm	65	70	175
Vessel steel type	C-Mn	C-Mn-Mo	9% Ni steel
Vessel height, m	9.5	23.96	26.75

Digitized by Google

bottom dome, which is hemispherical in shape, is penetrated by 87 nozzles, as follows:

32 superheater nozzles
34 nozzles that indicate the positions of control rods by ultrasonics
12 nozzles for neutron detectors
8 nozzles for startup heating and coolant inlet
1 nozzle that is a transport channel for control rods and fuel elements

The entire internal shell surface is clad with stainless steel by overlay welding, and the shell is penetrated by nozzles for feedwater, control-rod-drive piping, pressure-relief valves, emergency cooling piping, and canning leak-detection piping. The hemispherical upper head is penetrated by three nozzles for television cameras and the large central nozzle supporting the charging machine. The vessel closure system is unique and is illustrated schematically in Fig. VI-9. The design is such that all forces acting in the fixed flange rings pass through one point, thus giving no moment in the ring.

The pressure vessel for the 600-Mw(e) BASHFUL reactor, which is an advanced design of a boiling heavy-water-moderated reactor, has an inside diameter of 6680 mm and a total height of 24,750 mm. The vessel would be shipped to the site in at least two pieces. After installation of the internals at the site, the parts of the vessel would be joined by welding and locally heat-treated. At the present time no welding electrode has been developed that is fully satisfactory with the 9% nickel steel proposed for the vessel, but the reference states that such electrodes are expected to be developed in the near future.

Directions of Future Developments

The direction of development of the pressure-vessel heavy-water-moderated power reactor appears to be largely dependent on the future program in Sweden, as well as on the Norwegian work, although there apparently is also some activity on the reactor type in Germany.[17] Sweden, probably because it is relatively well endowed with water power, anticipates a slow buildup of nuclear capacity in the near future but a rapidly accelerating one later. Reference 18 assumes that Sweden will have an installed nuclear capacity of 200 Mw in 1970, 1000 Mw in 1975, and 4000 Mw in 1980. The figures seem to indicate that, when nuclear energy is finally

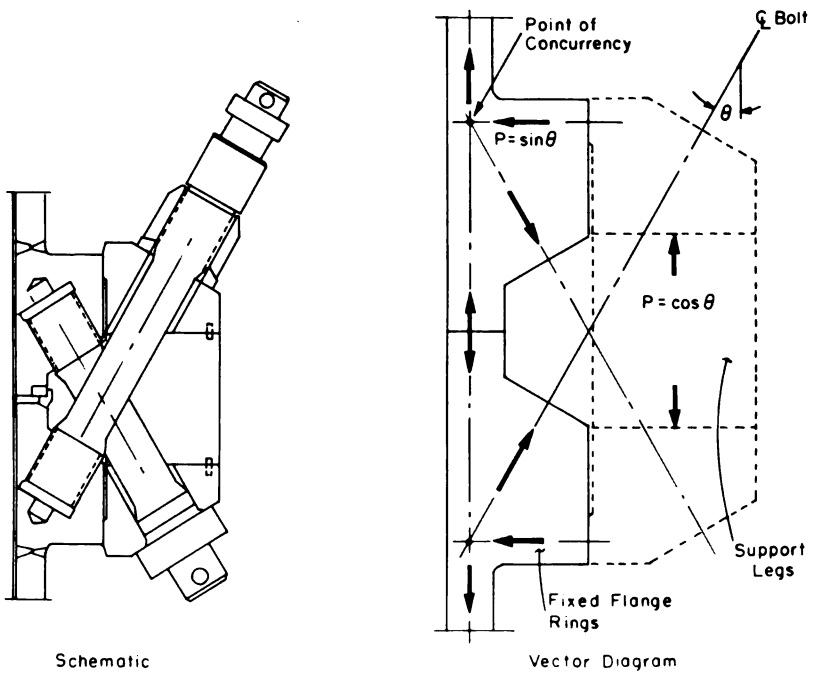

Fig. VI-9 Details of Marviken vessel-closure flange.[15]

Digitized by Google

Table VI-6 PARAMETERS CHARACTERIZING ADVANCED SWEDISH REACTORS[18]

	Marviken	BHWR*		PHWR	BASHFUL†
		Natural U	Enriched U		
Thermal efficiency	0.287	0.314	0.314	0.283	0.371
Specific power, kw/kg of U	18.0	18.0	27.0	35.6	24.0/41.2
Enrichment, wt.% ^{235}U					
Initial	1.00	0.71	1.17	1.50	1.05/2.17
Final	0.25	0.25	0.25	0.40	0.2/0.92
Rod diameter, mm	12.5	14.0	11.5	10.4	11.5/8.5
Plutonium, g/kg of U	5.6	4.7	6.6	6.0	6.3/6.9

*The BHWR is a 300- to 500-Mw(e) reactor producing saturated steam.
†BASHFUL is a reactor similar to Marviken in the 400- to 1000-Mw(e) power range. The numerator of the fractional entries pertains to the parameters of the boiling region, and the denominator pertains to the superheating region.

needed, it will be badly needed. This is substantiated in the reference, which states that domestic sources of fossil fuels in Sweden are lacking.

The Marviken reactor represents the 1970 commitment approximately. Beyond this date the reactor type to be built is open; pressurized heavy-water reactors (PHWR),[19] saturated boiling heavy-water reactors (BHWR), and boiling and superheating reactors of the Marviken type (BASHFUL)[18] are all under study. Reference 18 is a discussion of the economics of these various types, and some of the proposed design parameters are given in Table VI-6. Fuel costs are given in Table VI-7. Table VI-7 illustrates the importance of on-power refueling, since this is said to be responsible for the difference in cost between the PHWR and the remaining reactors. The PHWR costs were arrived at by assuming multizone, batch loading, whereas the remaining plants were assumed to be continuously refueled. The penalty can be seen in the enrichment values given for the PHWR, as contrasted to the remaining plants. The processing of fuel appears to be of marginal value, as Table VI-7 shows that the cost of processing about equals the plutonium value.

The Swedish fuel-cycle philosophy is now characterized as follows:[18]

> Use of slightly enriched uranium for normal operation but possibility of optional operation with natural uranium.
>
> Once-through uranium cycle without reprocessing of spent fuel but with possibility of future recycling of plutonium in a self sustained cycle.

The option for use of natural uranium is somewhat peculiar to Sweden but is of general interest. If 4000 Mw(e) is in fact the installed capacity in 1980 and if the annual increase is 800 Mw(e), the net import requirements for natural uranium would amount to $8 million per year, compared to $13 million for enriched uranium. If the nuclear electricity were being generated with conventional BWR's, the corresponding figures, as given in Ref. 18, would be $40 million per year for Zircaloy-clad fuel and $63 million

Table VI-7 FUEL COSTS* FOR DIFFERENT REACTOR TYPES[18]

	Marviken	BHWR		PHWR	BASHFUL
		Natural U	Enriched U		
Cost item, mills/kw-hr					
Fuel consumption	0.51	0.39	0.63	1.04	0.67
Manufacturing	0.88	1.23	0.89	1.10	0.79
Fixed	0.20	0.13	0.13	0.14	0.13
Processing	0.29	0.44	0.26	0.30	0.23
Credit on uranium	0	0	0	−0.04	−0.09
Credit on plutonium	−0.43	−0.55	−0.46	−0.47	−0.38
Once-through (items 1 to 3)	1.59	1.75	1.65	2.28	1.59
Net credit (items 4 to 6)	−0.14	−0.11	−0.20	−0.21	−0.24
Total cost	1.43	1.64	1.45	2.07	1.35

*Basic assumptions: burnups, 15 Mwd per kilogram of uranium, except for natural uranium, which is 9 Mwd per kilogram of uranium; feed cost, $8 per pound; separative work, $30 per kilogram of uranium; interest rate, 7%; fixed costs at 6000 h/g and 60% of initial core; processing, $30 per kilogram of uranium; plutonium credit, $8/g total.

Digitized by Google

for stainless-clad fuel. These numbers might be important in considerations involving trade balance or emergency situations, but the reference assigns them a "minor importance." Nevertheless, the requirement that the reactor be capable of operation with natural uranium is allowed to compromise the optimization of the reactor fueled with enriched uranium, and this is noted in the reference.[18]

Czechoslovak Nuclear Power Station

The remaining heavy-water power reactor of the pressure-vessel type is the gas-cooled reactor of the Czechoslovakian nuclear power station. Few design details were presented at the conference, but coverage had been reasonably thorough at the Second Geneva Conference. Reference 20 reports on some design and construction problems of the reactor and discusses the charge-discharge machine, control-rod tests, top biological shield design, steam-generator tests, main blower tests, and steam-turbine design. The plant has been scheduled[21] to be critical in 1965. No other dates are given to suggest that this time schedule will not be met, although it is mentioned in Ref. 20 that the construction time has been "elongated."

The pressure vessel for the Czechoslovakian nuclear power station is discussed in Ref. 16 and is shown in Fig. VI-10. The figure does not illustrate the upper head details, but there are approximately 200 nozzles through the head for control and refueling. The reactor is D_2O moderated, and the CO_2 coolant is piped through 12 inlet and 12 exit nozzles. The reference contains much information on stress analysis, material properties, and test results that would be of interest to the specialist. The pressure-vessel steel is designated "CSN 13030," and is composed of <0.20% carbon, 1.10 to 1.14% manganese, <0.10% cobalt with titanium and aluminum added "... for increasing of structural stability and finegrainedness ..."[16] The reference describes the manufacture of a shortened version of the pressure vessel. The vessel is the same as the one shown in Fig. VI-10 but does not include some of the ring sections.

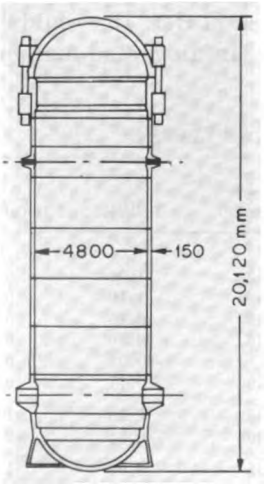

Fig. VI-10 Pressure vessel for the first Czechoslovakian power station.[16]

References

The references that contain A/Conf. numbers are papers that were presented at the Third United Nations International Conference on the Peaceful Uses of Atomic Energy, Geneva, September 1964.

1. P. I. Nylander, P. Hjertberg, and B. Larson, Manufacturing and Installation Experience of the Heavy-Water Systems of the Agesta Nuclear Power Plant, A/Conf.28/P/602.
2. G. Granelli, G. Fagerlund, S-O Brunzell, and G. Frŏman, Fuel-Handling Equipment for the Agesta D_2O-Moderated Pressure Vessel Reactor, A/Conf.28/P/808.
3. P. H. Margen, L. Leine, and R. Nilson, The Design of the Marviken Boiling Heavy Water Reactor with Nuclear Superheat, A/Conf.28/P/603.
4. P. H. Margen, The Development Work Leading up to the Marviken Nuclear Power Station, Lecture to the Swiss Nuclear Society, June 22, 1963, Reprint from *New Techniques*, 5(12): 699-714 (1963).
5. G. Apelqvist, P. E. Blomberg, O. Nylund, and R. Persson, Reactor Physics Studies and Comparisons Between Reactor Physics Data from Calculations and Mock-up Studies and from Measurements in the Agesta Nuclear Power Plant, A/Conf.28/P/682.
6. N. Rydell, P. Blomberg, and E. Ericsson, Experience from the Commissioning, the Criticality Experiments and the Power Operation of the Agesta Nuclear Power Plant, A/Conf.28/P/679.
7. E. Jamne, J. A. Firing, M. Øvreeide, and T. Wullum, Operational Experience on the 2nd Charge for the Halden Boiling Heavy Water Reactor, A/Conf.28/P/594.
8. H. Mogard, S. Djurle, I. Multer, H. P. Myers, B. Nelson, and U. Runfors, Fuel Development for Swedish Heavy Water Reactors, A/Conf.28/P/608.
9. G. Oestberg and H. P. Myers, Aspects of Swedish Studies of Cladding Materials for Water-Cooled Reactors, A/Conf.28/P/419.
10. S. Aas and K. Videm, Improved Aluminum Alloys as Fuel Cladding Material in Water-Cooled Power Reactors, A/Conf.28/P/591.

Digitized by Google

11. L. Hammar, R. Rose, and G. M. Allison, Water Chemistry Research at HBWR, A/Conf.28/P/595.
12. S. Ericsson and B. Ahlnaes, Design, Development and Manufacture of Control Rod Drives for Heavy Water Power Reactors, A/Conf.28/P/809.
13. B. Aarset, H. P. Olson, R. D. Smith, and O. Vapaavuori, In-Core Instrument Development in the HBWR Programme, A/Conf.28/P/859.
14. H. Ager-Hanssen and R. D. Smith, Advanced In-Core Instrumentation from Halden, *Nucleonics*, 22(4): 49-56 (April 1964).
15. O. Hellstroem, Design and Manufacture of the Reactor Pressure Vessels for the Agesta and Marviken Power Stations and Some Future Developments, A/Conf.28/P/810.
16. J. Hauer, St. Havel, J. Nemec, and St. Stěpánek, Pressure Vessel for the First Czechoslovak Nuclear Power Station, A/Conf.28/P/522.
17. A. Ziegler, Objectives in the Development of D_2O Pressure Vessel Reactors, A/Conf.28/P/779.
18. L. Zettergren and B. Pershagen, Fuel Cycle Physics and Economics for Heavy Water Reactors, A/Conf.28/P/417.
19. A. Jonsson and B. McHugh, A Large Swedish Nuclear Power Station with a Pressurized Heavy Water Reactor with an Open Uniform Lattice Core, A/Conf.28/P/605.
20. J. Hůlovec, J. Jůza, A. Komárek, J. Kořenek, V. Křížek, J. Tomčík, and K. Wagner, Development and Construction Problems of the First Czechoslovak Nuclear Power Station, A/Conf.28/P/523.
21. *Directory of Nuclear Reactors, Vol. IV: Power Reactors*, International Atomic Energy Agency, Vienna, 1962.

Digitized by Google

Section

VII

Power Reactor Technology

Gas-Cooled Clad-Fuel Reactors

By Walter Mitchell III

General Status

The Geneva information on gas-cooled reactors that employ metallic fuel jackets deals almost exclusively with reactors developed in the United Kingdom and France. Consequently, this article reviews the status, the significant developments, and the indicated directions of future development in terms of the British and French programs.

Some basic information on specific reactors of the type is presented in Table VII-1. The reactors, all of which are CO_2 cooled and graphite moderated, are classified as "British designed" or "French designed," but the reactors in the former category are not all located in the British Isles. Although the majority of the stations listed are multiple-reactor installations, as indicated in the first column of Table VII-1, the net electric outputs listed pertain to single reactors. The date of power operation for a particular station gives the year in which the first reactor in a multiple-reactor installation began or will begin operation.

The large number of British reactors of the CO_2-cooled graphite-moderated type built or being built and the steady progression in reactor output are striking results of the British program, which has up to now concentrated heavily on this reactor type. The improvements in the type, as indicated by the parameters listed in Table VII-1, illustrate rather vividly the technological advances that occur as a re-

Table VII-1 GENERAL INFORMATION ON GAS-COOLED CLAD-FUEL REACTORS[1-16]

Station (number of reactors in parentheses)	Date of first reactor on power	Net electric output per reactor, Mw	Net efficiency, %	Primary coolant nominal pressure, psia	Primary coolant temperature at reactor outlet, °F	Fuel rating, Mw(e)/ metric ton of U	Capital cost, $/kw
British-designed reactors							
Calder Hall (4)	1956	54	23.5	100	652		
Chapelcross (4)	1959	54	23.5	100	652		
Berkeley (2)	1962	138	24.4	140	653	0.59	521
Bradwell (2)	1962	150	28.2	147	739	0.63	492
Latina (1)	1963	200+	28.4	197	739		
Hinkley Point (2)	1964	250	26.4	195	705	0.72	420
Hunterston (2)	1964	150	28.3	161	744	0.60	
Trawsfynydd (2)	1964	250	29.4	246	735	0.85	384
Dungeness (2)	1965	275	32.9	284	770	0.92	319
Tokai (1)	1965	149	26.8	223	739		
Sizewell (2)	1965	290	30.5	282	770	0.91	300
Oldbury (2)	1966	300	33.6	365	770	1.02	302
Wylfa (2)	1968	590	31.5	400	770	1.00	280
AGR (1)	1962	27.3	27.3	285	977		
French-designed reactors							
G2 (1)	1959	40	16.0	215	644		
G3 (1)	1960	40	16.0	215	644		
EDF-1 (1)	1963	70	23.3	406	670		
EDF-2 (1)	1964	200	23.6	385	716	0.80	
EDF-3 (1)	1966	480	30.8	435	770	1.14	240
EDF-4 (1)	1968	480	29.1	435	752	1.08	

Digitized by Google

sult of the research engendered by a large building program and the experience gained through reactor operations. The French program, although considerably smaller than the British effort, has resulted in rather remarkable advances also. Indeed, the predicted performances of the French reactors presently under construction are fully as impressive as those of the British. For example, a comparison of the data in Table VII-1 for the Sizewell and EDF-3 plants, which are scheduled for on-power operation in 1965 and 1966, respectively, shows that the bulk outlet gas temperatures from the reactors are the same. Pressure and fuel rating in EDF-3 exceed the comparable values in Sizewell by a large margin. Comparisons of cost estimates from different countries can be misleading, but, if the estimates for Sizewell and EDF-3 are comparable, they indicate a considerable advantage for the French design, perhaps because of the larger reactor output.

That the British are proceeding with such a vigorous construction program is not surprising in view of the fact that, even under conservative assumptions, nuclear power in that country is expected to command a place in the generating system on solely economic grounds in the period 1970 to 1975. An indication of the relative costs of nuclear and conventional power in Great Britain is given in Ref. 9 by the statement that the replacement generation cost per day for Bradwell was $75,500 in January 1963 and $36,400 in July 1963. (The replacement cost is the incremental fuel cost per day of the next available stations in the order of merit needed to replace Bradwell's 300 Mw.) Although one would expect the January figure to be high, since this is a peak-load time of the year and the conventional plants available for service are the old and expensive plants, the July figure represents a period of low load during which time it appears reasonable that some fairly good conventional plants would be available for use. The January 1963 replacement generation cost is equivalent to a fuel cost of over 10 mills kw-hr. It is interesting to note that even the very large conventional power stations that will be commissioned in Great Britain during the period 1965 to 1970 are estimated to have fuel costs[13] of between 4.1 and 5.8 mills kw-hr.

An interesting trend has developed in the use of the prestressed-concrete pressure vessel for this reactor type. In the British program, all reactors down through Sizewell use metal pressure vessels, whereas Oldbury and Wylfa use prestressed concrete in conjunction with the "integral-plant" arrangement described later in this article. The French, despite (or perhaps because of) previous experience with concrete vessels in the G2 and G3 reactors, reverted to metal enclosures for the EDF-1 and EDF-2 reactors. Then, for EDF-3, they changed again—to a concrete version of the conventional pressure vessel, i.e., a vessel that encloses only the reactor proper. Finally, in the EDF-4 plant, the concrete-vessel integral-plant concept is used. Thus it appears that the evolution of the reactor type in the United Kingdom and France, after having proceeded along somewhat dissimilar paths, has now reached a point in time at which the gross features of the plants under construction are comparable. In the course of this evolution, it seems that the British may have displaced the French as the boldest exponents of the concrete pressure vessel, since they expect to put the integral concept into service in 1966 in the Oldbury plant, two years before EDF-4.

The large gas-cooled reactors have proved their reliability through the years. For some time now, utilization factors of 90% and greater have been common for long periods in the operating history of the Calder Hall reactors, and, as shown in Table VII-2, even the relatively young Berkeley and Bradwell plants are exhibiting a satisfactory degree of reliability. The "utilization factor" is defined as

$$\frac{\text{Units sent out} \times 100}{\text{Design sent-out capacity} \times \text{time}} \%$$

The performance of Berkeley and Bradwell during the period from startup to February 1964 is presented in Table VII-3 in terms of the utilization factor.

The reactors listed in Table VII-1, with the exception of the Advanced Gas Cooled Reactor (AGR), are fueled with natural-uranium metal clad in a relatively low-temperature alloy. The fuel elements are massive, to the extent that the entire cross section of a process channel contains only a single fuel element, and the specific power and power density are consequently low. These characteristics result from the use of metallic uranium, since the massive elements not only promote the attainment of the

Digitized by Google

Table VII-2 PERFORMANCE OF BERKELEY AND BRADWELL STATIONS DURING PEAK LOADING OF U. K. CENTRAL ELECTRICITY GENERATING BOARD SYSTEM[9]

	Berkeley		Bradwell	
	Nov. 1962 to Feb. 1963	Nov. 1963 to Feb. 1964	Nov. 1962 to Feb. 1963	Nov. 1963 to Feb. 1964
Design sent-out capacity, Mw	275	275	300	300
Maximum sent-out capacity achieved, Mw	231	241	278	311
Units sent out, kw-hr × 10^{-6}	528	557	552	807
Utilization factor, %	67	70	64	93
On-power dates	Reactor 1, June 1962 Reactor 2, Oct. 1962		Reactor 1, June 1962 Reactor 2, Nov. 1962	

Table VII-3 ANALYSIS OF PERFORMANCE FROM STARTUP TO FEBRUARY 1964, BERKELEY AND BRADWELL STATIONS[9]

	Berkeley, %		Bradwell, %	
Utilization factor		52		60
Utilization losses				
Output restrictions				
Nuclear fuel temperature		4.8		5.8
Nonnuclear pressure drop in superheaters		8.0		0
Plant nonavailability				
Nuclear				
Reactor trips	0.4		0.4	
Spurious reactor trips	1.1		0.6	
Flux scan tube failure	0		1.8	
Absorber, fuel, etc., movements off load	2.6		2.1	
Fuel failures	0.7	4.8	0.4	5.3
Nonnuclear				
Modification of superheaters	9.6			
Turbines, boilers, etc.	6.3	15.9	7.0	7.0
Planned maintenance		3.6		9.0
External causes		0.2		0.3
All other causes (load changing, startup, fuel integrity tests, etc.)		10.7		12.6
		100		100

necessary reactivity but also keep the fabrication component of the fuel cost at a reasonable level, despite the short exposure lifetime. The logical development of the reactor type, as embodied in the AGR, is a reactor capable of developing considerably higher gas temperatures and much higher power density, along with much extended fuel life. This is accomplished principally through the use of different fuel and cladding materials but requires the use of enriched fuel. Details of the AGR, in which the fuel consists of slightly enriched-uranium dioxide pellets encased in thin stainless-steel cans, assembled in clusters, are in Ref. 17. Fuel loading of the AGR commenced[8] in August 1962, and since February 1963 the reactor has operated at or above its designed power. The designed gross electrical generation of 33 Mw was achieved at startup, and within weeks the output was increased to 37 Mw, the limit of the installed generating plant. The experimental nature of the AGR has required the reactor to be shut down on several occasions, but, despite these periods of shutdown, the plant load factor (utilization factor) for the first year of operation has been a very satisfactory 74.1%. The plant availability factor, defined as the proportion of time for which the reactor was operating at full power, or for which the plant was fully available but was shut down or operated at reduced power for experimental purposes, has been 86.6%. These values, as well as the reasons for losses of equivalent full-power time, are shown in Table VII-4.

In summarizing the current status of the gas-cooled graphite-moderated reactor, one can really state only the obvious things: that a large number of the reactors have been built; that the reactors which have been built have operated satisfactorily and have proved that

Table VII-4 CAUSES OF REACTOR OUTAGE OF THE AGR[8] (FEBRUARY 1963 TO FEBRUARY 1964)

(Losses As Percent of Equivalent Time at Full Power)

Planned annual maintenance and inspection, %	4.5
Unplanned maintenance, %	
Control-rod sleeve faults	4.6
Electrical/mechanical faults	2.8
Instrument faults	0.03
Human errors	1.5
Total operational losses, %	13.4
Operational availability, %	86.6
Off load or reduced power handling of irradiation experiments, %	11.7
Power reduction for physics experiments, %	0.8
Total experimental losses, %	12.5
Plant load factor, %	74.1

Digitized by Google

the type is reliable; that, typically, original performance capacities are exceeded by technological improvements which are incorporated in the existing plants; that the advanced reactors represented by the British AGR appear to have a sound basis for future development; and, finally, that the development of the technology has proceeded as might have been expected. Thus the very considerable gains that can be made by choosing a reactor type and building and developing it intensively have been demonstrated. If the type still appears to be less than economically competitive in countries like the United States, it is not because of any failure to equal or exceed the early expectations but because of inherent characteristics of the type.

Fuel Elements

The Magnox reactor, which is defined as a graphite-moderated gas-cooled reactor fueled with metallic uranium in Magnox cans, is the "standard" reactor discussed here. The cost reductions that have been achieved in the development of this reactor type are discussed in a paper by Smith et al.[7] which, although written to apply to those reactors developed in the United Kingdom, serves as an excellent guide to the directions of development and remaining areas of exploitability of the general reactor type. The comments that follow are taken largely from Ref. 7.

The primary factors in the cost reductions which have been achieved are increases in unit output, improvements in layout and detailed design, and increases in fuel rating. Since the fuel electrical rating (electrical megawatts per metric ton of uranium) determines the total weight of fuel in a plant of given capacity, it is a significant parameter in the cost of the first fuel charge and also influences strongly the reactor dimensions, which, in turn, are reflected in the cost of the reactor and its associated equipment. The fuel electrical ratings can be increased by increasing fuel heat ratings, by increasing reactor coolant temperatures and steam-cycle efficiencies, or by lowering blower power. The achievement of a net gain by any of the above three means while keeping materials constant requires improvement of the fuel-element heat-transfer performance and/or the coolant heat-transport performance; in the gas-cooled reactor, the most straightforward approach to such a gain is an increase in the coolant pressure. The trend toward higher pressures is illustrated in Fig. VII-1 for a majority of the Magnox reactors designed and built to date. The prestressed-concrete pressure vessels developed for the very large Magnox reactors have enabled the designer to select coolant pressure on the basis of economic optimization. All the high-output plants shown in Fig. VII-1 (Oldbury, Wylfa, EDF-3, and EDF-4) utilize the concrete vessel, and the attendant increase in fuel electrical rating is evident.

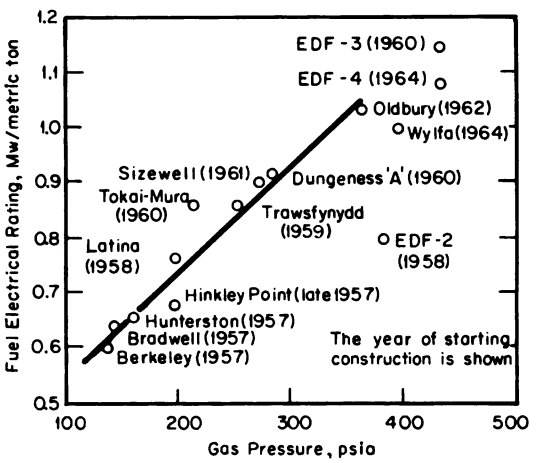

Fig. VII-1 Fuel ratings and gas pressures of various reactor designs.[3,7]

As stated in Ref. 7: "The scope for increasing thermal efficiency of Magnox stations is probably fully exploited, so attention is now focused on increasing the fuel heat rate." Much of the effort on fuel and fuel-element development has been directed toward finding designs that can yield the higher heat ratings simultaneously with a fuel-element life expectancy that is at least as long as the reactivity lifetime afforded by natural uranium.

Fuel Materials

Certainly one of the most significant developments in the Magnox-reactor fuel program has been the production of "adjusted" uranium by the British. In the earlier days of the Magnox reactor, core life was considered to be determined by the swelling in the natural-uranium metal fuel. It is now considered that the behav-

Digitized by Google

ior of the uranium is not a limitation in the operation of the Magnox fuel elements and that the lifetime limit will be determined by the available reactivity. Basically, adjusted uranium is uranium containing 400 to 1200 ppm aluminum and about 300 ppm iron and 600 ppm carbon. These additions of material produce the greatest individual effect in reducing swelling, but, in order to obtain the effect, it is necessary to quench the uranium from the beta phase and subsequently anneal it in the alpha phase. In uranium produced by this method, the fractional volume increases are remarkably small and are unaffected by fission rate (for a given total burnup). British data[18] indicate that the adjusted uranium is superior to uranium-molybdenum alloy in its swelling behavior and does not have the high-neutron-absorption penalty of the molybdenum alloy. Additionally, the molybdenum content of the uranium-molybdenum alloy presents a considerable problem in the chemical processing stage of the fuel cycle. Figure VII-2 illustrates the relation between the volume increases in uranium and uranium alloys. The adjusted uranium has been tested in thermal-cycling conditions of the amplitude and frequency expected in the Magnox reactors, and its swelling appears to be unaffected by such cycling.

Reference 18 contains an interesting dissertation on uranium swelling which, for the purposes of this discussion, can be said to be dependent largely on the size and distribution of fission-gas bubbles in the metal. In a rather crude sense, it can be said that the swelling of uranium can be held to a minimum by preventing the coalescence of fission-gas bubbles: in other words, although fission-gas generation is a function of irradiation, the effects of such generation can be minimized by preventing the migration and coalescence of the gas bubbles. In even simpler terms the desired condition within the fuel is one in which the number of gas bubbles is kept to a maximum and, consequently, the sizes of the individual bubbles are kept at a minimum. During the production of adjusted uranium, when the material is held in the beta phase, most of the particles of the intermetallic compound UAl_2 and all the particles of U_6Fe precipitated during casting are redissolved. When the material is quenched, the aluminum and iron are retained in solution and, during the subsequent alpha annealing, are reprecipitated as fine particles at the grain boundaries and within the grains of the material. The quenching and annealing apparently produce a fine intragranular and intergranular dispersion of UAl_2 particles with possibly some iron in solid solution. The reason for the excellent performance of the adjusted uranium is thought to be that this dispersion essentially "anchors" the fission-gas bubbles within the material so that migration and coalescence cannot take place.

Although the adjusted uranium has become the standard material used at the Springfields Works (the fuel-element production facility of the UKAEA),[19] and although the British consider[19] that other alloys now undergoing irradiation are unlikely to show an overall advantage as a fuel material when compared to the adjusted uranium, it is evident that the French

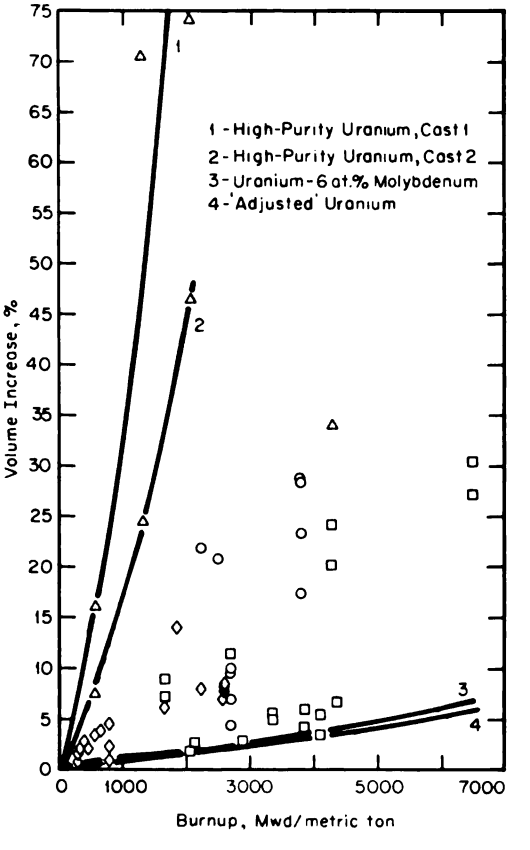

Fig. VII-2 Volume increases in uranium with no added aluminium, irradiated at 500 to 650°C. Curves for high-purity uranium, uranium–6 at.% molybdenum, and "adjusted" uranium are superimposed.[18] *○, U. S. results, direct irradiation. □, U. S. results, postirradiation annealing. ▽, AERE results, direct irradiation, 50 to 90 ppm carbon. ▢, AERE results, direct irradiation, 300 to 1000 ppm carbon.*

Digitized by Google

consider other alloys as the preferred Magnox-reactor fuel materials. The French flatly contradict the British proposition that the bubble-migration phenomenon is the dominant factor in the growth of uranium fuel elements and state[20] that no French experiments have ever shown evidence of such a phenomenon. In the later French reactors, the fuel is typically uranium-molybdenum alloy, with the molybdenum content ranging from 0.5 to 1.0%. These fuel elements are hollow-rod type elements with external cooling only. For their advanced fuel element, which has an annular cross section of uranium cooled internally and externally, the French propose a fuel made of uranium of "low alloy contents" in order to avoid the relatively high neutron absorption of the molybdenum alloys, since the mechanical strength of the molybdenum alloy is not required in the internally cooled annular elements. Perhaps the French philosophy on fuel-material development is that the uranium-molybdenum alloys possess a high mechanical strength at elevated temperatures and that this property makes them particularly suitable for use in the hollow-rod elements subjected to high external pressures. Furthermore, growth becomes negligible at temperatures around 525°C and appears to be independent of the type of alloy considered, although no inconvenient swelling has been observed in the uranium-molybdenum alloy during fuel-element tests.[6] Although the French are devoting a substantial effort to the development of the annular fuel element that utilizes less absorptive fuel than their typical uranium-molybdenum alloy, they clearly state[21] that the more conventional closed-tube elements such as those employed in the EDF-2, -3, and -4 reactors will not be abandoned.

Although development of fuel elements for the AGR in Great Britain is continuing, nothing very unusual has been reported concerning the fuel portion of these elements. High-density UO_2 is still the preferred fuel material, and research on this material is proceeding along fairly routine lines. The major emphasis in the development of these fuel elements is in the configuration and cladding materials, which will be discussed in following sections.

Fuel-Element Cladding and Structure

The policy adopted by the British for the development of critical items such as cladding alloy and structural alloy for fuel elements has been one of parallel development with alternative solutions. It appeared likely that the material used for cladding alloy since 1956 in the Calder Hall reactors would have a limited life because of failure by linkage of grain-boundary cavities at temperatures up to 300°C. This material, a coarse-grained magnesium–0.8% aluminum alloy called Magnox AL80, could be replaced by a fine-grained Magnox AL80 that exhibited a greater ductility and could be expected to have a longer life, but the fine-grained structure could be attained only by the controlled application of cold work which might be expected to be a hindrance to bulk manufacturing operations.[19] The principal alternative to the fine-grained Magnox AL80 alloy was an inherently fine-grained two-phase alloy containing 0.55% zirconium and called Magnox ZR55. Cladding made of bulk materials was produced for the Civil Reactor Program in Great Britain, and large-scale proving trials in the UKAEA reactors were begun. Meanwhile, the manufacture of the fine-grained AL80 cladding material was developed until the process was suitable for large-scale production of cans, and this development turned out to be a fortunate one for the program. Because of the diffusion of plutonium through the Magnox ZR55 cladding at irradiations above 1000 Mwd/ton, the operation of the burst-cartridge detection gear in the Magnox reactors was impaired. Consequently, the fine-grained Magnox AL80 has been adopted as the "standard" cladding material for use in the British reactors.

The requirements of some of the structural components of fuel elements are different than those of the cladding since the loadings are different. For instance, the end caps and associated fittings which support the axial loads acting on stacked elements require a high resistance to creep but demand less ductility than is required of the cladding alloys. To date, a 0.7% manganese alloy, Magnox MN70, has been the one most widely used for end caps and fittings,[22] and the most popular material for spreaders and braces has been heat-treated Magnox ZR55 (Ref. 19).

The French presented relatively little information at Geneva concerning the development of cladding and structural materials for the fuel elements of their gas-cooled reactors. Although they are aware of the fine-grained Magnox AL80 used by the British, the French ap-

Digitized by Google

pear to prefer[23] a magnesium-zirconium alloy similar, presumably, to the Magnox ZR55 considered by the British. Although the typical French fuel element does differ[21] from the British elements (in that, since EDF-2, the French have fitted their elements with a graphite sleeve), the plutonium diffusion problem must still remain. Little information was given concerning burst-cartridge detection in the French reactors, but the problem has apparently been reconciled with the operation of the reactors. Apparently the magnesium-zirconium alloy is used for the welded end caps[23] of the fuel elements as well as for the cladding material.

The development of cladding materials for higher temperature gas-cooled reactors (such as the AGR and the French gas-cooled heavy-water-moderated reactor EL-4) indicates that, at least for the fairly near future, reactors of this sort will utilize fuel that is clad with very thin stainless steel. Apparently, the British are not considering very seriously any material other than stainless steel for this high-temperature application, although some years ago beryllium had been considered for use in the AGR. The French, however, although resigned to the use of stainless steel at present, continue studies directed toward the development of beryllium as a cladding material and are investigating, in parallel efforts, other materials such as iron-aluminum alloys. Reference 24 contains descriptions of some of the recent work in France on the development of beryllium and indicates that some progress is being made on the problem of improving the ductility of beryllium in the direction perpendicular to the direction of extrusion.

Fuel-Element Configurations

The fuel-element configuration that has been used or specified most frequently in Great Britain is the solid rod in a polyzonal can, whereas the French ordinarily use the hollow rod in a polyzonal can, housed in a graphite sleeve. The British-designed Tokai reactor, however, has[25] a hollow-rod element and a graphite sleeve, and the Hunterston reactor also has the graphite sleeve.[25] Some of the fuel geometries that have been considered by the British are shown in Fig. VII-3. The arrangement of flat bars in a fuel element is one in which bars with different widths are held parallel to each other to "fill" approximately the circular-cross-section fuel channel. The investigation of these geometries has been prompted by the trend to higher heat ratings. A departure from the solid fuel geometry is required if the desired increases in rating are to be achieved. The British have apparently concluded that the flat-bar and tubular elements offer substantial savings in power-generation cost relative to the current solid-rod designs in very large reactors.[7] Of the two configurations the flat-bar approach is preferred because it appears to have fewer technical uncertainties and slightly better economic potential than the tube.[7] Of the solid-rod type elements used or specified to date, two types appear to have been used in the largest numbers. These are the polyzonal element with helical fins and the polyzonal element with herringbone fins. Drawings of the external appearance of elements of these types are shown in Fig. VII-4. As is indicated by the drawing, the herringbone element is considerably simpler mechanically than the helical type identified as a Dungeness Mark I element. Although the British have been quite cautious and have stated that the herringbone element has yet to demonstrate its stability in such mechanical form,[26] they do plan large-scale irradiation trials and state that the merits of the design[27] have re-

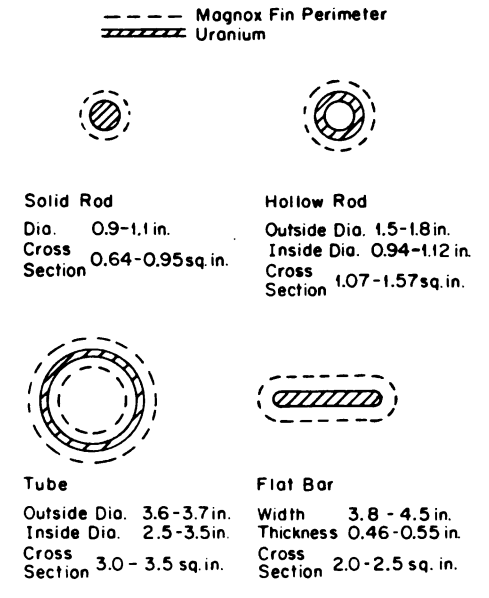

Fig. VII-3 Fuel geometries, British studies.[7]

Digitized by Google

sulted in its adoption for the second reactor at Sizewell.

The characteristics of French fuel elements for Magnox reactors are shown in Table VII-5, which indicates that the reactors in the EDF series all use hollow rods, that from EDF-2 onward graphite sleeves have been used, and that for the external surfaces of round elements the herringbone finning arrangement is preferred.

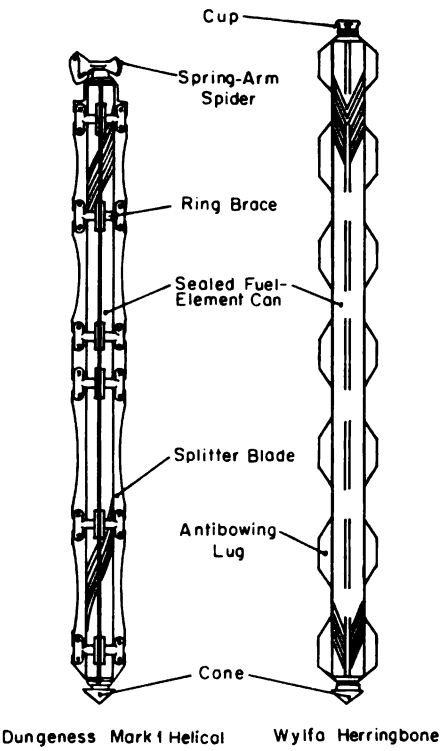

Fig. VII-4 British fuel elements.[26]

The "advanced" French fuel element that corresponds to the flat-plate type envisioned by the British is the annular element listed in Table VII-5 and shown in Fig. VII-5. As indicated in the drawing, this is a very large element, the distance across the span of the centering device being about 7 in. Its cross-sectional area of fuel and its inside and outside diameters correspond roughly to those studied by the British in their search for an advanced fuel element (Fig. VII-3). It is interesting to compare the maximum specific powers shown in Table VII-5 for the French fuel elements with the data presented in Fig. VII-6, which is based on information generated by the British and presented in Ref. 7. The comparative generation costs shown in the figure are based on optimized reactors of 500-Mw(e) output for each of four fuel geometries. Although it is stated that the fuel prices for the flat bar and the tube are nearly the same for their optimum designs,[7] the blowing power requirement at a given coolant pressure is lower for the flat-bar design than for the tube, and this more than offsets the costs associated with the requirement for a somewhat larger core when the flat-bar design is used.

With regard to the French fuel-element program, an interesting comparison of the relative costs of the various operations in preparing fuel elements for the reactors for G2 to EDF-3 is shown in Table VII-6. Since the "new uranium" cost should be the same for each ele-

Table VII-5 CHARACTERISTICS OF FRENCH FUEL ELEMENTS[21]

	EDF-1	EDF-2	EDF-3 and EDF-4	Annular element (INCA)
CO_2 pressure, psia	406	385	435	656
Fuel				
Alloy	U-Mo, 0.5%	U-Mo, 1%	U-Mo, 1%	Slightly alloyed U
Diameter, in.	0.55 × 1.38	0.71 × 1.57	0.90 × 1.69	3.03 × 3.74
Cross section, sq in.	1.24	1.55	1.55	3.88
Maximum specific power, Mw/ton	4.4	5.8	6	11
Can				
Type of fins	Longitudinal	Helical herringbone	Flat-sided herringbone	External, herringbone; internal, longitudinal or corrugated
Maximum heat flux, Btu/(hr)(sq ft)	178,000	260,000	257,000	External, 333,000; internal, 222,000
Element				
Individual support	None	Graphite sleeve	Graphite sleeve	Graphite sleeve
Length, in.	23.6	23.6	23.6	23.6
Number per channel	15	12	15	15

Digitized by Google

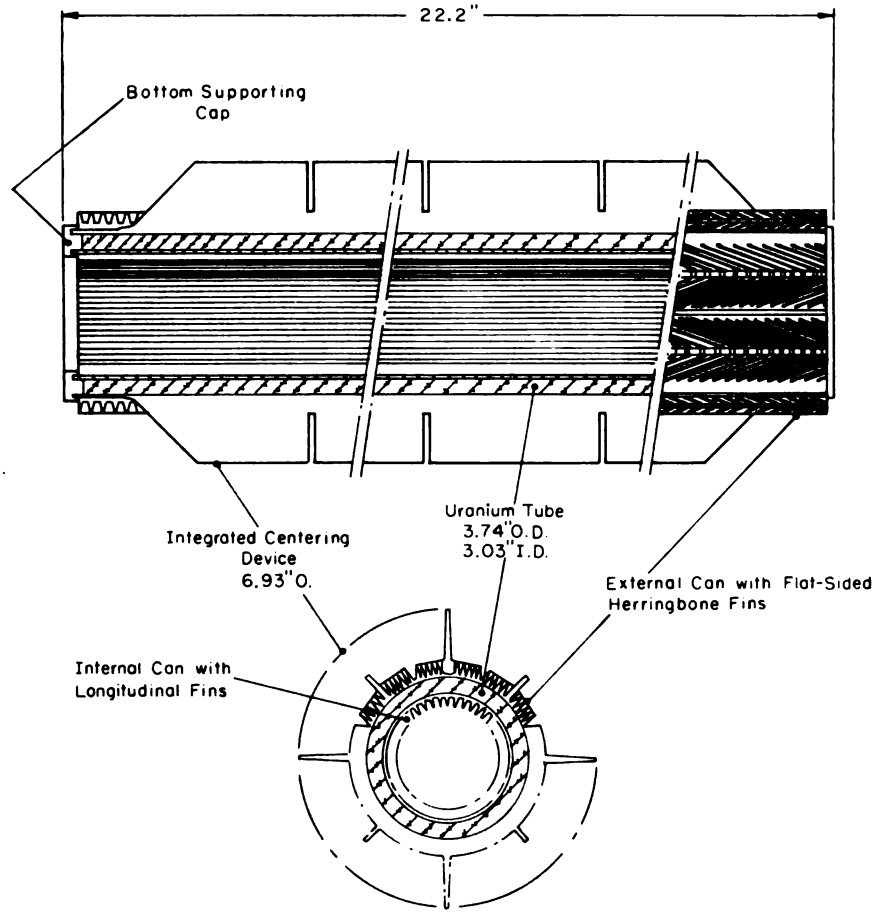

Fig. VII-5 The French annular element (INCA).[21]

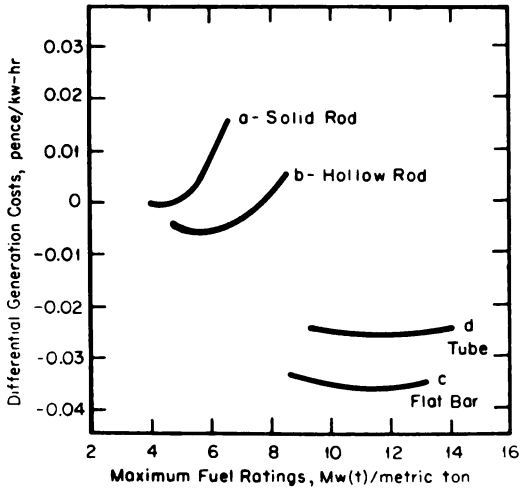

Fig. VII-6 Differential generation costs.[7]

ment type, the relative costs for the complete elements are easily derived.

It appears that no radical changes are forthcoming in the selection of fuel-element configurations for advanced gas-cooled reactors such as the AGR, and the continued use of multirod bundles of small-diameter fuel tubes may be expected.[28]

Pressure Vessels

The British reactor stations up to Sizewell have utilized steel pressure vessels. The fuel electrical rating has been increased significantly through this series of plants, as indicated in Fig. VII-1, and much of this increase has come about through increases in coolant

Digitized by Google

Table VII-6 BREAKDOWN OF FUEL CARTRIDGE COST IN FRANCE[23]

	Percent of fuel cartridge cost			
	G2 and G3 solid rod (dia., 1.22 in.)	EDF-1 hollow rod (dia., 0.55 to 1.38 in.)	EDF-2 hollow rod (dia., 0.71 to 1.57 in.)	EDF-3 hollow rod (dia., 0.90 to 1.69 in.)
New uranium (ingots)	72	58	56	54
Solid-rod and hollow-rod manufacture	6	7	6	7
Cans and plugs	4	7	4	5
Alumine pellets		1		
Centering grids			2	
Graphite sleeves			8	8
Manufacture and testing	18	27	24	28

pressure. But increases in design pressure have been limited by the difficulties met in procurement and in on-site welding and inspection of thick steel plate.[7] At the same time the trend in reactor capacity has been to high-capacity units that make possible significant reductions in capital cost, and the influence of this trend has been to increase reactor size despite the higher power density that has been achieved. Consequently the problem of increasing the pressure in order to increase the fuel rating, while at the same time larger and larger plants are achieved, has resulted in the conflicting requirements of higher pressures in larger vessels. An example of this is evident in the designs of the Bradwell and Dungeness reactors. For Bradwell, 3-in.-thick plate was specified at a working pressure of 147 psia. For Dungeness, about three years later, when 4-in.-thick plate was available, coolant pressure was limited to a value somewhat less than 300 psia, and pressure-vessel dimensions were at a maximum of approximately 60 ft in diameter. The use of prestressed-concrete pressure vessels has permitted the economic optimization of coolant pressure and vessel diameter, and it is obvious from inspection of Fig. VII-1 that the desired pressure of the larger and newer power plants is substantially greater than that which had been possible in the units up through Dungeness-A.

The impressive sizes of the concrete pressure vessels which have been specified for planned plants are illustrated by the data presented in Table VII-7. For example, the Wylfa pressure vessel has an internal diameter about half again as great as that of the largest steel vessels, and the nominal pressure of its primary coolant is more than a third again as great as that of the steel-vessel plants. The proponents of the concrete vessel claim that it has other advantages also. A fair body of opin-

Table VII-7 GAS-COOLED CLAD-FUEL REACTORS USING CONCRETE VESSELS[4,10]

Reactor	Date of first reactor on power	Thermal power, Mw	Primary coolant nominal pressure, psia	Primary coolant temperature at reactor outlet, °F	Pressure vessel		
					Shape of internal cavity	Dimensions of internal cavity, ft	Approximate minimum wall thickness, ft
G2	1959	250	215	644	Horizontal-axis cylinder	Diameter, 45.9; length, 51.5	9.8
G3	1960	250	215	644	Horizontal-axis cylinder	Diameter, 45.9; length, 51.5	9.8
EDF-3	1966	1560	435	770	Vertical-axis cylinder with truncated cone sections at top and bottom	Diameter, 62.3; height, 69.1	13.9
Oldbury	1966	890	365	770	Vertical-axis cylinder	Diameter, 77.0; height, 60.0	15.0
EDF-4	1968	1650	435	752	Vertical-axis cylinder with upper truncated cone section	Diameter, 62.3; height, 119.0	16.4
Wylfa	1968	1870	400	770	Sphere	Diameter, 96.0	11.0

Digitized by Google

ion among the British and French designers is that the steel pressure vessels used in the United States are, in fact, susceptible to sudden failure. In the opinion of these people, the maximum credible accident should logically be considered to be the sudden brittle fracture of the reactor pressure vessel; the mode of ultimate failure of concrete pressure vessels, however, is progressive and without sudden rupture.[29] Obviously this theory is not widely popular among the proponents of steel vessels.

Refueling Machines

The performance of refueling equipment in both the British and French reactors has been acceptable, and the development of refueling machines has been characterized by steady improvements based on operating experience gained with the machines used in the relatively early reactors. In the G2 and G3 reactors, the original machinery has been improved principally for increasing operational safety, but the improvements have also permitted increases in the refueling rates so that it is now possible to discharge nearly 27 fuel channels in 24 hr, or about three times the initial design rate of the machines.[1] The EDF-2 reactor is equipped with two refueling machines, the main machine and an auxiliary machine, whereas in EDF-3 the French have reverted to a single all-purpose device. Among the difficulties encountered by the designers of the equipment for these reactors is the problem of lifting of the last few elements in a particular channel when that channel is being unloaded under power. Important design features of the machines[30] are the baffling arrangements that are used to avoid levitation of the final elements by preventing a very high loss of head at the top end of the channel being refueled. The performance of the French refueling equipment will be interesting to observe in view of the fact that studies and tests are said to account for about 35% of the cost of the machines.

A British paper[31] relates the experience obtained with the Bradwell and Latina on-load fuel-handling equipment and discusses the influence of this experience on the design of later machines for the Dungeness and Oldbury reactors. It is sufficient here to point out two of the major conclusions of the paper. The first is that the time required for the machine to perform a certain number of reloading or charging operations is considerably longer in practice than is indicated by design calculations. These differences in time are illustrated by the data in Table VII-8 which show that the actual time is some 2½ times as great as the design time. It is felt that the required time may be reduced to a value of about twice the design time. The other conclusion drawn by the British is given in the following quotation from Ref. 31: "Massive rather than elegant devices give by far the best service."

Table VII-8 BRADWELL CHARGE-MACHINE OPERATING-CYCLE TIMES[31]

Operation	Actual time, hr	Design time, hr
Inspect three channels of fuel and load magazine	1½	
Load three channels of fuel into machine	2	1
Travel machine to gas supply and connect	½	¼
Pressurize machine	¾	
Reinstate previous standpipe and prepare new one	3	
Connect machine to standpipe	½	½
Discharge and reload three channels	8	3¾
Disconnect machine and travel to vent point	½	¼
Depressurize machine	½	2
Connect to discharge hole and unload three channels	2	
Travel to vent point and purge machine	½	
Travel to loading point and connect	½	¼
Total times	20¼	8

Control and Instrumentation

The development of larger and more complex reactor plants has had a number of effects on plant operating philosophy. There are trends (1) toward centralized control,[32] (2) toward a better understanding of, and consequently a closer approach to, the temperature limits of the various core materials,[33] and (3), because of the very large reactors currently under construction and operation, toward concentrating on the control and stability problems inherent in very large cores, particularly with regard to spatial variations.[34] The experience gained

Digitized by Google

through the years, while revealing some problems that had not been anticipated in the early designs, has served as both a firm foundation and an experimental basis for the future operation of power reactors.[35]

At the time the burst-cartridge detection gear was designed for the Calder Hall reactors, no operating experience existed to indicate the types of fuel-element failure which might occur. Consequently the systems supplied for the early reactors were designed to meet a few fundamental requirements for burst-cartridge detection and were not particularly suited to detecting properly the types of actual bursts that would be encountered during operation. As a consequence of reactor operation and the determination of the most likely modes of fuel-element failure, system specifications have been more clearly defined. The fast burst, a fuel-element failure that gives virtually instantaneous release of a significant quantity of fission products, has been identified as a particular failure type, and this type of burst makes important the quick-detection-and-location capability that has led to an increase in the frequency of group scanning at some expense to sensitivity. Since experience with the early reactors became available, the burst-cartridge detection systems for the British reactors have used a combination of the fast scan at low sensitivity with a single-channel scan of long cycle time. .Some of the features of systems designed for later British reactors are given in Table VII-9.

The French G2 reactor was initially equipped with a burst-cartridge detection installation similar to that used in the Calder Hall reactors.[1] On the strength of experience acquired with the G1 reactor, modifications to the G2 system and development of the G3 system have been based on a capability which the French feel is important: measuring the time rate of the signal as well as an instantaneous absolute value. The G3 reactor installation has performed satisfactorily and has served as the basis for the burst-cartridge detection systems that will be employed in the EDF reactors.

Advanced Concepts and Future Directions

The concepts that are classified here as "advanced" include the advanced gas-cooled reactor, typified by the Windscale AGR, and the integrated plant designs that utilize concrete pressure vessels to enclose the entire primary system.

The AGR has been described rather thoroughly in the literature, and here it will suffice to say that the reactor was commissioned essentially on schedule and that its operation since commissioning has been entirely satisfactory.

Table VII-9 DETAILS OF RECENT BRITISH BURST-CARTRIDGE DETECTION SYSTEMS[36]

	Dungeness	Sizewell	Oldbury	Wylfa
Reactor No. 1 on load	1964	1965	1966	1968
Channels in reactor	3932	3784	3308	6156
Channels per group sample	32	32	8	32
Period of group scan, min	6.7	Continuous	11	Continuous
Cycle time per sample, sec	25	60	25	60
Single-channel scan period, hr	3.7	4.25	4.0	7.1
Total precipitator units per reactor	20	18*	27	29*
Group sample flow rate at precipitator, lb/sec	0.115	0.037	0.115	0.031
Single sample flow rate at precipitator, lb/sec	0.042	0.017	0.042	0.026
Total circuit mass flow, lb/sec	1.6	5.2	2.4	7.3
Circuit pressure drop, psi	40–45	40	42–47	55
Transit time, channel to precipitator, sec	6	5.9	11	6.7
Sensitivity (M.D.A.)†				
Group, mm^2	10.0	3.5	2.5	3.8
Single, mm^2	0.57	0.11	0.57	0.13

*Eight chambers per precipitator unit.

†Minimum detectable area as determined by an alarm set 25% above background for a scanned system and 15% above background for a continuous system.

Digitized by Google

As mentioned briefly before, the AGR type fuel elements have undergone no major evolution in the past few years: the reactor type is apparently destined to use the multirod bundle type element. Since an element of this type involves relatively high fabrication costs per unit weight of uranium, favorable economic performance requires a rather long fuel life in the reactor. This requirement poses a difficult task for the designer if it is also imperative to design for the minimum possible fuel enrichment; for, in the absence of a good low-cross-section material for the fuel jacket, he must design for the minimum-thickness jacket of stainless steel. A fairly recent development in the AGR fuel program is the consideration of the use of plutonium[37] as the enriched component of the fuel, since it is felt in Great Britain that the stockpile of plutonium is growing at a rate which will ensure a more than adequate supply of the material when fast-breeder reactors become commercial. Consequently the British philosophy appears to be that the thermal reactors will be permitted to utilize this "extra" plutonium if it appears feasible.

The integrated plants, which are EDF-4, Oldbury, and Wylfa, are typified by their compact arrangements (if such a description can be applied to these huge reactors). Although all three reactor vessels contain all the principal components of the primary circuit, their shapes and arrangements are quite different, as indicated in Table VII-7. EDF-4, for example, utilizes a rather tall, thin configuration in which the steam generator is located below the reactor core. A disadvantage of this scheme is the lack of natural-circulation cooling in the event all CO_2 circulators are lost. With the over-and-under arrangement of the major components of the primary loop, it follows that the EDF-4 pressure-vessel internal space is relatively small in diameter and quite high, as indicated in Table VII-7. The basic arrangements in Oldbury and Wylfa resemble one another in that the steam generators are located peripherally around the reactor core and at about the same elevation as the core. The shapes of the internal cavities of the pressure vessels are different, however, with the Wylfa station retaining the traditional spherical shape of the earlier British stations and with Oldbury using a vertical-axis cylinder.

The directions of future development of the planned stations in both Great Britain and France are rather clearly shown by the information presented in Table VII-1 and by the increases in primary coolant pressure and fuel electrical rating shown in Fig. VII-1. What is not so clearly shown is the type reactor that will be employed for the "next generation" plants in these two countries.

At the time of its conception, the AGR was felt to be the logical successor to the Magnox stations in Great Britain. Although the AGR has performed as expected, there is still the problem of minimizing absorption in the fuel cladding in order to obtain long fuel lifetimes at low values of enrichment. When one makes the jump to enriched fuel, a variety of reactors enters the picture. Furthermore, although the AGR fuel has behaved well to date, the operation reported has carried the exposure only to the neighborhood of 4000 Mwd per metric ton of uranium, a long way from the economic optimum average burnup of around 20,000 Mwd per metric ton of uranium, or even the average value of 12,000 Mwd per metric ton of uranium which is stated[28] to be the target for the first charge of an early commercial station. Effort is being directed toward the further development of the AGR fuel element along such lines as thinner cladding material, basic studies in oxide fuels, and the development of plutonium enrichment for thermal-reactor fuel. At this time the preferred future concept for construction in Great Britain is not clear, although there have been some indications that the Magnox reactor has about reached the end of the line. Whether the AGR type plant will be built in large numbers as a second-generation gas-cooled-reactor type is uncertain. The selection of a preferred concept for the future will be based largely on economic considerations, but surely there will be a strong tendency toward the gas-cooled type because of the large amount of experience accumulated and the advances expected of the very large integrated plants utilizing concrete pressure vessels.

In France the directions of future development are clearer: the French like Magnox reactors, and, after some apparent early uncertainty, they have committed their gas-cooled program to the concrete pressure vessel. They are developing the integral plant concept with the EDF-4, and they will apparently adopt no other new concept in the very near future, although the performance of EL-4 will affect later plans. In France, then, it appears that the Mag-

Digitized by Google

nox reactor can look forward to a relatively bright future.

References

The references that contain A/Conf. numbers are papers that were presented at the Third United Nations International Conference on the Peaceful Uses of Atomic Energy, Geneva, September 1964.

1. R. Boussard, F. Conte, and J. Stoltz, Operating Experience with the G2–G3 Reactors at Marcoule and Starting Test Results for the Chinon EDF I Reactor, A/Conf.28/P/35.
2. J. Bourgeois and B. Saitcevsky, The Development of Natural Uranium Graphite Reactors, A/Conf. 28/P/36.
3. C. Bienvenu, P. Passerieux, and P. Bacher, Nuclear Power Stations E.D.F.2–E.D.F.3 and E.D.F. 4, A/Conf.28/P/38.
4. G. Lamiral, L. Laurent, R. Bonnelle, N. Beaujoint, and P. Faurot, The Prestressed Concrete Pressure-Vessels for French Natural Uranium-Graphite-CO_2 Gas Type Reactors, A/Conf.28/P/52.
5. R. Fays, L. Laurent, F. DeVathaire, J. Plisson, and J. Bussi, Safety of Natural Uranium-Graphite-Gas Type Reactors, A/Conf.28/P/81.
6. M. Englander et al., The Effect of Neutron Irradiation on Certain Fuels Used in Gas-Graphite Type Reactors, A/Conf.28/P/97.
7. D. R. Smith, P. D. Murphy, R. Rutherford, C. S. Lowthian, and J. M. Yellowlees, The Trend to Higher Ratings in the Magnox Reactor, A/Conf. 28/P/124.
8. K. Saddington, T. N. Marsham, and J. Moore, The Contribution of the Windscale Advanced Gas Cooled Reactor to the Development of a Commercial Power System, A/Conf.28/P/125.
9. D. R. R. Fair and R. L. Rutter, Early Operation of the C.E.G.B. Nuclear Power Stations, A/Conf. 28/P/128.
10. A. H. Brown, J. D. Hay, R. B. Hyde, and T. W. Spruce, The Design and Construction of Prestressed Concrete Pressure Vessels with Particular Reference to Oldbury Nuclear Power Station, A/Conf.28/P/140.
11. P. R. J. French, D. J. Millard, M. J. Cartmell, and B. K. Casterton, Experience in Relating the Observed Thermal Performance of Civil Magnox-Uranium Power Reactors to Design Predictions and Operating Criteria, A/Conf.28/P/171.
12. W. Penney, Nuclear Power in the United Kingdom, A/Conf.28/P/559.
13. P. W. Cash and F. Faux, Planning for Nuclear Power in the Central Electricity Generating Board's System, A/Conf.28/P/561.
14. A. Bertini, G. Gualtieri, G. Lesnoni, B. Zaffiro, M. Calcagno, and R. Negrini, Latina Nuclear Power Station: Commissioning and First Operational Experience, A/Conf.28/P/865.
15. J. Gaussens, A Few Present Economic Aspects of Nuclear Energy in France (Charge des Etudes Economiques Generales at the C.E.A.).
16. Power Reactors the World Around, *Nucleonics*, 21(2): 112-115 (August 1963).
17. *J. Brit. Nucl. Energy Soc.*, 2(2): (April 1963).
18. R. S. Barnes, R. G. Bellamy, B. R. Butcher, and P. G. Mardon, The Irradiation Behaviour of Uranium and Uranium Alloy Fuels, A/Conf.28/P/145.
19. J. C. C. Stewart, V. W. Eldred, T. J. Heal, D. O. Pickman, and H. Rogan, Review of Progress of Development, Manufacture, and Performance of Magnox Fuel Elements in the United Kingdom, A/Conf.28/P/560.
20. Y. Adda, J. Mustelier, and Y. Quere, Behaviour of Uranium Under Irradiation, A/Conf.28/P/62.
21. M. Salesse, J. Stohr, and G. Jeanpierre, Recent Developments Concerning French Fuel Elements for Natural Uranium-Graphite-CO_2 Reactors, A/Conf.28/P/60.
22. P. Greenfield, R. G. Coffin, G. C. E. Olds, B. Pickles, and T. C. Wells, Development of Magnesium Alloys for Fuel Elements in the United Kingdom, A/Conf.28/P/146.
23. R. Boussard, B. Boudouresques, and J. Nadal, The Manufacture of Fuel Elements in France, A/Conf.28/P/57.
24. J. M. Mallen-Herrero, Effect of Impurities of the High-Temperature Brittleness of Commercial Grade Beryllium, French Report CEA-R-2445, 1964.
25. R. Sagane, T. Yoshioka, N. L. Franklin, B. E. Eltham, P. T. Fletcher, and B. C. Woodfine, The Design and Development of the Tokai Hollow Rod Fuel Element, A/Conf.28/P/426.
26. J. W. Hughes, G. H. Inglis, C. H. Jones, and J. Price, The Development and Evaluation of Uranium Magnox Fuel Elements, A/Conf.28/P/147.
27. C. Cunningham, B. E. Boyce, T. Davis, and B. N. Furber, Heat Transfer and Pressure Drop Performance of Herringbone and Helical Fin Fuel Elements for Uranium/Magnox Reactors, A/Conf. 28/P/135.
28. G. B. Greenough, J. S. Nairn, and J. D. Thorn, Progress Towards the Design of A.G.R. Fuel Elements for Power Reactors, A/Conf.28/P/149.
29. R. S. Taylor and A. J. Williams, The Design of Prestressed Concrete Pressure Vessels, with Particular Reference to Wylfa, A/Conf.28/P/141.
30. B. Saitcevsky and D. Gaussot, Refueling Equipment in Natural Uranium-Graphite-Gas Reactors, A/Conf.28/P/54.
31. J. O. Joss, W. H. Shipley, G. H. Branch, and J. E. Taylor, Experience with Bradwell and Latina On-Load Fuel Handling Equipment and Its Influence on Future Designs, A/Conf.28/P/139.
32. D. S. Hiorns, T. O. Jeffries, D. Moore, H. Moores, and A. H. Weaving, Recent Developments in the Instrumentation and Control of Large Gas-Cooled Reactors, A/Conf.28/P/126.
33. H. A. Hughes, D. S. Briggs, R. Dodds, and R. M. Horsley, Temperature Limits and the Optimisation of Power Output in Calder and Chapelcross Reactors, A/Conf.28/P/178.
34. P. B. Branson, R. L. Carstairs, and A. J. Spurgin, Design of Control Rod Systems for Gas-Cooled Reactors, A/Conf.28/P/180.
35. H. A. Hughes, D. A. L. Clinch, R. M. Horsley, D. J. Millard, and R. Razzell, Experimental Basis of Power Reactor Operation, A/Conf.28/P/170.
36. B. Holmes and A. D. Boothroyd, The Development of Burst Cartridge Detection Systems with Particular Reference to Sizewell Nuclear Power Station, A/Conf.28/P/142.
37. B. Cutts, A Study of Fuel Cycles and Fuel Cycle Problems for Advanced Gas Cooled Graphite Moderated Reactors, A/Conf.28/P/177.

Digitized by Google

Section

VIII

Power Reactor Technology

Gas-Cooled Unclad-Fuel Reactors

The gas-cooled unclad-fuel reactors are characterized by high coolant temperatures and all-ceramic fuels. The two reactors of this type which are under construction, the Dragon experiment in England[1] and the Peach Bottom prototype in the United States,[2] have not changed markedly since their designs were described in past issues of *Power Reactor Technology*. Dragon was described in the December 1962 issue, 6(1): 74, and the Peach Bottom description appeared in the June 1962 issue, 5(3): 61. The Dragon reactor[3] achieved initial criticality on Aug. 23, 1964, and initial operation of the Peach Bottom plant[4] is expected in 1965.

The designation of Dragon as an "experiment" and of Peach Bottom as a "prototype" is explained by the difference in components provided for the two plants. The Dragon installation is not equipped with power-generating equipment—its heat is simply dumped to a heat sink—whereas the Peach Bottom plant is provided with the usual electric-power-generating components of a power plant. A comparison of the characteristics of the two reactors is given in Table VIII-1, which contains information taken largely from Refs. 4 and 5.

As seen in Table VIII-1, the coolant outlet temperatures for two reactors are identical. From an overall point of view, this is perhaps the most significant comparison that can be made between the two reactors since both use the same coolant gas and both have the attainment of high coolant temperature as a major design objective.

As indicated in Table VIII-1, the Dragon core will be loaded with two types of fuel elements. Since the core is quite small, its neutron leakage is very high, and it does not, as a whole, represent a core typical of larger power reactors. It uses a two-zone loading[6] to overcome this disadvantage and generate information applicable to larger cores. The seven center

Table VIII-1 CHARACTERISTICS OF DRAGON AND PEACH BOTTOM

Plant characteristics	Dragon	Peach Bottom
Reactor thermal power, Mw	20	115
Net electric power, Mw	None	40
Coolant gas	Helium	Helium
Pressure, psia	294	350
Inlet temperature, °F	662	652
Outlet temperature, °F	1382	1382
Reactor core	Vertical cylinder	Vertical cylinder
Height, ft	5.25	7.5
Diameter, ft	3.5	9.1
Average power density, kw/liter	14.0	8.3
Fuel elements	Seven-rod clusters	Individual tubes
Number	37	804
Fuel material	Uranium in driver elements; uranium and thorium in test elements	Uranium and thorium
Cladding material	Graphite	Graphite
Control elements	Rods	Rods
Number	24	36
Location	Radial reflector	Core
Poison material	B_4C	B_4C
Drive location	Top	Bottom
Refueling	At shutdown	At shutdown

Digitized by Google

elements of the core will be representative of those which would be used in a large power reactor and will be fueled with a uranium-thorium mixture. The remaining 30 elements, which surround the seven center elements, will contain no thorium and will serve as driver elements that must be replaced at relatively frequent intervals. By this means the center elements can be irradiated for several years and will effectively "see" conditions that would be typical of a large power-reactor core.

Materials developments for the reactor type in the United States and the United Kingdom have proceeded along quite similar paths. Graphites with helium permeabilities as low as about 10^{-3} cm^2/sec have been developed in both countries, and fuel-particle development has been directed principally toward the design of coated particles.[7,8] Particle-coating investigations are concerned with single, double, and triple coatings utilizing pyrolytic carbon and silicon carbide. In addition to the work on pyrolytic carbon and silicon carbide, work continues in both countries on the development of alumina and beryllia.

The well-known advantages of helium as a reactor coolant are restated in the following quotation from Ref. 2:

> Helium gas is used as the HTGR system's coolant because its chemical inertness and other properties contribute to reliable, easily maintainable, high temperature plant operation. Helium does not react with or corrode any structural material; it does not react with steam, water or air. It does not undergo a change in phase at operating temperatures, nor does it solidify at ambient temperature. Helium does not parasitically absorb in the reactor core, and cannot affect the physics of the reactor; it does not become radioactive . . . .

There are, however, disadvantages to the use of helium, and these center about the fact that it is a relatively high-priced gas. The pressure of the system must be relatively high in order to achieve good heat transfer and heat transport with reasonable pumping powers. High pressure, unfortunately, tends to aggravate the leakage problem that exists with helium. Leakage must be minimized because of cost considerations and, in reactors of the unclad-fuel type, because of the relatively high radioactivity of the primary coolant. Consequently, the ability to fabricate primary coolant systems with a very high standard of overall leaktightness has been of major importance in the Dragon and Peach Bottom plants. Recent tests of the Dragon facility[9] have been very encouraging in this respect since the actual leakage rates encountered were within the specified rate of 0.1% per day of the gas contained in the circuit.

Although technologies developed for Dragon and Peach Bottom have been extended to conceptual designs of large nuclear power plants, the actual directions of future development of plants of this type are not uniquely defined at this time. The developers of Peach Bottom consider a plant in which a fuel-element purge system is employed and fission-product release is encouraged in order to obtain conversion ratios greater than unity.[2] Actually, this is the approach that was used by the Dragon designers[5] in the early stages of the project—they envisaged a fuel element that emitted as many fission products as possible to the fission-product trapping system, thereby obtaining the maximum reactivity benefit through the removal of neutron poisons from the fuel. However, further work showed that some of the more important fission products tended to remain in the fuel, although enough did leave to require the use of a complicated purification system to limit primary coolant activity. Consequently, the Dragon project does have the purge and purification system, but the hoped-for reactivity benefits from the removal of neutron poisons have not materialized. Recent studies, which must be regarded as preliminary, indicate that there could be some cost benefit associated with the development of a fuel element which could be directly cooled by the main helium stream and which would not be supplied with the elaborate purging and purification systems currently employed in Dragon and Peach Bottom.

The pebble-bed reactor[10] represents a different version of the high-temperature gas-cooled concept. It also uses the fuel in completely ceramic form—probably in balls containing UC_2-ThC_2 particles coated with pyrolytic graphite, with a graphite shell surrounding each ball—but no attempt is made to draw off fission products. The reactor is fueled more or less continuously during power operation by adding balls to the top of the assemblage, which constitutes the active portion of the core, and draining off balls from the bottom. Of the balls removed, the most highly exposed and those which may be damaged are discarded, and the good balls of low exposure are recycled to the reactor. One of the developmental prob-

Digitized by Google

lems is to find a means of handling and sorting the balls.

The concept is being developed primarily in Germany, and an experimental power station of 15 Mw(e) (the AVR Reactor), built for a group of utility companies with financial support from the federal government, is reported to be near completion in the Federal Republic of Germany.[10] Development is also proceeding toward a large reactor of the type.

It would appear that the development of the high-temperature gas-cooled reactor, utilizing unclad fuel, must depend heavily on the experimental information and the operating experience gained from the plants now under construction or startup. Until this experience has been gained, speculation as to the future development of these already sophisticated designs should be considered as just that.

References

The references that contain A/Conf. numbers are papers that were presented at the Third United Nations International Conference on the Peaceful Uses of Atomic Energy, Geneva, September 1964.

1. Organisation for Economic Co-operation and Development, European Nuclear Energy Agency, O.E.C.D. High Temperature Reactor Project, Dragon, Fifth Annual Report, April 1, 1963–March 31, 1964.
2. General Atomic Division, General Dynamics, HTGR, The High Temperature Gas-Cooled Power Reactor, United States Technical Exhibit, Third United Nations International Conference on the Peaceful Uses of Atomic Energy, Geneva, August 31–September 9, 1964.
3. C. L. Rickard, G. Melese, and P. Fortescue, Gas-Cooled-Reactor Technology, *Nucl. News*, 7(10): 73-75 (October 1964).
4. F. de Hoffman and C. L. Rickard, High-Temperature Gas-Cooled Reactors, A/Conf.28/P/213.
5. C. A. Rennie, G. E. Lockett, and R. E. Reynolds, The Dragon Project, A/Conf.28/P/121.
6. L. R. Shepherd, H. de Bruijn, R. A. U. Huddle, and K. O. Hintermann, Review of Research and Development Work for the Dragon Project, A/Conf.28/P/122.
7. F. S. Martin, F. J. P. Clarke, R. W. M. D'Eye, and D. T. Livey, Preliminary Development of Dispersed Fuels in the U.K.A.E.A., A/Conf.28/P/152.
8. R. W. Dayton, W. V. Goeddel, and W. O. Harms, Ceramic-Coated-Particle Nuclear Fuels, A/Conf.28/P/235.
9. G. Franco, S. B. Hosegood, H. W. Muller, and L. H. Prytz, Review of Engineering Work for the Dragon Project, A/Conf.28/P/549.
10. C. B. von der Decken, J. D. Luders, O. Machnig, H. W. Schmidt, and R. Schulten, Development Project of a Pebble Bed Power Reactor, A/Conf. 28/P/536.

Digitized by Google

Section

IX

Power Reactor Technology

Sodium-Cooled Reactors

By J. R. Dietrich

Technology of Sodium Systems

The two currently important types of sodium-cooled reactors are the sodium graphite reactor and the fast breeder. They differ markedly from each other in some characteristics, and, moreover, there has been increasing interest during the past two or three years in fast breeders using other coolants. Nevertheless, the technology of sodium cooling is important enough to both types to justify discussing them together and in terms of the developments in sodium systems.

The Conference produced reviews of heat transfer[1,2] and corrosion[3,4] in liquid-metal systems, by both U. S. and Russian authors, of value to the designer of sodium-cooled reactors. The heat-transfer papers, which include such practical considerations as burnout, and heat transfer in rod bundles, will be particularly useful. The discussion here, however, will be confined to those aspects of sodium technology which affect the direction of reactor development in more obvious, qualitative ways.

Fission Products in Sodium

One of the important areas of new information is in the behavior of fission products in sodium. Investigations by Atomics International[5,6] have shown that liquid sodium will trap radioiodine quantitatively, and this characteristic is expected to be of considerable significance in determining siting criteria for sodium-cooled reactors. The Dounreay Fast Reactor (DFR) has utilized vented fuel elements, of a uranium–20 at.% molybdenum alloy, which purposely allow the escape of fission products into the sodium coolant.[7] Russian experience with the BR-5 reactor[8] has given other information on the behavior of fission products in the primary coolant system which is worthy of note. A brief summary follows.

The BR-5 reactor, which was fueled with plutonium oxide elements in stainless-steel jackets, began operation in 1959 and reached the design value of fuel burnup (2%) the following year. After a burnup of 2.4% it was noted that the residual activity of the sodium, after the decay of ^{24}Na (half-life, 15 hr), began to increase with fuel exposure. Previously the residual activity had all been attributable to the small amount of ^{22}Na (half-life, 2.6 years) formed by the $(n,2n)$ reaction on ^{23}Na. Most of the new activity was due to ^{137}Cs. Table IX-1 shows the growth of this activity, relative to the ^{22}Na activity, with fuel burnup, and this growth is plotted in Fig. IX-1 in terms of the total residual activity. During the period after the ^{137}Cs became apparent, ^{133}Xe was detected in the argon-gas blanket over the sodium. By the time the fuel burnup had reached 5%, alpha activity due to plutonium was found in the sodium (Table IX-1).

After 5% burnup the reactor was shut down because of trouble with a circulation pump, and all the fuel was removed. Of the total of 81 fuel assemblies, 18 were found to contain fuel elements showing gross leakage of fission products. After decay of ^{24}Na the sodium was drained from the primary system, but the drainage caused no substantial reduction in the activity of the primary system, indicating that the fission products were deposited on pipe walls and other surfaces in the system. The primary system was decontaminated by first washing with steam and then with solutions of 0.5% $KMnO_4$, 5% nitric acid plus 1% oxalic acid, and finally with distilled water. This treatment reduced the gamma background in the primary system cells from several thousand micro-

Digitized by Google

Table IX-1 GROWTH OF ^{137}Cs ACTIVITY IN BR-5 PRIMARY COOLANT,[8] RELATIVE TO THAT OF ^{22}Na

Fuel burnup, %	Residual activity induced by ^{22}Na, %	Residual activity induced by ^{137}Cs, %	Alpha activity (dis/min per gram of Na), %
2.00	100		
3.20	80	20	
3.90	60	40	
4.55	30	70	
5.00	5	95	50

roentgens per second to about 10 μr/sec. The major activities in the decontamination solutions were ^{137}Cs, ^{95}Zr, and ^{95}Nb. The reactor was reloaded with 63 of the original plutonium oxide fuel assemblies (some of which apparently contained leaky elements) and 50 new assemblies containing UO_2 elements. A bypass circuit was installed in the primary line which could be valved off at will to allow decay of ^{24}Na in the bypass line without interrupting operation of the reactor. A program of experiments on

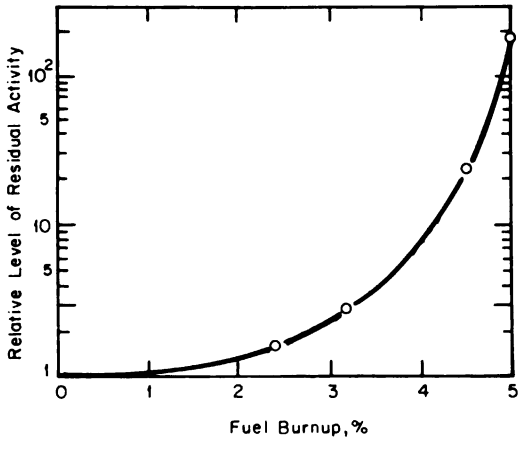

Fig. IX-1 Growth of the residual activity of the primary circuit of BR-5.[8]

the behavior of fission products produced the following results:

1. With the reactor operating at 100 kw with a sodium outlet temperature of 350°C, 90% of the residual gamma activity in the coolant was due to ^{137}Cs, 5% to ^{22}Na, and the remainder to ^{140}Ba, ^{95}Zr, ^{95}Nb, and ^{140}La. The cesium activity level was 4×10^5 dis/min per gram of sodium. Draining of sodium from the bypass line decreased the activity of the line by only 10 to 20%.

2. Changes in sodium temperature in the primary circuit and in sodium flow rate through the bypass section did not produce a noticeable effect on the concentration of cesium on the inner walls of the circuit.

3. Heating of the walls of the bypass section, while the coolant was circulating, decreased the concentration of ^{137}Cs on the inner walls by several times.

4. With the reactor shut down, after the decay of ^{24}Na, and with the oxide cold traps shut down, heating of the walls of the entire primary circuit caused the ^{137}Cs concentration in the coolant to increase by several times. After the cold traps were put into operation, the ^{137}Cs concentration quickly diminished to the initial level. In the steady state the cesium content of the coolant depends on the cold-trap operating conditions; an increase of cold-trap temperature from 110 to 185°C caused the ^{137}Cs activity in the coolant to increase by a factor of 3.

5. Items of equipment, such as pumps and level gauges, which had some parts submerged in the coolant and some parts in the cover gas, were found to be contaminated by ^{137}Cs in both regions. The contamination was a maximum in the region of the interface between sodium and cover gas.

6. The argon cover gas was found to contain the following radioactive isotopes in addition to ^{41}Ar: ^{133}Xe, ^{129m}Xe, ^{135}Xe, ^{135}Cs, ^{85}Kr, ^{85}Rb, and ^{88}Rb. The important contributors to the activity are ^{133}Xe and ^{135}Xe. The major components of the activity from a sampling during reactor operation at 1000 kw were as follows:

^{133}Xe	4.3 $\mu C/cm^3$
^{135}Xe	0.95 $\mu C/cm^3$
^{133m}Xe	0.05 $\mu C/cm^3$
^{85}Kr	0.017 $\mu C/cm^3$

The reference calls attention to the fact that no fission products with half-lives less than 2.5 hr were found in the cover gas, although the equipment was capable of detecting half-lives as short as 5 min.

Sodium Handling and Cleanup

The experience in the general handling, cleanup, and maintenance of quality of sodium has been much greater than the amount of reactor operation would indicate, and this phase of sodium technology appears now to be well understood. This was not the case, however,

Digitized by Google

when the DFR was first commissioned: considerable trouble was experienced in the initial cleanup of the system.[33] References 5 and 9 describe the filling and cleanup of the systems for the Hallam Nuclear Power Facility (HNPF), the Experimental Breeder Reactor (EBR-II), and the Enrico Fermi Fast Breeder Reactor (EFFBR). The Russian experience in reloading the fuel elements of BR-5 after examination is worth noting.[8] The residual sodium and sodium oxide were not removed from the fuel assemblies. The assemblies were reloaded, a few at a time, into the reactor sodium system, and the oxide was cleaned up by the normal system cold traps. The cleanup of carbon from the sodium of the Sodium Reactor Experiment (SRE) after it had been contaminated by the inleakage of Tetralin, as described in Ref. 5, is also of interest.

Despite the routine solution of sodium cleanup problems, it is still true that the protection of sodium systems from the intrusion of oxygen and other contaminants is a consideration of primary importance. The removal or replacement of components in sodium systems is always done with great care to preserve the cleanliness of the sodium system, and, even when the sodium is drained, care is taken to maintain the inert atmosphere of the cover gas throughout the system. Thus, when it was necessary to perform fairly extensive repairs to the hold-down mechanism of the EFFBR, these repairs were made by workmen who entered the drained reactor vessel through an air lock and worked in gastight suits. The scheme that has been used for removing a primary sodium pump from the EBR-II reactor, without contaminating the cover gas, is illustrated in Fig. IX-2. A system similar in principle has been used on the EFFBR for the removal and replacement of components.

Manipulations Under Sodium

Experience has continued to affirm that the manipulation of components under sodium—and particularly the handling of fuel elements in fast reactors, where rather high precision is required of the mechanisms—is one of the more difficult aspects of sodium technology. It has been pointed out frequently that the opacity of the sodium, and the resulting necessity of carrying out blind operations, adds considerably to this problem. Experience with the EFFBR[9] has shown that relatively minor malfunctions may lead to more serious results because of the difficulty of detecting them. Thus the offset handling mechanism was bent in the course of the preoperational test program when an attempt was made to move it laterally with a partially raised dummy subassembly still in the gripper. Damage also occurred to the hold-down mechanism during this program and appears to have been increased by the continued use of the mechanism after initial slight (and undetected) damage caused by the sticking of a dummy subassembly to one of the fingers of the mecha-

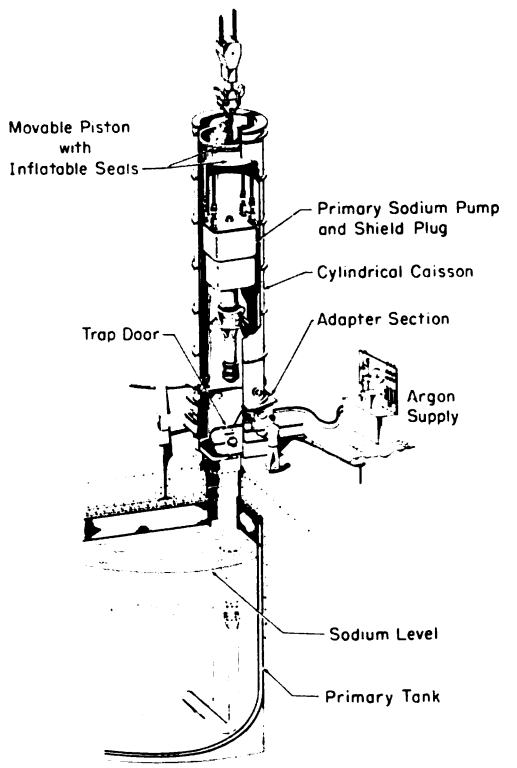

Fig. IX-2 Apparatus used to remove the EBR-II sodium pump.[9] The adapter section, which includes the gastight trap door, was installed, with a gastight seal, around the shield plug of the pump. The cylindrical steel caisson was sealed to the top of the adapter, was purged and filled with argon. The shield plug, with the pump attached, was then lifted slowly by the crane, while the caisson was kept gastight by the movable piston and argon was admitted to hold the pressure constant. After the pump cleared the trap door, the door was closed, resealing the reactor cover-gas system, and it was no longer necessary to maintain the argon atmosphere in the caisson. The operation was carried out with the reactor sodium temperature at 260°F. After the pump had been withdrawn and cooled to room temperature, it was transported to the cleaning and repair area inside the caisson.

Digitized by Google

nism. A "sweep arm" has been installed to prevent the recurrence of the latter difficulty. This sweep arm can be swept in a horizontal arc to determine that no core component is attached to the hold-down mechanism before lateral motion of the mechanism is initiated.

Preoperational tests of the fuel-handling equipment of EBR-II indicated the desirability of incorporating means of manual operation of the fuel-transfer arm to permit the operator to feel any interference that might be present.[9] This was accomplished by a system of counterweights to balance the weight of the rather heavy mechanism.

Although problems have been encountered with the fast reactor fuel-handling systems, it appears that they are problems of arriving at satisfactory designs for specific pieces of equipment rather than general feasibility problems. Indeed, the experience with practice handling of the fuel in both EBR-II and the EFFBR indicates that fuel handling is satisfactory once the specific troubles have been corrected. The British experience with fuel-element handling in the DFR appears to have been good from the beginning.[7]

Components

Outside of the reactor itself, the major components[10] common to sodium-cooled power reactors are the pumps, the steam generators, and the intermediate sodium-to-sodium heat exchangers. The use of the latter, along with the second set of pumps and piping required for the intermediate sodium circuit, must be reckoned as one of the economic handicaps of the sodium-cooled reactor. Apparently it will not soon be eliminated, for no recent design has appeared without the intermediate sodium system to isolate the radioactive primary sodium from the water in the steam generator. Technically, no serious problems have been found in the design of the intermediate heat exchanger, although the units built to date do not approach the capacities that will be required for plants of economic size and do not reach the temperatures that are ultimately hoped for. The three exchangers for the EFFBR plant, of 143 Mw(t) capacity each, are the largest so far. They operate with primary inlet and outlet temperatures of 900 and 600°F, respectively, and secondary inlet and outlet temperatures of 520 and 820°F.

The steam generators designed to date show great variety of concept. The HNPF and EBR-II units are natural-circulation boilers that use double-wall tubes. In the former the sodium is on the tube side, whereas in the latter it is on the shell side. The EFFBR unit is a once-through generator with the water in single-wall tubes and sodium on the shell side. The three HNPF generators, each of which has a capacity of 69 Mw(t) in the evaporator and 16 Mw(t) in the superheater to produce steam at 895 psig and 875°F, are the only ones that have operated at power. No difficulties have been experienced other than the necessity of controlling the water level very precisely (within ±1 in.) to give satisfactory operation without excessive carryover of water. The design, which utilizes reentrant tubes to circumvent thermal-expansion problems, has been described previously in *Power Reactor Technology*, 5(3): 44-47.

The once-through design of the three EFFBR steam generators is shown in Fig. IX-3. Before operation the tubes of one of these units were found to be cracked at the bends as a result of stress corrosion. The corrosion was attributed to residual cleaning solution containing sodium hydroxide and sodium nitrate. During isothermal operation, after about two weeks of test with maximum sodium flow, several tubes

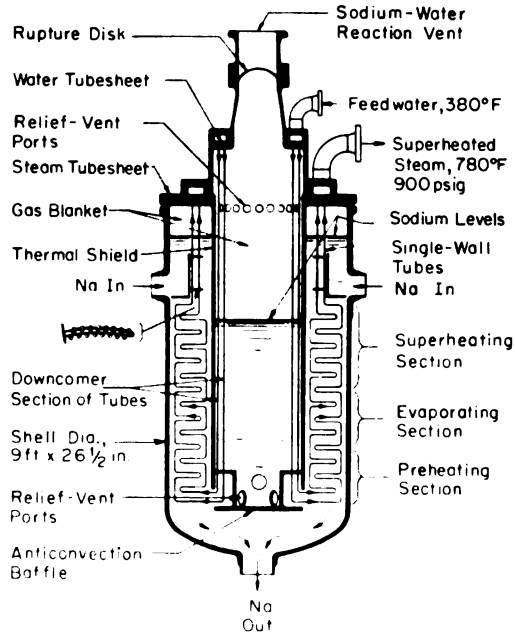

Fig. IX-3. Diagram of the EFFBR steam generator [143 Mw(t)].[7]

Digitized by Google

failed in another of the units. The resulting sodium-water reaction generated enough hydrogen to break the rupture disk (see Fig. IX-3), which was set at 60 psi. All systems designed to accommodate such a reaction functioned satisfactorily, and the separator collected all the sodium expelled from the unit. This inadvertent demonstration of the ability to accommodate a large sodium-water reaction is considered an important contribution to steam-generator development.[10] The tube failure was attributed to flow-induced vibration of the tubes opposite the sodium inlets. Baffles and tube clips have been installed to correct the trouble.

It is stated[11] in the description of the proposed BN-350 fast-breeder reactor in the USSR that the steam generator will be of the natural-circulation type, with a single separating wall between sodium and water. The choice of single-wall construction is said to have been substantiated by a number of experiments on wall ruptures, and sodium-water and sodium-steam interactions, in models of steam generators.

In the studies of large advanced sodium graphite plants,[5] there has evolved the concept of steam-generator systems made up of many low-capacity modules. Separate modules are proposed for the evaporator, superheater, and reheater functions, each with a capacity of 12 to 15 Mw(t). The superheat and reheat modules would be of stainless steel, and the evaporators would be of chrome-molybdenum steel. All modules are of vertical, once-through design, with single-wall tubes and with the sodium on the shell side. The problems of caustic and chloride stress corrosion are minimized by avoiding crevices and by the use of ferritic steels for the evaporator modules. The justification for the use of single-wall tubes is the choice of shell thickness adequate to contain full steam pressure for short periods of time, plus the provision of rupturable membranes, spaced axially along the shell length, to rupture below full steam pressure and direct any reaction products resulting from a tube break to a relief tank. The modular array is expected to allow the isolation and removal from service of any unit that may give trouble, with a minimum effect on plant availability.

The most definite development in sodium components seems to be the virtual abandonment of electromagnetic pumps in favor of mechanically driven centrifugal pumps. The characteristics of the pumps for HNPF, EBR-II, and EFFBR are listed in Table IX-2, and drawings of the primary pumps for the three

Table IX-2 DESIGN CHARACTERISTICS OF SODIUM PUMPS FOR HNPF, EBR-II, AND EFFBR

	HNPF	EBR-II	EFFBR
Primary system pumps			
Type	Mechanical free surface	Mechanical free surface	Mechanical free surface
No. of units	3	2	3
Capacity, gal/min	7200	5500	11,800
Dynamic head, ft	160	200	310
Design temperature, °F	1000	800	1000
Motor speed, rpm	900	1075	900
Motor power, hp	350	350	1060
Sealing arrangement	Mechanical shaft seal	Totally enclosed drive motor	Mechanical shaft seal
Material	304 S.S.	304 S.S.	304 S.S.
Type of speed control	Eddy-current coupling	Variable frequency and voltage	Wound rotor motor with liquid rheostat
Manufacturer	Byron-Jackson	Byron-Jackson	Byron-Jackson
Secondary system pumps			
Type	Mechanical free surface	A-c linear induction	Mechanical free surface
No. of units	3	1	3
Capacity, gal/min	7200	6500	13,000
Dynamic head, ft	170	142	100
Design temperature, °F	1000	700	1000
Motor speed, rpm	900	1180 (motor-generator set)	900
Motor power, hp	350	500 (motor-generator set)	350
Sealing arrangement	Mechanical shaft seal	Total metal enclosure	Mechanical shaft seal
Material	304 S.S.	304 S.S.	2¼ Cr–1 Mo
Type of speed control	Eddy-current coupling	Variable voltage (motor-generator set)	Eddy-current coupling
Manufacturer	Byron-Jackson	General Electric	Byron-Jackson

Digitized by Google

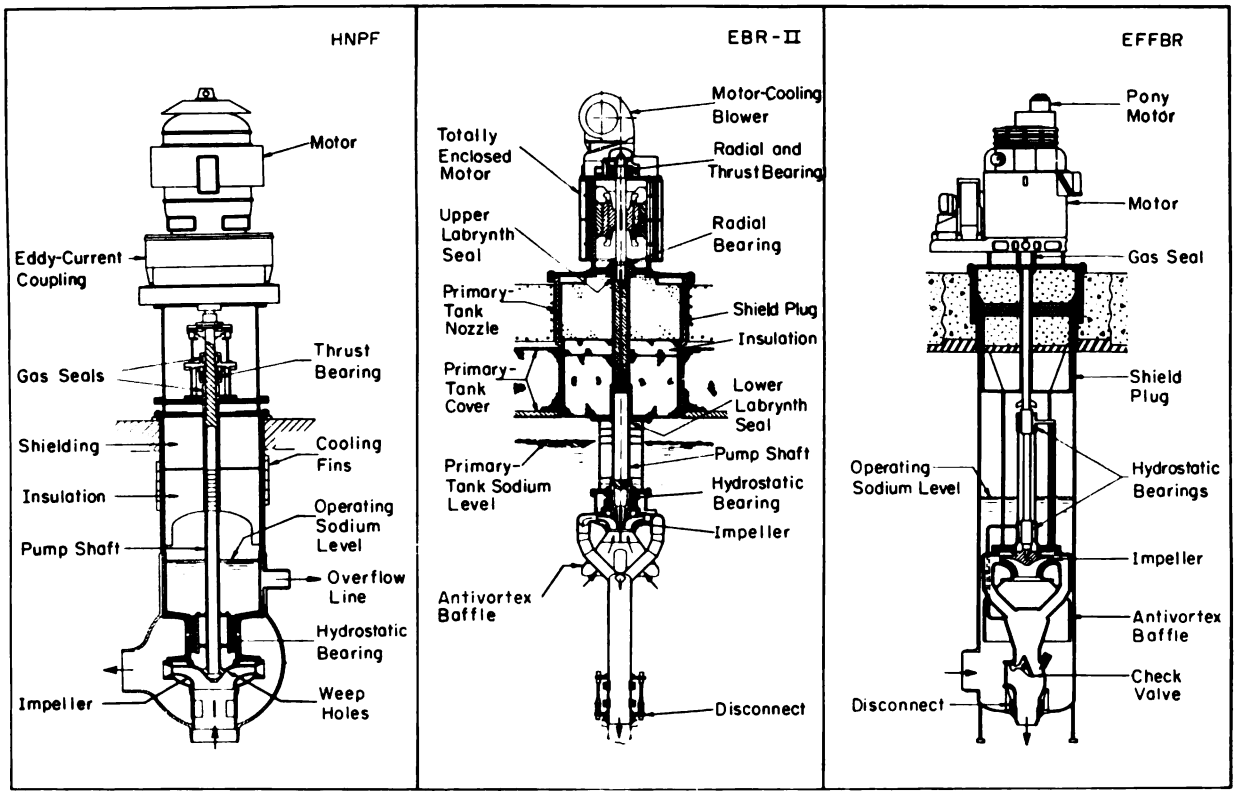

Fig. IX-4 Primary system sodium pumps for HNPF, EBR-II, and EFFBR.[10]

reactors are shown in Fig. IX-4. The EFFBR pumps have been operated for more than 7000 hr without difficulties. Some troubles with binding have been experienced with both the HNPF and EBR-II pumps, and, in both cases, insufficient clearances and misalignment (possibly due to uneven temperature distribution in the pump casing in HNPF and to warpage of the three-piece welded shaft in EBR-II) are judged to be at least partially responsible. The difficulties are believed to be incidental rather than basic, and extrapolation of centrifugal pump designs to large sizes is considered feasible.[10]

Sodium Graphite Reactors

Status and Operating Experience

The development of the sodium graphite reactor has centered around the SRE, a 20-Mw(t) experimental plant, and the HNPF, a 75-Mw(e) generating plant operated by the Consumers Public Power District of Nebraska for the Atomic Energy Commission. The SRE began operation in 1957, and most of the nonroutine items of operating experience have been reviewed in past issues of *Power Reactor Technology*. The major problems were those resulting from the leakage of Tetralin into the primary coolant system [*Power Reactor Technology*, 3(2): 60-64 (March 1960); 5(1): 84-87 (December 1961)] and the unexpected power coefficient of reactivity due to the bowing of fuel elements [*Power Reactor Technology*, 6(1): 57-61 (December 1962)]. Both of these problems were incidental rather than fundamental and have been corrected. The first core, of unalloyed uranium metal, was run to a maximum exposure of 1200 Mwd/ton, and the fuel exhibited volume changes of 8 to 9%. Exposures of about 5000 Mwd/ton have been attained with the second core, of metallic thorium-uranium fuel, with little dimensional change. The SRE is now being modified to raise the power level

Digitized by Google

from 20 to 30 Mw(t) and the sodium outlet temperature from 950 to 1200°F; the new fuel loading will consist of uranium carbide elements designed to operate at central temperatures in the range from 1700 to 2000°F.

The design of the HNPF was reviewed in *Power Reactor Technology*, 5(3): 39-51 (June 1962). The plant first attained the design power level in July 1963. The fuel elements, of uranium–10% molybdenum, have accumulated peak exposures of more than 1200 Mwd/ton. The main problems encountered in operation were the following:

1. Helium was entrained in the main secondary sodium loops from the cover gas in a tank that was provided to accommodate sodium expansion and to provide a low-velocity free surface for degasification. The entrainment occurred because of the formation of a vortex at the exit of the tank. The trouble was corrected by bypassing over 90% of the sodium flow past the tank. This does not negate the effectiveness of the tank for its intended function.

2. Leaks developed in one of the intermediate heat exchangers because of flow-induced vibration of the peripheral tubes. The trouble was corrected by installing support shims in all of the six heat-exchanger units.

3. Some of the Zircaloy-2 control-rod thimbles failed because of hydriding and resulting embrittlement. The hydrogen apparently came from titanium hydride shields placed in the thimbles to counter neutron streaming. The trouble was corrected by replacing the Zircaloy-2 thimbles with stainless-steel thimbles; the resulting reactivity loss was about 0.7%. A circulating-gas and hydrogen-removal system was also added to the control-rod-thimble gas-purge system.

The first of these difficulties, the entrainment of gas in the coolant, appears to be a potential problem to be aware of in the design of sodium systems. Both the DFR[33] and the BR-5 fast reactor[8] experienced troubles with cover-gas entrainment in the coolant of the primary loop.

Development of Uranium Carbide Fuel

Although uranium carbide fuel[12] may be attractive in other applications, its development has received the greatest impetus from the sodium graphite reactor program, and forecasts of future developments of the sodium graphite reactor are based on the use of the carbide fuel. The carbide is compatible with sodium and has the advantage, in comparison with uranium metal, of good stability under irradiation. Compared with uranium oxide, the carbide has the advantages of higher density (13.0 g/cm^3) and much higher thermal conductivity [about 0.23 watt/(cm)(°C)]. The latter advantages are particularly important in the sodium graphite reactor, where it is better to use rather massive fuel elements in order to minimize neutron losses to cladding and coolant, without sacrificing the high heat fluxes that the cooling properties of sodium make possible.

Ordinarily, uranium monocarbide (UC, 4.80 wt.% carbon) is used, but acceptable performance does not appear to depend upon the attainment of the exact stoichiometric composition. Most experience with the carbide elements has been accumulated with the slightly uranium-rich composition (hypostoichiometric) in arc-cast slugs with sodium-bonded stainless-steel jackets. The results of capsule irradiations are summarized in Table IX-3.

Reactor experience with full-size carbide elements began in June 1963 when two full-length elements were placed in the second core of the SRE. In September 1963, 10 full-size carbide elements began operation in the HNPF reactor. Experience to date with both groups of elements is described as entirely satisfactory.[12] The second full-core loading for the HNPF reactor will consist of 171 carbide elements, essentially the same in design as the 10 elements currently installed. The fuel-element design data for the HNPF carbide elements, and for two projected designs of large sodium graphite reactors (LSGR) are given in Table IX-4. The anticipated performance is believed to be compatible with test experience to date.[12] The design criteria that led to the data given in Table IX-4 are discussed in Ref. 5.

Higher specific powers than those shown in Table IX-4 are thought to be possible—linear power ratings up to 50 kw/ft, corresponding to central temperatures of about 2400°F—but close control of the carbide composition to the stoichiometric value would probably be necessary to yield high-burnup capability in this temperature range.[12]

Digitized by Google

Table IX-3 RESULTS OF CAPSULE IRRADIATION TESTS[12] OF URANIUM CARBIDE FUEL SAMPLES*†

Capsule	Cladding	Fuel comp., % C	Annulus width, in.	Bond	Fuel diameter, in.	Actual peak temperature, °C		Average fuel temperature, °C		Burnup (isotopic and/or radiochemical), 10^3 Mwd/metric ton of U	Increase in		Fission-gas release, % ^{85}Kr	Cladding carbon content, wt.%	
						Center	Surface	Center	Surface		Dia., %	Length, %		Preirrad. (nom.)	Postirrad. (max.)
BMI-23-2	304 S.S.		Wire basket	NaK	0.375 gnd‡									0.072	Not analyzed
T§		5.3				1000	580	750	490	5.6	0.9				
B¶		5.1				800	490	570	370	7.8	0.9				
BMI-23-3-B¶	304 S.S.	5.0	Wire basket	NaK	0.375 gnd	890	380	590	330	12.8	0.8			0.072	Not analyzed
BMI-23-5	304 S.S.		Wire basket	NaK	0.375 gnd									0.072	Not analyzed
T		4.6				720	535	720	470	8.6	0.8				
B		4.55				780	455	670	460	6.4	1.2				
BMI-23-6	304 S.S.		Wire basket	NaK	0.375 gnd										
T		4.8					560	780	435	7.0	0.5				
B		4.55					430	510	315	7.0	0.5				
AI-3-1	304 S.S.	4.4 to 4.7	0.015	Na	0.5 ac**	1340	870	980	675	6.5	2 to 6	2.5 to 3	2.3	0.072	0.16
AI-3-4	Ni	4.8 to 5.0	0.050††	Na	0.5 ac	1150	680	1010	535	15.0	1 to 4		0.18	0.10	0.07
AI-3-5	304 S.S.	4.2 to 4.4	0.015	Na	0.5 ac	1530	920	1150	730	13.0	3.8 to 7.6		21.6	0.072	0.32
AI-5-1	304 S.S.	4.8 to 5.0	0.005	NaK	0.5 ac	970	540				0.8	0.4	0.06	0.072	0.51
NAA-48-1	304 S.S.	4.8 to 5.0	0.005	NaK	0.5 ac	1260	780	940	570	9.1	1.4		Gas lost	0.072	1.26
								1180	690						
NAA-48-2	304 S.S.	4.8 to 5.0	0.005	NaK	0.5 ac	1090	670	480	295	23.9	0.6 to 5.0		1.3	0.072	0.84
								830	500						
NAA-48-3	304 S.S.	4.8 to 5.0	0.015	NaK	0.5 ac	1110	650	830	490	19.0	3 to 7		7.0	0.072	0.96
NAA-48-6	304 S.S.	4.8 to 5.0	0.015	NaK	0.5 ac	1290	755	950	575	6.4	3.2 to 4.4	0.6	0.74	0.072	1.39
NAA-81-3	304 S.S.	4.4 to 4.8	0.025	Na	0.5 ac	1040	600	980	570		1.0		0.26		
UNC 1-1	Nb–1 Zr	4.45	0.020	Na	0.375 ac	1150	735	1120	715	39.9	10.0				
		4.70				1165	800	1020	700	34.8	8.9		31		
		5.20				1160	790	980	660	36.0	5.7		5	Nb–1 Zr cladding	
UNC 1-2	Nb–1 Zr	4.45	0.020	Na	0.375 ac					22.9	11.0		30		
		4.70								22.9			7		
		5.20				1250	790	1120	720	22.9			4		
SU-20	304 S.S.	4.4 to 4.7	0.020	Na	0.5 ac	870	540	Data not reduced		Not examined					
SU-28	304 S.S.	4.4 to 4.7	0.020	Na	0.8 ac	940	690	Data not reduced		Not examined					

*Fuel enrichment was 10% in all capsules.
†Range of heat fluxes calculated at fuel surfaces: 9.15 to 13 × 10^5 Btu/(hr)(sq ft) (288 to 410 watts/cm^2).
‡gnd, the fuel surface ground after casting.
§T, the capsule top.
¶B, the capsule bottom.
**ac, the as-cast fuel-surface condition.
††Three 0.050-in.-diameter spacer wires in fuel-cladding annulus.

Digitized by Google

Table IX-4 DESIGN DATA FOR CARBIDE FUEL ELEMENTS FOR SODIUM GRAPHITE REACTORS[12]

	81-Mw(e) HNPF core I (operating)	200- to 250-Mw(e) LSGR prototype (projected)	1000-Mw(e) LSGR (projected)
Materials			
Fuel (all hypothetically UC)	4.4 to 4.8 wt.% C	4.5 to 4.8 wt.% C	4.6 to 4.8 wt.% C
Cladding	304 S.S.	304 S.S.	304 S.S.
Bond	Sodium	Sodium	Sodium
Enrichment, wt.% ^{235}U	3.7 and 4.9	3.8	3.6
Element			
No. of rods	8	18	18
U content, kg/element	146	124	124
Peak specific power, kw/kg of U	18	52	72
Fuel-slug diameter, in.	0.872 (2.22 cm)	0.500 (1.27 cm)	0.500 (1.27 cm)
Active fuel length, ft	13 (3.96 m)	14 (4.26 m)	14 (4.26 m)
Total fuel-rod length, ft	15 (4.57 m)	18 (5.49 m)	18 (5.49 m)
Cladding thickness, in.	0.010 (0.25 mm)	0.010 (0.25 mm)	0.010 (0.25 mm)
Sodium annulus thickness, in.	0.030 (0.76 mm)	0.025 (0.63 mm)	0.025 (0.63 mm)
Design criteria			
Fission-gas release, % of total produced	3	3	3
Maximum cladding strain, %	0.5	0.5	0.5
Peak cladding temperature, °F	1005 (542°C)	1250 (676°C)	
Peak fuel temperature, °F	1600 (870°C)	1750 (955°C)	2000 (1095°C)
Average burnup, Mwd/metric ton of U	15,000	25,000	25,000
Maximum fuel-volume increase, %	17	17	17
Fuel-diameter increase, %	7	5.3 (average)	5.3 (average)
Maximum rod linear power, kw/ft	28 (920 watts/cm)	24 (788 watts/cm)	35 (1150 watts/cm)
Maximum heat flux, Btu/(hr)(sq ft)	207,000 (128 watts/cm^2)	549,000 (173 watts/cm^2)	
Mixed mean temperature, coolant outlet, °F	945 (508°C)	1150 (620°C)	1150 (620°C)

Directions of Future Development

Studies by Atomics International on large sodium graphite reactors are the sources for projections of the direction of development for the reactor type. With regard to performance, the main effort is in the direction of higher specific power (Table IX-4) and higher temperature. Conversion ratios above about 0.5 are not predicted for the reactor type.[5] Reference 5 states that supercritical steam pressures can be justified economically for plants above 400 Mw(e) capacity, whereas subcritical pressures, from 1800 to 2400 psig, would be used for smaller plants. Table IX-5 shows projected conditions for reactors in the two size ranges. In either case the projection calls for an increase in the primary sodium outlet temperature to 1150°F, from the 945°F used in HNPF. As mentioned above, the modified SRE is to operate with a sodium outlet temperature of 1200°F.

Perhaps the most annoying problem of the sodium graphite reactor is that of separating the sodium from the graphite moderator. In the SRE and HNPF, the approach is to can the moderator in sizable units in zirconium or steel cans. The advanced design studies for large reactors use a calandria design, with the sodium flowing through the calandria tubes. This approach is expected to permit higher sodium temperatures and higher power density while the parasitic loss of neutrons is being reduced.

Standardization and modular construction are features of the advanced designs which are expected to reduce costs. A common height of

Table IX-5 TYPICAL PROCESS CONDITIONS FOR SMALL AND LARGE FUTURE SODIUM GRAPHITE PLANTS[5]

	200 to 400 Mw(e)	400 to 1000 Mw(e)
Steam conditions, psig/°F/°F (kg/cm^2/°C/°C)	2400/1000/1000 (168.5/538/538)	3500/1000/1000 (246/538/538)
Final feedwater temperature, °F (°C)	473 (245)	512 (267)
Reactor sodium outlet temperature, °F (°C)	1150 (621)	1150 (621)
Intermediate heat-exchanger log mean temperature difference, °F (°C)	75 (24)	90 (31)
Reactor sodium inlet temperature, °F (°C)	750 (400)	750 (400)
Net efficiency, %	41.8	43.6

Digitized by Google

14 ft is projected for reactors ranging in capacity from 200 to 1000 Mw(e), and a fuel-slug diameter of ½ in. is thought to be near the optimum. A basic loop of 250 Mw(e) capacity is considered to be a practical module for the primary coolant system. The modules for the steam generators are of much lower capacity, 12 to 15 Mw(t), as described in the preceding general discussion of sodium-system components.

Fast-Breeder Reactors

There is general agreement that the fast breeder will be needed in the long term, although opinion varies as to how soon the need will be serious. Most of the countries with major nuclear power programs are pursuing development programs aimed at achieving large, economically competitive, fast-breeder power plants in the next 10 to 15 years. In England and France, where the current nuclear power generation is based on natural uranium, the intention is to start the fast breeders on plutonium from the thermal reactors; and, indeed, some of the incentive for fast-breeder development seems to be the desire to do something with the accumulating plutonium. In the United Kingdom, at least, the plutonium stocks are expected to become large several years before enough fast breeders are in commercial use to absorb them.[13] In France the accumulation of plutonium is expected to be something over 4 tons by 1975. This amount is considered to correspond approximately to the supply for a first large breeder plant.[14]

In the United States and the USSR, where enriched uranium is the fuel for practically all single-purpose power reactors, no great emphasis has been placed on coordinating the development of fast breeders with the growth of the plutonium stockpile. In the United States a considerable analytical effort is devoted to determining the dollar value of plutonium for thermal-reactor fuel, in addition to substantial development efforts aimed at utilizing the plutonium in the thermal-reactor application. In the USSR the economic potential of the fast breeder seems to be regarded more highly than elsewhere, and the forecasts appear to predict its economic superiority even when fissile isotope is not in short supply.

The more favorable Russian estimates may be due, in part, to the different approach used in economic analyses. Instead of trying to evaluate a reactor type by fitting it into an existing complex of mining, transportation, fabrication, processing, and power transmission facilities, the Russians apparently try to evaluate the effort involved in setting up this entire complex for the reactor type in question. This type of approach is also used in evaluating nuclear power vs. coal power. Apparently much of the attractiveness of the fast breeder stems from the expectation that doubling times may be achieved which are short enough to provide for the expansion of nuclear plant capacity without requiring any large expansion of mining operations or enrichment facilities, as indicated by the quotation from Ref. 15:

> Most profitable and at the same time providing for the most effective use of nuclear fuel is a development of nuclear power with the priority given to fast 500 to 1000 MWe reactors with a mixed uranium and plutonium fuel cycle and the increase of the proportion of plutonium breeder reactors.
>
> Such a trend would require small scale industries for production and chemical reprocessing of core fuel elements and moderate capacities for production and chemical reprocessing of blanket fuel elements as well as for reenrichment of the core fuel with the plutonium produced in the reactor, enriched fuel being required only to provide the initial load of every new reactor and one or two of its refuelings.
>
> No constant expansion of uranium mining or enrichment industries will be required; nor practically will the power industry be dependent on these, because two or three sets of fuel cores are a sufficient "trigger pulse" for further operation of reactors that would be self sustaining and at the same time provide a certain plutonium excess for new capacities at the rate of eight to ten per cent of annual power increase. This rate can be considerably increased through the use of fissionable materials formerly intended for defense purposes. Such possibilities are opened up in the Statement made by N. S. Krushchev, Chairman, USSR Council of Ministers on the 21st April 1964.

The relatively low estimate of investment in fuel-cycle installations for the fast breeder (includes mining, ore processing, and transportation investment, as well as investment for chemical processing and fuel fabrication) is indicated in Table IX-6, which summarizes some of the results of a Russian study of future nuclear power possibilities.[15] Surprisingly enough, the unit investment in the power station itself is also estimated to be somewhat lower for the fast breeder than for the water-moderated reactor.

Digitized by Google

Table IX-6 ESTIMATES FOR THE FUTURE* OF REQUIRED UNIT INVESTMENTS AND POWER PRODUCTION COSTS FOR SEVERAL NUCLEAR PLANT TYPES IN THE USSR[15]

	Gas-cooled graphite natural-uranium reactors	Heavy-water organic natural-uranium reactors	Water-cooled graphite slightly enriched-uranium reactors with steam superheating in the core	Water-cooled water-moderated slightly enriched-uranium reactors	Fast sodium reactors
Mean unit investment, roubles/kw(e)					
Investments in nuclear power stations	179 (75%)	186 (80%)	114 (66%)	135 (66%)	127 (79%)
Investments in fuel-cycle installations	60 (25%)	46 (20%)	59 (34%)	70 (34%)	34 (21%)
Total investment	239	232	173	205	161
Mean power production cost, kopeks/kw-hr	0.40	0.42	0.43	0.48	0.33

*These estimates are from a study covering the period up to 1980. They are based on plants in the 500- to 1000-Mw(e) range.

Problem of the Large Reactor

Although there has been considerable development in fast breeders since the 1958 Geneva Conference, the significance of an important part of the development has been more in the revealing of basic difficulties than in the solution of them. Specifically, the developments in fast reactor physics and safety analysis, and their application in large-reactor design studies, have shown that there is a fundamental problem in extending the design of sodium-cooled fast breeders from small units to large ones: the problem of preserving an inherently negative power coefficient of reactivity under all credible circumstances.

In small fast reactors it was clear that, once the fear of a substantial positive Doppler coefficient of reactivity due to the fission resonances was allayed, the power coefficient of reactivity could always be made inherently negative, at least so long as the mechanical structure of the core remained intact. The major components of the power coefficient were due to: the linear expansion of fuel elements, which increases neutron leakage by reducing the average density of fuel in the core; the Doppler coefficient, either very small (if there was little fertile isotope in the core) or negative; and the reduction of sodium density by thermal expansion or boiling. The latter was a negative component because its major effect was to increase neutron leakage, and this effect was considerably larger than other, positive effects, such as the effect of neutron absorption by sodium. Experience with EBR-I had, of course, shown that the thermal bowing of fuel rods could lead to positive contributions [see *Power Reactor Technology*, 5(2): 24-29], but with suitable mechanical design this possibility could be eliminated. The designer could count on a negative power coefficient that, if large and fast acting, could be a substantial help in countering the effects of accidental power excursions or, if small or slow, would at least not compound the effect of such an excursion.

As much larger reactors were investigated, with relatively high ratios of fertile-to-fissile isotope in the core, it became clear that it was very difficult, if not impossible, to preserve the negative character of the sodium-voiding component of the power coefficient. Also, this component could be so large as to override all negative components and increase the reactivity by the order of dollars in some cases of substantial sodium loss from the core. This is partly because the neutron-leakage effect becomes smaller as the core size is increased. However, in the relatively "soft" neutron-energy spectrum that exists in the large dilute core, the "hardening" of the spectrum due to a decrease in moderation by sodium also results in a reactivity increase. The reactor physics aspects of the sodium coefficient and other reactivity coefficients were discussed at length in *Power Reactor Technology*, 7(2).

Once it is clear that a real threat of a net positive coefficient exists, the problems of evaluating it and its significance become very complex. It soon becomes evident, for example, that the overall sodium-void coefficient for the core is not the only consideration. The designer and the safety analyst must consider the local value of the coefficient at the point in the core

Digitized by Google

where boiling would start first in the event of a power excursion or a cooling interruption. Usually the coefficient is found to be more highly positive in these higher power regions of the core. The process of optimizing the power coefficient through the proper adjustment of design variables is a complex one because all components of the coefficient respond to changes in these variables, and the designer is apt to find, for example, that a design change which reduces the positive nature of the sodium-void coefficient will also reduce the magnitude of the desirable, negative Doppler coefficient. Finally, the evaluation of the coefficients by neutron physics analysis is a very complex problem that still involves large uncertainties.

Although fast reactor theory is, in many respects, the most sophisticated branch of neutron physics, its inadequacies become apparent when it is applied to the evaluation of complex reactivity coefficients. These inadequacies are not due to any deficiencies of fundamental understanding but to the sheer range and detail of data that must be handled (and must be available from experimental measurement). It is still possible that further developments in neutron physics may ease the problem of the power coefficient. For example, the French results summarized in Table IX-7 indicate that calculations which take into account the self-shielding of resonances predict a much more favorable sodium-void coefficient.

It should be made clear that the reactivity-coefficient problem does not appear to be a problem of normal reactor operation, but one that affects the prognosis for the course of a hypothetical accident. The seriousness with which the problem is viewed varies widely from group to group and from country to country, and reactions vary from a rather casual recognition of the problem to the initiation of searches for alternate fast reactor coolants.

In the United States there does not appear to be any widespread inclination to doubt sodium as the optimum coolant for fast breeders, but the problem of the sodium coefficient of reactivity is taken quite seriously. It appears unlikely that any easy solution of general applicability will be found. However, individual solutions for specific designs will be found through detailed and exhaustive safety analyses. This implies that fast reactor physics, safety experiments, and methods of safety analysis will continue to get much attention in the United States and probably abroad. The current emphasis on these fields is attested by the papers at the Conference, listed as Refs. 16 to 25. The papers are too detailed for review here, but they contain much pertinent and useful information.

Fast Reactor Fuels

Although most of the general considerations involved in the selection and development of fuels for thermal reactors apply also to fast breeders, their relative importance is different. In addition, in fast reactors the effects of the fuel on reactivity coefficients and on reactor behavior in hypothetical accidents must be considered carefully.

Even the largest fast breeders must use fuel of relatively high enrichment. For a given method of fuel processing, high enrichment leads to high processing costs (per unit of fuel comprising fissile-plus-fertile isotope) because

Table IX-7 INFLUENCE OF RESONANCE SELF-SHIELDING ON SODIUM-VOID COEFFICIENT AND BREEDING RATIO[14]

(Spherical, 2886-Liter Core with Oxide Fuel; Fuel Volume Is 35% of Core Volume; Fissile Isotope Is ^{239}Pu; and Fertile Isotope Is ^{238}U)

	$^{238}U/^{239}Pu$	Sodium-void coefficient,* 10^{-5} $(\delta k/k)/°C$				Internal breeding ratio	Total breeding ratio
		Diffusion	Absorption	Degradation	Total		
Without self-shielding	6.25	−0.736	+0.072	+1.361	+0.697	0.916	1.455
With self-shielding	6.86	−0.775	+0.080	+0.597	−0.098	0.874	1.408

*The calculation breaks the sodium-void coefficient down to the components of neutron diffusion (leakage), absorption by sodium, and the effect of sodium in degrading the neutron-energy spectrum. The calculations show a big reduction in the latter (positive) effect when resonance self-shielding is taken into account. The sodium-void coefficient is expressed in terms of a sodium-temperature coefficient, via the volumetric coefficient of expansion of sodium.

Digitized by Google

of the criticality problems and the high cost of fuel losses. Moreover, the high enrichment necessitates high specific power if fuel-inventory costs are to be kept within reasonable bounds. This in turn requires a highly subdivided fuel structure that usually involves high fabrication costs. Further increases in processing and fabrication costs (relative to thermal reactors) tend to result from the necessity for recycling plutonium (or ^{233}U) and possibly from the necessity of processing blanket fuel as well as core fuel. The attainment of low fuel cost in the fast reactor therefore appears to require either that inherently cheaper methods of processing and fabrication be found, relative to those used for thermal-reactor fuel, or that the exposure lifetime of the fuel be increased greatly beyond that which is acceptable for thermal reactors. The relative insensitivity of the neutron economy of the fast reactor to the presence of some materials that would absorb neutrons strongly in a thermal reactor assists in both these directions. It permits the use of fuel jackets that are rather thick relative to the fuel element. It also makes the neutron economy rather insensitive to the fission-product burden of the reactor, so that long exposures do not degrade the neutron-physics performance importantly; and it removes the neutron-physics requirement for complete fission-product removal during processing.

It appears to be the result of cost studies that if oxide fuel elements are used in fast breeders, the attainment of acceptable fuel costs requires average fuel exposures of about 100,000 Mwd/ton. Documentation of the conclusion is not easy to find, but it is implied by the frequent use of this exposure in economic studies of fast breeders. Processing and fabrication estimates for oxide elements should be more reliable than estimates for other types, because of the more extensive experience with oxide in the United States. Irradiation tests have indicated that exposure lifetimes of 100,000 Mwd/ton are indeed possible for mixed uranium-plutonium oxide elements of types acceptable for fast breeders.[26] Consequently it is tempting to conclude that oxide fuel elements are essentially proved as practical elements for the fast breeder. Certainly it appears that the oxide, although it may not ultimately prove to be best, offers the most straightforward approach to a feasible fast-breeder fuel element. But more extensive irradiation experience is required, and the gap in experience, between processing and fabrication of uranium oxide elements for thermal reactors and comparable experience with the uranium-plutonium oxide elements for fast breeders, must not be overlooked.

Design characteristics of fuel rods proposed for the Fast Ceramic Reactor (Table IX-8) are considered typical for oxide elements.[26] Preliminary estimates of the fabrication cost, for a production rate corresponding to 3000 Mw(e) of generating capacity, yield $211 per kilogram of uranium and plutonium in the core. This corresponds to a fuel-fabrication contribution to the power cost of 0.29 mill/kw-hr for an average exposure level of 100,000 Mwd/ton.

Table IX-8 PROPOSED DESIGN CHARACTERISTICS OF FUEL ELEMENTS FOR THE FAST CERAMIC REACTOR[26]

Form of element	Rod
Fuel composition	80 wt.% UO_2–20 wt.% PuO_2, solid solution
Form of fuel	0.220-in.-diameter pellets, pressed and sintered
Fuel density, % of theoretical density	95
Jacket	AISI 347 S.S. tubing
Jacket outside diameter, in.	0.250
Jacket thickness, in.	0.015
Fuel length, ft	2 to 4, depending on reactor design

British work on the irradiation of oxide fuels is summarized in Ref. 27. It calls attention to erratic behavior with respect to fission-gas release, and another British paper[28] cites oxide fuel-element designs for fast reactors in which plenum volumes are left in the element, for the accommodation of fission gases, of volume equal approximately to the volume of fuel.

With respect to reactivity coefficients, the Doppler component of the power coefficient is usually strongly negative in oxide fuels containing high proportions of fissile isotopes. This characteristic, which results from the strong dependence of the average fuel temperature on the power level, is of course desirable. It is usually assumed that no important negative component of the power coefficient due to axial expansion of the fuel can be counted on in oxide cores because of the uncertainty as to how an element composed of cracked oxide will expand thermally. The British irradiations have shown much less cracking of PuO_2-UO_2 samples than of pure UO_2 samples.[27] However, it is questionable whether this difference will be

Digitized by Google

significant from the point of view of the thermal-expansion behavior of the fuel element.

Metallic fuel elements have been used in the fast reactors EBR-I, EBR-II, EFFBR, and DFR. They have many attractive features for the fast-breeder application, but it seems questionable whether satisfactory resistance to radiation damage can be achieved, at least with plutonium-uranium elements.

In the United States the use of metal fuel has been coupled with the concept of pyrometallurgical processing of the fuel, and the EBR-II plant includes facilities for such processing and on-site remote fabrication by casting techniques. Although there are still large uncertainties in the costs of these processes for a large-scale plant—as indeed there are also uncertainties in the costs of processing and fabrication of oxide fuels for the fast breeder—the current U. S. paper on fast-breeder fuel economics[29] does not forecast substantial cost advantages for them. Consequently it appears that the exposure goals for the metal fuels must lie at least as high as 40,000 to 60,000 Mwd/ton, or, roughly, 4 to 6 at.% burnup.

The uranium-fissium* alloys show at least some encouraging performance under irradiation: at 600°C, for example, uranium–5 wt.% fissium alloy shows a swelling rate of about 8% volume increase per atomic percent burnup.[30] However, uranium-plutonium-iron alloys swell badly even at relatively low temperatures. The alloy uranium–20 wt.% plutonium–10 wt.% fissium, for example, increases about 20% in volume per atomic percent burnup at an irradiation temperature of 400°C (Ref. 30). It has been found possible, however, to restrain the swelling by the use of sufficiently strong jackets on the metallic fuel. Once the fuel swells to the point that it begins to press against the jacket, the internal pressure generated within the fuel by fission gases must be resisted, essentially by the strength of the jacket alone. The exposure lifetime then depends on the tensile strength of the jacket material, the diameter and thickness of the jacket, and the fractional void volume built into the element as an allowance for radial swelling. In its simplest form such an element is conceived as a rod of the fuel material inside a tube of the cladding material, with a sodium-filled annular space (initially) between fuel and jacket. Figure IX-5 shows the calculated effects of cladding-wall thickness and radial clearance (given in terms of the inner diameter of the jacket for a constant fuel diameter) on the achievable burnup for uranium-plutonium-iron elements.

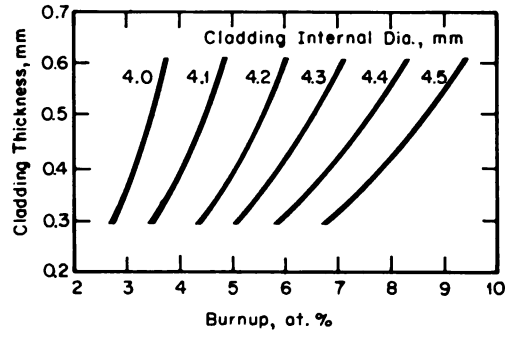

Fig. IX-5 Calculated effect of cladding thickness and internal diameter on the achievable burnup in 3.65-mm diameter uranium-plutonium-fissium alloy rods under EBR-II temperature conditions. A maximum allowable cladding stress of 30 kg/mm² was assumed.[30]

Thorium-rich thorium-uranium alloys show relatively good resistance to radiation-induced swelling, even at temperatures up to 750°C. Although irradiation results are not available at high temperatures for thorium-plutonium alloys, the few results that have been obtained at 450°C are promising.[30]

Although stainless steel was used as the fuel-jacket material in EBR-I, it has the undesirable property of forming a eutectic alloy with uranium, of relatively low melting point. As jacket materials for uranium metal, the nickel-base alloys have the same drawback. Of the refractory metals that do not present this problem, only vanadium appears completely satisfactory as an alloy base with respect to corrosion resistance and nuclear properties.[26] Currently, an alloy of vanadium–20% titanium appears very promising. Its fabrication into high-quality thin-walled tubing is difficult, however.

In the DFR, metallic fuel elements have been used in a number of design variations, but basically the elements consist of annuli of

*The term "fissium" is used to designate the mixture of fission products, comprising molybdenum, ruthenium, technetium, palladium, zirconium, rhodium, and niobium, left in the exposed fuel after pyrometallurgical processing.

Digitized by Google

uranium alloy with strong inner and outer jackets of niobium, originally designed to restrain swelling. The outer diameter of the annular element is approximately 0.75 in. The thicknesses of the fuel annuli have been varied during the development of the elements. The elements currently in the reactor use uranium–20 at.% molybdenum as the fuel alloy, with annuli 0.10 in. thick for the central region of the reactor core and 0.13 in. thick for the peripheral core regions. The elements are vented to allow those fission gases which may be released by the fuel to escape to the coolant. Irradiation tests have shown that the temperature of this fuel should be limited to 650°C if rapid swelling is to be avoided. Furthermore, it has been found that there is a lower temperature range, from 480 to 580°C, where rapid swelling of uranium-molybdenum alloys can occur during irradiation because of a transformation of the metastable gamma phase to alpha-plus-delta phases. If the fission density is high enough, however[30,31] [above 8×10^{13} fissions/(cm^3)(sec)], the formation is suppressed and irradiation stability does not suffer. One of the design goals therefore was to hold the fuel temperature below 480°C so long as the fission density is below 8×10^{13} fissions/(cm^3)(sec). The DFR experience has shown that these elements will operate satisfactorily up to a burnup of 1.2%, the maximum yet experienced, and probably considerably higher. These results are for a peak specific power of 205 watts/g. The niobium jacket material has shown some incompatibility with the sodium coolant. It has absorbed hydrogen from the coolant with resulting severe embrittlement when the jacket temperature is reduced to a low value. There is, however, a brittle-ductile transformation at 150 to 200°C, and therefore the properties are not impaired at operating conditions.[31] There is some corrosion of the niobium which is attributed to oxygen. The oxygen level in the DFR coolant has been about 10 ppm. A jacket temperature limit of 480°C is currently imposed on the elements to avoid this corrosion.

If metallic fuel bodies could be counted on to retain their structural integrity, they would offer the favorable property of a substantial negative component of the power coefficient of reactivity due to axial thermal expansion. Although this is probably the case early in fuel lifetime, it is questionable whether the property is retained after long exposure. In particular, if the jacket is relied upon to restrain fuel swelling, it seems improbable that the fuel would expand axially in proportion to its temperature and its normal temperature coefficient of expansion. Rather, it might be expected that the axial expansion would be governed by the jacket temperature, which is relatively insensitive to changes in power level. Compared to the ceramic fuels, the metallic fuels are unlikely to provide a large reactivity sink due to the Doppler effect before the fuel temperature rises to the point of fuel-element failure. This is particularly the case if the jacket material can form a low-melting eutectic alloy with the fuel.

The carbide fuels have been discussed briefly in the preceding paragraphs, primarily in connection with sodium-cooled thermal reactors. When these fuels are considered for fast reactors, interest is concentrated on the mixed uranium-plutonium carbides and on performance at very high levels of burnup. To date the irradiation results on uranium-plutonium carbides appear to be relatively few and to be limited to exposure levels of 30,000 Mwd/ton or lower.[12,28] However, the results have been encouraging and suggest that, at any given temperature, the rate of fission-gas release from carbide fuel is similar to or less than that from oxide.[28] If the temperature limits of the carbide are indeed comparable to those of the oxide, the carbide should allow the use of much more massive fuel-element designs, because of the high thermal conductivity of the carbide.

It appears that, for the fast reactor application, there may be considerably more emphasis on attaining the nominally stoichiometric composition of the monocarbides. It is pointed out in Ref. 28 that a more appropriate description of the desired composition is that of a single-phase alloy, since there may be small quantities of oxygen and nitrogen present as well as carbon. The desired composition is one in which the sum of the concentrations of oxygen, nitrogen, and carbon is close to 50 at.%. The hypostoichiometric (uranium-rich) compositions are to be avoided because it is believed that the accumulation of fission gas in any free metal that may be present will determine the swelling rate of the fuel body. The hyperstoichiometric compositions show poor compatibility with the common jacket materials

Digitized by Google

because of the transfer of carbon from the fuel body to the jacket.

The good conductivity of the carbide makes it worthwhile to consider elimination of the thermal resistance of the fuel-jacket gap through the use of some kind of thermal bonding. Sodium bonding may be used, but it accentuates the transfer of carbon from hyperstoichiometric carbides to the jacket. In the United Kingdom some development is being carried out on the metallurgical bonding of carbide fuel to the jacket.[28] There has been some success with copper- and nickel-based brazing alloys as the bonding material between uranium carbide and steel jackets, but there is some problem of cracking of the carbide under thermal cycling in the bonded elements.

Another approach to the fast reactor fuel problem is through the use of cermets. These are dispersions of fuel materials (fissile or fissile plus fertile) in ceramic form in a metallic matrix. The ceramic is usually the oxide of the fuel material. The basic concept is to take advantage of the irradiation stability of the ceramic while approximating the thermal conductivity and mechanical properties of a metal. It is desirable that the size of the ceramic particles in the dispersion be sufficiently large that only a small fraction of the fission gas can escape from the particles by fission recoil.

One of the main disadvantages of the cermets is that the ceramic component cannot usually be made to constitute the major fraction of the total material. Therefore, if both the fissile and fertile components of the fuel mixture are incorporated in the ceramic form, the amount of fertile material that can be incorporated is severely limited. This means that the internal breeding ratio of the reactor will be low, that the reactor will tend to lose reactivity rapidly with burnup, and that this reactivity loss must be taken care of either by strong control elements or by frequent partial refueling. The possibility of avoiding this difficulty by using the fertile element as the metal matrix and incorporating only the fissile element in the ceramic form is referred to in Ref. 26. This appears to be an attractive possibility from the point of view of nuclear performance, but restriction of the choice of the metal matrix to uranium, and possibly thorium, is a severe metallurgical limitation. Apparently there has been no extensive work on this concept.

The British have under way a program on cermet fuels[32] which is directed primarily toward the development of a fast reactor element and which has concentrated on the use of oxides in a steel matrix. The fissile and fertile materials are mixed in the oxide form, and the problem of achieving an acceptably high fertile content is attacked simply by attempting to use the highest possible oxide content in the cermet. The practical limit of oxide content appears to be about 50 vol.%.

The British experience has shown that, although the cermets can be formed by pressing and sintering the metal-oxide mixture, the densities attainable by this process alone are no higher than about 85% theoretical and that mechanical working is necessary to attain higher densities. Both hot rolling and hot swaging have been used for densification. Pin type elements are produced by mixing the oxide and steel particles, cold pressing into pellets and sintering at 1100 to 1300°C, sealing the pellets into a steel tube, and swaging at a temperature between 1000 and 1300°C (Ref. 32). Conceptually the objective in fabrication of the cermet is to produce an assemblage of oxide granules, each surrounded by a small, steel pressure vessel, and the whole bonded together as a structure. It is fairly obvious that this objective will be promoted if the oxide granules are spherical in shape, and the process does include the use of such granules. The spherical particles are produced by first pressing the oxide into green compacts about 1 cm in diameter with aluminum sterate binder. The green pellets are broken down to granules and sized, and the granules are spheroidized by abrasion in a gyrating dish coated with silicon carbide powder. The spherical particles are sintered at a peak temperature of 1600°C in an atmosphere of cracked ammonia. A further improvement in the cermet has been made by coating the sintered oxide spheroids with an organic binder that makes them sufficiently sticky to cause a layer of stainless-steel powder to adhere to each particle before the cermet is pressed. The material preferred for the metal matrix is type 316L (low carbon) stainless steel.

Plate type dispersion elements have been made by processes analogous to those used for the pins but with hot rolling substituted for the swaging process. Cermets have been made with both uranium oxide and plutonium-uranium oxide

Digitized by Google

mixtures and have been irradiation tested. The results with the plutonium fuels have not been as good as those with uranium, but the irradiation program has necessarily lagged behind the fabrication development, and the latest improvements have not yet been thoroughly tested. Results[32] to date suggest that the fabrication technology is capable of producing cermet plates and pins with 30 to 50 vol.% ceramic that will achieve a burnup of at least 10% heavy atoms without failure when the surface temperature is about 625°C.

Current Status and Future Directions

The fast reactors currently in operation or definitely planned are listed in Table IX-9. Since the Second Geneva Conference, reactors that have contributed new operating experience at substantial power levels are the British DFR[7] and the Russian BR-5.[8] In the United States the EBR-I continued in operation, and its latter-day operation was directed primarily to the rather specialized, but necessary, investigation of dynamic characteristics. These EBR-I results have been covered rather thoroughly in *Power Reactor Technology* in the past.

The escalation of power of the DFR to the design value of 60 Mw(t) was a long, troublesome process, which covered the time period from early 1960 to July 1963. It yielded, however, much useful information on sodium technology and metallic fuels.[33] The early problems had mainly to do with the entrainment of gas in the coolant and with the removal of gross impurities from the primary coolant system. The latter problem was finally solved by the use of hot-dumping operations in addition to the more usual cold-trapping processes. A "hot dump" consisted of heating the primary coolant to 250 to 300°C, transferring it to the dump tanks, cooling it to 80°C, and then returning it to the primary system through a filter. Twelve of these dump sequences were used after the fuel had been removed from the reactor.

A more fundamental obstacle to power escalation was the fuel performance, and full power was attained only after the original fuel elements had been replaced by redesigned elements. The original concept for the annular elements had been to accept a fuel alloy of relatively poor swelling resistance, to restrain the radial swelling by the walls of the element, and to accommodate the volumetric swelling by allowing the fuel material to extrude axially within the confines of the element walls. Early experience showed, however, that the axial extrusion was opposed by frictional forces great enough to exceed the creep strength of the jacket. Redesign of the element involved the substitution of a fuel alloy of higher swelling resistance (uranium–20 at.% molybdenum), reduction of the thickness of the fuel annulus to limit the maximum alloy temperature to 650°C, and the provision of a larger fuel-jacket clearance to allow for more radial swelling. The limit on the alloy temperature and a 480°C limit imposed on the jacket temperature to avoid corrosion have prevented attainment of the design value of coolant outlet temperature. It is suspected that the corrosion of the niobium jacket is accelerated by some impurity in the coolant, possibly carbon, which may be eliminated with time.

Although a number of problems had to be overcome to attain full power, all of them were recognized long before they resulted in operating difficulties, and operation has been smooth and without untoward incident within the recognized limits of the plant. The reactor is continuing operation and is being used extensively for the irradiation of improved fuel elements.

The BR-5 reactor, although much smaller than the DFR, has given valuable results on the behavior of plutonium oxide fuel elements, as well as information (discussed earlier) on the behavior of fission products in sodium systems.

The steel-jacketed, oxide fuel elements of BR-5 are described in Table IX-10. The reactor core operates at an average power density of about 300 kw/liter. The initial fuel loading of plutonium oxide elements operated to an average burnup of 2.4% of the plutonium before any evidence of fission-product leakage was detected. Thereafter the reactor operation was continued, with increasing evidence of fission products in the primary coolant and finally with plutonium alpha activity in the coolant, but without operating difficulty, to a maximum burnup of 5% (see Table IX-1). During this period the primary coolant outlet temperature had been raised from the initial 400 to 450°C level to 500°C. Thereafter the fuel assemblies containing gross failures were replaced by new assemblies of UO_2, and operation was continued at lower temperatures (outlet temperatures of

Digitized by Google

Table IX-9 FAST REACTORS IN OPERATION, OR UNDER CONSTRUCTION, OR DEFINITELY PLANNED*

Reactor	Country	Power, Mw(t)/Mw(e)	Status	Fuel	Remarks	Reference
Rapsodie	France (with Euratom)	20/none	Being built; full power expected before end of 1967	PuO_2-UO_2 pressed and sintered pellets, 5.7 mm in diameter, in 316L S.S. cans with 0.45-mm wall	The French program is directed toward 1000-Mw(e) fast breeders. It is expected that an intermediate size plant of 80 Mw(e) will be needed between Rapsodie and the large plants.[14] A large critical experiment (Masurca) and a source-calibration pile (Harmonie) are also under construction at Cadarache	34 34
DFR	U. K.	60/14	Operating at full power since July 1963	U–20 at.% Mo alloy in Nb jacket	The reactor is being used primarily to investigate the behavior of various Pu-based fuels and canning materials. The construction of a prototype large enough to demonstrate the core and fuel characteristics for a 1000-Mw(e) commercial plant is planned by the U. K.; this should be on power soon after 1970.[13] Two large critical assemblies are used in the U. K. program, Vera and Zebra [19]	7 33
BR-5	USSR	5/none	Operating at full power since July 1959	PuO_2 in S.S. jackets (See Table IX-10)	The previously announced BN-50 reactor has been eliminated from the USSR program, but plans have been announced to construct the BOR reactor, a 50- to 60-Mw(t) experimental fast reactor. Critical experiments for large dilute reactors are carried out at the "BFS"-stand [21]	8
BN-350	USSR	1000/350	Definitely planned but schedule not announced	PuO_2 in S.S. jackets (See Table IX-11)		11
EBR-II	U. S.	65/20	Critical November 1963. Power escalation under way	0.144-in. U-Fs alloy rods in type 304 S.S. jackets, Na bonded	Although the U. S. has a large program directed to the development of large fast breeders, no commitment has yet been made for the construction of a prototype. The program includes critical experiments on two facilities (ZPR-III and ZPR-VI)[20] and fuel-meltdown studies with the TREAT reactor.[25] Two experimental reactors are under development: FARET, primarily for the test of fuel systems at high temperature, and SEFOR, a 20-Mw(t) developmental reactor using PuO_2-UO_2 fuel[35] (the latter project has participation also by Gesellschaft für Kernforschung mbH and Euratom)	9
EFFBR	U. S.	300/100	Critical August 1963. Power escalation under way	0.158-in. U–10% Mo rods clad with metallurgically bonded Zr cladding		

*This table lists only the reactors that were discussed at the Conference. It does not include some of the older reactors, such as EBR-I.

Digitized by Google

Table IX-10 CHARACTERISTICS[36] OF FUEL ELEMENTS AND ASSEMBLIES IN THE FIRST LOADING OF BR-5

Fuel element	
Type	Rod
Fuel	Sintered plutonium oxide pellets
Jacket material	Stainless steel, type IX18H9T
Jacket outside diameter/ thickness, mm	5/0.4
Fueled length, mm	280
Thermal expansion space (at top of fueled section), mm high	2 to 3
Filling gas	Helium at atmospheric pressure
Fuel assembly	
Type	Hexahedral stainless-steel tube
Dimensions, mm	26, between parallel sides; 0.5, wall thickness
No. fuel elements per assembly	19
Method of supporting elements in assembly	Top and bottom grids

300 to 430°C) and various power levels to study the effects of fission-product contamination of the primary circuit. By Mar. 1, 1964, the maximum burnup in the original plutonium oxide elements that were still in the core was 5.8%.

At the time of fuel-assembly replacement, all assemblies were tested by pumping gas from them and checking it for radioactivity. Some showed activities thousands of times greater than the average. These were discarded (18 out of a total of 81) and replaced by the new UO_2 assemblies. The following quotation from Ref. 8 describes the condition of elements from the "discarded" and "undiscarded" assemblies:

> ...Two of the discarded subassemblies with a 4.9% burnup (one was processed with steam) and one subassembly with a 5% burnup out of the undiscarded were examined in the hot laboratory. Longitudinal cracks 8–10 cm long and up to 1.0 mm wide were detected on the surface of some elements of these subassemblies. The cracks, as a rule, continued in the plutonium dioxide. Mostly radial cracks were observed on the surface of cross sections of the disintegrated elements. No central cavities were found in any of the disintegrated elements. In the third subassembly examined all the elements turned out to be tight, the element canning was in good condition: the element surface was light-colored and bright and there were no visible defects.

In late 1964 and early 1965 it is planned to load the BR-5 with uranium monocarbide fuel. It is stated in Ref. 8 that the operation of the BR-5 reactor has already confirmed the practical feasibility of the reactor type for industrial installations. The announced decision[11] to bypass the previously planned 50-Mw(e) commercial plant BN-50 in favor of pushing on directly to the large 350-Mw(e) plant (BN-350) appears to be in harmony with this point of view. However, Ref. 11 also announces a project to construct a "fast pilot reactor," designated BOR, for general development work leading to large fast breeders. This reactor, of thermal capacity 40 to 60 Mw, will test advanced concepts and operating conditions: power densities up to 1500 kw/liter, sodium outlet temperatures to 630 to 650°C, and fuel burnup to 10% with thin-walled fuel elements that allow fission-gas leakage to the coolant. This suggests that the elimination of the "commercial" BN-50 may have been the result of a decision that the effort could be spent more effectively on a reactor of more experimental nature.

With the beginning of operation of EBR-II and the EFFBR, fast reactor progress in the United States should accelerate. Neither of these plants can be considered the prototype of an economic commercial fast breeder. Although the EFFBR will operate as a utility station, its fuel is far from satisfactory even on a nonrecycle basis. The shortcomings of the fuel have restricted the operating power level, in a manner reminiscent of the early DFR experience. The situation is summarized in the following quotation from Ref. 9:

> The present core was de-rated from 300 to 200 MW(t) because of an increase in the estimated pressure drop across the core resulting from a change in the fuel element support arrangement (see Fig. 6, P/2427). Experimental data obtained subsequent to this decision show that the pressure drop will be only 40 psi at 200 MW(t) whereas the subassembly and internals are capable of operating at 65 psi. A higher power level, therefore, is possible but cannot be justified economically because of the burnup limitation on the U–10 w/o Mo fuel alloy. As described in another paper, this alloy has not proven to have the irradiation damage resistance which early results suggested. It has been found that the allowable burnup decreases with increasing fuel temperature. Therefore, after demonstration of 200 MW(t) operation, it is planned to operate at an inlet sodium temperature of 450°F and at a power level of 110 MW(t) which is estimated to double the allowable burnup. Although these conditions are uneconomical for electric power generation, it will extend the fuel life of the two core loadings now on hand and permit use of

Digitized by Google

the reactor as a test bed for irradiation of experimental fast reactor fuels. Plans are proceeding to utilize the reactor initially for this purpose.

Although the British hope to have a prototype of a commercial fast reactor on power soon after 1970, the date is contingent on the development of a satisfactory fuel and decisions as to the main reactor design features.[13] Apparently only the USSR is committed far enough to a prototype (BN-350) at this time to announce its general features. These are summarized in Table IX-11. However, the construction schedule for the plant appears to be somewhat flexible, and it is not clear whether the current concept has lasting significance.

Table IX-11 CHARACTERISTICS OF THE BN-350 REACTOR[11]

Thermal power, Mw	1000
Core volume, approx., liters	2000
Average power density, kw/liter	500
Sodium volume in reactor vessel, m^3	165
Primary sodium temperature inlet/outlet, approximate, °C	300/500
Maximum sodium velocity in core, m/sec	10
No. of core fuel assemblies	211
No. of blanket assemblies	500
Axial and radial blanket thickness, cm	60
Core diameter/height, m	1.5/1.06
Sodium volume fraction in core, %	39
Fuel	Plutonium and uranium dioxide mixture (19% Pu)*
Critical mass, kg of Pu	780 (or 950 kg ^{235}U)
Fuel element	Rod type; oxide pellets in stainless-steel tube, as in BR-5†
Diameter/thickness of jacket tube, mm	5/0.4
Fuel assemblies	96 mm hexagons with wall thickness of 2 mm
No. of fuel elements per assembly	217
Method of spacing elements in assembly	Top and bottom grids plus ribs on element jackets
Breeding ratio, total/internal	1.5/0.62
Rate of reactivity loss, % k_{eff}/month	0.62 (one month gives about 0.5% burnup)
Control rods	Assemblies similar to fuel assemblies with enriched B_4C in place of fuel

*The first loading may employ enriched UO_2 (23% ^{235}U).
†It is stated that the average oxide density will be lower than in BR-5 to accommodate fission gases.

The key question in predicting the course of fast-breeder development is the selection of fuel type. Although the early experience has been predominantly with metal fuel, that experience has not been highly encouraging even for uranium metal, and the prospects for plutonium appear considerably less favorable. On the basis of current knowledge, the oxides appear to be the surest bet as potentially acceptable fast reactor fuels. The carbides, however, have inherent advantages in thermal conductivity and density, and it is primarily the lack of experience with them that puts them in a less favored position. It is, of course, conceivable that a number of acceptable fast breeders might be developed utilizing different basic fuel types. But for the moment it would be encouraging to be able to verify the completely satisfactory performance—in relation to breeding ratio, reactivity coefficients, and reactivity lifetime, as well as to the more obvious criteria such as fuel lifetime and fabrication cost—of any one fuel. Because of the growing interest in oxide fuels, the coming operation of Rapsodie in France[34,37] and of the Southwest Experimental Fast Oxide Reactor (SEFOR) in the United States[35] will be awaited with interest.

In whatever direction the fuel development goes, considerations of reactivity coefficients are expected to have an important influence on the design of large fast breeders. In particular, there will be efforts to attain a negative value for the sodium-void coefficient of reactivity or minimize its positive value and to provide as large a sink of reactivity in Doppler effect as possible. The effects of these considerations on reactor design are discussed in Ref. 24 and were reviewed at length in *Power Reactor Technology*, 7(2): 107-144.

Partly because of the difficulty with the sodium coefficient of reactivity and partly to circumvent problems and difficulties in sodium technology, some groups have investigated other coolants for fast reactors. The Karlsruhe proj-

Digitized by Google

ect is investigating cooling by helium and dry steam as well as by sodium,[38] and papers on gas cooling[39] and steam cooling[40] were also presented at the Conference by Swiss and Belgian groups, respectively. The latter is a direct-cycle system that utilizes dry steam as the reactor coolant. Part of the superheated steam from the reactor exit goes to the turbine, and another appropriate fraction is directed to a Loeffler boiler where it is quenched in the boiler water and produces dry saturated steam to feed the reactor inlet.

One of the problems with less efficient coolants is to design for the characteristic high specific power of the fast reactor. This may be not so much a problem of normal cooling as of emergency shutdown cooling, particularly upon loss of coolant pressure. In the gas-cooled concept[39] it is proposed to use water injection as a last-ditch emergency measure. Criticality can be avoided under these conditions by incorporating resonance absorbers in the reactor core. This would be relatively ineffective in the normal "fast" neutron spectrum but would absorb strongly if the spectrum were degraded by water injection. The problem sounds like a difficult one.

References

The references that contain A/Conf. numbers are papers that were presented at the Third United Nations International Conference on the Peaceful Uses of Atomic Energy, Geneva, September 1964.

1. O. E. Dwyer and R. N. Lyon, Liquid-Metal Heat Transfer, A/Conf.28/P/225.
2. V. I. Subbotin, P. A. Ushakov, P. L. Kirillov, M. K. Ibragimov, M. N. Ivanovsky, E. V. Nomophilov, D. M. Ovechkin, D. N. Sorokin, and V. P. Sorokin, Heat Removal from the Reactor Fuel Elements Cooled by Liquid Metals, A/Conf.28/P/328.
3. B. A. Nevsorov, V. V. Zotov, G. P. Fedortsev-Lutikov, D. M. Skorov, N. M. Beskorovagynii, Ju. S. Belomytsev, M. D. Abramovitch, E. V. Umnyashkin, V. A. Ivanov, V. E. Andreev, S. M. Golubenkova, V. K. Ivanov, E. I. Yakovlev, S. A. Iodkovskii, and N. M. Samarina, Corrosion Resistance of Constructional Materials in Alkali Metals, A/Conf.28/P/343.
4. D. H. Gurinsky, J. R. Weeks, C. J. Klamut, L. Rosenblum, and D. H. DeVan, Corrosion in Liquid Metal Systems, A/Conf.28/P/244.
5. C. Starr and S. Siegel, Sodium Cooled Thermal Reactors, A/Conf.28/P/206.
6. W. P. Kunkel, D. M. Elliott, and A. S. Gibson, In-Pile Experiments on Retention of Fission Products in 500°F Sodium, USAEC Report NAA-SR-9163, Atomics International, January 1964.
7. R. R. Matthews, J. L. Phillips, K. J. Henry, R. H. Allardice, D. M. Donaldson, and H. E. Tilbe, Performance and Operation of the Dounreay Fast Reactor, A/Conf.28/P/130.
8. A. I. Leipunskii, O. D. Kazachkovskii, M. S. Pinkhasik, N. N. Aristarkhov, M. S. Poido, A. V. Karpov, Y. P. Larin, I. A. Efimov, N. V. Krasnoyarov, B. S. Tymosh, M. P. Nikulin, D. I. Zhestkov, Y. A. Uralets, and V. I. Galkov, 5-Year Operation Experience on Reactor BR-5, A/Conf.28/P/312.
9. L. J. Koch, F. S. Kirn, G. W. Wensch, C. E. Branyan, and E. L. Alexanderson, Sodium Cooled Fast Breeder Reactors, A/Conf.28/P/207.
10. H. O. Monson, F. A. Smith, W. J. Hellett, and J. J. Morabito, Components for Sodium Reactors, A/Conf.28/P/228.
11. A. I. Leipunskii, O. D. Kazachkovskii, I. I. Afrikantov, M. S. Pinkhasik, N. V. Krasnoyarov, and M. S. Poydo, Sodium Cooled Fast Reactors, A/Conf.28/P/311.
12. H. Pearlman and R. F. Dickerson, Carbide Fuel Fabrication and Performance, A/Conf.28/P/234.
13. W. Penney, Nuclear Power in the United Kingdom, A/Conf.28/P/559.
14. G. Vendyres, The Fast Neutron Reactor Series in France, A/Conf.28/P/41.
15. N. M. Sinev, B. B. Baturov, and V. M. Shmelev, Trends of Nuclear Power Development in the USSR, A/Conf.28/P/294.
16. R. Avery, H. H. Hummel, R. N. Hwang, D. Meneghetti, P. A. Moldauer, A. B. Smith, P. Greebler, and J. B. Nims, Physics of Fast Reactors, A/Conf.28/P/259.
17. A. I. Leipunskii, O. D. Kazatchkovskii, M. V. Troyanov, N. V. Krasnoyarov, M. G. Kulakovskii, V. B. Lytkin, V. I. Matveev, V. M. Murogov, A. I. Novozhilov, L. M. Usatchev, N. M. Shagalin, and S. B. Shikhov, Some Physics Calculations on the Performance of Fast Power Reactors, A/Conf.28/P/369.
18. D. C. G. Smith, K. W. Brindley, D. Tait, and R. C. Wheeler, The Physics of the Dounreay Fast Reactor at Power, A/Conf.28/P/173.
19. R. D. Smith, A. R. Baker, E. P. Hicks, J. E. Mann, J. L. Rowlands, D. C. Smith, and J. Weale, Fast Reactor Physics, Including Results from U.K. Zero Power Reactors, A/Conf.28/P/166.
20. F. W. Thalgott, J. K. Long, W. G. Davey, W. Y. Kato, S. G. Carpenter, H. A. Morewitz, and G. H. Best, Fast Critical Experiments and Their Analysis, A/Conf.28/P/265.
21. A. I. Leipunskii, I. I. Bondarenko, O. D. Kazachkovskii, L. P. Abagyan, Yu. S. Aborin, N. O. Bazazyants, G. A. Batirbekov, V. V. Bondarenko, A. I. Voropaev, V. I. Golubev, E. F. Efimov, Yu. S. Zamyatkin, A. V. Zvonarev, V. P. Zinovyev, M. N. Zyzyn, V. V. Ivanov, N. V. Krasnoyarov, N. N. Krot, M. Ya. Kulakovskii, V. G. Liforov, V. F. Mamontov, B. K. Maslennikov, V. I. Matveev, V. N. Morozov, M. N. Nikolaev, M. Yu. Orlov, V. A. Parfyonov, V. V. Penenko, V. E. Ridkii, V. A. Semyonov, G. N. Smirenkin, A. P. Smirnov-Averin, V. P. Sokolov, M. F. Troyanov, O. P. Uznadze, F. I. Ukraintsev, L. N. Usachev, and N. N. Shagalin, Experimental Studies on Fast-Neutron Reactor Physics, A/Conf.28/P/368.
22. W. Häfele, K. Ott, L. Caldarola, W. Schikarski, K. P. Cohen, B. Wolfe, P. Greebler, and A. B. Reynolds, Static and Dynamic Measurements on

Digitized by Google

the Doppler Effect in an Experimental Fast Reactor, A/Conf.28/P/644.
23. J. Codd, J. E. Beardwood, D. C. Leslie, and H. M. Sumner, Studies of Resonance Absorption and the Doppler Phenomenon for Fast and Thermal Reactors, A/Conf.28/P/172.
24. D. Okrent, K. P. Cohen, and W. B. Loewenstein, Some Nuclear and Safety Considerations in the Design of Large Fast Power Reactors, A/Conf. 28/P/267.
25. W. J. McCarthy, Jr., C. E. Dickerman, A. E. Klickman, and R. B. Nicholson, Fast Reactor Safety Research, A/Conf.28/P/284.
26. R. E. Macherey, H. W. Alter, and A. A. Shoudy, Fabrication of Solid Fuels for Fast Reactors, A/Conf.28/P/238.
27. L. E. J. Roberts, P. Brock, J. R. Findlay, B. R. T. Frost, L. E. Russell, J. B. Sayers, and E. Wait, The Behaviour of UO_2 and of (U, Pu)O_2 Fuel Materials Under Irradiation, A/Conf.28/P/155.
28. L. E. Russell, B. T. Bradbury, H. J. Hedger, N. Parkinson, R. G. Sowden, and M. B. Waldron, Monocarbides as Reactor Fuels, A/Conf.28/P/154.
29. L. E. Link, G. J. Fischer, and E. L. Zebroski, Fuel Cycle Economics of Fast Reactors, A/Conf. 28/P/248.
30. J. H. Kittel, T. K. Bierlein, B. R. Hayward, and W. C. Thurber, Irradiation Behavior of Metallic Fuels, A/Conf.28/P/239.
31. S. A. Cottrell, E. Edmonds, P. Higginson, and W. Oldfield, Development and Performance of Dounreay Fast Reactor Metal Fuel, A/Conf.28/P/150.
32. B. R. T. Frost, L. H. Cope, J. B. B. Lambert, H. Lloyd, W. Long, J. E. Manson, and P. G. Mardon, Fabrication and Irradiation Studies of UO_2-Stainless Steel and (U,Pu)O_2-Stainless Steel Cermets, A/Conf.28/P/153.
33. J. L. Phillips, Achievement of Full Power Operation of the DFR, *Nucl. Eng.*, 9(92): 10-16 (January 1964).
34. G. Vendryes, Rapsodie, A/Conf.28/P/42.
35. W. Schnurr and J. R. Welsh, The SEFOR Reactor—Aspects of International Cooperation, A/Conf.28/P/533.
36. A. I. Leipunsky, V. G. Gravin, N. N. Aristarkhov, I. I. Bondarenko, O. D. Kazachovsky, O. L. Lubimtsev, S. A. Pashkov, M. S. Pinkhasik, K. K. Renne, U. Y. Stavissky, F. A. Ukraintsev, and L. N. Usachev, Experimental Fast Reactors in the Soviet Union, in *Proceedings of the Second United Nations International Conference on the Peaceful Uses of Atomic Energy, Geneva, 1958*, Vol. 9, pp. 348-357, United Nations, New York, 1958.
37. R. Abdon and M. Chaigne, Predicted Dynamic Behaviour of Rapsodie, A/Conf.28/P/79.
38. W. Häfele, K. H. Beckurts, E. Bojarsky, P. Engelmann, A. Jansen, K. Kummerer, A. Müller, K. Ott, K. E. Schroeter, D. Smidt, H. H. Vogg, and E. Windbühl, The Karlsruhe Fast Breeder Project, A/Conf.28/P/539.
39. P. Fortescue, R. Shanstrom, L. Meyer, W. Simon, and P. Fischer, Gas Cooling for Fast Reactors, A/Conf.28/P/694.
40. G. Tavernier, J. Chermanne, C. Descamps, M. Egleme, E. Fossoul, E. Jonckheere, J. Morelle, M. Stievenart, L. Tollet, and J. Van Dievoet, "HERMES" Fast Neutron Superheater Reactor, A/Conf.28/P/516.

Digitized by Google

Section

X

Power Reactor Technology

Maritime Reactors

Of the two nuclear-powered ships that are in operation, only the icebreaker *Lenin* was formally discussed at the Conference.[1,2] Other papers concerned the nuclear plant for the German nuclear-powered vessel *Otto Hahn*[3] and design studies of the VULCAIN[4–6] and NERO[7] reactors for marine propulsion.

The icebreaker is powered by three pressurized-water reactors, each capable of producing 90 Mw(t), although the vessel can be operated at design conditions with only two of the three reactors operating. The core of each reactor consists of 219 fuel assemblies arranged as shown in Fig. X-1. Each assembly is composed of 36 fuel pins fabricated of UO_2 pellets clad with zirconium alloy tubing having an outside diameter of 6.1 mm and a thickness of 0.75 mm. The fuel pins are contained in a flow tube that is fabricated of zirconium alloy, bearing ^{10}B as a burnable poison. The amount of poison is varied from tube to tube to reduce the radial power-peaking factor. The reactor is equipped with safety and control rods as well as a so-called "compensation system." Although details of the construction of these control components are not given in Ref. 1, a paper from the Second Geneva Conference[8] may be consulted for additional information.

Each reactor of the *Lenin* is equipped with two coolant loops, each containing a steam generator, two main circulating pumps, an emergency circulating pump, two electrically heated pressurizers, and an ion-exchange filter. Figure X-2, which is a photograph of part of the Russian exhibit, illustrates the reactor compartment of the ship. Although call-outs are not provided, the reader can see the positions of the three reactors in the center of Fig. X-2 as evidenced by their control- and safety-rod "thimbles" protruding above the upper shield structure. The six main coolant pumps and a cutaway showing one of the steam generators can be seen at the left. The loops are designated "bow" or "stern" loops in the reference, the reactor compartment in Fig. X-2 being arranged with the center line of the pumps in a fore-aft orientation. Table X-1 lists additional operating data for the reactors.

In general, the operation of the *Lenin* has been "quite successful." Much of the success perhaps results from the fact that the icebreaker application approximates an "ideal" application of nuclear energy. The vessel became operational in December 1959 and operated on its first fuel for over 11,000 hr, producing about 450,000 Mw(t)-hr. The average burnup reached about 12,000 Mwd per ton of uranium, with peak burnup reaching about 30,000 Mwd per ton of uranium. Refueling was done in the spring of 1963, and in May 1964 the vessel was operating with the second fuel charge. In 1961 the self-regulation of the reactor was demonstrated using the Doppler effect to com-

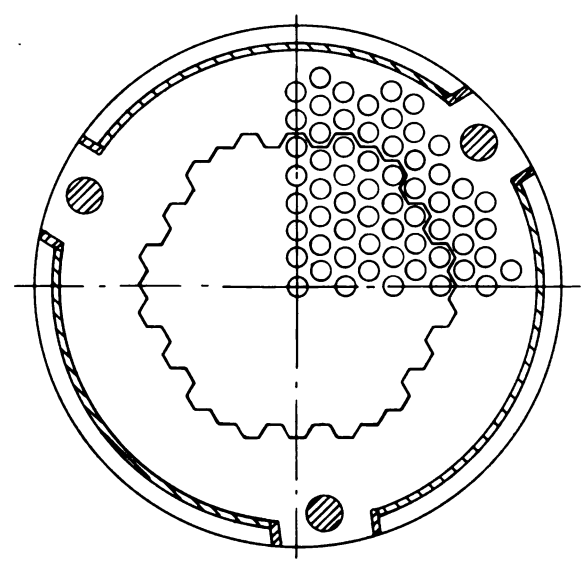

Fig. X-1 Lenin *reactor core cross section.*[2]

Digitized by Google

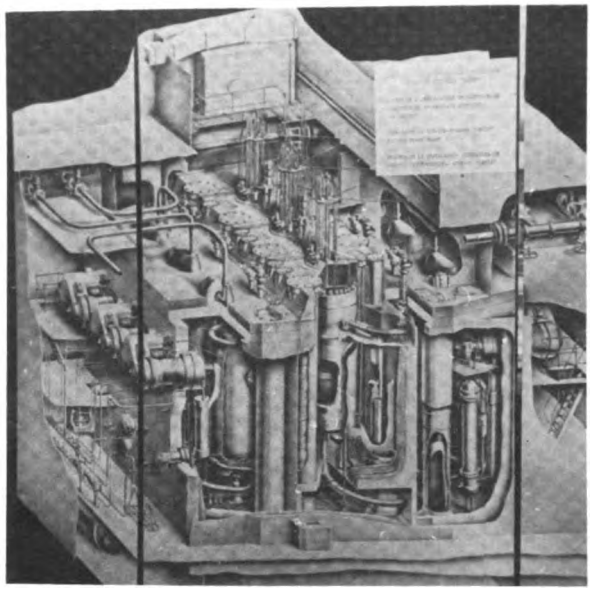

Fig. X-2 Photograph of part of the Russian Geneva exhibit illustrating the reactor compartment of the Lenin.

pensate for load changes. The primary components of the plant operated about 15,000 hr (including the year 1963) at working pressure (180 kg/cm^2). The main circulating pumps have operated up to about 8500 hr without inspection, although some pumps apparently have failed owing to shorting of the stator windings.

The primary circuit components that are permanently or periodically filled with potentially contaminated water are accommodated in the so-called "central compartment" of the plant. In Fig. X-2 this probably consists of the compartments containing the reactors and steam generators, and these compartments are hermetically sealed from the rest of the ship and ventilated separately. Some leakage has been experienced from the primary system. Reference 2 notes that this has come from the packing of various valves in the primary circuit. Contamination from fission gases and long-lived fission products is reported to be low.

Table X-1 OPERATIONAL DATA FOR THE *LENIN* REACTORS[2]

	Designed values for 65 Mw	Operation data for reactors 1, 2, and 3*		
Water flow in primary circuit loops, tons/hr	415	435/430	458/467	435/453
Reactor outlet temperature for loops, °C	317	311/311	312/313	311/313
Reactor inlet temperature for loops, °C	261	260	261	260
Steam output for loops, tons/hr	43.3/43.3	42/42	47/42	43/46
Steam pressure, kg/cm^2	29	32/31	31.5/30.5	31/31
Steam temperature, °C	307	310/309	308/308	308/308

*Fraction numerators refer to bow loop and the denominators to stern loop.

Reference 9, although not specifically directed toward the *Lenin* reactors, pertains to a control system that might be uniquely applied to the reactor type. The essence of the system is a reactor in which the coolant is separated from the moderator; the *Lenin* reactors are of this type with their flow-tube design. The principles of the control system are contained in the following quotation:[9]

> Let us consider a reactor core formed by a regular lattice of cylindrical fuel elements placed in a liquid moderator, say in H_2O. Let the top ends of all elements be fastened in some plane thus that any of them can turn independently around the fastening point. Let, further, these elements pass freely through the spacer plate, the holes in it forming a grid similar to that of fastening points. The lattice and the form of the cylindrical reactor do not depend on the distance between the plane of joints (fastening points) and that of the spacer plate. Let the plate be rotated in the horizontal plane around the reactor central axis. Then the core will have the form of a one-sheet hyperboloid of revolution and the fuel element lattice will be deformed thus that the surfaces of the constant spacing will turn out to be, with a greater accuracy, ellipsoids of revolution having one focus with the hyperboloid that forms the side boundary.
>
> The reactivity dependence on the core spacing in a cylindrical reactor is not monotone, it has optimum. When the spacing increases reactivity rises first, and then falls. Therefore to control a reactor by means of the core deformation it is possible to use either the "left" branch of the curve corresponding to the core spacing less than optimum or the "right" one corresponding to the spacing greater than optimum.

The reactivity of a reactor controlled in the above manner was studied both analytically and experimentally, and the reference may be consulted for details.

The power plant for the German research ship *Otto Hahn* is described in Ref. 3. It will be a pressurized-water reactor (PWR) having the characteristics shown in Table X-2. The ship was launched in June 1964, and the time schedule calls for the reactor to be installed in 1966 with power operation to commence in 1967. The normal power of the propulsion plant is 10,000 shp.

Digitized by Google

Table X-2 MAIN DATA OF REACTOR INSTALLATION FOR THE SHIP *OTTO HAHN*[3]

Core	
Diameter of active zone, mm	1150
Height of active zone, mm	1120
No. of fuel elements	16
No. of control rods	12
Fuel elements (side length), mm	270
No. of fuel rods installed	3128
Fuel-rod diameter, mm	10.9
Fuel-rod cladding thickness, mm	0.33
Total surface, m^2	120
Core entrance temperature, °C	266
Core exit temperature, °C	278
Maximum thermal output, Mw	38
Average reactivity lifetime, Mwd/ton	7200
Maximum reactivity lifetime, Mwd/ton	14,000
UO_2 fuel loading, tons	2.95
Enrichment in four zones, %	~2.5, 2.9, 3.5, and 4.3
Average enrichment, %	~3.6
Surface heat release, kcal/(m^2)(hr)	272,000
Average fuel temperature over lifetime, °C	460–680
Hot-channel load at central fuel melting, %	172
Absorbing material in control rods	Boron carbide in steel
Burnable poison	ZrB_2-ZrO_2 pellets
Excess reactivity (cold, unpoisoned), %	15
Excess reactivity (hot, unpoisoned), %	7
Excess reactivity (hot, poisoned), %	4.5
Shutdown reactivity of control rods, %	25
Pressure vessel	
Operating pressure, ata	63
Inside height, mm	8580
Inside diameter, mm	2360
Wall thickness and plating, mm	50 + 5
Coolant circulation, kg/hr	2.37×10^6
Steam generator	
Operating pressure, ata	31
Steam temperature, °C	273
Superheat, °C	36
Tube diameter, mm	19.4
Tube wall thickness, mm	1.2
Material	Inconel
Containment vessel	
Height, m	13.1
Diameter, m	9.5
Wall thickness, mm	30
Design pressure, ata	14.5
Weight including reactor parts, tons	930

The German maritime reactor[3] incorporates some of the advanced techniques described in the review of the Consolidated Nuclear Steam Generator and the Unified Modular plant in the Fall 1963 issue of *Power Reactor Technology*, 6(4): 106-117. These include self-pressurization and location of the primary heat exchangers within the pressure vessel. In addition, the primary pumps are arranged quite close to the core, probably in a manner similar to that shown in Fig. VII-3 of the above-mentioned *Power Reactor Technology* article. The fuel elements are of square geometry with a four-zone-loaded core to achieve power flattening. The pressure vessel will be fabricated by circumferential welding of several forged rings.

The objectives of the VULCAIN program, which is a joint UKAEA–BelgoNucléaire effort, are quoted as follows:

(i) The basic nuclear physics and engineering design parameters of a compact, highly rated core capable of operating to a peak burn-up of 40/50,000 MWD/TeU.
(ii) The development and manufacture of a VULCAIN core, of 40 MW/thermal output, for loading into the Belgian BR3 reactor later in 1964. The BR3 reactor will then be operated with a mixed D_2O/H_2O moderator and coolant throughout the three years life of the core.
(iii) The engineering design of a compact steam-raising unit of 20,000/25,000 shp suitable either as a single unit for marine propulsion, or as a multi-unit for small land-based power stations.

The physics portion of the work is concentrated in critical experiments in the VENUS zero-energy program and will conclude in 1965. The BR-3–VULCAIN power experiment is concerned with irradiation of a core in the BR-3 reactor. The fuel assembly and a so-called "moderator tube" of the reactor are shown in Fig. X-3, and the core layout is shown in Fig. X-4. The moderator tubes come in two lengths; 14 of them are about 1.4 m long and the remaining four are about 2.4 m. The long tubes house hydraulically operated absorber rods, and 10 of the short tubes house absorber rods actuated by existing BR-3 magnetic-drive mechanisms. The remaining four short tubes are used for instrumentation, sample tubes, and neutron sources (Fig. X-4). Additional core data are given in Table X-3.

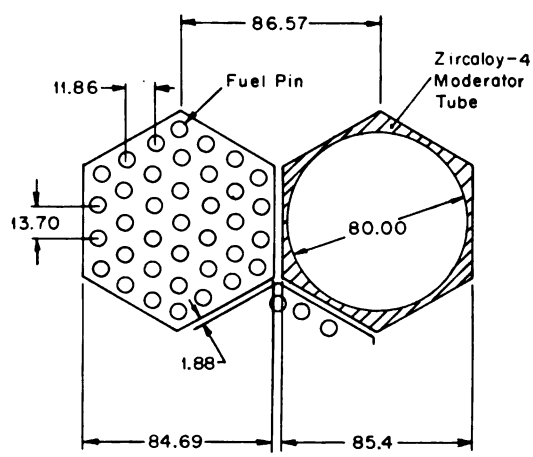

Fig. X-3 VULCAIN fuel assembly and moderator tube.[4] *(Dimensions are in millimeters.)*

Digitized by Google

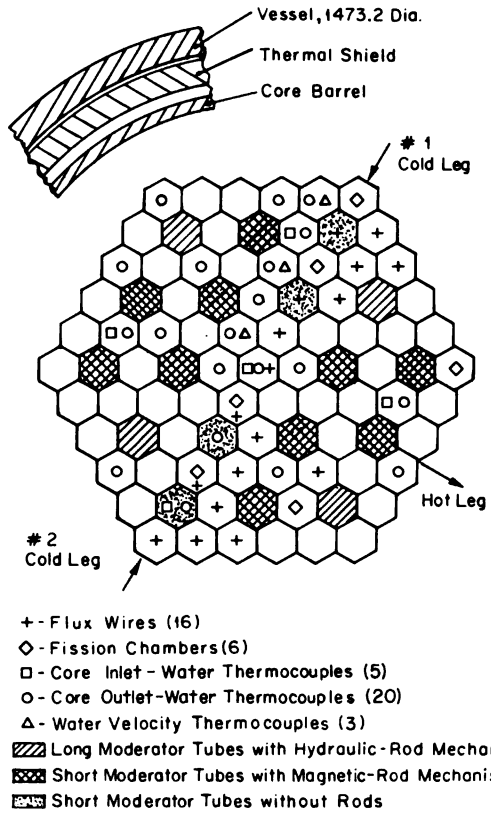
Vessel, 1473.2 Dia.
Thermal Shield
Core Barrel
1
Cold Leg
Hot Leg
2
Cold Leg
+ - Flux Wires (16)
◇ - Fission Chambers (6)
□ - Core Inlet - Water Thermocouples (5)
○ - Core Outlet-Water Thermocouples (20)
△ - Water Velocity Thermocouples (3)
Long Moderator Tubes with Hydraulic-Rod Mechanisms
Short Moderator Tubes with Magnetic-Rod Mechanisms
Short Moderator Tubes without Rods

Fig. X-4 BR-3—VULCAIN core cross section with in-pile instrumentation.[4]

The reactor normally will be operated without rods in the core and with the coolant containing about 85% D_2O at start of life. The burnup target is an average of about 25,000 Mwd per ton of uranium, and, as burnup proceeds, light water is added until the D_2O concentration is almost zero at end of life. The hydraulically operated absorber rods, described in Ref. 4, are located with their drives entirely within the pressure vessel. The operation is described as follows:

> In this type of hydraulic mechanism, the absorber rod moves up or stays in its top position because of the upwards flow inside the moderator tube created by the pressure differential between the tube inlet and the vessel outlet flow nozzle to which the top end of the tube is connected through a master valve. When the latter connects the tube top end with a higher pressure (vessel inlet flow nozzle), the moderator flow is reversed and the 10 kg rod drops into the core and stays there after being stopped by a dashpot in the bottom of the moderator tube. The H.P. and L.P. connections of the master valve are thus located entirely within the reactor vessel. The servo pressure actuating the spring-loaded master valve is transmitted by a pipe passing through the vessel collar from a pilot valve which is supplied by a high or low pressure to position the master valve for up or down movement of the rod, respectively. The system is thus fail safe, as failure of the servo-pressure, e.g., due to a pipe rupture, will cause insertion of the rod into the core.

The design of the VULCAIN reactor for marine propulsion also incorporates internal pressurization and integral heat exchangers. The design of the reactor is schematically illustrated in Fig. X-5. Provisions are made for gas pressurization, as well as self-pressurization, in order to reduce the in-core voids if desired.

The NERO reactor for ship propulsion was designed by the Reactor Centrum Nederland (RCN) in cooperation with Euratom. The NERO is a pressurized-water reactor having the characteristics shown in Table X-4. The reactor is a conventional PWR design with the exception of the primary flow loop. A system with internal recirculation, somewhat similar to that of a boiling-water reactor, is provided. The external primary flow is pumped to a ring of water ejectors located inside the reactor vessel in the downcomer region, and enough recirculating water is pumped to provide an internal circulation having about 1.5 times the mass flow in the external circuit. The reference states that the reason for this was to reduce the size of the external primary coolant system and still provide sufficient flow of coolant through the core in one pass. This design also provides a path for natural circulation entirely within the pressure vessel to facilitate emergency cooling. The NERO project

Table X-3 CORE DATA FOR THE VULCAIN–BR-3 POWER EXPERIMENT

Parameter	Value
Fuel material, mm	Dished UO_2 pellets
Outside diameter, mm	7.5
Fuel-cladding material	AISI 304 stainless steel
Thickness, mm	0.5
Active length, mm	1000
Total length, mm	1235
No. of pins/fuel element	37
No. of fuel elements/core	73
Absorber rod geometry	Tubular, unfollowed
Material	Unclad 18/16 stainless steel containing 2 wt.% natural boron
Inside diameter, mm	68
Outside diameter, mm	78
Length, mm	1035
Reactor power, Mw(t)	40.9
Coolant	D_2O-H_2O mixture
Pressure, kg/cm^2	140
Total core flow, m^3/hr	2500

Digitized by Google

has been under development since late 1961, when a contract was signed between RCN and Euratom. This contract covered critical experiments, irradiation studies of fuel rods, hydraulic experiments, shielding, and other studies. Design of the propulsion reactor also was undertaken, although the data given in Table X-4 are preliminary in nature.

References 10 and 11 pertain to investigations of the dynamic behavior of marine boiling-water reactors. Reference 10 discusses test results with an oscillating, boiling, natural-circulation loop called "Yo-Yo." Although many of the details are of specialized interest, the conclusions are quoted below for the generality:[10]

1) The error introduced by neglecting the direct g-effect upon slip is small. It should therefore be safe to assume that data from stationary rigs may be used with confidence in the design of natural circulation boiling water reactors for marine application.
2) No effects have been found which indicate any sudden transition from one flow regime to another.
3) No carry under has been produced in this geometry where the water velocity in the upper part of the downcomer was 0.2 times the circulation velocity.
4) A stabilizing effect may be achieved by increasing the single phase inertia.

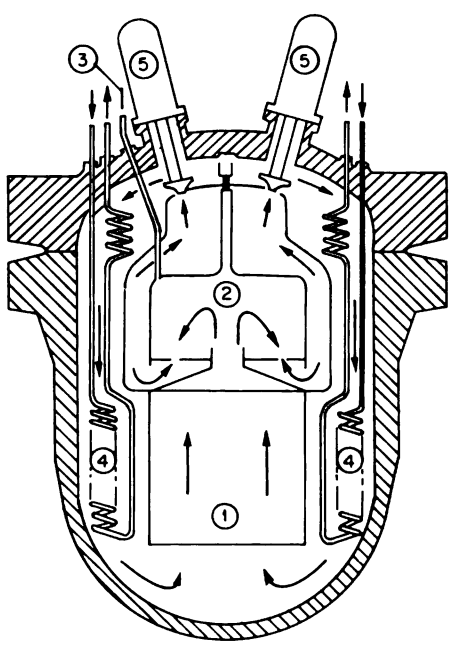

Fig. X-5 Principles of VULCAIN reactor.[5] (1) Core; (2) pressurizer; (3) pressurizing-gas piping; (4) steam generators; (5) pumps.

Table X-4 MAIN PARAMETERS OF NERO DESIGN[7]

General and primary system	
Reactor power, Mw(t)	67
Steam production, metric tons/hr	111.2
Steam pressure, kg/cm²	40
Temperature, °C	280
Reactor operating pressure, kg/cm²	151
Nominal reactor inlet temperature, °C	270
Nominal reactor outlet temperature, °C	299
Nominal inlet temperature reactor core, °C	288
Mass flow through reactor core, kg/sec	1155
Mass flow through each of two external circuits, kg/sec	220
Reactor core dimensions	
Core height, mm	1327
Core nominal diameter, mm	1128
No. of full-size fuel elements	30
No. of subsize fuel elements	12
Total No. of fuel rods	4218
Diameter of pellets, mm	10.03 ± 0.01
Total weight of UO_2, kg	4600
Cladding (Zircaloy) inside diameter, mm	10.2
Cladding (Zircaloy) outside diameter, mm	11.9
Pitch of fuel rods, mm	15.0
Core volume fractions	
UO_2	0.3352
H_2O	0.4402
Cladding boxes	0.1725
Control rods	0.0407
Core physics and heat transfer	
Average burnup, Mwd/metric tons of UO_2	16,600
Initial enrichment of central zone	4.4
Initial enrichment of outer zone	4.8
Amount of burnable poison, g of B_4C equivalent	1240
Maximum heat production, watts/cm of rod length	500
General dimensions	
Inside diameter of reactor vessel, m	2.0
Inside height of reactor vessel, m	5.5
Heat-transfer surface of steam generator, m² each	200
Heat-transfer surface of superheater, m² each	43.8
Inside diameter of containment, m	9.0

The reference also discusses the design of a steam injector-jet pump for use in the downcomer region of a boiling-water reactor. Reference 11 couples the neutronic and hydraulic behavior of a marine boiling-water reactor into a digital-computer code to study transient behavior of the reactor in a rolling and heaving ship. It is shown[11] that the results of the ship's motion produce large neutron-flux variations but affect fuel temperature, heat flux, coolant flow rate, reactor vessel pressure, and rate of steam flow to the turbine only a small amount.

References

The references that contain A/Conf. numbers are papers that were presented at the Third United Nations International Conference on the Peaceful Uses of Atomic Energy, Geneva, September 1964.

1. V. I. Neganov, B. G. Pologikh, and J. V. Sivintsev, Atomic Ships Safety Problems, A/Conf.28/P/378.
2. J. J. Aphrikantov, N. M. Mordvinov, P. D. Novikov, B. G. Pologikh, A. K. Sledzjuk, N. S.

Digitized by Google

Khlopkin, and N. M. Tsarev, Operating Experience of the Atomic Power Plant on the Icebreaker "Lenin," A/Conf.28/P/313.
3. W. Wiebe, H. Konig, and I. Weisbrodt, The Reactor Plant of the Research Ship of Gesellschaft fur Kernenergieverwertung in Schiffbau and Schiffahrt mbH, A/Conf.28/P/540.
4. J. Storrer and S. Rigg, The Vulcain Core Power Experiment, A/Conf.28/P/515.
5. R. P. Kinsey and P. E. Maldague, Technical Objectives of the Vulcain Reactor Project, A/Conf. 28/P/565.
6. J. Smith and F. de Waegh, Physics Problems of Water Reactors Moderated by a Variable H_2O/D_2O Mixture, A/Conf.28/P/176.
7. M. Bogaardt and M. Muysken, The NERO Reactor for Ship Propulsion, A/Conf.28/P/588.
8. A. P. Alexandrov, I. I. Afrikantov, A. I. Brandaus, G. A. Gladkov, B. V. Gnesin, V. I. Neganov, and N. S. Khlopkin, The Atomic Icebreaker "Lenin," in *Proceedings of the Second United Nations International Conference on the Peaceful Uses of Atomic Energy, Geneva, 1958*, Vol. 8, pp. 204-219, United Nations, New York, 1958.
9. G. A. Bat, G. B. Muhina, D. M. Parfanovich, D. C. Klochkov, V. C, Muhortov, H. M. Truhachev, and D. I. Sheffer, Compensation of Large Changes in Reactivity by Means of Core Lattice Deformation, A/Conf.28/P/376.
10. E. Kjelland-Fosterud, I. Bencze, B. Kierulf, and O. R. Kolberg, Two-Phase Flow Investigations for a Marine Boiling Water Reactor, A/Conf.28/P/801.
11. H. Christensen, K. O. Solberg, and A. O. Wagbø, On the Dynamic Behavior of Boiling Water Ship Reactors, A/Conf.28/P/748.

Digitized by Google

Section

XI

Power Reactor Technology

Other Reactors

A number of reactors discussed at the Conference have not been reviewed in the preceding sections, either because they are intended for special purposes or because their development is still at a stage too early to reveal their ultimate major characteristics. Some of these are discussed briefly in the following paragraphs.

Portable Power Plants

The Army Reactors Program in the United States has resulted in the construction and operation of five nuclear power plants that represent the U. S. effort in the development of portable reactor plants for applications other than space. The first reactor in the series began operation in April 1957. General information on the plants is given in Table XI-1, which is taken from Ref. 1. All the reactors are of the pressurized-water type, with operating pressures from 1200 to 1750 psi, and all use UO_2–stainless-steel cermet fuel.

The truly portable plants in the U. S. series were designed to be transported by a variety of means, such as truck, rail, boat, or aircraft. Consequently shipping modules were limited to a size of 8 by 8 by 30 ft and to a weight of 30,000 lb. About 18 modules of reactor and power-plant equipment, plus about 40 modules of support facilities and buildings, comprise a typical plant. For plant details the reader is referred to Ref. 1, to *Power Reactor Technology*, 6(3): 43, which presents a description of the PM-1 core design, and to Ref. 2, which contains details of all five plants in the portable-power-plant series. The design objectives of the U. S. portable reactor development program, as set forth in Ref. 1, are as follows:

—Minimum size and weight
—Minimum installation effort
—High reliability
—System simplicity
—Self-sufficient plant
—Capability of being relocated

The Russians have developed an interesting portable nuclear power plant, the organic-moderated ARBUS plant, which has been in operation since June 1963. The plant has about half the output of the U. S. plants, as shown in Table XI-2. The coolant used in ARBUS, a hydrostabilized gas-oil, has proved to be satisfactory, probably largely because of the incorporation in the ARBUS plant of a coolant "regeneration" system. Operation of the system is described in the following quotation from Ref. 3:

> ...The coolant comes from the primary circuit (200–250 liter/hour) to the regeneration system

Table XI-1 U. S. PORTABLE REACTOR POWER PLANTS IN OPERATION[1]

Designation	Location	Startup date	Power	Purpose
SM-1	Fort Belvoir, Va.	1957	10 Mw(t), 1860 kw(e)	Training, experimental
SM-1A	Fort Greely, Alaska	1962	20 Mw(t), 1640 kw(e) + 35×10^6 Btu/hr	Power and heat
PM-1	Sundance, Wyo.	1962	9.4 Mw(t), 1000 kw(e) + 7×10^6 Btu/hr	Power and heat
PM-2A	Camp Century, Greenland	1960	10 Mw(t), 1600 kw(e) + 1×10^6 Btu/hr	Power and heat
PM-3A	McMurdo Station, Antarctica	1962	9.5 Mw(t), 1500 kw(e)	Power

Digitized by Google

gas oil pump. Then the gas oil at a pressure of 45–60 atm is mixed with an inflow of circulating hydrogen. The latter is obtained by water electrolysis in an electrolyzer from which it is transported to the system by a displacement compressor of the regeneration system. The gas oil and hydrogen mixture is heated in the regenerative heat exchanger, and then it is heated up to the working temperature in an electric furnace. After that the gas oil and hydrogen mixture is fed to the reactor filled with catalyst. The hydrogen and regenerated gas oil mixture coming from the reactor transfers its heat in the heat exchanger, and is finally cooled down to 30–50°C in the cooler. Then the mixture is separated in a gas separator from which the gas oil comes through cermet and felt filters to the primary circuit feed tanks, and hydrogen flows to the circulating compressor. Owing to formation of destruction gas products (methane), small amounts of the circulating gas are continuously rejected to an exhaust stack. Hydrogen total flowrate is found to be 0.45 kg/hr, hydrogen in the amount of 0.36 kg/hr directly takes part in the reaction.

Table XI-2 ARBUS MAIN PARAMETERS[3]

Reactor output, kw	5000
Turbogenerator output, kw	750
Pressure in the primary-circuit pressurizer, psi	88
Coolant temperature	
At reactor inlet, °F	446
At reactor outlet, °F	469
Coolant flow rate of the primary circuit, metric tons/hr	600
Saturated steam temperature in steam generator, °F	433

Inital characteristics of the low-cost gas-oil coolant are given in Table XI-3. It is believed, however, that for the remote-station application of the plant the low melting point of the gas-oil (relative to that of the terphenyls usually used in the nuclear application) is considered at least as important as the low cost. It is believed also that the gas-oil is not being considered for central-station use because of its relatively poor high-temperature capability.

The ARBUS plant consists of separate factory-tested units, similar to the modules of the U. S. plants but apparently of slightly larger size. The plant consists of 19 units, each weighing 20 tons or less, and it is stated[3] that the weights and sizes of the units make possible their transportation to the building site by water or land. Setup of the plant on site requires two or three months,[3] a time that compares with the 77 days required[1] to erect the U. S. plant PM-3A. The ARBUS plant and the U. S. plants differ greatly in design, of course, but a particularly interesting difference is in one of the rather major

Table XI-3 HYDROSTABILIZED GAS-OIL CHARACTERISTICS[3]

Specific weight at 20°C, g/cm³	0.8558
Iodine number	Not greater than 1
Sulfurizing total, wt.%	30
Boiling initiation, °C	212
Boiling termination, °C	300
Carbon content, %	86.89
Hydrogen content, %	13.11
Hydrogen/carbon ratio	1.8
Sodium content, wt.%	2×10^{-5}
Sulfur content, wt.%	3×10^{-3}
Vapor pressure at 350°C, atm	4.85
Chemical compound	
Paraffin, %	30.12
Aromatic, %	30.03
Naphthene, %	39.85

features of the plants. Early in the design of PM-1, it was recognized that adequate sources of cooling water would not always be available at remote sites. For that reason heat rejection to the air was specified. In the ARBUS plant the condenser is water cooled.

The second Russian portable nuclear power plant,[4] the TES-3, has been in operation since 1961. TES-3, which has a pressurized-water reactor, is more advanced than the other portable plants in one respect: practically all the equipment is arranged in four large packages that are permanently mounted on track type vehicles. When the plant is readied for operation, biological shielding is provided by covering the two vehicles, which carry the reactor and the primary system, with the most convenient locally available shielding material, e.g., earth. The operation of TES-3 has apparently been successful and has confirmed the reliability, the good control characteristics, and the convenience for maintenance of such plants.[4] Principal characteristics of the plant are given in Table XI-4.

Table XI-4 THE MAIN CHARACTERISTICS[4] OF TES-3

Generator power, kw	1500
Reactor power, kw	8800
Pressure in the primary circuit, psi	1910
Temperature at the reactor inlet, °F	527
Temperature at the reactor outlet, °F	572
Parameters of the second circuit	
Pressure in the steam generator, psi	294
Temperature of steam superheat, °F	536
Pressure in the condenser, in. Hg	~3.9
Cooled water flow rate, metric tons/hr	1000
Weight of the plant equipment, metric tons	210
Weight of the transported shield if included, metric tons	28.5
Weight of all power truck-trailers, metric tons	310
Core life, days	250

Digitized by Google

Direct-Conversion Power Plants

The direct-conversion reactors discussed at Geneva, although not strictly the type of plant normally discussed in *Power Reactor Technology*, will be mentioned briefly for whatever bearing they may have on civilian power-reactor development.

A concise history of the SNAP-10A program is given in Ref. 5. The reactor is described, the direct conversion of heat to electricity is discussed, and the integration of the reactor heat source and a thermoelectric power-conversion system into a complete package is discussed. The characteristics of the thermal-neutron SNAP reactors are given in the paper, and Table XI-5 reproduces some of the SNAP-10A data. In mid-1964 the reactor and conversion subsystems had performed satisfactorily in independent tests, and preflight tests of the integrated plant had begun. Flight testing in the actual space environment is scheduled for 1965.

Table XI-5 SNAP-10A DESIGN CHARACTERISTICS[5]

Fuel-moderator elements (U-ZrH)	
Diameter, in.	1.25
Length, in.	13.0
N_H, H atoms/cm^3 × 10^{-22}	6.5
U (fully enriched ^{235}U), wt.%	10
Number of elements	37
Total ^{235}U, kg	4.3
Cladding thickness, in.	0.015
Reactor	
Core-vessel diameter, in.	8.94
Core-vessel height, nominal, in.	15.6
Be reflector thickness, nominal, in.	2
Number of control drums-safety elements	4
Core volume, cu ft	0.3
Weight with reflector control assembly, lb	250
Fuel-element spacing-triangular matrix, in.	1.26
Operating characteristics	
Coolant (NaK) flow, gal/min	13.1
Inlet temperature, °F	900
Outlet temperature, °F	1010
Maximum fuel temperature, °F	1085
Power, kw(t)	34
Power density, average, kw(t)/liter	4.0
Heat flux, average, Btu/(hr)(sq ft)	10,200
Neutron flux, average, neutrons/(cm^2)(sec)	1.7 × 10^{11}

The high-temperature direct-conversion reactor Romashka has operated as a complete system for about 500 hr in the Soviet Union, and the direct-conversion portion of the plant has been tested[6] with electric heat for over 1000 hr. In Romashka, heat generated in the fast reactor core is transferred by conduction radially to a reflector, and then from the lateral surface of the reflector to a semiconductor conversion device mounted coaxially and adjoining the reflector. The cylindrical reactor is built up of horizontal fuel elements, each of which is made of a graphite body and enriched fuel plates of uranium dicarbide. The radial reflector of the reactor is made of graphite and beryllium, and end-face reflectors are fabricated of metallic beryllium. The reactor is controlled by four rods that are inserted in the radial beryllium reflector and by movement of the lower end-face reflector. The cold junctions of the thermoelectric conversion devices are cooled by radiating fins. The average temperature at the bases of the fins is about 550°C. Some basic parameters of the Romashka reactor are given in Table XI-6, which is taken from Ref. 6.

Table XI-6 BASIC PARAMETERS OF THE DIRECT-CONVERSION REACTOR ROMASHKA[6]

Electrical output, kw	0.50 to 0.80*
Total thermal power, kw	40
Maximum temperature of beryllium reflector, °C	1200
Maximum temperature of external surface of beryllium reflector, °C	980
Maximum temperature of uranium dicarbide fuel elements, °C	1900
Charge of ^{235}U, kg	49
Worth of automatic control rod, %	0.2
Worth of manual control rod, %	0.4
Worth of safety rod, %	0.4
Worth of all control rods, %	1.4
Worth of mobile end-face reflector, %	3.5
Total neutron flux in core center, neutrons/(cm^2)(sec)	10^{13}
Total neutron flux at reactor core boundary, neutrons/(cm^2)(sec)	7 × 10^{12}
Neutron leakage from reactor, neutrons/(cm^2)(sec)	3 × 10^{11}

*Depending on temperature conditions.

One result of the Soviet experimental work that may be of interest to the reactor designer is given in Fig. XI-1, which shows the depen-

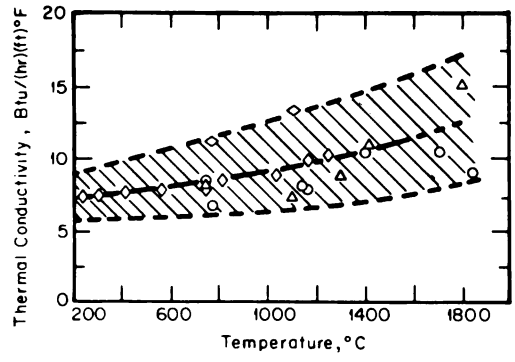

Fig. XI-1 Dependence of thermal conductivity of uranium dicarbide on temperature.[6]

Digitized by Google

Table XI-7 ADVANCED REACTOR TYPES UNDER CONSTRUCTION IN THE UNITED STATES[11]

	MSRE*	EBOR†	UHTREX‡	FRCTF§
Location	Oak Ridge, Tenn.	NRTS, Idaho	Los Alamos, N. Mex.	Los Alamos, N. Mex.
Contractor or laboratory	ORNL	General Atomic Div. of General Dynamics Corp.	LASL	LASL
Power, Mw(t)	10	10	3	20
Fuel	Molten solution of UF_4 and ZrF_4 in ^7LiF-BeF_2	62 UO_2–38 BeO	UC_2 coated particles in graphite	Molten Pu-Co-Ce
Fuel enrichment, % ^{235}U	25 to 93	62	93	
Maximum fuel temperature, °F	1225	1900	3000	1200
Cladding or container	INOR-8 (Hastelloy N)	Hastelloy X	None	Ta alloy
Primary coolant	Circulating fuel (LiF, BeF_2-ZrF_4-UF_4)	He	He	Na
Coolant exit temperature, °F	1225	1300	2000 to 2400	1157
Moderator	Graphite	BeO	Graphite	

*MSRE, Molten-Salt Reactor Experiment.
†EBOR, Experimental Beryllium Oxide Reactor Experiment.
‡UHTREX, Ultra-High-Temperature Reactor Experiment.
§FRCTF, Fast Reactor Core Test Facility of the Los Alamos Molten-Plutonium Reactor Project.

dence of the conductivity of uranium dicarbide on temperature.

Other papers concerning direct-conversion devices or techniques are listed as Refs. 7 to 10.

Advanced Concepts

A paper by Sievering[11] describes several advanced reactor concepts currently under development in the United States. The four advanced reactor types listed in Table XI-7 are being built as reactor experiments, and several other concepts are in the stage of laboratory development. The Molten Salt Reactor Experiment is expected to be in operation early in 1965, as is the Experimental Beryllium Oxide Reactor. The Ultra High-Temperature Reactor Experiment is planned to achieve initial criticality late in 1965, and the Fast Reactor Core Test Facility, which will be able to accommodate core-blanket combinations of various designs, is scheduled for initial operation in 1967.

Three papers are on advanced reactor concepts being investigated in the Federal Republic of Germany. One paper is concerned with the pebble-bed power reactor,[12] which has been previously mentioned in Sec. VIII, and the other two describe a sodium-cooled, zirconium hydride-moderated power-reactor experiment[13] and a molten-salt epithermal reactor,[14] respectively.

References

The references that contain A/Conf. numbers are papers that were presented at the Third United Nations International Conference on the Peaceful Uses of Atomic Energy, Geneva, September 1964.

1. M. A. Rosen, J. B. Roll, and R. D. McFarren, Portable Reactor Power Plants, A/Conf.28/P/211.
2. *Directory of Nuclear Reactors,* Vol. IV, Power Reactors, International Atomic Energy Agency, Vienna, 1962.
3. K. K. Polushkin, I. Ya. Emelyanov, P. A. Delens, N. V. Zvonov, U. N. Aleksenko, I. I. Grozdov, S. P. Kuznetsov, A. P. Sirotkin, U. I. Tokarev, K. P. Lawrovsky, A. M. Brodsky, A. R. Belov, E. V. Borisyuk, V. M. Gryazev, V. D. Tetyukov, D. N. Popov, U. I. Koryakin, A. G. Filippov, K. V. Petrochuk, V. D. Khoroshavin, N. P. Savinov, M. N. Meshcheryakov, V. I. Pushkarev, V. A. Suroyegin, P. A. Gavrilov, L. N. Podlazov, I. W. Rogozhkin, L. N. Podlazov, and I. N. Rogozhkin, The ARBUS—Organic Cooled and Moderated Nuclear Power Station, A/Conf.28/P/307.
4. N. M. Sinev, A. K. Krasin, I. F. Bichkov, O. I. Blokhin, D. L. Broder, V. N. Gabrussev, Yu. V. Dudnikov, V. A. Zhiltsov, M. A. Koptev, A. Ya. Komarov, A. P. Kotov, M. N. Lantsov, G. A. Lissochkin, G. V. Merzlikin, I. G. Morozov, Yu. I. Orekhov, Yu. A. Sergeev, P. N. Slyusarev, G. N. Ushakov, N. V. Fyodorov, V. Y. Chyornyi, and V. M. Shmelev, Small-Gabarit Atomic Power Plant TES-3, A/Conf.28/P/310.
5. H. M. Dieckamp, R. Balent, and J. R. Wetch, Reactor Direct-Conversion Units, A/Conf.28/P/218.
6. M. D. Millionshchikov, I. G. Gverdtsiteli, A. S. Abramov, L. V. Gorlov, Yu. D. Gubanov, A. A. Efremov, V. F. Zhukov, V. E. Ivanov, E. A. Koptelov, V. G. Kosovskii, N. E. Kukharkin, R. Ya. Kucherov, S. P. Lalykin, V. I. Merkin, Yu. A. Nechaev, B. S. Pozdnyakov, N. N. Ponomarev-Stepnoy, E. N. Samarin, V. Y. Serov, V. A. Usov, V. G. Fadin, V. V. Yakovlev, M. V.

Digitized by Google

Yakutovich, V. A. Khodakov, and G. V. Kompaniets, High-Temperature Direct Conversion Reactor "ROMASHKA," A/Conf.28/P/873.
7. P. D. Dunn and J. Adam, Fission-Heated Thermionic Diodes, A/Conf.28/P/132.
8. B. C. Lindley, Nuclear Magnetoplasmadynamic Energy Conversion, A/Conf.28/P/133.
9. E. W. Salmi, F. G. Block, G. M. Grover, H. D. Miller, R. W. Pidd, and V. C. Wilson, Thermionic Diodes for Direct Conversion Reactors, A/Conf.28/P/219.
10. I. I. Bondarenko, I. N. Gorelov, Yu. K. Gus'kov, V. M. Dmitriev, I. I. Kasikov, V. P. Karmasin, S. Ya. Lebedev, M. A. Lebedev, V. A. Malikh, S. A. Majev, V. Ya. Pupko, V. G. Petrovskii, V. P. Paschenko, E. E. Sibir, Y. Ya. Stavisskii, I. P. Stakhanov, A. S. Stepanov, and Yu. S. Yur'ev, Theoretical and Experimental Investigations Connected with Development of Thermionic Reactors — Converters, A/Conf.28/P/317.
11. N. F. Sievering, Jr., The U. S. Program for the Development of Advanced Reactor Concepts, A/Conf.28/P/212.
12. C. B. von der Decken, J. D. Lueders, O. Machnig, H. W. Schmidt, and R. Shulten, Development Project of a Pebble-Bed Power Reactor, A/Conf.28/P/536.
13. R. Harde and K. W. Stoehr, A Sodium-Cooled Power Reactor Experiment Employing Zirconium Hydride Moderator, A/Conf.28/P/537.
14. P. R. Kasten, The MOSEL Reactor Concept, A/Conf.28/P/538.

LEGAL NOTICE

This journal was prepared under the sponsorship of the U. S. Atomic Energy Commission. Neither the United States, nor the Commission, nor any person acting on behalf of the Commission:

A. Makes any warranty or representation, expressed or implied, with respect to the accuracy, completeness, or usefulness of the information contained in this journal, or that the use of any information, apparatus, method, or process disclosed in this journal may not infringe privately owned rights; or

B. Assumes any liabilities with respect to the use of, or for damages resulting from the use of any information, apparatus, method, or process disclosed in this journal.

As used in the above, "person acting on behalf of the Commission" includes any employee or contractor of the Commission, or employee of such contractor, to the extent that such employee or contractor of the Commission, or employee of such contractor prepares, disseminates, or provides access to, any information pursuant to his employment or contract with the Commission, or his employment with such contractor.

Digitized by Google

GIFT
APR 13 '

Digitized by Google

Digitized by Google

Digitized by Google

NUCLEAR SCIENCE ABSTRACTS

The U. S. Atomic Energy Commission, Division of Technical Information, publishes *Nuclear Science Abstracts (NSA)*, a semimonthly journal containing abstracts of the literature of nuclear science and engineering.

NSA covers (1) research reports of the U. S. Atomic Energy Commission and its contractors; (2) research reports of government agencies, universities, and industrial research organizations on a world-wide basis; and (3) translations, patents, books, and articles appearing in technical and scientific journals.

Complete indexes covering subject, author, source, and report number are included in each issue. These are cumulated quarterly, semiannually, and annually providing a detailed and convenient key to the literature.

Availability of *NSA*

SALE *NSA* is available on subscription from the Superintendent of Documents, U. S. Government Printing Office, Washington, D. C., 20402, at $30.00 per year for the semimonthly abstract issues and $22.00 per year for the four cumulated-index issues. Subscriptions are postpaid within the United States, Canada, Mexico, and all Central and South American countries, except Argentina, Brazil, British and French Guiana, Surinam, and British Honduras. Subscribers in these Central and South American countries, and in all other countries throughout the world, should remit $37.00 per year for subscriptions to semimonthly abstract issues and $25.00 per year for the four cumulated-index issues.

EXCHANGE *NSA* is also available on an exchange basis to universities, research institutions, industrial firms, and publishers of scientific information. Inquiries should be directed to the Division of Technical Information Extension, U. S. Atomic Energy Commission, P. O. Box 62, Oak Ridge, Tennessee, 37831.

Digitized by Google

TECHNICAL PROGRESS REVIEWS may be purchased from Superintendent of Documents, U. S. Government Printing Office, Washington, D. C., 20402. *Isotopes and Radiation Technology* at $2.00 per year for each subscription or $0.55 per issue; the other four journals at $2.50 per year and $0.70 per issue. The use of the coupon below will facilitate the handling of your order.

POSTAGE AND REMITTANCE: Postpaid within the United States, Canada, Mexico, and all Central and South American countries except as hereinafter noted. Add $0.50 per year, or $0.15 per single issue for the *Isotopes and Radiation Technology* journal and $0.75 per year or $0.20 per single issue for the other four journals for postage to all other countries, including Argentina, Brazil, British and French Guiana, Surinam, and British Honduras. Payment should be by check, money order, or document coupons, and MUST accompany order. Remittances from foreign countries should be made by international money order, or draft on an American bank, payable to the Superintendent of Documents, or by UNESCO book coupons.

order form

SUPERINTENDENT OF DOCUMENTS
U. S. GOVERNMENT PRINTING OFFICE
WASHINGTON , D. C., 20402

Enclosed:
document coupons ☐ check ☐ money order ☐

Charge to Superintendent of Documents No._____

Please send a one-year subscription to

☐ NUCLEAR SAFETY

☐ POWER REACTOR TECHNOLOGY

☐ REACTOR FUEL PROCESSING

☐ REACTOR MATERIALS

(Each subscription $2.50 per year; $0.70 per issue.)

☐ ISOTOPES AND RADIATION TECHNOLOGY

(Each subscription $2.00 a year; $0.55 per issue.)

SUPERINTENDENT OF DOCUMENTS
U. S. GOVERNMENT PRINTING OFFICE
WASHINGTON, D. C., 20402

(Print clearly)

Name _____

Street _____

City _____ Zone ___ State _____

Digitized by Google

y3.At7:
36[8-2
Eng.
TK
9202
.G4

POWER REACTOR TECHNOLOGY

ENGINEERING
NOV 17 '66
LIBRARY

3658

A Quarterly Technical Progress Review

...RMATION USAEC, by
...TRING INC., NUCLEAR DIVISION

Spring 1965

VOLUME 8

NUMBER 2

Digitized by Google

TECHNICAL PROGRESS REVIEWS

To meet the needs of industry for concise summaries of current atomic developments, the Atomic Energy Commission is publishing this series, Technical Progress Reviews. Issued quarterly, each of the reviews digests and evaluates the latest findings in a specific area of nuclear technology and science.

The five journals published in this series are:

Isotopes and Radiation Technology, P. S. Baker, A. F. Rupp, and associates, Oak Ridge National Laboratory

Nuclear Safety, Wm. B. Cottrell, W. H. Jordan, and associates, Oak Ridge National Laboratory

Power Reactor Technology, W. H. Zinn and J. R. Dietrich, Combustion Engineering, Inc., Nuclear Division

Reactor Fuel Processing, Stephen Lawroski and associates, Chemical Engineering Division, Argonne National Laboratory

Reactor Materials, R. W. Dayton, E. M. Simons, and associates, Battelle Memorial Institute

Each journal may be purchased from the Superintendent of Documents, U. S. Government Printing Office, Washington, D. C., 20402. *Isotopes and Radiation Technology* at $2.00 per year for subscription or $0.55 for individual issues; the other four journals at $2.50 per year and $0.70 per issue. See back cover for remittance instructions and foreign postage requirements.

The views expressed in this publication do not necessarily represent those of the United States Atomic Energy Commission, its divisions or offices, or of any Commission advisory committee or contractor.

Availability of Reports Cited in This Review

Unclassified AEC reports are available for inspection at AEC depository libraries and are sold by the Clearinghouse for Federal Scientific and Technical Information, National Bureau of Standards, U. S. Department of Commerce, 5285 Port Royal Road, Springfield, Va., 22151. Some of the reports cited are not available owing to their preliminary nature; however, the information contained in them will eventually be made available in formal progress or topical reports.

Unclassified reports issued by other Government agencies or private organizations should be requested from the originator.

Unclassified British and Canadian reports may be inspected at AEC depository libraries. British reports are sold by the British Information Service, 45 Rockefeller Plaza, New York, N. Y.; Canadian reports (AECL series) are sold by the Scientific Document Distribution Office, Atomic Energy of Canada, Ltd., Chalk River, Ontario, Canada.

Classified U. S. and foreign reports identified in this journal as Classified may be purchased by properly cleared Access Permit Holders from the Division of Technical Information Extension, U. S. Atomic Energy Commission, P. O. Box 1001, Oak Ridge, Tenn., 37831. Such reports may be inspected at classified AEC depository libraries.

Digitized by Google

POWER REACTOR TECHNOLOGY

A REVIEW OF RECENT DEVELOPMENTS

Prepared for DIVISION OF TECHNICAL INFORMATION, USAEC,
by W. H. ZINN and J. R. DIETRICH,
COMBUSTION ENGINEERING, INC., NUCLEAR DIVISION

SPRING 1965

VOLUME 8

NUMBER 2

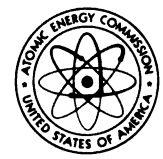

Digitized by Google

Foreword

This quarterly review of reactor development has been prepared at the request of the Division of Technical Information of the U. S. Atomic Energy Commission. Its purpose is to assist interested organizations in the task of keeping abreast of new results in reactor technology for civilian application.

Power Reactor Technology contains reviews of selected recently published reports that are judged noteworthy in the fields of power-reactor research and development, power-reactor applications, design practice, and operating experience. It is not meant to be a comprehensive abstract of all material published during the quarter, nor is it meant to be a treatise on any part of the subject. However, related reports from different sources are often treated together to yield reviews having some breadth of scope, and background material may be added to place recent developments in perspective. Occasionally the reviews are written by guest authors. Reviews having unusual breadth or significance are placed at the front of the issue as Feature Articles.

The intention is to cover the various areas of reactor development from the general viewpoint of the reactor designer rather than from the more detailed points of view of specialists in the individual areas. To whatever extent the coverage of *Power Reactor Technology* may occasionally overlap the fields of the other Technical Progress Reviews, the overlaps will be motivated by this objective of viewing current progress through the eyes of the reactor designer.

A degree of critical appraisal and some interpretation of results are often necessary to define the significance of reported work. Any such appraisal or interpretation represents only the opinion of the reviewer and (in the usual case, when the review is written by Combustion Engineering, Inc., Nuclear Division staff) the Editor. When the review is predominantly interpretive the reviewer is named; unless identified as a guest author, he is a member of the Combustion Engineering, Inc., Nuclear Division staff. Readers are urged to consult the original references to obtain all the background of the work reported and to obtain the interpretation of the results given by the original authors.

For timely coverage, *Power Reactor Technology* must often review fragmentary material. The fixed subject headings listed below have been adopted in the hope of maintaining some continuity and order in the material from one issue to another: all reviews except Feature Articles will be arranged under these headings. A particular issue will not necessarily contain all the headings but only those under which material is reviewed.

Economics, Applications, Programs
Resources and Fuel Cycles
Physics
Fluid and Thermal Technology
Fuel Elements
Materials
Control and Dynamics
Containment, Radiation Control, and Siting
Systems Technology
Components
Design and Construction Practice
Operating Experience
Specific Reactor Types
Specific Applications
Unconventional Approaches

W. H. Zinn, Vice-President
J. R. Dietrich, Editor
Combustion Engineering, Inc.

Digitized by Google

Contents

I Physics 109
Critical and Exponential Experiments . . 109
Age and Diffusion-Length Determinations 113
Cross Sections 115
Neutron Thermalization 115
References 116

II Fluid and Thermal Technology . . . 118
Conduction 118
Gases 121
Pressurized Water 121
Organic Fluids 123
References 124

III Fuel Elements 126
Cermet Fuels for Fast Reactors . . . 126
Fabrication of Various Fuel Assemblies 128
References 131

IV Components 133
EBR-II Control-Drive Mechanisms . . 133
Process Tubes and Fittings for the NPR 134
References 136

V Specific Reactor Types 137
Large Pressurized-Water Reactors . . 137
EBWR 147
Design Studies of a 1000-Mw(e) Fast Reactor 147
References 155

Issued quarterly by the U. S. Atomic Energy Commission. Use of funds for printing this publication approved by the Director of the Bureau of the Budget on October 14, 1963.

Digitized by Google

Digitized by Google

Letter to the Editor

WESTINGHOUSE ATOMIC POWER DIVISION
EXPERIENCE WITH STAINLESS-STEEL-CLAD FUEL ELEMENTS

In marked contrast to the VBWR results reported in *Power Reactor Technology*, 7, 4, Westinghouse has not observed failure of stainless steel cladding in a pressurized water reactor environment. Our operating experience to date is summarized in Table I. Stainless steel has clearly performed with distinction under exposures substantially in excess of those at which failures occurred in VBWR, regardless of whether the cladding was annealed or cold worked, freestanding or collapsed. Yankee environment was primary neutral, with periods of high *p*H and boric acid operation; Saxton and Selni are chemical shim systems (boric acid) having added alkali.

Table I IRRADIATION DATA ON STAINLESS-STEEL FUEL ELEMENTS IN WESTINGHOUSE REACTORS

Stainless type	Cladding thickness, in.	Peak exposure		Reactor
		Nvt >1 Mev	MWD/MTU	
Annealed 348	0.021 (freestanding)	7×10^{21}	30,000	Yankee
Cold worked 304	0.016 (freestanding)	3×10^{21}	20,300	Saxton
Cold worked 304	0.010 (collapsed)	1×10^{21}	10,000	Saxton
Cold worked 304	0.015 (freestanding)	1×10^{21}	6,000	Selni

A test assembly irradiated in Yankee Cores I and II is now under test in Core IV and will achieve a peak burnup of 41,000 MWD/MTU (fast flux >1 Mev = 11×10^{21} nvt) by September 1965. Fuel elements in the basic Saxton Core will achieve peak exposures of 25,000 MWD/MTU by June 1965. Selni fuel elements will achieve 16,000 MWD/MTU by July 1966.

Based on an extensive review of experimental data reported by other laboratories, we conclude that in-reactor failures of UO_2 fuel elements clad with commercial stainless steel have occurred only in a boiling water environment. Factors which must be evaluated in explaining the differences between stainless steel behavior in boiling and pressurized water reactors are as follows:

1. *System Pressure*

The higher system pressure in a pressurized water reactor produces a larger compressive stress component on the cladding surface. For example, the circumferential compressive stress contribution from 2,000 psi external pressure will be about 12,000 psi greater than in a boiling water system operating at 1,000 psi, assuming equivalent clad thickness and geometry. The higher system pressure thus prevents or delays the development of tensile stress in the cladding as a result of fission gas accumulation. Crack propagation cannot normally occur in the absence of a tensile stress.

2. *System Chemistry*

Typically, oxygen concentration in pressurized water is less than 0.01 ppm. In direct cyclic boiling systems, however, oxygen in the vapor stage varies from 20–40 ppm; in the liquid, oxygen concentration is typically 0.05 to 0.5 ppm. High oxygen concentrations have been shown in laboratory experiments to accelerate stress corrosion. Differences in corrosion behavior may also arise from differences in the equilibrium distribution of chemical species from radiolytic decomposition.

3. *Corrosion Product Deposition*

Corrosion products deposit on the surfaces of fuel elements irradiated in both boiling and nonboiling water environment (although the examination of the irradiated Yankee elements revealed almost no deposited corrosion product). The corrosion product deposited from a boiling coolant will be highly oxidized; ferric ions are known to be effective crack promoters.

Digitized by Google

4. *Local Thermal Stresses*

Fundamental heat transfer studies[1,2,3] have shown that rapid thermal fluctuations occur at surfaces where boiling is occurring. These local temperature fluctuations are caused by the growth and detachment of vapor bubbles which temporarily change the local heat transfer rates at the fuel element surface. Amplitude of the observed temperature variations ranges from a few degrees to about 30°F, occurring at somewhat irregular intervals of 3–50 milliseconds. The rate at which the temperature decreases during a local thermal fluctuation may be as high as 1500°F/sec. Although the strain resulting from these fluctuations is relatively small, the very high frequencies at which such a strain is cyclically applied may contribute to fuel element failure. Since bubble nucleation occurs preferentially at small surface crevices or pits, thermal cycling is focused on locations which are already sources of potential microcracks. The temperature will fluctuate at any fuel element surface experiencing nucleate boiling (either bulk or local). However, smaller fluctuations occur in a pressurized water system because of the higher pressure and greater forced convection cooling of the surface.

The relative importance of each of these mechanisms has yet to be fully assessed. However, controlled experiments are required to supplement engineering test data and to establish the relevance of these mechanisms to behavior of other cladding materials.

---

(1) F. D. Moore and R. B. Mesler, *A.I.Ch.E. J.*, 7: 4, 620 (1961).
(2) N. Madsen, Memo WWO 26-M31, Technische Hochschule, Eindhoven, 1964.
(3) T. S. Rogers and R. B. Mesler, *A.I.Ch.E. J.*, 10: 5 (September 1964).

R. J. Allio, Manager
Materials and Processes Development
Westinghouse Atomic Power Division

March 19, 1965

Digitized by Google

Section I

Power Reactor Technology

Physics

Critical and Exponential Experiments

Several reports of results of critical and exponential experiments have been issued since the last review of the subject in *Power Reactor Technology* [7(3): 206-212 (Summer 1964)]. These include some papers from the Third Geneva Conference.

Reference 1 describes a series of critical experiments with a close-packed D_2O-moderated lattice in the Special Power Excursion Reactor Test II (SPERT-II). These experiments were directed toward providing information needed for design of the final operational core and for analysis of power-excursion tests conducted with that core to investigate the influence of prompt-neutron lifetime on reactor kinetics. In addition to the effects of initial system pressure and temperature, planned kinetic experiments with the close-packed core configuration will investigate the dynamic response of the reactor during forced coolant flow. Fuel assemblies, spaced on a uniform square pitch of 6.0 in., consisted of 3-in.-square thin-walled aluminum cans containing 18 highly enriched, removable, flat fuel plates separated by heavy-water channels 0.094 in. thick. The fuel plates were of a uranium-aluminum alloy meat (0.020 by 2.54 by 24 in.) clad with 0.020 in. of aluminum. Each plate contained a nominal loading of 7 g of ^{235}U, and therefore each assembly had a total of approximately 126 g of ^{235}U. The facility was designed to permit operation up to moderately elevated temperatures and pressures, e.g., 400°F and 375 psig, respectively. The reference discusses critical loadings, flux maps, adjoint flux maps, and the reactivity coefficients of pressure, temperature, and voids.

Bucklings were measured[2] by substitution techniques in the Process Development Pile for fuel assemblies composed of clusters of 19, 31, and 37 natural UO_2 rods with various rod spacings within the cluster. The UO_2 rods were 0.500-in.-diameter sintered pellets (10.4 g/cm^3) stacked in aluminum tubes having an outside diameter of 0.547 in. and a wall thickness of 0.020 in. The hexagonal rod clusters were placed inside aluminum-housing tubes of circular and hexagonal cross section and were of such dimensions as to limit the coolant-flow area to realistic values. The various coolants investigated were Dowtherm A, polyethylene, H_2O, air, and D_2O. The single-region reference-core loading consisted of 31-rod UO_2 clusters contained in D_2O-filled aluminum-housing tubes; both the reference and test lattices were spaced on a 9.33-in. triangular pitch. Measurements were made by the successive substitution technique wherein effective critical water heights are determined after the substitution of one, three, and finally seven test assemblies. One-group perturbation and two-group flux-matching methods were used in the interpretation of the experimental data.

Reference 3 presents a summary of experimental and theoretical results obtained in the Heavy Water Lattice Project of the Massachusetts Institute of Technology (MIT) during the period October 1962 to September 1963. Experimental methods were developed during previous studies on lattices of 1-in.-diameter natural-uranium rods in the main subcritical (exponential) assembly. These methods were employed in the evaluation of the material buckling, fast-fission effect, and resonance and thermal captures in fuel lattices of 0.25-in.-diameter slightly enriched-uranium-metal fuel rods. The uranium metal was enriched to 1.03% ^{235}U and was clad with aluminum 0.028 in. thick. Values of the material buckling were evaluated for unreflected lattices of the 1.25-in. triangular pitch in both the 3- and 4-ft-diameter tanks

Digitized by Google

and with a 2.50-in. triangular pitch in the 4-ft-diameter tank. Preliminary results on measurements of the ratio of fissions of ^{238}U to fissions of ^{235}U, and on the ratio of epithermal to thermal fission of ^{235}U, are reported for lattice pitches of 1.25, 1.75, and 2.5 in. Results are compared with earlier results obtained in the Miniature Lattice Facility at MIT and with results obtained at Brookhaven National Laboratory with 0.25-in. rods in lattices moderated by H_2O. Measurements of the ^{238}U cadmium ratio, the ratio of ^{238}U capture rate to the ^{235}U fission rate, and intracellular distributions of neutron-capture rates in ^{238}U and copper are described and compared, where possible, to measurements made in the Miniature Lattice Facility. Experimental determinations of intracellular thermal-neutron distributions and comparisons with analytical results are discussed. In particular, the difficulties arising from the cylindrical approximation to the unit cell, mainly with the lattices of 1.25-in. triangular pitch, the use of improved energy-exchange kernels, and modifications of the THERMOS code to include the effects of radial and axial leakage are described. The progress on miniature lattices, two-region or substituted lattices, and pulsed-neutron studies is also discussed.

Experimental data were obtained at both the Savannah River Laboratory (SRL) and the Hanford Laboratories to establish standards for the prevention of accidental criticality in handling, storing, and processing uranium metal enriched to 3 wt.% ^{235}U. In the Hanford experiments the approach-to-critical and exponential methods were used to provide material bucklings and critical masses for H_2O-moderated lattices with fuel-rod diameters of 0.175, 0.300, 0.600, and 0.925 in. The SRL measurements, discussed in Ref. 4, employed subcritical exponential techniques to determine the material buckling for H_2O-moderated lattices containing metal rods of 2- and 3-in. diameters at several lattice pitches. The material buckling for fuel elements of a given diameter and lattice pitch was evaluated from measured values of the neutron relaxation lengths along the axes of assemblies having at least two different effective diameters. The use of assemblies with different effective diameters permitted an evaluation of the radial extrapolation distance without the measurement of transverse flux shapes. Tabulations of the extrapolation distance, transverse buckling, neutron relaxation length, material buckling, and critical mass are given for the configurations investigated at SRL. A summary of both the SRL and Hanford data for the 3 wt.% ^{235}U metal rods is given in Ref. 4.

The ZPR-III facility has been used to study the properties of very large fast power breeder reactors by a two-zone-core technique wherein a small subcritical portion of a large dilute system is positioned in the center of the critical-facility matrix and surrounded by a buffer region and an annular driver region. Reference 5 describes the measurements in assembly 42 which were designed to assess the validity of this technique. The central core area of assembly 42 had an effective radius of 9.22 in., a length of 34 in., and a composition identical to that of a previously run dilute simulated uranium carbide reactor (assembly 34). The buffer region consisted of a 0.5-in.-thick depleted uranium filter with a length equal to that of the inner zone. Surrounding the buffer zone radially, and with an axial length equal to that of the two inner regions, was a driver zone of 3.18-in. nominal thickness. This driver zone had a ^{235}U volume fraction approximately twice that of the central core region. A depleted uranium blanket surrounded the entire core assembly in both the axial and radial directions. Reactivity measurements performed in this assembly included determinations of plate-orientation worth, homogeneity corrections, reactor-segment worths, central reactivity coefficients, and radial worth distributions of axial columns of core materials. Spectral-index determinations included central fission ratios, nuclear track emulsion measurements, fission-counter traverses, Rossi-alpha measurements, sodium activation, and natural- and enriched-uranium foil measurements. Comparisons between results obtained for the central core region and assembly 34 are given.

The second two-zone core built in the ZPR-III facility (assembly 43) is described in Ref. 6. In this case the central region with its low-density axial blanket was designed to simulate a projected fast power breeder reactor employing uranium monocarbide with a high proportion of ^{238}U to promote internal breeding. The basic structural and coolant materials were stainless steel and sodium, respectively. The composition of the driver region was so chosen that the complete assembly would be critical within the ZPR-III inventory of enriched ura-

Digitized by Google

nium. The composition of the buffer region was then chosen, by calculation, to modify the spectrum of the neutrons diffusing in from the driver to a spectrum similar to that in the central zone. The low-density axial blanket behind the central zone was identical in composition to the central zone except that the enriched uranium was replaced with stainless steel. The remaining part of the core was surrounded by a depleted uranium blanket. In both the central and driver zones, experimental determinations were made for sodium void coefficients and reactivity effects resulting from the substitution of enriched and depleted uranium, ^{233}U, ^{239}Pu, simulated fission products, and various structural and control materials. Spectral indices were measured, and reaction-rate traverses and activation experiments were performed. The reactivity change due to the Doppler effect was measured by heating a large depleted uranium oxide sample.

In support of the Advanced Sodium Graphite Reactor program, a series of critical and exponential experiments[7,8] has been performed to determine values of the material buckling and k_{eff} for graphite assemblies fueled with slightly enriched uranium carbide. These assemblies employed triangular lattice pitches of 9, 11, and 12 in. and, in most cases, included control-channel mockups. The uranium carbide fuel elements each contained 18 fuel rods arranged in two concentric rings about a centrally located, voided, stainless-steel tube. The inner fuel ring consisted of 6 rods evenly spaced on a 1.47-in.-diameter circle, and the outer ring consisted of 12 rods evenly spaced on a 2.84-in. circle. Each fuel rod contained a 72-in. stack of 0.500-in.-OD uranium carbide pellets inside a 0.010-in.-thick 0.550-in.-OD stainless-steel tube. The uranium carbide had a density of 13.23 g/cm^3, a carbon weight fraction of 4.9%, and a ^{235}U enrichment of 3.02%. The region outside the fuel rods and within the 0.025-in.-thick 4.00-in.-ID process tube was filled with sodium to a height of 72 in. The number of uranium carbide fuel elements (24) was much less than the number required for a bare or reflected critical assembly; consequently it was necessary to employ a driver region surrounding the test lattice to achieve a critical configuration. Fuel elements for the graphite-moderated driver region consisted of hollow cylinders (1.026 in. in inside diameter and 1.730 in. in outside diameter) of uranium metal enriched to 2 wt.% ^{235}U and stacked inside a 0.040-in.-thick aluminum tube. Fuel assemblies in the driver region were spaced on a 10.6-in. triangular pitch regardless of the lattice pitch employed in the test region. The critical experiments provided data on source multiplication measurements for the test lattices as well as on the number of driver assemblies required for each lattice to achieve criticality. The former data were used to determine the k_{eff} for each uranium carbide test lattice. Lattice configurations identical to those employed as test regions in the two-region critical assemblies were employed in the exponential measurements. In addition, data were also obtained for the same lattice compositions, but with reduced radial dimensions, to permit an evaluation of the effective radial buckling for a given lattice composition. Material-buckling values inferred from the two-region critical measurements are compared with those obtained from the exponential measurements and with those obtained by multigroup and few-group calculational schemes.

A short description of the critical and exponential facilities at the Institute of Nuclear Research, Swierk, Poland, as well as a brief description of the Institute's research programs, is given in Ref. 9. The critical assembly ANNA is a heterogeneous water-graphite-moderated pile with a graphite reflector. The central region of the graphite pile has 45 cylindrical holes positioned on a square pitch of 14 cm, into which graphite plugs or fuel channels can be inserted. Each fuel element is composed of three aluminum-canned coaxial tubes of 20% enriched UO_2. ANNA serves primarily as a mockup facility of the high-flux reactor. The MARYLA reactor is a zero-power (1 kw) flexible pool type facility designed for the study of various light-water systems. The individual fuel assemblies consist of 15 or 16 fuel pins, each of which is 8 mm in diameter by 50 cm long and contains 8 g of ^{235}U. HELENA is a subcritical assembly designed to investigate the parameters of natural-uranium–graphite lattices. The fuel is in the form of aluminum-canned uranium slugs, 30 cm long by 2.5 cm in diameter.

The NPY Project is a joint undertaking in reactor physics between the International Atomic Energy Agency and research laboratories in Norway, Poland, and Yugoslavia. Reference 10 presents a description of the NPY lattices studied, the experimental techniques

Digitized by Google

used in the measurements of neutron-flux distributions, and comparisons between the experimental flux distributions and theoretical predictions. The rod type fuel elements employed in the zero-power facility NORA (Kjeller, Norway) have a fuel radius of 5.64 mm and consist of nonsintered UO_2 powder which has a density of 9.28 g/cm^3 and which is enriched to 3 wt.% ^{235}U. The cladding is type 304 stainless steel with a thickness of 0.71 mm. The lattices reported were moderated by D_2O (99.4 mole %) and employed square pitches of 10, 4.908, and 3.658 cm. The lattices employed in the above-mentioned zero-power assembly ANNA (Swierk, Poland) consist of H_2O-cooled annular elements moderated by graphite and positioned at a square pitch of 14 cm. The fuel element is composed of an inner aluminum support tube, three concentric fuel annuli clad with aluminum, and an aluminum tube that separates the outer water annulus from the graphite. Each fuel annulus is 2.3 mm thick and is composed of 38.5 wt.% UO_2 (enriched to 20% ^{235}U) and 61.5 wt.% aluminum. The fuel element employed in the RB zero-power reactor (Vincha, Yugoslavia) consists of a single fuel annulus that is enriched to 2 wt.% ^{235}U, clad with aluminum, and moderated and cooled by D_2O. The D_2O coolant at both surfaces of the fuel annulus is separated from the inner and outer D_2O-moderated regions by thin-walled aluminum tubing. Square lattice pitches of 8 and 17.9 cm were investigated. Experimental data on thermal-flux distributions measured at the three facilities are compared with analytical results obtained by various calculational techniques, e.g., THERMOS, one-group Amouyal-Benoist, and one-velocity P_3.

Reference 11 is a description of the ROSPO critical facility (Comitato Nazionale per l'Energia Nucleare) that was built for the PRO power-reactor project to test organic-moderated cores. This facility was designed to carry out critical experiments in various cores differing in size, geometry, and control-rod type. During operation the moderator temperature can be changed over a range from about 40°C above the melting point to about 20°C below the boiling point, e.g., 190 to 350°C for Santowax OMP. Over this range the moderator temperature can be maintained constant to within ±0.5°C. The moderator level can be varied and controlled to ±1.5 mm. Data to be obtained by means of the ROSPO facility are as follows: critical-mass values vs. core configuration and fuel enrichment; temperature coefficients, control-rod worth, and reactivity effects associated with structural components. In addition to a detailed description of the facility, Ref. 11 gives data on the following for the first core: critical loadings, worth of control rods and peripheral fuel elements, and temperature-coefficient and buckling measurements. The first core is of the plate type and is moderated and cooled by Santowax OMP. The fuel assemblies are square boxes (71 by 71 mm) fabricated from 0.78-mm-thick stainless-steel sheet. The fuel plates are 96.4 cm long by 0.72 mm thick and 70 mm wide. The meat is an enriched (90% ^{235}U) UO_2 dispersion in an AISI type 304 stainless-steel matrix; the cladding is AISI type 304L stainless steel.

Reference 12 presents a summary of results obtained by pulsed-neutron techniques on graphite- and H_2O-moderated systems and critical experiments on H_2O-UO_2 systems. The pulsed experiments were made on two reflected, highly subcritical systems: (1) a graphite-moderated and -reflected system in the semihomogeneous critical assembly at the Japan Atomic Energy Research Institute (JAERI) and (2) the light-water-moderated UO_2 subcritical reflected system at the Mitsubishi Atomic Power Industries (MAPI) research laboratories. Reasonable agreement between calculated and measured values of the prompt-neutron decay constant of the fundamental mode was reported. The light-water lattice studies were made by the Ozenji Critical Facility (OCF, Central Research Laboratory, Hitachi, Ltd.) and the Tank-type Critical Assembly (TCA, JAERI). Fuel elements used in the experiments at the OCF facility were of the rod type, containing 10-mm-diameter UO_2 pellets sheathed in 0.8-mm-thick aluminum tubes. The UO_2 enrichments were 1.5 and 2.5% ^{235}U. Rod type fuel elements were also used in the TCA. These elements had an effective diameter of 12.5 mm and contained 2.6% enriched UO_2. The results discussed in Ref. 12 for the various experiments include critical masses, flux distributions, spectral parameters, lattice and water-gap peaking, temperature and void coefficients, and space-dependent reactivity effects of fuel.

Two additional papers (Refs. 13 and 14) presented at the Third Geneva Conference are reviews that cover the work on critical experiments in the United States since the Second Geneva Conference in 1958. The first paper[13]

Digitized by Google

covers in detail the field of fast reactor critical experiments, and the second[14] does the same for the work on D_2O-moderated systems. An extensive list of references is included in each paper.

Age and Diffusion-Length Determinations

Measured and calculated values of the flux age of fission neutrons to the indium resonance energy (1.44 ev) in graphite have been reported in Ref. 15. The measurements were made in 8-ft-high hexagonal graphite assemblies having effective diameters of 5 and 7 ft. The assemblies were centered on a cylindrical graphite thermal column which was 5 ft in diameter and which extended $3\frac{1}{2}$ ft above the core of the 2-kw AE-6 water-boiler reactor. The graphite in the experimental assemblies was of AGOT grade and was cast in the form of 4-ft-long hexagonal logs with a distance across flats of 4 in. The graphite density was 1.697 ± 0.004 g/cm^3 as determined from the total weight and as-built dimensions of the assemblies. Two fission sources were employed; the primary source was $3\frac{1}{2}$ in. in diameter, and the secondary source was 1 in. in diameter. Each was fabricated from 4-mil-thick uranium enriched to 93.2 wt.% ^{235}U and was covered on the top side with a 20-mil-thick cadmium disk that served as a sink for thermal neutrons transmitted through the source from the reactor thermal column. Detector foils were 1 cm square by 5 mils thick and were composed of 40% indium and 60% tin; the cadmium boxes were 40 mils thick.

The various corrections investigated[15] experimentally included source perturbations, detector-foil perturbations, nonisotropic foil activation, and epithermal leakage from the graphite assemblies.

Theoretical values[16] of the spatial moments of the slowing-down density distribution at the indium resonance energy were determined by the TYCHE code, which is an infinite-medium slowing-down Monte Carlo program written in FORTRAN. The effects of both inelastic scattering and anisotropic elastic scattering are included in the calculation. Detailed descriptions of the cross sections employed in the code are given in Ref. 16. Comparison with experimental results requires an evaluation of the flux age, τ^{ϕ}. The latter quantity is related to the slowing-down age, τ^{q}, by the method of Goldstein,* which utilizes the Grueling-Goertzel relation to couple flux and slowing-down density.

$$\tau^{\phi} = \frac{M_2^{\phi}}{6} = \frac{M_2^{q}}{6} + \beta$$

where $\beta = \dfrac{\gamma D}{\xi \Sigma_s + \gamma \Sigma_a}$

$$\gamma = 1 - \frac{\alpha(\ln \alpha)^2}{2\xi(1-\alpha)}$$

$$\alpha = \left(\frac{A-1}{A+1}\right)^2$$

and the undefined symbols have the conventional definitions.

Table II-1 presents a comparison between the experimental and theoretical results described above and the previously reported values of the age in graphite. All results are normalized to a graphite density of 1.60 g/cm^3. The experimental values quoted for the present work (Ref. 15) were computed using a parabolic integration procedure over the experimental points as well as an extrapolation of the experimental points. Additional contributions to the uncertainty in the computed flux age including the uncertainties in graphite density, counting statistics, foil positioning, and extrapolated flux distribution. The comments in Table II-1, particularly those relating to the experimental references, give some indication of significant differences between the present and past work.

Measurements of the flux age of fission neutrons to the indium resonance energy in several zirconium-water mixtures are described in Ref. 17. The experimental techniques were similar to those employed in the measurement of the age of fission neutrons in H_2O [reviewed in *Power Reactor Technology*, 7(4): 331 (Fall 1963)]; i.e., the measurements utilized a plane fission source of finite dimension and effectively infinite-plane detectors to give a result equivalent to a measurement using axial detectors and an infinite-plane source. The fission source consisted of an enriched-uranium foil, $28\frac{3}{4}$ in. in diameter and 4 mils thick, masked down to

*H. Goldstein, J. G. Sullivan, Jr., R. R. Coveyou, W. E. Kinney, and R. R. Bate, Calculations of Neutron Age in H_2O and Other Materials, USAEC Report ORNL-2639, Oak Ridge National Laboratory, July 12, 1961.

Digitized by Google

Table II-1 AGE TO INDIUM RESONANCE ENERGY, FOR FISSION NEUTRONS IN GRAPHITE[15] (ρ = 1.60 g/cm^3)

	$\frac{1}{6}M_2$, cm^2	M_4, 10^6 cm^4	M_6, 10^{10} cm^6	Comments
Present work (Ref. 15)				
Experiment	307.8 ± 2.0	6.577	3.843	Foils, 1 by 1 cm; cadmium boxes, 40 mils thick
Theory	307.4 ± 1.0	6.59 ± 0.06	4.01 ± 0.09	Monte Carlo calculation
Experimental reference				
Fermi*	317.0			Large point source (293 g), thick (0.102 in.) cadmium boxes
Hill†	310.6 ± 3.0	6.89	4.4	Large (4 by 6.35 cm) foils, thick (0.135 in.) cadmium boxes
Davey‡	337.9			Source: planar distribution of natural-uranium rods
Hendrie§	312.6 ± 0.5	6.87	4.3	Uncertainty based in counting statistics only
Theoretical reference				
Joanou¶	305.0			Moments method
Goldstein**	304.0 ± 3.0			Monte Carlo calculation

*E. Fermi, J. Marshall, and L. Marshall, Slowing Down of Fission Neutrons in Graphite, CP-1084, Nov. 25, 1943.

†J. E. Hill, L. D. Roberts, and G. McCammon, Slowing Down of Fission Neutrons in Graphite, ORNL-187, Jan. 19, 1949.

‡W. G. Davey, J. C. Field, J. C. Gilbert, and A. L. Pope, An Experimental Study of the Slowing Down of Fissions Neutrons and the Diffusion of Thermal Neutrons in Graphite and in Heterogeneous Mixtures of Bismuth and Graphite, AERE-R/R-2501, March 1958.

§J. M. Hendrie, et al., Slowing Down and Diffusion Length of Neutrons in Graphite-Bismuth Systems, in *Progress in Nuclear Energy, Physics and Mathematics*, Series 1, Vol. 3, Pergamon Press, Inc., New York, 1959.

¶S. D. Joanou et al., Moments Calculations of the Fermi Age in Moderators and Moderator-Metal Mixtures, *Nucl. Sci. Eng.*, 13(2): 171-(1962).

**H. Goldstein, J. G. Sullivan, Jr., R. R. Coveyou, W. E. Kinney, and R. R. Bate, Calculations of Neutron Age in H_2O and Other Materials, ORNL-2639, July 12, 1961.

an effective diameter of 12 in. with cadmium. The homogeneous zirconium-water mixtures were simulated by 0.113-in.-thick zirconium plates arranged parallel to the fission source in a tank of water. The detector foils were $\frac{3}{4}$ in. in diameter by 0.005 in. thick and were composed of 40% indium and 60% tin; cadmium covers were 20 mils thick. In a given plane, parallel to the fission plate, the foils were spaced radially from the axis of symmetry of the experimental assembly. The relative infinite-plane activity $\phi(z)$ was obtained by numerical integration of the following equation:

$$\phi(z) = \int_0^\infty r\phi'(r,z)\,dr$$

where $\phi'(r,z)$ is the activity of a foil at a distance r from the axis of symmetry and in a plane at a distance z from the fission source. Detailed descriptions of the methods of data reduction and tabulations of data are given in the reference. For metal-to-water ratios, R, of 0.0, 0.348, 0.565, and 1.20, the measured ages are given by τ (cm^2) = 26.63 ± 19.23R.

Steady-state measurements of the effective thermal-neutron-absorption cross section and diffusion length in graphite, by means of a beryllium-antimony source, are reported in Ref. 18. The effective absorption cross section was evaluated by comparing the volume-integrated thermal-neutron distribution measured in a finite graphite assembly with that measured in an "infinite" water assembly containing the same beryllium-antimony source. Although this method does give a result relative to the absorption cross section of H_2O, it does not require any assumption as to the magnitude of the transport cross section of graphite. The diffusion lengths were also evaluated from the asymptotic flux distributions in both the graphite and water assemblies. The graphite assembly was an 8-ft-high stack of hexagonal AGOT-grade graphite logs forming a decahedron 12 ft across the flats. Since the finite dimensions of the graphite stack allowed thermal leakage in both directions, displaced source measurements were made to facilitate evaluations of leakage effects. A detailed discussion of the experimental procedures, data-reduction techniques, and correction factors, i.e., source absorption, foil depression, and leakage factors, are given in the reference. The average effective absorption cross section $\sigma_a(\hat{v})$, evaluated at the most probable velocity for a Maxwellian distribution at 20°C, was 4.42 ± 0.08 mb and is in good agreement with a value of $\sigma_a(\hat{v})$ = 4.38 mb deter-

Digitized by Google

mined by the use of the transport mean free path λ_{tr} (steady state) reported by Campbell.* The graphite cross section can be expressed as $\sigma_a = 0.01332\ \sigma_a(H)$, where $\sigma_a(H)$ is the absorption cross section of hydrogen. The average diffusion length, normalized to a graphite density of 1.60 g/cm^3 and measured in the direction parallel to the extrusion axis, was 54.77 ± 0.20 cm, and, in the direction perpendicular to the extrusion axis, it was 55.10 ± 0.15 cm. The former value is in good agreement with the values measured by Campbell in graphite assemblies on the thermal column of the AE-6 water boiler reactor, namely, 54.7 ± 0.3 cm, corrected to 55.02 ± 0.20 cm for infinite geometry by a diffusion cooling correction. The diffusion length for H_2O was 2.80 ± 0.02 cm.

Cross Sections

The fission cross section of ^{241}Pu becomes more important for neutron economy and long-term reactivity changes as fuel elements are developed to withstand increasing total exposures and more particularly if plutonium is recycled. Reference 19 reports measurements made with the Materials Testing Reactor fast chopper and presents the fission cross section of ^{241}Pu from 0.02 to 100 ev. A value of 962 ± 38 barns was measured at 0.0253 ev. Multilevel parameters to 10 ev are given. Reference 20 also reports ^{241}Pu fission cross sections, measured with the Rensselaer Polytechnic Institute linear accelerator. The range of measurement is from 2 to 100 ev, with sufficient resolution to permit multilevel analysis to be carried out for the neutron energies below 36 ev.

In Ref. 21, measurements of the integral cross section for the ^{9}Be$(n,2n)$ reaction in the upper end of the fission spectrum (above 2.7 Mev) are reported. The results are based on measurements of the total amount of helium produced during irradiation of BeO specimens in the Battelle Research Reactor. The value reported is 460 ± 60 mb.

The measurement was made as part of an investigation of the long-term effects of fast-neutron irradiation on polycrystalline beryllia. It is suspected that helium generated within the crystalline matrix may be the cause of the loss of mechanical strength that has been observed in BeO after high fast-neutron doses at temperatures in the range of 100 to 500°C. The $(n,2n)$ process is perhaps even more troublesome in beryllium metal because the resulting helium is responsible for the swelling of beryllium fuel jackets after substantial exposures at relatively high temperatures. The process is, of course, beneficial to the neutron economy of reactors that contain considerable beryllium in regions where the fast-neutron flux is high. The results reported in Ref. 21 are not inconsistent with the $(n,2n)$ cross sections assumed at the 1959 Conference on the Physics of Breeding (Ref. 22).

Measurements of cross sections for a number of threshold reactions, averaged over the ^{235}U fission spectrum, are reported in Ref. 23. The measurements were made by an activation technique. The target material was irradiated in a fission-flux converter, and a characteristic gamma emission from the product nucleus was counted. Most of the results of the measurements are summarized in Table II-2. The half-lives listed in the table were not measured in the experiments but were taken from other sources for use in reducing the data.

Table II-2 MEASURED AVERAGE CROSS SECTIONS FOR THRESHOLD REACTIONS IN A ^{235}U FISSION SPECTRUM[23]

Reaction	$T_{1/2}$	Gamma rays measured, Mev	Breeding ratio of gamma rays, %	Average cross section measured, mb
^{24}Mg$(n,p)^{24}$Na	15.05 hr	1.368	100	1.31 ± 0.06
^{27}Al$(n,p)^{27}$Mg	9.5 min	1.015	98	2.9 ± 0.5
^{27}Al$(n,\alpha)^{24}$Na	15.05 hr	1.368	100	0.60 ± 0.03
^{31}P$(n,p)^{31}$Si	2.56 hr			30.5 ± 1.2
^{32}S$(n,p)^{32}$P	14.3 days			60 ± 1.2
^{47}Ti$(n,p)^{47}$Sc	3.4 days	0.16	66	22.0 ± 1.5
^{48}Ti$(n,p)^{48}$Sc	44 hr	1.32	100	0.21 ± 0.016
^{54}Fe$(n,p)^{54}$Mn	314 days	0.835	100	66 ± 3.5
^{56}Fe$(n,p)^{56}$Mn	2.58 hr	0.845	99	0.90 ± 0.05
^{58}Ni$(n,p)^{58}$Co	71.3 days	0.81	100	105 ± 5
^{58}Ni$(n,p)^{58m}$Co	9.0 hr			30 ± 7
^{64}Zn$(n,p)^{64}$Cu	12.8 hr	0.51	38	27 ± 1.6
^{67}Zn$(n,p)^{67}$Cu	61 hr	0.184	45	0.9 ± 0.1
^{92}Mo$(n,p)^{92}$Nb	10.1 days	0.93	98	6.2 ± 0.4
^{95}Mo$(n,p)^{95}$Nb	35 days	0.765	99	0.13 ± 0.02

Neutron Thermalization

A general review of neutron thermalization, with attention to reactor applications, is given in Ref. 24. The paper also discusses various computer methods for representing scattering

*R. W. Campbell, Diffusion Length in SGR Graphite, USAEC Report NAA-SR-Memo-7415, Atomics International, May 29, 1962.

Digitized by Google

kernels and for determining the thermal-neutron characteristics in reactor lattices.

The "scattering-law" formulation for the handling of differential scattering data was discussed previously at some length in *Power Reactor Technology*, 6(1): 6-14 and 6(4): 46-53. New tabulations of scattering-law data (scattering cross section as a function of energy and momentum transfer) are given in Refs. 25 and 26 for H_2O and D_2O at temperatures of 22 and 150°C. The measurements were made at Chalk River with a neutron spectrometer with selected initial neutron energies ranging from 0.034 to 0.26 ev. A comparison with earlier measurements (Ref. 27) at 24°C shows good agreement; the later compilations (Refs. 25 and 26), however, cover a wider range of variables. Measurements made in the USSR on H_2O at 23 and 90°C, as well as measurements on monoisopropyl-diphenyl ($C_{15}H_{16}$) at 20°C are tabulated in Ref. 28.

References

1. J. A. McClure and R. L. Johnson, Critical Loading and Initial Static Experiments in the SPERT II Reactor with a Closed-Packed D_2O-Moderated Core, USAEC Report IDO-16996, Phillips Petroleum Company, June 1964.
2. F. D. Benton, Measurements of Bucklings and Void Effects in D_2O-Moderated, Organic- or H_2O-Cooled Lattices of UO_2 Rod Clusters, USAEC Report DP-873, E. I. du Pont de Nemours & Co., Inc., June 1964.
3. I. Kaplan, D. D. Lanning, and T. J. Thompson (Eds.), Heavy Water Lattice Project Annual Report, USAEC Report MITNE-46, Massachusetts Institute of Technology, Sept. 30, 1963.
4. W. B. Rogers, Jr., and F. E. Kinard, Material Buckling and Critical Masses of Uranium Rods Containing 3 Wt.% U-235 in H_2O, *Nucl. Sci. Eng.*, 20(3): 266 (November 1964).
5. P. I. Amundson, R. L. McVean, and J. K. Long, A Two-Zone Fast Critical Experiment (ZPR-III Assembly 42), USAEC Report ANL-6733, Argonne National Laboratory, January 1954.
6. J. M. Gasidlo, J. K. Long, and W. P. Keeney, Doppler Effect Measurements, Sodium Void Coefficients, and Critical Studies of a 5000-Liter Fast Power Breeder Reactor by the Two-Zone Method (ZPR-III Assembly 43), USAEC Report ANL-6838, Argonne National Laboratory, May 1964.
7. O. R. Hillig and D. W. Latham, Material Bucklings of Critical and Subcritical Uranium Carbide Fueled Graphite Assemblies, Part I, Experiment, USAEC Report NAA-SR-9771, Atomics International, Dec. 1, 1964.
8. E. R. Specht, Material Bucklings of Critical and Subcritical Uranium Carbide Fueled Graphite Assemblies, Part II, Theoretical Interpretation, USAEC Report NAA-SR-9772, Atomics International, Aug. 1, 1964.
9. L. Adamski, Z. Bajbor, W. Dabek, J. Koziel, and W. Suwalski, Critical and Exponential Assemblies at the Institute of Nuclear Research—Swierk, presented at the Third United Nations International Conference on the Peaceful Uses of Atomic Energy, Geneva, 1964, Paper A/Conf.28/P/807.
10. L. Adamski et al., Microscopic Neutron Flux Distributions in Unit Cells of Critical Assemblies of the NPY-Project, presented at the Third United Nations International Conference on the Peaceful Uses of Atomic Energy, Geneva, 1964, Paper A/Conf.28/P/499.
11. G. Bitelli, G. Gambardella, R. Martinelli, S. Nicosia, F. Orestano, A. Pulacci, E. Santandrea, P. Saya, and R. Zona, ROSPO—Organic Moderated Critical Experiments, presented at the Third United Nations International Conference on the Peaceful Uses of Atomic Energy, Geneva, 1964, Paper A/Conf.28/P/871.
12. K. Sumita et al., Subcriticality Measurements by Pulsed Method and Critical Experiments on Light Water System, presented at the Third United Nations International Conference on the Peaceful Uses of Atomic Energy, Geneva, 1964, Paper A/Conf.28/P/846.
13. F. W. Thalgott, J. K. Long, W. G. Davey, W. Y. Kato, S. G. Carpenter, H. A. Morewitz, and G. H. Best, Fast Critical Experiments and Their Analysis, presented at the Third United Nations International Conference on the Peaceful Uses of Atomic Energy, Geneva, 1964, Paper A/Conf.28/P/265.
14. J. L. Crandall, W. L. Brooks, I. Kaplan, F. L. Langford, Jr., and L. C. Schmid, Lattice Studies and Critical Experiments in D_2O Moderated Systems, presented at the Third United Nations International Conference on the Peaceful Uses of Atomic Energy, Geneva, 1964, Paper A/Conf.28/P/268.
15. R. W. Campbell, R. K. Paschall, and V. A. Swanson, The Age of Fission Neutrons to Indium Resonance Energy in Graphite, Part I, Experiment, USAEC Report NAA-SR-8683, Atomics International, June 15, 1964; also reported in *Nucl. Sci. Eng.*, 20(4): 445 (December 1964).
16. H. Alter, The Age of Fission Neutrons to Indium Resonance Energy in Graphite, Part II, Theory, USAEC Report NAA-SR-8684, Atomics International, Oct. 9, 1963.
17. R. K. Paschall, The Age of Fission Neutrons to Indium Resonance Energy in Zirconium-Water Mixtures, USAEC Report NAA-SR-9503, Atomics International, Sept. 15, 1964.
18. J. A. DeJuren, T. E. Stewart, and E. R. Specht, Measurements of Thermal Neutron Absorption Cross Section and Diffusion Length of Graphite Using an Sb-Be Source, USAEC Report NAA-SR-9803, Atomics International, Aug. 1, 1964.
19. T. Watanabe and O. D. Simpson, Low-Energy Neutron Fission Cross Section of ^{241}Pu, USAEC Report IDO-16995, Phillips Petroleum Company, June 1964.
20. T. Watanabe, M. S. Moore, O. D. Simpson, J. E. Russell, and R. W. Hockenbury, Experimental Measurements of the Fission Cross Section of ^{241}Pu, USAEC Report IDO-16976, Phillips Petroleum Company, Apr. 10, 1964.

Digitized by Google

21. F. F. Felber, Jr., D. R. Farmelo, and V. C. Van Sickle, The Integral $^{9}Be(n,2n)$ Cross Section, USAEC Report PWAC-433, Pratt & Whitney Aircraft Division, United Aircraft Corporation, May 19, 1964.
22. Wolf Haefele, The Fast Multiplication Effect Due to the $(n,2n)$ Reaction in Beryllium and Beryllium Oxide, in Proceedings of the Conference on the Physics of Breeding, October 19–21, 1959, USAEC Report ANL-6122, pp.163-176, Argonne National Laboratory.
23. J. W. Boldeman, Fission Spectrum Averaged Cross Sections of Threshold Reactions, *J. Nucl. Energy: Pt. A & B*, 18(8): 417-424 (August 1964).
24. J. R. Beyster, N. Corngold, H. C. Honeck, G. D. Joanou, and D. E. Parks, Neutron Thermalization and Reactor Applications, presented at the Third United Nations International Conference on the Peaceful Uses of Atomic Energy, Geneva, 1964, Paper A/Conf.28/P/258.
25. B. C. Haywood, A Compilation of the Scattering Law for Water at 22°C and 150°C, British Report AERE-R-4484, January 1964.
26. B. C. Haywood, A Compilation of the Scattering Law for Heavy Water at 22°C and 150°C, British Report AERE-R-4582, May 1964.
27. P. A. Egelstaff, Compilation of Early Scattering Law Data, British Report AERE-R-3931, January 1962.
28. V. I. Mostovoy, V. S. Dykarev, D. P. Eremeev, S. P. Ishmaev, I. P. Sadikov, Yu. S. Saltykov, V. A. Taraban'ko, and A. A. Chernyshov, Experimental Studies on Neutron Thermalization, presented at the Third United Nations International Conference on the Peaceful Uses of Atomic Energy, Geneva, 1964, Paper A/Conf.28/P/367.

Digitized by Google

Section

II

Power Reactor Technology

Fluid and Thermal Technology

Conduction

Reference 1 is a report on an analytical determination of the temperature distribution in long, cylindrical fuel elements cooled internally by several channels. This conduction problem has been treated in the past, and Ref. 2 is a recent article on the subject. The Ref. 2 article describes the derivation of the so-called ROB code for the determination of the steady-state temperature distribution for a heat-generating, circular cylinder cooled by a ring of holes. The ROB code provides for analytically calculating the temperature as a function of radius and azimuthal angle if the heat-generation rate in the cylinder is spatially independent. The particular geometry used in the ROB code is shown in Fig. II-1. The analytical derivation in Ref. 1 is similar to that

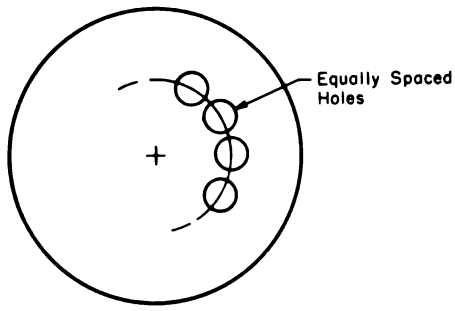

Fig. II-1 Cross section of cylinder illustrating geometry.[2]

in Ref. 2 except that a radially distributed heat-generation rate is provided for; Poisson's equation is solved by the method of "sources" and "sinks," with the assumption that the solid is isotropic. The reference presents the equations needed for calculating the temperature distribution for either an arbitrary radial distribution of the heat generation or a radial generation rate developed from neutron-diffusion theory.

Often in real cases the three-dimensional problem is important in elements of this kind; until the third dimension is incorporated into the analytical expressions, the designer must handle such problems as best he can. It may well be that the incorporation of a third dimension in the conduction equations would result in a prohibitively complex solution and that entirely numerical techniques will be required in calculation of the temperature distribution in the long, cylindrical fuel elements that are internally cooled.

References 3 and 4 present "large" conduction codes suitable for use on digital computing machines. Reference 3 presents a FORTRAN II code suitable for calculation of transient temperatures in a multiregion, axisymmetric, cylindrical configuration. The conduction code (ARGUS) allows up to 25 concentric regions, each region consisting of either a stationary or a turbulently flowing material having temperature-dependent properties. The stationary materials can have space- and time-dependent heat-generation rates, and temperatures are calculated at equally spaced nodal points. Material properties of the flowing materials are approximated by second-order polynomials. The thermal properties of the stationary materials must be constant except that, with appropriate heats of transformation, up to nine phase changes are allowed in these materials. Also allowed are 100 nodal points per radial row and up to 16 radial rows.

The IBM-650 code HEAT-1 presented in Ref. 4 is a one-dimensional time-dependent or steady-state heat-conduction code. The program obtains a numerical solution to the one-

Digitized by Google

dimensional heat-conduction equation in either slab or cylindrical coordinates by use of the finite-difference approximation to the partial differential equations. This program is somewhat smaller than the ARGUS code in that it can accommodate 10 regions and a maximum of 51 mesh points. The thermal conductivities and heat capacities are described by third-order polynomials, and a time-dependent and pointwise space-dependent heat source can be accommodated.

Apparently the thermal designer is accumulating a variety of machine codes that enable him to tackle many formidable conduction problems occurring in reactor design and analysis.

Reference 5 reports on the thermal conductivity of uranium dioxide fuel elements during irradiation. This reference deals with research at the Bettis Atomic Power Laboratory and is an extension of a program originally reported in USAEC Report WAPD-228. That report was reviewed in the March 1961 issue of *Power Reactor Technology*, 4(2): 39-43. Briefly the experiment was designed to measure the effective thermal conductivity of UO_2 and a zirconium oxide–uranium oxide mixture; the discussion here will be limited to those experiments employing only UO_2. Table II-1 gives the composition and density of the fuel materials used in the experiments, and Fig. II-2 illustrates the design of the capsule used for the in-pile measurements of the thermal conductivity. Table II-2 gives assembly and irradiation data on the several capsules. In Tables II-1 and II-2, the experiments designated "WAPD-22" are reported in WAPD-228, and the experiments designated "BETT" are reported in Ref. 5.

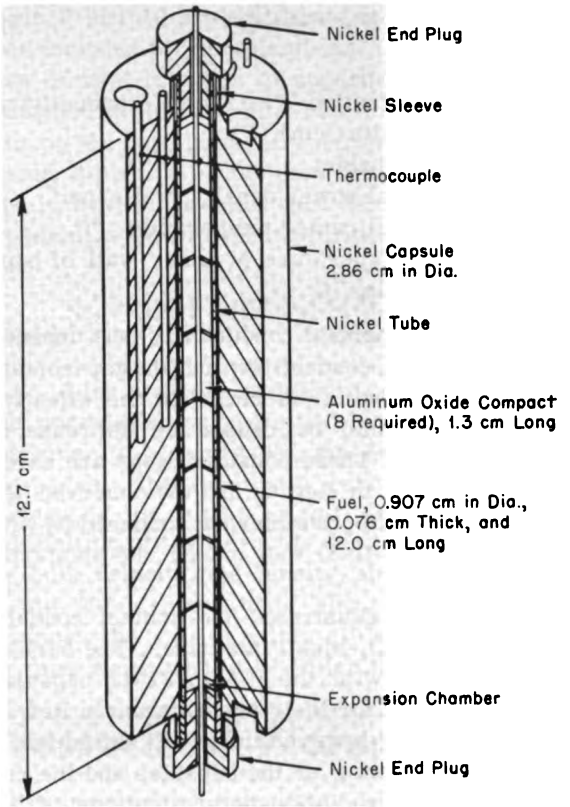

Fig. II-2 Capsule for in-pile measurement of the thermal conductivity of oxide fuels to high fission depletions[5] (BETT-69-4).

Table II-1 COMPOSITION AND DENSITY OF FUEL MATERIALS[5]

Experiment No.	Fuel	Wt.% ^{235}U in total U	^{235}U atoms/cm^3 ($\times 10^{-20}$)	Average fuel density	
				G/cm^3	% TD*
WAPD-22-11	UO_2 (natural)	0.7	1.65	10.4	95
BETT-69-1-C1	UO_2	21.0	50.0	10.6	97
BETT-69-4-C1	UO_2	21.4	51.0	10.6	97

* Percent of theoretical density.

The fuel cylinders were pressure bonded between the nickel capsule and a thin inner tube filled with BeO or Al_2O_3 (Fig. II-2). The capsule design was considerably different from the one employed for the WAPD-22 experiments, in which the fuel pellets were shrink fitted into type 304 stainless-steel capsules (Table II-2). The stainless-steel and nickel capsules had radial pairs of thermocouples for the determination of heat flux and a central thermocouple for the determination of the central temperature.

Figure II-3 illustrates BETT-69 capsule results for the effective thermal conductivity. The ordinate of Fig. II-3 shows the effective thermal conductivity, defined as follows:

Digitized by Google

$$K_{eff} = \frac{FP_f}{T_c - T_b} \quad (1)$$

where K_{eff} = effective thermal conductivity, watts/(cm)(°C)
F = constant
P_f = fuel power density, watts/cm^3
T_c = fuel center temperature, °C
T_b = temperature at inner wall of capsule, °C

The effective thermal conductivity thus depends on both the fuel conductivity and the gap-contact conductance, and a decrease in the effective conductivity could be caused by decrease in either quantity. These considerations are carefully explained in Ref. 5, and the observed decrease in the effective thermal conductivity with exposure (Fig. II-3) was indeed due primarily to irradiation.

Figure II-4 illustrates the contact conductances of the UO_2-metal interfaces. The earlier data obtained with the WAPD-22-11 capsules were reworked for their presentation in Ref. 5. This reworking involved improved estimates of the gamma heating of the capsules and the results of postirradiation determinations of the fuel-to-capsule gaps. Additional conclusions are quoted from Ref. 5 as follows:

1. The inpile thermal conductivities of UO_2 and UO_2 + ZrO_2 fuels at practical operating temperatures are essentially the same as their unirradiated conductivities up to fission depletions of about 10^{19} fissions/cc for operating temperatures near 500°C.

. . . . . .

3. For operating temperatures near 500°C, the thermal conductivities of UO_2, ZrO_2 + 34 w/o UO_2, and ZrO_2 + 46 w/o UO_2 decreased approximately 50, 25, and 35 percent, respectively, between 1×10^{19} and 25×10^{20} fissions/cc.

. . . . . .

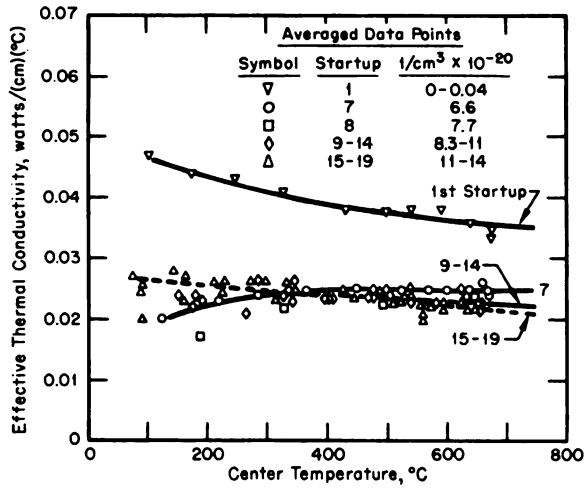

Fig. II-3 BETT-69-4 data for the effective thermal conductivity of UO_2 (Ref. 5).

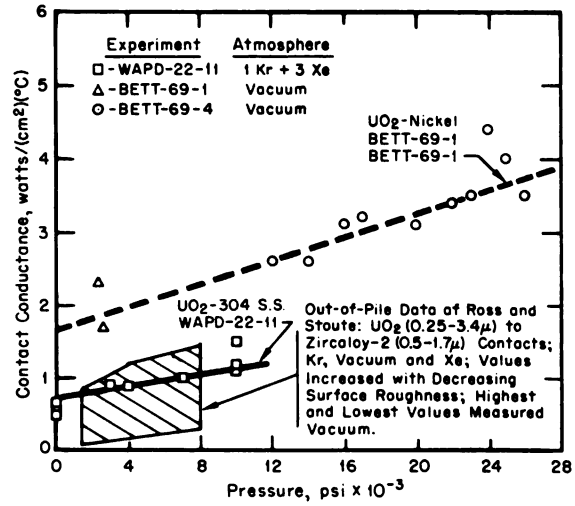

Fig. II-4 Contact conductances of UO_2-metal interfaces.[5]

Table II-2 ASSEMBLY AND IRRADIATION DATA[5]

Experiment No.	Capsule material	Gas-filling atmosphere	Fuel wall thickness, cm	Estimated total exposure, thermal neutrons/cm^2 ($\times 10^{-20}$)	Total burnup, fissions/cm^3 ($\times 10^{-20}$)	Remarks
WAPD-22-11	Type 304 S.S.	1 Kr + 3 Xe	0.365	4.0	0.35	Shrink-fitted fuel pellets
BETT-69-1-C1	Nickel	1 Kr + 3 Xe	0.365	2.0	5.4	Pressure bonded (thin internal cladding with powdered BeO in bore)
BETT-69-4-C1	Nickel	Vacuum	0.076	4.3	28	Pressure bonded (thin cladding supported by Al_2O_3 pellets shrink fitted after pressure bonding)

Digitized by Google

5. The initial inpile contact conductances of UO_2 + Zircaloy interfaces, derived from inpile data for UO_2 + nickel and UO_2 + type 304 stainless steel joints, are in good agreement with out-of-pile contact conductances of UO_2 + Zircaloy interfaces measured by Ross and Stoute [Canadian Report CRFD-1075]. Both the inpile data (for first start-ups) and the out-of-pile data indicate that, for interface pressures near 3000 psi, the contact conductance is approximately 1 watt/cm^2-°C for UO_2 + Zircaloy contacts between surfaces having surface roughnesses of less than 1 micron whether the interface is evacuated or filled with krypton and xenon. It is thought that the contact conductance decreases proportionally with the UO_2 conductivity, but additional data are needed to verify such decreases.

The thermal conductivity of uranium dioxide is also discussed in Ref. 6. This report presents an improved radial-heat-flow technique for the experimental determination of thermal conductivity, and a large section of the reference is a discussion of the technique and the results determined for Armco iron. However, the thermal conductivity of polycrystalline uranium dioxide was measured for the temperature range −57 to 1100°C. The uranium dioxide was prepared in the form of disks of nuclear-grade depleted UO_2 powder, cold pressed and sintered in hydrogen at 1850°C for 4 hr. The resulting pellets were 93.4% of the theoretical density (10.97 g/cm^3). The results indicated that the thermal resistivity, which is the reciprocal of the thermal conductivity, is linear between 200 and 1000°C with a slope of 0.0223 cm/watt. Between 1000 and 1100°C a slight deviation from the linear behavior was noted in the direction of increasing thermal conductivity, and the authors of Ref. 6 suggest that this may indicate a change in the composition of the material or a change in the basic heat-transport mechanism within the solid.

Gases

The following thermodynamic properties of helium are discussed in Ref. 7: pressure-volume-temperature and enthalpy relations, specific heat, viscosity, thermal conductivity, and Prandtl number. The compilation is an updating and expansion of previous work and includes recent information. In general, the property data are given for temperatures approaching 2000°F.

References 8 to 10 are British publications dealing with heat-transfer-coefficient calculations for gases at high temperatures. References 9 and 10 are not recent reports but have been included for completeness. The specialized case of heat transfer to superheated steam is presented in Ref. 11. This reference correlates data on the heat-transfer coefficient for superheated steam at 1000 psia flowing in a uniformly heated circular duct. The following expression is recommended for design purposes:

$$Nu_b = 0.021\ Re_b^{0.8}\ Pr_b^{0.6} \left(\frac{T_b}{T_w}\right)^{0.575} \qquad (2)$$

In Eq. 2 the symbols have their usual meanings. The correlation suggests that, as the wall temperature (T_w) increases, the Nusselt number decreases. The functional relation, which is derived by the author of Ref. 11, results from a definition of the Reynolds number in terms of the bulk velocity, the density, and the viscosity at the film temperature. The correlation reproduces the data to within ±10%, although only 18 runs were used to establish the correlation.

Pressurized Water

Fragmentary information on pressurized-water research of general interest was reported by Oak Ridge National Laboratory (Ref. 12) and Hanford Atomic Products Operation (Ref. 13). A dimensionless correlation was developed[12] for predicting the critical-heat-flux value for natural-convection burnout of water in a heated vertical channel closed at the bottom and open at the top to a liquid supply. Data were taken with tubes which were operated at atmospheric pressure and which had inside diameters from 0.086 to 0.25 in. and lengths from 6 to 48 in. This physical situation, although not of interest in reactor operations, might be encountered during the shutdown and depressurization of a power reactor. The correlation given in Ref. 13 is for the pressure drop occurring during local boiling. The experiments were conducted with a 19-rod electrically heated bundle; flow rates varied from 500,000 to 5×10^6 lb/(hr)(sq ft) at a pressure of 1200 psia.

References 14 and 15 deal with heat transfer to a fluid flowing in an annulus; Ref. 14 is concerned with water, whereas Ref. 15 deals with an arbitrary coolant. Annular-flow heat transfer was treated in the March 1961 issue of *Power Reactor Technology*, 4(2): 13-15, and the conclusion in that review was that under cer-

Digitized by Google

tain conditions the effect of the diameter ratio on the heat-transfer coefficients of the inner- and outer-wall surfaces was uncertain. In particular, Fig. IV-1 in that issue illustrates that the discrepancies by and large were between results obtained in this country and results obtained by Russian experimenters. After deriving theoretical expressions for heat transfer in an annulus, the author of Ref. 14 presents experimental data on the heat-transfer coefficients of inner- and outer-wall surfaces using average wall temperatures and calculated bulk water temperatures. The important result seems to be that the ratio of film coefficients of the inner- and outer-wall surfaces is dependent on the heat-flux level and the ratio of the inner and outer values of the heat flux. Accordingly the situation is somewhat more complex than was suggested in the earlier review. The author of Ref. 14 states that the theoretical predictions of Maloney, appearing in what is cited as an unpublished work, adequately fit the experimental results.

The analysis given in Ref. 15 extends consideration to heat transfer in an annulus with a variable circumferential heat flux. The treatment is completely analytical, and no experimental data are given. The analysis takes into consideration the resistance to circumferential mixing, with the assumption that in turbulent flow the eddy diffusivity in the circumferential direction is the same as that in the radial direction. Although no experimental support is given, the condition of a circumferentially varying heat flux is the usual one encountered in reactors.

Reference 16 is a report on the transient behavior of a natural-circulation loop operating near the thermodynamic critical point. The particular fluid studied in the report was Freon-114, primarily because it had a low critical temperature (294.2°F) and because thermodynamic data for the material were available. The analytical portion of the study consisted of writing one-dimensional conservation equations for a control volume and stacking the control volumes to obtain the simulated loop. The system of equations thus obtained was solved with the aid of a high-speed digital computer. The computer model, however, failed to represent the system adequately, primarily because of the assumptions used when the model was set up. The flow-stability results, however, are probably of general interest, and the following quotation from Ref. 16 serves to define them:

> It has been determined experimentally that operation of a single-phase, heat-transfer loop in the thermodynamic critical region of the fluid of the design studied in this experiment will produce pressure and flow fluctuations under certain conditions. The condition determined experimentally for the occurrence of sustained flow and pressure fluctuations was that the system fluid be passing through the thermodynamic region in which a maximum in the density-enthalpy product as a function of temperature, enthalpy, or density occurs. In this region it was found that as little as 1¼ kw of heating was necessary to obtain sustained flow oscillations. The loop would operate stably in the thermodynamic regions on either side of this maximum in the density-enthalpy product. It was noted experimentally that the magnitude and frequency of the pressure and flow fluctuations depended on whether the maximum in the density-enthalpy curve was being traversed from the low- or the high-temperature side. Approach from the low-temperature side resulted in a dominant frequency of 10 to 20 cps, which was 100 times the frequency found when traversing the maximum from the high-temperature side.

Reference 17 deals with the critical, or burnout, heat-flux determination in subcooled, boiling water flowing under forced convection. The reference contains a number of arbitrary correlations, mostly derived by manipulation of the Jens-Lottes equation. The existence of a number of correlations probably is caused by the attempt to correlate data taken from systems operating in various subcooled-boiling flow regimes. This is recognized by the author,[17] and as many as four different regimes are postulated. These are the nucleate-boiling flow regime, the stratified-bubble flow regime, the nonstratified-bubble regime, and froth flow. The nucleate-boiling flow regime probably is the most straightforward of all. In this case, which occurs only at subcoolings greater than about 50 Btu/lb, the nucleate bubbles are rapidly quenched by the liquid flow stream. Occurrence of the regime requires also a system pressure of at least 500 psi, mass velocity in excess of 0.9×10^6 lb/(hr)(sq ft), and an equivalent diameter in excess of ⅛ in. The stratified and nonstratified flow regimes are separated by a matter of degree rather than type, the stratified regime changing gradually to a nonstratified flow as the bubbles become dispersed in the bulk of the coolant. The stratified-bubble flow regime consists of unquenched bubbles which are concentrated close to the heat-transfer surface and which actively inhibit the frictional and heat-transfer effects of the turbulence caused by the nucleate boil-

Digitized by Google

ing. This "shield" minimizes the effect of the surface condition of the transfer surface, in contrast to the nucleate-boiling flow regime where a greater dependence of the critical heat flux with respect to the heat-transfer surface condition is encountered.[17]

Froth flow occurs at low subcoolings, with flow channels less than $\frac{1}{8}$ in. in diameter, or at pressures below 500 psi. The regime is characterized by relatively large amounts of unquenched bubbles, and the phase structures are somewhat similar to net vapor generation.

References 18 and 19 present design data pertinent to bundle type fuel assemblies. The particular geometry studied experimentally in Ref. 18 is illustrated in Fig. II-5; it consists of

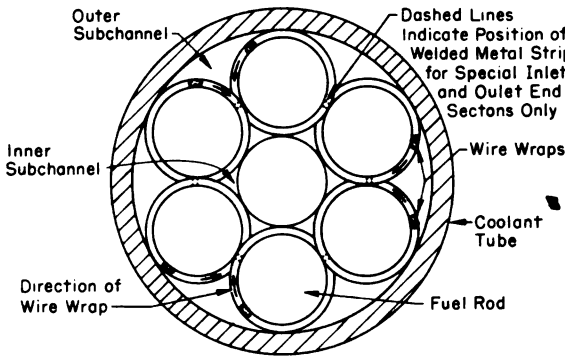
Outer Subchannel
Dashed Lines Indicate Position of Welded Metal Strips for Special Inlet and Oulet End Sectons Only
Inner Subchannel
Wire Wraps
Coolant Tube
Direction of Wire Wrap
Fuel Rod

Fig. II-5 Cross section of a wire-wrapped seven-rod bundle in a coolant tube.[18]

a wire-wrapped seven-rod bundle placed within a flow tube. The spiral wire wrappings are typical of rod-bundle construction and serve not only to promote mixing between the coolant subchannels but also to help maintain proper spacing between adjacent rods and between the rods and the flow tube. The geometry shown in Fig. II-5 is particularly germane to pressure-tube type reactors. The experiment was conducted by injecting a salt solution into the inner coolant channels of a 70-in.-long seven-rod bundle fitted into the flow tube. Tap water was introduced into the outer coolant channels, and samples were taken of the outer-coolant-channel fluid at several places along the length of the bundle for analysis of salt concentration. The measurements then could be converted into a determination of the amount of coolant mixing that resulted for various wire-wrap configurations. The wire wraps produced considerable interchannel mixing, and the amount of mixing varied with changes in the wire-wrap pitch, although the amount was relatively insensitive to the relative spacing between the wires on adjacent rods.

Reference 18 presents equations to determine the interchannel coolant-mixing rate and gives two illustrative problems on the use of the equations in a practical reactor design. It is shown, for example, that the use of the wire wraps reduces the temperature inequality between the inner- and outer-coolant-channel streams (for the particular design study) by about a factor of 6. Reference 19 discusses the effect of wire wraps on the pressure drop for axial turbulent flow through rod bundles. The experiments reported in Ref. 19 were done with two basic types of assemblies: one was similar to the bundle shown in Fig. II-5, and the second incorporated a wire wrapped around the entire rod bundle as well as on the individual rods. A 19-rod bundle with wraps on 12 rods plus the overall bundle was also tested. Data were taken with unwrapped rods, and the increase in pressure drop caused by wrapping the rods in the fuel bundle is presented graphically in the reference. It was determined that the ratio of the pressure drop with wrapped rods to the pressure drop for the nonwrapped rods was proportional to the square of the number of wire wraps per unit length of rod. Changing the relative spacing between wires on adjacent rods caused some change in the pressure drop along the rod bundle. The entrance and exit losses across the rod bundle and end fittings are presented in tabular form, and the reference states that the data show only "fair agreement" with generally accepted contraction-expansion loss coefficients.

Organic Fluids

Reference 20 presents data on the heat-transfer properties of organic coolants containing high-boiling (HB) residues. The coolants studied were Santowax R (a mixture of terphenyl isomers), a mixture of Santowax R and HB residues produced by the pyrolytic decomposition of Santowax R, mixtures of Santowax R and HB residue from the Organic Moderated Reactor Experiment (OMRE), and OMRE coolant. Data were taken in the range of Reynolds numbers from 10^4 to 10^5 and were found to correlate within ±8.5% by an equation given in the reference. In addition, several experiments

Digitized by Google

were carried out under subcooled boiling conditions. The coolants used for the experiment were the OMRE coolant and a 55% pyrolytic HB-residue mixture. The authors conclude that subcooled boiling of organic coolants containing HB residues is a complex phenomenon since the multicomponent fluids have a very wide range of boiling points; it is concluded[20] that "the advantages to be gained by operating a reactor in this region may be marginal." This conclusion is based on the fact that as boiling commences the heat-transfer coefficient often decreases and does not return to its nonboiling value until the wall temperature is about 70°C higher than that needed to initiate boiling. Although this conclusion may be peculiar to the experimental conditions and apparatus used in Ref. 20, it is an important one and probably justifies additional study. The investigation wherein the decrease in heat-transfer coefficient with the onset of boiling was observed utilized the 50% pyrolytic HB-residue mixture; when the OMRE coolant was used as the working fluid, small increases in the heat-transfer coefficient were noted at the onset of boiling. In any case the operation of an organic system in the nucleate-boiling regime appears questionable.

References 21 and 22 deal with the determination of heat-transfer and void correlations during the forced-circulation boiling of organic coolants. Reference 21 is primarily a discussion of the test loop used to determine the data, although it contains a correlation of the forced-convection heat transfer of Santowax R and an isopropyldiphenyl mixture. The same coolants were used in the experiments reported in Ref. 22 to determine boiling-heat-transfer behavior, and Santowax R was used as a coolant in the void-fraction measurements. Coolant velocities from 5 to 14 ft/sec were utilized at system pressures from 15 to 35 psia. The boiling-heat-transfer data were compared with correlations of Levy, Rohsenow, and Forster-Greif. Graphical comparisons are given in Ref. 22, and, in general, the equation of Levy represented the data best. The void-fraction data for Santowax R were classified into three regions: region I covering subcooled boiling for coolant subcoolings greater than 8°F, region II covering the transition from subcooled equilibrium bulk boiling, and region III covering equilibrium bulk boiling at qualities greater than 0.005. A correlation is developed in Ref. 22 for the subcooled and transitional boiling, and the bulk-boiling void fraction was correlated with the Lockhart-Martinelli curve. The reference concludes with a discussion of the physical properties of isopropyldiphenyl and Santowax R.

References

1. D. E. Amos and F. R. Zaloudek, Temperature Distribution in Long Cylindrical Fuel Elements Cooled Internally by Several Channels, USAEC Report HW-77681, Hanford Atomic Products Operation, May 1963.
2. J. C. Rowley and J. B. Payne, Steady-State Temperature Solution for a Heat-Generating Circular Cylinder Cooled by a Ring of Holes, *J. Heat Transfer*, 86(4): 531-536 (November 1964).
3. D. F. Schoeberle, J. Heestand, and L. B. Miller, A Method of Calculating Transient Temperatures in a Multiregion, Axisymmetric, Cylindrical Configuration. The Argus Program, 1089/RE248, Written in Fortran II, USAEC Report ANL-6654, Argonne National Laboratory, November 1963.
4. R. J. Wagner, Heat 1 — A One Dimensional Time Dependent or Steady State Heat Conduction Code for the IBM-650, USAEC Report IDO-16867, Phillips Petroleum Company, April 1963.
5. R. C. Daniel and I. Cohen, In-Pile Effective Thermal Conductivity of Oxide Fuel Elements to High Fission Depletions, USAEC Report WAPD-246, Westinghouse Electric Corp., Bettis Atomic Power Laboratory, April 1964.
6. T. G. Godfrey, W. Fulkerson, T. G. Kollie, J. P. Moore, and D. L. McElroy, Thermal Conductivity of Uranium Dioxide and Armco Iron by an Improved Radial Heat Flow Technique, USAEC Report ORNL-3556, Oak Ridge National Laboratory, June 1964.
7. D. R. Doman, High-Temperature Thermodynamic Properties of Helium, USAEC Report HW-78724, Hanford Atomic Products Operation, December 1963.
8. A. R. Pickering, Turbulent Heat Transfer to Fluids with Variable Physical Properties — A Review, British Report AEEW-R-290, February 1964.
9. N. Sheriff, P. Grumley, and J. France, Heat-Transfer Characteristics of Roughened Surfaces, British Report TRG-Report-447, Mar. 7, 1963.
10. A. C. Rapier, Forced Convection Heat Transfer in Passages with Varying Roughness and Heat Flux Around the Perimeter, British Report TRG-Report-519, Mar. 6, 1963.
11. W. A. Sutherland, Heat Transfer to Superheated Steam, USAEC Report GEAP-4528, General Electric Company, Atomic Power Equipment Department, May 1963.
12. Oak Ridge National Laboratory, July 7, 1964. (Unpublished)
13. M. M. Hendrickson and J. K. Green (Eds.), Research and Development Programs Executed for the Division of Reactor Development, Quarterly

Digitized by Google

Progress Report, July, August, September 1963, USAEC Report HW-79280, Hanford Atomic Products Operation, October 1963.

14. A. R. Pickering, Forced Convection Heat Transfer to Water in an Annulus, British Report AEEW-R-295, February 1964.
15. W. A. Sutherland and W. M. Kays, Heat Transfer in an Annulus with Variable Circumferential Heat Flux, USAEC Report GEAP-4571, General Electric Company, Atomic Power Equipment Department, May 1964.
16. Darrel G. Harden, Transient Behavior of a Natural-Circulation Loop Operating Near the Thermodynamic Critical Point, USAEC Report ANL-6710, Oklahoma State University, Argonne National Laboratory, and Associated Midwest Universities, May 1963.
17. R. J. Weatherhead, Nucleate Boiling Characteristics and the Critical Heat Flux Occurrence in Subcooled Axial-Flow Water Systems, USAEC Report ANL-6675, Argonne National Laboratory, March 1963.
18. E. D. Waters, Fluid Mixing Experiments with a Wire-Wrapped 7-Rod Bundle Fuel Assembly, USAEC Report HW-70178(Rev.), Hanford Atomic Products Operation, November 1963.
19. E. D. Waters, Effect of Wire Wraps on Pressure Drop for Axial Turbulent Flow Through Rod Bundles, USAEC Report HW-65173(Rev.), Hanford Atomic Products Operation, June 1963.
20. A. G. Debbage, M. Driver, and P. R. Waller, Heat Transfer Properties of Organic Coolants Containing High-Boiling Residues, British Report AEEW-R-261, January 1963.
21. F. Bergonzoli (Ed.), Flow-Stability Test Loop, USAEC Report NAA-SR-8610, Atomics International, Mar. 1, 1964.
22. F. Bergonzoli and F. J. Halfen, Heat Transfer and Void Formation During Forced Circulation Boiling of Organic Coolants, USAEC Report NAA-SR-8906, Atomics International, June 15, 1964.

Digitized by Google

Section

III

Power Reactor Technology

Fuel Elements

Cermet Fuels for Fast Reactors

Development at the Oak Ridge National Laboratory (ORNL) of fuel-fabrication processes[1] for core B of the Enrico Fermi reactor has been concentrated[2] on 0.112-in.-thick flat cermet plates containing 35 wt.% UO_2 dispersed in, and clad with, type 347 stainless steel. Spheroidal oxide fuel particles with diameters of 105 to 149 μ (−100 +140 mesh) were used.[2] In the development program different tendencies for fragmentation and stringering were observed for different batches of the spheroidal UO_2 during roll-bonding operations. An attempt[3] was made to establish a specification that would permit the consistent purchase of spheroidal UO_2 with a high degree of reliability to minimize fragmentation and stringering during roll bonding. A number of control tests were devised in an attempt to characterize different batches of powder. The method of evaluation was to compare metallographically the stringering and fragmentation in rolled plates made with material from each batch of UO_2 with that of rolled plates fabricated with fused and ground material. Oxide batches with performances equal to or poorer than the standard were rated as unacceptable, and those with performances superior to the reference were classified in their relative order of quality. Results of the characterization tests reported in Ref. 3 are summarized as follows:

1. Microhardness. Good particles with low porosity and high bulk density cracked severely. No correlation with performance during roll bonding could be established.

2. Attrition. Correlations could not be established.

3. Crushing strength. Results of simple test procedures were capable of differentiating good from poor batches. Differentiation of a large amount of material in the intermediate category could not be made. However, it was felt that more exotic test procedures, requiring large expenditures of time and effort, might be developed to permit better differentiation of the intermediate batches.

4. Grain size. No correlations could be established.

5. Surface area. The Brunauer-Emmett-Teller (BET) method, using N_2 and krypton, was employed. No correlations could be found. It is interesting to note that differences as great as 40% were observed between BET measurements made at ORNL and fuel vendors, although repetitive measurements at ORNL exhibited reasonably high degrees of reproducibility.

6. Bulk density. Mercury-pycnometer measurements were capable of differentiating between the highest and lowest grades of UO_2 but were not capable of separating acceptable material from intermediate grades of UO_2.

7. Solid embedment. Density determinations on particles embedded in epoxy resin, when combined with empirical density corrections based on metallographic observations, provided the best correlations.

On the basis of the above evaluations, it was concluded that the mercury-pycnometer method would provide gross classification of obviously acceptable and unacceptable batches. A minimum density of 10.1 g/cm^3 was set as a lower limit for grade-A material, and material with a density below 9.8 g/cm^3 was classified as unacceptable. Material having intermediate densities was classified as grades B or C. The solid-embedment technique could then be used to classify batches between these limits.

Uranium dioxide powder that was classified[3] in various grades below the optimum, as a result of the preceding test procedures, was heated in hydrogen for 1 hr at 1750°C. Internal

Digitized by Google

porosity decreased, and the quality of all powder batches was increased as a result of this treatment.

A rolling temperature of 1200°C was previously established for the Fermi prototype fuel elements on the bases that the shape of the UO_2 particles was retained and that the condition of the plate surfaces was acceptable. A reevaluation of rolling temperatures from 900 to 1250°C was made[3] using the standard Fermi prototype rolling schedule, the best-rated UO_2 powder batches, and a loading of 33 wt.% UO_2.

Results are summarized as follows:

1. Surface finish. Rolling above 1050°C produced a mat finish, whereas lower rolling temperatures provided a satin-smooth finish that was free of pits.

2. Fragmentation and sintering. In all cases this was not excessive but increased with decreasing rolling temperature.

3. Density of cermet fuel. In all cases this was insensitive to the rolling temperature within the range evaluated.

4. Core-cladding bond. Bonding occurred at all temperatures. Grain coarsening became excessive at temperatures greater than 1150°C.

On the basis of the preceding results, it was concluded that the optimum rolling temperature was 1150°C. Other investigations[3] indicated that cold rolling severely fragmented the cermets made with either optimum- or poor-quality oxide and that fragmentation of the oxide was enhanced if too small an initial reduction was used in plate rolling. It was demonstrated[4] that the performance of fuel elements containing UO_2–stainless-steel cermets clad with stainless steel is, under thermal-cycling conditions somewhat comparable to those anticipated during large changes in reactor power levels, a function of the fabrication method employed. Investigations centered on stainless-steel-clad cermet fuel plates containing 40 to 50 vol.% UO_2. These studies included evaluation of hot compacted, as well as cold compacted and sintered, cermet cores and clad plates that were hot rolled at 1100°C to reductions in area from 60 to 90%. The cermet cores in these rolled plates were fabricated either from random-mixed or homogenized-mixed* cermet cores.

*Random-mixed cores are formed from mixtures of UO_2 and stainless-steel particles. Homogenized-mixed cores are formed from mixtures of stainless-steel powder and UO_2 spheres which have been precoated with stainless-steel powder.

The thermal-cycling tests performed[4] on these materials employed a hot-leg temperature of 800°C with the cold leg either at 250°C or at room temperature. Holding times and transfer times were varied in the different tests; however, the most significant results were obtained from tests of up to 1000 cycles at a heating rate of 60 to 70°C/sec and a cooling rate of 250°C/sec.

Examination of the as-rolled plates indicated excessive stringering in the random-mixed cores and a relatively uniform dispersion of the UO_2 in the homogenized-mixed cores. Stringering in the random-mixed cores increased with increasing reductions. In the homogenized-mixed cores, there was no evidence of large agglomerates, stringering, or cracking of the UO_2. Performance of the homogenized-mixed samples during cycling was superior to that for the random-mixed cores. Sigma-phase formation was observed in the type 316L stainless-steel core. The amount of sigma increased with increasing number of cycles and was probably associated with the amount of time at 800°C in each cycle. On the basis of the observed distribution of carbides and sigma phase after cycling, it was concluded that these would not be deleterious to performance.

Although additional details are not given in Ref. 4, it is stated that new fabrication methods had been developed to produce plates of improved quality which would provide better thermal-cycling stability.

It was concluded[4] that stainless-steel-clad cermets containing 40 to 50 vol.% UO_2–stainless steel, prepared by the homogenized-mixed-core process, could withstand 1000 thermal cycles up to 800°C at heating and cooling rates up to 70 and 250°C/sec. The following conditions must be met[4] to provide good resistance to thermal cycling:

1. Elimination of continuous interparticle networks in the core

2. Use of spheroidal UO_2 that is well dispersed in the core

3. Use of spheroids with minimum internal stress and high resistance to fragmentation

4. Good initial bonding between cermet core and picture-frame cladding

The use of Dynapak and a combination of Dynapak plus swaging is under development[5] at Los Alamos for the fabrication of refractory-metal-clad 45 vol.% UO_2–tungsten cermet fuels. The program is aimed at determining the fea-

Digitized by Google

sibility of coextruding refractory-metal-clad cermet fuel elements. Work has been concentrated on a cermet made from 2-μ tungsten powder and 20-μ UO_2 powder which was hydrostatically pressed into 1¼-in.-diameter cylinders at either 50,000 or 70,000 psi. These compacts were induction sintered at 2200°C for 2 hr. Slow heating (4 hr) and cooling (2½ hr) cycles were required to minimize thermal-stress cracking. After the pellets were sintered, they were machined to dimensions of 1 in. in diameter by 1 in. long; their density was 85% of theoretical. Coextrusion billets were prepared by loading the machined pellets with a light press fit into cans of either molybdenum, 70 wt.% molybdenum–tungsten, or 25 wt.% molybdenum–tungsten and then electron-beam welding the lids. These billets were extruded in air, with glass wool as a lubricant, after they were preheated in H_2 to about 2000°C. Typical conditions included a fire pressure of 750 to 900 psi, velocity at contact from 460 to 540 in./sec, and extrusion ratios of 4 to 9. Typical yields ranged from 75 to 100% for finished lengths and diameters from 4¾ to 7¼ in. and 0.47 to 0.75 in. Although the cermet bond was uneven as a result of the penetration of UO_2 particles into the cladding, core-to-cladding bonding was generally good for all rods, and the bond quality increased with increasing extrusion ratio.

One rod clad with 25% molybdenum–tungsten and coextruded to a reduction in area of 89% was further reduced 75% in area by swaging at 1800°C (first third of reduction) and then at 1500°C. The surface appearance and bond quality were good. It was indicated that further reductions were possible.

It was suggested[5] that improvements in both fabrication and performance could be achieved with a 25 wt.% molybdenum–tungsten alloy for the cermet as well as for the cladding. Advantages claimed for this alloy are compatibility with H_2 and UO_2, availability, low relative cost, good high-temperature strength, and a melting point in excess of 3100°C. Furthermore, this alloy is less dense and is simpler to fabricate than tungsten. The success to date with Dynapak extrusions, as well as the potential advantages that can be gained through the use of the 25 wt.% molybdenum–tungsten alloy, have led to suggested programs at Los Alamos involving the extrusion of other shapes, the use of higher UO_2 loadings, and thinner cladding.

Fabrication of Various Fuel Assemblies

As part of the Fuel Cycle Program of the U. S. Atomic Energy Commission (AEC), the Atomic Power Equipment Department (APED) of the General Electric Company initiated a program aimed at extending the performance capabilities of UO_2 fuel elements in boiling-water reactors. Under this program 12 special assemblies have been fabricated and inserted in the Vallecitos Boiling Water Reactor (VBWR) for irradiation testing. Detailed descriptions of the fabrication of 3 of these special assemblies are given in Refs. 6, 7, and 10. The APED work under the Fuel Cycle Program has been reviewed previously in *Power Reactor Technology*, 7(1): 27-50, and 7(4): 354-355. The reports reviewed here present fabrication details not available when the earlier reviews were prepared; some repetition has been allowed for convenience of reading.

The AEC Fuel Cycle Special Assembly 8L, containing 16 fuel rods in a 4 by 4 array, was aimed[6] at demonstrating the performance of very thin (0.005 in.) type 304 stainless-steel cladding. The selection of the 0.005-in.-thick cladding for the program was based upon the realization that this represented the thinnest available stainless-steel tubing capable of performing a cladding function. Of the 16 fuel rods in the 8L assembly, 12 contained UO_2 with thin cladding. The corner rods had heavier cladding (0.015 in.) to reduce the probability of damage to the fuel assembly during handling. The 12 test rods, about 46 in. long, contained 4.58% enriched-UO_2 pellets which were 0.370 in. in diameter and which were clad with ¼-hard stainless-steel tubing. A 7-in.-long fission-gas plenum was designed to accommodate 100% gas release at twice the target burnup. In an effort to minimize wrinkling of the cladding, the cladding was swaged over the pellets, providing a nominal rod diameter of 0.380 in. Target heat flux and burnup were 500,000 Btu/(hr)(sq ft) and 10,000 Mwd/ton, respectively. At this heat flux a differential diametral expansion between the fuel and the cladding of 0.0035 in. was calculated, which would result in plastic straining of the cladding. Cladding-stress calculations, materials specifications, element design, cladding fabrication and evaluation, fuel-pellet fabrication, fuel-rod fabrication, and results of preirradiation tests

Digitized by Google

are discussed and described in detail in Ref. 6. Irradiation testing of this special element was begun in November 1961 and was terminated in December 1963 as a result of the final shutdown of the VBWR.

The AEC Fuel Cycle Special Assembly 9L contained UO_2-molybdenum cermet fuel.[7] Molybdenum additions were made in an attempt to increase the thermal conductivity of UO_2. Vacuum hot-pressing techniques were used to produce the two types of cermet pellets utilized in this assembly: (1) pellets containing 20 vol.% molybdenum fibers had densities of 94 to 95% of theoretical and (2) pellets fabricated from molybdenum-coated UO_2, containing approximately 16 vol.% molybdenum, had densities of 84 to 96% of theoretical. Radial orientation of the molybdenum fibers in the pellets was achieved by means of unidirectional compaction. Hot pressing of the molybdenum-coated UO_2 particles provided a continuous molybdenum network. The forms of UO_2-molybdenum cermets selected for the program were based on the intent to cover the largest possible range of difference in the mode of metal-phase distribution. Three fuel rods fabricated with each of the two types of uranium-molybdenum cermets were combined with two rods of conventional UO_2 pellet design to form the eight-rod Special Assembly 9L. All fuel cladding was type 304 stainless steel with an outside diameter of 0.515 in., a wall thickness of 0.020 in., and a pellet-to-cladding diametral clearance of 0.003 to 0.004 in. The objective of this test was to compare the performances of the cermet fuels and UO_2 after operation at a surface heat flux of 500,000 Btu/(hr)(sq ft) and a burnup approaching 15,000 Mwd/ton. Irradiation testing was begun in the VBWR in September 1962 and was terminated at the final shutdown of the VBWR in December 1963. The impetus for this series of irradiation tests was based on out-of-pile thermal-conductivity data[8,9] obtained for UO_2-Mo and UO_2-ThO_2-Nb (10 to 30 vol.% metal) which indicated potential improvements of 300%. Calculations of axial and radial temperature profiles anticipated for the cermet rods and the bulk UO_2 rods indicated substantial differences. Relative performance could then be judged by an analysis of microstructure data. Details of these calculations, as well as fuel-element-design characteristics, materials specifications, fabrication procedures, and results of preirradiation evaluations, are given in Ref. 7.

The AEC Fuel Cycle Special Assembly 11L contained[10] sintered UO_2 extrusions prepared independently under two different projects. One project was sponsored by the United States–Euratom Joint Research and Development Program at Compagnie Industrielle des Combustibles Atomiques Frittés (CICAF). The other project was a joint effort of the Allis-Chalmers Mfg. Co. and The Electric Autolite Co. (AC-EA) as part of the AEC Fuel Cycle Program. Fuel densities achieved were 97.6 and 96.2% of the theoretical density for the CICAF and AC-EA sintered extrusions. A 16-rod (4 by 4) assembly was fabricated for testing in the VBWR at a surface heat flux of 400,000 Btu/(hr)(sq ft). It contained 12 rods fabricated with sintered extrusions (6 from each program) and 4 pellet rods for comparison. The cladding was $\frac{1}{8}$-hard type 304 weld-drawn stainless steel with an outside diameter of 0.540 in. and a wall thickness of 0.022 in. Extrusion processes, descriptions of extrusions, fabrication and assembly procedures for fuel rods, irradiation design criteria, materials specifications, and results of preirradiation examinations are reported in considerable detail in Ref. 10. Results of some of the VBWR irradiations are summarized in two 1964 Geneva Conference papers (Refs. 11 and 12).

Hanford has published detailed specifications for swage compaction[13] and vibratory compaction (VIPAC)[14] of mixed oxide (UO_2-PuO_2) fuel in Zircaloy cladding for the Mark I-M, 19-rod clusters being irradiated in the Plutonium Recycle Test Reactor (PRTR). Fuel for the swaging process and the VIPAC process is a mixture of UO_2 and PuO_2 formed by a high-energy-rate pneumatic-impaction (NUPAC) method that yields fuel particles with a density greater than 97% of the theoretical density.

Ten full-sized sodium-bonded uranium carbide fuel assemblies of hypostoichiometric composition were fabricated[15] by Atomics International for testing in the Hallam Nuclear Power Facility. The objectives of the program, in addition to the irradiation testing of sodium-bonded fuel elements in the Hallam reactor, included the development of fabrication methods for carbide, the evaluation of storage conditions for cast carbide, and the development of sodium-bonding techniques and nondestructive test methods.

Each clad fuel rod[15] was about 182 in. long and 0.952 in. in diameter and contained a

Digitized by Google

uranium carbide fuel column 0.872 in. in diameter and 156 in. long. The radial sodium annulus between the fuel and the type 304 stainless-steel cladding was 0.030 in.; helium gas at 1 atm occupied the region above the sodium level. Each fuel assembly contained eight fuel rods. Uranium carbide enrichment in eight assemblies was 3.7%, and in the remaining assemblies, 4.9%. One of the eight assemblies with the 3.7% enrichment contained thermocouples located within the fuel and on the cladding surface.

The fabrication and inspection methods used for these sodium-bonded fuel elements are described in detail in Ref. 15. A number of significant observations are summarized below:

1. Uranium dioxide feed was converted to UC melt stock by the carbothermic reaction.

2. Better control of carbon content was attained for melt stock containing less than 500 ppm oxygen. The melt stock of lower oxygen content gave less splatter of the melt on the graphite electrode and thus less erratic carbon pickup.

3. Compensation of carbon pickup from the electrode was made by means of uranium-metal additions.

4. Metallographic determinations of carbon content near stoichiometric (4.6 to 4.8 wt.% carbon), based on comparison with controls, were more accurate than the analytical methods employed.

5. Dry storage was demonstrated to be effective, provided that prescribed fuel-preparation and fuel-storage conditions are followed.

6. Dry cutting methods were developed.

7. Proper fuel cleanliness was a necessary prerequisite for good sodium bonding.

Zircaloy-2-clad tubular fuel elements containing thorium–2.5 wt.% uranium (93.2% enriched)–1 wt.% zirconium fuel alloy were fabricated[16] for irradiation testing in the P-7 high-temperature high-pressure water loop of the Engineering Test Reactor (ETR). Fabrication development, including arc-melting techniques, coextrusion procedures, metallurgical evaluation, and fuel-element-assembly procedures, is described. It was shown that the zirconium addition to the base fuel composition improved the surface quality of arc-cast ingot, improved uranium homogeneity, lowered the fuel-alloy hardness, and was beneficial in consumable-electrode fabrication. Fully bonded tubular fuel, 1.750 in. in outside diameter by 1.050 in. in inside diameter with 0.025-in.-thick Zircaloy cladding on both the outside and inside diameters, was produced by coextrusion at 760°C at a reduction ratio of 17 to 1. Fuel elements 8 in. in length were closed by brazing Zircaloy-2 end caps with 5 wt.% beryllium–Zircaloy-2 alloy, followed by electron-beam welding of the braze line. Three fuel elements were charged in the P-7 loop in April 1963 and were operating at a maximum specific power of 230 kw/ft, a peak heat flux of 1.12×10^6 Btu/(hr)(sq ft), and a maximum calculated fuel temperature of 620°C. Interim measurement of fuel density will be made throughout the irradiation in which the target has a burnup of 3 at.%, or approximately 26,000 Mwd/ton.

Information on the potential for plutonium-enriched fuel in pressurized-water reactors will be obtained[17] as a result of the Saxton Plutonium Project. Nine fuel assemblies containing PuO_2-UO_2 are to be irradiated at the center of the Saxton core, and 12 stainless-steel-clad assemblies containing UO_2 are to be irradiated at the core periphery. Two of the plutonium fuel assemblies will contain PuO_2-UO_2 fuel that has been vibratorily compacted into Zircaloy-4 tubes; the remaining plutonium fuel assemblies will contain PuO_2-UO_2 pellets in a Zircaloy-4 cladding. Zircaloy was selected over stainless steel as the cladding material for the plutonium-containing elements because it provides higher initial reactivity and longer lifetime for a given plutonium enrichment. Equal heat ratings are contemplated for both types of plutonium-containing fuel elements. Descriptions of the fuel and fuel rods are summarized in Tables III-1 and III-2. Nuclear Materials & Equipment Corp. will supply the pelletized plutonium-containing fuel elements, and the VIPAC fuel elements will be fabricated[17] by Hanford from feed material prepared by the Dynapak process.

Table III-1 FUEL-ROD DETAILS FOR THE SAXTON PLUTONIUM PROJECT[17]

	Plutonium	Uranium
Cladding material	Zircaloy	304 S.S.
Cladding thickness, in.	0.023	0.015
Cladding outside diameter, in.	0.391	0.391
Diametral gap, in.	0.005 for pelletized 0.0 for VIPAC	0.004

Digitized by Google

Table III-2 FUEL DETAILS FOR THE SAXTON PLUTONIUM PROJECT[17]

Material	6 wt.% PuO_2–94 wt.% UO_2	6 wt.% PuO_2–94 wt.% UO_2	UO_2
Type	Pelletized	VIPAC	Pelletized
Diameter, in.	0.340	0.345	0.357
Density, % of theoretical	94	88	93
Enrichment	6 wt.% Pu	6 wt.% Pu	5.7 wt.% ^{235}U

Isotopic content of Pu, %

^{239}Pu	90.46
^{240}Pu	8.60
^{241}Pu	0.90
^{242}Pu	0.04

Insertion of the plutonium-containing fuel assemblies in the Saxton reactor is scheduled for July, and plans are that these fuel assemblies will be irradiated for two years. Post-irradiation examination and analysis are scheduled for the period January 1968 to February 1969. A maximum fuel-rod heat rating of 16 kw/ft has been established[18] for the Zircaloy-4-clad PuO_2-UO_2 fuel rods. The following comments on hydrogen pickup and oxide thickness on the cladding are quoted from Ref. 17:

The hydrogen pickup by the Zircaloy clad and the thickness of the ZrO_2 coating formed in-pile were calculated for linear rod powers of 16 kw/ft and assuming 40% down time for the reactor. The results showed that the hydrogen level at the end of life, 130 ppm, will be considerably below the level at which hydride problems occur. The ZrO_2 coating thickness and the temperature drop across the coating were found to be negligible.

Also from Ref. 17 a survey of performance of VIPAC fuel in other test programs is summarized as follows:

1. Based on technology already developed at the national laboratories, no defects in vibrationally compacted fuel rods are anticipated.

2. The results of the national laboratory experiments show that no significant fuel washout and no waterlogging results from defects in rods containing loose powder fuel.

3. The economic incentives for developing vibratory compacted PuO_2-UO_2 fuels and the present state-of-the-art provide strong motivation for carrying out engineering demonstration tests in the Saxton reactor.

References

1. J. E. Cunningham et al., Specifications and Fabrication Procedures for APPR-1 Core II Stationary Fuel Elements, USAEC Report ORNL-2649, Oak Ridge National Laboratory, Feb. 11, 1959.
2. J. H. Cherubini et al., Fabrication Development of UO_2–Stainless Steel Composite Fuel Plates for Core B of the Enrico Fermi Fast Breeder Reactor, USAEC Report ORNL-3077, Oak Ridge National Laboratory, Apr. 18, 1961.
3. A. J. Taylor et al., Characterization of Spheroidal UO_2 Particles and Studies of Fabrication Variables for Core B Fuel Plates of the Enrico Fermi Fast Breeder Reactor, USAEC Report ORNL-3645, Oak Ridge National Laboratory, August 1964.
4. J. M. Davies and C. Steer, Thermal Cycling of UO_2–Stainless Steel Cermets, British Report AERE-M-1253, January 1964.
5. J. M. Dickinson and T. J. Ready, Feasibility Study of the Co-Extrusion of Refractory Metal Clad Reactor Fuel Elements, USAEC Report LAMS-3065, Los Alamos Scientific Laboratory, Apr. 12, 1964.
6. J. P. Hoffman, Design and Fabrication of Pellet Fuel Rods Clad with Thin-Wall Stainless Steel, USAEC Report GEAP-4407, General Electric Company, Atomic Power Equipment Department, February 1964.
7. S. Y. Ogawa, AEC Fuel Cycle Program—Design and Fabrication of Special Assembly 9-L, Irradiation Performance Test of UO_2-Cermet Fuel, USAEC Report GEAP-4435, General Electric Company, Atomic Power Equipment Department, March 1964.
8. S. J. Paprocki et al., Preparation and Properties of UO_2 Cermet Fuels, USAEC Report BMI-1487, Battelle Memorial Institute, Dec. 19, 1960.
9. Y. Baskin et al., Some Physical Properties of Thoria Reinforced by Metal Fibers, *J. Am. Ceram. Soc.*, 43: 489-492 (September 1960).
10. F. H. Megerth, Design and Fabrication of Fuel Rods Containing Sintered UO_2 Extrusions, Assembly 11L, USAEC Report GEAP-4556, General Electric Company, Atomic Power Equipment Department, February 1964.
11. S. Naymark and C. N. Spalaris, Oxide Fuel Fabrication and Performance, presented at the Third United Nations International Conference on the Peaceful Uses of Atomic Energy, Geneva, 1964, Paper A/Conf.28/P/160.
12. W. P. Chernock, R. M. Mayfield, and J. R. Weir, Jr., Cladding Materials for Nuclear Fuels, presented at the Third United Nations International Conference on the Peaceful Uses of Atomic Energy, Geneva, 1964, Paper A/Conf.28/P/255.
13. Hanford Atomic Products Operation, Specifications for Swage-Compacted, Mixed Oxide (UO_2-PuO_2), Fuel Elements for the PRTR (Mark I-M), USAEC Report HW-79290, Oct. 1, 1963.
14. Hanford Atomic Products Operation, Specifications for Vibrationally Compacted, Mixed Oxide

Digitized by Google

(UO_2-PuO_2), Fuel Elements for the PRTR (Mark I-L), USAEC Report HW-79291, Oct, 1, 1963.
15. W. Draganchuk, UC Fuel Element Design and Fabrication, USAEC Report NAA-SR-9988, Atomics International, Aug. 1, 1964.
16. R. S. Kemper et al., Fabrication of Zircaloy-2 Clad Thorium–Uranium Alloy Fuel Elements, USAEC Report HW-79843, Hanford Atomic Products Operation, March 1964.
17. N. R. Nelson, Saxton Plutonium Program, Quarterly Progress Report for the Period Ending September 30, 1964, USAEC Report WCAP-3385-1, Westinghouse Atomic Power Division, October 1964.

Digitized by Google

Section

IV

Power Reactor Technology

Components

EBR-II Control-Drive Mechanisms

The Experimental Breeder Reactor II (EBR-II) is controlled by 12 hexagonal-shaped control subassemblies, moved vertically by 12 rack-and-pinion type electromechanical drive mechanisms. These are capable of scramming the control assemblies with an acceleration of 1.5 *g*, with a pneumatic cylinder providing the assist to attain this acceleration. The design stroke for the mechanism is 14 in. The control assembly was described in the EBR-II hazards summary report (Ref. 1) that was issued in May 1957. Some of the novel features of the mechanism (shown in Fig. IV-1) are as follows:

1. The mechanism has internal and external bellows seals that are fabricated from 0.010-in.-thick stainless-steel sheet to maintain vessel integrity.

2. A sensing-device shaft is used to indicate whether the control assembly is engaged to the mechanism. This sensing shaft is housed within the 26-ft-long main shaft.

3. A pneumatic cylinder at the top of the main shaft is used to accelerate the control assembly during a scram. Normal pressure in the cylinder is 30 psig.

4. An oil-filled dashpot decelerates the control assembly during the final $4\frac{1}{8}$ in. of scram.

5. All the control-assembly drive mechanisms are mounted on a single platform. This platform can be raised 3 in. to check the control-assembly grippers to ensure that they are disengaged and are clear of the adapters of other subassemblies in the core. The platform is lowered $\frac{7}{8}$ in. from its normal operating position to engage the control assemblies.

6. A labyrinth seal is used to limit the flow past the shaft bearing in the vessel cover.

Extensive testing was performed on 2 prototype drive mechanisms and on 1 of the 14

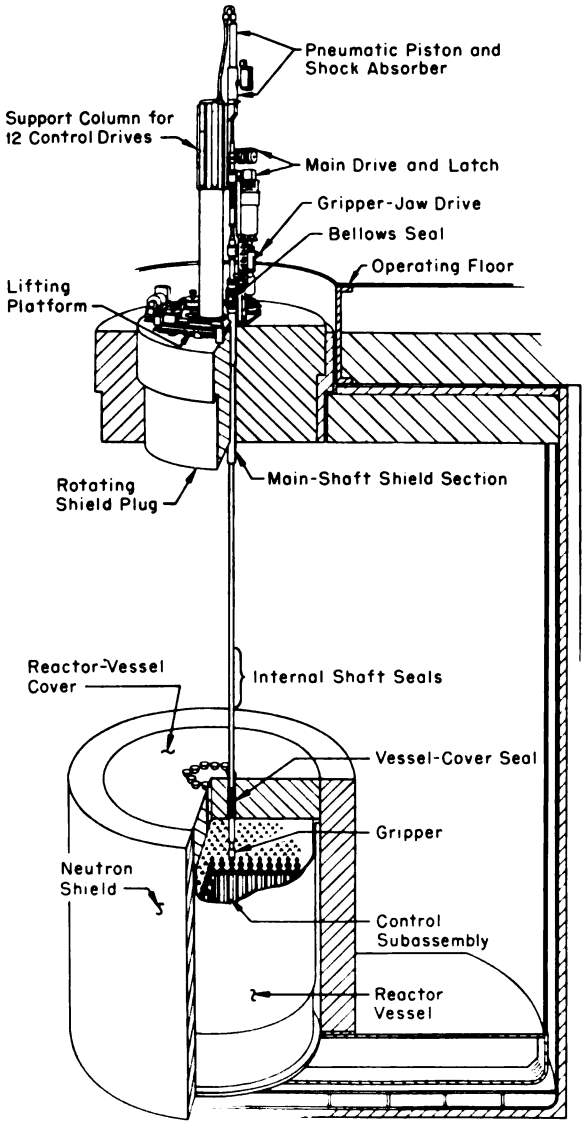

Fig. IV-1 Simplified drawing of components of the EBR-II control-rod drive.[2]

Digitized by Google

production mechanisms that were fabricated.[2] Table IV-1 summarizes the testing details.

Table IV-1 CONTROL-MECHANISM TESTING[2]

Rod	Environment	Temperature, °F	No. of full-stroke cycles	No. of gripper operations	No. of scrams
P-1	Air	Room	300		
	Sodium	300 to 900	13,200		24
P-2	Air	Room	31,440		
	Sodium	300 to 900	1,680	15	35
F-1	Air	Room	900	20	120
	Air	800	700	6	5
	Sodium	750	1,100	18	80

All these tests were performed with no significant problems. Furthermore, all the production rods were tested in place, and only minor adjustments were required. However, during a recent scram of the EBR-II, 2 of the 12 rods became stuck (rods 7 and 9).[3] Rod 9 was broken loose by applying a 200-lb force. The rod was then exercised by using a lifting force of 350 to 550 lb and slight mallet taps to assist its downward travel. After some exercise it resumed normal operation. Rod 7 required the fabrication of special tools to break it loose. It was determined that the main shaft for the rod was sticking in a $29\frac{1}{8}$-in.-long Stellite sleeve in the reactor-vessel cover. This sleeve is the lower guide bearing for the control-assembly shaft (Fig. IV-2) and also serves as a seal between the sodium inside the reactor vessel and the bulk storage outside the vessel. So that the leakage can be reduced, each main shaft contains 23 labyrinth grooves, as shown in the figure. The nominal radial clearance between the outside diameter of the main-shaft lands and the inside diameter of the sleeve is 0.015 in. It is reported in Ref. 3 that a special tool, which applied axial and rotational forces to the stuck shaft, performed successfully the task of loosening the seized shaft.

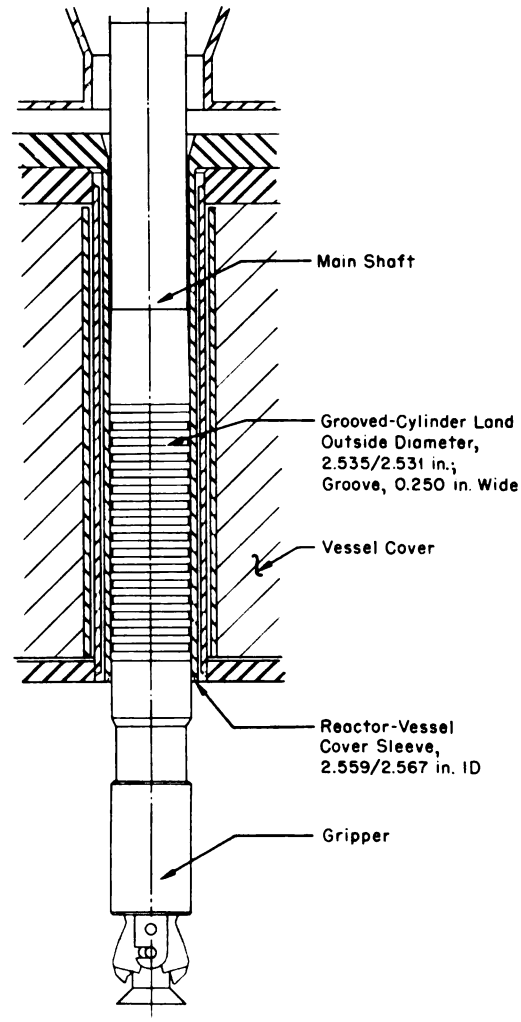
Main Shaft
Grooved-Cylinder Land Outside Diameter, 2.535/2.531 in.; Groove, 0.250 in. Wide
Vessel Cover
Reactor-Vessel Cover Sleeve, 2.559/2.567 in. ID
Gripper

Fig IV-2 Main-shaft seal through the EBR-II reactor-vessel cover.[2]

Process Tubes and Fittings for the NPR

The New Production Reactor (NPR; also called the N Reactor) is a graphite-moderated pressure-tube reactor designed to operate at a coolant pressure of 1600 psi and a temperature of 300°C. The reactor requires 1064 Zircaloy-2 pressure tubes that are 57 ft long, 3.25 in. in diameter, and 0.25 in. in wall thickness, as well as a considerable number of fittings, connectors, and transition joints. Reference 4 is a descriptive summary of a development pilot order and a competitive-bid program for procurement of the pressure tubes. The procedures used for this program were required because of the lack of manufacturing technology and industrial experience with this relatively high-cost material and because of the stringent quality and dimensional requirements specified.

The initial phase of the program consisted of developmental contracts to three vendors on a best-efforts basis. The second, or pilot order, phase was awarded to the three vendors on a negotiated basis. The final phase was accomplished on the basis of a competitive-bid,

Digitized by Google

product-guaranteed, fixed-price contract. This procurement effort developed an industrial capability for producing heavy-walled Zircaloy tubing to reactor-application specifications[4] and covered the full range of processes from ingot to finished product. The effort included the development of (1) specifications that indicate the level of quality to which such tubing can be produced and (2) commensurate inspection and quality-control requirements.

Technical problems in the selection, manufacture, installation, and testing of primary-loop fittings are discussed in Ref. 5. The fittings included the rolled-joint connections between Zircaloy and carbon steel, a mechanical "make-and-break" coupling, a venturi assembly, manifold piping, and valve-body material. The leak-tight roller joint, shown in Fig. IV-3, was

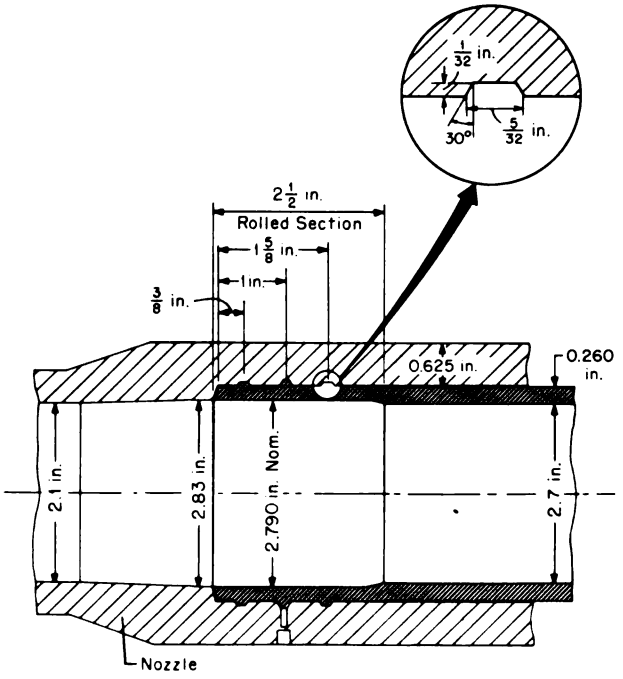

Fig. IV-3 NPR inlet rolled joint.[5]

designed for 1800 psi at 600°F and to withstand thermal shock from sudden coolant-temperature changes. This joint was selected over eight other mechanical type joints on the basis of superior strength and low-leakage qualities. In this type of connection, the Zircaloy tube is rolled into the grooved carbon-steel nozzle by means of an expander mandrel that provides for a 12% wall-thickness reduction. The rolling process forces Zircaloy into the grooves and provides a joint that is judged to be structurally sound and reliably leakproof.

The quick-connection make-and-break mechanical coupling was required to minimize the maintenance time at the faces of the reactor. Of 15 various candidate assemblies evaluated, the Grayloc type coupling was chosen for this application because of its ruggedness and resistance to leakage under different stress conditions and its clean internal-surface configuration. It features a two-stud split-clamp arrangement that causes axial loading of a tapered metal-seal member within the tapered bores of the coupling flanges. Spherical convex nuts and temporary shims are used during assembly of the coupling to minimize cocking and to maintain parallelism. Figure IV-4 shows the connector-coupling components.

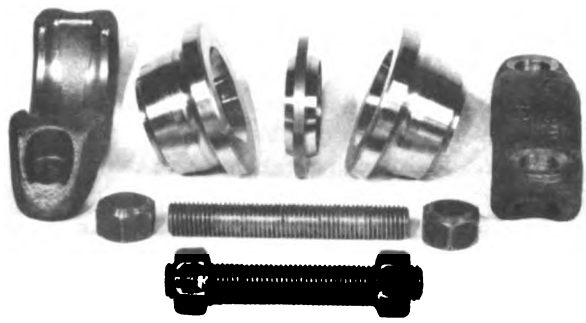

Fig IV-4 NPR connector-coupling components.[5]

The venturi throat assembly is used to monitor continuously the coolant flow in each of the connector pipes. The original design of this component specified a type 316 stainless-steel throat section to be mounted in a carbon-steel body by means of an interference fit. However, subsequent heat-treating operations caused loosening of the throat. The design was modified by substituting Inconel for stainless steel on the throat section, thus minimizing the differential thermal expansion. Extending the tap connection into the throat component corrected the loosening of the throat component.

The manifold piping on the NPR consists of over 100,000 ft of carbon-steel tubing of $2\frac{5}{8}$-in. outside diameter by 0.260-in. wall thickness. The piping connects the individual process tubes

Digitized by Google

to the 18-in. inlet and outlet headers. The connectors did not meet impact-strength requirements after bending. This deficiency was attributed to limitations of the heat-treatment equipment used in the manufacture.[5] It was subsequently corrected by additional heat-treatment, and thereafter the tubing met specified impact-strength requirements. The valve bodies of both forged and cast types failed to meet the impact-strength requirements specified. In some cases an additional grain-refinement treatment at 1550°F completely refined the structure, and notch toughness was raised above minimum values. In other cases detailed analysis of the metallurgical deficiency showed the need for a much more extensive modified heat-treatment procedure, in addition to some pre-heat-treatment machining operations, to bring the product above specified impact- and tensile-strength values.

References

1. L. J. Koch, W. B. Loewenstein, H. O. Monson, D. Okrent, M. Levenson, W. R. Simmons, J. R. Humphreys, J. Haugsnes, and V. C. Jankus, Hazard Summary Report, Experimental Breeder Reactor-II, USAEC Report ANL-5719, Argonne National Laboratory, May 1957.
2. E. Hutter and G. Giorgis, Design and Performance Characteristics of EBR-II Control Rod Drive Mechanisms, USAEC Report ANL-6921, Argonne National Laboratory, August 1964.
3. Argonne Staff, Reactor Development Program Progress Report, October 1964, USAEC Report ANL-6965, Argonne National Laboratory, Nov. 15, 1964.
4. T. C. Aungst and D. H. Curtiss, Procurement of Zircaloy-2 Process Tubes for N-Reactor, USAEC Report HW-80566, Hanford Atomic Products Operation, March 1964.
5. Staff of the N-Reactor Project, Technical Problems in Fittings for N-Reactor Primary Loop, USAEC Report HW-79616, Hanford Atomic Products Operation, November 1963.

Digitized by Google

Section

V

Power Reactor Technology

Specific Reactor Types

Large Pressurized-Water Reactors

The trend toward interconnected power systems in the electric-utility industry has greatly increased the opportunities for reducing unit power-generating costs through the use of very large plants. This trend has also focused attention on the question of the maximum capacity available from a single reactor in a nuclear plant. References 1 and 2 present the results of a study by the Westinghouse Atomic Power Division for the U. S. Atomic Energy Commission (AEC) to evaluate the technical feasibility and economic potential of a 1000-Mw(e) all-nuclear power plant incorporating a single pressurized-water reactor. The work was performed during the period May 1962 to March 1963. The results of the study command particular attention since the work was clearly based on the extensive Large Closed Cycle Water Reactor Research and Development (LRD) Program that Westinghouse has been conducting since 1960 in association with the San Onofre Nuclear Generating Station of the Southern California Edison Company. It is stated that the design philosophy adopted for the study represents a modest extension of the technology to be employed in the 375-Mw(e) Southern California Edison* and the 465-Mw(e) Round 3A† plants. The conclusion from the study is that the 1000-Mw(e) reactor is technically feasible and economically practical and that 1970 is a reasonable date for the commercial operation of the plant. A $10.5 million research and development program is outlined. The principal development problems lie in the area of core physics and core development and result from the increased core size.

Except for size the plant is similar to the present generation of pressurized-water reactors under contract, such as those for the San Onofre and Malibu stations. The plant has the following capabilities:

Reactor, Mw(t)	3220
Gross electrical generation, kw	1,058,000
Net electrical generation, kw	1,002,400
Cycle heat rate, Btu/kw-hr	10,377
Full-load net station heat rate, Btu/kw-hr	10,363
Net plant efficiency, %	31.1

Of the principal reactor-plant components, only the reactor vessel represents a measurable extension of present-day fabrication techniques. Although the 615-ton vessel can be shop fabricated and erected at the hypothetical site selected for the study,‡ transportation might be a limitation for less favorable sites. The pressure-vessel-design condition was 2500 psi at 650°F, and the vessel was to be designed, manufactured, inspected, and stamped in accordance with Sec. VIII of the *ASME Boiler and Pressure Vessel Code*. Since this study was completed, Sec. III, Rules for Construction of Nuclear Vessels, was approved and issued by the American Society of Mechanical Engineers. A discussion of the principal difference between the two code sections is presented in Ref. 3. The new Sec. III permits better utilization of the reactor-vessel material, resulting in a lighter weight vessel. For example, a reduction of more than 2 in. in thickness of the 202-in.-ID cylindrical section of the 1000-Mw(e) vessel can be achieved. Reference 3 concludes that the new code permits design of nuclear vessels for water-reactor plants up to 1500 Mw(e).

*The Malibu Plant of the City of Los Angeles Department of Water and Power.

†The Connecticut Yankee Atomic Power Company.

‡The "Middletown" site employed in the AEC evaluation studies of utility reactors since 1959.

Digitized by Google

In the design study presented in Ref. 1, seven primary coolant loops are employed. Each loop contains a vertical U-tube steam generator having 32,726 sq ft of heat-transfer surface and a canned-motor single-speed centrifugal pump with a design flow capacity of 61,000 gal/min against a 280-ft head. The pump volute contains an integral center-guided check valve positioned between the suction nozzle and the impeller. No main coolant block valves are used. In present-day plants the use of the block valves seems to be a customer choice; Connecticut Yankee uses them, but Malibu does not. The main coolant piping is 27-in.-ID rolled and welded carbon steel clad internally with stainless steel. The 3240-cu ft pressurizer vessel is connected to the hot leg of one reactor loop. The steam-generator design data are tabulated in Table V-1.

Table V-1 DESIGN DATA[1] FOR STEAM GENERATOR

Type	Vertical U tube with integral steam drum
Heat-transfer load, Btu/hr	15.729×10^8
Steam flow, lb/hr	2.014×10^6
Design pressure, tube side, psia	2500
Operating pressure, tube side, psia	2050
Tube material	Inconel
Coolant flow in each side, lb/hr	22.86×10^6
Coolant inlet temperature, °F	598
Coolant outlet temperature, °F	546
Shell-side full-load pressure at outlet, psia	700
Full-load steam temperature at outlet, °F	503
Maximum moisture at outlet (full load), %	¼
Shell-side design pressure, psia	1000
Feedwater temperature at full load, °F	442
Logarithmic mean temperature difference, °F	65.5
Heat-transfer surface area, sq ft	32,726
Dry weight, lb	503,800
Flooded weight, lb	738,800

The reactor-plant containment is provided by a reinforced-concrete vertical right-circular cylindrical structure with a flat base and hemispherical dome. The dome has an inside radius of 81 ft, and the total inside height is 211 ft. The structure is lined with a steel membrane ¼ in. thick to make the container vaportight and gastight. The containment is similar in design to the one built at Parr Shoals for the Carolinas-Virginia Nuclear Power Associates, Inc.

The turbine-generator represents a significant extension of current practice. The turbine is of 4-cylinder single-shaft design, operates at 1800 rpm, and turns a single 1,300,000-kva hydrogen-intercooled generator. The throttle pressure condition is 650-psia saturated steam as in current practice. Exhaust from the single double-flow high-pressure cylinder passes through six moisture separators and is reheated with steam at the throttle condition before being expanded in the three double-flow low-pressure cylinders. The entire high-pressure-turbine casing and the last five stages of each low-pressure-turbine casing are lined with stainless steel to minimize moisture corrosion. The low-pressure-turbine rotors are too large to ship completely assembled. The last two stages of each low-pressure turbine are bladed in the field. Similarly, because of size and weight, final assembly of the generator rotor and stator is performed in the field.

The estimated power-generation cost for the plant based on a net generation of 1,002,400 kw is 5.77 mills/kw-hr, made up as follows:

Capital	3.42
Land, working capital, and nuclear insurance	0.27
Fuel	1.83
Operation and maintenance	0.25
	5.77

The estimated total capital cost of the plant is $165,084,000, including land and land rights, interest during construction, and contingency; the resulting unit cost is $165 per kilowatt. The 1.83 mills/kw-hr fuel cost is based on an equilibrium core utilizing zirconium-clad fuel. The first-core fuel-cycle cost for the reference elastically collapsed stainless-steel-clad core is 2.13 mills/kw-hr. The first-core fuel-cycle cost for the alternative freestanding stainless-steel-clad core is 2.23 mills/kw-hr. Fuel cost estimates were based on government ownership of uranium.

The principal improvements and advances over current pressurized-water-reactor technology are in the area of the core and the associated reactor arrangement. Two designs were carried through in the study. The reference design utilized short Zircaloy followers for the control-rod blades and elastically collapsed thin-walled stainless-steel cladding on the fuel. The less-advanced alternate design

Digitized by Google

employed full-length control-rod followers and freestanding stainless-steel cladding. Slightly enriched UO_2 is used as fuel in both designs. The alternate design resulted in an increase of reactor-vessel length of 8 ft. The consequent increase of reactor-coolant-system holdup was 9%, and the increase in plant-container volume was 11%. The estimated capital-cost saving incurred by choice of the reference design is approximately $3 million. Figure V-1 shows the reactor-vessel assembly for both the reference and the alternate designs.

The reference-design core is roughly cylindrical in shape with an active height of 11 ft and an equivalent diameter of 12.8 ft. The individual fuel elements consist of UO_2 pellets, 0.354 in. in diameter by 0.708 in. high, enclosed in stainless-steel tubes of 0.010-in. wall thickness. The cladding operates under an elastically collapsed condition, as described in Ref. 1:

In order to reduce the amount of steel in the reactor core and improve neutron economy, elastically collapsed 304 stainless steel was selected for the clad material. The normal fuel rod has an inside diameter of 0.358 inches with a wall thickness of 0.010 inches ±0.0005. The collapsed clad is designed to be elastically buckled between 1000 – 1500 psia pressure. At zero power conditions the maximum stress in the clad will be localized at the inner surface of the vertices of the buckled clad and will approach the yield strength of the material. However, it is expected that the clad will be pushed back toward a circular shape by the fuel pellets as the reactor is brought from zero power to full power and that the maximum clad stress will be below the yield strength during normal operations.

The fuel assemblies of the reference core consist of a basic 16-by-16 square array of fuel rods with 20 rods omitted from the periphery of the assembly to provide space for control rods. A cross section of the fuel assembly and control rod is shown in Fig. V-2. The outermost row along the periphery of each

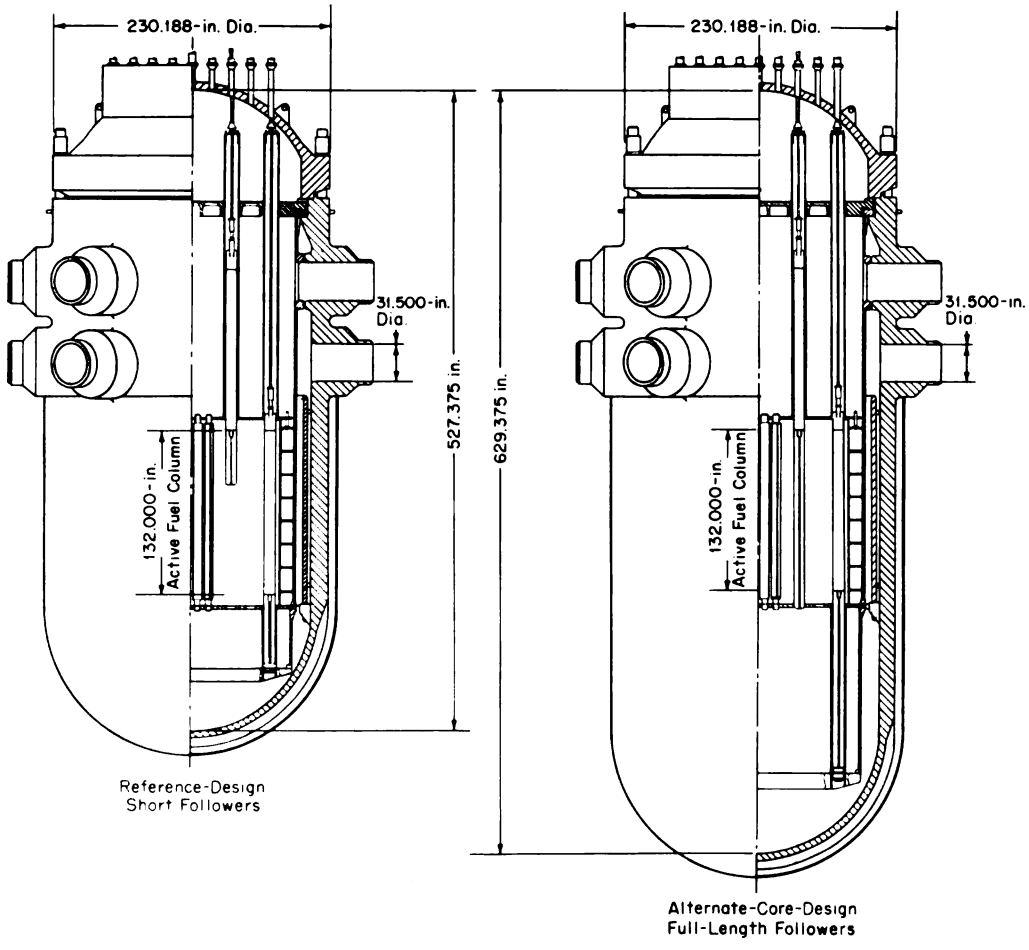

Fig. V-1 Reactor-vessel assembly for both the reference and alternate designs.[1]

Digitized by Google

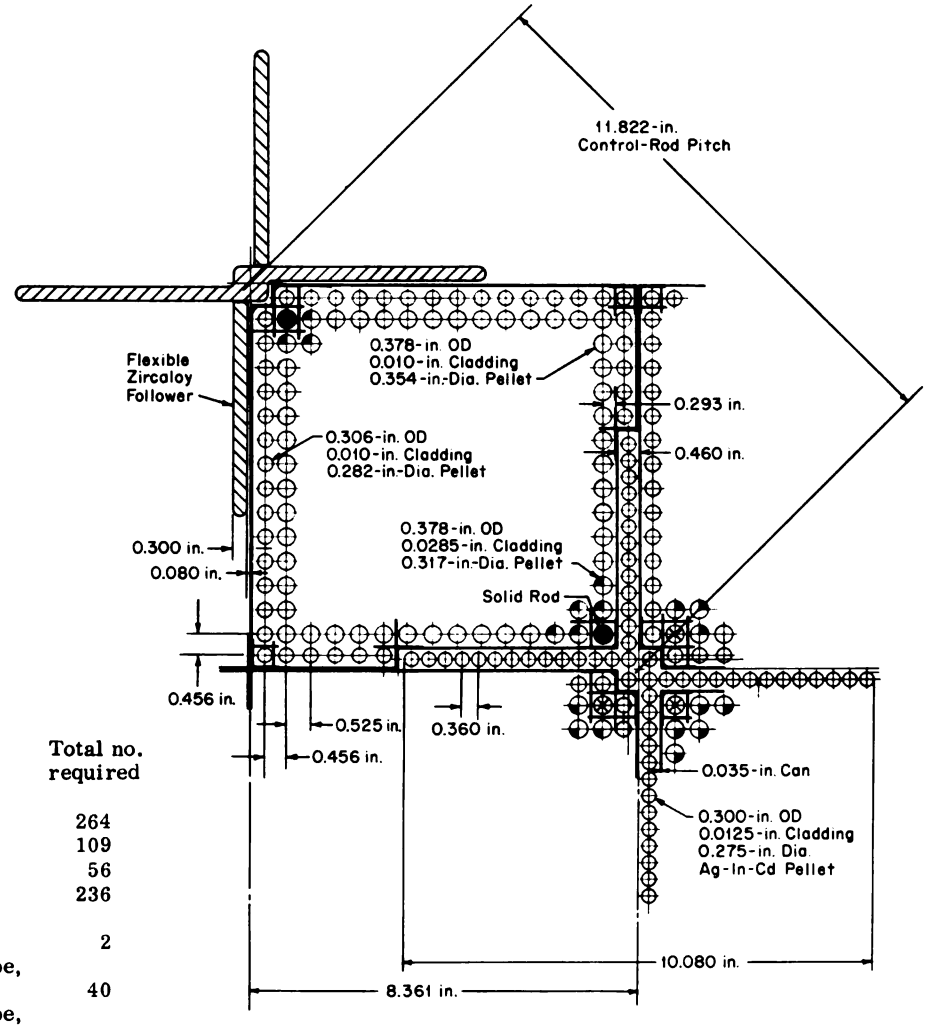

	Total no. required
Fuel assemblies	264
Control-rod slots	109
Tubes per control rod	56
Rods per fuel assembly	236
●, solid stainless-steel corner rods	2
○, 0.306-in.-OD fuel tube, 0.010-in. cladding	40
◴, 0.378-in.-OD fuel tube, 0.0285-in. cladding	8
○, 0.378-in.-OD fuel tube, 0.010-in. cladding	186

Fig. V-2 A cross section of the fuel assembly and control rod.[1]

fuel assembly consists of fuel rods reduced in outside diameter from the normal 0.378 in. to 0.306 in. In addition, two corner rods of each assembly in the vicinity of the greatest flux peaking were replaced by solid-steel rods, and thick cladding was used on eight fuel rods in selected high-power-density positions so that the fuel-pellet area was reduced to 80% of the normal area. All the fuel rods within an assembly have the same enrichment. The assortment of fuel-rod sizes was not needed in the alternate core that used full-length control-rod followers since the water gap producing high peaking factors in the adjacent fuel elements was greatly reduced. The alternate core has the same active fuel length and equivalent diameter as the reference core.

The individual fuel rods are held mechanically within the fuel assembly by a method generally similar to that being developed for the Round 3A plants. Support for the fuel rods is provided by a grid-clip assembly. Rows of clips are interlocked, as in an eggcrate design, and are furnace brazed to form the grid. The grids are welded to a boxlike structure that forms the exterior of the fuel assembly. The structure is perforated to minimize the amount of steel in the system and to allow coolant flow between adjacent assemblies. Fuel rods are inserted through the grids and are held in place by clips or fingers extending from the grid pieces. The clip support is lateral only, and the rods are free to expand axially between the end plates. The end plates and nozzles are

Digitized by Google

welded to the unit after all the fuel rods are inserted to complete the fuel assembly.

Figure V-3 shows the core cross section. The core contains 264 identical fuel assemblies and 109 individually driven cruciform control rods. The rod pattern is such that every internal fuel assembly has a rod centered adjacent to each of two corners on the diagonal of the assembly. The absorber section is fabricated from 0.275-in.-diameter rods of 80-15-5 silver-indium-cadmium alloy inserted into stainless-steel tubes. The tubes are welded together to form a cruciform, as shown in Fig. V-2. Zircaloy followers are attached to the bottom of the absorber section. In the reference core the follower is 3.7 ft long. In the alternate core the length of the follower is equal to the full core length of 11 ft. The function of the short follower in the reference core is to reduce bypass flow in the control-rod slot and to promote flow mixing between the fuel assemblies.

The nuclear design of the core is tied intimately to the intended method of fuel management because of the large size and high fuel burnup. The fuel loading is 125 metric tons of uranium. The average burnup for the equilibrium core is 24,000 Mwd per metric ton of uranium. This corresponds to a core life of 22,370 EFPH (effective full-power hours) or about 7,460 hr per refueling cycle and results in a refueling period of 12.7 months on the basis of an 0.80 plant factor.

The Westinghouse workers studied[2] several methods of cycling the fuel assemblies in the core. Their purpose was to determine a suitable means of achieving the lifetime requirements while holding the maximum-to-average radial power-density ratio to the limit of 1.5, which is required before the design thermal output can be reached. As is usually the case for reactors of large size and high burnup, the regionwise out-to-in cycling methods were relatively unattractive. The results of the survey of various refueling methods are summarized in Table V-2. The uniform-batch core was calculated for comparison only. Both the 3-region–3-cycle and 5-region–5-cycle shuffles failed to meet either the burnup with the selected feed enrichment or the power-distribution requirements. The 3-region 3-1-2 shuffle, in which fresh fuel assemblies are inserted in the intermediate region, was tried since the results of the out-in cycle studies indicated that the coupling between fresh and burned fuel must be increased to obtain higher burnup and satisfactory power distribution. The trial was unsuccessful, and it was concluded that, whenever a sizable fraction of a large core is replaced by fresh fuel, a large power peak always occurs in that region, and the remainder of the core serves as a multiplying reflector. The method of fuel management proposed, which avoids regionwise cycling, is designated "Roundelay multibatch." In the equilibrium cycle fresh elements are inserted in a uniform

Table V-2 CHARACTERISTICS OF DIFFERENT REFUELING METHODS FOR A 1000-MW(e) PRESSURIZED WATER REACTOR[2]

(Feed Enrichment Is 3.4 Wt.% in All Cases)

Refueling method*	Discharge burnup	Burnup/ batch burnup	Power ratio $P_{max,(radial)}/P_{av.}$	$K_{initial}$ (no Xe)
Uniform batch	15,250	1.00	1.99	1.229
Out-in				
3 region–3 cycle	20,440	1.34	1.96	1.126
5 region–5 cycle	21,960	1.44	1.92	1.095
3-region 3-1-2	21,740	1.43	2.28	1.158
Roundelay 3-batch	23,290	1.53	1.35†	1.116
Roundelay 5-batch	25,830	1.69	1.22†	1.081

*In the out-in refueling method, fresh fuel is fed to the outermost of several concentric fuel regions and subsequently moved inward at each refueling cycle. Spent fuel is removed from the innermost region. The 3-region 3-1-2 method is a variation in which fresh fuel is loaded into the intermediate region of a 3-region core. The numbering sequence taken in inverse order identifies the region in which the fuel is successively placed, the regions being numbered from out to in. In the Roundelay method the core is divided into a large number of adjacent regions, each of which has a number of fuel batches (usually one assembly is a batch). At every refueling cycle a spent fuel batch is removed and replaced by a fresh batch in each region. The partially spent fuel is never moved.

†These values do not include local "ripple" effects.

Digitized by Google

distribution throughout the core at each refueling operation. For example, with Roundelay 3-batch, every third element is replaced, and the other elements are left in place. In Fig. V-3 the fuel assemblies are numbered in the order

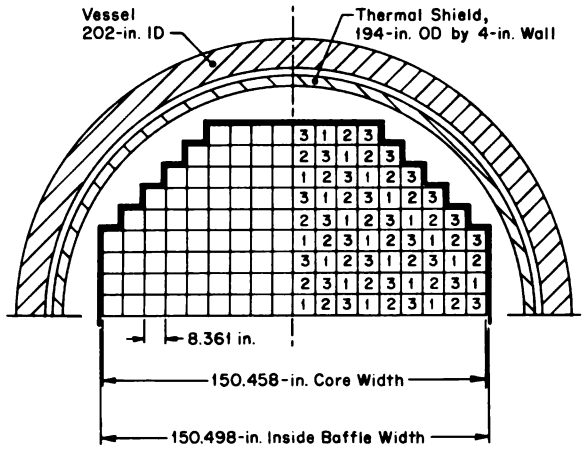

Fig. V-3 Cross section of vessel core.[1]

in which they might be replaced in the reference core; during one refueling all No. 1 fuel assemblies would be replaced, and so on. It was found that the mixing of the fresh and burned fuel assemblies produces strong coupling between them and permits improved power production from the burned elements. The improved burnup is evident in the results shown in Table V-2. The favorable values of maximum-to-average power ratio are illusory, however, since the survey study did not take into consideration the "ripple" on the overall power distribution resulting from significantly different power production from adjacent fuel assemblies with greatly different burnup. As a result the reference core failed to meet the design criteria, although two changes were proposed to permit it to do so, as follows.

1. Reduce the local power ripple by increasing the number of fuel assemblies. A 673-fuel-assembly core with a 10-by-10 fuel-rod array showed a much improved power distribution.

2. Select a core array that has a center fuel assembly so that the replacement of the central group of four elements forced by symmetry would be eliminated. A very poor power distribution results from the power spike produced when the four fuel assemblies adjacent to the center are replaced together.

With Roundelay 3-batch refueling, it was found that after six refueling steps the core conditions are essentially those of the equilibrium cycle.

The thermal and hydraulic characteristics for both the reference and alternate cores are presented in Table V-3. A review of these parameters gives the best insight into the methods by which the rather remarkable power density of 80 kw/liter is expected to be achieved in these very large cores. No single item makes a large contribution to improved performance, but a substantial improvement is expected from a combination of many small items, with careful attention to their detailed interaction. This attention to detail extends not only to the physical arrangements of core components (e.g., the array of different type fuel rods within one assembly) and to a more uniform approach to design limitations over the core volume (e.g., promoting interchannel mixing to reduce enthalpy-rise hot-channel factors) but also to a reexamination of the limitations themselves. For example, the design limitation of a DNB (departure from nucleate boiling) ratio of 1.25 at 115% of full power represents less margin than is used in current practice. Evidently the belief is that operational experience from present-day plants plus adequate in-core instrumentation will permit satisfactory operation within these margins.

The composition of F_q, the ratio of maximum heat flux to average heat flux in the core, used for design purposes, is[1]

Subfactor	F_q
Axial	1.60
Radial	1.50
Local power peaking	1.30
Transient hot-channel factor	1.02
Engineering	1.045
Design overall factor	3.33

For $F_{\Delta H}$, the ratio of maximum coolant enthalpy rise to average coolant enthalpy rise over the total length of the core, the composition is[1]

Subfactor	$F_{\Delta H}$
Radial	1.5
Transient factor	1.02
Engineering	
Net hot cell	1.07
Uncertainty	1.03
Flow distribution	1.07
Design value total	1.8

Digitized by Google

Table V-3 THERMAL AND HYDRAULIC CHARACTERISTICS OF THE CORE[1]

	Reference design (short followers)	Alternate design (full-length followers)
Total heat output		
Mw	3220	3220
Btu/hr	10.99×10^9	10.99×10^9
Heat generated in fuel, %	97.4	97.4
System pressure, nominal psia	2050	2050
Hot channel factors in steady-state		
Heat flux, F_q	3.33	2.94
Enthalpy rise, $F_{\Delta H}$	1.80	1.80
Coolant conditions		
Total flow rate, lb/hr	160.0×10^6	160.0×10^6
Effective flow rate for heat-transfer, lb/hr	144.0×10^6	144.0×10^6
Flow area for heat-transfer flow (unit cells), sq ft	69.77	68.2
Average velocity along fuel rods, ft/sec	12.7	13.0
Average mass velocity along fuel rods, lb/(hr)(sq ft)	2.06×10^6	2.11×10^6
Coolant temperature, °F		
Nominal inlet	546	546
Maximum inlet due to instrumentation error and dead band	550	550
Average rise in vessel	52	52
Average rise in core	57	57
Average in vessel	572	572
Average in core	574.5	574.5
Nominal outlet of hot channel	639	639
Maximum outlet quality of hot channel, wt.%	2.0	2.0
Maximum outlet enthalpy of hot channel, Btu/lb	687	687
Saturation enthalpy at minimum steady-state pressure, Btu/lb	675	675
Average film coefficient, Btu/(hr)(sq ft)(°F)	4850	5040
Average film-temperature difference, °F	34	30
Heat transfer		
"Active" heat-transfer surface, sq ft	65.5×10^3	70.9×10^3
Average heat flux, Btu/(hr)(sq ft)	163.5×10^3	151.0×10^3
Maximum heat flux, Btu/(hr)(sq ft)	544.3×10^3	444.0×10^3
Maximum thermal output, kw/ft	16	13.2
Average fuel temperature in core, °F	1535	1537
Heat transfer (continued)		
Maximum rod-surface temperature at nominal pressure, °F	645	645
DNB ratios*		
Average q''-DNBR at 100% power at 2050 psia	1.51	1.76
Average q''-DNBR at 115% power at 2200 psia	1.39	1.62
H-DNBR at 100% power at 2050 psia	1.49	1.53
H-DNBR at 115% power at 2200 psia	1.23	1.26

	Normal rod	Small rod	
Fuel rod (cold dimensions)			
Outside diameter, in.	0.378	0.320	0.3884
Cladding thickness, in.	0.010†	0.010	0.0152
Diametral gap, in.	0.004	0.004	0.004
Pellet diameter, in.	0.354†	0.296	0.354
Density of UO_2, % of theoretical density	96.5	96.5	96.5
Fuel length (pellets only), in.	132	132	132
Pitch, in.	0.525	0.456	0.523
Rod array in assembly	16 × 16		16 × 16
Rod per assembly	194	40	240
Total number fuel rods in assemblies	51,216	10,560	63,360
Hydraulic equivalent diameter of unit cell, ft	0.0469		0.0424
Additional water gap at edge of assembly, in.	0.0305	0.029	0.0305
Control rod			
Number of slots	109		109
General			
Total core area (inside core baffle), sq ft	128.2		133.9
Equivalent core diameter, ft	12.8		13.1
Maximum diameter of core, in.	166.0		169.3
Core length, between fuel ends, ft	11.0		11.0
Length-to-diameter ratio of core	0.86		0.84
Water-to-uranium ratio, unit cell	3.29		3.12
Fuel weight, lb of UO_2	289.3×10^3		314.8×10^3
Pressure drop, psi			
Across core	36		46
Across vessel, including nozzles	51		57
Core power density			
Kw/liter of core	80.7		77.2
Kw/kg of U	27.8		25.6

*The DNB ratios are based on the correlations presented in Ref. 20 and are minimum ratios, within the core, of the DNB condition to the actual condition. The heat-flux DNB ratio, q''-DNBR, applies to the subcooled regions of the core. The enthalpy-rise DNB ratio, H-DNBR, applies to quality regions of the core.

†Eight rods have a 0.0285-in. cladding thickness and a 0.317-in. pellet diameter.

Digitized by Google

In both tabulations above the transient factor provides for rod motion required for a 5% step change in load at 95% power level. It is expected that coolant mixing within the core, both between channels and between fuel assemblies, will be required to achieve the $F_{\Delta H}$ design value. Provision has been made in the core to promote mixing. Flow mixing is promoted between fuel assemblies to cool the channels at the assembly edge, where the power peaks, by mixing vanes installed on the grids within the upper 5 ft of the core and by staggering the grids in this region. Bulk boiling at the exit of the hot channel is permitted, to the extent of 2 wt.% quality, to keep the coolant-flow requirements within the capabilities of a seven-loop primary system.

In a study associated with the 1000-Mw(e) pressurized-water-reactor (PWR) design, the effects of core height, enthalpy rise, and burnup on the axial power distribution were investigated. The following quotation from Ref. 2 states the general problem:

> In designing very large reactor cores, it is important to understand the dependence of power distribution on core height, enthalpy rise, and burnup. To illustrate this point, consider the following hypothetical situation. Suppose a reactor with a core height of 10 feet has been designed to produce a given power output. If a new reactor design is required which has a 10% higher output, one might propose an increase in the core height to 11 feet, maintaining the same average power density. However, the axial hot channel factor might be greater in the 11 ft. core; if the increase in hot channel factor is 10%, the power capability is not increased at all in going from a 10 ft. to an 11 ft. core, assuming a burnout heat flux limitation. The power distribution might be expected to become worse as the enthalpy rise is increased since the water density becomes more non-uniform.

The conclusions (Ref. 2) drawn as a result of the study were as follows:

1. In the first core, which contains only fresh fuel, the axial peaking increases slightly with core size. At a burnup of a few thousand MWD/MTU, there is little variation in peaking factor with core size. Beyond 3000 MWD/MTU, the larger cores may have slightly less axial peaking than smaller cores.
2. In a cycle typical of equilibrium, the peaking factor appears to increase substantially with core size; however, burnup effects have reduced the equilibrium peaking factor to a low value in all cases so that the peaking is not serious, even in the larger cores.
3. All steady state power distributions which were studied had axial peaking factors less than 1.60, which is the design value for the 1000 MWe PWR.

Reactivity control of the reactor is provided by a combination of the mechanically actuated neutron-absorbing control rods and a chemical neutron poison dissolved in the reactor coolant. The soluble poison is boron in the form of boric acid. Rapid reactivity changes resulting from rapid load changes, safety shutdown, Doppler, and other rapid transient effects are controlled by the rods. The slower acting reactivity changes due to fuel depletion, samarium, xenon, and gross temperature effects are accommodated by adjusting the concentration of the neutron poison in the primary coolant. The principal advantages in using a soluble poison are the improved core power distribution resulting from being able to withdraw most of the control rods during operation and the reduced total reactivity compensation required of the control rods since they are no longer required to shut down the reactor to the cold clean condition by themselves. The principal disadvantages are the large volume of primary coolant that must be handled when bleed-and-feed dilution is used to reduce the boron concentration and the influence of the poison in reducing the moderator coefficient of reactivity or even causing it to change sign. In connection with the latter point, the criteria for the reference design permit the moderator coefficient of reactivity to vary from positive to negative during core life. It is proposed that the stability of the reactor be preserved through the combination of the Doppler effect and the coolant temperature controller.

The estimated boron concentrations for the first and equilibrium core cycles are[1]

Condition	Boron concentration, ppm	
	1st cycle	Equilibrium
Refueling shutdown; rods in; $k = 0.90$	3880	2930
Cold normal shutdown; rods in; $k = 0.97$	2880	1960
Hot normal shutdown; rods in; $k = 0.97$	2670	1550
Hot full power; no rods; no poison	2780	1810
Hot full power; no rods; Xe poison	2310	1370
Hot full power; no rods; Xe and Sm	2150	1240
End of life	≈ 0	≈ 0

In recent operation the Yankee Atomic Electric Co. reactor at Rowe, Mass., has been successfully employing soluble-poison shim

Digitized by Google

control, and other reactors have run in this manner on an experimental basis. The degree to which the soluble poison is employed in the reference large PWR, however, is significantly greater than in systems that have been run to date.

With the heavy dependence on soluble shim control, it might seem that the reference design employs an unusually large number of control rods (109). The large number results from uncertainties regarding spatial instabilities in the large core, which might conceivably arise from either sustained xenon oscillations or Doppler oscillations. The possibility of both was studied. It was found that for the conditions normally existing in a PWR, i.e., negative Doppler coefficient, no Doppler oscillations are possible, even for a very large reactor. In regard to xenon oscillation, the conclusions were not as definite and were summarized in Ref. 2 as follows:

> 1. The nominal temperature coefficient is sufficiently negative to prevent sustained Xe oscillations of constant or increasing amplitude, even with pessimistic assumptions for the degree of flux flattening.
> 2. With the minimum temperature coefficient and a pessimistic degree of flux flattening, the calculations predict the 1000 MWe core is near the threshold for sustained oscillations.
> 3. Damped oscillations are predicted in all directions for both the nominal and minimum temperature coefficients. Damped oscillations do not represent a serious operational problem if the degree of damping is sufficient to quickly reduce the amplitude of the oscillation. With the nominal temperature coefficient, the damping is probably sufficient to prevent any serious problem; however, with the minimum coefficient, very little damping is expected and operational problems could occur. These conclusions must be qualified since no definite standards have been established regarding the degree of damping required for satisfactory reactor operation....

It is further stated in Ref. 2 that the possibility of xenon oscillations is not believed to be a feasibility problem of the 1000-Mw(e) PWR since reactors have been operated in the presence of such oscillations.

In-core instrumentation is proposed to detect nuclear flux tilts as well as to monitor reactor-coolant temperatures. Neutron fluxes at selected locations in each of the 66 fuel assemblies in one quadrant of the core and at 3 positions in each of the remaining quadrants would be measured by miniature in-core neutron detectors. Temperatures at the outlets of each of the 66 fuel assemblies in one quadrant of the core and at 34 selected positions in the other three quadrants would be measured by sheathed Chromel-Alumel thermocouples.

A second alternate core design aimed principally at an improvement in control-rod features was proposed, although a complete core design was not developed in the study (Ref. 1). This alternate is based on replacing the separate cruciform control rods by a cluster of poison elements arranged in one or more rings and located within the fuel assembly instead of between the fuel assemblies. The individual poison elements are approximately the size of the fuel tubes and move in thimbles located within the fuel assembly. This "rod-cluster-control" (RCC) concept eliminates the necessity for followers and makes the use of canless fuel assemblies more attractive. A model of the rod-cluster-control assembly is shown in Fig. V-4. The RCC fuel assembly requires no change in the basic fuel lattice, and the spring-clip grids for holding the fuel rods in the lattice are retained. The guide tubes in which the individual control elements move are permanently fixed within the lattice of the fuel assembly. The individual control elements are fastened together above the fuel assembly by means of a spider, as shown in Fig. V-5, and all elements within an assembly move up and down together. The guide tubes within the fuel assembly are perforated over a substantial length to provide for coolant flow. The venting is controlled at the bottom of the tube to serve as a dashpot during scramming of the control element. The rod-cluster control-guide tube is shown in Fig. V-6. Advantages of the rod-cluster control are summarized in Ref. 1:

> 1. Improved power distribution due to (a) separation of interassembly peaking from control slot peaking and (b) breakup of control slot peaking by distributing the control material as individual rods throughout the lattice.
> 2. More control per weight of absorber provided the most favorable geometry can be selected.
> 3. More uniform distribution of control. This will result in better power distribution control in the event of unstable power distribution and better temperature and pressure dead-band control because of the lower worth per rod step.
> 4. Less parasitic absorption if elimination of the stainless steel can is successful which will improve the fuel cycle costs.
> 5. Complete elimination of followers.
> 6. Reduced coolant bypass flow.
> 7. Simplification in mechanical design.

Although rod-cluster control is considered only as an alternative in the 1000-Mw(e) PWR

Digitized by Google

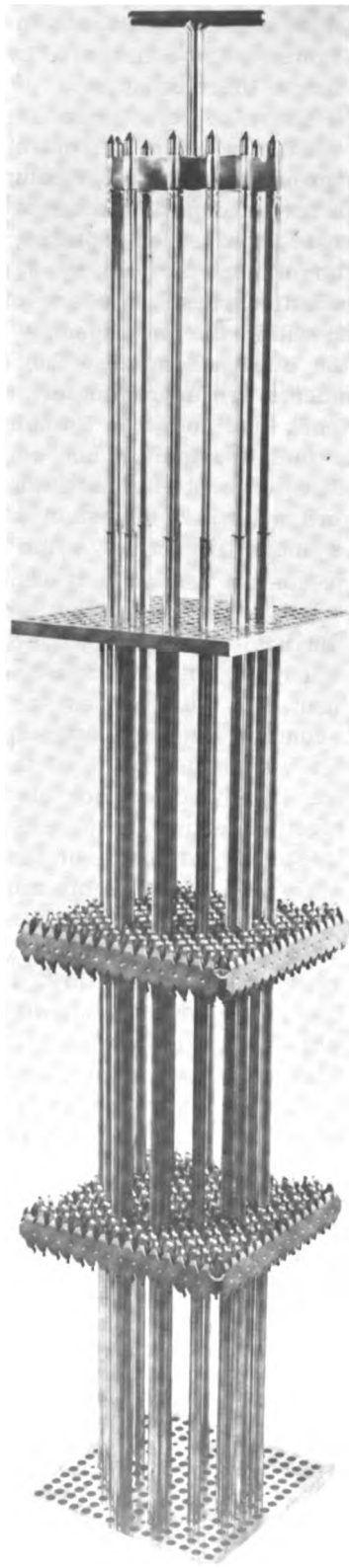

Fig. V-4 Fuel-assembly model for rod-cluster control.[1]

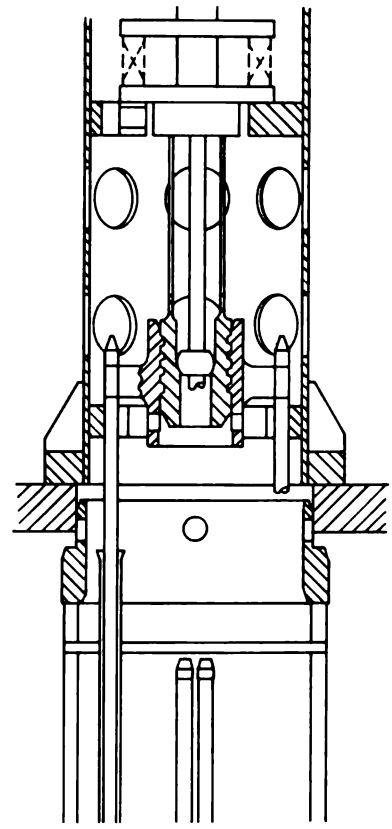

Fig. V-5 Coupling for rod-cluster control.[1]

study, significant development has been devoted to the concept, and it has been incorporated in the design of the San Onofre reactor (Ref. 15). Rod-cluster control could reasonably be expected to be adopted for the Connecticut Yankee and Malibu reactors also.

As mentioned earlier in this review, this 1000-Mw(e) Closed Cycle Water Reactor Study should rest on firmer ground than the usual run of reactor-feasibility studies because it is based on information generated under the massive LRD Program being conducted for the San Onofre reactor. References 4 to 15 are progress reports on this program. Topical reports, Refs. 16 to 39, on the same program treat the reactor subjects covered in the 1000-Mw(e) study (Refs. 1 and 2) in greater depth and are keyed, of course, to the San Onofre reactor. For example, a number of mechanically assembled fuel assemblies have been irradiated in the Saxton reactor, and additional assemblies have been prepared for irradiation. These included two rod-cluster-control assemblies, one a 3-

Digitized by Google

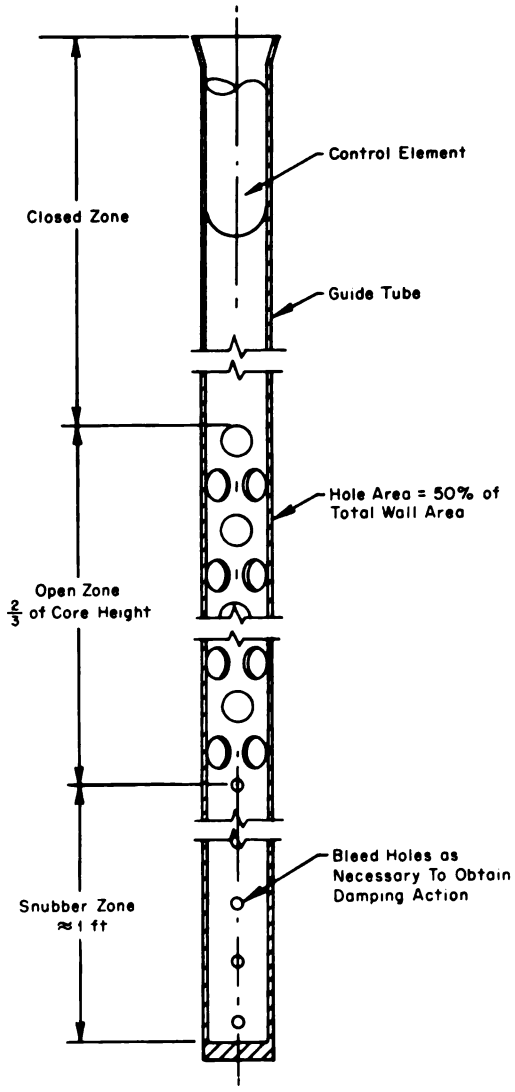

Fig. V-6 Guide tube for rod-cluster control.[1]

by-3 and the other a 9-by-9 array. Fuel cladding of these assemblies included both thin-walled stainless steel and Zircaloy.

A general comment appears appropriate on the size of components for large pressurized-water reactors. At the time this 1000-Mw(e) PWR study was conducted, a 1000-Mw(e) power level was believed to be the highest achievable from a single reactor vessel in the relatively near future. Similarly, seven coolant loops were required because of restrictions on the maximum size of steam generators and main coolant pumps. Recent indications are that manufacturers are now capable of providing these key components in higher unit ratings. As previously mentioned, pressure vessels for 1500-Mw(e) units appear to be feasible.[3] Steam generators of almost twice the capacity used in the study are being discussed. If coolant pumps are not restricted to canned-motor units, the remaining restriction would be only the size of volute that can be cast. This would permit pumps of increased capacity.

EBWR

Operation of the Experimental Boiling Water Reactor (EBWR) at power levels up to and including 100 Mw(t) has been previously reviewed in *Power Reactor Technology*, 7(3): 317-320, on the basis of several topical reports. Reference 40 contains a collection of the detailed test reports that cover operation since the modification of the reactor and plant for the higher power up through operation for brief periods at 100 Mw(t). The test reports contain detailed accounts of the loading sequence and initial critical testing. Physics tests included critical control-rod-position determination, rod calibrations, and measurements of temperature and void coefficients and flux distribution. The response of the reactor to step reactivity changes was determined with reactor periods ranging from 15 to 40 sec and peak power levels near 1 Mw(t). Analytical correlation of the peak power and energy production during these transients with the reactor period was obtained using an energy-production-dependent reactivity feedback. Inspection of the control rods irradiated during prior operation of the EBWR is described, including metallurgical and radiochemical examinations. Thermal and hydraulic testing included temperature measurements in the reactor, determination of recirculation rate, measurements of steam-volume fractions in the core and riser, as well as investigation of steam carry-under and moisture carry-over.

Design Studies of a 1000-Mw (e) Fast Reactor

Four independent design studies (Refs. 41 to 44) were made for the AEC on a 1000-Mw(e) ceramic-fueled fast breeder reactor cooled with liquid sodium. In two of the studies the fuel was UO_2-PuO_2, whereas in the other two studies UC-PuC was used. These studies, which were focused on the reactor and primary heat-

Digitized by Google

removal systems, represent the first phase in AEC's program to develop basic fast breeder concepts for large commercial power stations. The objectives in the studies were to develop designs that optimized fuel-cycle costs, obtained attractive fuel-doubling times, and permitted high-temperature steam conditions at the turbine, consistent with safety requirements in fast reactors. The studies thus included core physics and thermal-hydraulic analysis, mechanical design features, fuel-handling concepts, and fuel-cycle economics. The following ground rules were common to all studies:

1. The performance was to be evaluated for equilibrium cores.

2. The fuel cladding was to be a stainless steel.

3. The primary sodium temperature was to be sufficiently high to produce 1000°F steam, taking into account the temperature drop in the intermediate heat exchanger.

4. The breeding ratio was to be greater than 1.2, with a reasonable doubling time.

5. The fuel was to be considered government owned with a 4¾% rental charge.

6. The value of $10 per gram was to be used for ^{239}Pu and ^{241}Pu in the form of the nitrate.

7. The feed material to the plant for the equilibrium core was to be depleted uranium containing 0.3 wt.% ^{235}U.

In a recent feature article by Okrent[45] in *Power Reactor Technology*, various problems were discussed which affect the performance of large sodium-cooled ceramic-fueled fast reactors. In general, the considerations introduced by economics, breeding, and safety give rise to conflicting requirements in optimizing the design of such reactors. A ceramic fuel after exposure in the reactor cannot be considered to provide the reliable axial thermal expansion that, in smaller metal-fueled reactors, is responsible for a significant rapidly acting negative reactivity coefficient. On the other hand, the presence of oxygen or carbon in the ceramic softens the neutron spectrum so that a sizable negative Doppler coefficient of reactivity can be obtained. The change in reactivity upon loss of sodium from the core becomes more positive with increasing reactor size because the positive reactivity effects associated with changes in neutron spectrum become more important relative to the negative neutron-leakage effect. The buildup of ^{240}Pu and fission products in the equilibrium core increases the positive reactivity effects due to sodium voiding, as would also the substitution of niobium for steel structures. Any measure that increases the neutron leakage from the core also tends to shift the sodium void coefficient in the negative direction for two reasons. First, the increase makes the effect of sodium on the neutron leakage more important. Second, an increase in the concentration of fissile isotope is required; this, therefore, results in a harder spectrum that is less sensitive to changes in sodium density. The higher leakage has other, unattractive consequences: if brought about by a thinning of the breeder blanket, it decreases the total breeding ratio, and, if brought about by the use of high-leakage core geometry, it decreases the internal breeding ratio and increases the rate of reactivity loss with fuel burnup. The Doppler reactivity coefficient can be improved by the addition of a fixed moderator to the core, such as BeO, to soften the neutron spectrum; however, this is detrimental to the breeding ratio and doubling time.

Among the other problems that required consideration in these studies were the limitations of the stainless-steel fuel cladding at the high temperature required to obtain the 1000°F steam temperature specified for high thermodynamic efficiency, the utilization of the fuel at high burnup and high heat ratings for attractive fuel-cycle economics, thermal-stress problems in the reactor vessel and primary system imposed by high-velocity sodium operating at temperature differences in the range of 200 to 300°F, and reliable methods of refueling without excessive reactor downtime.

The four fast reactor design studies were evaluated by the AEC[46] with the assistance of the Argonne National Laboratory and the Los Alamos Scientific Laboratory. A very brief summary description of the four reactor concepts was presented in a paper by Koch et al.[47] A summary of the nuclear and safety characteristics of the reactor concepts was compiled by Okrent et al.,[48] and the fuel-cycle economics were evaluated by Link et al.[49] A paper by Klotz and Miller described the Allis-Chalmers design.[50]

A brief description is given below of the four 1000-Mw(e) concepts. The core arrange-

Digitized by Google

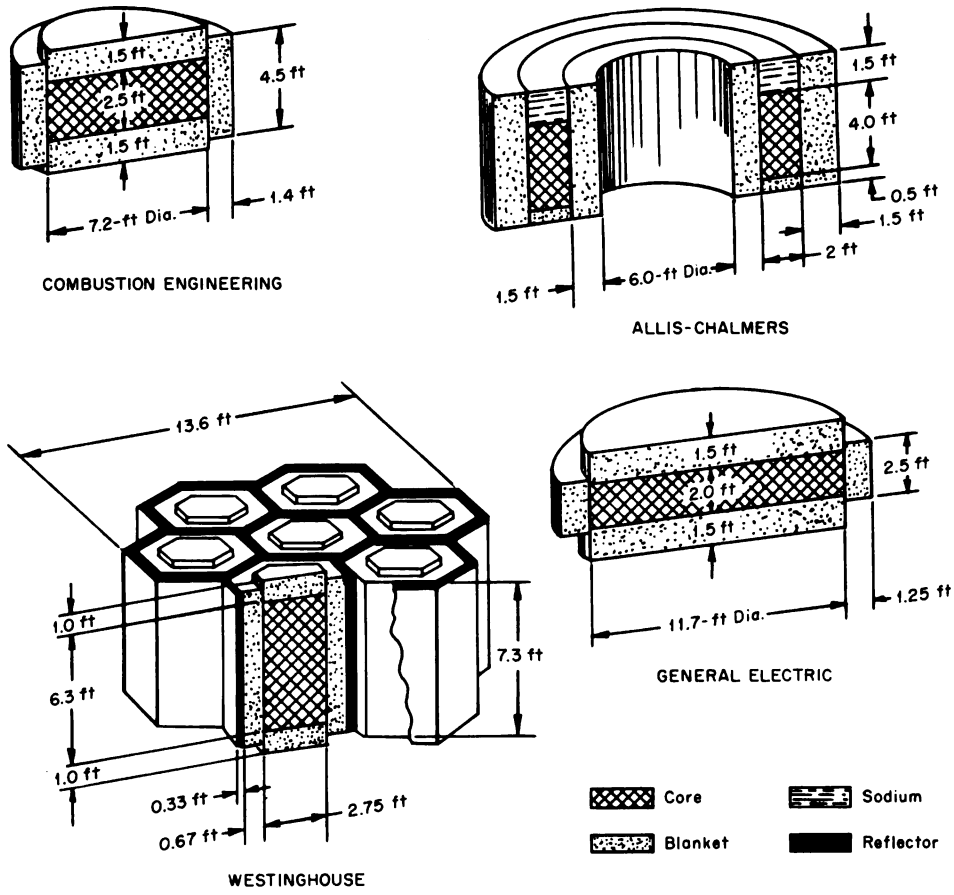

Fig. V-7 Reactor-core arrangements for four 1000-Mw(e) design studies.

ments are shown diagrammatically in Fig. V-7, and the major characteristics of the four concepts are presented in Table V-4.

Allis-Chalmers Reactor Concept

To reduce the sodium void coefficient as much as possible, this concept uses a thin annular core having high neutron leakage. The core annulus is 2 ft thick, 13 ft in outside diameter, and 9 ft in inside diameter, with a volume of 7720 liters. The sodium void coefficient is decreased even further because no breeder blanket is used above the core region; instead a sodium space is provided at the top of the core with a layer of B_4C above the sodium. The fuel pins contain UO_2-PuO_2 pellets that are distributed axially in 3-in. compartments within the pins to minimize reactivity effects from fuel compaction. The fuel pellets have hollow centers to permit a maximum heat rating of 13 kw/ft with a cladding temperature of 1420°F. There are 123 fuel pins in the hexagonal fuel assembly which are held in place by six grids, 12 in. apart, along the length of the assembly, with tie rods at alternate corners of the assembly. The fuel assemblies are held down hydraulically and are individually orificed to obtain a uniform sodium exit temperature. Heat is removed from the 1200°F primary sodium by means of six external loops.

For refueling the fuel elements are located by double rotating and indexing shield plugs. After the reactor is cooled to 350°F and the sodium level is lowered, direct visual observation of the core is possible for grappling the fuel elements. The fuel is removed to an argon-cooled cask, is cleaned with steam to remove the sodium, and is then transferred to an on-site reprocessing plant. The blanket is shuffled in an out-in manner to match the orificed sodium flow with the power generation in the elements. This avoids large changes in exit sodium temperature in the blanket assemblies

Digitized by Google

Table V-4 CHARACTERISTICS OF THE 1000-Mw(e) CERAMIC-FUELED FAST REACTOR CONCEPT

	Allis-Chalmers[41]	Combustion Engineering[42]	General Electric[43]	Westing-house[44]
Core and blanket				
Core geometry	Annulus	Flat cylinder	Flat cylinder	7 modules
Core volume, liters	7520	2895	6030	7050
Axial blanket volume, liters	960	3500	9050	2400
Radial blanket volume, liters	17,700	4800	4200	19,850
Fuel form				
Core and axial blanket	Oxide	Carbide	Oxide	Carbide
Radial blanket	Oxide	Carbide	Oxide	Oxide
Active height of core, ft	4	2.5	2.0	6.3
Blanket thickness				
Axial blanket, ft	0.5	1.5	1.5	1.0
Radial blanket, ft	1.5	1.4	1.3	0.7
Composition of core and axial blanket				
Fuel, %	29.4	25.6	34.8*	29.4†
Sodium, %	40	66.5	46.4	55.1
Steel, %	30.6	7.9	18.8	15.5
Composition of radial blanket				
Fuel, %	55	45	50.7	55
Sodium, %	30	43	32.1	25
Steel, %	15	12	17.2	20
Core fissile metal, kg	3690	1155	2304	3686
Blanket fissile metal				
Axial blanket, kg	6	32	58	23
Radial blanket, kg	260	83	80	171
Core load (metal), kg	17,760	8913	12,828	23,420
Blanket loading (metal)				
Axial blanket, kg	2210	10,696	19,242	7800
Radial blanket, kg	84,566	27,886	24,300	56,886
Core load (ceramic), kg	20,200	9400	14,600	25,200
Blanket loading (ceramic)				
Axial blanket, kg	2510	11,250	21,900	8200
Radial blanket, kg	96,100	29,400	27,500	59,800
Power, Mw(t)				
Total	2500	2500	2500	2500
Core	2125‡	1950	2125	2170
Axial blanket		200	300	35
Radial blanket	375	350	75	295
General				
Core irradiation level, Mwd/metric ton of U	100,000	110,000	110,000	100,000
Breeding ratio§	1.32	1.42	1.25	1.57
Doubling time,§ years	19.5	6.2	15.8	11.7
Sodium void worth¶ (100% core voided), $\%\Delta k$	0.0	1.0	0.4	0.3
Doppler coefficient, $-T(dk)/(dT) \times 10^{+3}$	2.6	5	5	12
Fuel-cycle cost,§ mills/kw-hr	0.69	0.30	0.57	0.28
Size, ft				
Reactor diameter	16.0	10.0	14.2	13.6
Reactor height	6.0	5.5	5.0	8.3
Vessel diameter	20.0	16.5	18.0	18.0
Vessel height	25.0	40.7	33.0	36.0
Thermal parameters				
Specific power, kw/kg				
Core U + Pu ceramic material§	100	198	150	86
Core fissile material¶	640	1680	920	520
Power density in core,§ Kw(t)/liter	282	695	365	308
Temperature, °F				
Core inlet	950	850	800	979
Cladding peak	1330	1400	1332	1400
Fuel peak	4615	2600	4700	2184
Core outlet	1200	1120	1100	1200
Fuel bond	Helium	Sodium	Helium	Sodium
Coolant				
Sodium flow, (lb/hr) $\times 10^{-6}$	114	113.6	95.4	128
Core velocity, ft/sec	10	20	11.1	26.5
Loop pressure drop, psi	90	59.8	40	113

Digitized by Google

Table V-4 (Continued)

	Allis-Chalmers[41]	Combustion Engineering[42]	General Electric[43]	Westinghouse[44]
Fuel				
Fuel-pin-cladding outside diameter, in.				
Core and axial blanket	0.30	0.30	0.25	0.30
Radial blanket	0.607	0.45	0.50	0.464
Cladding thickness, in.				
Core and axial blanket	0.028	0.011	0.015	0.010
Radial blanket	0.015	0.016	0.020	0.020
Sodium-bond gap, in.				
Core and axial blanket		0.010		0.006
Radial blanket		0.011		
Pellet outside diameter, in.				
Core and axial blanket	0.24	0.259	0.22	0.268
Radial blanket	0.574	0.396	0.45	0.420
Pellet, inside diameter, in.	0.10		0.06**	
Active core height, in.	48	30	24	75
Active blanket height, in.				
Axial blanket	6	36	36	24
Radial blanket	72	54	36 and 60	87
Assemblies				
Distance across flats, in.	4.45	6.241	8.75	5.104
Triangular pitch of pins, in.				
Core and axial blanket	0.375	0.468	0.338	0.426
Radial blanket	0.69	0.539	0.565	0.496
No. of pins per assembly				
Core and axial blanket	123	169	470	120
Radial blanket	37	127	208	91
No. of assemblies in region				
Core and axial blanket	498	157	225	252
Radial blanket	858	156	108	357
Total no. of pins in region				
Core and axial blanket	61,254	26,533	105,750	30,240
Radial blanket	31,709	19,812	22,464	19,812
Feed enrichment, average, %				
Core	20.8	13.0††	18.0††	15.7
Blankets	0.3	0.3	0.3	0.3

*Includes BeO.
†Includes cermet.
‡Includes bottom axial blanket.
§Per contractor calculations.
¶Per evaluator calculations.
**Formed during operation.
††Zoned.

with the rapid buildup of plutonium associated with the high radial neutron leakage from the core.

Combustion Engineering Reactor Concept

This concept uses a conventional cylindrical core that has a volume of 2895 liters. The core is 2.5 ft high and is 7.2 ft in diameter, with a length-to-diameter ratio of 0.35. The carbide fuel is sodium bonded to the 11-mil-thick cladding made of type 19-9 DL stainless steel. The sodium bond permits higher heat fluxes for a given maximum temperature limit on the fuel and also accommodates the swelling of the fuel with burnup. The top and bottom axial blankets are integral with the core. A 15-in. gas space is provided on top of the upper axial blanket to accommodate a gas release of 11% over the 100,000 Mwd/ton exposure of the element. The carbide is slightly hyperstoichiometric, i.e., carbon content is greater than 4.8 wt.%, to limit swelling and gas release in fuel operating at a maximum temperature of 2600°F. Several methods are proposed to prevent the carburization of the cladding. The hexagonal fuel assemblies in the core each contain 169 fuel pins that are held together by band wraps. The radial blanket is also carbide fuel, with a residence time three times that of the core. Halfway through its life each blanket element is rotated 180° to equalize its exposure and to increase the coolant flow to accommodate the higher heat generation.

For refueling the fuel elements are located by a single rotating and indexing plug and a manipulator arm and are transferred under sodium to an adjacent decay storage pool of sodium. After three months' decay the elements are removed, steam cleaned to remove sodium, and prepared for shipment off-site in a water-cooled cask.

Digitized by Google

There are six conventional primary loops outside the reactor vessel. The pump is at the outlet to minimize the pressure of the cover gas in the reactor vessel.

Combustion Engineering also presents an advanced design featuring a voided radial gap between the core and blanket to obtain a negative sodium coefficient for complete voiding of the core coolant. The theoretical basis for the gap was described in a recent paper (Ref. 51).

General Electric Reactor Concept

To obtain high neutron leakage from the core, this concept uses a highly "pancaked" core, 2 ft high and 11.7 ft in diameter, which has a volume of 6000 liters. There are three radial zones of fissile plutonium enrichment for power flattening. The maximum heat rating of 22.7 kw/ft is obtained with oxide fuel that has a hollow cored center, formed during initial reactor operation. The maximum temperatures for the fuel and the type 316 stainless-steel cladding are 4700 and 1330°F, respectively. The fuel pins are fastened to a grid in the fuel box by use of a T slot in the lower end plug and a mating bar in the grid. The pins are positioned along their length by means of slotted spacer tubes that contact the three surrounding fuel pins. There is an upper shield-plug section that is integral with the fuel pins so that the fuel elements are held down by their own weight. The core contains 7 vol.% beryllium oxide to increase the magnitude of the Doppler coefficient by softening the neutron spectrum. The entire primary system, including the reactor core, the six heat exchangers, and the six pumps, is immersed in a large tank of sodium, 52 ft in diameter, so that problems associated with sodium leakage and thermal expansion in the primary piping are minimized.

A shielded inert-gas-filled cell with manual manipulators is provided directly over the reactor for refueling. The vessel head is removed and the fuel is transferred under sodium using hot-cell techniques. After they have decayed in a storage tank, the fuel elements are removed and shipped under sodium without any cleaning.

General Electric also presents an advanced core without beryllium oxide to obtain a higher breeding ratio. The fuel burnup in this design is 200,000 Mwd/ton.

Westinghouse Reactor Concept

The reactor consists of seven hexagonal cylindrical modules, each containing a high-leakage core that is 2.75 ft in diameter and 6.3 ft high, with a total core volume of 7000 liters. Each core is surrounded by an 8-in.-thick blanket of UO_2 and a 4-in.-thick layer of graphite that decouple the modules from each other. The fuel consists of pressed and sintered carbide pellets of 90% density; the carbide is hypostoichiometric, carbon content less than 4.8 wt.%, to avoid carburizing the type 316L stainless-steel cladding. The pellets are compartmentalized in the pins to minimize reactivity effects from compaction of the ceramic fuel. The axial blankets containing UC form an integral part of the fuel pins. The maximum temperatures for the fuel and the cladding are 2184°F and 1400°F, respectively. Iron is added to the fuel to combine with the free metallic phase forming $(U\text{-}Pu)Fe_2$. This is to avoid forming in the cladding a plutonium-iron eutectic that has a melting point of only 770°F and also to tie up any free plutonium in the grain boundaries to minimize fuel swelling. The fuel is assembled in what is called a Controlled Fuel-Expansion Assembly to provide a negative reactivity coefficient due to thermal expansion and thus supplement the negative Doppler coefficient. Each ceramic fuel pin is made in two pieces; one piece is attached to the upper assembly plate, and the other is attached to the lower assembly plate. A small gap is left in the center. The size of this gap is controlled by the thermal expansion of seven cermet type fuel pins in each assembly which tie the upper and lower grip plates together. The cermet is 20 vol.% UO_2 in stainless steel with a ^{235}U enrichment of 30%.

The fission-product gases are vented from the fuel pins to the primary sodium coolant to minimize the stresses in the cladding. The fuel assemblies are held down in the reactor by means of a push-pull latching device at the bottom of the assembly.

The reactor vessel is designed with a coaxial arrangement for the inlet-outlet pipes to minimize stresses in the vessel from thermal expansion and to minimize the number of penetrations. As a result of the high neutron leakage into the radial blanket of each module, the plutonium content, and therefore the power generation in the blanket elements, increases

Digitized by Google

markedly with exposure in the reactor. Hence provision is made for periodic adjustments in the sodium flow to the blanket elements. For refueling the reactor-vessel head is removed, and by hot-cell techniques the fuel is transferred visually, using gas cooling, to an antimony-lead-filled cask for shipping.

Nuclear and Safety Characteristics

All four reactors have neutron lifetimes in the range from 3 to 6 $\times 10^{-7}$ sec, effective delayed-neutron fractions of about 0.004, and sizable negative Doppler coefficients. The power coefficients of reactivity are all negative and in the range from -1 to -3×10^{-6} Δk/Mw. Relatively flat radial power distributions are obtained in the cores with low length-to-diameter ratios (the Combustion Engineering and General Electric cores) by radial zoning of the plutonium concentration. The tall thin cores (the Allis-Chalmers annular core and the Westinghouse modules) have favorable radial power distributions without fuel zoning. A brief description is given below of the distinguishing characteristics of the four concepts, using parameters obtained from the design reports (Refs. 41 to 44). Note that the values differ from those listed in Table V-4 for the cases where the table values are taken from the AEC evaluation report (Ref. 46) (see Table V-5 for comparison).

The *Allis-Chalmers concept* has a breeding ratio of 1.32, giving a doubling time of 20 years for the fuel inventory. The core conversion ratio is 0.52; an excess reactivity of 0.06 Δk is required for the reactivity decrease between partial reloadings of the core when one-third of the fuel is replaced. A major design basis for this concept is minimizing the possibility of large reactivity insertion should the sodium in the reactor boil, even in the absence of a scram. The voiding of all the sodium in the core gives a reactivity increase of 0.002 Δk. If the sodium boiling occurs in such a way that the upper axial sodium gap is also voided, the reactivity decreases. The Doppler effect will compensate for 0.0017 Δk reactivity before all the oxide fuel reaches the melting point. Control in the annular core requires that several control rods be moved as a coordinated unit because of the small coupling between different sections of the core.

In the *Combustion Engineering concept* the breeding ratio is 1.42, and the specific power in the core is 1680 kw per kilogram of fissionable plutonium; the resulting doubling time is seven years. With the core internal conversion ratio of 0.85, the reactivity change with fuel burnup is only 0.0003 Δk per 1000 Mwd/ton. The reactivity increase for complete loss of sodium from the core is 0.024 Δk, whereas the loss of all the sodium from the core and blankets as well gives no reactivity change. It was calculated that the reactor by means of the Doppler effect can safely absorb a step reactivity increase of 1 dollar and 24 cents without any melting of the fuel or boiling of the sodium. The reactor is partially refueled every two and two-thirds months to replace one-eighth of the core elements so that the reactivity to be controlled is only 0.004 Δk or 1 dollar. Also, sources of potential reactivity addition have been similarly limited; the maximum reactivity worth of a control rod is 1 dollar, and the worth of a fuel assembly is 93 cents. In the event of total loss of coolant flow, it is required that the control rods scram to prevent boiling of the core sodium.

A major objective of the *General Electric concept* is the achievement of a large negative Doppler coefficient of reactivity to counteract reactivity increases that would result from voiding the sodium starting at the core center, even for implausible accidents. Enhancement of the Doppler coefficient is even more important for the oxide fuels, which operate at higher temperature than the carbide fuels, since the Doppler coefficient usually decreases with increasing temperature. The beryllium oxide in the core softens the spectrum so that the Doppler coefficient is enhanced; the Doppler effect will compensate for 0.005 Δk reactivity when the fuel is heated from operating temperature to an average temperature of 4700°F. Voiding all the sodium in the core adds 0.008 Δk, with a maximum increase of 0.014 for some configuration of partial voiding.

It has been calculated that a step reactivity increase of 1 dollar and 70 cents will not cause fuel damage or sodium boiling. The blockage of coolant flow in the core at full power will cause boiling to start at the center with a maximum reactivity gain of less than 1 dollar so that the reactor does not become prompt critical. Up to 3 dollars and 50 cents of reactivity can be inserted at a rate postulated for a refueling accident without any sodium boiling in the core. The energy yield on core meltdown,

Digitized by Google

which inserts reactivity at the rate of 50 dollars/sec, is equivalent to 200 lb of TNT.

In this reactor of softer spectrum, the breeding ratio is 1.25, with an internal conversion ratio of 0.69. The doubling time is 16 years. The core is refueled every 6 months, when one-sixth of the fuel is replaced; 0.33 Δk excess is provided for fuel burnup.

In the *Westinghouse concept* the sodium coefficient for complete voiding of the core sodium has been made very small, -0.001 Δk, by the use of seven small very loosely coupled core modules, each with its own blanket. A partial voiding of the sodium can increase reactivity by 0.0032 Δk, which is below prompt critical. The controlled-expansion fuel elements provide a reactivity coefficient of $-0.75 \times 10^{-5}/°F$, which supplements the Doppler coefficient of $-0.69 \times 10^{-5}/°F$ at operating temperature. The reactivity sharing between the modules reduces the effect of a reactivity insertion in any one module. The coupling in a clean core is only 0.003 Δk, which increases in the equilibrium core to 0.025 Δk as plutonium builds up in the blanket. The monitoring and control of the modular core may require extensive in-core instrumentation.

The breeding ratio is 1.57, the core conversion ratio is 0.54, and the doubling time is 11 years. The reactor is shut down for refueling every 7 months to replace one-sixth of the core. The reactivity decrease between refuelings, because of fuel burnup, is 0.009 Δk.

Physics and Fuel-Cycle Evaluation

In the course of the AEC's evaluation[46] of the four studies, comparative calculations were performed on breeding ratio, Doppler coefficient, and sodium void coefficient, using consistent cross-section data and calculational methods. The fuel-cycle costs were also recomputed for each concept[49] by applying common procedures for estimating the cost of fuel processing, shipping, and fabrication, taking into account such factors as the diameter, length, and cladding thickness of the fuel pins.

Table V-5 PHYSICS AND FUEL-CYCLE EVALUATION

	Allis-Chalmers concept	Combustion Engineering concept	General Electric concept	Westinghouse concept
Reactivity change for complete voiding of core sodium, Δk				
Contractor calculation	0.001	0.024	0.008	−0.001
Evaluator calculation	0	0.010	0.004	0.003
Doppler coefficient, $-T(dk/dT) \times 10^3$				
Contractor calculation	2.9	5	10	12
Evaluator calculation	4.3	5.4	5.4	3.3
Breeding ratio				
Contractor calculation	1.32	1.42	1.25	1.57
Evaluator calculation	1.20	1.41	1.21	1.38
Doubling time, years				
Contractor calculation	18.4	6.9	13.5	13
Evaluator calculation	30	7.2	20	19
Fuel-cycle cost, mills/kw-hr				
Contractor calculation	0.78	0.30	0.57	0.28
Evaluator calculation	0.70	0.43	0.54	0.43

A common burnup of 100,000 Mwd/metric ton was used, as well as a load factor of 80%. The plutonium credits, however, reflect the contractors' estimate of breeding ratio rather than the normalized values obtained in the evaluation. A comparison with the contractors' values is presented in Table V-5. Except for inventory charges that depend on specific power and plutonium credits that depend on breeding ratio, the other components of the fuel-cycle costs in mills per kilowatt-hour are nearly the same for all concepts: fuel fabrication, 0.4; core capitalization, 0.1; shipping, 0.1; and reprocessing, 0.1. Inventory charges are in the range from 0.1 to 0.3 mill/kw-hr and plutonium credits, based on the normalized breeding ratios, are in the range from 0.2 to 0.4. The Allis-Chalmers study proposes that the fuel be reprocessed on the reactor site. This would lower the fuel-cycle cost for that reactor in Table V-5 by 0.1 mill/kw-hr.

Digitized by Google

The differences between the contractors' values and those calculated by the AEC evaluators are to some extent indicative of the state of the art in the physics of large fast reactors. Several conclusions are drawn in the AEC evaluation of the four 1000-Mw(e) fast breeder reactors. It is stated in the evaluation that each of the four concepts could be used as the basis of a technically feasible design. A choice cannot yet be made between the mixed-carbide and mixed-oxide fuels because the potential advantages of the carbides depend on information yet to be obtained in development programs. Additional work that should be done prior to committing a 1000-Mw(e) ceramic-fueled fast breeder is outlined in the evaluation. Included are further preliminary designs and optimizations covering the entire plant, safety studies to establish criteria and to predict the course of accidents, physics studies to include cross-section measurements and integral experiments, fuel and materials development, and fuel-handling development.

References

1. Westinghouse Electric Corp., Atomic Power Division, 1000-Mw(e) Closed Cycle Water Reactor Study, Vol. I, USAEC Report WCAP-2385, March 1963.
2. Westinghouse Electric Corp., Atomic Power Division, 1000-Mw(e) Closed Cycle Water Reactor Study, Vol. II, USAEC Report WCAP-2385, March 1963.
3. A. L. Gaines and L. Porse, Problems in the Design and Construction of Large Reactor Vessels, presented at the Third United Nations International Conference on the Peaceful Uses of Atomic Energy, Geneva, 1964, Paper A/Conf.28/P/227.
4. J. C. Rengel, Project Manager, Large Closed-Cycle Water Reactor Research and Development Program, Progress Report for the Period December 1, 1960 to May 31, 1961, USAEC Report WCAP-3703, Westinghouse Electric Corp., Atomic Power Division.
5. J. C. Rengel, Project Manager, Large Closed-Cycle Water Reactor Research and Development Program, Progress Report for the Period June 1, 1961 to August 31, 1961, USAEC Report WCAP-3706, Westinghouse Electric Corp., Atomic Power Division.
6. N. R. Nelson, Project Manager, Large Closed-Cycle Water Reactor Research and Development Program, Progress Report for the Period September 1, 1961 to November 30, 1961, USAEC Report WCAP-3707, Westinghouse Electric Corp., Atomic Power Division.
7. N. R. Nelson, Project Manager, Large Closed-Cycle Water Reactor Research and Development Program, Progress Report for the Period December 1, 1961 to February 28, 1962, USAEC Report WCAP-3708, Westinghouse Electric Corp., Atomic Power Division.
8. N. R. Nelson, Project Manager, Large Closed-Cycle Water Reactor Research and Development Program, March 1, 1962 to June 30, 1962, USAEC Report WCAP-3710, Westinghouse Electric Corp., Atomic Power Division.
9. Westinghouse Electric Corp., Atomic Power Division, 1962. (Unpublished)
10. Westinghouse Electric Corp., Atomic Power Division, 1962. (Unpublished)
11. Westinghouse Electric Corp., Atomic Power Division, 1963. (Unpublished)
12. Westinghouse Electric Corp., Atomic Power Division, 1963. (Unpublished)
13. Westinghouse Electric Corp., Atomic Power Division, 1963. (Unpublished)
14. Westinghouse Electric Corp., Atomic Power Division, 1963. (Unpublished)
15. C. Roderick, Project Manager, Large Closed-Cycle Water Reactor Research and Development Program, Progress Report, January 1, 1964 to March 31, 1964, USAEC Report WCAP-3269-2, Westinghouse Electric Corp., Atomic Power Division.
16. D. E. Byrnes and W. E. Foster, Literature Values for Selected Chemical/Physical Properties of Aqueous Boric Acid Solutions, USAEC Report WCAP-1570, Westinghouse Electric Corp., Atomic Power Division, January 1961.
17. W. D. Fletcher, A. Krieg, and P. Cohen, The Behavior of Austenitic Stainless Steel Corrosion Products in High Temperature Boric Acid Solutions, USAEC Report WCAP-1689 (Rev.), Westinghouse Electric Corp., Atomic Power Division, May 1961.
18. P. Cohen and G. R. Taylor, Ion-Exchange with Equilibrium and Decay, USAEC Report WCAP-1700, Westinghouse Electric Corp., Atomic Power Division, January 1961.
19. A. N. Nahavandi and G. B. Killinger, Primary System Pressure Response Study Due to Power Unbalance (TOPS Code), USAEC Report WCAP-1831, Westinghouse Electric Corp., Atomic Power Division, September 1961.
20. L. S. Tong, H. B. Currin, and A. G. Thorp II, New DNB (Burnout) Correlations, USAEC Report WCAP-1997 (Rev. 2), Westinghouse Electric Corp., Atomic Power Division, May 1963.
21. J. E. Olhoeft, The Doppler Effect for a Non-Uniform Temperature Distribution in Reactor Fuel Elements, USAEC Report WCAP-2048, Westinghouse Electric Corp., Atomic Power Division, July 1962.
22. A. S. Kitzes, Design and Hazards Report, LRD Irradiation Test Number 1, USAEC Report WCAP-3701, Westinghouse Electric Corp., Atomic Power Division, July 15, 1963.
23. W. Zernik, H. B. Currin, E. Elyash, and G. Previti, "THINC," A Thermal Hydrodynamic Interaction Code for a Semi-Open or Closed Channel Core, USAEC Report WCAP-3704, Westinghouse Electric Corp., Atomic Power Division, February 1962.
24. R. A. Dannels and Dermot J. Bredin, Compilation of a Muft Library (Library 567), USAEC Report WCAP-3709, Westinghouse Electric Corp., Atomic Power Division, December 1962.
25. W. J. Eich, H. T. Williams, Jr., and H. Aisu, The Heterogeneous Representation of Control Rods in Light Water Lattices: A Comparison of Analysis and Experiment, USAEC Report WCAP-3711,

Digitized by Google

Westinghouse Electric Corp., Atomic Power Division.
26. D. E. Byrnes, Some Physicochemical Studies of Boric Acid Solutions at High Temperatures, USAEC Report WCAP-3713, Westinghouse Electric Corp., Atomic Power Division, September 1962.
27. J. S. Moore, and B. H. Axelson, Reactor Control and Protection System Study for Chemical Shim Operation of a Large Closed Cycle Water Reactor, USAEC Report WCAP-3714, Westinghouse Electric Corp., Atomic Power Division, October 1962.
28. W. D. Fletcher, Ion Exchange in Boric Acid Solutions with Radioactive Decay, USAEC Report WCAP-3716, Westinghouse Electric Corp., Atomic Power Division, November 1962.
29. R. E. Wolf and J. F. Noonan, RENEWED: A Program for Nuclear Reactor Fuel Cycle Analysis, USAEC Report WCAP-3717, Westinghouse Electric Corp., Atomic Power Division, November 1962.
30. D. L. Miller, Control Rod Programming in a Large Multiregion Core, USAEC Report WCAP-3719, Westinghouse Electric Corp., Atomic Power Division, October 1962.
31. P. G. Lacey, Reactivity Dependence Upon Moderator Temperature and Boron Concentration in Large PWR Cores Controlled by Chemical Shim, USAEC Report WCAP-3720, Westinghouse Electric Corp., Atomic Power Division, November 1962.
32. A. N. Nahavandi, B. H. Axelson, G. B. Killinger, and A. H. Killinger, A Digital Computer Analysis of Closed Cycle Water Nuclear Power Plant Start-Up Using Natural Circulation (THERMO-SYPHON Code) Vols. I and II, USAEC Report WCAP-3722, Westinghouse Electric Corp., Atomic Power Division, February 1962.
33. P. G. Lacey, Fine Structure Power Peaking in a Critical Experiment Mockup of a Chemical Shim Core, USAEC Report WCAP-3723, Westinghouse Electric Corp., Atomic Power Division, March 1963.
34. H. Aisu, R. F. Barry, and P. G. Lacey, Load Variation Restrictions in a Chemically Poisoned Large PWR Core, USAEC Report WCAP-3724, Westinghouse Electric Corp., Atomic Power Division, March 1963.
35. D. L. Miller, Control Rod Requirements in a Chemical Shim Core, USAEC Report WCAP-3727, Westinghouse Electric Corp., Atomic Power Division, August 1963.
36. L. F. Picone, The In-Pile Test of Chemical Shim, USAEC Report WCAP-3729, Westinghouse Electric Corp., Atomic Power Division, June 1963.
37. L. F. Picone, D. D. Whyte, and G. R. Taylor, Radiotracer Studies of Hideout at High Temperature and Pressure, USAEC Report WCAP-3731, Westinghouse Electric Corp., Atomic Power Division, June 1963.
38. L. E. Strawbridge and R. E. Wolf, Optimization Study for Large Pressurized Water Reactor Cores, USAEC Report WCAP-3733, Westinghouse Electric Corp., Atomic Power Division, Apr. 8, 1964.
39. R. A. Dean, Coolant Mixing in Open Lattice Reactor Cores, USAEC Report WCAP-3735, Westinghouse Electric Corp., Atomic Power Division, August 1963.
40. EBWR Project Group, EBWR Test Reports (100-MWT Operation), USAEC Report ANL-6703, Argonne National Laboratory, January 1964.
41. Allis-Chalmers Mfg. Co., Atomic Power Development Associates, Inc., and The Babcock & Wilcox Co., Large Fast Reactor Design Study, USAEC Report ACNP-64503, January 1964.
42. Combustion Engineering, Inc., Liquid Metal Fast Breeder Reactor Design Study, USAEC Report CEND-200, Vols. I and II, January 1964.
43. General Electric Company, Atomic Power Equipment Department, Liquid Metal Fast Breeder Reactor Design Study, USAEC Report GEAP-4418, Vols. I and II, January 1964.
44. R. B. Steck (Comp.), Liquid Metal Fast Breeder Reactor Design Study, USAEC Report WCAP-3251-1, Westinghouse Electric Corp., Atomic Power Division, January 1964.
45. David Okrent, Neutron Physics Considerations in Large Fast Reactors, *Power Reactor Technol.*, 7(2): 107-137 (Spring 1964).
46. Chicago Operations Office, Reactor Engineering Division, An Evaluation of Four Design Studies of a 1000-MWe Ceramic-Fueled Fast Breeder Reactor, USAEC Report COO-279, Dec. 1, 1964.
47. L. J. Koch, F. S. Kirn, G. W. Wensch, C. E. Branyan, and E. L. Alexanderson, Sodium Cooled Fast Breeder Reactors, presented at the Third United Nations International Conference on the Peaceful Uses of Atomic Energy, Geneva, 1964, Paper A/Conf.28/P/207.
48. David Okrent, K. P. Cohen, and W. B. Loewenstein, Some Nuclear and Safety Considerations in the Design of Large Fast Power Reactors, presented at the Third United Nations International Conference on the Peaceful Uses of Atomic Energy, Geneva, 1964, Paper A/Conf.28/P/267.
49. Leonard E. Link, George J. Fischer, and Edwin L. Zebroski, Fuel Cycle Economics of Fast Reactors, presented at the Third United Nations International Conference on the Peaceful Uses of Atomic Energy, Geneva, 1964, Paper A/Conf.28/P/248.
50. C. E. Klotz and R. S. Miller, The Design of a 1000 MWe Fast Breeder Reactor, *Trans. Am. Nucl. Soc.*, 7(1): 196 (June 1964).
51. L. S. Noderer and Sidney Visner, Effect of a Voided Gap on Reactivity Coefficient for Voiding Core Sodium in a Fast Reactor, *Trans. Am. Nucl. Soc.*, 7(2): 238 (November 1964).

LEGAL NOTICE

This journal was prepared under the sponsorship of the U. S. Atomic Energy Commission. Neither the United States, nor the Commission, nor any person acting on behalf of the Commission:

A. Makes any warranty or representation, expressed or implied, with respect to the accuracy, completeness, or usefulness of the information contained in this journal, or that the use of any information, apparatus, method, or process disclosed in this journal may not infringe privately owned rights, or

B. Assumes any liabilities with respect to the use of, or for damages resulting from the use of any information, apparatus, method, or process disclosed in this journal.

As used in the above, "person acting on behalf of the Commission" includes any employee or contractor of the Commission, or employee of such contractor, to the extent that such employee or contractor of the Commission, or employee of such contractor prepares, disseminates or provides access to, any information pursuant to his employment or contract with the Commission, or his employment with such contractor.

Digitized by Google

Digitized by Google

Digitized by Google

NUCLEAR SCIENCE ABSTRACTS

The U. S. Atomic Energy Commission, Division of Technical Information, publishes *Nuclear Science Abstracts (NSA)*, a semimonthly journal containing abstracts of the literature of nuclear science and engineering.

NSA covers (1) research reports of the U. S. Atomic Energy Commission and its contractors; (2) research reports of government agencies, universities, and industrial research organizations on a world-wide basis; and (3) translations, patents, books, and articles appearing in technical and scientific journals.

Complete indexes covering subject, author, source, and report number are included in each issue. These are cumulated quarterly, semiannually, and annually providing a detailed and convenient key to the literature.

Availability of *NSA*

SALE *NSA* is available on subscription from the Superintendent of Documents, U. S. Government Printing Office, Washington, D. C., 20402, at $30.00 per year for the semimonthly abstract issues and $22.00 per year for the four cumulated-index issues. Subscriptions are postpaid within the United States, Canada, Mexico, and all Central and South American countries, except Argentina, Brazil, British and French Guiana, Surinam, and British Honduras. Subscribers in these Central and South American countries, and in all other countries throughout the world, should remit $37.00 per year for subscriptions to semimonthly abstract issues and $25.00 per year for the four cumulated-index issues.

EXCHANGE *NSA* is also available on an exchange basis to universities, research institutions, industrial firms, and publishers of scientific information. Inquiries should be directed to the Division of Technical Information Extension, U. S. Atomic Energy Commission, P. O. Box 62, Oak Ridge, Tennessee, 37831.

Digitized by Google

TECHNICAL PROGRESS REVIEWS may be purchased from Superintendent of Documents, U. S. Government Printing Office, Washington, D. C., 20402. *Isotopes and Radiation Technology* at $2.00 per year for each subscription or $0.55 per issue; the other four journals at $2.50 per year and $0.70 per issue. The use of the coupon below will facilitate the handling of your order.

POSTAGE AND REMITTANCE: Postpaid within the United States, Canada, Mexico, and all Central and South American countries except as hereinafter noted. Add $0.50 per year, or $0.15 per single issue for the *Isotopes and Radiation Technology* journal and $0.75 per year or $0.20 per single issue for the other four journals for postage to all other countries, including Argentina, Brazil, British and French Guiana, Surinam, and British Honduras. Payment should be by check, money order, or document coupons, and MUST accompany order. Remittances from foreign countries should be made by international money order, or draft on an American bank, payable to the Superintendent of Documents, or by UNESCO book coupons.

order form

SUPERINTENDENT OF DOCUMENTS
U. S. GOVERNMENT PRINTING OFFICE
WASHINGTON, D. C., 20402

Enclosed:

document coupons [ ] check [ ] money order [ ]

Charge to Superintendent of Documents No._____

Please send a one-year subscription to

[ ] NUCLEAR SAFETY

[ ] POWER REACTOR TECHNOLOGY

[ ] REACTOR FUEL PROCESSING

[ ] REACTOR MATERIALS

(Each subscription $2.50 per year; $0.70 per issue.)

[ ] ISOTOPES AND RADIATION TECHNOLOGY

(Each subscription $2.00 a year; $0.55 per issue.)

SUPERINTENDENT OF DOCUMENTS
U. S. GOVERNMENT PRINTING OFFICE
WASHINGTON, D. C., 20402

(Print clearly)

Name _____

Street _____

City _____ Zone ____ State _____

Digitized by Google

Y3.At7:
36 8-3

Eng.

TK
9202
.G4

ENGINEERING
NOV 17 '66
LIBRARY

POWER REACTOR TECHNOLOGY

A Quarterly Technical Progress Review

Prepared by DIVISION OF TECHNICAL INFORMATION, USAEC,
in cooperation with COMBUSTION ENGINEERING, INC., NUCLEAR DIVISION

Summer 1965

● VOLUME 8

● NUMBER 3

Digitized by Google

TECHNICAL PROGRESS REVIEWS

To meet the needs of industry for concise summaries of current atomic developments, the Atomic Energy Commission is publishing this series, Technical Progress Reviews. Issued quarterly, each of the reviews digests and evaluates the latest findings in a specific area of nuclear technology and science.

The five journals published in this series are:

Isotopes and Radiation Technology, P. S. Baker, A. F. Rupp, and associates, Oak Ridge National Laboratory

Nuclear Safety, Wm. B. Cottrell, W. H. Jordan, and associates, Oak Ridge National Laboratory

Power Reactor Technology, formerly prepared and edited by W. H. Zinn and J. R. Dietrich, Nuclear Division, Combustion Engineering, Inc. (a new contractor will take over preparation of this journal beginning with Vol. 8, No. 4).

Reactor Fuel Processing, Stephen Lawroski and associates, Chemical Engineering Division, Argonne National Laboratory

Reactor Materials, R. W. Dayton, E. M. Simons, and associates, Battelle Memorial Institute

Each journal may be purchased from the Superintendent of Documents, U. S. Government Printing Office, Washington, D. C., 20402. *Isotopes and Radiation Technology* at $2.00 per year for subscription or $0.55 for individual issues; the other four journals at $2.50 per year and $0.70 per issue. See back cover for remittance instructions and foreign postage requirements.

The views expressed in this publication do not necessarily represent those of the United States Atomic Energy Commission, its divisions or offices, or of any Commission advisory committee or contractor.

Availability of Reports Cited in This Review

Unclassified AEC reports are available for inspection at AEC depository libraries and are sold by the Clearinghouse for Federal Scientific and Technical Information, National Bureau of Standards, U. S. Department of Commerce, 5285 Port Royal Road, Springfield, Va., 22151. Some of the reports cited are not available owing to their preliminary nature; however, the information contained in them will eventually be made available in formal progress or topical reports.

Unclassified reports issued by other Government agencies or private organizations should be requested from the originator.

Unclassified British and Canadian reports may be inspected at AEC depository libraries. British reports are sold by the British Information Service, 45 Rockefeller Plaza, New York, N. Y.; Canadian reports (AECL series) are sold by the Scientific Document Distribution Office, Atomic Energy of Canada, Ltd., Chalk River, Ontario, Canada.

Classified U. S. and foreign reports identified in this journal as Classified may be purchased by properly cleared Access Permit Holders from the Division of Technical Information Extension, U. S. Atomic Energy Commission, P. O. Box 1001, Oak Ridge, Tenn., 37831. Such reports may be inspected at classified AEC depository libraries.

Digitized by Google

POWER REACTOR TECHNOLOGY

A REVIEW OF RECENT DEVELOPMENTS

Prepared by DIVISION OF TECHNICAL INFORMATION, USAEC,
in cooperation with
COMBUSTION ENGINEERING, INC., NUCLEAR DIVISION

SUMMER 1965

VOLUME 8

NUMBER 3

Digitized by Google

Foreword

This is an interim quarterly review assembled by the Division of Technical Information, U. S. Atomic Energy Commission, from material supplied by Combustion Engineering, Inc., prior to the termination, at their request, of their contract to prepare the review. A new contractor will assume responsibility for the preparation of *Power Reactor Technology* beginning with the Fall issue, Vol. 8, No. 4.

Power Reactor Technology contains reviews of selected recently published reports that are judged noteworthy in the fields of power-reactor research and development, power-reactor applications, design practice, and operating experience. It is not meant to be a comprehensive abstract of all material published during the quarter, nor is it meant to be a treatise on any part of the subject. However, related reports from different sources are often treated together to yield reviews having some breadth of scope, and background material may be added to place recent developments in perspective. Occasionally the reviews are written by guest authors. Reviews having unusual breadth or significance are placed at the front of the issue as Feature Articles.

The intention is to cover the various areas of reactor development from the general viewpoint of the reactor designer rather than from the more detailed points of view of specialists in the individual areas. To whatever extent the coverage of *Power Reactor Technology* may occasionally overlap the fields of the other Technical Progress Reviews, the overlaps will be motivated by this objective of viewing current progress through the eyes of the reactor designer.

A degree of critical appraisal and some interpretation of results are often necessary to define the significance of reported work. Any such appraisal or interpretation represents only the opinion of the reviewer. Readers are urged to consult the original references to obtain all the background of the work reported and to obtain the interpretation of the results given by the original authors.

For timely coverage, *Power Reactor Technology* must often review fragmentary material. The fixed subject headings listed below have been adopted in the hope of maintaining some continuity and order in the material from one issue to another; all reviews except Feature Articles will be arranged under these headings. A particular issue will not necessarily contain all the headings but only those under which material is reviewed.

Economics, Applications, Programs
Resources and Fuel Cycles
Physics
Fluid and Thermal Technology
Fuel Elements
Materials
Control and Dynamics
Containment, Radiation Control, and Siting
Systems Technology
Components
Design and Construction Practice
Operating Experience
Specific Reactor Types
Specific Applications
Unconventional Approaches

U. S. Atomic Energy Commission
Division of Technical Information

Digitized by Google

Contents

I Physics 157
Measurements on Operating Reactors . . 157
Resonance Absorption 159
Heterogeneous Graphite-Moderated Reactors 160
Reduced-Delayed-Neutron-Group Representation 161
References 162

II Fluid and Thermal Technology . . . 163
Liquid Metals 163
Two-Phase Systems 164
References 170

III Fuel Elements 172
Fuel-Performance Evaluations 172
Incoloy 800 Cladding. 174
References 175

IV Components 176
Liquid-Metal-Level Probes 176
Pressure-Tube Fretting Corrosion . . . 177
References 182

V Specific Reactor Types 183
Sodium-Graphite Reactors: Steam Cycles 183
Reference 185

VI Unconventional Approaches . . . 186
Fast Supercritical Water Reactor . . . 186
Hanford Graphite Superheat Reactor . . 193
References 198

NOTE: The Commission regrets to announce that, at the request of Combustion Engineering, Inc., their contract to prepare *Power Reactor Technology* has been terminated. This issue was assembled by the AEC Division of Technical Information from material supplied by Combustion prior to the time the contract expired. A new contractor, Argonne National Laboratory, will assume responsibility for preparation of *Power Reactor Technology* beginning with Vol. 8, No. 4, and the distribution of that issue will be delayed. Please direct any communications regarding this issue to the USAEC Division of Technical Information, Washington, D. C., 20545.

Issued quarterly by the U. S. Atomic Energy Commission. Use of funds for printing this publication approved by the Director of the Bureau of the Budget on October 14, 1963.

Digitized by Google

Digitized by Google

Section I

Power Reactor Technology

Physics

Measurements on Operating Reactors

On installation of the second core in the Sodium Reactor Experiment (SRE), a test program was initiated to develop and evaluate techniques for measuring the nuclear parameters of the core and for checking core stability. An objective of this program is to make possible reliable interpretation of measured changes in control-rod positions in terms of reactivity values. A method of monitoring for abnormal behavior would then be available from the comparison of calculated and measured reactivity variations. References 1 and 2 describe some of the work directed toward this purpose.

Reference 1 presents test results that show the feasibility of a technique developed for calibrating shim rods during normal reactor power operation. When compared with other rod-calibration methods that have been used in the past, the new technique is said to have the following advantages: (1) increased plant availability, (2) elimination of operational hazards, (3) use of inexpensive equipment, and (4) elimination of special devices to drive the control rod or elimination of the need for a pile oscillator within the core. The technique utilizes an analog computer that is programmed to simulate the reactor. Six groups of delayed neutrons with a fuel-temperature feedback loop are included in the simulation. For a rod-calibration measurement, the reactor flux is manually cycled by moving the shim rod in equal increments about the critical position. A signal is taken from the shim-rod position indicator and is scaled with a potentiometer to give the shim-rod differential worth, which becomes the reactivity input for the computer. The computer output is the simulated-reactor-flux signal. The differences in actual reactor flux and simulated reactor flux are recorded on a strip chart. The shim-rod differential worth is given by the setting of the shim-rod-worth potentiometer, which results in agreement of the computer-flux response with the actual reactor-flux response. In practice the fuel-temperature feedback constants in the simulation circuit are adjusted until the system indicates the same differential rod worth for all frequencies of rod travel. Results of tests at 12 Mw(t) show that rod worths can be determined within ±5% of the true value. This compares with resolutions of ±2% obtained at zero power with normal period-measurement techniques. Reactor-flux noise was an important limiting factor to the attainment of higher accuracy with the on-line shim-rod-calibration technique.

Reference 2 describes the experiments performed to obtain the reactivity coefficients of core 2 of the SRE. From the results of transfer-function measurements at 10, 15, and 20 Mw(t), it was clearly demonstrated that the positive prompt power coefficient associated with fuel-rod bowing was eliminated when the clusters were constrained to prevent bowing. Through analyses of the reactivity variations introduced by a flow ramp and an inlet temperature ramp, the combined fuel-and-coolant temperature coefficient and the inlet temperature coefficient were determined. The combined coefficient was found to be −0.12 cents/°F, a value that agrees very well with the sum of the calculated Doppler and coolant coefficients. A simple lag model was used in the analysis of the inlet-temperature-ramp data. Although good agreement with calculations was obtained, it is recognized that the simple model used is not entirely adequate because the slow change in inlet temperature used in the experiment results in interactions with the reactivities associated with core temperatures. Other pertinent measurements are described, e.g., shim-rod

Digitized by Google

calibrations, xenon transient, and isothermal core temperature.

Reference 3 presents the results of a number of performance tests conducted at the Plutonium Recycle Test Reactor to investigate the operating characteristics of the plutonium-fueled D_2O-moderated reactor. The test results were obtained during initial operation with a three-zone configuration comprising natural UO_2 elements in the central region surrounded by an annulus of plutonium-aluminum elements and an outer region of UO_2 elements. Reactor refuelings to compensate for burnup were made by charging fresh plutonium-aluminum elements in the intermediate zone. When a steady-state loading was finally achieved, the intermediate plutonium-aluminum zone was somewhat expanded, as compared to the initial loading, at the expense of a reduced central zone of the UO_2 elements. Measurements were made of the change in reactivity with fuel burnup. The rate of loss of reactivity per unit of energy production increased with the inventory of plutonium in the reactor, as expected from the results of diffusion-theory perturbation calculations. As the steady-state loading was approached, the fraction of the total core fissions rate due to the plutonium was about 55%.

Measurements were made of the radial power distribution by computing individual tube power outputs from flow and temperature-rise data; data are presented for exposures of 0, 1000, and 2000 Mwd. As a result of the method of charging the plutonium-aluminum elements in the intermediate zone of the three-zone core (outside-in method), the radial power flattening improved with increasing exposure.

Measurements of the photoneutron flux were observed to decay at a rate determined by a fission-product decay curve derived from the work of Perkins and King;[4] the curve represented a simulation of the decay rate of gamma flux from the emitters giving gammas of energy greater than 2.2 Mev, the threshold energy for the (γ, n) reaction in deuterium. Measurements of the shim-rod worths, using the partial water-height method, showed decreasing total worth as operation of the reactor progressed to the steady-state three-zone fuel loading, i.e., as the plutonium-fission ratio increased. Random-noise techniques were used to measure the reactor transfer function and thus to obtain β/l. The measurements indicated a decrease in β/l as the plutonium inventory in the reactor was increased. The combined fuel-plus-coolant temperature coefficient and the moderator temperature coefficient were observed to become much less negative as the plutonium inventory was increased during the approach to the steady-state configuration. A contributing factor to the decreases in negative temperature coefficients was the gradual degradation of the primary coolant from 99.75% to 95% D_2O during the course of reactor operation. The decreases in negative coefficient values were not considered large enough to affect reactor safety.

References 5 and 6 report on the recent successful operation of the Experimental Breeder Reactor No. 1 (EBR-I) with a plutonium loading (Mark IV). The results of a stability analysis, based essentially on transfer-function and power-coefficient measurements, are presented in Ref. 5, wherein it is noted that there is nothing inherently unsafe or dangerous in the operation of a plutonium-fueled system. The results of breeding-gain measurements, which demonstrate directly the superiority of plutonium as a fuel, are treated in Ref. 6.

Oscillator-rod measurements were conducted on EBR-I, Mark IV, to obtain the zero-power and load-power transfer functions. From the transfer functions a separation was made of the reactivity feedback corresponding to the various reactor power levels and inlet coolant temperatures. Reference 5 describes the reactivity-feedback function by a mathematical model characterized by the following two terms: (1) prompt, small, and associated primarily with power changes in the fuel (axial expansion of fuel, NaK expulsion, radial expansion of the Zircaloy jackets, fuel-slug bowing, and jacket bowing); and (2) relatively delayed, strong, and associated with expansion effects in the coolant, structure, and upper portion of the blanket region. Substitution of the experimental data into the mathematical model results in a set of time constants and power coefficients that adequately describes the experimentally derived reactivity-feedback function for a given set of operating conditions. In all cases the values of the fitted time constants are consistent with values estimated from heat-transfer considerations.

The fitted power-coefficient values for the delayed term greatly exceed the corresponding values established for the prompt fuel-

Digitized by Google

expansion term. This empirical result is surprising and is attributed to slug-bowing effects that cancel nearly all the usual prompt negative effects. That slug bowing is an important mechanism is also indicated by the static measurements of the power coefficient. Insofar as the stability and safety of the system are concerned, it is concluded that the effects of slug bowing are not particularly important. In all cases studied the overall power coefficient was strongly negative and was still sufficiently rapid in action to prevent strong reinforcement of input and feedback reactivities. Changes in coolant inlet temperature were found to effect strong changes in the feedback, apparently a consequence of temperature-sensitive clearances.

Reference 5 concludes that, in general, a system fueled with plutonium would tend to be more sensitive to reactivity perturbations than one fueled with uranium. For a feedback that reinforces the input, the neutron kinetics are such that the system tends to be less stable (relative to ^{235}U fuel). However, for a feedback that cancels a portion of the input, the system would tend to be more stable. Hence, if slug-bowing and rod-bowing effects could be eliminated, it is possible that the kinetic behavior of a plutonium-fueled system would be more stable than that of its ^{235}U-fueled counterpart.

The experimental methods used for the breeding-gain measurements on EBR-I, Mark IV, are described in detail in Ref. 6. The method is based on integration of the various fission and capture patterns over the system volume. The mapping technique requires observation of activities generated in thin metallic foils of uranium and plutonium inserted in the core and blanket regions of the assembly. The counting operations for the various types of foils and the operations involved in the organization of the counting data for integration purposes are described. Spatial distributions were established for plutonium, ^{235}U, and ^{238}U fissions and captures. It should be noted that specific measurements of captures in plutonium and ^{235}U were not carried out on the Mark IV loading. Instead, use was made of the results of measurements by Kafalas et al.,[7] who established values of α for ^{239}Pu and ^{235}U as a function of radial distance and elevation in a ^{235}U-fueled loading in EBR-I.

The breeding ratio is defined as the ratio of ^{239}Pu and ^{241}Pu production to ^{235}U, ^{239}Pu, and ^{241}Pu destruction. The value of breeding ratio arrived at from the measurements is 1.27 ± 0.08. This value demonstrates the importance of ^{239}Pu as a fast reactor fuel since earlier measurements of the conversion ratio of essentially the same system fueled with ^{235}U gave values of the order of unity. The marked increase is directly attributable to a much higher value of ν for ^{239}Pu and a much lower value of α. The results also indicate the beneficial aspects of threshold fissions in ^{238}U and ^{240}Pu. Reference 5 concludes that the results obtained provide tangible proof that a reactor fueled with ^{239}Pu can produce useful power and regenerate substantially more fuel than is consumed.

Resonance Absorption

In the case of isolated rods in the *NR-NR* approximation, collision theory yields

$$RI = \int \left[P_0 \frac{\sigma_p}{\sigma_0} + (1 - P_0) \right] \sigma_a \, dE/E$$

where σ_0, σ_a, and σ_p are the total, absorption, and potential scattering of the fuel, and P_0 is the nonescape probability from the fuel region. If the Wigner rational approximation is used, i.e.,

$$P_0 = \frac{x}{1 + x}$$

where x is the average optical chord length of the rod for a given energy, then the heterogeneous resonance integral is equivalent to the homogeneous resonance integral in which a new potential scattering is defined as

$$\sigma_p' = \sigma_p + \frac{\sigma_0}{x}$$

Reference 8 investigates the use of three better approximations to P_0 that are rational forms in x, namely:

1. From Booth,

$$P_0 = \frac{x(x + c)}{(x + b)^2}$$

2. From Carlvik and Fukai,

$$P_0 = \frac{2x}{x + 2} - \frac{x}{x + 3}$$

Digitized by Google

3. From Sauer,

$$P_0 = 1 - \frac{1}{x}\left[1 - \left(1 + \frac{x}{n+1}\right)^{-(n+1)}\right]$$

by comparison with the exact escape probabilities.

None of these methods can easily take into account differences in resonance parameters. Reference 9 considers the exact escape probability

$$P_0(x) = 1 - P_0(x) = \left[1 + \frac{x}{A(x)}\right]^{-1}$$

and obtains an average

$$\overline{A} = \frac{1}{I}\int_{-\infty}^{\infty} A\, dI$$

where I is the effective resonance integral for a particular resonance. Because the Doppler effect in each resonance is not proportional to its resonance integral, the use of the same relation for P_0 for a series of resonances in ^{238}U, for example, could lead to relatively large errors in temperature coefficients.

A form of the Dancoff factor based on cell calculations with white boundaries—i.e., all neutrons striking the cell boundary are returned with a cosine azimuthal distribution and do not follow the laws of specular reflection—is shown, in Ref. 8, to lead to results in good agreement with Monte Carlo calculations. The paper also justifies the use of the white-boundary condition on theoretical grounds.

Heterogeneous Graphite-Moderated Reactors

A design calculation method for gas-cooled graphite-moderated reactors has been coded in FORTRAN II in the ARGOSY program.[10] The principal approximations are:

1. Spatial effects in fuel and moderator are ignored, and mean fuel and mean moderator effects only are evaluated.

2. The generalized heavy-gas approximation is used to treat neutron thermalization.

3. Resonance integrals are not evaluated in the method but are obtained (in the case of ^{238}U) from tabular data.

Three energy groups with upper-energy cutoffs of 4 ev, 10 kev, and 10 Mev are used.

Thermal-Group Calculation

A three-region cylindrical cell, with fine structure within the fuel region reduced by simple flux-weighting factors, is used with about 100 energy points. An interpolation between narrow and wide resonance theory is used to compute fluxes through the plutonium resonance range. The thermalization in both fuel and moderator is approximated by the operator

$$L\phi = \xi\Sigma_s\, d/dx\{f(x)\,[x\phi'(x) + (x-1)\phi(x)]\} \qquad (x = E/kT)$$

where $f(x)$ is adjusted for crystal-binding effects as a function of plutonium concentration and moderator temperature. The coupled fuel and moderator equations are integrated using a finite-difference scheme.

Resonance-Group Calculation

Tabular values for the ^{238}U effective resonance integral as a function of fuel temperature and σ_{ex} are utilized.

$$\sigma_{ex} = \frac{\gamma S_{eff}}{4N_{238}\overline{V}_{fuel}}$$

where γ is a factor to correct for inaccuracies in the normal Wigner rational approximation and S_{eff} is the effective surface of the fuel element or cluster. These tables were made for uranium oxide and metal by considering for each resonance the proper mixture of narrow and wide resonance for potential scattering cross sections of uranium and oxygen. For ^{235}U and ^{239}Pu resonances, the infinite resonance integrals are reduced by factors allowing for self-shielding and shielding by ^{238}U and other isotopes. These can reduce the dilute values by about 20%. The spectrum in this group is not calculated, but effects of other absorbers are taken into account.

Digitized by Google

Fast-Group Calculation

A collision-probability approach is used in obtaining reaction rates in fuel and moderator for each of three energy subgroups where a spatially flat fission source in the fuel is assumed. This yields flux-weighted capture, fission, and removal cross sections. Diffusion coefficients for all groups are modified by streaming factors in the radial and axial directions.

Point core criticality can be achieved through changes in leakage, absorption, or fission source. Equivalent control-rod cross sections are evaluated by determining the extrapolation distance from blackness coefficients as a function of energy. A simple point burnup calculation can also be performed. The IBM-7090 time required for a complete calculation including burnup is about 5 min.

Reduced-Delayed-Neutron-Group Representation

In the analysis of the dynamic behavior of a reactor, considerable simplification results from the use of a reduced number of delayed-neutron groups, often with little sacrifice in accuracy. The selection of the reduced-group parameters (delayed-neutron yield and decay constant) generally depends on the type of transient being investigated. Reference 11 develops a reduced-group model chosen so that the resulting representation matches the reactor transfer function exactly in the limit of both very-low and very-high frequency. This requirement leads to the so-called "asymptotic" representation, the parameters for which are obtained from the following relations:

$$\sum_{j=1}^{m} \beta_j = \sum_{i=1}^{n} \beta_i \tag{1}$$

$$\sum_{j=1}^{m} \beta_j \lambda_j = \sum_{i=1}^{n} \beta_i \lambda_i \tag{2}$$

$$\sum_{j=1}^{m} \frac{\beta_j}{\lambda_j} = \sum_{i=1}^{n} \frac{\beta_i}{\lambda_i} \tag{3}$$

$$\sum_{j=1}^{m} \frac{\beta_j}{\lambda_j^2} = \sum_{i=1}^{n} \frac{\beta_i}{\lambda_i^2} \tag{4}$$

where β = delayed-neutron yield
λ = decay constant
i = group index of the physical-decay groups
n = number of the physical-decay groups
j = group index of the reduced groups
m = number of the reduced groups

Equations 1 and 2 result from matching the transfer function in the high-frequency limit, and Eqs. 3 and 4 result from matching the low-frequency limit. The equations as given hold for any number of reduced groups, but at least two groups must be used to satisfy all four conditions.

In some cases it is necessary to represent a particular group explicitly, for example, the longest lived group in cases where reactor shutdown is of interest or the shortest lived group for very rapid transients. In such a case the remaining groups are selected to satisfy Eqs. 1 to 4. Reference 12 contains a compilation of reduced-group parameters for various fissile isotopes with one reduced group (Eqs. 1 and 3), two groups (Eqs. 1 to 4), and three groups (Eqs. 1 to 4 with either the longest or shortest lived delay group represented explicitly).

Reference 13 reports a method of obtaining reduced-delay-group parameters by a least-squares fit. The parameters are chosen such that the integral

$$\int_{\omega} \left\{ 1 - \frac{\mathrm{Re}\,[F(j\omega)]}{\mathrm{Re}\,[G(j\omega)]} \right\}^2 d \ln \omega$$

is minimized where $G(j\omega)$ is the transfer function with all six delay groups and $F(j\omega)$ is the transfer function with the reduced groups. Results for two, three, and four reduced groups are tabulated for all fissile isotopes with the least-squares fit over a range of frequencies (ω) of 0.001 to 10 radians/sec. A comparison of the reduced-group parameters obtained from the asymptopic and the least-squares approach as determined in Ref. 13 is given in Table I-1. In addition, Ref. 13 compares calculations of both the reactor transfer function and the reactor response to positive- and negative-

Digitized by Google

reactivity steps with the reduced-group models and the full six-delay-group model.

Table I-1 COMPARISON OF REDUCED-DELAYED-NEUTRON-GROUP PARAMETERS FOR ^{235}U (THERMAL FISSION)[13]

	Asymptotic	Least squares
Two groups		
λ_1	0.0252	0.0410
λ_2	0.566	0.540
β_1	0.00194	0.00293
β_2	0.00459	0.00360
Three groups (longest lived group isolated)		
λ_1	0.0124	0.0124 (0.0278)*
λ_2	0.0342	0.0512 (0.0231)
λ_3	0.609	0.590 (1.568)
β_1	0.00022	0.00022 (0.00185)
β_2	0.00263	0.00299 (0.00364)
β_3	0.00367	0.00332 (0.00104)

*Three-groups straight least-squares fit.

References

1. E. A. Moore and C. L. Peckinpaugh, On-Line Shim Rod Calibration, USAEC Report NAA-SR-9511, Atomics International, Aug. 1, 1964.
2. M. R. Pellet, Core II Physics Tests on the Sodium Reactor Experiment, USAEC Report NAA-SR-9510, Atomics International, Aug. 1, 1964.
3. V. W. Gustafson, Plutonium Recycle Test Reactor Power Test Results, USAEC Report HW-80253, Hanford Atomic Products Operation, December 1963.
4. J. F. Perkins and R. W. King, Energy Release from the Decay of Fission Products, *Nucl. Sci. Eng.*, 3(6): 726-746 (June 1958).
5. R. R. Smith, R. O. Haroldsen, and F. D. McGinnis, Stability Considerations for a Plutonium Loading in EBR-I, USAEC Report ANL-6863, Argonne National Laboratory, May 1964.
6. R. R. Smith, R. O. Haroldsen, R. E. Horne, and R. G. Matlock, The Breeding Ratio of a Plutonium Loading in EBR-I, USAEC Report ANL-6789, Argonne National Laboratory, February 1964.
7. P. Kafalas et al., Determination of the Ratio of Capture to Fission Cross Sections in EBR-I, *Nucl. Sci. Eng.*, 2(5): 657 (September 1957).
8. D. C. Leslie, J. G. Hill, and A. Jonsson, Improvement to the Theory of Resonance Escape in Heterogeneous Fuel. 1. Regular Arrays of Fuel Rods, British Report AEEW-R-353, 1964.
9. J. M. Otter, Escape Probability Approximations in Lumped Resonance Absorbers, USAEC Report NAA-SR-9744, Atomics International, August 1964.
10. J. G. Tyror, A Method of Lattice Calculation for Gas-Cooled Graphite-Moderated Reactors, British TRG-Report-754(W), 1964.
11. R. E. Skinner and E. R. Cohen, Reduced Delayed Neutron Group Representations, *Nucl. Sci. Eng.*, 5(5): 291-298 (May 1959).
12. R. W. Albrecht and C. Metelmann, The Use of Reduced Delayed Neutron Group Representations in Nuclear Reactor Simulation, USAEC Report HW-81076, Hanford Atomic Products Operations, March 1964.
13. T. E. Springer, Delayed Neutron Reduced Groups by Least Squares, USAEC Report LA-3082, Los Alamos Scientific Laboratory, December 1961.

Digitized by Google

Section

II

Power Reactor Technology

Fluid and Thermal Technology

Liquid Metals

References 1 and 2 are literature reviews of the engineering properties of various liquid metals. They contain data on properties such as density, thermal conductivity, electrical resistivity, specific heat, surface tension, vapor pressure, and viscosity for metals such as mercury, sodium, sodium-potassium, potassium, rubidium, and lithium. Reference 1 is directed specifically to liquid-metal heat transfer by forced convection and presents a comparison of theoretical and experimental results. The report presents "recommended" equations suitable for the engineering calculation of heat transfer in fully developed turbulent flow in circular tubes, heat transfer in fully developed turbulent flow through tubes of noncircular cross section, and heat-transfer-coefficient correlations for flow parallel to bundles of circular rods and across a staggered tube bank. The discrepancies between experimental and theoretical results are discussed, and several reasons for the discrepancies are suggested.

Data on forced-convection heat transfer and pressure drop for boiling potassium are given in Ref. 3. The particular system considered in the reference is quite specialized in that the experiments were done to obtain design data for a potassium boiler constructed of serpentine tubes. Nevertheless, the reference gives insight into the difficulties of experimentation with liquid metals and the techniques employed to determine heat-transfer coefficients in rather complex systems. Figure II-1 illustrates the forced-convection local-boiling heat-transfer coefficients for potassium boiling inside serpentine tubes. The figure shows the "best-fit" correlation. The data, which show considerable scatter, are not reproduced here, but are given in Ref. 3. The range of experimental parameters is shown in Table II-1.

It is interesting to note that the stability of the boiling loop proved to be a continuing problem in the experiments. The loop, which was constructed of Haynes 25 alloy, consisted of a preheater, a test boiler, a superheater, and an air-cooled condenser, coupled with an electromagnetic flowmeter and pump. Much of the instability problem was said to originate in the preheater-preboiler portion of the loop as the result of subcooled nucleate boiling, despite the fact that a rather large pressure drop was established by use of a throttle valve just downstream of the electromagnetic pump. The authors conclude that the stability of two-phase

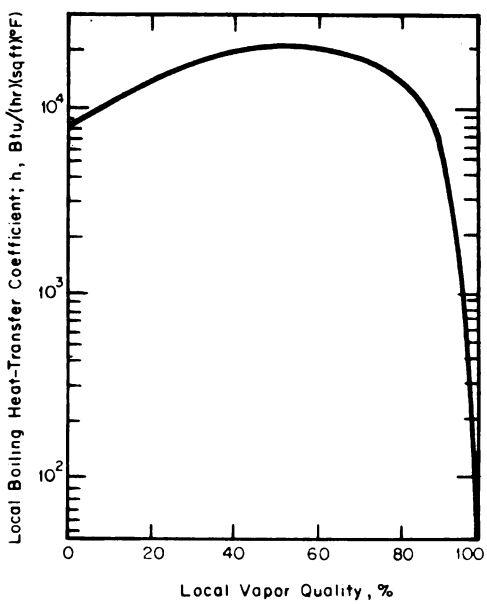

Fig. II-1 Forced-convection local-boiling heat-transfer coefficients for potassium inside a serpentine tube.[3]

Digitized by Google

Table II-1 RANGE OF EXPERIMENTAL PARAMETERS IN BOILING POTASSIUM EXPERIMENT[3]

Potassium flow rate, lb/hr	17 to 25
Vapor quality, %	0 to 100
Boiling ΔT, °F	2 to 170
Boiling temperature, °F	1625 to 1725
Heat flux in test boiler, Btu/(hr)(sq ft)	17,000 to 52,000
Max. heat flux in preboiler	64,000
Boiling pressure, psia	42 to 62
Max. vapor velocity, ft/sec	330
Test duration, hr	3625
Boiling hours	980

potassium systems cannot be studied by simulation with water or other common fluids. The pressure-drop data taken during the experiments were found to correlate within ±20% by the Lockhart-Martinelli correlation.

Reference 4 presents data on the boiling-heat-transfer coefficients and burnout heat fluxes for pool boiling of sodium. The reference describes in some detail two sodium loops, the larger of which accommodates an instrumented electric heating element on which accurate surface-temperature measurements can be made at heat fluxes up to 10^6 Btu/(hr)(sq ft) in boiling sodium. The test-section portion of this large loop, called the "working loop" in Ref. 4, is fabricated of graphite, electrically insulated with a boron nitride sleeve. The test section, which is heated by the resistance of the graphite, is capable of working to the heat flux of 10^6 Btu/(hr)(sq ft); a second test section heated by electron bombardment is being developed to extend the heat flux limit to 5×10^6 Btu/(hr)(sq ft). The data recorded in Ref. 4 on heat-transfer coefficients and burnout heat flux are of a preliminary nature but nevertheless would be of interest to the specialist.

Reference 5 reports on the determination of void fractions, slip ratios, and flow rates for liquid-vapor metal systems in pipes under critical-flow conditions. The Fauske model is applied to calculate the void fraction, the slip ratio, and the two-phase critical flow rates for mercury, cesium, rubidium, potassium, sodium, and lithium under the postulate that the mechanisms causing critical flow in the liquid-vapor systems are the same as in steam-water systems. Figure II-2 illustrates, for example, the theoretical prediction of the slip ratio for rubidium under critical-flow conditions. According to Ref. 5, no experimental data exist pertinent to the critical flow of liquid metals; it is therefore not possible to compare the theoretical predictions with experimental results.

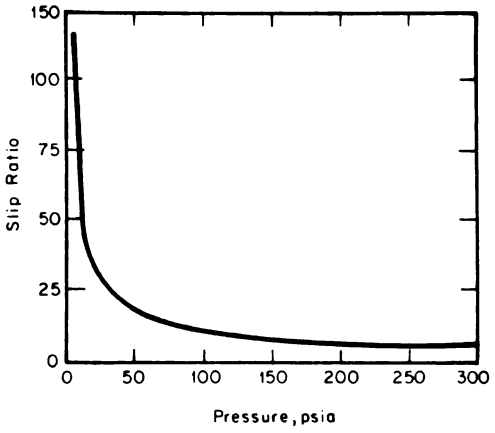

Fig. II-2 Theoretical prediction of slip ratio for rubidium under critical-flow conditions.[5]

Two-Phase Systems

The relatively large volume of literature pertinent to two-phase flow indicates continued interest in the associated phenomena. Reference 6 is an extensive annotated bibliography on the heat transfer and hydraulics of gas-liquid systems. A total of 2843 documents are cited in the bibliography, and the subjects covered represent a wide range of interests. These include such items as the critical heat flux, flow patterns, nozzles, phase and velocity distribution, pressure drops, separation of mixtures, transients and instability, turbulent flow, and visual observations. The references were published between 1950 and 1962 in *Nuclear Science Abstracts*, *Chemical Abstracts*, *Science Abstracts — Section A*, *Engineering Index*, and *Applied Mechanics Reviews*. It is believed that the volume will prove to be a valuable asset to workers in the field of two-phase hydraulics and heat transfer.

References 7 to 12 are somewhat specialized and will not be reviewed in detail. The consideration of the group as a whole, however, indicates the basic lines of attack in attempts to discover basic information on two-phase flow and heat transfer. References 7 and 8 deal with pool boiling. References 9 and 10 are air-water studies pertaining to annular, two-phase flow. References 11 and 12 deal with flow regimes. Reference 12 is particularly interesting in that it reports on an experimental program to determine the transition point between slug- and annular-flow regimes at elevated pressures.

Digitized by Google

The Armadilla loop at Argonne National Laboratory was used to produce a steam-water mixture at pressures up to 600 psig. Conductivity measurements were made in the riser of the test loop by means of a suitably designed probe. This probe measured the electrical resistance between the center of the pipe and the wall; when the probe was dry, the resistance was very high, and, when wet, the resistance was relatively lower. Figure II-3 is indicative of the results obtained in the study. The figure shows the superficial vapor velocity plotted against the superficial liquid velocity and indicates that the transition between the slug- and annular-flow regimes was not a step change, but that there existed a region designated as "transition" wherein the major mode of liquid transport corresponded to slugs with a large number of bubbles entrained in them. As the superficial vapor velocity was further increased, fully developed annular flow was established. It was found that the transition between the slug- and annular-flow regimes at a given pressure occurred at almost constant quality, independent of flow range, provided that the following relation was satisfied:

$$\frac{V_{gs}^2 \rho_g}{gD \rho_f} \geq 2.0$$

where V_{gs} is the superficial vapor velocity, D is the pipe diameter, and ρ_f and ρ_g are the liquid and vapor densities, respectively. The quality at which the transition occurred ranged from 8.6% at 215 psia to about 18% at 615 psia. The following quotation serves to summarize the results:[12]

> ... Physically, the picture that emerges from these experiments is as follows. When the quality is passed through at which slugs can form, they do. As the annular flow region is approached, these slugs begin to lose liquid to the wall as they rise, ultimately being completely consumed if the pipe is long enough.... If the heat flux were higher, or perhaps if the region in which slug flow could exist were shorter, slug flow might never develop, and one could go right from bubbly to annular flow.
>
> Repeated attempts to obtain bubbly flow in this apparatus always were unsuccessful. Either the heat flux was too low or the pump too small for this condition ever to exist. In the 0.375-in. ID pipe, the maximum inlet liquid velocity was only 10 ft/sec. This is apparently insufficient to give bubbly flow as the fully developed condition. In addition, the water was very pure, which also made it difficult to obtain bubbly flow. It would appear that bubbly flow is an important flow regime only when the pressure and/or the heat flux is very high.

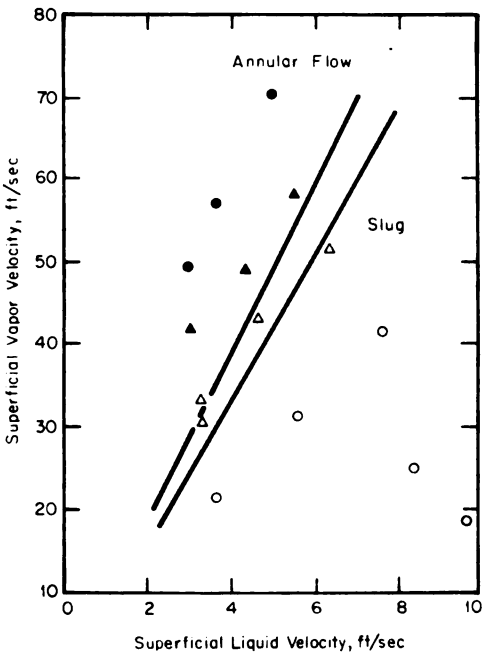

Fig. II-3 Flow-regime map for 0.375-in. pipe.[12] Pressure is 615 psia. (The open symbols are slug flow, and the solid symbols are annular flow.)

It is natural that both the analyst and the experimenter would like to "see" what is going on within the test section; indeed, the author of Ref. 12 does present pictures of air-water flow tests at low pressure. References 13 to 15 are devoted to results of photography and X radiography of two-phase flow systems. A perusal of these documents indicates that the problems in optics connected with photographing gas-liquid mixtures probably are as formidable as the problems of analyzing the results obtained from such experiments. The technique discussed in Ref. 14, that of radiography, appears quite promising in that it does allow studies using opaque tubing and high pressures. The discussion in that reference is devoted to a large extent to the mechanics of obtaining the X-ray photographs, although a few results of the experiments are given pictorially. The positive prints of the X-ray plates shown illustrate that it is remarkably easy to tell the positions of the liquid and gas phases (in this case air) within the tube, and the pictures show various flow regimes.

Reference 15 reports on experiments designed to study boiling flow of steam-water mixtures at atmospheric pressures. High-speed motion pictures were made for a variety of flow rates

Digitized by Google

and heat fluxes utilizing a transparent rectangular channel heated by a strip of metal at one side of the flow channel. The reference reproduces a relatively large number of frames of motion pictures which illustrate bubble-, coalescing slug-, and annular-flow regimes. An unusual procedure was developed for measuring the velocities of the various liquid and vapor phases. The reference also contains a quantitative discussion of the important variables affecting the transitions between the different flow regimes.

A relatively large number of publications (Refs. 16 to 23) pertain to the hydrodynamics of two-phase flow. Included are papers on two-phase pressure drop,[16,17] nozzle flow,[18,19] and the prediction of critical flow rates for two-phase mixtures.[20–23] Reference 16 compares a number of analytical methods for the prediction of two-phase pressure drop with experimental results. The analytical techniques were those of Levy, Marchaterre, and Martinelli and Nelson. Experimental pressure drops were measured for circular and annular channels. The results are compared graphically, and no single correlation was found to represent the data adequately. Neither the Martinelli and Nelson nor the Levy correlation provides for the effect of the mass flow on the pressure drop, and this effect appeared to be a relatively large one in the experimental results.

The information in Ref. 17 includes two-phase pressure-drop data as experimentally determined for a variety of piping components such as bends, tees, expansions, contractions, and valves. Most of the data were obtained at 1200 psia (although a few points were run at 800 and 1600 psia) at mass velocities from 1 to 4 million lb/(hr)(sq ft) and at qualities up to 24 wt.%. Pressure-drop ratios were determined for straight-pipe flow and were found to be correlated "favorably" by the Levy model. The effect of flow rate on the pressure-drop ratios was negligible, and the author mentions that this behavior is not consistent with the results of other investigators. The author[17] suggests that this comes about because of the relatively large pipe diameter — 2 in. — used in his measurements. The reference presents a correlation relating the two- to single-phase pressure-drop ratio of bends to the ratio for straight pipes over the pressure range 800 to 1600 psia. Resistance coefficients were obtained for contraction and expansion losses on the assumption of a homogeneous mixture, and the coefficients agreed reasonably well with the data presented in standard engineering textbooks. The ratio of the two- to single-phase pressure drop for flow through an orifice at 1200 psia was calculated by the homogeneous model, and the results appeared to agree fairly well with the experimental data. The pressure losses in flows through gate and globe valves, however, did not correlate very well with calculations based on the homogeneous model.

The expansion of two-phase fluids through converging-diverging nozzles is discussed in Refs. 18 and 19. The emphasis in these two papers is not on reactor design, although the information they present could be applied to mass-flow-rate determination. References 20 to 23 pertain to the predictions of critical flow of single- and two-phase mixtures. These references contain both experimental and analytical predictions of critical flow rates in a variety of geometries; the results may be useful in the field of nuclear safety, since two-phase critical flow usually would occur in the discharge of coolant from a pipe or pressure-vessel break into the reactor containment system. Reference 21, for example, reports on experimental determination of the discharge of steam-water mixtures from short lengths of pipe at upstream pressures approaching 2000 psia. The reference[21] presents an equation correlating experimentally determined data.

The subject of boiling burnout is covered in Refs. 24 to 27. Reference 24 gives the results of an investigation into forced-convection burnout in Freon and deals with the uniformly heated round tubes utilizing vertical upflow. The use of Freon (also called "Acton" in the reference) is an attempt to gain an insight into the mechanism and important parameters affecting burnout in steam-water systems without encountering the many experimental difficulties involved with the actual use of steam and water. The material (Freon-12) has low vapor pressure and a low latent heat. This combination of physical properties enabled the Freon loop to operate at low pressures and temperatures with low power requirements. The reference reports experimental data and compares them to results obtained in steam-water experiments, with the following conclusions:[24]

> The qualitative similarity in shapes of functions and detailed effects between the Acton 12 data at 155 pounds per square inch and data for water at

Digitized by Google

1000 pounds per square inch indicates a high probability of success in developing model techniques at least for the study of burn-out in high-pressure water systems.

References 25 to 27 all deal with experimental studies of burnout in bundles of heated rods. This subject was previously considered in the Spring 1964 issue of *Power Reactor Technology*, 7(2): 154-165. This previous review concluded that the experimental results for burnout in multirod geometry were not well understood. Part of the problem was believed to lie in the difficulty of determining the amount of mixing from one flow subchannel to another within the multirod bundle. Accordingly the information appearing in Ref. 25 is of interest in that it reports boiling burnout data taken with two different types of rod spacers, "wires" and "warts." The Hanford tests done with the wire-wrapped bundle were reviewed in the earlier issue of *Power Reactor Technology*, and the data given in Ref. 25 compare results obtained when the wire wrapping on the rods is replaced by the so-called warts. The warts were made of alumina having a length of $^{9}/_{16}$ in., a width of 0.17 in., and a thickness of 0.048 in. and were positioned on the heated rods by placing them in slots cut in Inconel ferrules soldered to the heated rods. The test section was housed in a horizontal 3.25-in.-ID pressure tube, and pressure was controlled to 1200 psig. Results indicated that "there is no discernible difference in the burnout heat fluxes between the test sections with rods spaced with wire wraps and the test sections with rods spaced with warts."[25] The authors comment[25] that this was somewhat unexpected, in that they believed that the degree of mixing would be increased by the use of the wire-wrapped test section and that this increase would result in higher burnout heat fluxes. A number of explanations offered for the lack of difference in the two sets of data include the following: (1) the amount of mixing between the subchannels is the same with the wire wrap as with the warts; (2) a spacing effect predominates over mixing in determining the burnout conditions; (3) the increased mixing caused by the wires is offset by the tendency of the wires to strip the liquid film from the rods.

Reference 26 reports on burnout experiments employing a 19-rod bundle as a test section and using "fog" as a coolant. A cross section of the bundle is shown in Fig. III-1 of *Power Reactor Technology*, 7(2): 154. The test section used to take the data in Ref. 26 employed the wart type spacers to ensure that the rod-to-rod spacing (0.074 in.) was maintained. Experiments were conducted at pressures of 1000 and 1200 psia with flow rates from 500,000 to 2 million lb/(hr)(sq ft). One of the test sections had a "flow diverter" present (about 14 in. upstream of the heated length) which was designed to direct the coolant flow to the interior of the bundle at that point; the second test section was similar but was constructed without the presence of the flow diverter. The presence of the flow diverter had little effect on the burnout heat flux when the coolant at the inlet was fog, but the diverter did increase the value of the burnout heat flux some 10 to 20% for subcooled water. Possibly the most important piece of information coming from the tests[26] was the demonstration of the importance of the hydraulic stiffness of the system on the value of the burnout heat flux. Figure II-4 illustrates the burnout heat flux as a function of the outlet enthalpy for a pressure of 1200 psia. The discontinuities in the curves shown in Fig. II-4 were believed to be caused by the presence of a compressible medium, steam, in that portion of the test loop between the steam generator and the test section. The presence of this instability complicates the data and makes their comparison to other results difficult. Of more importance, it indicates extreme care must be taken in applying laboratory data to reactors whose hydraulic characteristics may be different from those of the laboratory apparatus.

In British work[27] on the effect of rod spacing on burnout in a simulated rod bundle, the test section simulated the gap between the rod type

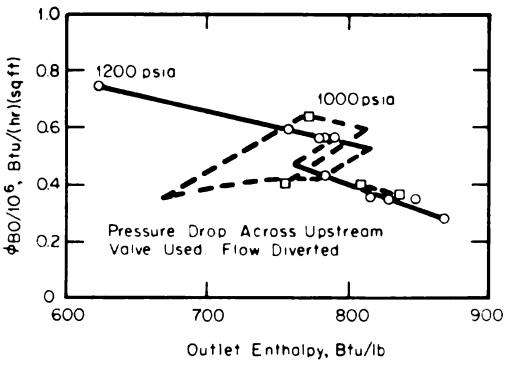

Fig. II-4 Effect of system pressure on boiling burnout for 19-rod bundles at a flow rate[26] of 500,000 lb/(hr)(sq ft).

Digitized by Google

elements in a multirod bundle by means of a "dumbbell" test section. The cross section of the dumbbell test section is shown in Fig. II-5; the use of such a mock-up permits experiments to be carried out in loops of reduced power capability. The heat generation at the

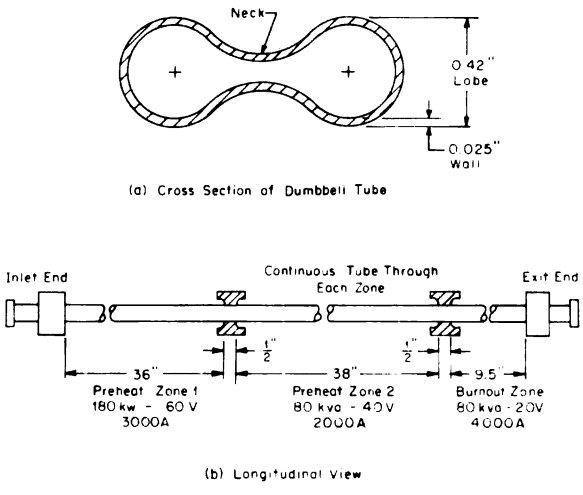

Fig. II-5 Details of the dumbbell test section.[27]

neck of the dumbbell test section was increased for some of the runs by fixing a strip of stainless steel to each neck, and tests were run at a pressure of 960 psia, with a mass velocity of 2 million lb/(hr)(sq ft) and vertical upflow of water. Tests were also made with a tubular test section of the same diameter as the lobe of the dumbbell test section. The total length of the test section was about 7 ft, with the first 6 ft being utilized as a preheater and the last 9.5 in. being instrumented to detect burnout. The surfaces of the neck portion of the test section could be forced closer together by insulating blocks, and the gap therein varied from about 0.04 to 0.2 in. The results indicated that for tests with uniform peripheral heat flux the value of the gap was unimportant for gaps ranging within the values just mentioned. Burnout occurred at the exit end of the test section and on the lobe rather than at the neck. Additional tests were done with local increases of heat flux at the neck of the test section, and an arbitrary increase of 40% in heat flux was made by the inclusion of the metal strips. The effect of the gap was again small, although in these runs burnouts did take place in the region of the test-section neck. Correlation of the tubular burnout data[27] with the data from the dumbbell illustrated that burnout occurred in the two test sections at equivalent values of heat flux.

The remaining group of reports[28–32] deals with experimental and analytical studies of the dynamics of two-phase systems. Three of the reports[28–30] cover analytical studies, and the remaining two reports discuss experimental results. The analytical approaches are all based on the fundamental conservation equations dealing with mass, energy, and momentum plus an equation of state. They are different in the techniques used to solve the equations and the models of the system upon which the equations are based. The treatment in Ref. 28, for example, uses the simplified model illustrated in Fig. II-6, and the differential equations are solved by the "modified-Euler" integration process combined with appropriate iterative procedures. The author of Ref. 29 considers the idealized natural-circulation system shown in Fig. II-7, and the solution of the equations is accompanied by perturbation theory. Figure II-8 illustrates the system studied in Ref 30, in which perturbation theory is again used to achieve a solution. The treatment in Ref. 28 is quite complete; reactivity feedback in the reactor is provided and is coupled into the time-dependent solutions. Separate energy-conservation equations for the fuel, cladding, and the heat exchanger are also included, and separated flow is assumed. The author of Ref. 29 obtains the void-reactivity feedback by integrating the product of the perturbed void fraction, both spatially

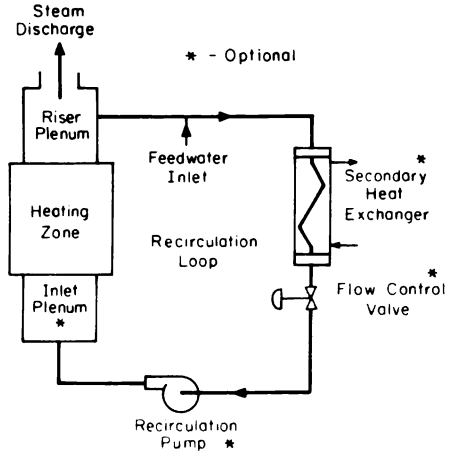

Fig. II-6 Idealized boiling-water system.[28]

Digitized by Google

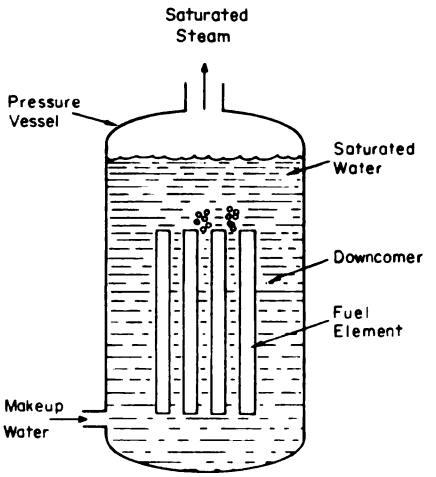

Fig. II-7 Model of a natural-circulation boiling-water reactor.[29]

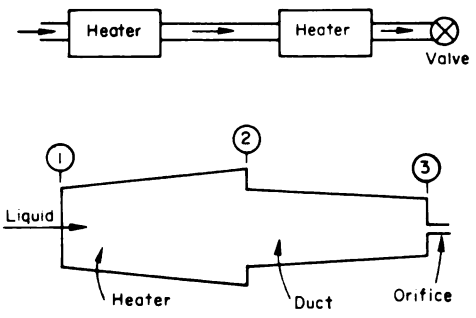

Fig. II-8 Configuration of system studied in Ref. 30.

and temporally, and the reactivity worth of the voids. The treatment of power generation in Ref. 30 assumes that the rate of vapor generation in the heater is constant or is proportional to the system density at point 2 (see Fig. II-8).

It is feasible here only to mention a few of the general results of the rather complex dynamic analyses. The mathematical model developed in Ref. 28 is compared to experimental results obtained at General Electric Company, Atomic Power Equipment Department. The authors conclude that "the period of oscillations and threshold of instability predicted by the present analysis are in good agreement with the test results." The analyses are then applied in studying the response of a "typical" boiling-water reactor to a variety of perturbations. In Ref. 29 the analytical solutions obtained are applied to several specific problems, namely, the dependence of stability on steady-state conditions, the effect of pressure drops in the downcomer and at the inlet to the channel, and the stability of a parallel-channel system with a common downcomer. The effect of the channel length on the dynamic behavior of the system is also studied.[29] The author of Ref. 30 has specialized his solution to the case of a short heater followed by a long insulated duct and orifice, and also a long heater immediately followed by an orifice with no insulated duct. Briefly the author concludes that, whenever a fluid density ratio greater than about 3 exists across an evaporator, there is a possibility of the development of flow oscillations.

The experiments reported in Ref. 31 are preliminary in nature and were done with two parallel heated channels. Both single-phase liquid (subcooled water) at atmospheric pressure and steam-water mixtures were employed as feed to the test sections. Heating was accomplished by the condensation of steam at pressures ranging from 20 to 50 psi. The results illustrate that a negative slope of the curve of mass flow rate vs. pressure is not a necessary condition for the occurrence of oscillatory instabilities. The authors also conclude that, when there is net quality in the feed to the heated test section, no oscillatory instabilities will occur. This conclusion appears to disagree with the data presented in Ref. 26; in that study the presence of steam in the piping between the steam generator and the test section was believed to have allowed flow oscillations in the test section. The problem is complicated, however, by the fact that the "springiness" of the entire test loop depends on its constructional details; and, although the test loop used to take the data appearing in Ref. 31 did employ two-phase mixtures at the test-section inlet, it may well be that the flow loop nevertheless was "stiff."

The test section utilized in Ref. 32 was an electrically heated stainless-steel tube (0.045 in. in inside diameter and 4.5 in. long). Although the tests were run at 200 psia, a pressure lower than that ordinarily used for water type reactors, the results still are of general interest. The author notes that at low values of subcooling it is possible to obtain high void fractions due to the presence of unquenched bubbles. The bubbles exist because, as the subcooling of zero is approached, the temperature driving force

Digitized by Google

transferring heat from the bubbles to the bulk liquid becomes small, with the result that the bubbles have relatively long lifetimes. The presence of the nonequilibrium situation within the flow channel resulted in a departure from the characteristic burnout pattern in subcooled water. The most noticeable result of this was the reduction of the burnout heat flux to relatively low values. The author suggests that this is due to the initiation of "froth flow" as the unquenched bubbles are entrained in the liquid. The reference presents a table of critical-heat-flux data taken with the apparatus, and each burnout point is accompanied by a description of a hypothesized local flow regime. The local flow regimes were identified by consideration of the behavior of the test-section instrumentation and the past history of a particular run. Some idea of the technique can be obtained by considering Fig. II-9. Figure II-10 illustrates the effect of instabilities on the burnout heat flux for the hypothesized annular flow. The author comments on the figure as follows:

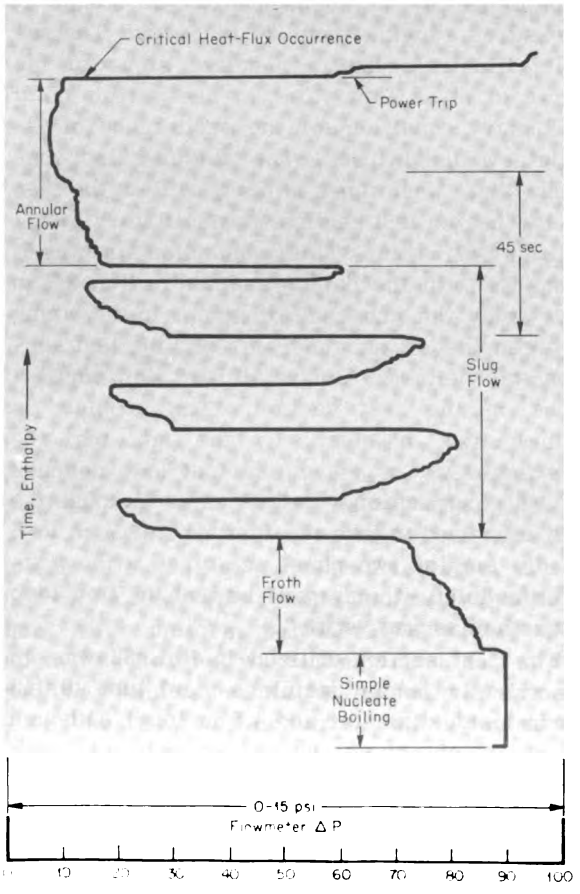

Fig. II-9 Froth flow, periodic vapor slugging, and stable annular flow during net steam generation.[32]

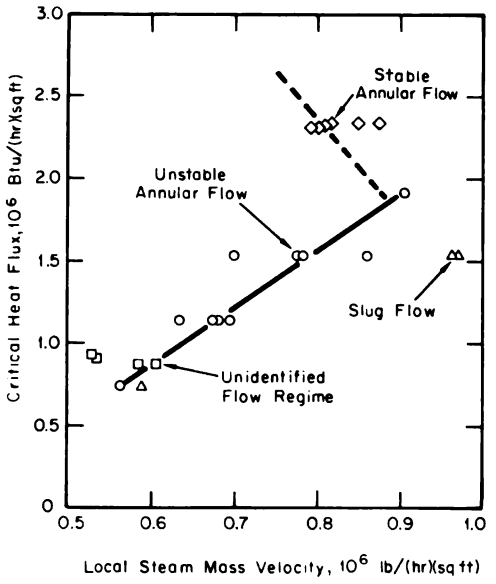

Fig. II-10 Effect of flow regime and degree of hydrodynamic instability upon critical-heat-flux occurrence during net steam generation[32] *at 200 psia.*

> The positive slope of the critical heat flux-steam mass velocity relationship [see Fig. II-10] which is characteristic of unstable annular flow, is directly counter to the negative slope typical for stable flow. Since the slug-flow data follow a similar behavior, this characteristic may be applied to distinguish between stable and unstable flow conditions in systems using high-damping, slow-response secondary flow meters, such as mercury manometers.

This was one of the points made in the review article in the Fall 1964 issue of *Power Reactor Technology*, 7(4): 335.

References

1. R. Herrick, Liquid Metal Heat Transfer by Forced Convection, British TRG-Report-546, July 2, 1963.
2. G. F. Burdi, Snap Technology Handbook, Volume I. Liquid Metals, USAEC Report NAA-SR-8617 (Vol. I), Atomics International, Aug. 1, 1964.
3. E. Bernstein, J. P. Petrek, G. J. Rose, and J. J. Horan, Experimental Results of Forced Convection Boiling Potassium Heat Transfer and Pressure Drop Tests, USAEC Report PWAC-429, Pratt & Whitney Aircraft Division, United Aircraft Corp., July 16, 1964.
4. R. C. Noyes, Boiling Studies for Sodium Reactor Safety. Part I. Experimental Apparatus and Results of Initial Tests and Analysis, USAEC Report NAA-SR-7909, Atomics International, Aug. 30, 1963.

Digitized by Google

5. Hans K. Fauske, Two-Phase Critical Flow with Application to Liquid-Metal Systems (Mercury, Cesium, Rubidium, Potassium, Sodium, and Lithium), USAEC Report ANL-6779, Argonne National Laboratory and Associated Midwest Universities, October 1963.
6. Robert R. Kepple and Thomas V. Tung, Two-Phase (Gas-Liquid) System: Heat Transfer and Hydraulics, An Annotated Bibliography, USAEC Report ANL-6734, Argonne National Laboratory, July 1963.
7. W. R. Beasant and H. W. Jones, The Critical Heat Flux in Pool Boiling Under Combined Effect of High Acceleration and Pressure, British Report AEEW-R-275, July 1963.
8. W. L. Owens, Jr., An Analytical and Experimental Study of Pool Boiling with Particular Reference to Additives, British Report AEEW-R-180, May 1963.
9. L. E. Gill, G. F. Hewitt, and P. M. C. Lacey, Sampling Probe Studies of the Gas Core in Annular Two-Phase Flow: Part II. Studies of the Effect of Phase Flow Rates on Phase and Velocity Distribution, British Report AERE-R-3955, June 1963.
10. G. F. Hewitt and P. M. C. Lacey, The Breakdown of the Liquid Film in Annular Two-Phase Flow, British Report AERE-R-4303, August 1963.
11. A. A. Kudirka, Two-Phase Heat Transfer with Gas Injection Through a Porous Boundary Surface, USAEC Report ANL-6862, Argonne National Laboratory, March 1964.
12. Peter Griffith, The Slug-Annular Flow Regime Transition at Elevated Pressure, USAEC Report ANL-6796, Argonne National Laboratory, November 1963.
13. K. D. Cooper, G. F. Hewitt, and B. Pinchin, Photography of Two-Phase Flow, British Report AERE-R-4301, May 1963.
14. R. T. P. Derbyshire, G. F. Hewitt, and B. Nicholls, X-Radiography of Two-Phase Gas-Liquid Flow, British Report AERE-M-1321, January 1964.
15. John H. Vohr, A Photographic Study of Boiling Flow, USAEC Report NYO-9650, Columbia University, Oct. 25, 1963.
16. M. Muscettola, Two-Phase Pressure Drop—Comparison of the "Momentum Exchange Model" and Martinelli and Nelson's Correlation with Experimental Measurements, British Report AEEW-R-284, May 1963.
17. D. E. Fitzsimmons, Two-Phase Pressure Drop in Piping Components, USAEC Report HW-80970 (Rev. 1), Hanford Atomic Products Operation, Mar. 20, 1964.
18. E. S. Starkman, V. E. Schrock, K. F. Neusen, and D. J. Maneely, Expansion of a Very Low Quality Two-Phase Fluid Through a Convergent-Divergent Nozzle, *J. Basic Eng.*, 86: 247-256 (June 1964).
19. Joseph A. Vogrin, Jr., An Experimental Investigation of Two-Phase, Two-Component Flow in a Horizontal, Converging-Diverging Nozzle, USAEC Report ANL-6754, Argonne National Laboratory, July 1963.
20. K. Goldmann, R. Hankel, and R. P. Stein, An Equation for the Critical Mass Velocity of Homogeneous Vapor-Liquid Mixtures at Low Pressures, *J. Appl. Mech.*, 31(3): 380-382 (September 1964).
21. F. R. Zaloudek, Steam-Water Critical Flow from High Pressure Systems. Interim Report, USAEC Report HW-80535, Hanford Atomic Products Operation, January 1964.
22. F. R. Zaloudek, The Critical Flow of Hot Water Through Short Tubes, USAEC Report HW-77594, Hanford Atomic Products Operation, May 1963.
23. S. Levy, Prediction of Two-Phase Critical Flow Rate, *J. Heat Transfer*, 87(1): 53-58 (February 1965).
24. G. F. Stevens, D. F. Elliott, and R. W. Wood, An Experimental Investigation into Forced Convection Burn-Out in Freon, with Reference to Burn-Out in Water. Uniformly Heated Round Tubes with Vertical Up-Flow, British Report AEEW-R-321, January 1964.
25. J. M. Batch and G. M. Hesson, Comparison of Boiling Burnout Data for 19-Rod Bundle Fuel Elements Spaced with "Wires" and "Warts," USAEC Report HW-80391 (Rev. 1), Hanford Atomic Products Operation, Jan. 15, 1964.
26. G. M. Hesson, D. E. Fitzsimmons, and J. M. Batch, Boiling Burnout Experiments with Fog-Cooled Nineteen-Rod Bundle Test Sections, USAEC Report HW-80523 (Rev. 1), Hanford Atomic Products Operation, March 1964.
27. D. H. Lee and R. B. Little, U. K. Atomic Energy Authority. (Unpublished)
28. A. N. Nahavandi and R. F. von Hollen, A Space-Dependent Dynamic Analysis of Boiling Water Reactor Systems, *Nucl. Sci. Eng.*, 20(4): 392-413 (December 1964).
29. Chathilingath K. Sanathanan, Dynamic Analysis of Coolant Circulation in Boiling Water Nuclear Reactors, USAEC Report ANL-6847, Argonne National Laboratory, April 1964.
30. A. H. Stenning, Instabilities in the Flow of a Boiling Liquid, *J. Basic Eng.*, 86: 213-217 (June 1964).
31. D. J. Pulling and J. G. Collier, Instabilities in Two-Phase Flow. Preliminary Experiments, British Report AERE-M-1105, July 1963.
32. R. J. Weatherhead, Heat Transfer, Flow Instability, and Critical Heat Flux for Water in a Small Tube at 200 psia, USAEC Report ANL-6715, Argonne National Laboratory, June 1963.

Digitized by Google

Section

III

Power Reactor Technology

Fuel Elements

Fuel-Performance Evaluations

An engineering proof test of seven UO_2 fuel rods, which were 0.412 in. in diameter and which were clad with type 304 stainless steel, was successfully completed[1] in a borated pressurized-water loop in the Westinghouse Testing Reactor (WTR). The loop conditions[1] are summarized below:

Average coolant inlet temperature, °F	560 to 580
Coolant pressure, psi	2000
Flow rate, gal/min	62
Chlorine, ppm	<0.1
Boron (as H_3BO_3), ppm	1500 ± 50
Hydrogen, cm^3 (STP) per kilogram of H_2O	30
Oxygen, ppm	<0.1

The elements were irradiated to a maximum burnup of 4000 Mwd per metric ton of uranium at a maximum heat flux of 340,000 Btu/(hr)(sq ft) for the purposes of demonstrating the feasibility of boron chemical shim and the performance of fuel rods in the large-plant design of the Large Closed Cycle Water Reactor Research and Development (LRD) Program.* The fuel bundle was fabricated as a simulation of a four-rod segment of the fuel assembly in the large plant. The 2.07% enriched UO_2 fuel pellets, of 0.379-in. diameter, were fabricated to 96% of the theoretical density and were clad with 10% cold-worked type 304 stainless steel that was 0.016 in. thick. The fuel-cladding diametral gap of 0.004 in. was filled with air. An attempt to measure in-pile thermal expansion of the UO_2 fuel column by means of markers inside the cladding, to differentiate between the performance of dished and flat pellets, did not succeed. Postirradiation evaluation indicated satisfactory performance, and the results of fission-gas-release measurements and postirradiation microstructure evaluations were consistent with those generally anticipated for UO_2 fuel rods operating under comparable conditions.

The rods that achieved an average burnup of 6.4×10^{20} fissions/cm^3 in the blanket of the Shippingport reactor at the end of the third seed life have been examined.[2] One of these rods operated at an average cladding-surface temperature of 515°F and a lifetime average surface heat flux of 155,000 Btu/(hr)(sq ft). Although the lifetime average heat flux of 139,000 Btu/(hr)(sq ft) noted for the second rod would appear to provide little additional interest, it was found that a heat flux of 428,000 Btu/(hr)(sq ft) had occurred in this rod for about 200 equivalent full-power hours.

Results of postirradiation examinations indicated no cladding failures, no changes in fuel-rod diameters, and fission-gas release less than 1% of that generated. In addition, there was no evidence of structural change in the UO_2 when it was compared with unirradiated microstructures. The range of hydrogen concentration in the cladding of these fuel rods was 51 to 73 ppm; this represents only a very small increase in the hydrogen content when compared with a nominal content of about 40 ppm in the as-vacuum-annealed unirradiated cladding. All hydrides were in a random orientation. The range of oxide film thickness was 47 to 99 μin.

Results of irradiation tests of multicomponent tubular UO_2 fuel elements have been reported.[3] A tube-and-rod assembly was irradiated in a test loop in the Engineering Test Reactor (ETR) at a target maximum surface heat

*The LRD Program was discussed in Sec. V of *Power Reactor Technology*, 8(2).

Digitized by Google

flux of 320,000 Btu/(hr)(sq ft). During early stages of the irradiation, a burnout occurred which was the result of locally reduced coolant flow caused by a crossover of two thermocouples. A nested tubular element (tube-tube-rod) fabricated by vibratory compaction of UO_2 into 0.060-in.-thick Zircaloy-2 cladding, to densities in the range of 83 to 88% of the theoretical density, was irradiated at 350,000 Btu/(hr)(sq ft). After 10 reactor scrams and inadvertent severe thermal transients, fission-gas leakage was noted. Visual examination of the element failed to indicate defects. During disassembly of the components of the test elements, a fibrous material was found lodged between the rod and the inner tube and adjacent to a cladding failure. It was concluded that failure was induced by flow blockage caused by entrapped foreign matter. Extensive hydriding was noted at the cladding failure and further substantiated the postulated cause of failure. The appearance of the microstructure of both the fuel and the cladding in the region of the failure indicated that failure resulted from interference with surface heat transfer rather than from excessive local heat generation. A third element, containing the tube-tube-rod array similar to that described immediately above, was irradiated to its target burnup of 1360 Mwd per ton of UO_2 at a maximum surface heat flux of 400,000 Btu/(hr)(sq ft). Post-irradiation evaluations indicated that less than 10% of the fission gases and less than 50% of the sorbed gases were released.

Evaluation[4] of the influence of irradiation on the ductility of Zircaloy tubing by means of mechanical burst, weld-shear, and bend tests has indicated no effective loss in ductility after exposure to an integrated fast flux of 10^{20} neutrons/cm^2 at less than 100°C. Tubular fuel elements up to 2 ft long, with outside and inside diameters of about $2\frac{1}{4}$ and $1\frac{1}{2}$ in., were fabricated with Zircaloy-2 or low-nickel Zircaloy-2 cladding. The fuels used were vibratory-compacted and vibratory-compacted-and-swaged UO_2. The following conclusions are quoted from Ref. 4:

> The results of these tests indicate that large diameter tubular elements should not fail by either sheath rupture or weld separation due to irradiation embrittlement. In this event, calculations have shown that the limiting stress should be that stress required to cause sheath collapse. The tests also showed that the irradiation exposures, up to approximately 10^{20} nvt, had no noticeable effect on the sheath ductility, as measured by mechanical burst tests.
>
> These conclusions would be invalid, however, if severe hydriding, such as was previously observed in the . . . test series, were present.

Prototype fuel elements for the first Mobile Low Power Plant No. 1 (ML-1) core loading have been irradiation tested[5] in a gas-cooled General Electric Test Reactor (GETR) loop. The ML-1 core contains 61 fuel elements that are arranged in 61 pressure tubes located in the reactor calandria. Each fuel element contains 19 pins, with 1 unfueled pin in the center surrounded by two concentric rings containing 6 UO_2 and 12 BeO-UO_2 fuel pins. The objectives of these tests, in addition to providing irradiation performance data, included verification of design calculations concerning hot-spot limits and determination of in-pile corrosion resistance of Hastelloy X to the coolant gas. It was also noted[5] that the closed Brayton cycle used in the ML-1 plant was highly sensitive to pressure losses. For example, an increase of 1 psi in the system pressure drop resulted in a loss in net thermodynamic output of 6 kw. Hence another objective of the tests was to evaluate the influence of corrosion-product buildup or changes in fuel-element configuration on pressure drop.

The conditions in the gas loop are summarized below:[5]

Element power, kw	55
Inlet coolant temperatures, °F	800
Outlet coolant temperatures, °F	1200
Mass flow rate, lb/hr	1560
Loop operating pressure, psia	315

Two fuel elements, one of which was instrumented, were irradiated for 6415 hr in a coolant gas that was 99.5 wt.% N_2 and 0.5 wt.% O_2. The irradiation testing of the uninstrumented fuel element was continued in air for an additional 3736 hr.

Results[5] of cladding-temperature measurements indicated good agreement with previous calculations, and it was concluded that the hot-spot limit of 1750°F would not be exceeded at the full element power of 55 kw. Results of pressure-drop measurements during the test indicated no problems with respect to possible reductions in the net thermodynamic output of

Digitized by Google

the cycle. Postirradiation examination of the cladding microstructure indicated the formation of a massive second phase, which was due to an apparent reaction between nitrogen and Hastelloy X in all fuel pins that were instrumented. It was postulated that leaks were present at the brazed joints between the fuel and thermocouples and that the coolant gas permeated the inside of the fuel rods; nitrogen was measured in these rods. It was further postulated that the fuel gettered the O_2, leaving an oxygen-free N_2 atmosphere that reacted with the Hastelloy X to form a second phase which, in some cases, formed a continuous layer on the inside surface of the cladding and extended intergranularly through the thickness. All tubes that contained this second phase were severely embrittled. It was stated[5] that problems of this nature are not anticipated in the operating reactor.

The fuel pins in the 19-rod fuel assembly were spaced by means of spirally wrapped spacer wires on each pin. As a result of a 300°F difference in temperature between the fuel pin and the spacer wire, spiral bending of the fuel pins was observed, after irradiation, on a pitch that was almost the same as that of the wire wrap. It was concluded that the pin bending was a result of unequal expansion of the fuel pins and spacer wires.

An understanding of the performance of sodium-bonded hypostoichiometric UC fuels during transients has been obtained[6] through capsule testing in the Transient Reactor Test Facility (TREAT). Rods resembling the second Hallam fuel loading and containing 0.872-in.-diameter carbide fuel (4.58% carbon) clad with stainless steel of 0.952-in. outside diameter and 0.010-in. wall thickness were subjected to a total of five transients. A summary of results is given in Table III-1.

Evidence of uranium migration was not found even after bursts that provided fuel temperatures in excess of 2700°F. Bursts that increased the temperature to about 4200°F did not provide evidence of melting. However, a decrease in the amount of free uranium was noted, and it is postulated[6] that uranium became redissolved in the UC. Temporary boiling of the sodium, which probably occurred during the final transient, was rapidly quenched by cooler sodium located about the boiling region. The integrity of the fuel rod was such that it was concluded that "power levels of fuel rods of this type can reach values which are 100 times maximum steady-state levels for pulse duration of about 1 second without serious consequence."[6]

Incoloy 800 Cladding

Incoloy 800 is being evaluated[7] as a possible fuel-cladding material for use in nuclear superheat reactors. Procurement, quality control, fabrication, and metallographic evaluation of Incoloy 800 are described in detail in Ref. 7. Prior to 1962 there was little information on the fabrication of this material into thin-walled tubing.

Some of the first tubing received in the welded and drawn condition exhibited unhomogenized weld zones and disturbed surface layers. It was shown that the weld zone was a potentially weaker area than the base metal. It was concluded that the microstructure of all incoming Incoloy 800 tubing should show:[7]

1. No dendritic segregation in the weld zone.
2. Equal grain size in the weld zone and parent metal.
3. Grain size smaller than ASTM Number 5.

Complete recrystallization of the weld zone could be achieved by annealing in the tempera-

Table III-1 RESULTS OF TREAT TESTS* OF SODIUM-BONDED URANIUM CARBIDE FUEL RODS[6]

Transient number	TREAT energy, Mw/sec	Initial reactor period, sec	Peak central fuel temp. (measured), °F	Peak fuel temp.,† °F	Peak bond temp. (measured), °F	Peak pressure increase in fuel section, psi
1	30.7	0.259	1025	1060	845	3
2	63.3	0.157	1380	1520	980	8
3	180.0	0.158	2540	2760	1475	16
4	31.4	0.259	1030	1030	835	2
5	293.0	0.101	3970	4200	1840	20

*Initial temperature about 700°F; initial pressure about 32 psia (fuel section and inner capsule).

†Each value represents the maximum temperature at any position in the fuel since, as a result of flux depression, the peak transient temperature would not be expected to occur in the center of the fuel slug. Values are based on analog calculations and the measured central temperature.

Digitized by Google

ture range of 1900 to 2100°F, but the dendritic structure could only be eliminated after two cold reductions of approximately 20 to 30% followed by annealing at 2000 to 2100°F. The grain size could then be reduced by subsequent cold working and annealing.

The ductility of Incoloy 800 was reduced after 1000 hr at temperatures above 1050°F as a result of an aging phenomenon associated with the precipitation of titanium- and aluminum-containing intermetallics. As a result of this information, the titanium and aluminum content was specified as 0.1% maximum. Cold-worked Incoloy 800 was insensitive to annealing temperatures below 1000°F. Softening was initiated at 1400°F and was reasonably complete in 10 to 15 min at 1800°F. Rapid grain growth occurred at temperatures above 1850°F. Solution annealing occurred at 2050 to 2100°F after 1 to 2 hr. It was necessary to water quench through the 1100 to 1600°F temperature range in order to prevent carbide precipitation.

Typical chemical and physical properties for Incoloy 800 are indicated in Tables III-2 and III-3.

A monograph on the use of Incoloy 800 for fuel-element cladding has been prepared[8] which includes: mechanical properties, physical metallurgy, metallography and electron-microscopy techniques, radiation damage, strain-cycle fatigue, corrosion, and irradiation results of fuel elements (clad with Incoloy 800) exposed in the superheat environment. Performance in superheated-steam environments has been superior to that for the austenitic stainless steels, and Incoloy 800 has been selected as the reference cladding in some nuclear superheat applications.

Table III-2 CHEMICAL COMPOSITION[7] OF INCOLOY 800

Constituent	Weight percent
Nickel	30 to 35
Chromium	19 to 23
Iron	Balance
Carbon	0.10 maximum
Manganese	1.50 maximum
Sulfur	0.03 maximum
Silicon	1.00 maximum
Copper	0.75 maximum

Table III-3 MECHANICAL PROPERTIES OF EXTRUDED INCOLOY TUBES[7]

Condition	Tensile strength, 1000 psi	Yield strength (0.2% offset), 1000 psi	Elongation in 2 in., %
As extruded	75-105	25-50	50-30
Annealed	75-100	25-55	50-30

References

1. D. R. McClintock and C. J. Kubit, Fabrication and Irradiation of Stainless Steel Clad UO_2 Fuel Rods (The LRD In-Pile Chemical Shim Loop Experiment), USAEC Report WCAP-3734, Westinghouse Electric Corp., Atomic Power Division, April 1964.
2. L. R. Lynam, Metallurgical Examination of PWR Core 1 Blanket Fuel Rods at the End of the Third Seed Life, USAEC Report WAPD-TM-433, Bettis Atomic Power Laboratory, August 1964.
3. M. K. Millhollen, G. R. Horn, and W. J. Flaherty, Multicomponent Tubular UO_2 Fuel Element Irradiations, USAEC Report HW-80291, Hanford Atomic Products Operation, November 1963.
4. M. R. Louthan, Jr., Destructive Evaluation of Irradiated Zircaloy Sheathing, USAEC Report DP-888, Savannah River Laboratory, May 1964.
5. J. S. Brunhouse et al., Army Gas-Cooled Reactor Systems Program, USAEC Report IDO-28616, Aerojet-General Nucleonics, June 1964.
6. S. J. Stachura, M. Silberberg, and R. N. Cordy, Uranium Carbide Transient Heating Experiments — Phase 1, USAEC Report NAA-SR-9508, Atomics International, Aug. 1, 1964.
7. R. F. Kirby, D. F. Macmillan, and J. R. Punches, Fabrication of Fuel Cladding from Incoloy Alloy 800, An Evaluation of Methods, USAEC Report GEAP-4557, General Electric Company, Atomic Power Equipment Department, April 1964.
8. C. N. Spalaris (Comp.), Incoloy-800 for Nuclear Fuel Sheaths (A Monograph), USAEC Report GEAP-4633, General Electric Company, Atomic Power Equipment Department, July 1964.

Digitized by Google

Section

IV

Power Reactor Technology

Components

Liquid-Metal-Level Probes

Some significant improvements have been made in resistance type probes for determining the level of high-temperature liquid metals in a vessel. Reference 1 reports on an investigation of the various types of probes that can be used for determining the level of liquid metals and concludes that the resistance type is promising. The J probe that was developed utilized a tube with alumina-insulated stainless-steel-clad nickel wires. A straight tube probe, similar in operation and construction to the J probe, but which indicates one discrete level only and is called an I probe, also was studied.

The J probe indicates the level of the liquid metal over the range from the top of the unsupported leg of the J to the bottom of the J. This is accomplished by passing a direct current through one of the insulated internal wires in the tube to the tip of the J as shown in Fig. IV-1. The negative wire from the power supply is connected to the metal vessel. A potential is then impressed between the tip of the J and the vessel and the resistance between these two points is changed as the liquid-metal level around the unsupported leg is changed. The maximum resistance exists when the level is lowest, and the current must pass through the sheath of the J tube. The potential between the tip of the J and the tank is measured by a second insulated internal wire to the tip of the J and a wire to the tank. Unfortunately the resistances of the stainless-steel sheath and the probe wires vary with temperature. In the design shown in Fig. IV-1, compensation is accomplished by maintaining a constant voltage across the entire probe and internal current lead. Figure IV-2 is a refinement of this design wherein the temperature-compensation circuit is connected inside the J tube and the resistance of the current lead is increased. The increased length of the lead is in the same temperature gradient as the probe, and compensation is obtained by maintaining a constant voltage between the tip of the probe and the internal splice.

The I probe, which indicates whether the liquid-metal level is above or below a certain point, is shown in Fig. IV-3. A potential is impressed between the end of the probe and the vessel, and an amplifier connected in parallel to this circuit actuates a relay to signify that the level of the liquid metal is below the probe end. When the liquid metal comes in contact with the end of the probe, a new circuit with less resistance is established and the decrease in voltage causes the amplifier to drop the relay.

In addition to the problem of attaining correct temperature compensation, there is a problem of obtaining thermoelectric voltage if

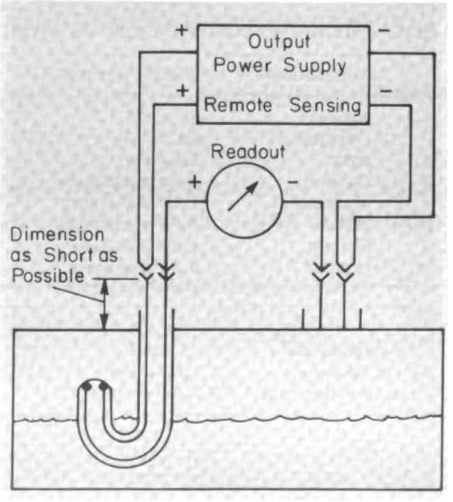

Fig. IV-1 Two-wire J probe with externally connected temperature-compensation circuit.[1]

Digitized by Google

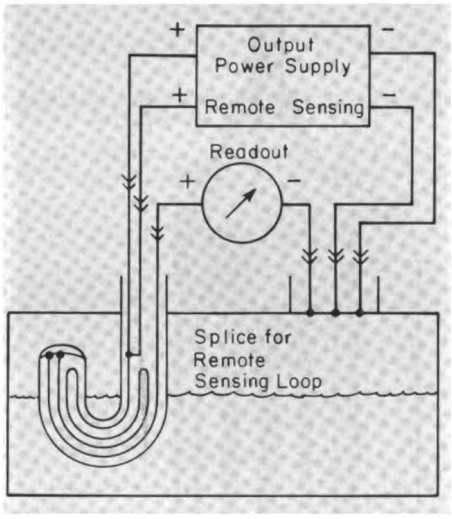

Fig. IV-2 J-probe design with internally connected temperature-compensation circuit and increased-resistance remote sensing loop.[1]

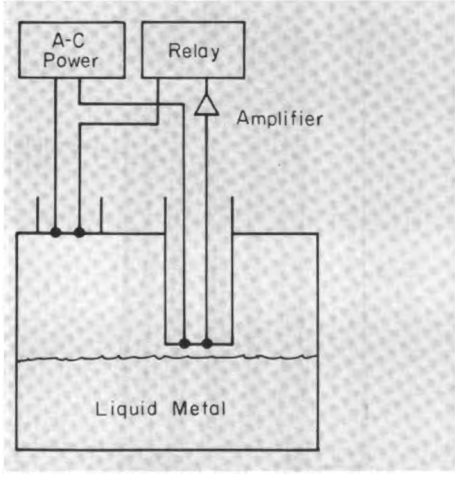

Fig. IV-3 I probe for one-point-level determination.[1]

materials are not carefully selected. Further, complete wetting of the surface of the probe requires careful attention to the preparation of the surface before immersion. Reference 1 indicates that if the probe can be completely wetted, an accuracy within 1% can be achieved.

Pressure-Tube Fretting Corrosion

A continuing surveillance program is being conducted on the Plutonium Recycle Test Reactor (PRTR) to monitor fretting corrosion of the pressure tubes. A summary of results of (1) programs designed to detect and determine the extent of in-reactor fretting attack and (2) associated tests outside the reactor is presented in Ref. 2. The PRTR[3] is a heavy-water-moderated pressurized-heavy-water-cooled reactor that operates at 70 Mw(t). The moderator is contained at low pressure and temperature in an aluminum calandria tank, with 85 calandria tubes arranged vertically. Zircaloy-2 pressure tubes, containing fuel assemblies, are installed in the calandria tubes. The coolant enters the bottom of the pressure tubes at a temperature of 248°C and a pressure of 1090 psig and discharges at the top at 277°C and 1080 psig. The maximum flow rate per pressure tube is 123 gal/min. The Zircaloy-2 pressure tubes are 3.250 in. in inside diameter, with a minimum wall thickness of 0.146 in. The tubes are flanged at the upper end to permit attachment of outlet-nozzle jumper assemblies and are tapered at the bottom for attachment of inlet jumpers. Before installation the pressure tubes were autoclaved to provide a zirconium dioxide surface film.

The fuel assemblies are 19-rod clusters, as shown in Fig. IV-4, and both metallic (aluminum-plutonium) and ceramic (UO_2 and PuO_2-UO_2) Zircaloy-2-clad rods are used. Spacing between rods is maintained with top and bottom brackets and spirally wound spacer wires around the outside of selected fuel rods. The aluminum-plutonium and the PuO_2-UO_2 fuel assemblies are bound with circumferential bands, whereas a wire wrap is used on the UO_2 fuel assembly. A pressure tube containing a fuel assembly is shown in Fig. IV-5. The fuel assembly is attached to an upper hanger that is supported near the outlet nozzle and is free to expand downward. Clearance between the fuel assembly and the pressure tube is a nominal 0.015 in., but it can be as much as 0.050 in. Portions of the fuel assembly that could come in contact with the pressure tube include the following: the three equidistant centering feet on both the top and bottom end brackets; the wire wrap (bundle or individual rods); circumferential bundle bands if the centering feet are sufficiently worn; and the individual fuel rods if the wire wraps and centering feet are sufficiently worn.

A rather comprehensive program[4–6] has been conducted, on a continuing basis, to determine

Digitized by Google

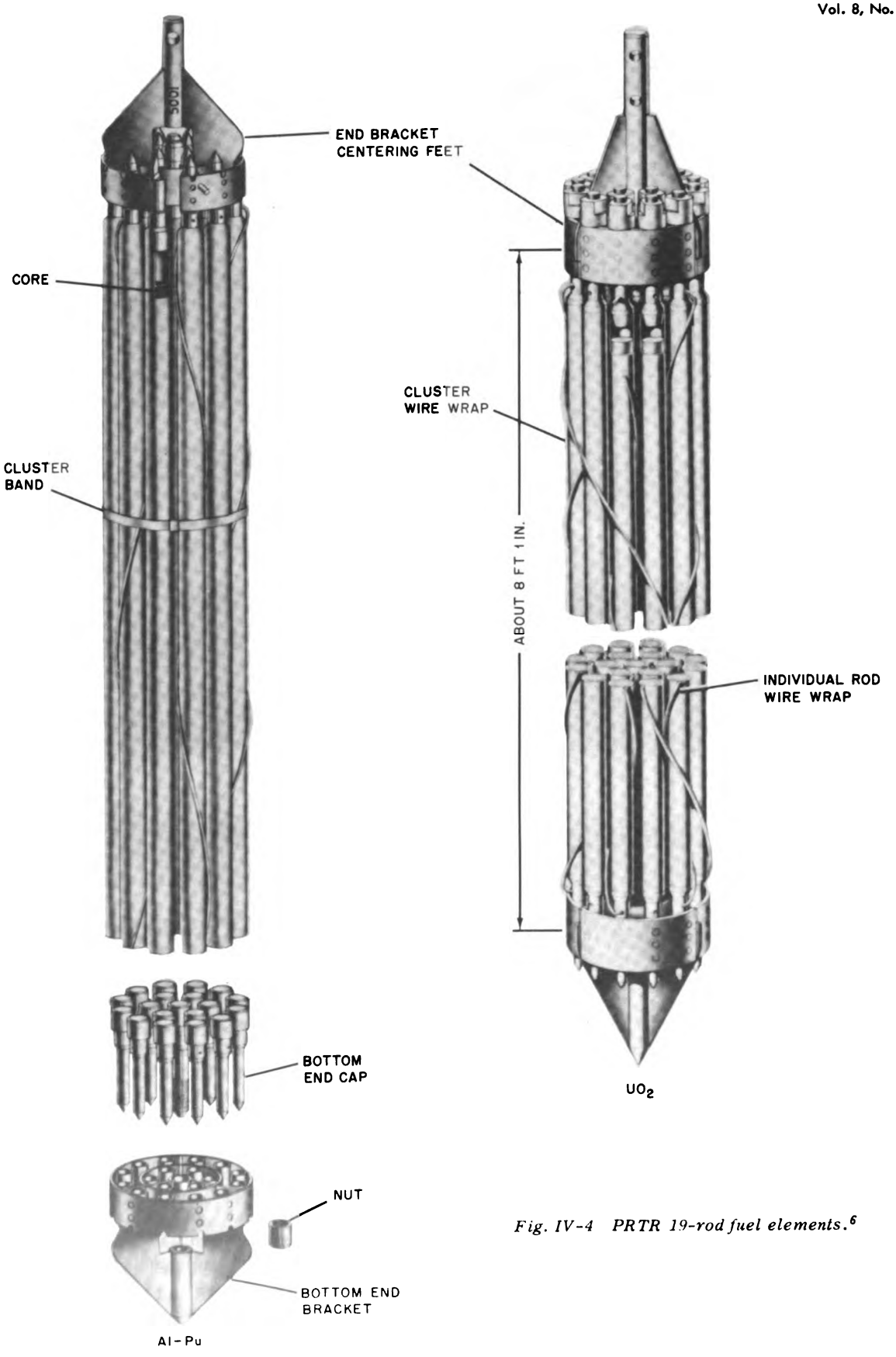

Fig. IV-4 PRTR 19-rod fuel elements.[6]

Digitized by Google

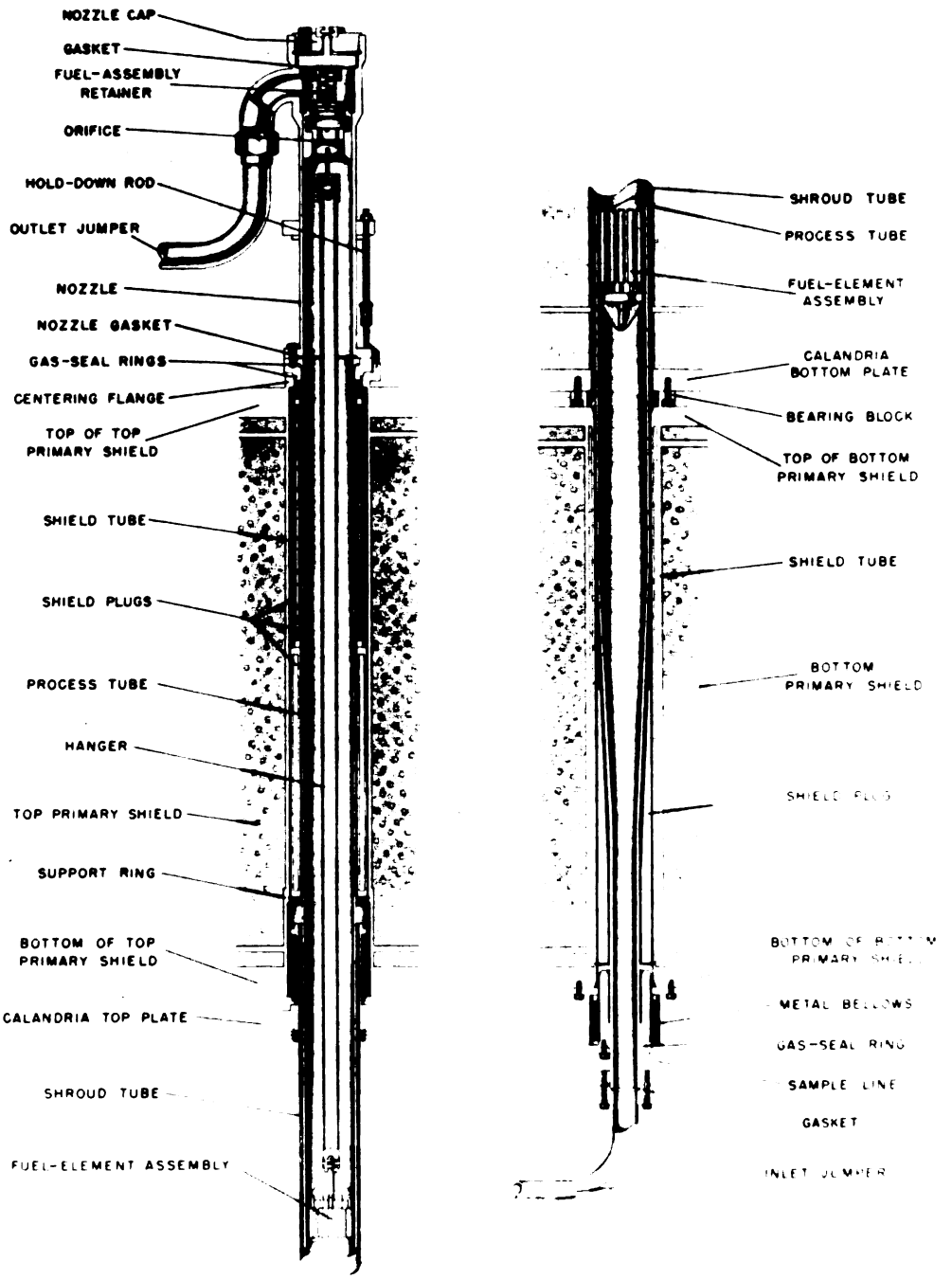

Fig. IV-5 Pressure-tube assembly.[2]

Digitized by Google

the magnitude of fretting corrosion and to establish methods of minimizing pressure-tube wear. The program consisted of out-of-reactor tests and in-reactor examination. The initial phase of the out-of-reactor program consisted of flow tests in a high-temperature high-pressure facility and autoclave tests. The initial test specimen was a Zircaloy-2 tube with a spirally wound Zircaloy-2 wire. The wire was fastened at one end and was free at the other end. After two weeks of exposure in recirculating water at 300°C and 25 ft/sec, grooves approximately 0.001 to 0.005 in. deep were noted on the tube, and the wire was worn approximately 0.020 in. where the moving wire could contact the stainless-steel housing. This and other similar tests showed that the relative movement induced by flow could result in localized corrosion areas at the point of contact between two surfaces. Sliding- and impact-wear tests were conducted in autoclaves in deionized water at 1500 psi. The sliding-wear test, consisting of a rotating disk in contact with a stationary rod, showed that disk penetration and rod wear increased with increasing temperature in the range from 100 to 400°C. The test also showed that the wear increased with contact pressure from 5 to 15 psi and also with rotational speed of the disk. The impact-wear test consisted of a solenoid-activated cylindrical plunger tipped with Zircaloy-2 impacting against a Zircaloy-2 flat plate. Results indicated over twice the plunger wear with an increase in the water temperature from 200 to 400°C.

An out-of-reactor test facility, shown in Fig. IV-6, was utilized to test an individual reactor pressure-tube fuel-element assembly at operating flow and temperature. Fretting marks found after facility operation prompted additional tests in vertical test sections. Initial tests were conducted with a Zircaloy-2 collar mounted at the bottom of a steel rod suspended in a tube lined with Zircaloy-2. The fretting attack was found to be independent of water velocity in the range from 15 to 30 ft/sec but quite sensitive to clearance between the three centering feet on

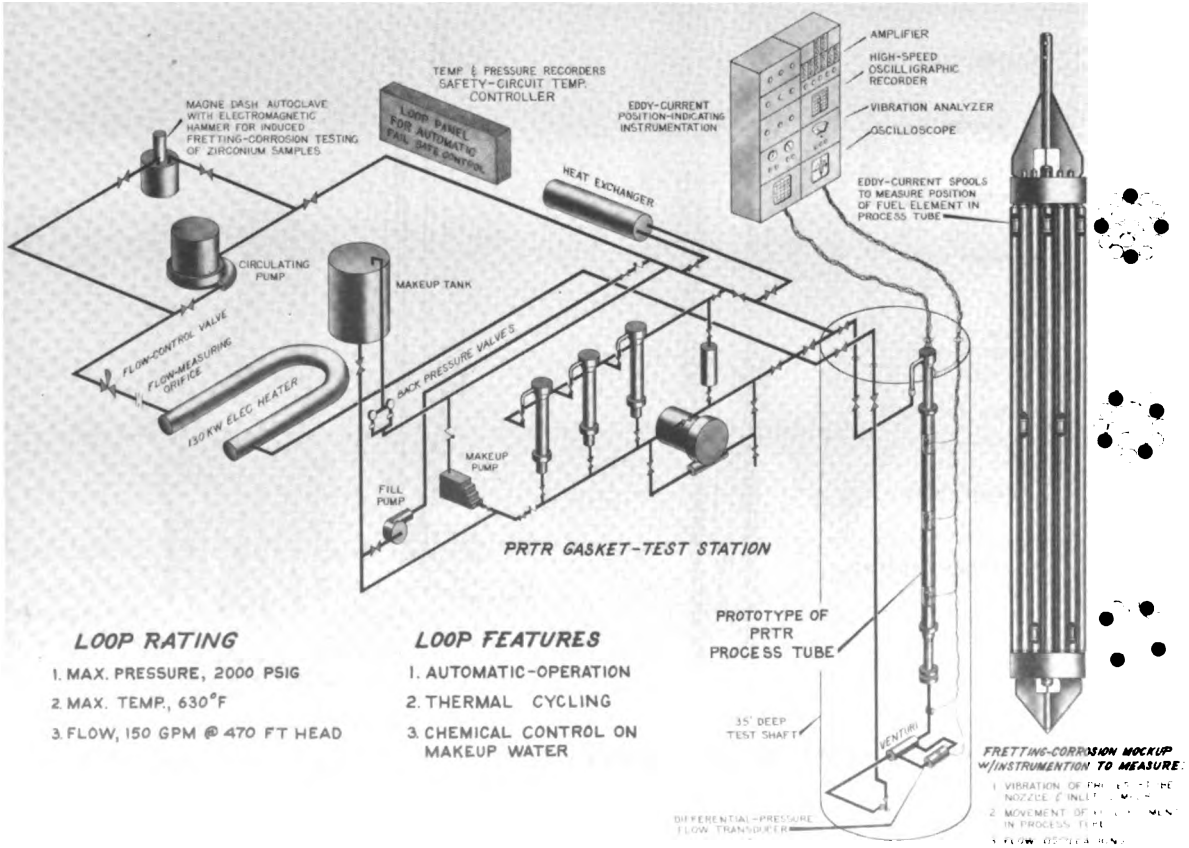

Fig. IV-6 Out-of-reactor test facility.[2]

Digitized by Google

the collar and the tube. The attack also increased with temperature and with a superimposed external vibrating force. Later tests were conducted in a vertical test assembly consisting of the upper 10 ft of a PRTR pressure tube containing a fuel assembly. Water at 300°C was circulated upward through the fuel assembly at at a flow rate of 123 gal/min. After two weeks fretting marks, approximately 0.005 in. deep, were noted at the contact points between the pressure tube and the centering feet of the fuel-assembly end brackets. Continued testing did not always increase the depth of penetration, indicating that the process may be intermittent. Increasing the contact surface tended to decrease the penetration.

The out-of-reactor tests generally have shown that fretting attack is increased with increased temperature, vibration, and clearance. The process seems to be one of removing the protective oxide film mechanically and thus permitting progressive oxidation of the Zircaloy.

The in-reactor examination of the condition of the pressure tubes consisted of visual inspection and measurement of the depth of observed marks.[4–6] A television-camera–borescope arrangement was used to examine the inner surface of the pressure tube and to read a dial indicator used to measure the depth of marks. The number and location of fretting marks are given in Table IV-1, and an example of one of the more severe fretting marks is shown in Fig. IV-7. This mark was detected during an examination of all the pressure tubes in May and June of 1962. The diagonal fretting mark is the result of contact with a wire wrap around a fuel assembly and is approximately 0.025 in. deep. The wire wrap was worn sufficiently to allow two of the fuel rods to contact the tube wall, and the vertical fretting mark resulted.[5]

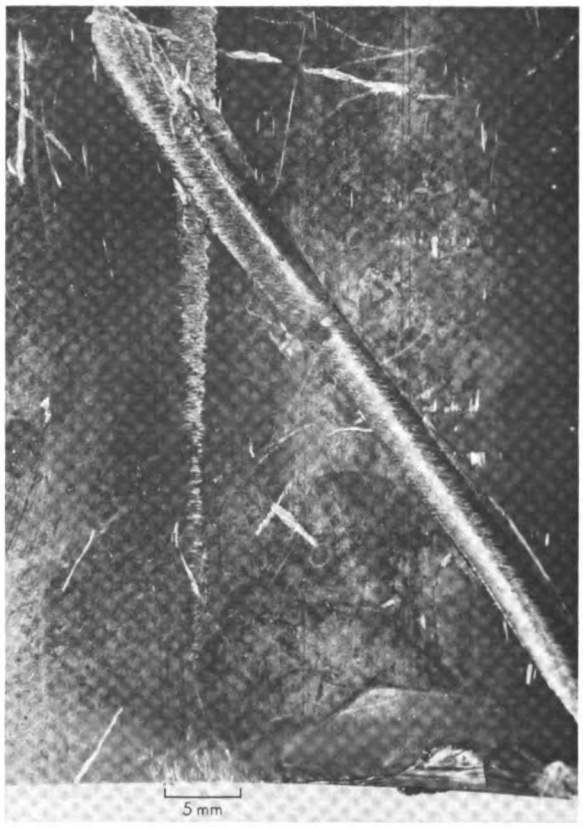

Fig. IV-7 Pressure-tube fretting mark.[2]

The severity of fretting corrosion has decreased as some of the causes have been discovered and corrected. For example, the width of the centering feet on the fuel assemblies has been increased on new fuel, and this has decreased the severity of the fretting.[6] Some of the fretting was attributed to a failed flow-straightening baffle, which has been replaced. Tests are continuing to define more precisely the reasons for fretting attack and to find methods for minimizing or eliminating this

Table IV-1 NUMBER AND LOCATION OF PRESSURE-TUBE FRETTING MARKS[2]

Fuel-element component making mark	9/60 to 6/62*		7/62 to 11/63*		Total*	
	No.	%	No.	%	No.	%
Centering feet, upper end bracket	327	20.0	418	24.2	745	22.1
Centering feet, lower end bracket	484	29.6	524	30.3	1008	30.0
Wire wraps	674	41.2	788	45.5	1462	43.5
Unclassified	150	9.2	1		151	4.4
	1635	100.0	1731	100.0	3366	100.0

*Includes marks found on tubes that have been removed from the reactor.

Digitized by Google

problem. Techniques are under development for continuous monitoring of PRTR pressure tubes to detect excessive fretting attack — for example, monitoring of the zirconium content of the water shows some promise.[7] Of the analytical methods available (emission spectrographic, radiochemical, and spectrophotometric), emission spectrography is considered most reliable for measuring zirconium contents as low as 0.10 ppb. Work is continuing on the correlation of the results of this technique with fretting attack. Recently a vibration-monitoring program has also been started. Velocity type transducers have been installed on the inlet jumpers of selected pressure tubes; sufficient data have not been obtained as yet to enable a correlation between vibration measurements and zirconium concentration in the coolant water.

References

1. S. J. Fanciullo, Development of Liquid Metal Level Probes, USAEC Report PWAC-423, Connecticut Aircraft Nuclear Engineering Laboratory, April 1964
2. W. K. Winegardner, Fretting Corrosion in the Plutonium Recycle Test Reactor, USAEC Report HW-80021, Hanford Atomic Products Operation, March 1964.
3. N. G. Wittenbrock, P. C. Walkup, and J. K. Anderson, Plutonium Recycle Test Reactor Final Safeguards Analysis, USAEC Report HW-61236, Hanford Atomic Products Operation, Oct. 1, 1959.
4. D. R. Doman and P. J. Pankaskie, In-Reactor Monitoring of Zircaloy-2 PRTR Pressure Tubes, Part I, September 1960–May 1962, USAEC Report HW-73701(Rev.), Hanford Atomic Products Operation, May 1962.
5. D. R. Doman and P. J. Pankaskie, In-Reactor Monitoring of Zircaloy-2 PRTR Pressure Tubes, Part II, May and June 1962, USAEC Report HW-74731, Hanford Atomic Products Operation, August 1962.
6. P. J. Pankaskie, In-Reactor Monitoring of Zircaloy-2 PRTR Pressure Tubes, Part III, July 1963–November 1963, USAEC Report HW-80158, Hanford Atomic Products Operation, December 1963.
7. T. F. Demmitt, Zirconium Concentration Measurements in the PRTR Primary Coolant: Interim Report, December 8, 1962 to June 30, 1963, USAEC Report HW-78080, Hanford Atomic Products Operation, July 1963.

Digitized by Google

Section

V

Power Reactor Technology

Specific Reactor Types

Sodium-Graphite Reactors: Steam Cycles

A recent steam-cycle optimization study[1] has been made for sodium-graphite nuclear power plants to determine optimum steam conditions and sodium-system parameters for plants in the 350- to 400-Mw(e) size range. The general results are summarized as follows:

1. For plant ratings up to approximately 350 Mw(e), a 2400-psig steam pressure results in the most economical operating condition.
2. For plant ratings above 350 Mw(e), a 3500-psig steam pressure results in the most economical operating condition.
3. The highest justifiable initial and reheat steam temperatures are 1000°F each for reheat cycles at a reactor outlet temperature of 1150°F.
4. For most economical operation the sodium temperature rise across the reactor should be in the range of 350 to 375°F.
5. For the 2400-psig steam cycle, the most economical log mean temperature differential of the intermediate heat exchanger is 65 to 80°F. For the 3500-psig steam cycle, this range is 85 to 95°F.

The optimum (most economical) cycles for a fuel-cycle cost of $0.20 per 10^6 Btu and a reactor sodium outlet temperature of 1150°F, in the 400-Mw(e) size, are summarized in Table V-1.

In this study heavy emphasis was given the steam portion of the plant, inasmuch as the costs of the reactor and related sodium systems are relatively insensitive to the steam pressure used, once the outlet sodium temperature for the reactor has been fixed. The major components of the power-generating system considered are shown schematically in Fig. V-1, along with typical sodium and steam temperatures and pressures.

The steam-cycle study was divided into three phases. During phase I studies were made for steam pressures of 1450, 1800, 2400, and 3500 psig for a 350-Mw(e) plant. The basis of comparison was the total evaluated cost, made up of major-equipment costs and capitalized energy costs.

Bases are given in Ref. 1 for costs of such items as heat-exchanger surfaces, feedwater

Table V-1 CHARACTERISTICS OF OPTIMUM STEAM CYCLES FOR 400-Mw(e) PLANTS[1]

	7% capital-charge rate	14% capital-charge rate
Steam throttle pressure, psig	3500	3500
Initial and reheat steam temperatures, °F	1000 each	950 each
Type of steam cycle	Double reheat	Double reheat
Type of steam turbine (last-stage blading size)	Cross compound double flow (30 in.)	Tandem compound four flow (30 in.)
Net station heat rate, Btu/net kw-hr	7665	7870
Fuel-cycle cost at $0.20 per 10^6 Btu, mills/net kw-hr	1.53	1.57
Reactor sodium ΔT, °F	350	350
Intermediate heat exchanger log mean temperature difference, °F	95	95

Digitized by Google

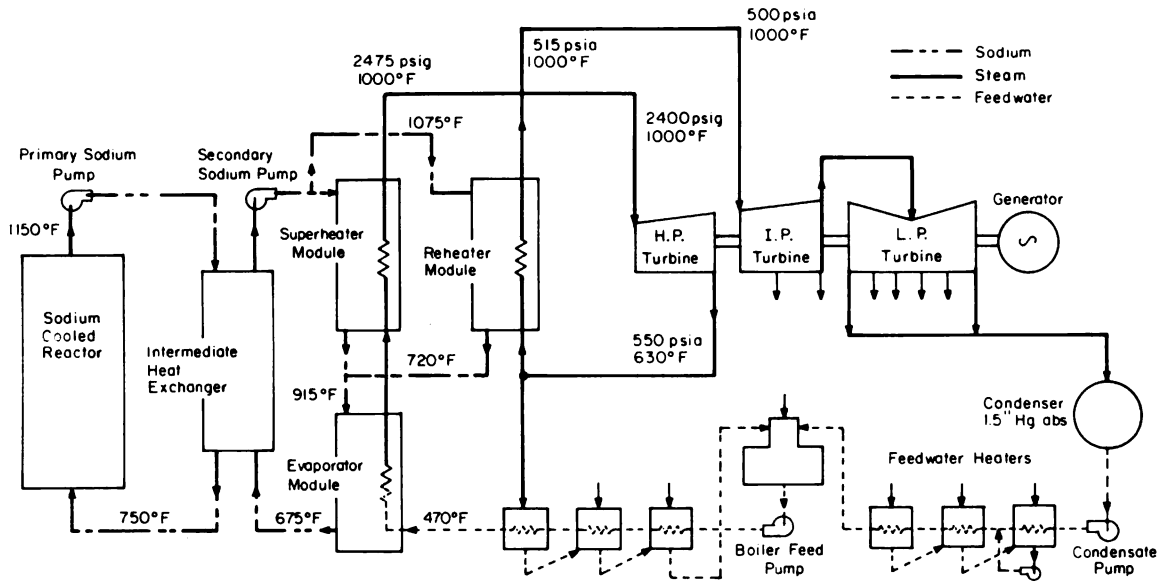

Fig. V-1 Typical schematic of sodium-graphite nuclear power-generating system.

heater-supply and treatment systems, and the steam-condensate systems. Variations in reactor thermal rating due to changes in cycle efficiency were accounted for by use of a reactor cost differential of $50,000 per 1% change in reactor rating. For the phase I study, all fuel-cycle costs were based on $0.20 per 10^6 Btu. Other assumptions used for evaluating fuel-cycle costs are also presented.[1]

Phase I results are summarized as follows:

1. The steam-pressure condition with the lowest cost at a 14% capital-charge rate is 2400 psig; the next best pressure is 3500 psig.

2. At a 7% capital-charge rate, the steam-pressure condition with the lowest cost is 3500 psig, followed by the 2400-psig pressure condition.

3. At a 14% capital-charge rate, the best steam-temperature condition is 950°F; at a 7% capital-charge rate, either 950 or 1000°F is recommended.

During phase II a system pressure of 2400 psig was used for a more detailed study of various parameters of a 350-Mw(e) plant.

The following summarizes phase II results:

1. A 350°F sodium-temperature differential across the reactor is optimum.

2. A 65 to 80°F log mean temperature difference for the intermediate heat exchanger is optimum.

3. Although the cross-compound turbine generators with 1800-rpm low-pressure sections are more efficient and provide improved turbine-cycle heat rates over the tandem-compound machines at 3600 rpm, the significantly higher cost of the cross-compound unit more than offsets the savings in operating costs for $0.20 per 10^6 Btu fuel costs.

4. The optimum feedwater temperature is 475°F.

5. As fuel costs increase from $0.20 to $0.25 per 10^6 Btu, the trend is toward the more efficient cycle (steam pressure of 2400 psig and initial and reheat steam temperatures of 1000°F).

6. As the plant-capacity factor decreases from 80 to 60%, the trend is to the less efficient cycle (steam pressure of 2400 psig and initial and reheat steam temperatures of 950°F.

7. It is difficult to justify the added capital cost of high-pressure feedwater heaters for feedwater temperatures above 475°F with $0.20 per 10^6 Btu fuel costs.

In phase III the basic effort was to study in detail the merits of 2400- vs. 3500-psig steam for a 400-Mw(e) plant with 14 and 7% capital-charge rates. For these studies the reactor-sodium outlet temperature was held at 1150°F. Areas investigated were generally similar to those in phase II.

Digitized by Google

Results for the phase III study are summarized as follows:

1. The 3500-psig double-reheat plant with 1000°F steam temperatures and a 7% capital-charge rate provides savings of $1,485,000 over the 2400-psig case.

2. The 3500-psig plant with 950°F steam temperatures and a 14% capital-charge rate appears to provide savings of $292,000 and $444,000 for single and double reheat, respectively, over the single-reheat case with 2400-psig steam. However, additional analyses would be required to verify this trend.

3. A 1050°F steam temperature is not justified for any steam-pressure condition studied.

4. The tandem-compound four-flow turbine with a 30-in. last-stage blade is the best selection at 14% capital-charge rates: the cross-compound double-flow unit with a 43-in. last-stage blade is the best with the 7% capital-charge rate.

Naturally any generalized study of this kind can be only as valid as the assumptions on which it is based, and the author of Ref. 1 has pointed out the need for basing the steam conditions in an actual plant design upon the specific site and ground rules as related to a specific utility company. It is also well to recognize that optimum conditions are strongly affected by the particular designs of some of the components in the sodium system.

The economic results of the study would not apply to other sodium-cooled reactors because the effects of changes in reactor capital costs and fuel costs were not investigated over a wide range. For example, the much lower fuel cost of a sodium-cooled fast reactor plant would tend to justify lower steam-cycle temperature conditions and therefore lower optimum cycle efficiencies than those found for the sodium-graphite case.

Reference

1. G. A. Schneider, Steam Cycle Optimization Study for Large Sodium Graphite Nuclear Power Generating Stations, USAEC Report NAA-SR-9488, Atomics International, Aug. 31, 1964.

Digitized by Google

Section

VI

Power Reactor Technology

Unconventional Approaches

Fast Supercritical Water Reactor

As a part of the continuing study effort for the U. S. Atomic Energy Commission's Division of Reactor Development, Hanford Atomic Products Operation issued a report by Aase et al.[1] describing the design and economic evaluation of a 300-Mw(e) fast supercritical-pressure water reactor. The fast supercritical-pressure power-reactor (FSPPR) design employed a fast breeder-reactor concept, a plutonium-uranium fuel cycle, and supercritical water as the coolant. Hanford has been involved in the design of supercritical-pressure power reactors for some time, and an earlier design,[2] the supercritical-pressure power reactor (SPPR), was reviewed in *Power Reactor Technology*, 6(3): 73-78 June (1963). The SPPR is quite different in design than the FSPPR in that it is a thermal reactor employing UO_2 as the fuel material. The earlier work was utilized in the preparation of Ref. 1, however, to establish the design of the auxiliary systems for the FSPPR.

The FSPPR was designed for a power of 677 Mw(t) with a net efficiency of 44.3%. The reactor core is fueled with plutonium and uranium oxides with a moderator-segmented-core design and axial and radial blankets. The moderator-segmented-core design was expected to overcome some of the safety considerations that must be dealt with in a fast reactor design and will be discussed shortly. A direct-cycle system provides supercritical-pressure water coolant with turbine-inlet conditions of 3500 psig and 1050°F. Figure VI-1 shows a simplified feedwater-and-steam-system schematic for the FSPPR. It can be seen that two stages of reheat are employed using regenerative heat exchangers and a cross-compound turbine. The reactor incorporates three coolant passes with temperature control at the inlet to the second and third passes. This coolant-temperature-control system was intended primarily to compensate for the changes in power distribution expected during the life of the core. Shown in Fig. VI-2 are one reactor core, a portion of the piping, and the containment vault. The containment vault is designed to contain two reactors in a tandem arrangement. This tandem arrangement allows refueling of one core while the other core is in operation, although simultaneous operation of the two cores was not intended. It was felt that this type of design should reduce reactor downtime quite significantly and thereby increase the productive period of the plant. A single FSPPR core was designed for approximately 4.9 full-power years, equivalent to approximately 6.1 calendar years. The volume between the two main reactor vaults in Fig. VI-2 is a basin to be used in fueling operations. One of the FSPPR cores can be seen in the upper portion of the figure; below the reactor core is the fuel-transfer pot to be used in refueling. A series of headers is placed at the top of the reactor-core assembly to deliver and remove the supercritical coolant from the various passes of the reactor core. Numerous jumper assemblies are utilized, a few of which are shown in Fig. VI-2, to connect the toroidal headers to the core fuel assemblies.

The internal composition of the core can be seen in Figs. VI-3 and VI-4. The cross section of the core in Fig. VI-3 shows the two core regions that are refueled with uranium oxide and plutonium oxide and separated by an absorber region that contains moderator tanks. The control rods for the core are located in the moderator tanks, and a radial blanket is

Digitized by Google

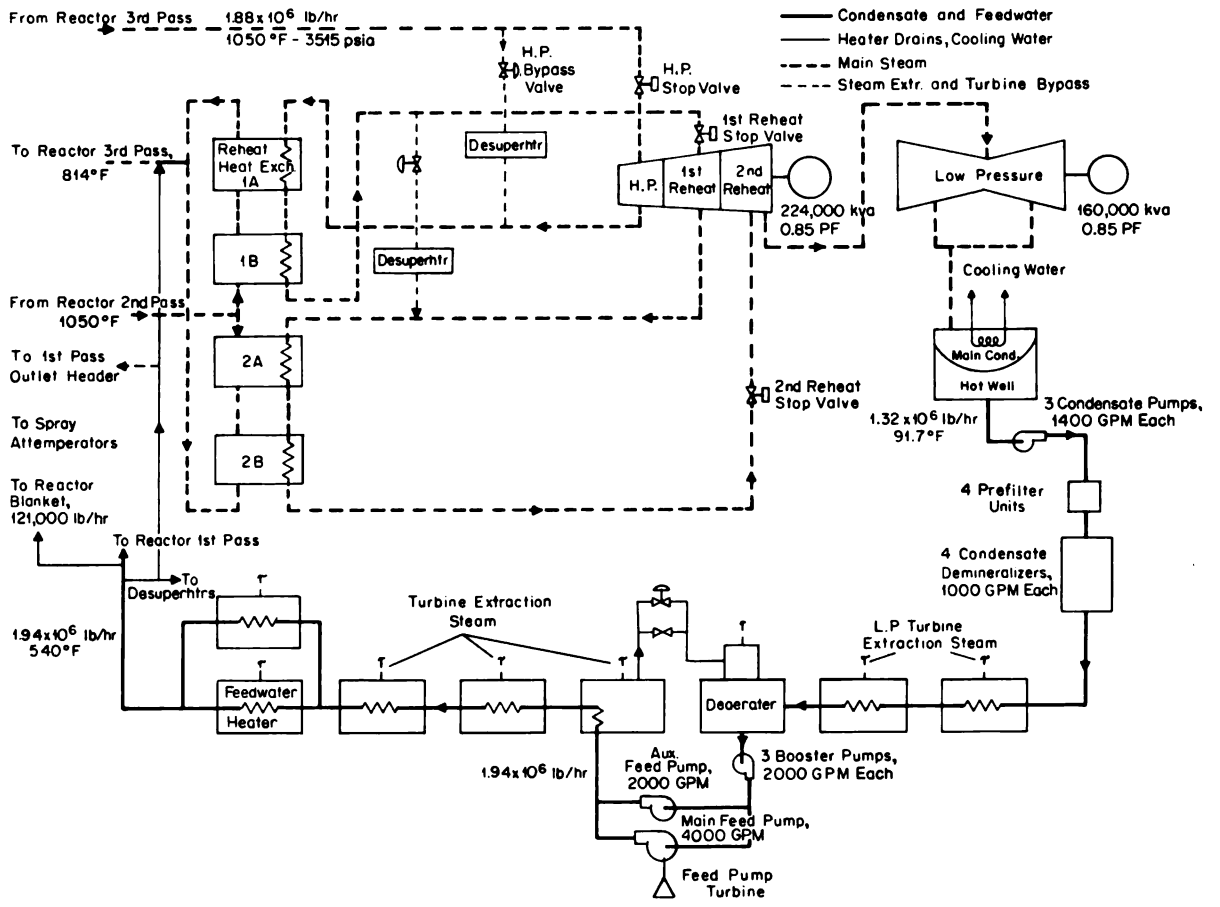

Fig. VI-1 Simplified feedwater and steam system of the FSPPR.

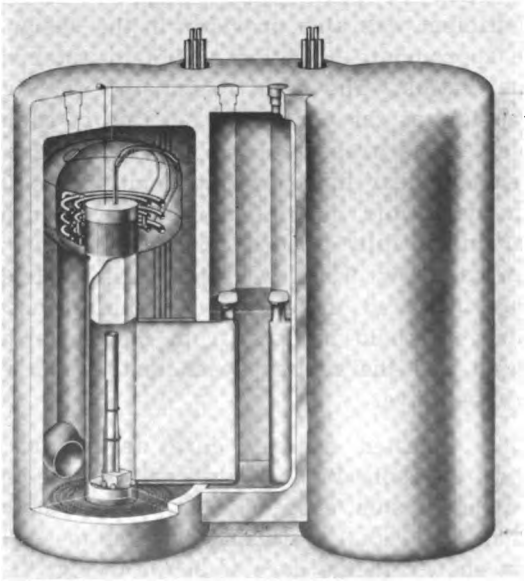

Fig. VI-2 The FSPPR.[1]

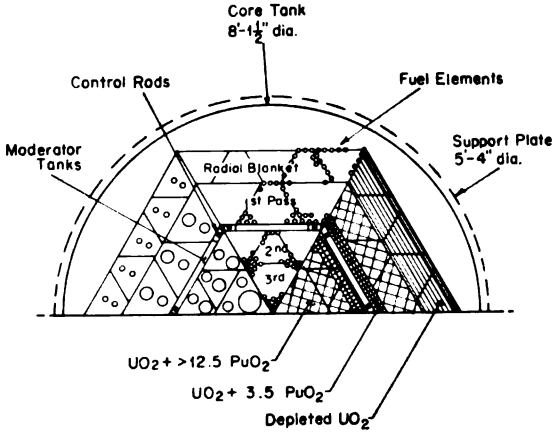

Fig. VI-3 Core layout of the FSPPR.[1]

Digitized by Google

placed around the core assembly. Three coolant passes are provided for the central section of the core, and coolant also is delivered to the radial blanket. The upper and lower axial blankets can be seen in Fig. VI-4. These fuel assemblies are provided either in equilateral triangular shapes or in trapezoidal shapes. Coolant flows to the fuel elements at the outer rows of tubes of the elements, flows down the elements to a mixing chamber at the bottom, and returns up the central portion of the element. The top and bottom of the elements are closed with porous plugs to allow the escape of fission gases.* The fastening plate on the inlet and outlet fuel-element pipes is connected to the top support plate of the reactor, with the fuel elements being suspended from the reactor top support plate. The characteristics of the FSPPR are given in Table VI-1.

The nuclear design of the FSPPR utilized the previously mentioned moderator-segmented-core concept to overcome some of the difficulties associated with the use of a moderating material, water, as the coolant. The amount of water in the reactor core was kept as low as possible to maintain a sufficiently hard neutron spectrum to permit economic operation. The use of a moderator-segmented core reduced the interaction between the coolant and the neutrons by enhancing the internal leakage effect of the core. The coolant flow was arranged such that the lower density flow occurred at the center of the core. The core composition that was used for the moderator-segmented design is shown in Fig. VI-3 and consisted of a layer of absorbing material placed on either side of the moderator tanks to form an annular volume between "fast" core regions. This core segmentation allowed productive core leakage upon coolant voiding, with the net effect of coolant voiding being a reduction of reactivity. A negative flooding coefficient was also provided in the design by the appropriate selection of fuel-to-water volume ratios. The total calculated reactivity behavior of the core as a function of coolant inventory is presented in Fig. VI-5. It can be seen that near the operating point the coolant reactivity void coefficient is nearly zero and that in the fully flooded condition the core is approximately 9% $\Delta k/k$ subcritical. Calculations indicated that a considerable amount of hydrogen could be lost from the moderator region and the coolant coefficients would remain negative.

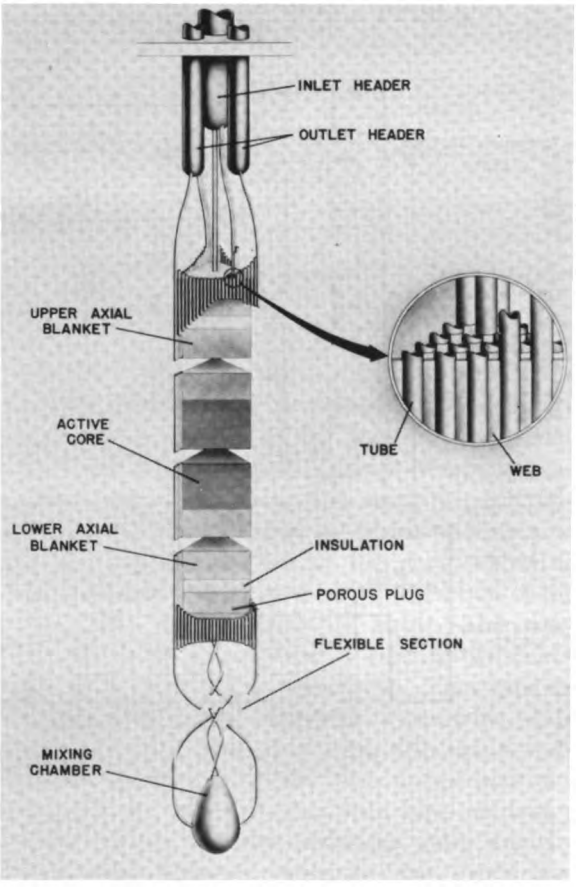

Fig. VI-4 Fuel-element assembly of the FSPPR.[1]

The detailed nuclear core description is shown in Table VI-2. At the center of the core a mean fission energy of 82 kev was calculated. The radial distribution of the mean fission energy in the core is shown in Fig. VI-6, and the calculated initial and end-of-life radial power distributions are shown in Fig. VI-7.

*It is expected that, in order for fast breeder reactors to compete with existing reactors, high fuel burnups of the order of 80,000 to 100,000 Mwd/ton may be required. The resulting fission-gas release, coupled with the potentially weakened cladding condition after long irradiation, magnifies the internal-pressure problem in fuel-element design. Fission-gas volumes provided to accommodate this release become large and unwieldy for the compact cores envisaged. Faced with these problems some designers are talking of concepts in which "controlled venting" of fuel-element fission gases would be employed. Gases would be collected and separated from the cover gas and processed.

Digitized by Google

Table VI-1 CHARACTERISTICS OF THE CONCEPTUAL FAST SUPERCRITICAL-PRESSURE POWER-REACTOR (FSPPR) PLANT

General characteristics	
Thermal power, Mw	677
Net electric power, Mw	300
Net efficiency, %	44.3
Gross efficiency, %	47.1
Auxiliary power, Mw	2.83
Equivalent main feed-pump power, Mw	9.93

	General	First pass	Second pass	Third pass	Radial blanket
Reactor dimensions					
Outside dimension of each region, in.		34.8	22.8	13.3	43.5
Core height, in.	60				
Core + axial-blanket height, in.	$75\frac{3}{4}$				
Core volume, liters	3095				
Flux-trap thickness, in.	~8.75				
Reactor fuel inventory					
Depleted uranium, kg	30,895				15,407
Total plutonium, kg	1559				
Fissile plutonium, kg	1059				
Reactor power density, kw/liter of core + blanket	218.7				
Reactor specific power, kw/kg of uranium + plutonium	50				
Fuel-element assembly					
Fuel material	PuO_2 + depleted UO_2				
Initial enrichment, % plutonium		14.5	12.5	12.5	
Fuel density, g/cm³	9.3				
Flux-trap material	PuO_2 + depleted UO_2				
Enrichment, % plutonium	3.8				
Fuel-element type	Equilateral triangle or trapezoid				
No. of fuel elements	72	18	18	6	30
No. of cooling tubes per fuel element		1216	686	730	43
Fuel-element active length, ft	5				
Fuel-element overall length, ft	15.25				
Cooling-tube material	René 41				
Cooling-tube inside diameter, in.		0.146	0.160	0.204	0.286
Cooling-tube wall thickness, in.		0.013	0.022	0.027	0.030
Cooling-tube spacing, in. (on triangular pitch)		0.291	0.269	0.358	1.20
Weight of fuel per fuel element, lb of oxide		1544	523	906	1132
Fuel-cladding material	René 41				
Cladding thickness, in.		0.090	0.083	0.080	0.090
Heat removal					
Maximum heat flux, Btu/(hr)(sq ft) ($\times 10^{-5}$)	8.93	8.73	7.00	6.43	
Average heat flux, Btu/(hr)(sq ft) ($\times 10^{-5}$)	2.91	2.98	2.27	4.14	
Average core power density, kw/liter	230				
Maximum fuel temperature, °F	2260	2260	1740	1930	
Maximum pressure-tube temperature, °F	1385	1300	1385	1320	

Digitized by Google

Table VI-1 (Continued)

	General	First pass	Second pass	Third pass	Radial blanket
Coolant conditions					
Pass inlet temperature, °F		514	804	820	
Pass outlet temperature, °F		804	1050	1050	
Pass inlet pressure, psig		4360	4330	4100	
Turbine throttle pressure, psig	3515				
Coolant flow rate, lb/hr × 10^{-6}	1.88				
Coolant *p*H	8.7 to 9.0				
Nuclear characteristics					
Core life					
Full-power years	4.85				
Calendar years	6.06				
Average fuel irradiation level at discharge, Mwd/metric ton	83,700	69,160	96,840	122,500	
Initial fuel isotopic composition					
^{239}Pu, % of total plutonium	55				
^{240}Pu, % of total plutonium	32				
^{241}Pu, % of total plutonium	13				
Neutron lifetime, sec	8.7×10^{-7}				
Effective neutron fraction	0.0041				
Final fuel isotopic composition					
^{239}Pu, % of total plutonium		63.0	64.0	54.6	
^{240}Pu, % of total plutonium		28.0	25.0	32.1	
^{241}Pu, % of total plutonium		9.0	11.0	13.3	
Initial flux-trap enrichment, % plutonium	3.8				
Final flux-trap enrichment, % plutonium	5.2				
Fuel-temperature effect, m*k*	−20				
Other temperature effects, m*k*	2				
Total safety-rod strength, m*k*	50				
Total control-rod strength, m*k*	25				
Breeding ratio, core + blankets	1.14				
Moderator characteristics					
Moderator material	YH_x or $ZrH_x + H_2O$				
YH_x or ZrH_x, vol.%	70				
Reactor heat in moderator, Mw	1.3				
Control					
No. of control rods	6				
Control-rod material	Stainless steel–1.25% natural boron				
Control-rod diameter, in.	3/4				
No. of safety rods	6				
Safety-rod material	Stainless steel–1.10% B^{10}				
Safety-rod diameter, in.	3/4				
Coolant	H_2O (same as used for moderator)				
Power-cycle components					
Turbine type	Cross compound				
No. of reheats	2				
High-pressure-stage conditions, °F/psi	1050/3515				
First-reheat conditions, °F/psi	1000/912				
Second-reheat conditions, °F/psi	1000/299				
Exhaust pressure, in. Hg	3.5				
Condenser size, sq ft	110,000				
No. of feedwater stages, including deaerator	7				
No. of feedwater pumps	2				

Digitized by Google

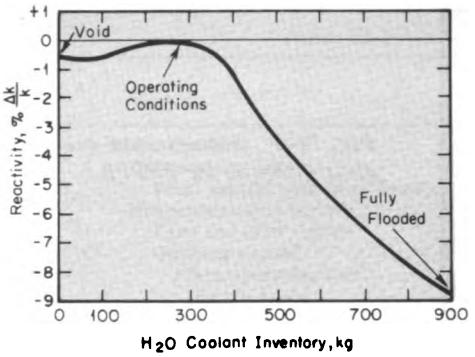

Fig. VI-5 Reactivity change vs. coolant inventory for the FSPPR.[1]

although differences in reactivity values indicate that perhaps diffusion theory gave more conservative results."

In calculating the pressure drops of the fuel-element cooling channels, it was determined that a large variation between the minimum and maximum pressure drops within an element existed; however, when the maximum pressure drop was used, the calculated core total pressure drop was 658 psi, and the total pressure drop across the reactor, including turbine reheat exchanges and associated piping, was about 800 psi. The heat-transfer correlations of Chalfant* were used at pressures above

Table VI-2 NUCLEAR CORE-DESIGN DATA[1]

Region	Radius, cm	Description	Enrichment, % plutonium	Coolant pass	Coolant density, g/cm³	Composition, vol.%				
						Fuel	Coolant	Tube	Wall	Void
1	30.8	Third reactor core	12.5	3	0.108	46.4	30.9	18.4	1.7	2.6
2	44.2	Second reactor core	12.5	2	0.121	46.0	30.7	18.4	1.9	3.0
3	51.2	Absorber region, low plutonium enrichment	3.8	2	0.121	46.0	30.7	18.4	1.9	3.0
4	54.2	Zirconium hydride moderator, water cooled		Low-pressure water		70, ZrH_x	30			
5	61.2	Absorber region, low plutonium enrichment	3.8	1	0.445	63.9	21.3	12.8	0.9	1.1
6	80.4	First reactor core	14.5	1	0.445	63.9	21.3	12.8	0.9	1.1
7	100.4	Depleted uranium	0.0	1	0.445	85.9	5.7	2.2	2.9	3.3

The dimensions and worths of the control and safety rods are presented in Table VI-1. Some radial enrichment zoning was done in the absorber region to reduce power peaking in this region over core lifetime. A fuel-temperature coefficient of reactivity was computed for the Doppler broadening of the ^{238}U resonances only as $-2 \times 10^{-5} \Delta k/(k)(°C)$. It was recognized that a further positive contribution to the fuel-temperature coefficient would be available from ^{239}Pu and that a negative contribution would be available from ^{240}Pu; however, these were not calculated. Fuel- and cladding-expansion effects were estimated to be approximately $10^{-6} \Delta k/(k)(°C)$. The majority of the static reactor-physics calculations were done utilizing diffusion-theory codes, and some checking of the validity of diffusion theory for a core of this type with a moderator region located internally was done using a multigroup transport code. The results[1] obtained from the two methods of calculations "... generally confirmed the data yielded by diffusion theory, 4000 psia. Similarly the correlation of McAdams* was used at pressures from 3500 to 4000 psia. The maximum heat flux in all cases was limited by the pressure-tube wall temperature.

The proposed refueling scheme involves fueling one of the tandem reactors before the other reactor is shut down. The newly loaded reactor then begins operation while the exposed fuel is allowed to decay for a period of two to three months in the reactor core. The fluid jumpers for the individual fuel elements are remotely cut, and the fuel elements are transferred to the fuel storage basin. Plugs are then placed in severed coolant jumpers until the time of refueling, at which time the jumpers are temporarily frozen with liquid nitrogen and the coolant jumpers of the new fuel elements are welded in place. Removal of the frozen coolant

*The reader may wish to refer to Refs. 7 and 8 of Ref. 1 for these correlations.

Digitized by Google

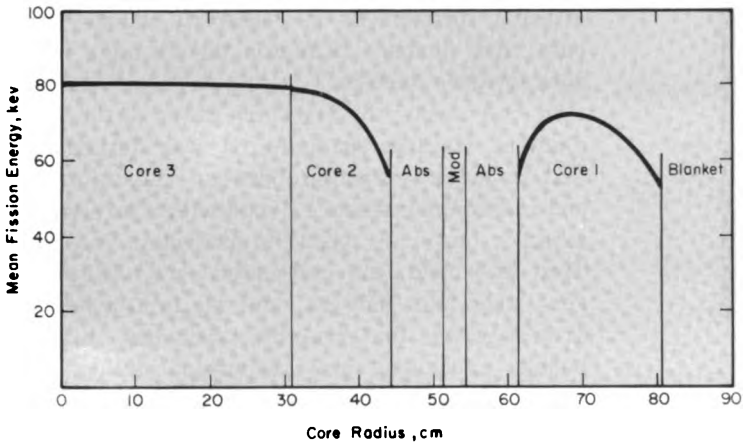

Fig. VI-6 Mean-fission-energy distribution in the FSPPR.[1]

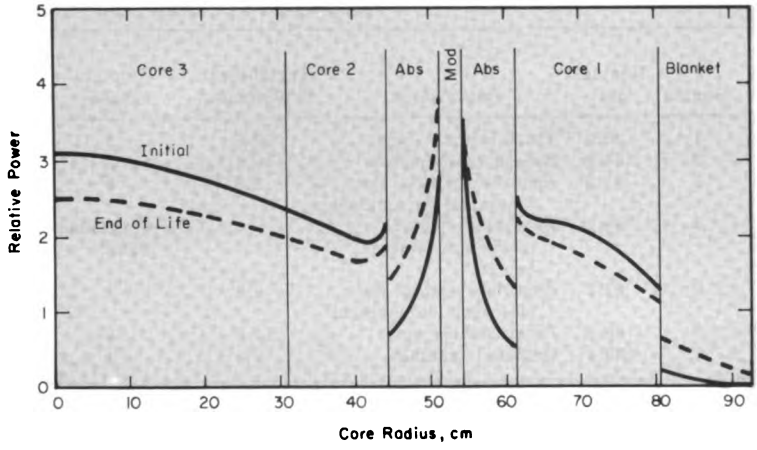

Fig. VI-7 Power distribution in the FSPPR.[1]

then restores the function of the coolant passages.

Startup of the reactor involves first purging the water in the coolant channels with low-density steam to reduce the large shutdown margin. The approach to criticality is made by control-rod withdrawal, and on reaching criticality the design power is approached by simultaneously programmed manipulations of rod position, pressurization, and flow. During normal operation the load changes are accomplished by positioning of the turbine admission valve, and the reactor power level is automatically adjusted, using a banked-control-rod configuration, to hold the coolant outlet temperature constant. Additional control and safety systems are provided to ensure safe operation at power.

The power-generation costs that were computed for the FSPPR are shown in Table VI-3. The cost data given in the "Guide to Nuclear Power Cost Evaluation" handbook were used to arrive at the computed unit cost of power generation of approximately 5.12 mills/kw-hr.

The following required technological developments are enumerated:[1]

(1) Analytical and experimental verification of a practical and economical moderator segmented core design.

(2) Demonstration of the Doppler effect as a reliable prompt negative coefficient in fast ceramic-fueled reactors.

(3) Demonstration of a high endurance (greater than 80,000 Mwt days per tonne) internally cooled ceramic-fueled element.

(4) Development of high strength alloys and fabrication techniques for complex pressure tube assemblies that are reliable under high exposures and fast neutron irradiation.

(5) Development of water treatment cleaning and decontamination techniques that avoid fouling and carry-over problems in a once through cooling system.

(6) Demonstration of reliable and economical remote fuel and pressure piping replacement methods.

Digitized by Google

Table VI-3 POWER-GENERATION COSTS FOR FSPPR[1]

	Capital cost, $	Rate, %	Annual cost, $	Unit cost,* mills/kw-hr
Fixed charges				
Depreciating capital				
Total capital cost (less land)	51,373,000	14.46	7,429,000	3.534
Nondepreciating capital				
Land and land rights	360,000	13.0	47,000	0.022
Working capital				
Plant operation and maintenance	130,000	13.0	17,000	0.009
Fuel-cycle operations	4,015,000	13.0	522,000	0.248
Nuclear liability insurance			280,000	0.133
Subtotal: fixed charges			8,295,000	3.946
Operating costs				
Operating and maintenance cost			889,000	0.423
Fuel cost			1,572,000	0.748
Subtotal: operating costs			2,461,000	1.171
Total power-generation costs			10,756,000	5.117

*Plant factor is 80%.

Hanford Graphite Superheat Reactor

The N-Reactor Project Section of the Hanford Atomic Products Operation[3] has recently reported results of a design and evaluation study for a Hanford graphite superheat reactor (HGSR). These studies involved consideration of two basic reactor sizes, a 300-Mw(e) plant and a 1000-Mw(e) plant, both utilizing pressurized process tubes, vibratory-compacted uranium dioxide fuel, graphite-moderator blocks, and a once-through boiling-superheating coolant passage.* Since the 1000-Mw(e) plant design is quite similar to the smaller plant design, a detailed description of the smaller plant will be presented first, followed by some indications of the differences that were encountered in the design of the larger plant.

The process tubes, fuel elements, and coolant routing are shown in Fig. VI-8, and further descriptive material is presented in Table VI-4. As shown in Fig. VI-8, the process tube would be supported by the top primary shield, and the seal assembly on the fuel element would transmit the load of the fuel to the nozzle. This seal assembly would separate the 400°F water that enters the fuel element and flows down its outer peripheral flow channel from the steam that passes up the central flow channel of the element and exhausts from the nozzle assembly. The tube that separates the water and steam is formed in a 360° helix around the fuel-element supporting rod, thereby eliminating the need to penetrate the steam-tube wall. Subcooled water passes down the outer flow channel, and then the boiling water returns up the two inner annuli where it is further vaporized and superheated. A 10-mil Incoloy cladding is proposed for the fuel that would be uranium dioxide vibratorily compacted to approximately 92% of the theoretical density. The process tubes would be manufactured from Zircaloy (in the active core region) and stainless steel (above the core).

The general arrangement of process tubes, control rods, graphite stack, and coolant-flow zones is shown in Fig. VI-9. Further information is contained in Table VI-4. As shown in Fig. VI-9, the graphite stack is composed of horizontal layers of blocks of graphite with successive layers oriented at right angles to each other. The process tubes and the continuous-chain control rods then pass through the openings provided for them in the graphite stack. The dimensions of the graphite blocks are such that ventilating voids are provided

*These designs bear some similarities to the graphite-moderated superheating reactor located at the USSR Beloyarsk Power Station. This reactor was described in *Power Reactor Technology*, 8(1): 28-34 (Winter 1964-1965), and the reader may wish to refer to that review for a comparison. Some of the major differences in the two designs involve the general mechanical arrangement of the fuel, the fuel enrichment, and the coolant-flow-passage arrangement.

Digitized by Google

throughout the graphite stack, which would serve as steam vent volumes in the event of a process-tube rupture. Steam would escape through the core by the lifting of the layer of the stack in which the rupture occurred. Steam would then travel to a plenum located in the reflector which could carry the steam outside the reactor block. The top, bottom, and side reflectors are also composed of graphite, and they maintain the same basic layer formation with the exception that the steam-vent spaces are filled with graphite to increase the reflecting ability. Thermal and biological shields are arranged around the graphite stack. Flow to the process tubes would be controlled in 5 flow-control zones (shown in Fig. VI-9). Each of the 5 zones is divided into two halves that are supplied by headers located on opposite sides of the reactor. Each flow-control zone would theoretically contain tubes of equal power; thus by supplying a control valve on each of 10 supply headers, flow control could be maintained to one-half of a zone. Fuel charging and discharging would be managed along the same zone plan.

The locations of the control-rod blocks are also shown in Fig. VI-9. The control-rod design incorporates a flexible endless chain, with poison sections attached to it, and a bottom drive that would be supplied power by a hydraulic motor. This particular flexible rod design provides for a minimum of storage height when the poison is out of the reactor and also allows assistance from gravity in holding the control material in the reactor. Dimensional details and other information on the control rods are in Table VI-4. Cooling water would be supplied to the tubes containing the control rods, and poison could be injected into the rod coolant passages for backup reactivity control; a flow diagram of the poison system is shown in Fig. VI-10.

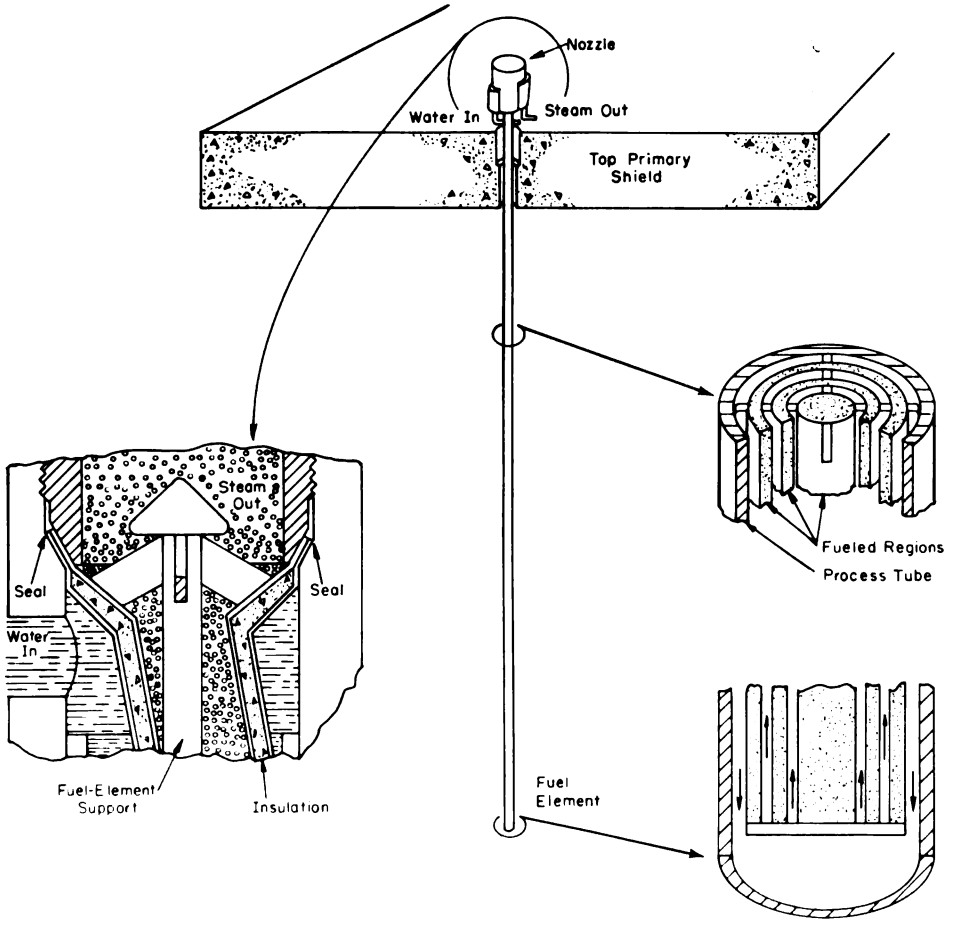

Fig. VI-8 Recentrant type process-tube coolant connections in the HGSR.[3]

Digitized by Google

Table IV-4 DATA SUMMARY FOR 300- AND 1000-Mw(e) HGSR PLANTS[3]

	300-Mw(e) plant	1000-Mw(e) plant
Gross thermal, Mw(t)	840	2700
Gross electrical, Mw(e)	321	1030
Net electrical, Mw(e)	311	1000
Exit steam condition	1100 psig, 1000°F	Same
Inlet steam condition	1525 psig, 400°F	Same
Steam flow, lb/hr	2.48×10^6	8.10×10^6
Reactor Description		
Reactor core		
Active width, ft	~18	~28
Active length, ft	~18	~26
Lattice spacing, in.	9.25	10.5
Total UO_2 loading, kg	50,600	156,000
Fuel initial enrichment	2.391 wt.%	2.37 wt.%
Reflector material	Graphite	Same
Reflector thickness	2 ft 11½ in.	2 ft 10½ in.
Fuel element		
Fuel material (~92% of theoretical density)	UO_2	Same
Fuel-element dimensions (UO_2), in.		
Outer cylinder	OD, 2.279 ID, 1.690	OD, 2.644 ID, 2.055
Inner cylinder	OD, 1.457 ID, 0.80	OD, 1.603 ID, 0.950
Rod diameter	0.50	0.490
Cladding material (base case)	Incoloy	Incoloy
Cladding thickness, in.	0.010	Same
Process-tube material	Zircaloy-2	Same
Process-tube dimensions, in.	ID, 2.475 Wall, 0.234	ID, 2.907 Wall, 0.275
Reactor-control material	Boron steel	Same
No. of control elements	64	140
Control-rod OD, in.	1.5	Same
Control-rod effective length, ft	18.2	26
Reactor mass velocities (average), lb/(hr)(sq ft)		
Boiler pass	1.22×10^6	1.38×10^6
Superheat pass	1.06×10^6	9.46×10^5
Reactor bulk-coolant inlet temperature, °F	400	Same
Reactor maximum coolant outlet temperature, °F	1115	Same
Steam coolant flow, lb/hr	2.48×10^6	8.10×10^6
Maximum fuel temperature, °F	4100	4700
Maximum cladding temperature, °F	1200	1260
Maximum heat flux, Btu/(hr)(sq ft)(°F)		
Boiler pass	4.70×10^5	4.88×10^5
Transition pass	4.84×10^5	5.21×10^5
Average heat flux, Btu/(hr)(sq ft)(°F)		
Boiler pass	2.09×10^5	2.17×10^5
Transition pass	2.15×10^5	2.32×10^5
Peak-to-average power ratio		
Axial	1.5	Same
Radial	1.5	Same
Relative radial flux distribution in fuel element		
Outer cylinder	1.29	Same
Inner cylinder	1.08	Same
Rod	1.00	Same
Average core velocity, ft/sec		
Inlet	6.5	7.2
Outlet	200	195

Digitized by Google

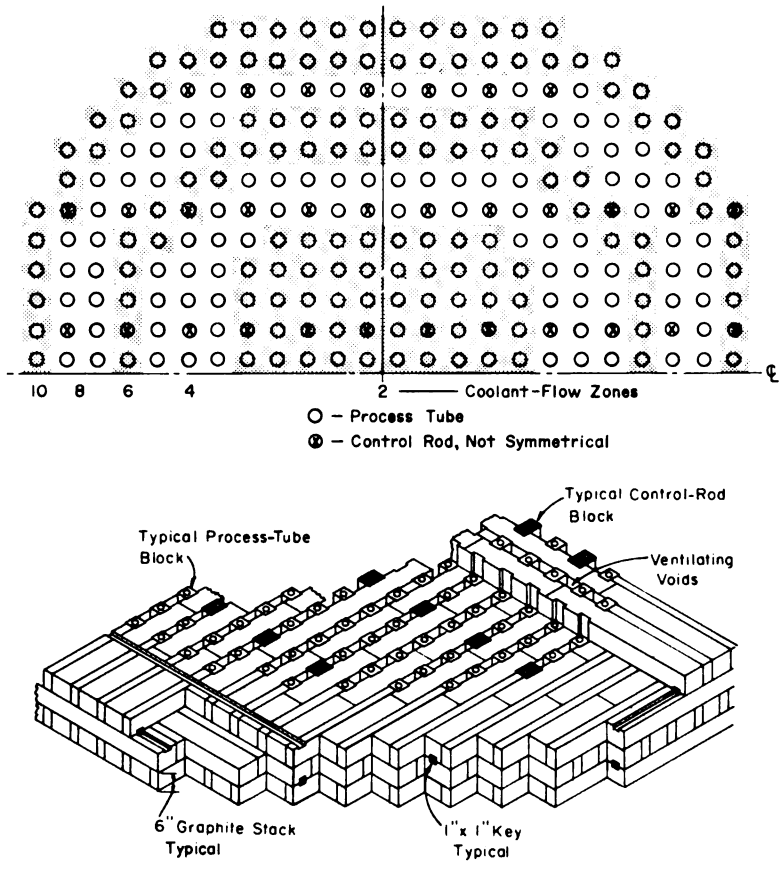

Fig. VI-9 General arrangement of fuel, control rods, graphite stack, and coolant-flow zones in the HGSR.[3]

The IBM-7090 program FLEX-II was used to obtain most of the physics analysis. The computed operational reactivity variations and reactivity coefficients are shown in Table VI-5. Control requirements are minimized because of an assumed staggered discharge scheme wherein about 10% of the fuel would be discharged at a time; a fuel exposure of 22,000 Mwd/ton would be obtained. As reported in Ref. 3: "... If the reactor is loaded with 2.39% enriched material, its reactivity will exceed the capacity of the control system. Therefore, some poison must be charged in the new reactor ..." It is proposed[3] that natural uranium dioxide elements be used as control material to be periodically replaced with the reference enrichment until the equilibrium fuel-management phase is achieved. Computed peak-to-average power ratios are included in Table VI-4.

The flow diagram for the steam- and feedwater-supply system, as well as for some of the auxiliary systems, is shown in Fig. VI-10. A helium-gas system is supplied for the HGSR to provide a chemically stable environment for the process tubes and the graphite moderator and to provide a means of detecting small steam or water leaks within the pile. The helium would also serve as a carrier of corrosion inhibitors to protect the process tubes from gas hydriding. Analytical instruments are provided in the gas loop to control the carbon monoxide and the water-vapor level. During the initial 20 sec following scram or shutdown, cooling would be provided by the coastdown of the feedwater pump; thereafter a shutdown-cooling system takes over. The fuel-element-rupture monitoring system consists of a gamma spectrometer, which analyzes gas from the primary coolant, and a delayed-neutron detector. Location of the particular process tubes containing ruptured fuel would be by means of traps located in each outlet nozzle. Superheated steam flows to the 1800-rpm tandem

Digitized by Google

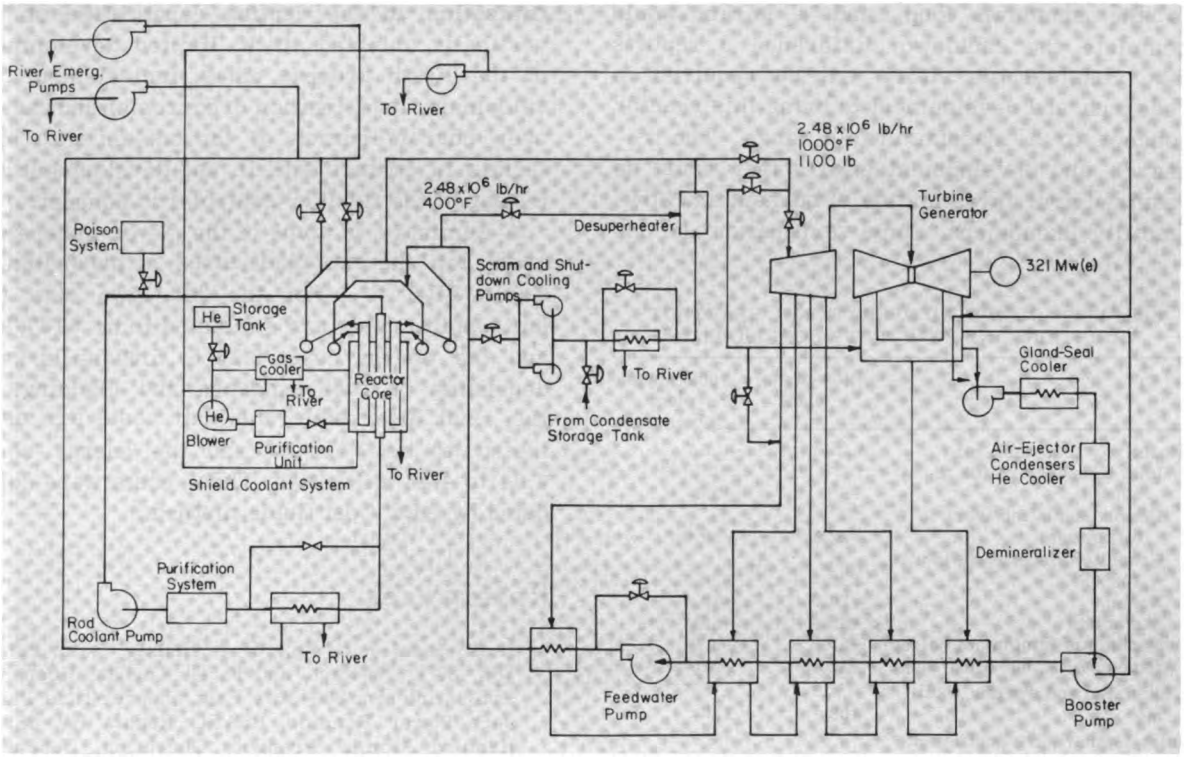

Fig. VI-10 Flow diagram of the 300-Mw(e) HGSR.[3]

compound turbine with inlet conditions of 1000°F and 1100 psig.

As previously mentioned, the 1000-Mw(e) design is quite similar to, and in many instances identical to, the smaller design. Only those differences which are considered significant will be mentioned here. The flow diagram shown in Fig. VI-10 is the same as the schematic for the 1000-Mw(e) plant with appropriate changes made in the various ratings. Table VI-4 describes some of the parameters that were changed in the 1000-Mw(e) plant. The length of the uranium-bearing section of the fuel elements was increased to slightly over 26 ft, the active width of the core was increased to approximately 28 ft, additional control rods were added, and the coolant flow was divided into three flow-control zones. Computed operational reactivity variations and reactivity coefficients for the 1000-Mw(e) HGSR are shown in Table VI-5. The larger design required doubling the capacity of the liquid-poison system, and this was accomplished by installing two systems identical to the ones used in the smaller plant. The circulation rate of the helium-gas system was doubled for the larger design; this maintained the same gas velocity through the reactor and the same frequency of gas exchange within the reactor. Steam for the larger unit would be supplied to two turbine-generators at the same inlet-throttle conditions. Nuclear control instrumentation would utilize the same low-level and intermediate-level systems; however, eight power-level channels would be utilized.

The HGSR was designed to operate at approximately a constant load; therefore the reactor operation would be at an approximately constant pressure and temperature. Manual control-rod movement would be used for level-load operations. The procedure that was envisioned for the cold startup involved maintaining the reactor flow rate at its normal operating value during the startup. The startup was estimated to require approximately 4 hr; the hot startup was estimated to require approximately 1 hr. Normal shutdown would be accomplished by gradual power reduction and corresponding flow reduction with steam going through the bypass to the turbine condenser. When the power level was approximately 10% of full power, the cooldown would be transferred

Digitized by Google

to the shutdown loop, and a scram would complete the shutdown. Reference 3 reports that considerable effort will be required in research and development to bring this reactor concept to a manufacturable stage. The research and development efforts that would be required are: investigation of burnout and flow-stability phenomena, some verification and optimization of the venting capabilities of the vertically oriented stack, limited development of the HGSR process tubes, fuel-element development, investigation of corrosion and carry-over characteristics of the coolant with materials in contact with it, and development and testing of the flexible-control-rod concept.

A summary of some of the power-generation costs for the two plant sizes is presented in Table VI-6. "... For the 300 Mwe size, the unit capital costs are estimated to be $147/kw, and the energy costs 5.13 to 5.60 mills/kwh, depending on fuel exposure and cladding. In the 1000 Mwe size, the unit costs are estimated to be $112/kw and the energy costs 4.04 to 4.43 mills/kwh. These costs were computed by AEC Cost Guide method."

Table VI-5 COMPUTED OPERATIONAL REACTIVITY VARIATIONS AND REACTIVITY COEFFICIENTS*

	300-Mw(e) plant	1000-Mw(e) plant
Reactivity transient, mk		
Inlet temperature (68 to 400°F)	−9.5	−9.4
Power escalation (zero to full power)	−22.5	−39.6
Graphite temperature (68 to 1085°F)	29.5	32.5
Xenon	−26.9	−30.4
Samarium	−6.3	−6.3
Neptunium (plutonium holdup)	−3.4	−3.4
Exposure (22,000 Mwd/ton)	−320.0	−280.0
Calculated rod worths (total), mk	109	120
Inlet-temperature coefficient,* $\Delta k/(k)$(°F)	-2.85×10^{-5}	-2.82×10^{-5}
Power coefficient,*† $\Delta k/(k)$(Mw)	-2.74×10^{-5}	-1.43×10^{-5}
Graphite coefficient,* $\Delta k/(k)$(°F)	2.90×10^{-5}	3.20×10^{-5}

*These values are at "average" conditions, i.e., in a reactor containing fuel of all exposures from 0 to 22,000 Mwd/ton.

†This includes effects of water density and fuel temperature.

References

1. D. T. Aase, J. C. Fox, R. J. Hennig, R. E. Peterson, S. L. Stewart, and K. G. Toyoda, Economic Evaluation of a 300-Mwe Fast Supercritical Pressure Power Reactor, USAEC Report HW-78953, Hanford Atomic Products Operation, December 1963 (first unrestricted distribution, April 1964).
2. H. Harty, J. J. Regimbal, K. G. Toyoda, and R. D. Widrig, Economic Evaluation of 300-Mw(e) Supercritical Pressure Power Reactor, USAEC Report HW-68420(Rev.), Hanford Atomic Products Operation, June 1961.
3. Hanford Atomic Products Operation, Hanford Graphite Superheat Reactor (HGSR), Design Study and Evaluation, USAEC Report HW-73130, January 1960.

Table VI-6 POWER-GENERATION COSTS FOR 311-Mw(e)* AND 1000-Mw(e) HGSR PLANTS

		311-Mw(e)* plant			1000-Mw(e) plant		
	Rate, %	Capital cost, $1,000	Annual cost, $1,000	Unit cost, mills/kw-hr	Capital cost, $1,000	Annual cost, $1,000	Unit cost, mills/kw-hr
Fixed charges							
Depreciating capital							
Total capital cost (less land and land rights)	14.5	45,810	6,640	3.04	112,100	16,260	2.32
Nondepreciating capital							
Land and land-rights working capital	13.0	360	47	0.02	360	47	0.01
Plant operating and maintenance	13.0	159	21	0.01	540	70	0.01
Fuel-cycle operation	13.0	2,100	273	0.13	4,490	584	0.08
Nuclear liability insurance			289	0.13		340	0.05
Annual fixed charges, subtotal			7,270	3.33		17,301	2.47
Operating costs							
Operating and maintenance			890	0.41		2,280	0.32
Fuel cost			3,020	1.39		8,760	1.25
Operating costs, subtotal			3,910	1.80		11,040	1.57
Total power-generation costs			11,180	5.13		28,341	4.04

*The exact value of 311 Mw(e) was used in computing these costs instead of the rounded-off "300 Mw(e)" that appears throughout this article.

Digitized by Google

LEGAL NOTICE

This journal was prepared under the sponsorship of the U. S. Atomic Energy Commission. Neither the United States, nor the Commission, nor any person acting on behalf of the Commission:

A. Makes any warranty or representation, expressed or implied, with respect to the accuracy, completeness, or usefulness of the information contained in this journal, or that the use of any information, apparatus, method, or process disclosed in this journal may not infringe privately owned rights; or

B. Assumes any liabilities with respect to the use of, or for damages resulting from the use of any information, apparatus, method, or process disclosed in this journal.

As used in the above, "person acting on behalf of the Commission" includes any employee or contractor of the Commission, or employee of such contractor, to the extent that such employee or contractor of the Commission, or employee of such contractor prepares, disseminates, or provides access to, any information pursuant to his employment or contract with the Commission, or his employment with such contractor.

Digitized by Google

640
GIFT

NOV 2 '65

Digitized by Google

NUCLEAR SCIENCE ABSTRACTS

The U. S. Atomic Energy Commission, Division of Technical Information, publishes *Nuclear Science Abstracts (NSA)*, a semimonthly journal containing abstracts of the literature of nuclear science and engineering.

NSA covers (1) research reports of the U. S. Atomic Energy Commission and its contractors; (2) research reports of government agencies, universities, and industrial research organizations on a world-wide basis; and (3) translations, patents, books, and articles appearing in technical and scientific journals.

Complete indexes covering subject, author, source, and report number are included in each issue. These are cumulated quarterly, semiannually, and annually providing a detailed and convenient key to the literature.

Availability of *NSA*

SALE *NSA* is available on subscription from the Superintendent of Documents, U. S. Government Printing Office, Washington, D. C., 20402, at $30.00 per year for the semimonthly abstract issues and $22.00 per year for the four cumulated-index issues. Subscriptions are postpaid within the United States, Canada, Mexico, and all Central and South American countries, except Argentina, Brazil, British and French Guiana, Surinam, and British Honduras. Subscribers in these Central and South American countries, and in all other countries throughout the world, should remit $37.00 per year for subscriptions to semimonthly abstract issues and $25.00 per year for the four cumulated-index issues.

EXCHANGE *NSA* is also available on an exchange basis to universities, research institutions, industrial firms, and publishers of scientific information. Inquiries should be directed to the Division of Technical Information Extension, U. S. Atomic Energy Commission, P. O. Box 62, Oak Ridge, Tennessee, 37831.

Digitized by Google

TECHNICAL PROGRESS REVIEWS may be purchased from Superintendent of Documents, U. S. Government Printing Office, Washington, D. C., 20402. *Isotopes and Radiation Technology* at $2.00 per year for each subscription or $0.55 per issue; the other four journals at $2.50 per year and $0.70 per issue. The use of the coupon below will facilitate the handling of your order.

POSTAGE AND REMITTANCE: Postpaid within the United States, Canada, Mexico, and all Central and South American countries except as hereinafter noted. Add $0.50 per year, or $0.15 per single issue for the *Isotopes and Radiation Technology* journal and $0.75 per year or $0.20 per single issue for the other four journals for postage to all other countries, including Argentina, Brazil, British and French Guiana, Surinam, and British Honduras. Payment should be by check, money order, or document coupons, and MUST accompany order. Remittances from foreign countries should be made by international money order, or draft on an American bank, payable to the Superintendent of Documents, or by UNESCO book coupons.

order form

SUPERINTENDENT OF DOCUMENTS
U. S. GOVERNMENT PRINTING OFFICE
WASHINGTON , D. C., 20402

Enclosed:
document coupons [ ] check [ ] money order [ ]

Charge to Superintendent of Documents No. _____

Please send a one-year subscription to

[ ] NUCLEAR SAFETY

[ ] POWER REACTOR TECHNOLOGY

[ ] REACTOR FUEL PROCESSING

[ ] REACTOR MATERIALS

(Each subscription $2.50 per year; $0.70 per issue.)

[ ] ISOTOPES AND RADIATION TECHNOLOGY

(Each subscription $2.00 a year; $0.55 per issue.)

SUPERINTENDENT OF DOCUMENTS
U. S. GOVERNMENT PRINTING OFFICE
WASHINGTON, D. C., 20402

(Print clearly)

Name _____

Street _____

City _____ Zone ___ State _____

Digitized by Google

Y3.At7:
368-4

Eng.

TK
9202
G4

ENGINEERING
NOV 17 '66
LIBRARY

4004

POWER REACTOR TECHNOLOGY

A Quarterly Technical Progress Review

Prepared for DIVISION OF TECHNICAL INFORMATION, USAEC, by
ARGONNE NATIONAL LABORATORY

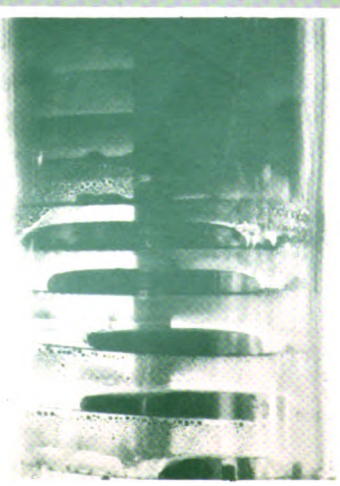

Trapping liquid-metal vapor ... see page 259

Fall 1965

● VOLUME 8

● NUMBER 4

Digitized by Google

TECHNICAL PROGRESS REVIEWS

To meet the needs of industry for concise summaries of current atomic developments, the Atomic Energy Commission is publishing this series, Technical Progress Reviews. Issued quarterly, each of the reviews digests and evaluates the latest findings in a specific area of nuclear technology and science.

The five journals published in this series are:

Isotopes and Radiation Technology P. S. Baker, A. F. Rupp, and associates
Oak Ridge National Laboratory

Nuclear Safety Wm. B. Cottrell, W. H. Jordan, and associates
Oak Ridge National Laboratory

Power Reactor Technology
Argonne National Laboratory

Reactor Fuel Processing Stephen Lawroski and associates
Chemical Engineering Division, Argonne National Laboratory

Reactor Materials R. W. Dayton, E. M. Simons, and associates
Battelle Memorial Institute

See the back cover for availability information.

The views expressed in this publication do not necessarily represent those of the United States Atomic Energy Commission, its divisions or offices, or of any Commission advisory committee or contractor.

Availability of Reports Cited in This Review

Unclassified AEC reports are available for inspection at AEC depository libraries and are sold by the Clearinghouse for Federal Scientific and Technical Information, National Bureau of Standards, U. S. Department of Commerce, 5285 Port Royal Road, Springfield, Va., 22151. Some of the reports cited are not available owing to their preliminary nature; however, the information contained in them will eventually be made available in formal progress or topical reports.

Unclassified reports issued by other Government agencies or private organizations should be requested from the originator.

Unclassified British and Canadian reports may be inspected at AEC depository libraries. British reports are sold by the British Information Service, 45 Rockefeller Plaza, New York, N. Y.; Canadian reports (AECL series) are sold by the Scientific Document Distribution Office, Atomic Energy of Canada, Ltd., Chalk River, Ontario, Canada.

Classified U. S. and foreign reports identified in this journal as Classified may be purchased by properly cleared Access Permit Holders from the Division of Technical Information Extension, U. S. Atomic Energy Commission, P. O. Box 1001, Oak Ridge, Tenn., 37830. Such reports may be inspected at classified AEC depository libraries.

Digitized by Google

Contents

Power Reactor Technology

Vol. 8, No. 4

UNCONVENTIONAL APPROACHES	Liquid-Metal MHD Topping Cycles	199
PHYSICS	Evaluating Heavy-Atom Cross Sections for Plutonium-Recycle Calculations	210
	Critical and Exponential Experiments with Plutonium	211
	Use of Soluble Poisons in Critical Experiments	214
	Water-Reactor Data Generally Verify Theory	214
	Reactivity Changes with Long Irradiation	215
	Improvements in Resonance-Integral Theory	217
CONTROL and DYNAMICS	Reactor Control Experience	221
FLUID and THERMAL TECHNOLOGY	Heat-Transfer Conference Highlights	228
MATERIALS	Effect of Hydriding on Zircaloy Properties	245
FUEL ELEMENTS		
Letters to the Editor	Stainless-Steel Cladding in Boiling-Water Reactors	252
	Rebuttal	254
	Re-rebuttal	255
COMPONENTS	Vapor Traps Protect Liquid-Metal Systems	259
OPERATING EXPERIENCE	Operational Problems and Solutions	271
	Hallam Operation in Retrospect	279
SYSTEMS TECHNOLOGY	Advancements in Organic Coolants	290
INDEX	Volume 8	297

This issue of *Power Reactor Technology* is behind schedule because of problems attendant to the assumption of editorial and writing responsibility by Argonne National Laboratory and because of scheduling problems at the AEC production facility. It is expected that future issues will soon return to a proper seasonal schedule.

Issued quarterly by the U. S. Atomic Energy Commission. Use of funds for printing this publication approved by the Director of the Bureau of the Budget on October 14, 1963.

Digitized by Google

Statement by the New Editors

This quarterly review of developments in reactor technology has been prepared at the request of the Division of Technical Information of the U. S. Atomic Energy Commission. It is intended to help designers of power reactors stay abreast of significant progress and experience in their field. Thus its scope includes research and development in the various technical specialties in the field as well as design and construction practices, reactor concepts, applications, economics, and operating experience.

Although they are not meant to be comprehensive abstracts of all information published during the quarter, the articles in each issue will call to the reader's attention various publications that merit study. In addition, some articles will summarize and critically evaluate individual reports. Other articles will review a topic more broadly so that designers can interpret new developments and trends against the perspective of the state of the art. Because any appraisal involves the reviewer's opinion of the significance of the work reported, readers are urged to consult the references for additional information and the judgments of the original authors. If a reader has information that causes his evaluation to reinforce, modify, or contradict the opinions of our reviewers, he is encouraged to write to the Editor.

For reasonably timely coverage, articles often must be based on fragmentary information. Thus continuity will be maintained from one issue to another by use of the following subject headings whenever appropriate:

Economics, Evaluations, Programs
Specific Applications
Unconventional Approaches
Fuel Resources and Cycles
Physics
Control and Dynamics
Fluid and Thermal Technology
Containment, Radiation Control, Siting
Materials
Fuel Elements
Design and Construction Practice
Specific Reactor Types
Components
Operating Experience
Systems Technology

Because reactors are being developed and considered for power applications other than the generation of central-station electricity — and because of the similarity and transferability of the technology — the content of future issues will be broadened to include progress in reactor systems for process heat, desalting, undersea, space and other advanced applications.

This is the first issue prepared by Argonne National Laboratory. The new editors wish to express their appreciation to the previous editors, W. H. Zinn and J. R. Dietrich of Combustion Engineering, Inc., for earning *Power Reactor Technology* its respected stature in the field. Only from the experience of preparing an issue can their accomplishment be truly comprehended.

The Reactor Engineering Division (L. J. Koch, Director) has the principal responsibility for the preparation of *Power Reactor Technology*, with the regular assistance of the Reactor Physics Division (R. A. Avery, Director) and the occasional assistance of other Laboratory divisions (Metallurgy, Chemical Engineering, Chemistry, Reactor Operations, and Idaho). Thus, unless noted otherwise, the reviewers and authors of articles are Laboratory staff members. The editors will welcome interpretive review articles contributed by readers outside the Laboratory.

JAMES J. DUTTON, Editor; DAVID H. LENNOX, Technical Editor;
EDWARD J. CROKE and RAYMOND GOLD, Associate Editors
Argonne National Laboratory

Digitized by Google

Section

I

Power Reactor Technology

Unconventional Approaches

Liquid-Metal MHD Topping Cycles

By Michael Petrick

For all practical purposes, development of the steam cycle has reached a plateau. Further gains in efficiency by increasing steam pressure and temperature do not appear very profitable. Thermodynamically, steam is a poor working fluid because it absorbs too little heat at the maximum cycle temperature. However, no other single fluid is superior when all factors are considered. A logical improvement would be to use a binary system in which a second working fluid is used in a "topping" cycle.

A promising binary concept couples a liquid-metal topping cycle with a conventional steam bottoming cycle. In the topping cycle a liquid-metal magnetohydrodynamic (MHD) generator is tied directly to a liquid-metal-cooled reactor that heats the working fluid to 1500°F or possibly to as high as 2000°F.

Recent advances in magnetohydrodynamics show that an MHD device is a feasible way to convert heat into electricity. Although the plasma MHD cycle has a formidable obstacle to overcome—the attainment of adequate electrical conductivity within practical temperature limits—liquid metals have electrical conductivities five orders of magnitude higher than the electrical conductivity of plasma. The power density of an MHD generator is directly proportional to the fluid conductivity times the squares of fluid velocity and magnetic flux. Thus, even though the velocities that can be achieved in a liquid-metal generator are about a hundred times lower than with a plasma, liquid-metal MHD systems have a greater potential for compact or low-capital-cost generators than do plasma MHD systems.

The introduction of a topping cycle above 1000°F creates problems that must be resolved, e.g., high-temperature-material limitations affect component fabrication, cost, reliability, and, most important, longevity. The lifetimes of power equipment of various maximum operating temperatures are shown in Fig. I-1, which depicts typical experience with commercial rotating equipment, ducted gases, and reactors, as well as the goals of ambitious programs for space power using thermionics and alkali-metal cycles.[1] It appears that a turboelectric topping cycle would be limited to a range of 900 to 1400°F because of turbine reliability

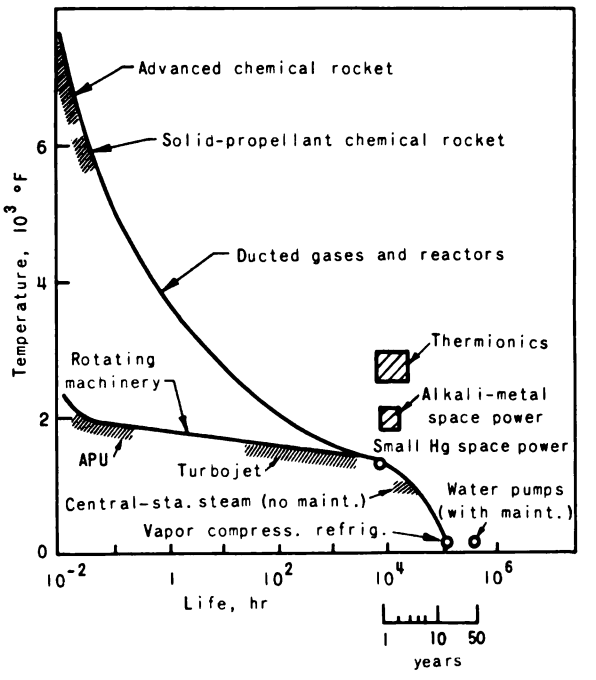

Fig. I-1 Operating temperature affects life of power equipment.[1]

Digitized by Google

problems. Unlike the conventional turboelectric generator, the MHD generator contains no moving parts that are subject to extreme temperature and dynamic stress and require close machine tolerances. As a result the MHD generator should be able to operate under conditions that conventional energy-conversion devices could not tolerate for prolonged times.

Liquid-Metal MHD Cycles

Five types of cycles have been proposed for liquid-metal MHD power systems. They are similar in that they are based on the conversion of thermal energy into kinetic energy, which then is converted into electric energy by an MHD generator. The cycles differ primarily in the way the thermal energy is converted to kinetic energy.

Two-Loop Two-Fluid Cycle. In the MHD cycle first proposed by Elliott[2] (of the Jet Propulsion Laboratory) as a space power cycle (Fig. I-2), one metal circulates in the vapor loop and another circulates in the liquid loop. The fluid circulating in the vapor loop leaves the condenser as condensate and is pumped (by an electromagnetic pump) to the mixer, where it vaporizes on contact with the liquid; the vapor expands with the liquid through a two-phase nozzle, separates from the liquid in the separator, and recondenses in the condenser. Cycle efficiency is raised by a heat exchanger that cools the vapor while it preheats the condensate. In the liquid loop the liquid is heated in the reactor heat source, is cooled as it vaporizes the condensate in the mixer, is accelerated by the vapor in the nozzle, separates from the vapor in the separator, decelerates by producing electricity in the MHD generator, and returns through the diffuser to the heat source.

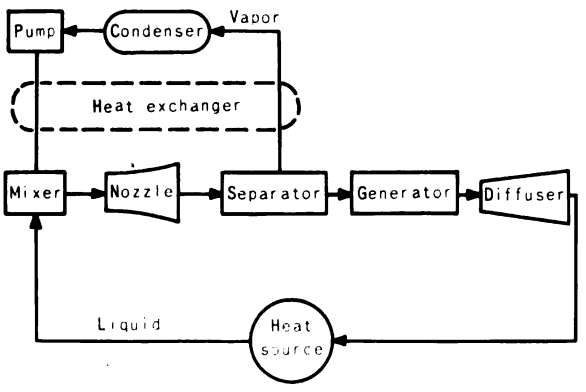

Fig. I-2 In the two-loop two-fluid MHD cycle proposed by Elliott,[2] one metal circulates in the vapor loop and another circulates in the liquid loop. Condensate from the vapor loop vaporizes when it mixes with hot liquid before both expand through a two-phase nozzle.

Two-Loop One- or Two-Fluid Cycle. The cycle proposed by Prem at Atomics International is also bicyclic.[3] It can be operated with either one or two fluids. The single-fluid version (Fig. I-3) is especially suited for large power

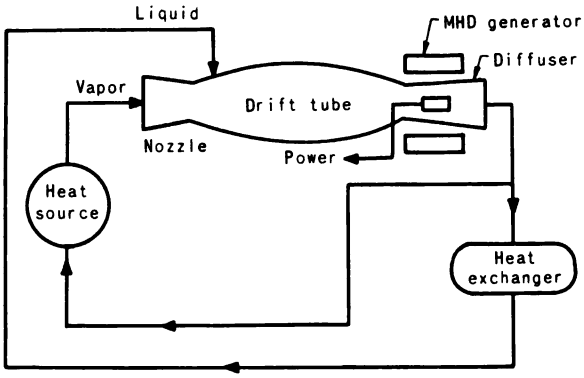

Fig. I-3 In the single-fluid version of the two-loop single- or two-fluid MHD cycle proposed by Prem,[3] hot partially vaporized fluid expands through a supersonic nozzle before cooler atomized liquid is injected to form mostly liquid stream.

stations. After the liquid metal in the first loop is partially vaporized by the heat source, the two-phase fluid expands by passing through a supersonic nozzle to transform the thermal energy to kinetic energy. Downstream of the nozzle, considerably cooler atomized liquid from the second loop is injected into the two-phase high-velocity stream. Momentum exchange accelerates the injected stream, and mass and heat transfer between the two streams condenses the vapor component of the two-phase fluid. The resulting high-velocity predominantly liquid stream enters the generator, where most of the fluid kinetic energy is transformed into electric energy. The second loop carries a portion of the liquid metal through a heat exchanger, where cycle waste heat is rejected.

One-Loop One-Fluid Cycle. A simplified single-fluid version (proposed by Petrick[4] at Ar-

Digitized by Google

gonne) of the two-fluid cycle is shown in Fig. I-4. After the velocity of a two-phase mixture or a saturated vapor from the reactor is increased by being passed through the nozzle, the two-phase fluid passes directly through the MHD generator to produce electric energy. When the fluid has been condensed, it goes through a diffuser and back through the reactor. This cycle has fewer parts and is more efficient than the two-fluid cycle of Fig. I-2 because of potentially lower friction losses and elimination of the vapor loop. Solubility and entrainment problems are also eliminated.

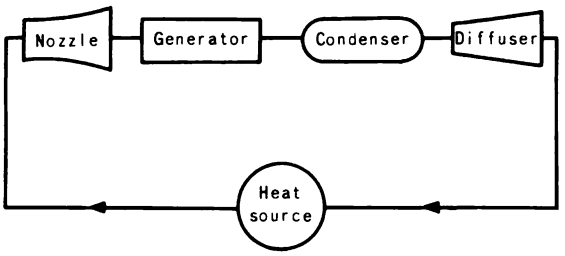

Fig. I-4 In a simpler single-loop single-fluid version (proposed by Petrick[4]) of the two-fluid MHD cycle, heat converts liquid metal to a two-phase mixture or a saturated vapor before velocity is raised in the nozzle. There is no separate vapor loop, mixer, or separator.

Two-Loop One-Fluid Condensing-Injector Cycle. The condensing-injector single-fluid MHD power cycle proposed by MIT's Jackson and Brown[5] (Fig. I-5) consists of a vapor loop (heating loop) and a liquid loop (heat-rejection loop). The vapor is generated in the reactor heat source and passes into the condensing injector, where it condenses in mixing with the liquid emerging from the waste heat exchanger to give a high-velocity liquid that passes through the MHD generator, where the kinetic energy is converted to electric energy. Then the liquid separates into two streams; one returns to the reactor, where it is vaporized, and the other stream goes to the liquid loop, where waste heat is rejected.

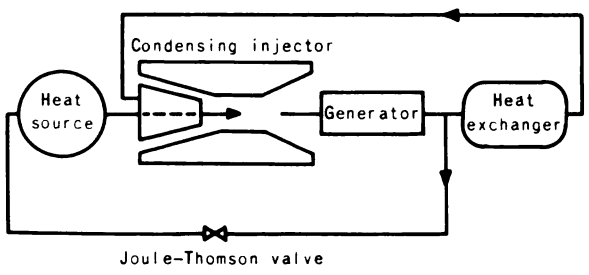

Fig. I-5 In the two-loop one-fluid condensing-injector MHD cycle proposed by Jackson and Brown,[5] vapor generated by heat condenses when it mixes with cooler liquid in the condensing injector before the fluid passes through the generator.

Slug-Generator Cycle. This cycle, proposed by Powell and coworkers at Brookhaven,[6] is similar in principle to a conventional steam-engine cycle. In this cycle (Fig. I-6) the vapor expands to accelerate liquid slugs through the generator.

The two modes of operation are either (1) to keep the intake valve open during the expansion stroke and irreversibly exhaust the high-pressure vapor through a Joule–Thomson isoenthalpic expansion to a condenser, or (2) to close the intake valve partway through the cycle and continue an adiabatic isentropic expansion to condenser conditions. The latter is more efficient and is used in conventional steam engines.

Potential Cycle Efficiencies

Calculated efficiencies for the various liquid-metal MHD cycles are reported in Refs. 6 to 9. Although the primary emphasis in this review is on the performance of the MHD cycle as a topping unit on a central-station power plant, the results of these studies also can be applied to compact power systems. Data are presented on the following working fluids: mercury, mercury–potassium alloy (40 mole % potassium), potassium, cesium, and lithium.

Two-Loop Two-Fluid Cycle. The efficiency of the Elliott cycle[9] employing cesium and lithium is shown in Fig. I-7. Assumptions made in the analysis are that: (1) the kinetic energy is converted to electric energy in the generator with 70% efficiency, including the effect of all fluid friction losses between the separator and the generator and between the generator and the diffuser; (2) diffuser efficiency is 85%; (3) the vapor-loop pump is 50% efficient; and (4) the pressure drops across the reactor, radiator, and mixer are each 10 psi.

Figure I-7 shows how cycle efficiency (defined as MHD generator output minus vapor-loop pump input divided by reactor thermal power) varies with sink temperature when the nozzle inlet is at 2000°F. Under the stated assumptions, cycle efficiency reaches a maxi-

Digitized by Google

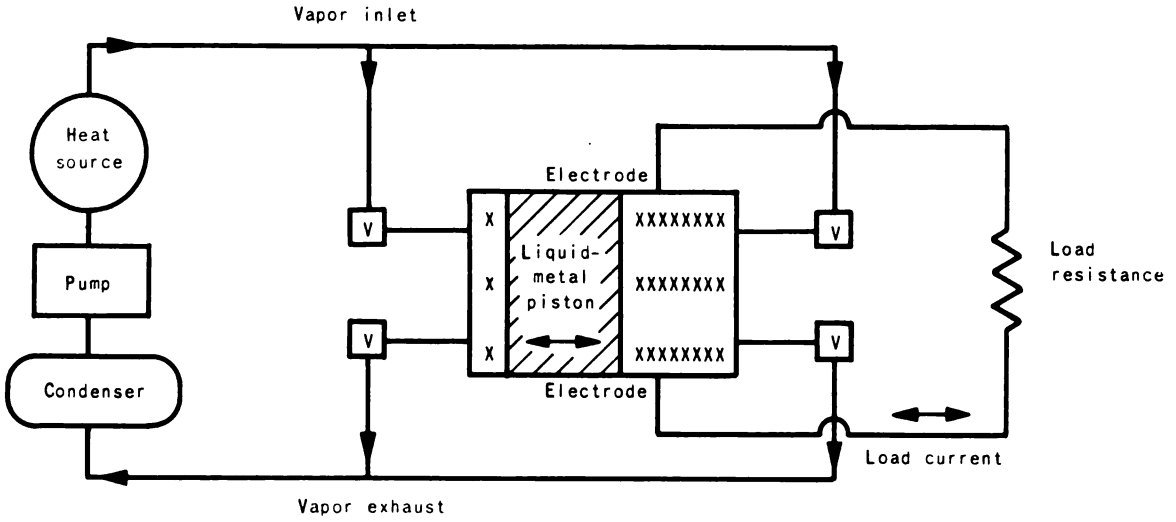

Fig. I-6 In the slug-generator MHD cycle proposed by Powell et al.,[6] liquid-metal vapor expansion pushes liquid slugs through the generator in a manner reminiscent of a conventional steam-engine cycle. V designates valves for liquid metals; X represents transverse magnetic field.

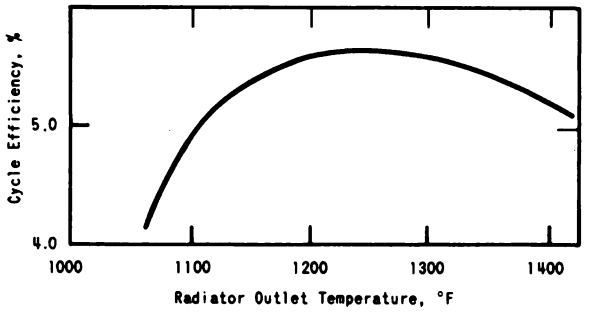

Fig. I-7 The efficiency of the two-loop cesium–lithium MHD cycle proposed by Elliott reaches a maximum of 5.7% when the sink is at approximately 1270°F (this curve is for 2000°F cesium–lithium at the nozzle inlet).[9]

mum of 5.7% when the sink is at approximately 1270°F. [At 30 kw(e) the flow rates are about 19 lb of cesium per second and 120 lb of lithium per second.] The efficiency decreases at higher sink temperatures because the Carnot efficiency decreases; it decreases at lower sink temperatures because the separator area increases and more lithium vapor enters the radiator.

Figure I-8 shows the cesium–lithium cycle efficiency as a function of the liquid and gas flow rates, exit nozzle pressure, and generator efficiency.[8]

It is apparent that this cycle has low efficiency. The maximum pressure of the system, and consequently the inlet pressure to the nozzle, is set by the working fluids used. For a cesium–lithium system, the temperature and pressure before the nozzle were set at 2010°F and 150 psia. Thus the maximum theoretical cycle efficiency is approximately 16% if the nozzle exit pressure is 0.25 psi and the generator is 100% efficient; but the maximum practical cycle efficiency is only approximately 7.5% with a more realistic exit nozzle pressure of 10 psi and an 80%-efficient generator.

Two-Loop One- or Two-Fluid Cycle. Efficiency analyses for both the single- and two-fluid versions of the Prem[7] cycle are shown in Fig. I-9; no attempt was made to optimize the cycle. Optimum cycle efficiency occurs at approximately 10% quality for a single-fluid system and supersonic nozzle inlet conditions of 2000°F and an outlet temperature equal to the vaporization temperature of the fluid at 14.7 psia. The upper three curves represent predicted efficiencies for the two-fluid cycle using an immiscible cesium–lithium mixture. The top curve shows how efficiency improves if the working fluid is expanded to 3 psia instead of 14.7 psia; the lower two curves (both of which are for 14.7-psia nozzle outlet pressures) show the importance of reducing average radiator temperature from 1050 to 780°F.

The predicted cycle efficiencies shown are based on assumed efficiencies of 70% for elec-

Digitized by Google

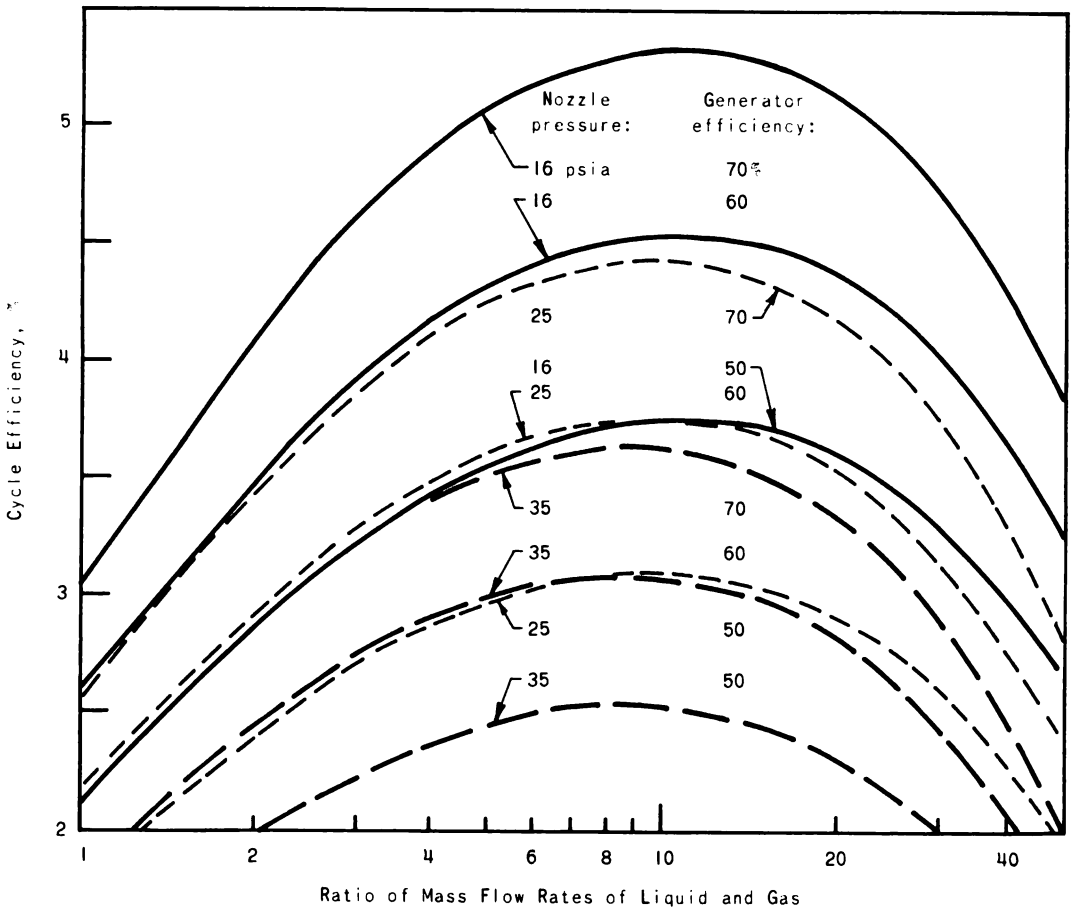

Fig. I-8 How efficiency of two-loop cesium–lithium MHD cycle varies with liquid and gas flow rates, exit nozzle pressure, and generator efficiency.[8]

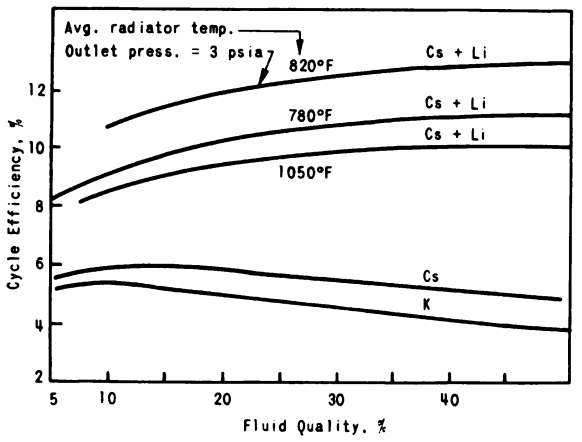

Fig. I-9 The efficiency of the two-loop MHD cycle of Prem with two fluids (upper three curves) is greater than with single fluids (lower two curves).[7] *Nozzle inlet is at 2000°F; outlet temperature is equal to the vaporization temperature at 14.7 psia, except for 3 psia for the top curve.*

trical conversions. The mechanical efficiency allows for losses in the nozzle plus frictional losses throughout the system; the electrical efficiency includes end losses in the generator and the magnetization current for producing the magnetic field.

One-Loop One-Fluid Cycle. Typical predicted cycle efficiencies for mercury, mercury–potassium, and potassium are shown in Figs. I-10 to I-12. The maximum efficiency in the cycle occurs with 100% vapor quality at the nozzle inlet.

Within the boundary conditions specified, mercury gives the highest efficiencies for the one-fluid cycle. The overall cycle efficiency is 22.5% with the source at 1540°F, the sink at 540°F, and the efficiencies of the MHD generator and the nozzle are 75 and 80%, respectively. For the potassium–mercury mixture,

Digitized by Google

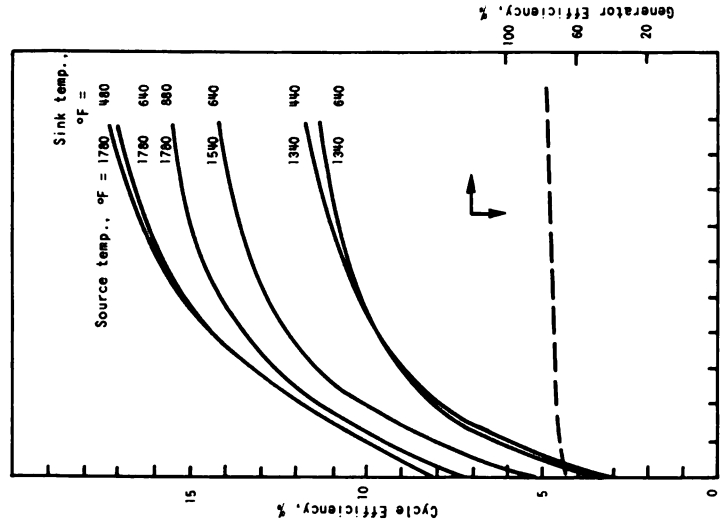

Fig. I-12 Cycle efficiency with potassium as the single fluid in the single-loop MHD cycle by Petrick.[8]

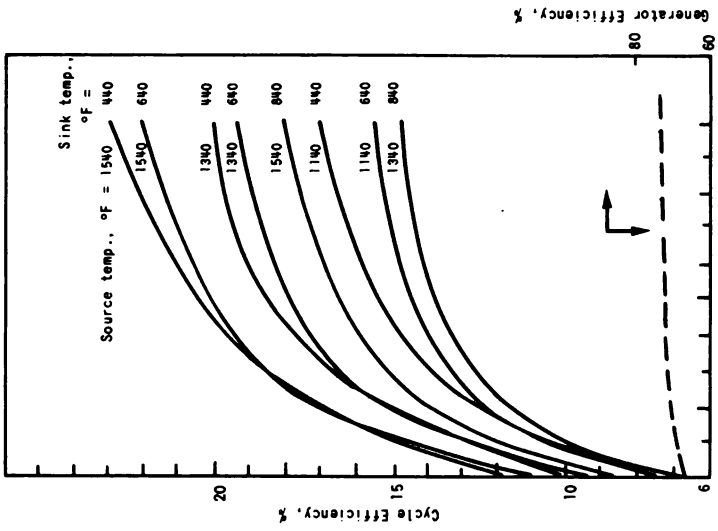

Fig. I-11 Cycle efficiency with a mercury–potassium alloy eutectic as the single fluid in the single-loop MHD cycle by Petrick.[8]

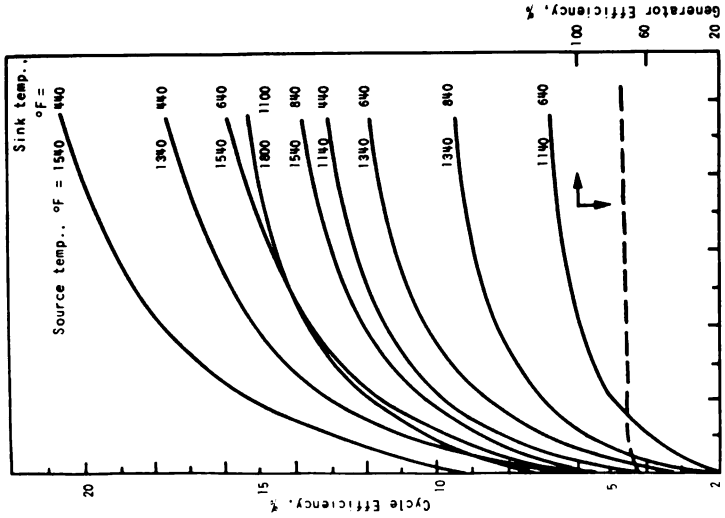

Fig. I-10 Cycle efficiency with mercury as the single fluid in the single-loop MHD cycle by Petrick.[8]

Digitized by Google

cycle efficiencies are approximately 10 to 25% lower and are much more sensitive to the source and sink temperatures.

In comparison with alkali metals, mercury and the mercury–potassium eutectic have lower boiling points, which permit operating temperatures nearer present technological limits. This advantage rapidly diminishes for the pure-mercury system because the vapor pressure of mercury increases rapidly with temperature; at 1540°F its pressure is 1762 psi. At the same temperature the vapor pressure of the mercury–potassium eutectic is only 198 psi.

Of the alkali metals, the best fluid for the one-component cycle apparently is potassium, whose calculated maximum cycle efficiency is approximately 20% over the range 2240 to 1160°F. Although cesium gives essentially the same efficiency as potassium, its lower electrical conductivity reduces its effectiveness in the MHD generator. The conductivity of sodium is higher than that of cesium or even potassium, but sodium as a working fluid yields the lowest cycle efficiencies.

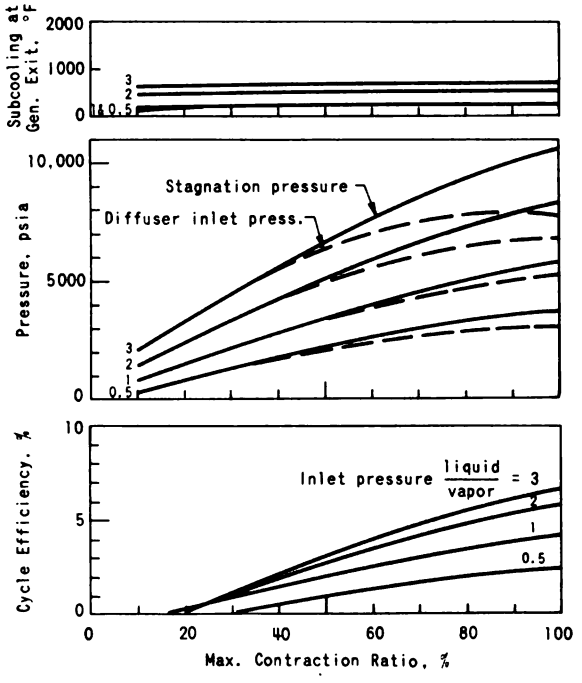

Fig. I-13 Efficiency with mercury in the condensing-injector MHD cycle when the source is at 1860°F, the sink is at 860°F, and the liquid-to-vapor mass flow ratio is 5. For inlet liquid-to-vapor pressure ratios of 0.5, 1, 2, and 3, maximum contraction ratios are 35, 49.2, 69.4, and 84.8, respectively.[8]

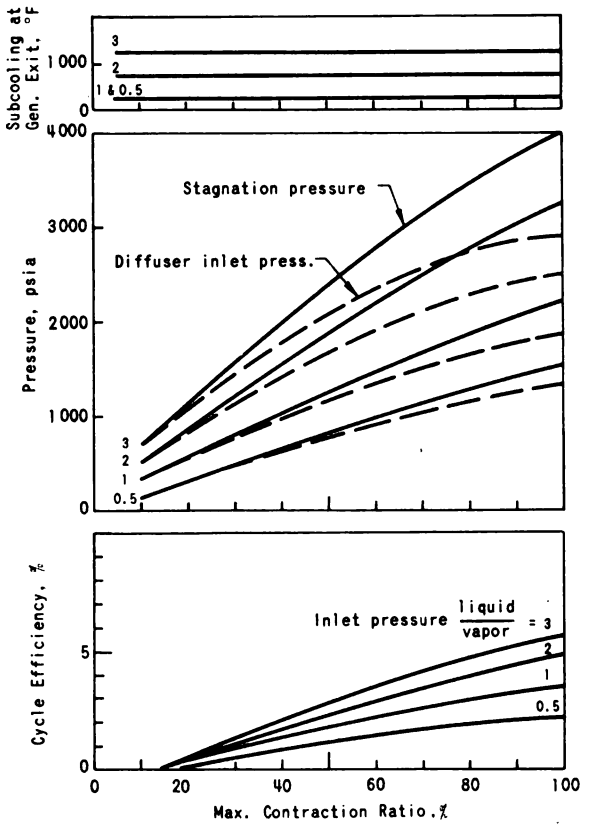

Fig. I-14 Efficiency with potassium in the condensing-injector MHD cycle when the source is at 2700°F, the sink is at 1060°F, and the liquid-to-vapor mass flow ratio is 3. For inlet liquid-to-vapor pressure ratios of 0.5, 1, 2, and 3, maximum contraction ratios are 23.2, 33.0, 46.7, and 57.2, respectively.[8]

Two-Loop One-Fluid Condensing-Injector Cycle. Figures I-13 and I-14 show typical estimated efficiencies of the condensing-injector cycle with mercury and potassium.[8] For these computations it was assumed that the MHD generator is 80% efficient and that the actual pressure rise in the condensing injector is 80% of theoretical. The cycle data show that mercury as a working fluid produces the highest cycle efficiency, 10%, and that it is followed closely by cesium at 8%. Sodium has the lowest performance potential. The ratio of the cycle efficiency to Carnot efficiency is in the range 0.17 to 0.25.

Some noteworthy trends derived from the cycle analysis are that: (1) cycle efficiency increases with injector contraction ratio and inlet stagnation pressure ratio but decreases with mass flow ratio (however, the variation of these parameters is limited by the second law

Digitized by Google

of thermodynamics); (2) cycle efficiency decreases with sink temperature and increases with heat-source temperature; (3) increasing the velocity from the condensing injector so that the total stagnation head is caused mostly by the kinetic head requires the injector geometry to give a contraction ratio greater than 50% of the maximum so that the MHD generator can be of the variable-area type, and thus it and the injector can be designed for much lower pressures.

Slug-Generator Cycle. Figure I-15 shows the calculated maximum ideal cycle efficiency for the slug-generator cycle,[6] assuming no generator losses, for adiabatic and isopressure expansions with potassium vapor. Note that isopressure expansion is about half as efficient as adiabatic expansion. As with all cycles, efficiency increases with vapor temperature.

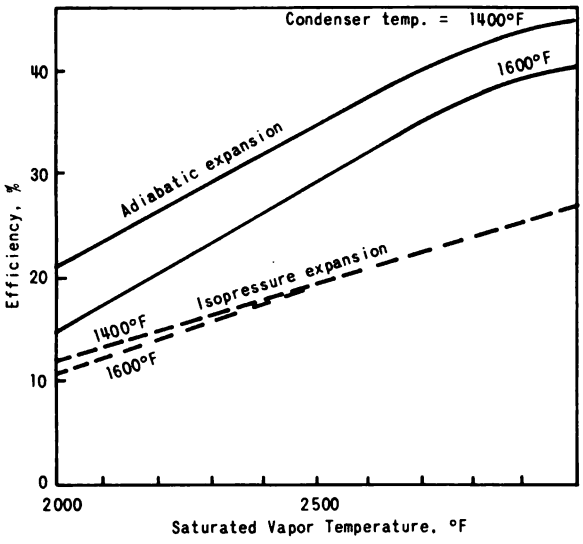

Fig. I-15 Ideal efficiencies for the slug-generator cycle with potassium vapor show that adiabatic expansion is nearly twice as efficient as isopressure expansion.[6]

Overall Plant Efficiency

The overall efficiency of a binary power system that has an MHD topping cycle and a normal steam cycle as the sink or bottoming cycle can be estimated by combining the efficiencies:

$$\epsilon_C = \epsilon_{MHD} + (100 - \epsilon_{MHD})\,\epsilon_{SC}$$

where ϵ_C is the binary cycle efficiency, ϵ_{MHD} applies to the topping cycle, and ϵ_{SC} is the efficiency of the steam bottoming cycle.

From this analysis the following conclusions are reached:

1. The potential overall efficiency of a central-station nuclear power system employing a liquid-metal MHD topping cycle appears to be excellent. (A fossil-fired boiler using a liquid-metal coolant also could be used as the heat source, in which case the boiler could operate at high cycle temperatures with the low vapor pressures possible with liquid metals.)

2. With an alkali metal as the working fluid, the maximum potential overall cycle efficiency appears to be 55% and results from either a potassium–steam or a cesium–steam binary cycle. The liquid-metal topping cycle operates between 2240 and 1100°F and produces 33% of the total power. The bottoming steam plant is the equivalent of a modern supercritical plant, such as the Eddystone unit, operating at 4000 psi and 1050°F; the efficiency of the steam plant is estimated to be approximately 45% and is based on upgrading the published Eddystone efficiency of 40.7% by eliminating boiler and stack losses.

3. The maximum potential efficiency of the mercury–steam binary cycle is approximately 53%, which is slightly lower than the cesium–steam or potassium–steam binary cycle. This efficiency is based on the source being at 1540°F and the condenser at 1100°F. If the sink temperature is dropped to 440°F, the overall cycle efficiency drops to approximately 47% even though the efficiency of the topping cycle increases substantially. Although mercury is thermodynamically the superior working fluid, it has several major drawbacks: (*a*) vapor pressure rises rapidly with temperature, (*b*) the use of additives to improve the wettability and heat transfer tends to increase operational problems considerably, (*c*) limited availability, and (*d*) relatively high cost. Thus the feasibility of the high-pressure mercury system is questionable.

4. For the medium-temperature range (1100 to 1600°F), mercury–potassium alloy and potassium appear to be the most promising working fluids for the liquid-metal cycle. Overall cycle efficiencies could be as high as 50%; the efficiency of the MHD topping cycle alone could be as high as 15% at a maximum working pressure below 75 psi.

Digitized by Google

Economics. Although no detailed economic studies have been reported, a preliminary study[8] indicates two major areas in which MHD topping cycles could save money: (1) the capacity of the steam bottoming plant could be reduced in proportion to the power generated in the MHD topping cycle, and (2) fuel costs would be lower because of the increased efficiency. The money saved in these two areas is available for converting the steam plant to the binary cycle and thus is a measure of the economic incentive for doing so.

For illustrative purposes, Fig. I-16 shows the total savings that would result from adding an MHD topping cycle to a base steam plant as a function of fuel cost and increase in plant efficiency. The values shown are for a 1000-Mw(e) plant operating with a 90% load factor, a cost of $30/kw(e) for the steam turbine-generator plant, and a 14.7% capitalization charge on the annual fuel savings (which transfers the annual fuel savings to an equivalent capital expenditure). As an example of the savings from a 20% increase in overall plant efficiency on a steam plant whose efficiency was 40%, the break-even point is approximately $25 million for a fuel cost of $0.20/$10^6$ Btu. The 20% increase in cycle efficiency can be achieved by an MHD topping cycle whose efficiency is 12.5%, which could be obtained with a maximum cycle temperature near 1600°F.

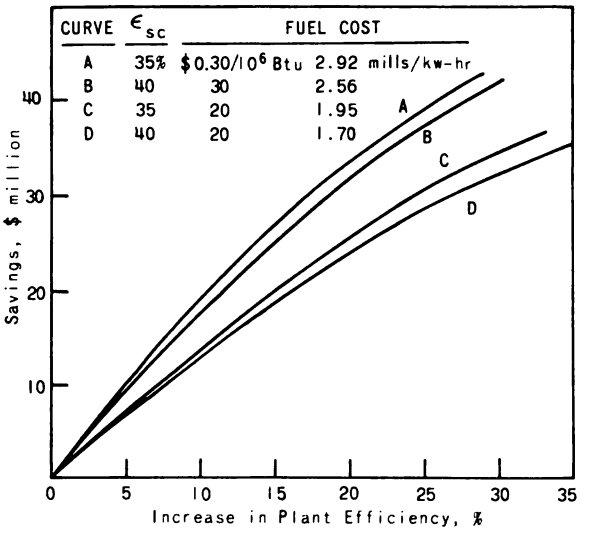

Fig. I-16 Savings from increasing plant efficiency by adding MHD topping cycle to a base steam plant.[8]

Liquid-Metal MHD: State of the Art

Active experimental programs are under way at Jet Propulsion Laboratory, Atomics International, Brookhaven National Laboratory, Massachusetts Institute of Technology, and Argonne National Laboratory to resolve uncertainties concerning the efficiencies of the various liquid-metal MHD cycles and components that have been proposed.

The Jet Propulsion Laboratory program to develop a space power source is the most comprehensive effort in liquid-metal MHD research that has been reported. In addition to tests on the MHD generator with NaK as the working fluid, the nozzle, separator, and diffuser have been tested with water and nitrogen. The nozzle has delivered 90% of isentropic exit velocity, the separator had about 1% liquid loss and 20% velocity loss, the diffuser was 75% efficient, and the generator operated at approximately 50% efficiency. Potential lifetime limitations due to erosion and to insulator loss were also investigated in water-flow and lithium-capsule tests; results indicated negligible material loss up to 1000 hr.[9,10]

The Atomics International development program is studying (1) the simultaneous mass heat-transfer and momentum-transfer process, which occurs in their "drift tube"; (2) the electrical resistivity of two-phase mixtures under various pressures, temperatures, void fractions, and impurities; and (3) generator types and performance. (Analyses and research toward the development of an MHD electric generator suitable for utility applications are being sponsored by the Edison Electric Institute.) The only results reported pertain to the acceleration and momentum-transfer process. Studies with sand and air indicate that the acceleration is accomplished very rapidly, reaching 60% of the air velocity at a distance of 30 to 40 cm from the injection point.[11] A potassium test-loop facility has been built to demonstrate the overall power-conversion process.

The Argonne National Laboratory program is studying the performance of liquid-metal generators and evaluating the condensing injector. The generator experiments will provide data on its efficiency with a dispersed two-phase entering fluid for various generator geometries, angles of incidence of the entering

Digitized by Google

fluid, and phase distributions. A second study, with a single-phase fluid, will confirm end losses in variable-area generators and establish maximum generator efficiencies, develop means to minimize end losses, and investigate the fluid mechanics of the generator. These investigations will provide data for defining the actual efficiencies of the condensing injector and two-phase single-fluid cycles.

At Massachusetts Institute of Technology, Jackson and Brown have concentrated on developing the condensing injector and the a-c generator. Brown has shown that a large pressure rise across the condensing injector is possible if a convergent mixing section is used. Jackson and coworkers[12,13] have developed the theory and outlined the performance limitations of the a-c induction generator. Experimental equipment is being fabricated to obtain extensive data on the performance characteristics of the a-c generator.

The Brookhaven National Laboratory program is oriented primarily toward investigating a slug generator.[6] Extensive studies of slug stability were made using high-speed movies of water, methanol, and mercury slugs accelerated through rectangular channels. Measurements of hydrodynamic and hydromagnetic wave growth rates agree approximately with theory. A mercury slug generator has reached an output of 100 watts, and, although its efficiency was only 10%, work is under way on an alkali-metal slug generator whose efficiency is expected to be 90% or greater. Also, work is being done on a reciprocating solid-piston MHD generator.

Others. Although programs are also being conducted at Allgemeine Elektrizitätsgesellschaft in Germany and at Space Technology Laboratories in the United States, they have not been reported in detail.

When these experiments have been completed, it should be possible to make a more thorough appraisal of the merits of the various liquid-metal MHD power cycles. Both efficiencies and needed materials development will be more clearly defined.

Comparison of Liquid-Metal and Plasma MHD Cycles

Because most of the work done in the field of magnetohydrodynamics has been on the plasma MHD cycle, the major problem areas and limitations of this concept have been pinpointed.

Efficiency and Temperature. Gunson et al.[14] have described a detailed study of a binary plasma MHD–steam power plant. Rosa and Kantrowitz[15] have calculated efficiencies for a closed-cycle plasma MHD–steam binary system, as well as for a purely MHD system; Fig. I-17 is based on their study. Both studies involved a helium cycle. Gunson reports a net efficiency of 47.1% for a plasma MHD–steam binary cycle operating with a top temperature of 3000°F.

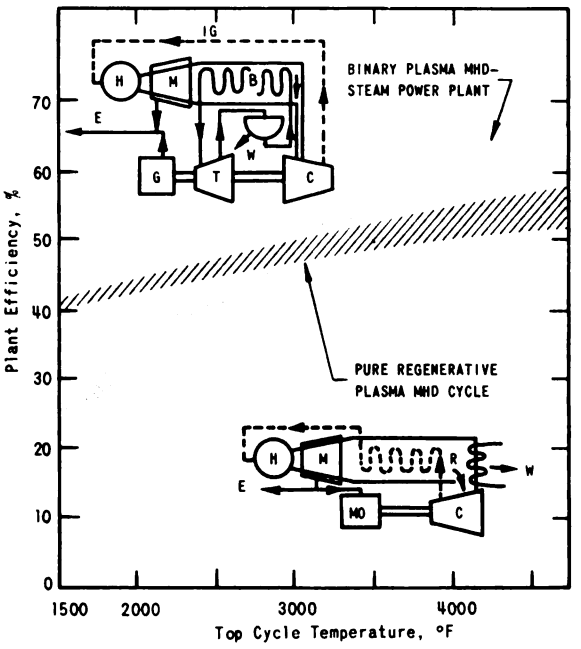

Fig. I-17 Plant efficiency with a closed-cycle plasma MHD–steam binary system exceeds that with a pure regenerative plasma MHD cycle when the top cycle temperature exceeds 2500 to 3500°F. Symbols: B, boiler; C, compressor; E, electrical output; G, generator; H, heat source; IG, inert gas; M, MHD generator; MO, motor; R, regenerator; T, turbine; and W, waste heat.[14]

For the same condition, Fig. I-17 indicates a value of approximately 51%. Thus, to better the efficiency of a modern steam plant, the temperature of a binary plasma MHD–steam plant must approach 3000°F. Temperatures must approach 4000°F to achieve overall cycle efficiencies of 55%. It also is interesting to note that the pure regenerative plasma MHD cycle (also shown in Fig. I-17) must approach 4000°F to achieve 50% efficiency. In studies of the open-cycle combustion-fired plasma MHD cycle, Way and Young[16] indicate that the overall efficiency of a binary system is 43 to 50% for a cycle top temperature of 4500°F; the highest efficiency would be achieved with a supercritical steam plant as the bottoming cycle. In comparison, liquid-metal MHD–steam binary system overall efficiencies of 50% appear possible at approximately 1600°F, and efficiencies of approximately 55% appear possible below 2200°F.

A major factor that tends to reduce the efficiency of the plasma MHD cycle is that it is essentially a Brayton cycle, and so a large fraction of the power generated is required for the compressors circulating the gas. For example, in the study made by Gunson et al., about 25% of the total electricity generated was used by the compressors. Seeding techniques and heat sources greater than 3200°F probably will be required to achieve an adequate

Digitized by Google

conductivity of the plasma in the plasma closed-cycle system. Although the development of a commercial reactor to operate at 3200°F appears possible, there are many unanswered questions about fuel performance and structural behavior.

Magnet Size and Cost. In addition to efficiency at reasonable temperatures, the liquid-metal MHD cycle offers other potential advantages. The power density achievable in a liquid-metal generator might be an order of magnitude higher than for a plasma generator; consequently smaller and less expensive magnets or coils (superconducting or normal) are feasible. Because the magnet or coil is a major cost item in an MHD plant, these potential savings are important.

Direct A-C Generation. Because d-c to a-c converters are expensive, the possibility of direct a-c generation is especially attractive. Jackson and Pierson[12] have shown that the feasibility of an MHD induction generator depends on a high magnetic Reynolds number, which is based on the wavelength of the field structure and the velocity difference between the wave and the fluid. Ionized gas flows in the conductivity range attainable now have very low magnetic Reynolds numbers, approximately 10^{-2}, and therefore direct a-c generation with such gases does not appear to be feasible. On the other hand, a characteristic magnetic Reynolds number of a liquid-metal generator would be approximately 10; thus the probability of producing a-c power directly is much more promising.

References

1. An Evaluation of Systems for Nuclear Auxiliary Power, USAEC Report TID-20079, January 1964.
2. D. G. Elliott, Two-Fluid Magnetohydrodynamic Cycle for Nuclear-Electric Power Conversion, *Am. Rocket Soc. J.* (June 1962).
3. L. L. Prem and W. E. Parkins, A New Method of MHD Power Conversion Employing a Fluid Metal, in *Proceedings of the International Symposium on MHD Electric Power Generation, Paris, France*, European Nuclear Energy Agency, Paper 63, July 1964.
4. M. Petrick and Kung-You Lee, Performance Characteristics of a Liquid Metal MHD Generator, USAEC Report ANL-6870, Argonne National Laboratory, July 1964.
5. W. D. Jackson and G. A. Brown, Liquid Metal Magnetohydrodynamic Power Generator Utilizing the Condensing Ejector, Patent Disclosure, Massachusetts Institute of Technology, October 1962.
6. J. R. Powell et al., Summary of Direct Conversion Work, USAEC Report BNL-8199, Brookhaven National Laboratory, March 1964.
7. L. L. Prem, Atomics International, private communication, September 1964.
8. M. Petrick and Kung-You Lee, Liquid Metal MHD Power Cycle Studies, USAEC Report ANL-6954, Argonne National Laboratory, June 1965.
9. D. G. Elliott, D. J. Cerini, et al., Liquid MHD Power Conversion, Vol. IV, JPL Space Programs Summary No. 37-27, Jet Propulsion Laboratory.
10. D. G. Elliott, D. J. Cerini, and E. Weinberg, Investigation of Liquid MHD Power Conversion, in *AIAA Third Biennial Aerospace Power Systems Conference, September 1–4, 1964*, Paper 64-760.
11. L. L. Prem, Fluid-Metal MHD/Steam Binary Cycle Developed, *Electrical World* (Oct. 19, 1964).
12. W. D. Jackson and E. S. Pierson, Operating Characteristics of the MPD Induction Generator, in *Proceedings of the IEE Magnetoplasmadynamic Electrical Power Generation Conference, New Castle upon Tyne, England, September 6–8, 1962*, Institution of Electrical Engineers Conference Report Series No. 4, pp. 38-42, 1963.
13. W. D. Jackson, E. S. Pierson, and R. P. Porter, Design Considerations of MHD Induction Generators, in *Proceedings of the International Symposium on MHD Electric Power Generation, Paris, France*, European Nuclear Energy Agency, Paper 61, July 1964.
14. W. E. Gunson et al., MHD Power Conversion, *Nucleonics*, 21(7): 43-47 (July 1963).
15. R. Rosa and A. Kantrowitz, MHD Power, *Intern. Sci. Tech.*, pp. 80-92 (September 1964).
16. S. Way and W. E. Young, The Feasibility of Large Scale MHD Power Generation, in *Proceedings of the International Symposium on MHD Electric Power Generation, Paris, France*, European Nuclear Energy Agency, Paper 98, July 1964.

Digitized by Google

Section

II

Power Reactor Technology

Physics

Evaluating Heavy-Atom Cross Sections for Plutonium-Recycle Calculations

By Edwin M. Pennington

Reactivity calculations were made[1] for Yankee critical experiments and for Hanford experiments that involved plutonium fuel. The calculational methods were standard. But significant is the fact that large reactivity differences were obtained by using different cross sections in the same computational model.

Experiments

The Yankee criticals studied consisted of four lattices with H_2O-to-UO_2 volume ratios varying roughly from 1 to 3.5. The UO_2 contained 2.73 at.% ^{235}U and was in 122-cm-high pins of 0.381-cm radius; the pins were clad with stainless steel 0.0407 cm thick.

Hanford criticals had PuO_2-UO_2 in 123-cm-high pins of 0.472-cm radius clad with zirconium 0.0685 cm thick; the isotopic enrichments were 1.366 at.% ^{239}Pu, 0.117 at.% ^{240}Pu, 0.011 at.% ^{241}Pu, 0.219 at.% ^{235}U, and 98.287 at.% ^{238}U. Four lattices were examined with H_2O-to-UO_2 volume ratios varying from 1 to 5.

Subcritical experiments at Hanford used 1.82 wt.% plutonium–aluminum fuel, with the plutonium consisting of 93.97 wt.% ^{239}Pu, 5.58 wt.% ^{240}Pu, and 0.44 wt.% ^{241}Pu. The pins were 111.3 cm high, of 0.635-cm radius, and were clad with zirconium 0.0762 cm thick. Five water-moderated lattices with hydrogen-to-plutonium atom ratios varying from 630 to 1418 were investigated.

Calculations

The calculational model of Ref. 1 involved three fast groups and a thermal group. Fast-group constants were obtained from the GAM-I code[2] using the original library,[3] except that versions of ^{240}Pu and ^{235}U having resonance parameters were used, and the Hanford RBU library[4] values were used for ^{238}U. When ^{239}Pu was involved, self-shielding factors calculated with the RIC code[5] were input to GAM-I. The RIC code computes resonance integrals in a manner similar to the Adler–Heinman–Nordheim method[6] used in GAM-I.

A preliminary SOFOCATE[7] problem using the actual isotopic densities as input provided thermal-group constants. The resulting cross sections were then used in a DSN[8] cell calculation with an extra scattering region to mock-up the isotropic return at the cell boundary. A final SOFOCATE problem using the DSN flux-weighted isotopic densities as input provided the thermal-group cross sections. Thermal-neutron cross sections for ^{235}U, ^{240}Pu, and ^{241}Pu for the SOFOCATE library were taken from Ref. 9. For ^{239}Pu, σ_f values from Ref. 9 were used with values of α^{49} adjusted as described in Ref. 1.

The four-group cross sections obtained as described above were used in one-dimensional diffusion theory (REX) calculations to obtain k_{eff} for the experimental radius. Values of k_{eff} were within approximately 1% of experimental values for all cases.

Comparisons

For the Yankee critical experiments, calculations were done both with the RBU library version of ^{238}U and the original GAM-I ^{238}U. Figure II-1 shows the calculations and provides a striking example of the reactivity differences

Digitized by Google

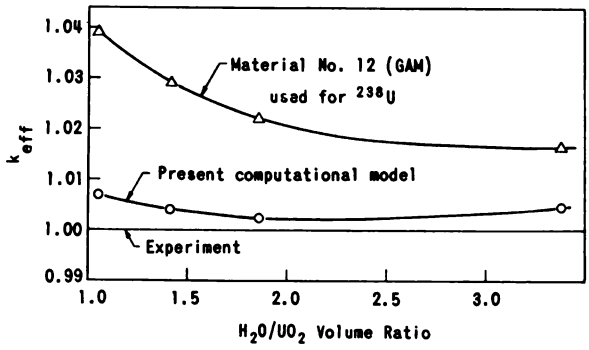

Fig. II-1 Comparison of computational model with Yankee critical experiments.[1]

that can result from using different cross sections in the same calculational model. Values of k_{eff} for the tightest lattice differ by over 3%, whereas it is desirable to calculate with an error of not more than about 1%. Even larger differences result[10] from using various cross sections in the same model for the highly undermoderated high-conversion critical experiments.[11–13]

For undermoderated light-water lattices, in which above-thermal processes are of considerable importance, uncertainties in cross sections are of more significance than errors produced by using approximate calculational methods. There is need for further work to determine basic cross-section data for use in reactor-physics computations.

Critical and Exponential Experiments with Plutonium

By Karl E. Plumlee

Plutonium produced by modern nuclear power plants significantly affects their economy. Various uses are made of recycled plutonium. Some has been used to enrich depleted uranium (as will be described). Plutonium also can be used for fuel spikes, driver regions, and full cores in reactors that require the larger number of neutrons produced per fission in plutonium than in uranium; in comparison with uranium, this characteristic tends to produce higher neutron fluxes without increasing the power level, which is an advantage for research and production reactors. On the other hand, if plutonium composition varies spatially, as it does during the operation of many cores, it poses a challenge to the physicist or engineer who is interested in determining the flux and power throughout such a core.

The Need for Data

Recent reports of critical and subcritical experiments indicate growing interest in plutonium-enriched cores and in the use of plutonium recovered from spent fuel.[14–24] Development of more durable fuel elements permits longer fuel exposures and greater plutonium utilization before the spent fuel must be reprocessed. Such highly exposed fuel contains plutonium having sizable concentrations of ^{240}Pu and ^{241}Pu (the ^{240}Pu is formed by nonfission capture of neutrons in ^{239}Pu, and the ^{241}Pu, by capture in ^{240}Pu). Because ^{240}Pu has a large capture resonance for 1-ev neutrons, its reaction rate varies nonlinearly with neutron-energy distribution as well as concentration (because of self-shielding). Thus differences in geometry, and operating variables, such as moderator temperature, affect the ^{240}Pu reaction rate. Designers must know the extent of these effects if plutonium is to be used economically.

Predictions of reactivity, power and temperature coefficients, burnup, and power and flux distributions are quite complicated for plutonium systems—particularly in the often-encountered situation in which both plutonium and uranium are in the core. Consequently experiments are needed to develop and check analytical approximations.

Experiments

Because there are several variables to be considered, measurement of the reactivity effects in plutonium cores requires carefully designed experiments and various fuel samples. But the elaborate procedures and equipment required with plutonium make fuel preparation and critical experimentation difficult. The extreme toxicity of plutonium limits permissible contamination to very low levels; the rapid accumulation of radioactive daughter elements severely limits the exposure time permitted during fuel handling.

In addition to showing the kinds of work being done, a review of the experiments being con-

Digitized by Google

ducted will indicate rates of progress and the problems encountered, even though some of the work is preliminary.

UO_2–PuO_2, Water Moderated. Critical and subcritical water-moderated experiments, fueled by rods of 1.5 wt.% PuO_2 blended with depleted UO_2 (0.22 wt.% ^{235}U in uranium), have been performed at Hanford.[14] Part of this fuel is being used in the Plutonium Recycle Program in the EBWR (Experimental Boiling Water Reactor), which will involve lengthy operation of the reactor to study reactivity trends, fuel burnup, and operational problems with a plutonium-fueled region. The 4-ft-high fuel rods are clad with Zircaloy-2 tubing 0.37 in. in diameter and 0.03 in. in wall thickness. The oxide-fuel content averages 827 g, of which approximately 86.7 wt.% is uranium and 1.3 wt.% is plutonium; the plutonium isotopic composition is 91.4 wt.% ^{239}Pu, 7.8 wt.% ^{240}Pu, and 0.73 wt.% ^{241}Pu.

The fuel rods were loaded in the subcritical experiment with hexagonal pitches of 0.55, 0.60, 0.71, 0.80, 0.90, and 0.93 in.; as much as 96% of the critical mass was accumulated so that inverse multiplication methods could be used to extrapolate the data to criticality. These extrapolated subcritical-experiment loadings indicated 2 to 5% smaller critical masses than predicted by calculations that were made using computer codes (GAM-I, HRG, TEMPEST, and THERMOS for cross sections, and HFN for criticality). Critical experimentation using the 0.7-in. fuel spacing indicated a somewhat larger critical loading (496 fuel rods) than did the subcritical experiment with the same spacing (484 rods). The change was mainly the result of component modifications, such as substitution of polycarbonate for Lucite plastic grids (or templates) to space the fuel rods.

Uranium and Plutonium Alloys, Graphite Moderated. A series of measurements was made at Winfrith in subcritical plutonium- and uranium-metal-fueled graphite-moderated assemblies that were representative of up to 4000 Mwd/metric ton fuel exposure.[15] The facilities, which were called Scorpio-I and Scorpio-II, were designed for buckling measurements and for fine flux and power-distribution measurements at 20 to 390°C; the experiments were planned to yield data for evaluating methods of calculating reactivity and temperature coefficients in power reactors. Plutonium compositions of ¼ and ½% of the uranium content were employed, with 2.5 to 3.2% ^{240}Pu in the plutonium; composition of ^{235}U was 0.42 to 0.44% in the uranium rods. In some cases the plutonium was present in plutonium–aluminum alloy strips, whereas in others plutonium–uranium rods were used; fuel-rod diameters were typically 1.1 to 1.2 in., and the length was 18 in. Volume ratios of moderator to fuel were from 17 to 108. Square lattice pitches were 7, 8, 9.9, and 11.3 in. Scorpio-I was the larger assembly with minimum dimensions of 84 by 84 by 84 in.; there were a few significantly larger arrays; the largest reported was 98 by 112 by 91 in. Details of the techniques used to measure power distribution in Scorpio-II have been described.[16]

Sample Measurements in Reactors. Related experiments were carried out by introducing a variety of 18-in.-long samples (similar to those described in Ref. 15) into an insulated cell in the uranium–graphite reactor Hector.[17] Because only samples are needed rather than complete uniform lattice loadings, this technique offers the advantage of savings in cost of fuel and in preparation.

Reactivity differences were measured over the range 20 to 450°C. Analysis of the results yielded values of k_∞ agreeing within 0.5% with the values obtained from uniformly loaded lattices. The report indicates that the effects of small perturbations in fuel composition (presence of small amounts of plutonium) can be compared without large corrections being applied in the analysis of results—provided the lattice spacing is large, typically 8.5 in. or larger. A comparison of the experimental results with the Tracer method of lattice calculation shows good agreement for room-temperature reactivities, but the calculation gave k_∞ values 1.5% lower than those measured at 400 to 450°C.

Experiments in France

A list of French CEA-operated critical facilities and typical experiments has been published.[18] Two graphite-moderated facilities are mentioned: Marius, which is operated at room temperature, and Cesar, which is operable at high temperatures. Aquilon is a D_2O facility, and both Alize and Azur are H_2O experiments. Alecto-I and Alecto-II are homogeneous-solution experiments.

Digitized by Google

Marius is a natural-uranium–graphite reactor that has been used for survey work, including variation of lattice pitch (19 to 38 cm), diameter of fuel channels (7 to 14 cm), and fuel-element geometry, including both annular and rod type fuel.[19] Tubular fuel elements were 3 to 10 cm in diameter, and fuel rods were 3 to 6 cm in diameter. The data have been used to develop improved methods of calculation, particularly in regard to large annular fuel elements. The development program requires measurements of relative fission rates in ^{239}Pu and ^{235}U and of their reactivities by oscillation and by substitution methods with plutonium–uranium fuel, irradiated fuel, and enriched and depleted samples. Experimental data and methods of analysis for obtaining reactivities, migration lengths, and related information have been reported.[19]

Marius and EDF-1. Measurements and analyses of flux fine structure and of indexes of neutron-energy spectrum, including some elevated-temperature experiments in the EDF-1 power reactor, as well as in Marius, have been reported.[20] The first part of the report details methods of fine-structure measurement and interpretation using ^{235}U, ^{239}Pu, and ^{115}In bare and cadmium-covered detectors, as well as comparison with calculated fuel and moderator flux ratios obtained by the Amouyal–Benoist–Hurwitz method. The second part concerns spectral index measurements (including ^{239}Pu, ^{235}U, indium, manganese, europium, and lutetium detectors), details of data treatment, and environmental conditions.

Marius and Minerve. Systematic experiments using oscillation techniques have been used to determine the reactivities as functions of sample composition of ^{235}U (enrichments up to 86%), ^{239}Pu, and boron (up to 12 ppm), for comparison with irradiated fuel samples.[21] The changes in effective cross sections of fuel as functions of neutron-energy spectrum and exposure will be studied by sample irradiation in the EL3 (D_2O) reactor, followed possibly by reactivity measurements in Minerve and by chemical and isotopic analysis. The precision of various techniques used to measure small reactivities, including sinusoidal- and square-wave input of reactivity or source, and also pulsed-source methods, has been studied.[22] Time requirements for equivalent accuracy are estimated for comparable methods. Limitations of the various methods are analyzed and reported, and sensitive areas are pointed out.

Aquilon-II. Bucklings and migration areas with depleted, natural, enriched, and plutonium-alloyed uranium lattices have been measured[23] in the D_2O reactor Aquilon-II. Progressive substitution measurements were made as the reference cores (natural-uranium lattices) were replaced by fuels containing 0.69, 0.71, 0.83, or 0.86% ^{235}U, and natural uranium plus 0.043% plutonium. Uranium pieces were 23.4 cm long and 2.9 cm in diameter; when assembled with aluminum containers, the rods were 240 cm long and 3.2 cm in diameter. The plutonium–uranium assemblies included double aluminum jackets and were also 240 cm long but 3.4 cm in diameter. Lattice pitches were 12, 13, 17, 19, and 21 cm. The analysis indicates consistent results by use of standard treatment. An interesting technique involves using the spontaneous neutron emission rate to measure the uniformity of the plutonium in the plutonium–uranium elements.

Homogeneous Experiments

Critical experiments have been conducted with H_2O solutions of 90% enriched uranyl nitrate and of plutonium nitrate.[24–28] The experiments provide data needed for safely handling fissionable material in solution. Typical geometries were cylinders and annuli. In addition to bare and H_2O-reflected systems, there were thick reflectors of wood and concrete and thin shells of cadmium. Experimental and calculated compositions of solutions involved plutonium in the range 19 to 104 g/liter. Experimental measurements are given for several geometries;[24] values of k_{eff} calculated by two- and four-group diffusion theory are also given for several cores; critical-height measurements are also compared with calculated values. Agreement was within 1% in most of the plain-geometry experiments. Further calculations were by the transport code TDC employing the S-4 approximation and four neutron-energy groups with RZ geometry. Monte Carlo calculations also are reported, and these indicate that 20 to 30 min of computer time is required to obtain a precision of approximately 1.2% in k_{eff} for complicated geometries involving plutonium solutions.

Homogeneous plutonium–hydrogen critical-mass measurements performed at Hanford over

Digitized by Google

the past few years have been summarized.[29] Data are reported for hydrogen-to-plutonium atomic ratios ranging from 15 to 870. The effect of nitrate was studied for concentrations as high as 460 g of NO_3 per liter. Assemblies were made with bare spherical geometry, with cadmium liners, and with reflectors of H_2O, paraffin, or concrete. A number of PuO_2–polystyrene plastic assemblies were reported, particularly for lower hydrogen-to-plutonium ratios. Information helpful in understanding the physics of the plutonium homogeneous systems was developed. Experimental techniques included standard critical-mass measurements, noise measurements, pulsed-source experiments, and spectral-index measurements with foils. Temperature variations also were studied.

Use of Soluble Poisons in Critical Experiments

By Karl E. Plumlee

Boric acid was used to poison the moderator of the Alize-II critical facility.[30] This was done to obtain measurements of temperature coefficients and excess reactivities at various temperatures; boric acid concentrations ranged from 20 to 300 ppm boron. Fuel was aluminum-clad enriched-uranium–aluminum alloy containing 12.8 g of ^{235}U per fuel plate. Plate size was 0.1 by 7.9 by 65 cm. Core composition was varied by assembling aluminum, boron–aluminum, and zirconium components, as well as fuel plates, into boxes. The boxes were inserted into grid positions to form cores. Different grids were available, providing a selection of box spacings. Numerous details are given of the steps taken to control the boron solutions. Measurements of boron deposition rates on aluminum, zirconium, and coated surfaces are reported for various conditions of temperature, concentration, etc. Residual amounts in the core were reported, as well as methods of analysis for less than 1-ppm boron concentration in rinse water. Degassing of the moderator to prevent bubble formation during temperature-coefficient measurements is also described.

Soluble-poison studies also have been conducted with cadmium sulfate solutions.[31] Cadmium solutions, which are alternatives to boron solutions as reactor poisons, were studied in detail to determine the circumstances under which irreversible deposition occurs on reactor components. Quantitative laboratory measurements were made with various surface finishes, both aluminum and zirconium components, and with variations of temperature, *p*H, etc., with 13-ppm cadmium solutions.

Water-Reactor Data Generally Verify Theory

By Charles N. Kelber

The growth of low-enrichment light-water-cooled and -moderated power-reactor technology has in large measure been predicated upon a massive amount of experimental and theoretical work in reactor physics. Although some discrepancies remain, a recent summary[32] demonstrates basic agreement between theory and experiment for these systems. Thus reactor theory can be used confidently as the major predictive tool in the design of these systems.

Material Buckling

Material-buckling measurements and calculations are compared and examined for systematic error. Two methods are in common use for measuring material buckling: "flux shape" and "variable loading." The flux-shape method, which uses a fit to activation traverses, has a major difficulty in that data from points near the lattice boundary must be rejected and, especially in small systems, the detector response depends on the system size. The variable-loading method involves measuring the axial flux distribution for each of many different-sized loadings of the lattice. A two-parameter least-squares fit to the axial buckling vs. lattice radius yields the reflector savings and material buckling. The basic assumption that leads to systematic error is the constancy of the radial-reflector savings. Theory predicts that this is not so, but to remove this assumption requires a three-parameter least-squares fit, with a loss of accuracy, in general.

Similarly, a number of systematic errors were found in theoretical analysis. Three chief sources were (1) use of incorrect thermal-neutron cross sections for ^{235}U, (2) neglect of the effect of cladding on the Dancoff correction,

Digitized by Google

and (3) overestimation of the fast effect. Buckling data were sorted for 96 lattices, and theory was compared with the experiment. For the 11 lattices with the smallest reported error in buckling, the predicted k_{eff} had an average value of 0.9992 ± 0.0016 instead of 1.0. For 55 lattices the average predicted k_{eff} is 0.9988 ± 0.0027. The greatest discrepancy, as expected, is in predicting the properties of closely packed lattices. The authors conclude that the "usual four-group theory" systematically underestimates the worth of the radial reflector.

Ratio of ^{238}U to ^{235}U Fissions

A quantity directly related to the fast effect is the ratio of fissions in ^{238}U to those in ^{235}U, δ^{28}. The determination of δ^{28} depends on knowledge of a function $P(t', t)$, the ratio of measured activity per fission in ^{235}U to that from ^{238}U; t' is the irradiation time, and t is the time between shutdown and measurement of the activity. Uncertainties in $P(t', t)$ contribute an error of 5% to δ^{28}. For specific fission products such as ^{140}La, the function $P(t',t)$ is a constant, but the relative yields are uncertain.

Fast-effect calculations are fundamentally homogeneous-mixture calculations, but heterogeneity calculations show that the rod advantage factor can yield as much as 1% in k_{eff} and 25% in δ^{28}. These effects can be treated accurately enough by a one-group treatment of neutrons above the fast-fission threshold in ^{238}U. Monte Carlo calculations using the MOCA-2 code[33] agree excellently with experiments. A simple relation can be obtained from a two-region representation of the lattice cell. The fast advantage factor (ratio of average flux in the fuel to that in the moderator) ξ^{28} can be represented by

$$\xi^{28} = 1 + V_1/V_0\beta\Sigma_1 l_0$$

where V_1 = moderator volume
V_0 = fuel volume
Σ_1 = removal plus absorption cross section of the moderator
l_0 = mean chord length of the fuel
β = a numerical factor that can be related to the chord-length distributions in fuel and moderator
β = 0.67 for a single rod and approximately 0.45 for typical light-water lattices

A second result is that δ^{28} (effects of leakage neglected) is given by

$$\delta^{28} = \delta^{28}_{\infty}\,\bar{l}/(\gamma + \bar{l})$$

where $\bar{l}$ is $l_0 + V_0/\Sigma_1 V_1$, γ is the mean free path in the fuel augmented by fast fission, and δ^{28}_{∞} is the fission ratio in an infinite block of fuel. This representation works best for closely spaced lattices.

Resonance Capture in ^{238}U

Measurement of this quantity or of the related ratio ρ^{28} (epicadmium to subcadmium capture ratio) is too inaccurate to evaluate the various theoretical methods available. Although some progress is being made, the authors feel that "... new and improved experimental methods are necessary to resolve the problems of resonance-neutron capture in light-water lattices."

Thermal-Neutron Distributions

Errors in measurement of thermal-neutron spatial and spectral distribution by means of foil activation stem in part from perturbations of the flux by the foil holder. Another source of error is reduced by careful selection and calibration of foils. Theoretical techniques in common use are the MARC-2B (Ref. 34) and THERMOS[35] codes and the Nelkin scattering kernel.[36] Predicted and measured spectra and distributions are in good agreement, but discrepancies of 1 to 5% in the disadvantage factors remain.

An important source of theoretical error is the treatment of the boundary, especially in closely packed lattices. Use of a condition of isotropic return eliminates most of this source of error.

Reactivity Changes with Long Irradiation

By Bernard I. Spinrad

As plant capital costs go down, reactor fueling costs become a larger fraction of power cost. Therefore the incentive to reduce fuel-cycle costs in reactors becomes greater, and

Digitized by Google

the impact of even small cost reductions becomes more significant. The ability to understand and predict the isotope and reactivity history of the reactor and its fuel is the major physics contribution to fuel economy.

Fuel-Management Methods

There are three general regimes of fuel management, and these depend on the specific power of the reactor. For reactors of low specific power and long fuel residence times (several years), reactivity changes are small over appreciable lengths of time; then, because the problem is to schedule fuel loading and unloading most advantageously, reactivity-change studies emphasize the achievement of criticality under steady-state fuel management. (The same situation holds for higher specific-power reactors if they have rapid fuel-change mechanisms, as do CANDU and the newer British gas-cooled reactors.)

For reactors of somewhat higher specific power, such as most of the higher power water reactors, refueling is not done frequently enough to be used as the major means of reactivity control. Because fuel residence times are from one year to a few years, reactivity changes appreciably during irradiation, requiring the use of control systems for major shimming. The change of flux shape and spectrum under irradiation, coupled with the fact that these changes also depend on the means of control adopted, become important. However, appreciable reactivity is also manageable by zoned or other forms of graded fuel loading, and some relocation of fuel elements at reloading times is possible.

At very high specific power, refueling time becomes a major economic factor; unless on-line fueling is adopted, fuel lifetime is limited by the excess reactivity loaded and the method of controlling this reactivity. One or two, or at most three, running periods exist between load and discharge of an element, and only very limited fuel management can be employed. The physics of control and of isotope — and flux — change as a function of position becomes the overriding problem.

A survey of papers presented at the Geneva Conference provides the opportunity of reviewing this important field. Future issues of this journal may then report further progress.

Prediction and Measurement

Four major papers were presented on this subject — one each from the United States, United Kingdom, Canada, and France.

Light-water reactor physics was emphasized in a bibliographic review of the status of U. S. technology.[37] Light-water power reactors tend to have rather high specific powers and long refueling times. Therefore the emphasis is on calculation of reactor changes over long irradiation, with fuel-management studies being less developed. References are given to the depletion and flux-evolution codes that have been used and are recommended. Because the detailed evaluation of a three-dimensional reactor, with control system, as a function of time is an expensive process even with modern computing machinery, there has been a recent trend toward reactivation of few-group diffusion theory and few-region flux synthesis, with very good results reported. These methods are all cited in the paper's bibliography. The authors conclude that calculational methods are, by and large, adequate and that the next improvement in predictive capability will come from isotopic analysis of irradiated fuel and its correlation with improved basic cross-section data.

Gas-cooled-reactor fuel management was studied in the United Kingdom.[38] Because these reactors are capable of virtually continuous refueling, the details of flux-shape evolution are unimportant, and the scheduling of regional fuel relocation is the major problem. No recommendations are made; the antagonistic aims of uniform power (maximum equilibrium reactivity on the reactor fringes) and maximum fuel residence time (maximum reactivity at the center) must be evaluated in detail for any set of reactor economic criteria.

Experimental burnup physics studies were described in a status report on the French program.[39] The report is of value, first, as a bibliography of pertinent French work (mostly CEA reports), and, second, as a good example of the sort of coordinated experimental program required to understand integral properties of irradiated fuels. To calibrate single-sample measurements on irradiated samples, the program features measurement of clean plutonium–uranium fuels as regional lattices in substitution experiments. The fuel enrichments are low, as would be employed in heavy-water reactors.

Digitized by Google

The D_2O reactors, particularly CANDU, benefit from comparisons of theoretical and experimental isotope—and reactivity—changes in D_2O reactors. The Canadian program, which is possibly the most integrated one of theory and measurement for a single reactor type, was described in detail.[40] The computational model used is the standard two-group four-factor formula with, however, each term rationalized for both logical correctness and experimental verifiability. As irradiation proceeds, effective cross sections and resonance integrals are varied to account for changes in neutron spectrum and isotopic concentrations. Fission-product cross sections have been measured and reported. The effect of radial nonuniformity of burnup in a rod has been investigated and found to be small owing to canceling effects of plutonium and fission products. The conclusion is that reactivity change in a D_2O reactor can be predicted closely—0.1% or so in reactivity, corresponding to ±10% of a 10,000 Mwd/metric ton lifetime.

Operating Experience

The measurement and prediction of reactivity changes in British gas-cooled reactors were described in some detail.[41] By frequent rod recalibration, both reactivity change and temperature coefficient of reactivity have been followed up to several hundred megawatt-days per metric ton. Reasonably good theoretical fit is obtained with a two-group reactor model, in which the neutron temperature is obtained by a thermal-spectrum calculation and self-shielding of plutonium resonances is computed in detail as a function of local plutonium concentration.

Reactivity experiments after irradiation of natural uranium, ^{235}U, and ^{233}U in the Materials Testing Reactor (MTR) were reported.[42] Although the irradiation spectrum in the MTR is not very characteristic of a power-reactor history, the results of the natural-uranium irradiations provide a valuable checkpoint for theoretical methods since they extend to 15,000 Mwd/metric ton. This work has been reported previously.[43] The experiments agree well with a standard depletion code. The ^{235}U and ^{233}U experiments serve as measures of the effective cross section of stable and long-life fission products (after the xenon transients, which they also measured, had decayed). An effective $1/v$ cross section of approximately 50 barns (for each fission caused by 2200 m/sec neutrons, *not* per fission product), in good agreement with theory, is found for several irradiations. A resonance integral between approximately 170 and 210 barns per fission is also reported, which is about 10% lower than theoretically estimated.

Burnup experience with the Novo-Voronezh reactor (WWER) was described without going into details of fuel or control management or of evaluation methods.[44] An initial fuel enrichment of 2% permits operation to a discharge burnup of 12,000 Mwd/metric ton.

Calculations

A method for calculating global flux changes during irradiation was reported without presentation.[45] The method uses two-group theory and a simplified method for solving the Helmholtz equations in a few-region system.

Local reactivity as calculated by standard depletion codes fits remarkably well to a quadratic in flux time.[46] With this simplifying assumption, analytic expressions for reactivity lifetime can be obtained for a variety of fuel-management schemes. Amusingly, this paper cites no Western references, even though the work is similar in spirit to Canadian and U. S. work reported at the 1955 Geneva Conference.

The use of soluble and burnable poison in water reactors was evaluated.[47] No reactivity experience is listed in the paper, which is to be considered rather as a bibliographic source. Soluble- and burnable-poison control-physics calculations are key problems in reactivity calculations for high-specific-power reactors because the errors in predicting control margin are comparable to the normal errors in reactivity-change prediction.

Improvements in Resonance-Integral Theory

By Paul F. Gast

During the slowing-down process, neutrons may be captured by the reactor materials

Digitized by Google

through the action of resonances. Because such captures in ^{238}U or thorium make important contributions to fissionable-material production, they have been studied extensively. Thus neutron-capture rates in ^{238}U and thorium can be computed satisfactorily for simple fuel shapes by semiempirical methods. However, captures in other materials or in more complicated fuel shapes require theoretical treatment, at least in the exploratory conceptual design stages. Work on resonance-integral theory began in the University of Chicago Metallurgical Laboratory days. Some recent developments are reported here.

It is now possible to calculate resonance integrals for isolated resonances to an accuracy limited only by a knowledge of the resonance parameters and by the time and effort appropriate for the case in hand. Monte Carlo methods have been available for some time; recently, numerical analytical techniques have been applied to these problems.

The collision densities and fluxes for homogeneous mixtures of uranium and carbon have been obtained for the 6.7-, 21.0-, and 36.8-ev resonances of ^{238}U by numerical solution of the integral equation.[48] A well-moderated case and one with very little moderation were considered. Although the results are unlikely to find direct application in reactor design, the paper has considerable didactic value because the six cases considered nicely illustrate most of the features of resonance absorption that are neglected in the usual approximations.

A similar solution for a uranium cylinder in a graphite lattice has been worked out for the 6.7-ev resonance only.[49] Details of the method have not been published, but isotropic scattering was assumed, and a polynomial approximation of the transport kernel was used.

In reactor design work such calculations are not usually feasible, so most theoretical attention has been directed toward less laborious methods that give accuracies appropriate for reactor work. The intermediate-resonance method[50] has been extended to the heterogeneous case[51] by the use of equivalence principles. A physical interpretation of the method[52] permits easy computation of the "width parameter" and extension to Doppler-broadened cases.

Equivalence principles rest on two approximations: (1) the assumption of a flat source in computing the escape probabilities from the absorber and (2) the use of a rational approximation to represent the resulting probabilities. The errors arising from the flat-source assumption have been examined.[51,53] The basic approach is the same in both papers, but the method of Ref. 53 has the advantage of not being limited to thin slabs. Table II-1 shows the results obtained by numerical integrations, which depend on the amount of resonance scattering and the slab thickness (in potential scattering mean free paths). Presumably, similar values would apply for other simple convex shapes with the same surface-to-volume ratio; appreciable errors occur when the resonance is a strongly scattering one.

Table II-1 PERCENT ERRORS FROM FLAT-SOURCE APPROXIMATION[53]

Slab thickness	Neutron width/resonance width, Γ_n/Γ			
	0.2	0.4	0.6	0.8
0.0	1.1	2.7	5.5	11.5
0.3	1.3	2.9	5.7	11.7
0.6	1.6	3.2	6.0	11.9

Improvements in the rational approximation are the subject of continuing investigation, and three recent efforts were described in the Summer 1965 issue of *Power Reactor Technology*.[54] An additional formulation has been reported,[55] and its extension to nonblack tubular absorbers has been developed.[56]

References

1. D. P. Moon, Consistent Heavy-Atom Cross-Section Evaluation for Plutonium Recycle Calculations, USAEC Report ANL-6972, Argonne National Laboratory, December 1964.
2. G. D. Joanou and J. S. Dudek, GAM-I: A Consistent P_1 Multigroup Code for the Calculation of Fast Neutron Spectra and Multigroup Constants, USAEC Report GA-1850, General Dynamics Corp., June 28, 1961.
3. G. D. Joanou et al., Nuclear Data for GAM-I Data Tape, USAEC Report GA-2451, Vols. I and II, General Dynamics Corp., Aug. 22, 1961.
4. R. C. Liikala, Updated RBU Basic Library, USAEC Report HW-75716, Vols. 1, 2, 3, Hanford Atomic Products Operation, 1963.
5. D. A. Klopp and W. E. Zagotta, Resonance Integral Determination, ARF Progress Report A-1918-8, Illinois Institute of Technology, Armour Research Foundation, March 1962.
6. F. T. Adler, G. W. Hinman, and L. W. Nordheim, The Quantitative Evaluation of Resonance Integrals, in *Proceedings of the Second United Na-*

Digitized by Google

tions International Conference on the Peaceful Uses of Atomic Energy, Geneva, 1958, Vol. 16, pp. 155-171, United Nations, New York, 1958.
7. H. Amster, The Calculation of Thermal Constants Averaged Over a Wigner-Wilkins Flux Spectrum: Description of the SOFOCATE Code, USAEC Report WAPD-TM-39, Westinghouse Electric Corp., Bettis Atomic Power Laboratory, January 1957.
8. B. Carlson, C. Lee, and J. Worlton, The DSN and TDC Neutron Transport Codes, USAEC Report LAMS-2346, Los Alamos Scientific Laboratory, February 1960.
9. D. J. Hughes, B. A. Magurno, and M. K. Brussel, Neutron Cross Sections, USAEC Report BNL-325 (2nd ed.) (Suppl. 1), Brookhaven National Laboratory, Jan. 1, 1960.
10. E. M. Pennington, Argonne National Laboratory, in preparation.
11. Q. L. Baird and A. R. Boynton, Bucklings, Disadvantage Factors, and δ^{28} Measurements in Some Undermoderated Slightly Enriched Cores, *Trans. Am. Nucl. Soc.*, 6(1): 258 (1963).
12. Q. L. Baird et al., Initial Conversion Ratio and ρ_c^{28} Measurements in Very Undermoderated Slightly Enriched Oxide Cores, *Trans. Am. Nucl. Soc.*, 7(1): 80 (June 1964).
13. A. R. Boynton, Experimental Thermal-Disadvantage Factors in Some Very Undermoderated, 3%-Enriched Water-Uranium Oxide Lattices, *Trans. Am. Nucl. Soc.*, 8(1): 249 (June 1965).
14. L. C. Schmidt, R. C. Liikala, W. P. Stinson, and J. R. Worden, Critical Masses and Bucklings of $PuO_2-UO_2-H_2O$ Systems, *Trans. Am. Nucl. Soc.*, 7(2): 216 (1964); USAEC Report HW-83187, Hanford Atomic Products Operation, July 1964; USAEC Report HW-84608, Hanford Atomic Products Operation, June 15, 1965.
15. D. H. Carter et al., Buckling and Reaction Rate Experiments in Plutonium/Uranium Metal Fueled, Graphite Moderated Lattices at Temperatures Up to 400°C, Part I. Experimental Techniques and Results, British Report AEEW-R-318, July 1964.
16. D. H. Carter, B. J. Puckett, and A. E. Richards, Measurements of $Pu^{239}:U^{235}$ Fission Ratio Using Foils at Temperatures Up to 400°C, British Report AEEW-M-447, May 1964.
17. R. C. Bannerman, H. H. W. Pitcher, and R. Richmond, Analysis of the Results of Reactivity Change Measurements on Plutonium-Uranium Fuel Elements, British Report AEEW-M-441, July 1964.
18. D. Breton and P. LaFore, Experimental Methods in Thermal Reactor Physics, presented at the Third United Nations International Conference on the Peaceful Uses of Atomic Energy, Geneva, 1964, Paper A/Conf.28/P/102.
19. F. Congé, Mesures Globales de Reseau a Graphite dans l'Empilement Critique Marius, French Report CEA-R-2478, August 1964.
20. F. Cogné and J. Journet, Mesures Fines dans les Reseaux Graphite, French Report CEA-R-2479, 1964.
21. O. Tretiakoff et al., Mesure des Sections Efficaces Effectives d'Echantillons Fissiles par une Methode d'Oscillation dans les Assemblages Critiques, French Report CEA-R-2487, August 1964.
22. J. Valat and T. E. Stern, Analyse de la Precision de Certaines Methodes de Mesure des Tres Basses Reactitivities, French Report CEA-R-2229, August 1964.
23. R. Naudet et al., Experiences Critiques dans Aquilon Portant sur des Combustibles Legerement Enrichis en U^{235} et en Plutonium, French Report CEA-R-2477, August 1964.
24. M. F. Ithurralde et al., Interpretation des Experiences de Criticite sur des Solutions Homogenes de Plutonium et d'Uranium, French Report CEA-R-2488, August 1964.
25. D. Breton and C. Clouet d'Orval, Etudes de Criticite, presented at the Third United Nations International Conference on the Peaceful Uses of Atomic Energy, Geneva, 1964, Paper A/Conf.28/P/84.
26. J. G. Bruna et al., Alecto, Experiences de Criticalite sur une Solution de Plutonium. Resultats Experimentaux, Cuve No. 1, French Report CEA-2274, 1963.
27. J. G. Bruna et al., Alecto 1—Experience de Criticite sur une Solution de Plutonium et d'Uranium Enrichi a 90%. Resultats Experimentaux et Calculs Concernant la Cuve No. 2, French Report CEA-R-2453, June 1964.
28. E. Deilgat et al., Experiences de Criticite sur des Cylinders Annulaires Contenant des Solutions de Plutonium, French Report CEA-R-2495, June 1964.
29. E. D. Clayton, Progress in Plutonium Critical Mass Physics, USAEC Report HW-83603, Hanford Atomic Products Operation, October 1964.
30. J. Bailly et al., Etude des Reseaux a l'Eau Legere par la Methode d'Empoisonnement Homogene au Bore, French Report CEA-R-2489, August 1964.
31. O. Croix et al., Utilisation du Cadmium en Solution dans le Moderateur du Reacteur EL_4, Fixation Irreversible du Cadmium sur les Surfaces Metalliques, French Report CEA-R-2504, August 1964.
32. Glenn A. Price and R. L. Hellins, Lattice Studies in Light Water Moderated Systems, presented at the Third United Nations International Conference on the Peaceful Uses of Atomic Energy, Geneva, 1964, Paper A/Conf.28/P/264.
33. H. Rief, An IBM 704 Monte Carlo Code To Calculate the Fast Effects in Homogeneous and Heterogeneous Systems, USAEC Report BNL-647, Brookhaven National Laboratory, Jan. 1, 1961.
34. E. M. Gelbard, H. B. Ondis, and J. Spanier, MARC—A Multigroup Monte Carlo Program for the Calculation of Capture Probabilities, USAEC Report WAPD-TM-273, Westinghouse Electric Corp., Bettis Atomic Power Laboratory, May 1962.
35. H. C. Honeck, THERMOS. A Thermalization Transport Theory Code for Reactor Lattice Calculations, USAEC Report BNL-5826, Brookhaven National Laboratory, September 1961.
36. M. Nelkin, Scattering of Slow Neutrons by Water, *Phys. Rev.*, 119(2): 741-746 (July 15, 1960).
37. G. H. Minton and H. W. Graves, Jr., Calculation of Criticality, Power Distribution, and Fuel Burnup in Thermal Power Reactors, presented at the Third United Nations International Conference on the Peaceful Uses of Atomic Energy, Geneva, 1964, Paper A/Conf.28/P/266.
38. B. Cutts, A Study of Fuel Cycles and Fuel Cycle Problems for Advanced Gas Cooled Graphite

Digitized by Google

Moderated Reactors, presented at the Third United Nations International Conference on the Peaceful Uses of Atomic Energy, Geneva, 1964, Paper A/Conf.28/P/177.

39. O. Tretiakoff, Burn Up Physics, presented at the Third United Nations International Conference on the Peaceful Uses of Atomic Energy, Geneva, 1964, Paper A/Conf.28/P/77.
40. M. F. Duret et al., Fuel Burn-Up and Reactivity Changes, presented at the Third United Nations International Conference on the Peaceful Uses of Atomic Energy, Geneva, 1964, Paper A/Conf.28/P/26.
41. H. A. Hughes, D. A. L. Clinch, R. M. Horsley, D. J. Millard, and R. Razzell, Experimental Basis of Power Reactor Operation, presented at the Third United Nations International Conference on the Peaceful Uses of Atomic Energy, Geneva, 1964, Paper A/Conf.28/P/170.
42. R. G. Nisle, D. R. deBoisblanc, E. Fast, J. C. Connor, and S. B. Gunst, Fission-Product Build-up and Long-Term Reactivity Effects, presented at the Third United Nations International Conference on the Peaceful Uses of Atomic Energy, Geneva, 1964, Paper A/Conf.28/P/269.
43. S. B. Gunst, E. D. McGarry, and J. J. Scoville, The Reactivity of Natural UO_2 Irradiated to 6×10^{21} n/cm^2, *Nucl. Sci. Eng.*, 7: 407-418 (1960).
44. L. V. Kommisarov, G. L. Lunin, A. N. Novikov, V. A. Sidorenko, and V. P. Sidorenko, Physical Studies of Novo-Voronezh Atomic Power Station, presented at the Third United Nations International Conference on the Peaceful Uses of Atomic Energy, Geneva, 1964, Paper A/Conf.28/P/585.
45. F. Accinni, R. Bonalumi, C. Bruschi, F. Palazzi, S. Rubbia, and G. B. Zorzoli, The Physics of a Steam-Water Mixture-Cooled Heavy Water Power Reactor, presented at the Third United Nations International Conference on the Peaceful Uses of Atomic Energy, Geneva, 1964, Paper A/Conf.28/P/625.
46. V. Bartosek, M. Hron, V. Lelek, and M. Neprasove (Prague), On Some Physical Problems of Uranium Burnup in Heavy Water Reactors, presented at the Third United Nations International Conference on the Peaceful Uses of Atomic Energy, Geneva, 1964, Paper A/Conf.28/P/630.
47. A. Radkowsky and R. J. Creagan, Poison Control of Thermal Reactors, presented at the Third United Nations International Conference on the Peaceful Uses of Atomic Energy, Geneva, 1964, Paper A/Conf.28/P/274.
48. Hans-Jürgen Siegert, Das Neutronenspektrum in der Umgebung von Resonanzen, *Nukleonik*, 6(6): 307-310 (October 1964).
49. F. T. Adler and E. E. Lewis, Comparison of Exact and Approximate Treatments of Resonance Effects in Cylindrical Lattices, *Trans. Am. Nucl. Soc.*, 7(1): 29 (June 1964).
50. R. Goldstein and E. R. Cohen, *Nucl. Sci. Eng.*, 13(2): 132 (June 1962).
51. R. Goldstein and H. Brooks, Intermediate Resonance Absorption in Nonhomogeneous Systems, *Nucl. Sci. Eng.*, 20(3): 331-337 (November 1964).
52. Guido Forti, Evaluation of Resonance Integrals in Homogeneous and Heterogeneous Systems — An Intermediate Approximation, *Nucl. Sci. Eng.*, 19(4): 449-457 (August 1964).
53. J. Berg, The Flat Source Approximation in Resonance Integral Calculations, *Nukleonik*, 6(4): 202-209 (July 1964).
54. *Power Reactor Technol.*, 8(3): 159-160 (Summer 1965).
55. H. Neltrup, An Approximate Collision Probability Formula for Resonance Integrals, *J. Nucl. Energy, Pt. A & B*, 18: 704-708 (December 1964).
56. H. Aisu, Effective Surface of a Tubular Absorber in the Calculation of Resonance Integrals, *Nucl. Sci. Eng.*, 21(2): 250-255 (February 1965).

Digitized by Google

Section

III

Power Reactor Technology

Control and Dynamics

Reactor Control Experience

By Joseph M. Harrer

Control-system designers sometimes introduce plant features that, although good in principle or in laboratory tests, do not always work out according to plan when the plant is operated. Thus the experience with control equipment and the failure analyses that were aired at the Conference on Reactor Operating Experience (sponsored by the Reactor Operations Division of the American Nuclear Society) are significant for designers. One attendee's summary and interpretations are given here.

Reactor Accident Frequency

The general opinion exists that reactor accidents are unusual occurrences. Over a period of a little more than 20 years, all types of reactors and critical experiments have amassed a total of more than 1000 years of operating history. Despite the fact that many of these devices were of new or experimental configurations, no member of the general public has ever been overly exposed to radiation or suffered inconvenience from a reactor accident.[1] But during these 20 years there have been about 20 accidents or incidents that resulted in prompt criticality, crew fatalities, or massive damage to the plant. At least half of these accidents would not have occurred if the reactor safety systems had operated correctly.

Components Have Been Reliable. In an effort to prevent reactor excursions, reactors still are being built with equipment that automatically checks safety-system performance as frequently as once per second. The object of these tests is to detect safety-component failure before any reactor excursion occurs. But the actual record of one uncontrolled excursion per million operating hours shows that not one of them resulted from failure of a safety-system component.

The System Must Be Able. Some excursions occurred when the safety system lacked proper input information; several failures resulted from slow response by the safety system. In at least two cases, the safety system was paralyzed by the accident; in another case the accident was intensified by safety action—and in still another case the accident was caused by an attempt to scram the reactor. Thus, rather than being related to component failure or lack of reliability, these performance failures occurred because the safety systems were inherently unable to protect the reactors. Clearly, although it is impossible to anticipate or simulate the exact conditions under which the safety system must perform, much more must be done to make tests uncover more than just component failure. In this way designs and operating procedures can be corrected so as to prevent uncontrolled excursions.

Although the statistical experience of one uncontrolled excursion per million hours was acquired with all sorts of reactors and critical experiments—and thus is not really applicable to the situation in which we are operating proved and stably operated reactors—its importance can be appreciated from the facts that (1) most reactors today have higher powers and greater fission-product inventories and (2) direct extrapolation of these statistics would indicate (improperly, however) that, over a 25-year life, one out of four reactors would suffer an uncontrolled excursion that results in massive damage.

Digitized by Google

Perhaps a significant question is, "Have we been learning enough from experience?" Simple component testing is not the answer. Operators and designers must devolve tests and corrections that will prevent accidents more effectively.

Rod Problems

The primary safety device has always been control rods. Thus tests that detect impending trouble in control rods are important for preventing accidents. But how dependable is a test that simply assures the time for scram is less than a predetermined value? Not very dependable, according to experience with the UMRR (University of Missouri at Rolla, Reactor), a 10-kw swimming-pool reactor,[2] and with the 61-Mw Heavy Water Components Test Reactor (HWCTR) at Savannah River Laboratory.[3]

UMRR Rod Swelling. Each of the original shim-safety rods consisted of a type 304 stainless-steel shell lined with 30 mils of cadmium and filled with B_4C powder. Because such rods elsewhere have a history of failure, the UMRR rods were checked closely by measuring rod-drop times at six-month intervals. These tests were expected to yield information on the condition of the rods, particularly about swelling, as well as simultaneously checking the scram circuit.

But during one routine startup, control-panel instruments indicated that a control rod would not withdraw beyond 17 in. Inspection showed that the rod was hung at a partially withdrawn position. After the reactor was shut down, rod-drop times were measured and found to be normal for withdrawals of up to 16 in. After the core was dismantled and the suspect control rod was removed, measurement with a micrometer showed an 8.6% increase in rod thickness, which was enough to cause the rod to bind in its channel. Although similar measurements showed that the other two shim-safety rods had swelled 3.2 and 3.0%, rod-drop times gave no indication of this swelling.

A possible failure mechanism is that a shell leak allows water to accumulate in the rod, radiation decomposes the water, the gas pressure seals the hole by forcing damp B_4C powder into it, and subsequent water decomposition raises the pressure, which swells the shell.

The original rods in the UMRR have now been replaced by solid rods consisting of 18-18 stainless steel alloyed with 1.5% boron. As expected, these new rods have a measured worth 80% that of the original B_4C rods. This is more than adequate for the excess reactivity used in the UMRR. And, because of the greater reliability of the new rods, safer operation results.

The UMRR reactor staff concludes that, although rod-drop-time tests provide a good monitor on the total scram circuitry, they are not adequate for monitoring control-rod condition; for this, periodic direct inspection and measurement of rod dimensions are necessary.

HWCTR Rod-Guide-Tube Ruptures. The time measured in rod-drop tests is often judged as satisfactory if it is less than some standard value for a particular rod system. But experience at the HWCTR shows that a simple go—no-go test does not guarantee that failure is not in progress.[3] Safety-rod drop times were measured at HWCTR before each startup, analyzed for unusual results, and compared with previous results to indicate trends. When rod-drop time decreased, loss of snubbing action was the cause; the problem was traced to rupture of the Zircaloy-2 guide tubes for four of the six safety-rod assemblies. The rods had been in service for nearly three years.

The failures consisted of longitudinal splits starting at a transition in size of the guide tube. These tubes are 11.3 ft long, but the inside diameter of the bottom 3.4 ft is 1.310 in. (rather than 1.375 in. as in the upper section) to provide a $\frac{1}{4}$-in.-high transition piece for hydraulic snubbing action when the control rod drops. The splits were attributed to a combination of high residual stress in the necked-down area and cumulative tensile-stress pulses when the rods were snubbed.

The existence of residual stresses might have been expected. The upper and lower sections were of the same thickness, and the design called for absorbing the snubbing forces in tension in the lower section. This in itself leads to the second observation, that tension pulses contributed to the failure. It is well known that considerable tensile stress will develop under those conditions. The vertical tensile stress could have been eliminated by a bottom support for the guide tube, but the hoop stress that initiated the failures would remain. The correction involved lengthening the transition section from $\frac{1}{4}$ to 1 in. and changing the

Digitized by Google

specifications to assure less residual stress and higher ductility.

Further study of the tubes showed that D_2 content of the Zircaloy was 100 to 300 ppm, which is considered high; generally, the D_2 content at the transition piece was at the higher value. Other Zircaloy tubes that had endured the same reactor environment — but which were of low nickel content — did not display this high D_2 pickup and remained much more ductile when tested by completely collapsing the tubes. They did not crack even when fully collapsed. On the basis of these tests, an overall conclusion is that either Zircaloy-4 or low nickel Zircaloy-2 would be much better for use under the HWCTR conditions, which are 200 to 250°C, *p*D of 10 to 11 (at 25°C), chlorides less than 0.1 ppm, O_2 less than 0.1 cm^3 per kilogram of D_2O (0.14 ppm).

Gravity-Independent Rods

Gravity rod-insertion systems are as old as reactors themselves. But what if you do not have gravity acting in the proper direction at all times? A gravity-independent system with springs provided one answer.[4] The need arose because the Aerospace Shield Test Reactor (ASTR) had to be rotatable in two planes and positionable vertically for various shielding experiments. Thus, rather than heavy rods (on which gravity usually has a beneficial effect), a lighter rod had to be found for this reactor. Optimum performance was obtained by selecting a minimum thickness of silver–indium–cadmium by means of critical-experiment tests; in these tests a 0.200-in.-thick absorber was first tried in the critical assembly; then the silver–indium–cadmium was machined to 0.18, 0.15, 0.12, and finally to 0.100 in., at which thickness a sharp drop in effectiveness was observed. With the 0.125-in. thickness selected, each 24-in.-long rod weighs only 13 lb. Spring forces vary between 30 and 80 lb, with the higher force when the rod is fully withdrawn. Thus maximum and minimum forces are 6 and 2 *g*. Even if the reactor and rod are completely inverted so that gravity acts against the rod springs, the basic 1 *g* is always present to hold the rods in the shutdown position.

Springs Vs. Pneumatics. Gravity-independent rods are widely used on critical experiments, especially for fast reactors — where the assembly and the rods are operated horizontally (to make it easy to assemble fuel in trays), but in air rather than in water as is the ASTR. Many designers feel that air cylinders provide an adequate and neat stored-energy package and prefer them to springs. Assemblies of springs usually are much more bulky, and some mechanical designers do not consider them more reliable than a well-designed pneumatic system. But the big objection to pneumatic systems is that an oil explosion could suddenly wreck the entire system and rapidly remove the stored energy force. Although oil explosions in air storage systems can be prevented by using pumps that do not need an oil lubricant, self-lubricating pistons (for example, graphite rings) would also be needed in the scram cylinders. The pistons could be lubricated with high-flash-point oil, but this would not be an ideal solution.

The use of springs or pneumatic systems for stored energy in gravity-independent systems remains an open question. Designers and users are well-advised to keep abreast of pertinent experience and observe any failures realistically. It may well be that springs could be far superior when one considers the long-term maintenance problem and the fact that catastrophic failure of a spring is not likely if inspection is adequate.

Control of Critical Assemblies by Moderator Level

Usually the dumping of moderator from a critical assembly is considered a backup for control rods. But experience with moderator control at the Westinghouse Reactor Evaluation Center shows that variation of moderator level can be a useful primary control method.[5] The important principle is to vary the moderator level so that at the operating point the k_{eff} is approximately unity due to the upper reflector. Then the upper portion of the reflector is of decisive importance; lowering it will produce negative reactivity immediately even with the rods partially controlling the reactivity.

Use of the moderator as the basic control device is desirable when the cores being studied have nonhomogeneous fuel enrichments, dimensions, and cladding. Criticality is achieved first by movement of control rods and then by the exchange of reactivity in control rods and moderator until the rods are fully withdrawn.

Digitized by Google

Advantages. The achievement of uniform lattices requires complicated design and fabrication efforts if rods are used at all. Fueled followers (for control-rod slots) tend to produce core uniformity. But if any fuel protrudes into the lower reflector, nonuniformity is introduced. The coupling of control material to fuel represents a potential source of weakness in the rod structure, and, because a hazard is created, the absorber follower section could fall through the core. This type of problem calls for a meticulous design effort to assure safety. For a reduction in this time-consuming and costly work, and at the same time for an increase in the inherent safety, it is much better to rely on moderator-level control completely.

The most probable and most severe accidents considered in hazard analyses for critical facilities and reactors are presumed to come from rapid (step) movement of control material. Thus, in terms of positive insertion of reactivity, operation by moderator control is a significant step in the direction of safer operations because it eliminates a possible accident-creating component.

The ramp rate one obtains from moderator control is a single continuous variable, whereas the ramp rates of control rods vary with radial location; thus, for a given core, the operator does not have to be concerned with there being different ramps available at his fingertips. There is only one method of adding reactivity, and any mechanical failure in the moderator-fill system (leak, pipe failure, etc.) results in moderator loss and reactivity loss.

It has been argued that, with a high moderator level, the moderator reactivity differential effectiveness is low and then one has no rapid means of inserting negative reactivity. However, this argument tends to be countered by the fact that under such circumstances fast insertion of positive reactivity is not even possible.

The whole problem as discussed in Ref. 5 gives one side of one of the oldest arguments in critical-facility operation. Should one raise water with rods withdrawn ready to stop an uncontrolled reaction, or, knowing that the rods will prevent an uncontrolled reaction, should one leave the rods in place until the water moderator is fully in?

The usual method is a compromise. One or two rods are removed, then the water is raised, and later the other rods are raised to achieve a critical assembly. If moderator level alone is used, it is argued that first all rods should be raised and then the raising of the moderator should begin. However, in many assemblies this cannot be done without violating interlocks.

A strong case can be made for moderator-only control, but it is very difficult to prove that by itself it assures safety. If rods are present or even possible, it seems safer to use them in some way to limit the bulk moderator effect and then later achieve a uniform core by changing moderator level and exchanging moderator reactivity for rod reactivity as they are drawn out of the core.

Subcriticality Measurement

All reactor operators want a simple and sure way of measuring subcriticality during shutdown. Although this is one of the most difficult measurements to make in a power reactor, it can be done relatively well in "clean" critical assemblies and in low-power multiplication experiments. As always, the key factor is instrumentation—but, in theory, the measurement is always possible.

The measurement consists in comparing the neutron statistical variation at two or more frequencies. As the ratio of the low-to-high frequency amplitude increases, criticality is approached. But in a power reactor, the high gamma background makes this measurement difficult if not impossible. As a step toward circumvention of this problem, an experiment was performed in which a conventional 12 count/(sec)(nv) BF_3-filled detector was connected to a 20-Mc wide-band video amplifier by a 75-ohm-impedance transmission line.[6] A pulse width of about 100 $\mu\mu$sec was observed. Although neutron counting rates were higher, even with the wide-band electronics there was no significant improvement in gamma tolerance. This led to use of a lower-multiplication gas tube.

A boron-lined detector about 9 in. long by $\frac{1}{4}$ in. in diameter was selected. For greater sensitivity and efficiency, four prototype tubes were operated in parallel. One tube had a boron-coating thickness of 1 mg/cm^2 and was filled with argon–isobutane at a pressure of 250 mm Hg; the other three tubes were filled with argon–carbon dioxide to the same pressure, but their coating thicknesses were 0.8, 1, and 1.2 mg/cm^2. The detectors were checked

Digitized by Google

with a neutron source, and spent fuel elements served as a gamma source. The typical count-rate response for various pulse-height settings shown in Fig. III-1 indicates only slight desensitization of the detector in a gamma field of 19,000 r/hr. Thus the author concludes that extension of the wide-band techniques with miniature boron-lined detectors will permit measurement of the reactivity of shutdown power reactors by noise-analysis techniques.

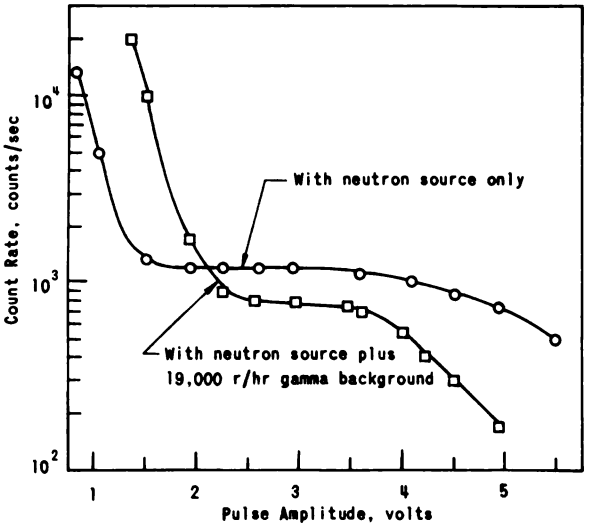

Fig. III-1 Count-rate response at various pulse-height settings for four miniature prototype boron-coated detectors operating in parallel shows that 19,000 r/hr gamma field desensitizes detector only slightly.[6]

Liquid-Poison Injection

Even with good instrumentation, fast safety circuits, and control rods to prevent and stop any uncontrolled excursion, reactor designers have always tried to install a backup system that could be used if the rods failed to control the reactor. A survey of the methods of backup protection used on reactors is given in *Nuclear Safety*, 7(1): 45-52. This backup often is in the form of a neutron-absorbing liquid poison, such as boric acid, that could be forced into the reactor coolant or moderator. But the design of such a system calls for a special approach. How fast should it operate? Should it be automatic or under procedural control? Is stored high-pressure gas a good force to inject poison into a pressurized reactor system? Experience with liquid-poison injection systems at Savannah River Laboratory can help answer such questions.

In the HWCTR[3] protection comes from injecting poison ($K_2B_4O_7-4H_2O$) into the coolant (D_2O) stream. The operator would actuate this system if the neutron flux fails to decrease after a scram signal. The solution has the same reactivity worth as the control rods, a minimum of 24% $\Delta k/k$. If uniformly distributed in the full 7000 gal of D_2O in the primary system, the poison would keep the reactor subcritical under all conditions.

The system was tested at least once a year during an outage by replacing the poison solution with D_2O and timing an injection; poison injection was never actually required during reactor operation.

As the system was originally designed and built, poison solution was delivered rapidly from a storage tank pressurized by helium from an external source. It was planned to adjust the helium pressure for the proper injection time, depending on whether the reactor was pressurized or unpressurized, and to determine the proper helium pressures experimentally during prestartup tests. These tests showed that this arrangement would not deliver the poison properly under certain combinations of reactor pressure and flow. On several occasions with the reactor unpressurized and when some D_2O was blown out of the tank, the main D_2O circulating pumps became gasbound by large volumes of helium.

These problems were avoided by the following changes: the pressure between the reactor gas space and the storage tank was equalized by connecting the reactor gas space to the poison storage tank, which was elevated about 50 ft above the reactor so that gravity would provide the driving force; an orifice was installed in the injection line to control the injection time. After these changes the remaining variable that affected the injection time was the coolant flow through the reactor. About half the system pressure drop is across the core—and thus between the reactor gas space and the moderator space where the poison is injected. Therefore the coolant flow in the reactor directly affects the driving force for injection.

Injection time must be quite a bit longer than the recirculation time of coolant to assure that enough poison is always in the reactor core. If too-rapid injection were allowed, each coolant-

Digitized by Google

flow cycle could sweep the poison completely out of the core and result in a power excursion. Table III-1 shows the amount of poison injected and compares its injection time to the D_2O circulation time for full flow and shutdown flow. This method was proved by test, and there was no gas binding in the pumps.

Table III-1 HWCTR POISON-INJECTION CHARACTERISTICS

	D_2O full flow	D_2O shutdown flow
D_2O circulation time, min	0.6	2.0
Poison total injection time, min	3.6	3.9
Total poison injected, gal	73	60

Actual injection of another neutron-absorber liquid was tested in a production reactor at Savannah River Laboratory.[7] This system injects $Gd(NO_3)_3$–D_2O solution directly into the D_2O moderator.

Important mechanical features of the system are that: (1) it operates on self-contained pneumatic power that is independent of other pneumatic or electrical networks, (2) injection is not automatic, but rather is initiated from the reactor control room in accordance with specified procedures, and (3) injection of $Gd(NO_3)_3$ starts not less than 5 sec after initiation of the signal but then is completed within 3 sec after injection is begun.

In a special test in a production reactor operating at power, reactor power began to decrease 3.5 sec after the system was actuated and had decreased to 50% after 6.5 sec. Reactor response to the poison injection is shown in Fig. III-2. (The poison was subsequently removed from the moderator by ion exchange.)

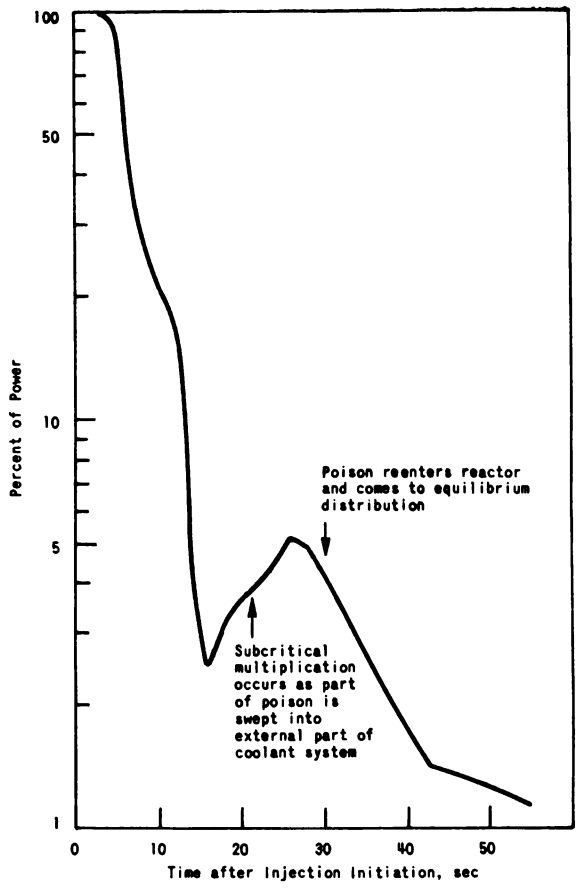

Fig. III-2 Rapid shutdown occurred when neutron-absorbent liquid was injected into reactor moderator.[7]

Computer Applications

The work of compiling a large amount of data accurately, quickly, and selectively is obviously the job for a computer. At Savannah River, the application of modern computer technology is helping ease operational problems.

An on-line digital computer[8] at the K production reactor there improves reactor safety and operating efficiency by providing more thorough surveillance and by compiling accurate operating information much faster than could be obtained otherwise. Signals from about 3200 thermocouples, flow and pressure meters, flux monitors, and other sensors provide information from all regions of the reactor.

Two types of data scans are provided: (1) a sequential scan of 2400 temperatures and flows in the 600 reactor-lattice positions, and (2) a random-access scan for nuclear instruments, in-core flux sensors, and miscellaneous sensors in the D_2O primary and H_2O secondary (river water) coolant systems.

Surveillance of reactor operating limits is an important function of the computer. Several types of fuel elements can be used in one reactor charge, and each may have distinct hydraulic characteristics and operating limits. Alarm programs compare reactor data with the appropriate limits for coolant flow, temperature, temperature rise, and bulk moderator (D_2O) temperature. An alarm is typed in red if an operating limit is exceeded. A periodic print-

Digitized by Google

out of the margin from the nearest limits is used by reactor operators to adjust reactor power level. Complicated limits, such as proximity to burnout heat flux, are calculated on demand with axial flux data from in-core sensors and fuel-coolant temperature data stored by the computer.

An analog system[9] was used to compute the safety margin from burnout in a special high-flux core [$> 4.3 \times 10^{15}$ neutrons/(cm^2)(sec)] in one of the D_2O-cooled and -moderated production reactors at the Savannah River Plant. The power density of greater than 130 kw per gram of ^{235}U was controlled with the aid of a direct-reading analog-computer circuit that displayed the safety factor against burnout of the fuel surface within an accuracy of 5%. The circuit compares the operating heat flux [$\sim 2.5 \times 10^6$ Btu/(hr)(sq ft)] to the heat flux at burnout as defined by the correlation

$$HF_B = 463{,}000(1 + 0.04V)[1 + 0.0167(T_s - T_b)]$$

where HF_B = heat flux at burnout in British thermal units per hour per square foot
V = coolant velocity in feet per second
T_s = coolant saturation temperature in degrees Fahrenheit
T_b = coolant bulk temperature in degrees Fahrenheit

For the burnout safety factor, the computer circuit solves the simplified equation

$$(BOSF)_x = \frac{(C_1 - C_2 x)\sum_{i=1}^{5} \Phi_i}{\Phi_x \Delta T} - \frac{C_3 \sum_{i=0}^{x-1} \Phi_i}{\Phi_x} - C_4$$

where Φ_x = relative power intensity measured by gamma-flux monitors at five vertical locations (x) equally spaced along the fuel surface
$\Phi_i = 0$ for convenience of notation
C_1 to C_5 = constants for fuel design, pressure, and velocity
ΔT = coolant temperature rise

For more information on control experience discussed at the same ANS meeting, see the article that begins on page 271.

References

1. E. P. Epler, Safety System Performance Failures, *Trans. Am. Nucl. Soc.*, 8(Suppl.): 49-50 (1965).
2. D. R. Edwards, Experience with Rod Drop Times at the UMRR, *Trans. Am. Nucl. Soc.*, 8(Suppl.): 53 (1965).
3. C. P. Ross, Performance of HWCTR Safety Systems, *Trans. Am. Nucl. Soc.*, 8(Suppl.): 50 (1965).
4. J. T. Pancoast, A Gravity Independent Reactor Control System, *Trans. Am. Nucl. Soc.*, 8(Suppl.): 51-53 (1965).
5. G. N. Hamilton, E. G. Taylor, and D. F. Hanlen, Design Considerations in Safety Analysis of Partial Moderator-Level Controlled Reactors, *Trans. Am. Nucl. Soc.*, 8(Suppl.): 49 (1965).
6. Irwin Bluestein, Neutron Measurements in High Gamma Backgrounds, *Trans. Am. Nucl. Soc.*, 8(Suppl.): 24 (1965).
7. L. A. Heinrich, Gadolinium Nitrate Injection as an Auxiliary Shutdown System for Savannah River Reactors, *Trans. Am. Nucl. Soc.*, 8(Suppl.): 58 (1965).
8. K. L. Gimmy and F. R. Field, On-line Computer Assists Reactor Operation at Savannah River Plant, *Trans. Am. Nucl. Soc.*, 8(Suppl.) 53-54 (1965).
9. E. S. Occhipinti, P. E. Mix, J. S. Stutheit, and F. R. Field, Analogue Computer Simplifies Operation of Savannah River High Flux Charge, *Trans. Am. Nucl. Soc.*, 8(Suppl.): 54-55 (1965).

Digitized by Google

Section

IV

Power Reactor Technology

Fluid and Thermal Technology

Highlights of the 8th National Heat Transfer Conference

By David Miller

Many papers of fundamental and applied interest for reactor technology were presented and discussed at the 8th National Heat Transfer Conference, Los Angeles, Aug. 9–11, 1965, which was jointly sponsored by the American Institute of Chemical Engineers and the American Society of Mechanical Engineers. Although many of the studies were sponsored by the U. S. Atomic Energy Commission (AEC) and have been published in project reports, most were being reported for the first time.

Topics discussed ranged from applications such as heat exchangers, packed beds, desalinization, and loss-of-coolant accidents in reactors to more fundamental studies of boiling and condensation, two-phase flow and pressure drop, and radiation and thermophysical properties.

Boiling and Two-Phase Flow

Boiling, two-phase flow, and stability received a major share of attention. In particular, studies of critical heat flux are of interest to reactor designers.[1–8]

Pertinent to the design of a greater than 600-psia forced-convection water-reactor system is a study in which the coolant entered cylindrical test sections of 0.1- and 0.2-in. inside diameters as a subcooled liquid and during certain tests left as superheated steam.[2] Emphasis was placed on the region with wall temperature higher than that corresponding to the critical heat flux where the surface temperature oscillations were not large; this region is often called the transition or partial film-boiling region. Experiments covered the pressure range 2420 to 3120 psia, mass flows of 0.5 to 2.5 $\times$ 10^6 lb/(hr)(sq ft), heat fluxes of 0.1 to 0.65 $\times$ 10^6 Btu/(hr)(sq ft), and exit qualities of 7 to 100%. These data were combined with other data[9] that extended down to 580 psi to obtain the equation

$$\left(\frac{hD}{k}\right)_f = 0.0193 \left(\frac{DG}{\mu}\right)_f^{0.80} \left(\frac{C_p\mu}{k}\right)_f^{1.23} \left(\frac{\rho_v}{\rho_b}\right)^{0.68} \left(\frac{\rho_v}{\rho_L}\right)^{0.068}$$

for flows of greater than or equal to 0.8 $\times$ 10^6 lb/(hr)(sq ft) over the range 580 to 3190 psia for steam qualities as high as 100%. This correlation has a 2σ probability limit of $\pm$19%. Density was calculated with a void-fraction-weighted sum of the gas and liquid densities; a homogeneous model was used to calculate the void fraction. This study showed that the two-phase entrance length and the length-to-diameter ratio have an important effect on heat transfer. Thermodynamic nonequilibrium found at low flows [0.5 $\times$ 10^6 lb/(hr)(sq ft)] was attributed to unevaporated water droplets passing through the test section; low-flow-rate data were not included in the correlation. The maximum heat-transfer coefficient after the critical heat flux occurred near or at 100% quality.

For a fog-cooled reactor concept, the "dry-out" heat flux (a term used to describe the critical or burnout heat flux at high steam qualities) was measured at mass velocities of 0.5 to 1.4 $\times$ 10^6 lb/(hr)(sq ft) and outlet qualities in the 38 to 78% range.[3] For two-phase inlet conditions, dry-out behavior of geometries simulating reactor fuels was investigated with: (1) angular misalignment of 0 to 60° between an unheated bundle upstream of the 19.25-in.-long heated bundle, (2) two bundle end geometries (CANDU-reactor type and flat-end), and (3) bundle-mounted stripping rings intended to

Digitized by Google

remove the parasitic water film from the unheated flow tube and redistribute it to the heated rods. All experiments were for a 19-rod bundle cooled by steam–water fog at 515 psia. Angular misalignment reduced the dry-out heat flux on some surfaces (usually inner elements) by as much as 20% but increased it on others (usually outer elements) by up to 70%. Stripping rings raised the dry-out heat flux by up to 100%.

The effects of upstream compressibility on subcooled critical heat flux were investigated.[4] Moderate upstream volumes of subcooled water were shown to have sufficient compressibility to promote oscillatory behavior, which greatly reduces the subcooled critical heat flux for a single channel. This oscillatory instability can be avoided only by operation to the right of the minimum in the overall pressure drop–flow curve characteristic of the heated section. Usually a flow restriction at the inlet of the heated section is needed to alter the overall characteristic so that stable critical heat fluxes can be obtained.

Although inlet-fitting losses make some systems inherently stable, it usually is necessary to provide another restriction at the heated-section inlet. The necessary throttling at the inlet can be estimated readily from

$$\frac{\partial(\Delta P)_{TS}}{\partial w} = 0$$

[where $(\Delta P)_{TS}$ is the pressure drop across the test section in pounds per square inch] if the heated-section hydraulic characteristics are known.

The influence of axially nonuniform heat fluxes on the departure from nucleate boiling (DNB) was studied.[7] Heat-flux distributions studied are shown in Fig. IV-1. For a limited range of parameters, the results are given in the form of a correction factor

$$F = \frac{C}{q''_{DNB,local} + 1 - \exp(-CL_{DNB})} \times \int_0^{L_{DNB}} q''(z) \exp\left[-C(L_{DNB} - z)_{dz}\right]$$

Here C is a coefficient defined as $h/\rho v s c_p$. Because the components of C are not known well enough to permit analytical evaluation, C was correlated by the equation

$$C = 0.44\,(1 - x_{DNB})^{7.9}/(10^{-6}\,G)^{1.72}\ \text{in.}^{-1}$$

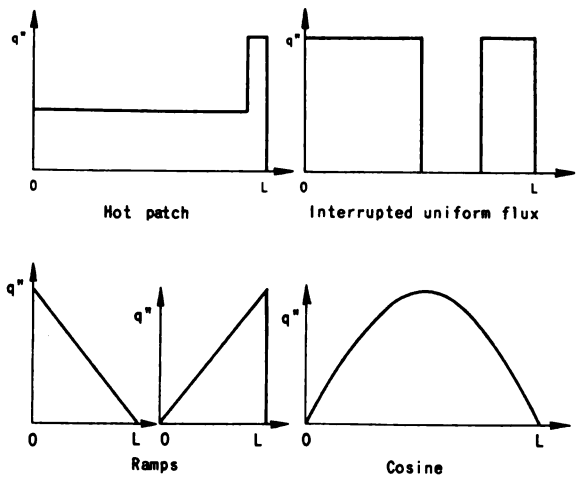

Fig. IV-1 Four shapes of heat-flux distributions were considered in studying how axially nonuniform heat fluxes influence the departure from nucleate boiling.[7]

Pool-boiling critical heat flux was studied by various investigators.[1,5,6,8] Saturated pool boiling on horizontal wire heaters of 0.0025 to 0.254-in. radii was measured[1] over a reduced-pressure (pressure divided by critical pressure) range of 0.0010 to 0.0197. The peak and minimum boiling heat fluxes were correlated with pressure and heater configuration (horizontal and vertical wires and flat horizontal plates) for five fluids: methanol, isopropanol, acetone, benzene, and water. All data can be represented by a single three-dimensional surface that is the product of a function of geometrical scale and a function of pressure. The function of pressure appears to be the same in any configuration. The effect of radius on critical heat flux for small wires at low pressures is significant and complex.

Experimental and analytical investigations of critical heat flux in pool boiling show that the addition of small amounts of calcium sulfate to distilled and deionized water allows increased boiling heat fluxes from stainless-steel heaters.[5] For a $\frac{1}{16}$-in. cylindrical stainless-steel heater coated with calcium sulfate, the critical heat flux was increased by 35%. Pool-boiling tests in water, with a porous graphite heater having air flow through its wall, decreased critical heat flux by 37% over the same heater with no air flow. If it is assumed that departure from nucleate to film boiling occurs when the heater surface becomes nonwetting at a temperature equal to the maximum

Digitized by Google

possible superheat for the liquid, it is possible to postulate a critical-heat-flux equation for the special case of a small-diameter heater. Significant variation in the critical heat flux with heater properties is predicted by this equation, which contains several coefficients that must be determined experimentally.

When the effects of thermal conduction on the critical heat flux and pool boiling were measured,[6] the critical heat flux of propanol that was boiling at atmospheric pressure on heater strips mounted horizontally in a saturated pool was seen to increase by a factor of 2 as the element conductance parameter, *kt* (which is the thermal conductivity times "effective" thickness of heater), increased in the range of 4.5 to 1680×10^{-4} watts/°C. A proposed analytical model qualitatively predicts these trends but does not agree quantitatively with the experimental data. The authors conclude that the prime reason that thin heat-transfer elements have lower critical heat fluxes is lower conductance and not lower heat capacity.

Designers concerned with space power units, fast reactor safety, and advanced reactor technology will be interested in studies of the critical heat flux for boiling liquid-metal systems.[8] Eighteen critical-heat-flux experimental data points were presented: two for sodium, eight for rubidium, and eight for water, all taken in the same apparatus. A correlation that represents 60 data points also includes data of other investigators for sodium and potassium; from it results the nondimensional equation

$$\left(\frac{q_c'' C_p \sigma}{\lambda^2 \rho_v k}\right) = 1.18 \times 10^{-8} \left(\frac{\rho_L}{\rho_v}\right)^{0.71}$$

where all values are at saturation conditions. This expression was modified by introducing the Prandtl number to the 0.71 power to include both metallic and nonmetallic data in a single dimensionless correlation

$$\left(\frac{q_c'' C_p \sigma}{\lambda^2 \rho_v k}\right) \mathrm{Pr}^{-0.71} = 1.02 \times 10^{-6} \left(\frac{\rho_L - \rho_v}{\rho_v}\right)^{0.65}$$

that is recommended for predicting the critical heat flux over a range of Prandtl numbers from 0.004 to 11; this correlation is shown in Fig. IV-2.

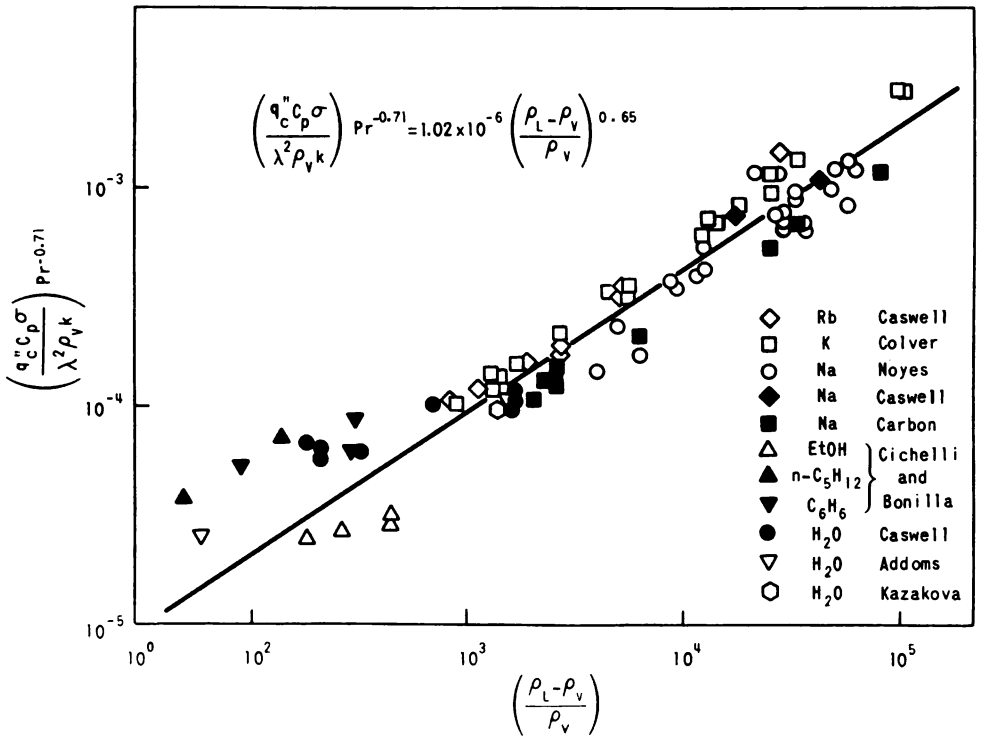

Fig. IV-2 Critical heat flux (q_c'') for various metallic and nonmetallic boiling fluids can be determined by means of a single dimensionless correlation.[8]

Digitized by Google

The boiling behavior of metallic liquids was also investigated.[10-12] How boiler surfaces ranging from highly polished mirror finishes to coarse, porous coatings affect nucleate pool boiling of sodium was studied.[12] Heat fluxes as high as 236,000 Btu/(hr)(sq ft) were attained at pressures below 1 atm with sodium at 1200 to 1500°F. The qualitative effects of roughness, aging, and hysteresis were determined. For reproducible data to be obtained, it was essential to employ uniform cleaning and filling procedures. Incipient nucleate-boiling heat flux vs. wall superheat were discussed, as were the effects of pressure and pool depth on the nucleate-boiling curve. The surface roughness and past history were found to affect significantly the incipient boiling, the nucleate-boiling wall superheat, and the slope of the boiling curve of sodium. The wall superheat required to initiate sodium nucleate boiling is significantly greater (at least a factor of 5) than that required to sustain it. Natural convection for a horizontal disk in pool boiling, particularly at low boiling heat fluxes, may appreciably influence sodium heat transfer. Clearly, nucleate-boiling heat-transfer data cannot be correlated without including the effect of surface conditions.

In a companion theoretical study of nucleate-boiling instability for alkali metals, a simplified theoretical model for bubble nucleation stability was proposed and an approximate stability criterion was developed.[10] This criterion contains both fluid and surface properties and predicts that nucleation for sodium should be unstable. Measurements of the effects of surface material and its chemical treatment, heat flux and cavity geometry on nucleation stability agreed with theoretical predictions. The stability criterion developed from an analysis of the bubble nucleation and dynamics is unique in that it includes the thermal properties of the surface, the cavity geometry, and the wetting behavior of the fluid. Inertial effects have been omitted. Only double reentrant type cavities appeared to be effective in maintaining nucleation stability of sodium. Thus an artificial nucleating site (such as a doubly reentrant type cavity, a patch of porous plate or porous weld, or a "hot finger") might be used to maintain stability in alkali-metal boilers.

A transient-quenching method of determining the critical heat flux and heat-transfer coefficients in film- and nucleate-boiling magnesium was presented.[11] A tungsten sphere, instrumented with thermocouples, was heated to 3100°R and then quenched in a boiling pool. As the sphere cools, its surface temperature and heat flux follow the boiling curve for the liquid metal being studied. Critical heat flux and heat-transfer coefficients in the transition- and nucleate-boiling regimes for subcooled (265°F) pool-boiling magnesium are included. Analytical predictions of the critical heat flux, however, were a factor of 5 to 10 higher. It was hypothesized that the low measured value of critical heat flux of magnesium was caused by the lack of wetting of the tungsten sphere by the magnesium during transition boiling.

Stability of Flow in Heated Channels

The interaction between hydrodynamics and heat transfer was studied analytically[13] and experimentally.[14] A very restrictive set of assumptions was applied in a theoretical calculation of the dynamic stability of flow oscillations in a heated channel.[13] The stability of this channel was investigated by applying the Hurwitz criterion after a perturbation solution of the usual equations. The resulting third-order characteristic equation shows that, under certain operating conditions, there exists both upper and lower stability bounds on the stability map. The analysis was applied to correlate experimental data of other investigators and to study the effects of various system parameters on system stability. The trends predicted agree with the limited range of experimental conditions (five points for two pressures by one investigator) for which the comparison was attempted.

Flow stability in multitube forced-convection vaporizers was investigated with a transparent closed test loop having Freon-113 as the test fluid.[14] Dimensionless simulation criteria were defined on the basis of the significant parameters determined from a literature survey. Conclusions and discussions are based on the measured data and high-speed photographs of two-phase flow in a five-tube boiler whose tubes had twisted-tape inserts. Stable flow was achieved by inserting an orifice at the entrance of each boiler tube to give pressure drops between 20 and 160% of the two-phase pressure drop. The importance of visual observations was stressed.

Digitized by Google

Theoretical Boiling Studies

Reactor designers will be interested in theoretical studies of boiling phenomena, including film boiling and bubble formation in nucleate boiling.

Film boiling was explored by several investigators.[15-18] The relation between bubble diameter and frequency of removal from a heated sphere during film boiling in saturated liquid nitrogen was studied,[15] as was the Leidenfrost phenomenon of film boiling of drops on a hot surface.[16-18] The vibrations and breakup of such a drop corresponded to those calculated from spherical-shell theory.[16] An analytical model for boiling heat transfer to waterdrops on a flat-plate-covered heat transfer to the waterdrop, heat transfer from the plate, and the heat-transfer coefficient for the special case where radiation can be neglected.[17] The effect of film boiling for large drops was measured experimentally and compared to theoretical analyses.[18] The maximum drop diameter and the minimum temperature difference for stable film boiling were predicted by stability considerations—similar methods have been suggested for nucleate boiling. These studies may be useful to estimate fuel-element cooling time after a reactor accident.

Bubble phenomena relevant to nucleate-boiling heat transfer were discussed.[19-21] The delay time, growth rate, contact diameter, and bubble size and shape at departure are interrelated.[19] A longer delay brings about faster growth, a larger contact diameter, and a bigger bubble at departure. Spherical bubbles have little or no delay time, slow growth, little contact area, and small size at departure; hemispherical bubbles have a long delay time, very fast growth, a large contact area, and a very large bubble volume at departure; oblate bubbles have intermediate values for all these factors.

Bubble shapes apparently can be explained in terms of inertial and surface-tension forces. For spherical bubbles, the surface-tension force is always greater than the inertial force, but for hemispherical bubbles the inertial force is dominant. For oblate bubbles, either can be dominant. Bubble departure diameters, departure velocities, and contact angles were measured by means of high-speed motion pictures of steady-state boiling.[20] A zirconium-ribbon heater insulated at its undersurface and edges was immersed in a pool of the liquid maintained at saturation temperature. Data for various liquids at subatmospheric pressure were represented by

$$D_d = 0.028\beta \left[\frac{g_c\sigma}{g(\rho_L - \rho_v)}\right]^{0.5} \left[1 + 0.0025\left(\frac{dD}{dt}\right)^{1.5}\right]$$

Mixtures are of interest for increasing boiling heat transfer and for determining the relative importance of thermal and diffusional resistances in the growth and formation of a bubble. Bubble growth rates were given for two mixtures.[21]

Condensation

Studies of condensation are of interest for the design of reactor equipment and, additionally, represent a phase change that is the inverse of boiling.

Laminar film condensation in two-phase channel flow was investigated in an analytical study that includes the interaction between the vapor and liquid interfaces and that proposes a dimensionless criterion for neglecting inertia and convection effects in the condensate film.[22] A relation was derived with the use of a universal velocity profile for predicting condensate-film heat-transfer coefficients for various surface-roughness heights.[23] Two regions were found—an upper limit corresponding to fully developed rough flow and a lower limit corresponding to hydraulically smooth flow. Some experimental data on the condensation of water gave results that fall between these two boundaries.

Film condensation of metal vapors has shown consistently lower heat-transfer coefficients than predicted from Nusselt's classical theory[24] or from more recent modifications of that theory. Kinetic-theory calculations to resolve this discrepancy between theory and experiment show that a significant thermal resistance can exist at the liquid–vapor interface of liquid metals.[25] This resistance increases with decreasing vapor pressure and depends on the value of an accommodation coefficient, named the "condensation coefficient." Experiments to verify this liquid–vapor interfacial-resistance hypothesis used mercury condensing on a vertical nickel surface at low pressures in the

Digitized by Google

absence of noncondensable gases. Because the condensation coefficient is a function of the state of the liquid surface, it is probably influenced by contamination in the experimental system and may vary with vapor pressure and temperature. Calculations for condensing metals at pressures significantly less than 1 atm should include the condensation coefficient. In practice, particular attention must also be paid to the presence of noncondensable gases in experiments and in operating equipment.

In certain cryogenic applications, heat exchange between condensing and boiling streams is limited by the condensing-side heat-transfer performance. This occurs primarily at high heat fluxes because condensing coefficients decrease with increasing heat flux. The Nusselt equation for film type condensation on a horizontal tube suggests that the coefficient increases in a multi-g acceleration field. More improvement would be expected if the resistance of the condensate layer to heat flow were reduced by a thin porous coating on the condensing surface. Results of condensation experiments in smooth and porous coated tubes under acceleration agree with the theory.[26] At the highest test acceleration of 325 g's, the condensing coefficient improved by a factor of at least 4.25 over that for 1 g with the same temperature driving force. At heat fluxes greater than 10,000 Btu/(hr)(sq ft), experimental coefficients were better than theory predicted; this was attributed to rippling of the condensate film with consequent enhancement of the heat-transfer coefficient. At 325 g's and with a heat flux of 20,000 Btu/(hr)(sq ft), condensation on a porous aluminum surface was 4.5 times better than on a smooth surface. Therefore the combined improvement over a smooth tube at 1 g was a factor of 19.1.

Experiments showed that radially grooved rotating disks reduced the condensing film resistance by some 65% but improved the rate of heat transfer through the disks by only 12 to 14%. In these experiments only a relatively small amount of the feed was evaporated, and thus most of the resistance to heat transfer was on the evaporating side.[27]

Dropwise condensation was discussed by Westwater in an invited lecture and in his papers,[28,29] which showed renewed interest in this method of improving condensing heat transfer. Dropwise condensation of water was shown to occur at active nucleation sites (and therefore should be termed nucleate condensation) whose number depends on the surface preparation and its subcooling.[28] The heat flux may be greater than, less than, or equal to that for filmwise condensation at the same temperature difference, depending on the active-site population. Exact calculation of the heat flux requires an involved iterative technique to account for the nucleation, growth, and coalescence of every drop. The functional relation between the temperature difference and active-site population is unknown for any surface. Oleic acid[29] promoted dropwise condensation of ethylene glycol on a copper condenser when the surface was cooler than 290°F. Correlation of data over a wide range of variables was achieved through modification of an Isachenko[30] equation to

$$\mathrm{Nu} = 1.46 \times 10^{-6} (\mathrm{Re}^*)^{-1.63} \Pi_k^{1.16} \mathrm{Pr}^{0.5}$$

where

$$\mathrm{Re}^* = k_L \Delta T / \mu_L \lambda \Pi_k = 2 g_c \sigma (d\sigma/dT) T_s / J \lambda \mu_L^2$$

and

$$\mathrm{Pr} = (C_p \mu / k)_L$$

This study also indicates there may be as many as 7 million active nucleation sites per square inch during dropwise condensation. A drop may experience an estimated 400,000 coalescences in reaching its final size. Thus the liquid-film fracture theory of dropwise condensation is rejected.

Two-Phase Pressure Drop

Reactor thermal and safety analyses frequently involved predictions of the properties of two-phase fluids. That interest in this subject continues strong was evidenced by seven papers.[31-37] Two-phase frictional pressure drop was correlated on the basis of data for mercury–nitrogen, water–air, and three sets of data for steam.[37] The ratio of two-phase to all-liquid pressure-drop gradient was expressed as

$$\Phi_{L_0}^2 = \frac{(\Delta P/\Delta L)_{TP}}{(\Delta P/\Delta L)_L}$$

where the subscript 0 stands for total mass flow rate. The relation between this two-phase

Digitized by Google

multiplier and the Lockhart–Martinelli[38] correlation

$$\Phi_L^2 = \frac{(\Delta P/\Delta L)_{TP}}{(\Delta P/\Delta L)_L}$$

is given by

$$\Phi_{L_0}^2 = \Phi_L^2(1-x)^{1.8}$$

where x, the quality, is the ratio of gas (or vapor) mass flow rate to total flow rate, for both single- and two-component flow. The correlation consists in a plot of the two-phase multiplier as a function of the property index, $(\mu_L/\mu_g)^{0.2}/(\rho_L/\rho_g)$, with quality as a parameter for mass velocities from 0.25 to 3×10^6 lb/(hr)(sq ft). This correlation was based on 129 experimental points and the mass-flow-rate data of Sher and Green[39] for 2000-psia steam. The latter set of curves shows a rather unusual behavior and cannot be represented by any analytical expression.

Experimental pressure-drop and void-fraction data are compared with this correlation for water–air, kerosene–air, diesel oil–air, NaK–nitrogen, potassium (in a horizontal serpentine and an annulus with a helical tape), and steam. No effort was made to include the effect of changing flow patterns in the correlation. However, because the two-phase multiplier ratio may both increase and decrease at a given mass velocity and quality as the property index increases, this unusual aspect of the correlation may implicitly include the effects of flow-pattern changes. Application of the correlation to data on boiling potassium required the use of a previous correlation[40] to predict liquid fraction.

Bubbling mixtures in turbulent flow within a vertical plexiglass tube were used in an experiment that included analyses and separate measurements of frictional, hydrostatic, and momentum pressure drops.[35] Calculational procedures are suggested. The authors found the simplest correlation for bubbling-flow wall shear stress is obtained when a Reynolds number and friction factor are defined by use of the actual mixture velocity and density along with the liquid viscosity. The resulting friction factors are then approximately 10% above the Moody smooth-pipe friction factor. Momentum fluxes in bubbling flow were found to be not necessarily bounded by the homogeneous and separated flow models. The momentum fluxes were found to be better correlated by the separated model but would always be 5 to 25% larger than predicted by that model.

When the void fraction was less than 25%, bubbles formed at the wall diffused only slowly toward the center, giving rise to slip ratios less than 1. This behavior is characterized as "developing flow"; however, the length required for fully developed flow is not known. Photographs helped define a map of the boundary between bubbly flow and unsteady exit flow on the coordinates of superficial liquid velocity vs. superficial gas velocity. For large volumetric flow concentrations, the void fraction approaches the slug-flow limit.

The transition from the slug-annular to two-phase flow was studied with an electrical-conductivity probe.[34] The purpose of this study was to identify the flow pattern for correlations of pressure drop and heat transfer. Simultaneous void measurements indicate that the transition occurs when the void fraction is between 80 and 90%. For superficial liquid velocities greater than about 1 ft/sec, the mass quality at transition is a constant that depends only on pressure. For low superficial liquid velocities, transition occurs at a superficial gas velocity that depends on pipe diameter. When the liquid flow is small, transition is unaffected by a reduction in liquid surface tension or the effects of liquid impurities. The liquid viscosity does not significantly affect the transition line.

During the discussion of this paper, it was mentioned that substantial subcooling eliminates slug flow to give transition directly from bubbly to annular flow. As an alternate to the electrical-conductivity probe, a study of the power spectral density of pressure fluctuations at the wall was suggested for determining the flow regime.

Void fractions in a developing two-phase flow system with flowing and nonflowing liquid phases were investigated for steam–water mixtures flowing vertically in a large unheated duct over a wide range of flow conditions.[36] The scope of the experiment covered superficial liquid velocities of 0 to 20 ft/sec and pressures of 600 to 1500 psig. A gamma attenuation system was used to measure chordal void fractions, which were integrated to give an average. Also, a manometer technique was evaluated for giving the average void fraction.

Digitized by Google

Void distributions obtained with the variable-density model of Bankoff[41] (this reference was incorrectly cited in the paper) were compared with those from the film–exponential model. The latter model assumes a thin film of liquid at the wall. The average void fractions were compared with slip-ratio correlations of Marchaterre and Hoglund[42] and the kinematic-wave model of Zuber and Findlay.[43] In the discussion of this paper, the question of flow development was raised again. For an explanation of the slip ratios of less than 1, it is necessary to assume that the vapor was near the wall where velocity is least. Experimentally it was found, however, that there was liquid at the wall. It was also pointed out that equations for two-phase flow should include the dependence between velocity and void profiles. Fluctuations in velocity and density give rise to terms similar to the Reynolds stresses in turbulence theory.

The phase velocities in boiling flow systems are given by their relation for minimum voids in terms of phase densities and parameters related to the velocity distribution by use of a total energy balance.[31] The correlating interval (which is a function of the quality and the vapor- and liquid-phase viscosities and densities) was derived from diffusion theory. A simple relation was obtained between quality, vapor fraction, and power input per unit flow volume in the test section. Qualitative predictions of void variation with heat flux and hydraulic diameter were said to agree with data from the literature. In the discussion of this paper, it was pointed out that application of minimization principles without rigorous justification could lead to serious errors. Kinetic-energy distribution factors dependent on velocity distributions were introduced in this model; they varied from 0.5 to 1, and the variation depended on whether the flow was laminar or fully turbulent. If the flow pattern in each of the phases cannot be specified, these constants may only serve to curve-fit the data.

Sudden contraction in two-phase flow in round pipes caused pressure drops that were measured and reported as functions of system pressure, flowing-mixture quality, contraction-area ratio, and mass velocity.[32] No void measurements were made, and water at saturation pressures of 200 to 500 psia was the only fluid studied. Pressure drop caused by the contraction was correlated in terms of a contraction coefficient that was independent of mass velocity over the range of conditions studied. The homogeneous model gave the best correlation of the data, but it was about 20% high, supposedly because of a large amount of mixing in the reexpansion after the vena contracta.

Two-phase heat transfer was simulated by the bubbling of air through the wall of a porous heated tube into water and into ethylene glycol flowing upward at room temperature and atmospheric pressure.[33] A simplified superposition type model based on microconvection, vapor–liquid exchange, and "convection-area-reduction" mechanisms was found to predict the trends of the air bubbling rate on heat transfer. Heat transfer increases over that of pure forced convection at low and moderate bubbling rates compared favorably with those caused by pool nucleate boiling when convective heat-transfer rates were relatively low. Photographs of pool boiling and air bubbling from identical tubes in a tank of Freon-11 showed qualitatively that bubble diameters and flow formations were similar in both processes. The result of this theory suggests that the enhancement in heat transfer and boiling could be considered as hydrodynamic in nature, thus making latent-heat transport unimportant as a heat-transfer mechanism.

Heat Exchangers

A lively commercial and technical interest in heat-exchanger design and operation is indicated by the large number of relevant papers that were presented.

Experimental heat-transfer coefficients were presented[44] for in-line, turbulent flow of NaK along the surface of an unbaffled bundle of nineteen $\frac{1}{2}$-in.-diameter rods arranged on an equilateral triangular pattern with a pitch-to-diameter ratio of 1.75. The shell and all rods in the bundle were heated electrically to provide equal and uniform heat fluxes of 18,000 to 30,000 Btu/(hr)(sq ft) throughout the bundle. Tests covered conditions of fully established velocity and temperature profiles and also conditions where entrance effects were important. These results agreed with theoretical predictions and earlier similar experiments with mercury except at very low flow rates corresponding to Peclet numbers less than 500. It was hypothesized that the low heat-

Digitized by Google

transfer coefficient (~10% below theory) was caused by gas collection and incomplete wetting at the heated surface.

An analytical study of the wall and fluid temperature field in a counterflow heat exchanger includes the effects of longitudinal conduction in the wall and unbalanced flow.[45] In addition to the general solution, balanced flow and insulated boundary conditions are considered. Longitudinal conduction in the wall separating the fluids distorts the temperature-distribution curves for both streams and produces a larger temperature difference at the ends; the minimum difference is at some point between the ends. With these exact solutions and the temperature-distribution plots, it is possible to determine how thermal performance is affected at low flow rates.

The effectiveness (the ratio of the enthalpy actually transferred to the maximum possible) and temperature difference of the unmixed fluid in "split cross-flow" heat exchangers were determined analytically.[46] Of particular interest is the "split–mixed crisscrossed–unmixed" heat exchanger, which provides the most uniform exit temperature distribution of the unmixed fluid among the simple-configuration cross-flow heat exchangers (Fig. IV-3). Effectiveness and temperature distribution are compared with conventional cross-flow heat exchangers. Heat exchangers with one shell pass and n tube passes, where n is an even number, are often referred to as 1-n exchangers. A generalized equation[47] has been derived for the effectiveness, ϵ, of 1-n exchangers in terms of the capacity-rate ratio, R, and number of transfer units, NTU. Values of ϵ at small intervals of R and NTU are tabulated for the 1-2 exchanger together with correction factors to give ϵ for each 1-n exchanger through $n = 12$. Deviations from 1-2 exchanger effectiveness increase with n and NTU. Thus, in addition to the significant effect that these deviations have on thermal stability and control of exchangers, the correction factor is particularly important in the design and selection of large heat exchangers whose purpose is the economic recovery of heat from a fluid. Because economic evaluations of such exchangers often involve the difference between two large numbers, the accuracy of the deviations and correction factors is an essential factor. The use of analog and digital computers to design plate type

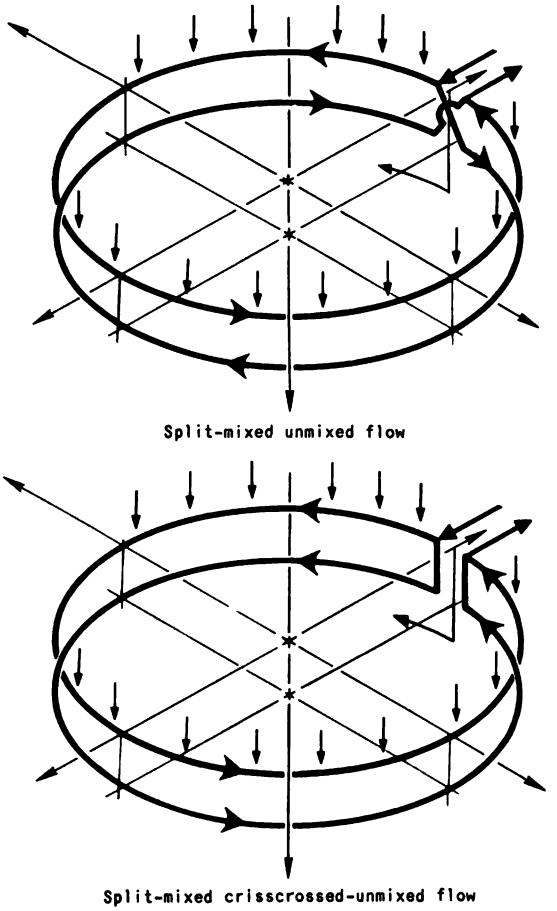

Fig. IV-3 Schematic of flows in split cross-flow heat exchangers within cylindrical envelopes.[46]

exchangers by the ϵ–NTU method was described.[48] The techniques were outlined in detail, and some results were given.

Finned tube heat-exchanger design data and procedures were given in seven papers.[49–55] Pressure drop of air flowing across triangular-pitch banks of finned tubes is correlated in the form of a friction factor as a function of a Reynolds number and a pitch-to-diameter ratio.[54] Measurements are reported of convective heat transfer and flow friction for nine pin–fin surfaces with square spacing of 2, 3, and 4 times the fin diameter and with plate spacing of 4, 8, and 12 times the diameter.[52] Vibration was found to be important, and intense noise occurred at certain flow velocities because of vortex shedding, which may have been coupled with a natural frequency in the heat exchanger. Vibrations increased the friction factor but did not significantly affect

Digitized by Google

the heat transfer. Natural frequencies of the heat exchangers may be either acoustical or mechanical. Free-convection heat transfer to a new type of extended surface covered with rows of finned pins was studied.[51] With an average temperature excess of 200°F at the roots of the pins, the rate of heat transfer from such an extended surface was 475% higher than that from the basic surface without the finned pins.

The problem of optimizing finned geometry to maximize free-convection heat transfer in air at atmospheric pressure, taking into account nonuniform fin temperatures, was investigated[49] by introducing the fin effectiveness into the Elenbaas[56] solution for uniform fin temperature. This yields an optimum fin spacing for the nonuniform case, together with optimum values for fin thickness and tube diameter for a tube with square fins. A theoretical analysis of optimization of parabolic-shaped fins considers the combined effect of conduction, radiation, and solar irradiation.[50] The governing differential equation is reduced to an equivalent double-integral equation that yields the relation between the finned geometry and weight parameters. The resulting geometry of least mass is plotted as a function of the dimensionless irradiation parameter and the structure-to-weight ratio (total weight to the weight of the fins).

A novel lightweight heat-rejection system for vapor was reported.[55] It uses cooling fins made of plastic film to condense the vapor coolant for a portable direct-conversion energy system. The plastic film can accommodate changes in heat input by changing shape or by partially collapsing. The durability and long-term performance of finned tubes under steady-state and thermal-cycling conditions were evaluated by means of tests on both extruded-fin tubes and tension-wound-fin tubes (in each specimen the fin and tube were of different metals).[53] Single-tube heat-transfer and strain-gauge tests were run both at the original contact pressures and at the isothermal tube-wall temperatures at which the fin-to-tube contact was lost.

A dynamic analysis was made of a concentric-tube heat exchanger with a time-varying flow as the forcing function.[57] The mathematical model agrees well with experiments for step, square wave, and sinusoidal changes in the tube flow rate. Errors introduced by linearization of the equations were investigated to determine the accuracy of the approximation.

Two novel heat-exchange devices were reported.[58,59] The Spiralator uses a rotating twisted tape to scrape the interior wall of tubes containing viscous or fouling liquids.[58] Small-diameter flexible-tube Teflon* heat exchangers offer high corrosion resistance, smooth slippery surface, tube flexibility, and inertness.[59] The favorable nucleation characteristics of Teflon for boiling and condensation and the fact that about 200 sq ft of surface area per cubic foot of shell volume can be built into a small tube exchanger stimulate interest in this new development. The higher thermal resistance of the Teflon wall can be offset by the lack of fouling for crystalline deposits and the versatility of its use.

Packed Beds

Relevant to some advanced reactor concepts are several papers on packed-bed heat transfer and pressure drop. Heat-transfer and pressure-loss characteristics of glass–ceramic matrices for regenerative heat exchangers were measured.[60] The steady-state axial temperature distributions in moving-bed fluid-to-particle heat exchange was determined analytically for a vertical duct of constant area in cocurrent and countercurrent flow.[61] If the regeneration principle is used, the distance over which the gas and solid temperatures are different and heat is transferred can be predicted. The small value of the effective length indicates that such a fluid-to-particle heat exchanger would be very compact. An analysis of unsteady-state heat transfer to a fluid flowing through porous heated solids provides solutions for both solid and fluid temperatures, some of which were verified experimentally.[62] Theory and experiments were reported for the heat-transfer and flow-friction characteristics of air-cooled matrices of high porosity that were heated by radiation which gives an exponential heat source.[63] A transient solution of simultaneous convection and radiation heat-transfer equations, when used with experimental data taken in the steady state, gave volumetric heat-transfer coefficients for convection only in the matrices. Correlations were obtained with

*Trademarked name for Du Pont fluorocarbon resin copolymer.

Digitized by Google

Reynolds numbers, based on a characteristic length obtained by equating pressure drop to the sum of viscous and inertial resistance terms. A related but more theoretical paper reported a study of the time-dependent temperature distribution for incompressible flow past a sphere.[64] A numerical solution of the diffusion equation showed that the temperature gradients at a spherical surface, as well as the time required to approach steady state, depend markedly on the value of the Peclet number.

Desalinization

The possibilities of the desalting of seawater as an auxiliary process while generating power in a dual-purpose nuclear plant have been receiving considerable attention from reactor designers. The interest in such technology is indicated by the six papers presented on this subject.[65-70] The thickness of a laminar liquid film draining from a vertical wall can be found analytically for the case of a constant evaporation rate from the surface of the film.[65] Transient as well as steady-state expressions are found that show the location where the film vanishes, the rate of evaporation, and the total mass evaporated.

The U. S. Department of the Interior's Plant No. 1 at Freeport, Tex., for desalting seawater by the falling-film distillation process was described thoroughly.[70] Reference 70 gives a description of the process, analysis of pilot-plant data and a report on evaporator performance. An alternate method of heat transfer in desalinization involves a multiphase exchanger that uses direct-contact heat transfer from a nonvolatile immiscible liquid to change the phase of a volatile fluid.[69] The initial diameter of pentane droplets evaporating within an immiscible water medium in a 3-phase (pentane, water, and pentane vapor) heat exchanger was found to affect the overall heat-transfer coefficients. The heat-transfer coefficient increased with a decrease in droplet size, and, apparently, surface tension and excess pressure from curvature are relevant parameters. Although scraped or wiped falling-film evaporators have been used industrially for some years, little has been published about their heat-transfer performance. An experimental study of evaporation at a scraped surface found that the Nusselt number was proportional to Reynolds number to the 0.25 power, to a rotary Reynolds number to the 0.43 power, to the Prandtl number to the 0.33 power, and to the number of the blades to the 0.33 power.[68]

Deposits formed beneath bubbles during nucleate boiling of radioactive calcium sulfate solution were found in detailed studies to be related to heat transfer and the problem of fouling of surfaces during evaporation of salt water.[66] Calcium sulfate is of interest because of its scale-forming ability. Studies of such deposits show that the bubble behavior is consistent with the microlayer vaporization hypothesis proposed by Moore and Mesler.[71] The relative distribution of the deposits revealed by autoradiographs indicates that there is more evaporation beneath the bubble (as was suggested by Moore and Mesler) than there is in evaporation at the triple interfaces (as was proposed by Partridge and White).[72] A second study of heat transfer and fouling rates during pool boiling of calcium sulfate solution shows the deposition rate is proportional to the square of the heat flux and nearly constant in time at constant heat flux.[67] It follows that the deposition rate is proportional to the concentration driving-potential squared, as proposed by Miyauchi.[73] Deposition of $CaSO_4$ on a surface in nucleate boiling creates additional nucleate-boiling sites, which raises the heat-transfer coefficient during part of the operating time—although the eventual result of fouling is to reduce heat transfer. Thin polyhydrocarbon coatings retarded scaling by an order of magnitude and increased the overall coefficient of heat transfer during calcium sulfate deposition. Polymerization fouling, which was also studied, produces a temperature–time behavior completely different from that of crystalline fouling and is not well understood. The heated surface temperature remained constant for a time that depended on the heat flux and polymer concentration. It then increased 350 to 400°F within 1 to 2 min and began oscillating with an amplitude of 40°F and a period of about 0.1 min.

Radiation

Interest in radiation heat transfer continues to grow because of the increase in design temperatures of reactor systems and because of the importance of this mechanism for heat sinks for space power plants.

Digitized by Google

A method was presented for calculation of radiative exchange in enclosures whose surface reflectance can be approximated by the sum of a diffused and a specular component.[74] Heat transfer by simultaneous internal conduction and surface radiation in plates with specular reflection was treated in terms of a nonlinear integro-differential equation that was converted to an integral equation and then solved numerically.[75] Solutions have been obtained for a wide range of conditions, including those for which diffuse reflection results are available. Reflection and transmission intensities from gray slabs were found by use of the powerful invariant embedding method that was developed for phenomena such as neutron transport.[76] Problems of simultaneous convection and radiation in a laminar boundary layer on a flat plate were formulated and solved.[77] In these solutions it was assumed that the plate surface is black and that the fluid medium is a perfect gas for which the mass absorption coefficient for radiation is independent of frequency and temperature. The iterative solution includes the effect of viscous dissipation, secondary emission and absorption, and incident external radiative fluxes.

Thermophysical Properties

A novel use of heat-transfer techniques enables the measurement of thermophysical properties at extremely high temperatures. The thermal conductivities of noble gases in the range 1500 to 5000°K were determined by measurement of heat-transfer rates from heated gases to the end wall from a reflected shock wave.[78] Consideration of density variation in the thermal boundary layer was found to be significant in evaluation of the data; some previous investigations had neglected this effect. The thermal conductivity of hydrogen from 2000 to 4700°F and 15 to 150 psia was determined from the measured effective conductivity of porous tungsten specimens filled with pressurized hydrogen;[79] thermal conductivity as determined by subtracting the solid conductivity contribution compares within a factor of 2 with existing experimental and theoretical work. Heat transfer through porous ceramics in a thermally degraded ablation material was measured and tested against different theories.[80] If the correct model is assumed, the apparent conductivity is the sum of the separate contributions of solid and gas conduction in radiation. The radiant portion of the conductance is proportional to the product of the mean temperature cubed times the average pore size.

Other Heat-Transfer Studies

Studies important to cryogenic heat transfer were described.[81,82] Heat transfer from laminar boundary layers was considered, with emphasis on large free-stream velocity gradients and highly cooled walls.[83] In experiments on how free convection affects laminar forced-flow heat transfer in a uniformly heated horizontal tube, the free-convection-flow component that caused secondary flow was observed as a decrease in the wall-to-bulk fluid temperature difference required to transfer heat as compared to the pure forced flow.[84] Local as well as average heat-transfer coefficients between an isothermal flat plate and impinging two-dimensional jets were measured for both single jets and arrays of jets.[85] Viscous and thermal boundary-layer behavior on the electrically insulating wall of a rectangular magnetohydrodynamic channel was analyzed theoretically by use of momentum and energy integral approximations.[86] Measurements of the way in which asymmetrical heating in a parallel-plate channel affects fully developed turbulent heat transfer show it to be qualitatively as predicted analytically.[87] An analysis of a thermal flowmeter includes the normally neglected effect of axial conduction along the tube.[88] Transient heat transfer between a thin circular tube and the incompressible fluid moving through it was analyzed for constant inlet fluid temperature;[89] both radial conduction in the wall and the heat loss at the outer surfaces of the cylinder were included. The effect of heat conduction on wall temperature was determined for a well casing passing vertically through a planar heat source of constant temperature.[90]

An approximate calculation was presented for natural-convection melting of an ice-water system.[91] Although an analytical study of transient heat transfer to a Bingham plastic (a material with a finite yield stress and linear stress–strain curve) in laminar flow in a circular tube with energy generated internally was given with a justification of its applicability to slurry reactors, experiments reported in the paper generally agree poorly with the theory, showing wall temperatures 30% lower to 100% higher

Digitized by Google

than predicted plus a different transient response.[92] Equations were given for the temperature of moving solid materials undergoing heating or cooling.[93,94] The determination of the surface heat flux from the measured-temperature history inside a heat-conducting solid is called the inverse heat-conduction problem; this problem becomes nonlinear if the thermal properties depend on temperature and was solved by a finite-difference method.[95] A stable, explicit numerical solution of the conduction equation for multidimensional nonhomogeneous media was presented.[96] This method, which may be called an alternating-direction explicit procedure, takes less computational time than the alternating-direction implicit procedure and appears to combine the computational ease of the explicit methods with the stability of the implicit methods.

Evaporation rates from hot vertical flat plates, which are relevant to reactor safety analyses, were analyzed.[97] It was concluded that a correction factor accounting for the effect of transverse mass flux must be incorporated in the correlation expression for pure heat transfer. Also of potential importance to reactor safety is an experimental study of transient heat transfer to liquids in cylindrical enclosures.[98]

The thermal-control techniques and the thermal-design calculations for the Nimbus satellite were reviewed.[99] Movable insulation panels provide active temperature control of exterior surfaces. The analytical methods described agree with thermal model tests and actual space-flight data.

Loss-of-Coolant Accidents

One facet of heat transfer directly related to reactor safety and containment was discussed by a panel. Most of the discussion concerned the LOFT (Loss-of-Fluid Test) program that is part of the reactor safety program of the AEC. For this program a 50-Mw(t) pressurized-water reactor and test facility are being built in Idaho to learn how a reactor is affected by a sudden loss of coolant and the extent of any resulting radioactivity release. Phillips Petroleum Company is responsible for building and testing the LOFT blowdown facility; Kaiser Engineers, a Division of Henry J. Kaiser Co., is designing the LOFT facility.

R. P. Rose (of Phillips) described the proposed five-phase test program: (1) containment pressure and leak tests, (2) coolant blowdown tests with a dummy core, (3) low-power physics tests and power operation, (4) loss-of-coolant test, and (5) facility cleanup and posttest examination. Rose pointed out that the many unknowns associated with the blowdown program have suggested the need for a scale model to mock up the LOFT geometry before the full-scale tests. He discussed the scaling down of the LOFT physical dimensions for the proposed blowdown test facility, which would preserve the relative dimensions of the piping, vessel, and core rather than the time scale. As a result the metastable fluid behavior during blowdown may be affected because linear three-dimensional scaling involves shortening of the time scale.

J. S. Busch, W. D. Harrington, and S. Fabic (of Kaiser) discussed analyses that gave the system boundary conditions for transient containment as well as for the primary-loop transients resulting from blowdown; generalized digital-computer programs and subsequent parametric analyses were used.

S. Esleak (of The Babcock & Wilcox Co.) discussed some of the more important problems pertaining to a loss-of-coolant accident: (1) two-phase critical flow, (2) two-phase pressure drop, (3) dynamic effect in the core, and (4) coolant expansion and degree of separation in the reactor vessel. The bases of his discussion are available in a recent state-of-the-art report.[100]

Specific phenomena pertaining to the loss-of-coolant accident were discussed by J. A. Redfield, P. J. Moody, and H. Fauske. Redfield (of Bettis Atomic Power Division, Westinghouse Electric Corp.) presented a simplified model for fuel-element heat transfer during a loss-of-coolant accident which has been applied to the Zircaloy-clad oxide-rod fuel elements for LOFT. He concluded that more data are needed for transient heat transfer under conditions of rapidly falling pressure, rapidly rising coolant quality, and highly unsteady flow conditions.[101]

Moody (of General Electric Company) discussed an idealized model for estimating critical flow rates and pressure drops for given vessel conditions and flow break geometry. Although this ideal-nozzle model agreed well with one previous test (for the Humboldt Bay nuclear power plant), it clearly overpredicted another test (for the Bodega Bay plant). An extension of the energy model to include fric-

Digitized by Google

tion losses yielded fair agreement with the recent data of Fauske.[102]

Fauske (of Argonne) evaluated existing models for calculating maximum escape rates of reactor coolant. On the basis of recent measurements of voids at critical flow conditions, he concluded that previously formulated models (Fauske,[102] Levy,[103] and Moody[104]) are physically incorrect and that their good predictions resulted from the high values of velocity ratios, which compensated for metastability effects. A new model was suggested, including both the effects of slip and metastability.

Nomenclature

A = area, sq ft
C_p = heat capacity, Btu/(lb)(°F)
D = test-section diameter, ft
D_d = diameter of bubble at departure
g = local acceleration, ft/sec^2
g_c = gravitational conversion factor, 32.16 lb_{mass}-ft/sec^2/lb_{force}
G = mass velocity, lb/(hr)(sq ft)
h = heat-transfer coefficient, Btu/(hr)(sq ft)(°F)
J = mechanical equivalent of heat = 778 ft-lb/Btu
k = thermal conductivity, Btu/(hr)(ft)(°F)
L = length, ft
NTU = number of transfer units = $AU_{av.}/(C_p w)_{min.}$
P = pressure, psi
q'' = heat flux, Btu/(hr)(sq ft)
q''_c = critical heat flux, Btu/(hr)(sq ft)
R = capacity-rate ratio = $(C_p w)_{hot\ fluid}/(C_p w)_{cold\ fluid}$
s = liquid-layer thickness, ft
t = time, sec
t = effective thickness of heater, ft
T = temperature, °F
U = overall heat-transfer coefficient, Btu/(hr)(sq ft)(°F)
v = velocity, ft/sec
w = weight rate of flow, lb/hr
x = vapor weight fraction, lb vapor/lb fluid
z = distance from inception of local boiling, measured in the direction of flow, ft
β = contact angle, deg
ϵ = heat-exchanger effectiveness, heat transferred/maximum possible heat transfer
λ = latent heat, Btu/lb
μ = viscosity, lb/(ft)(hr)
ρ = density, lb/cu ft
σ = surface tension, Btu/sq ft = 778 × lb/ft
Φ = two-phase flow multiplier

Subscripts

$av.$ = average
b = bulk
c = critical
DNB = departure from nucleate boiling
f = film conditions
g = gas
L = liquid
S = saturation
TP = two-phase
v = vapor
max. = maximum
min. = minimum

References

Most of these papers were presented at the 8th National Heat Transfer Conference, Los Angeles, Calif., Aug. 9–11, 1965, sponsored jointly by the American Institute of Chemical Engineers and the American Society of Mechanical Engineers; they are marked with the initials of the appropriate society.

Individual papers are available from the two societies; some of the ASME papers will appear in the ASME Journal of Heat Transfer; but all the AIChE papers will appear in a volume in the Chemical Engineering Progress Symposium Series.

1. J. H. Leinhard and K. Watanabe, On Correlating the Peak and Minimum Boiling Heat Fluxes with Pressure and Heater Configuration. (ASME)
2. A. A. Bishop, R. O. Sandberg, and L. S. Tong, Forced Convection Heat Transfer at High Pressure After the Critical Heat Flux. (ASME)
3. E. O. Moeck, F. Stern, G. A. Wikhammer, and R. T. Dempster, Dryout in a 19-Rod Bundle Cooled by Steam/Water Fog at 515 psia. (ASME)
4. R. S. Daleas and A. E. Bergles, Effects of Upstream Compressibility on Subcooled Critical Heat Flux. (ASME)
5. W. J. Frea, G. S. Dzakowic, J. M. Hamelink, and W. S. Harjala, Some Experimental and Analytical Investigations on the Critical Heat Flux in Pool Boiling. (AIChE)
6. M. Carne and D. H. Charlesworth, Thermal Conduction Effects on the Critical Heat Flux in Pool Boiling. (AIChE)
7. L. S. Tong, H. B. Currin, P. S. Larsen, and O. G. Smith, Influence of Axially Non-Uniform Heat Flux on DNB. (AIChE)
8. B. F. Caswell and R. E. Balzhiser, The Critical Heat Flux for Boiling Liquid Metal Systems. (AIChE)
9. Z. L. Miropol'skii, Heat Transfer in Film Boiling of a Steam–Water Mixture in Steam-Generating Tubes, *Teploenerg.*, 10: 99 (1963) (in Russian). Also available as USAEC Report AEC-tr-6252.
10. P. J. Marto and W. M. Rohsenow, Nucleate Boiling Instability of Alkali Metals. (ASME)
11. J. M. Adams, An Investigation of Heat Transfer to Pool-Boiling Magnesium. (ASME)
12. P. J. Marto and W. M. Rohsenow, Effects of Surface Conditions on Nucleate Pool Boiling of Sodium. (ASME)
13. M. N. Ozisik and T. Cebeci, Dynamic Stability of Flow Oscillations in a Heated Channel. (ASME)
14. P. J. Berenson, An Experimental Investigation of Flow Stability in Multitube Forced-Convection Vaporizers. (ASME)
15. T. H. K. Frederking and D. J. Daniels, The Relation Between Bubble Diameter and Frequency of Removal from a Sphere During Film Boiling. (ASME)
16. G. J. Schoessow and K. J. Baumeister, Liquid Drop Model Vibrations and Simulated Fission. (AIChE)
17. K. J. Baumeister, T. D. Hamill, F. L. Schwartz, and G. J. Schoessow, Film Boiling Heat Transfer to Water Drops on a Flat Plate. (AIChE)
18. B. M. Patel and K. J. Bell, The Leidenfrost Phenomenon for Extended Liquid Masses. (AIChE)

Digitized by Google

19. M. A. Johnson, J. de la Peña, and R. B. Mesler, Bubble Shapes in Nucleate Boiling. (AIChE)
20. R. Cole and H. L. Shulman, Bubble Departure Diameters at Sub-Atmospheric Pressures. (AIChE)
21. J. M. Yatabe and J. W. Westwater, Bubble Growth Rates for Ethanol-Water and Ethanol-Isopropanol Mixtures. (AIChE)
22. G. J. Hordmann and Kwang-Tzu Yang, Laminar Film Condensation in Two-Phase Channel Flow. (ASME)
23. J. O. Medwell and A. A. Nicol, Surface Roughness Effects on Condensate Films. (ASME)
24. W. Nusselt, Die Oberflaschen Kondensation Des Wasserdampf, *Z. Ver. deut. Ing.*, 60: 541, 569 (1916).
25. S. P. Sukhatme and W. M. Rohsenow, Heat Transfer During Film Condensation of a Liquid Metal Vapor. (ASME)
26. D. W. Weiler, A. M. Czikk, and R. S. Paul, Condensation in Smooth and Porous Coated Tubes Under Multi-G Accelerations. (AIChE)
27. L. A. Bromley, R. F. Humphreys, and W. Murray, Condensation on and Evaporation from Radially Grooved Rotating Disks. (ASME)
28. J. L. McCormick and J. W. Westwater, Drop Dynamics and Heat Transfer During Dropwise Condensation of Water Vapor on a Horizontal Surface. (AIChE)
29. A. C. Peterson and J. W. Westwater, Dropwise Condensation of Ethylene Glycol. (AIChE)
30. V. P. Isachenko, Mechanism and Criteria Equations of Heat Transfer in the Condensation of Steam in Drops, *Teploenerg.*, 9: 81 (1962) (in Russian).
31. E. E. Polomik, Phase Velocities in Boiling Flow Systems by Total Energy and by Diffusion. (ASME)
32. G. E. Geiger and W. M. Rohrer, Sudden Contraction Losses in Two-Phase Flow. (ASME)
33. A. A. Kudirka, R. J. Grosh, and P. W. McFadden, Two Phase Heat Transfer in a Tube with Gas Injection from the Walls. (ASME)
34. R. E. Haberstroh and P. Griffith, The Slug-Annular Two-Phase Flow Regime Transition. (ASME)
35. S. C. Rose, Jr., and P. Griffith, Flow Properties of Bubbly Mixtures. (ASME)
36. K. F. Neusen, Void Fractions in a Developing Two-Phase Flow System with Flowing and Non-flowing Liquid Phase. (ASME)
37. C. J. Baroczy, A Systematic Correlation for Two-Phase Pressure Drop. (AIChE)
38. R. W. Lockhart and R. C. Martinelli, Proposed Correlation of Data for Isothermal Two-Phase, Two-Component Flow in Pipes, HART, *Chem. Eng. Progr.*, 45: 39 (1949).
39. N. C. Sher and S. J. Green, Boiling Pressure Drop in Thin Rectangular Channels, Chemical Engineering Progress Symposium Series, No. 23, p. 61, American Institute of Chemical Engineers, 1959.
40. C. J. Baroczy, Correlation of Liquid Fraction in Two-Phase Flow with Application to Liquid Metals, Chemical Engineering Progress Symposium Series, No. 57, p. 179, American Institute of Chemical Engineers, 1965.
41. S. Bankoff, A Variable Density Single-Fluid Model for Two-Phase Flow with Particular Reference to Steam Water Flow, *J. Heat Transfer*, 82: 265 (1960).
42. J. F. Marchaterre and B. M. Hoglund, Correlation for Two-Phase Flow, *Nucleonics*, 20(8): 142 (August 1962).
43. N. Zuber and J. A. Findlay, The Effects of Nonuniform Flow and Concentration Distributions and the Effect of the Local Relative Velocity on the Average Volumetric Concentration in Two-Phase Flow, USAEC Report GEAP-4592 (EURAEC-1096), General Electric Company, April 1964. [See also *J. Heat Transfer*, 87: 453 (1965).]
44. S. Kalish and O. E. Dwyer, Heat Transfer to NaK Flowing In-Line Through a Bundle of Circular Rods. (ASME)
45. C. L. Pan and N. E. Welch, Exact Analytical Wall and Fluid Temperature Field for a Counterflow Heat Exchanger with the Effect of Longitudinal Heat Conduction. (ASME)
46. H. Kamei, Effectiveness and Temperature Distribution of Split Cross Flow Heat Exchangers. (ASME)
47. A. D. Kraus and D. Q. Kern, The effectiveness of Heat Exchangers with One Shell Pass and Even Numbers of Tube Passes. (ASME)
48. B. W. Jackson and R. A. Troupe, Plate Heat Exchanger Design by ϵ-NTU Method. (AIChE)
49. D. R. Fairbanks and M. Mark, An Optimization Procedure for Finning in Free Convection. (ASME)
50. K. Kotan and O. A. Arnas, On the Optimization of the Design Parameters of Parabolic Radiating Fins. (ASME)
51. S. T. Hsu, B. C. Vatsaraj, and C. Hsieh, An Extended Surface with Finned Pins Under Free Convection Cooling. (ASME)
52. G. Theoclitus, Heat-Transfer and Flow-Friction Characteristics of Nine Pin-Fin Surfaces. (ASME)
53. E. C. Smith, S. P. Victory, and A. Y. Gunter, Evaluation of Fin Tube Performance Under Steady State and Thermal Cycling Conditions. (ASME)
54. K. K. Robinson and D. E. Briggs, Pressure Drop of Air Flowing Across Triangular Pitch Banks of Finned Tubes. (AIChE)
55. W. R. Martini, A Light Weight Vapor-Fin Heat Rejection System. (AIChE)
56. W. Elenbaas, Heat Dissipation of Parallel Plates by Free Convection, *Physica*, 9: 1 (1942).
57. W. J. Privott and J. K. Ferrell, Dynamic Analysis of a Flow-Forced, Concentric Tube Heat Exchanger. (AIChE)
58. W. R. Penney, The Spiralator—Initial Tests and Correlations. (AIChE)
59. R. E. Githens, W. R. Minor, and V. J. Tomsic, Small Diameter Flexible Tube Heat Exchangers. (AIChE)
60. F. J. Bayley and C. Rapley, Heat Transfer and Pressure Loss Characteristics of Matrices for Regenerative Heat Exchangers. (ASME)
61. L. E. Sissom and T. W. Jackson, Temperature Distribution of Solids and Fluid in Fluid-to-Particle Heat Exchange. (ASME)
62. F. T Hung and R. G. Nevins, Unsteady-State Heat Transfer with a Flowing Fluid Through Porous Solids. (ASME)
63. J. P. Chiou and M. M. El-Wakil, Heat Transfer

Digitized by Google

and Flow Characteristics of Porous Matrices with Radiation as a Heat Source. (ASME)
64. M. Bentwich, G. Szwarcbaum, and S. Sideman, Time Dependent Temperature Distribution in Flow Past a Sphere. (ASME)
65. J. R. O'Loughlin, Evaporation from a Draining Liquid Film. (ASME)
66. N. B. Hospeti and R. B. Mesler, Deposits Formed Beneath Bubbles During Nucleate Boiling of Radioactive Calcium Sulfate Solutions. (AIChE)
67. J. W. Palen and J. W. Westwater, Heat Transfer and Fouling Rates During Pool Boiling of Calcium Sulphate Solutions. (AIChE)
68. T. R. Bott and M. R. Sheikh, Evaporation at a Scraped Surface. (AIChE)
69. S. Sideman, G. Hirsch, and Y. Gat, Direct Contact Heat Transfer with Change of Phase: Effect of the Initial Drop Size in 3-Phase Heat Exchangers. (AIChE)
70. D. I. Dykstra, Desalination of Sea Water by the Falling-Film Distillation Process. (AIChE)
71. F. D. Moore and R. B. Mesler, The Measurement of Rapid Surface Temperature Fluctuations During Nucleate Boiling of Water, *A.I.Ch.E. J.*, 7: 620 (1961).
72. E. P. Partridge and A. H. White, Mechanism of Scale Formation of Calcium Sulfate Boiler Scale, *Ind. Eng. Chem.*, 21: 835 (1929).
73. T. Miyauchi and T. Moriyama, Rate of Anhydrous $CaSO_4$ Scale Formation in Seawater Evaporators, *Kagaku Kogaku*, 25: 531 (1961) (in Japanese).
74. A. F. Sarofim and H. C. Hottel, Radiative Exchange Among Non-Lambert Surfaces. (ASME)
75. R. G. Hering, Radiative Heat Exchange Between Conducting Plates with Specular Reflection. (ASME)
76. J. O. Mingle, Reflection and Transmission Intensities from Gray Slabs Utilizing Invariant Imbedding Methods. (AIChE)
77. C. C. Oliver and P. W. McFadden, The Interaction of Radiation and Convection in the Laminar Boundary Layer. (ASME)
78. D. J. Collins and W. A. Menard, Measurement of the Thermal Conductivity of Noble Gases in the Temperature Range 1500 to 5000 Deg Kelvin. (ASME)
79. S. L. Israel, T. D. Hawkins, R. T. Salter, and S. C. Hyman, Thermal Conductivity of Hydrogen from 2000 to 4700°F. (AIChE)
80. C. M. Pyron, Jr., and C. D. Pears, The Mechanisms of Heat Transfer Through Porous Materials at Elevated Temperatures. (ASME)
81. R. F. Barron and L. S. Han, Heat and Mass Transfer to a Cryosurface in Free Convection. (ASME)
82. J. C. Burke and A. H. Rawdon, An Experimental Study of Heat Transfer to Two-Phase Film-Boiling Nitrogen. (ASME)
83. L. H. Back and A. B. Witte, Prediction of Heat Transfer from Laminar Boundary Layers, with Emphasis on Large Free-Stream Velocity Gradients and Highly Cooled Walls. (ASME)
84. S. T. McComas and E. R. G. Eckert, Combined Free and Forced Convection in a Horizontal Circular Tube. (ASME)
85. R. Gardon and J. C. Akfirat, Heat Transfer Characteristics of Impinging Two-Dimensional Air Jets. (ASME)
86. W. C. Moffatt, Approximate Solutions for Skin Friction and Heat Transfer in MHD Channel Flows. (ASME)
87. E. M. Sparrow, J. R. Lloyd, and C. W. Hixon, Experiments on Turbulent Heat Transfer in an Asymmetrically Heated Rectangular Duct. (ASME)
88. G. E. Zinsmeister and J. R. Dixon. Thermal Flowmeters: The Effect of Axial Conduction. (ASME)
89. N. Hayasi and K. Inouye, Transient Heat Transfer Through a Thin Circular Pipe Due to Unsteady Flow in the Pipe. (ASME)
90. P. J. Closmann, Effect of a Heat-Conducting Well Wall on Temperature Distribution in an Observation Well. (ASME)
91. Chi Tien and Yin-Chao Yen, An Approximate Solution of a Melting Problem with Natural Convection. (AIChE)
92. C. D. Henning and W. J. Yang, Transient Heat Transfer to Laminar Bingham-Plastic Flow in a Circular Tube with Internal Energy Generation. (AIChE)
93. J. A. Clumpner, Equations for Calculating the Temperature of Moving Solid Plates and Cylinders Undergoing Heating or Cooling. (AIChE)
94. L. E. Erickson, L. T. Fan, and L. C. Cha, The Cooling of a Moving Continuous Flat Sheet. (AIChE)
95. J. V. Beck and H. Wolf, The Nonlinear Inverse Heat Conduction Problem. (ASME)
96. S. R. Allada and D. Quon, A Stable, Explicit Numerical Solution of the Conduction Equation for Multi-Dimensional Non-Homogeneous Media. (AIChE)
97. F. S. Li and W. H. Gauvin, Evaporation from Vertical Flat Plates in High-Temperature Surroundings. (AIChE)
98. L. B. Evans and N. E. Stefany, An Experimental Study of Transient Heat Transfer to Liquids in Cylindrical Enclosures. (AIChE)
99. A. London, Heat Transfer as Applied to the Thermal Design of the Nimbus Control System. (AIChE)
100. C. E. Parks, Blowdown Models Applicable to the Loss-of-Fluid Test Facilities (LOFT), USAEC Report BAW-1195-4, The Babcock & Wilcox Co., June 1965.
101. S. G. Margolis and J. A. Redfield, Heat Transfer Aspects of the Loss of Coolant Accident, USAEC Report WAPD-T-1811 (CONF-650920-1), Westinghouse Electric Corp., Bettis Atomic Power Laboratory, August 1965.
102. H. Fauske, The Discharge of Saturated Water Through Tubes, Chemical Engineering Progress Symposium Series, No. 59, p. 210, American Institute of Chemical Engineers, 1964.
103. S. Levy, Prediction of Two-Phase Critical Flow Rate, *J. Heat Transfer*, 87: 53 (1965).
104. F. J. Moody, Maximum Flow Rate of a Single Component, Two-Phase Mixture, *J. Heat Transfer*, 87: 134 (1965).
105. M. R. El-Saden, Theory of Nonequilibrium Thermodynamics with Application to the Transport Processes in a Solid. (ASME)
106. G. S. Springer and R. Ratonyi, Heat Conduction from Circular Cylinders in Rarefied Gases. (ASME)
107. V. P. Tyagi, Laminar Forced Convection of a Dissipative Fluid in a Channel. (ASME)

Digitized by Google

108. B. F. Elam, Heat Transfer in Honeycomb-Core Sandwich Panels. (ASME)
109. J. V. Beck and A. M. Dhanak, Simultaneous Determinations of Thermal Conductivity and Specific Heat. (ASME)
110. W. R. Stubstad, Thermal Contact Resistance Between Thin Plates in Vacuum. (ASME)
111. W. R. Wilcox and R. L. Duty, Macroscopic Interface Shape During Solidification. (ASME)
112. K. C. Cheng, Analog Solution of Laminar Heat Transfer in Noncircular Ducts by Moire Method and Point-Matching. (ASME)
113. T W. Jackson and K. R. Purdy, Resonant Pulsating Flow and Convective Heat Transfer. (ASME)
114. J. M. Davies, Input Power Determined from Temperatures in Simulated Skin Protected Against Thermal Radiation. (ASME)
115. B. Koh and J. E. A. John, The Effect of Interfacial Metallic Foils on Thermal Contact Resistance. (ASME)
116. D. H. Elliott, Thermal Conduction Across Aluminum Bolted Joints. (ASME)
117. J. R. Larson and R. J. Schoenhals, Turbulent Free Convection in Near Critical Water. (ASME)
118. H. A. Blum and G. J. Moore, Transient Phenomena in Heat Transfer Across Surfaces in Contact. (ASME)
119. J. H. Van Sant and M. B. Larson, Convection Heat Transfer for Turbulent Flow in Subsonic Diffusers. (ASME)
120. L. Hoogenboom, Electrical Analog Model of Two-Dimensional Transient Heat Conduction. (ASME)
121. E. Talmor, Film Cooling of Small Diameter Throat Tubes. (AIChE)
122. D. Gidaspow and B. S. Baker, Heat Transfer in a Fuel Cell Battery. (AIChE)
123. D. A. Willoughby and T. J. Dwyer, Heat and Mass Transfer with an Exothermic Chemical Reaction in a Tubular, Laminar Flow Reactor. (AIChE)

Digitized by Google

Section

V

Power Reactor Technology

Materials

Effect of Hydriding on Zircaloy Properties

By C. Roger Sutton

Zirconium-base alloys and austenitic stainless steels have been the preferred materials for the cladding of water-cooled power-reactor fuel elements. In choosing between them, reactor designers balance the lower cost and simpler fabrication of the stainless steels against the better neutronic efficiency of the zirconium alloys—thus the cladding for each reactor is selected on the basis of economic considerations. Today's economic conditions often favor the use of Zircaloy. With the transition to private ownership of fuel in the 1970's, there is expected to be a still clearer economic advantage for zirconium alloys. Zircaloy-2, the reference zirconium-base alloy for the fuel cladding of water-cooled reactors for many years, has very good corrosion resistance and usually adequate mechanical and physical properties. Nevertheless, anything that changes the properties of the cladding material can have a profound effect on the life and economics of the fuel.

Occurrence of Hydride

One factor affecting the life and properties of Zircaloy, and thus the economics of its use, is the formation of zirconium hydride. Investigations of failed Zircaloy-2 cladding on fuel rods has indicated that the presence of oriented zirconium hydride caused brittle failure.[1,2] When the hydrides are oriented perpendicularly to the stress axis, both ductility and strength are decreased appreciably.[3] Preferential orientation of the zirconium hydride platelets can be caused by strains during fabrication[4] or by the application of stresses greater than some threshold intensity while the hydrides are precipitating.[3,5]

Sources of Hydride

Zirconium-base alloys usually contain little hydrogen (10 to 25 ppm) of the melting and fabrication procedures as a result. When the alloys are exposed in oxidizing aqueous media, additional hydrogen is generated continuously by the reaction

$$Zr + 2H_2O \rightarrow ZrO_2 + 4H$$

In a system that is not degassed continuously, some of this hydrogen diffuses into the zirconium alloy. Because the solubility[6] of hydrogen in zirconium is very limited (see Fig. V-1), a second phase ($ZrH_{1.53}$) precipitates, usually in the form of platelets. The amount, size, distribution, and orientation of this precipitated

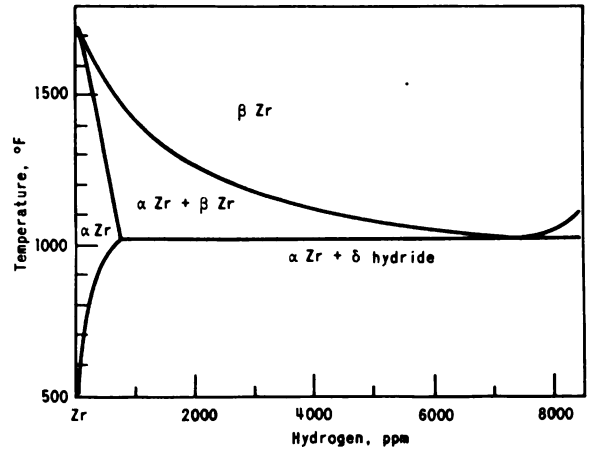

Fig. V-1 Zirconium–hydrogen phase diagram shows that solubility of hydrogen in zirconium increases with temperature up to about 1020°F, above which hydrides will not accumulate.[6]

Digitized by Google

phase may have a pronounced effect on the mechanical properties of the zirconium alloy.

Factors Affecting Hydrogen Uptake

Kirk[7] predicts that 30 to 50% of the available corrosion-product hydrogen will be absorbed by Zircaloy-2 and Zircaloy-4. Other data[8–10] indicate that 50% is probably the high side of the range and that absorption may be as low as 5%, depending on temperature, pressure, irradiation field, and other factors.

The dominant factors affecting the rate and amount of hydrogen uptake of available corrosion-product hydrogen are: zirconium-alloy composition, temperature, characteristics of the oxide film, radiation field, and coolant chemistry.

Alloy Composition. In discussing Zircaloy-2, nickel-free Zircaloy-2, and Zircaloy-4, Kass[11] states that hydrogen absorption is enhanced by the presence of nickel in the alloy. He reports that nickel-free Zircaloy-2 and Zircaloy-4 are superior to Zircaloy-2 in less than or equal to 680°F water because of their lower hydrogen pickup and decreased sensitivity to hydride failure but that above 750°F Zircaloy-2 has better oxidation resistance; beta quenching permits all three alloys to be used up to 850°F. Klepfer and Douglass[12] demonstrated that zirconium-base alloys containing copper and iron have less long-term hydrogen pickup than Zircaloy-2 (Table V-1). Greenberg and Youngdahl[9] report the combined effect of alloying and heat-treatment on hydrogen uptake (Table V-2); they conclude that hydrogen absorption in a particular alloy is primarily sensitive to exposure temperature and that a zirconium-base alloy containing 1.1% copper and 1.2% iron merits further study. Freer, Silvester, and Wanklyn[10] show the effect of 1% copper on hydrogen uptake at 932°F (Figs. V-2 and V-3). Weinstein and Holtz[13] determined the hydrogen pickup of various alloys in 680°F water and 750°F steam (Tables V-3 and V-4).

Temperature. Greenberg and Youngdahl[9] show (Table V-2) that hydrogen absorption by zirconium alloys after long exposure to steam is relatively insensitive to heat-treatment and composition of the alloys but very sensitive to temperature at least above about 1000°F. The percentage of corrosion-product hydrogen absorbed is much less at 1200°F than at 1000°F.

Table V-1 EFFECT OF TEMPERATURE ON LONG-TERM HYDRIDING OF THREE ZIRCONIUM ALLOYS*[12]

Alloy, at.%	Hydride rate, 10^{-2} mg/(dm^2)(day) At 750°F	At 930°F
Zircaloy-2	1.8	41.6
Zr–1 Nb–1 Cu–0.3 Fe	1.4	4.4
Zr–1.1 Cu–0.3 Fe	0.068	6.1

*In 1000-psi low-velocity flowing steam containing 20 ppm O_2 and 2.5 ppm H_2. Exposure time: rate data taken "posttransition," 1000 to 3000 hr. Specimens were fabricated from sponge by double consumable arc melting, forged and hot rolled at 1450°F, water quenched, 20% cold rolled, and alpha annealed 8 hr at 1050°F.

This result[6] is to be expected since zirconium hydride is unstable at temperatures above about 1020°F (see Fig. V-1).

Oxide Film. Gulbransen and Andrew[14] found that oxide films may inhibit the gaseous hydriding of zirconium by factors of 1000 or more. Smith[15] showed that the hydrogen pickup rate is inversely proportional to the ZrO_2 film thickness. Freer, Silvester, and Wanklyn[10] studied hydrogen uptake during initial stages of corrosion in superheated steam at 930°F. They suggest that reactions at the steam–oxide film interface, rather than bulk oxide films, control hydrogen entry into the alloy. Figure V-4 shows typical hydrogen uptakes[10] in steam at 932°F.

Irradiation. Exposure of zirconium alloys to irradiation conditions in a reactor can either increase or decrease hydrogen pickup. By contributing to a slow but steady buildup of oxide film on the surface of zirconium alloys (by means of radiolytically produced oxygen and activation of the surface), radiation can retard hydrogen pickup. MacDonald and Parry[16] found that the ZrO_2 film on alpha-annealed Zircaloy-2 fuel sheaths that had been irradiated 13,000 hr in less than or equal to 480°F pressurized water (the fuel was run at $\int_{T_1}^{T_2} k\,dT \leq 40$ watts/cm until a burnup of 10,000 Mwd per metric ton of uranium was attained) was 2 to 3 μm thicker than expected from out-of-reactor tests. This caused hydrogen pickup to be considerably less (3 to 20%) than the 50% pickup predicted by out-of-reactor tests.

In general agreement with MacDonald and Parry,[16] Burns and Maffei[17] state that a fast-neutron exposure of 0.3 to 8.2×10^{20} neutrons/cm^2 increases greatly the average corrosion

Digitized by Google

Table V-2 HOW COMPOSITION AND HEAT-TREATMENT OF ZIRCONIUM ALLOYS AND THE TIME AND TEMPERATURE OF THEIR EXPOSURE TO SUPERHEATED STEAM AFFECT THEIR ABSORPTION OF CORROSION-PRODUCT HYDROGEN[9]

Alloy, wt.% heat-treatment*	Exposure to 600-psi steam: Temperature, °F	Exposure to 600-psi steam: Time, days	Weight gain, mg/cm²	H_2 concentration, ppm	Hydrogen absorbed, %
Zr–3 Ni–0.5 Fe (initially contained 20 ppm H_2)					
As cast	1000	35	0.8	80	93
As cast	1000	97	1.8	119	56
Zr–3.1 Ni–0.6 Fe (initially contained 22 ppm H_2)					
As hot rolled	1000	1	1.1	166	45
As hot rolled	1000	7	1.9	203	41
H, Q, A	1000	108	5.30	666	55
H, Q, A	1200	88	9.38	348	14
H, Q	1200	88	9.19	330	14
H, C, Q, C	1000	108	6.88	1451	61
H, C, Q, C, A	1000	108	7.51	1320	53
Zr–2.1 Ni–0.6 Fe (initially contained 16 ppm H_2)					
As hot rolled	1000	117	8.63	1208	67
H, Q, A	1000	108	6.58	875	62
H, C	1000	117	9.69	1518	63
H, C, Q, C	1000	108	7.68	868	40
H, C, Q, C, A	1000	108	7.22	940	43
Zr–1.1 Cu–0.7 Fe (initially contained 22 ppm H_2)					
H, Q, A	1000	108	9.81	980	46
H, C, Q, C	1000	108	10.8	1175	41
Zr–0.5 Cu–1.0 Fe (initially contained 18 ppm H_2)					
H, Q, A	1000	108	6.21	641	47
H, C, Q, C	1000	108	4.80	356	25
H, C, Q, A	1000	108	7.25	1080	62
Zr–1.1 Cu–1.2 Fe (initially contained 21 ppm H_2)					
As hot rolled	1000	1	0.60	30	7
As hot rolled	1000	7	1.20	38	8
H, Q, A	1000	108	6.90	716	44
H, Q, A	1200	88	8.53	131	5.5
H, Q	1200	88	8.30	90	3.6
H, C, Q	1000	108	6.71	583	32
H, C, Q, A	1000	108	7.42	932	49

*H = hot rolled; Q = quenched from 1650°F; A = aged for 1 hr at 1290°F, then air cooled in capsule; C = cold rolled with <20% reduction.

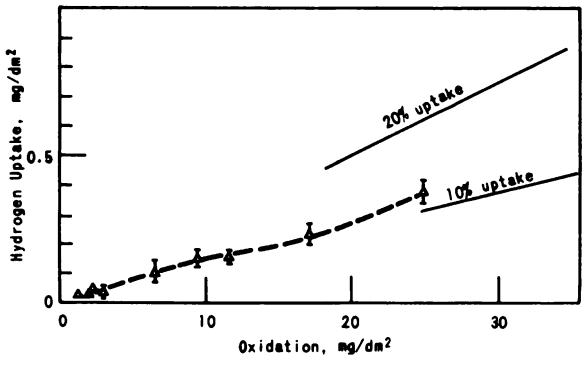

Fig. V-2 Hydrogen uptake of crystal-bar zirconium in 932°F steam of atmospheric pressure.[10]

rates of Zircaloy-2 in 540°F water having *p*H = 10, but that the fraction of corrosion–hydrogen pickup remains in the low part of the range normally found in the absence of radiation. They note that the corrosion proceeds at a nearly uniform rate above an as-yet-undetermined threshold flux rate.

On the other hand, under coolant flow and temperature conditions that erode the oxide film or encourage hydride pickup, the surface activation and hydrogen produced by irradiation can cause more total hydrogen to be picked up. Tobin[18] shows in Fig. V-5 that Zircaloy-2 at 540°F in a reactor loop picks up markedly more hydrogen than it does in an out-of-reactor loop at the same temperature; but he states that percentage uptake in the reactor is on the low side of the out-of-reactor results.

Water dissociates radiolytically. The amount and types of net steady-state dissociation products depend on at least two reactions: (1) a forward reaction that depends primarily on the intensity and type of radiation and (2) a back reaction that depends on temperature, the con-

Digitized by Google

centration of decomposition products, the type and intensity of radiation, the type and concentration of impurities in the water, and possibly on catalytic effects of materials in the immediate zone of dissociation.

In high-temperature pressurized-water reactors, the net dissociation is very low. It is probable that the only hydrogen available to react with the zirconium alloy is the small residual amount from reaction of equilibrium oxygen with metallic surfaces.

Coolant Chemistry. Dalgaard[19] states that zirconium–2.5% niobium alloys, with or without 0.5% copper, are very sensitive to LiOH in water of $pH = 10$; he also reports that small concentrations of oxygen or oxidizing agents in water or steam may depress hydrogen uptake significantly.

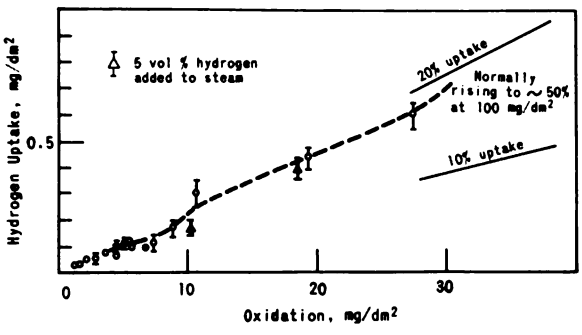

Fig. V-3 Hydrogen uptake of zirconium–1% copper alloy in 932°F steam of atmospheric pressure.[10]

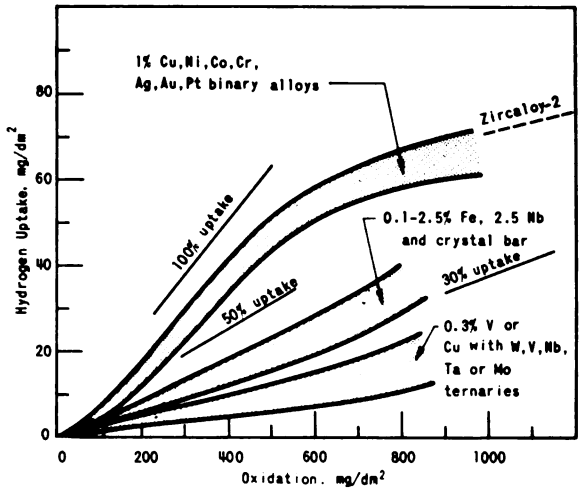

Fig. V-4 Hydrogen-uptake ranges of zirconium alloys in 932°F steam.[10]

Table V-3 HYDROGEN PICKUP AND TENSILE STRENGTH OF ZIRCONIUM ALLOYS IN 680°F WATER FOR 200 DAYS[13]

Composition, wt.%	Hydrogen pickup			Ultimate tensile strength (at 680°F), psi
	Weight gain, mg/dm²	Total H_2, ppm	Pickup, %	
Zircaloy-2	68.47	183	46	27,800
Zr–1 Cr–0.25 Te	35.79	54	15	32,800
Zr–1 Sb–0.5 Nb	68.59	63	12	
Zr–1 Sb–0.25 Te	49.66	62	17	30,300
Zr–1 Sb–0.25 Ge	52.85	38	8	32,700
Zr–0.5 Sn–0.25 Ge	36.98	51	18	25,100
Zr–0.5 Sn–0.25 Te	42.84	55	18	30,200
Zr–0.5 Nb–0.25 Te	46.88	65	22	30,700

Table V-4 HYDROGEN PICKUP AND TENSILE STRENGTH OF ZIRCONIUM ALLOYS IN 750°F STEAM FOR 125 DAYS[13]

Composition, wt.%	Hydrogen pickup			Ultimate tensile strength (at 750°F), psi
	Weight gain, mg/dm²	Total H_2, ppm	Pickup, %	
Zircaloy-2	87.96	256	50	26,500
Zr–1 Fe–0.25 Cr	51.81	126	55	24,800
Zr–1 Fe–0.25 Te	68.84	204	71	22,300
Zr–1 Fe–0.5 Nb	88.60	212	58	30,200
Zr–1 V–1 Fe	72.00	163	50	31,800
Zr–3 Cr–1 Fe	65.43	158	50	30,000
Zr–3 Cr–0.25 Te	67.03	141	43	32,700
Zr–0.5 Nb–0.25 Cr	97.47	79	13	27,900
Zr–0.5 Nb–0.25 Te	66.95	94	30	27,200

Digitized by Google

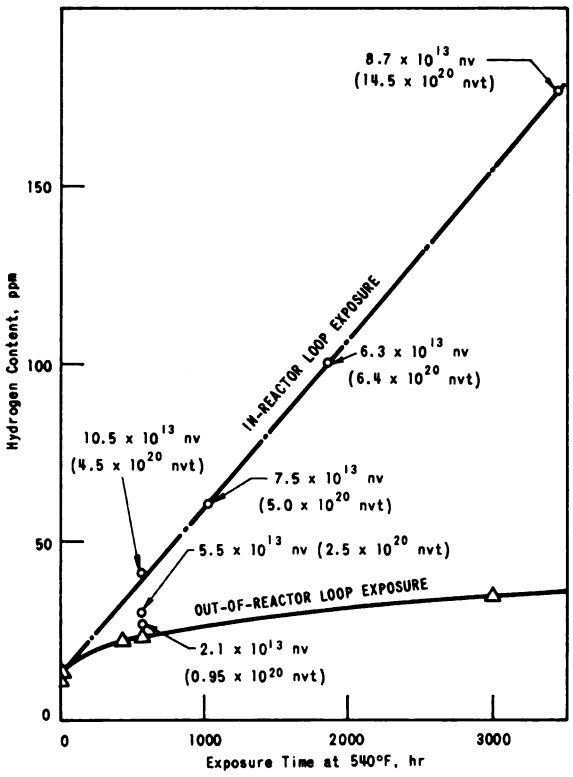

Fig. V-5 Much more total hydrogen is picked up by Zircaloy-2 in a reactor loop with 540°F water than in an out-of-reactor loop with same-temperature water.[18]

How Hydrides Affect Properties

The major effect of adversely oriented hydrides is to decrease ductility,[20] but tensile strength[20] and stress-rupture life[21] also might be reduced. From studies of the effect of irradiation on Zircaloy-2 containing 0 to 200 ppm H_2 and zirconium–2.5% niobium containing 0 to 300 ppm H_2, Sawatzky[22] concludes that hydrogen has little effect on tensile strength at 77 to 832°F. He also found that hydrogen decreased the ductility of both alloys, but the effect was less than that of irradiation to 10^{21} neutrons/cm^2 ($E > 500$ ev) at 536°F. Sawatzky also noted that deuterium and hydrogen have the same effect on the impact strength of Zircaloy-2 on an atom-for-atom basis.

By means of drop-weight tests on unirradiated pressurized tubes, Farrow and Watkins[23] found that 20%-cold-worked Zircaloy-2 containing less than 100 ppm H_2 does not support crack propagation at room temperature, but that tubes having 200 ppm H_2 exhibit crack propagation below 250°F. Standard drop-weight tests on the same material indicated a ductile–brittle transition temperature of 230°F; Zircaloy-2 with as much as 800 ppm H_2 has a ductile–brittle transition temperature less than 445°F, which is well below the operating temperatures of power reactors.

Babyak, Bourgeois, and Salvaggio[8] show that increased hydrogen content causes little loss of necking strain in Zircaloy-2 at 500°F. They also note that beta-quenched Zircaloy-2 with uniformly distributed hydrides shows greater necking strain than material to which no hydrogen has been added. At room temperature the necking strain of alpha-annealed Zircaloy-2 containing 500 ppm H_2 is about half the initial (low hydrogen) value, regardless of morphology, but beta-quenched material with uniformly distributed hydrides shows little effect. Samples containing 200 to 300 ppm H_2 in the form of grain-boundary hydrides show a decrease to only 1 to 2% strain.

Causes and Control of Orientation

Data presented by Burton[24] and by Mehan and Wiesinger[25] indicate (1) little if any effect of hydrogen content (up to at least 500 ppm) on the tensile strength of annealed Zircaloy-2 from room temperature to 600°F and (2) no effect on ductility above about 300°F. But if the hydride is situated in the grain boundaries or, particularly, if the hydride platelets are preferentially oriented in a direction perpendicular to the stress direction, brittleness develops.[5]

Marshall and Louthan[3] also report that, like the effect prior strain has on hydride orientation, stress applied during hydride precipitation causes the hydride platelets to orient preferentially—and, when the treatment produces hydrides oriented perpendicularly to the stress axis, both strength and ductility decrease significantly.

Marshall and Louthan[3] also observe that unfavorable orientation can be corrected by applying stress (in a direction perpendicular to the platelets) during hydride precipitation (precipitation occurs when the material is cooled below the hydrogen solubility temperature or during the longer times while the alloy is absorbing more than a soluble amount of hydrogen); the amount of stress needed depends on fabrication history. Although Louthan and Marshall[5] found that for highly susceptible material the minimum transverse stress to change hy-

Digitized by Google

dride orientation may be as low as 6000 psi, Wootton[20] shows that a stress of 16,000 psi appears to be somewhat below that required. But both investigators agreed that hydrides oriented parallel to the applied stress are unaffected by as much as 16,000 psi. Parry and Evans[4] found that the hydride precipitated parallel to the direction in which grains are deformed and that a minimum strain of 7% is required to produce directionality.

Significance

From the data described it can be concluded that reactor designers can avoid or alleviate the problems of hydride-induced brittleness and loss of strength in Zircaloy: (1) by selecting alloys and the surface films and water conditions that reduce hydrogen absorption, (2) by choosing operating temperatures that prevent hydride formation or accumulation, and (3) by designing components and specifying fabricating methods that cause any hydride platelets that do form to precipitate either in random orientation or parallel to the principal operational stress.

Slow Hydrogen Absorption. Much effort is being exerted to learn techniques to reduce the rate by which corrosion-induced hydrogen is absorbed by zirconium alloys. The fact that many reactor cores of pressurized- and boiling-water reactors have performed satisfactorily with Zircaloy-2 at about 600°F or less is prima facie evidence that either the reaction rate

$$Zr + 2H_2O \rightarrow ZrO_2 + 4H$$

is very slow below this temperature or that the diffusion rate of hydrogen through the existing oxide film is very low, or both. Above 600°F the amount of hydrides formed is, in many instances, sufficient to cause concern. The removal of nickel from Zircaloy-2 and other slight modifications has resulted in an alloy designated as Zircaloy-4. It is slightly less corrosion resistant than Zircaloy-2, but it is substantially less susceptible to hydriding. Although other alloys, notably zirconium–2.5% niobium, have been proposed, they have not yet been specified for a reactor core.

As noted by Burns and Maffei[17] and by MacDonald and Parry,[16] neutron irradiation lowers the percentage uptake of hydrogen, thus tending to offset any increased concentration of hydrogen in the coolant resulting from possible increased in-reactor oxidation rate of the zirconium alloy. Tobin[18] showed higher total hydrogen uptake under irradiation owing to increased corrosion rates but stated that the percentage uptake is on the low side of the out-of-reactor results.

Prevent Hydride Formation. Designers can select alloys and operating temperatures such that the solid solubility limit of hydrogen is not exceeded (so that zirconium hydride will not form and precipitate). In the intermediate-temperature range of interest for reactor application, moderate hydrogen pickup may not be deleterious because the solubility of hydrogen increases with temperature. For example, Fig. V-1 shows that, at 750°F, up to about 250 ppm H_2 can be accommodated without hydride formation; at 1000°F about 800 ppm can be tolerated. The designer can take advantage of this phenomenon if the operational conditions maintain the zirconium alloy above the temperature corresponding to the predicted hydrogen saturation level.

If the zirconium-alloy component operates at a temperature above that at which the zirconium hydride phase becomes unstable (~1020°F; see Fig. V-1), the hydride will accumulate slowly, if at all. This is supported by Greenberg and Youngdahl,[9] who report only a 5.5% uptake of corrosion-product hydrogen at 1200°F in out-of-reactor tests. However, the relief from hydride problems above about 1020°F is usually only of academic comfort because of oxygen embrittlement and loss of strength at such temperatures.

Random or Parallel Orientation. The orientation of the precipitated zirconium hydride phase in either a completely random fashion or in preferred orientations related to the operational stress is the factor that most readily lends itself to control by the designer. Although the presence of hydrogen, per se, in zirconium alloys has little effect on the metal properties, there is a pronounced deleterious effect if zirconium hydride precipitates as platelets either in the grain boundaries or preferentially oriented perpendicular to the principal stress. This behavior corresponds in many ways to the ductile–brittle transition in steel.

In fully alpha-annealed or beta-quenched zirconium alloys, the hydrides present at the

Digitized by Google

annealing or quenching temperature tend to precipitate randomly. However, slow cooling from these temperatures tends to cause the hydride platelets to accumulate in the grain boundaries, thus resulting in brittleness. If the metal is free of stress, corrosion-product hydrogen will form randomly oriented hydrides. However, when the metal is in a stressed condition, the hydrides precipitate preferentially in an orientation perpendicular to tensile stresses and parallel to compressive stresses; in fact, the preferential orientation can be changed by reversing the stress direction in service.[5] Hence it is important that the designer specify production and fabrication methods that yield optimum orientation of the hydride platelets. He also should design Zircaloy reactor internals in a manner that ensures platelet orientation parallel to the principal stress axis during operation.

References

1. A. S. Bain, G. M. Allison, L. M. Howe, and A. Ridal, Failure of Swaged UO_2 and Co-extruded U_3Si Specimens Irradiated in X-2 Loop (Test X-2-q), Canadian Report CRMet-904, Appendix III, 1959.
2. G. R. Caskey, Jr., G. R. Cole, and W. G. Holmes, Failures of UO_2 Fuel Tubes by Internal Hydriding of Zircaloy-2 Sheaths, in Proceedings of the Symposium on Powder Packed Uranium Dioxide Fuel Elements, Windsor, Conn., 1961, USAEC Report CEND-153, Vol. II, pp. 77-101.
3. R. P. Marshall and M. R. Louthan, Jr., Tensile Properties of Zircaloy with Oriented Hydrides, *Trans. Am. Soc. Metals*, 56: 693 (1963).
4. G. W. Parry and W. Evans, The Effect of Strain on the Directional Precipitation of Zirconium Hydride in Zircaloy-2, Canadian Report CRGM-1135 (AECL-1707), December 1962.
5. M. R. Louthan, Jr., and R. P. Marshall, Control of Hydride Orientation in Zircaloy, *J. Nucl. Mater.*, 9(2): 170-184 (1963).
6. D. H. Stone, Some High Temperature Mechanical Properties of Zircaloy-2, Type 304 Stainless Steel, and AM-350 Stainless Steel, USAEC Report NAA-SR-11047, Atomics International, June 15, 1965.
7. W. W. Kirk, Corrosion and Hydrogen Pickup of Zircaloy-2 and Zircaloy-4, in Zirconium Highlights, USAEC Report WAPD-ZH-21, pp. 8-14, Bettis Atomic Power Laboratory, Westinghouse Electric Corp., December 1959.
8. W. J. Babyak, W. F. Bourgeois, and G. J. Salvaggio, Effect of Hydride Morphology on the Tensile Properties of Zircaloy-2, in *Corrosion of Zirconium Alloys*, American Society for Testing and Materials, Special Technical Publication No. 368, pp. 76-100, 1964.
9. S. Greenberg and C. A. Youngdahl, Superheated Steam Corrosion of Zirconium Alloys Containing Small Amounts of Iron and Copper or Nickel, *Corrosion*, 21(4): 113-124 (April 1965).
10. D. W. Freer, D. R. Silvester, and J. N. Wanklyn, Hydrogen Uptake of Zirconium and Its Alloys During Early Stages of Corrosion in Steam, *Corrosion*, 21(4): 137-142 (April 1965).
11. Stanley Kass, The Development of the Zircaloys, in *Corrosion of Zirconium Alloys*, American Society for Testing and Materials, Special Technical Publication No. 368, pp. 3-27, 1964.
12. H. H. Klepfer and D. L. Douglass, The Factors Limiting the Utilization of Zirconium Alloys in Superheated Steam, in *Corrosion of Zirconium Alloys*, American Society for Testing and Materials, Special Technical Publication No. 368, pp. 118-142, 1964.
13. D. Weinstein and F. C. Holtz, Development of Improved Zirconium Alloys for Use in Superheated Water and Steam, USAEC Report GEAP-4089, Vol. 1, Paper 6, General Electric Company, Vallecitos Atomic Laboratory, Nov. 30, 1962.
14. E. A. Gulbransen and K. F. Andrew, Diffusion of Hydrogen and Deuterium in High Purity Zirconium, *J. Electrochem. Soc.*, 101: 560-566 (1954).
15. T. Smith, Hydrogen Permeation of Films on Zirconium, USAEC Report NAA-SR-6267, Atomics International, May 15, 1962.
16. R. D. MacDonald and G. W. Parry, Zircaloy-2 Clad UO_2 Fuel Elements Irradiated to a Burnup of 1000 MWd/Tonne U, Canadian Report CRFD-1178 (AECL-1952), January 1964.
17. W. A. Burns and H. P. Maffei, Neutron Irradiation and Cold Work Effects on Zircaloy-2 Corrosion and Hydrogen Pickup, in *Corrosion of Zirconium Alloys*, American Society for Testing and Materials, Special Technical Publication No. 368, pp. 101-117, 1964.
18. J. C. Tobin, Progress on the Irradiation Damage to Reactor Metals Program. A Summary of Hanford Laboratories Achievements in This Program under General Electric Company Management, 1962-1964, USAEC Report HW-83615, p. 28, Hanford Atomic Products Operation, Dec. 15, 1964.
19. S. B. Dalgaard, Factors Affecting Oxidation and Hydriding of Zirconium Alloys, *Trans. Am. Nucl. Soc.*, 6(2): 370 (November 1963).
20. G. C. Wootton, The Effect of Oriented Hydride on the Mechanical Properties of Zircaloy-2 Tubing, Canadian Report AECL-1989, March 1964.
21. R. C. Aungst, Stress Rupture Tests of Zircaloy-2 Pressure Tubes, USAEC Report BNWL-8, Battelle-Northwest, January 1965.
22. A. Sawatzky, The Effect of Neutron Irradiation on the Mechanical Properties of Hydrided Zirconium Alloys, Canadian Report AECL-1986, June 1964.
23. M. Farrow and B. Watkins, The Effect of Hydrogen on the Embrittlement of Zirconium-base Pressure Tubes, British Report TRG-Report-774, Apr. 23, 1964.
24. H. H. Burton, Hydrogen Effects of Zircaloy-2 Tensile Properties, USAEC Report HW-61077, Hanford Atomic Products Operation, July 10, 1959.
25. R. L. Mehan and F. W. Wiesinger, Mechanical Properties of Zircaloy-2, USAEC Report KAPL-2110, Knolls Atomic Power Laboratory, Feb. 1, 1961.

Digitized by Google

Section

VI

Power Reactor Technology

Fuel Elements

Letters to the Editor

Boiling-Water Environment Not Necessarily Detrimental to Stainless-Steel Cladding

In the letter by R. J. Allio in *Power Reactor Technology*, 8(2), the successful application of stainless-steel cladding in pressurized-water reactors (PWR) is contrasted with the experience with such cladding reported from the Vallecitos Boiling Water Reactor (VBWR).[1] It is the purpose of this communication to review the statements in the reference letter concerning the differences between PWR and BWR cladding behavior and, further, to examine in some detail why the VBWR data are *not* applicable to BWR's in general.

1. *System Pressure*

"Higher pressure prevents or delays development of tensile stress." The 12,000-psi compressive stress corresponds to an incremental strain of approximately 5×10^{-4} in./in., which with UO_2-fueled rods corresponds to an increase in allowable burnup of about 250 Mwd per metric ton of uranium. Since the PWR fuels cited exceeded the VBWR burnups by factors of 2 and 3, clearly the increased compression on the cladding due to the higher pressure cannot explain the difference in behavior.

"Crack propagation cannot normally occur in the absence of a tensile stress." Both tensile and compressive stresses lead to failure via cracking in *cold-worked* austenitic stainless steel even in oxygen- and chloride-free water.[2]

2. *System Chemistry*

"High oxygen concentrations have been shown in laboratory experiments to accelerate stress corrosion." This statement is erroneous unless qualified by the statement "in the liquid phase and in the presence of chloride ion."[3] The concentration of oxygen in the vapor phase in BWR's is immaterial to this discussion and, depending upon the residence time of the coolant in the core, reactor power density, system pressure, etc., can be an order of magnitude smaller than the 20 to 40 ppm cited. However, oxygen does not always act in a detrimental manner; some metals, including the austenitic stainless steels, form a highly impervious oxide film that provides resistance to further attack,[4] and oxygen has been employed to passivate steels in high-temperature water.[5]

3. *Corrosion-Product Deposition*

System chemistry and corrosion-product deposition are inseparable aspects of intermeshing phenomena and system design philosophy and criteria. Hence such an arbitrary separation is inappropriate to a technical discussion. The evidence indicates that corrosion-product deposition on stainless-steel claddings in both PWR's and BWR's has been negligible[6] and that only after relaxation of water purification specifications did the VBWR exceed negligible deposition.[7] Only in the Experimental Boiling Water Reactor (EBWR)[8] was scaling of fuel elements appreciable, and this was due to aluminum oxide formed in the core from the aluminum–nickel alloy dummy fuel elements.

One could argue that the dynamic action of nucleate-boiling bubble formation, at the fuel-element surface in BWR's, should "scour" the surface free of "crud"; therefore the "crud bursts" and short-term high-coolant impurity levels encountered in PWR's after thermal shocks should not occur in a BWR.

Digitized by Google

4. *Local Thermal Stresses*

The thermal fluctuations cited in the reference letter are based on measurements made under conditions (1) of atmospheric pool boiling, (2) of very low heat flux—to permit the study of individual bubble histories, and (3) of specially prepared poorly nucleating surfaces—again to study the life cycles of individual bubbles. The effect of pressure on boiling superheat (wall temperature minus saturation temperature) results in a decrease in required superheat, at equal heat fluxes, of factors of 3 for subcooled boiling,[9] and of 3.7 for bulk boiling;[10] thus the maximum magnitude of these fluctuations falls from the 30°F claimed to 8 to 10°F at 1000 psia. The effect of increasing heat flux at atmospheric pressure, according to the Eindhoven research,[11] is to decrease the amplitude and increase the frequency of thermal fluctuations; therefore higher heat fluxes cause damping even at low pressure where the driving force is large. Fuel-element surfaces are characteristically "rough" by laboratory standards, providing numerous, randomly spaced and random-sized nucleating sites (the "small surface crevices or pits" of the reference letter as well as grain boundaries, discontinuities in the oxide layer, etc.). With numerous nucleating sites scattered randomly over a surface, the surface temperature in a representative region will be the result of summing the thermal fluctuations from the surrounding bubble generating sites, each of which is randomly producing bubbles at various stages in their life cycles. Thus "real" surfaces tend to damp both the severity (amplitude) and frequency of thermal fluctuations.

In addition to these basic arguments, the measurements cited are inapplicable because they ignore the effect of coolant velocity on the bubbling layer adjacent to the heated surface. The large increase in frictional pressure drop with nucleate boiling is graphic evidence of increased shear in the bubble layer. A recent study[12] confirms that bubbles migrate on the heated surface under the influence of coolant velocity. Therefore, during the life cycle of a bubble, it may not remain at the nucleation site, and that site, therefore, cannot experience the full thermal fluctuation proposed in the reference letter.

VBWR Data Not Applicable to BWR's in General

We have discussed the points raised and have shown that the arguments against BWR's are questionable. It is appropriate, however, to examine why the VBWR fuel elements did fail and to show that the VBWR experience is atypical of BWR practice. The behavior of stainless steels in water-cooled nuclear reactor environments has been extensively studied. The results obtained to date may be conveniently summarized graphically[13] as shown in Fig. VI-1. Two regions may be defined: that below an exposure of approximately 10^{21} neutrons/cm^2 and that beyond this level. In the first region the effects of water chemistry (corrosiveness of coolant), degree of cold-work initially imposed on

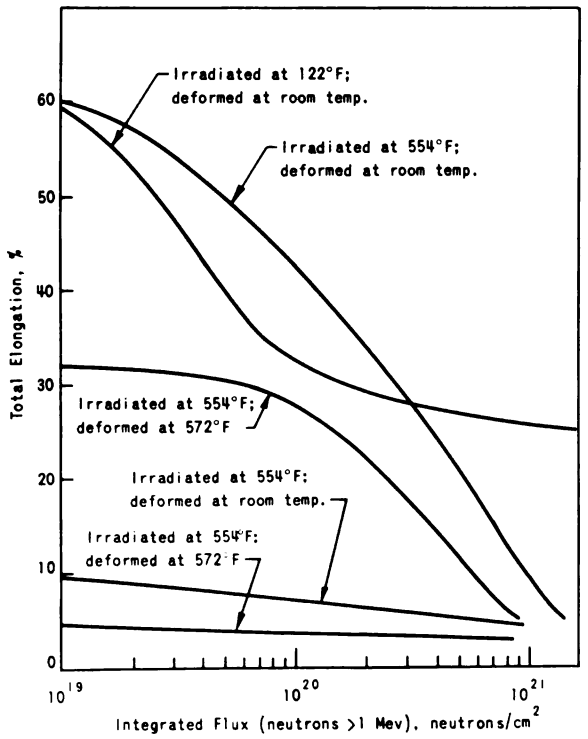

Fig. VI-1 Effects of radiation on ductility of type 348 stainless steel; upper three curves are for annealed samples; lower two curves are for 25% cold-worked samples.[13]

Digitized by Google

the metal, and stress imposed by the mechanical design all play an important role. This is the region in which all the VBWR failures lie. If a fuel-element design and the environment are both favorable, exposures in excess of 10^{21} neutrons/cm^2 (>1 Mev) may readily be attained, as shown by the PWR experience cited. The history of the J-10 loop (ETR) pressure tube[14] shows that thermal cycling and stress, of themselves, do not cause failure.

Despite the reported low level of chloride ion in the VBWR coolant,[15] coolant chemistry control must have been grossly inadequate, since chemical analysis of the crud deposited on some VBWR elements revealed up to 4000 ppm chloride ion.[16,17] This is not the whole story, however. Three classes of fuel cladding were irradiated in the VBWR: highly cold-worked, commercially annealed, and fully annealed. Although the VBWR personnel refer[18] to the commercially annealed cladding as annealed, they had measured the residual stress level in this tubing at 10,000 to 20,000 psi. Commercial annealing consists of a 10-min exposure to 1800°F; full annealing requires at least an hour at 1800°F for 300-series steels.[19] Both the cold-worked (residual stress of 10,000 to 40,000 psi) and commercially annealed tubing failed in the VBWR tests. However, a series of elements had been prepared by Nuclear Metals, Inc., by coextrusion of the UO_2 and type 304 stainless steel at temperature high enough (>1800°F) to assure full annealing of the cladding; these were irradiated under the same environmental conditions as the other elements, and, although the density of the UO_2 was higher (97 vs. 95% of theoretical) and these elements had no gap between the UO_2 and steel, none failed.[16,17] Thus we have evidence of the value of fully annealed cladding relative to the cold-worked varieties under irradiation, extending the out-of-pile experience previously reported.[20] In addition, the high chloride-ion content of the crud testifies to the hostile coolant environment in the VBWR. The inescapable conclusion is that the VBWR environment embrittled stainless-steel claddings causing intergranular and transgranular cracking.

To show that high-quality coolant ensures satisfactory BWR cladding performance, consider the experience in the Elk River reactor. Although the strength of the cladding has been compromised by incorporation of 600 ppm boron (as burnable poison), exposures have exceeded levels at which similar elements (0.003-in. diametral gap and 95% theoretical density UO_2) had failed in the VBWR without any failures.

Thus the assertion that the boiling-water environment is necessarily detrimental to stainless-steel cladding cannot be substantiated.

L. Bernath and B. W. Colston
Atomics International

Rebuttal: Boiling Water Is Detrimental to Stainless-Steel Cladding

I commend Messrs. Bernath and Colston for their attempts to provide additional insight into the behavior of stainless-steel-clad fuel elements in water-reactor environments. However, the validity of my original position, to wit, that a boiling-water environment is detrimental to stainless-steel cladding, has recently been affirmed by other knowledgeable investigators.[21,22] Nevertheless, the reader may appreciate our identification of several fallacies Bernath and Colston attempt to promulgate.

1. *System Pressure*

Both PWR and BWR stainless-steel-clad fuel elements are normally designed to have a 0.003 to 0.006-in. diametral fuel-cladding gap. In such fuel elements the primary source of stress is fission-gas accumulation. Thus a simple calculation of fission-gas release as a function of burnup shows that an increase in external pressure of 1000 psi may permit even a "factor of 2 and 3" increase in burnup, assuming exposure to be limited by the attainment of a specific tensile stress. The Bernath and Colston calculation of 250 Mwd per metric ton of uranium may refer to a fuel swelling phenomenon, which is not relevant to the fuel elements under discussion.

Crack propagation normally occurs only when the resulting decrease in elastic strain energy is greater than the energy required to create new surface. Bernath and Colston have misinterpreted their Ref. 2, which does not provide evidence for "crack propagation in the absence of a tensile stress." Nor does their Ref. 2 demonstrate that "compressive stresses lead to failure." Explicit interpretation of the experimental results of their Ref. 2 is not possible because of the failure of the authors to define the actual stress state at the surface. Stress state in the specimens tested will be determined by the sum of residual stresses introduced by the heat-treatment and cold-hardening process, local mechanical stress caused by the roller separating the specimens, and the gross bending load. Cracking kinetics will also be determined by strain energy of the specimen. Thus their Ref. 2 appears to demonstrate only that stainless steel can corrode intergranularly in high-temperature water under certain conditions.

Digitized by Google

2. *System Chemistry*

The presence of chloride was implicit in my observation that high oxygen concentration accelerates stress corrosion, as shown, for example, by the work of Williams and Eckel.[23] Moreover, the suggested qualification of "in the liquid phase" is unnecessary, as shown by the same research.

I cannot possibly disagree with the contention that "oxygen does not always act in a detrimental manner." Unfortunately the examples cited by Bernath and Colston deal with mass corrosion and are not germane to the matter of crack initiation and propagation.

3. *Corrosion-Product Deposition*

It is hardly sporting in a technical discussion to place heavy emphasis on evidence from privy sources, the validity of which cannot be verified by the reader (namely, Bernath and Colston Refs. 6, 15, and 18). Corrosion-product deposition is apparently adjudged to be "negligible"—by what standard, may I ask?

Bernath and Colston may choose to argue that nucleate-boiling bubble formation scours the surface. I prefer to accept the experimental evidence[24] that nucleate boiling in fact promotes crud formation.

4. *Local Thermal Stresses*

The thermal fluctuations measurements cited in my original letter were indeed performed at low heat flux and pressure. Although the magnitude of measured thermal fluctuations will diminish with increasing pressure, the finite mass and dimensions of the thermocouples result in a significant underestimate of the true thermal fluctuations at a point in the cladding surface. Furthermore, the implied generalization that increasing heat flux decreases the amplitude of thermal fluctuation is a gross simplification. In thermal transient phenomena the amplitude of thermal fluctuation is a complex function of not only heat flux but also thermal capacitance, thermal resistance, and source frequency.

The study of the effect of coolant velocities quoted in their Ref. 12 was limited to low pressure, low heat flux, and large bubbles; whereas bubble migration under these conditions cannot be extrapolated directly to behavior under PWR or BWR conditions. In any case, after the sudden growth of a bubble at a heat-transfer surface, liquid inertia will tend to pull the bubble away from the surface. The horizontal shear force associated with high coolant velocity will cut the bubble close to the surface, introducing cooler liquid. Collapse of the remaining bubble will still produce a large thermal fluctuation.

VBWR Data

The relevance of VBWR data to BWR's in general has been confirmed,[1,2] as noted previously.

Figure VI-1, showing decreases in total elongation of stainless steel with increasing neutron exposure (hardly a revelation), surely does not constitute a summary of the "behavior of stainless steels in water cooled nuclear reactor environments." For that matter, total elongation is not even a suitable measure of cladding ductility. I suggest that the relevance of the figure to the Bernath and Colston mechanism for failure is obscure at best.

The addition of boron to stainless steel does not compromise strength.[25] Fuel-element integrity in any event is not a unique function of cladding strength. Moreover, the exposure to date of Elk River fuel elements is insufficient to disprove the generalization that boiling-water environment is detrimental to stainless-steel cladding.

R. J. Allio, *Manager*
Materials and Processes Development
Westinghouse Atomic Power Division

Re-Rebuttal: Readers Can Decide Relevance

We are faced with the onerous task of affirming the factual and rejecting the extraneous and misleading from Allio's rebuttal. The difficulty arises from the fact that Allio's original letter was propaganda and, as such, was a melange of fact and "smoke-screen" against *all* BWR's.

Allio's rebuttal, Refs. 21 and 22, in fact, confirm our position by stressing the importance of the coolant environment. Allio has extracted, out of context, one statement to support his position, namely. "Contrary to initial expectations, Type-304 stainless steel clad fuels have proven unsatisfactory for boiling water reactor service above peak exposures of 15,000 Mwd/tonne." He fails to note, in the same sources, that "Type-304 stainless steel clad was found susceptible to intergranular cracking *in at least some water-reactor environments*," and he omits the table in Ref. 21, which shows that *four* BWR's have been operated to between 7500 and 17,000 Mwd/metric ton exposures

Digitized by Google

and that these are continuing to perform satisfactorily. Allio prefers to cite the VBWR experience as typical, to the possible embarrassment of the GE–San Jose people, who cannot fully defend themselves without admitting to a very cavalier treatment of the pertinent mechanical properties of the cladding as well as of coolant purity requirements. This may have been deliberate on the part of GE—at the initial of the VBWR tests, it was desired to show that no special care was required. It was precisely this situation that prompted us to cite the facts omitted by Allio and to present an objective assessment of the VBWR results.

1. *System Pressure*

Allio cites the existence of a 0.003- to 0.006-in. diametral gap between fuel and cladding to support his contention of the beneficial effects of increased system pressure. What he does not consider is that the cited gap exists only in the cold, as-fabricated condition; simple calculation of the differential expansions of UO_2 and stainless steel, at operating conditions, shows that at zero burnup this gap disappears and that as much as 0.1% strain may be imposed on the cladding. Thus fuel growth or swelling with increasing exposure is most pertinent to the discussion, refuting Allio's opinion that it is not relevant. In fact, Allio's coworkers agree (see page 320 of his Ref. 24) that dimensional stability of UO_2 (which determines the stress condition of the cladding with increasing burnup) is a function of such parameters as "burnup, heat rating, fuel density and grain size, and clad restraint."

As Allio points out, our original Ref. 2 was subject to interpretation. Obviously then, his statements that we have misinterpreted the reference are his opinion and are very much open to question. There is, however, significant merit to his further comments, namely, "Stress state in the specimens tested will be determined by the sum of residual stresses..." It was to summarize these effects, plus the effect of water chemistry and irradiation, that we included our figure of "obscure" relevancy.

2. *System Chemistry*

Allio's allegation that "the presence of chloride was implicit in my observation, etc." cannot be accepted, as repeated reading of his original letter fails to substantiate any appreciation of the effects of chloride ion. He glosses over his misconceptions relative to oxygen concentrations in BWR's and implies that vapor-phase stress corrosion is observed under high coolant purity conditions.

3. *Corrosion-Product Deposition*

Allio not only ignores the evidence we cited, but he also distorts the direct findings of his coworkers (his Ref. 24). The experimental evidence he cites is based on five out-of-pile tests at low bulk velocity and relatively low heat flux, in which ferrous hydroxide was injected to simulate in-reactor corrosion; the validity of this simulation is unsubstantiated. The results obtained are highly suspect since calculation of the density of the deposit (page 4.32 of Ref. 24) indicates a value of approximately 0.5 g/cm^3 rather than the customary one of approximately 3 g/cm^3, a factor of 6 that cannot be explained. The results show (page 4.42 of Ref. 24) that when vigorous boiling occurred (the 1000-psi test condition) the pressure drop across the test section decreased, confirming a significant removal of deposited material (scouring action?).

4. *Local Thermal Stresses*

Allio persists in his belief in the existence of large local thermal stresses in boiling. To buttress his case, he equates the "low heat flux and pressure" of the pool boiling data he cited [10,000 to 30,000 Btu/(hr)(sq ft) and atmospheric pressure] with our Ref. 12, channel flow data [~100,000 Btu/(hr)(sq ft) and 200 psi]; the ratio of liquid-to-vapor density in these two cases, which is a paramount factor in bubble dynamics, differs by more than an order of magnitude, 1600 in the former and 124 in the latter. Allio insists on "sudden growth of a bubble at a heat transfer surface" while ignoring the effects of high coolant velocity to keep bubbles small and to move them along the surface during their growth cycle. Collapse of the bubble, which can only occur in subcooled nucleate boiling, may produce a "thermal fluctuation," but such collapse occurs in the bulk of the fluid, not at the surface!

VBWR Data

The relevance of VBWR data to BWR's in general and of our figure showing the total elongation of stainless steel with increasing neutron exposure is discussed in the second paragraph.

We do wish to thank Mr. Allio for his one useful comment. We agree that the addition of boron to stainless steel does not compromise the strength. We inadvertently used the word "strength," instead of "ductility." The pertinence of our comment concerning the Elk River cladding is, however, substantiated in Allio's Ref. 25. It is shown in this reference that irradiated boron stainless steel shows large (70 to 90%) decreases in elongation after irradiation with the degree of deterioration increasing with thermal-neutron exposure and concentration of boron. We are sure that Mr. Allio is also aware of the recent work in this field.[26,27]

Digitized by Google

An argument such as this can only deteriorate — my father can lick your father — to the point where even the interpretation of the same results can be disputed with vehemence. We suggest, therefore, that only the individual readers of our comments can decide relevance and that each will utilize the discussion to delve into the referenced material to the extent of his immediate interest.

Again, we thank you for the opportunity, via publication of our letter, to present what we feel is a more objective interpretation of the VBWR results.

L. Bernath and B. W. Colston
Atomics International

Editors' Comment

Inasmuch as the objectives of *Power Reactor Technology* are to call its reactor-designer readers' attention to data of concern to them — and to venture interpretation and evaluation in the form of opinions as to the applicability of the data — we particularly welcome contributions from readers that either offer their original evaluations or interpretations that differ with those expressed in articles or letters in our issues. We believe the usefulness of our pages will be enhanced by expressions of differing opinions, which in turn will encourage our authors to venture and verify their interpretations more vigorously. As more data become available to substantiate or refute evaluations presented in our pages, we hope that readers will call them to our attention. In this light, we thank Messrs. Allio, Bernath, and Colston for their useful exchange and invite other readers to volunteer articles or communications on matters of mutual interest.

References

1. Stainless-Steel-Cladding Failures in VBWR, *Power Reactor Technol.*, 7(4): 354-355 (Fall 1964).
2. P. A. Akol'zin and L. V. Korneeva, Study of Corrosion Under Stress of 1Kh18N9T Steel Depending on the Composition of the Medium and State of the Metal, in Corrosion of Reactor Materials: A Collection of Articles, USAEC Report AEC-tr-5219, pp. 124-145, V. V. Gerasimov (Ed.), translated from a Russian publication of the State Publishing House of Literature in the Field of Atomic Science and Technology, Moscow, 1960.
3. D. J. DePaul (Ed.), Stress Corrosion, in Corrosion and Wear Handbook for Water Cooled Reactors, USAEC Report TID-7006, pp. 187-223, March 1957.
4. F. L. LaQue and H. R. Copson (Eds.), *Corrosion Resistance of Metals and Alloys*, 2nd ed., p. 378, Reinhold Publishing Corporation, New York, 1963.
5. Ya. M. Kolotyrkin, G. M. Florianovich, P. S. Petrov, N. K. Smirnova, and L. M. Vyazankin, Use of Oxygen for Protecting Steel from Corrosion in Water at High Temperatures, in Corrosion of Reactor Materials: A Collection of Articles, USAEC Report AEC-tr-5219, pp. 26-40, V. V. Gerasimov (Ed.), translated from a Russian publication of the State Publishing House of Literature in the Field of Atomic Science and Technology, Moscow, 1960.
6. T. J. Pashos, General Electric Company, Atomic Power Equipment Department, unpublished, September 1963.
7. F. J. Brutschy, H. W. Dreyer, and W. L. Pearl, Vallecitos Boiling Water Reactor, Coolant Technology, *Ind. Eng. Chem.*, 51: 1262-1264 (October 1959).
8. C. R. Breden et al., Water Chemistry and Fuel Element Scale in EBWR, USAEC Report ANL-6136, Argonne National Laboratory, November 1960.
9. W. H. Jens and P. A. Lottes, Analysis of Heat Transfer, Burnout, Pressure Drop and Density Data for High-Pressure Water, USAEC Report ANL-4627, Argonne National Laboratory, May 1, 1951.
10. W. M. Rohsenow, A Method of Correlating Heat Transfer Data for Surface Boiling of Liquids, *Trans. ASME*, 74: 969-976 (1952).
11. University of Eindhoven, Final Report on the Research Programme on Heat Transfer and Stability Studies in Boiling Water Reactors, USAEC-Euratom Report EURAEC-335, p. 22, February 1965.
12. G. J. Kirby et al., A Visual Study of Forced-Convection Boiling, Part I, British Report AEEW-R-281, March 1965.
13. J. E. Irvin et al., The Combined Effects of Temperatures and Irradiation on the Mechanical Properties of Austenitic Stainless Steel, in *Flow and Fracture of Metals and Alloys in Nuclear Environments*, pp. 236-250, American Society for Testing and Materials, Special Technical Publication No. 380, 1964.
14. William E. Murr, Frederic R. Shober, Robert Lieberman, and Ronald F. Dickerson, Effects of Large Neutron Doses and Elevated Temperature on Type 347 Stainless, USAEC Report BMI-1609, Battelle Memorial Institute, Jan. 21, 1963.
15. T. J. Pashos, GE-San Jose, personal communication, Dec. 16, 1963.
16. W. H. Arlt and S. R. Vandenberg, Fuel Failure Examinations and Analyses in the High Power Density Program, USAEC Report GEAP-4360,

Digitized by Google

General Electric Company, Vallecitos Atomic Laboratory, Sept. 16, 1963.
17. General Electric Company, Atomic Power Equipment Department, Nuclear Superheat Project. Nineteenth Quarterly Report, February–April 1964, USAEC Report GEAP-4619, May 1964.
18. T. J. Pashos, GE–San Jose, personal communication, Dec. 16, 1963.
19. V. V. Gerasimov, A. I. Gromova, and E. T. Shapovalov, Corrosion Cracking of 1Kh18N9T Steel, in Corrosion of Reactor Materials: A Collection of Articles, USAEC Report AEC-tr-5219, pp. 146-151, V. V. Gerasimov (Ed.), translated from a Russian publication of the State Publishing House of Literature in the Field of Atomic Science and Technology, Moscow, 1960.
20. A. V. Stanyukovich and E. E. Levin, Causes of Failure of Steam Superheater Pipes Made from 18 Cr/12 Ni/1 Ti steel, British Report TRG-Inf-Ser-191, 1963, translated from *Energomashinostroenie*, 10: 27-30 (1961).
21. T. J. Pashos, H. E. Williamson, and R. N. Duncan, Fuel Performance in Boiling Water Reactors, *Trans. Am. Nucl. Soc.*, 8(2): (1965).
22. T. J. Pashos (Comp.), Stainless Steel Failure Investigation Program. First Quarterly Progress Report, February 15–June 30, 1965, USAEC–Euratom Report GEAP-4915, General Electric Company, Atomic Power Equipment Department, Aug. 1, 1965.
23. W. Williams and J. Eckel, *J. Am. Soc. Naval Engrs.*, 68(93): (February 1965).
24. C. Roderick, Large Closed-Cycle Water Reactor Research and Development Program. Progress Report, April 1–June 30, 1964, USAEC Report WCAP-3269-3, Westinghouse Electric Corporation, Atomic Power Division, 1964.
25. W. K. Anderson and J. Theilacker, Neutron Absorber Materials for Reactor Control, *Naval Reactors, Division of Reactor Development*, Washington, 1962.
26. W. R. Martin and J. R. Weir, Effects of Elevated Temperature Irradiation on Hastelloy N, *Nucl. Appl.*, p. 160, April 1965.
27. R. S. Barnes, Embrittlement of Stainless Steels and Nickel Based Alloys at High Temperature Induced by Neutron Radiation, *Nature*, p. 1307, June 1965.

Digitized by Google

Section

VII

Power Reactor Technology

Components

Vapor Traps Protect Liquid-Metal Systems

By David H. Thompson

Instruments and equipment in liquid-metal systems are damaged if the liquid-metal vapor entrained in the inert cover gas condenses out on them. Vapor condensation also can plug gas supply, vent, or instrument lines. Traps that will prevent such damage or plugging are installed in the gas circuits of liquid-metal systems to remove the metal vapor.

We will consider here the principles of such traps, early versions, the variety of types and ways they are used in reactors and other dynamic systems, some recent developments, and conclusions and recommendations concerning their use and the need for improved technology for future reactors. Experience with traps for static systems also is discussed briefly in connection with fume traps for spent-reactor-fuel melt-refining furnaces.

Trapping Principles

Among the phenomena that have been studied for vapor traps are stagnation, impingement, condensation, adsorption, chemical reaction, and repulsion. Vapor traps now used in dynamic systems depend on condensation to remove liquid-metal vapor from the flowing inert gas; stagnation and impingement also are involved in trap operation. Table VII-1 summarizes the features of such traps.

Table VII-1 PRINCIPLES OF CONDENSING VAPOR TRAPS

Type (and temperature)
Configuration
Maintenance of operation
Examples
ACCUMULATING CONDENSER (outlet gas cooler than vapor freezing temperature)
Impingement–condensing type
Cylinder filled with mesh, shot, or liquid NaK; trap is cooled by natural or forced convection
Heated to remove accumulated Na when trap plugs — or replace trap internals
EBR-I, EBR-II, Fermi, SRE, Hallam, SCTI, FARET, SEFOR, SIG
Stagnation–condensing type
Lengths of relatively large diameter pipe
Heated to remove accumulated Na when trap plugs
STF, LAMPRE
CONTINUOUSLY REFLUXING CONDENSER (outlet gas slightly hotter than vapor freezing temperature)
Impingement–condensing type
Cylinder filled with mesh, shot, and/or baffles
After liquid metal agglomerates on trap surfaces, it runs off and is returned to system
FRCTF, Pratt & Whitney research, ANL research

In a condensing vapor trap, natural- or forced-convection cooling reduces the tempera-

Digitized by Google

ture of the inert gas passing through, which results in the metal vapor condensing on surfaces within the trap. The amount of metal vapor that passes through such a vapor trap is a function of the vapor pressure of the liquid metal at the trap outlet temperature—and is extremely small if gas temperatures are kept near the metal freezing point.

In impingement—condensing vapor traps, the extended surfaces formed by the mesh, shot, or baffles force the vapor-laden gas to follow a tortuous path, which promotes both heat transfer from the gas and condensation of the metal vapor.

In stagnation—condensing vapor traps, the relatively large-diameter lengths of pipe lack the extended-surface inner packing or fill of the impingement–condensing vapor traps. They operate most satisfactorily in systems that have slow flows of relatively cool gas.

Early Versions

In early work with sodium and NaK experimental facilities, it was postulated that the relatively large amount of sodium and NaK entrained in the gas was caused by the formation of a stable sodium or NaK aerosol that did not readily condense onto the surfaces over which it passed.[1] Another theory suggested that oxygen present with the inert gas reacted with the sodium vapor to form a stable aerosol of sodium oxide. The conditions required for aerosol production and the nature of the aerosol itself still are not fully understood. However, if aerosol is present in the cover gas of liquid-metal systems, it apparently is not present in concentrations large enough to influence vapor-trap effectiveness.

Some attempts at vapor trapping included experiments with a copper-coil condenser, an electrostatic precipitator, and a NaK bubbler.[1] Gas flow through these devices ranged from 130 to 1560 cu in./hr, and vapor was produced by passing purified argon over a 1500°F sodium pool. The room-temperature NaK bubbler operated effectively over the entire flow range (maximum velocity was ~1 ft/sec), but the condenser (a 16-turn 2-in.-diameter coil of $\frac{1}{4}$-in. copper tubing maintained at 235°F in an oil bath) allowed vapor to pass at high gas flows. The electrostatic precipitator was the least effective vapor trap for dynamic conditions, but it proved satisfactory under static conditions. In work predating the Sodium Reactor Experiment (SRE), it was shown that the stainless-steel wool- or mesh-filled trap could be very effective,[2] but these experiments showed that effectiveness depends on gas temperatures and flows.

Gas Systems, Trap Applications

Much of the developmental effort on vapor traps has been directed toward a particular system or systems for individual reactor projects. Thus most of the concepts, design details, and experience with them have not been reported in the literature. Because of the increasing need for dependable large fast reactor systems, it is worthwhile to describe in some detail the inert-gas blanket systems and vapor-trap installations at a number of liquid-metal-cooled facilities. In this discussion no attempt is made to distinguish between aerosol and vapor or to define the exact nature of the trapping action, whether it be technically termed a filter, trap, or condenser.

EBR-I, EBR-II, FERMI

These first-generation breeder reactors use metallic fuels and have reactor-coolant-outlet temperatures of less than 900°F. All three reactors have argon as the inert cover gas for the primary coolant system, and the gas-supply system of each was constructed with NaK-bubbler type purification units followed by a stainless-steel wool- or mesh-filled vapor trap. However, because the Experimental Breeder Reactor No. 2 (EBR-II) facility is supplied with relatively pure liquid argon, rather than bottled argon as originally proposed, the NaK-bubbler purifier has not been operated. At the Experimental Breeder Reactor No. 1 (EBR-I), the primary-system cover gas was continuously recirculated, whereas, at both EBR-II and the Enrico Fermi Fast Breeder Reactor, the cover-gas systems are operated on a demand type basis and provide for recovery and recirculation of the gas transferred from the primary vessel.

EBR-I. Because EBR-I used NaK, which is liquid at room temperature, as both the primary and secondary coolants, there was only a limited need for vapor traps. During operation a continuous downward flow of argon gas through the reactor top plate was maintained to retard

Digitized by Google

upward diffusion and condensation of NaK vapor on the surfaces near the top of the vessel. The NaK vapor was removed from the recirculating argon primary cover gas by a centrifugal separator and strainer near the inlet to the parallel centrifugal blowers.[3] The strainer tank, approximately 2 ft in diameter and 4 ft high, was fitted near the bottom with a perforated plate and was filled with steel wool. In operation the oxides and NaK liquid trapped in the strainer formed a semisolid mass that allowed little liquid to be withdrawn during draining attempts. When flow through the strainer became restricted, rapping the tank with a hammer was sufficient to restore free flow. This strainer fulfilled the EBR-I trapping requirements, without replacement, for the operation of all four cores. In addition to this strainer, a small-diameter stainless-steel-mesh-filled trap was installed ahead of the piston type positive-displacement depressurizing pump in the gas-transfer line.

Fermi. In addition to the purification-unit vapor trap, Fermi has (1) a Dowtherm-cooled vapor trap in the gas-recirculating system, (2) a vapor trap in the line to the fission-product detector, and (3) lengths or coils of pipe used as vapor traps in the gas lines having slow flows, such as instrument lines. The Dowtherm-cooled vapor trap and other components of the recirculating gas system are located in the Fermi inert-gas building; gas is conveyed from the reactor building to the inert-gas building through a resistance-heated gas line in an underground tunnel. In the gas building the gas flows into a 500-cu ft vacuum tank, then to the Dowtherm-cooled vapor trap, which protects the compressors from liquid-metal entrainment.

As shown in Fig. VII-1, this trap consists of a 26-in.-OD inner shell that is surrounded by a 41.5-in.-OD outer shell charged with Dowtherm A as coolant.[4] The contacting surface of the vapor trap is increased by a 6-ft section of stainless-steel wool enclosed between perforated baffle plates. Downstream from the vapor trap is a cyclone separator, followed by three gas compressors in parallel. Although the line downstream from the vapor trap is not equipped with a sampling means to check trap effectiveness, there has been no evidence of sodium reaching the compressor diaphragms, which are changed periodically.

The EBR-II primary-gas system, like that of Fermi, operates on a demand type basis, with

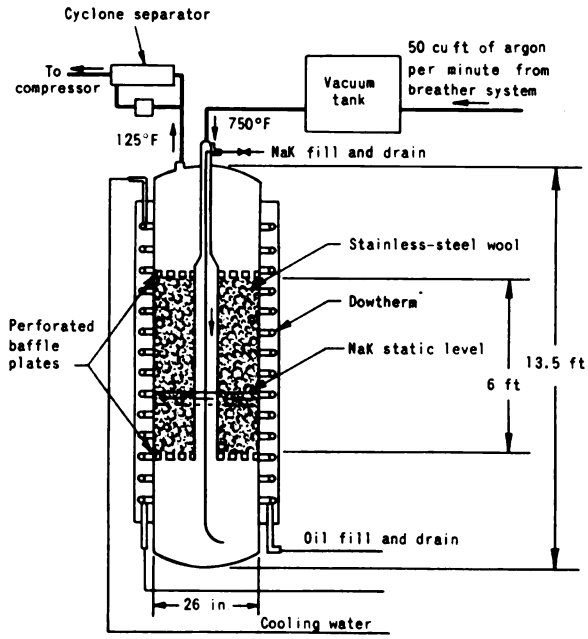

Fig. VII-1 Fermi vapor trap in gas recirculation system bubbles argon through NaK and passes it through stainless-steel wool; water-cooled Dowtherm in annulus cools trap and gas.[4]

the primary-tank argon pressure controlled by a floating-head tank. When gas volume changes because of temperature fluctuations, the floating head in the tank moves to maintain the cover-gas pressure constant.

Figure VII-2 shows the two stainless-steel-mesh-filled vapor or aerosol traps in the EBR-II argon cover-gas system.[5] These traps are not equipped with heaters, and therefore, if plugging occurs, the gas flow can be rerouted through a bypass line to keep the system operative while the traps or their mesh are replaced. Gas discharged from the primary tank passes up through a cleanout or access flange, then through the small vapor trap, through a silicone-oil-cooled heat exchanger that cools the argon to 150°F; then it passes through the large vapor trap and on to the floating-head tank. If the volume change exceeds the capacity of the floating-head tank, one of the two parallel blowers pumps gas into the argon receiver tank for future use (the second blower is a standby unit).

The traps see little flow except when the system is purged. When the primary tank was purged with the system still at approximately 700°F, the small vapor trap became plugged.

Digitized by Google

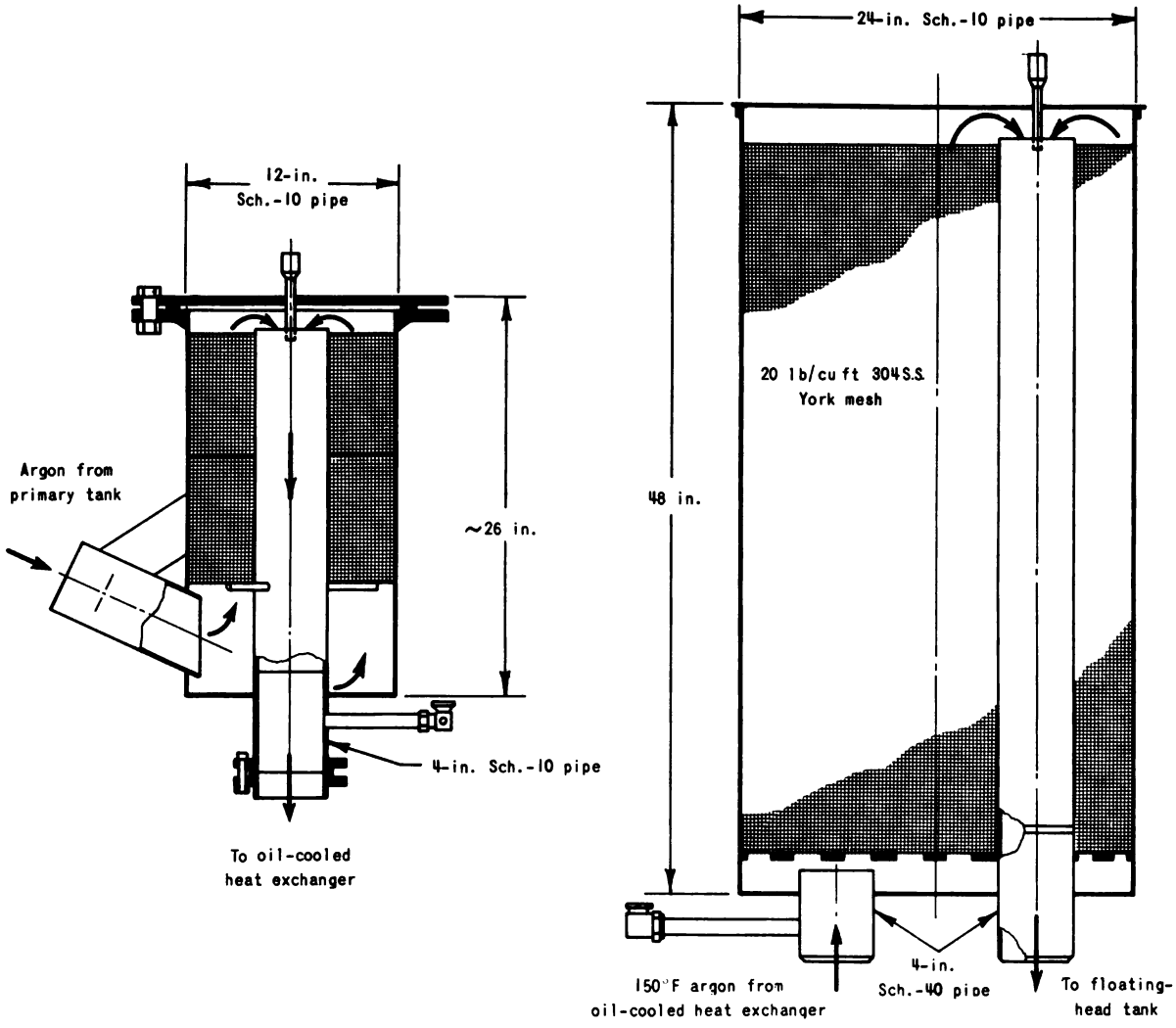

Fig. VII-2 EBR-II vapor or aerosol traps for primary-system argon are packed with stainless-steel mesh; heat exchanger in circuit between the traps cools the gas.[5]

When the operators removed the two-piece mesh packing through the flanged upper end of this vapor trap, they found that the lower section of mesh was plugged for approximately 1 in. from the mesh surface near the inlet nozzle, but the remainder of the mesh packing was relatively free of accumulated sodium. Although the operators removed the plugged-mesh piece and left only the upper piece of mesh in place, the trap has worked satisfactorily since.

The EBR-II fueling machine is cooled by an argon system, most of whose components are in an area depressed beneath the main operating floor. This argon system, which is separate from the reactor cover-gas system, includes two turbine type blowers, a multiple-tube natural-convection argon-to-air heat exchanger, a stainless-steel-mesh-filled vapor trap, and two molecular sieves in parallel. The vapor trap and molecular sieves, which are beds of crystalline sodium aluminosilicate pellets, remove vapor and fission-product gases from the argon drawn from the reactor vessel into the system piping during fuel-handling operations.

As shown in Fig. VII-3, mounted on the fueling-machine carriage are another lead-shielded vapor trap and molecular sieve, similar to the units in the argon system, for treating argon that is drawn directly into the fueling machine. Subassembly-heated argon (210 to 450°F) from the fueling machine passes through

Digitized by Google

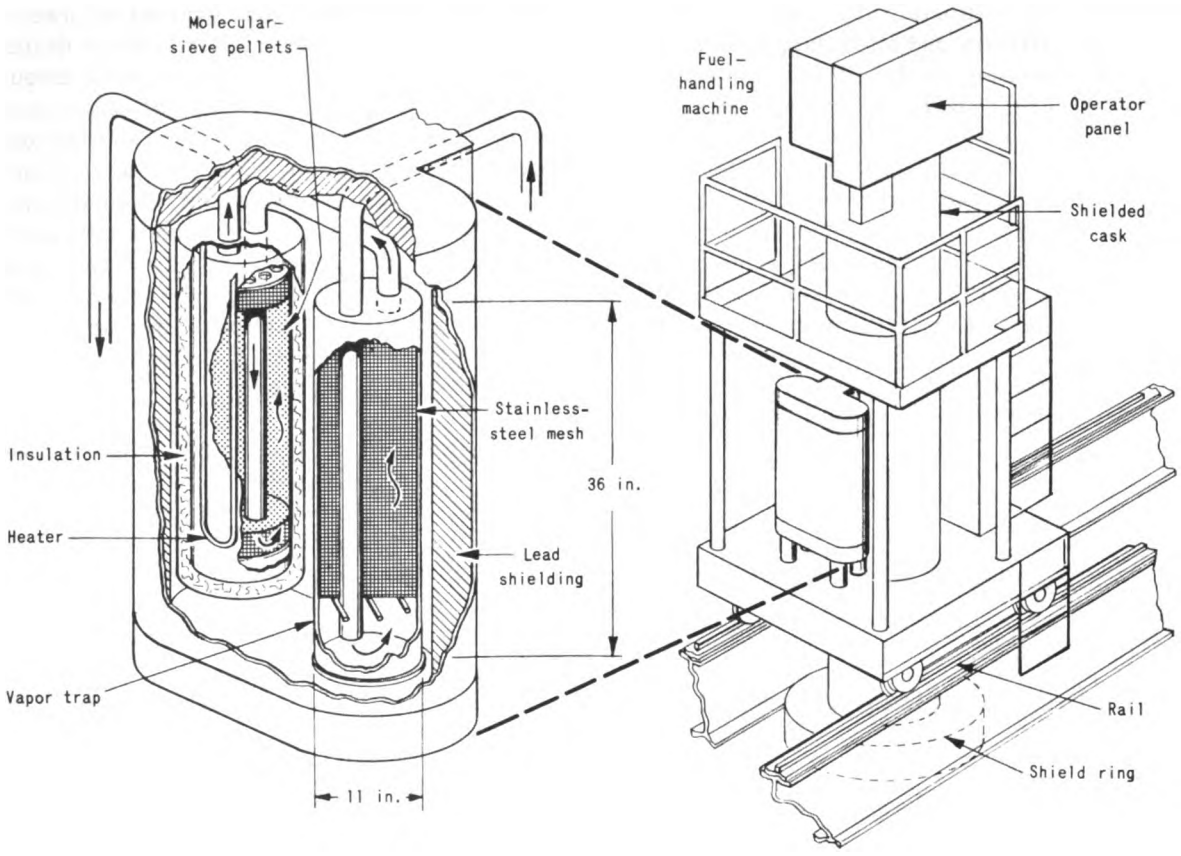

Fig. VII-3 EBR-II fueling machine has shielded vapor trap and molecular sieve to remove vapor and fission-product gases from argon drawn directly into machine.[5]

a 200-in.-long flexible hose to the heat exchanger, is cooled to approximately 100°F, and then enters the main turbine type blower (the smaller blower serves as a standby unit).

The vapor trap on the fueling machine has partially plugged once. Inspection revealed that the stainless-steel mesh had not plugged, but the lower opening of the gas-inlet tube had become blocked by sodium that had condensed onto the trap cold internal surfaces beneath the mesh.

The vapor trap in the depressed area also has plugged once. Operation was restored by removing the flanged outlet end of this horizontally installed trap and replacing the stainless-steel-mesh packing. When one of the turbine type blowers was disassembled recently to correct a manufacturing error, a fine white powder was seen in the piping and blower. This substance has not been analyzed, but its talcum-powder texture indicates that it is probably powder from the pellets in the molecular sieves and not sodium oxide.

Fission-Gas Monitor. When difficulty was experienced in obtaining vapor- and aerosol-free gas samples for the EBR-II fission-gas monitor that detects fuel-cladding failures, an 8-in.-diameter vapor trap containing a 4-in. thickness of stainless-steel mesh was installed in the gas line to the monitor and has operated satisfactorily. Argon enters this trap at 230°F and leaves at ambient temperature; gas flow is less than 200 cm^3/sec.

SRE, HALLAM, FARET, SCTI

These facilities can operate at temperatures up to 1200°F, where the vapor pressure is approximately 20 times greater than at 900°F. This is reflected in a wider use of vapor traps at these facilities than at EBR-I, EBR-II, or Fermi.

Digitized by Google

Hallam. Approximately 10 vapor traps are used in the primary and secondary sodium systems of the Hallam Nuclear Power Facility. As shown in Fig. VII-4, these traps are constructed with a 10-in.-diameter pipe within a 12-in. pipe fitted with pipe caps; vapor-laden gas enters the annular region and flows horizontally through the mesh, reverses direction, passes through the interior cylindrical volume, then exits through the outlet nozzle. These traps are equipped with heaters to melt the accumulated sodium when plugging occurs or when the rising pressure drop across the vapor trap indicates that the trap is becoming plugged.

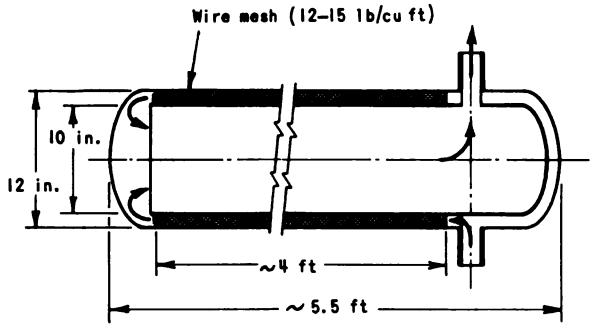

Fig. VII-4 Hallam vapor traps pass vapor horizontally through stainless-steel mesh in annular region, then through interior cylindrical volume; cooling is by natural convection. Heaters melt sodium when plugging occurs.[6,7]

The criterion for designing the Hallam vapor traps was to provide sufficient heat capacity and heat-transfer surface in the trap that the heat from the gas passing through the trap could be absorbed and dissipated rapidly enough to cool the gas below the melting point of sodium. Summary evaluation of the Hallam traps[6] indicates that "Operation of the vapor traps, installed in the system to prevent sodium vapor from entering and clogging the helium lines, has been satisfactory except at high reactor venting rates, such as when control-rod thimble leaks developed. Trap design and efficiency should provide many years of satisfactory maintenance-free service, but consideration should be given to the installation of more heaters."

The vapor trap in the reactor vent line plugged about four times during Hallam operation.[7] To unplug the trap, personnel entered the primary-system pipe gallery to insulate the plugged trap, which then was heated until sufficient sodium melted and drained to restore proper operation. The melted sodium drained directly into the liquid-metal system through the trap inlet nozzle. Although the plugging occurred during changes in reactor-operating conditions, no reactor shutdowns were caused specifically by the plugging of a vapor trap. If it had been necessary to shut down the reactor specifically to unplug the vent-line trap, an approximately 10-day waiting period would have been required for the radioactivity of the sodium in the primary pipes to decay enough for personnel to enter the gallery.

SRE. Atomic International's SRE at Santa Susana has mesh-filled vapor traps (one in the primary system, two in the secondary). Although SRE has operated without the trap becoming plugged, when the reactor vent line was removed for system modifications, it was discovered that approximately two-thirds of the cross-sectional area within the vent pipe was blocked with sodium. Nevertheless, the original mesh-filled vapor trap in the SRE primary system has been retained in modifications made recently to improve plant reliability and to permit reactor power to be increased from 20 to 30 Mw, with reactor-coolant temperature[8] raised from 960 to 1200°F.

SCTI. The vapor traps for the Sodium Components Test Installation (SCTI) at Atomic International's Santa Susana site differ from those at Hallam because of uncertainty concerning the flow rates through the SCTI gas system.[9] The cylindrical SCTI vapor traps are 6 in. in diameter and 3 to 4 ft high. Installed vertically, they are filled with $\frac{1}{8}$-in.-diameter steel shot to increase the heat capacity.

FARET. Vapor traps in the Argonne's Fast Reactor Test Facility will be of the annular design, similar to the Hallam traps, but the gas flow will be reversed so as to use the quiescent central volume of the trap as a refluxing condenser before the vapor-laden gas passes through the annular mesh. The design objective is to cool the outlet gas below 200°F regardless of whether the gas system has a slow flow of hot gas (to satisfy normal "breathing" requirements) or a fast flow of cool gas (such as during purging). As shown in Fig. VII-5, these traps will be installed with the longitudinal axis inclined 10° from the horizontal to facilitate

Digitized by Google

draining; they will be covered with 1-in.-thick insulation.

FARET vapor traps will be located in the argon supply and vent lines for the main secondary sodium system, auxiliary secondary sodium system, wet-fuel-storage tank, NaK drain tank, wet-fuel cooling system, and reactor-annulus drain tank—as well as on the argon supply line for the main primary sodium system and on the vent of the drain tank in the primary sodium system.

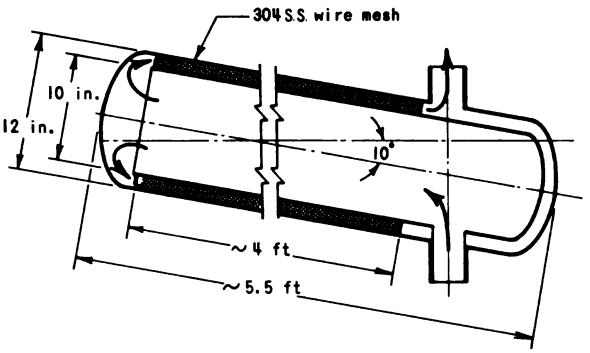

Fig. VII-5 FARET vapor traps, like those at Hallam, will be of annular design, but argon will flow first through quiescent central zone (which will serve as a refluxing condenser) before passing through mesh-filled annulus; 10° inclination will facilitate draining sodium.[10]

The coolant-gas-system equipment for the FARET fuel-handling machine, including the compressors, filters, vapor trap, heat exchangers, and argon supply tank, will be located in the transfer tunnel beneath the operating floor of the primary-containment cell and will be connected to the carriage of the fuel-handling machine by flexible metal hoses approximately 50 ft long.[10] For this system the functions of vapor trap and heat exchanger will be combined in a single unit that has an ammonia evaporative coil immersed in NaK maintained at 40°F; it is designed for gas flows of up to 60 cfm.

STF, LAMPRE, FRCTF

Los Alamos Scientific Laboratory has had notable success using stagnation type vapor traps on its 2-Mw Sodium Test Facility and the Los Alamos Molten Plutonium Reactor Experiment.[11] These facilities are relatively small, tight systems that do not require high gas flows and in which the gas is drawn from system locations where the sodium temperatures are relatively low. In general, the stagnation type vapor traps are pipes 4 to 5 ft long and greater than or equal to 3 in. in diameter that connect the liquid-metal system with smaller diameter gas piping. The traps are equipped with heaters to clear accumulated sodium when necessary.

The gas system of the Los Alamos Fast Reactor Core Test Facility is designed to recirculate the primary-system cover gas continuously. For this higher gas-flow system, it is planned to use continuously refluxing impingement type vapor traps.[12] Each of these reflux condensers will consist of a 1-in. pipe whose 30-in. length will be filled with $\frac{1}{8}$-in.-diameter stainless-steel balls. In the annulus between this 1-in. central pipe and an outer 2-in. pipe will be NaK that is cooled by air or water to maintain the outlet gas at approximately 300°F.

SEFOR

Vapor traps for the Southwest Experimental Fast Oxide Reactor, being designed by the General Electric Company for construction in Arkansas, will be 2- to 8-in.-diameter pipe sections that are packed with stainless-steel mesh for lengths[13] of approximately 18 in. These configurations, which were chosen as the result of General Electric experience with sodium loops and with the prototype power plant for the nuclear submarine *Seawolf*, are sized to maintain gas velocity less than 1 ft/sec. Although the larger traps will be equipped with heaters, sufficient heat is expected to be transferred through the short lengths of pipe between the vapor sources and the smaller vapor traps that heaters will not be required on these units.

LARGE TREAT SODIUM LOOP

The large sodium loop in the Transient Reactor Test Facility, located at the National Reactor Testing Station in Idaho, will be used to test unirradiated and preirradiated fast reactor fuels to failure under variable coolant temperature and flow conditions.

Possible contamination will be localized during fuel tests by operation of the loop on a once-through mode—sodium coolant will flow from a storage vessel through the test section and then to a dump vessel. A vapor-trapping

Digitized by Google

demister, molecular sieve, and liquid-nitrogen-cooled charcoal trap in the gas system remove gaseous fission products and entrained sodium or sodium vapor from the helium cover gas transferred between vessels during the once-through flow. The demister is constructed of a 12-in. length of 4-in.-diameter pipe fitted with knitted stainless-steel wire mesh having a bulk density of 20 lb/cu ft; the molecular sieve is a 9-in.-deep bed of $\frac{1}{8}$-in.-diameter sodium aluminosilicate (Linde 4A) pellets in an 8.5-in.-diameter container. Neither the demister nor the molecular sieve has heating or cooling provisions but are valved and flanged for replacement when necessary. Gas transfer through the system may reach 20 cfm at temperatures up to 900°F but will be sustained for a duration of only several minutes.

MELT-REFINING FURNACES

In conjunction with the development of the melt-refining process for purifying discharged EBR-II fuel, screening tests were conducted to determine the capability of various materials to trap alkali-metal vapors[14] as hot as 1470°F. Although the application was to statically trap sodium vapors and other condensible volatiles released by the melt-refining process, the materials were tested in a dynamic system. Argon gas was bubbled through a vaporizer containing a shallow pool of alkali metal and then through the bed material until breakthrough occurred; breakthrough was detected by white oxide fumes formed when the untrapped metal vapor reacted with oxygen at the end of the bed. The tests indicated that simple condensation alone is ineffective for retaining vaporized sodium but that nearly all surface-active materials, such as molecular sieves, activated carbon, and activated alumina, were effective.

Although molecular-sieve beds initially were used as fume traps for the EBR-II fuel melt-refining furnaces, their maintenance in a remotely operated plant would require additional handling equipment. Thus a simpler disposable fume trap was sought. Tests of an absorber type trap consisting of a molded, porous Fiberfrax (aluminum silicate ceramic fiber) cup showed it to retain sodium vapors quite effectively.[15,16] This trap works on the principle of absorption and chemical reaction of the sodium with the trap surface; the reacted layer can be seen in Fig. VII-6.

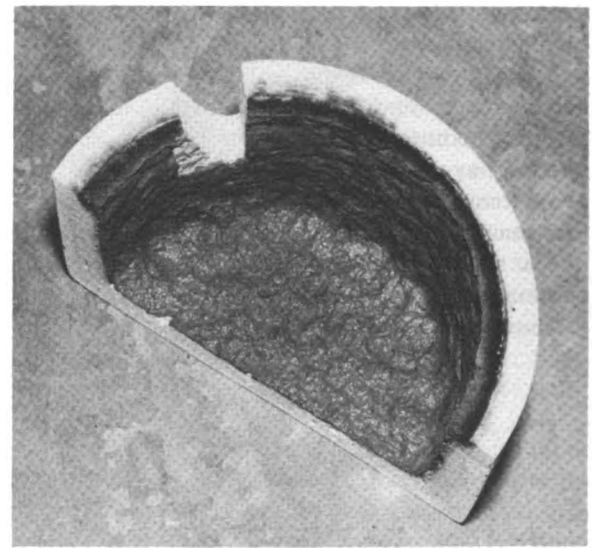

Fig. VII-6 Melt-refining-process development work for reprocessing spent EBR-II fuel showed that a porous Fiberfrax molded cup effectively traps sodium vapor by absorption and chemical reaction.[15]

Recent Developments

Recent research on vapor traps has been reported by Pratt & Whitney (CANEL) and by Argonne National Laboratory (ANL), with both efforts directed toward developing continuously refluxing vapor traps.

P&W. The lack of suitable design criteria can be seen in recent developmental work on vapor traps that was being conducted for the Lithium Cooled Reactor Experiment (LCRE).[17,18] Gas-system tolerances were to be defined as a result of long-term system testing, but, unfortunately, this work ceased when the LCRE project was terminated.

Four separate operating regimes had been defined for the LCRE vapor-trap tests: (1) 1000°F lithium vapor in 60 to 100 cu ft of helium per hour, (2) 120 to 1000°F lithium vapor in approximately static helium, (3) 700 to 1000°F NaK vapor in 30 to 50 cu ft of helium per hour, and (4) 100 to 300°F NaK vapor in approximately static helium. Air- or nitrogen-cooled traps were being developed to prevent more than an arbitrarily chosen 2-ppm (by weight) vapor carry-over; screening tests were made on a number of vapor-trap designs, including shell-and-tube heat exchanger, baffle, continuous-refluxing bubbler, mesh-packed, and helical-fin types. Most promising of these was

Digitized by Google

the continuous-helical-fin type vapor trap. Thus five helical-fin vapor traps were fabricated for tests to determine how helix pitch (1/4 to 3/4 in.) and fin-surface slope affect trap performance; Fig. VII-7 describes their geometries. These lithium tests showed the trap with 1/4-in. pitch to be the most efficient: approximately 80% for 1000°F lithium and approximately 99% for 1000°F NaK; Fig. VII-8 shows this trap. Figures VII-9 and VII-10 show the transparent housing for visually observing condensation in the helical-fin vapor traps and the tendency of the condensed liquid metal to agglomerate before draining back to the vapor source.

Stringent gas-purity requirements for the LCRE were to be met by the use of various settling, impingement, and filter devices downstream and in series with the 1/4-in.-pitch helical-fin trap. Mesh-filled settling chambers were tested with the helical-fin traps for about 400 hr, but the LCRE termination prevented completing these evaluation tests.

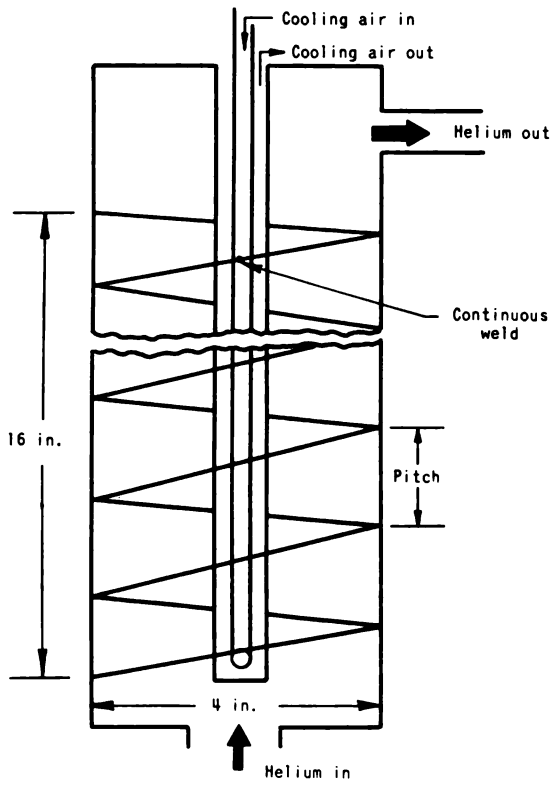

Fig. VII-7 When LCRE vapor-trap screening tests indicated that continuous-helical-fin type refluxing trap promises best efficiency, five such traps were built to test effect of helix pitch and fin slope. Fins of one trap were conical and on 1/2-in. uniform pitch. Flat fins on each of other three were uniform 1/4, 1/2, and 3/4 in.; Fig. VII-9 shows the fifth trap, whose flat fins had nonuniform pitch.[18]

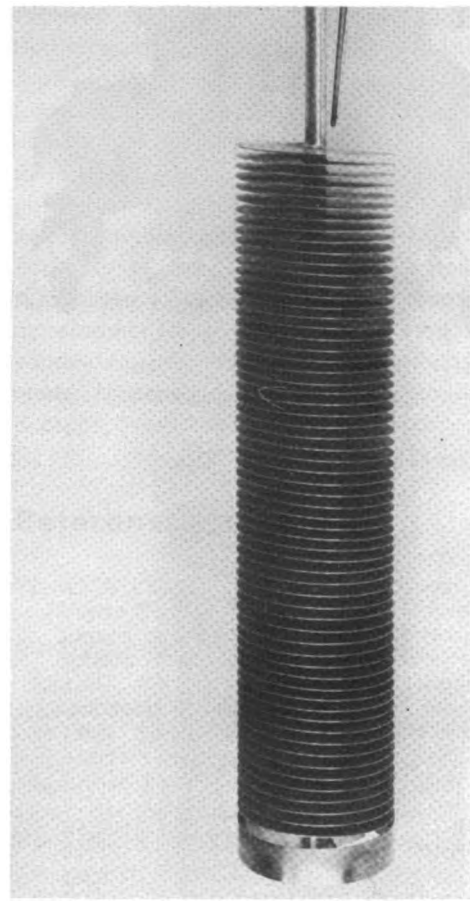

Fig. VII-8 Most efficient of the vapor traps tested by Pratt & Whitney for LCRE lithium vapor in helium was helical-flat-fin type trap having 1/4-in. uniform pitch.[18]

ANL. Recent work on the development of a 1200°F sodium vapor trap at ANL has been reported.[19] Two experimental vapor traps were constructed. Figure VII-11 shows the second, mechanically improved vapor trap. It was tested with gas flows up to 40 cu ft/hr from a sodium tank maintained at 1200°F; vapor-removal efficiency was as high as 99.8%. Sodium condensation rates were determined by radiography of a calibrated U-tube beneath the vapor-trap inlet. At a gas flow of 20 cu ft/hr, the condensation rate was 13.6 cm^3/hr; it increased to 86 cm^3/hr when gas flow was 40 cu ft/hr.

These test results indicate that vapor-trap configuration and temperature can be adjusted

Digitized by Google

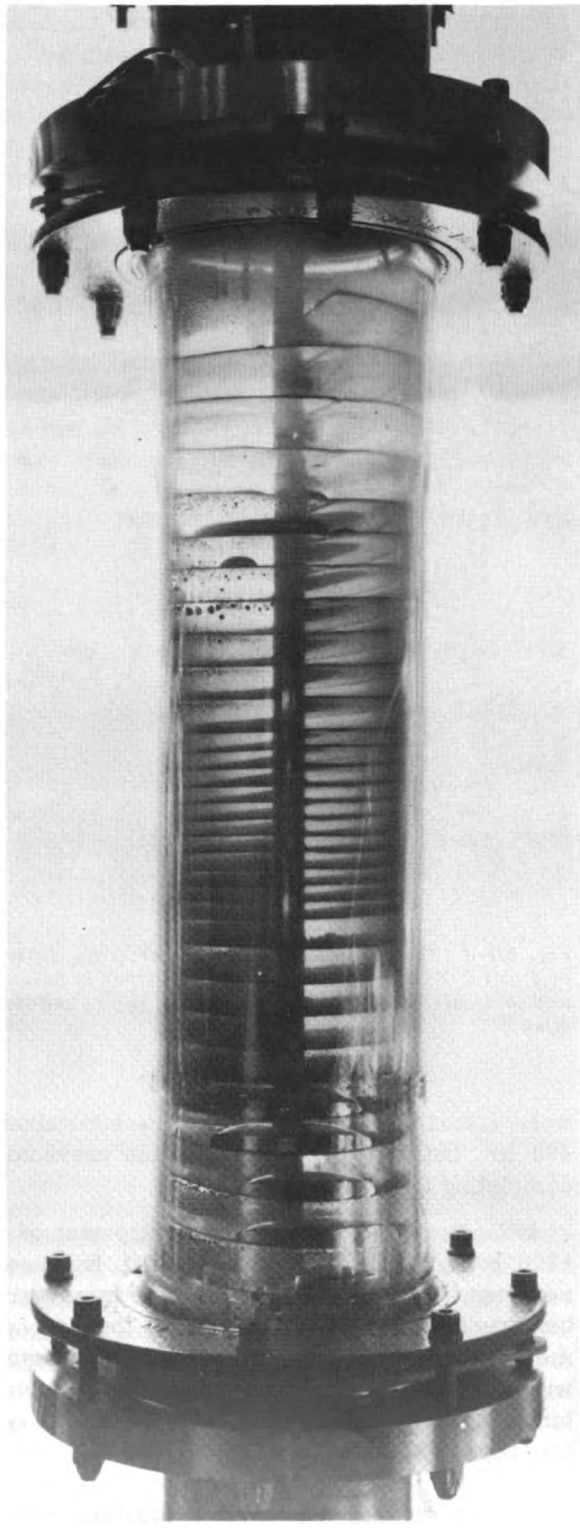

Fig. VII-9 Pyrex transparent shell permits observation of nonuniform pitch of this helical-flat-fin trap: 1/4 in. for middle 3 in. of helix, 1/2 in. for next 3.5 in. upper and lower, and 3/4 in. for top and bottom ends.[18]

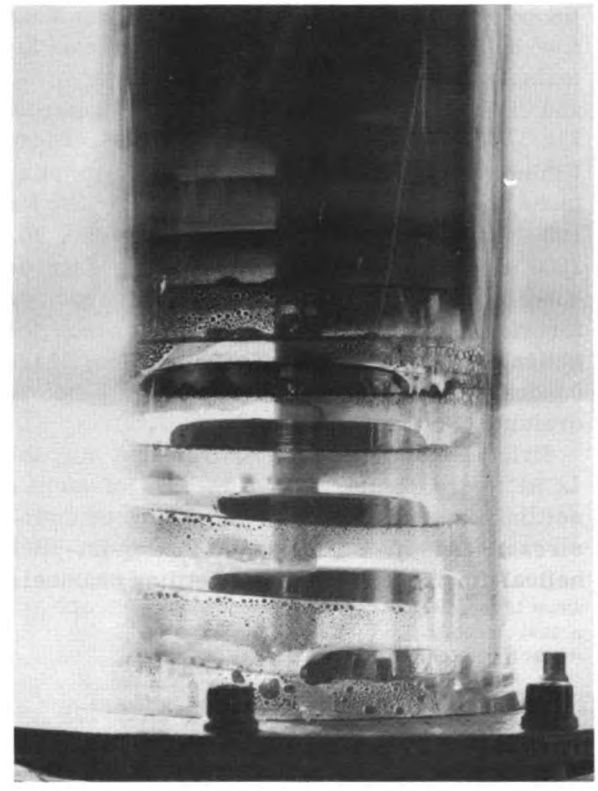

Fig. VII-10 Condensed liquid metal in helical-flat-fin trap tends to agglomerate on fins before draining back to vapor source, which in this case and in Fig. VII-9 was 1000°F NaK; photographs were taken[18] after trap operated 5 hr.

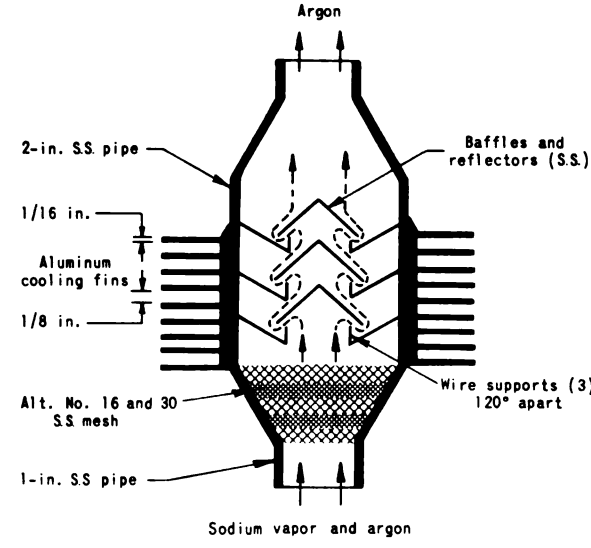

Fig. VII-11 Refluxing type impingement-condensing trap being developed at Argonne for 1200°F sodium vapor has cooling fins and internal baffles as well as mesh.[19]

Digitized by Google

to provide continuous refluxing of sodium vapor. In addition to avoiding trap plugging, this would permit reducing trap size and cost. But this trap would not operate satisfactorily if the gas contained an oxide aerosol because oxide accumulation on the limited condensing surface would plug the trap.

A larger trap with a 2-in. inlet is being tested now. It has operated for about 650 hr at 570°F and 800 hr at 1020°F. The major operating problem has not been with the vapor trap, but with maintenance of the tank heaters.

Recommendations for System Design

Vapor traps should be located near the vapor sources to minimize sodium plugging or obstruction of gas lines. However, because traps for handling appreciable gas volumes are rather bulky, and space within containment cells is often at a premium, traps cannot always be positioned next to sodium-containing vessels. Thus system designers must ensure that the gas piping has enough heat capacity to overcome liquid-metal accumulation and plugging and that the entrapped liquid metal can be drained from the piping.

Trap Design. Field experience with replaceable mesh-filled vapor traps indicates that plugging occurs in a small volume of the mesh near the gas inlet and that most of the mesh volume in a plugged trap remains relatively free of liquid-metal accumulation. This experience suggests that trapping capacity might be improved by the use of graduated-density or zoned-density packings. Another improvement on current practice might be to increase the frontal-area-to-volume ratio of the mesh packing, such as by arranging the mesh packing in a relatively thin annulus through which the gas would pass radially.

Conclusions: Development Needed

The mesh-filled vapor trap has found almost universal application in liquid-metal-reactor systems where large volumes of gas are transferred. The operation of these traps can be described as tolerable or even acceptable, but in few installations have they proven to be completely satisfactory.

There has not been a significant change in vapor-trap technology during the past decade. The early experimental work with vapor traps covered almost the entire spectrum of devices that are being used now. The first impingement type units were purposely oversized to compensate for lack of adequate design criteria and uncertainties surrounding the nature of the sodium vapor or aerosol, and this approach persists today. However, the vapor-trapping requirements of liquid-metal-cooled systems continue to rise as system size and operating temperatures increase. Thus a comprehensive developmental program is needed to provide vapor-trap and reactor-system designers adequate information upon which to base their designs.

References

1. A. J. Erickson, C. L. Gregory, and P. M. Lang, Vapor Traps for Handling Liquid Sodium, USAEC Report AECU-3200, MIT Engineering Practice School, Aug. 25, 1951.
2. J. C. Cochran (Ed.), Sodium Graphite Reactor Quarterly Progress Report, July–September 1955, Section B, USAEC Report NAA-SR-1513, Atomics International, Mar. 15, 1956.
3. R. O. Haroldsen, F. D. McGinnis, M. Novick, R. R. Smith, and F. W. Thalgott, Safety Analysis Report, EBR-I, Mark IV, USAEC Report ANL-6411, Argonne National Laboratory, February 1963.
4. Power Reactor Development Company, Enrico Fermi Atomic Power Plant Revised License Application, Part B, Technical Information and Hazards Summary Report, Report NP-10458, Vol. 1, pp. 107.7–107.12, July 1961.
5. L. J. Koch, W. B. Loewenstein, and H. O. Monson, Addendum to Hazard Summary Report Experimental Breeder Reactor-II (EBR-II), USAEC Report ANL-5719(Add.), Argonne National Laboratory, Jan. 7, 1964.
6. J. E. Price, Final Evaluation Report — Hallam Nuclear Power Facility, USAEC Report NAA-SR-9777, Atomics International, 1964.
7. G. L. Ballew, Hallam Nuclear Power Facility, personal communication, Aug. 31, 1965.
8. W. J. Freede and J. K. Roberts (Eds.), Sodium Reactor Experiment. Power Expansion Program — Heat Transfer Systems Modifications, USAEC Report NAA-SR-10379, Atomics International, Oct. 9, 1964.
9. R. Cygan, Atomics International, personal communication, Sept. 22, 1965.
10. W. R. Simmons et al., Argonne National Laboratory, unpublished, 1965.
11. L. A. Whinery, Los Alamos Scientific Laboratory, personal communication, Aug. 12, 1965.
12. B. J. Melton, Los Alamos Scientific Laboratory, personal communication, Sept. 22, 1965.
13. H. N. Bass, Atomic Power Equipment Department, General Electric Company, personal communication, Aug. 31, 1965.
14. J. Wolkoff and A. A. Chilenskas, The Melt Refining of Irradiated Uranium, Application to EBR-

Digitized by Google

II Fast Reactor Fuel. IX. Sorption and Retention of Sodium and Cesium Vapor on Stationary Beds at Elevated Temperature, *Nucl. Sci. Eng.*, 9(1): 71-77 (January 1961).
15. S. Lawroski, W. A. Rodger, R. C. Vogel, and V. H. Munnecke, in Chemical Engineering Division Summary Report for January, February, March 1960, USAEC Report ANL-6145, p. 32, Argonne National Laboratory, 1960.
16. J. C. Hesson, M. J. Feldman, and L. Burris, Description and Proposed Operation of the Fuel Cycle Facility for the Second Experimental Breeder Reactor (EBR-II), USAEC Report ANL-6605, Argonne National Laboratory, April 1963.
17. H. J. Banach, LCRE Auxiliary Systems Termination Report, USAEC Report PWAC-416, Pratt & Whitney Aircraft, Mar. 9, 1964.
18. E. H. Donnelly, Final Report on the Design and Development of Lithium and NaK Vapor Traps, Report PWAC-400, Pratt & Whitney Aircraft, Mar. 3, 1964. (Classified)
19. E. L. Kimont, Engineering Development of a Practical 1200°F Sodium-Vapor Trap, *Trans. Am. Nucl. Soc.*, 8(1): 147 (1965).

Digitized by Google

Section

VIII

Power Reactor Technology

Operating Experience

Operational Problems and Solutions

By Rolf C. Skaardal

Reactor designers should be interested to learn what reactor operators have found out about their products. Some reactor operational difficulties traced to design, fabrication, and inspection were reported at the Conference on Reactor Operating Experience sponsored by the Reactor Operations Division of the American Nuclear Society (ANS). Some of the "nuts-and-bolts" type problems are reported here. Most of these involved hydraulically induced vibrations, corrosion, leaks in components, and control-system peculiarities. Repair methods, control of oxygen in heavy water, and changes to research-reactor experimental facilities also are of interest to operators and designers and therefore are taken into account in this review.

Control Systems

Difficulties have occurred with neutron-absorber rods and control circuitry at various power reactors.

Control Rods. During a routine license test with the Indian Point reactor shut down, one control rod stuck when it was being inserted.[1] After borating the water, cooling the system, and removing the vessel head, the operators found that a tapered stainless-steel pin ($1\frac{3}{4}$ in. long by $\frac{5}{32}$ to $\frac{9}{32}$ in.) had wedged between the upper grid plate and a blade of the cruciform control rod. They removed the pin, of unknown origin, with a 19-ft-long slender wrench when the control rod was jacked from below.

Also at Indian Point, when it was time to remove the 12 boron–stainless-steel fixed shim rods that had been installed in the first core to limit reactivity during the early part of core life, several blades were found to be stuck.[1] The rods were freed by partially removing, as a unit, all four fuel elements around each rod. The sticking was caused by considerable buckling of the rods, which apparently occurred because of radiation-induced growth of the shim blades relative to their rigidly attached nonborated stainless-steel tips. These shim rods had been in the reactor for only 189 effective full-power days.

Specimens of Elk River reactor control rods of a similar material (2% boron–stainless steel) also suffered radiation damage, in this case, ductility loss.[2] About a year after the plant reached full power, the control rod was replaced because tests on a specimen of the rod material indicated that it might no longer meet the technical-specification requirement of 3.4% elongation. However, visual inspection of the removed rod showed no apparent mechanical damage. Studies are under way to determine (1) how much rod embrittlement is tolerable and (2) whether periodically changing the core location of the rods to expose all rods uniformly would be a more practical program than replacing each rod as it reaches its limiting ductility.

When the nickel plating on the silver–indium–cadmium control rods of the Yankee reactor failed to protect the silver from corrosion, radioactive silver corrosion products circulated and deposited throughout the primary system.[3] This caused maintenance problems, particularly during the first refueling. After the reactor pit was flooded (to provide shielding for the refueling crew) and the vessel lid was removed, the radioactive silver in the reactor water got into the pit water and plated out on the stainless-steel liner. To avoid the problem

Digitized by Google

thereafter, the operators replaced the original rods with hafnium rods. For two years they also have successfully used two experimental silver–indium–cadmium rods that are clad with Inconel and now have installed two new silver–indium–cadmium rods clad with stainless steel.

Chemical Shim. Yankee, like Indian Point, was designed to use boric acid solution in the coolant–moderator to reduce reactivity during cold shutdown. As an extension of this, during operation with the second core, the Yankee operators experimented with boric acid injection as a chemical shim method.[3] Although the experiments were successful, for some unexplained reason the boric acid in the operating reactor system was accompanied by higher crud concentrations and appeared to cause oxygen generation in the pressurizer. While the causes are being investigated, the solution at Yankee has been to arrange for degassing from the top of the pressurizer and recombination by reinjecting into the main coolant system with 25 cm^3 of hydrogen per liter in the coolant.

Temperature Sensor. The Elk River reactor experienced several spurious scrams caused by a malfunctioning temperature bulb and pressure switch.[2] After tests indicated this equipment was sensitive to radiation, it was replaced by a thermocouple system.

Level Control. When a water-level indicator in the Special Power Excursion Reactor Test No. 3 (SPERT-III) 2500-psi 650°F pressurizer reported that the water was more than 2 ft higher than it actually was, the electric heaters became partly uncovered and superheated the steam to 1000°F. This caused the pressurizer-vessel material to fail in creep and ruptured its seam weld.[4] The error illustrates the mutual dependence of instrumentation and mechanical-hardware designs. The signal from a differential-pressure cell was used to sense the water level. Compensation for the effect of density changes on the water-level indication was provided through a temperature signal received by the automatic controller from a single sensor near the top of the normal water level. Unfortunately this signal did not recognize the water-temperature stratification that occurred when certain operating conditions led to diminished internal circulation of the pressurizer water.

Reliable water-level control in the new pressurizer is to be obtained by (1) electric heaters staged to operate at different elevations so as to circulate the water by convection (heater response is delayed only slightly) and (2) taps for the differential-pressure cell located such that the normal operating water level is 25% of the differential range above the bottom tap. Although this increases the safety margin, temperature–density compensation is still necessary for water levels other than normal.

Electrical Circuit. Routine checks of the SPERT-III scram circuit five years after installation revealed abnormal operation and relay chatter.[5] After wiring checks did not find the cause, a complete evaluation of the system disclosed that electrical leakage to ground through faulty insulation could actuate relays that should be deenergized (such as the rod-withdrawal circuit). This failure by leakage to ground occurred on leg *a* of the "floating-ground" power-distribution system (Fig. VIII-1),

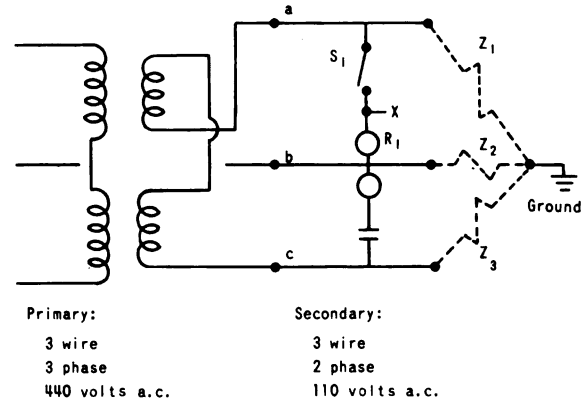

Fig. VIII-1 Original power-distribution scheme for SPERT-III proved "fail-unsafe" when the wire insulation deteriorated, permitting a short circuit in the wiring to override the control-rod switch by effectively shorting it closed.[5]

where the insulation on the wiring in the control-rod drives was particularly susceptible to deterioration because of exposure to vibration, heat, and moisture.

Because the leakage impedance Z on any of the three lines shown in Fig. VIII-1 was made up of both the resistance path through deteriorated insulation and the strong inherent capacitance built into the a-c control system by its long wiring runs to ground, an accident

Digitized by Google

could result (because the switch S_1 is effectively shorted by impedance Z_1, the relay R_1 cannot be deenergized) if a failure to ground occurs near point X in Fig. VIII-1. Although R_1 is a 110-volt relay, 60 volts will energize it, and it will remain energized down to 45 volts. Despite the intention to design a fail-safe system, the discovery that ground failures might not deenergize certain relays meant that the system was not, in fact, fail-safe.

Because of the hazard, the control-system power-distribution circuit was modified as shown in Fig. VIII-2 so that wiring deterioration can be detected before serious consequences result. The transformer neutral line

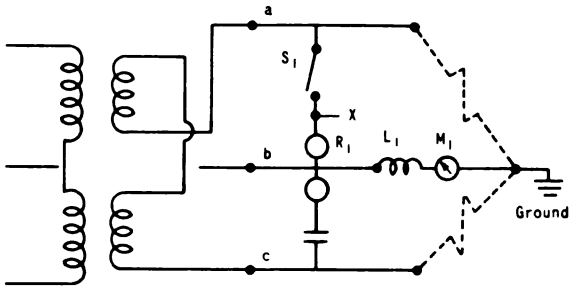

Fig. VIII-2 Modified circuit for SPERT-III alarms if deteriorated insulation permits leakage to ground. Thus insulation can be repaired before a short circuit occurs and overrides the switch.[5]

b was grounded through a current-limiting lamp L_1 in series with an ammeter M_1. Any leakage to ground from either of the high-voltage legs *a* or *c* then completes the circuit and causes current to flow through the lamp and meter. Although this system cannot prevent faults, it does keep the reactor operator informed as to the condition of the system and provides an alarm if an abnormality occurs.

This ground-loop problem at SPERT-III taught several lessons applicable to any electrical system. For instance, operators must bear in mind that the usual insulation checks are d-c measurements that will not detect capacitance paths, which are serious for a-c systems. Designers must consider the operating characteristics of components, such as relays, and the likelihood of large capacitance in their leads. Because of the impossibility of designing a completely failproof system and the chance of practical problems such as insulation deterioration, systems must be designed so that failures will not have serious consequences.

For more information on control experience discussed at the same ANS meeting, see page 221.

Flow Oscillations

The Elk River reactor[2] has exhibited flow pulsations ever since the initial power-escalation runs in 1963. The oscillations, which are well defined and repeatable, apparently are caused by surges in the feedwater flow at around 50% of rated power. These flow oscillations cause the reactor power to vary less than 2.5%. Although the conditions are adjudged to present no operational hazard to the reactor, studies are continuing to permit better understanding of the phenomenon.

Flow-Induced Vibrations

Flow of the coolant at high speeds through a reactor can buffet components and cause them to vibrate and wear. Failures resulting from this at the Big Rock Point, Yankee, General Electric Test Reactor (GETR), and SPERT-III reactors emphasize the need for designers to assess potential vibration sources, components that are susceptible to such damage, and ways to keep broken items out of the pumps and the core.

Excessive vibration loosened, and in some cases dislodged, bolts connecting fuel channels to channel support tubes in the high-power-density forced-circulation reactor in the Big Rock Point Nuclear Power Plant.[6] Investigations using accelerometers and strain gauges showed that the vibration was caused by inadequate distribution of the water coolant as it entered the reactor vessel. The manner in which the problem was solved by adding a baffle and by modifying the core support plate and 72 fuel channels will be described in an article on reactor-modification methods in the next issue of *Power Reactor Technology*. That article also will discuss modifications to the thermal-shield support in the Big Rock Point reactor.[7] These were required when several studs fractured by thread-root fatigue after fretting had enlarged clearances. The fretting occurred when small pressure fluctuations across the large surface of the thermal shield caused significant wear forces between line-contact sliding surfaces.

Digitized by Google

Hydraulically induced fretting corrosion was found when the Yankee power reactor was first refueled.[3] Zircaloy to stainless-steel joints on the fuel elements had corroded to a depth of more than 0.1 in. Later, stainless-steel tubes of the in-core instrumentation package were found to have been damaged by fretting corrosion to a depth of 0.040 in. Evidence also has been found that the Yankee control rods had fluttered, causing notches to be worn into the stainless-steel rubbing straps.

Steps to prevent such hydraulic problems at Yankee have included substitution of stainless steel for Zircaloy in parts that might rub, replacement of the 24 guide tubes, and installation of impact sleeves to act as cushions or vibration absorbers, and at the same time to give larger (100-fold in some cases) surfaces for dissipating impact.

The problem caused by hydraulic flow at Yankee has been the failure of 10 holders for irradiation coupons. Four were recovered in 1963, but the other six holders and basket parts remained lodged in uncertain positions in the reactor vessel until they were recovered during the 1965 refueling.

In the GETR,[8] hydraulically induced vibrations of control-rod guide tubes caused excessive wear of aluminum core-component spacer pads (see Fig. VIII-3). The pads provide lateral support for the upper ends of the fuel elements and beryllium filler pieces; there is no upper grid plate. The ½-in. 8-cps vibration of the guide tubes affected the reactor log-N period instrument, causing large-period recorder oscillations as the spacer pads ablated. When the reactor was operating at a steady 30 Mw, the recorder showed periods as short as ±30 sec, which caused repeated alarms.

Reactor modifications to stop the vibration consisted in bolting the free upper ends of the control-rod guide tubes to the coolant-flow distributor, replacing the guide-tube aluminum spacer pads with stainless-steel bands (fitted into slots milled circumferentially around each aluminum guide tube in the pad region), and installing complete stainless-steel top ends on the beryllium pieces.

No significant log-N period oscillations have been observed since; at a steady 30 Mw, recorder oscillations indicate periods of ±400 sec (for reference, the period indication is ±1000 sec with the reactor shut down). No pad wear could be detected after operation for one year.

In the SPERT-III reactor primary system, vibrations broke loose a thermowell.[5] Fortunately this failure occurred downstream of the pumps, and the 8-in.-long piece of ½-in. pipe was caught below the core. This occurrence, together with earlier fatigue failures of in-core instrumentation (due to vibration of small parts exposed to the turbulent coolant stream), caused concern about the 17 remaining thermowells in the primary system. Investigation revealed that none of these conformed with vendor's drawings. Strain-gauge tests showed that 9- and 6-in. wells were excited at their natural fre-

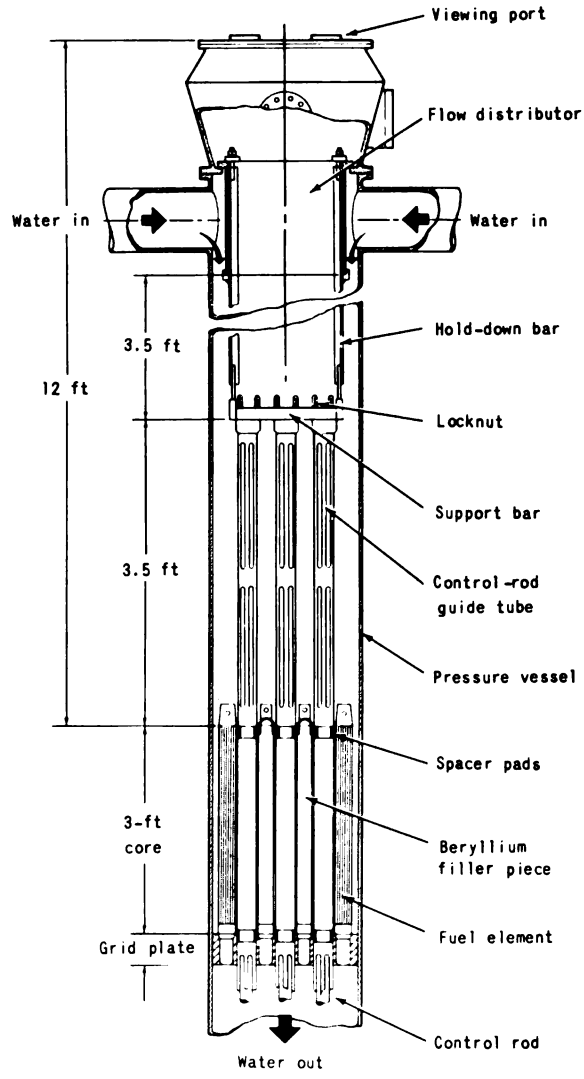

Fig. VIII-3 The GETR, which does not have an upper grid plate, employed aluminum spacer pads for lateral support of the upper ends of the core components.[8]

Digitized by Google

quencies, but 5-in. wells showed essentially no excitation. Thus 5-in. wells have been installed, and no further thermowell problems have been encountered.

Corrosion Problems

A mysterious form of corrosion of Inconel has been discovered at the Ågesta Nuclear Power Plant in Sweden.[9] The Ågesta reactor, a pressurized D_2O-cooled and -moderated reactor, has a flat hollow lid that is filled with light water for cooling the lid and for radiation shielding. This lid is penetrated by 188 Inconel pipes for heavy water; 11 of these pipes, used for charging irradiation specimens, are located at the periphery and barely pass through the inside of the lid (Fig. VIII-4). Leakage of heavy water into the lid was discovered and found to be caused by corrosion of three of these peripheral tubes.

Examination revealed intercrystalline stress-corrosion cracking on the tube surface, originating from the light-water side. The lid-water chemistry had been harmless—*p*H was maintained between 9.5 and 10.5 by addition of LiOH. Chloride-ion concentration was ≤0.5 ppm, and stresses were less than 20% of yield stress. Thus this stress-corrosion phenomenon is not fully understood; the damaged tubes are being examined metallurgically. In this reviewer's opinion the cause for this "abnormal" stress corrosion might be traced to the Inconel-tube manufacturing process itself.

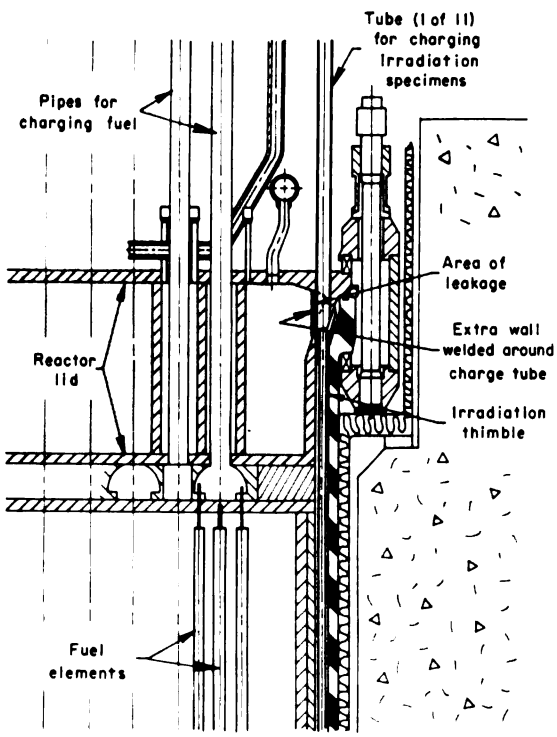

Fig. VIII-4 Extra wall section was welded around each of 11 Inconel specimen-charging tubes in the shield lid of the Ågesta reactor after three tubes cracked due to stress corrosion.[9]

Leaks in Mechanical Components

The Yankee and SPERT-III pressurized-water-reactor systems have experienced a variety of difficulties with leaks in mechanical components and resulting troubles.

At Yankee, early problems were encountered with leaks from canned-motor-pump flanges and from stem-leakoff type valves.[3] The flange leakage, which was caused by differential thermal expansion, is prevented by the use of the thermal expansion itself for final tightening of the closure; the operators do not pressurize the primary system when fluid temperature is low. For any cold hydraulic test of the system, the operators must adjust the pump flange by tightening the bolts. When the inner packing on the leakoff type valves could not control the leakage to desirable levels, it was necessary to remodel the valves to provide deeper inner packings. Leakage from the refueling water cavity and the ion-exchange pit at Yankee presented vexing problems. Also, one 2-in. stainless-steel pipe in the charging line failed by cracking due to suspected vibration and fatigue, and eight socket welds and seal welds have leaked. As the plant has become "broken in," such problems have tapered off—Yankee has now logged two complete one-year cycles without a primary-system cooldown or depressurization.

The SPERT-III reactor has experienced leaks from valves, gaskets, and piping.[5] The desirability of waterproofing all control-system electrical connections was demonstrated by the failure of a single tube fitting in the primary-coolant system. Extensive damage from short circuits resulted from the complete drenching of control-system wiring.

An unusual kind of leakage was experienced with one of the four canned-motor pumps in the SPERT-III primary system. During a plant cooldown in November 1964, a pump circuit breaker dropped out. Inspection showed that

Digitized by Google

water had leaked through the seals of the stator-winding terminal posts and short-circuited the windings. The rotor can, stator liner, and stator were damaged, and the motor section had to be completely rebuilt. Although no cause for the leak has been ascertained, it is believed that the pump had operated for some time with a damaged rotor can. Thus the initial damage might have been caused either by a foreign particle entering the motor from the primary system or by a piece corroded from the nitrided surface of the thrust disk. This latter is considered more likely because some corrosion has been observed on the thrust disks of all four pumps. The operators are considering replacing the nitrided 17-4 PH material on the thrust-bearing disks by Stellite 19, which better resists pitting corrosion.

All gaskets in the SPERT-III system, except the heat-exchanger head gaskets (which are solid stainless steel), are of the spiral-wound asbestos-filled stainless-steel type (Flexitallic); diameters range from 1 to 53 in. Although experience with this type of gasket has been generally satisfactory, some flanged connections leak slightly during the cooldown portion of about the first three cycles after gasket installation. Thus retightening during each cycle is necessary until the gasket firmly seats. Also, if this type of gasket is installed without an inside-diameter retaining surface, water flow tends to unwind the gasket and pieces break off. This adds tramp metal to the system as well as weakening the gasketed joints.

The SPERT-III experience with metal gaskets has not been satisfactory. The heat-exchanger stainless-steel gaskets leak slightly and erratically at operating temperature. Although the primary control valves originally were fitted with solid-metal gaskets and welded canopy seals, frequent leaks and repair difficulties have prompted their replacement by Flexitallic type gaskets.

Stem galling and leakage through valve seats also occurred at SPERT-III. The motor-operated temperature-control valves were furnished with chrome-plated type 304 stainless-steel valve stems and Stellite 6 bonnet bushings and lantern rings. After about a year of service, a valve stem seized and the motor force, in addition to the 2500-psi internal pressure, broke the packing-gland bolts, necessitating an emergency shutdown. After the valve stems were overlaid with Colmonoy 6 and new bushings of bearing bronze were fitted with greater clearance, there were no further troubles of this kind.

Repair Procedures

At Indian Point, two maintenance jobs involved welding in high-radiation areas.[1] One job was the modification of the nuclear boilers secondary-side blowdown piping (the original design did not provide for differential thermal expansion relative to the boiler shell). To protect the welder from the 1.5 to 3 r/hr radiation field, a special lead shield on four wheels was made of 3- by 3-ft 0.25-in.-thick lead plates stacked as many as eight thick; the shield was just high enough for the welder to position himself under it and "turtle" along while doing the work, which required two to three weeks to complete. The other task involved rewelding of an inspection cover on a control-rod guide tube in the upper grid-plate assembly. This plate is located 4 ft below the reactor-vessel flange. The radiation field was 10 r/hr with the water level lowered to just below the plate. A 3- by 4- by 4-ft lead box, with its top open and a small round hole in the bottom was made from 0.25-in. lead sheets. The welder did his work through this hole. He spent an uninterrupted 30 min and received only a very low radiation dose.

At the Ågesta Nuclear Power Plant, an unusual repair job was accomplished in connection with the peculiar stress-corrosion cracking of Inconel-600 tubes in the shield lid.[9] These tubes, which are part of the D_2O circuit, penetrate the periphery of the H_2O-filled lid over the reactor vessel; they serve as charging pipes for irradiation specimens. Only 3 of the 11 peripheral tubes were cracked by the intercrystalline corrosion, which originated on the H_2O side, but it was decided to protect all 11 tubes from further attack by enclosing each within an extra wall section that would be welded to the inside of the lid (Fig. VIII-4). This repair work was extremely difficult because the work area was severely restricted by the heavy-water piping on the lid. Further, the lid structure permitted holes of only approximately 6 in. in diameter to be made for access to the welding area. Thus it was necessary to use mirrors and bent electrodes. The repairs took four months, including demonstration of an efficient repair method and recommissioning of the lid.

Digitized by Google

The radiation levels in the work area were moderate, 1 to 5 mr/hr, and were chiefly from crud deposits in the heavy-water piping atop the lid. The fuel contributed to the background only slightly and, therefore, was not discharged from the core during the repair. No worker received more than 0.7 rem.

Control of Oxygen in D_2O

Operators of the Plutonium Recycle Test Reactor (PRTR) reported difficulties in reducing the oxygen content of the helium-blanketed heavy-water systems.[10] The oxygen came from radiolysis of the D_2O and air leaks. The excess oxygen quickly disperses through all the D_2O systems because of the common surge tank, for the helium, which is the pressurizing medium for the reactor coolant, provides an inert atmosphere over the moderator and reflector, as well as serving as blanket gas between the calandria and shields.

The usual method for reducing the excess oxygen involved recombination by adding "shots" of hydrogen gas directly into the D_2O coolant. Although chromatographic analyses of the helium showed that these injections partially reduced the oxygen, they also unexplainably decreased the indicated content of hydrogen in the gas. Investigations employing mass-spectrometric analyses showed that the chromatograph was inaccurate (at equilibrium before H_2 was injected, no H_2 was present and only 12 to 17% as much D_2 as the chromatograph had indicated total H_2 plus D_2) and that the oxygen in the gas preferred to combine with the H_2 injected into the water rather than with the D_2 already present in the gas.

When it became clear that injecting hydrogen gas into the coolant still did not sufficiently reduce the oxygen content of the D_2O, tests were made to learn the effectiveness of a uniform concentration of excess hydrogen in the helium supply. Although calculations indicated that an initial concentration of 0.3% H_2 would be enough to combine with the oxygen from radiolytic dissociation and air inleakage, it only very slowly reduced the O_2 concentration in the D_2O. Increasing the H_2 concentration to 0.6% produced faster results, but only after reactor systems reached equilibrium temperature after startup. Since a 1% H_2 concentration in the helium was selected for routine operation, there has been very little problem with excess oxygen.

Research-Reactor Modifications

Designers of reactor experiments will be interested in considering the modifications made to irradiation facilities at two pool type research reactors to increase their usefulness for certain types of experiments.

Rabbit Facility. An interesting pneumatic irradiation system has been operated in the thermal column of the Industrial Reactor Laboratories (IRL) 5-Mw pool type research reactor.[11] It permits samples to be inserted and removed from the 10^{11} neutrons/(cm^2)(sec) flux in the column during full-power operation. The unique feature of this rabbit facility is that the track and 1- by ½-in. vent line were machined from graphite and assembled to form two 4- by 4- by 51-in. standard graphite pieces (Fig. VIII-5) which, when connected end-to-end, fully penetrate the thermal column. The 1⅜-in.-diameter track has an S shape to prevent radiation streaming. The low-friction graphite track is ideal for rabbit travel; no liner is needed that might perturb the flux or cause contamination problems in the column.

A maximum rabbit-surface contamination of 0.05 μc/cm^2, due mainly to the 12.9-hr ^{64}Cu and 2.58-hr ^{56}Mn from impurities in the AGOT graphite, has presented no serious handling problems.

Figure VIII-6 shows the pneumatic system used in inserting and returning the rabbit.

D_2O Reflector. A vented rectangular aluminum tank[12] containing 45 gal of heavy water has been installed along one full face of the core of the University of Michigan reactor (Fig. VIII-7). When the core size was reduced, installation of the tank converted two radial beam ports into tangential ports, increased the thermal-neutron flux at the beam-port source planes by 80%, and improved the signal-to-background ratio by factors of 2.8 and 4.7. Figure VIII-8 shows how the installation of the heavy-water reflector influenced the ionization-chamber readings.

When tests showed that the D_2O-filled-tank reactivity worth (compared to H_2O) was only half the +0.04 $\Delta k/k$ prediction calculated, the operators increased the core operating mass by 12% so as to provide enough excess reactivity for routine operation at 2 Mw.

The maximum credible accident is postulated to involve the release into the reactor pool of tritium produced in the D_2O tank. Thus the

Digitized by Google

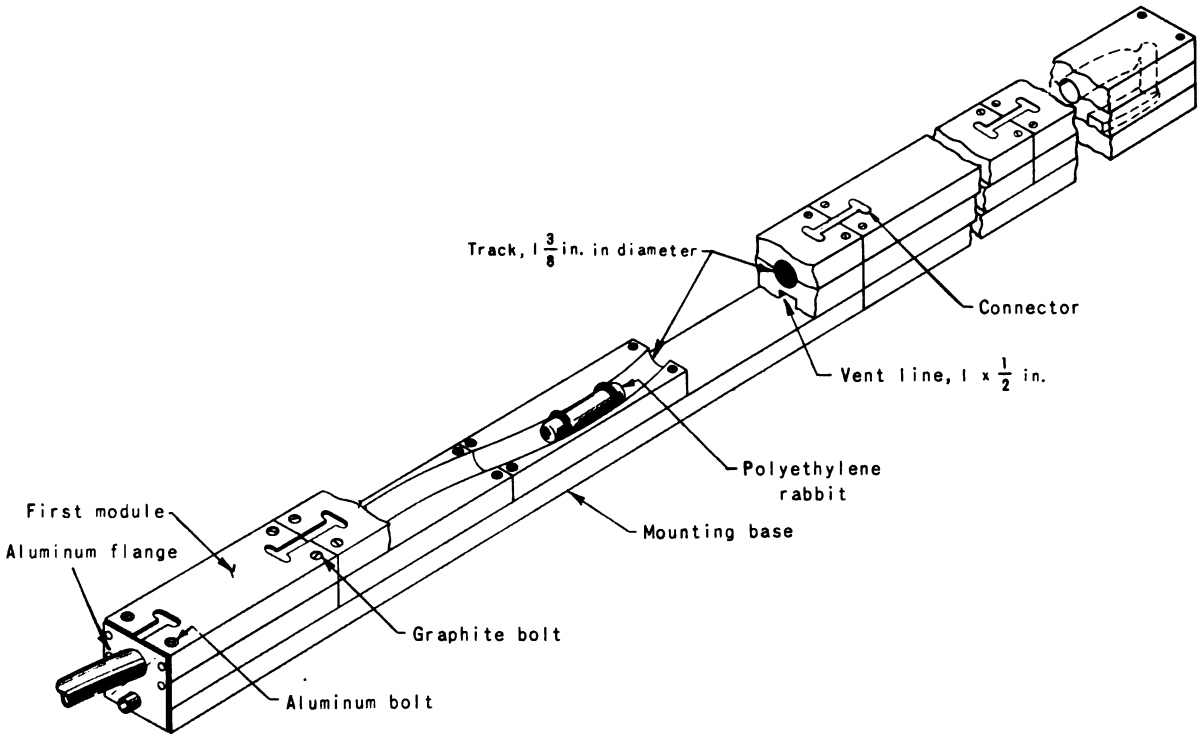

Fig. VIII-5 Assembly of graphite modules for rabbit-travel guide in IRL reactor thermal column. Graphite modules, each 12¾ in. long, are mounted on two 1- by 4- by 51-in. graphite pieces placed end-to-end.[11]

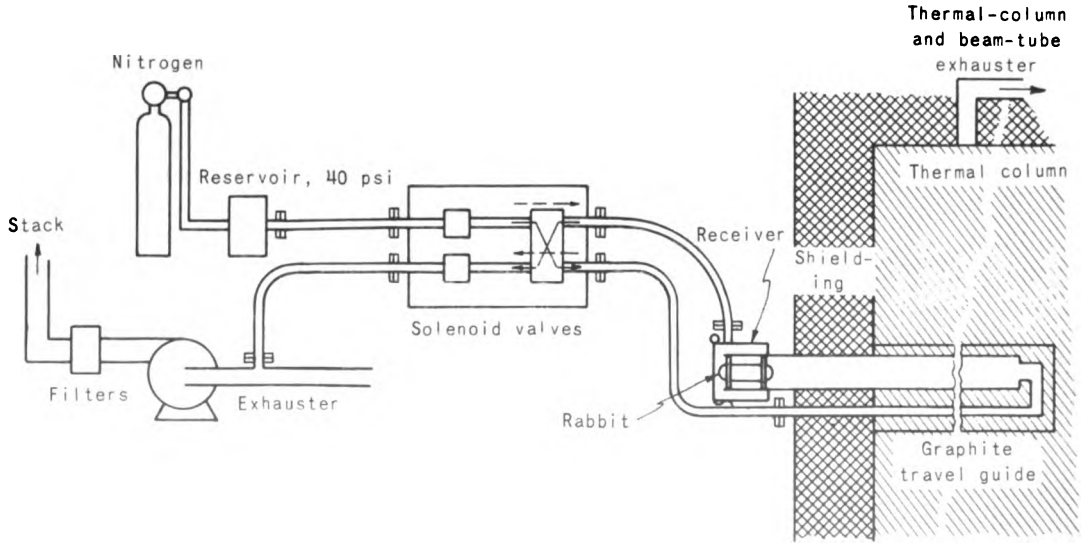

Fig. VIII-6 Pneumatic system controlled by solenoid valves supplies 40-psi nitrogen pulse for insertion and return of rabbit.[11]

Digitized by Google

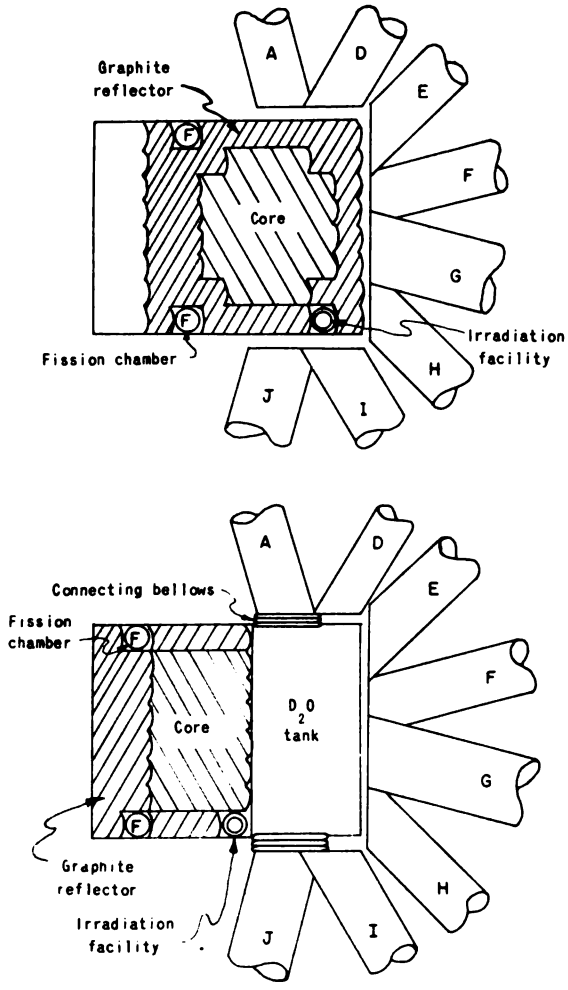

Fig. VIII-7 Arrangement of core, graphite reflector, and beam tubes of the University of Michigan reactor was modified from standard configuration (top) by adding D_2O reflector next to north face of core (bottom).[12]

tritium content in the tank will be checked every 800 Mw-hr to ensure that it does not exceed 50 curies; production-rate measurements predict that the D_2O will not need reprocessing or replacement until the reactor has operated 15,800 Mw-hr. Calculations had predicted a neutron-flux peak in the tank of twice the core flux, but preliminary measurements in the tank show that no peak occurs. No evidence of D_2O radiolysis has been detected.

Hallam Operation in Retrospect

By Fred A. Smith

The future operation of the Hallam Nuclear Power Facility has been under serious consideration since the reactor was shut down in September 1964, after failure of seven moderator elements,[13,14] and August 1965, when the U. S. Atomic Energy Commission announced termination of its operating contract with the Consumers Public Power District of Nebraska. Nevertheless, the operating experience gained in starting up and operating the 250-Mw(t) sodium-cooled graphite-moderated reactor is well worth reviewing because of its applicability to other reactors, particularly those cooled by sodium.[15–22]

On the basis of a review of the information on Hallam testing, startup, operation, problems encountered, corrective steps, and recommendations for improving plant performance and reliability, I have summarized highlights and

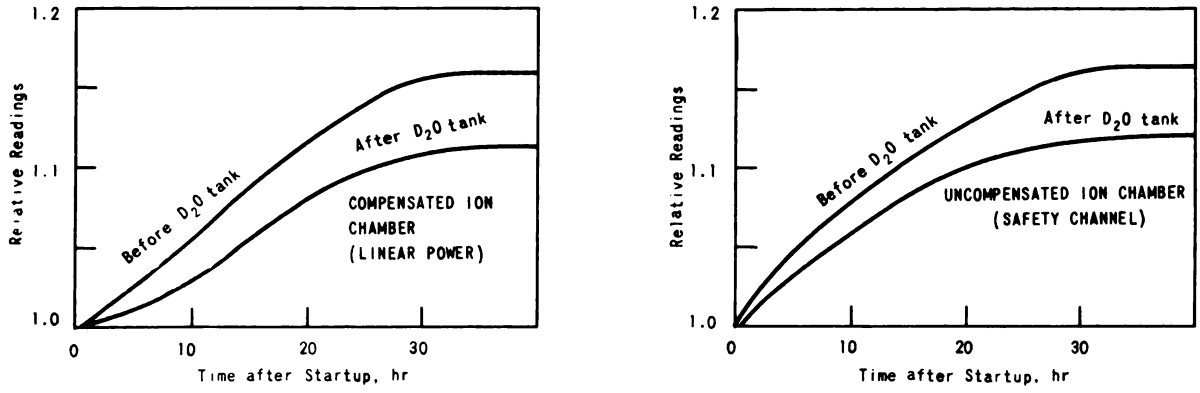

Fig. VIII-8 Effect of D_2O reflector on reactor ionization-chamber readings (average data from 10 runs before and after tank installation).[12]

Digitized by Google

have attempted to evaluate the significance of this experience. For convenience, I have considered the experience in three categories: normal operation, difficult component problems, and unresolved problems.

Summary

In general, the 80-Mw(e) plant performed well until the moderator elements failed.[14,23-25] Figure VIII-9 summarizes the plant operating history. The measured core-physics parameters agreed well with predictions. Although the sodium-heated steam generators operated safely, they were not in service long enough to appraise realistically their operating and maintenance costs. The numerous difficulties encountered in operating with sodium components, and some caused by sodium chemistry, emphasize the need for progress in these technologies.

Normal Operating Experience

As with the startup and early operation of most power plants, many Hallam activities and components gave no trouble, and others caused minor difficulties that required modifications involving only modest cost and time to make.

Plant Preoperational Tests. These tests, which involved 57 systems or functions,[20] began after "beneficial occupancy" of the facility in August 1961. Dry criticality was achieved in January 1962. Then seven months of system checkout were required before wet criticality was attained on Aug. 25, 1962. Rise-to-power tests followed; electricity was generated May 29, 1963, and full power was reached in July 1963. Thus the total time to take this plant from postconstruction occupancy to full power spanned 23 months. This accomplishment must be classed as a successful, normal operating experience much like that which should be expected for any nuclear plant of this size and complexity. Although some of the systems tested contained components whose operation later proved to be difficult or presented unresolved problems, the plant test program represents a successful joint venture between Atomics International, Consumers Public Power District, and the U. S. Atomic Energy Commission.

Initial Sodium Fill. The primary and secondary systems were initially filled with 741,500 lb of sodium in a problem-free operation similar to the large-scale transfers of sodium at Fermi and Experimental Breeder Reactor No. 2 (EBR-II). An electrically heated oil-circulation system liquified the sodium, which was pumped electromagnetically from railroad tank cars. Plant cold traps reduced the oxide content of the sodium enough that the sodium plugging temperature was brought below 250°F after only approximately 24-hr operation in the secondary system and approximately 36 hr in the primary system.

Nuclear Tests. In general, calculated and measured nuclear reactivity values agreed excellently. In criticality tests[26,27] sodium worth at 350°F in a 53-element core was measured as $-6.1\%\ \Delta k/k$; the value calculated was $-5.5\%\ \Delta k/k$. For the 140-element cold, clean core, k_{eff} was measured as 1.109 ($9.8\%\ \Delta k/k$); the predicted value was 1.069 ($6.5\%\ \Delta k/k$). Measurements of zero-power temperature coefficients of reactivity[28] showed the isothermal coefficient of reactivity to be +0.123 cent/°F at 400°F and +0.088 cent/°F at 500°F. With 20% sodium flow in the primary system, the "prompt" power coefficient is −0.4 cent/Mw(t) and is −0.05 cent/Mw(t) at 240 Mw(t) with 96% sodium flow.

The peak of ^{135}Xe buildup[29] occurs approximately 4.5 hr after a scram from full power and is worth −263 cents of reactivity. Samarium-149 has a peak buildup of 160 full-power days and an equilibrium worth of −122 cents.

For power operation, investigations of control-rod patterns[30] indicate that the axial power distribution has a range of peak-to-average ratios of 1.40 to 2.62.

Plant Control System. A number of minor problems were experienced. These related to faulty components, fabrication errors, and design shortcomings.

Of 13 interrelated subsystems of the plant control system, 7 demonstrated satisfactory operation without any corrective action. The satisfactory systems were the (1) plant power control, (2) nuclear power control, (3) fuel-temperature and coolant-flow ("convection power") control, (4) outlet steam ("attemperator") control, (5) steam-generator pressure-relief control, (6) primary block-valve control, and (7) secondary-flow control. Minor modifications were required to the division-of-load

Digitized by Google

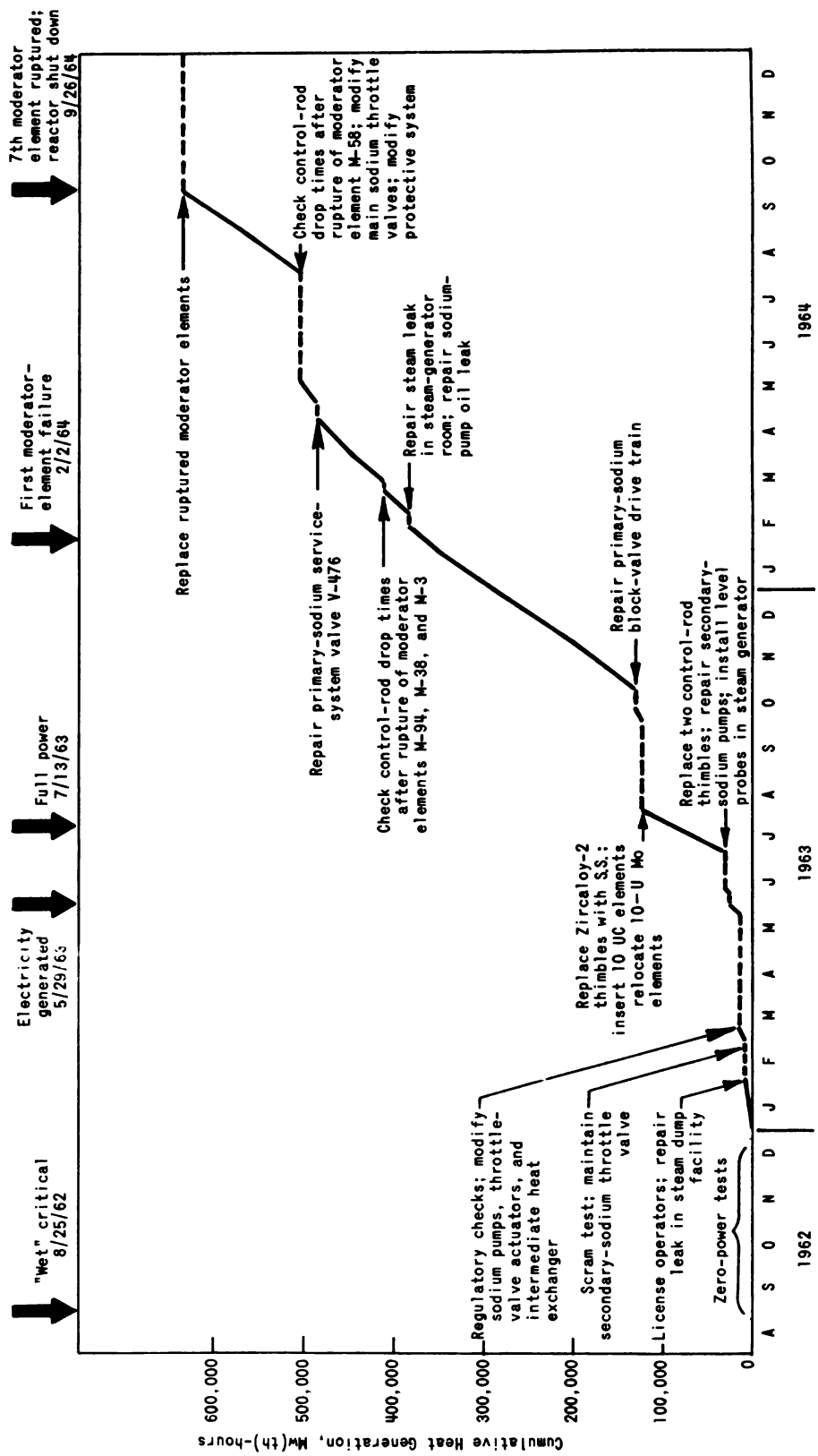
"Wet" critical 8/25/62
Electricity generated 5/29/63
Full power 7/13/63
First moderator-element failure 2/2/64
7th moderator element ruptured; reactor shut down 9/26/64
Cumulative Heat Generation, Mw(th)-hours
0
100,000
200,000
300,000
400,000
500,000
600,000
A S O N D J F M A M J J A S O N D J F M A M J J A S O N D
1962
1963
1964
Zero-power tests
License operators; repair leak in steam dump facility
Regulatory checks; modify sodium pumps, throttle-valve actuators, and intermediate heat exchanger
Scram test; maintain secondary-sodium throttle valve
Replace Zircaloy-2 thimbles with S.S.; insert 10 UC elements relocate 10-U Mo elements
Replace two control-rod thimbles; repair secondary-sodium pumps; install level probes in steam generator
Repair primary-sodium block-valve drive train
Check control-rod drop times after rupture of moderator elements M-94, M-38, and M-3
Repair primary-sodium service-system valve V-476
Replace ruptured moderator elements
Repair steam leak in steam-generator room; repair sodium-pump oil leak
Check control-rod drop times after rupture of moderator element M-58; modify main sodium throttle valves; modify protective system

Fig. VIII-9 Summary of Hallam reactor operating performance shows cumulative thermal power generated vs. time and reasons for various outages. Before the last shutdown, moderator-element failures during 1964 seriously affected operations; a 1668-hr outage followed failure of moderator element M-58. Two other 1964 outages lasted 230 and 253 hr; 12 others lasted less than 100 hr each.[59]

Digitized by Google

computer, moderator–coolant control, and steam-dump control systems. Although the primary-sodium flow control system has operated satisfactorily, the need for the existing recorder–controllers for this system should be evaluated more completely for actual plant load-following conditions.

The neutron-flux control system encountered difficulties because of below-average reliability of components. However, after more reliable plug-in components were installed, the neutron-flux control system operated uninterruptedly longer and was easier to maintain. Feedwater-level control posed a difficult problem; because level control was limited by the lack of vertical head in the horizontal steam generator, it was really a problem of steam-generator design rather than of instrument control.

In general, the overall control system has responded excellently to intentional transients.[31] On one occasion the operator manually overrode the instruments, which resulted in a reactor scram. Subsequent investigation revealed that the automatic control-rod response had been legitimate.

On another occasion, when both the conventional and nuclear plants were operating simultaneously and the conventional boiler suddenly dropped off the line, nuclear response was immediate. As designed, the reactor picked up the full turbine load faster than approximately 20%/min.

Control-Rod Operation. The control-rod design speeds were verified by preoperational tests in air.[32] No change in drive speed and no malfunctions were found when the control rods were tested again during the plant rise to power.[33] There were small differences in design-vs.-actual rod drop times for the 9-ft free fall and full drop-to-snubber closure, but they were well within specifications.

Faulty magnets, shorted coils, and improper limit switches caused spurious scrams of the control rods. After the causes of these problems were corrected, the control rods worked perfectly. Although the difficulties with the rod drives involved normal installation adjustments, the original control-rod-drive thimbles, which were to keep the control rods in a dry helium atmosphere, failed; they are discussed further under the subsection Unresolved Problems.

Reactor Heat-Transfer Systems. Overall performance of the heat-transfer system has been equal to or better than design. Total heat losses were independent of load and remained at approximately 1.5 Mw(t), which is less than a 1% loss at full load. High-temperature, high-flow, and low-pressure operation has been effected satisfactorily for prolonged periods. Reactor operation as a load-following plant has been very successful.

Sodium Mechanical Pumps. Both during preoperational testing and after plant power operations, the six vertically mounted overhung mechanical type pumps had to be removed for maintenance.[19] Subsequently, these centrifugal and free-surface pumps (the primary and secondary systems each have three) were modified to: (1) loosen the diametral running clearances of the impeller upper and lower wear rings, (2) make more uniform the temperature distribution of the exterior casings of the pumps so as to prevent impeller binding, (3) provide greater area for sodium flow from the bearings to the pump suction, and (4) install sintered metallic filters to prevent foreign material (beads from the welding rods that had been used in fabricating the steam generators) from entering the secondary-system pumps. Since the corrections, overall performance of the pumps has been satisfactory. Fortunately, like the EBR-II and Fermi mechanical pumps, the Hallam pumps were designed so that that the impeller and shaft can be removed relatively easily from the volute casing, making field maintenance possible.[19] It is easier to remove, maintain, and replace a sodium pump than a deep-well pump, a boiler feedwater pump, or a similar major pump.[34]

Leakage Through Sodium Valve Seats. For plant safety the sodium in the reactor drain and fill lines must be kept molten by heating the lines. However, seepage of radioactive sodium across the drain-line valves limited personnel access to the sodium service cell (where the cold and hot traps are located) during reactor operation. To avoid the problem, a bypass line has been installed in the primary-sodium service system to connect each main coolant loop to the drain tanks without passing through the sodium service cells.

Bellows-Seal Valves. The bellows in about 11% of the 2-in. (or less) sodium valves in the cold-trap and drain circuits have failed. Most of the leaks occurred on valves that were

Digitized by Google

partially open for throttling service—none of the bellows valves that normally are either fully open or closed failed. The bellows-seal valves that have not leaked were operated subsequently as stop valves. The failed valves have been replaced with freeze-seal valves or fixed orifices, both of which are recommended for future installations. It also has been recommended[35] that the number of throttle valves should be minimized in future sodium plants and that any bellows-seal valves be tested thoroughly at various openings and with sodium turbulence to be certain that any bellows will not oscillate.

Plugging Meters. These units, which indicate the oxide concentration in sodium, have operated well in each of the primary and secondary systems. However, to eliminate poor flushing of the plugged area when the oxide saturation temperature approaches the bulk sodium temperature, a minor modification would be desirable—a heater should be added to raise the temperature of the sodium flowing through the meter above the bulk sodium temperature.[36]

Handling of Core Components. These handling operations have involved the movement of fuel elements and control-rod thimbles and, more recently, the removal of moderator elements. Facilities for cleaning and inspecting core components have operated as designed.[37,38] The fuel-handling machine and its gantry and trolley assembly were tested with a core mockup vessel before delivery to the site.[39] Thus the system has operated well with only minor changes required since installation. This success indicates the desirability of pretesting full-size components. Hallam experience with handling damaged core components points up the desirability of handling-equipment designers giving thought to being able to dislodge and remove damaged core components expeditiously.

Difficult Component Problems

The operation of some components and systems revealed considerable or sustained difficulties that involved substantial cost and time to correct.

Nuclear Instruments. Electrical noise interference, high instrument temperatures, and difficulty in achieving rapid response have been problems. Power-range instruments required only minor modifications. But the intermediate-range log-N instruments encountered difficulties caused by poor design and poor quality control. Because the average signal-to-noise ratio was only 5:1, the startup-range channels initially provided readings with fluctuations of far greater magnitude than normally associated with nuclear statistics.

These instrument problems were greater than should be expected. An evaluation[40] report recommends more stringent performance specifications for future plants to eliminate extensive testing, repair, and modification of nuclear instrumentation.

Plant Protective Instruments. The main functions of this system,[41] which is separate from the plant regular control systems, are to prevent inadvertent hazardous operation and to detect off-normal conditions and then act automatically to prevent damage to the reactor system or heat-transfer-system components.

Tests and use of the plant protective system[42] led to numerous improvements that eliminated (1) noise caused by poorly regulated a-c power, (2) noise caused by the grounding pattern, (3) drift related to insufficient cooling, (4) short lifetime of mechanical "choppers" in the amplifier, and (5) interaction between protective-system components. With these modifications the system proved to offer adequate protection against potentially hazardous conditions. For future designs of such systems, it has been recommended that electric power be regulated at the point of end use rather than at the source with a common regulator.[43] Future designs also should be studied closely for clear definitions of the purpose and function of protective-system components.

Control-Rod Thimbles. The control-rod thimbles were intended to isolate the rods from the reactor sodium by containing them in a pressurized helium atmosphere.[41] The reason for the selection of a dry control-rod system was the state of development of mechanisms in sodium at the time the design was fixed. However, the Zircaloy-2 walls of 3 of the 19 thimbles cracked early in the prestartup tests of the primary sodium system. Study indicated[44] that a possible cause of the failure was hydrogen embrittlement due to the diffusion into the Zircaloy-2 of hydrogen from the titanium hydride used as a shielding material in the control-rod-drive housing. (For more informa-

Digitized by Google

tion on hydrogen embrittlement of Zircaloy, see page 245.) It is interesting to note that earlier engineering proof tests of the control-rod-drive mechanism and thimbles in sodium were conducted without the titanium hydride shielding installed. The problem was solved when all 19 Zircaloy-2 thimbles in the reactor were replaced with thimbles of type 304 stainless steel.

Throttle Valves. The Hallam primary-system throttle valves are freeze-seal ball valves actuated by a double jackscrew driven by an air motor.[45] Difficulties were encountered with the valve actuator, shafts, torque limiter, and jackscrews. Although the various modifications eventually resulted in satisfactory operation, the problems were bothersome and both they and the corrective measures involved an extended period of time.

Intermediate Heat Exchangers. Vibration caused a tube to fail in one of the three intermediate heat exchangers—which convey heat from the radioactive primary-system sodium to the nonradioactive sodium in the secondary system—in November 1962, which was before the reactor was used to produce power. Analysis indicated that failure was caused by flow-induced vibration in the shell (secondary) side near the sodium inlet baffles.[46] The natural frequency of vibration was changed when shims were installed between tube rows in the 12 to 15 ft/sec sodium inlet area. Subsequent tests and operations indicate that the vibration ceased. Nevertheless this internal modification was difficult to make.

More favorable was the fact that the heat transferred by the intermediate exchangers was within 12% of the value predicted,[26] and it did not vary significantly over the plant history. Pressure drops were greater than predicted—6 vs. 1.2 psi on the primary side and 14 vs. 6.8 psi on the secondary side. These greater than predicted drops are of little concern because the pump head is sufficient to achieve the flows required.

Steam Generators. These units, of which there are three, are described in Refs. 19, 20, 41, 47, and 48. When plant auxiliary steam was used to preheat the steam generators to 300°F before they were filled initially with sodium, the steam did not distribute the heat evenly over the entire steam generator. This relatively minor problem was corrected by maintaining a partial vacuum on the steam generator while admitting the preheat steam; this procedure distributed the heat so that temperatures were within ±25°F.

A more difficult problem arose during the tests for the initial rise to power. The three steam generators had 0.60 to 0.70% liquid water in the steam leaving the separator, which exceeded the maximum acceptable moisture carry-over of 0.25%. After numerous tests,[49,50] it was found that the water level was dropping enough that some of the horizontal sodium-heated tubes did not have water over them. Water level was varying as much as 5 in. at full power. Thus carry-over was limited by the installation of more precise control equipment to hold the water level in the evaporator section within ±0.7 in. at full power. With these conditions the steam separators have little capacity above their steam rated capacities of 251,000 lb/hr.

Although it is significant that the overall heat-transfer coefficients for steam generation have remained essentially constant (which means no fouling has occurred) and that the steam generators have not leaked sodium to air or to water (which testifies to the safety of the design bases and the fabrication quality control), the need for the numerous tests and modifications to solve the moisture carry-over problem makes it necessary to consider the experience with Hallam steam generators as having been difficult.

Gas Entrainment in Sodium Expansion Tank. Originally, all sodium in the three secondary-system parallel loops flowed through an expansion tank in each loop. During preoperational tests, it was discovered that helium cover gas in the expansion tanks became entrained by the sodium and circulated through the system. Although this problem was eliminated by modifications that caused 96% of the sodium flow to bypass the expansion tanks,[51] this type of design deficiency cannot be considered normal; the modifications required approximately three months to complete. One of these expansion tanks cracked during later operation; because this problem has not been rectified, it is discussed in the next subsection.

Unresolved Problems

Operating experience uncovered some problems that either have no positive means of

Digitized by Google

correction or whose resulting difficulties have not yet been corrected.

Crack in Sodium Expansion Tank. The shell of one of the three expansion tanks in the secondary systems cracked near a nozzle.[52] The crack was caused by weld-rod coating entrapment at an internal baffle plate (the lesson learned from this is that internal welds require specifications similar to external sodium-containment welds). Analysis of the nature of this sodium-leakage failure indicates the desirability of replacing all three tanks if the plant is to resume operation.[53] Such a change would be a relatively minor task.

Cold Traps for Oxide. Although the initial efficiency of the cold traps, estimated as nearly 100%, shows their ability to keep the oxide content of the sodium low, the operator must either periodically replace the 10 to 12 plugged cold traps or install larger traps. The original traps plugged relatively rapidly because of the oxide that formed in the sodium during the repairs and modifications to the secondary system and the intermediate heat exchanger.

Because of mechanical interference, maintenance men must enter the cell to remove the primary-system cold traps.[54] This is no problem now, but, if a fuel cladding fails and leaks fission products into the sodium, remote methods might have to be devised to replace the traps.

Hot Traps for Carbon. To monitor the carbon content of the primary-system sodium, operators placed type 304 stainless-steel tabs at the sodium inlet of a carbon trap. After being held at 1200°F in the 30 to 40 gal/min sodium flow for 100 hr, the tabs were removed and analyzed chemically and metallurgically. These tabs showed no evidence of carburization.[55] In contrast, when fresh type 304 stainless-steel tabs were exposed statically at 1200°F for 100 hr to a sodium sample withdrawn from the carbon trap, the tabs invariably carburized to a range of 4 to 147 ppm. Obviously, the problem of understanding and measuring the chemical effects of various forms of carbon in sodium is still unsolved.

Freeze Traps for Sodium Vapor. Condensation or freeze traps are installed at high points in the reactor auxiliary sodium systems to remove sodium vapor from the cover gas that is vented or purged when the sodium system is being drained or filled.[56] Each of these traps contains a sodium-level float valve that controls the leakage of cover gas to the vent; the valve opens the gas path to the vent when the rising sodium level raises the float, which engages a cam that operates a shaft running through a sodium "freeze seal." However, the shaft packing that contains and backs up the freeze seal has leaked helium and permitted some liquid sodium to leak through the shaft annulus into the vent, which plugged it. Also, because of the variable resistance of the freeze seal, excessive manual pressure has been applied to this shaft, which broke on several occasions.

Although these problems have not been so severe as to warrant redesign of the Hallam system, a better system for venting and filling inert gas is needed for future sodium plants. (For more information on inert-gas systems and vapor traps, see page 259.)

Fuel-Channel Orifices. Adjusting the coolant flow by means of variable orifices in each fuel channel in the core allowed the operators to hold coolant exit temperature from each channel to within 15°F of the average.[41,57] Flow through the orifice could be adjusted 30 to 100% by moving the orifice plug its full 4-in. stroke; at 100% flow, 4-in. travel changes sodium temperature at the channel exit 90 to 150°F. However, the inability to move some of the plugs, due primarily to sodium oxide, has limited the use of these devices. Twelve orifices became either fully closed (but there is also a bypass), stuck, or broken. In other cases, when the drive cable would remain in tension after turning was difficult, the orifice plug would "creep" so that further adjustment would be necessary.

Although these fuel-channel variable orifices could be improved by replacing the flexible shaft with a rod or by installing a bellows, it was not practical to make changes on the initial core.

Moderator-Element Failure. Leakage of the type 304 stainless-steel cladding on the graphite moderator elements[41,58] was a significant event of major proportion in that it necessitated shutting down the plant for core repairs. By the end of September 1964, the cladding on seven moderator elements had failed and had flooded

Digitized by Google

the elements with sodium; Fig. VIII-10 shows the core locations of the failed and suspect moderator elements.[34] This flooding reduced core reactivity, tilted the flux, and depressed the power, by which means the failures were detected and the suspect failed elements were identified[59] (see Table VIII-1); these tests indicated that 8 and possibly 9 moderator elements had failed, but subsequent examination with boroscopes and electromagnetic probes showed that only 7 elements had failed. However, this leakage also permitted the sodium to react with the graphite, which swelled the elements and caused 19 fuel elements to become stuck in place (none of the thimble-enclosed control rods stuck.)

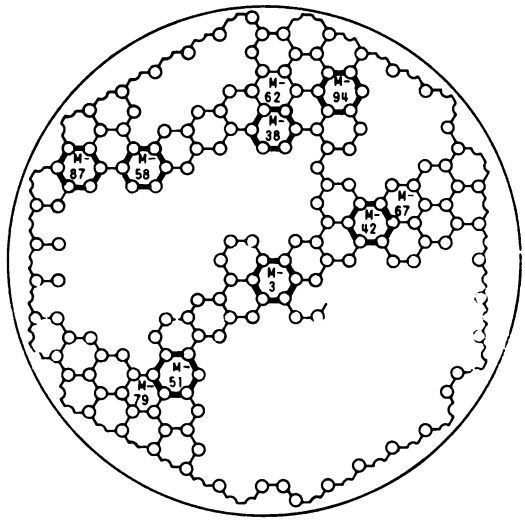

Fig. VIII-10 Locations in the core of the failed and suspect moderator elements.[34] The seven cans that actually failed are shown with heavy borders. Element M-87 was not suspected initially. On the basis of flux patterns, M-62 and M-67 were suspected, and M-79 was regarded as a possible failure, but examination showed that all three were intact.

Subsequent core-repair work removed the 19 stuck fuel elements; the 7 failed moderator elements, together with 3 others that suffered damage in the handling operations, were replaced with 10 new moderator elements by July 12, 1965.

A review of the moderator-element design, material specifications, and inspection and fabrication methods that was made before the failed elements were removed uncovered no obvious reasons for the failures, although it cast suspicion on rewelds that were made on initially defective welds.[60] Although the final report on the detailed examination and analysis of the cans was not available as of this writing, Fig. VIII-11 shows a typical crack,[61] which occurred approximately 3 in. from the top of the element in core position M-42. Six element cans cracked in similar locations; metallographic study of the type 304 stainless steel near the cracks revealed little or no

Table VIII-1 REACTIVITY REDUCTIONS WHEN MODERATOR-ELEMENT CANS CRACKED AND SODIUM ENTERED ELEMENTS[34]

Moderator-element location	Date ruptured	Date of additional disturbance	Reactivity reduction, cents: Actually observed	Corrected for rod-calibration error	Predicted worth*
M-94	2/2/64		3	4	4
M-38 and M-62	2/2/64 and 2/20/64–2/22/64		9 } 25	10.5 } 29	20 (M-38) 11 (M-62) } 31
		3/6/64–3/12/64	9	10.5	
		3/29/64–4/5/64	7	8	
M-3	3/4/64		18	21	21
M-58	5/15/64		16	19	18
M-51	9/9/64		23	23	20
M-42 and M-67	9/26/64		25 } 43	25 } 43	23 (M-42) 20 (M-67) } 43
		9/27/64–9/30/64	18	18	
Total			128	139	137

*Predicted worth is determined by flux weighting to corrected-observed worth of M-3 as base.

Digitized by Google

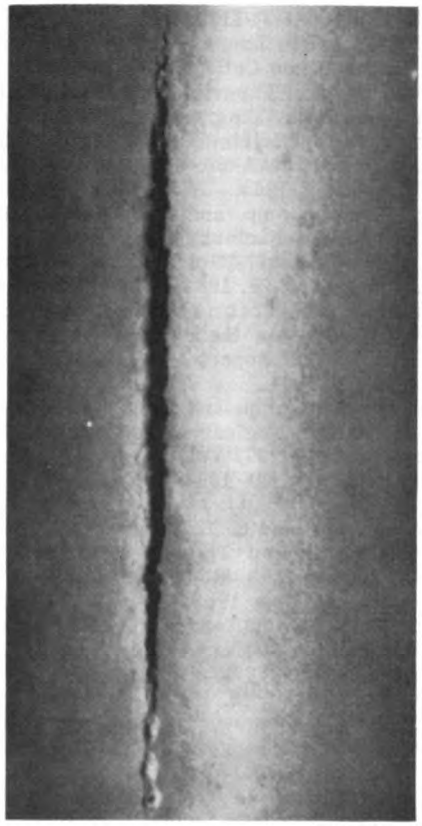

Fig. VIII-11 Crack that occurred near the top of the can on moderator element in core position M-42 is typical of the cracks in six of the seven failed cans.[34]

thinning or grain distortion[62] but found intergranular separation of the type that occurs from long-term stress in the range of creep deformation (below the yield stress). In this area near the top of the cans, which contain a vacuum, the thin type 304 stainless steel is not supported by the graphite. Although a series of "fingers" is intended to support the cladding wall, in six of the failed cans some of the fingers did not give support.[63] (The seventh element failed rapidly when the swelling of the other elements damaged a process tube, which gouged the seventh can.)

The plant designers believe the problem can be solved by eliminating the vacuum in the 141 moderator cans.[63] This could be done within about six months by installing on each moderator element an 11-ft snorkel tube that would vent it to the inert cover gas above the sodium surface in the reactor vessel.

From studies made of the design of the failed moderator elements,[64] it is now clear that the Hallam design does not represent an engineering extrapolation of the moderator elements used in the Sodium Reactor Experiment.[65] Future liquid-metal-cooled reactor designs must be considered carefully to determine precisely which features are truly represented by previous experience and to identify design features that involve advancements in the state of the art and therefore constitute a performance risk.

References

1. J. A. Prestele, Operating Experience at Indian Point, *Trans. Am. Nucl. Soc.*, 8(Suppl.): 30-31 (1965).
2. Robert Campbell and Joseph A. Signorelli, Elk River Reactor Operations, *Trans. Am. Nucl. Soc.*, 8(Suppl.): 31 (1965).
3. Glen A. Reed, Major Operating and Refueling Problems at the Yankee Atomic Electric Company Rowe Power Plant, *Trans. Am. Nucl. Soc.*, 8(Suppl.): 28 (1965).
4. R. E. Heffner, Failure of SPERT III Pressurizer Vessel, *Trans. Am. Nucl. Soc.*, 5(1): (1962); also USAEC Report IDO-16743, Phillips Petroleum Company, January 1962.
5. R. E. Heffner, Six-Years Operating Experience with PWR Plant Components, *Trans. Am. Nucl. Soc.*, 8(Suppl.): 29-30 (1965).
6. J. I. Riesland and E. A. Gustafson, Work Performed on Fuel Channels and the Core Support Plate at Big Rock Point Nuclear Power Plant, *Trans. Am. Nucl. Soc.*, 8(Suppl.): 5-9 (1965).
7. L. M. Hausler, R. L. Haueter, and R. C. Christianson, In-Vessel Modification of Irradiated Reactor Internals at Big Rock Point, *Trans. Am. Nucl. Soc.*, 8(Suppl.): 3-5 (1965).
8. C. Arthur Dalke, Elimination of Hydraulically Induced Core Vibrations in the General Electric Test Reactor, *Trans. Am. Nucl. Soc.*, 8(Suppl.): 2 (1965).
9. Nils Rydell, Some Aspects of Operating Experience at Ågesta Nuclear Power Plant, *Trans. Am. Nucl. Soc.*, 8(Suppl.): 31-32 (1965).
10. R. V. Dulin, Control of Oxygen in PRTR Helium Systems, *Trans. Am. Nucl. Soc.*, 8(Suppl.): 46-47 (1965).
11. Arthur de Saint Maurice and Richard Canfield, Thermal-Column Pneumatic Facility, *Trans. Am. Nucl. Soc.*, 8(Suppl.): 1 (1965).
12. Robert D. Martin, Operating Experience with a Heavy-Water-Reflector Tank, *Trans. Am. Nucl. Soc.*, 8(Suppl.): 46 (1965).
13. Consumers Public Power District, HNPF Monthly Operating Report No. 36, p. 1, July 1965.
14. R. H. Davidson, Moderator Element Failures in the HNPF, *Trans. Am. Nucl. Soc.*, 8(Suppl.): 35 (1965).
15. Consumers Public Power District, HNPF Monthly Operating Reports, A Series, Nos. 1–37.
16. Atomics International–AEC Chicago Operations Office, HNPF Reactor Operating Analysis Reports, USAEC Reports, A Series, Nos. 1–28.
17. R. C. Gerber, Hallam Nuclear Power Facility, in Symposium Proceedings on Sodium Reactors

Digitized by Google

Technology, Lincoln, Nebraska, May 24–25, 1961, USAEC Report TID-7623, pp. 73-88.
18. W. P. Venable, Integration of Hallam Nuclear Power Facility into Consumers Public Power District of Nebraska System, in Symposium Proceedings on Sodium Reactors Technology, Lincoln, Nebraska, May 24–25, 1961, USAEC Report TID-7623, pp. 89-96.
19. H. O. Monson et al., Components for Sodium Reactors, presented at the Third United Nations International Conference on the Peaceful Uses of Atomic Energy, Geneva, 1964, Paper A/Conf.28/P/228.
20. Atomics International, Final Evaluation Report, Hallam Nuclear Power Facility, USAEC Report NAA-SR-9777(Vols. I–VI), 1964.
21. L. E. Keller and R. H. Davidson, Hallam Operating Experience, *Nucl. Safety*, 7(2): 236-242 (Winter 1965–1966).
22. K. K. Brown, Operating Hallam, *Nucleonics*, 22(9): 41-46 (September 1964).
23. J. D. Cochran, Operating Experience at Hallam Nuclear Power Facility, in *American Power Conference, Chicago, Illinois, March 26–28, 1963*, Vol. XXV, pp. 204-212.
24. J. D. Cochran and J. E. Owens, Initial Operation of the Sodium Graphite Reactor at the HNPF, in *26th Annual American Power Conference, Chicago, Illinois, April 14–16, 1964*, Vol. XXVI, p. 201.
25. Emerson Jones and J. D. Cochran, HNPF Operating Experience and Testing to 250 Mw(t) to November 1, 1963, USAEC Report TID-20396, November 1963.
26. J. E. Price (Comp. and Ed.), Final Evaluation Report, Hallam Nuclear Power Facility, USAEC Report NAA-SR-9777(Vol. I), p. 34, Atomics International, Sept. 29, 1964.
27. J. E. Price and J. W. Rocke (Eds.), Final Evaluation Report, Hallam Nuclear Power Facility, Wet Excess Fuel Loading, AI-PC-710, USAEC Report NAA-SR-9777(Vol. VI), Atomics International, June 12, 1964.
28. *Ibid.*, Zero Power Coefficients of Reactivity, AI-PC-760.
29. *Ibid.*, Xenon Poisoning, AI-PC-840.
30. *Ibid.*, Power Coefficient, AI-PC-770.
31. P. F. Shaw, HNPF Control System Response During Transient Conditions, USAEC Report NAA-SR-9584, Atomics International, June 15, 1964.
32. J. E. Price and J. W. Rocke (Eds.), Final Evaluation Report, Hallam Nuclear Power Facility, Control Rod Drive and Actuator Assemblies, AI-P-1145, USAEC Report NAA-SR-9777(Vol. III), Atomics International, June 12, 1964.
33. J. E. Price and J. W. Rocke (Eds.), Hallam Nuclear Power Facility, Master Schedule Including Rise-to-Power, AI-PC-830, USAEC Report NAA-SR-9777(Vol. VI), Atomics International, June 12, 1964.
34. Ivan O. Sunderman, Consumers Public Power District, personal communication, Sept. 17, 1965.
35. J. E. Price (Comp. and Ed.), Final Evaluation Report, Hallam Nuclear Power Facility, USAEC Report NAA-SR-9777(Vol. I), p. 17, Atomics International, Sept. 29, 1964.
36. *Ibid.*, Sodium Service System, AI-P-1104.
37. J. E. Price and J. W. Rocke (Eds.), Final Evaluation Report, Hallam Nuclear Power Facility, Wash Cells, AI-P-1133, USAEC Report NAA-SR-9777(Vol. III), June 12, 1964.
38. *Ibid.*, Maintenance Cell., AI-P-1139.
39. W. A. Kaspic, Experimental Testing of Core Component Handling Equipment and Handling Techniques for Hallam Nuclear Power Facility, USAEC Report NAA-SR-7785, Atomics International, Sept. 15, 1964.
40. J. E. Price (Comp. and Ed.), Final Evaluation Report, Hallam Nuclear Power Facility, USAEC Report NAA-SR-9777(Vol. I), p. 69, Atomics International, Sept. 29, 1964.
41. Atomics International, Final Summary Safeguards Report for the Hallam Nuclear Power Facility, USAEC Report NAA-SR-5700, pp. 257-269, Apr. 15, 1961.
42. J. E. Price (Comp. and Ed.), Final Evaluation Report, Hallam Nuclear Power Facility, USAEC Report NAA-SR-9777(Vol. I), p. 60, Atomics International, Sept. 29, 1964.
43. *Ibid.*, p. 63.
44. R. K. Wagner and S. L. Essglebert, Results of HNPF Control Rod Thimble Examinations, USAEC Report NAA-SR-TDR-9142, Atomics International, October 1963.
45. J. E. Price (Comp. and Ed.), Final Evaluation Report, Hallam Nuclear Power Facility, USAEC Report NAA-SR-9777(Vol. I), pp. 13-17, Atomics International, Sept. 29, 1964.
46. R. E. Durand, Operating Experience with Intermediate Heat Exchangers at HNPF, USAEC Report NAA-SR-9718, Atomics International, June 15, 1964.
47. Robert W. Dickinson and John B. Williams, Trends in Sodium Equipment, *Nucleonics*, 19(1): 65-70 (January 1961).
48. Frank Boni and Philip S. Otten, Fermi and Hallam Steam Generators, *Nucleonics*, 19(6): 58-61 (June 1961).
49. Consumers Public Power District, HNPF Operating Report for December 1963.
50. Atomics International, HNPF Reactor Operations Analysis Program, Semiannual Progress Report No. 2, March 1–August 31, 1963, USAEC Report NAA-SR-9265, pp. 105-111, Mar. 1, 1964.
51. J. E. Price (Comp. and Ed.), Final Evaluation Report, Hallam Nuclear Power Facility, Main Heat Transfer System, AI-P-1103, pp. 12-29, USAEC Report NAA-SR-9777(Vol. I), Atomics International, Sept. 29, 1964.
52. Consumers Public Power District, HNPF Monthly Operating Report No. 26, October 1964.
53. Consumers Public Power District, HNPF Monthly Operating Report No. 28, December 1964.
54. J. E. Price (Comp. and Ed.), Final Evaluation Report, Hallam Nuclear Power Facility, USAEC Report NAA-SR-9777(Vol. I), p. 52, Atomics International, Sept. 29, 1964.
55. Atomics International, HNPF Reactor Operations Analysis Program, Semiannual Progress Report No. 1, September 1, 1962, to February 28, 1963, USAEC Report NAA-SR-8401, July 1, 1963.
56. J. E. Price (Comp. and Ed.), Final Evaluation Report, Hallam Nuclear Power Facility, USAEC Report NAA-SR-9777(Vol. I), p. 54, Atomics International, Sept. 29, 1964.
57. J. E. Price and J. W. Rocke (Eds.), Final Evaluation Report, Hallam Nuclear Power Facility, Radial Power Distribution and Fuel Channel

Digitized by Google

Orifice Adjustment, AI-PC-800, USAEC Report NAA-SR-9777(Vol. VI), Atomics International, June 12, 1964.
58. *Power Reactor Technol.*, 5(3): 39-51 (June 1962).
59. Atomics International, HNPF Reactor Operations Analysis Program, Semiannual Progress Report No. 4, February 29–September 30, 1964, USAEC Report NAA-SR-10743, May 15, 1965.
60. *Ibid.*, pp. 61-69.
61. Consumers Public Power District, HNPF Monthly Operating Report No. 35, June 1965.
62. John J. Purcell, AEC Chicago Operations Office, Sodium Components Development Program, Project Coordination Report, Hallam Nuclear Power Facility, p. 12, August 1965.
63. *Nucl. Ind.*, 12(9): 11 (September 1965).
64. *Reactor Handbook*, 2nd ed., Vol. IV, Engineering, p. 677, edited by Stuart McLain and J. H. Martens, John Wiley & Sons, Inc., New York, 1964.
65. *Reactor Handbook*, 2nd ed., Vol. IV, Engineering, p. 665, edited by Stuart McLain and J. H. Martens, John Wiley & Sons, Inc., New York, 1964.

Digitized by Google

Section

IX

Power Reactor Technology

Systems Technology

Advancements in Organic Coolants

By J. E. Sawyers, Combustion Engineering, Inc.

The investigations in organic-coolant technology have involved seven general aspects: (1) decomposition by radiolysis and pyrolysis, (2) additives to improve resistance to decomposition, (3) reclamation methods for used coolant, (4) fouling-film formation, (5) corrosion properties, (6) heat-transfer properties, and (7) possible new coolant materials. Although biphenyl and other organics have been studied, the major work has concentrated on the terphenyls, especially Santowaxes OMP and R. Much of the work summarized here is discussed[1] in detail in a comprehensive analysis of the status of organic-coolant technology through mid-1964.

Decomposition

Experiments on pyrolysis of biphenyl, orthoterphenyl, and metaterphenyl included limited investigations of gamma radiolysis.[2]

The pyrolytic exposures involved various durations at 750 to 825°F in an autoclave controlled within 5°F. After pyrolysis products were analyzed and molecular-weight distributions were measured, rate constants and heats of reaction were calculated. Orthoterphenyl pyrolyzes about five times faster than biphenyl and metaterphenyl. The data indicate that pyrolysis is a first-order reaction. Rate constants for all three materials increase with temperature and fit reasonably well to an Arrhenius plot. Calculated heats of reaction are 93 kcal/mole for biphenyl, 89 kcal/mole for orthoterphenyl, and 83 kcal/mole for metaterphenyl.

Probable mechanisms are discussed on the basis of reaction-product analyses. Calculations of entropies of activation (at 800°F) suggest formation of a high-entropy complex that subsequently reacts or decomposes to give the products observed.

The radiolysis experiments were conducted by surrounding the autoclave with spent reactor fuel elements. Low-temperature (below 500°F) experiments, where pyrolysis is not significant, indicate that radiolysis depends on temperature—but there were insufficient data to determine this effect quantitatively. In a 775°F radiolysis experiment, exposure to 2.5 Mr/hr for 840 hr (2.1×10^9 r total dose) decomposed approximately twice as much organic as did pyrolysis alone in a control sample. Analysis of the radiolytic decomposition products suggests that the reaction mechanisms change as temperature increases. Gases produced by gamma irradiation in the absence of air include acetylene, ethylene, propylene, and propane. The observations that radiolysis rate and reaction mechanisms depend on temperature agree with work summarized earlier.[3]

The dose-rate effect on the radiolysis of paraterphenyl was investigated by exposing samples at approximately 660°F to electrons from a Van de Graaff generator.[4] Values of $G_{polymer}$, defined as the number of molecules of paraterphenyl converted to less-volatile material per 100 ev absorbed, were 0.17 to 0.26; G_{gas} values, defined analogously for conversion to gaseous products, were 0.017 to 0.037. Dose rates between 0.24 and 10 watts/g did not affect either $G_{polymer}$ or G_{gas}.

Reactor irradiations of Santowax OMP at 600°F in a loop in the MIT reactor have been reported.[5] After initial buildup of high boilers, unirradiated organic was added to maintain

Digitized by Google

their content at approximately 33 wt.%. Total irradiation time was approximately seven months (equivalent energy dose to the coolant was not reported); specimens were taken throughout this time. Coolant viscosity, density, and average molecular weight remained essentially constant because of the coolant replacement. The Santowax OMP degraded to higher boiler at the rate of 0.15 molecule per 100 ev absorbed.

Seventeen organic compounds, including 12 condensed-ring polyaromatics, biphenyl, orthoterphenyl, metaterphenyl, and paraterphenyl, and bibenzyl, were studied in pyrolytic and radiolytic experiments.[6] The objectives were to determine their general decomposition behavior and parameters that correlate with it. All experiments were performed in vacuum and in the range 375 to 840°F. A ^{60}Co gamma facility and the Brookhaven Graphite Research Reactor (BGRR) were used for the irradiations. Gamma-irradiated samples were exposed to 7×10^8 rads over 7 days; reactor-irradiated samples were exposed to 2.1×10^9 rads over 19 days.

Gas production increases with temperature in gamma radiolysis and in pyrolysis (no provision was made for measuring gas from the BGRR samples). For many compounds, pyrolysis and gamma radiolysis produced markedly different concentrations of hydrogen and methane. In general, the most common gases produced were ethylene and propane, with less consistent or smaller amounts of ethane, acetylene, and about eight other gases.

The decomposition rate usually increases with temperature, and the amount of decomposition in the radiolytic experiment always exceeded that from the control samples, in which only pyrolysis occurred. Data for decomposition rate as a function of temperature reveal the same general relation for all compounds—there is a temperature "breakpoint," below which the increase in decomposition rate with temperature is not very substantial and above which the increase becomes very marked. For a given compound this apparent breakpoint occurs at about the same temperature during radiolysis as in pyrolysis, but it occurred at lower temperatures for the reactor-radiolyzed samples than for the gamma-radiolyzed samples. This difference is attributed to the threefold difference in irradiation times.

Experiments showed that, in general, aromatic carbon–carbon bonds are more stable against both radiolysis and pyrolysis than are aliphatic carbon–carbon bonds. The control pyrolysis experiments show that pyrolytic decomposition rate increases with time, that is, pyrolysis products form increasingly quickly as pyrolysis products build up. Thus the investigators concluded that the results of short-term pyrolysis studies cannot be extrapolated meaningfully to long exposures. On the basis of breakpoint observations, they recommend that the maximum operating temperature for these organic materials be in the neighborhood of 750°F to avoid extensive decomposition.

Several attempts were made to obtain a correlation between radiolytic stability and other compound parameters. Two of these parameters, singlet–triplet excitation energy and electron affinity, were reported to indicate some reasonable degree of correlation with radiolytic decomposition rate.

Six-Mev electrons have been used[7] to irradiate biphenyl, the three terphenyl isomers, and Santowax OMP at approximately 600°F to decompositions of approximately 40%. Five specific conclusions are reported: (1) second-order kinetics best describe the radiolysis reaction; (2) paraterphenyl is more stable than metaterphenyl, which is more stable than orthoterphenyl; (3) rate constants increase for successive steps in biphenyl radiolysis reactions; (4) concentration of molecular-weight multiples of the starting material (biphenyl or terphenyl) rises rapidly in the radiolysis-product fraction; and (5) there is a linear relation between total dose and molecular weight (up to $\sim 1.5 \times 10^{10}$ rads). Nuclear magnetic-resonance measurements were interpreted to suggest that part of the hydrogen generated during radiolysis might react with the polymeric products.

Additives

Irradiations with 6-Mev electrons were performed to determine the effects of selected additives on the radiolytic stability of terphenyl.[7] Total dose was 0.5 to 1.0×10^{10} rads at approximately 650°F. Additives that contribute substantial stability against electron radiolysis can be broadly described in three general groups: (1) elemental sulfur and compounds containing divalent or tetravalent sulfur; (2) fused-ring

Digitized by Google

compounds structurally related to anthracene, in which either none of the rings, the end rings only, or the center ring only is hydrogenated and in which 9 and 10 positions of the center ring are occupied by sulfur, nitrogen, and carbon (or, in a few cases, oxygen) atoms; and (3) hydrogenated or partially hydrogenated fused-ring compounds not necessarily related to anthracene. They reduce electron radiolysis by approximately 10 to 25% when added to terphenyls in concentrations of 3 mole % or less. Compounds of the second group depend only slightly on concentration, but those of the first and third groups depend greatly on concentration — elemental sulfur is most effective at 0.7 mole %. Effectiveness of none of the better additives appears to depend much on temperature.

Electron and reactor irradiations have been used to measure how various additives affect the decomposition of biphenyl, Santowax R, and paraterphenyl.[8] The addition of small (10 to 20%) portions of paraquaterphenyl to biphenyl slows the decrease in biphenyl degradation by electrons slightly (≤20%) but does not significantly affect the reactor-irradiation results. In reactor irradiation of paraterphenyl, gas and high-boiler formation was slowed 10 to 20% by the addition of approximately 0.5% of any of various additives, including ferrocene, phthalocyanine, iron, copper, and cobalt phthalocyanines.

Coolant Reclamation

Catalytic hydrocracking has been studied as a means to reclaim used organic coolant.[9–11] In catalyst-screening experiments, cobalt molybdate, nickel oxide, platinum, and cobalt oxide plus vanadia (all on low-surface alumina, 50 to 80 m^2/g) proved to be efficient catalysts for terphenyls at 600 to 900°F and 500 to 1000 psig. Catalytic efficiency increased with phenyl chain length; nickel oxide on alumina was the most selective to chain length. Further experiments were performed with the cobalt molybdate and nickel oxide using coolant from core 2 of the Organic Moderated Reactor Experiment (OMRE) and several other synthetic terphenyl mixtures. Continuous-flow hydrocracking of OMRE core 2 coolant (23% high boilers) at 900°F and 1000 psig removed 90 to 100% of the high boilers and recovered 85 to 95 wt.%. of the feed as usable product (some material was lost as light ends and some deposited on the catalyst). The average molecular weight of the product was 205 to 225, compared to 270 for uncracked core 2 coolant.

Radiolytic stability of the cracking products was investigated by use of a linear accelerator for irradiations of 0.48 to 1.3×10^{10} rads at 650°F. The selectively hydrocracked material was slightly more stable than Santowax OMP. Although the hydrocracked material released up to four times as much gas as did Santowax OMP, the gas amounted to only approximately 0.3 wt.% of the sample, and total radiolytic decomposition was significantly less for the hydrocracked material. Pyrolytic stability of the reclaimed coolant also was studied in 48-hr experiments. No thermal high boiler was measured up to 650°F; results are interpreted to suggest a "threshold" for pyrolysis at 750 to 825°F.

Cost estimates were performed for a 1000-Mw [300 Mw(e)] organic-moderated and -cooled reactor that produces high boilers at either 25,000 or 50,000 lb/day. On the basis of equipment amortization within seven years, total cost for manufacturing hydrocracked usable coolant would be $0.083/lb (later revised to $0.07/lb) for the 25,000 lb/day case and $0.053/lb for the 50,000 lb/day case, compared to fresh terphenyl coolant costing $0.17/lb. Advantages of the hydrocracking reclamation process would be (1) reductions in coolant-makeup and waste-disposal requirements and (2) removal of film-forming material that would foul the fuel elements; these improvements would reduce overall operating costs. A disadvantage would be the possible net buildup in the coolant of biphenyl, whose high vapor pressure might cause reactor operating difficulties.

Economics estimates have been performed for catalytic hydrocracking processes to reclaim damaged coolants from the 11.4-Mw(e) Piqua Nuclear Power Facility.[12] Three hydrocracker feed schemes were considered: feed supplied from the bottoms of a flash tank, from the bottoms of the presently installed distilling column, and directly from the main coolant stream. Selective hydrocracking of either concentrated high boilers or total coolant would be efficient and economical, but flash-tank feed is recommended as the most economical. The plant for the flash-tank-fed hydrocracker recommended for Piqua would cost $300,000. It could maintain high-boiler concentration in the coolant below 10% and ash concentration at 0.3

Digitized by Google

ppm. Without interest or taxes, payout time would be approximately 4.6 years, with a subsequent power-cost saving of 1.08 mills/kw-hr before taxes (0.52 mill/kw-hr after taxes), assuming full-power reactor operation 60% of the time.

Also studied briefly were the economics of a flash-tank-fed hydrocracker for a 500-Mw(e) organic-cooled D_2O-moderated reactor that operates at full power 60% of the time. If a hydrocracker is used instead of a distillation system to maintain coolant quality, the estimated saving is $205,400/year, and the payout time is 1.0 year if there are no taxes on the saving (or 1.9 years with taxes) and if the unit is amortized over 7.5 years.

The study also evaluated whether hydrogen could be recovered from radiolytic gases to reduce hydrocracker operating costs. Although technically feasible, such a process would be economically advantageous only with plants larger than Piqua.

Film Formation

Pyrolytic capsules were used for fouling tests performed to evaluate the film-forming tendencies of OMRE core 2 coolant.[13-14] These tests consisted essentially of maintaining coolant samples at 600°F for 24 hr under a nitrogen blanket while a stainless-steel tube held at 1050°F was immersed in the coolant, after which the amount of film deposited on the tube was measured. Results indicated that some coking did take place on the heaters and that ^{60}Co and ^{54}Mn concentrated on the heater surface to approximately 500 times their concentration in the coolant. Preliminary screening of adsorbents that might be useful in removing ^{35}S and ^{32}P from organic coolants indicated that metals and reduced oxides might be useful, and, in particular, a reduced nickel oxide hydrogenation catalyst showed good removal efficiencies for the concentrations used.

Engineering-scale equipment and static capsules were used for fouling studies and iron and water solubility studies.[6] In the static-capsule fouling tests, no fouling-film deposits nor detectable traces of alpha iron were found on the type 304 stainless-steel heater test specimens exposed to individual terphenyl isomers at 500 to 800°F. No correlation was apparent between the test conditions and the presence or absence of small amounts of alpha iron. Terphenyl generally absorbed or reacted with 1 vol.% oxygen placed in the cover gas. In the iron and water solubility studies, purified orthoterphenyl and paraterphenyl were covered with argon containing up to 6.5 vol.% water. No iron was found in the coolant. Water added to the coolant to a maximum concentration of 68 ppm did not noticeably affect iron solubility. Although water was slightly soluble in orthoterphenyl, no water was found in paraterphenyl.

Mechanisms of fouling-film formation were studied by testing Santowax OMP and coolant fluid from core 2 of the OMRE in pyrolytic capsules or in a circulating loop in which the organic was irradiated with 6-Mev electrons.[7] Also studied were the effects of temperature, flow, pressure, cover gas, and various preventive additives.

In regard to mechanisms, the study indicated that film formation on hot surfaces comes from (1) mass transfer of iron from the container and pipes and (2) deposition of a composite material that forms when high-molecular-weight polymers adhere to either soluble or insoluble iron in the coolant — and that "to a limited degree, certain higher molecular weight high boilers were more effective in fouling."

The pyrolytic capsule tests showed that film formation increases exponentially with surface temperature, but bulk temperature is also important and is greatly speeded by temperature "spikes" of less than 1-min duration.

In the electron-irradiation loop, film formation was (1) not affected greatly by blanket-gas pressures over the range 400 to 700 psig, (2) inversely proportional to coolant velocity, (3) enhanced by surface roughness or projections into the coolant stream, and (4) affected by the radiation intensity. When the blanket over the fluid was hydrogen, rather than nitrogen, the film was heavier and had greater thermal conductivity.

Corrosion Properties

Out-of-pile tests in a tilting-furnace apparatus were used to test the corrosion properties of type 304 stainless steel, A-285C mild steel, 1100 aluminum, Al-288, and SAP M-257 in 500 to 800°F paraterphenyl and 500 to 710°F orthoterphenyl.[6] On the basis of rather sketchy data, it was concluded that these materials are highly resistant to corrosive and mass-transfer attack by the terphenyls.

Digitized by Google

The combined effects of exposure to both an organic moderator–coolant and reactor radiation were measured on specimens of various materials that had been placed in the core of the OMRE for 26 months.[15] Specimens included SAE 1020 carbon steel, SAE 4130 low-alloy steel, types 410 and 304 stainless steels, aluminum, and magnesium. High-boiling-point impurities in the organic were allowed to rise to nearly 30%, at which level they were held during most of the last half of the exposure. The SAE 1020 and 4130 steels corroded at the rate of approximately 0.0001 in./year. Aluminum and types 410 and 304 stainless steels were quite resistant to corrosion. Magnesium was the only metal that corroded appreciably; these measurements seemed to confirm that magnesium, whether anodized or not, is unsuitable for organic-reactor service. It was concluded that measurements of corrosion rates in an out-of-pile laboratory can predict in-pile corrosion rates with sufficient accuracy for design purposes.

Corrosion of iron by terphenyl was investigated with a variety of organic mixtures and reagent-quality iron wire.[7] Clean terphenyl, either irradiated (by 6-Mev electrons) or unirradiated, does not corrode iron, but it becomes corrosive upon oxidation by air. Two commercial automotive motor-oil detergents were tested for preventive effects, but first indications were unfavorable.

Autoclave and loop tests have been used to determine the corrosion rates of structural materials exposed to commercially available terphenyls (Santowax mixtures); potential corrosion inhibitors also were evaluated.[16] Santowax R was used in agitated autoclave tests, and Santowax OMP was used in the loop tests. Corrosion rates usually decrease with exposure and depend on fluid velocity and temperature. Although the corrosion rates of the various alloys seem relatively insensitive to water additions, water did seem to promote a more adherent oxide scale in the autoclave tests.

Steel corrosion rates were insensitive to water content up to 2000 ppm, which contrasts to the OMRE experience in which particulate-formation rates depended directly on water or air contamination. Corrosion rates that can be expected for carbon or SAE 4130 steels as a function of organic bulk temperature are reported as 0.05 to 0.06 mg/(cm^2)(month) at 600°F, 0.10 mg/(cm^2)(month) at 650°F, and 0.20 to 0.25 mg/(cm^2)(month) at 750°F. Of the three steels tested, annealed, or sensitized, type 304 stainless steel is the most corrosion resistant (it shows negligible corrosion in both the autoclaves and the loop), and carbon steel is less resistant than ferritic type 410 stainless steel. Limited tests with type 406 stainless steel (13% chromium–4% aluminum) indicate a corrosion rate as low as that for type 304 stainless steel. One advantage of type 406 stainless steel is that it absorbs approximately 25% fewer thermal neutrons than type 304.

Aluminum and specimens made from sintered aluminum powder (called SAP or APM) were almost inert to terphenyls with normal water content. Type 1100 aluminum oxidized only when water content exceeded 1000 ppm. Although the tests indicated that magnesium and its alloys might be attractive as water-removal agents, they are unsuitable for use in organic reactors because they are readily corroded by organic coolants.

Protective coatings were evaluated in autoclave tests. None of a wide variety of coatings on zirconium alloys was able to prevent hydriding of the zirconium. Copper and brass corrodes faster than carbon steel, but beryllium appears to be quite inert. Although niobium apparently corrodes more than carbon steel, it might be an effective diffusion barrier between aluminum cladding and metallic-uranium fuel.

Contaminants. The results of these tests and other considerations show that, in general, the presence of water, hydrogen, air (oxygen), or sulfur in terphenyl enhances corrosion and film formation. Although the effects of minor air contamination were negligible in the laboratory experiments, experience at the OMRE indicates that air contamination of irradiated coolant tends to increase fouling. The fouling tendency of coolants can be reduced if (1) the water or oxygen content is minimized, (2) the access of air and water to the coolant system is strictly controlled, and (3) larger and more effective particulate-removal systems are used.

Sampling. For these experiments the workers developed a significantly improved technique for sampling Santowax to determine its water content. The difficulty had been caused by the ability of water to flash off from the Santowax at 750°F when the pressure was reduced. A

Digitized by Google

sampler that simulated a flow sample from the autoclave was developed to avoid this problem.

Heat-Transfer Properties

Forced-circulation heat transfer in organic systems has been studied extensively.[17] Boiling heat transfer with forced-circulation Santowax R and isopropyl diphenyl has been measured in an out-of-pile test loop having an electrically heated vertical test section;[18] Table IX-1 shows

Table IX-1 CONDITIONS IN BOILING HEAT-TRANSFER EXPERIMENTS[18]

Conditions	Isopropyl diphenyl	Santowax R
Heat flux, Btu/(hr)(sq ft)	40,000–100,000	27,000–110,000
Mass velocity, lb/(sec)(sq ft)	325–630	280–750
System pressure, psia	21–33	15–28
Flow direction	Up only	Up and down
Subcooling, °F	0–17	0–57

the range of variables investigated. Data for Santowax R heat transfer correlated best with Levy's equation;[19] Rohsenow[20] and Forster–Greif[21] equations were less successful. The correlation was insensitive to flow direction. Data for isopropyl diphenyl correlated within 10% using Levy's equation; the Rohsenow and Forster–Greif relations were not tried because of uncertainty concerning the surface tension of isopropyl diphenyl.

Void fraction was measured in the Santowax R experiments by an X-ray transmission technique. With greater than 8°F subcooling, these data were correlated using a modified form of Maurer's equation.[22] An expression was developed and used with moderate success to correlate void-fraction data near equilibrium bulk boiling. For equilibrium boiling the experimental results were consistent with predictions from a modified Martinelli model.[23]

Possible New Coolants

Attempts have been made to find an inexpensive organic coolant with properties similar to the terphenyls.[7,24] A large group of high-boiling distillates from the petroleum industry which were studied included recycled oils from some catalytic-cracking operations, highly aromatic fractions used as feed for producing carbon black in furnaces, and coal-tar distillates. Irradiation with 6-Mev electrons usually liberated more gas from these oils than from Santowax OMP. Radiation resistance of these oils ranged from somewhat lower to somewhat greater than Santowax OMP. In general, their thermal stabilities were unsatisfactory above 650°F.

When these petroleum-base stocks had been hydrodealkylated and the coal-tar stocks hydrodesulfurized, they had pyrolytic thresholds approximately 50°F less than terphenyl. Radiolysis of coolants prepared in this manner formed polymer only 50 to 75% as fast as did terphenyl but liberated gases several times faster than terphenyl. Viscosities, vapor pressures, densities, and hydrogen densities were very similar to terphenyl. The film-forming tendency of these materials has not been tested, but no coking was observed up to 750°F. Although estimates based on these data indicate that these coolants could be produced cheaply enough that inventory and makeup costs would be somewhat less than for terphenyl in a conventional steam plant where bulk temperatures do not exceed 700°F, these experiments did not include in-pile or neutron irradiations. Thus the results are only indicative.

Acknowledgments

The author gratefully acknowledges the assistance of reviewers at Atomics International for their help with, and further organization of, this article.

References

1. R. F. Makens (Ed.), Organic Coolant Summary Report, USAEC Report IDO-11401, Idaho Operations Office, December 1964.
2. D. G. Kuper, Organic Coolant Degradation Studies, USAEC Report IDO-16851, Phillips Petroleum Company, Mar. 25, 1963.
3. *Power Reactor Technol.*, 6(3): 71 (June 1963).
4. A. W. Boyd, The Radiation and Thermal Stability of Some Potential Organic Moderator-Coolants, Part VII. The Effect of Radiation Intensity on the Decomposition of Paraterphenyl by Fast Electrons, British Report AERE-R-4048, August 1963.
5. E. A. Mason and C. D. Sawyer, Irradiation Loop Studies of Organic Reactor Coolants, Progress Report, January 1–September 30, 1962, USAEC Report MITNE-29(IDO-11106), Massachusetts Institute of Technology, Feb. 15, 1963.
6. H. Susskind et al., Organic Reactor Coolant Studies, USAEC Report BNL-7650, Brookhaven National Laboratory, June 30, 1963.
7. J. C. Hillyer, Organic Coolant Research Summary

Digitized by Google

Report, July 1, 1960–March 31, 1963, USAEC Report IDO-16911, Phillips Petroleum Company, Oct. 1, 1963.
8. W. G. Burns, C. R. V. Reed, and J. A. Winter, The Radiation and Thermal Stability of Some Potential Organic Moderator-Coolants. Part VIII. Pile and Electron Irradiation of Various Polyphenyl Mixtures and Work with Additives, British Report AERE-R-4072, November 1963.
9. L. E. Gardner, Reclamation of Damaged Nuclear Reactor Coolant by Catalytic Hydrocracking, USAEC Report IDO-16853, Phillips Petroleum Company, Mar. 29, 1963.
10. L. E. Gardner, Evaluation of Catalysts for Selective Hydrocracking of Polyphenyls, USAEC Report IDO-16858, Phillips Petroleum Company, Apr. 25, 1963.
11. L. E. Gardner, Catalytic Hydrocracking of High Boiler in Nuclear Reactor Coolant, USAEC Report IDO-16877, Phillips Petroleum Company, May 20, 1963.
12. J. L. Griffith and G. J. Russell, Economics of Hydrocracking Damaged Coolant from Organic Reactors, USAEC Report IDO-11400, Idaho Operations Office, November 1963.
13. J. F. Black, M. E. Conn, and P. R. Geissler, First Semi-Annual Progress Report on Organic Coolant Technology During May Through October 1962, USAEC Report IDO-11221, Esso Research and Engineering Company, Dec. 14, 1962.
14. P. R. Benson, Development of the Pyrolytic Fouling Test for Organic Reactor Coolants, USAEC Report NAA-SR-7362, Atomics International, Nov. 30, 1962.
15. R. S. Neymark, Performance of Structural Materials Exposed to the Coolant in the OMRE, USAEC Report NAA-SR-9796, Atomics International, Aug. 1, 1964.
16. R. S. Neymark, Corrosion of Structural Materials in Impure Santowax, USAEC Report NAA-SR-7755, Atomics International, May 15, 1963.
17. Atomics International, Organic Reactor Heat Transfer Manual, USAEC Report NAA-SR-Memo-7343, Dec. 1, 1962.
18. F. Bergonzoli and F. J. Halfen, Heat Transfer and Void Formation During Forced Circulation Boiling of Organic Coolants, USAEC Report NAA-SR-8906, Atomics International, June 15, 1964.
19. S. Levy, Generalized Correlation of Boiling Heat Transfer, ASME Paper 58-HT-8, *J. Heat Transfer*, 81: 37-42 (1959).
20. W. M. Rohsenow, A Method of Correlating Heat Transfer Data for Surface Boiling Liquids, *Trans. Am. Soc. Mech. Engrs.*, 74: 969-976 (1952).
21. H. K. Forster and R. Greif, Heat Transfer to a Boiling Liquid: Mechanism and Correlations, ASME Paper 58-HT-11, *J. Heat Transfer*, 81: 43-53 (1959).
22. G. W. Maurer, A Method of Predicting Steady-State Boiling Vapor Fraction in Reactor Coolant Channels, in Bettis Technical Review—Reactor Technology, USAEC Report WAPD-BT-19, Westinghouse Electric Corp., Bettis Atomic Power Laboratory, June 1960.
23. R. W. Lockhart and R. C. Martinelli, Proposed Correlation of Data for Isothermal Two-Phase, Two-Component Flow in Pipes, *Chem. Eng. Progr.*, 45(1): 39-48 (January 1949).
24. L. E. Gardner, W. M. Hutchinson, and J. C. Hillyer, Low Cost Organic Moderator-Coolants for Nuclear Reactors, USAEC Report IDO-16907, Phillips Petroleum Company, Dec. 23, 1963.

Digitized by Google

Index

Power Reactor Technology

Volume 8

Note: The page range for each of the four issues of Vol. 8 is as follows: No. 1, pages 1 to 108; No. 2, pages 109 to 156; No. 3, pages 157 to 198; and No. 4, pages 199 to 296.

A

Accidents
  frequency, 221-22
  loss-of-coolant, 240-41
Aerosols
  formation in NaK systems, 260
  traps for, 259-70
Air
  effects on corrosion by polyphenyls, 294
  reactivity effects, 109
Air-water systems
  flow, techniques for observing, 165
Aluminum
  corrosion by polyphenyls, 293-94
Aluminum alloys
    (see also SAP)
Aluminum alloys (Al-Pu)
  criticality, 210, 212
Aluminum oxide systems (Al_2O_3-UO_2)
  radiation effects, 8
Analog computers
  use for reactor control, 227
Annuli
  heat transfer in, 121-22
Argonne National Laboratory
  liquid-metal magnetohydrodynamic research, 207-8
ARGOSY code
  for graphite-moderated reactor core design, 160-61
ARGUS code
  thermal conductivity calculations, 118
Atomics International
  liquid-metal magnetohydrodynamic system research, 207

B

Bellows
  failures in Hallam Power Reactor, 282-83
Beryllium
  corrosion by polyphenyls, 294
Beryllium-9
  integral cross section, 115
Beryllium oxide systems (BeO-UO_2)
  radiation effects, 8
Beryllium oxide systems (BeO-UO_2) (Hastelloy-X-clad)
  fuel elements, evaluation, 173
Bibliographies
  two-phase flow, 164
Biphenyl
  heat transfer properties, 295
  pyrolysis, 290
  radiolysis, 290-92
Boiling, 14-17
  bubble growth and control, 256
  burnout in Freon, 166
  burnout in Na, 164
  burnout in steam-water systems, 166-70
  heat transfer, 235
  heat transfer from K, 163-64
  phase velocity in two-phase flow, 235
  stability in two-phase flow, 228
  subcooled, burnout heat flux in, 122-23
Boiling (film)
  heat transfer coefficients, 231
  theoretical studies, 232
Boiling (nucleate)
  bubble phenomena, 232
  convection effects, 235
  effects on frictional pressure drop, 253
  heat flux effects on, 229
  heat transfer in brines, 238
  liquid metal instability, 231
Boiling (pool)
  effects of heat flux, 229-30
  heat transfer, 253
Boric acid
  use as chemical shim, 272
  use as soluble poison, 214
  use of solution for reactor shutdown, 225
Boron
  use as soluble poison, 10-12
Brass
  corrosion by polyphenyls, 294
Breeding blankets
  design for large fast breeder reactors, 147-52
Brines
  deposit formation in boiling, 238
Brookhaven National Laboratory
  liquid-metal magnetohydrodynamic system research, 208
Bubbles
  effects on heat transfer, 253
  effects on thermal stresses, 255
  formation and control in boiling, 256
  formation rate during boiling, 235
  phenomena in nucleate boiling, 232
  in turbulent flow, 234-35
Buckling
  experiments, 109-10
  fuel elements, UC, 111
  materials, in light-water reactors, 214-15
Burnable poisons
    (see Poisons)
Burnout, 14-17
  in boiling Na, 164
  in fog-cooled reactors, 228-29
  in Freon, 166
  safety margin computation, 227
  in steam-water systems, 166-70
  in water, 121-23
Burnup
  fuel elements, Magnox-clad, 62
  measurements, 216-17

C

Cadmium sulfates
  solution, use as poison, 214
Calcium sulfates
  deposits in boiling solutions, 238
Catalytic hydrocracking
  reclaiming of organic coolants, 292
Ceramics
    (see Fuel elements (ceramic))
Cermets
    (see Fuel elements (cermet))
Cesium (liquid)
  thermal, thermodynamic, and flow properties, 164
Channels
  burnout of water in vertical, 121
  fluid flow stability in heated, 231
Chloride ions
  corrosive effects on stainless steels, 254
Coatings
  corrosion by polyphenyls, 294
Cold traps
  for oxides in Hallam Power Reactor, 285
Components
  reliability, 221
Computer codes
  ARGOSY, 160-1
  ARGUS, 118
  GAM-I, 210, 212
  HEAT-1, 118
  HFN, 212
  HRG, 212
  MARC-2B, 215
  MOCA-2, 215
  REX, 210
  ROB, 118
  SOFOCATE, 210
  STOKE, for heavy water reactor simula-

Digitized by Google

tion, 35
TEMPEST, 212
THERMOS, 212, 215
TYCHE, 113
Computers
use for reactor control, 226-27
Condensation
dropwise, of ethylene glycol, 233
dropwise, of water, 233
of laminar films, 232
of liquid metals, 232-33
vapor traps utilizing, 259-60
Conductivity
(see Thermal conductivity)
Control, 221-27
calibration for EBR-I, with Pu core, 158
calibration for SRE, second core, 157
computer use for, 226-27
critical assemblies using moderator level, 223-24
gas-cooled reactors, 68-69
poisons, 10-12, 214, 217, 225-26
Control rods
drive mechanisms for EBR-II, 133-34
gravity independent, 223
operation in Hallam Power Reactor, 282
radiation effects, 271
reliability, 221-22
thimble failure in Hallam Power Reactor, 283-84
Control systems, 272-75
ASTR, 223
development, 18
Elk River Power Reactor, 271-72
Hallam Power Reactor, 280, 282
Indian Point Power Reactor, 271
large pressurized-water reactors, 144-46
Yankee Power Reactor, 271-72
Convection (forced)
in boiling K, 163-64
burnout heat flux in subcooled boiling water, 122
effects in boiling, 235
fluid flow stability, 231-32
two-phase flow, 228
Convection (free)
burnout of water in vertical channel, 121
coolant loop transient behavior, 122
effects on film condensation, 232
heat transfer coefficients for ice-water systems, 239-40
heat transfer at cryogenic temperatures, 239
heat transfer to finned tubes, 236-37
liquid metal boiling in, 231
Coolant loops
fluid flow stability, 122
transient behavior under free convection, 122
Coolants
(see also Potassium alloys (K-Na) (liquid))
contamination in Dounreay Fast Reactor, 75
flow oscillations in Elk River Power Reactor, 273
loss accidents, 240-41
Na, 75-96
Coolants (organic)
corrosive effects, 293-94
film formation by, 293-94
heat transfer properties, 123-24, 295
pyrolysis, 290-91
radiolysis, 290-94
reactivity effects of Dowtherm A, 109
reclamation, 292-93
Cooling systems
Hallam Power Reactor, 282
Copper
corrosion by polyphenyls, 294
Cores
radiation effects on lifetime, 216
Cores (graphite moderated)
physics calculations, 160-61
Corrosion
by nitrogen, 173-74
by organic coolants, 44-45, 293-94
in Agesta Reactor, 275
of ceramic fuel elements (Zircaloy-2-clad), 177-82
of Hastelloys, 23, 173-74
of Incoloy-X, 23
of Nb alloys, 42-45
of stainless steels, 254-55, 293-94
of steels, 9-10, 293-94
of Yankee Power Reactor control rods, 271-72
Corrosion products
deposition in reactors, 252, 256
Cracks
propagation in boiling water reactor fuel elements, 254
Critical assemblies
control by moderator level, 223-24
perturbations in graphite-moderated, 115
Critical assemblies (Anna)
design, 111-12
Critical assemblies (Helena)
design, 111
Critical assemblies (OCF)
pulsed neutrons in, 112
Critical assemblies (ROSPO)
design, 112
Critical assemblies (Scorpio I)
criticality measurements in, 212
Critical assemblies (Scorpio II)
criticality measurements in, 212
Critical assemblies (TCA)
pulsed neutrons in, 112
Critical experiments, 109-13, 210-14
Critical facilities (Alize-II)
use of soluble poisons in, 214
Cross sections, 114-15
absorption, thermal neutrons in graphite, 114-15
calculations, 210, 212
fission, of ^{241}Pu, 115
fission spectrum, of ^{235}U, 115
integral, of ^{9}Be, 115
neutron capture, of Pu isotopes, 211
Crud
analysis from VBWR, 254, 256
Cryogenics
heat transfer, 232-33

D

Decontamination
sodium reactor coolants, 75-77
Delayed neutrons
calculations, 161-62
Departure from nucleate boiling
effects of nonuniform heat flux on, 229
Desalination
deposits during boiling and heat transfer through films, 238
Diffusion length
thermal neutrons in graphite, 114-15
Digital computers
use for reactor control, 226
Diphenyl
(see Biphenyl)
Direct power conversion
plants, 105-6
"Dowtherm A" coolant
reactivity effects, 109

E

Economics
of catalytic hydrocrackers for organic coolant reclamation, 292-93
fast breeder reactors, 85
radiation effects on core lifetime, 216
sodium graphite reactors, 185
Electrical circuits
SPERT-3, failure, 272-73
Electrons
radiation effects on polyphenyls, 291-92
Electrostatic precipitations
use with NaK vapors, 260
Energy conversion (direct)
plants, 105-6
Ethylene glycol
condensation, dropwise, 233
Excursions, 221-22
Exponential experiments, 109-13, 211-14

F

Fission parameters
calculations, 161-62
Fission products
contamination at Dounreay Fast Reactor coolant, 75
gases, monitor for, 263
Fluid flow, 14-17, 118-25, 163-71, 228-44
effects on boiling, 253
large pressurized water reactors, 142-44
oscillations in Elk River Power Reactor, 273
Fluid flow (annular)
transition to two-phase, 234
Fluid flow (froth)
occurrence and characterization, 123
Fluid flow (turbulent)
bubble studies, 234-35
heat transfer in annuli, 122
Flowsheets
Halden Reactor, 50
soluble poison control systems, 11
Forced convection
(see Convection (forced))
Free convection
(see Convection (free))
Freeze traps
for Na in Hallam Power Reactor, 285
Freon systems
boiling burnout in, 166
Froth flow
(see Fluid flow (froth))
Fuel assemblies
design for large pressurized-water reactors, 139-41
Fuel cycles
evaluation for large fast breeder reactors, 154-55
Fuel elements
Agesta Reactor, 51-52
burnout of rods, 167
criticality of pins, 210
design, 3, 6-9
design for AGR Reactor, 62
design for Anna Critical Assembly, 112
design for BONUS Reactor, 27
design for NORA Reactor, 112
design for RB Reactor, 112
development for fast breeder reactors, 86-91
development of SAP, 37, 39
fabrication, 126-31
failures in boiling water reactors, 254-56

Digitized by Google

failure due to internal pressure, 252
failure in VBWR, 252-54, 256
Marviken Reactor, 51-52
radiation effects, 7-8, 62, 82, 255-56
thermal conductivity, 118-21, 129
Fuel elements (Al-Pu)
criticality in graphite lattices, 212
Fuel elements ($BeO-UO_2$)(Hastelloy-X-clad)
evaluation, 173
Fuel elements (ceramic)
design, 3, 6-9, 147-52
evaluation, 172-74
Fuel elements (ceramic)(Zircaloy-2-clad)
fretting corrosion, 177-82
Fuel element (cermet)
development, 89, 126-28
fabrication, 129
thermal conductivity, 129
Fuel elements (enriched U)
criticality in D_2O lattices, 213
Fuel elements (Incoloy-800-clad)
evaluation for superheating reactors, 174-75
Fuel elements (Magnox-clad)
burnup, 62
design, 63-66
radiation effects, 62
Fuel elements ($Mo-UO_2$ cermet)
fabrication and thermal conductivity, 129
Fuel elements ($Mo-W-UO_2$ cermet)
development, 128
Fuel elements ($Nb-ThO_2-UO_2$ cermet)
thermal conductivity, 129
Fuel elements (Pu)
criticality in graphite lattices, 212
Fuel elements (Pu-U)
criticality in graphite lattices, 212-13
Fuel elements (PuC-UC)
design for large fast breeder reactors, 147-49, 151-52
Fuel elements (PuO_2-UO_2)
criticality in water, 212
design for large fast breeder reactors, 149-52
specifications, 129
Fuel elements (PuO_2-UO_2)(Zircaloy-2-clad)
fretting corrosion, 177-82
Fuel elements (PuO_2-UO_2)(Zr-clad)
criticality, 210
fretting corrosion, 177-82
Fuel elements (stainless steel-clad)
design, 3, 6-9
Fuel elements (stainless steel-UO_2 cermet)
development, 126-27
Fuel elements (Th-U)
development for fast breeder reactors, 89
Fuel elements (Th-U-Zr)(Zircaloy-2-clad)
fabrication, 130
Fuel elements (ThO_2-UO_2)
design, 3, 6-9
Fuel elements ($W-UO_2$ cermet)
development, 127-28
Fuel elements (U)
criticality in graphite lattices, 212-13
Fuel elements (UC)
buckling studies, 111
development for sodium graphite reactors, 81-83
radiation effects, 82
Fuel elements (UC)(stainless steel-clad)
evaluation, 174
fabrication of Na-bonded, 129-30
Fuel elements (UO_2)
design, 3, 6-9
fabrication, 129
thermal conductivity, 119-21
Fuel elements (UO_2)(enriched)
pulsed neutron studies, 112
Fuel elements (UO_2)(stainless steel-clad)
evaluation, 172
fabrication, 128-29
Fuel elements (UO_2)(Zircaloy-2-clad)
evaluation, 172-74
fretting corrosion, 177-82
Fuel elements (Zircaloy-clad)
design, 3, 6-9
evaluation, 18
Fueling machines
Bradwell Reactor, operation, 68
EBR-2, vapor traps for, 262-63
design, 68, 141-42

G

Gadolinium nitrates
use of solutions for reactor shutdown, 226
GAM-I code
criticality and cross section calculations, 210, 212
Gases
entrainment in Hallam Power Reactor, 284
fission product monitoring, 263
thermodynamic properties, 121, 239
Graphite
criticality of Pu alloys in lattices of, 212-13
moderator, pulsed neutron studies in, 112-13
thermal neutron absorption cross section and diffusion length in, 114-15
Gravity
control rod independence from, 223

H

Hastelloy-C alloy
corrosion in superheating reactors, 23
Hastelloy-X alloy
corrosion by N_2, 173-74
HEAT-1 code
thermal conductivity calculations, 118
Heat exchangers
concentric tube, dynamic analysis of, 237
design, 236-37
efficiency, 236
failures in Hallam Power Reactor, 284
finned tube, 236-37
heat transfer coefficients for NaK, 235-36
Heat transfer, 14-17, 118-25, 163-71, 228-44, 253
large pressurized-water reactors, 142-44
organic coolants, 123-24, 295
Heavy water
chemistry of, 39-40
control of oxygen in, 277
criticality studies in lattices of, 213
moderator, pulsed neutron studies in, 113
reactivity effects, 109
reflector, in University of Michigan Reactor, 277, 279
Heavy Water Lattice Project
buckling experiments, 109-10
Helium
thermodynamic properties, 121
HFN code
cross section calculations, 212
Hot traps
for carbon in Hallam Power Reactor, 285
HRG code
cross section calculations, 212
Hydriding
Zr alloys, 9, 246-51
Hydrogen
effects on corrosion by polyphenyls, 294
reactions with Zircaloys, 245-46
thermal conductivity at high temperatures, 239

I

Ice-water systems
free convection melting, heat transfer calculations, 239-40
Impingement
vapor traps utilizing, 260
Incoloy-800 alloy
testing for fuel element cladding, 174-75
Inconel-X alloy
corrosion in superheating reactors, 23
Indium resonance energy
flux age, 113-14
TYCHE code, determination by, 113
Instrumentation
gas-cooled reactors, 68-69
Hallam Power Reactor, 283, 285
large pressurized water reactors, 145-47
level controllers, failure, 272
liquid metal level indicators, 176-77
neutron detectors, 224-25
pressure switches, failure, 272
temperature sensors, failure, 272
Integral cross sections
^9Be, 115
Iron
corrosion by polyphenyls, 294

J

Jet Propulsion Laboratory
liquid-metal magnetohydrodynamic system research, 207

L

Leaks
Hallam Power Reactor, 282
pressure vessels, 3
SPERT-3, 275-76
Yankee Power Reactor, 275-76
Level controllers
SPERT-3, failure, 272
Level indicators
for liquid metals, 176-77
Light water
(see Water)
Liquid metals
(see Metals (liquid))
Lithium (liquid)
thermal, thermodynamic, and flow properties, 163-64
Loss-of-coolant
accident analysis, 240-41

M

Magnesium
corrosion by polyphenyls, 294
Magnesium alloys
corrosion by polyphenyls, 294
Magnesium oxide systems ($MgO-PuO_2$)
radiation effects, 8

Digitized by Google

Magnetohydrodynamic systems, 199-209
Maintenance
  handling of Hallam Power Reactor core components, 283
MARC-2B code
  thermal neutron distribution calculation, 215
Massachusetts Institute of Technology
  liquid-metal magnetohydrodynamic system research, 208
Melt Refining Process
  vapor traps, 266
Mercury
  condensation in Ni surfaces, 232-33
  thermal, thermodynamic, and flow properties, 163-64
Metals (gaseous)
  film condensation, 232-33
Metals (liquid)
  boiling behavior, 231
  level indicators, 176-77
  pumps for, 282
  thermal, thermodynamic, and flow properties, 163-64
  use in magnetohydrodynamic systems, 199-209
  vapor traps for use with, 259-70
Meters
  plugging in Hallam Power Reactor, 283
MHD system
  (see Magnetohydrodynamic systems)
MOCA-2 code
  criticality calculation, 215
Moderators
  criticality control with, 223-24
  element failure in Hallam Power Reactor, 285-87
Molybdenum systems (Mo-W-UO_2 cermets)
  development for fuel elements, 128
Molybdenum systems (Mo-UO_2 cermets)
  fabrication into fuel elements and thermal conductivity, 129
Multiplication factors
  for EBR-I, with Pu core, 158-59

N

NaK
  (see Potassium alloys (K-Na)(liquid))
Natural convection
  (see Convection (free))
Neutrons
  age determination, 113-15
  delayed, 161-62
  detector design, 224-25
  flux measurements, 157-58
  pulsed, 112-13
  scattering, 116
  thermal, 114-15, 215
  thermalization, 115-16
Nimbus Satellite
  thermal design calculations, 240
Niobium
  corrosion by polyphenyls, 294
Niobium alloys (Nb-Zr)
  corrosion, 42-45
  hydriding stress allowance, 9
  use in pressure tubes, 41
Niobium systems (Nb-ThO_2-UO_2 cermets)
  thermal conductivity, 129
Nitrogen
  corrosive effects, 173-74
Noble gases
  thermal conductivity at high temperature, 239
NPY Project, 111-12

O

Organic coolants
  (see Coolants (organic))
Orifices
  operating problems in Hallam Power Reactor, 288
Oxide films
  effects on hydriding of Zr alloys, 246-48
Oxygen
  control of concentration in D_2O, 277
  effects on corrosion by polyphenyls, 294

P

Packed beds
  heat transfer, 237-38
Petroleum distillates
  development for reactor use, 295
Physics, 109-17, 154-55, 157-62, 210-20
Plates
  evaporation rates from hot, 240
  heat transfer from at cryogenic temperatures, 239
Plutonium
  critical experiments, 211-14
  neutron capture cross sections, 211
Plutonium-239
  neutron capture cross sections, 211
Plutonium-240
  neutron capture cross sections, 211
Plutonium-241
  fission cross sections, 115
  neutron capture cross sections, 211
Plutonium alloys
  criticality in D_2O lattices, 213
Plutonium alloys (Al-Pu)
  criticality, 210, 212
Plutonium alloys (Pu-U)
  criticality in lattices, 212-13
Plutonium carbide systems (PuC-UC)
  design of fuel elements for large fast breeder reactors, 147-49, 151-52
  radiation effects, 8
Plutonium carbides (PuC)
  radiation effects, 8
Plutonium nitrates
  criticality of solution, 213-14
Plutonium oxide systems
  critical experiments in water lattices, 210
Plutonium oxide systems (MgO-PuO_2)
  radiation effects, 8
Plutonium oxide systems (PuO_2-UO_2)
  critical experiments in water lattices, 210, 212
  design of fuel elements for large fast breeder reactors, 149-52
  fuel elements, fretting corrosion of Zircaloy-2 cladding, 177-82
  fuel elements, specifications, 129
  radiation effects, 8
Plutonium oxide systems (PuO_2-ZrO_2)
  radiation effects, 8
Plutonium oxides
  criticality in polystyrene, 214
Pneumatic systems
  use in control systems, 223
Poisons, 10-12
  boric acid, 214, 225
  $CdSO_4$ solution use, 214
  $Gd(NO_3)_3$, 226
  use in water-moderated reactors, 217
Polyethylene
  reactivity effects, 109
Polyphenyls, 123-24, 290-95
Polystyrene
  moderating effects on PuO_2, 214
Potassium (liquid)
  thermal, thermodynamic, and flow properties, 163-64
Potassium alloys (K-Na)(liquid)
  aerosol formation in, 260
  heat transfer coefficients, 235-36
  thermal, thermodynamic, and flow properties, 163
Power conversion (direct)
  plants, 105-6
Pressure
  effects on boiling superheat, 253
Pressure drop
  of air in finned-tube heat exchangers, 236-37
  turbulent flow through wire-wrapped, seven-rod fuel assemblies, 123
  two-phase, 166, 233-35
Pressure switches
  Elk River Power Reactor, failure, 272
Pressure tubes
  design, 40-41
  fretting corrosion, 177-82
Pressure vessels, 12-14
  design for large pressurized water reactors, 138-39
  design for Magnox reactors, 66-68
  KRB Reactor, 12-13
  leaks, 3
  SENA Reactor, 12-13
SENN Reactor, 12-13
SEP Reactor, 12
WWER-1 Reactor, 9-10, 12-14
Pressurized water
  burnout calculations, 121-23
Pumps
  development for reactors, 18
  liquid metal, for Hallam Power Reactor, 282
  Hallam Power Reactor, 282
Pyrolysis
  organic coolants, 290-91

R

Rabbit facility
  design and fabrication, 277
Radiation (thermal)
  heat transfer calculations, 238-39
Radiation effects
  biphenyl, 290
  control rods, 271
  core lifetime, 216
  fuel elements, 7-8, 62, 82, 255-56
  hydriding of Zr alloys, 246-48
  polyphenyls, 290-91, 293-94
  reactivity, 217
  SAP, 38
  Zircaloy-2, 38, 41
Radiolysis
  organic coolants, 290-94
Reactivity
  calculations, 217
  changes with irradiation, 216
  effects on, 109-10
  measurements in reactors, 157-59
Reactors
  (see also Critical...)
  corrosion product deposition in, 252
  future development, 17-20
  reactivity, 216-17
  subcriticality measurement during shutdown, 224-25
Reactors (Advanced Gas Cooled)(AGR)
  design, 58
  fuel element design, 62
  operation, 60
Reactors (Advanced Sodium Graphite)
  buckling studies, 111

Digitized by Google

Reactors (Aerospace Shield Test)(ASTR)
control system, 223
Reactors (Agesta)
corrosion in, 275
design, 47-48, 52-53
repair procedures, 276
Reactors (AKB)
design, 36
Reactors (Aquilon-II)
criticality measurements in, 213
Reactors (ARBUS)
design and operation, 103-4
Reactors (AVR)
design, 73-74
Reactors (Bashful-600)
design, 53, 55-56
Reactors (Beloyarsk-1)
design, 28-34
Reactors (Beloyarsk-2)
design, 28-34
Reactors (Big Rock Point Power), 6
design, 4, 7
flow-induced vibrations, failures from, 273
operating experience, 3
pumps, 18
Reactors (BN-350)
design, 94
status, 92
Reactors (Bodega Bay Power)
design, 4
Reactors (Boiling, Experiments-5) (BORAX-5)
design, 23
Reactors (Boiling heavy-water)
design, 55
Reactors (boiling-water), 3-29
corrosion product deposition in, 256
fuel element failure, 254-56
radiation effects on fuel elements, 255
water quality control, 254
Reactors (BONUS)
design, 23, 25, 27
Reactors (BR-3)
design, 5
use of soluble poison control, 10, 12
Reactors (BR-5)
coolant contamination, 75-76
status, 95
Reactors (Berkeley)
design, 58
performance, 60
Reactors (Bradwell)
design, 58
performance, 60
refueling machine operation, 68
Reactors (Calder Hall)
design, 58
Reactors (CANDU), 37-44
physics, 217
Reactors (Chapelcross)
design, 58
Reactors (Connecticut Yankee Power)
design, 5
Reactors (Czechoslovakian Heavy Water)
design, 56
Reactors (DON)
design, 36
Reactors (DOR)
design, 36
Reactors (Dounreay Fast)
fission product contamination of coolant, 75
status, 92
Reactors (Dragon)
design, 72-73
Reactors (Dresden Power), 6
design, 4, 7
operating experience, 3
pumps, 18
Reactors (Dungeness)
design, 58
Reactors (EDF-1)
criticality studies in, 213
design, 58
Reactors (EDF-2)
design, 58
Reactors (EDF-3)
design, 58
pressure vessel, 67
Reactors (EDF-4)
design, 58
pressure vessel, 67
Reactors (EL-4)
design, 36
Reactor (Elk River Power)
control system, 271-72
coolant flow oscillations, 273
design, 4
instrument failure, 272
Reactors (Enrico Fermi Fast Breeder)
auxiliary systems, 77-78
coolant decontamination, 77
design, 78-80
operation, 78
status, 92
vapor traps, 261
Reactors (Experimental Beryllium Oxide) (EBOR)
development, 106
Reactors (Experimental Boiling Water) (EBWR)
operation, 147
scaling, 252
Reactors (Experimental Breeder-I) (EBR-I)
nuclear parameters for Pu core, 158-9
vapor traps, 260-61
Reactors (Experimental Breeder-2) (EBR-2)
control rod drive mechanisms, 133-34
design, 78-80
coolant decontamination, 77
status, 92
vapor traps, 261-63
Reactors (fast breeder), 84-95
criticality studies, 110
design of large, 147-55
gas coolant, 95
Reactors (Fast Supercritical Pressure Power)(FSPPR)
design, 186-93
Reactors (Fast, Test)(FARET)
vapor traps, 264-65
Reactors (First Atomic Power Station)
design, 28-29
Reactors (fog-cooled)
heat transfer, 228-29
Reactors (G2)
design, 58
pressure vessel, 67
Reactors (G3)
design, 58
pressure vessel, 67
Reactors (gas-cooled), 56, 58-74
design of fast breeders, 95
operating experience, 216
physics, 216
Reactors (General Electric Test)(GETR)
flow-induced vibrations, failures from, 273-74
Reactors (graphite-moderated), 28-34
core physics calculations, 160-61
Reactors (Halden)
flowsheets, 50
operation, 50-51
water chemistry, 52
Reactors (Hallam Power)
coolant decontamination, 77
design, 78-80
operation, 81, 279-80, 282-88
vapor traps, 264
Reactors (Hanford Graphite Superheat) (HGSR)
design, 193-98
Reactors (heavy-water), 35-37
oxygen concentration control in coolant, 277
physics, 217
Reactors (Heavy Water Components Test) (HWCTR)
control rod-guide-tube rupture, 222-23
shutdown with boric acid, 225
Reactors (Hector)
criticality measurements in, 212
Reactors (Hinkley Point)
design, 58
Reactors (Humboldt Bay Power), 6
design, 4, 7
operating experience, 3
Reactors (Hunterston)
design, 58
Reactors (Indian Point Power) (CETR), 6
control system, 271
operating experience, 3
repair procedures, 276-77
Reactors (Industrial Reactor Laboratories)
rabbit facility design and fabrication, 277
Reactors (JPDR)
design, 4
Reactors (Kahl Superheating)
design, 22, 24
Reactors (KBWP)
design, 5
Reactors (KRB)
design, 4
pressure vessel, 12-13
Reactors (La Crosse Boiling Water) (LACBWR)
design, 4
Reactors (Large Closed Cycle Water)
fuel element evaluation, 172
Reactors (Latina)
design, 58
Reactors (Lenin)
design and operation, 97-98
Reactors (liquid metal-cooled), 75-96
Reactors (Lithium Cooled, Experiment) (LCRE)
vapor traps, 266-67
Reactors (Los Alamos Fast, Core Test Facility)(FRCTF)
vapor traps, 265
Reactors (Los Alamos Molten Plutonium, Experiments)(LAMPRE)
vapor traps, 265
Reactors (Loss-of-Flow Test)(LOFT)
program analysis, 240-41
Reactors (Lucens)
design, 36
Reactors (Magnox), 58-71
Reactors (Malibu-1 Power)
design, 5
Reactors (marine), 97-102
Reactors (Marius)
criticality measurements in, 213
Reactors (Maryla)
design, 111
Reactors (Marviken)
design, 47, 49, 52-55
Reactors (Minerve)
criticality measurements in, 213
Reactors (ML-1)
fuel element evaluation, 173-74
Reactors (Molten Salt, Experiment) (MSRE)

Digitized by Google

development, 106
Reactors (NERO)
design, 100-1
Reactors (New Production)(NPR)
tubes and fittings, 134-36
Reactors (Nine Mile Point Power)
design, 4
Reactors (NORA)
fuel element design, 112
Reactors (Novo-Veronezh)(WWER)
burnup, 217
Reactors (NPD), 35-44
Reactors (NRX)
testing of reactor materials in, 38
Reactors (Oldbury)
design, 58
pressure vessel, 67
Reactors (Organic Cooled, Heavy Water Moderated Power)
design, 36
Reactors (Otto Hahn)
design, 98-99
Reactors (Oyster Creek Power)
design, 4
Reactors (Parr Shoals Power)
design, 36
Reactors (Pathfinder Power)
design, 23
Reactors (Peachbottom Power)
design, 72-73
Reactors (pebble bed)
design, 73-74
Reactors (Plutonium Recycle Test) (PRTR)
control of oxygen in D_2O system, 277
nuclear parameters, 158
pressure-tube fretting corrosion, 177-82
Reactors (PM-1)
status, 103
Reactors (PM-2A)
status, 103
Reactors (PM-3A)
status, 103
Reactors (portable power), 103-4
Reactors (pressure-tube), 35-45
Reactors (Pressurized Heavy Water)
design, 51-53, 55
Reactors (pressurized-water), 3-29
development and design of large, 137-47
use of soluble poisons for control, 10-12
Reactors (Puerto Rico Power)(BONUS)
design, 23, 25, 27
Reactors (R-1)
design, 36
Reactors (R-2)
design, 36
Reactors (R3/Adam)
(see Reactors (Agesta))
Reactors (Rapsodie)
status, 92
Reactors (RB)
fuel element design, 112
Reactors (Romaska)
design, 105-6
Reactors (RWE)
design, 4
Reactors (San Onofre Power)
design, 5
pumps, 18
Reactors (Savannah River)
burnout computation, 227
Reactors (Saxton Power)
design, 5, 7
operating experience, 3
use of soluble poison control, 12
Reactors (SELNI)
design, 5
Reactors (SENA)
design, 5
pressure vessel, 12-13
Reactors (SENN)
design, 4
pressure vessel, 12-13
Reactors (SEP)
design, 4
pressure vessel, 12
Reactors (Shippingport Pressurized Water) (PWR), 6
design, 5
fuel element performance, 172, 252
operating experience, 3
use of burnable poison, 12
Reactors (Sizewell)
design, 58
Reactors (SM-1)
status, 103
Reactors (SM-1A)
status, 103
Reactors (SNAP-10A)
design, 105
Reactor (Sodium, Experiment)(SRE)
nuclear parameters of second core, 157-58
operation, 80-81
vapor traps, 264
Reactors (sodium graphite), 80-84
steam cycles, 183-85
Reactors (Southwest Experimental Fast Oxide)(SEFOR)
vapor traps, 265
Reactors (Special Excursion, Tests-2) (SPERT-2)
critical experiments with, 109
Reactors (Special Power Excursion, Tests-3) (SPERT-3)
electrical circuits, failure, 272-73
flow-induced vibrations, failures from, 273-75
leaks, 275-76
level controller failure, 272
Reactors (Steam Generating Heavy Water)
design, 36
Reactors (superheating), 22-34
design of HGSR, 193-98
fuel element development, 174-75
Reactors (Tarapur)
design, 4
Reactors (TES-3)
operation, 104
Reactors (Tokai Mura)
design, 58
Reactors (Transient, Test Facility) (TREAT)
vapor traps, 265-66
Reactors (Trawsfynydd)
design, 58
Reactors (UEM)
design, 5
Reactors (Ultra High Temperature, Experiment) (UHTREX)
development, 106
Reactors (Ulyanovsk)
design, 25-26
Reactors (University of Michigan)
D_2O reflectors, 277, 279
Reactors (University of Missouri at Rolla) (UMRR)
control rod swelling, 222
Reactors (Vallecitos Boiling Water) (VBWR)
fuel element failure in, 252-54, 256
Reactors (Vallecitos Superheat)
design, 22, 24
Reactors (VULCAIN)
design, 99-101
Reactors (water-cooled), 3-29
material buckling in, 214-15
physics, 216
Reactors (water-moderated), 3-29
material buckling in, 214-15
physics, 216
use of poisons in, 217
Reactors (WWER)
design, 5
operating experience, 3
Reactors (WWER-1)
design, 19-20
pressure vessel, 9-10, 12-14
Reactors (WWER-2)
design, 19-20
Reactors (Wylfa)
design, 58
pressure vessel, 67
Reactors (Yankee Power), 6
control system, 271-72
critical experiments, 210
design, 5
flow-induced vibrations, failures from, 273-74
leaks, 275-76
operating experience, 3
pumps, 18
use of soluble poison control, 12
Reactors (ZPR-3)
core design, 110-11
Reflectors
D_2O in University of Michigan Reactor, 277, 279
Resonance absorption
mathematical analysis, 159-60
Resonance capture
in U-238, 215
Resonance Integral Theory
calculations, 218
REX code
criticality calculations, 210
ROB code
thermal conductivity calculations, 118
Rubidium (liquid)
thermal, thermodynamic, and flow properties, 163-64

S

Safety
accident frequency, 221-22
burnout computation in Savannah River Reactors, 227
coolant flow oscillations in Elk River Power Reactor, 273
fast breeder reactors, 85-86, 153-54
Hallam Power Reactor, 280
instrument failures, 272-73
leaks, 275-76, 282
loss-of-coolant accidents, 240-41
shutdown, emergency, 225-26
University of Michigan Reactor, 279
University of Missouri at Rolla Reactor, 222
vibrations, flow-induced, 273-75
Salt solutions
heat transfer to, from wire-wrapped, seven-rod fuel element bundles, 123
Santowax
sampling techniques, 294-95
Santowax OMP
corrosive effects, 294
film formation by, 293-94
radiolysis, 290-91
use in ROSPO Critical Assembly, 112
Santowax-R
corrosive effects, 294
heat transfer properties, 123-24, 295
radiolysis, 291-92
SAP

Digitized by Google

corrosion by polyphenyls, 293-94
development for reactor fuels, 37, 39
radiation effects, 38
Satellites (man-made)
Nimbus, thermal design calculations, 240
Seals
pressure vessel, leaks, 3
use of freeze, in Hallam Power Reactor, 283
Shims (chemical), 10-11
Yankee Power Reactor, 272
Shutdown (emergency)
use of boric acid, 225
use of gadolinium nitrate, 226
Sintered aluminum products
(see SAP)
Sodium (gaseous)
freeze traps for, 285
Sodium (liquid)
heat transfer from boiling, 164
reactor cooling, 75-96
thermal, thermodynamic, and flow properties, 163-64
Sodium alloys (K-Na)(liquid)
aerosol formation in, 260
heat transfer coefficients, 235-36
thermal, thermodynamic, and flow properties, 163
Sodium Components Test Installation
vapor traps, 264
Sodium Test Facility
vapor traps, 265
SOFOCATE code
criticality calculations, 210
Specifications
fuel elements, PuO_2-UO_2, 129
pressure vessels, 13-14
Spiralator
heat exchanger, design, 237
Springs
use in control system, 223
Stagnation
vapor traps utilizing, 260
Stainless steel systems (stainless steel-UO_2 cermets)
development for fuel elements, 126-27
Stainless steels
cladding for fuel elements, 3, 6-9
corrosion of, 254, 293-94
effects of boiling water on, 255
performance in water-cooled reactors, 254, 256
Steam
effects on hydriding of Zr alloys, 246
Steam (superheated)
heat transfer, 40, 121
Steam generators
design for large pressurized water reactors, 138
operating problems in Hallam Power Reactor, 284
Steam-water systems
boiling burnout in, 166-67
flow and heat transfer, 165, 166-70
Steels
corrosion, 9-10, 293-94
STOKE code, 35
for heavy water reactor simulation, 35
Stress corrosion
effects of oxygen concentration, 255
Stresses
(see also Thermal stresses)
effects on cracking, 252, 255
Subcriticality
measurement, 224-25
Sulfur
effects on corrosion by polyphenyls, 294
Superheated steam
(see Steam (superheated))
Superheating
pressure effects on boiling, 253
Surfaces
effects on boiling, 231, 253

T

Tanks
failure of Na expansion, in Hallam Power Reactor, 285
Teflon
flexible tube heat exchangers, 237
Temperature sensors
failure in Elk River Power Reactor, 272
TEMPEST code
cross section calculations, 212
Terphenyl
heat transfer properties of irradiated, 123-24
Thermal conductivity
effects on pool boiling, 230
fuel elements, 118-21, 129
heat transfer calculations, 239
hydrogen at high temperatures, 239
noble gases at high temperature, 239
Thermal neutrons
absorption cross section and diffusion length in graphite, 114-15
distribution in light-water reactors, 215
Thermal radiation
heat transfer calculations, 238-39
Thermal stresses
in fuel elements, 253, 255
Thermometers
failure in Elk River Power Reactor, 272
THERMOS code
cross section calculations, 212
thermal neutron distribution calculations, 215
Thorium alloys (Th-U)
fuel element development for fast breeder reactors, 89
Thorium alloys (Th-U-Zr)(Zircaloy-2-clad)
fabrication of fuel elements, 130
Thorium oxide systems (Nb-ThO_2-UO_2 cermets)
thermal conductivity, 129
Thorium oxide systems (ThO_2-UO_2)
fuel element design, 3, 6-9
radiation effects, 8
Traps
for aerosols, 359-70
for carbon, oxides, and Na in Hallam Power Reactor, 285
for liquid metal systems, 259-70
Tubes
(see also Pressure tubes)
burnout, 16-17
burnout of water in, 121
heat transfer from, at cryogenic temperatures, 239-40
Tubes (finned)
use in heat exchangers, 236-37
Tungsten systems (Mo-W-UO_2 cermets)
development for fuel elements, 128
Tungsten systems (W-UO_2 cermets)
development for fuel elements, 127-28
Turbulent flow
(see Fluid flow (turbulent))
Two-phase flow
(see Fluid flow)

U

Uranium
criticality in D2O lattices, 213
criticality in graphite lattices, 212-13
radiation effects on reactivity, 217
Uranium-233
radiation effects on reactivity, 217
Uranium-235
fission ratio to U-238, 110
fission spectrum cross section, 115
radiation effects on reactivity, 217
Uranium-238
fission ratio to U-235, 110
resonance capture, 215
Uranium (enriched)
criticality in D_2O lattices, 213
Uranium alloys (Pu-U)
criticality in lattices, 212-13
Uranium alloys (Th-U)
fuel element development for fast breeder reactors, 89
Uranium alloys (Th-U-Zr)(Zircaloy-2-clad)
fabrication of fuel elements, 130
Uranium carbide systems (PuC-UC)
design of fuel elements for large fast breeder reactors, 147-49, 151-52
radiation effects, 8
Uranium carbides (UC)
buckling studies, 111
development for fuel elements for sodium graphite reactors, 81-83
evaluation for fuel elements, 174
fabrication of Na-bonded fuel elements, 129-30
radiation effects, 8, 82
Uranium nitrides (UN)
radiation effects, 8
Uranium oxide systems
critical experiments in water lattices, 210
Uranium oxide systems (Al_2O_3-UO_2)
radiation effects, 8
Uranium oxide systems (BeO-UO_2)
radiation effects, 8
Uranium oxide systems (BeO-UO_2)
(Hastelloy-X-clad)
fuel elements, evaluation, 173
Uranium oxide systems (Mo-UO_2 cermets)
fabrication into fuel elements and thermal conductivity, 129
Uranium oxide systems (Mo-W-UO cermets)
development for fuel elements, 128
Uranium oxide systems (Nb-ThO_2-UO_2 cermets)
thermal conductivity, 129
Uranium oxide systems (PuO_2-UO_2)
critical experiments in water lattices, 210, 212
design of fuel elements for large fast breeder reactors, 149-52
fuel elements, fretting corrosion of Zircaloy-2 cladding, 177-82
fuel elements, specifications, 129
radiation effects, 8
Uranium oxide system (stainless steel-UO_2 cermets)
development for fuel elements, 126-27
Uranium oxide systems (ThO_2-UO_2)
fuel element design, 3, 6-9
radiation effects, 8
Uranium oxide systems (W-UO_2 cermets)
development for fuel elements, 127-28
Uranium oxide systems (UO_2-ZrO_2)
radiation effects, 8
Uranium oxides (UO_2)
evaluation, 172-74
fretting corrosion, 177-82
fuel elements, design, 3, 6-9
fuel elements, evaluation, 172-74
fuel elements, fabrication, 128-29
fuel elements, thermal conductivity,

Digitized by Google

GIFT
JUN 22 '66

119-21
pulsed neutron studies, 112
radiation effects, 8
Uranium silicides (U_3Si)
radiation effects, 8
Uranium sulfides (US)
radiation effects, 8
Uranium systems
criticality in water lattices, 210-11
Uranyl nitrate
criticality of solutions, 213

V

Valves
performance in Hallam Power Reactor, 282-84
Vapor traps
for liquid metal systems, 259-70
Vaporizers
flow stability in forced convection, 231-32
Vena contracta
mixing during reexpansion, 235
Vertical channels
(see Channels)
Vibrations
flow-induced, failures from, 273-75

W

Water
burnout heat flux under forced convection, 122
condensation, 233
corrosion of steel, 9-10
criticality studies in lattices of, 210-212
dissociation, effects on hydriding of Zr alloys, 248
effects on corrosion by polyphenyls, 294
moderator, pulsed neutron studies in, 113
quality control, 254
reactivity effects, 109-10
Water (pressurized)
burnout calculations, 121-23
Water-air systems
flow, techniques for observing, 165
Water-ice systems
free convection melting, heat transfer calculations, 239-40
Water-steam systems
boiling burnout in, 166-67
flow and heat transfer, 165, 166-70

Z

Zircaloy alloy
cladding for fuel elements, 3, 6-9
effects of hydriding on properties, 245
Zircaloy-2 alloy
corrosion, 42-45
effects of hydriding on properties, 245, 248-49
hydriding, control of, 249-50
hydrogen absorption, 246
radiation effects, 38, 41
use in pressure tubes, 41
Zircaloy-2 alloy (Ni-tree)
hydrogen absorption, 246
Zircaloy-4 alloy
hydriding, control of, 250
hydrogen absorption, 246
Zirconium alloys
hydriding, 246-51
Zirconium alloys (coated)
corrosion by polyphenyls, 294
Zirconium alloys (Nb-Zr)
corrosion, 42-45
hydriding stress allowance, 9
use in pressure tubes, 41
clad)
Zirconium alloys (Th-U-Zr)(Zircaloy-2-clad)
fabrication of fuel elements, 130
Zirconium hydride
formation in Zircaloys, 245-46
orientation, 250-51
Zirconium oxide systems (PuO_2-ZrO_2)
radiation effects, 8
Zirconium oxide systems (UO_2-ZrO_2)
radiation effects, 8

LEGAL NOTICE

This journal was prepared under the sponsorship of the U. S. Atomic Energy Commission. Neither the United States, nor the Commission, nor any person acting on behalf of the Commission:

A. Makes any warranty or representation, expressed or implied, with respect to the accuracy, completeness, or usefulness of the information contained in this journal, or that the use of any information, apparatus, method, or process disclosed in this journal may not infringe privately owned rights; or

B. Assumes any liabilities with respect to the use of, or for damages resulting from the use of any information, apparatus, method, or process disclosed in this journal.

As used in the above, "person acting on behalf of the Commission" includes any employee or contractor of the Commission, or employee of such contractor, to the extent that such employee or contractor of the Commission, or employee of such contractor prepares, disseminates, or provides access to, any information pursuant to his employment or contract with the Commission, or his employment with such contractor.

Digitized by Google

NUCLEAR SCIENCE ABSTRACTS

The U. S. Atomic Energy Commission, Division of Technical Information, publishes *Nuclear Science Abstracts* (*NSA*), a semimonthly journal containing abstracts of the literature of nuclear science and engineering.

NSA covers (1) research reports of the U. S. Atomic Energy Commission and its contractors; (2) research reports of government agencies, universities, and industrial research organizations on a worldwide basis; and (3) translations, patents, books, and articles appearing in technical and scientific journals.

Complete indexes covering subject, author, source, and report number are included in each issue. These are cumulated quarterly, semiannually, and annually providing a detailed and convenient key to the literature.

Availability of *NSA*

SALE *NSA* is available on subscription from the Superintendent of Documents, U. S. Government Printing Office, Washington, D. C., 20402, at $30.00 per year for the semimonthly abstract issues and $22.00 per year for the four cumulated-index issues. Subscriptions are postpaid within the United States, Canada, Mexico, and all Central and South American countries, except Argentina, Brazil, British and French Guiana, Surinam, and British Honduras. Subscribers in these Central and South American countries, and in all other countries throughout the world, should remit $37.00 per year for subscriptions to semimonthly abstract issues and $25.00 per year for the four cumulated-index issues.

EXCHANGE *NSA* is also available on an exchange basis to universities, research institutions, industrial firms, and publishers of scientific information. Inquiries should be directed to the Division of Technical Information Extension, U. S. Atomic Energy Commission, P. O. Box 62, Oak Ridge, Tennessee, 37830.

Digitized by Google

TECHNICAL PROGRESS REVIEWS may be purchased from Superintendent of Documents, U. S. Government Printing Office, Washington, D. C., 20402, at $2.50 per year for each journal or $0.70 per issue. The use of the coupon below will facilitate the handling of your order.

POSTAGE AND REMITTANCE: Postpaid within the United States, Canada, Mexico, and all Central and South American countries except Argentina, Brazil, British and French Guiana, Surinam, and British Honduras. For these Central and South American countries and all other countries, add $0.75 for each annual subscription or $0.20 for a single issue. Payment should be by check, money order, or document coupons, and MUST accompany order. Remittances from foreign countries should be made by international money order or draft on an American bank payable to the Superintendent of Documents or by UNESCO book coupons.

order form

SUPERINTENDENT OF DOCUMENTS
U. S. GOVERNMENT PRINTING OFFICE
WASHINGTON, D. C., 20402

Enclosed:
document coupons ☐ check ☐ money order ☐

Charge to Superintendent of Documents No. _____

Please send a one-year subscription to

- ☐ NUCLEAR SAFETY
- ☐ POWER REACTOR TECHNOLOGY
- ☐ REACTOR FUEL PROCESSING
- ☐ REACTOR MATERIALS
- ☐ ISOTOPES AND RADIATION TECHNOLOGY

(Each subscription $2.50 per year; $0.70 per issue.)

SUPERINTENDENT OF DOCUMENTS
U. S. GOVERNMENT PRINTING OFFICE
WASHINGTON, D. C., 20402

(Print clearly)

_____
Name

_____
Street

_____
City, State, ZIP Code

Digitized by Google

Y 3, At 7:
369-1

ENGINEERING
NOV 17 '66
LIBRARY

Eng
TK
9202
.G4

POWER REACTOR TECHNOLOGY

4076

A Quarterly Technical Progress Review

Prepared for DIVISION OF TECHNICAL INFORMATION, USAEC, by
ARGONNE NATIONAL LABORATORY

Winter 1965-1966

● VOLUME 9

● NUMBER 1

Digitized by Google

TECHNICAL PROGRESS REVIEWS

To meet the needs of industry for concise summaries of current atomic developments, the Atomic Energy Commission is publishing this series, Technical Progress Reviews. Issued quarterly, each of the reviews digests and evaluates the latest findings in a specific area of nuclear technology and science.

The five journals published in this series are:

Isotopes and Radiation Technology P. S. Baker, A. F. Rupp, and associates
Oak Ridge National Laboratory

Nuclear Safety Wm. B. Cottrell, W. H. Jordan, and associates
Oak Ridge National Laboratory

Power Reactor Technology
Argonne National Laboratory

Reactor Fuel Processing Stephen Lawroski and associates
Chemical Engineering Division, Argonne National Laboratory

Reactor Materials R. W. Dayton, E. M. Simons, and associates
Battelle Memorial Institute

See the back cover for availability information.

The views expressed in this publication do not necessarily represent those of the United States Atomic Energy Commission, its divisions or offices, or of any Commission advisory committee or contractor.

Availability of Reports Cited in This Review

Unclassified AEC reports are available for inspection at AEC depository libraries and are sold by the Clearinghouse for Federal Scientific and Technical Information, National Bureau of Standards, U. S. Department of Commerce, 5285 Port Royal Road, Springfield, Va., 22151. Some of the reports cited are not available owing to their preliminary nature; however, the information contained in them will eventually be made available in formal progress or topical reports.

Unclassified reports issued by other Government agencies or private organizations should be requested from the originator.

Unclassified British and Canadian reports may be inspected at AEC depository libraries. British reports are sold by the British Information Service, 45 Rockefeller Plaza, New York, N. Y.; Canadian reports (AECL series) are sold by the Scientific Document Distribution Office, Atomic Energy of Canada, Ltd., Chalk River, Ontario, Canada.

Classified U. S. and foreign reports identified in this journal as Classified may be purchased by properly cleared Access Permit Holders from the Division of Technical Information Extension, U. S. Atomic Energy Commission, P. O. Box 1001, Oak Ridge, Tenn., 37830. Such reports may be inspected at classified AEC depository libraries.

Digitized by Google

Contents

Power Reactor Technology

Vol. 9, No. 1

APPLICATIONS	Ocean Technology and Nuclear Power	1
PHYSICS	Advances in Power-Reactor Shield Analysis	19
CONTROL and DYNAMICS	Measuring Neutron-Flux Distribution in Operating Reactors	25
FLUID and THERMAL TECHNOLOGY	What's New in Two-Phase Flow	35
	How Coolant Dynamics Affect Fast-Reactor Safety	46
SPECIFIC REACTOR TYPES	UHTREX Operation Near	51

Issued quarterly by the U. S. Atomic Energy Commission. Use of funds for printing this publication approved by the Director of the Bureau of the Budget on October 14, 1963.

Digitized by Google

Power Reactor Technology is a quarterly review of developments in reactor technology—including new concepts and applications as well as research results, analysis, and experience with existing or new components and systems. Prepared by Argonne National Laboratory at the request of the Division of Technical Information of the U. S. Atomic Energy Commission, *Power Reactor Technology* is intended for reactor designers and other technical specialists concerned with the interplay among reactor development, design, construction, operation, and economics. Thus this quarterly journal reports and interprets progress in the power-reactor field in terms of its significance to the reactor designer. Its scope includes research and development in the various technical specialties in the field as well as design and construction practices, reactor concepts, applications, economics, and operating experience.

Some articles summarize and critically evaluate reported developments; others review a topic broadly so that designers can interpret new developments, experience, and trends. All, however, call the reader's attention to reports and publications that merit study. Because any appraisal involves the reviewer's opinion of the significance of the work reported, readers are urged to consult the references for additional information and the judgments of the original authors. If a reader has information that causes his evaluation to reinforce, modify, or contradict the opinions of our reviewers, he is encouraged to write to the Editor.

For reasonably timely coverage, articles often must be based on fragmentary information. Thus, whenever appropriate, continuity will be maintained from one issue to another by use of subject headings that reflect parts of the following scope of the journal:

> CONCEPTS and APPLICATIONS: Progress in evaluating the applicability and economics of various reactor types and systems (including unconventional approaches), as well as of fuel resources and cycles, for utility central-station generation of electricity, auxiliary power, process radiation and heat, desalting, and propulsion—and for terrestrial, undersea, aerospace, and other advanced uses.
>
> ANALYSIS and EXPERIMENTATION: Advancements in the techniques of reactor physics, fluid and thermal technology, power conversion, fuel elements, materials, mechanics, control and dynamics, reactor and radiation safety, containment, and siting.
>
> SYSTEMS and COMPONENTS: Experience as reflected in design and construction practice, components, systems technology, and operating experience of various specific types of reactors—including pressurized- and boiling-water reactors, molten-salt, organic-, gas-, and liquid-metal-cooled reactors, as well as generally applicable aspects of research and test reactors.

At Argonne National Laboratory, the Reactor Engineering Division (L. J. Koch, Director) has the principal responsibility for the preparation of *Power Reactor Technology*, with the regular assistance of the Reactor Physics Division (R. A. Avery, Director) and the occasional assistance of other Laboratory divisions (Metallurgy, Chemical Engineering, Chemistry, Reactor Operations, and Idaho). Thus, unless noted otherwise, the reviewers and authors of articles are Laboratory staff members. The editors will welcome interpretive review articles contributed by readers outside the Laboratory.

JAMES J. DUTTON, Editor; DAVID H. LENNOX, Technical Editor;
EDWARD J. CROKE and RAYMOND GOLD, Associate Editors;
BARBARA A. SCHMEH, Assistant Editor

Argonne National Laboratory

Digitized by Google

Section

I

Power Reactor Technology

Applications

Ocean Technology and Nuclear Power

By Edward J. Croke

Oceanography originated as a basic science devoted to the study of the dynamics of ocean behavior on and beneath the surface, the mapping of depths and shorelines, and studies of the history and composition of the ocean floor and undersea ecological system. The fishing industry, national defense, and offshore oil industry have given rise to an oceanographic technology that is based on the application of both conventional techniques of naval architecture and technological developments from the aerospace and atomic-energy programs to the mastery of the ocean environment.

The growth of ocean science, technology, and industry is leading to a need for power sources of various kinds. The nature of these needs suggests that the features of nuclear power can be adapted in numerous ways to enable the exploitation of ocean resources.

Oceanic Power Needs

Ocean technology requires power sources ranging from data sensors consuming a few milliwatts to undersea industrial equipment demanding power by tens of megawatts. In general, the potential areas of application for nuclear power can be divided into (1) the remote and unmanned long-duration systems, such as buoys and beacons, that must operate for several years without attention and (2) the manned and relatively short-duration systems that include submersible vehicles and industrial facilities. The long-duration systems involve low-power sources in the 1-mw to 100-watt range, but the short-duration systems tend to have kilowatt or megawatt requirements. Thus both isotope and reactor power supplies offer promise for many of the projected tasks that will be encountered in the conquest of inner space.

Isotopic power sources, such as certain of the Systems for Nuclear Auxiliary Power (SNAP) systems, can be expected to yield up to 100 watts (electrical) or a few thermal kilowatts over extended times, whereas isotopic steam engines may supply power in quantities on the order of 100 kw(t). Nuclear reactors could provide power in the range up to tens of thermal megawatts. The SNAP-10A (Fig. 1) power generator and the naval submarine propulsion plants (Fig. 2) are representative of these classes of reactor power sources.

The potential applications of undersea nuclear power are many and varied. Undersea construction, submarine laboratories, oil drilling and production operations, mining and dredging, submersible-vehicle propulsion, navigational aids, and undersea pumping facilities for petroleum or water are among the more obvious and immediate uses for reliable electric- or thermal-power supplies. Thus the future of nuclear-powered commercial industry under the sea lies in three basic types of applications: (1) the extractive industries, (2) the harvesting of protein resources, and (3) underwater construction.

THE EXTRACTIVE INDUSTRIES

These include petroleum and mining (exploration and production) operations, ocean versions of which are becoming increasingly valuable.

Digitized by Google

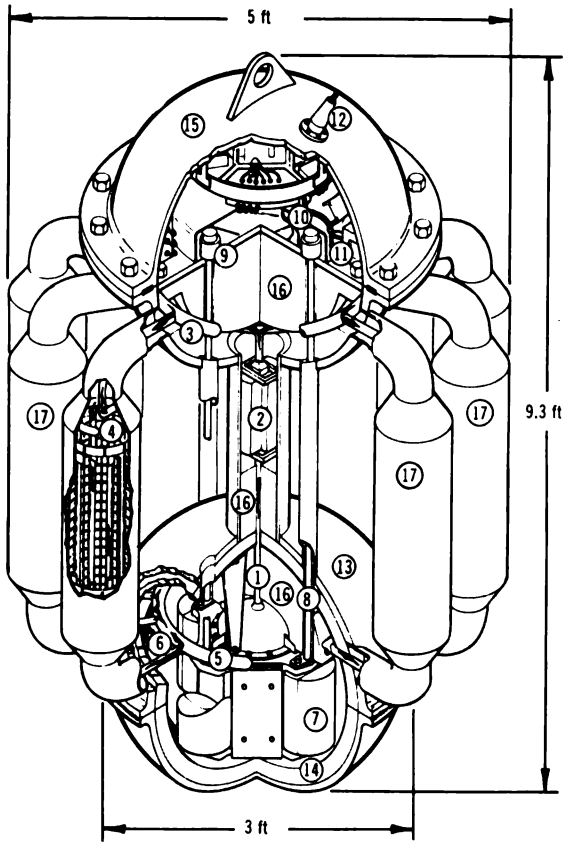

Fig. 1 The SNAP-10A reactor power generator, adapted to marine use, is designed to produce 500 watts with three thermoelectric converter assemblies and 2000 watts with 12 converter assemblies; design life would be more than five years.

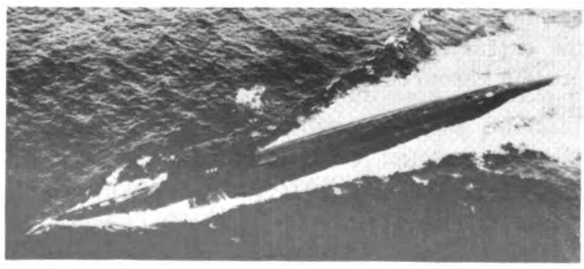

Fig. 2 Triton, largest U. S. nuclear submarine, is propelled by twin reactors of pressurized-water type designed for AEC by Knolls Atomic Power Laboratory.

Petroleum. Offshore oil production in the United States began in 1938 from the Creole field off the Louisiana shoreline. The development of the California and Texas offshore fields began shortly thereafter. Today, throughout the world, underwater oil and gas fields are also producing in many inland bodies of water, such as Lake Erie, and large-scale penetrations of the continental shelves have been made in the Persian Gulf, off the coasts of Saudi Arabia, in the Gulf of Suez, off Venezuela, Japan, Mexico, Trinidad, and Peru. As extensive exploration of the continental shelf areas continues, petroleum production operations are expected to expand both geographically and in depth. In the essentially unexplored coastal depths between 100 and 600 ft, several hundred new oil and gas fields are expected to be discovered eventually.[1]

Drilling activities at sea have always been conducted from fixed offshore towers or from floating rigs. These have the problem of station-keeping in the face of surface turbulence and weather. In the future, undersea drilling from submerged platforms or submersibles is envisioned. The freedom of the undersea drill rig from the influence of weather, the potential for sinking wells at much greater depths (deeper than 600 ft) than has been possible with floating surfaces, and the resultant extension of the area available for exploitation all make the prospects of undersea drilling most attractive. The only "if" is that such operations be proven to be economically feasible, which is an almost direct function of the technology available.

A submerged drilling rig with life-support facilities has been estimated to require approximately 25% more power than a comparable surface platform.[2] The larger surface rigs operating now require about 6000 shp (shaft horsepower), so an undersea operation would involve a continuous demand of about 7500 shp per rig. An additional 500 hp would be required approximately every three years for major on-site equipment overhauls, and about 10 hp would be required for monthly routine maintenance (such as paraffin removal).

Pressurization of the oil field would be required during production. If seawater were used for this, the power requirement would be 500 to 600 shp; gas pressurization would require 2000 to 15,000 shp, depending on the size and nature of the field. If the petroleum product were transported to shore by pipeline, a pump-

Digitized by Google

ing power ot about 3000 hp would be required, depending on local conditions, depth, and pumping distance.

The first application of nuclear power to offshore petroleum production went into operation on June 21, 1965, on an oil and gas platform in the Gulf of Mexico. A 60-watt SNAP-7F isotopic electricity generator built by the Martin Co. (Fig. 3) replaced a diesel-powered generator on an offshore installation owned jointly by the Phillips Petroleum and Kerr-McGee Companies. As a result of the joint, no-cost, research and development contract between the AEC and Phillips, the SNAP unit is powering two flashing-light beacons and a foghorn during a two-year test. This modest beginning might be regarded as a first step in the development of a nuclear-powered deep-sea petroleum industry.

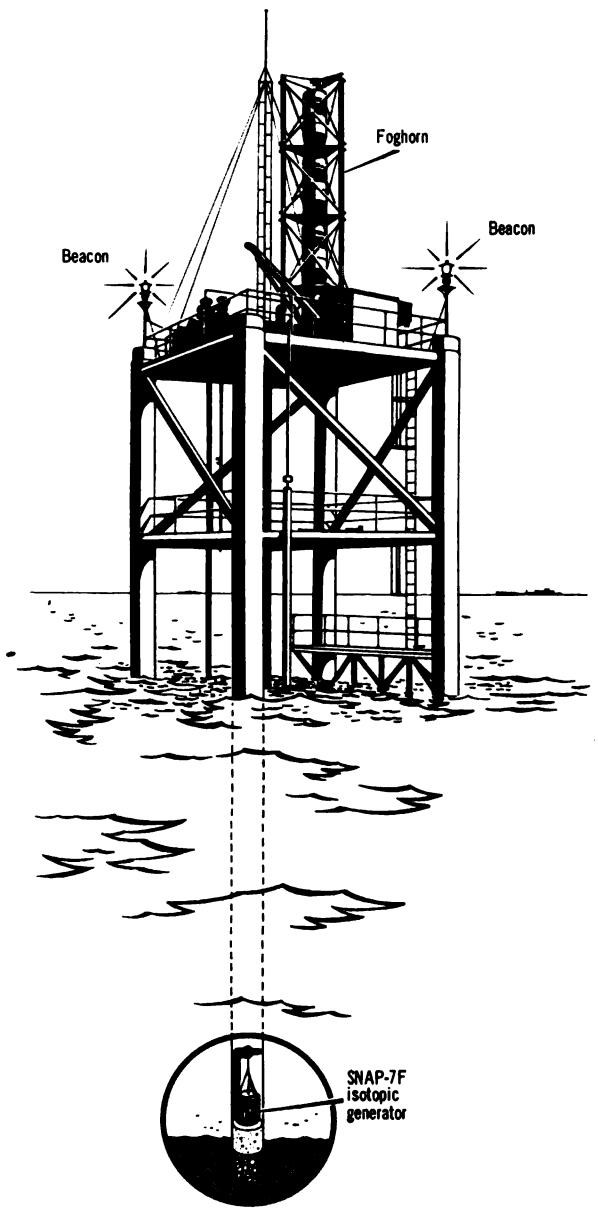

Fig. 3 The SNAP-7F isotopic power generator, in one of four tubular piles that support unmanned oil and gas platform in the Gulf of Mexico, produces 60 watts to power navigation aids. Design life is five years without refueling.

Mining. Since the British oceanographic vessel "Challenger" dredged manganese dioxide nodules from the sea floor in 1870, abundant evidence of the mineral wealth of the oceans has been revealed. At present approximately $200,000 worth of diamonds are recovered monthly along the South African coast; tin is dredged from the shallow seas in the Indonesian Archipelago; Japan mines iron from its coastal waters; and heavy minerals are taken from beaches and near-beach areas of the United States, Australia, and India. Sulfur is found in the Gulf of Mexico, and coal is mined from tunnels under the seas off Canada and England. Bromine, magnesium, iodine, and common salt are recovered commercially from seawater. Furthermore, manganese dioxide nodules, phosphorites, gold, platinum, and tin are found on the continental shelves and on the deep-sea floor.

The major obstacle to the large-scale exploitation of the minerals of the oceans has been economic in nature. For example, in most cases, the cost of extracting minerals from the sea is prohibitively high. All marine mining operations have been carried on in relatively shallow waters, less than 400 ft deep, to allow the use of conventional dredging equipment.[1] However, private industry is supporting efforts to develop practical methods for undersea mining.

In a unique arrangement that reverses the usual funding pattern, three major firms have provided the Bureau of Mines of the Department of the Interior with funds and manpower to support research and development in marine mining systems. The Bureau of Mines has supplied project leadership and facilities in a research program with the Merritt-Chapman & Scott Corp., the Lockheed Missiles and Space Company, and the International Mining and Chemical Corporation.[3] In September 1965, the Bureau signed a contract for a cooperative exploration of the Pacific continental shelf with

Digitized by Google

the latter two firms.[4] E. P. Wheaton of Lockheed estimates that undersea mining stands today where the offshore petroleum industry stood 15 years ago.

Mineral Exploration. The most immediate interest in ocean mining is in alluvial deposits close to or within 200 ft of the ocean floor and orthogenic deposits (phosphates and manganese) on the ocean floor. Nuclear techniques of mineral detection through the liquid overburden appear both promising and necessary because conventional in situ sampling systems cannot differentiate between nodular mineral deposits and the surrounding sand or mud. In situ neutron-activation-analysis devices and neutron or beta-particle backscatter detectors must be developed to detect and identify mineral deposits qualitatively and quantitatively. Preliminary investigation of such detection systems is being performed by the Bureau of Mines. A nuclear density probe for in-place measurement of deep-sea sediments has been described.[5]

This probe was developed for in situ measurement of bulk sediment density on the deep-sea floor. Measurement is based on the scattering of gamma rays from a source in the probe. The intensity of the backscatter is detected by a G-M counter assembly and recorded photographically by a camera in the instrument. The amount of backscatter indicates sediment density. After the probe has penetrated the sea floor, the source and detector automatically move vertically within the lower barrel of the probe and thereby give a density profile. Approximately 60 stations can be occupied during a single lowering of the device. The self-contained probe is approximately 26 ft long and weighs approximately 700 lb in air.

The nuclear technique used in this instrument involves total absorption or scattering (partial absorption) of gamma rays and the subsequent detection of the backscattered rays by a detector. The source is 100 mc of ^{137}Cs and the detector consists of a bundle of 30 G-M tubes. An 11.11-in. tungsten–aluminum shield separates the source and detector. This device, developed by the Lane-Wells Co., under contract to the AEC, has proven to be capable of measuring densities ranging from 1 to 2 g/cm^3 with an accuracy of 1%.

Mineral Production. Because open-ocean mining involves navigation and site marking, undersea beacons are needed to signal the location of abandoned or temporarily inactive sites, to mark the boundaries of mineral deposits, and to guide automatic mining equipment. Isotope-powered sonic buoys that can operate continuously for years in the marine environment are appropriate for these tasks. Present SNAP systems appear overly elaborate and too expensive for the purpose; however, they constitute the best available power sources for the durations required.

Recovery of minerals from the sea floor will involve any of several conventional types of dredge, suction, or airlift systems. In special cases, submersible barges will be needed to recover minerals on or beneath the sea floor. Water-lift mining techniques are suitable at depths less than 1000 ft where power supplies in the range of 250 to 1000 kw(e) would be appropriate. For deep-water recovery at depths from 1000 to 20,000 ft, power sources of 11 to 30 Mw(e) would be required.[6]

Strip, drift, slope, or shaft mining of the sea floor may involve the establishment of semipermanent facilities and perhaps processing plants on the ocean floor. An underwater strip-mining operation might require 3500 shp for a unit capable of handling 900 cu yd of sand or similar material per hour. Core bores or large-scale sample collection would require some 200 shp for a borer and 5000 shp for a large dredger. The processing and cleaning of ores would demand power in excess of several hundred shaft horsepower; thus undersea mine operations can be expected to involve a continuous demand for 200 to 5000 shp.[2]

For shallow-water mining operations, nuclear power sources cannot, at present, compete with fossil fuels. For deep-water operations at a range of 2100 miles from fossil-fuel ports, nuclear power approaches the economic break-even point as compared to fossil fuels.[6] The problems of station-keeping, power transmission from the surface, surface turbulence, required mobility, and power duration may enable nuclear power to become competitive with fossil fuels on the basis of sheer necessity.

PROTEIN HARVESTING

The sea produces approximately 40 million tons of protein annually. This yield is being harvested by the world fleet of trawlers, factory ships, and whaling vessels that use methods analogous to those employed by primitive hunters and food gatherers on land. For the

Digitized by Google

fishing industry to improve its efficiency of harvest and the yield of sea protein (as it must to accommodate an expanding world population), scientific "farming" of the sea, aided by modern technology, must be implemented. The most immediate and promising application of nuclear power in the fishing industry is in the supply of propulsion and facility power for mother ships or factory ships. An estimate based on upgrading the largest class of modern mother ship indicates that 10,000 shp would be required for propulsion and another 10,000 shp for electric fishing equipment, cannery power, fish pumps, fish-meal processors, and irradiation equipment.[7]

Small submersibles having crews of two or more might be used with the mother ship for herding fish or for exploring for biological resources. Such craft would have mission durations ranging from one day to three months and could involve power requirements from 20 to several thousand shaft horsepower. Seagoing fish-processing plants with refrigeration facilities, packing capability, or chemical processing plants could require 2000 to 30,000 shp, depending on vessel size, range, and mission.[2]

CONSTRUCTION

The power requirements for undersea construction of bridges, piers, or hydrophonic platforms are comparable to those associated with the extractive industries but require shorter durations.

A VARIETY OF OCEAN POWER NEEDS

Nuclear instruments such as sediment density probes would use an isotopic gamma-ray source, such as ^{137}Cs, in amounts equivalent to a few hundred millicuries. However, sensing instruments that are not themselves nuclear, such as magnetometers, tide gauges, temperature sensors, seismometers, tsunami detectors, anemometers, various transducers, and their associated amplifiers or telemetry systems, may require from a few milliwatts to several watts of power over times ranging from a few days or weeks in manned research facilities to five years for unmanned remote stations.

Long-term power sources are required for unmanned buoys and floating or submerged stations that function in such diverse capacities as acoustic beacons for navigation or site marking, lighthouses, foghorns, weather stations, communication and surveillance systems, recoverable sonobuoys, offshore oil equipment, and cathodic protection.[8] These devices will require power from 10 to several hundred electrical watts, depending on their specific task, and will be required to function without attention for up to five years.

Small manned undersea dwellings for research or industrial operations will require power for heating, cooking, and air regeneration. Power supplies yielding anything from a few kilowatts up to 100 kw(t) are appropriate for these purposes. Fortunately much of the power required by these stations can be used at relatively high efficiency in thermal form rather than through thermoelectric conversion systems. Heated scuba gear for prolonged work in cold water appears to be a possiblility.

Steam engines in the 1-kw(t) range can be used for industrial or research operations involving undersea drilling, pumping, valve controls, and work-assist devices.

Small research submarines or industrial work vehicles having 1 to 15 shp will be needed for manned or remote operation. Seawater shielding of nuclear plants offers a possibility of obtaining reasonably good power-to-weight ratios with such vehicles. Operating times from a few days to several months would be required, depending on system use. Table 1 summarizes these power requirements and indicates the approximate duty cycle of potential undersea nuclear energy sources.

Table 1 TYPICAL POWER AND ENDURANCE REQUIREMENTS FOR OCEAN POWER[2]

Activity	Power demand	Endurance
Petroleum		
Drilling	6000 hp + 25%	1 to 3 months
Workover	10 to 500 hp	1 day to 2 weeks
Repressurization	500 to 15,000 hp	Continuous
Tanker transport	20,000 hp	1 week/trip
Pipelining	Pumping, depending on design	Continuous
Mining		
Dredging	3500 hp	30 days
Boring	200 to 2000 hp	30 days
Protein		
Small research vehicles	20 hp	1 day
Large research vehicles	2000 to 3000 hp	3 months
Processing vessels	2000 to 30,000 shp	7 to 45 days
Sea habitats		
Hotel load	10 kw/man	1 to 6 weeks
Work load	Depends on activities	1 to 6 weeks

Undersea Work Methods

The extension of man's ability to work in the sea involves the use of four basic methods of

Digitized by Google

operation: (1) the diver, (2) the remotely controlled and unmanned submersible, (3) the manned submarine, and (4) the undersea station. The power requirements of each of these can be estimated with some confidence.

DIVERS

The diver in a scuba suit or hard-hat rig is the most versatile undersea operator in situations where a high degree of manipulatory skill is involved and risks are acceptably small. Recent experience with the Sealab has emphasized the significant problem of maintaining body warmth when a man is exposed to the ambient ocean; in the low temperatures of deep water, the working time of a scuba diver is limited to about 30 min. A suit heater that would permit a man to remain in the water indefinitely would consume about 300 watts (thermal).[9]

REMOTE-CONTROL VEHICLES

Remotely controlled submersibles, equipped with television cameras and manipulators and capable of operating at depths and carrying loads greater than a diver could tolerate, can be expected to be used in situations that do not require a high degree of manipulatory skill or in which a diver or manned vehicle would not be risked. Examples might be the transport and placement of explosives in mining operations or the preliminary exploration of an undersea site. The robot might be controlled through an umbilical cable from a surface vessel. If the mission power demand were sufficiently great, the vehicle could contain an integral power supply; otherwise the umbilical connection could transmit both control signals and power. If the robot contained an integral power supply, the umbilical connection might be omitted in favor of preprogrammed control or sonic control from the surface. The power requirement for remotely controlled submersibles depends greatly on the mission, but a fairly large vehicle might require up to 50 kw(e).

MANNED SUBMERSIBLES

Submarines for exploration, research, or industrial work will probably constitute the primary means of exploiting undersea resources. These vehicles will range in size from small one- or two-man vessels with mission durations of a few days to large industrial work platforms equipped with cranes and manipulators or cargo-carrying submarines weighing many tons. Small submersibles with crews of one to six persons will cruise at maximum speeds of about 8 knots and will consume approximately 50 kw(e) for propulsion and 10 kw(e) for life-support facilities. Larger vehicles for transporting petroleum or other products to shore-based processing plants would require 3000 to 5000 shp.[2]

Vehicle Design. Although the technology of deep-submergence-vehicle design is still relatively young, more than 22 such vehicles have been or are in the process of being built (Table 2); Fig. 4 illustrates a typical vessel intended for research and exploration. All, except the U. S. Navy *NR-1*, are powered by conventional electrochemical sources and are limited to a marked extent by the endurance capability of their power supplies. For example, the bathyscaphe *Trieste* can remain submerged for a maximum of about two days if it does not engage in significant maneuvering, or it can travel at approximately 1.5 knots for 5 hr using a conventional electric-power supply. The first deep-submergence research vehicle designed to overcome the power-supply limitation will be the nuclear-powered *NR-1*.

Fisheries Research. A nuclear submersible conceptual design was completed recently by the Electric Boat Company under the auspices of the Bureau of Fisheries Biological Laboratory in Honolulu.[11] This agency is charged with exploring and developing the fishery resources of the central Pacific Ocean. As presently understood these resources consist of several species of tuna and other large pelagic fishes.

It has become apparent that neither the tuna resource nor the oceanic environment can be understood fully from observations made from surface vessels. A fishery and oceanography submarine was proposed as a better platform for tuna research. The known behavior and distribution of tuna indicate that such a vehicle should have a 20-knot speed, a 1000-ft operational depth, and a submerged endurance of six weeks. Provisions for direct viewing of fish, continuous environmental sampling, and quiet operation are essential.

The feasibility and conceptual design study of the vessel shows it to be 163.5 ft long, 23 ft in diameter, nuclear powered, manned by a crew of 24, and able to carry 7 scientists. Innova-

Digitized by Google

Table 2 EXISTING OR PROJECTED DEEP-SUBMERGENCE VEHICLES[13]

Vehicle name Owner/operator	Operating depth, ft	Speed, knots Cruise	Speed, knots Max.	Propulsion endurance, hr/at knots	Propulsion No. of propulsion units	Propulsion Energy source	Dimensions, ft Length	Dimensions, ft Beam	Dimensions, ft Height
Aluminaut									
Reynolds International, Inc. (1965)	15,000	3	3.8	32/3	Two 5 hp horiz. (tail plane); one 5 hp vert. (amidships)	Four 77-cell 32,500 amp-hr silver–zinc (internal)	55	8	14.25
Alvin I									
Office of Naval Research/Woods Hole Oceanographic Institution (1965)	6,000	2.5	4	8/2	Two 5-hp hydraulic motors powered by pumps driven by two oil-encased electric motors	Three external oil-encased lead–acid pressure compartments	22	8	13
American Submarine Co. Model 300									
American Submarine Co. (1961)	300	1	6	3/3	One 3 hp; 12 to 24 volts	Four 6-volt lead–acid	13	4.2	4.75
American Submarine Co. Model 600									
American Submarine Co. (1963)	600	1	6	6/3	One 3.5-hp oil-immersed motor	Four 6-volt nickel–cadmium	13	5.5	5.2
Archimede									
French Navy (1961)	36,000	3			One 30 hp, 110 volts (horiz.); one 5 hp (vert.); one 6 hp (direction control)	Two 110-volt 860-amp-hr oil-encased alkaline batteries (outside pressure hull)	69	13	26.5
Auguste Piccard									
Swiss Natl. Expos. Corp. (1964)	2,500	1 to 2	6	8/6	One 80 hp	Two 2000-amp-hr 110-volt lead–acid batteries	93.5	19.7	24
Benthos V									
Lear Siegler, Inc. (1963)	600	2		2/2	Two 1 hp, 24 volts	One silver–cadmium	11.3	6.1	6
Cubmarine PC3A									
Perry Submarine Bldrs., Inc./Ocean Systems, Inc. (1964)	300	3	4.25	8/2; 3/3	One 7 hp	Six 6-volt 210-amp-hr lead–acid	18.5	3.5	6
Cubmarine PC3B									
Perry Submarine Bldrs., Inc./Ocean Systems, Inc. (1964)	600	2	4	2/4; 4/2	One 7 hp, 36 volts	Fifty 1.5-volt 250-amp-hr silver–zinc	22	3.5	6
Deep Jeep									
Naval Ordnance Test Station, China Lake, Calif. (1964)	2,000	2	2	4–6/2	Two 0.75 hp, 24 volts (variable); oil-immersed	Eight 6900-watt-hr lead–acid	10	8.5	8
Deep Star 4000									
Westinghouse Electric Corp. (under construction)	4,000	1	3	6/3; 12/1	Two 4.5 hp a-c free-flooded	Three lead–acid 400-amp-hr in 62 2-volt cells (inverter)	18	11.5	7
Diving Saucer									
Westinghouse Electric Corp. (1959)	1,000	1	1	4/1	One 2-hp motor driving centrifugal water pump; two jets provide thrust	Three 104-amp-hr lead–acid batteries	9.5	9.5	5.5
Dolphin AG(SS)555									
U. S. Navy (under construction)					One diesel–electric	Three silver–zinc batteries; two diesel–electric	152	19	
Kuroshio II									
Hokkaido Univ., Japan (1960)	650	2		Tethered	One 440-volt a-c motor	Electric from surface through cable	36.7	7.15	10.4
Moray									
U. S. Naval Ordnance Test Station, China Lake, Calif. (1964)	6,000	6	15	3.6/6	One 90-hp battery-operated torpedo motor; counter-rotating propellers	Bank of 240 silver–zinc secondary cells	33	5.3	5.3
Severyanka									
USSR/All Union Inst. of Marine Fishery and Oceanography (1958)	550	15		16,500-mile range	Diesel–electric	Diesel–snorkel; lead–acid	240	22	15
Star I									
General Dynamics Corp. (1963)	200	0.75		3/0.75	Two side-mounted; 0.25 hp, 18 volts	Two external 18-volt d-c lead–acid	10.1	6	5.8
Star II (Asherah)									
General Dynamics Corp. (1964)	600	1	4	10/1; 2/4	Two side-mounted; 2 hp, 24 volts	External 24 volt lead–acid	17	7.7	7.6
Star III									
General Dynamics Corp. (under construction	2,000	1	4	10/1; 2/4	7.5-hp single-screw stern drive; one 2-hp bow thruster; one 2-hp vert. hovering motor	115-volt 30-kw-hr oil-immersed lead–acid	24.5	6	8
Trieste II									
U. S. Navy (1964)	20,000*	2		5/2	Two 10-hp aft; one 2-hp bow thruster	External 145 kw-hr lead–acid	67	15	18
Yomiuri									
Yomiuri Shimbun Newspaper, Tokyo, Japan (1964)	1,000	4		6/4	One electric (a-c); two diesel	Diesel–electric; auxiliary diesel for battery charging; alternator for a-c power	48	8.2	9.2
NR-1									
U. S. Navy	Continental shelves			Indefinite	Two or more	Pressurized-water nuclear reactor			

*With Terni pressure sphere; 36,000 ft with alternate Krupp sphere.

Digitized by Google

Fig. 4 Research submarine designed to take 7000-lb payload to 6000-ft depths. This 50-ton 40-ft-long electrochemically powered vehicle is being developed and built by Lockheed Missiles and Space Company.

tions include an observation sphere, 2 research laboratories, several deep-sampling devices, and a 4-pod motor arrangement. Table 3 summarizes the characteristics of this vehicle.

Argonne National Laboratory (ANL) also studied a nuclear submarine concept for oceanographic research.[12] The ANL design featured

Table 3 PROPOSED FISHERIES-RESEARCH NUCLEAR SUBMARINE[11]

Hull material	HY-80 steel
Hull diameter	23.0 ft
Length, overall	163.5 ft
Power	3240 shp total
Per motor pod	810 shp
Reactor	17.0 Mw(t)
Displacement, normal surface	1265 tons
Net submerged	1407 tons
Stability and trim lead	37 tons (2.9%)
Margin lead	145 tons (11.5%)
Main ballast	142 tons
Reserve buoyancy	11.2%
Maximum speed, submerged	20 knots
Surfaced	11 knots
Turning radius at slow speeds	150 ft
Depth, operating	1000 ft
Collapse	1500 ft
Dive duration	9 weeks
Forward laboratory space (cylindrical)	
Volume	2900 cu ft
Floor area	290 sq ft
Aft laboratory space (cylindrical)	
Volume	1450 cu ft
Floor area	65 sq ft

a 7.75-Mw pressurized-water reactor (Fig. 5) that could supply 2000 shp for the propulsion of a 100-ft-long 15-ft-diameter vehicle.

UNDERSEA STATIONS

Small undersea facilities, such as ocean-floor laboratories, will require thermal and electric power for lighting, heating, cooking, and life support. The total power demand is

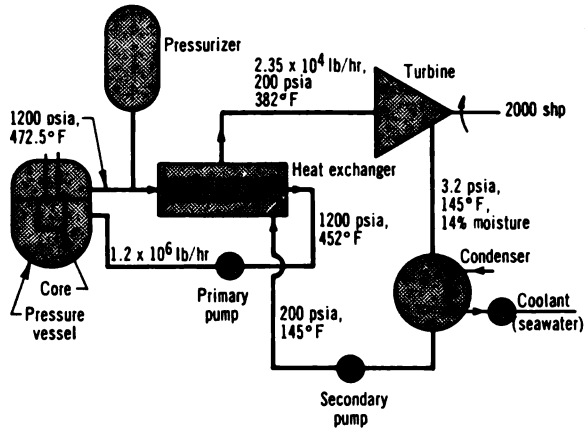

Fig. 5 Fisheries-research submarine concept studied by Argonne would be propelled by 7.75-Mw pressurized-water-reactor system; shield diameter would be 10 ft and propulsion system would be 27 ft long overall.[12]

expected to be approximately 25 kw(e) for a crew of 10 divers.

Large undersea processing plants for the separation of oil and gas or the benefaction of ores might require several thousand kilowatts of energy for hotel functions alone.[2] Integral or detached stationary power supplies (Fig. 6) will accompany such facilities.

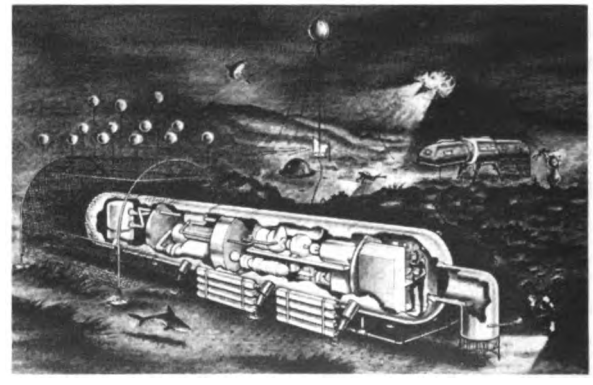

Fig. 6 Typical undersea utility plant envisioned by Aerojet-General Nucleonics might supply electric power, potable water, interior heating, hydraulic power, and oxygen for undersea plants that process oil, gas, or ores.

Oceanic Power Sources Available

Power sources for undersea use are limited to methods that neither produce exhaust fumes nor require abundant air supplies but which can supply relatively large quantities of power.

Digitized by Google

Thus batteries, fuel cells, and nuclear sources are the only reasonable possibilities at this time. Both endurance and the power required must be considered when the various chemical and nuclear sources are compared in the light of anticipated oceanic missions.

Comparison. Figure 7 provides a comparison among various 50-kw(e) power sources in terms of system weight and operating time.[2]

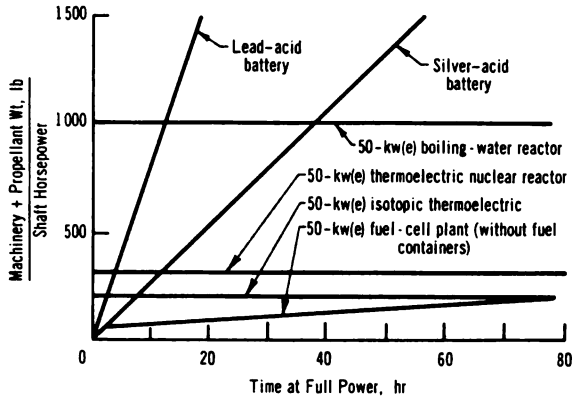

Fig. 7 Comparison of system weights and operating time of various 50-kw(e) power sources.[2]

Thus, at the 50-kw(e) power level, it is evident that fuel cells and isotopic electric systems offer a clear weight advantage for missions longer than one day.

For higher powers, such as those associated with large submersibles, or for undersea tasks, such as mining operations, where there is a continuous high power demand over an extended time and weight is not of major significance, nuclear sources are more than competitive. Although the power threshold at which the nuclear reactor becomes competitive with other sources on a power-to-weight ratio basis has not been absolutely established, a report[13] of the Interagency Committee for Oceanography of the Federal Council for Science and Technology concludes that, for large undersea vehicles requiring power plants of 1000 shp or more and an endurance greater than 400 hr, nuclear power is "indicated." Even for smaller vessels with more modest requirements, 30 shp and 30 hr, the report concludes that batteries usually will not be practical. The report finds that the alternatives are various types of power sources, including nuclear sources, all of which would require considerable development effort.

Nuclear Power in the Sea. Among the means considered for supplying power over the broad range of undersea technology are a number of thermomechanical, thermoelectric, and turboelectric energy systems that use isotope or reactor power. Their relative merits depend strongly on the weight, duration, shielding, and power required for a given mission or task. A number of nuclear power supplies have already been used in oceanographic missions, and other nuclear oceanic systems are being developed.

ISOTOPES AT SEA

Relatively few isotopes satisfy the criteria for use as marine power sources. These criteria include a half-life exceeding 100 days, a thermal power density greater than 0.1 watt/g, ready availability, and relatively low cost. The AEC is focusing its attention on four isotopes that meet these requirements: ^{90}Sr, ^{137}Cs, ^{144}Ce, and ^{60}Co. Table 4 shows the pertinent characteristics of these isotopes. Plutonium-238 and ^{147}Pm are also possibilities for limited application. It appears that the national output of these isotopes will be such that several thousands of kilowatts of isotope power will be made available annually. AEC isotope-application programs span a power range from 20 μw(e) to 10 kw(e) and include thermal, thermoelectric, and thermodynamic energy-conversion systems.

Isotopic Thermal Power. A joint AEC–Air Force program to investigate the application of isotope power to life-support systems, including water recovery, carbon dioxide removal, oxygen recovery, heating, cooling, and particle removal, is being conducted by Garrett Corporation. The system is designed to use a radioisotopic heat source. Isotopes being evaluated for this program are ^{238}Pu at Mound Laboratory and ^{147}Pm at the Hanford plant. Management of the development effort is performed by the Thermal Applications Branch of the AEC Division of Isotopes Development (DID). Although this program is primarily oriented toward space-flight applications, the system also is regarded by the DID as a possible undersea-laboratory life-support system.[9]

Evaluation of a proposed isotope-powered thermoacoustic system for an undersea sonic beacon is in progress at the DID, which is

Digitized by Google

Table 4 ISOTOPIC POWER SOURCE DATA[16]

	$^{90}Sr-Y$	$^{137}Cs-Ba$	$^{144}Ce-Pr$	^{147}Pm	^{60}Co
Half-life, years	27.7	30	0.78	2.6	5.2
Radiation	β	β,γ	β,γ	β	β,γ
Power, curies/watt (thermal)	148	207	126	2790	65
Typical fuel form	$SrTiO_3$	Glass	CeO_2	Pm_2O_3	Metal
Density	3.7	3.1	6.3	6.6	8.7
Power, watts (thermal)/cm^3	0.8	0.24	20	1.8	27
Possible availability, kw(t)/year					
1965	12	5	8	0.4	100
1970	90	48	800	10	150
1980	650	620	4200	56	
Cost, $/watt (thermal)					
1965 AEC price	112	104	126	4900	33
1966 AEC price[23]	30	26	19	556	33
Future estimate	19	21	0.90	93	10
Cost, $/kw-hr					
Thermal	0.40	0.40	0.20	15.00	0.40
Electrical	10.0	10.0	30.0		10.00

considering a study of candidate systems for directly converting heat into sound. If such a system proves feasible, it would be less costly and complex than comparable heat–electricity–acoustic energy systems. A system proposed by the Martin Co. envisions the use of heat from a ^{90}Sr source to boil water. The steam would power a hydroacoustic transducer that produces sound from the flow of oil through an orifice in a diaphragm. The entire system could fit into a lightweight 1-cu ft box and has a projected life[9,14] of 10 years.

An isotope-heated scuba suit, being developed at Mound Laboratory, combines a 300-watt ^{238}Pu heat source with a fluid-flow heat exchanger; the fluid would transmit the heat through veinlike tubes embedded in the scuba suit. This heating unit will weigh approximately 15 lb and is designed to be backpacked. It will extend the useful immersion time of a diver from approximately 30 min/day up to the limit of his physical ability to perform underwater work.[9] This development program also is being sponsored by the Thermal Applications Branch of the DID.

A possible application of ^{90}Sr as an undersea heat source is being investigated at Oak Ridge National Laboratory (ORNL). Although this heater, essentially an encapsulated isotope brick pile, has been proposed as a heat source for the second phase of the Sealab experiment, no decision to develop or use it has been announced.

In view of the prospective requirements for larger sources of thermal energy for undersea-facility heating and power sources, it is reasonable to expect that the present relatively modest AEC effort along these lines will be expanded as the oceanographic (and aerospace) programs progress.

Isotopic Thermoelectric Systems. The AEC has concentrated considerable effort on the development of isotopic thermoelectric systems. A family of such power supplies has been built and is being used in various marine capacities; more advanced systems are also being developed.

Several prototype ^{90}Sr-fueled lead telluride thermocouple systems have been placed in operational test by the AEC. These generators, spanning the power range of 7.5 to 60 watts, were developed under the SNAP-7 program by the Martin Co.

The SNAP-7A device (Fig. 8), a 10-watt generator that supplies power for a Coast Guard navigational buoy at Curtis Bay, Md., contains 40,000 curies of ^{90}Sr in the form of strontium titanate pellets. This fuel is contained within two layers of Hastelloy C to form a total thickness of 0.5 in. Sixty pairs of lead telluride thermocouples, having a hot-junction temperature of 800°F and a cold-junction temperature of 115°F, supply 10 watts at 5 volts direct current. The entire unit, including biological shielding, weighs 1840 lb, of which the fuel, generator, and containment capsules weigh only 121 lb.

The SNAP-7B (Fig. 9) is a 60-watt lead telluride thermocouple generator fueled with 225,000 curies of strontium titanate. The fuel is encased in a double layer of Hastelloy C and shielded by 3 in. of depleted uranium. The unit, including shielding, weighs 4600 lb. The SNAP-

Digitized by Google

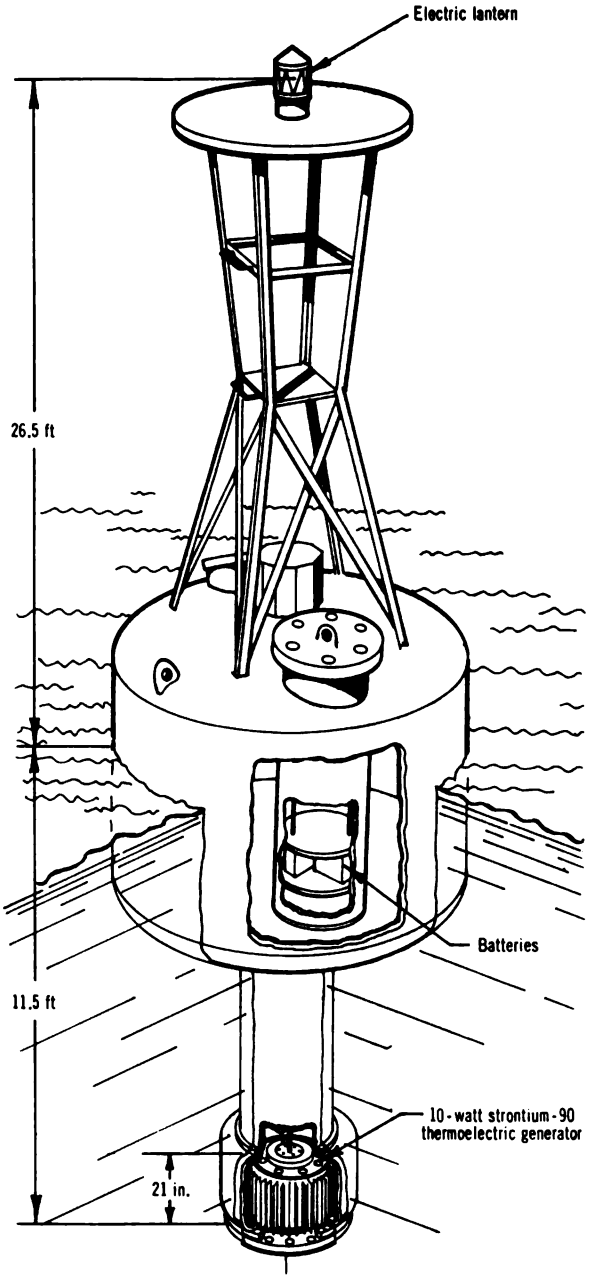

Fig. 8 The SNAP-7A isotopic thermoelectric power system, in base of buoy, generates 10 watts to recharge batteries in Coast Guard navigational buoy at Curtis Bay, Md.

7B is in service as the power supply for the Baltimore lighthouse in Chesapeake Bay.

The SNAP-7C system, a 10-watt unit that is essentially identical to the SNAP-7A, supplies power for a U. S. Navy automatic weather station in the Antarctic.

The SNAP-7D, a 60-watt generator similar to SNAP-7B, powers a floating Navy automatic

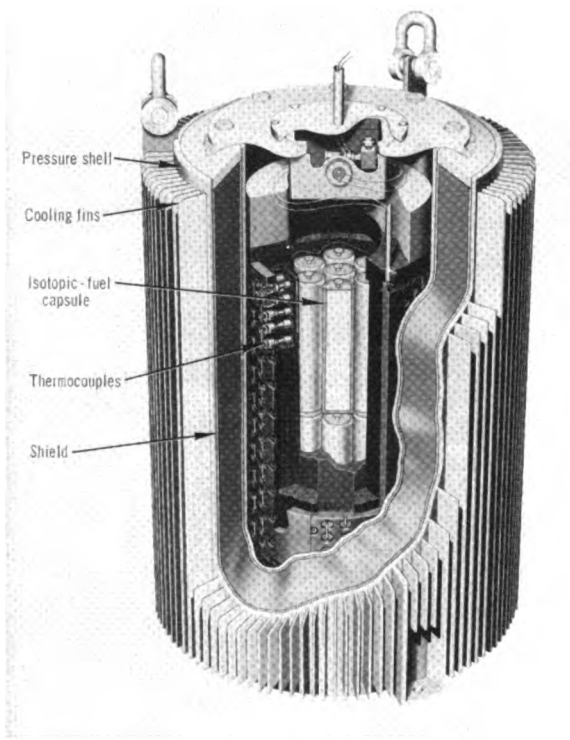

Fig. 9 The SNAP-7B isotopic thermoelectric power system has 120 pairs of lead telluride thermocouples to convert heat from 14 fuel capsules to 60 watts that power Coast Guard's Baltimore Light.

weather station in the Gulf of Mexico (Fig. 10). This buoy system, called NOMAD (Navy Oceanographic and Meteorological Automatic Device), is a forerunner of a network of such installations planned by the Navy.

The SNAP-7E (Fig. 11), which is essentially similar to the 7A and 7C units but with an output of 7.5 watts, provides power for a navigational sonobuoy on the 15,000-ft-deep floor of the Atlantic Ocean near Bermuda. Unlike the 7A and 7C units, SNAP-7E has a forged-steel pressure vessel to withstand the 8000-psi ambient pressure at its operational site.

The SNAP-7F generator (Fig. 3) is a 60-watt device that has powered navigational aids on an offshore oil and gas platform in the Gulf of Mexico. This operational test unit is similar to the other 60-watt generators in the SNAP-7 series.

A second generation of marine SNAP systems to produce powers of 10 to 60 watts is being developed. These are the SNAP-21 units that will operate in pressures up to 10,000 psi for at least five years without maintenance.

Digitized by Google

Fig. 10 The SNAP-7D isotopic thermoelectric generator provides 60 watts to power weather instruments and telemetry system on a Navy unmanned weather boat in the Gulf of Mexico.

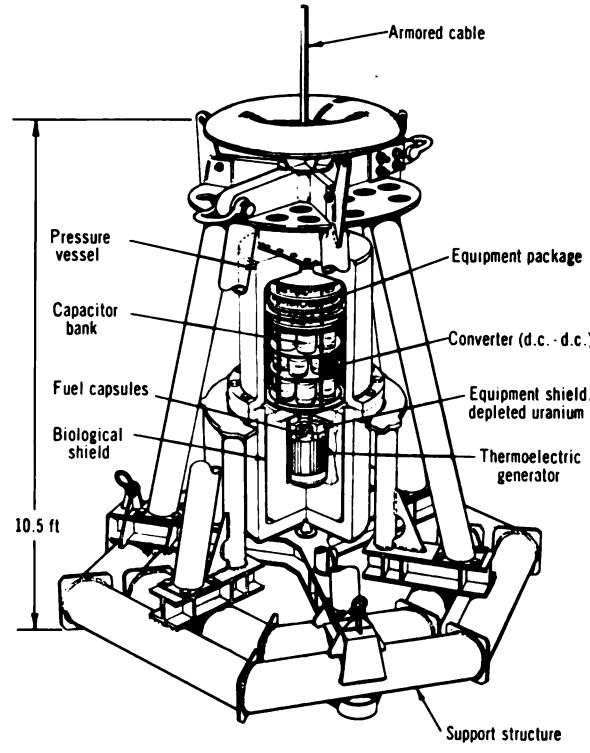

Fig. 11 The SNAP-7E isotopic thermoelectric generator, which is on sea floor at 15,000 ft depth in the Atlantic Ocean, produces 7.5 watts to power a Navy navigational sonobuoy that is about 3000 ft above the generator.

The SNAP-21 units will be developed for 10-, 20-, and 60-watt powers and will be fueled with ^{90}Sr. The Minnesota Mining & Manufacturing Co. has undertaken the development effort, which is scheduled to produce a 10-watt prototype unit in 1966. The use of improved thermoelectric materials, higher hot-junction temperature, and improved thermal insulation and design will result in second-generation systems whose cost and weight will be an order of magnitude less than the SNAP-7 series. For example, the 7.5-watt SNAP-7 unit weighs 6000 lb, but the 10-watt SNAP-21 will weigh only about 500 lb (Ref. 15).

The AEC also is planning an Advanced Large Milliwatt Generator Program. The first phase of the program would yield conceptual designs for 150-, 600-, and 900-mw generators that could power sonic pingers for wellhead locators and other such low-power devices.[15]

The SNAP-15 program involves development of a 1- to 3-mw thermoelectric generator weighing less than 1 lb. Such a power constitutes the lower useful limit for undersea energy sources, but SNAP-15 could power a variety of instruments and data sensors. The General Atomic Division of General Dynamics Corp. is the contractor for the development of this ^{238}Pu-fueled generator.

Isotopic Engines. Thermodynamic engines that can supply power in the range 10 to 100 kw(t) will find use in small submersible propulsion systems, turbodrills, and work-assist devices.

A conceptual design study of an isotopic heat source integrated with a propulsion engine for undersea craft is in progress at Aerojet-General Nucleonics under a cooperative contract with the DID. This RISE (Radioisotope Submersible Engine) program will provide the first demonstration of a thermodynamic isotopic ocean power system having a cycle efficiency two to four times that of existing thermoelectric conversion devices.[8]

The RISE concept, for which ^{60}Co has been tentatively selected as the heat source, envi-

Digitized by Google

sions a turbine-Rankine-cycle system using Dowtherm A as the working fluid in a direct (single-loop) power-conversion system that will consist of a combined rotating unit that includes a turbine–alternator, condensate pump, regenerator, and condenser. The power-conversion system will be sealed to prevent leakage of working fluid or contamination of the system. Current effort in the RISE program involves the conceptual design, detailed program planning, and initial research and development for a 3-kw(e) or 4-shp demonstration engine. The system design, like the heat source, will be scalable to about 20 kw(e) or 26.8 shp. This proof-of-principle engine probably will use a 16-kw(t) isotope source with design potential for being upgraded[9] to 100 kw(t).

In an associated effort the Savannah River Laboratory is performing a source-selection trade-off study, including research and development, on the production and use of ^{60}Co for this purpose. A study of ^{90}Sr as an alternative heat source is in progress at ORNL.

An isotope-heated steam piston engine also has been studied at Aerojet-General Nucleonics.[16,17] This system features a 12-shp two-cylinder steam engine weighing approximately 3800 lb, including 2900 lb of shielding. Figure 12 and Table 5 illustrate the system and delineate its characteristics. Isotope steam engines similar to this propulsion power package are also being studied for underwater mechanical power supplies and work-assist devices.

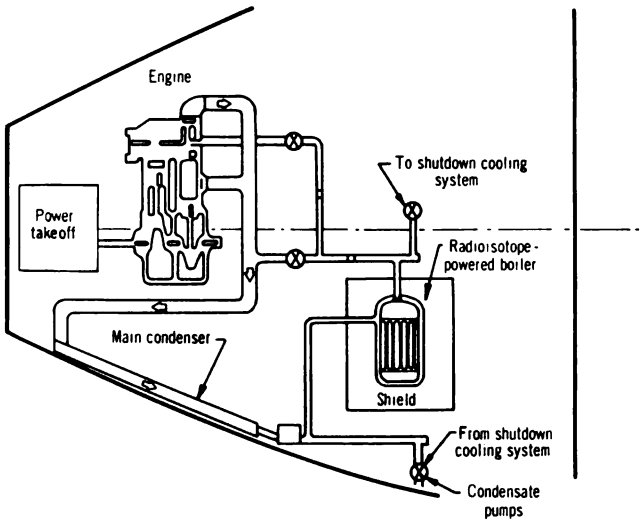

Fig. 12 Radioisotope-powered steam piston engine could propel small submarines or power turbodrills or other work-assist devices.

Table 5 SUMMARY OF RADIOISOTOPE-ENGINE CHARACTERISTICS[17]

Cycle characteristics	
Shaft power output	12 kw
Maximum pressure	1200 psia
Maximum temperature	567°F
Minimum temperature	141°F
Ideal efficiency	34.8%
Boiler characteristics	
Fuel	Cerium-144 as CeO_2
Cladding material	Hastelloy C
Fuel-element configuration	19 pins in hexagonal array
Pin size	1.5 in. in diameter by 7.9 in. long
Total fuel volume	250 cu in.
Maximum thermal power	71 kw
Minimum thermal power	45 kw
Shield material	Natural or depleted uranium
Engine characteristics	
Type	Reciprocating, double acting, compound 2-cylinder
Speed	2000 rpm
Auxiliaries	
Condensers	Natural convection to seawater
Feed pumps	2 steam-driven reciprocating pumps; 2 electrically driven gear pumps

REACTOR-POWERED SYSTEMS

The high power range of reactor systems has been effectively exploited for the propulsion of ships and large submarines. However, for the smaller research submersibles intended for deep penetration of the ocean, no suitable reactor power or propulsion systems are available now. Vehicles ranging in size between the large combat submarine and the very small (< 300 tons) submersibles would lend themselves well to reactor power. Of interest for this application is a class of reactors in the SNAP-10A family, which was originally developed for space-flight applications and generates 500 watts (thermal), and the higher powered SNAP-8, which produces 100 kw(t) and could generate 20 to 50 kw(e).

SNAP-10A is a uranium–zirconium hydride-fueled reactor that contains 4 kg of ^{235}U. Weighing approximately 1000 lb, SNAP-10A measures 5 ft at the base and is 12 ft high. Its NaK coolant is circulated by a thermoelectric pump, and power is converted by silicon–germanium thermoelectric modules with 885°F hot junctions and 235°F cold junctions.

An adaptation of SNAP-10A that would yield 500 to 2000 watts (electrical) has been studied

Digitized by Google

for stationary undersea use (Fig. 1). Total weight of the 2000-watt version of this marine reactor is 8200 lb (with shielding for retrieval); the 500-watt version would weigh 7200 lb. The SNAP-10A reactor was developed by Atomics International under contract to the AEC.

Larger versions capable of delivering 300 to 2000 kw(e) have been developed and might be adapted for undersea use. Such reactors could be of service in large operations such as undersea construction; benthic laboratories; offshore oil drilling; and production, mining, and dredging.

The NR-1 manned submersible represents the only large-scale effort now being made to develop a reactor-powered deep-sea research vehicle. Although it is expected that the proven nuclear technology of the combat submarines will contribute materially to the configuration of the *NR-1* pressurized-water reactor, little power-plant design information is available.

Supercritical-Water Reactor. A reactor configuration that might be appropriate for propulsion and auxiliary power in a deep-submergence vehicle was studied by Battelle Memorial Institute.[18] This supercritical-water reactor (SWR) plant, whose design is summarized in Table 6, has a number of features that make it attractive as an undersea power supply. The heat capacity of supercritical water averages twice that of ordinary water and six times that of sodium. This large heat capacity, coupled with a large temperature rise, results in low flow requirements and thus smaller pumps and piping.

Water is a good neutron moderator and good heat-transfer medium; the relatively high fluid temperature associated with the system leads to high efficiency and a lightweight power-conversion system. Moreover, the SWR is a natural extension of the pressurized-water-reactor concept for which considerable design and operating experience exists. The usual requirement for a thick pressure vessel for a water reactor is less severe in the SWR design because ocean pressure can be used to partially balance working-fluid pressure at operating depths.

SWR Vehicle. A research vehicle was considered for missions to 10,000 ft. Composed of three adjacent 10-ft-diameter spheres with the supercritical-water-reactor power package suspended below them, the entire system would be surrounded by a hydrodynamic firing. One of the spheres houses the operating crew, another is for the research crew, and the third is for personnel-support equipment. Radiation shielding is supplied by approximately 8 ft of seawater in addition to the reactor

Table 6 SUPERCRITICAL-WATER REACTOR DESIGN DATA[18]

Core	
Active diameter	12 in. equivalent
Height	18 in.
Structural material	Type-347 stainless steel
Core power	1440 kw
Reflector thickness	2.5 in.
Control	Stainless-steel-clad boron carbide vanes in reflector
Fuel elements	
Type	UO_2 coupons in stainless-steel plate
Meat	93% dense UO_2, fully enriched
Fuel coupon thickness	40 mils
Cladding thickness	7 mils
Coolant-channel width	15 mils
Element size	1.125 in. square, including 20-mil can
Plates per element	15
Number of elements	45
Initial fuel loading	64.8 kg of ^{235}U
Maximum meat temperature	1170°F
Maximum surface temperature	1140°F
Heat-transfer data (design conditions)	
Coolant	
Pressure, average	4340 psia
Inlet temperature	300°F
Outlet temperature	1000°F
Core pressure drop	<1 psia (without orifices)
Flow rate	4400 lb/hr
Core flow area	0.07 sq ft
Heat flux (average)	29,000 Btu/(hr)(sq ft)

Digitized by Google

thermal shield and pressure vessel. A reactor and power-conversion package providing 250 kw(e) for propulsion and auxiliary electric power for extended missions has a mass of approximately 15,700 lb at a specific gravity of approximately 1.8.

Surface-Ship Propulsion. Reactor propulsion for surface vessels has been a reality for some time. The nuclear merchant ship *Savannah* (Fig. 13), the aircraft carrier *Enterprise* (Fig. 14), the cruiser *Long Beach,* the destroyer *Bainbridge,* and the Russian icebreaker *Lenin* have amply demonstrated the operational feasibility of nuclear surface propulsion.

Gas-Cooled Reactor. The gas-cooled type of reactor has been evaluated by several organizations as a promising hydrospace power source for stationary installations. An Aerojet-General Nucleonics study[19] indicates that, for near-term and low-power (<1 Mw) requirements, an optimum configuration would consist of a heterogeneous light-water-moderated reactor cooled by a breathing-gas mixture (helium, nitrogen, and oxygen). In addition to serving as both the reactor coolant and as the hull-pressurizing medium, such a gas mixture could be replaced on site by use of the breathing-gas generation system. Power would be converted by a Brayton-cycle system with a split-turbine-driven alternator and recuperator. Plant output would be 100 kw(e) net plus 100 kw(e) for auxiliaries and hotel load. A precooler would provide the cycle heat sink; a natural-convection seawater heat exchanger would provide the ultimate heat sink. The reactor compartment would be flooded to provide shielding for the power-conversion compartment.

Fig. 13 The N.S. Savannah, a 22,000-ton vessel, was the first cargo-passenger ship to be propelled by nuclear power.

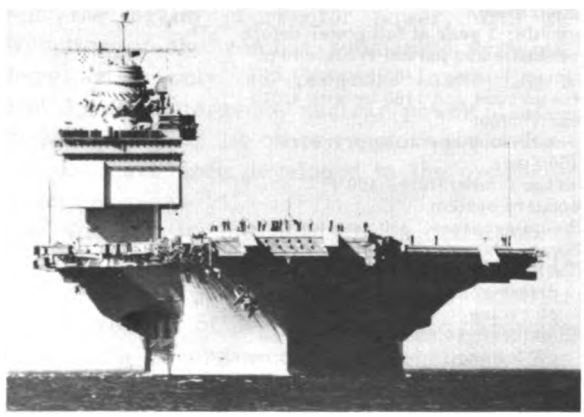

Fig. 14 The USS Enterprise has demonstrated benefits of nuclear power for aircraft carriers.

MH-1A. A possible precursor of the large industrial undersea nuclear power plant of the future is the Army MH-1A floating nuclear power plant (Fig. 15). This 10-Mw(e)-reactor electricity-generating system was designed and built by the Martin Co. under contract to the Army Corps of Engineers. Installed in a Liberty Ship hull, the MH-1A will provide a floating power supply that can be towed to any port in the world to supply or augment electric power for emergency conditions. Table 7 summarizes system characteristics.[20]

TURPS. A somewhat smaller reactor thermoelectric power system is being studied by the Martin Co. under contract to the Surface Nuclear Power Group of the Air Force Weapons Laboratory. This TURPS (Terrestrial Unattended Reactor Power System) was proposed as a power source for Air Force remote radar installations; however, it also is being evaluated as an undersea power plant.

The TURPS concept has a uranium–zirconium hydride reactor that is cooled by natural circulation of tetraphosphorus trisulfide. Its rated thermal power is 1.56 Mw, or 100 kw(e). Shielding is accomplished with earth or water and two shield plugs above and below the reactor; a shield sleeve surrounds the reactor during transportation. The cylindrical core measures 13 by 13 in., and the entire assembly is 4 ft in diameter and 19 ft long. The weight of the system[21] is 18,700 lb. According to the Martin Co., TURPS would be about 200 times more powerful than any direct-conversion system now operating and would be able to operate for five years at full power without refueling.

From this enumeration of reactor power plants can be seen the considerable variation

Digitized by Google

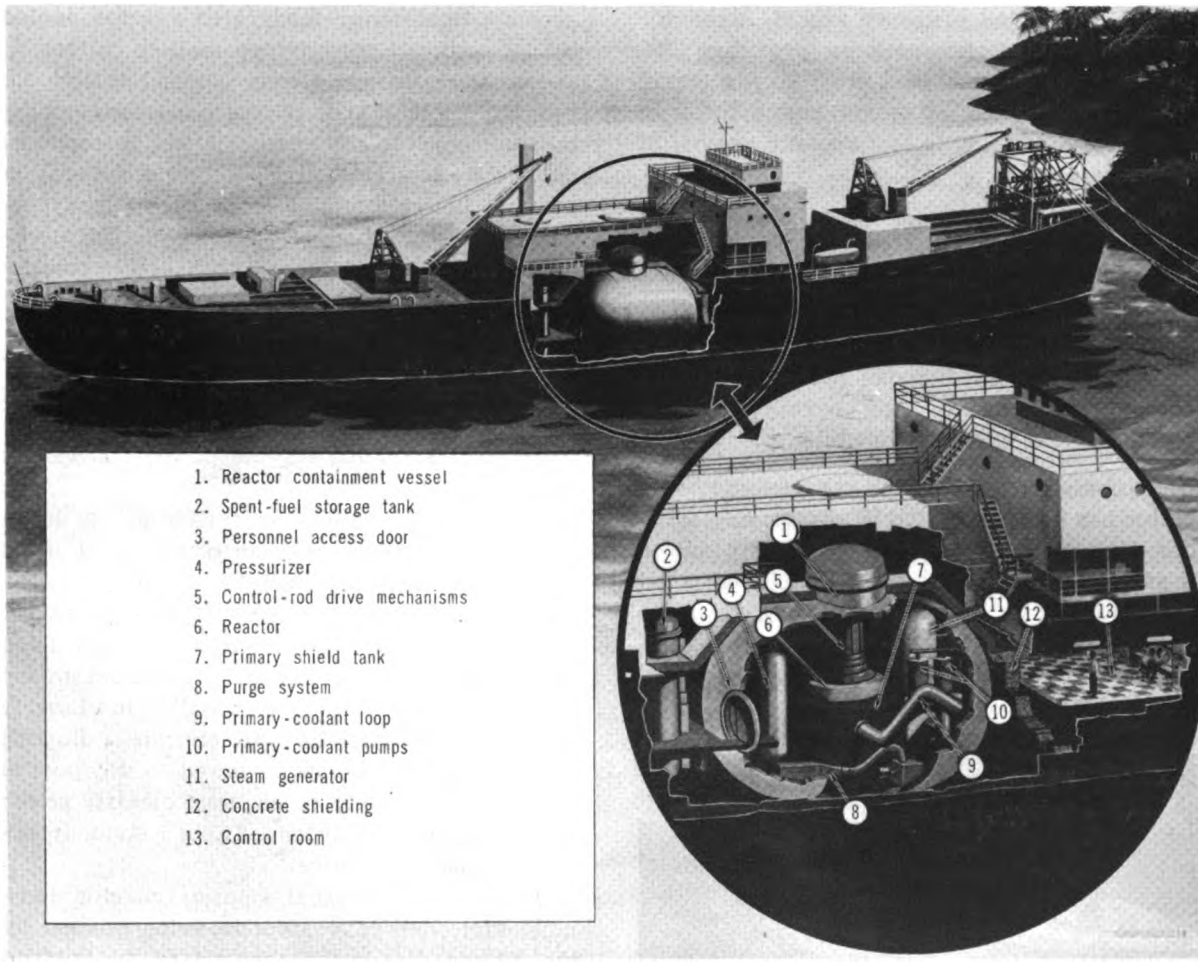

Fig. 15 The MH-1A floating nuclear power plant provides 10 Mw(e) to any area to which a barge can be towed.

Table 7 MH-1A FLOATING NUCLEAR POWER PLANT[20]

Length: Overall 441.5 ft, beam 65 ft Displacement: 8254 tons Gross output: 45 kw(t) Net output: 10,000 kw(e) Containment: Reactor system is completely contained in steel containment vessel; additional safety is provided by special collision and grounding barriers in hull Shielding: 600 tons of lead and polyethylene and 880 tons of concrete surrounding the steel containment vessel Plant design life: 20 years Core type: stainless-steel tubes containing UO_2 fuel pellets Reactor type: pressurized water Fuel elements: 3328 stainless-steel tubes 39 in. long and 0.507 in. in diameter; fuel pellets are low-enrichment UO_2 Core size: 30 in. high, 45 in. in equivalent diameter; 36 in. in active height	Control rods: 12 cruciform cross-section rods of boron–stainless-steel alloy Core life: 1 year at full power before reshuffle and partial replacement Uranium loading: 1460 kg with 4.65% enrichment and 1460 kg with 4.07% enrichment Primary-loop operating pressure: 1500 psia Average temperature: 490°F Secondary system Steam pressure: 330 psia (throttle) Steam generator: Verticle U tube Turbine-generator: 3600 rpm direct-connected; 13,529 kva at 60 cycles Electrical: 10,000 kw(e) net at 60 cycles and 13,800 volts; 8083 kw(e) net at 50 cycles and 11,500 volts

Digitized by Google

among the reactor configurations that are being considered for use in the ocean. Except for naval reactors, all the systems available now are essentially land-based systems modified for a maritime setting. Until additional experience with nuclear power in an oceanographic framework is accumulated, it will be difficult to identify the specific characteristics and peculiarities of an optimum undersea nuclear power plant.

The AEC has initiated a program for the development of low-power nuclear reactor systems that initially will cover the 100-kw(e) to 2-Mw(e) range and be applicable to a variety of uses, such as oceanographic power plants.[22]

Conclusions

The development of nuclear power sources for use in the ocean is progressing steadily along a broad, if somewhat discontinuous, front. In the extremely low-power range, nuclear or nuclear-powered instrumentation technology has received less attention than it deserves. Isotope-thermoelectric intermediate-power source development is well into the proof-of-principle stage and is being advanced in a vigorous and systematic way, probably because of the impetus of the aerospace program.

Although isotope thermal and thermodynamic power sources have been investigated, experiments have been performed, and analyses have been made, most of these devices are still in the laboratory or conceptual-design stage and much work remains to be done. The lack of a specifically defined immediate requirement for such systems has probably delayed their development.

In the realm of reactor power, with the exception of the combat submarine systems, there exists only one program to develop a true deep-submergence nuclear power plant—the *NR-1* project. No other reactors for undersea use have been developed to the proof-of-principle stage.

In addition to the need for a definition of oceanographic objectives, the basic obstacle to nuclear ocean power is cost. Less familiar is the problem of designing nuclear hardware to operate in the marine environment. The solution to both depends on resolving the old problems of system efficiency, compactness, and weight—especially shield weight. As the need for nuclear ocean systems becomes more evident, the incentive will lead to solutions to these problems.

It is clear that nuclear-powered devices have a definite and often undisputed place in the exploration and exploitation of the oceans. Wherever long-endurance power is required, nuclear systems are serious competitors with fossil fuel and electrochemical energy sources. Although the development of nuclear power for the sea is still in a very early stage, the results thus far have been so promising, and the variety of potential applications of nuclear power so great, that continued and expanded research and development in this area appear nearly inevitable for the future.

References

1. Interagency Committee on Oceanography, Oceanography, Ten Years Ahead. A Long Range National Oceanographic Plan, 1963–1972, Pamphlet No. 10, June 1963.
2. J. V. Harrington, Underwater Uses for Power Sources in Industrial Applications, presented at the Marine Technology Society Meeting, Washington, June 1965.
3. W. S. Beller, Trend Is Toward Useful Applications, *Missiles and Rockets*, 17(10): 23-25 (Sept. 6, 1965).
4. Lockheed Missiles and Space Company, News Release No. 190-64, Sept. 16, 1965.
5. G. H. Kellar, Nuclear Density Probe for the In-Place Measurement in Deep-Sea Sediments, presented at the Marine Technology Society Meeting, Washington, June 1965.
6. E. P. Wheaton, Ocean Mining and Commercial Resources Development, presented at the Atomic Industrial Forum, Washington, Nov. 15, 1965.
7. E. E. Duckstad, Potential Applications of Nuclear Energy in a Marine Environment, Stanford Research Institute Report on Project No. IU-2754, August 1959.
8. Aerojet-General Nucleonics Testimony Before the Joint Committee on Atomic Energy, Aug. 10, 1965.
9. R. W. Shivers, Atomic Energy Commission, Division of Isotopes Development, personal communication, Oct. 26, 1965.
10. Reference deleted.
11. D. W. Strasburg, A Submarine for Research in Fisheries and Oceanography, presented at the Marine Technology Society Meeting, Washington, June 1965.
12. J. Madell, Application of Nuclear Power to an Oceanographic Research Submarine, presented at the Torpedo Propulsion Conference, sponsored by the American Institute of Astronautics and Aeronautics, Newport, R. I., July 22–26, 1963.
13. Pamphlet No. 18 of the Interagency Committee for Oceanography of the Federal Council for Science and Technology, October 1965.
14. Power from Radioisotopes, U. S. Atomic Energy Commission Publication, Division of Technical Information.

Digitized by Google

15. Robert Carius, Terrestrial and Space Power Branch, U. S. Atomic Energy Commission, personal communication, Sept. 27, 1965.
16. E. E. Fowler and N. F. Sievering, Nuclear Power for Ocean Applications — Its Potential and Availability, presented at the Marine Technology Society Meeting, Washington, June 1965.
17. E. E. Buck, A Radioisotope Engine for Submersible Vehicle Propulsion, presented at the Marine Technology Society Meeting, Washington, June 1965.
18. J. W. Ray and J. W. Chastain, A Supercritical Water Reactor for Propulsion and Auxiliary Power in a Deep Submersible Research Vehicle, presented at the Marine Technology Society Meeting, Washington, June 1965.
19. P. Grisel, Aerojet-General Nucleonics, personal communication, Oct. 18, 1965.
20. Martin Co. Publicity Release No. 3801, July 3, 1964.
21. Martin Co. Publicity Release No. 3948, Sept. 16, 1965.
22. AEC Authorizing Legislation for Fiscal Year 1967, Hearing Before the Joint Committee on Atomic Energy, 89th Congress of the United States, Second Session, page 406.
23. AEC Press Release H-222, Oct. 11, 1965.

Digitized by Google

Section II

Power Reactor Technology

Physics

Advances in Power-Reactor Shield Analysis

By Phillip S. Mittelman, United Nuclear Corporation*

Power-reactor shields are massive structures designed to reduce external radiation heating, radiation dose, and radiation activation to acceptable limits. Because the reactor shield represents a significant cost and also influences the design of the reactor building and containment structure, it is worthwhile to optimize the shield design so as to minimize both direct and indirect costs.

Toward this end there has been a slow but steady advance in the state of the art of power-reactor shield analysis. Accurate prediction of shield performance is the first step in an optimization program—and in itself can reduce costs by eliminating the need for extra shield thickness to compensate for calculational uncertainties.

Advances in shield analysis have consisted mainly of transforming feasible methods of shield analysis into practical methods by the use of computers. Most of the fruitful activity has been associated with: (1) improved techniques for analyzing bulk shields and (2) analysis of complex geometries by means of the point-kernel or Monte Carlo method.

Bulk-Shield Analysis

A substantial portion of a power-reactor shield can be regarded as a one-dimensional (slab, sphere, or cylinder) multilayer assembly of material surrounding a source region of similar geometry. A shield-analysis technique attempts to determine the neutron and gamma-ray leakage from such a shield, taking account of secondary gammas produced by neutron interactions in the shield. In addition, the radiation heating and activation of shield components are also desired outputs.

Several very useful approaches have been developed in recent years to study bulk shields quickly and accurately. In general, these methods have replaced the older techniques that involved the performance of power and geometrical transformations[1] on experimental bulk-shield configurations. They are more accurate and can be performed for situations in which experimental data are not available. Because a complete bulk-shield analysis can be completed in less than 15 min of IBM-7090 time, the effects of design modifications can be studied easily.

The most widely used methods combine a removal theory and multigroup diffusion theory. The United Kingdom RASH codes,[2] the Swedish NRN method,[3] and the Hanford MAC program[4] divide the high-energy region into a number of energy groups and assume that source neutrons are attenuated exponentially. Energy-dependent removal cross sections are employed; neutrons "removed" from the high-energy groups slow down in the shield and lead to secondary gamma sources. In the RASH procedure, continuous slowing down is used, whereas NRN and MAC permit slowing down from one group to any other group. In these programs the capture-gamma sources are determined, and then gamma-ray transmission is calculated to determine the leakage gamma flux.

The RASH and MAC programs calculate gammas by point-kernel techniques with approximate multilayer buildup factors. However,

*Present address: Mathematical Applications Group, Inc., 221 East Hartsdale Ave., Hartsdale, N.Y.

Digitized by Google

NRN uses a highly efficient slab-geometry Monte Carlo program that provides gamma heating and leakage data. Figures 1 to 3 show some typical results obtained with the RASH, MAC, and NRN codes. When these methods are applied to water-reactor shields consisting of water, iron, and concrete, they can predict fast-neutron and gamma doses that are accurate within a factor of about 3. Both RASH and NRN have been coded for Ferranti mercury computers; MAC is a FORTRAN program that is usable on the IBM-7090–7094 series and can be adapted easily to other large computers. The latest version[5] of NRN is programmed in FORTRAN IV and is operational on the IBM-7044. The latest version of RASH, RASH-F, is being programmed in FORTRAN and should soon be available.

MULTIGROUP TECHNIQUES

It is tempting to use the multigroup diffusion and transport programs[6–8] familiar to reactor analysts to perform the shield analysis. Such programs are useful to determine capture-gamma sources in the inner shield layers but are inadequate to handle deeper penetration. Generally, high-energy radiation scattered through small angles is responsible for the dose at the outer shield layers, and reactivity programs underestimate it. Analysts have obtained useful shielding results by performing multigroup calculations with P_1 theory or the Carlson S_n methods and then normalizing the high-energy fluxes or doses to the results of accurate high-energy calculations, i.e., moments method or Monte Carlo method. The P_1MG method[9] uses this technique, and Tomonto[10] has reported on a similar calculation combining the Monte Carlo and S_n methods.

The P_3MG program[11] uses a P_3 rather than a P_1 approximation to the transport equation and appears to be accurate at deep penetration (~150 cm) in slab shields without needing normalization to more refined methods.

Special versions[12,13] of the Carlson S_n program have been prepared for shielding applications. These programs can incorporate highly anisotropic angular distributions following elastic scattering and thus are able to treat more

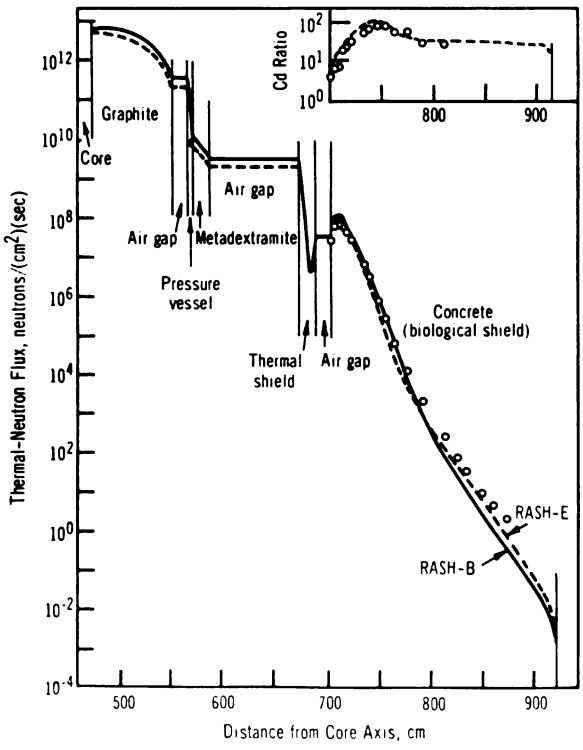

Fig. 1 Thermal-neutron flux distribution through radial bulk shield of No. 1 reactor at Calder Hall operating at 180 Mw(t) showing values calculated by RASH codes and measured data points.[27]

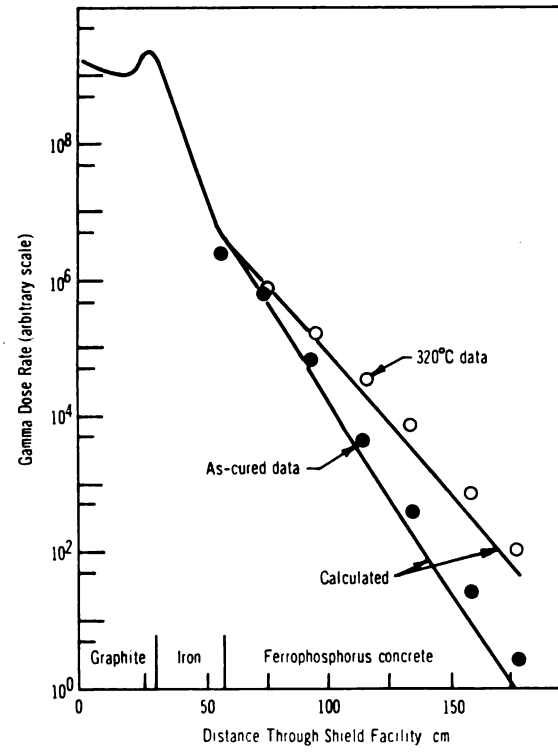

Fig. 2 Gamma distribution through Hanford Shield Facility showing points measured[28] *and curves calculated by MAC code.*[4]

Digitized by Google

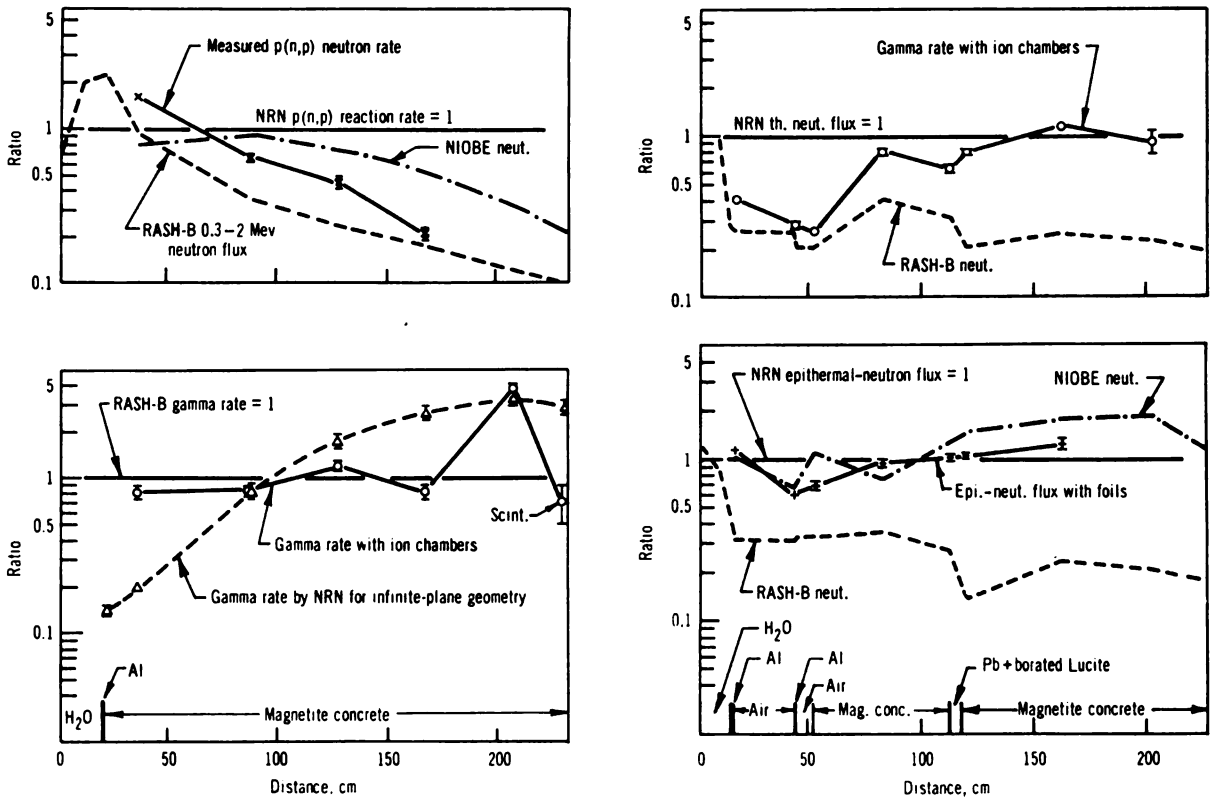

Fig. 3 Comparison of NRN, NIOBE, and RASH-B calculations with measurements for two shield configurations.[15] Note that all neutron fluxes are presented as ratios of those data to the NRN prediction. Gamma data are presented as ratios of exposure rates to the RASH-B prediction.

accurately the high-energy neutron-transport problems. Although they have not yet been applied to full power-reactor shields, they have been used successfully for limited depths of penetration, and DTF-IV has been successful in calculating gamma-ray penetration.

The NIOBE program (Numerical Integration of the Boltzmann Equation)[14] represents perhaps the most ambitious attempt at the numerical solution of the Boltzmann transport equation for neutrons and gamma rays in spherical multilayer assemblies. It has been used successfully in Europe to study power-reactor shields and to check out the RASH[2] and NRN[15] methods. The requirements of 2.5 hr of IBM-7094 time and the absence of a thermal group have restricted its application for water-reactor shields.

Complex-Geometry Problems

In power-reactor shielding the designer often is faced with the problem of determining the radiation leakage or streaming through shield penetrations, such as coolant lines or ducts, instrument tubes, and gaps around shield plugs. Shield heating problems often require that the energy deposition in particular locations in the inner shield be determined fairly accurately (within 20 to 30%). In these instances a one-dimensional representation of the shield is not adequate, and two- or three-dimensional representations are needed. Generally such problems are handled by the use of one of the following techniques: (1) point kernel, (2) combination point-kernel–multigroup, or (3) Monte Carlo.

POINT-KERNEL METHODS

The point-kernel programs break the source region into a number of equivalent point sources and determine the contribution of all such points to one or more detectors. The contribution of any point to any detector is a function of the distance between source and detector and the amount and type of material on the line joining them. A "kernel" predetermined from experiment or more exact calculation provides the material attenuation information.

Digitized by Google

The most useful application of point-kernel programs is for estimating fast-neutron dose or gamma dose. For fast-neutron dose the method is primarily used for shields containing a thick final layer of hydrogenous material. The attenuation of other layers is accounted for by the use of removal cross sections,[16] and a special kernel is used for the hydrogenous layer.[17] Nonhydrogenous shields (carbon and beryllium) have been analyzed with some success by the use of kernels derived from moments-method calculations.[18]

For gamma-ray dose calculations, the kernel is the product of the uncollided dose and a buildup factor. The latter is taken to be the buildup factor appropriate for the last layer, or one of several multilayer-buildup-factor formulas is used.[19,20] Typical programs are the GE-14-0 program[21] and the Los Alamos QAD program.[22] Each of these programs handles complicated figures of revolution.

When the radiation actually travels along the rays in question, point-kernel methods can give accurate answers. At times, however, the detector response is predominately caused by radiation that has scattered around local shielding. Then the point-kernel methods can be orders of magnitude wrong. Each problem must be examined to see if such possibilities exist. If so, then Monte Carlo techniques should be used. In fact, it would be good practice to check a point-kernel calculation for a particular shield against Monte Carlo or to experiment before this technique is used extensively.

COMBINATION POINT-KERNEL–MULTIGROUP METHODS

The various kernels discussed above generally yield information on dose, heating, or some other integral quantity. If more detailed spectral information is required, it generally can be obtained when (1) a one-dimensional problem is solved with an approximate representation of the shield layers present between the core and the detector in question and (2) the fluxes are scaled so that the computed dose equals the dose determined from a point-kernel calculation for the same detector point. The RASH, NRN, MAC, P_1MG, P_3MG, or DTF calculations can be used for the one-dimensional analysis.

MONTE CARLO METHODS

When accurate answers for complex geometries are required, the Monte Carlo programs can be used. These programs track radiation through space and simulate its actual interactions with matter. To the extent that good cross sections are available, these programs can give highly accurate answers to the shielding problem.

Two factors must be kept in mind when a complex-geometry Monte Carlo program is used: (1) if improperly used, the program will give answers with an apparently small statistical uncertainty but with a large absolute error, and (2) the running time for problems may be of the order of hours on machines in the IBM-7094 class.

The potential inaccuracy arises from the possibility that important spatial and energy radiation sources are not properly sampled. For instance, the neutron dose outside a thick water shield is produced largely by those neutrons whose initial energies are greater than 6 Mev. The Monte Carlo program may pick its source neutrons in the reactor core from a fission-spectrum energy distribution. If 1000 particles are being followed, the probability of picking a neutron above 6 Mev is so low that only approximately 20 will be picked. If these 20 are picked isotropically, few, if any, may actually enter the shield. In this situation a low emergent dose will be calculated, and the code user will be unaware of the error. An experienced shield physicist or engineer would certainly run a special high-energy-source problem to ensure that the important source energies are sampled properly.

There are several complex-geometry neutron and gamma-ray Monte Carlo programs in routine use today. The principal programs are: 05R,[23] FMC,[24] ADONIS,[25] and UNC–SAM.[26]

Some of the important characteristics of these programs are tabulated below. Because both 05R and UNC–SAM still are growing in capabilities, it is suggested that potential users contact the originating group to determine the applicability of the program to their specific problem.

Any organization contemplating the use of a complex-geometry Monte Carlo program should allow a learning period of several man-years before the program will be operational. These programs should be regarded more as experimental shielding facilities than as computer programs. They require skilled scientists or engineers for operation and continuous maintenance and adjustment by programmers to fit

Digitized by Google

new problems. These programs should be kept up-to-date as new techniques of importance sampling and routines for representing nuclear interactions are developed.

05R

Computer: Operational on CDC-1604A and IBM-7094.
Language: Combination of FORTRAN and machine language.
Geometry capability: Handles a three-dimensional array of figures bounded by planes and quadric surfaces.
Radiations: Neutrons.
Output: Produces interaction tapes that can be edited by user to evaluate fluxes, secondary gamma sources, heating, etc.
Variance reduction methods: Splitting or Russian roulette on region weights as functions of energy and position.

UNC–SAM I

Computer: Operational on CDC-1604A and Aberdeen BRLESC.
Language: FORTRAN.
Geometry capability: Handles a three-dimensional array of bounding boxes, each of which can contain up to seven boxes, spheres, cylinders, or wedges. Each of the latter can contain up to seven figures, which in turn can contain seven figures and so on. Orientation of figures inside bounding boxes is arbitrary.
Radiations: Neutrons and gamma rays.
Output: Neutron and gamma fluxes in each region or at specified points as functions of energy. Interaction tape yields secondary neutron and gamma sources and serves as source tape for secondary problem. Response functions are dose, heating, etc. Transmitted particle tape contains phase space coordinates of radiation leaving emergent face of configuration and can be used to continue problem into additional regions.
Variance reduction methods: Splitting or Russian roulette on region weights as functions of energy and position.
Cross sections for neutrons: 18 Mev to 0.037 ev (80 energy intervals) plus one thermal group; isotropic or anisotropic elastic scattering; level or continuum inelastic scattering; absorption; $(n,2n)$ reactions in beryllium. Gamma rays attenuated by Compton scattering and absorption by photoelectric and pair-production processes.
Special features: Subroutines for preparation of cross-section data from point data and to simplify geometry input.

ADONIS

Computer: Operational on IBM-7090–7094.
Language: FORTRAN and FAP.
Geometry capability: Handles a three-dimensional array of boxes.
Radiations: Neutrons and gamma rays.
Output: Neutron and gamma fluxes in each region as functions of energy. Interaction tape yields secondary gamma and neutron sources and serves as source tape for secondary problem. Response functions are dose, heating, etc. Transmitted particle tape contains phase space coordinates of radiation leaving emergent face of configuration and can be used to continue problem into additional regions.
Variance reduction methods: Splitting or Russian roulette on region weights as a function of position only.
Cross sections for neutrons: Same as UNC–SAM except that no thermal group is present.

FMC-N and FMC-G

Computer: Operational on IBM-704 and IBM-7090.
Language: Machine language.
Geometry capability: Handles a three-dimensional array of figures bounded by quadric surfaces.
Radiations: Neutrons and gamma rays.
Output: Radiation fluxes in volumes; leakage tallies; energy deposition.
Variance reduction methods: Splitting or Russian roulette on region weights as functions of energy and position; exponential transformation; statistical estimation of fluxes and leakages.
Special features: Allows reflecting boundaries to simplify geometry description.

Conclusions

Techniques are available to study water-reactor bulk shields rather quickly and with accuracies of factors of about 3 for the neutron- and gamma-leakage doses. These techniques are embodied in a variety of computer programs which, with the exception of P_3MG, use a transport kernel for the high-energy neutrons and a continuous slowing-down or multigroup slowing-down model to determine low-energy fluxes and capture gamma sources.

If geometrical considerations are important, approximate answers can be obtained by the use of point-kernel programs. These operate in a few minutes of IBM-7090 time but are of unknown accuracy. They should be normalized to either experimental results or Monte Carlo results in the same geometry.

Monte Carlo methods are available for the complex-geometry problems associated with ducts, plugs, and structural heating. When used properly, these programs are capable of accuracies of factors of 2 for neutron and gamma doses.

References

1. E. P. Blizard and T. A. Welton, The Shielding of Mobile Reactors. II. USAEC Report ORNL-1133 (Pt.2), Oak Ridge National Laboratory, June 1952.
2. A. F. Avery et al., Methods of Calculation for Use in the Design of Shields for Power Reactors, British Report AERE-R-3216, February 1960.
3. L. Hjaerne et al., A User's Manual for the NRN Shield Design Method, Swedish Report AE-145, June 1964.

Digitized by Google

4. E. G. Peterson, MAC—A Bulk Shielding Code, USAEC Report HW-73381, Hanford Atomic Products Operation, April 1962.
5. E. Aalto (Ed.), A Preliminary User's Manual for the NRN Shield Design Method in FORTRAN IV Language, Swedish Report FFA-673, RFN-213, November 1965.
6. H. P. Flatt and D. C. Baller, AIM-5, A Multigroup One-Dimensional Diffusion Code, USAEC Report NAA-SR-4694, Atomics International, March 1960.
7. B. G. Carlson et al., DTF User's Manual, UNC-Phys/Math-3321, Vol. 1, United Nuclear Corporation, November 1963.
8. W. R. Caldwell, PDQ-4, A Program for the Solution of the Neutron-Diffusion Equations in Two Dimensions on the Philco-2000, USAEC Report WAPD-TM-230, Westinghouse Electric Corporation, Bettis Atomic Power Laboratory, June 1961.
9. D. C. Anderson and K. Shure, Thermal Neutron Flux Distributions in Metal-Hydrogenous Shields, *Nucl. Sci. Eng.*, 8(3): 260-269 (1960).
10. J. R. Tomonto et al., Comparison of Neutron-Attenuation Calculations Using Monte Carlo, Transport and Diffusion-Theory Methods, *Trans. Am. Nucl. Soc.*, 8(1): 188 (June 1965).
11. K. Shure, P-3 Multigroup Calculations of Neutron Attenuation, USAEC Report WAPD-T-1563, Westinghouse Electric Corporation, Bettis Atomic Power Laboratory, May 1963; also in *Nucl. Sci. Eng.*, 19(3): 310-320 (July 1964).
12. J. H. Alexander, G. W. Hinman, and J. R. Triplett, GAPLSN—A Modified DSN Program for the Solution of the One-Dimensional Transport Equation, USAEC Report GA-4972, General Atomic Division, General Dynamics Corp., March 1964.
13. K. D. Lathrop, DFT-IV, A FORTRAN IV Program for Solving the Multigroup Transport Equation with Anisotropic Scattering, USAEC Report LA-3373, Los Alamos Scientific Laboratory, July 1965.
14. S. Preiser et al., A Program for the Numerical Integration of the Boltzmann Transport Equation NIOBE, Report UNUCOR-632, United Nuclear Corporation, March 1963.
15. E. J. Aalto, A Comparison of Shielding Calculations with Absolute Measurements in Massive Shields, *Nucl. Appl.*, 1(4): 359 (1965).
16. L. K. Zoller, Fast Neutron Removal Cross Section, *Nucleonics*, 22(8): 128 (1964).
17. R. D. Albert and T. A. Welton, A Simplified Theory of Neutron Attenuation and Its Application to Reactor Shield Design, USAEC Report WAPD-15, Westinghouse Electric Corporation, Atomic Power Division, November 1950.
18. A. D. Krumbein, Summary of NDA Unclassified Results of Moments Calculations for the Penetration of Neutrons Through Various Materials, USAEC Report NDA-92-2(Rev.), Nuclear Development Associates, Inc., April 1958.
19. H. Goldstein, *Fundamental Aspects of Radiation Shielding*, Addison-Wesley Publishing Company, Inc., Reading, Mass., 1959.
20. Yu. A. Egorov, Some Problems of Biological Shielding in Reactors, in *Reactor Shielding*, Technical Report Series, No. 34, pp. 108-122, International Atomic Energy Agency, Vienna, October 1964 (STI/DOC/10/34).
21. J. T. Martin et al., Shielding Computer Programs 14-0 and 14-1, Reactor Shield Analysis, USAEC Report TID-14360 (XDC-59-2-16), General Electric Company, Aircraft Nuclear Propulsion Department, January 1959.
22. D. M. Peterson, Los Alamos Scientific Laboratory, no formal reports available. Contact ORNL Shielding Information Center.
23. D. C. Irving et al., 05R, A General-Purpose Monte Carlo Neutron Transport Code, USAEC Report ORNL-3622, Oak Ridge National Laboratory, February 1965.
24. J. J. Loechler and J. E. MacDonald, Flexible Monte Carlo Programs FMC-N and FMC-G, USAEC Report APEX-706, General Electric Company, Flight Propulsion Laboratory Department, April 1961.
25. B. Eisenman and E. Hennessy, ADONIS—An IBM Monte Carlo Shielding Code, Report UNUCOR-635, United Nuclear Corporation, March 1963.
26. B. Eisenman and F. Nakache, UNC-SAM: A FORTRAN Monte Carlo System for the Evaluation of Neutron or Gamma-Ray Transport, Report UNC-5093, United Nuclear Corporation, August 1964.
27. J. Butler, The Status of Theoretical Methods for Reactor Shield Design, British Report AEEW-R-361, March 1964.
28. E. G. Peterson, Shielding Properties of Ferrophosphorus Concrete as a Function of Temperature, USAEC Report HW-64774, Hanford Atomic Products Operation, July 15, 1960.

Digitized by Google

Section

III

Power Reactor Technology

Control and Dynamics

Measuring Neutron-Flux Distribution in Operating Reactors

By Glenn F. Popper

Reactor economics, safety, or experimental control often provide the incentive for accurately and continuously measuring the distribution of neutron flux within a reactor core. Thus designers of both power and research reactors find it worthwhile to consider instrument systems for making such measurements.[1]

Reasons for Monitoring Flux

Greater power, burnup uniformity, safety, and radiation monitoring are among the purposes for measuring flux distribution.

Core uprating is an economic reason for monitoring the flux in a power reactor. The flux-mapping system used in the Yankee Rowe reactor, for example, confirmed a conservatism of at least 20% in the calculated maximum-to-average heat fluxes under the most unfavorable control-rod conditions.[2] On the basis of this information, the AEC authorized Yankee to increase plant gross output from 392 to 485 Mw(t) in June 1961. Power operation of core 2 began Sept. 21, 1962. Again, as happened in core 1, the in-core instruments confirmed that higher powers could be achieved. Throughout a significant portion of core 2 life, the reactor[3,4] operated at 540 Mw(t). Core 4 is expected to be able to operate at 600 Mw(t) solely because of the information obtained from the flux-monitoring system.

The economic success of the Yankee power-reactor system stimulated designers to incorporate flux-monitoring systems, of one kind or another, in the design of other reactors, such as San Onofre, Saxton, and Connecticut Yankee.[5] The Connecticut Yankee reactor, to be operational in 1967, will incorporate insertion drives similar to the Yankee flux-monitoring system but will substitute miniature ion chambers for activation wires.[6] These detectors were satisfactorily tested in the Saxton reactor in 1964. However, the Saxton reactor routinely uses a flux-wire system similar to the Yankee Rowe system. San Onofre is scheduled to use an "Aeroball" system[7] (described later).

Another example of the successful use of a flux-monitoring system to economic advantage was in the Dresden 1 reactor.[8] As a result of work with in-core ion chambers, the Dresden core was actually taken to rated power [630 Mw(t)] with 7.5% of the fuel removed. These examples show that the ability to determine experimentally, and with reasonable accuracy (~5%), the local flux distribution can create long-term economic savings that more than compensate for the high initial cost (usually greater than $50,000) of the instrument system. Other reactors that are using in-core flux-monitoring systems are Big Rock Point, Humboldt Bay, SENN, and the Japanese Power Demonstration Reactor.[9]

Uniform fuel burnup also can lead to substantial savings in either power or research reactors. With the information derived directly from the flux-monitoring-instrument system, the reactor operator can usually adjust the control rods to flatten the shape of the flux across the whole core and thereby obtain a more uniform burnup that will result in a

Digitized by Google

smaller fuel inventory and a lower fuel-management cost.

From the standpoint of reactor design, the engineer or physicist can better evaluate the core performance from fuel and thermal considerations if flux maps are available.[10] For example, wire irradiations in the SENN core have provided data that can be used either to verify present calculational methods or to provide correlation factors for use in future reactor designs. In this way, advanced designs can be realized without extreme conservatism.

SAFETY CONSIDERATIONS

Safety in large power reactors can also be an important reason for requiring in-core flux monitoring.[11] The Dresden nuclear power plant contains an operational in-core monitoring system of 64 points as required by the AEC license. This system is connected directly to the safety logic circuits. All future large prototype power reactors will probably be required to have a flux-mapping system connected to the safety system.

In the Halden Boiling Water Reactor (HBWR), core power was limited to 20 Mw(t) because of expected hot-channel factors. In-core flux measurements made with gamma thermometers verified that, with only a few in-core flux monitors connected to the safety circuit, an increase in power to 30 Mw(t) could easily be justified.[12] This 50% power increase, according to the report, represents almost $4 million per year in additional revenue.

IRRADIATION MONITOR

The experimenter using a test or research reactor for irradiation studies is almost always faced with two serious problems. First, because of the very frequent changes in the experimental equipment installed within the reactor and the subsequent control-rod-position changes required or because fuel-loading changes are necessary, an intermediate measurement of the neutron flux available at any particular irradiation location is not obtainable. The second problem is that, even after the flux has been determined, continuous changes occur with time. Hence installation of a flux-monitoring system is one solution to these problems. As a matter of convenience and economy, it would be preferable for the reactor facility to provide such a system for continuous neutron-flux-distribution measurements. However, no research or test reactor that will provide such continuous measurements is known.

Measurement Techniques in Use

Now that the reasons for making these measurements have been considered, it is appropriate to review some of the techniques with which to make neutron-flux-distribution measurements. By far the most familiar and popular method involves activation techniques.[13] This method uses any material that can detect neutrons by being measured for induced radioactivity after exposure in a neutron environment and is classed as a steady-state technique giving integral flux measurements. Materials that have well-defined absorption cross sections are usually used. Gold, indium, manganese, copper, cobalt, sulfur, and phosphorus are some common solid materials used. However, liquids or gases could also be used. The solid materials take the shape of foils, wires, pellets, or spheres; most are available commercially.[14]

FOILS

Counting techniques are readily available for foil-activity determinations, and foils are being successfully used in many reactors for neutron-flux measurements.[15] For example, gold and indium foils have been installed in the Oak Ridge Graphite Reactor for neutron-flux determinations.[16] Similar measurements[17] using both foils and wires were made in EBR-II. The activants used were ^{235}U and ^{238}U.

Wires and spheres or pellets are gaining favor over foils as a solid activant shape. Two of the reasons behind this trend are that they can be inserted into and removed from a reactor core more easily, even during reactor operation, and the commercial availability of complete wire- and ball-drive systems (Refs. 2, 7, 9, 18).

WIRES

A wire technique is used successfully in the Yankee reactor.[2] Activation wires made of carbon steel with approximately 0.5% manganese can be installed in any of 22 core positions, as shown in Fig. 1. Three separate irradiations of the eight available flux wires are required for a complete core mapping. After the wires have been irradiated about

Digitized by Google

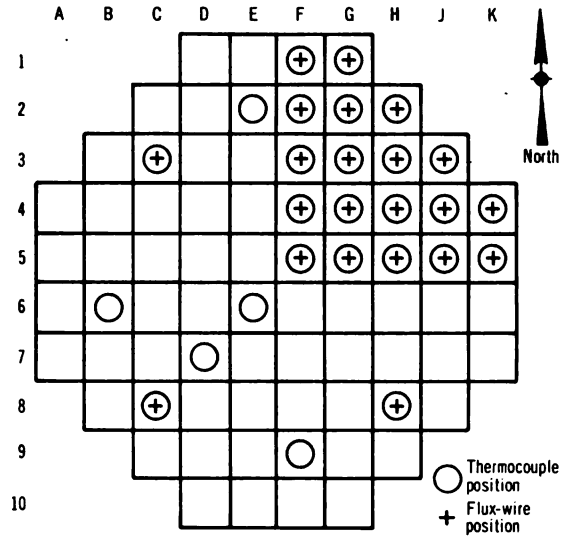

Fig. 1 Yankee in-core instrumentation showing 22 core positions into which activation wires can be inserted.[2]

4 min at 392 Mw(t), which corresponds to a time-integrated thermal flux of approximately 4.3×10^{15} neutrons/cm^2, they are withdrawn from the core and stored approximately 1 hr while the short-lived radioactive isotopes decay. The gamma activity from ^{56}Mn is then scanned with a NaI scintillation crystal–photomultiplier-tube combination. The tube current output is displayed directly on an $x-y$ plotter (x is axial core position; y is neutron flux), but it is also fed to an integrator where the integrated flux is plotted against axial core position on another $x-y$ recorder.

Activity buildup in the wires in numerous irradiations, ^{56}Mn decay during the elapsed time between irradiation and counting, wire inhomogeneity, and activation during insertion and removal require that corrections be applied to the data during reduction. These necessary corrections complicate the analysis and make fully automated data-reduction equipment expensive.

Complicated and often unique mechanisms are required for traveling-wire activation and analysis.[19] The typical mechanism shown in Fig. 2 was used in the Vulcain core experiments in the BR-3 reactor. Such a device adds significantly to the cost of the entire flux-monitoring system. The accuracy to which a wire is positioned is limited by the flexibility of the manipulation cable in the thimble and can vary by as much as 1 in. Silver or stainless-

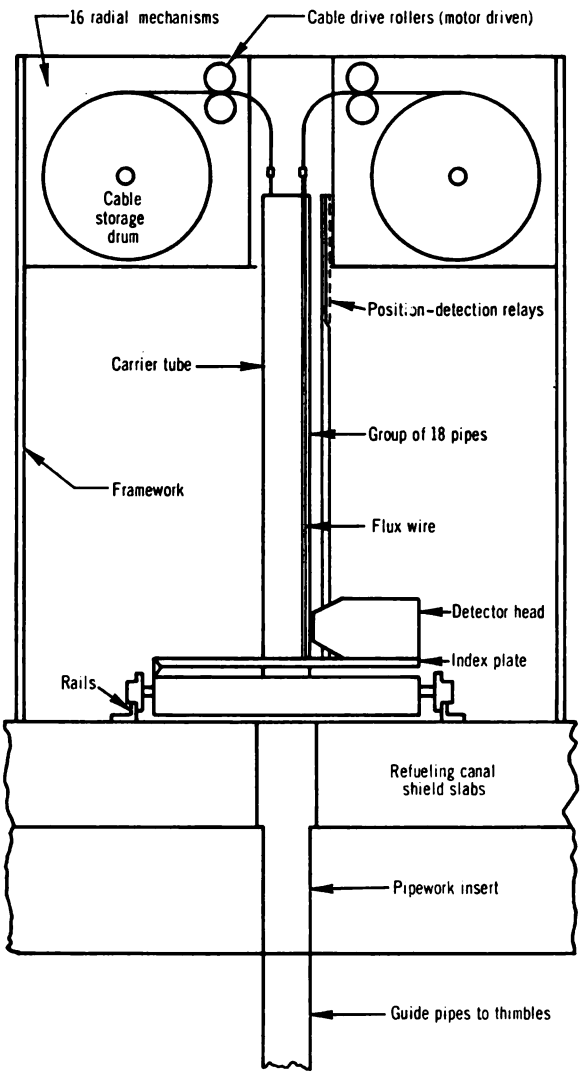

Fig. 2 Typical mechanism for traveling-wire activation and analysis showing general arrangement of flux-plotting machine[12] *for the BR-3 reactor.*

steel neutron absorbers have been fixed to the detector thimbles at the top and bottom of the core to overcome these positioning errors (by providing fixed reference points on the wire). Position accuracy,[20] determined by the absorber-placement accuracy, is 0.06 in.

SPHERES

A spherical shape is also being used for activation and has certain advantages over wires.[7,12,21] The very small sphere has sufficiently low radioactivant concentration to keep self-shielding low and approaches the ideal point detector for isotropic flux determination.

Digitized by Google

This shape eliminates obliquity variations and results in insignificant flux depression and perturbation factors. Because the spheres are inserted into and withdrawn from the reactor core pneumatically, there is no need for the expensive and bulky shielding that is necessary for the highly activated portions of the manipulation cable used with wire-drive systems. The pneumatic system, however, must be vented to an exhaust stack. Because of the positive thimble stops, the chain of spheres can be positioned very inexpensively, quickly, and more accurately in the core than can wires. The spheres are also particularly adaptable to a cheaper automatic-analysis technique because the system can count individual spheres. Correlation between each sphere and core position is well defined and limited only by the measurement accuracy of the ball or head stops. However, when individual spheres are counted, a direct indication of relative flux distribution is not available.

EBWR EXPERIENCE

Small, approximately 0.063-in.-diameter, aluminum–1% cobalt spheres (Fig. 3) were inserted pneumatically into six tubes located in selected core positions in the EBWR.[21] The spheres were encapsulated in small pieces of stainless-steel tubing, 0.096 in. in inside diameter, by forming the tubing over the end beads of 0.058-in. commercial stainless-steel bead chain, and thereby provided an easy means for accurately spacing the activant spheres. One disadvantage was that the capsules had to be machined open with a small lathe in a glove box to retrieve the spheres. This problem could be overcome by the use of aluminum or plastic tubing that is opened with a simple cutter. A sample changer was used so that individual spheres could be pneumatically transferred to a detector assembly, counted, and then returned to an indexed storage location in the changer. A multichannel analyzer with automatic printout was used for routine analysis of each sphere. Plans to use a slightly modified version of the system for the Plutonium Recycle Test Program are being made.

AEROBALL SYSTEM

More recently Westinghouse has developed the "Aeroball" system, in which in-core flux monitoring is accomplished by the pneumatic

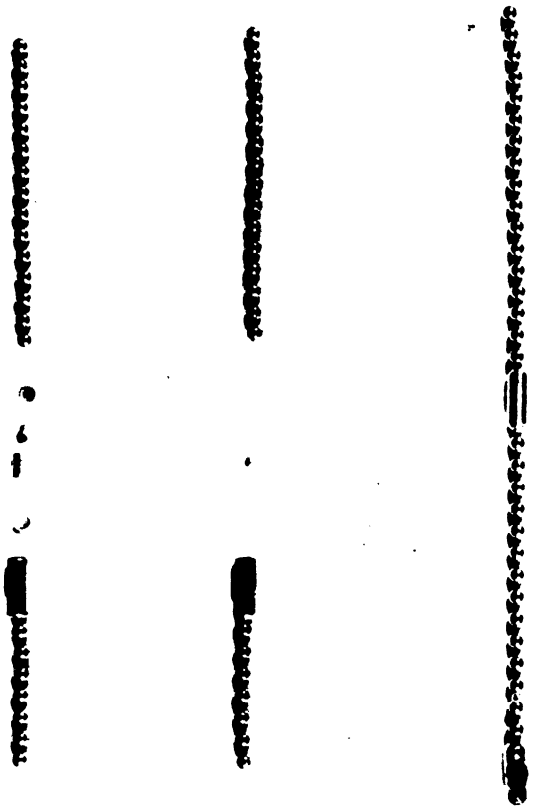

Fig. 3 Stainless-steel tubing encapsulates aluminum–1% cobalt spheres inserted into six tubes located in selected EBWR core positions.[21]

movement of a column of separate 0.063-in.-diameter balls into the core for irradiation and then to a scintillation detector for scanning. This system is being used in the SELNI reactor in Italy and in the San Onofre reactor.[7,12] The Aeroball thimbles, shown in Fig. 4, enter the San Onofre vessel through five spare control-rod ports and are then routed into selected core positions. The ball set used in each thimble is irradiated, put into storage, and then moved individually by diverter valves to a rotary readout table for detection. The ball set to be scanned enters the table and is formed into a horizontal circle around the counting table. The table then rotates past the scintillation detector and the 1-in.-wide collimator; 16 balls are scanned at a time, and the integral flux is plotted. Results from the SELNI system show that a more detailed flux profile can be obtained with a narrower collimator.

GAS ACTIVANTS

Gases are also being used as activants.[22] Argon is an excellent monitor of thermal-

Digitized by Google

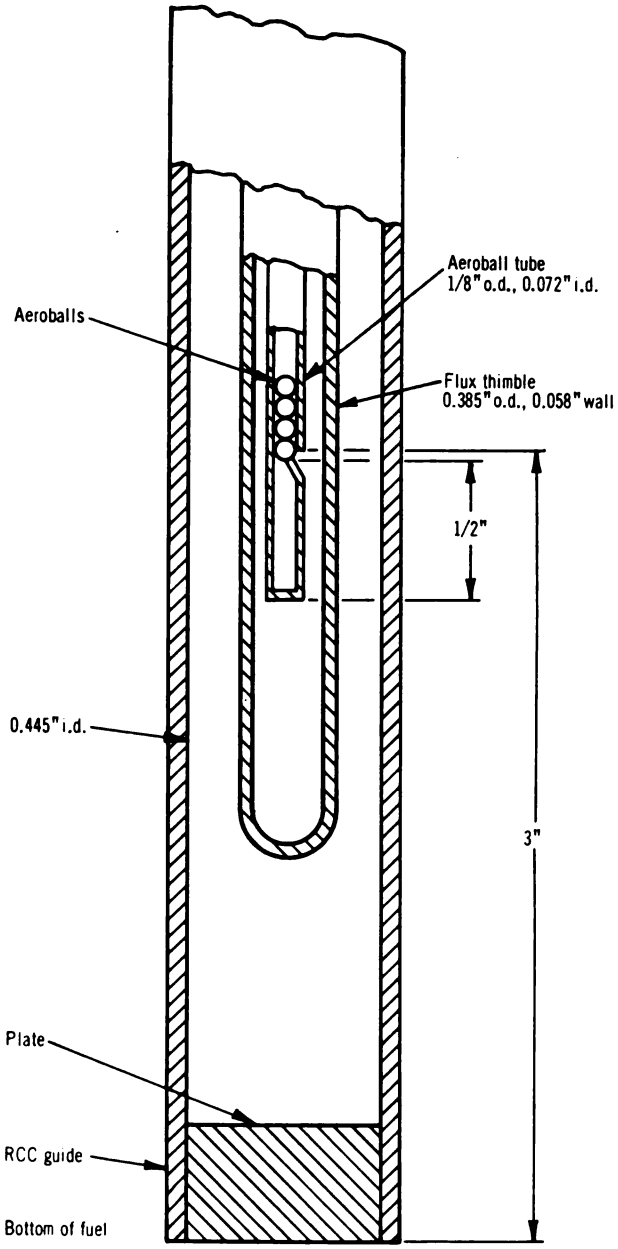

Fig. 4 Aeroball system for monitoring flux uses 0.063-in.-diameter balls that are moved pneumatically in thimbles within core, irradiated, then scanned by scintillation detector.[7] This system will be used in the SELNI and San Onofre reactors.

neutron flux. The only significant isotope, ^{40}Ar (99.6%), has a 0.53-barn thermal-neutron-absorption cross section with no resonance peaks. The other isotopes do not decay with gamma emission after neutron capture. Neutron capture transmutes ^{40}Ar into ^{41}Ar, which decays by emitting a 1.29-Mev gamma photon in 99% of the disintegrations. Since argon decays to stable daughters, it is not a source of contamination and can also be used as an inert protective atmosphere.

This argon-activation method was used to measure neutron flux in an irradiation experiment in the ORR. The argon gas flows in and out of the irradiation capsule through concentric tubes that are small compared to the capsule. This size difference produces a much higher gas flow rate through the tubes, compared to the flow through the capsule, and causes a lower activation in the tubes for a given flux density. Since most of the tubes are located in a much lower neutron flux than the capsule, all the activation can be assumed to occur within the capsule. However, since exposure time is sensitive to capsule temperature, an empirical correction must be made. The delay time between activation and detection, usually only a few seconds, depends on the gas flow rate and the flow path length between capsule and detector. The largest error in flux determination is attributed to the approximate 10% accuracy of the gamma-spectrometer detector. Moving the capsule in the irradiation thimble permitted neutron-flux distributions to be obtained.

NEUTRON SPECTRUM

The various analytical methods used to determine a neutron spectrum from activation measurements range from simple calculations, requiring minimum cross-section information, to complex computer techniques, requiring detailed information that reproduce the spectrum with high-energy resolution. The five basic methods currently being considered are:[13] (1) a resonance-reaction method, (2) an age-measurement method, (3) an effective threshold-reaction method, (4) a polygonal or polynomial method, and (5) an orthonormal-expansion method. In all cases the selection of a specific radioactivant material to define a desired neutron energy is a great problem. Additional work is needed in this area of material selection, especially for measurements to be made in the 10^3-ev neutron region.

MINIATURE ION CHAMBERS

Although activation techniques will continue to be necessary for neutron-spectrum measurements, miniature ion chambers are rapidly replacing activants as in-core flux-distribution

Digitized by Google

detectors. These ion chambers are small (some with diameters <0.090 in. and only 1 in. long) and have linear response and continuous outputs. Nearly the entire flux range [from about 10^4 neutrons/(cm^2)(sec) up to about 10^{14} neutrons/(cm^2)(sec)] of today's cores can be monitored by in-core ion chambers.[23]

Fixed-position in-core ion chambers, as shown in Fig. 5, have been used to monitor neutron-flux distribution in the Dresden 1 reactor (Refs. 8, 11, 20, 24, 25). The Dresden in-core power-monitoring array consists of 16

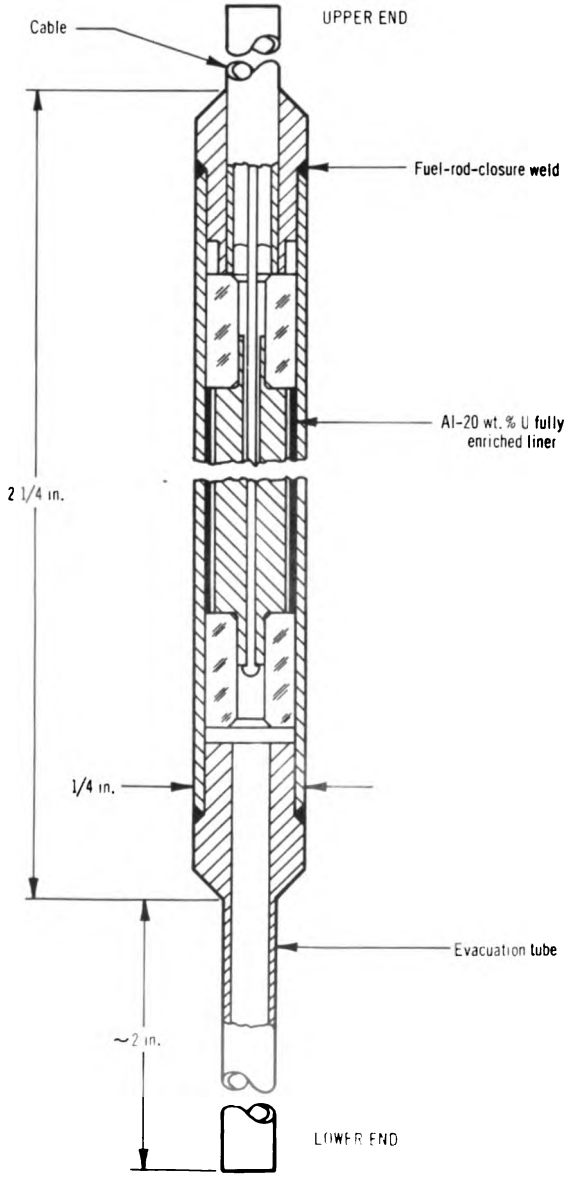

Fig. 5 Fixed-position in-core ion chambers of the type used to monitor neutron-flux distribution in the Dresden 1 reactor.[20]

assemblies for determination of radial distribution, each of which includes four ion chambers distributed at discrete elevations to determine axial distribution. A dry thimble to accept an activation wire for calibration purposes is also included in each assembly. The chambers are calibrated at low power to correct for variations in the "as-built" sensitivity. Calibration is accomplished by the insertion of a copper–titanium wire in each of the 16 ion-chamber guide thimbles during operation at approximately 50 Mw(t) and by irradiation for about 3 hr. The relative calibration of each ion chamber is then attained when the individual outputs are corrected to give a flux distribution equal to that obtained from the irradiated-wire distributions. Thereafter accuracy of about 5% is achieved. Calibrations are made as needed for correction of burnup of the fissionable uranium coating used in the chamber to render it neutron sensitive. The coating is an aluminum–20 wt.% fully enriched uranium alloy. The life of such a chamber is relatively short; 50% uranium-coating burnup corresponds to an integrated neutron flux of approximately 10^{21} neutrons/cm^2, approximately nine months in the Dresden reactor.[20]

Traversing ion chambers are rapidly becoming the most popular means of monitoring neutron-flux distribution in reactor cores.[9] Much longer lives are achieved because of the shorter core-exposure time. A system that uses activation wires for low-power operation [~10^9 to 10^{11} neutrons/(cm^2)(sec)] and traversing ion chambers for high-power operation [~10^{11} to 10^{13} neutrons/(cm^2)(sec)] was planned for the Experimental Gas-Cooled Reactor.[24,26] The ion chambers were to be used as the primary means of monitoring neutron flux in the core. The chamber-cable probes would be inserted into 18 thimbles, and a flexible multiple-strand cable would serve to position the chambers in the core. The center of this cable would be filled with a triaxial electrical lead. The outer wire strand of the cable would be an open helix and would mesh with a geared drive wheel either manually or electrically driven.

The chamber components and wires of the cable would be made of commercially pure titanium; quartz fiber was specified as electrical insulation in the cable. Forsterite would act as an electrical insulator in the chamber which was lined with ^{10}B and would have a thermal capability of 1200°F. This ^{10}B coating

Digitized by Google

was selected to minimize the radioactivity of the chamber assembly after withdrawal from the core. The relatively rapid burnup of the boron (33% at 10^{20} neutrons/cm^2) is acceptable because the probes would be used for periodic traverses only. Recorders in the control room plot neutron flux against position along the path of travel through the core. The positioning accuracy would be the same as with wire-drive systems.

THERMOMETERS

Gamma and neutron thermometers have also been applied to the measurement of neutron flux.[19,20] By this method, measurement is made of the temperature rise above ambient caused by fission or gamma heating. Several practical devices have been developed, but none are known to be available commercially.[27–30] Nevertheless, thermometer type sensors continue to be alluring as detectors. The obvious advantages of basic simplicity, easy construction, and simple readout systems are joined with the possibility of making a detector that physically resembles the fuel element. This could result in a power monitor, in contrast to a neutron-flux monitor. The problem of analytically relating the neutron flux to local power could then be eliminated, if local power actually is the desired parameter.

The neutron thermometer[20] used by Du Pont at Savannah River is shown in Fig. 6. This consists of a thermocouple with a uranium–aluminum button welded to the hot-junction end. The heat generated in the button increases the temperature of the sample thermocouple above that of the reference. The difference signal is proportional to the neutron flux. Although this thermometer has shown a sensitivity of about 5°C per 10^{12} neutrons/(cm^2)(sec), it is limited by the uranium burnup. Sensitivity would be reduced about 10% at 5×10^{22} neutrons/cm^2. The time response is about 0.5 sec.

SOLID-STATE DEVICES

Solid-state devices[31,32] have proved useful as compact neutron detectors for measuring flux distribution in critical experiments and in reactors in which the flux is in the range of 10^4 to 10^{11} neutrons/(cm^2)(sec). Operation in high flux is impractical because a dose of 10^{13} neutrons/cm^2 damages the semiconductor crystal lattice. For example, the device has a life of only 100 sec in a flux of 10^{11} neutrons/(cm^2)(sec). The operators overcame this difficulty by removing the semiconductor from the reactor core but leaving a fissionable target within an evacuated tube that extends into the core region.[33] The detector then counts fission fragments from the target, and the neutron-flux distribution can be plotted if the target and tube are moved within the core. This method measures neutron flux directly within 3%, and the target position is accurately known. This method can be used in fluxes up to approximately 10^{15} neutrons/(cm^2)(sec).

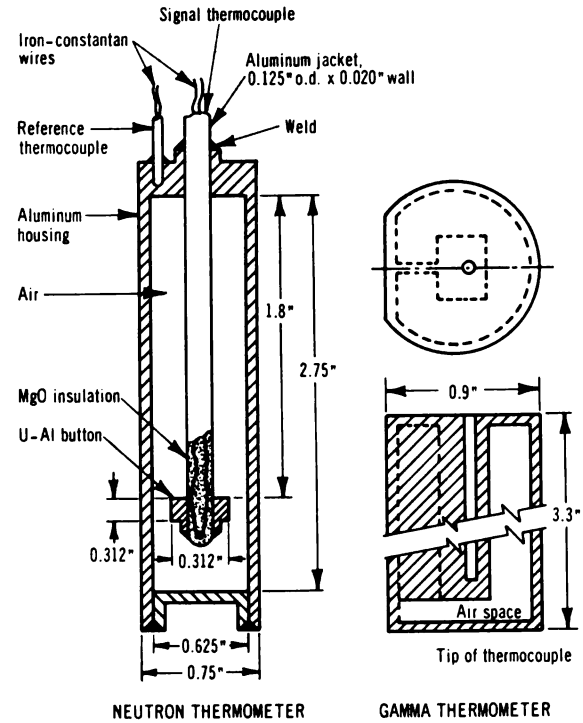

Fig. 6 Neutron and gamma thermometers. Heat generated in uranium–aluminum button raises temperature above that of reference thermocouple, and the neutron flux is determined from the difference signal, which is proportional to the neutron flux.[20] Gamma thermometer measures temperature rise above ambient caused by gamma heating.

Advanced Techniques

All the previously discussed devices or systems have been or are now being used.

Self-powered neutron detectors are being developed for advanced systems.[34,35] The neutron detector is made in the form of a coaxial cable, as shown in Fig. 7. The current produced in the detector comes from neutron-induced radioactivity. Detectors using ^{27}Al, ^{115}In, ^{109}Ag, and other elements have been built, and operational data are available. With a rhodium emitter this

Digitized by Google

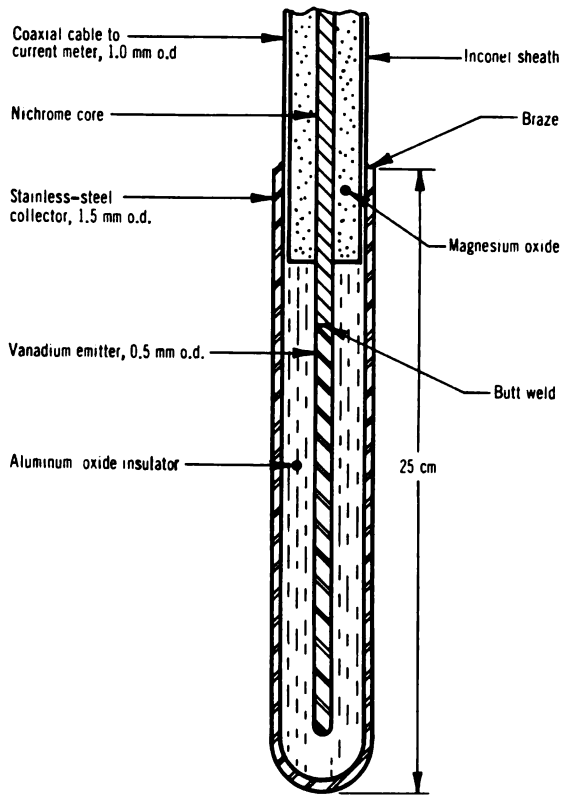

Fig. 7 Self-powered neutron detector is constructed in coaxial cable form; current is produced when emitter, in this case vanadium, becomes radioactive by neutron capture.[12]

detector is predicted to have a life 4 times longer than ^{235}U-coated detectors and 30 times longer than those coated with ^{10}B. However, it has only recently been introduced as a commercially available device.[36]

Noise systems. The neutron-induced current in an ion chamber is caused by a large number of individual pulses. The current is composed of the steady-state and the varying or noise components. The average noise power, or steady-state signal, is proportional to the neutron flux, and the average deviation, or noise component, is proportional to the square root of flux.[37,38] A practical system using the noise component has been developed.[23] This system improves gamma discrimination and eliminates d-c cable leakage interference currents. Hence it can be used in higher temperature and higher flux applications.

Microwave techniques are also being investigated as a method for neutron-flux measurements.[39–44] The basic applicable principle is that the propagation characteristics of microwave energy change as the waves traverse a gas that is ionized by neutron bombardment. These effects can be feasibly exploited for a practical system. The first suggests that the attenuation and/or velocity of propagation of microwaves traversing a gas plasma is a function of the degree of gas ionization. The second predicts that there will be cross coupling of microwave energy between two wave guides piercing a common plasma and is likewise dependent on plasma ionization. The third effect simply is that a wave guide surrounded by an ionized plasma will have induced in it microwave noise signals that can be measured. Laboratory measurements have confirmed the first two effects under simulated reactor conditions. Research on these detectors is in the early stages, but the results are encouraging.

Regenerative detectors. The useful life of a neutron detector is often limited if activant or fissionable materials are used. The useful lifetime during which neutron detectors can provide accurate, reliable in-core measurements can be substantially prolonged if the sensing element incorporates regenerating materials such that new fissile atoms are created from fertile atoms as the original fissile atoms are depleted.[45–47] Detector life can be increased by a factor of over 2.5 under certain conditions,[48] e.g., in ion chambers using a mixture of both ^{234}U and ^{235}U as the fissionable material. The mixture used will depend on the type of reactor being instrumented. In addition to extending the lifetime of in-core flux monitors, regenerating detectors will minimize the need to calibrate the system as often as for fully enriched ^{235}U detectors.

Factors Affecting Method Choice

Before a designer can select any particular method for measuring neutron-flux-distribution data, usage must be planned. Since neutron flux is three dimensional, measurements must usually be made in both the axial and radial directions. The reactor design greatly influences the choice of an instrument. The instrument system must be able to withstand the temperature, pressure, neutron-flux level, and medium. Cost and available manpower are both important factors because the development of new systems can be very expensive. Table 1 summarizes the techniques used for neutron-flux-distribution measurements and lists some of the limitations and significant characteristics.

Digitized by Google

Table 1 CHARACTERISTICS OF NEUTRON-FLUX-DISTRIBUTION MEASUREMENT TECHNIQUES

Technique	Detector available commercially	System available commercially	Approximate cost of detector system	Neutron-flux range, neutrons/(cm²)(sec)	Detector life in 10^{13} neutrons/(cm²)(sec) flux	Axial resolution	For safety circuits	Readout
			Activants					
Foils	Yes	Yes	< $1000–10,000	$10^3 - 10^{15}$	<3 months	Limited	No	Integrated
Wires				$10^3 - 10^{15}$	<1 year	Continuous	No	
Stationary	Yes	Yes	$1000–10,000					Integrated
Traveling	Yes	Yes	> $50,000					Delayed
Spheres	Yes	Yes	< $1000–50,000	$10^3 - 10^{15}$	<3 months	Limited	No	Delayed
Gas	Yes	No	< $1000–10,000	$10^3 - 10^{15}$	<1 day	Limited	Yes	Delayed
			Sensors					Continuous
Stationary		Yes	> $50,000			Limited	Yes	
Traveling		Yes	> $50,000			Continuous	No	
Ion chambers								
Stationary	Yes		$1000–10,000	$10^{10} - 10^{14}$	<1 year			
Traveling	Yes		$1000–10,000	$10^{10} - 10^{14}$	<1 year			
Noise	Yes		$1000–10,000	$10^7 - 10^{14}$	<1 year			
Regenerative	Yes		$1000–10,000	$10^{10} - 10^{14}$	>1 year			
Gamma, neutron thermometers	No				<1 year			
Solid-state	?		< $1000	$10^4 - 10^{11}$	<1 day			
Self-powered	Yes		< $1000	$10^9 - 10^{15}$	>1 year			
Microwave	No			Experimental	>1 year			

References

1. *Power Reactor Technol.*, 4(4): 34-36 (September 1961).
2. A. J. Kompanek, Jr., and E. C. Tarnuzzer, Neutron-Activated Wires Plot Fluxes in Yankee Core, *Nucleonics*, 20(2): 44-46 (February 1962).
3. H. W. Graves, Jr., and J. E. Howard, Nuclear Performance of Yankee Core I, USAEC Report TID-7672, pp. 1-32, February 1964.
4. J. D. McGaugh and R. H. Chastain, Power Density and Burnup Distributions in Yankee Core I, USAEC Report WCAP-6051, Westinghouse Electric Corporation, Atomic Power Division, January 1963.
5. R. A. Creagan and A. R. Jones, How Far Can We Go with PWRs?, *Nucleonics*, 21(6): 64-67 (June 1963).
6. Connecticut Yankee Atomic Power Company, Design and Engineering Annual Report, July 1964–June 1965, USAEC Report TID-22288, August 1965.
7. W. D. Leggett III, In-Core Instrumentation for the San Onofre Nuclear Generating Station, USAEC Report WCAP-3269-46, Westinghouse Electric Corporation, Atomic Power Division, March 1965.
8. J. Forster, Ion-Chamber Systems, *Nucleonics*, 20(2): 50-51, 54 (February 1962).
9. J. J. Forster, In-Core Neutron Flux Instrumentation, *IEEE Trans. Nucl. Sci.*, NS-12(6): 8-14 (December 1965).
10. C. E. Foreman, SENN Wire-Irradiation System Used To Evaluate Power-Distribution Calculations, *Trans. Am. Nucl. Soc.*, 8(Suppl.): 23-24 (July 1965).
11. Proceedings of the Power Reactor In-Core Instrumentation Meeting, Washington, D. C., April 28–29, 1960, USAEC Report TID-7598, p. 55, March 1961.
12. Symposium on In-Core Instrumentation, Oslo, Norway, June 15–19, 1964, Report CONF-640607, Vols. I and II.
13. J. Moteff, Neutron Flux and Spectrum Measurement with Radioactivants, *Nucleonics*, 20(12): 56-60 (December 1962).
14. Data Sheet B-11, Reactor Experiments, Inc., Belmont, Calif.
15. C. W. Tittle, Slow Neutron Detection by Foils—I, *Nucleonics*, 8(6): 5-9 (June 1951).
16. E. D. Klema and R. H. Ritchie, Thermal Neutron Flux Measurements in Graphite Using Gold and Indium Foils, *Phys. Rev.*, 87(1): 167 (July 1952).
17. F. S. Kirn and W. B. Loewenstein, EBR-II Wet Critical Experiments, USAEC Report ANL-6864, Argonne National Laboratory, October 1964.
18. C. Roderik (Ed.), Large Closed-Cycle Water Reactor Research and Development Program, Progress Report, January 1–March 31, 1956, USAEC Report WCAP-3269-12, Westinghouse Electric Corporation, Atomic Power Division.
19. Advanced Course on In-Core Instrumentation for Water Cooled Reactors, organized by the Netherlands'–Norwegian Reactor School at Institutt for Atomenergi, Kjeller, Norway, August 21–September 1, 1961, Report NP-11754 (Vol. I), 1961.
20. R. W. Bowring (Ed.), Proceedings of the Boiling Water Reactor In-Core Instrumentation Meeting, Halden, May 15–18, 1961, Norwegian Report HPR-16, December 1961.
21. W. G. Knapp, Method for Neutron Flux Studies in an Operating Power Reactor Using Bare and Cadmium Covered Radioactivants, USAEC Report ANL-7011, Argonne National Laboratory, March 1965.
22. R. M. Carroll, Argon Activation Measures Irradiation Flux Continuously, *Nucleonics*, 20(2): 42-43 (February 1962).
23. R. A. DuBridge and W. K. Green, A Full-Range In-Reactor-Core Neutron Monitoring System Employing Ion Chambers, USAEC Report GEAP-

Digitized by Google

4643, General Electric Company, Atomic Power Equipment Department, June 1964.
24. L. E. Link (Ed.), Reactor Technology, Selected Reviews—1964, USAEC Report TID-8540, July 1964.
25. Commonwealth Edison Company and General Electric Company, Test Operation of the Dresden Reactor at Power Levels to 315 Mw, Report No. 3, Report NP-14271, Apr. 27, 1960.
26. Oak Ridge National Laboratory, Revisions to Experimental Gas Cooled Reactor, Final Hazards Summary Report, Volume I, Description and Hazards Evaluation, USAEC Report ORO-586 (Vol. I)(Suppl. 1), April 1965.
27. A. C. Lapsley and R. R. Ingham, Internal Flux Measurements, in Proceedings of the Sixth Tripartite Instrumentation Conference, Chalk River, Ontario, April 20–24, 1959, Canadian Report AECL-801, pp. 55-60, Dec. 5, 1960.
28. C. K. Smith, C. V. Weaver, J. W. Chastain, and S. L. Fawcett, The Development of a Thermal-Neutron-Flux Measuring Instrument, USAEC Report BMI-1083, Battelle Memorial Institute, Apr. 12, 1956.
29. J. Ager-Hanssen and R. D. Smith, Advanced In-Core Instrumentation from Halden, *Nucleonics*, 22(4): 49-56 (April 1964).
30. R. A. DuBridge, Detectors for In-Core Power Monitoring, USAEC Report GEAP-4222, General Electric Company, Atomic Power Equipment Department, Apr. 1, 1963.
31. R. V. Babcock, R. E. Davis, S. L. Ruby, K. H. Sun, and E. D. Wolley, Coated Semiconductor in Tiny Neutron Detector, *Nucleonics*, 17(4): 116-122 (April 1959).
32. R. Steinberg, Rapid Flux Mapping in MTR Fuel Elements, *Nucleonics*, 19(4): 102-104 (April 1961).
33. V. Ajdacic, M. Kurepa, and B. Lalovic, Semiconductor Measures Fluxes in Operating Core, *Nucleonics*, 20(2): 47-49 (February 1962).
34. J. W. Hilborn, Self-Powered Neutron Detectors for Reactor Flux Monitoring, *Nucleonics*, 22(2): 69-72, 74 (February 1964).
35. General Electric Company, Nuclear Materials and Propulsion Operation, Reactor Instrumentation and Control Progress Report No. 88, USAEC Report GEMP-88, May 28, 1965.
36. Engineering Data Sheet, RSN-202-M1, 1965 Reuter–Stokes Electronic Components, Inc., Cleveland, Ohio.
37. N. R. Campbell, *Proc. Cambridge Phil. Soc.*, 15: 117, 310, 513 (1909–1910).
38. R. A DuBridge, Mean Square Voltage Fluctuation Measurements with Neutron Sensitive Ion Chambers, *Trans. Am. Nucl. Soc.*, 6(2): 306-307 (November 1963).
39. M. M. Hendrickson and J. K. Green (Eds.), Research and Development Programs Executed for the Division of Reactor Development, Quarterly Progress Report, July–September 1963, USAEC Report HW-79280, Hanford Atomic Products Operation, October 1963.
40. J. K. Green (Ed.), Research and Development Programs Executed for the Division of Reactor Development, Quarterly Progress Report, October–December 1963, USAEC Report HW-80284, Hanford Atomic Products Operation, April 1964.
41. J. K. Green (Ed.), Research and Development Programs Executed for the Division of Reactor Development, Quarterly Progress Report, January–March 1964, USAEC Report HW-81984, Hanford Atomic Products Operation, September 1964.
42. J. K. Green (Ed.), Research and Development Programs Executed for the Division of Reactor Development, Quarterly Progress Report, April–June 1964, USAEC Report HW-83298, Hanford Atomic Products Operation, November 1964.
43. J. K. Green (Ed.), Research and Development Programs Executed for the Division of Reactor Development, Quarterly Progress Report, July–September 1964, USAEC Report HW-84384, Hanford Atomic Products Operation, December 1964.
44. J. K. Green (Ed.), Research and Development Programs Executed for the Division of Reactor Development, Quarterly Progress Report, October–December 1964, USAEC Report HW-84609, Hanford Atomic Products Operation, December 1964.
45. D. E. Hegberg, Feasibility Study of In-Core Neutron Flux Monitoring with Regenerating Detectors, USAEC Report HW-73335, Hanford Atomic Products Operation, June 1962.
46. W. L. Bunch, Technique for Optimizing the Composition of Regenerating Neutron Flux Monitors, *Trans. Am. Nucl. Soc.*, 7(2): 319 (November 1964).
47. W. R. Loosemore and J. A. Dennis, The Continuous Measurement of Thermal-Nuetron Flux Intensity in High-Power Nuclear Reactors, *J. Brit. Nucl. Energy Soc.*, 1: 109 (April 1962).
48 W. L. Bunch and M. R. Wood, Initial Operating Characteristics of Regenerating In-Core Neutron Chambers, USAEC Report BNWL-14, Pacific Northwest Laboratory, January 1965.

Digitized by Google

Section

IV

Power Reactor Technology

Fluid and Thermal Technology

What's New in Two-Phase Flow

By Hans K. Fauske

Two-phase flow is a key factor in both thermal- and fast-reactor design and safety. However, because flow problems occur in many industries and branches of engineering, it is difficult for engineers concerned with two-phase flow to keep abreast of the progress reported in diverse publications. Thus the Symposium on Two-Phase Flow that was held at Exeter, England, June 21–23, 1965, provided a needed opportunity for about 200 engineers of various specialties from different countries to communicate concerning the latest developments in this area.

The symposium concentrated heavily on "microscopic" aspects of two-phase flow. Although a few of the papers presented information in a form that can be used in reactor design, most of them indicated methods and approaches for discovering basic information on two-phase flow and heat transfer. More specifically, they contributed importantly toward the displacement of classical two-phase-flow empirical engineering by sound physical and theoretical mathematical approaches that can be extrapolated with much greater assurance to pressures, flows, fluids, and geometries other than those tested.

A summary of the 40 papers presented at the symposium, which was sponsored by the University of Exeter, will acquaint reactor designers with some of the topics discussed, which included flow regimes, wave mechanics, void fractions and holdup, two-phase flow characteristics, nucleate and film boiling, entrainment, flooding, critical flow, and two-phase flow dynamics.

Flow Regimes

Detailed descriptions of the flow regimes and the regions at which transition takes place from one regime to the next must be known to describe adequately the heat transfer and pressure drop in two-phase systems.

An experimental study[1] of air–water mixtures included observations on flow regimes and their transitions (Fig. 1). The slug–churn transition and the churn–annular transition were described in detail.

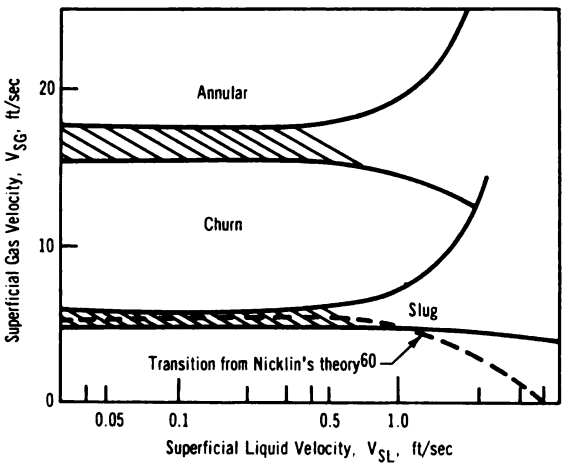

Fig. 1 Visually observed flow regimes and transitions of air–water mixtures,[1] as compared to transition predicted by Nicklin's theory.[60]

VERTICAL FLOW

In an investigation of adiabatic upward flow of gas–liquid mixtures, measurements were made of droplet entrainment by the gas core and the mean film thickness.[2] Interface aspects were observed, and the ratio between liquid film and total liquid flow rates were related to volumetric kinetic energy of the gas ($\rho_G V_{SG}^2/2$), the

Digitized by Google

liquid flow rate, and liquid physical properties. The mean film thickness depended on gas volumetric kinetic energy, but not on the total liquid flow rate.

Aspects of mass transfer of entrained liquid in vertical upflow of air–water were investigated[3] in a 0.375-in.-bore tube with column inlet pressures of 25 to 40 psia. Some conclusions were: (1) a certain minimum length of tube is required before entrainment starts, (2) no apparent equilibrium is established even after long lengths, and (3) for a particular gas flow rate, there is a critical liquid flow rate below which entrainment does not occur. Order-of-magnitude estimates were made of droplet mass-transfer coefficients.

Flow regimes, entrainment, mass interchange, and liquid deposition are critically important to the understanding of the burnout phenomenon in high-quality mixtures. Because two-component mixtures were used in the tests, the results cannot be applied directly. However, the data are useful in predicting the forms and trends to be expected in burnout data.

HORIZONTAL FLOW

An experimental and analytical study[4] used air and mineral oil to determine how the rate of atomization (liquid film), equilibrium ratio (between liquid flowing as film and liquid flowing as mist), and pressure drop in horizontal mist–annular flow is affected by fluid properties and pipe diameter in the range 51 to 140 mm. Atomization increased with film flow rate and gas velocity but decreased with pipe diameter. For the equilibrium fraction, $1-\psi_e$, the correlation was established that:

$$(1-\psi_e) = 1.247 + 1.04 \ln [Re_G^{1/3} Re_L^{2/3} We^{1/3} \times (M_L/M_G)^{1/3} (\rho_G/\rho_L)^2]$$

where Re_G equals $\rho_S V_{SG} D/\mu_G$, Re_L equals $\rho_L V_{SL} D/\mu_L$, and We equals $\rho_G V_{SG}^2 D/\sigma$.

The film thickness was calculated from measured pressure drop and film flow rate.

A test facility has been built at Queen Mary College, University of London, to study the annular flow regime and the mechanism of dry-out of the liquid film.[5] The high-pressure-steam heat source makes operation possible under dry-out conditions. The facility, which has a wide variety of instrumentation and permits visual observation of test-section flow, will enable experiments that should contribute significantly toward the solution of the burnout problem in the net boiling regime.

Two-Phase Wave Mechanics

The symposium concentrated heavily on "microscopic" aspects of two-phase flow, as illustrated by the papers dealing with studies of the mechanism of wave formation. Although these papers do not furnish design criteria directly, they are extremely important contributions toward the overall understanding of two-phase flows. They are prime examples of the kinds of experiments and analyses that are needed to improve the technology.

A theoretical analysis that concentrated mainly on the regime of roll waves was presented.[6] The method is intended to predict the wave size, speed, spacing, local film thickness, and the corresponding two-phase pressure drop. A new experimental facility will be used for measurements of the variables predicted by the analysis; it will test air–water and water–oil mixtures.

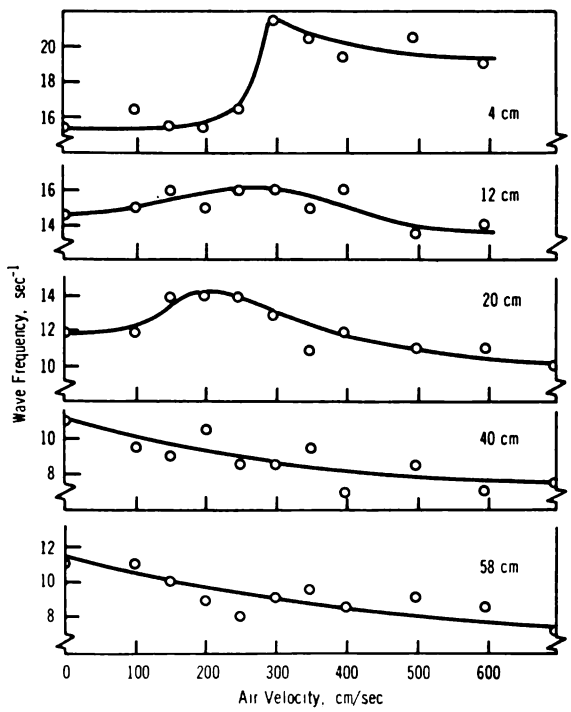

Fig. 2 Effect of countercurrent air velocity on free-surface wave frequencies of a liquid film falling down (Re_L = 80) a vertical surface, as measured at various tube positions.[7]

Digitized by Google

The effect of a countercurrent stream of air on the free-surface profile of a liquid film falling down a vertical surface was described.[7] A sensitive light-absorption technique was used to measure wave properties such as frequency, amplitude, and velocity as functions of liquid Reynolds number and vertical distance fallen by the film. The effects of countercurrent air velocities up to 750 cm/sec were examined; Fig. 2 shows the effect of air velocity on wave frequencies.

Measurements of turbulence-intensity correlation coefficients and local shear stress at several gas Reynolds numbers and positions from a wavy boundary were reported.[8] The influence of the liquid-film wave behavior on the gas phase was simulated with a flexible sheet that mechanically created standing waves that could be oscillated at adjustable frequencies (Fig. 3). Spectral analysis of the measurements suggested that one mode by which the interface acts is to shift the scale of turbulence and that for certain conditions the fluid receives energy from the interface, resulting in a shear stress in the gas phase that is less than would be expected if there were no oscillation at all.

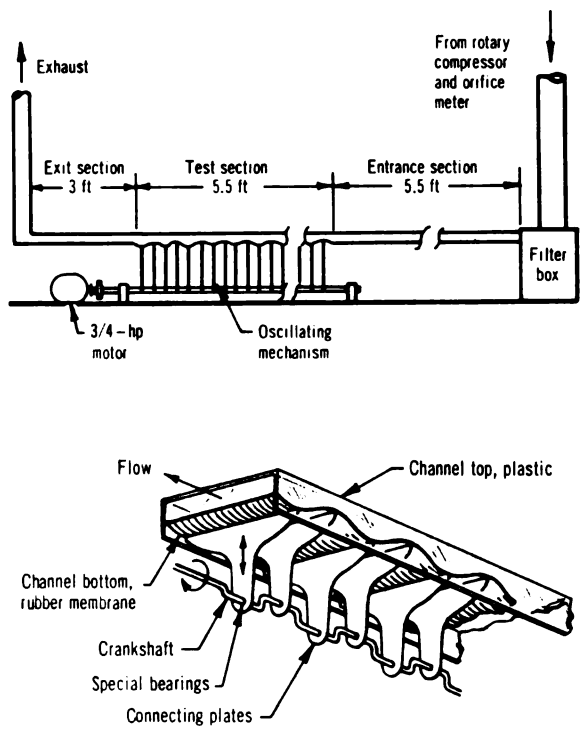

Fig. 3 Flexible sheet mechanically forms standing waves that can be oscillated at various frequencies to simulate influence of liquid-film wave behavior on gas phase.[8]

INTERFACIAL CONDITIONS

The following interfacial conditions were observed in the horizontal flow of air–liquid mixtures: (1) smooth interface, (2) two-dimensional waves, (3) three-dimensional waves, (4) roll waves, and (5) atomization.[9] Laws governing pressure variations and shear-stress variations over a wavy surface were discussed. Detailed descriptions of models explaining the physical processes responsible for the transitions from one type of interfacial structure to another were presented and supported by experimental observations.

Void Fractions and Holdup

Efforts to determine void volume in two-phase systems received strong attention at the symposium.

EFFECT OF GEOMETRY

Because of the lack of adequate data for industrial design and scale-up, the liquid volume fraction was investigated for vertically upward gas–liquid flow in tubes of 0.4 to 12 in. diameter.[10] The liquid holdup was determined by a quick-closing-valve technique. Generally accepted methods, like the Martinelli–Nelson[11] and the Hughmark[12] correlations, were shown to predict the liquid volume fraction inaccurately over a wide range of air and water velocities and column diameters. New correlations were presented that included different relations for bubble, slug, and froth–annular flow.

Experiments with rod bundles of annular and circular geometries were used to investigate liquid volume fraction in gas–liquid adiabatic systems.[13] In the experiments, which emphasized the bubble and dispersed-annular flow regimes, argon, water, and ethyl alcohol were used as the working fluids at pressures ranging from atmospheric to 400 psia. The effects of the liquid volume fraction on mass flow rate, quality, gas density, surface tension, and equivalent diameter were examined. Figure 4 compares previous correlations with the one proposed on the basis of these experiments:

$$\frac{1-\alpha}{1-\beta} = 1 + \frac{1.35\beta^{n}}{1 + 0.335\,\frac{G}{\alpha}\,D^{0.5}}\left(\frac{1}{\rho_G}\right)^{0.25}$$

where n equals $0.9 + 0.05\sigma$. This empirical correlation is within 15% of the data obtained.

Digitized by Google

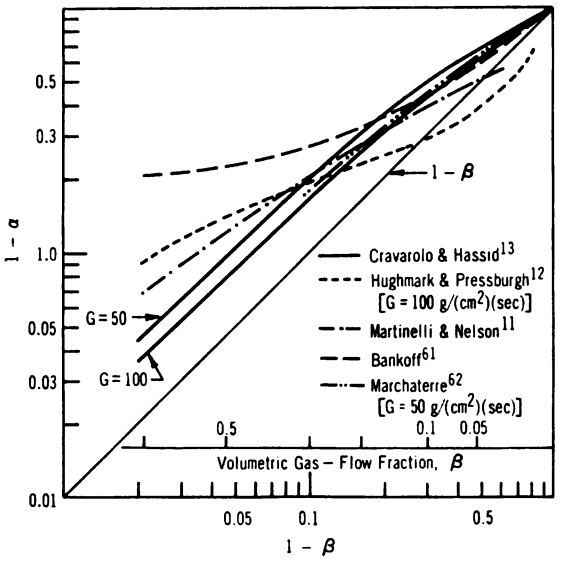

Fig. 4 Comparison of correlations for predicting the effects of liquid volume fraction on mass flow rate, quality, gas density, surface tension, and equivalent diameter for a steam–water mixture at 70 kg/cm² absolute pressure in a 2.5-cm-diameter tube. The new Cravarolo and Hassid correlation agrees within 15% with data.[13]

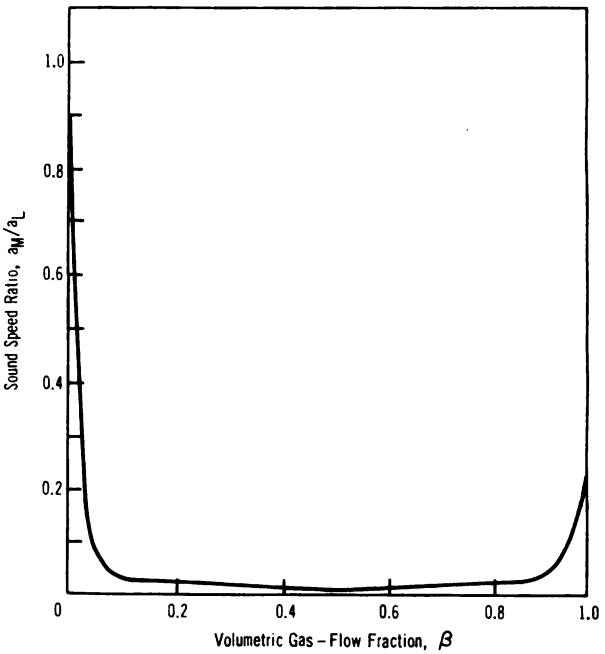

Fig. 5 Theoretically, measurements of sound velocity in air–water mixtures at atmospheric pressure can determine the vapor volume fraction.[17]

MEASUREMENT TECHNIQUES

A dilatation technique was used in an open loop to measure total steam volume fractions in heated channels.[14] The simplicity of this technique makes it easier to use in complicated geometries than other techniques (X-ray or gamma-ray attenuation). Preliminary data of total average steam volume fractions in heated round ducts were presented.

The (γ,n) reaction was applied to boiling heavy water to measure void volume fractions in the region of subcooled and low-quality boiling.[15] The investigators explored pressures from 10 to 50 bars, mass velocities from 50 to 1450 kg/(m²)(sec), heat fluxes from 30 to 90 watts/cm², subcooling from 30 to 0°C, and steam qualities from 0 to 15%. Pressure, heat flux, and mass velocity effects on void fraction were noted in the subcooled and net boiling regimes. A comparison of this large amount of data with Bowring's model[16] indicated large discrepancies, particularly for lower mass velocities.

Changes in acoustical properties were discussed as another method for measuring voids in liquid–gas systems.[17] Expressions were derived for the speed of sound and damping in bubble mixtures. Figure 5 shows the possibility, in principle, of determining the volume fraction of vapor in mixtures from measurements of sound velocity; preliminary experiments with air–water mixtures at atmospheric pressure prove the technique feasible for very small void fractions.

Two-Phase Flow Characteristics

Theoretical explanation and satisfactory prediction of two-phase flow necessitate detailed descriptions of the flow processes within the system. A number of papers dealt with these problems.

A study of cocurrent vertical mercury–nitrogen flow included measurements of local liquid velocities and gas fractions.[18] Power-law continuity expressions were derived, and velocity and void profiles were given for the Hg–N_2 system; Fig. 6 shows typical void-fraction profiles. Levy's mixing-length theory[19] was compared with computed intensities of density and liquid velocity fluctuations.

An electrical-resistivity probe was used to detect the presence of bubbles in a detailed study of the statistical properties of two-phase flow, primarily in the bubble-flow regime.[20] The study showed that the order of the Erlangian distri-

Digitized by Google

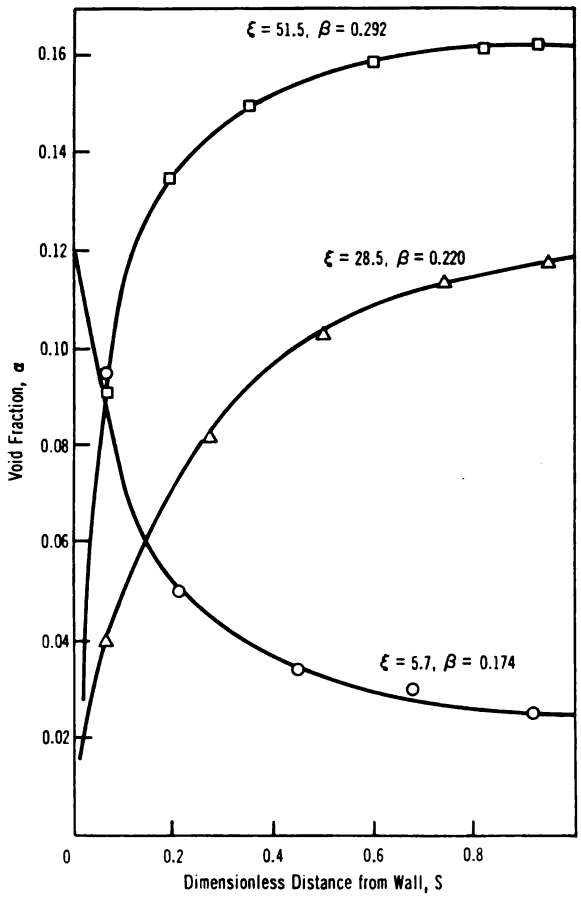

Fig. 6 Void fraction as a function of radial distance for various axial positions.[18]

bution of the bubble-arrival intervals at a given point is a statistical criterion for flow-pattern identification.

A theoretical model was presented to describe the heat-transfer and fluid-flow characteristics in vertical boiling channels.[21] The equations for continuity, momentum, and energy and the equation for diffusion and growth of bubbles were formulated for the unsteady-state case. Radial distributions were assumed for the velocity, temperature, and bubble density to obtain solutions for the steady-state case with given geometry and inlet conditions. Preliminary comparisons with experimental data obtained at the University of Eindhoven have been encouraging.

A number of existing two-phase dynamic models and data were examined from the viewpoint of the commonly adopted assumptions that (1) thermal equilibrium prevails and (2) local pressure variations can be neglected.[22] Evidence shows that failure to include nonequilibrium and compressibility effects in the analysis can lead to erroneous results. Thus these assumptions clearly should be verified for future analyses of two-phase flow; the effect of compressibility and nonequilibrium, particularly, should be included in future analyses describing the coolant behavior in nuclear reactors during rapid power excursions.

PRESSURE-DROP PREDICTION

In a survey lecture Levy[23] discussed three types of analytical models for predicting pressure drop in two-phase flow: (1) one-dimensional models, including the homogeneous and Martinelli–Nelson types and those based on momentum and energy exchange; (2) two-dimensional models, illustrated by the Bankoff variable-density model and Levy's mixing-length model; and (3) flow-pattern models, which are based on specified flow regimes (bubble, slug, annular, etc.). Levy concluded that considerably more research is needed on two-phase flow, especially in interface mechanics, and he singled out the flow-pattern model as the most promising approach for improving the prediction of pressure drop in two-phase flow.

Boiling Heat Transfer

The high heat fluxes obtained by boiling continue to attract the attention of numerous investigators.

NUCLEATE BOILING

Experimental and theoretical results were reported on the kinematic behavior of a bubble column originating at a single site during boiling of saturated liquid.[24] From the study of vapor-removal kinematics during nucleate and film boiling, it was concluded that, during vapor removal by gravity, the volume flow rate is proportional to $[g(\rho_L - \rho_G)\sigma]^{0.25}$ in both boiling regimes, so long as the individual bubble column is undisturbed.

The relation between local wall-temperature fluctuations and the formation of isolated bubbles was discussed for pool-boiling of water at atmospheric pressure.[25] Experiments indicate that the temperature drops correspond to the bubble growth and that the bubble departure has no perceptible effect on surface temperature. A proposed model for the bubble-formation mechanism was outlined.

Digitized by Google

From experiments and motion pictures concerning microconvection in boiling water, and from the determination of liquid volume exchanged in bubble growth and vapor removal, it appears that in subcooled boiling the liquid acceleration is related to the mechanism of bubble condensation (not growth).[26] In contrast to the situation with subcooled boiling, in saturated boiling there is no violent acceleration of liquid. Therefore only the buoyancy forces and the inertial forces related to the bubble growth period cause a slow liquid transport.

SIMULATED NUCLEATE AND FILM BOILING

An experimental investigation simulated nucleate and film boiling by bubbling gas from a heated porous disk in a pool of water at atmospheric pressure.[27] From studies of how the heat-transfer coefficients vary with air-injection rate, water temperature, diameter of the porous disk, and ratio of the pool diameter to the porous-disk diameter, it was concluded generally that: (1) an increase in the air-injection rate is accompanied initially by an increase in the heat-transfer coefficient; (2) when air injection reaches approximately 1.3 ft/sec, a transition from bubbles to a layer of air occurs, and the heat-transfer coefficient decreases (see Fig. 7), simulating the transition from nucleate to film boiling; (3) with a constant air-injection rate, a rise in water temperature causes the heat-transfer coefficient to increase; and (4) variations in disk diameter or pool diameter do not significantly affect the heat-transfer coefficient.

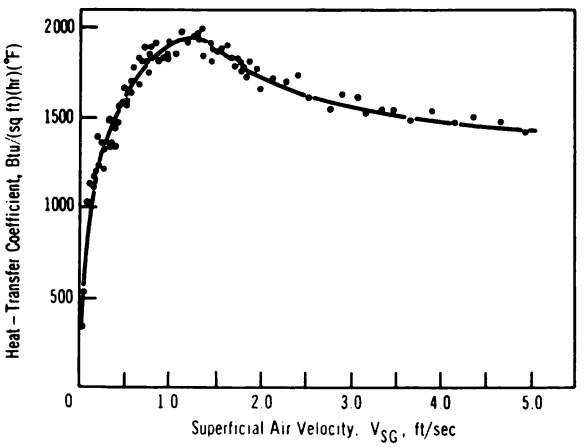

Fig. 7 Transition from nucleate to film boiling, simulated by bubbling various amounts of air through a porous disk in a water pool, causes heat-transfer coefficient to decrease when air changes from bubbles to a layer of air.[27] For the test shown, disk temperature was 112°F and diameter was 2.5 in., pool diameter was 4.75 in., Prandtl number was 4.0, and Crassman number was 1.8×10^{11}.

In a lecture on heat-transfer regimes, Kutateladze[28] reviewed various aspects of his own criteria for predicting the transition from nucleate to film boiling. He made an interesting comparison between the actual boiling process and the one simulated by bubbling an inert gas through a heated surface that is transferring heat to a nonboiling liquid. In agreement with Akturk,[27] he concluded that the analogy between the two is good. Kutateladze discussed the phenomena associated with "burnout" or heat-transfer "crisis" under conditions of high-velocity liquid flow. He also presented useful dimensionless groups for defining two-phase flow patterns.

FILM BOILING

A study of interface dynamics in stable film boiling emphasized the frequency of generation of waves at a stagnation point.[29] Analysis indicated that the phenomenon is dominated by acceleration effects in the vicinity of the stagnation point, rather than by viscous effects. Photographic and motion-picture studies showed that the effect of the stagnation point is felt throughout the laminar-flow region.

Another problem related to film boiling—that of waterdrops resting or impinging on a hot metal surface (Leidenfrost phenomenon)—was examined for measurement of: (1) evaporation rate of drops lying on a hot surface, (2) heat transfer to droplets during their impact with a hot surface, and (3) heat transfer from a hot surface to a transverse spray flow.[30] When the vapor layer that forms between the liquid and the hot wall is thicker than the roughness of the metal surface, the measured evaporation rate appears to be predictable by a simple model.

Entrainment

The problem of entrainment of a liquid in a gas, or vice versa, caused by incomplete separation has interested the nuclear and chemical industries for some time.

Because of concern with the detrimental effect of steam entrainment in the downcomer of a natural-circulation boiling reactor, data were taken in both a large-scale atmospheric-pres-

Digitized by Google

sure air–water loop and in a high-pressure steam–water loop.[31] The entrainment, represented by the void volume in the downcomer, was given in terms of the independent variables: superficial downcomer water velocity, superficial riser steam velocity, water level, riser–downcomer area ratio, and pressure. Statistical correlation equations useful for reactor design were presented.

The opposite problem of liquid entrainment in the vapor phase, which may occur when vapor is forced through a liquid region above an orifice of a sieve tray, was treated.[32] The mechanism by which entrainment is formed was reported, and a model based on this mechanism was formulated for predicting and extrapolating entrainment data.

The maximum water flow possible, without gas entrainment in vertical pipes from a vessel, was graphed as a function of downcomer diameter.[10] The experiments involved various gases and liquids and pipe diameters ranging from 1 to 12 in. Figure 8 shows the effect of the pipe diameter on the critical flow rate.

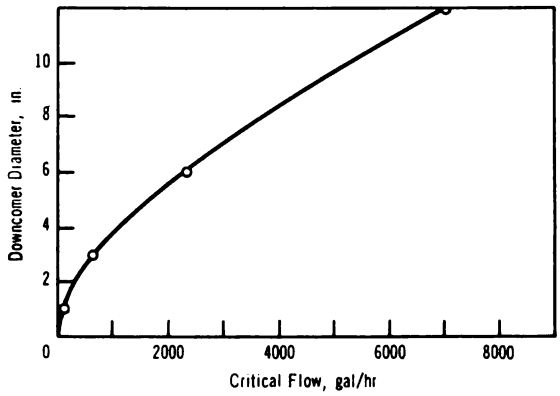

Fig. 8 Effect of pipe diameter on critical flow rate for air–water mixture.[10]

Flooding

When a liquid flows downward and gas flows upward in a vertical passage, there is a limiting condition known as "flooding." Two papers dealt specifically with this problem.

Experiments were conducted to study various aspects of the transition from falling-liquid-film flow to climbing-film flow in the presence of a rising gas stream.[33] The flooding transition was found to be a strong function of the channel length. Figure 9 shows that the flooding velocities obtained were usually higher than those predicted by the theories of Schutt[34] or Davidson and Shearer[35] and that they spanned the predicted values of Wallis.[36] Continuous measurements of the liquid-film thickness and the pressure gradient resulted in a detailed characterization of the flooding phenomenon.

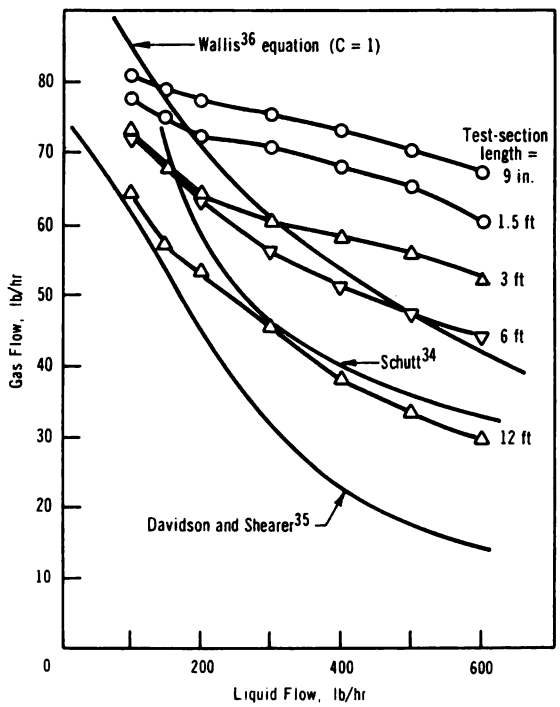

Fig. 9 The gas flow at which flooding occurs at atmospheric pressure depends on the test-section length and usually exceeds theoretical predictions.[33]

Because of concern that flooding could be detrimental to the cooling of fuel elements in a nuclear reactor during emergencies, a series of experiments was conducted on single tubes and rod clusters.[37] Flooding was found to depend strongly on geometry. Although the nondimensional velocities proposed by Wallis[36] were useful in correlating the data, it was concluded that the mechanism of flooding is far from being well understood.

Critical Flow

Critical and high-speed two-phase flows are important in applications such as nuclear reactor safety, in the analysis of flow from geothermal wells, and in devices for metering two-phase mixtures.

Digitized by Google

CHANNEL FLOW

Experiments on critical air–water flows in tubes and channels at low pressures were reported for a large range of qualities.[38] Data included critical flow rates, critical pressures, and exit void fractions. As Fig. 10 shows, the void-fraction measurements lead to much lower

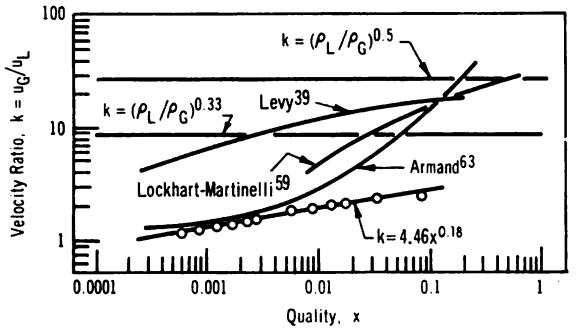

Fig. 10 Experimental and calculated velocity ratios of air–water mixtures for 17-psia critical pressure.[38]

values of the velocity ratios than had been predicted by empirical and analytical expressions used in previous critical-flow models. The previous models[39-41] agreed well with the previous data because the high values of velocity ratios compensate for metastability effects in the models used. A nonequilibrium-slip model was presented that agrees well with existing steam–water data.

The vapor choking model was recommended as being applicable to thermal-equilibrium critical mist flow, as in geothermal wells.[42] Equations were written suitable for a step-by-step solution of the mixture properties as the well exit is approached. Although exit slip and effective flow areas were calculated for critical-flow conditions, no general test of the theory was possible because of the lack of suitable experimental data.

NOZZLE FLOW

The difference in mass-limiting two-phase flow in straight tubes and nozzles was discussed, with particular emphasis on the effect of back-pressure on the mass flow rate and pressure profiles when mass-limiting flow conditions are approached.[43] Figure 11 shows some of the data and indicates that each geometry has different characteristics at the near mass-limiting con-

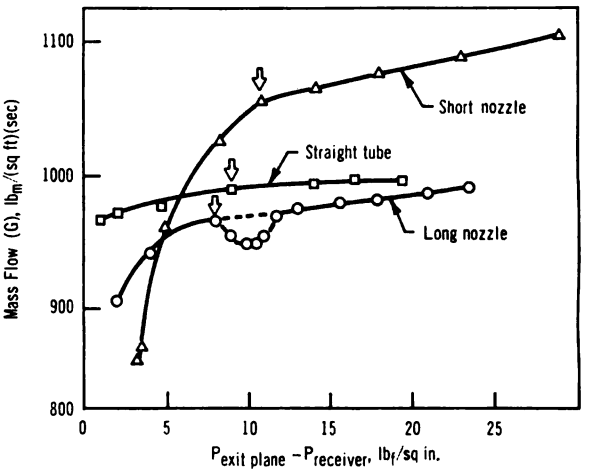

Fig. 11 Mass flow as a function of exit-plane-to-receiver pressure differential.[43] Flow-control tap conditions were 53.8 lb_f/sq in. and 0.116 quality; the vertical arrows show the approximate point of change of slope.

ditions. Although the straight tube shows conventional choking characteristics, large pressure differentials between the exit plane and the receiver are required to produce mass-limiting conditions in nozzles.

ORIFICE FLOW

Data were presented for the flow of steam–water mixtures through sharp-edged orifices; correlations of the data are useful for flowmeter applications.[44] For steam–water mixtures with steam qualities up to 10% and with 24 to 198 psia upstream pressures of the orifice plates, the data can be correlated within 10% by:

$$M_{LS}/M_L - 1 = a(YF)^b$$

where $Y = (X/1 - X)(M_{LN}/M_{VN})$

$$F = 1.414\left(\frac{1-r}{n}\right)^{0.5}\left(\frac{n+1}{2}\right)^{n+1/n-1}$$

$$a = 1.6d^{0.4}$$

$$b = 0.91 - \log a$$

Orifice inclination had no effect on the data.

Two-Phase Flow Dynamics

The transient behavior of two-phase flow systems, which was considered in a number of papers, is of great importance in the design, control, and safety of boilers and nuclear power reactors, as well as in the performance of gas–

Digitized by Google

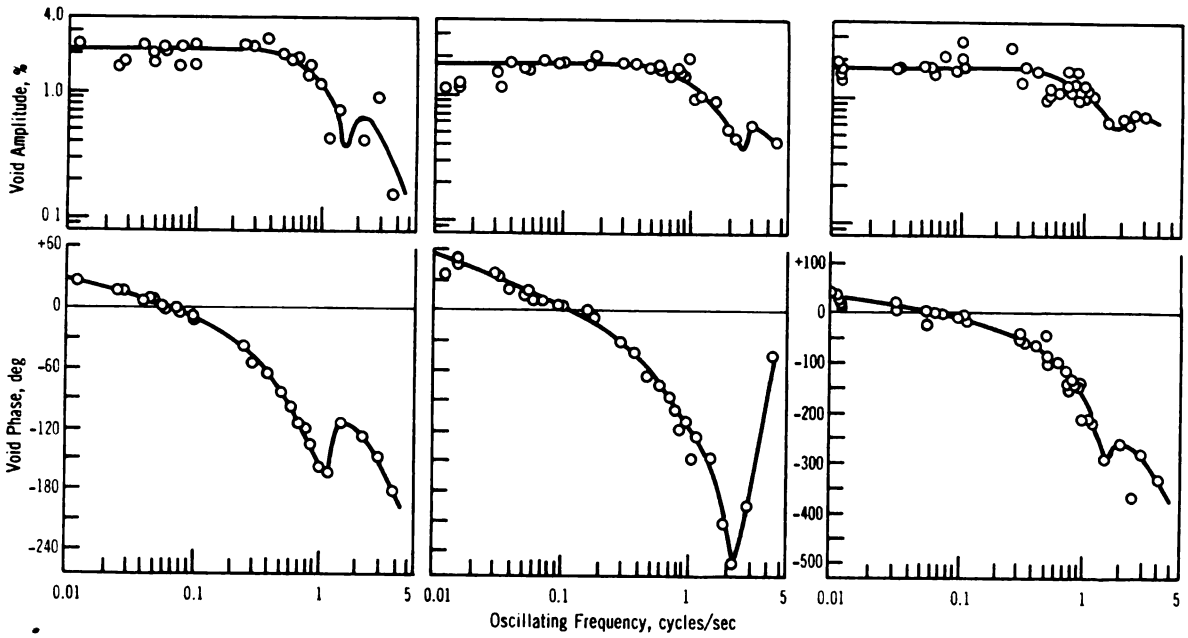

Fig. 12 Power-to-void transfer functions measured in steam–water mixtures within a vertical rectangular heated test section.[46] For the three runs shown (left to right), average void fractions were 46.4, 34.5, and 52.6%, and the axial distances were 0.834, 0.467, and 0.834, respectively.

liquid contacting operations such as distillation and gas absorption.

NUCLEAR REACTOR APPLICATIONS

Power-to-void transfer functions were measured in steam–water mixtures within a vertical rectangular test section that was heated electrically;[45] Fig. 12 shows typical data.[46]

Transient-void data were obtained by a "one-shot" gamma-attenuation technique; conditions investigated included 200 to 800 psia pressures, 2.52 to 3.78 ft/sec inlet flows, 2.28 to 9.12 × 10^4 Btu/(hr)/(sq ft) heat fluxes, and 0.8 to 12.4°F inlet subcoolings. Because the data deviated considerably from previous theoretical models,[47–50] a new model was constructed.

Similar transfer-function measurements, but limited to 140 psia and to tubular test sections, were also reported.[51] Transient-steam-volume fractions were obtained by a dilatation technique in closed-loop operation. Good agreement was claimed between the data and available models for two-phase flow dynamics.

Consideration was given to neglecting body and friction forces in the mathematical description of unsteady steam–water flow in a heated channel.[52] Although the frequency responses of the void fraction and steam and water velocities were computed, a numerical example, based on the Halden Boiling Water Reactor, illustrated the need for including the body and friction forces in two-phase flow analysis.

The onset of flow instability in a natural-circulation loop with two electrically heated parallel round ducts was discussed.[53] Uniform power distribution was applied along the 4300-mm heated length of 20-mm-diameter channels at 50-bars pressure with 6°C subcooling. The data were discussed in terms of investigated loss coefficients in different parts of the loop.

The dynamics of two-phase systems were examined in a study that concluded that flow oscillations cannot occur unless a maximum in the density–enthalpy product is obtained in the heater.[54,55]

DISTILLATION APPLICATIONS

In contrast to the papers that dealt primarily with nuclear reactor applications, several papers considered the dynamic behavior of gas–liquid contacting devices as used in distillation operations. One paper described a two-dimensional hydrodynamic-stability analysis of the oscillations in a gas–liquid mixture on a sieve plate.[56] The solution, which is based on numerous assumptions, indicated that neutral and am-

Digitized by Google

plified oscillations can occur only in distinct regions of the wave number.

The need for the sieve-tray design to be based on dynamic, rather than on steady-state, concepts was illustrated by experiments that showed large fluctuations in froth pressure drop in normal sieve-tray operation.[57] The amplitude of the fluctuations, which increased with the gas rate, reached 80% of the mean pressure drop.

The liquid on the sieve tray was demonstrated to behave in either a stable or an unstable way, depending on the sieve-tray geometry and the resulting flow regimes.[58] In the unstable regime the liquid-level wavelengths and oscillation frequencies were studied as functions of liquid height and gas flow.

In view of the enormous complexity of the many two-phase flow phenomena, it seems appropriate to conclude that many of the symposium papers are preliminary and intermediate and that many more investigations are necessary to obtain data suitable for various design problems.

Symbols

a_L = sonic liquid velocity
a_M = sonic mixture velocity
C = Crassman number
D = diameter of tube
d = diameter of orifice
G = mass flow
g = gravitational constant
k = velocity ratio = u_G/u_L
M_G = gas mass rate
M_L = liquid mass rate during two-phase flow
M_{LN} = liquid mass rate by weight during single-phase flow with unit contraction coefficient and two-phase pressure drop
M_{LS} = liquid mass rate by weight during single-phase flow with normal contraction coefficient and two-phase pressure drop
M_{VN} = vapor mass rate by weight during single-phase flow with unit contraction coefficient and two-phase pressure drop
n = index of isentropic expansion
P = pressure
P_C = critical pressure
r = ratio of backpressure to initial pressure
Re_G = gas Reynolds number
Re_L = liquid Reynolds number
S = dimensionless distance from wall
V_G = average gas velocity
T_S = porous surface temperature
V_{SG} = superficial gas velocity
V_{SL} = superficial liquid velocity
N_{Pr} = Prandtl number
We = Weber number
X = quality
α = void fraction
β = volumetric gas-flow fraction
ρ_G = gas density
ρ_L = liquid density
ξ = dimensionless axial distance
μ_G = gas viscosity
μ_L = liquid viscosity
σ = surface tension

References

Papers in the *Proceedings of the Symposium on Two-Phase Flow, Exeter, England, June 21—23, 1965*, are identified below by "(Exeter)". The two-volume proceedings are available for $24.00 from P. M. C. Lacey, Department of Chemical Engineering, University of Exeter, Exeter, Devon, England.

1. A. B. Chaudhry, A. C. Emerton, and R. Jackson, Flow Regimes in the Co-current Upwards Flow of Water and Air. (Exeter)
2. M. Truong Quang and J. Huyghe, Some Hydrodynamical Aspects of Annular Dispersed Flow: Entrainment and Film Thickness. (Exeter)
3. L. B. Cousins, W. H. Denton, and G. F. Hewitt, Liquid Mass Transfer in Annular Two-Phase Flow. (Exeter)
4. C. J. Hoogendoorn and W. A. Welling, Experimental Studies on the Characteristics of Annular-Mist Flow in Horizontal Pipes. (Exeter)
5. G. D. McPherson, A Test Facility for the Study of Dry-Out in Water Steam Flow. (Exeter)
6. H. S. Chung and W. Murgatroyd, Studies of the Mechanism of Roll Wave Formation on Thin Liquid Films. (Exeter)
7. F. P. Stainthorp and R. S. W. Batt, The Wave Properties of Falling Liquid Films with Countercurrent Air Flow. (Exeter)
8. N. Houze and A. E. Dukler, The Effect of a Moving Interface on Gas Phase Turbulence. (Exeter)
9. T. J. Hanratty and D. E. Woodmansee, Stability of the Interface for a Horizontal Air-Liquid Flow. (Exeter)
10. J. E. Ellis and E. L. Jones, Vertical Gas-Liquid Flow Problems. (Exeter)
11. R. C. Martinelli and D. B. Nelson, Prediction of Pressure Drop During Forced-Circulation Boiling of Water, *Trans. Am. Soc. Mech. Engrs.*, 70: 695 (1948).
12. G. A. Hughmark and B. S. Pressburgh, Holdup and Pressure Drop with Gas-Liquid Flow in a Vertical Pipe, *A.I.Ch.E. J.*, 7(4): 677 (December 1961).
13. L. Cravarolo and A. Hassid, Liquid Volume Fraction in Two-Phase Adiabatic Systems. (Exter)
14. G. Possa, G. Valli, and J. B. van Erp, Measurement of Total Steam Volume in a Heated Channel. (Exeter)
15. S. Z. Rouhani, Void Measurements in the Region of Subcooled and Low-Quality Boiling. (Exeter)
16. R. W. Bowring, Physical Model, Based on Bubble Detachment, and Calculation of Steam Voidage in the Subcooled Region of a Heated Channel, Norwegian Report HPR-10, December 1962.
17. F. v. d. Walle, A. J. Verheugen, V. J. M. Haagh, and M. Bogaardt, A Study of the Application of Acoustical Methods for Determining Void Fractions in Boiling Water Systems. (Exeter); also published in *A.I.Ch.E. J.*, 11(4): 624-635 (July 1965).
18. L. G. Neal and S. G. Bankoff, Local Parameters in Co-current Mercury-Nitrogen Flow, Parts I and II. (Exeter)

Digitized by Google

19. S. Levy, Prediction of Two-Phase Pressure Drop and Density Distribution from Mixing Length Theory, Paper No. 62-HT-6, *J. Heat Transfer*, 85: 137 (May 1963).
20. C. Lackmê, Some Statistical Properties of Two-Phase Flow in Vertical Tubes. (Exeter)
21. F. v. d. Walle, C. L. Spigt, H. J. Lamein, and M. Bogaardt, A Theoretical Study on Two-Phase Flow Characteristics. (Exeter)
22. H. Christensen and K. O. Solberg, Incomplete Thermal Equilibrium in Two-Phase Flow. (Exeter)
23. S. Levy, Pressure Gradient in Two-Phase Flow Systems. (Exeter)
24. T. H. K. Frederking, Gravity Effects on Interfacial Kinematics in Ordinary Boiling Systems. (Exeter)
25. R. Morin, Wall Temperature Fluctuations During Bubble Generation in Boiling. (Exeter)
26. A. Bähr, The Micro-Convection in Boiling Water Induced by Single Bubbles. (Exeter)
27. N. U. Akturk, Heat Transfer from a Heated Porous Surface to a Pool of Liquid with Gas Injection at the Interface. (Exeter)
28. S. S. Kutateladze, Criteria for the Prediction of the Transition from Nucleate to Film Boiling. (Exeter)
29. W. S. Bradfield, Wave Generation at a Stagnation Point in Stable Film Boiling. (Exeter)
30. L. H. J. Wachters, The Heat Transfer from a Hot Wall to Water Drops in the Spheroidal State. (Exeter)
31. E. Kjelland-Fosterud, I. Bencze, and J. Skaug, Void Fractions in Down-Flow in the Entrance Region. (Exeter)
32. R. D. Nielsen, M. R. Tek, and J. L. York, Mechanism of Entrainment Formation in Distillation Columns. (Exeter)
33. G. F. Hewitt, P. M. C. Lacey, and B. Nicholls, Transitions in Film Flow in a Vertical Tube. (Exeter)
34. J. B. Schutt, A Theoretical Study of the Phenomenon of Bridging in Wetted-Wall Columns, Ph. D. Thesis, University of Rochester, Rochester, N. Y., 1959.
35. J. F. Davidson and C. J. Shearer, Flooding in Wetted Wall Columns: Its Relation to the Formation of a Standing Wave Due To Gas Flowing Upwards Over a Vertical Liquid Film, to be published in the *Journal of Fluid Mechanics;* also, C. J. Shearer, Flooding in Wetted Wall Columns: Its Relation to the Formation of a Standing Wave Due To Gas Flowing Upwards Over a Vertical Liquid Film, Ph. D. Thesis, Cambridge University, Cambridge, England, 1964.
36. G. B. Wallis, Flooding Velocities for Air and Water in Vertical Tubes, British Report AEEW-R-123, December 1961.
37. G. L. Shires and A. R. Pickering, The Flooding Phenomenon in Countercurrent Two-Phase Flow. (Exeter)
38. H. K. Fauske, Two-Phase Two- and One-Component Critical Flow. (Exeter)
39. S. Levy, Predictions of Two-Phase Critical Flow Rate, *J. Heat Transfer*, 87: 53 (February 1965).
40. F. J. Moody, Maximum Flow Rate of a Single Component, Two-Phase Mixture, *J. Heat Transfer*, 87: 134 (February 1965).
41. H. K. Fauske, Critical Two-Phase, Steam–Water Flows, in *Proceedings of the Heat Transfer and Fluid Mechanics Institute*, Preprint Edition, Paper No. 79, Stanford University Press, Stanford, Calif., June 1961.
42. D. J. Ryley, Two-Phase Critical Mist Flow in Geothermal Steam Wells. (Exeter)
43. D. K. Edmonds and R. V. Smith, Comparison of Mass Limiting Two-Phase Flow in a Straight Tube and in a Nozzle. (Exeter)
44. D. Chisholm and G. G. Watson, The Flow of Steam/Water Mixtures Through Sharp-Edged Orifices. (Exeter)
45. C. C. St. Pierre, M. Petrick, and S. G. Bankoff, Response of a Boiling Water Channel to Power Modulation. (Exeter)
46. C. C. St. Pierre, Frequency-Response Analysis of Steam Voids to Sinusoidal Power Modulation in a Thin-Walled Boiling Water Coolant Channel, USAEC Report ANL-7041, Argonne National Laboratory, May 1965.
47. R. W. Wright and S. M. Zivi, Power-Void Transfer Function Measurements in a Simulated SPERT IA Modulator Coolant Channel, USAEC Report ANL-6205, pp. 45-73, Argonne National Laboratory, November 1960.
48. H. Christensen, Power-to-Void Transfer Functions, USAEC Report ANL-6385, Argonne National Laboratory, July 1961.
49. K. O. Solberg, The "Kjeller Model" for the Dynamics of Coolant Channels in Boiling Water Reactors, Part I: Theory, in *Symposium on Two-Phase Flow, Steady-State Burnout, and Hydrodynamic Instability, Studsvik, Norway, October 1–3, 1963,* European Atomic Energy Society.
50. C. K. Sanathanan, Dynamic Analysis of Coolant Circulation in Boiling Water Nuclear Reactors, USAEC Report ANL-6847, Argonne National Laboratory, April 1964.
51. G. Possa and J. B. van Erp, Measurement and Analysis of Two-Phase Flow Dynamics. (Exeter)
52. W. Ciechanowicz, On the Dynamics of a Boiling Water Reactor Coolant Channel. (Exeter)
53. R. P. Mathisen, An Experimental Study of Natural Circulation in a Loop with Parallel Flow Test Sections. (Exeter)
54. J. R. Bode and D. G. Harden, Associating the Hydrodynamics of Two-Phase Flow with the Density-Enthalpy Relationship. (Exeter)
55. D. G. Harden, Transient Behavior of a Natural-Circulation Loop Operating Near the Thermodynamic Critical Point, USAEC Report ANL-6710, Argonne National Laboratory, May 1963.
56. J. O. Hinze, Oscillations of a Gas-Liquid Mixture on a Sieve Plate. (Exeter)
57. B. T. Davies and K. E. Porter, Some Observations on Sieve Tray Froths. (Exeter)
58. W. J. Beek, Oscillations and Vortices in a Batch of Liquid Sustained by a Gas Flow. (Exeter)
59. R. W. Lockhart and R. C. Martinelli, Proposed Correlation of Data of Isothermal Two-Phase, Two-Component Flow in Pipes, *Chem. Eng. Progr.*, 45: 39 (1949).
60. D. J. Nicklin, Two-Phase Flow in Vertical Tubes, Ph. D. Thesis, Cambridge University, Cambridge, England, 1961.
61. S. G. Bankoff, A Variable Density Single-Fluid Model for Two-Phase Flow with Particular Reference to Steam–Water Flow, *J. Heat Transfer*, 82: 265 (November 1960).

Digitized by Google

62. J. F. Marchaterre and B. M. Hoglund, Correlation for Two-Phase Flow, *Nucleonics*, 20(8): 142 (August 1962).
63. A. A. Armand, The Resistance During the Movement of a Two-Phase System in Horizontal Tubes, British Report AERE-tr-828, translated by V. Beak from *Izv. Vses. Teplotekhn. Inst.* (Russia), 15: 16-23 (1946).

How Coolant Dynamics Affect Fast Reactor Safety

By Ralph M. Singer

The safe operation of a fast reactor can be affected adversely by two general types of occurrences: (1) loss of cooling capability and (2) power excursions caused by reactivity insertions. The good safety experience with fast reactors is based on substantial design and operations-management efforts to assure retention of cooling capability and to prevent unplanned insertions of reactivity. However, as more and larger fast reactors are planned, it becomes increasingly desirable to understand and predict the consequences of such events if they should occur despite the precautions. Then inherent design features can be incorporated to assure reactor safety.

If the extent of the consequences is to be understood and predicted when cooling capacity is lost or unwanted reactivity is inserted, it is necessary to understand and predict the role of each mechanism that would affect reactor behavior—and also to know the precise sequence of these various mechanisms as well as the effects of their interactions. Then it would be possible to predict which specific accidents, such as pump failures, fuel-rod bowing, or coolant-system leaks, could damage the system.

Although the probable sequence of events that would follow cooling loss or a power excursion in a fast reactor is of vital interest to reactor designers, little information is available on specific mechanisms relating to coolant dynamics and heat transfer.

Sequence of Events

Figure 1 shows the possible sequences of events that would follow a loss of cooling or a power excursion in a fast reactor. Although many sequences are possible, the sequence that actually would occur would depend on the specific details of the accident and on the reactor system itself.

EXAMPLE

A sufficiently rapid rate of insertion of reactivity can cause the fuel and cladding temperatures to rise so fast and high that the fuel and/or cladding will melt before enough energy transfers to the coolant to cause boiling. The melting of the fuel can result in at least three events: (1) the coolant may vaporize, (2) a pressure pulse may occur, or (3) the core may disassemble. If the coolant vaporizes after the core melts, there may result a pressure pulse and coolant expulsion, either of which can result in additional core damage. Expulsion of coolant could cause an additional reactivity increase that could lead to further damage.

If the initial reactivity insertion rate is moderate, sufficient energy could be trans-

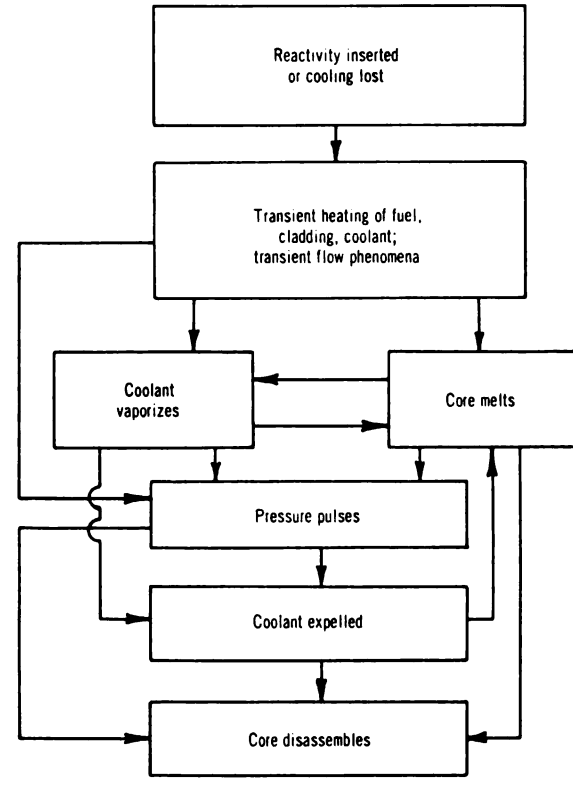

Fig. 1 Possible sequence of events that could follow loss of cooling or a reactivity-insertion-induced power surge in a fast reactor, excluding reactivity-feedback effects.

Digitized by Google

ferred to the coolant to vaporize it before the fuel melts; then the vapor could insulate the fuel, causing it to melt. Alternatively, a transient power surge in the core could suddenly expand the fuel and pressurize the coolant so that the coolant is directly expelled, which could cause the core to melt and disassemble.

Other sequences of events are undoubtedly possible, but the example indicates the complexity of the situation and the need for understanding not only the individual processes but also the interrelations among them. It is worthwhile to consider the status of our knowledge of transient heating of the core and single-phase behavior of the coolant, transient heat transfer and coolant hydrodynamics, transient vaporization of the coolant, pressure-pulse generation, and coolant expulsion.

Transient Core Heating and Single-Phase Behavior

If the energy generated in a reactor fuel is to be transferred to the reactor coolant, the heat must be conducted through the fuel material, the bonding material (if any), and the cladding material. Because the space–time variation of the temperature in the core must be known if core behavior is to be predicted, the first step in a safety analysis should be a study of transient heat conduction in multidimensional nonhomogeneous media, including the effects of internal energy generation and phase changes.

An excellent survey has been made of the available digital-computer codes which can calculate transient temperatures in various geometric regions and which consider coupling to reactor kinetics and coolant hydrodynamics.[1] The survey emphasizes the four codes, ARGUS, FORE, TIGER-V, and TER-4, and discusses their applications and limitations in detail. An additional code, TRANSFUGUE-I, deals with transient hydrodynamics and heat transfer.[2] All existing codes involve approximations and limitations that restrict their general applicability. Perhaps the most glaring deficiency in all the codes is their complete neglect of compressibility effects (critical flow and low sonic velocity) in two-phase mixtures. In certain situations sonic velocity in two-phase mixtures can be as low as 5 ft/sec, which can cause channel choking as soon as voids are formed. A recent paper discusses this problem analytically.[3]

Another recent paper, which presents a new numerical method for solving multiregion conduction problems, claims to combine the computational ease of explicit methods with the stability of implicit methods.[4] Use of this technique should be investigated in any future transient analysis codes. A reasonably detailed survey[5] of methods for predicting fuel-element and coolant behavior under reactor transient conditions summarizes studies conducted before 1961.

The prediction of incipient fuel melting or coolant vaporization has been simplified by the development of methods for predicting temperature transients of the fuel and single-phase coolant.[6] The simplified analytical techniques can be used to describe heat transfer in typical fuel channels and to obtain a rational extrapolation of existing empirical information to boiling sodium flow through heated channels.

Coolant Vaporization

When the space–time history of temperatures in a reactor core has been predicted for a specific incident, the next step is to determine whether any phase changes occur in the fuel or coolant. Prediction of the conditions under which the coolant will vaporize, and thus prediction of void-reactivity and other effects, requires a knowledge of (1) the amount of superheat needed to initiate boiling and (2) the factors that affect the superheat. For liquid metals, large superheats may be necessary to initiate boiling—and, when voids start to form, void growth can be extremely rapid.[7,8] Although work that was conducted before 1965 has been reviewed,[9] only a very limited amount of experimental information is available.

Once nucleate boiling begins, liquid metals have been observed to behave very unstably, with large variations in wall temperature and fluctuation between nonboiling and boiling states.[8,10] Apparently this instability is caused by the physical characteristics of the heated surface as well as by the properties of the fluid.[10] However, this instability has not been observed by all experimenters.

Data on transient boiling (pool and forced flow) of liquid metals are vital to designers for prediction of the space–time history of voids and temperatures. Although there are no

Digitized by Google

data for liquid-metal systems undergoing rapid heating transients, it might be possible to extrapolate to liquid metals the limited amount of information that exists on the transient boiling of water from a ribbon.[11–18] Extrapolation, of course, has inherent uncertainties and should be pursued cautiously.

A recent analytical description of transient boiling during fast reactor power transients leads to the conclusion that: (1) voiding in a reactor channel starts near the upper boundary of the core and grows axially along the fuel channel, (2) vapor production is so rapid that transient self-pressurization of the fuel channel occurs, and (3) the resulting two-phase flow is strongly unstable hydrodynamically.[19] Under certain circumstances, power sufficient just to initiate boiling can result in complete voiding of the channel without further increase in power.

The importance of coolant vaporization in fuel-meltdown studies, suggestions for needed work, and some answers for the following questions are described[20] in a survey report: (1) What abnormal conditions may lead to coolant vaporization? (2) Which phenomena associated with coolant vaporization are most important in each of the various possible accidents? (3) What are the important characteristics of each phenomenon, and what methods are available to predict them?

Generation of Pressure Pulses

For a safe design to be obtained, it is essential to know what pressures are attainable if the reactor operates under abnormal conditions. The SPERT tests show that destructive pressure transients can be generated in water reactors, although the mechanisms causing them are still matters for discussion. Programs that are under way at Argonne National Laboratory,[21] TRW Space Technology Laboratories,[22] and elsewhere are aimed at determining and understanding these mechanisms. Although experimental work so far has been limited to water systems, many of the pressure-generation mechanisms considered could apply equally well to liquid metals. Several of these mechanisms involve: sudden thermal expansion of the fuel and immediately adjacent coolant, rapid water–metal reactions that evolve hydrogen, pressure amplification caused by the collapsing of voids, and sudden void formation. However, much experimental and theoretical work must still be done before it is possible to predict accurately the severity of pressure transients that can result from specific accidents in specific reactors.

Coolant Expulsion

After a pressure pulse is generated in the coolant, the coolant will be expelled from the vicinity of the high-pressure source. Before the expulsion velocity can be predicted (assuming that the pressure-generating mechanism is known), it is necessary to understand the transient mechanics of two-phase flow. Although the theoretical tools are not yet developed sufficiently for two-phase flow, the expulsion velocity of a single-phase fluid can be estimated if enough is known about the initial pressure pulse. It is not known whether such an estimate would be accurate enough for confident predictions of reactivity feedback effects.

Apparently there is no experimental information on liquid-metal expulsion and only extremely limited data on water expulsion.[23,24] Motion pictures conclusively show that critical flow (choking) occurred in a two-phase system in which superheated water was ejected from a vertical tube.[24] The water was superheated by means of overpressurizing; the pressure suddenly decreased by rupturing a diaphragm, and the result was boiling and ejection of the water. An expulsion experiment under way at Argonne employs a large power surge in an electric heater to boil water in an annulus. It will produce data on expulsion velocities, pressure generation, and void growth rates and will lead into related experiments with sodium.

Conclusions

From this brief review of the effects of coolant dynamics on fast-reactor safety, it can be concluded that:

- The transient thermal and hydrodynamic behavior of the core and coolant is reasonably understood if no phase changes occur.
- There is a lack of data on how fuel melting (with or without cladding failure) affects the thermal and hydrodynamic behavior of the coolant.
- Data are needed on the degree of superheat needed to cause nucleate boiling of liquid metals under various conditions.

Digitized by Google

• Data on the transient nucleate boiling of water from a ribbon have not been rationally extrapolated to predict the transient nucleate boiling of liquid metals from a fuel surface (if at all possible).

• Data are lacking for the transient boiling (pool and forced flow) of liquid metals after a power surge; data on heat-transfer rates and void-formation rates are required.

• A generally accepted explanation of the mechanisms that can generate destructive pressure transients is not available; the available data for water systems should be rationally extrapolated to liquid-metal systems, and data should be obtained on liquid-metal systems.

• Data on coolant expulsion rates are extremely sparse.

The transient behavior of the coolant is probably the least understood phenomenon occurring in a reactor. However, the papers and discussions on the subject at the Conference on Safety, Fuels, and Core Design in Large Fast Power Reactors, which was held at Argonne in October 1965, indicate that there was general agreement among U. S. and European engineers concerning the proper direction of research needed to resolve the problems. Thus the results of current and planned research programs soon will yield an improved understanding of these complex problems.

References

1. A. H. Kazi and B. H. Cherry, Survey of Current Methods for Analysis of Fast Reactor Transients Including Meltdown, USAEC Report UNC-5092, United Nuclear Corporation, Aug. 28, 1964.
2. R. C. Noyes, J. G. Morgan, and H. H. Cappel, TRANSFUGUE-I, A Digital Code for Transient Two-Phase Flow and Heat Transfer, USAEC Report NAA-SR-11008, Atomics International, July 25, 1965.
3. M. Fischer and W. Häfele, Shock Front Condition in Two-Phase Flow Including the Case of Desuperheat, presented at the Conference on Safety, Fuels, and Core Design in Large Fast Power Reactors, USAEC Report ANL-7120, Argonne National Laboratory, Oct. 11–14, 1965.
4. S. R. Allada and D. Quon, A Stable, Explicit Numerical Solution of the Conduction Equation for Multi-Dimensional Non-Homogeneous Media, presented at the Eighth National Heat Transfer Conference and Exhibit, Aug. 8–11, 1965, sponsored by the ASME–AIChE, AIChE Preprint 27.
5. F. E. Beers, Review of Investigations Pertinent to the Prediction of the Thermal Behavior of Fast Reactors Under Abnormal Operating Conditions, USAEC Report NDA-2147-4, Nuclear Development Associates, Inc., Mar. 15, 1961.
6. R. P. Stein, Studies Related to Predicting Coolant Behavior for Fast Reactor Safety, USAEC Report NDA-2147-8, Nuclear Development Associates, Inc., Aug. 31, 1961.
7. R. E. Holtz, A Study of the Initiation of Nucleate Boiling in the Liquid Metals, USAEC Report ANL-6980, Argonne National Laboratory, December 1964.
8. H. W. Hoffman and A. I. Krakoviak, Studies in Boiling with Liquid Potassium, USAEC Report ORNL-P-35 (CONF-537-2) Oak Ridge National Laboratory, 1963.
9. T. G. Hersum and S. A. Schellin, Initiation of Nucleate Boiling in Liquids (An Annotated Bibliography), AMU–ANL Summer Engineering Practice School Report, Associated Midwestern Universities, Inc., and Argonne National Laboratory, July 2, 1965.
10. P. J. Marto and W. M. Rohsenow, Nucleate Boiling Instability of Alkali Metals, presented at the Eighth National Heat Transfer Conference and Exhibit, Aug. 8–11, 1965, sponsored by the ASME–AIChE, ASME Paper No. 65-HT-22.
11. R. Cole, Investigation of Transient Pool Boiling Due to Sudden Large Power Surge, Report NACA-TN-3885, Lewis Flight Propulsion Laboratory, December 1956.
12. M. W. Rosenthal and R. L. Miller, An Experimental Study of Transient Boiling, USAEC Report ORNL-2294, Oak Ridge National Laboratory, May 24, 1957.
13. A. J. Bendler, J. K. Roros, and N. H. Wagner, Fast Transient Heating and Explosion of Metals Under Stagnant Liquids, USAEC Report AECU-3623, Columbia University, Engineering Research Laboratories, Feb. 12, 1958.
14. H. A. Johnson, V. E. Schrock, S. Fabic, and F. B. Selph, Transient Boiling Heat Transfer and Void Volume Production in Channel Flow, USAEC Report SAN-1007, University of California, Berkeley, March 1963.
15. H. A. Johnson, V. E. Schrock, F. B. Selph, J. H. Lienhard, and Z. R. Rosztoczy, Temperature Variation, Heat Transfer, and Void Volume Development in the Transient Atmospheric Boiling of Water, USAEC Report SAN-1001, University of California, Berkeley, January 1961.
16. T. Sato et al., Experimental Studies on Transient Boiling, Japanese Report No. 98, September 1962.
17. S. Hayashi, A. Sakurai, and T. Iwazumi, Transient Heat Transfer in the Heterogeneous Water Reactor, Part I, Report NSJ-Tr-1, translated from *Nippon Genshiryoku Gakkaishi*, 5: 403-411 (May 1963); Part II, USAEC Report ANL-Trans-237, translated from *Nippon Genshiryoku Gakkaishi*, 6: 399-405(1964).
18. P. Spiegler, J. Hopenfeld, M. Silberberg, and C. F. Bumpus, Inpile Experimental Studies of Transient Boiling with Organic Reactor Coolant, USAEC Report NAA-SR-9010, Atomics International, Jan. 30, 1964.
19. R. C. Noyes et al., The Development and Growth of In-Core Voids Due to Boiling During Fast Reactor Transient, presented at the Conference on Safety, Fuels, and Core Design in Large Fast Power Reactors, USAEC Report ANL-7120, Argonne National Laboratory, Oct. 11–14, 1965.
20. A. J. Goldman, A Survey of Coolant Vaporization Effects Important to Fast Reactor Safety, USAEC

Digitized by Google

Report UNC-5021, United Nuclear Corporation, June 30, 1962.
21. C. E. Dickerman and W. Stephany, Correlation of In-Pile Transient Pressure Measurements, *Nucl. Struct. Eng.*, 1(3): 342-344 (1965).
22. C. T. Molloy, L. G. Neal, N. C. Pate, L. B. Wentz, and R. W. Wright, Kinetic Studies of Heterogeneous Water Reactors, Annual Summary Report, 1964, USAEC Report STL-372-13, TRW Space Technology Laboratories, Dec. 30, 1964.
23. C. E. Dickerman, Argonne National Laboratory, personal communication, Oct. 22, 1964.
24. G. Friz, Coolant Ejection Studies with Analogy Experiments, presented at the Conference on Safety, Fuels, and Core Design in Large Fast Power Reactors, Argonne National Laboratory, Oct. 11–14, 1965.

Digitized by Google

Section

V

Power Reactor Technology

Specific Reactor Types

UHTREX Operation Near

By Barton M. Hoglund

A novel gas-cooled reactor concept, with the acronym UHTREX (Ultra High Temperature Reactor Experiment), is expected to achieve criticality in October 1966 at the Los Alamos Scientific Laboratory.[1] Among its unique features of interest to reactor designers are:

- An annular core that is rotatable to facilitate refueling during reactor operation,
- Articulated control rods that can be inserted directly into the core regardless of its angular position,
- Simple graphite fuel elements that hold promise for fuel economies, but that lead to
- Normal operation with a contaminated primary coolant, and
- Use of an extensive on-line coolant-cleanup system to limit the amount of contamination in the coolant.

Purpose and Potential

The UHTREX, a 3-Mw(t) helium-cooled graphite-moderated reactor experiment, has been built so that operating experience can be acquired with a gas-cooled reactor system that employs simple graphite type fuel elements of various types. In planning the experimental program to be conducted in UHTREX, Los Alamos is considering using the fuel-loading flexibility of the reactor to determine the operational performance of various fuel materials. For example, to determine how neutron economy would benefit if gaseous fission products were released from the fuel during reactor operation, the experimental program might employ fuel elements that release fission products more rapidly than coated-particle fuels that will be used initially.

"Should fuel simplification outweigh the difficulties arising from the operation of a contaminated coolant circuit, UHTREX may provide the basis for significant economic gains to be made in future gas-cooled reactors for both power and process-heat applications."[2] In addition to power and high-temperature process heat for such uses as coal gasification, this concept might be a useful energy source for magnetohydrodynamic (MHD) devices or for high-temperature Brayton-cycle applications. The hope has been expressed[1] that, by development of high-temperature reactor technology beyond current applications, the applications technology would be stimulated to "catch up."

HISTORY

UHTREX is a continuation of the TURRET reactor experiment,[2] which was first proposed as a nitrogen-cooled reactor to drive a gas turbine in a closed cycle.[3] The proposal later was revised[4] to make TURRET a helium-cooled reactor having an operating pressure of 500 psia and an exit temperature of 2400°F. The TURRET program was terminated in January 1961; the UHTREX program began in May 1961. The UHTREX has been constructed on a site about 2.5 miles southeast of Los Alamos.

Design Description

The UHTREX facility (Fig. 1) includes operating and control areas, a fuel-handling area, and a containment structure.[5] All pressurized equipment containing contaminated helium is within the containment, which is a single concrete structure that is lined with a steel membrane and is divided into (1) a separately

Digitized by Google

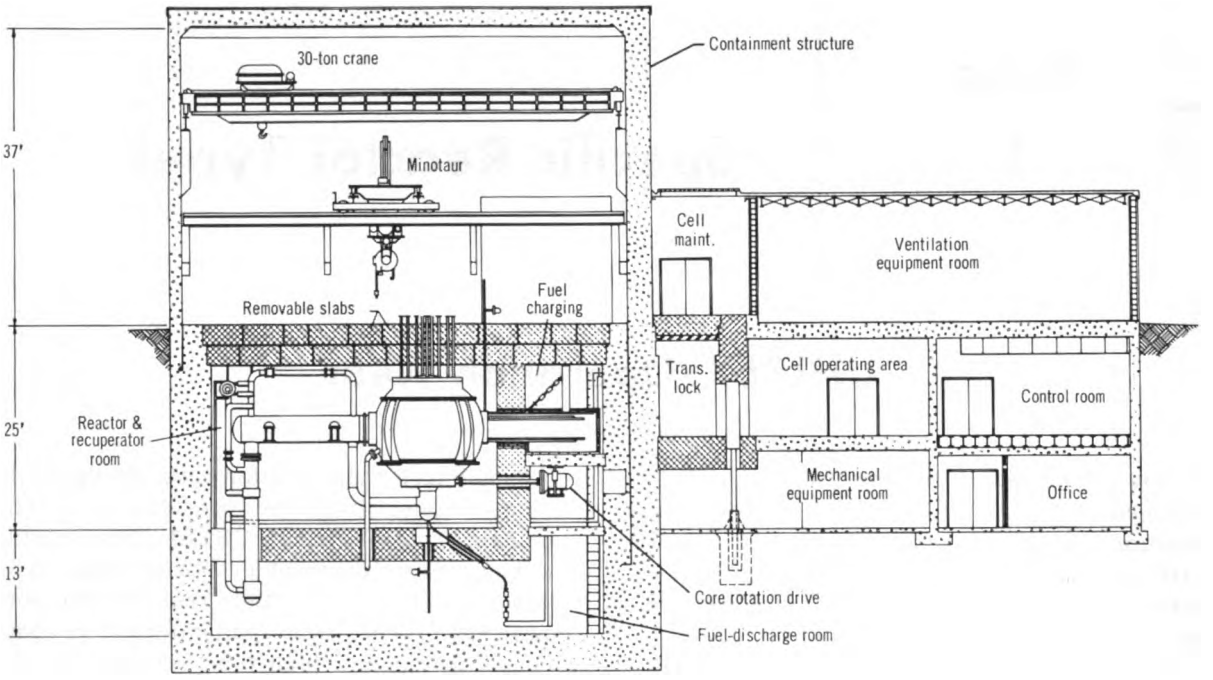

Fig. 1 The UHTREX facility consists of reactor primary system, containment structure, and control and service equipment rooms. The containment encloses reactor cell, primary coolant loop, fuel-loading apparatus, and fuel-discharge and gas-cleanup rooms.[5]

shielded reactor cell for the reactor, primary coolant loop, and fuel-loading apparatus; (2) a fuel discharge room; (3) a gas-cleanup room; and (4) two gas-cleanup piping rooms.

The UHTREX reactor (Figs. 2 and 3), which has a vertical cylindrical core surrounded by a reflector and insulation, is housed in a spherical pressure vessel with top-mounted control-rod drives. Fuel elements are loaded through one side of the reactor and discharged from the bottom. Table 1 (page 5) summarizes the parameters.

Fuel Elements

Each of the initial fuel elements to be used in UHTREX consists of an extruded hollow cylinder made of a mixture of graphite and 93% enriched UC_2 particles. The 5.5-in.-long cylinder has an inside diameter of 0.5 in. and an outside diameter of 1 in. Four of these fuel cylinders can be positioned end-to-end in the reactor horizontal fuel channels, each of which is 23.5 in. long and has a diameter of 1.1 in.

COATED-PARTICLE FUEL

The UC_2 particles are coated with pyrolytic carbon (PyC) to retard the release of fission products. The diameter range of the coated particles is about 350 to 450 μ, resulting from 100 to 110 μ of PyC coating on 147- to 208-μ UC_2 cores. This range represents a compromise between (1) the requirements for good particle strength and fission-product retention and (2) the need to keep the particle size and volume fraction of particles small to avoid difficulties in fabrication by the extrusion process. The PyC on the UC_2 particles is a General Atomic "Triplex" coating in which the 20- to 30-μ inner coating is a buffer layer of low-density PyC to catch fission recoils, to dissipate stresses caused by differential dimensional changes, and to provide a void volume that will minimize fission-gas pressure buildup. The 35- to 45-μ middle layer consists of "isotropic" (randomly oriented) PyC with low permeability to fission gases and good resistance to radiation damage. The outer layer is fine-grained columnar PyC. The interface between the isotropic and columnar layers is intended to retard the propagation of any cracks that might develop.[8] Fuel-element properties and fabrication methods and equipment have been described.[9]

MEASURING URANIUM CONTENT

The uranium content of each fuel element is determined nondestructively after fabrication

Digitized by Google

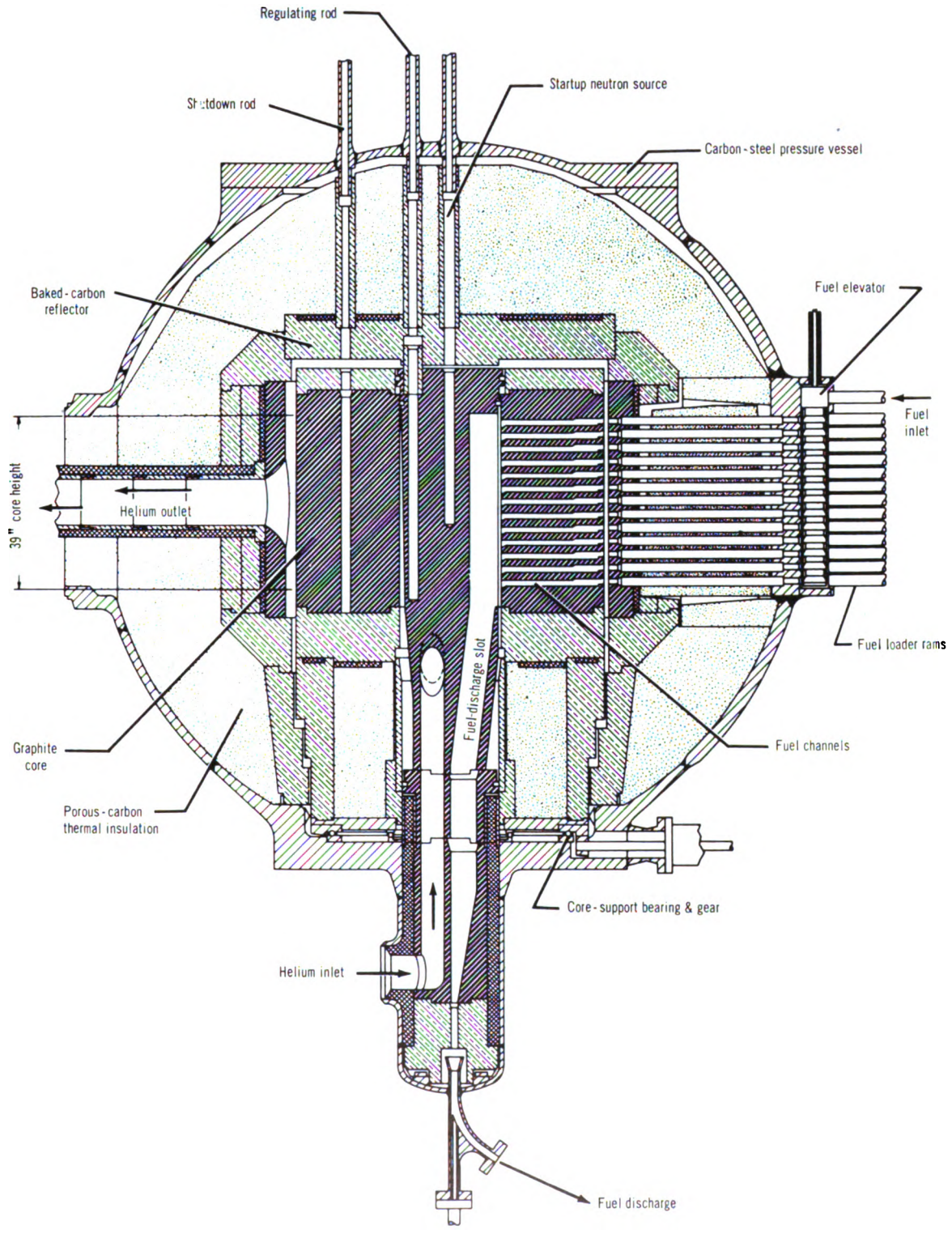

Fig. 2 Vertical cutaway of reactor shows horizontal fuel channels in annular core and vertical slot in stationary tapered central plug, through which discharged fuel elements drop when displayed by new element inserted by rams at right.[19]

Digitized by Google

by measurement of the gamma emission from the uranium with a NaI scintillator detector that completely surrounds the element. The integrated current produced in scintillator phototubes relates directly to the uranium content. Less than 2 min is required for a measurement with a relative standard deviation[8] of 0.3%.

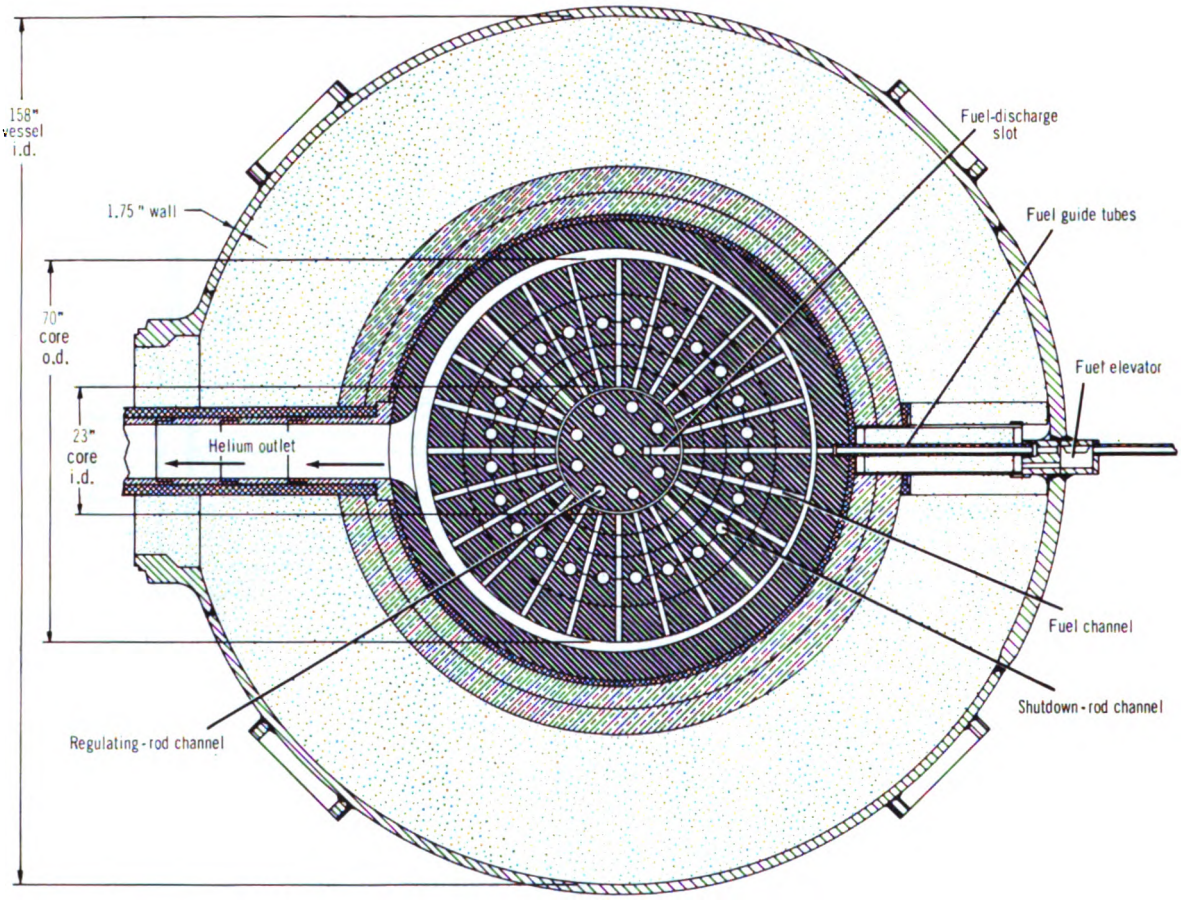

Fig. 3 Horizontal cutaway shows stationary central plug with fuel-discharge slot and eight channels for regulating rods (plus center channel for startup source), rotatable annular core with radial fuel channels and 24 vertical shutdown-rod channels, the outer reflector, insulation, and vessel wall.[19]

Reactor Core

The annular rotatable core is a hollow vertical cylinder (70 in. in outside diameter by 23 in. in inside diameter by 39 in. high) in which graphite serves as both the structural material and the moderator. The cylinder is made up of five concentric hollow cylinders so as to limit the thermal stresses across each piece of graphite. The fuel channels, which are 1.1-in.-diameter holes bored radially through the cylinder at 15° intervals in 13 horizontal planes, are separated vertically 3 in. center-to-center. Surrounding the core is a 16-in.-thick reflector made of 4 in. of graphite and 12 in. of dense ungraphitized carbon. Porous carbon between the reflector and the 13.5-ft-OD carbon-steel pressure vessel serves as insulation.

The hollow axial region of the core contains a tapered graphite plug; the taper leaves a plenum between the plug and the core through which the helium coolant enters the core to flow radially outward through the fuel channels. The entire annular core, together with portions of the reflector and insulation, can be rotated about the cylindrical axis so that fuel can be loaded and unloaded from the various channels. The movable portions (Fig. 4) rotate on a large-diameter dry-film-lubricated ball bearing whose integral

Digitized by Google

Table 1 SUMMARY OF UHTREX REACTOR CHARACTERISTICS[1,7]

Reactor type	Experimental, high-temperature, gas-cooled, unclad fuel
Rated power	3 Mw(t)
Fuel elements	Graphite cylinders, 1 in. OD, 0.5 in. ID, 5.5 in. long; pyrocarbon-coated fully enriched UC_2 particles dispersed in graphite
Moderator	Vertical graphite cylinder, 39 in. high, 70 in. OD, 23 in. ID
Reflector	4 in. of graphite plus 12 in. of dense carbon
Reactor vessel	Carbon-steel sphere, 13.2 ft ID, 1.75-in. wall, internally insulated
Fuel channels	312 radial, horizontal holes, each of 1.1 in. diameter, 23.5 in. length; 4 fuel elements/channel
Critical loading	11 kg 93% enriched uranium at design power and temperature and equilibrium poison; 5.7 kg 93% enriched uranium at zero power and 70°F
Temperature coefficient of reactivity	-1.52×10^{-5} Δk/°C in operating region (prompt) -1.05×10^{-4} Δk/°C in operating region -1.2×10^{-4} Δk/°C average from ambient to operating temperature
Power coefficient of reactivity	-9.2×10^{-6} $\Delta k/k$/kw (−0.13 ¢/kw)
Thermal-neutron flux	2 to 4×10^{13} neutrons/(cm²)(sec)
Fuel specific power	272 watts/g of ^{235}U (average)
Core power density	1.3 watts/cm³
Fuel burnup	10 to 50%
Refueling	At power
Rate	1 to 6 fuel elements/day; cycle time about 6 min/element
Excess reactivity required to compensate for temperature coefficient	~20% Δk
Control-rods material	B_4C in central rods; 1.9% boron–stainless steel in articulated core rods
Total worth	22% Δk
Withdrawal	18 in./min
Coolant maximum temperature	Helium at 500 psia max.; 10,250 lb/hr max. 1600°F inlet; 2400°F outlet

ring gear is mounted at the bottom of the pressure vessel.

Reactor Vessel

The spherical pressure vessel supports the core, moderator, reflector, insulation, and external components, including the fuel-loading mechanism and the control-rod drives (Fig. 2). The ASTM A-212B carbon-steel vessel is 13.4 ft in outside diameter with a 1.75-in. wall; it is designed for operating conditions of 650°F and 550 psig and for a test pressure of 825 psig.

As shown in Figs. 2 and 3, penetrations for the fuel loader and helium outlet nozzle are on the center line at opposite sides of the vessel. The fuel-elevator housing and a massive section penetrated by fuel-loading holes, both integral parts of the vessel wall, set up severe thermal stresses in the shell that are accommodated by a 3-in.-thick segment of the vessel wall. On the opposite side of the vessel is a short, 38-in.-ID nozzle for joining the recuperator to the pressure vessel. The vessel top is closed by an 11.7-ft-OD flanged cap that is bolted and seal welded; no gasket is used in the joint. The control-rod nozzles penetrate the cap. At the vessel bottom is a cylindrical extension that has a side nozzle to the helium inlet line and a dished bottom head that is penetrated by the fuel-discharge channel. There are two additional penetrations in the lower half of the sphere—one for instrumentation leads and one for the core indexing mechanism.

Reactor Control

Critical experiments show that the control system has a total rod worth of about 22% Δk. This is achieved by the insertion of 4 of the 12 control rods into the rotatable core region. Development of articulated control rods cleverly solved this alignment design problem.

As shown in Fig. 3, the 12 control rods hang in vertical holes arranged in two circles centered about the core axis;[1,11] the inner 8 holes are at a radius of 7.9 in. from the axis (and are in the stationary central plug), and the outer 24 holes are 23 in. from the center (and thus are in the rotatable core).

REGULATING RODS

The inner eight control rods, whose channels are within the stationary central graphite plug, are calculated[12] to be worth 14% Δk. These central rods will be used for control and safety

Digitized by Google

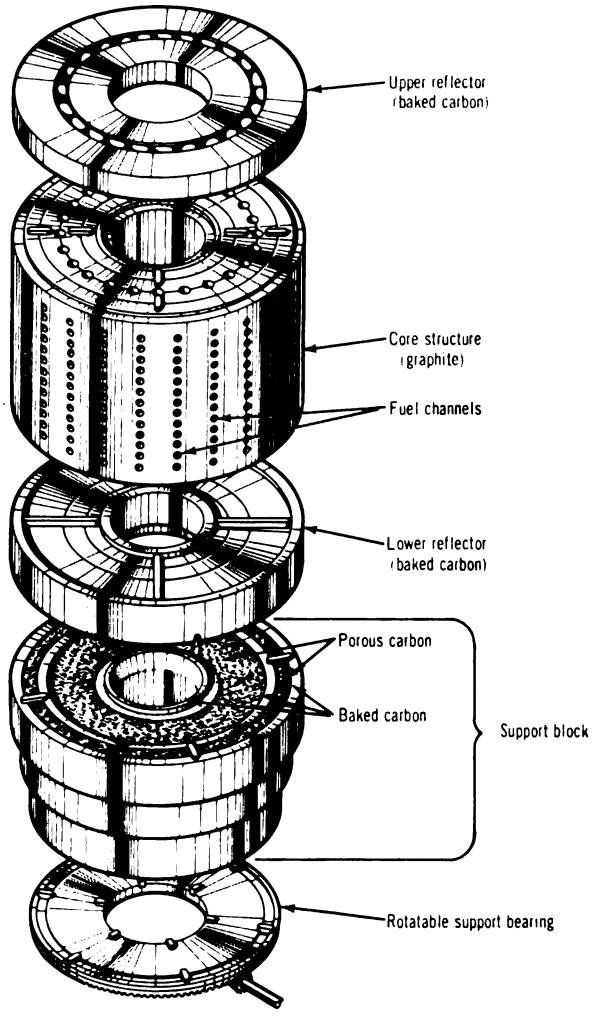

Fig. 4 Annular core as well as upper and lower reflectors and support block are mounted on support bearing that can be rotated to align horizontal fuel channels with refueling rams.[10]

during reactor operation as well as for shutting down the reactor.

Because these central regulating rods are in the hot reactor atmosphere during operation, they are made of refractory materials (Fig. 5). Each regulating-rod assembly, whose diameter is 1 in. and active length is 40 in., consists of pressed B_4C cylinders mounted on a 0.25-in.-diameter niobium support rod that has a flange swaged onto its lower end (because niobium-weld areas embrittle when exposed to impure 2400°F helium,[8] the support rod and end flange had to be swaged rather than welded). The regulating rod in Fig. 5 has a graphite sheath, but scram deceleration stresses have required that the design be changed to a niobium sheath.[13]

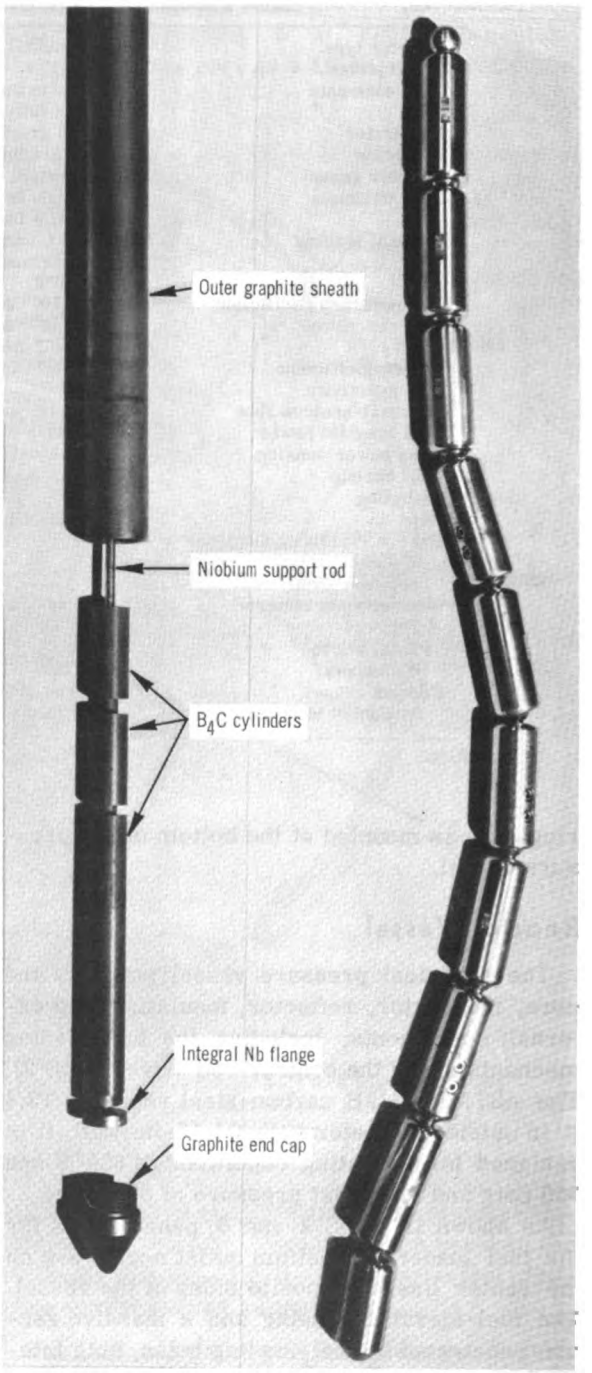

Fig. 5 The regulating rod (left), which moves within stationary central graphite region during reactor operation, is made of refractory materials; in newer design, outer sheath is niobium rather than graphite. The shutdown rod (right, but not to same scale), which is made of type 304 stainless steel—1.9% boron alloy and is inserted into channels in rotatable core only during extended shutdowns or for emergencies, consists of 4-in.-long ball-jointed segments that can go into channel if rod and channel are aligned[1] within 7.5°.

Digitized by Google

CORE SHUTDOWN RODS

The outer set of four control rods, whose 24 channels are within the rotatable core region, normally will be completely withdrawn from the core during reactor operation — they will be inserted only in case of an emergency or for extended shutdowns, when the reactor cools enough that additional shutdown reactivity is required to override the negative temperature coefficient of reactivity.

Analysis indicates that the eight central (in the stationary plug) regulating rods are adequate to bring the reactor subcritical at temperatures well below 900°F. Thus, by allowing the core to cool below 1800°F before inserting the core shutdown rods, the designers avoid having to make these articulated rods of refractory materials.

Each of the core rods, made of type 304 stainless steel–1.9% boron alloy, has a 1.4-in. outside diameter and a 40-in. active length.[14] These four rods are made of assemblies of 4-in.-long ball-jointed segments (Fig. 5) to provide flexibility so they can be inserted into the core even if the channels are not aligned with the rod-drive mechanisms. The core has 24 vertical channels into which the four shutdown rods can be inserted (Fig. 3) to permit up to 7.5° of rod-to-channel misalignment; these vertical channels are spaced at 15° intervals and pass between the horizontal radial fuel channels. If necessary, the core can be rotated as much as 15° with the articulated rods inserted.[10] Thermal-cycling tests show that all the ball joints remain free-acting throughout 1542 cycles.[15,16] The maximum temperature at which these rods can be inserted into the core is 1800°F, above which significant socket scaling occurs. Contamination of the graphite moderator by boron from the shutdown rods will be negligible because core temperature will drop after shutdown and these articulated rods will be in only line contact with the holes.

CONTROL-ROD DRIVES

One basic type of control-rod-drive mechanism has been designed for both the central regulating rods and the articulated shutdown rods.[7] The drive consists of an a-c hysteresis synchronous motor, with a d-c brake, driving a rack-and-pinion through a 940 : 1 ratio planetary gear train at a single drive speed of 18 in./min. The gear rack is machined on a ball spline that is used for the vertical guide. The entire drive mechanism is within the high-pressure primary coolant region, which eliminates seal problems.

Free-fall scram of the eight central rods is triggered by interrupting electric power to a stationary magnetic clutch that normally engages the gear train to the pinion. The free-falling control rods are decelerated in the control-rod dashpot by $\frac{1}{16}$-in.-diameter hardened and ground steel balls that collectively act as a "semi-fluid." Successful tests were run on a device with a 0.95-in.-diameter knob on the end of a 0.75-in.-diameter shaft that fell through a 1.625-in.-OD tube containing these balls.[17] A "spring" formed by a 12-turn helical path cut into the wall of the impact tube eases the initial deceleration shock.[13]

Analytical results indicate that the reactor is stable and that the overall system is well behaved. Typical thermal time constants are in the range[6] 100 to 1000 sec. Although thermal excursions in the core might arise from difficulties in the coolant loops, metallic components in the loops would be affected much more rapidly and radically than the refractory core would be. Thus action must be taken to protect the coolant loop from thermal effects well before the reactor itself would suffer damage.[7]

Fuel-Handling System

Figure 6 shows the entire fueling system for UHTREX. The short horizontal conveyor brings fuel elements from the fuel-handling cell; a dual-valve gas lock admits them into the containment. The sloping conveyor raises each element to the top of the gas-lock sequence, through which it enters the reactor coolant system. The top ram in the loader mechanism advances the element into the fuel elevator on the side of the reactor vessel; the elevator positions it at any of the 13 levels of horizontal fuel channels. Then the electrically powered loading ram at the desired level pushes the element into the outer edge of the core and, in so doing, pushes the innermost element so that it drops through the vertical slot in the central core plug, passes down through the vessel extension and lower gas lock, and is removed by the discharge conveyor. After the discharged element drops through the two valves to leave the containment enclosure, the long horizontal conveyor carries it into the fuel-handling cell. To align various fuel channels for refueling, the core can be rotated about its vertical axis by the electrically powered indexing mechanism.[10]

Digitized by Google

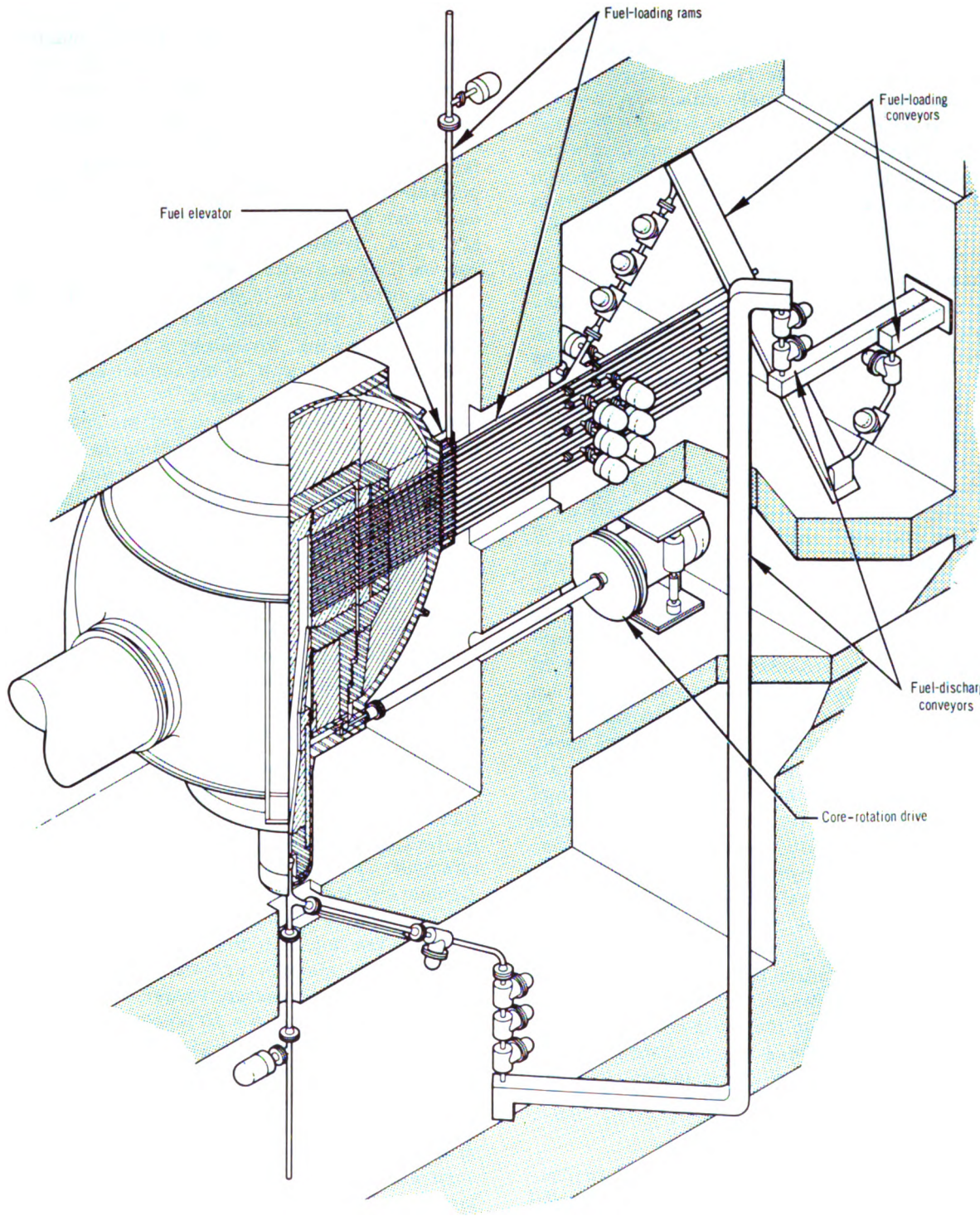

Fig. 6 Incoming fuel on conveyors enters containment and reactor system through two sets of gas-valve locks. The elevator (on right side of reactor vessel) aligns fuel element vertically with proper channel in core. When ram inserts new element, displaced spent element falls through central slot, leaves reactor, and is conveyed from primary system and containment through two sets of gas-valve locks.[10]

Digitized by Google

GAS VALVES

Considerable development work and testing have gone into the design of ball valves for the gas locks in the reactor coolant system. It was concluded[16] that "it is not possible to devise an all-metallic seal with a leakage consistently less than 10^{-5} standard cm^3/sec at 500 psi differential pressure under severe service conditions in which abrasive particles are introduced into the valve as it is operated through several thousand cycles. Soft metal seals were found to be effective initially, but the introduction of traces of particulate matter caused them to leak badly, even after cleaning wipers were employed. The hard metal seals were not so adversely affected by abrasive particles but under 500 psi pressure differential, they never seal very well, even initially."

The prototype ball valve has a hard metal seal that holds pressure from either direction. Under a continuing series of endurance tests,[14] this valve survived 2500 cycles under a 250-psi pressure differential with leakage of only 10^{-3} cm^3/sec. After the seat was relapped, the valve endured 4500 more cycles with a 500-psi differential before helium leakage exceeded 1.3×10^{-3} cm^3/sec. Primary coolant leakage past a primary valve is bled to a low-pressure receiver for storage until it is pressurized and returned to the primary coolant system.[1]

Cooling System

At full reactor power, two closed-cycle helium loops in series (Fig. 7) remove 3 Mw of heat from the reactor core and dissipate it to the atmosphere. The primary coolant loop forms a closed system inside the containment. Heat passes from the primary loop to the secondary cooling loop through the main heat exchanger; the secondary loop takes the heat to an air-cooled heat exchanger outside the reactor building. Helium flow rates in the two loops are matched.

In the primary coolant loop, 1600°F helium enters the reactor central plenum, from which it passes radially outward through the fuel channels, where it is heated to 2400°F. The helium is cooled to 1400°F as it passes through the hot side of the recuperator, one end of which is bolted and seal-welded directly to the

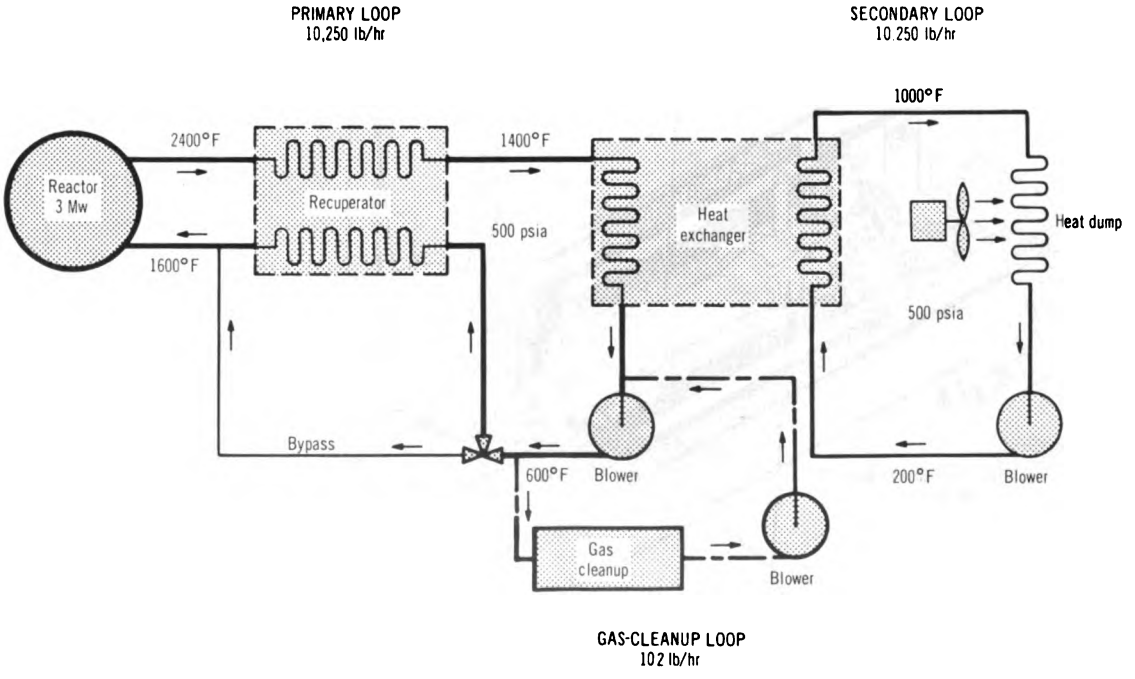

Fig. 7 In primary loop, hot helium from reactor passes through recuperator (which cools it 1000°F) and heat exchanger (which transfers heat to clean helium in secondary loop); blower circulates primary-system helium back to reactor through recuperator. The secondary clean-helium loop dissipates heat through radiator to atmosphere. Cleanup loop removes fission products from primary-system helium.[10]

Digitized by Google

reactor vessel; the other end is connected to the main heat exchanger.

THE RECUPERATOR

This internally insulated regenerative heat exchanger made of graphite in a carbon-steel pressure shell cools the outlet helium to temperatures tolerable in the stainless-steel heat exchanger. Heat exchange in the recuperator is achieved in a 2- by 2- by 8.7-ft block of graphite that is penetrated by 440 holes bored parallel to the long axis. The 0.5-in.-diameter holes are drilled on $^{15}/_{16}$-in. centers arranged in 22 columns. The hot and cold gases flow countercurrently through adjacent holes.[19]

MAIN HEAT EXCHANGER

From the recuperator the helium flows to the main heat exchanger where it is cooled to 600°F by transferring heat to the secondary coolant loop. The main heat exchanger is made of type 316 stainless steel and has bayonet tubes to avoid thermal-stress problems. The 87 bayonet-tube assemblies each consist of three concentric tubes. When the 1400°F primary coolant enters the exchanger, it flows down the innermost tube, reverses direction at the bottom, and then flows up through the outer tube, where it exchanges heat with the secondary coolant in the main shell. The intermediate tube in the bayonet assembly serves only to provide a stagnant helium gap that acts as a thermal insulator between the entering and exiting primary coolant; a sample wire that can be inserted into the annulus of the bayonet assembly can be withdrawn periodically for radiochemical analyses to measure the rate of fission-product buildup in the heat exchanger.

MAIN BLOWER

When the primary coolant leaves the heat exchanger, it passes through the main circulating blower, then back to the recuperator inlet. The helium blower (Fig. 8) is driven by a three-

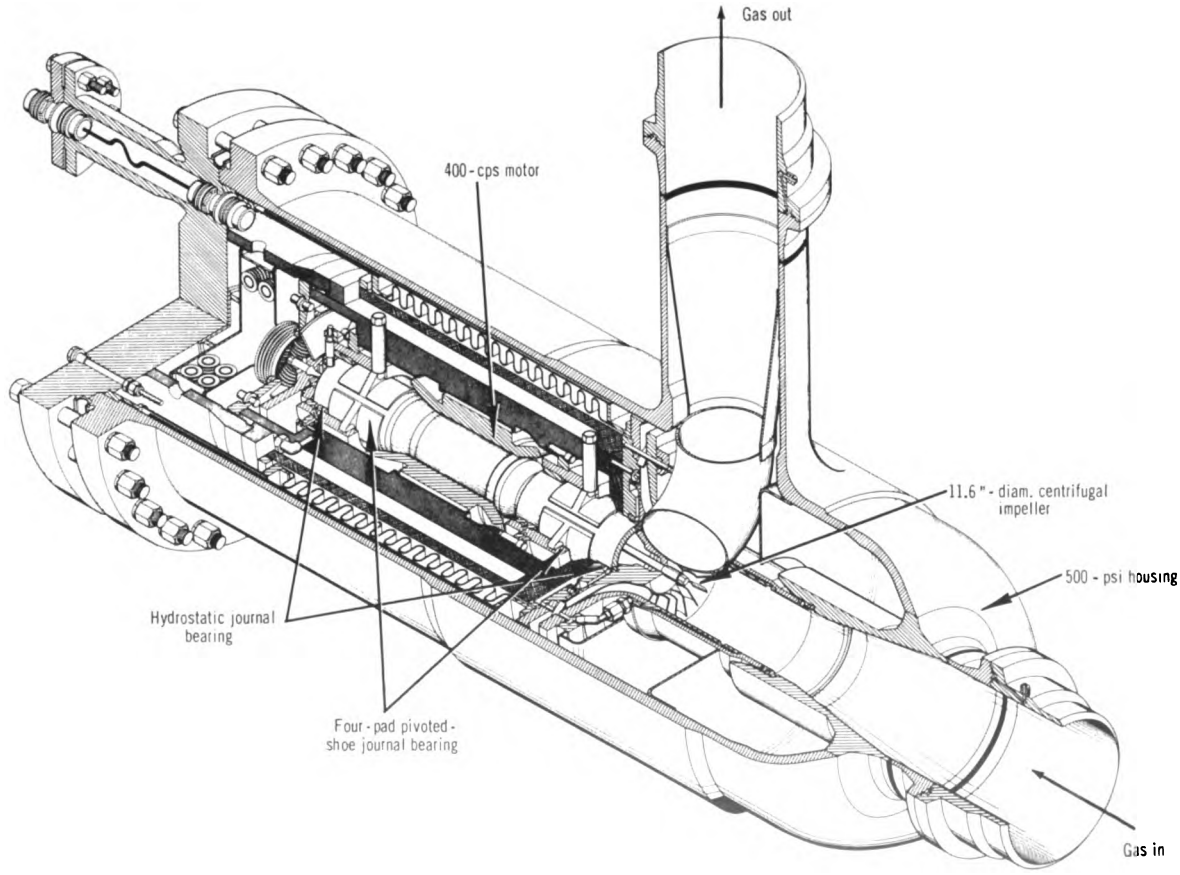

Fig. 8 The main blower raises pressure of 10,250 lb/hr of 510-psi helium 8 psi between heat exchanger and recuperator inlet. Helium serves as lubricant for blower bearings, and a water-cooled heat exchanger (not shown) cools by-passed helium that in turn cools shaft journals and motor.[7]

Digitized by Google

phase two-pole squirrel-cage induction motor rated at 65 hp at 1200 rpm. The open-face impeller on the centrifugal blower has an 11.6-in. diameter and 19 vanes. Helium-lubricated hydrodynamic bearings support the rotor, and hydrostatic pressure is applied during starts and stops; a centrifugal fan circulates helium through a water-cooled heat exchanger to cool the shaft journals and motor.[18] A variable-frequency alternator, magnetically coupled to two 75-hp 60-cycle motors, drives the blower motor. Each 75-hp motor can carry the alternator load and is supplied by a separate power source to prevent loss of pumping power if one of the main power feeders fails. With helium at 500 psi and 600°F, the blower is designed to deliver 10,250 lb/hr with a pressure rise of 8 psi.

Gas-Cleanup System

The chemical inertness of the coolant is preserved, and the amount of volatile long-life fission-product contamination in the primary loop is reduced, by the continuous purification of 102 lb of the helium stream per hour in the gas-cleanup system, a sidestream of the primary loop (Fig. 9).

Helium from the primary loop enters the cleanup system through a replaceable stainless-steel filter that removes particulate matter as small as 0.5 μ in diameter, is heated to 1200°F in an electrical preheater, then flows into a copper oxide bed, where carbon and hydrogen compounds in the helium are oxidized to CO_2 and H_2O, respectively. After leaving the copper oxide bed, the helium is cooled to 100°F and enters the tubes of a water-cooled decay heat exchanger. Activated carbon packed in these tubes delays passage of the krypton and xenon fission products by gas chromatography and adsorbs any iodine or bromine fission products. The radioactive decay of the fixed halogens and delayed noble gases liberate about 12 kw of heat.

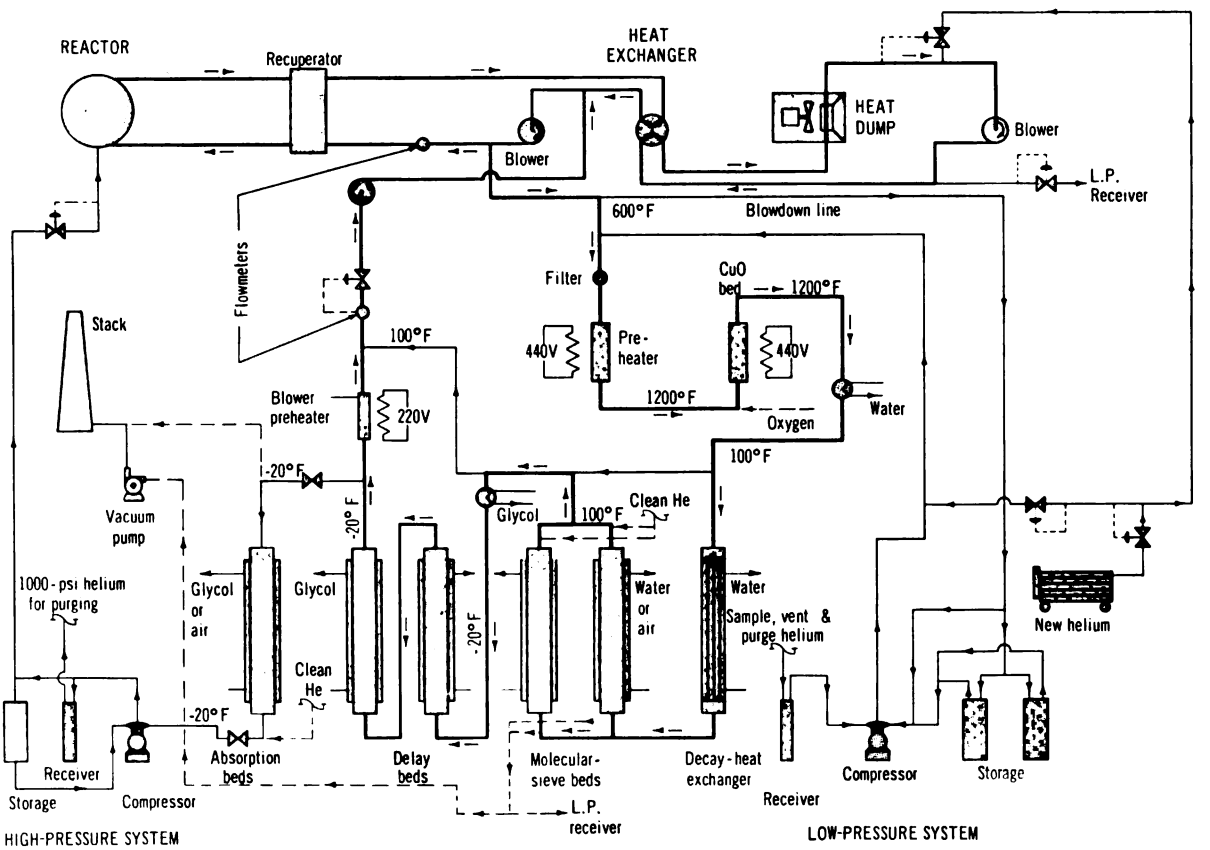

Fig. 9 Gas-cleanup system in 102 lb/hr sidestream of primary loop removes carbon and hydrogen impurities and removes or delays long-life volatile fission products in the helium by means of filters, absorbers, gas chromatography, oxidizing beds, molecular sieves, and delay beds.[10]

Digitized by Google

This decay heat exchanger protects both the downstream molecular sieve and the delay beds from localized overheating.

The molecular sieves reduce the concentration of CO_2 and water in the helium to less than 1 ppm. After leaving the sieve beds, the 100°F helium is refrigerated to –20°F, the operating temperature of the carbon beds. These carbon delay beds, which are packed with activated carbon and are maintained at –20°F by refrigerated ethylene glycol in external jackets, delay krypton for 43.6 hr (10 half-lives of ^{85}Kr) and xenon for 1790 hr (14 half-lives of ^{133}Xe). When the helium leaves the delay beds, the blower preheater heats it to 100°F and then the cleanup-system blower returns it to the primary loop.

Critical Experiment

A critical experiment used an assembly of the actual core, reflector, and fuel elements and a close simulation of the reactor control rods. First criticality with the assembly was achieved on June 9, 1965.

The observed critical mass of 6.5 kg was considerably larger than the calculated 4-kg critical mass.[17] Studies of these results attribute the deviation from calculations to (1) neglect of the effect of streaming through the exit coolant hole and the fuel-element slot, (2) uncertainties in the total effective cross section of the fabricated graphite, (3) a need for more careful treatment of the neutron-thermalization and the self-shielding effects of the fuel elements, and (4) the absence in the critical experiment of the additional reflector provided by the carbon insulation in UHTREX.

On-Line Computer

An on-line process computer will aid in the operation of the reactor, the reactor-coolant loops, and the coolant-purification system.

The computer system includes a central processor with 4000 words of magnetic-core memory, 32,000 words of drum memory, an input–output typewriter, and a paper-tape punch and reader; there are four logging typewriters and one visual-display unit. The system samples 600 analog and 300 digital inputs and sets 24 analog and 444 digital outputs. Twenty interrupt channels allow time-sharing of input–output equipment and initiate special programs that depend on UHTREX system conditions.[6]

The computer samples analog channels at a rate of 200 channels/sec and monitors them for out-of-limit conditions. It can prepare logs, perform on-line calculations, keep reactor fuel and other system histories, and monitor reactor-operator activities. The computer also has the capability of sequencing valves in operations such as fuel loading and can control coolant flow and thermal output of the cooling system. In addition, system diagnostic programs and emergency-shutdown programs will be available to assist in operation of the system.[6]

References

1. John H. Russell, K-Division, Los Alamos Scientific Laboratory, personal communications, Aug. 11, 1965, and Apr. 12, 1966.
2. The TURRET Experiment, *Power Reactor Technol.*, 2(4): 83-85 (September 1959).
3. R. P. Hammond et al., TURRET: A High Temperature Gas-Cycle Reactor Proposal, USAEC Report LA-2198, Los Alamos Scientific Laboratory, Jan. 23, 1958.
4. R. P. Hammond and J. R. Cody (Eds.), A Preliminary Study of the TURRET Experiment—An Operating Test of Unclad Fuel at High Temperature, USAEC Report LA-2303, Los Alamos Scientific Laboratory, March 1959.
5. Los Alamos Scientific Laboratory, Quarterly Status Report on Ultra High Temperature Reactor Experiment (UHTREX) for Period Ending February 20, 1962, USAEC Report LAMS-2678, March 1962.
6. H. B. Demuth, F. P. Schilling, and L. Weintraub, Ultra High Temperature Reactor Experiment On-Line Process Computer, USAEC Report LADC-6891 (Conf. 650413-1), Los Alamos Scientific Laboratory, presented at the Symposium on Neutron Dynamics and Control, Tucson, Arizona, April 1965.
7. Los Alamos Scientific Laboratory, Ultra High Temperature Reactor Experiment (UHTREX) Hazard Report, USAEC Report LA-2689, March 1962.
8. Los Alamos Scientific Laboratory, Quarterly Status Report on Advanced Reactor Technology (ART) for Period Ending January 31, 1964, USAEC Report LA-3244-MS, February 1965; W. V. Goeddel, Development and Utilization of Pyrolytic-Carbon-Coated Carbide Fuel for the High-Temperature Gas-Cooled Reactor, *Nucl. Sci. Eng.*, 20(2): 201-218 (October 1964).
9. J. M. Taub et al., Coated Particle Fuel Elements for UHTREX, USAEC Report LA-3378, Los Alamos Scientific Laboratory, July 1965.
10. Los Alamos Scientific Laboratory, Status Report on Ultra High Temperature Reactor Experiment (UHTREX) for Four-Month Period Ending September 20, 1962, USAEC Report LAMS-2782, October 1962.
11. Los Alamos Scientific Laboratory, Quarterly Status Report on Ultra High Temperature Reactor Experiment (UHTREX) for Period Ending May 20, 1962, USAEC Report LAMS-2722, June 1962.
12. Los Alamos Scientific Laboratory, Quarterly

Digitized by Google

Status Report on Ultra High Temperature Reactor Experiment (UHTREX) for Period Ending December 20, 1963, USAEC Report LAMS-3036, January 1964.
13. Los Alamos Scientific Laboratory, Quarterly Status Report on Advanced Reactor Technology (ART) for Period Ending January 31, 1966, USAEC Report LA-3482-MS, February 1966.
14. Los Alamos Scientific Laboratory, Quarterly Status Report on Ultra High Temperature Reactor Experiment (UHTREX) for Period Ending September 20, 1964, USAEC Report LA-3190-MS, October 1964.
15. Los Alamos Scientific Laboratory, Quarterly Status Report on Ultra High Temperature Reactor Experiment (UHTREX) for Period Ending March 20, 1963, USAEC Report LAMS-2894, April 1963.
16. Los Alamos Scientific Laboratory, Quarterly Status Report on Ultra High Temperature Reactor Experiment (UHTREX) for Period Ending June 20, 1963, USAEC Report LAMS-2933, July 1963.
17. Los Alamos Scientific Laboratory, Quarterly Status Report on Advanced Reactor Technology (ART) for Period Ending July 31, 1965, USAEC Report LA-3370-MS, August 1965.
18. Los Alamos Scientific Laboratory, Quarterly Status Report on Ultra High Temperature Reactor Experiment (UHTREX) for Period Ending September 20, 1963, USAEC Report LAMS-2984, October 1963.
19. Los Alamos Scientific Laboratory, Quarterly Status Report on Ultra High Temperature Reactor Experiment (UHTREX) for Period Ending December 20, 1962, USAEC Report LAMS-2835, January 1963.

LEGAL NOTICE

This journal was prepared under the sponsorship of the U. S. Atomic Energy Commission. Neither the United States, nor the Commission, nor any person acting on behalf of the Commission:

A. Makes any warranty or representation, expressed or implied, with respect to the accuracy, completeness, or usefulness of the information contained in this journal, or that the use of any information, apparatus, method, or process disclosed in this journal may not infringe privately owned rights; or

B. Assumes any liabilities with respect to the use of, or for damages resulting from the use of any information, apparatus, method, or process disclosed in this journal.

As used in the above, "person acting on behalf of the Commission" includes any employee or contractor of the Commission, or employee of such contractor, to the extent that such employee or contractor of the Commission, or employee of such contractor prepares, disseminates, or provides access to, any information pursuant to his employment or contract with the Commission, or his employment with such contractor.

Digitized by Google

Digitized by Google

Digitized by Google

640
GIFT
SEP 14 '68

Digitized by Google

NUCLEAR SCIENCE ABSTRACTS

The U. S. Atomic Energy Commission, Division of Technical Information, publishes *Nuclear Science Abstracts* (*NSA*), a semimonthly journal containing abstracts of the literature of nuclear science and engineering.

NSA covers (1) research reports of the U. S. Atomic Energy Commission and its contractors; (2) research reports of government agencies, universities, and industrial research organizations on a worldwide basis; and (3) translations, patents, books, and articles appearing in technical and scientific journals.

Complete indexes covering subject, author, source, and report number are included in each issue. These are cumulated quarterly, semiannually, and annually providing a detailed and convenient key to the literature.

Availability of *NSA*

SALE *NSA* is available on subscription from the Superintendent of Documents, U. S. Government Printing Office, Washington, D. C., 20402, at $30.00 per year for the semimonthly abstract issues and $22.00 per year for the four cumulated-index issues. Subscriptions are postpaid within the United States, Canada, Mexico, and all Central and South American countries, except Argentina, Brazil, British and French Guiana, Surinam, and British Honduras. Subscribers in these Central and South American countries, and in all other countries throughout the world, should remit $37.00 per year for subscriptions to semimonthly abstract issues and $25.00 per year for the four cumulated-index issues.

EXCHANGE *NSA* is also available on an exchange basis to universities, research institutions, industrial firms, and publishers of scientific information. Inquiries should be directed to the Division of Technical Information Extension, U. S. Atomic Energy Commission, P. O. Box 62, Oak Ridge, Tennessee, 37830.

Digitized by Google

TECHNICAL PROGRESS REVIEWS may be purchased from Superintendent of Documents, U. S. Government Printing Office, Washington, D. C., 20402. *Nuclear Safety* at $3.00 per year for each subscription or $1.00 per issue; the other four journals at $2.50 per year or $0.70 per issue. The use of the coupon below will facilitate the handling of your order.

POSTAGE AND REMITTANCE: Postpaid within the United States, Canada, Mexico, and all Central and South American countries except Argentina, Brazil, Guyana, French Guiana, Surinam, and British Honduras. For these Central and South American countries and all other countries, add $0.75 for each annual subscription or $0.20 for a single issue. Payment should be by check, money order, or document coupons, and MUST accompany order. Remittances from foreign countries should be made by international money order or draft on an American bank payable to the Superintendent of Documents or by UNESCO book coupons.

order form

SUPERINTENDENT OF DOCUMENTS
U. S. GOVERNMENT PRINTING OFFICE
WASHINGTON, D. C., 20402

Enclosed:
document coupons ☐ check ☐ money order ☐

Charge to Superintendent of Documents No._____

Please send a one-year subscription to

☐ ISOTOPES AND RADIATION TECHNOLOGY

☐ POWER REACTOR TECHNOLOGY

☐ REACTOR FUEL PROCESSING

☐ REACTOR MATERIALS

(Each subscription $2.50 per year; $0.70 per issue.)

☐ NUCLEAR SAFETY

(Each subscription $3.00 per year; $1.00 per issue.)

SUPERINTENDENT OF DOCUMENTS
U. S. GOVERNMENT PRINTING OFFICE
WASHINGTON, D. C., 20402

(Print clearly)

_____
Name

_____
Street

_____
City, State, ZIP Code

Digitized by Google

E119
TK
9202
.A4

POWER REACTOR TECHNOLOGY

ENGINEERING
FEB 17 '67
LIBRARY

A Quarterly Technical Progress Review

Prepared for DIVISION OF TECHNICAL INFORMATION, USAEC, by
ARGONNE NATIONAL LABORATORY

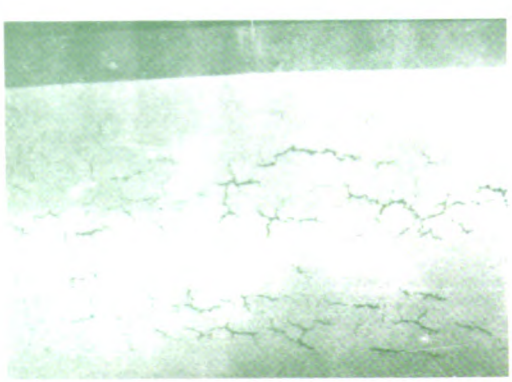

How serious are vessel cladding failures? ... see page 101

Summer 1966

● VOLUME 9

● NUMBER 3

Digitized by Google

TECHNICAL PROGRESS REVIEWS

To meet the needs of industry for concise summaries of current atomic developments, the Atomic Energy Commission is publishing this series, Technical Progress Reviews. Issued quarterly, each of the reviews digests and evaluates the latest findings in a specific area of nuclear technology and science.

The journals published in this series are:

Isotopes and Radiation Technology P. S. Baker, A. F. Rupp, and associates
Oak Ridge National Laboratory

Nuclear Safety Wm. B. Cottrell, W. H. Jordan, J. P. Blakely, and associates
Nuclear Safety Information Center, Oak Ridge National Laboratory

Power Reactor Technology
Argonne National Laboratory

Reactor Materials E. M. Simons and associates
Battelle Memorial Institute

See the back cover for availability information.

The views expressed in this publication do not necessarily represent those of the United States Atomic Energy Commission, its divisions or offices, or of any Commission advisory committee or contractor.

Availability of Reports Cited in This Review

Unclassified AEC reports are available for inspection at AEC depository libraries and are sold by the Clearinghouse for Federal Scientific and Technical Information, National Bureau of Standards, U. S. Department of Commerce, 5285 Port Royal Road, Springfield, Va., 22151. Some of the reports cited are not available owing to their preliminary nature; however, the information contained in them will eventually be made available in formal progress or topical reports.

Unclassified reports issued by other Government agencies or private organizations should be requested from the originator.

Unclassified British and Canadian reports may be inspected at AEC depository libraries. British reports are sold by the British Information Service, 45 Rockefeller Plaza, New York, N. Y.; Canadian reports (AECL series) are sold by the Scientific Document Distribution Office, Atomic Energy of Canada, Ltd., Chalk River, Ontario, Canada.

Classified U. S. and foreign reports identified in this journal as Classified may be purchased by properly cleared Access Permit Holders from the Division of Technical Information Extension, U. S. Atomic Energy Commission, P. O. Box 1001, Oak Ridge, Tenn., 37830. Such reports may be inspected at classified AEC depository libraries.

Digitized by Google

Contents

Power Reactor Technology

Vol. 9, No. 3

COMPONENTS — How Serious Are Vessel Cladding Failures? 101
Edward A. Wimunc

OPERATING EXPERIENCE — Nuclear Plant Performance—Good and Getting Better 110
George F. Bierman and Walter J. Miller

FLUID AND THERMAL TECHNOLOGY — Applying High-Temperature Instrumentation in Liquid-Metal Experiments 123
Paul A. Lottes

SPECIFIC REACTOR TYPES — Advances in Materials for Organic-Cooled Reactors 137
Edmund S. Sowa

CONTROL AND DYNAMICS — Two Advances in Reactor Neutron-Noise Analysis 142
Charles E. Cohn

PHYSICS — Water-Reactor Lattice Calculations and Measurements 145
Edwin M. Pennington

APPLICATIONS — Nuclear Power To Explore the Ocean Deeps 150
Edward J. Croke

LIMITED COVERAGE OF FUEL PROCESSING

The Technical Progress Review *Reactor Fuel Processing* is being terminated with the Vol. 9, No. 4, issue. Limited coverage of fuel processing will continue in *Power Reactor Technology* beginning with the Winter issue, Vol. 10, No. 1.

Issued quarterly by the U. S. Atomic Energy Commission. Use of funds for printing this publication approved by the Director of the Bureau of the Budget on July 8, 1966.

Digitized by Google

Power Reactor Technology is a quarterly review of developments in reactor technology—including new concepts and applications as well as research results, analysis, and experience with existing or new components and systems. Prepared by Argonne National Laboratory at the request of the Division of Technical Information of the U. S. Atomic Energy Commission, *Power Reactor Technology* is intended for reactor designers and other technical specialists concerned with the interplay among reactor development, design, construction, operation, and economics. Thus this quarterly journal reports and interprets progress in the power-reactor field in terms of its significance to the reactor designer. Its scope includes research and development in the various technical specialties in the field as well as design and construction practices, reactor concepts, applications, economics, and operating experience.

Some articles summarize and critically evaluate reported developments; others review a topic broadly so that designers can interpret new developments, experience, and trends. All, however, call the reader's attention to reports and publications that merit study. Because any appraisal involves the reviewer's opinion of the significance of the work reported, readers are urged to consult the references for additional information and the judgments of the original authors. If a reader has information that causes his evaluation to reinforce, modify, or contradict the opinions of our reviewers, he is encouraged to write to the Editor.

For reasonably timely coverage, articles often must be based on fragmentary information. Thus, whenever appropriate, continuity will be maintained from one issue to another by use of subject headings that reflect parts of the following scope of the journal:

> CONCEPTS and APPLICATIONS: Progress in evaluating the applicability and economics of various reactor types and systems (including unconventional approaches), as well as of fuel resources and cycles, for utility central-station generation of electricity, auxiliary power, process radiation and heat, desalting, and propulsion—and for terrestrial, undersea, aerospace, and other advanced uses.
>
> ANALYSIS and EXPERIMENTATION: Advancements in the techniques of reactor physics, fluid and thermal technology, power conversion, fuel elements, materials, mechanics, control and dynamics, and reactor safety.
>
> SYSTEMS and COMPONENTS: Experience as reflected in design and construction practice, components, systems technology, and operating performance of various specific types of reactors—including pressurized- and boiling-water reactors, molten-salt, organic-, gas-, and liquid-metal-cooled reactors, as well as generally applicable aspects of research and test reactors.

At Argonne National Laboratory, the Reactor Engineering Division (L. J. Koch, Director) has the principal responsibility for the preparation of *Power Reactor Technology*, with the regular assistance of the Reactor Physics Division (R. A. Avery, Director) and the occasional assistance of other Laboratory divisions (Metallurgy, Chemical Engineering, Chemistry, Reactor Operations, and Idaho). Thus, unless noted otherwise, the reviewers and authors of articles are Laboratory staff members. The editors will welcome interpretive review articles contributed by readers outside the Laboratory.

JAMES J. DUTTON, *Editor*
DAVID H. LENNOX, *Technical Editor;* KARL K. BROWN, *Managing Editor*
EDWARD J. CROKE and RAYMOND GOLD, *Associate Editors*
BARBARA A. SCHMEH, *Assistant Editor*

Argonne National Laboratory

Digitized by Google

How Serious Are Vessel Cladding Failures?

By Edward A. Wimunc

Defects have been discovered in the thin stainless-steel claddings that line the carbon-steel pressure vessels in three water-reactor systems. Historically, the principal function of reactor-vessel cladding has been to prevent vessel corrosion that would lead to the circulation of radioactive corrosion products through the system; i.e., the principal function of the cladding is to protect the coolant, not the vessel. Although the cladding defects found are not of sufficient area to pose operating problems because of corrosion-product radioactivity, their presence raised questions concerning their cause and their potential for weakening the vessel wall by means of crack propagation or localized corrosion.

In vessel design the thin cladding is not considered to impart any strength to the vessel. Therefore the presence of cracks in the cladding does not impair the vessel strength. However, the possibility of crack propagation into the thick carbon-steel wall led to extensive investigations. The investigations indicate that none of the cracks extend into the carbon steel, that the mechanisms causing the cladding failures are unlikely to cause cracking of the carbon steel, and that the corrosion of the carbon steel is unlikely to jeopardize the integrity of these pressure vessels, all of which are considerably thicker than is dictated by design of boiler and pressure-vessel code requirements.

Careful surveillance programs are being conducted to verify the continuing validity of these conclusions. Their findings will prove invaluable in guiding future design and fabrication practices for reactor vessels. In the meantime it is worthwhile to consider the studies made of the causes and limits of these cladding defects.

The Vessels

The four pressure vessels in which cladding failures have been detected are (1) the Experimental Boiling Water Reactor (EBWR) vessel,[1] (2) the Yankee-Rowe reactor vessel,[2] (3) the Yankee-Rowe reactor-system pressurizer,[3,4] and (4) the Elk River reactor vessel.[5,6] In all but the Yankee reactor vessel, where the cladding was ground down by the friction of loose parts in the bottom of the vessel, the failures were in the form of cracks in the cladding. Although the cracks, porosity, and inclusions in the Elk River reactor cladding that were discovered in 1961 before startup were repaired then, further cracks have been found recently in a section of the weld-overlay cladding known to have a martensitic structure. Thus the Elk River, EBWR, and both Yankee vessels now have cladding defects. About 1 sq ft of the EBWR SA-212B carbon-steel vessel wall is exposed, including areas from which cladding samples were removed for the investigation; only about 2 sq in. of the A-302B carbon-steel reactor-vessel wall is exposed at Yankee.

Because each of these vessels has a different history of construction and operation, it is interesting to consider the cladding methods employed and the locations where the failures occurred.

Cladding Methods

Figure 1 illustrates the principles of the three methods that have been used to line carbon-steel vessel material with stainless steel. The stitch-weld method, which was used to clad the EBWR and Yankee reactor vessels and the Yankee pressurizer vessel, leaves a nonbonded gap between the cladding and base metal. This communicating gap permits a leak in one location to expose much of the carbon steel to reactor water. The stitch-weld technique was discarded several years ago in favor of the weld-overlay cladding method, which, in fact, was also used to clad the nozzle and flange complex areas in all four of these vessels. The roll-bonding process was used to clad the straight shell sections and the heads of the Elk River reactor vessel.

The cracks in the Yankee pressurizer and in the EBWR vessel were in the stitch-welded cladding only (not in the weld-overlay areas, which had been clad

Digitized by Google

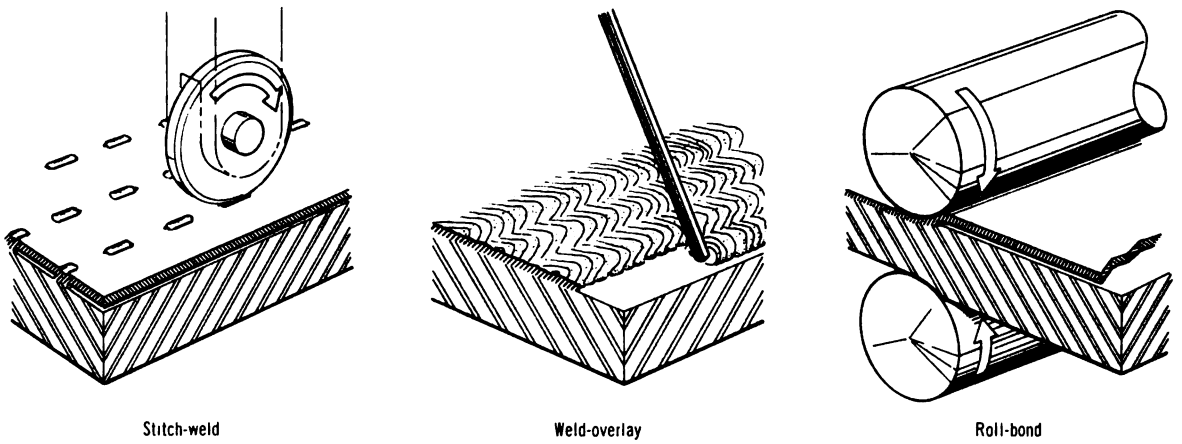

Fig. 1 Three methods for applying stainless-steel cladding to carbon steel for reactor vessels. In the "stitch-weld" method, sheets of stainless steel are resistance-welded to carbon-steel plates in a pattern of spot-welds; after forming, the edges of the panels are butt-welded to each other to form the vessel wall, and the sheets are butt-welded to form a single liner. The weld-overlay technique consists of depositing an overlapping series of arc-melted stainless-steel strips on the carbon steel (and, sometimes, then machining the surface smooth). Roll cladding diffusion-bonds the cladding and base metal by compressing the metals together at suitable temperature.

with a double pass), whereas the porosity, inclusions, and cracks in the Elk River reactor vessel were in the single-pass weld-overlay cladding only (none in the roll-bonded cladding), particularly at the junction of the weld-overlay cladding with the roll-bonded cladding and in certain questionable regions of the weld overlay.

Examining the EBWR

The EBWR operated in the boiling-water-reactor development program from 1956 until 1960 at powers up to 20 Mw(t) and up to 100 Mw(t) in 1961 and 1962 (Refs. 7 and 8). During that time the vessel experienced 15,665 hr (1.8 years) of service when steam was being generated at 489°F and 600 psig.[9] When plans were made to use the facility in the plutonium-recycle fuel-development program (to learn how isotopic distribution in fuel rods varies as burnup proceeds in a boiling-water reactor), the reactor vessel was examined in 1965 to determine its suitability for further service. However, because the reactor had operated, the core support structure and vessel thermal shield were quite radioactive even after the uranium core was removed. For this reason, thorough inspection was limited to the upper half of the interior walls of the vessel. The visual examination revealed evidence of hairline cracking on the surface of the stitch-weld cladding at locations shown in Fig. 2.

CLADDING PROCESS

The 2.44-in.-thick SA-212B carbon-steel plates for the EBWR vessel shell were clad by spot-welding 0.109-in.-thick 304 stainless-steel sheets to the plates by the intermittent-power pulse (stitch-weld) process while both plate and sheet were submerged in water. The cladding and plate edges were later butt-welded to adjacent similar panels to obtain a continuously clad cylindrical surface. The 4-in.-thick lower headplate was clad in a similar manner before being cut into a circular blank for the head-forming operation. The upper ring forging and upper head were clad by a double pass of the submerged-arc weld-overlay process; no cracks have been found in this cladding.

The fabricator established the integrity of the stitch-weld cladding by introducing 900-psi nitrogen into the annular gap between the cladding and base plate while watching for leakage bubbles in a soap solution applied on the cladding surface. By this means, several cracks were detected in the cladding; these cracks were rewelded before the vessel was shipped to the reactor site. (Further details of EBWR vessel design and construction have been reported.)[10]

Beginning in 1956 the reactor and vessel operated satisfactorily in the boiling-water-reactor development program until no longer needed and was decommissioned in 1962. Before reactor startup again for the plutonium-recycle development program, examination of the vessel indicated that there were fine cracks in the cladding.

INSPECTION AND ANALYSIS

Visual and dye-penetrant inspections of the stitch-clad plates in the upper half of the vessel revealed the cladding cracks, approximately 75% of which were in the steam region (the upper quarter of the vessel). Although the cladding of five of the eight panels contained surface cracks (most of which were near the manually deposited weld overlays that joined abutting

Digitized by Google

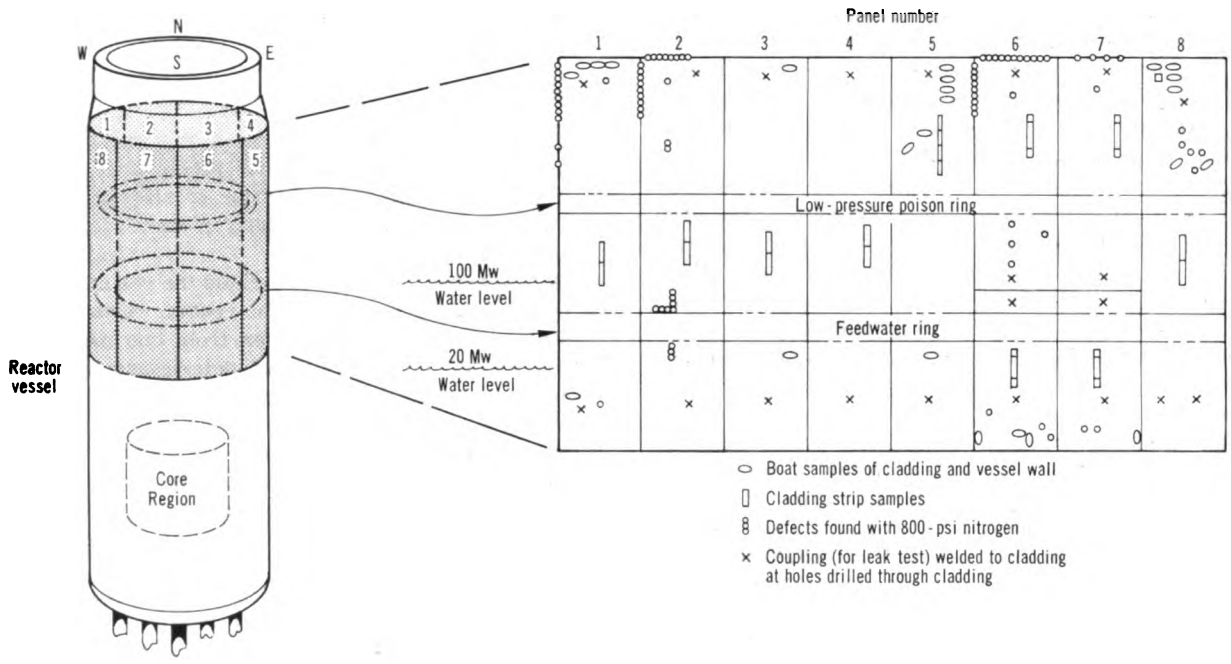

Fig. 2 Cracks were found in the cladding of five of the eight panels that make up the upper half of the EBWR vessel wall. Approximately 75% of the cracks were in the steam region in the top quarter of the vessel; few cracks were found below the waterline.[1]

panels of cladding sheet), few cracks were found below the waterline.

At first it was postulated that the cracks had been caused by service conditions during the most recent years of reactor operation. Fortunately other stitch-clad test plates and vessel-fabrication remnants were available (one of the test remnants had been exposed to the reactor environment for 11,225 hr until it was removed in 1960; a 2-in. plate, fabricated in the same way in 1959 for welding practice prior to a vessel modification,[11–13] had been stored outdoors ever since). Inspection of these plates and remnants negated the postulate. The discovery that the cladding on these plates had cracked (Fig. 3), apparently to an even greater degree than those in the vessel, when exposed not to a reactor environment but only to Illinois weather, was cause for reevaluation. When areas of the test-plate cladding were ground out and repaired by welding to develop methods for repairing the vessel cladding, the cladding cracked severely and extensively.

Initially it was not clear from the visual and dye-check inspections of the vessel whether the crack indications were surface "decorations" or actual cracks. The vessel cladding was leak tested with pressurized nitrogen to check this, as it had been just after fabrication; this test showed that the surface decorations were actually cracks through the cladding. Nearly all the cracks were in the wrought cladding adjacent to the spot-welds, although six cracks either crossed or terminated in the spot-weld

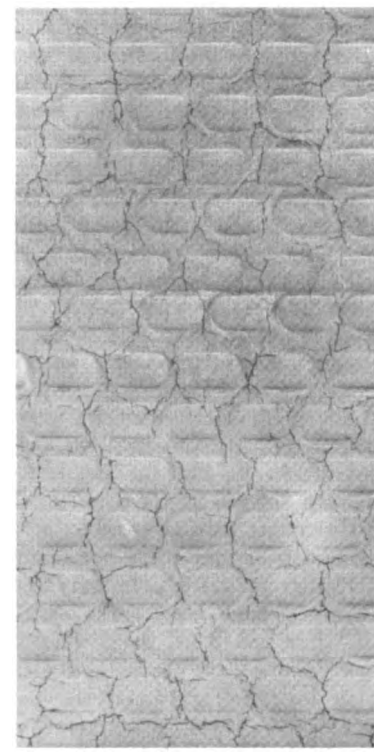

Fig. 3 Fine cracks in surface of 304 stainless-steel cladding on 2-in.-thick practice plate, which became visible after application of dye penetrant, showed that reactor conditions were not necessary to cause cracking.

Digitized by Google

"thumb print"; none of the through cracks started within the cladding spot-weld nuggets.

The condition of the vessel wall was investigated by grinding out to the carbon steel some of the through cracks in the stainless steel, with dye-penetrant tests interspersed during the process. The cracks appeared to increase in length, width, and number as the cladding was removed, suggesting that they might have originated at the base of the cladding adjacent to the weld areas (at the cladding interface with the gap). However, many cracks started within the cladding — at points remote from either surface (it was recognized that this characteristic of the cracks might have been caused by a changing stress pattern in the cladding as material was removed). The cladding fracture edges were square breaks with little visible ductile flow; many fractures were progressive. Although approximately 40 linear feet of cracks were ground down to and slightly into the base metal, no evidence of crack propagation into the carbon steel was found.

When the surface of the carbon steel between weld nuggets was examined for evidence of corrosive attack, a thin adherent film of black "mill scale" (Fe_3O_4) was found; but there was no evidence of local pitting or of gross generation of red rust (Fe_2O_3). Chloride concentrations detected were low.

Similar tests on the fabrication remnants and on the practice plate showed similar cracking but, again, with no evidence of crack propagation into the base metal. Metallographic examination of these specimens suggested that the cracking originated at the exposed, rather than the cladding-gap, interface. Because at least as much red Fe_2O_3 was found on the carbon steel of these test plates as black Fe_3O_4 on the carbon steel of the vessel itself, and because the test plates were exposed to an entirely different environment (the atmosphere), it was concluded that the reactor environment did not significantly influence corrosion at the interface.

SAMPLING

Numerous "boat" and strip samples were removed from the reactor vessel. The location and extent of sampling are shown in Fig. 2. The boat samples, about 0.5 in. wide and 2.5 in. long, were cut from the vessel with a circular slitting saw so as to include both cladding and base metal; the boat samples were examined metallographically, primarily to determine any cracking in the base metal. The strip samples, about 0.5 in. wide and 8 in. long, were of cladding only and were removed for chemical analysis. Additional samples for chemical analysis were milled from the 4-in.-thick lower headplate remnant and from the 2-in.-thick practice plate. The lower headplate remnant had cladding cracks similar to those found in the vessel. In addition, a crescent-shaped section of the reactor-vessel wall retained from a vessel modification was inspected; no cracks were found in this cladding section or in the vessel panel from which it had been cut.

TEST RESULTS

The chemical analyses showed that the cladding met *ASME Boiler and Pressure Vessel Code* materials requirements,[14] except for a slightly higher sulfur content (0.035 vs. 0.030% in the Code) in the vessel cladding.

Metallographic studies confirmed the results of the grinding explorations inside the reactor vessel. They showed that the cladding, even from one panel believed to be "crack-free" as determined by dye-penetrant examinations, contained numerous unsurfaced cracks. All the cracks in the cladding on the boat samples and the test panels were intergranular, except for a few hot tears inside the weld nuggets. In all cases both the microstructures and Strauss Reagent tests showed that the stainless steel was severely sensitized. Neither the intranugget nor the transgranular cracks in the cladding propagated into the carbon steel. In the bonded region the fusion boundary of the weld kernel stopped all the cracks in the cladding.

Examination of the cladding nuggets (spots where cladding and base metal fused) revealed regions of great complexity (Figs. 4 and 5). In all cases, only the stainless-steel cladding material in the nugget area had been melted by the passage of welding current. Although all the stainless-steel nuggets contained a dendritic kernel that originally was wrought material, the kernels were islands of cast material

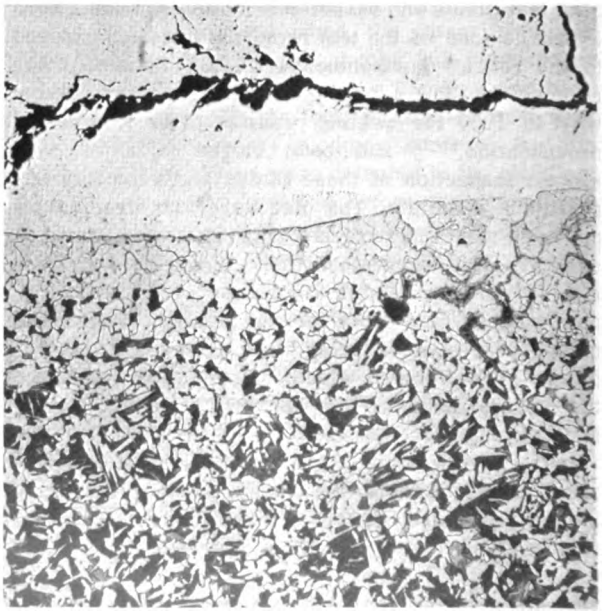

Fig. 4 Lamellar cracks in the EBWR cladding material paralleled the surface.[1]

Digitized by Google

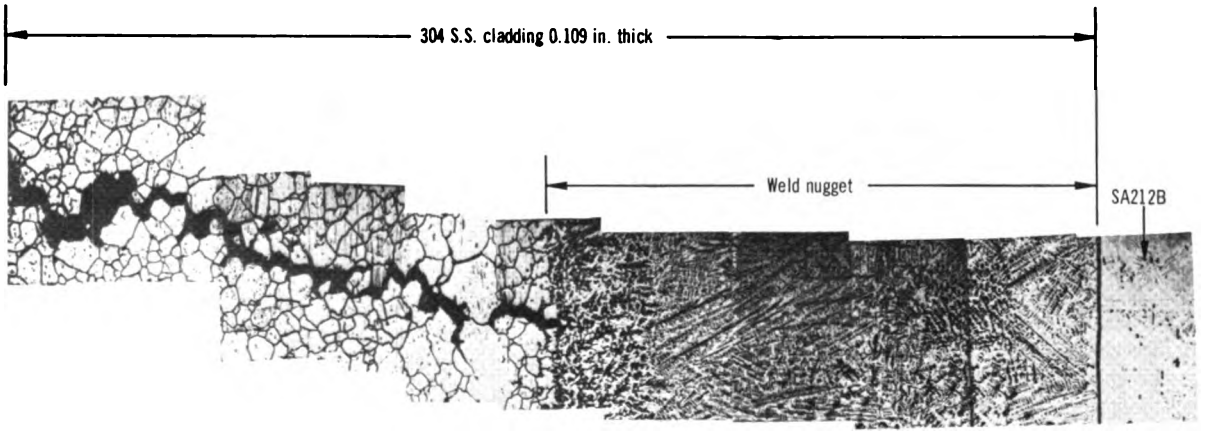

Fig. 5 Cracks in the 304 stainless-steel cladding of EBWR are arrested at the weld nugget by the absence of continuous grain boundaries.[1]

bounded by wrought stainless-steel cladding and the carbon steel. The wrought cladding surrounding the cast kernel contained numerous unsurfaced cracks radiating from the kernel interface as shown in Fig. 6. These cracks, which are usually perpendicular to the surface of the kernel, are primarily due to grain-boundary liquation. No radial cracks were found at the type 304 stainless steel–SA-212B steel interface. However, a thin zone of the cladding, about 0.001 in. thick, was carburized in the bonded zone at the weld nuggets; but this is not considered significant regarding either crack propagation or vessel strength.

Fig. 6 Unsurfaced cracks in the EBWR wrought cladding radiate from the interface with islands of cast cladding material (weld nuggets).[1]

Although the cracking of the vessel cladding was of great interest, all samples examined were searched primarily for evidence of concurrent cracking of the carbon-steel vessel plate. Several microcracks were found in the carbon steel. As shown in Figs. 7 and 8, a number were filled with intruded stainless steel from the cladding process. Metallographic studies conclusively showed that these microcracks existed before the cladding was applied and were probably formed in the initial fabrication of the plate. Specimens examined showed no evidence of propagation from the surface microcracks.

The hardness survey of the stainless steel and the carbon steel, supporting calculations, and the results of bend tests have been reported.[1] The bend tests on samples of the 2-in. plate attempted to force superficial surface cracks across the cladding and into the carbon steel. For these tests the SA-212B steel was bent back permanently to extend the crack in the 304 stainless-steel cladding. Intermittent incremental bending of a sample that had an intranugget crack only propagated the crack within the cladding to the unbonded interface; continued bending merely opened the crack without propagating it across the interface. Similar results were obtained from the forced development of an embryo crack in the wrought region of the cladding over the cast structure of the weld kernel; the kernel fusion line stopped the crack.

CRACKING MECHANISMS

Chloride stress corrosion, which requires the simultaneous presence of oxygen, stress, and concentrated chloride ions, was considered as a possible cause for the cracking of the austenitic 304 stainless-steel cladding of the EBWR vessel. But it was rejected as the probable primary cause because many unsurfaced and lamellar cracks (Figs. 4 to 6) were found within the stainless steel—and the through cracks in the cladding started at either surface or internally and are intergranular (rather than being

Digitized by Google

the classical branched "forked lightning" transgranular cracks). Because the evidence indicates a mechanical failure mode, and because a stress analysis shows that the spot-welded cladding might have been stressed beyond the ultimate tensile strength of the stainless steel when the upper and lower vessel courses cooled from the ~1700°F normalizing temperature (at which the courses were rolled vertically to improve concentricity), it was concluded that the cracking within the cladding most probably was caused initially by thermally induced stress ruptures during vessel fabrication and that these unsurfaced cracks propagated by low-cycle fatigue during reactor operation.[15] It also is believed that the mechanism that caused cladding failure would not be different in the inaccessible areas of the vessel. Evaluation of the information available and consideration of the fracture mechanics, radiation effects, temperature, and corrosion phenomena led to the conclusion that the integrity of the vessel has not been significantly impaired by the cracking of the cladding.

Continued operation of the reactor probably will cause more cracks to surface, and efforts to weld the existing cracks or sampled cladding areas would cause more severe cracking. Regardless of the mode of fracture, it is highly improbable that cracks in the stainless steel will propagate into the carbon steel. From the corrosion standpoint, the vessel is believed suitable for further service without the wall being reclad because at its thinnest spot (where boat samples were cut out) the carbon steel is $^{9}/_{16}$ in. thicker than is required by design codes; all SA-212B surfaces that were sampled have been contour-ground to eliminate notches. Nevertheless, a careful surveillance program has been instituted to study the corrosion of the bared steel walls and to verify the continued adequacy of the vessel.[16]

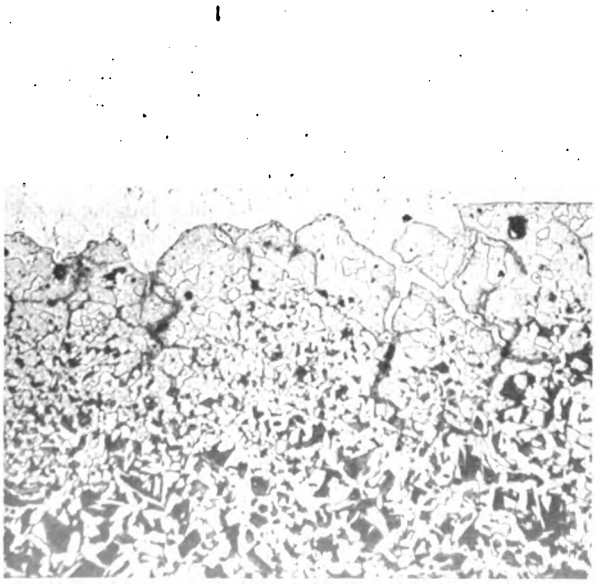

Fig. 7 Microcracks existed in the EBWR vessel SA-212B plate prior to cladding. Some of those under the weld spots became filled with 304 stainless steel in the cladding process.[1]

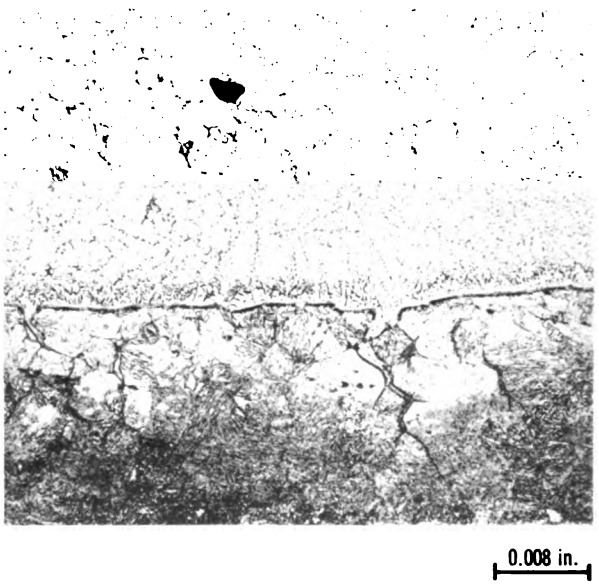

Fig. 8 Microcracks existed in the EBWR vessel SA-212B plate prior to cladding. Some of those under the weld spots became filled with 304 stainless steel in the cladding process.[1]

Yankee Inspections

The foregoing findings and analyses for the EBWR reactor vessel are corroborated by experience at Yankee, where both the reactor vessel and the pressurizer have been inspected and evaluated.[2-4] The major similarity between these two vessels and the EBWR vessel is the method by which cladding was applied—resistance spot welding.

PRESSURIZER VESSEL

Except for the absence of radiation, the service conditions of the Yankee pressurizer approximate those of the EBWR. Exploratory investigations with dye penetrant showed numerous cracks in the pressurizer cladding.[3,4] The checkerboard crack patterns were identical to the EBWR findings, and it is believed that the pressurizer had some cracks in the cladding after it was fabricated.

Explorations in the spot-weld nugget areas showed that the cracks in the cladding do not continue into the carbon-steel vessel material. Analyses of pressurizer operating conditions and all foreseeable effects

Digitized by Google

of the cracked cladding showed that the pressurizer cracks will not affect operation or present any kind of a safety hazard.

REACTOR VESSEL

Coolant flow within the Yankee reactor vessel caused six holder rods for material irradiation specimens and three locating baskets to break loose. Although four complete irradiation capsules with holders and several locating baskets were recovered in 1963, and four were recovered from within the baffle in 1965, one capsule with its holder rod and two baskets remained in the lower head area until the 1965 refueling.[17,18] At that time it was discovered that several small areas in the lower head cladding had been worn away. As reported by Reed and Tarnuzzer,[19] "When the bottom hemispherical head of the vessel was examined closely, one of the worries of leaving the loose irradiation specimen assemblies (Fig. 9) in the reactor vessel came into view. We found two small holes (Fig. 10) worn about 0.020 in. through the 0.109-in.-thick cladding. These two holes in the ... cladding resulted in extensive crevice-, galvanic-, and general-corrosion investigations and an extensive evaluation of hydrogen-embrittlement potential. Fortunately all of these investigations turned out favorably and indicated no combination of circumstances that could lead to a potential problem."

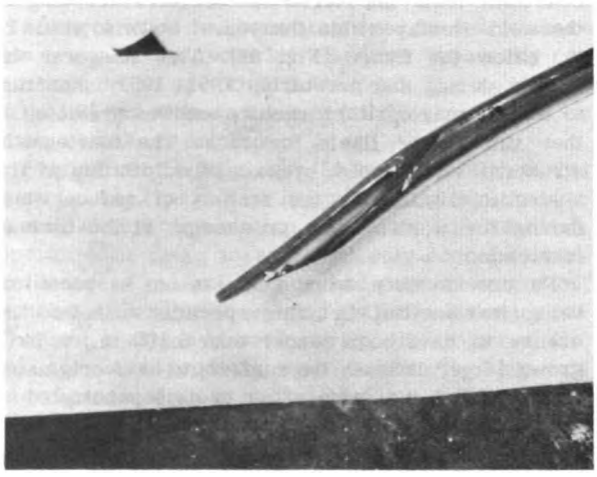

Fig. 9 Irradiation-specimen support rods that broke loose in the Yankee vessel were ground as they whirled around on the vessel bottom. Taper ground on rod shown is radius of bottom section of vessel.[19]

Casts of the worn areas in the lower head were made with a curable silicone rubber compound.[2] From these the maximum depth of the penetration from the surface of the cladding measured to be 0.115 in. It was assumed that 0.010 in. of wear had taken place in the 304 stainless-steel cladding in the general area around the penetrations, and therefore the reduction in the 4.219-in. thickness of the SA-302B carbon-steel vessel wall is approximately 0.016 in.

Fig. 10 Carbon steel of Yankee vessel, exposed when debris wore hole in cladding, is seen as light "8"-shape area in this underwater photo.[19]

Repair of these penetrated areas would be difficult because during shutdown, when the pit above the reactor is flooded, the lower head is under about 55 ft of water. Thus the approach was to analyze all possible operational problems that could be foreseen; from this analysis it was concluded that there are no safety problems involved in the continued operation of the vessel with the cladding defects. Details of the analytical methods that led to this conclusion, including mechanical and structural considerations and studies of the sources and effects of hydrogen on the walls of the vessel, various corrosion factors, and effects of the additional radioactive corrosion products, have been reported.[4]

Studies of the effects of the exposed carbon steel in the EBWR vessel and the Yankee vessels corroborate each other.

Elk River Findings

Cracks and other defects were detected in the single-pass weld-overlay cladding in the Elk River reactor vessel after prestartup tests in 1961 during which the system had been heated up nonnuclearly to test piping flexibility.[5,20] The 164 defect areas were ground to the base of the cracks to learn whether the cracks propagated into the carbon steel (they didn't). After the inspection was completed, all the ground areas were filled by a rewelding procedure[5,6] before reactor startup. Since then, the reactor has operated for approximately 1 full-power year,

Digitized by Google

after which additional cracks were found in the cladding.[21]

VESSEL FABRICATION

Plate material used in the straight shell section and in the heads for the Elk River reactor vessel[22] was clad by a roll-bonding process that complied with ASTM Specification A264 for stainless-steel roll-clad carbon-steel plate; no cracks have been found in this roll-bonded cladding. The 3-in.-thick plate material is A-302B carbon steel, and the cladding is 304 stainless steel. However, the forged material used in the flanges and nozzles is A105-2 carbon steel that was clad with a single-pass weld overlay of 308L stainless steel; the shell flange was overlaid and machined before it was butt-welded to the shell, whereas the head flange was butt-welded to the head before the overlay was applied. Nevertheless, both the shell- and head-flange areas had defects in the overlay cladding.

PRESTARTUP INSPECTION

A systematic inspection program[5] was pursued in 1961 and 1962. All crack or porosity indications were photographed. Because the overlay cladding on the flanges contained defects, 100% of the weld-overlay cladding, including the 10- and 16-in. nozzles, was dye-checked. (Because the reactor had not been operated before the inspection, the vessel was not radioactive and all areas were accessible after most of the vessel internals were removed.) Chemical analyses and hardness measurements were made. On the vessel shell, 109 suspect cladding areas were ground out; another 55 areas were ground out on the reactor-vessel head. A dye check was used in each area after each incremental layer of cladding metal was removed; this procedure was repeated until the carbon steel of the vessel was exposed.

PRESTARTUP TEST RESULTS

It was concluded that the dye-penetrant indications on the vessel shell were caused by porosity or slag inclusions, except for one cladding crack found in one of the 16-in. nozzles and a second crack in a sample adjacent to the first sample. These two cracks apparently resulted from hot shortness (brittle fracture at the high welding temperature) in a local cladding area. Except for these two cracks in this nozzle and one pinhole, all indications had the same appearance and all occurred in the junction of the weld-overlay cladding with the roll-bonded cladding.

When the weld-overlay surfaces of the head flange and head nozzles were examined by dye check, some aligned porosity was seen along the juncture of the Inconel and 308L stainless-steel overlays at the face of the head flange; some random areas of porosity also were seen in the surface of the manual overlay on the ends of all the nozzles. But in none of the ground patches were any unsatisfactory conditions detected in the carbon steel.[20]

The chemical and metallurgical data[20] obtained from the Elk River reactor-vessel patch-grinding program indicated that certain layers of some of the weld overlays contained martensite. No gross cracking was found in the weld overlays. The cracks found in the 16-in. nozzle overlays were hot-short in nature and were confined to the first layer; they did not extend into the base metal.

1966 INSPECTION

After the Elk River reactor had operated for approximately 1 full-power year [27,887 Mwd(t)], all accessible areas of the vessel were inspected again.[21] Inspection of weld-overlay cladding in the shell nozzles (borescopic, visual, and dye penetrant) and the head nozzles and flange (visual and dye penetrant) showed no evidence of cracks. However, although visual inspection of the weld-overlay 20 in. below the shell flange did not show any cracks, dye-penetrant tests uncovered considerable cracking in the weld-overlay within the vessel down to about 10 in. below the flange (Fig. 11). This area was observed during the prestartup 1961–1962 inspection to have a martensitic structure and was predicted at that time to be likely to crack. The martensitic structure was caused by excessive dilution of the austenitic overlay by the melting of carbon steel during the weld-overlay processing at the time of fabrication.

No cracks were found in areas not suspected of being martensitic. Grinding operations showed no cracks to have been deeper than 0.192 in., to have grown larger beneath the surface, to have originated other than at the surface, or to have penetrated as far as the carbon steel. Although the cracks appeared to be intergranular in nature, because they initiated

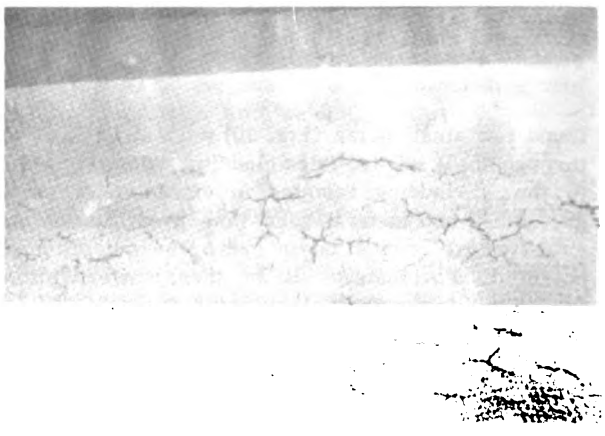

Fig. 11 Cracks in martensitic stainless-steel weld-overlay cladding just below flange in Elk River reactor vessel were discovered by dye-penetrant inspection in May 1966 (Ref. 21).

Digitized by Google

at the surface in the martensitic region and not in areas known to have high (0.08%) carbon content, they are believed caused by stress corrosion of martensitic material rather than intergranular corrosion of material with excess carbon content.

It is believed[21] that the reactor can be "operated without removal or repair of the cracks because of the following reasons: (1) No cracks were found which penetrated to the base metal; (2) The cracking observed was confined to an area of relatively low stress; (3) The plant is operated under conditions which prevent brittle fracture propagation; (4) Data available indicate that such defects will not propagate in low cycle fatigue at strain levels present at this location." Continued surveillance is planned during each refueling of the reactor.

Conclusions

Cracks have been found in stainless-steel cladding that was applied to the carbon steel of four reactor vessels by two methods: the stitch-weld process and the weld-overlay process. Although the stitch-weld cladding method has been abandoned for future reactor vessels, weld-overlay claddings apparently can continue to be specified if the deposition conditions and steel constituents are carefully controlled and/or a double pass is employed.

Studies of the four vessels have established that the cladding cracks have not propagated into the base metal, a fact of prime importance for continued safe operation of these vessels. But only continued surveillance of general, pitting, and galvanic corrosion, coupled with water-chemistry evaluations that include frequent analyses of water purity, *p*H, gross activity, and corrosion products, can establish the long-time significance of these vessel-cladding defects. In any case it seems appropriate for reactor-vessel designers and reactor operators to provide for careful inspection of vessel-cladding integrity and to be watchful for new research and performance data on vessel materials.

References

1. N. Balai et al., Inspection, Evaluation, and Operation of the EBWR Reactor Vessel, USAEC Report ANL-7117, Argonne National Laboratory, November 1965.
2. Westinghouse Electric Corp., Atomic Power Division, Evaluation of Yankee Vessel Cladding Penetrations, Report WCAP-2855, Oct. 15, 1965.
3. Westinghouse Electric Corp., Atomic Power Division, Yankee Pressurizer Cladding Evaluation, Report WCAP-2859, Nov. 2, 1965.
4. Westinghouse Electric Corp., Atomic Power Division, Yankee Pressurizer Cladding Evaluation, Report WCAP-2859, Supplement 1, Nov. 23, 1965.
5. K. J. Henry, Investigation of Integrity of Overlay Cladding and Structural Welds of Reactor Vessel and Head, USAEC Report ACNP-62513, Allis-Chalmers Mfg. Co., Mar. 9, 1962.
6. Elk River Reactor Vessel Repaired, Startup Near, *Nucleonics*, 20(7): 68 (July 1962).
7. Reactor File No. 1: EBWR, *Nucleonics*, 15(7): 53 (July 1957).
8. The Experimental Boiling Water Reactor (EBWR), *Power Reactor Technol.*, 1(1): 36-38 (December 1957).
9. N. Balai et al., Summary of the 1965 Partial Inspection of the EBWR Vessel: Cracking of Cladding, *Trans. Am. Nucl. Soc.*, 9(1): 221 (June 1966).
10. Argonne National Laboratory, The Experimental Boiling Water Reactor, USAEC Report ANL-5607, May 1957.
11. J. M. Harrer and T. L. Kettles, Modifying EBWR Vessel for 100-Mw(th) Operation, *Nucleonics*, 19(8): 50-53 (August 1961).
12. Modifications of the EBWR, *Power Reactor Technol.*, 3(3): 62-67 (June 1960).
13. T. L. Kettles and N. Balai, EBWR Reactor Pressure Vessel Revisions for Instrumentation and Increased Steam Output, USAEC Report ANL-6162, Argonne National Laboratory, January 1962.
14. *ASME Boiler and Pressure Vessel Code*, Section II, Material Specifications, 1952 Rev.
15. C. R. Sutton et al., Examination and Evaluation of Experimental Boiling Water Reactor Pressure-Vessel Cladding, *Trans. Am. Nucl. Soc.*, 9(1): 222 (June 1966).
16. R. F. Jones et al., Reactor Vessel Surveillance Program for the Plutonium Recycle Experiment, *Trans. Am. Nucl. Soc.*, 9(1): 222 (June 1966).
17. R. C. Skaardal, Operational Problems and Solutions, *Power Reactor Technol.*, 8(4): 274 (Fall 1965).
18. G. A. Reed, Major Operating and Refueling Problems at Yankee Atomic Electric Company Rowe Power Plant, *Trans. Am. Nucl. Soc.*, 8(Suppl.): 28 (1965).
19. G. Reed and E. Tarnuzzer, Examining Yankee Plant Performance in 1965, *Nucleonics*, 24(3): 42-47 (March 1966).
20. A. L. Schaeffler, Elk River Reactor—Chemical and Metallurgical Aspects of Investigation of Overlay Cladding and Structural Welds of Reactor Vessel, USAEC Report ACNP-62514, Allis-Chalmers Mfg. Co., Mar. 9, 1962.
21. E. B. Norris, The First Inspection of the Elk River Reactor Pressure Vessel After Operation, USAEC Report SWRI 1228-9-8, Southwest Research Institute, June 10, 1966.
22. Allis-Chalmers Mfg. Co., Elk River Reactor Vessel Cladding Defects, USAEC Report TID-13083, May 19, 1961.

Digitized by Google

Nuclear Plant Performance—Good and Getting Better

By George F. Bierman, Metropolitan Edison Co., and Walter J. Miller, Yankee Atomic Electric Co.

Electric utilities evaluate generating plants on the basis of cost of the power produced and reliability of the plant to produce power when needed. Utilities express the reliability of a plant in terms of its "availability" for operation. Utility-system reserve requirements, plant installation and retirement schedules, and production costs are influenced by plant availability. For nuclear plants, with their lower fuel costs and higher fixed charges (and they are certainly higher, if you remember to include first-core cost), high plant availability is especially desirable. But what availability can we expect, and how can we ensure it?

Study of the operating data for six U. S. utility-operated central-station nuclear power plants that have generated more than 500,000 Mw-hr each (Fig. 1 and Table 1) shows that the availability of a nuclear plant can compare favorably with that of a fossil-fired unit of the same size and degree of maturity. Nuclear plant availability has been adversely affected most by refueling operations, maintenance, and testing. The number and length of outages have decreased as the plants have been debugged and procedures have improved. For example, excluding refueling, the Dresden[1] reactor experienced only one outage — a 4-hr period to test a stuck control rod — during all of 1965, for an availability of greater than 99%. Earlier performance, like that for other plants, was not as spectacular[1-4] (Tables 2 to 4).

From the experience with and performance of these six plants, the following overall judgments can be made:

- Schedules for refueling and plant maintenance outages can be dovetailed with system requirements, as can nuclear plant output.
- Operating, refueling, and maintenance procedures for a water-cooled reactor appear to mature (but not stabilize) after two core lifetimes.
- Refueling can be shortened by design that provides ready access to the core with simple handling equipment.
- Shutdowns caused by malfunctions of fail-safe subsystems should diminish as designs improve.
- Substitution of water type reactors for conventional boilers reduces materials problems for plant operators — because reactor and turbine conditions are much less severe.
- The time it will take future nuclear plants to reach operational maturity will depend on such factors as (1) operating pressure and temperature, (2) quality control during fabrication and construction, and (3) use of components and systems proven by reactor experience or equivalent testing.
- High plant availability for future large plants will come with the modular design approach; more fuel elements, control-rod assemblies, rod drives, coolant loops, etc., can be added, rather than radically changed, to increase capacity.

Although these judgments stem from experience with just six plants, and not from probability mathematics (any sample involving less than 20 plants, nuclear or fossil fired, is regarded[5] as totally unreliable), they seem sound. The growing pains of future plants may be aggravated by their greater power and size, but proper interpretation of the family histories can lead to the best design choices. Then new plants will mature quickly and have high availability.

Evaluating Plant Performance

Plant performance data, summarized in Table 1, can be evaluated in terms of (1) plant capacity factor, which indicates how much power the plant actually generated as compared with how much power it could have generated if it had operated at maximum power

Digitized by Google

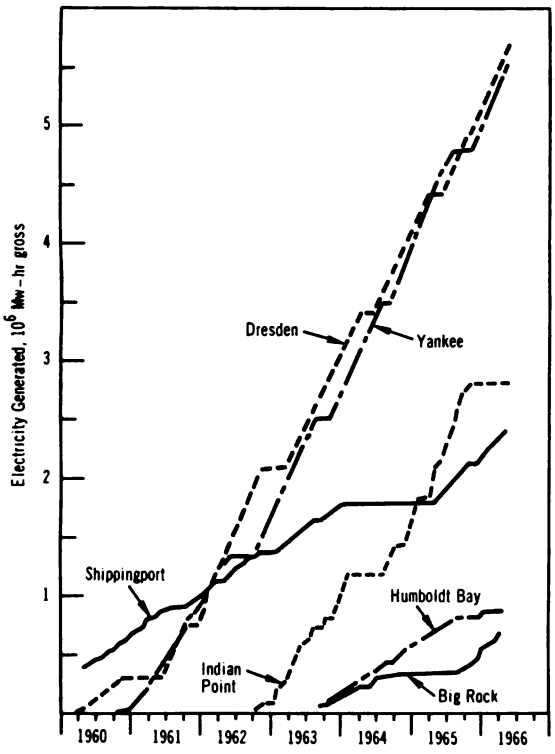

Fig. 1 Electricity generated by these six nuclear central-station power plants totals more than 18 Mw-hr (18×10^9 kw-hr). Refueling operations, maintenance, and testing are the principal drags and cause the flat spots in the curves of power generation.

during all of the period in question (and thus depends on load demand as well as plant reliability); (2) plant availability, which tells the portion of a time period during which a plant was capable of generating electricity; and (3) reactor availability, the portion of a time period during which a reactor was able to make steam. Tables 2 and 3 indicate the major factors affecting plant and reactor availability for five of these stations.

INTERPRETING THE DATA

If the purpose of evaluating the capacity and availability factors is to predict future performance of these or future plants, their operating goals and philosophies must be borne in mind. Specifically, the generation of test information—not electricity—has been the principal goal at Big Rock Point[6–9] and at Shippingport.[10–15] And testing not only reduces capacity factor but also invariably delays system debugging and involves instrument limit settings that cause frequent shutdowns. (Thus evaluation of the operational performance of plants that have dual functions requires careful study.) Dresden, Indian Point, and Shippingport have been load-following plants; as a result, their capacity factors were lower than they might have been, and these plants experienced some shutdowns (e.g., during load swings) that would not have occurred if the plants had been operated to supply the base load demand. On the other hand, Yankee was base-loaded and thus had practically as high a capacity factor as was possible.[16]

Table 1 CAPACITY AND AVAILABILITY FACTORS* FOR SIX MAJOR WATER-REACTOR PLANTS

	Power, Mw(e) net	Date critical	Factors during each year, %							
			1958	1959	1960	1961	1962	1963	1964	1965
Shippingport	60–140 equiv.	12/7/57								
Capacity factor			37	34	45	59	62	66		62†
Plant availability			53	50	50	64	76	81		69†
Reactor availability			68	67	50	64	76	81		71.5†
Dresden	200	10/15/59								
Capacity factor					21.8‡	33	73	53.8	56.2	55.4
Plant availability					32.9‡	38.1	78.6	75.6	80.9	78.7
Reactor availability					58.7‡	40.2	80.6	80.7	82.7	78.3
Yankee	175	8/19/60								
Capacity factor						76‡	55	69	80	65
Plant availability						89‡	64	78	88	73
Reactor availability						90‡	65	78	90	74
Indian Point	255	8/2/62								
Capacity factor							28‡	38	25	47.6
Plant availability										62.2
Reactor availability								67	48	64.0
Big Rock Point	71.5	9/27/62								
Capacity factor								35‡	42	29
Plant availability								39‡	43	30.1
Reactor availability								42‡	56	30.7
Humboldt Bay	50	2/16/63								
Capacity factor								78‡	83	60
Plant availability								81‡	87	77
Reactor availability								82‡	89	79

*Capacity factor = $\frac{\text{Power generated, Mw-hr}}{\text{Max. dependable capacity, Mw} \times \text{period, hr}}$

Plant availability = $\frac{\text{Period, hr} - \text{plant outage, hr}}{\text{Period, hr}}$

Reactor availability = $\frac{\text{Period, hr} - \text{reactor outage, hr}}{\text{Period, hr}}$

†Portion of year after plant modified (5/3/65) to raise power from 60 Mw(e) to 140 Mw(e) equivalent.

‡Portion of year after start of full-power operation.

Digitized by Google

Table 2 REACTOR-SYSTEM OUTAGES, HOURS (AND NUMBER)

Year	Shippingport			Dresden			Yankee				Big Rock Point			Humboldt Bay		
	Instruments		Other	Instruments	Steam drum	Control-rod drive	Instruments	Valve-stem leaks	Misc. leaks	Other	Instruments	Control-rod drives	Modifications	Instruments	Tests	Other
Forced outages																
1958	14 (3)		26 (2)													
1959	65 (2)		83 (1)													
1960	50 (8)		0	0	23 (2)	1127* (1)										
1961	6 (2)		12 (3)	0	0	3670	5 (2)	105 (3)	36†	6 (1)						
1962	19 (2)		15 (2)	0	18 (1)	0	0	0	0	0						
1963	4 (1)		4 (1)	5 (1)	0	0	7 (2)	0	148 (5)	22 (1)	34 (1)	80 (1)		12 (3)	25‡ (1)	2 (1)
1964	Plant modifications			0	0	0	15 (1)	0	0	22 (1)	30 (1)	0		9 (2)	55 (3)	0
1965	27 (4)		7 (1)	0	0	0	0	0	0	0	0	0	5921 (1)	0	0	4 (1)

Year	Tests	Shippingport Instruments	Shippingport Maintenance	Shippingport Other	Dresden Tests	Dresden Training and licensing	Dresden Maintenance	Yankee Tests	Yankee Vapor control	Yankee Control rods	Yankee Other	Big Rock Point Instruments	Big Rock Point Tests	Big Rock Point Inspections	Big Rock Point Maintenance	Humboldt Bay Instruments	Humboldt Bay Tests	Humboldt Bay Licensing
Scheduled outages																		
1958	710 (8)	231 (3)	1690 (5)	117 (4)														
1959	831 (5)	0	0	0														
1960	1472 (10)	0	79 (2)	25 (4)	274 (3)	1005 (4)	1283 (1)											
1961	1541 (10)	14 (1)	0	27 (2)	0	67 (1)	1544 (1)	625 (4)	9 (4)	19 (6)	4 (1)							
1962	1465 (6)	20 (1)	0	20 (1)	41 (1)	0	261 (4)	7 (1)	0	0	0							
1963	969 (7)	50 (2)	331 (3)	46 (2)	0	0	0	0	0	0	69 (1)	14 (1)	1420 (6)	0	2274§ (1)	0	79 (1)	0
1964	Plant modifications				104 (1)	0	0	21 (1)	0	0	0	0	1095 (3)	764§	1930§ (0)	0	325¶ (1)	16 (1)
1965	244 (8)	22 (1)	81 (2)	1348 (2)	0	0	4 (1)	68 (1)	9 (4)	0	0	0	0	0	151§ (1)	35 (2)	112 (1)	0

*Shutdown continued into following year.
†Extension of shutdown for other purposes.
‡Includes scheduled outage extensions for testing.
§Includes extension after shutdown for other reason.
¶Includes forced-outage extension.

Table 3 NONREACTOR-SYSTEM OUTAGES, HOURS (AND NUMBER)

Year	Shippingport	Dresden		Yankee			Big Rock Point			Humboldt Bay	
	All causes	Leaks	Other	Control valves	Instruments	Other	Bypass valve	Turbine	Other	Instruments	Other
Forced outages											
1958	122 (2)										
1959	0										
1960	4 (1)	150 (3)	0								
1961	0	0	0	94 (7)	7 (3)	10 (1)					
1962	0	29 (1)	44 (1)	115 (3)	0	0					
1963	0	0	97 (4)	22 (1)	0	7 (2)	26 (2)	0	195* (5)		
1964	Plant modifications	146 (2)	9 (2)	4 (1)	5 (1)	20 (3)	327 (5)	886* (1)	7 (1)		
1965	14 (1)	320 (4)	31 (1)	0	0	15 (1)	0	0	34 (1)	21 (1)	8 (2)

Year	Shippingport Maintenance	Shippingport Other	Dresden Tests	Dresden Inspections	Dresden Turbine	Dresden Other	Yankee All causes	Yankee Turbine	Humboldt Bay Tests	Humboldt Bay Other
Scheduled outages										
1958	1230 (3)	0								
1959	1421† (2)	44 (1)								
1960	43 (1)	0	35 (4)	7 (1)	78 (2)	132 (2)				
1961	0	0	0	0	59 (1)	79 (1)	0			
1962	0	4 (1)	0	122 (2)	0	0	0			
1963	9	25 (1)	173 (1)	0	97 (2)	119 (2)	1 (1)	0	0	2070‡ (4)
1964	Plant modifications		0	0	0	39 (1)	2 (1)	0	14 (2)	5 (1)
1965	64 (3)		0	0	(2)	60* (1)	8 (1)	18 (1)	0	74 (1)

*Includes extension after shutdown for other reason.
†Shutdown continued in following year.
‡Prior to commercial operation for miscellaneous plant modifications including reactor systems.

Digitized by Google

Table 4 DAYS REQUIRED FOR REFUELING, OVERHAULING, AND TESTING VARIOUS REACTORS EACH YEAR

Year	Shippingport	Dresden	Yankee	Humboldt Bay
1958	0			
1959	86.3*			
1960	101.5†	0		
1961	54.2	0	0	
1962	36*	54.5*	126.5	
1963	11.1†	68.6†	72	0
1964	‡	57.5	35.6	28.2
1965	0	62.1	93.5	71.8§

*Shutdown continued into following year.
†Includes extension of shutdown from previous year.
‡Plant modifications.
§Length determined by containment-system modifications; refueling was completed in 22 days.

In Tables 2 and 3 we have tried to categorize all outages according to the principal reason for the outage or its extension. However, invariably, scheduled outages have been planned for a combination of reasons; during many of the extended outages, repairs and tests have been made concurrently. Shutdowns frequently have been extended by on-the-spot decisions to perform maintenance work or to run tests. Thus delays not related to the initial cause of an outage are in some cases included as separate outages. Except when noted otherwise, refueling periods are included in determining capacity and availability factors. During outages for reactor tests at zero power and for operator training, the reactor and (therefore) the plant are assumed to be unavailable for generation. Thus time required for testing, inspecting, and training is regarded here as being related to a plant's period of immaturity. Actually, test programs are shrinking as the accuracy of core calculation methods is verified and as experience is gained with cores and system components. But not all test-time eliminated is time saved because maintenance work is often done concurrently with testing; savings vary from 50 to 100% of the test-time eliminated, depending on plant and core age.

MAJOR OUTAGES

Each of the four plants in operation before 1963 has had four or five shutdowns that have had more effect on plant availability factors than have the combined remaining shutdowns. These appear as flat spots in the generation curves in Fig. 1. Although most lengthy shutdowns were for refueling (several were for plant modifications), maintenance usually lengthened the outages.

Except for a 1958 outage to repair a turbine moisture separator and a test and training period at the end of 1962, the major Shippingport outages before 1964 were all during refueling periods.[11,15] The major Dresden outages in 1961 were for control-rod-drive modifications and inspection; however, subsequent major outages were for refueling. Much of Yankee's downtime has occurred at refueling periods; actually, the duration of Yankee's 1962 and 1965 refuelings were extended about 2 months because of maintenance problems and needed modifications.[16,17] The long Indian Point outage in 1964 resulted from a decision to make plant modifications at that time.

MATURITY

Experience shows that reduced maintenance requirements can be expected by the time a plant has operated through two core lifetimes. This is true for maintenance performed during refueling as well as for that performed during shutdowns specifically for maintenance. The eventual refueling time can be estimated fairly accurately after a plant has been refueled twice, by which time procedures will have been established, personnel trained, and equipment debugged. Therefore further improvements can be expected in availability factors for the Humboldt Bay, Big Rock Point, and Indian Point plants. Of course, design improvements will also permit future plants to benefit from this evolution.

Refueling Outages

The major factor limiting availability is scheduled maintenance, which is usually labeled "refueling" but often also includes turbine-generator inspection and overhaul and, with young plants of a new design, extensive modifications. Table 4 summarizes these outages, which greatly reduce overall availability.

IMPACT ON AVAILABILITY

Experience at Dresden 1, which was refueled in 1962, 1964, and 1965 (Fig. 2), is especially significant when examined on a fuel-cycle basis. Although plant availability for a calendar year has not exceeded 80.9%, during Cycle 2 the plant availability was 93.4% and during Cycle 3 it was 96.2%. (During Cycle 2, which extended from Mar. 10, 1963, to Apr. 12, 1964, Dresden generated 1,327,341 Mw-hr of electricity; during Cycle 3, June 7, 1964, to Mar. 28, 1965, the plant generated 983,981 Mw-hr.) But downtime during the first Dresden refueling (after Cycle 1, which lasted 36 months and 23 days) required approximately 123 days; this included turbine inspection and overhaul. The second refueling (96 elements) took only about 57 days, including approximately 1 week for a containment-sphere pressure test.

The third refueling (200 elements) of Dresden 1 began on Mar. 28, 1965. Turbine inspection and overhaul were performed concurrently, and the unit was returned to service on May 29, for a total of approximately 62 days of scheduled-outage time, including another 20-psig pressure test of the plant containment—which illustrates the incentive for devising ways to speed such routine tests. Exclusive of refueling, during 1965 the only outage, either forced or scheduled, involving the reactor was a 4-hr period required to test a stuck control rod. Thus, considering only the reactor, its availability during 1965

Digitized by Google

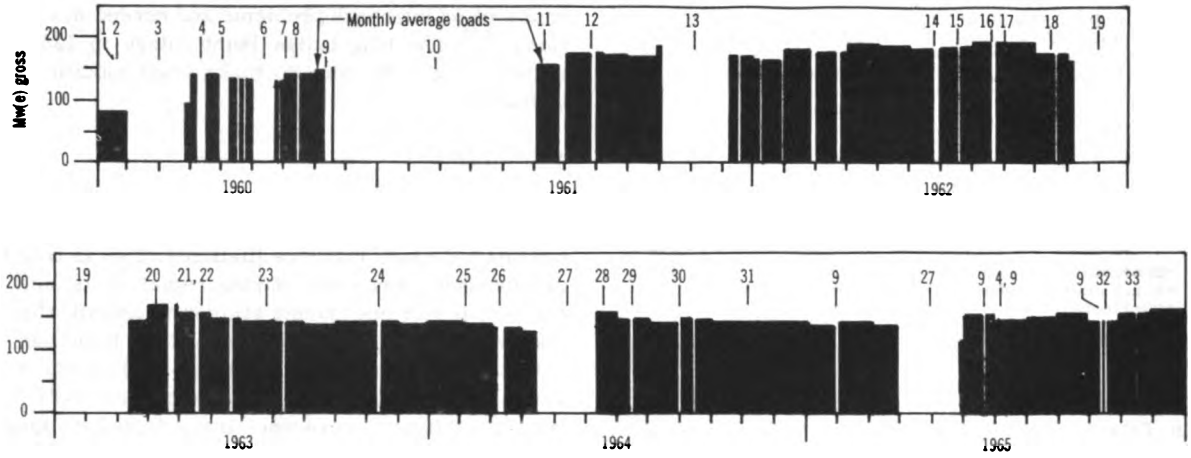

Fig. 2 Dresden Station Unit No. 1, Commonwealth Edison Co., plant outages were for the following reasons:

1. Low drum level and turbine rub
2. Leak in secondary drain
3. Remove test fuel and revise guide tubes
4. Reactor turbine test
5. High drum level and turbine drain
6. Personnel training and miscellaneous repairs
7. Recirculating pump leak (derating)
8. High-pressure turbine drain leak
9. Repair secondary-system leaks
10. Modify control-rod drives
11. Reactor testing (derating)
12. License examinations and turbine maintenance
13. Control rod and drive and inspect reactor internals
14. Scram, friction and temperature-coefficient tests
15. Leak in "D" extraction steam line
16. Motor-generator transient and temperature-coefficient tests
17. Low-drum-level scram
18. Fuel depletion (derating)
19. First refueling and turbine overhaul
20. Condensate demineralizer limitation
21. Scram, pressure-regulator sensing line
22. Turbine vibration and condensate pump leak
23. Repair transformer No. 1 lightning arrester
24. Repair turbine oil system
25. Fuel depletion (derating)
26. Nuclear testing
27. Refueling and sphere test
28. Loss of feedwater pumps
29. Moisture-removal-line leak
30. Extraction and gland line leaks
31. Minimize fuel failures (derating)
32. Control rod stuck
33. Transmission-line storm damage

was 83% including refueling and greater than 99% exclusive of refueling time; overall plant availability was 78.3% including refueling and 94% exclusive of refueling time.

Refueling experience at Dresden,[16] Shippingport,[11,15] and Yankee (Rowe)[17,18] shows that the actual replacement of the fuel need not be a particularly time-consuming operation if the fuel-handling equipment is of reasonably straightforward design for such repetitive operations. But the problems of gaining access to the fuel are another matter, although such difficulties are susceptible to solution by design improvements or evolution of operational procedures. Some steps that can reduce downtime for refueling are:

- Use hydraulic stud tensioners instead of bolt heaters to remove the bolts that fasten the reactor-vessel head.
- Mount control-rod drives on the bottom of the reactor vessel so they will not have to be disconnected from the rods before the vessel head is removed.
- Arrange vessel penetrations for instrumentation connections through the vessel itself or the bottom head, rather than through the vessel head, so that they will not have to be disconnected before the head is removed.
- Minimize and simplify above-core vessel internal structures so that access to the core can be achieved more readily.
- Locate coolant-flow-adjusting orifices in the core grid support structure, rather than on each fuel subassembly, so that it will not be necessary to change orifices when fuel is being "shuffled" during partial refuelings.
- Design and use the simplest and most rugged refueling tools consistent with the precision and handling care needed so that they will function reliably for the repetitive operations required of them.
- Design each fuel subassembly with more and longer fuel rods so as to reduce the number of handling operations per core.

EXPECTATIONS FOR NEW UNITS

Future pressurized-water reactors, with bottom-mounted control-rod drives and instrumentation, few vessel internals above the core, and reasonably straightforward refueling equipment, have been esti-

Digitized by Google

mated by Yankee Atomic Electric Co. to be refuelable in approximately 16 days. Routine refueling at Yankee (Rowe) now is expected to require about 4 weeks and to be accomplished concurrently with turbine-generator maintenance; the fact that the first four refuelings at Yankee (Rowe) took longer than this (Table 4) is attributable mostly to reactor modification and plant maintenance.

cleanup. In the reactors for the new Dresden 2 and 3 units (Fig. 3), each fuel bundle will produce twice as much power as a Dresden 1 fuel bundle; this will be accomplished by lengthening fuel rods (from 9) to 12 ft and using 49 rods per assembly instead of 36 — and will shorten refueling time by 2 to 4 days.

Table 5 shows our "guesstimates" of scheduled outages for new units using boiling- or pressurized-

Fig. 3 Dresden 2 and 3 will dwarf the present 200-Mw(e) plant (background). Both the new units, scheduled for service in 1969 and 1970, are initially rated at 715 Mw(e) and might stretch to 810.

The second unit at Dresden, which will have an initial capacity of 715 Mw(e) net and an ultimate rating of 793 to 810 Mw(e), is expected to need only 15 to 20 days for refueling, and the forced-outage rate is predicted to be about 1%. The pressure-suppression type containment should halve the down-time for containment leak testing. Thus unit availability should be about 94%.

Unlike Dresden 1, where spent fuel is transferred through canals from the reactor building to a separate storage building, the designs of the new units include spent-fuel storage facilities which are adjacent to the reactors and which eliminate canals and reduce water reactors. Note that the most extended outage comes in the third year, when the reactivity-holddown neutron absorbers (rods or curtains) are removed and the first partial fuel change is made.

Yankee (Rowe)

Yankee experience shows the advisability of using proven materials and designs where possible and the need for adequate testing where in-pile experience is unavailable.[17–23] Although fretting wear in mechanical joints was not experienced during control-rod-motion proof-tests by the designer, it was discovered during

Table 5 ESTIMATED SCHEDULED OUTAGES FOR LARGE WATER-REACTOR POWER PLANTS*

Plant power and part requiring outage	Days of outage during each year after reactor begins producing power									
	1	2	3	4	5	6	7	8	9	10
600-Mw(e) capacity										
Reactor	0	0	24	18	18	18	18	18	18	18
Turbine†	28 (HP,G)	18 (LP)	18 (LP)	18 (LP)	18 (G)	21 (HP)	18 (LP)	18 (LP)	18 (LP)	18 (G)
800-Mw(e) capacity										
Reactor	0	0	27	20	20	20	20	20	20	20
Turbine†	28 (HP,G)	18 (LP)	18 (LP)	18 (LP)	18 (G)	21 (HP)	18 (LP)	18 (LP)	18 (LP)	18 (G)
1000-Mw(e) capacity										
Reactor	0	0	31	23	23	23	23	23	23	23
Turbine†	28 (HP,G)	28 (HP,G)	24 (2LP)	18 (LP)	18 (LP)	28 (HP,G)	28 (HP,G)	24 (2LP)	18 (LP)	18 (LP)

*Based on three-shift operation with experienced and unlimited manpower.
†HP designates high-pressure turbine; LP is low-pressure turbine; G is generator.

Digitized by Google

the first refueling, when it caused a 6-week delay.[18] Most of the component failures that caused major delays during refuelings were due to vibration caused by hydraulic forces (Big Rock Point has had similar problems).[24,25] Control-rod rubbing straps, shim-rod surfaces, and in-core instrumentation thimbles fretted and required design modifications. Irradiation specimens became detached in the vessel, and some thermal-shield joint bolts have broken because of vibration caused by hydraulic forces. Activated corrosion products have caused serious delays by contaminating the refueling systems, a delay not anticipated during preirradiation tests. Other delays have been caused by difficulties in debugging the complex fuel-handling equipment. Fortunately, these problems have been recognized and in general have been eliminated.

Fig. 4 Yankee (Rowe), with a capacity of 175 Mw(e) net, has generated approximately 5 million Mw-hr since initial criticality Aug. 19, 1960.

During 1961 the Yankee plant experienced various problems that caused relatively short shutdowns (Figs. 4 and 5 and Tables 2 and 3). Downtime for tests to confirm performance calculations reduced plant availability by about 7%. Plant availability was reduced another 3% by all other shutdowns because of such factors as (1) primary-system valve-stem leakage, (2) turbine control-system malfunction, (3) the need to interchange the control rods, or (4) decisions to inspect equipment.

By 1962 many of the causes of the early shutdowns had been eliminated, and the extensive testing required with Core 1 was no longer required. Modifications of the valve-stem packings have prevented

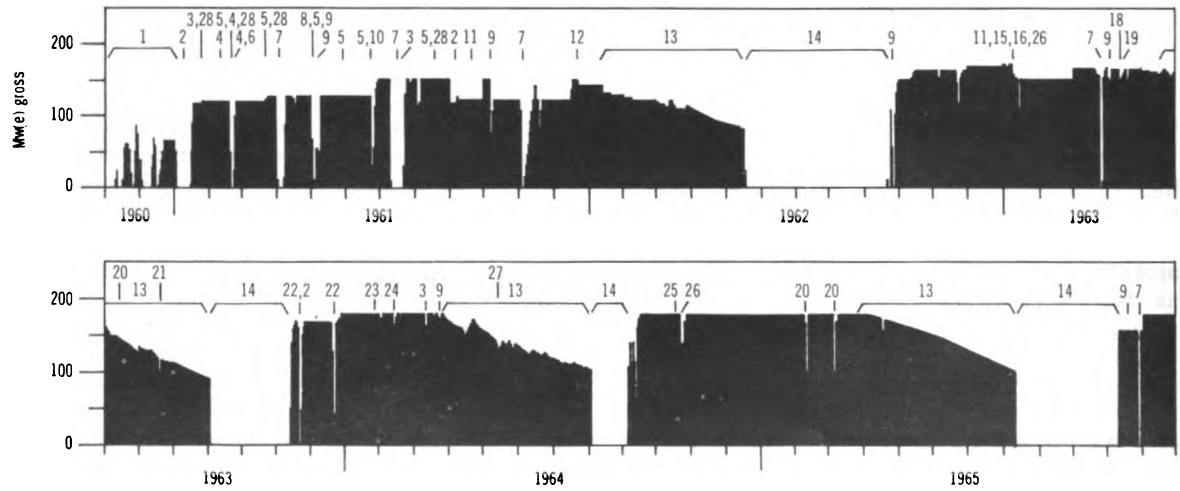

Fig. 5 Yankee (Rowe), Yankee Atomic Electric Co., plant outages had the following principal causes:

1. Initial test operation
2. Turbine vibration
3. Scram by moisture-separator switch
4. Valve stem leak-off
5. Control-rod interchange
6. Scram by instrument noise
7. Scheduled physics testing
8. Modified pressurizer instrumentation
9. Erratic turbine control valves
10. Throttle-valve sticking
11. Boron test
12. Scram by false flow signal
13. Core "stretch-out"
14. Refueling
15. Charging-line relief-valve leak
16. Primary drain-valve leak
17. Primary and secondary maintenance
18. Scram when control rod dropped
19. Flowmeter pipe leak
20. Transmission line fault
21. Scram-detector cable damage
22. Head adapter leak
23. Faulty turbine trip mechanism
24. Control-rod drop tests
25. Condenser bottle
26. Instrument ..on scram
27. Low condensate pressure
28. Inspection in vapor container

Digitized by Google

leakage. The need for shutdown to interchange control rods has been eliminated by operating with soluble boron control and with rods fully withdrawn. There is now no need to shut down for routine inspection of equipment in the vapor container.

For the years in which the plant was refueled, 1962 to 1965, plant availability was 64, 78, 88, and 73%. Except for the effect of core stretch-outs, availability is expected to be comparable with that of fossil-fired plants of like size. The forced-outage rate for these years was 2, 3, 0.8, and 0.2%. Excluding refueling and the effect of stretch-out, reactor availability was 99.8, 97.5, 99+, and 99+% in 1962 to 1965.

REFUELINGS

The major portion of all Yankee maintenance was performed during refuelings (Table 4). At the first refueling the Zircaloy control-rod followers were found to have worn by fretting at the stainless-steel-to-Zircaloy joint where they attach to the control rods. For this reason the followers were replaced with new ones having stainless-steel adapters designed to eliminate wear; but this work delayed operation 6 weeks. Fortunately, the modification proved to be successful. Another week was lost during repair of in-core instrumentation damaged during the refueling. The refueling shutdown extended 2 weeks more because radioactive silver that corroded from the first control rods contaminated the refueling area. These rods have since been replaced by rods that resist corrosion better.[18,25]

At the end of the second refueling shutdown, 14 days were lost to remove the vessel head so that a stuck control rod could be modified to prevent a recurrence; 7 days were used in the inspection of core components and vessel internals. Additional delay was caused by difficulties in attaching the shafts to the control rods. By now, most of these problems appear to have been solved.

The third refueling took 35 days. Three of these 35 days were for unplanned extensions to leak-test neutron sources and to inspect the irradiation specimens. Four days were consumed by difficulties in latching shim rods to their extensions and in coupling drive shafts to control rods. During the fourth refueling, which took 93 days, the core barrel was pulled to provide access to the entire inside of the vessel, the thermal-shield joint was modified, and a secondary core support was installed.[17]

Shippingport

Designed for operation either as a base-loaded or load-following plant, Shippingport (Fig. 6) has been successful in both operating modes. However, tests to determine overall station performance and to evaluate individual systems and components have used large portions of operating time[10–15] (Fig. 7) which have decreased plant capacity factor and caused outages that would not have been experienced had the plant remained base-loaded. For example, the large number of fail-safe protective devices installed for tests often led to spurious shutdowns during power changes and also demanded considerable operator attention because the set points are close to normal operating conditions.

Although the shutdowns resulting from instrument actions or failures were numerous, they were short; the plant may even have profited from these early problems. The 22 forced shutdowns and 7 scheduled shutdowns because of instrument action or need for repairs are more important in considering reliability (to take or hold load) than in calculating capacity factor. Plant forced-outage rates were 3, 4, 1.2, 0.3, 0.5, and 0.1% in the years 1958 to 1963. In 1964 the plant was down for modifications to increase its capacity to 140 Mw(e) net equivalent. For the last 8 months in 1965, the forced-outage rate was 1.2%. (The forced-outage rate of conventional plants is approximately 2%.) Shutdowns decreased as instrumentation systems were debugged and as the design of some components was improved. Improvements made apparent by experience at Shippingport are being made in other plants.

TESTING AND MAINTENANCE

Except when maintenance was clearly related to a test, it was difficult during Seed 1 operation to attribute outages to either maintenance or testing. In most cases they were performed concurrently. However, in Tables 2 and 3 outages are identified with whichever need appeared to be the most pressing. During a very significant percentage of the time Seed 1 was in use, the plant was devoted to testing; station capacity factor was 37%, plant availability was 45%, and reactor availability was 75%. Approximately 12% of Seed 1 operation was spent on maintenance of the moisture separator. Modifications have been made, and similarly modified separators installed at Yankee have had no problems. Another 10% of Seed 1 operation was spent on reactor-systems maintenance; 7% was spent on turbine-plant maintenance. Problems encountered early with governor control valves, steam generators, and main coolant pumps appear to have been solved.

TESTING TAKES TIME

The time spent for testing and training was almost doubled during operation with Seeds 2, 3, and 4 (note item 11, Fig. 7). The outage time attributed to maintenance has become a negligible influence on the plant availability factor. While operating with Seeds 2, 3, and 4, plant capacity factors were 70, 77, and 75% and plant availability was 79, 83, and 82%. Excluding downtime for testing, training, and refueling, reactor availability during each of these periods was 97%. Tables 2 and 3 show that, since the start of operation with Seed 2 early in 1960, the outages for

Digitized by Google

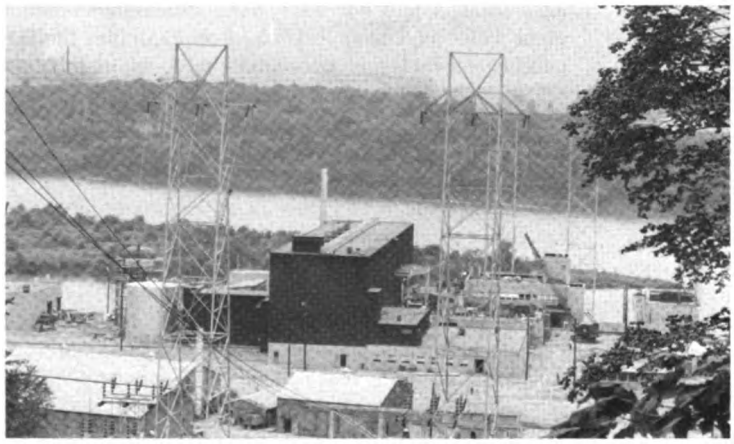

Fig. 6 Shippingport is a much modified nuclear power station. Initially built for tests and 60 Mw(e), the vessel now has a new head and a core that generates 140 Mw(e) net equivalent. Turbine generators can only use part of the steam; 50 Mw(e) net equivalent is dumped.

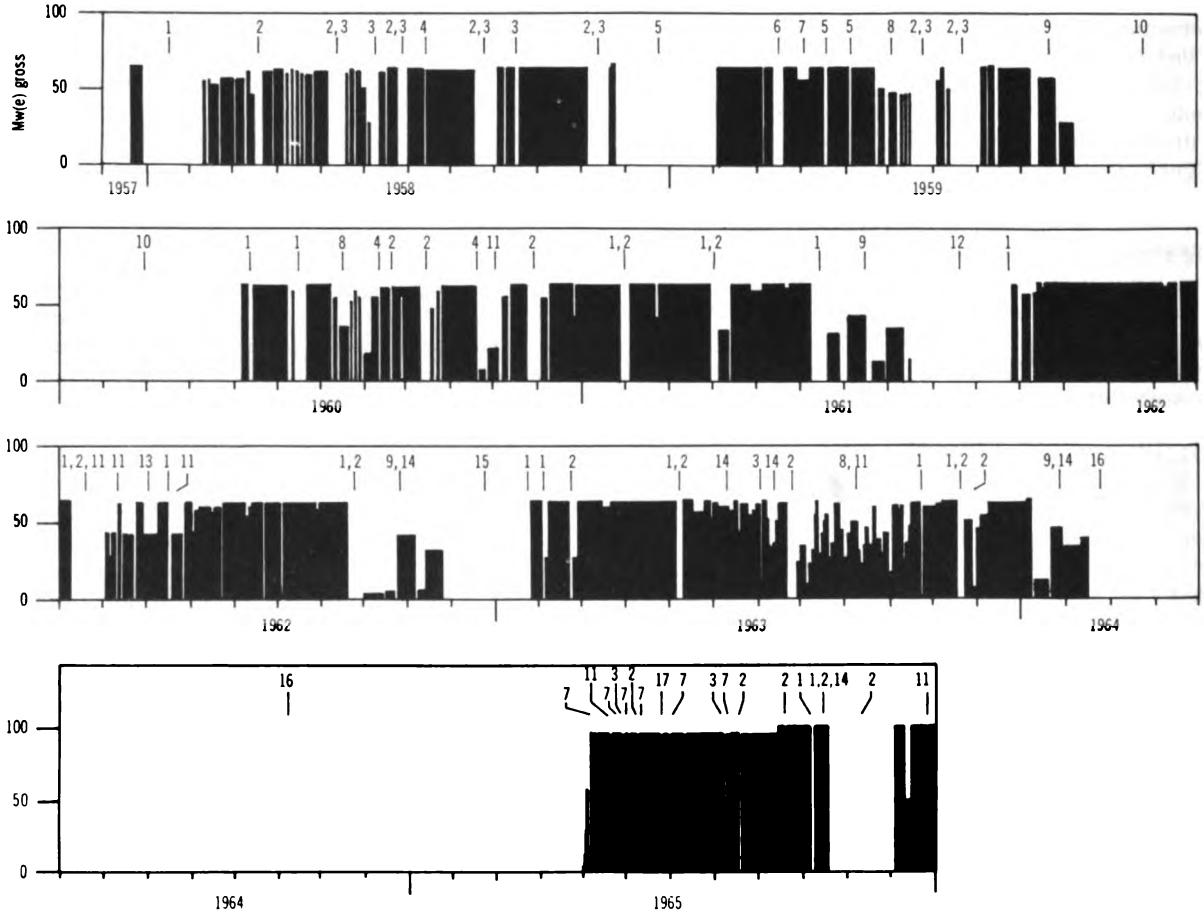

Fig. 7 Shippingport Atomic Power Station, Duquesne Light Co., plant outages were for the following principal reasons:

1. Hot plant and physics testing
2. Plant maintenance
3. Low-power physics testing
4. Returning a reactor coolant loop to service
5. Turbine-blading and moisture-separator repair
6. Turbine governor-valve deficiency
7. Nuclear instrumentation failure
8. System load requirements
9. Extended-life operation at reduced temperature
10. Seed 1 to Seed 2 refueling
11. Training
12. Seed 2 to Seed 3 refueling
13. Xenon oscillation testing
14. Heat-dissipation system testing
15. Seed 3 to Seed 4 refueling
16. Core 1 to Core 2 refueling and plant modifications
17. Control-rod sequence change

Digitized by Google

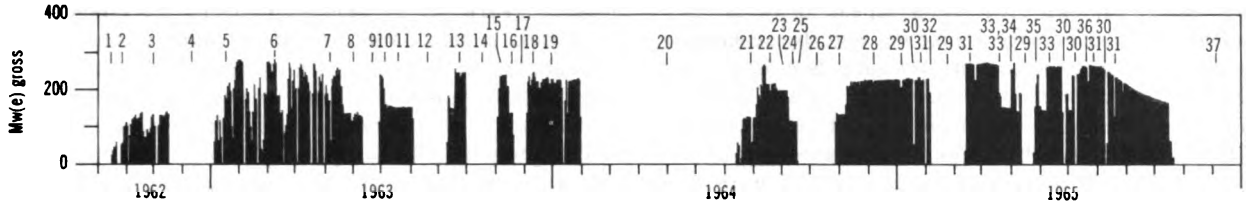

Fig. 8 Indian Point Station, Consolidated Edison Co., plant limits and outages were as follows:

1. First power operation
2. Ascending power tests
3. Limit 50%, single superheater
4. Control-start superheater piping
5. Ascending power tests
6. Load not limited, 89 days
7. Limit 92.5%, coolant pump 122
8. Limit 50%, single superheater
9. Generator hydrogen-seal brackets
10. Limit 85.8%, coolant pumps 122, 131
11. Limit 58%, water pump 12
12. Coolant pumps and circulating-water pumps
13. Limit 92%, primary pump 132
14. Nuclear boiler 14
15. Limit 92%, primary pump 132 (continuous)
16. Limit 50%, single superheater
17. Main-turbine steam-lead crack
18. Limit 92%, primary pump 132 (continuous)
19. Limit 84%, primary pump 132
20. Pool lining, gamma scanning, shim removal
21. Limit 50%, single superheater
22. Load not limited, 10 days
23. Limit 78%, nuclear boiler 11
24. Limit 71%, nuclear boiler 11, primary pump 122
25. Limit 44.5%, nuclear boilers 11 and 14, primary pump 122
26. Nuclear boilers 11 and 14, primary pumps
27. Limit 50%, single superheater, nuclear boiler 11
28. Limit 78%, nuclear boiler 11
29. Rod drive
30. Reactor instrument
31. Plant electrical
32. Weekend and rod drive
33. Control system
34. Deaerator level
35. Condenser leak
36. Superheater
37. Refuel
38. Stretch-out

purposes other than refueling or testing have, with one exception, had an insignificant effect on plant availability factors. The exception was a 10-day shutdown in 1963 for maintenance and test, which influenced availability factors by only 3%. Other maintenance has been performed but was not the primary reason for the outages.

Both plant availability and capacity factor would increase if testings were reduced to a minimum and if the plant were base-loaded, a fact demonstrated when the plant has been base-loaded; a drastic reduction in test operations would result in an increase of around 8% in plant availability. By improving procedures it has been possible to reduce refueling time to 2 months. With the uncomplicated vessel head installed with Core 2 (the older head was complex, designed for test use), it is anticipated that refueling can be accomplished in less than 6 weeks. Quite possibly the plant can continue to operate with no more than two forced shutdowns per year and to have a plant availability of 87%, which compares favorably with experience with fossil plants of this size.

Dresden

In the first two calendar years of Dresden operation (Fig. 2), extensive outages occurred for component modifications and removal of test assemblies (7624.2 hr) and for personnel training (1072 hr). By far the most significant item was the 4797.5 hr required for control-rod-drive mechanism changes. The resulting forced-outage rate for 1960 and 1961 was 38.4%. From 1962 to 1965 the forced-outage rates were 1.3, 1.5, 2.2, and 4.9%, whereas plant availability was 78.6, 75.6, 80.9, and 78.3%.

Practically all outage time in the turbine-condenser portion of the Dresden plant, either scheduled or forced, was precipitated by leaks in piping and flanges; approximately 300 hr were required to repair these leaks and about 60 hr were spent on condenser-tube leaks.[3]

Indian Point

The Indian Point Station (Figs. 8 and 9) had been in operation[26–28] slightly over 3 years when the data

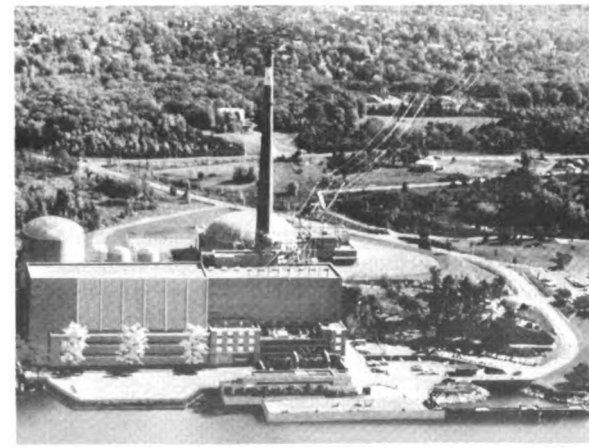

Fig. 9 New Indian Point Station (drawn in at left), 873 Mw(e) net, is to be completed by 1969.

Digitized by Google

were reviewed. All difficulties appear to be fairly conventional and readily remedied, e.g., by changing gasket materials on pumps. Because few data are available on refueling, estimates of future availability are subject to considerable error. An extended outage to load the reactor with a redesigned core and reactor internals started in October 1965. For 1965, including the 2.5-month shutdown in late 1965, plant availability was 62%.

The 173-day shutdown in 1964, item 20 in Fig. 8, was by far the longest shutdown in over 3 years of operation. It was extended 1 month beyond the time required to remove core shims by a license requirement that the hot fuel be gamma-scanned to confirm core performance calculations. Additional downtime resulted from installation and leak-testing of a stainless-steel pool liner, a step taken to reduce potential radiation and contamination problems. During this outage the oil-fired superheaters were partially retubed.

On completion of the initial 50% power operations in 1962, the plant was down 48 days to modify piping for parallel operation of the oil-fired superheaters. After completion of the ascending power tests to 100% power on Jan. 25, 1963, the plant was not load-limited for 89 days. During this period the plant output was varied considerably, and its performance was satisfactory.

COMPONENTS

Leakage past the thermal barrier of a primary coolant pump on May 6, 1963, caused the load limit to be reduced by 7.5%. This problem has caused six similar reductions for a total of 156 days in 2 years. During a 39-day shutdown starting in September 1964, the thermal barriers in the three pumps were modified and leaks in two nuclear boilers were repaired. In the 2 years of operation, boiler problems caused 22% reduction of load limit during 105 days.

Conventional plant equipment caused an appreciable reduction in plant load factor; superheater problems caused a load limit of 50% for a total of 62 days; circulating-water-pump problems caused a 58% limit for 30 days. The main coolant pumps were repaired during the 38-day shutdown starting in August 1963. A main-turbine steam-lead crack caused a 13-day outage for repairs.

Fail-safe controls caused numerous fast control-rod insertions and scrams that resulted from instrument faults and temporary spurious signals initiated within the systems themselves during operating manipulations. Such outages, which were relatively short, decreased in number as the systems were debugged.

Big Rock Point

This 50-Mw(e) boiling-water-reactor plant (Fig. 10) achieved full power in March 1963. In the research and development program scheduled over the next several years, it is planned to raise the output to 75 Mw(e). In this same period the plant, under AEC contract, is to be available for an extensive irradiation program to test UO_2 fuels that cost less to fabricate, operate to greater burnups, and produce more power per unit volume of core (45 to 60 kw/liter).[6–8] Refinements in fuel-element fabrication made possible by this program will result in improved economics and operation of future cores for this and similar reactors. Operation of Big Rock Point plant also is intended to furnish data on stability, power distribution, fluid flow, and heat transfer.

WIDE DESIGN PARAMETERS

Although the initial rated output for this reactor is 157 Mw(t) at a system pressure of 1050 psia, all components have been designed for operation at 240 Mw(t) and 1470 psia. Obviously, operation over this wide range of conditions can be accomplished only with a highly flexible design. Coupled with provisions for development of high power densities, the result is a reactor that is not optimized for routine power generation; therefore it probably will not achieve the availability expected in a more conventional installation.

VIBRATION

Modifications to the thermal shield and installation of a new thermal-shield seal were completed in August 1965. This outage started in October 1964 when 6 of the 12 thermal-shield holddown studs failed by fatigue; investigation disclosed that coolant flow induced a self-excited vibration of the shield. A new seal design and location of the seal on top of the shield eliminated the problem. Close attention to mechanical design and testing of vessel internals can eliminate a repetition of this experience.[24]

Fig. 10 Big Rock Point plant, following initial criticality in September 1962, has pursued an extensive research and development program designed to uprate core power density with improved fuels.

Digitized by Google

After the thermal-shield modification was made, one forced outage of 34 hr and two scheduled outages of 169 hr were recorded in 1965. The forced outage was caused by a defective tone relay on a 138-kv transmission line. The scheduled outages were brought about by leaks in the turbine drain manifold, a defective 138-kv circuit breaker, and a need to modify 22 control-rod drives.

Humboldt Bay

Initially licensed to operate at 165 Mw(t) and authorized in May 1965 to increase power to 70 Mw(e) gross [240 Mw(t)], the Humboldt Bay boiling-water reactor began commercial operation Aug. 1, 1963 (Figs. 11 and 12). Routine operation at the uprated power is expected to begin after the 1966 refueling. Experience indicates that a normal refueling operation, not requiring special core work such as removal of poison curtains (large curved plates used to shape flux in new cores), could be completed in 14 to 18 days.

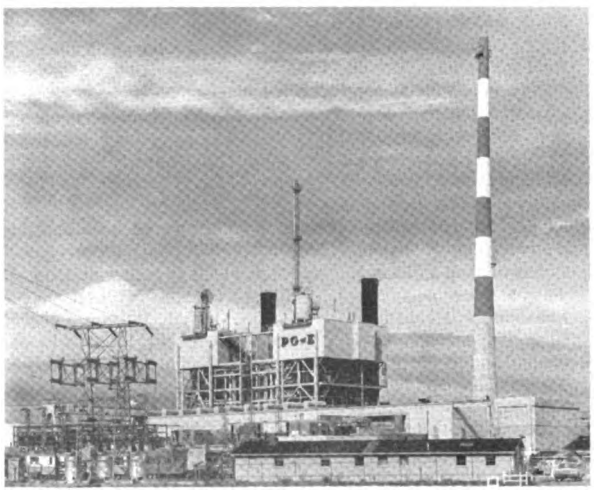

Fig. 11 Humboldt Bay includes two 50-Mw(e) fossil-fired units and the nuclear power plant, Unit No. 3. The 50- to 70-Mw(e) BWR at right uses an underground pressure-suppression containment system.[30]

During the 3672 hr of commercial operation in 1963, plant availability was 81.2%, scheduled-outage time was 660 hr, and the forced outage was 1.2% (Tables 1 to 4).

Scheduled outages in 1964 totaled 1038 hr and included 677.5 hr for the removal of poison curtains, the addition of 14 fuel assemblies, miscellaneous maintenance, operational testing, and the completion of construction work; 1964 included 64 hr of forced outages (for a rate of 0.8%). Plant availability was 87.3%.

In 1965 there were 1945 hr recorded as scheduled outages, including 1724 hr assigned to refueling, containment modification and leakage-rate testing, turbine overhaul, miscellaneous maintenance, and operational testing. Other scheduled outages included scram-system maintenance, testing of turbine trip and reactor protective system, and repair of a turbine-casing joint leak. These required approximately 220 hr, for a total scheduled-outage time of 1945 hr. Forced-outage time for the year was 37 hr. Plant availability, including the time lost for refueling, was 77.4%; excluding refueling, it was 79.5%.

Forced outages in 1965 amounted to 37 hr, but only 6 hr affected reactor availability. Thus, whereas the reactor forced-outage rate was less than 0.1%, the plant forced-outage rate was 0.55%.

Actual availability for the first 38 months of operation, including downtime for refueling, has been 86%. Analysis of experience indicates an availability of greater than 90% can be anticipated over the life of the plant.

Prognosis

The Humboldt Bay plant and the other plants reviewed here are typical in that outages required

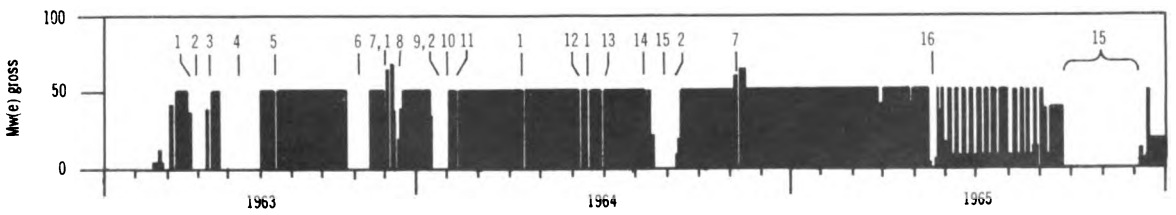

Fig. 12 Humboldt Bay, power plant Unit No. 3 (Units 1 and 2 are fossil-fired), Pacific Gas & Electric Co., plant outages were are follows:

1. Spurious reactor control system scram
2. Turbine leak
3. Scram-pressure transient
4. Reactor head leak and core changes
5. Turbine steam bypass valve stuck
6. Modify reactor head closure
7. Scram during test, low water level
8. Uprating tests
9. Reactor test and turbine leak
10. Scram during startup, low water level
11. Operator license examination
12. Turbine trip test
13. Scram, turbine control system
14. Turbine test
15. Refueling
16. Drywell vacuum breaker

Digitized by Google

during the early years of plant life to modify and debug systems should not reappear in future operations. As concluded in a recent report of the Federal Power Commission,[29] future operations of water-reactor stations are expected to demonstrate dependability, flexibility, and availability comparable to modern fossil-fired stations.

* * *

This article is based partly on a paper presented at the Annual Meeting of the American Nuclear Society, June 20–23, 1966. Data in both the paper and this article were obtained primarily by means of questionnaires and with the cooperation of the six utilities operating the plants discussed.

References

1. Operating Experience: Dresden, *Power Reactor Technol.*, 6(2): 60-64 (March 1963).
2. Operating Experience: Dresden, *Power Reactor Technol.*, 5(2): 56-59 (March 1962).
3. Dresden Turbine Inspected and Overhauled, *Nucleonics*, 21(4): 78 (April 1963).
4. The Dresden Nuclear Power Station, *Power Reactor Technol.*, 4(4): 56-58 (September 1961).
5. Report on Equipment Availability for the Five-Year Period 1961–1965, EEI Publication No. 65-35, Edison Electric Institute, New York, May 1965.
6. R. L. Haueter et al., Operating Big Rock Point, *Nucleonics*, 22(11): 41 (November 1964).
7. R. N. Duncan et al., Advances in High-Power Density BWR's — Part I, Toward Low-Cost High Performance BWR Fuel, *Nucleonics*, 23(4): 50 (April 1965).
8. N. H. Barth and R. K. Haling, Advances in High-Power-Density BWR's — Part II, Power Flattening Techniques Boost BWR Core Capabilities, *Nucleonics*, 23(5): 72 (May 1965).
9. Walter Mitchell III, Humboldt Bay and Big Rock Point, *Power Reactor Technol.*, 7(1): 70-84 (Winter 1963–1964).
10. Operating Experience: Shippingport, *Power Reactor Technol.*, 7(2): 193-196 (Spring 1964).
11. R. E. Barclay and W. J. O'Brien, Third Shippingport Refueling Still Faster, *Nucleonics*, 21(9): 70 (September 1963).
12. Operating Experience: Shippingport, *Power Reactor Technol.*, 6(3): 49-56 (June 1963).
13. Operating Experience: Shippingport, *Power Reactor Technol.*, 6(2): 64-67 (March 1963).
14. Operating Experience: Shippingport, *Power Reactor Technol.*, 5(4): 61-72 (September 1962).
15. J. J. Dutton, Two Shippingport Refuelings, *Nucleonics*, 20(4): 66-70 (April 1962).
16. Operating History of U. S. Nuclear Power Reactors, USAEC Report TID-8214, 1964.
17. G. A. Reed and E. Tarnuzzer, Examining Yankee Plant Performance in 1965, *Nucleonics*, 24(3): 42 (March 1966).
18. K. K. Brown, Three Yankee Refuelings Point Toward Minimum Downtime, *Nucleonics*, 23(1): 64-70 (January 1965).
19. Operating Experience: Yankee, *Power Reactor Technol.*, 6(4): 82-91 (Fall 1963).
20. W. D. Craig, Inspecting Water Reactors, *Nucleonics*, 20(4): 57-60 (April 1962).
21. Yankee Operators Discover Reactivity Anomalies, Prepare to Refuel, Hope to Raise Power, *Nucleonics*, 20(3): 84, 86 (March 1962).
22. R. J. Coe, G. A. Reed, and D. E. Vandenburgh, Yankee Reactor Operates on Schedule, Below Budget, *Nucleonics*, 19(3): 53-55 (March 1961).
23. Yankee Nuclear Power Station, *Power Reactor Technol.*, 4(3): 47-55 (June 1961).
24. F. H. Martens, Design Foresight Can Simplify Reactor Modifications, *Power Reactor Technol.*, 9(2): 74-79 (Spring 1966).
25. R. C. Skaardal, Operational Problems and Solutions, *Power Reactor Technol.*, 8(4): 271-279 (Fall 1965).
26. Consolidated Edison Nuclear Steam-Generating Station, *Power Reactor Technol.*, 7(3): 313 (Summer 1964).
27. Nucleonics Reactor File No. 14, Indian Point on the Line, *Nucleonics*, 21(4): (April 1963).
28. Consolidated Edison Nuclear Steam Generating Station, *Power Reactor Technol.*, 6(3): 28-48 (June 1963).
29. National Power Survey, Federal Power Commission, Washington. October 1964.
30. J. C. Carroll and J. O. Schuyler, Humboldt Bay Reactor Operating Experience, *Nucl. Safety*, 6(4): 441-451 (Summer 1965).

Digitized by Google

Applying High-Temperature Instrumentation in Liquid-Metal Experiments

By Paul A. Lottes

Liquid-metal technology stands today where water technology stood about 15 years ago. Rapid evolution is needed because liquid metals at high temperatures are of great importance for fast breeder reactors (at ~1200°F) and also for space power systems (at ~2000°F). Only in the past few years have data in significant quantities been reported, notably at the more recent of a series of conferences on high-temperature liquid-metal heat-transfer technology.[1,2] The earlier conferences[3,4] formulated many of the plans and ideas from which the recent data have grown. The latest conference emphasized instrumentation but also included many experimental results. Topics discussed included thermodynamic and heat-transfer measurements, vapor-quality and volume-fraction measurements, bearing-film measurements, and liquid-level and impurity measurements.

Instrumentation

Because liquid metals are difficult to handle and temperatures are high, exotic loops and heaters[5,6] are required, as are unusual pressure-measuring devices.[7,8] Void-fraction measurements[9] are made with gamma,[10,11] electromagnetic,[12,13] and X-ray[11] methods and calorimeters.[14] Bearing-film measurements, of special interest for aerospace application,[15] rely heavily on eddy-current methods,[16,17] although magnetic inductance[13] underlies some instruments. Unique equipment is being used for liquid-level and impurity measurements[18–22] and for cavitation damage studies.[23]

HEATERS

Experimental techniques for delivering large heat fluxes to flowing liquid metals include a thermal-radiation heater and an electron-bombardment heater.[5] The thermal-radiation heater is a d-c-heated tantalum sheet capable of delivering heat fluxes up to 62,000 Btu/(hr)(sq ft) for coolant temperatures up to 1400°F. The electron-bombardment heater uses a 20,000-volt 10-amp power supply and directs a uniform stream of high-velocity electrons against the inside wall of an evacuated tube to achieve heat fluxes up to 20,000 Btu/(hr)(sq ft) in a sodium-cooled system; since the conference, the heater has achieved 350,000 Btu/(hr)(sq ft) and is expected to generate 10^6 Btu/(hr)(sq ft).

A conduction type electric heater capable of delivering 5 Mw to flowing lithium at temperatures near 2000°F has also been developed.[6] The design was based on high-temperature electrical-breakdown data for fired ceramics and requires heat generated in the current element to be transferred by conduction across an electrical insulator and metal sheath to the liquid-metal stream.

Breakdown strength and insulator leakage currents for swaged ceramics were reported for a small test heater[6] that had a 0.125-in.-diameter tantalum center, 0.070 in. of swaged alumina insulation, and a 0.38-in.-diameter niobium–1% zirconium sheath. Resistivity measurements of the alumina after 500 hr of testing at 2540°F centerline temperature with a surface flux of 130 watts/sq in. [37,800 Btu/(hr)(sq ft)] showed a linear relation between leakage current and applied potential up to approximately 3 volts/mil. The average resistivity was 0.25×10^5 ohm-cm at approximately 2270°F, whereas the value in the literature for fired alumina at this temperature is 10^5 ohm-cm. The author concludes that swaged conduction heaters can be used at elevated temperatures with field strengths up to 3 volts/mil across the ceramic.

PRESSURE-MEASURING DEVICES

A device for measuring pressures before and after blade rows in a potassium-vapor turbine has been

Digitized by Google

developed.[7] Used to measure total and static pressure in a two-stage 200-hp potassium turbine at the inlet and outlet, the static pressures between all blade rows, and the total flow rate of potassium vapor to the turbine, the device is based on flowing a metered amount of inert gas through a 0.005-in.-diameter orifice in the sensor lines to pressure taps. The flow of inert gas prevents the diffusion of potassium vapor into the sensor lines. In this way the potassium vapor is contained within the experimental facility, and the pressure transducers operate in an inert-gas environment at moderate temperature.

In another pressure transducer for liquid-metal systems, a thermionic diode sensor converts the motion of a pressure-actuated refractory-alloy capsule into a suitable electric output.[8] It was developed to be capable of operating in liquid potassium up to 1800°F. Main problem areas include the high-temperature diaphragm-deflection characteristics, diaphragm compatibility with liquid metals, and the accuracy and sensitivity of the thermionic diode sensor. Figure 1 shows the transducer design, and Fig. 2 shows typical diode characteristics. The alloys selected for investigation as diaphragm materials were C-129 (Nb–10 W–10 Hf–0.1 Y), FS-85 (Nb–28 Ta–10 W–1 Zr), T-222 (Ta–10 W–2.5 Hf), and W–25 Re. Test results on compatibility, accuracy, and sensitivity are detailed.[8]

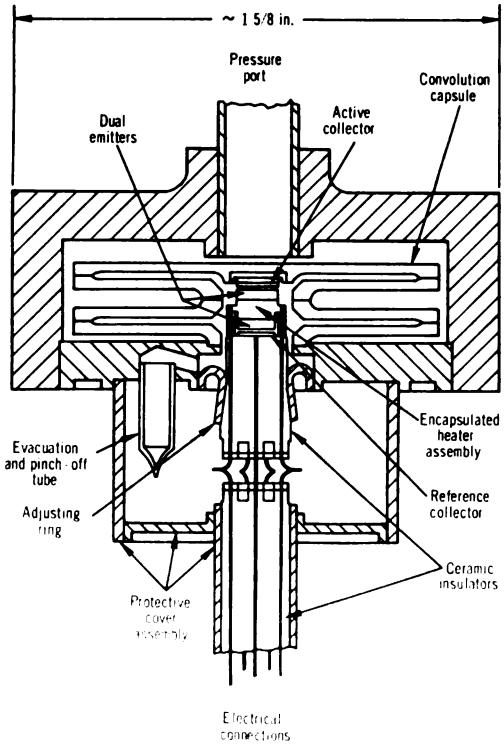

Fig. 1 Pressure transducer incorporates a double-convolution pressure capsule and a thermionic diode sensor.[8]

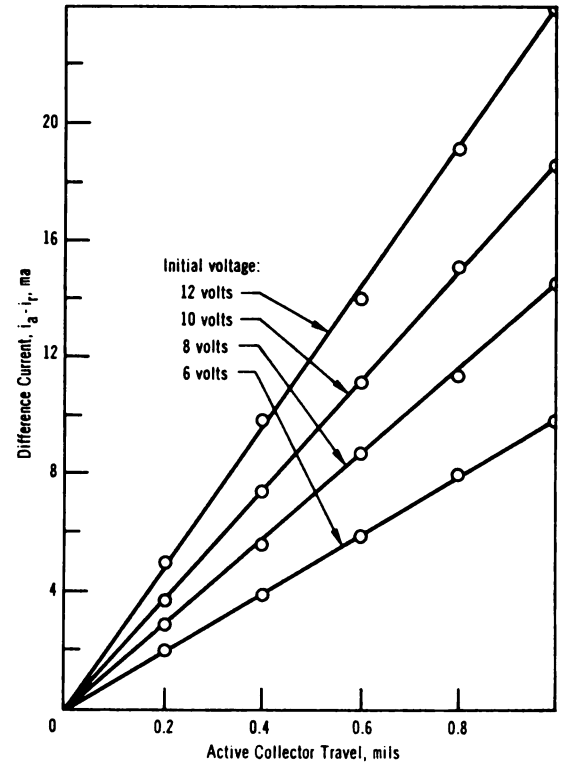

Fig. 2 Calibration data for a thermionic diode sensor show that it is suitable for use in a pressure transducer.[8]

VOLUME-FRACTION MEASUREMENTS

Numerous techniques have been described for volume-fraction measurements. These include gamma attenuation,[10,11] electromagnetic flowmeters,[12,13] X-ray methods,[12] and calorimeters.[14]

Gamma-Attenuation Methods. Volume fractions have been measured in a two-phase boiling sodium system both by gamma attenuation and with electromagnetic flowmeters. These methods and the accuracy involved under various conditions have been examined.[9,10]

One-shot gamma-attenuation methods (in which all the cross section of a flow channel is studied at once) are simple and easy to use, although they are less accurate than the traversing-beam methods. As a result of recent efforts to improve the accuracy of these techniques, design criteria have been developed that will reduce errors[11] to less than or equal to 5%. The shape of the collimator used in one-shot techniques is reported to greatly affect the dependence of the void-fraction measurement on the void distribution in a flow channel.

Electromagnetic Methods. In addition to the volume-fraction application mentioned above,[10] electromagnetic flowmeters have been used in the SNAP-10A flight system.[13] The NaK flow rates were mea-

Digitized by Google

sured electromagnetically by utilizing a secondary set of electrodes located approximately 0.25 in. from the main electrodes on a thermoelectric-powered d-c conduction pump. Pressure was indirectly monitored during the SNAP-10A flight by measuring the position of the bellows in two expansion compensators. Temperatures were measured with resistance type detectors and with chromel–constantan thermocouples. Data on bellows position (pressure indication) and system temperatures were given as a function of flight time (up to 1000 hr).

Observation of thermoelectric effect associated with the use of an electromagnetic flowmeter in a condensing alkali-metal test loop was reported but not explained.[24] A flowmeter output of approximately 10 μv was observed for zero-flow conditions. Also reported was the time required for the flowmeters and a-c conduction pumps to reach steady-state performance. Less than half an hour was required with a type 316 stainless-steel loop operating at 300°F, but an 8-hr soak at 800 to 1000°F was required with a refractory-metal loop (Nb–1% Zr).

X-Ray Methods. These techniques for determining void fractions in water systems can be extended for use in liquid-metal systems.[12] Estimates of attainable accuracy and space and time resolution are given for a measurement system used with a liquid-potassium laboratory experiment. In this feasibility experiment, liquid potassium was boiled in an induction-heated stainless-steel test section (0.218 in. in inside diameter by 0.016 in. in wall thickness). More than 10^8 X-ray quanta/sec (roughly equivalent to a radioactive source of 1000-curie strength) were detected with a beam area of 0.02 sq in., X-ray mean energy of approximately 47 kev, and energy width at half maximum of approximately 5 kev. The X-ray intensity in 1 msec was measured to within 0.2% accuracy, corresponding to an accuracy of better than

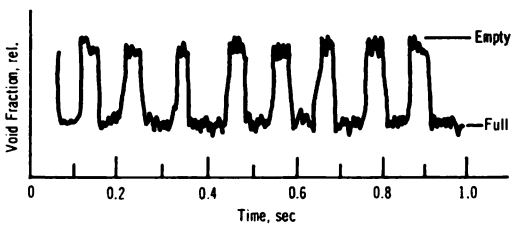

Fig. 3 X-ray measurements demonstrate periodic voiding of liquid potassium;[12] test was at atmospheric pressure, 50,000 Btu/(hr)(sq ft).

1% in the void fraction. Figure 3 demonstrates the void-measurement response.

Pressure and Void Fraction. Instrumentation for these measurements, and also data on two-phase friction factors and volume fractions for two-phase liquid-metal coolants, are given in Ref. 9. Gamma attenuation of ^{170}Tm is used to measure void fraction. Pressure drops were measured with a Taylor transmitter connected to a stainless-steel diaphragm assembly that contained a pressure-transmitting eutectic NaK.

Flow-Rate Calorimeter. Of more interest to liquid-metal turbine designers than to reactor designers, a flow-rate calorimeter has been described in, which a known amount of heat is added to a flowing stream of wet liquid-metal vapor.[14] The device determines vapor dryness (or percent moisture by weight in vapor) and is quite useful for measuring "quality" in the region from 80 to 100%. Moisture content is deduced from a heat balance (accurate physical properties and accurate temperature measurements are required). The preliminary tests discussed were performed with steam as the working fluid. Scheduled future tests will use 1500°F potassium, and more advanced tests are proposed at 2000°F.

BEARING-FILM MEASUREMENTS

Although reactor designers may not have a direct interest in liquid-metal turbine bearings, techniques described in some of these measurements should be of use in other applications. The status of bearing problems related to high-speed applications has been comprehensively reviewed;[15] the review includes an excellent discussion of the fundamentals of bearing design as well as an up-to-date evaluation of problems remaining to be solved.

Eddy Currents. An eddy-current technique was developed to measure potassium film thickness and to detect film discontinuities.[16] The transducer configuration was that of a small flat coil of wire buried in an electrically nonconducting bearing sleeve near the inner surface. Electric currents are induced in the adjacent liquid potassium and bearing journal. Then the effect of this induced current upon the apparent impedance of the transducer coil is used to determine the film thickness.

Reference 17 reports the development of a film-thickness transducer of the eddy-current type that is capable of measuring the radial motion of a potassium turbine shaft rotating at up to 24,000 rpm. The measuring system is accurate to ±0.00005 in. and will operate at 650°F. Shaft motion is detected by sensing the thickness variation of a 0.015-in. nominal thickness film of potassium located between the transducer and the shaft. Design features and curves along with some actual turbine performance data were included.

Magnetic Inductance. A magnetic-inductance transducer has been developed which consists of a coil of wire surrounding a core of ferromagnetic material specially chosen to exhibit a large Villari effect (strain dependence of permeability).[18] In operation, potassium film pressure deflects a thin diaphragm

Digitized by Google

in the bearing sleeve, thus straining the Villari-effect core that restrains the back side of the diaphragm. When properly calibrated, the transducer measures film pressure.

LIQUID-LEVEL MEASUREMENTS

A system capable of sensing and tracking the level of liquid metals (Fig. 4) uses a scanning eddy-current probe to sense level and a servo to position the device on the level.[18] The probe position is transmitted electrically to a remote indicator which can be calibrated (in percent or inches). The eddy-current probe is capable of sensing through vessel walls up to 0.2 in. thick. With the use of a stainless-steel tube to contain the liquid metal, and with air cooling, the system is capable of continuous operation at 1800°F and is accurate to 0.1 in. of liquid level.

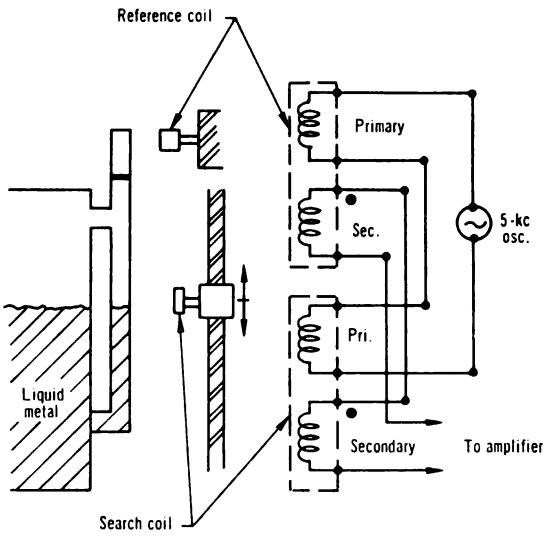

Fig. 4 Level detector for liquid metals uses two electrically identical coils, each containing primary and secondary, and is wired so that eddy currents indicate level.[18]

A similar probe developed as a level-seeking device (operating as an eddy-current unit that is motor driven to follow the liquid level) has been used in an experimental facility.[20] Advantages of the probe are that it requires a minimum of headroom, has a continuous linear response with level, operates automatically over the entire range (no switching, no manual manipulation), and operates in a thimble so that complete removal is simple. The probe is not exposed to sodium vapor and is easy to lubricate. Disadvantages are that the probe may require temperature compensation, is sensitive to sodium impurities, and is exceedingly slow.

Portable Unit. A battery-operated portable system with a hand-held probe for determining the liquid level in shipping containers, locating freeze or oxide plugs, etc., was described.[18] The probe has been used for detecting liquid levels in a 1600°F potassium system. Eddy-current sensor output is approximately 250 μv for a 2-in. travel (combined sensor travel of 1 in. above and 1 in. below the liquid level).

Pressure Transducers. Problems related to both instrumentation and control are emphasized in Ref. 19, which discusses experience with industrial pressure transducers in a potassium system. Temperature variations along condenser tubes (in a radiation-cooled condenser simulating a space power plant condenser) were detected qualitatively by taking photographs of the condenser with 9000 A Polaroid infrared-sensitive film. Results indicated that substantial temperature differences (of the order of 100°F) are easily detected (see Fig. 5). No indication was given regarding the smallest possible variation that could be detected. The object, however, was to detect large temperature imbalances in the parallel tube bank of the condenser, and hence the method proved to be quite useful.

Liquid-level devices of various types—resistance, inductive, and ultrasonic—were discussed. Figure 6, which indicates the sensitivity achieved in liquid-level determinations with an I-tube in one of the test systems, is typical for these devices.

IMPURITY MEASUREMENTS

Sodium oxide determinations were made by the technique of using a plugging valve.[20] The particular valve used differed from other designs in that the bellows sealed the sodium vapor from all parts having relative motion. The valve was also fabricated with relaxed tolerances which eliminated binding at high temperatures.

Dissolved-Oxygen Monitor. An on-line instrument for continuously measuring the effective oxygen content in liquid metals is capable of detecting concentration changes of a few parts per million.[21] The sensor of the instrument is installed directly in an operating system and provides a continuous indication of changes in oxygen activity without the necessity for sampling and chemical analysis. The sensor consists of an electrode assembly made from a solid electrolyte (thoria–yttria tube) and a copper–copper oxide reference electrode located inside the bottom of the assembly tube. Figure 7 shows the relative size and location of the assembly parts. In practice the meter must be calibrated if it is to be used for measuring absolute values of oxygen concentration.

The author states that the meter measures the thermodynamic activity of dissolved oxygen (effective oxidizing potential of the liquid metal) in liquid metals. Since oxygen activity, rather than total oxygen, effectively determines corrosion rates, the usefulness of the meter is evident for monitoring oxygen activity in liquid-metal systems in which low corrosion rates must be maintained.

Digitized by Google

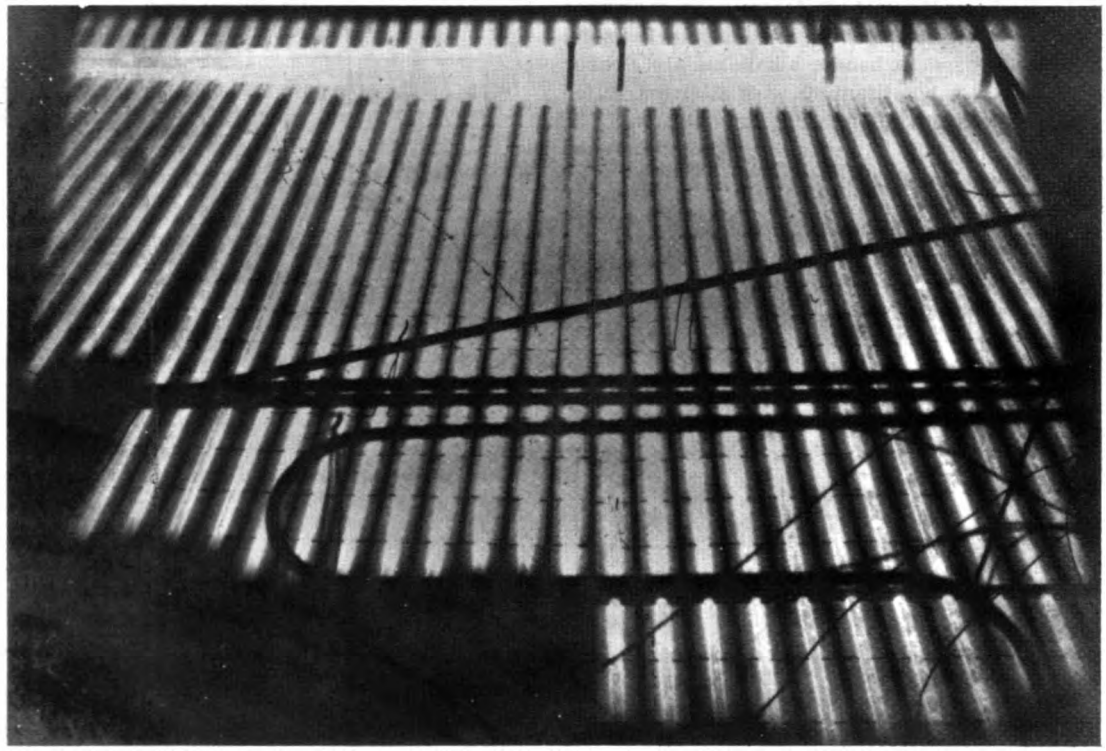

Fig. 5 Nonuniform loading of radiator tube banks is recorded in photograph taken with 9000 A Polaroid infrared film.[19]

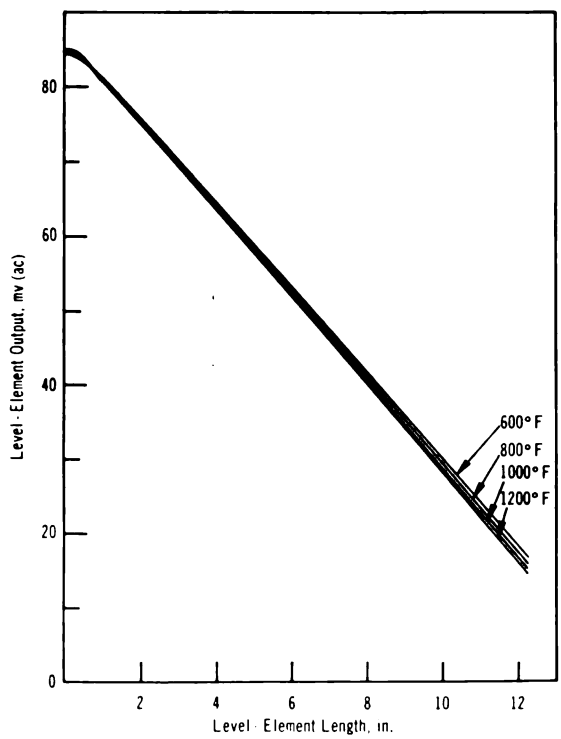

Fig. 6 Results for a resistance type liquid-level manometer, showing instrument sensitivity.[19]

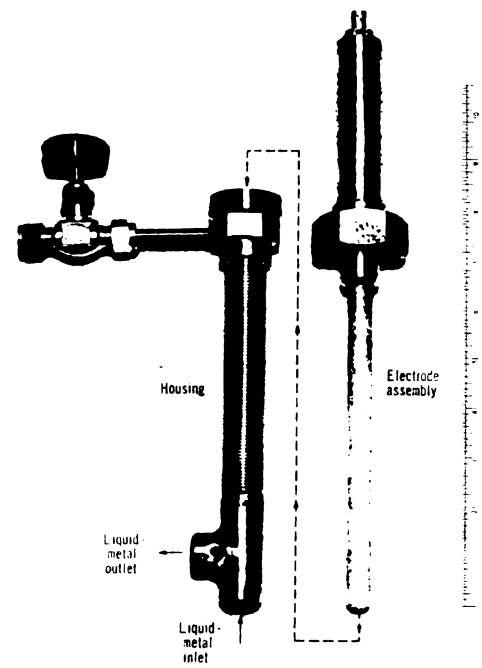

Fig. 7 Sensor for a liquid-metal oxygen meter. Key elements in the electrode assembly are a solid-electrolyte thoria–yttria tube and a copper–copper oxide reference electrode.[21]

Digitized by Google

Monitoring Inert Gases. Reference 22 describes an inert-gas purity meter that is particularly useful in glove boxes used to handle alkali metals. Sensor in the device is a hot titanium wire filament. Lifetime of the filament, which is consumed by oxidizing impurities in the gas, is a measure of the total concentration of such impurities. Figure 8 shows a typical calibration chart for the meter.

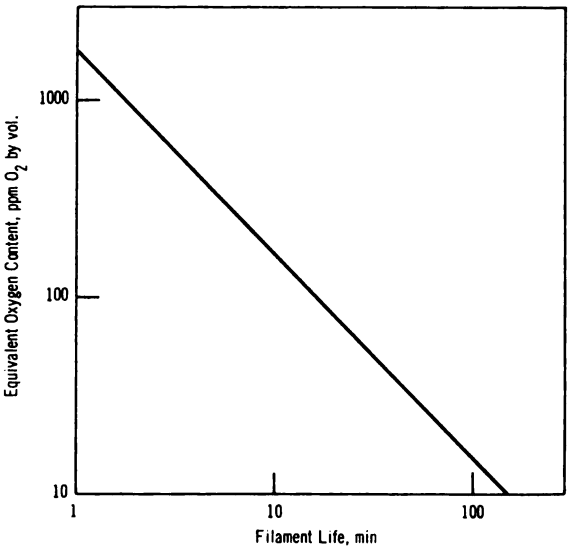

Fig. 8 Calibration chart for a gas-purity tester that measures equivalent oxygen content with a hot-wire filament that is consumed by oxidizing impurities.[22]

CAVITATION DAMAGE STUDIES

A complete description is given of an apparatus designed to impart small-amplitude sinusoidal vibrations to test specimens of various metals submerged in pools of liquid alkali metals.[23] The facility described is capable of maintaining a test retort of liquid sodium at temperatures up to 1500°F for an 8-hr period with an oxide purity of approximately 35 ppm. The particular mode of vibration chosen for the test rods allowed an experimental determination of the velocity of sound in the test pieces. From the values thus determined, it was possible to deduce the modulus of elasticity of the test pieces. Table 1 shows the results; Fig. 9 illustrates the apparatus used, and some of the results of the tests are given in Figs. 10 and 11.

Table 1 TEST PARAMETERS OF HIGH-FREQUENCY FATIGUE SPECIMENS

Metal	Temp., °F	Wavelength, in.	Modulus of elasticity, 10^6 psi	Specimen length, in.	Resonant frequency, cps
316 stainless steel	1000	12.2	21.8	5.500	14,140
	1500	11.3	18.5	5.125	14,080
TZM alloy	1000	15.0	42.0	7.000	13,990
	1500	14.5	39.0	6.750	14,080

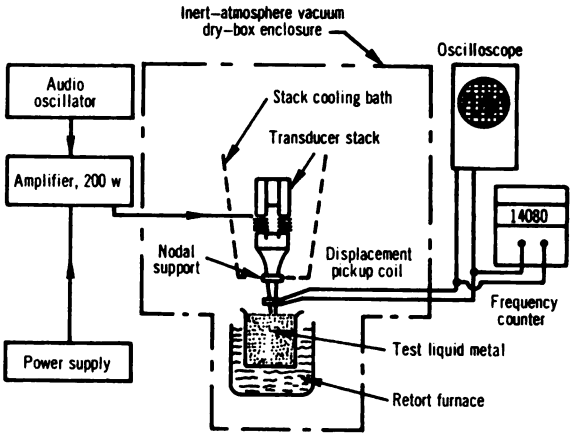

Fig. 9 Magnetostriction apparatus used for cavitation damage tests and for high-frequency fatigue tests.[23]

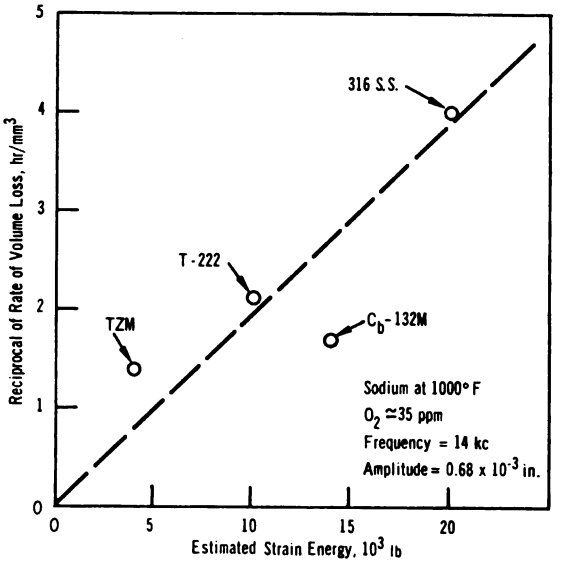

Fig. 10 Relation between cavitation damage resistance and estimated strain energy[23] at 1000°F.

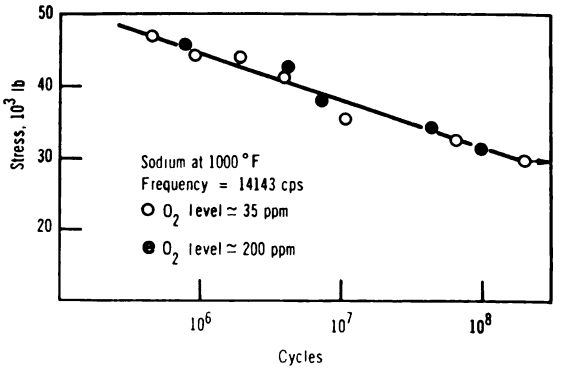

Fig. 11 High-frequency fatigue curve for type 316 stainless steel in 1000°F liquid sodium.[23]

Digitized by Google

Theory and Experiment

Although emphasizing instrumentation, the Conference included many papers that focused on theoretical and experimental heat transfer and fluid flow.

LOCAL HEAT FLUX

A new method has been developed for determining local heat flux and fully developed local overall heat-transfer coefficients in liquid metals for laminar-flow double-pipe heat exchangers.[25] The method is based on the application of basic physical principles rather than on the use of the customary heat-transfer coefficient. The mathematical solution uses expressions for the fluid temperature distribution which involve infinite series of exponential functions of the heat-exchanger axial position multiplied by an "eigenvalue." As a result, when the logarithm of a suitably expressed outer-wall temperature difference is plotted vs. axial position, the graph exhibits a linear portion that corresponds to the fully developed region of the heat exchanger—if such a region exists. From this slope it is possible to deduce the local overall heat-transfer coefficient. Methods are outlined for application to both cocurrent- and countercurrent-flow double-pipe heat exchangers, as well as to an idealized version of a liquid-metal-cooled or -heated condenser or boiler.

INVERSE TEMPERATURE PROFILES

Nonequilibrium inverse temperature profiles have been observed in boiling two-phase flow of potassium.[26] For certain tests the fluid centerline temperature at a given axial position was higher than the wall temperature at the same axial position. Test conditions where this phenomenon was noticed covered the following ranges: mass velocity, 3 to 10×10^5 lb/(hr)(sq ft); potassium temperature, 1510 to 1650°F; boiling pressure, 28 to 42 psia; vapor quality, 0.7 to 17.0%; boiling heat flux, 10,200 to 81,700 Btu/(hr)(sq ft). Measured differences between the inner-wall temperature and the fluid centerline temperature ranged from +4 to −9°F. Errors in instrumentation were eliminated by checking single-phase flow conditions which gave positive temperature differences up to approximately 30°F as expected.

Cause. The observed negative temperature differences are suggested to result when nonequilibrium exists between liquid and vapor and there is a decrease in pressure (and corresponding saturation temperature) along the flow channel, i.e., the observed phenomenon merely reflects the state of nonequilibrium. The vapor essentially does not have sufficient time to transfer its heat back to the liquid (at lower saturation temperature downstream). A very steep temperature gradient in the flow direction is needed for this phenomenon to exist. Figure 12 shows some of the data that exhibit nonequilibrium conditions.

SUPERHEAT IN BOILING SYSTEMS

Very high liquid superheats are possible in boiling liquid-metal systems.[27] For potassium boiling on an as-received (commercially smooth) surface, the superheat measured ranged from 500°F at a saturation temperature of 1500°F down to 230°F at a saturation temperature of 1770°F. Wall-temperature oscil-

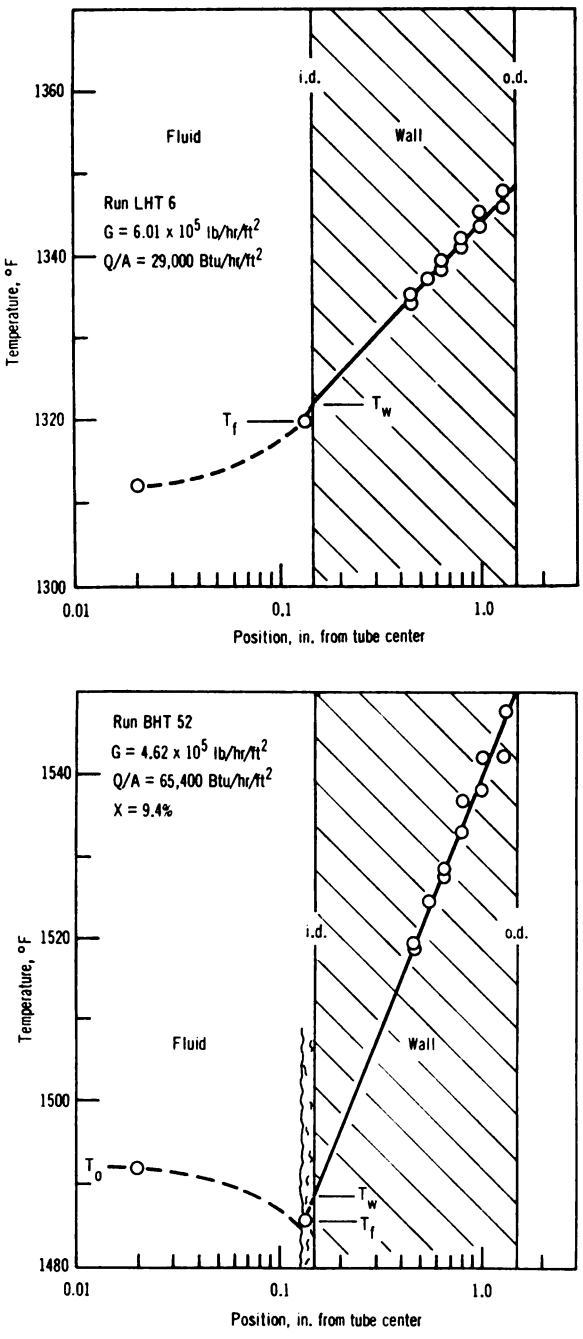

Fig. 12 Boiling-temperature profiles. These experimental data, for both liquid (left) and two-phase flow, show the inverse profile (right) in the fluid during two-phase flow.[26]

Digitized by Google

lations, which occurred in the presence of these large superheats, were 170 to 300°F at a frequency of 1.5 cycles/min. Owing to maximum-temperature limitations, sodium could not be boiled on this as-received surface.

Surface Effects. Significant reductions in both the magnitude of the superheat and the amplitude of the wall-temperature fluctuations were achieved by modifying the boiling surface. A surface containing 0.006-in.-diameter by 0.040-in.-deep drilled holes effectively reduced the superheat by a factor of 40. A porous surface formed by sintering stainless-steel particles on the inner surface of one of the tubes was less effective than the surface with the drilled holes, but still showed appreciable reduction in superheat during boiling. Similar results were obtained with sodium.

Over the limited range of the experiments, the superheat data (for both potassium and sodium) correlated reasonably well with predictions based on a model involving a spherical vapor bubble in thermal equilibrium within a liquid pool of uniform temperature. The theory was presented;[27] typical data are shown in Figs. 13 and 14.

Vaporization. Large wall superheats (150 to 200°F) were required to initiate vaporization in sodium boiling studies that used a single tube-in-shell counterflow heat-exchanger test section.[28] Boiling took place in a ½-in.-ID by 4-ft-long inner tube; pressurized sodium was used in the shell as the heating fluid. Tests up to 2000°F were conducted using a niobium–1% zirconium loop in a vacuum. Two types of vaporization resulted: (1) an apparent flashing, with large liquid superheats and (2) a more normal boiling with low wall superheats and qualities

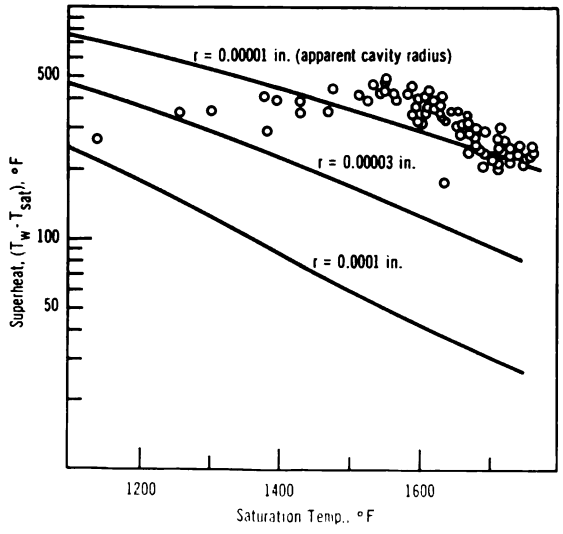

Fig. 13 Liquid superheat with potassium boiling on as-received (commercially smooth) surfaces.[27]

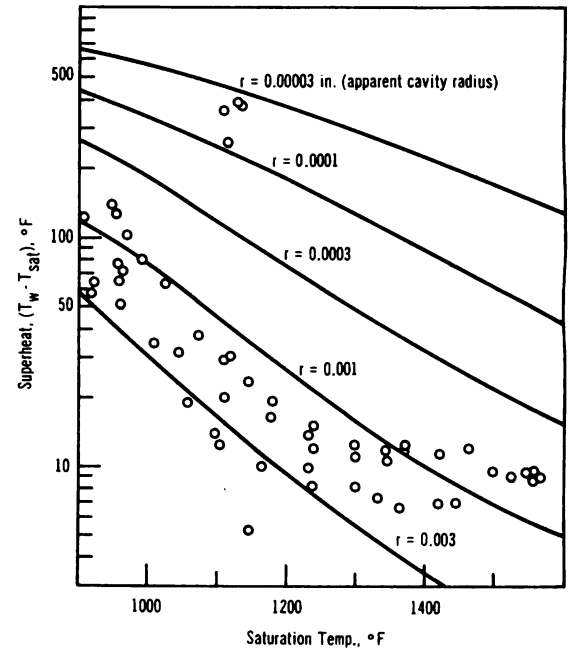

Fig. 14 Liquid superheat with potassium boiling on a pitted surface that was formed by drilling 0.006-in.-diameter holes 40 mils deep on 2-in. centers.[27]

up to 80%. Liquid-phase convective heat-transfer data and pressure-drop results were also obtained.

The protective vacuum environment for the refractory-metal components was noteworthy. Despite large outgassing sources, pressures of 10^{-7} torr were obtained at loop operating conditions.

RESULTS FOR POTASSIUM

Two-phase pressure-drop data were reported[29] for boiling potassium in forced-convection flow through a vertical circular tube. The data from a single series of measurements on a 6-ft-long tube with pressure taps at 1-ft intervals over the last 4 ft of length were compared with existing correlations from the literature for nonmetallic fluids. Calculated exit pressures from these correlations compared favorably with the measured values.

Figure 15 compares potassium data with Martinelli type correlations.[9] Figure 16 compares the various liquid-fraction correlations available in the literature. Slip ratio is shown in Fig. 17 as a function of void fraction and quality. Of interest is the fact that the authors report much higher slips for the metallic systems than those ordinarily experienced with nonmetallic flows. No explanation was offered other than the possible effects of wetting.[11]

Boiling potassium heat-transfer and pressure-drop data have been obtained in a radiant-heated niobium-alloy facility at temperatures up to 2100°F and in a two-loop sodium-heated Haynes 25 facility up to 1750°F (Ref. 30). Tests were reported for exit vapor

Digitized by Google

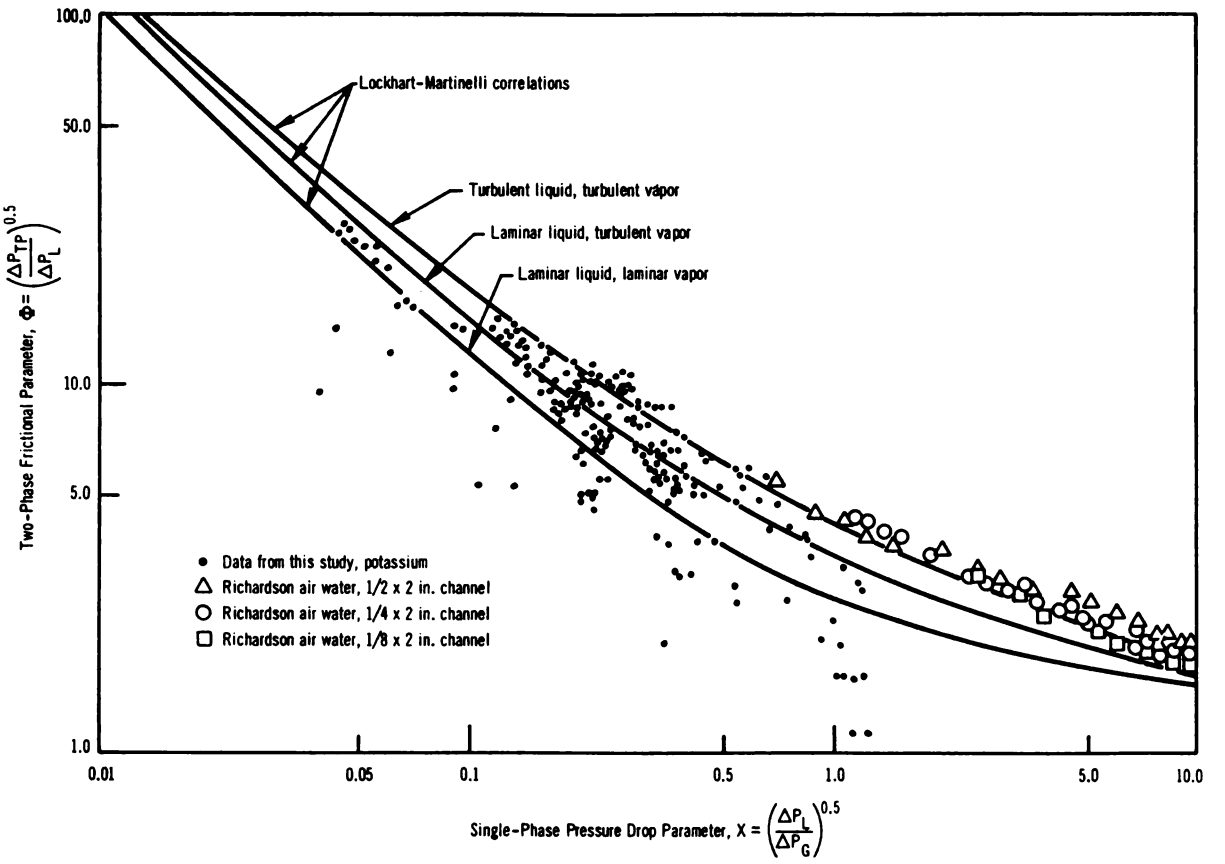

Fig. 15 Martinelli type plot of potassium two-phase frictional pressure-drop data.[9]

conditions up to about 200°F superheat. Various diameters of tubing were used with and without instrumented vortex-generator inserts. The single-tube test section in the Haynes 25 facility was a tube-in-shell heat exchanger instrumented so that both local and average heat-transfer and pressure-drop data could be obtained. Test conditions were chosen to simulate those encountered by a large space power system.

Although instrumentation and measurement techniques were described, greater emphasis was placed on the data collected. Heat-transfer data in the nucleate, transition, and film-boiling regions, and some measurements of critical heat flux were presented. Typical pressure-drop data are shown in Fig. 18, potassium transition boiling data in Fig. 19, and critical-heat-flux data in Fig. 20. The value of a_R in Figs. 19 and 20 represents the radial acceleration of the fluid at the tube wall developed by the helical inserts used in the experiments. The method of calculating a_R and the quality and limitations of the data are treated in detail.[30]

Condensing potassium experiments have used both nickel[31] and HS-25 condensers.[28] Potassium studies that have emphasized the experimental techniques used to obtain local condensing heat-transfer data in thick-wall high-purity nickel condenser tubes, and in which the radial temperature profile was measured at two axial locations, have yielded local values of heat flux and tube inner-wall temperature. A $\frac{1}{4}$-in.-ID instrumented tubular insert was centered in the $\frac{5}{8}$-in.-ID condenser tube to measure the potassium axial temperature distribution.

RESULTS FOR SODIUM

Recent Argonne National Laboratory work on two-phase flow of boiling sodium[10] covers the following range of variables: pressure, 2 to 17 psia; temperature, 1300 to 1650°F; inlet velocity, 1 to 5 ft/sec; boiler power density, 0 to 200 kw/liter; liquid superheat, 10 to 100°F; quality, 0.0005 to 0.01; vapor volume fraction, 0 to 0.87; slip ratio, 5 to 100; frictional pressure loss, 0 to 40 in. H_2O; boiling operation, 1000 hr. In this system, flowing sodium was heated by electrical resistance heaters within the coolant. Volume fractions were measured with gamma-attenuation techniques and electromagnetic flowmeters. Typical measured liquid superheats (Fig. 21) are substantially lower than those reported in Ref. 27. However, as Fig. 22 shows, the systems are quite different. Sodium experiments both with pool boiling and forced

Digitized by Google

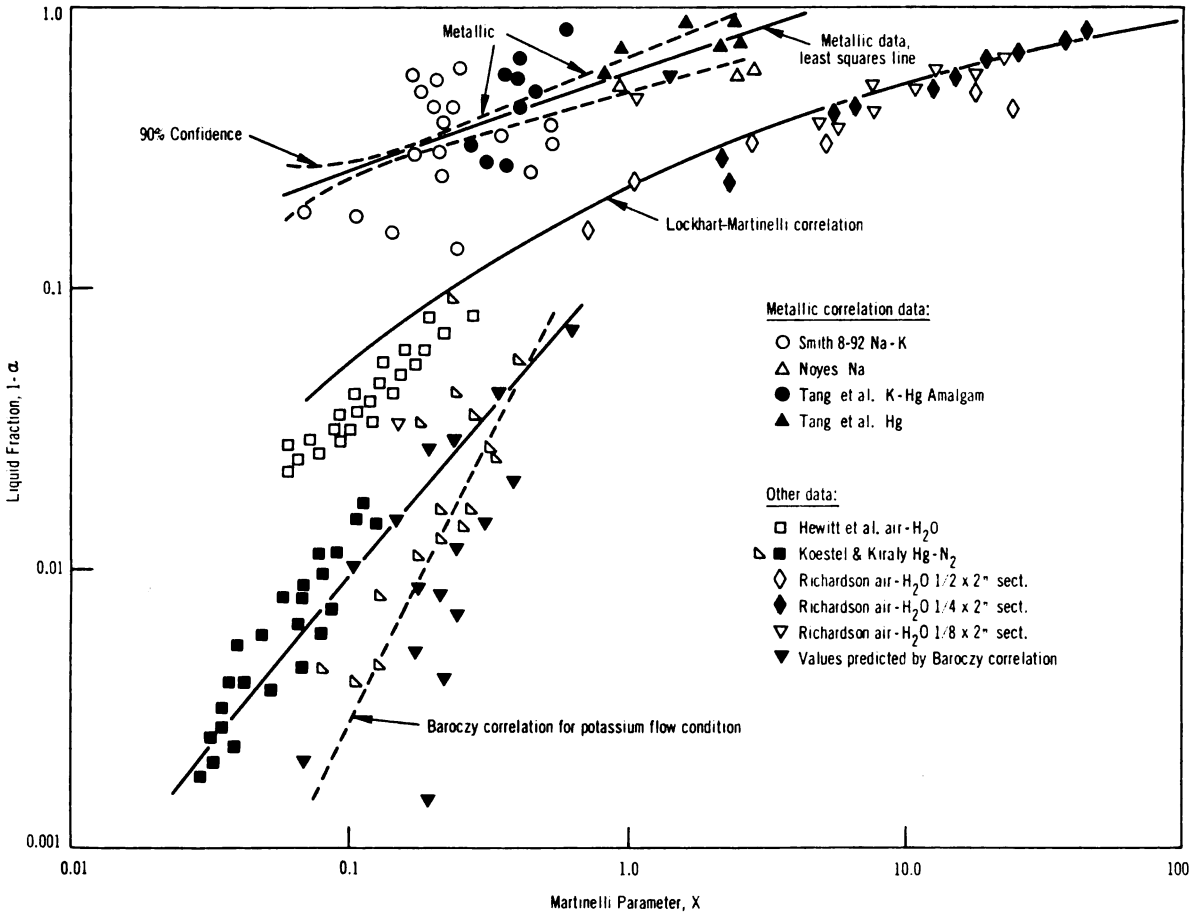

Fig. 16 Metallic liquid-fraction correlations compared with other data and correlations. Although the data scatter appreciably, they consistently yield lower void fractions than nonmetallic fluids.[9]

convection were summarized.[32] The test section for the pool-boiling experiments was a ¼-in.-diameter horizontal cylinder, whereas the forced-flow apparatus utilized an annular vertical test section formed with ¼- and ½-in.-diameter tubes 27 in. long. Other forced-convection heat-transfer data for NaK are reported[5] for the Peclet-number range from 9 to 200, which covers the laminar, transition, and turbulent regions.

Pool-boiling data for sodium and potassium at up to 10^6 Btu/(hr)(sq ft) have been reported.[28] Similar data up to 1.6×10^6 Btu/(hr)(sq ft) were also reported for a forced-convection system for inlet velocities between 0.5 and 6.0 ft/sec, pressures of 1.5 to 10 psia, average subcoolings to 116°F, and qualities up to 14% (Ref. 28). Pressure drop and void fraction were measured in an unheated vertical section of the loop over approximately the same range of conditions. Most of the data, summarized in seven figures, are compared to other reported results (pressure-drop data to Martinelli type correlations). Generally speaking, trends are similar to those for nonmetallic liquids; however, slip ratios proved much higher than for nonmetallic fluids (as in other findings).[9]

RESULTS FOR MERCURY

The mercury boiler for the SNAP-8 system (Rankine-cycle) has been extensively described;[33] summary findings are:

- The initial boiler performance characteristics (thermal load) depend on the condition of the internal-wall surfaces of the mercury flow passages and on the thermal and dynamic conditions imposed by the flow-passage geometry.
- High-velocity liquid-phase vortex flow at the preheat section end point, combined with similar dynamic conditions in the low-vapor-quality section, demonstrate excellent boiler-conditioning effects when the mercury flow passage is cleaned by established methods prior to mercury injection.
- The boiling heat-transfer results obtained from a fully conditioned boiler are in close agreement with the predictions established by the dropwise dry-wall boiling heat-transfer correlations.

Digitized by Google

- The two-phase flow pressure-drop data are correlated by means of a technique similar to the Martinelli method.
- The introduction of a tight preheat-section plug insert to obtain annular flow and high liquid velocity also improved the boiler performance stability significantly. (The plug insert caused liquid to flow in annular flow.)
- Mercury inventory variations (variation in liquid holdup) were minimized with the tight plug-insert geometry.

An X-ray movie has been filmed that presents a visual insight into two-phase flow patterns in a NaK-heated mercury boiler.[34] The prototype boiler had four tubes, each one with an internal swirl wire turbulator throughout the boiling section and a plug insert in the low-quality boiling section. The significant observation of the deconditioned state (when poorer heat transfer is obtained) was the existence of slug flow.

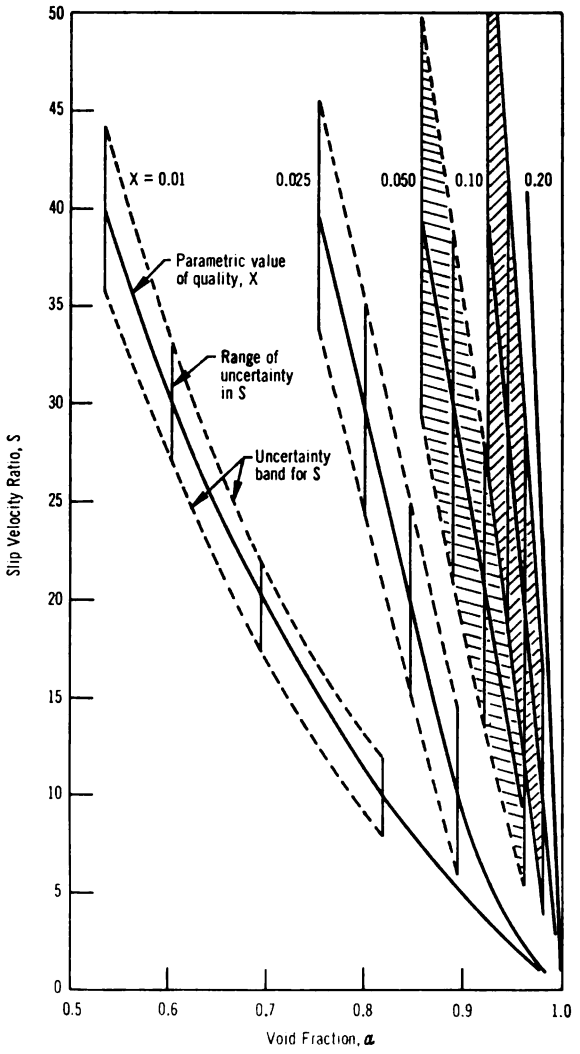

Fig. 17 Uncertainty in slip ratios increases with void fraction and quality (X). These data, obtained with radiation-attenuation techniques, are of value for qualities below approximately 0.15 (Ref. 9).

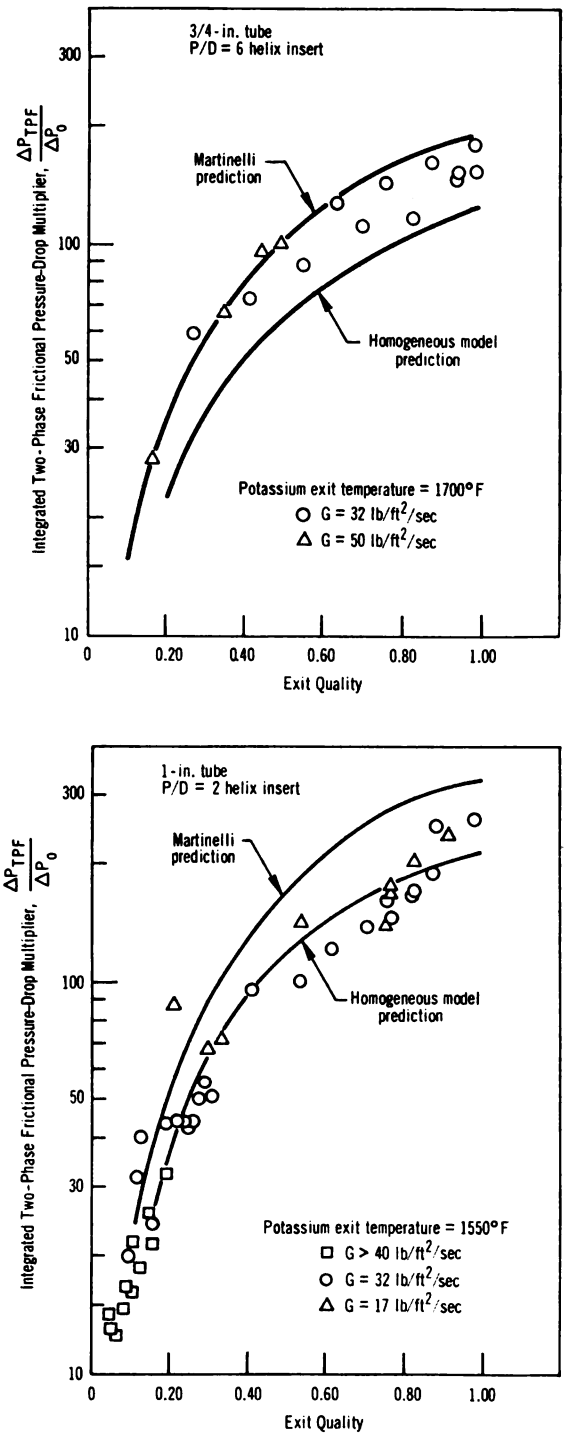

Fig. 18 Typical two-phase potassium frictional pressure-drop multipliers calculated from experimental data are compared to curves of predictions from models.[30]

Digitized by Google

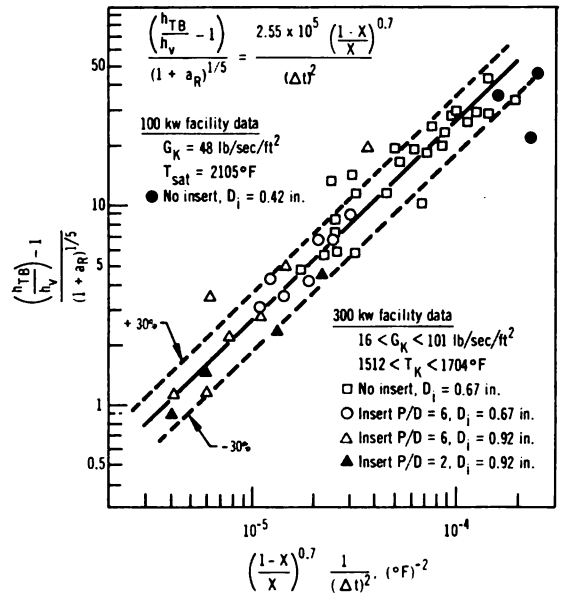
$\left(\frac{h_{TB}}{h_v} - 1\right) / (1 + a_R)^{1/5} = 2.55 \times 10^5 \left(\frac{1-X}{X}\right)^{0.7} / (\Delta t)^2$
100 kw facility data
G_K = 48 lb/sec/ft²
T_{sat} = 2105°F
● No insert, D_i = 0.42 in.
300 kw facility data
16 < G_K < 101 lb/sec/ft²
1512 < T_K < 1704°F
□ No insert, D_i = 0.67 in.
○ Insert P/D = 6, D_i = 0.67 in.
△ Insert P/D = 6, D_i = 0.92 in.
▲ Insert P/D = 2, D_i = 0.92 in.
+ 30%
- 30%
50
10
5
1
0.5
10^{-5}
10^{-4}
$\left(\frac{1-X}{X}\right)^{0.7} \frac{1}{(\Delta t)^2}$, (°F)⁻²
$\left(\frac{h_{TB}}{h_v}\right) - 1 / (1 + a_R)^{1/5}$

Fig. 19 Potassium transition boiling data obtained for various test geometries and plotted in terms of the empirical equation given.[30]

An activation method of determining vapor quality with trace amounts of ^{203}Hg (half-life of 48 days) has been studied[13] and is estimated to be accurate within 1% at a vapor quality of 95%.

Haynes 25 Surfaces. Performance of Haynes 25 surfaces with mercury has been studied in a series of boiler conditioning experiments.[13] Conclusions are:

- Exposure of clean Haynes 25 surface at 1200°F to air for a few hours had no deleterious effect on pool-boiling heat transfer at a mercury saturation temperature of 950°F for heat fluxes to at least 200,000 Btu/(hr)(sq ft).
- Pool-boiling heat transfer for a descaled-and-pickled Haynes 25 surface is essentially the same as for a degreased and cleaned surface except for an initial period of lower performance for the descaled-and-pickled surface.
- Degreased-and-cleaned and descaled-and-pickled surfaces remained wetted when cooled to room temperature after being at 950°F.
- The wetting of a clean Haynes 25 surface is not likely to be uniform.
- Contamination of a Haynes 25 surface with even a trace of oil will reduce the pool-boiling heat-

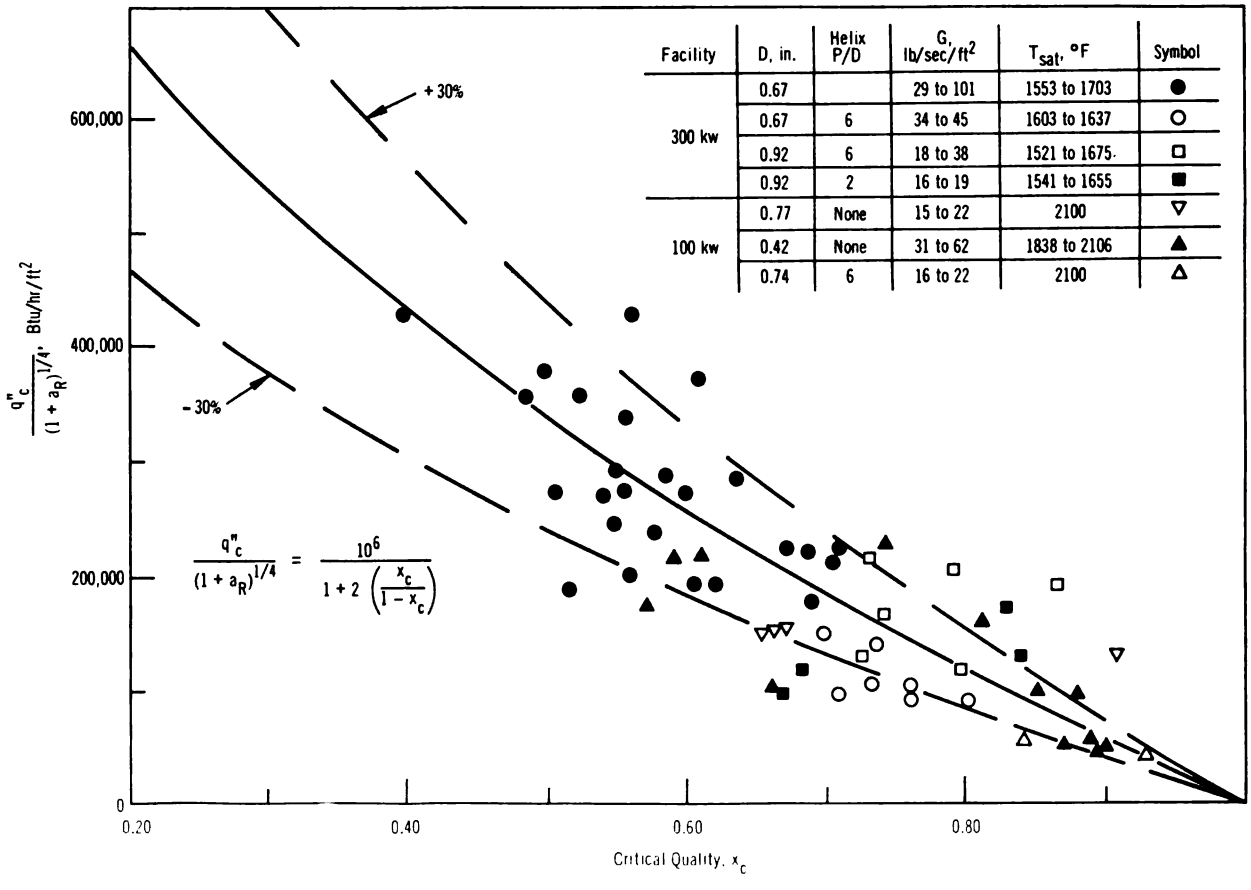

Fig. 20 Potassium critical heat-flux data show a trend toward decreasing heat flux with increasing vapor quality.[30]

Digitized by Google

transfer performance of the surface. However, the reduction is fairly small, and restoration to the performance of a clean surface may be possible with operating time.

- Gross contamination of a Haynes 25 surface with oil effects a drastic reduction in pool-boiling heat-transfer performance at mercury saturation temperatures greater than 650°F, a moderate reduction below approximately 650°F.
- A clean Haynes 25 heat-transfer surface will not remain clean in an oil-contaminated mercury system even when kept completely submerged in the liquid mercury.
- Degree of wetting and pool-boiling heat-transfer performance are directly related.

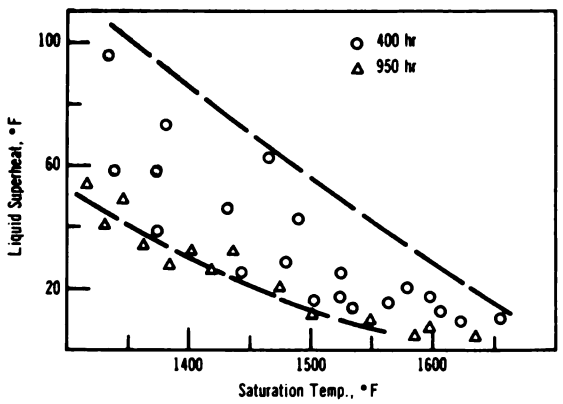

Fig. 21 Liquid superheat measurements indicate a decrease (with time) in the amount of superheat required to initiate boiling.[10]

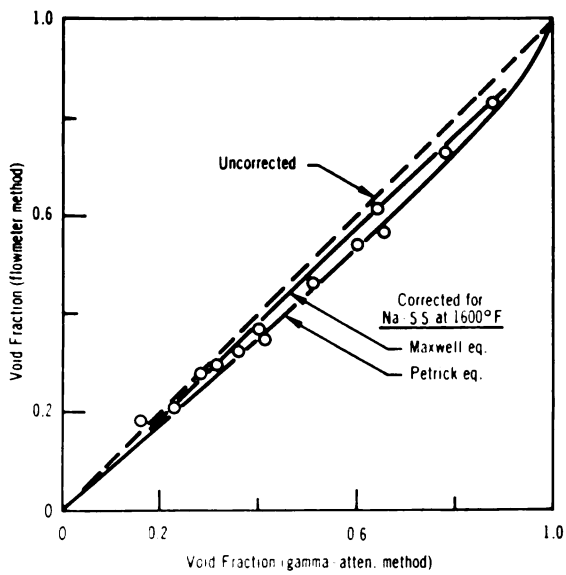

Fig. 22 Void-fraction data. Results indicate that the electromagnetic flowmeter is adequate for vertical upflow of two-phase liquid metals.[10]

RUBIDIUM AND CESIUM

Some preliminary data were presented[24] for condensing rubidium and cesium in horizontal and vertical flow for heat fluxes up to 140,000 Btu/(hr)(sq ft) and temperatures in the range of 1000 to 1400°F. The maximum temperature difference for condensing under any set of test conditions was found to be 13°F, but most of the data were less than 5°F.

References

References 5 through 34 are papers published in Ref. 2

1. Oak Ridge National Laboratory, Proceedings of 1963 High-Temperature Liquid-Metal Heat Transfer Technology Meeting, September 4–6, 1963, USAEC Report ORNL-3605. November 1964.
2. Argonne National Laboratory, Proceedings of the Conference on Application of High Temperature Instrumentation to Liquid-Metal Experiments, September 28–29, 1965, USAEC Report ANL-7100.
3. Argonne National Laboratory, Meeting on High Temperature Liquid Metal Heat Transfer Technology, June 14–15, 1961, USAEC Report ANL-6507, February 1962. (Classified)
4. Brookhaven National Laboratory, Proceedings of 1962 High-Temperature Liquid-Metal Heat Transfer Technology Meeting, May 17–18, 1962, USAEC Report BNL-756.
5. R. E. Holtz (Argonne National Laboratory), Heating Techniques for Liquid Metal Loops, USAEC Report ANL-7100, p. 9.
6. L. G. Hayes (Jet Propulsion Laboratory), Electrical Heater for Liquid Metals at Elevated Temperatures, USAEC Report ANL-7100, p. 23.
7. G. C. Wesling, R. J. Rossbach, and W. M. Shaffernocker (General Electric Company), Development of Efflux Measuring Device for Performance Evaluation of Potassium Vapor Turbine, USAEC Report ANL-7100, p. 127.
8. A. J. Cassano and R. E. Engdahl (Consolidated Controls Corporation), Pressure Transducer for Liquid Metal Applications, USAEC Report ANL-7100, p. 165.
9. R. E. Balzhiser and L. R. Smith (University of Michigan), Instrumentation for Two Phase Metallic Flows, USAEC Report ANL-7100, p. 217.
10. J. B. Heineman (Argonne National Laboratory), Forced Convection Boiling Sodium Studies at Low Pressure, USAEC Report ANL-7100, p. 189.
11. J. K. Ferrell and J. W. McGee (North Carolina State University), An Accurate One-Shot Gamma Attenuation Technique for Measuring Void Fractions, USAEC Report ANL-7100, p. 247.
12. L. B. Wentz, L. G. Neal, and R. W. Wright (TRW Systems), X-Ray Measurement of Void Dynamics in Boiling Liquid Metals, USAEC Report ANL-7100, p. 195.
13. H. H. Hanlin (Atomics International), High Temperature Liquid Metal Instrumentation at Atomics International for: (1) The SNAP 10A Flight System, (2) Boiler Conditioning Experiments and Mercury Vapor Quality Measurement for Mercury Rankine Systems, USAEC Report ANL-7100, p. 641.
14. P. Tauson and R. L. Ammon (Westinghouse Electric Corporation), Development of Alkali Metal Quality Meter, USAEC Report ANL-7100, p. 271.
15. E. B. Arwas, F. K. Orcutt, and B. Sternlicht (Mechanical Technology Inc.), Approaches to the Measurement of the Steady State and Dynamic Performance Characteristics of Liquid-Metal Lubricated Bearings, USAEC Report ANL-7100, p. 331.
16. D. R. Grieser (Battelle Memorial Institute) and J. L. Morris (Air Force Aero Propulsion Laboratory),

Digitized by Google

Liquid-Metal Lubricated Bearing Instrumentation, USAEC Report ANL-7100, p. 291.
17. L. W. Stillwell and R. Herman (AiResearch Manufacturing Co.), Development of Performance-Measuring Instrumentation for a Liquid-Metal Turbine-Driven Bearing Test Rig, USAEC Report ANL-7100, p. 307.
18. L. W. Stillwell (AiResearch Manufacturing Co.), Liquid-Metal Level Detector and Indicator, USAEC Report ANL-7100, p. 367.
19. H. J. Metz and M. M. Yarosh (Oak Ridge National Laboratory), Experiences and Developments in Instrumentation for Liquid Metal Experiments, USAEC Report ANL-7100, p. 379.
20. A. G. Hosler (Chicago Operations Office) and F. A. Smith (Argonne National Laboratory), Impurity and Liquid Level Measurements for the Faret Loop, USAEC Report ANL-7100, p. 413.
21. B. Minushkin (United Nuclear Corp.), The Liquid Metal Oxygen Meter, USAEC Report ANL-7100, p. 427.
22. J. McKee (United Nuclear Corp.), An Inert Gas Purity Tester, USAEC Report ANL-7100, p. 443.
23. H. S. Preiser and A. Thiruvengadam (Hydronautics, Inc.), Instrumentation for Evaluating Cavitation Damage Resistance and High Frequency Fatigue of Refractory Alloys in High Temperature Liquid Alkali Metals, USAEC Report ANL-7100, p. 455.
24. C. R. Fisher and J. H. Moskowitz, Jr. (Aerojet-General Nucleonics), Flow Instrumentation and Operating Experience in a Condensing Alkali Metals Test Loop, USAEC Report ANL-7100, p. 45.
25. R. P. Stein (Argonne National Laboratory), A Method for the Determination of Local Heat Fluxes in Liquid Metal Heat Exchangers, USAEC Report ANL-7100, p. 483.
26. J. C. Chen (Brookhaven National Laboratory), Existence of Non-Equilibrium Inverse Temperature Profile in Boiling Two-Phase Flow, USAEC Report ANL-7100, p. 499.
27. J. A. Edwards and H. W. Hoffman (Oak Ridge National Laboratory), Superheat with Boiling Alkali Metals, USAEC Report ANL-7100, p. 515.
28. J. P. Lewis (National Aeronautics and Space Administration), Experimental Studies of Boiling of Sodium and Condensing of Potassium, USAEC Report ANL-7100, p. 513.
29. R. P. Wichner and H. W. Hoffman (Oak Ridge National Laboratory), Pressure Drop with Forced-Convection Boiling of Potassium, USAEC Report ANL-7100, p. 535.
30. J. A. Bond, J. R. Peterson, and F. E. Tippets (General Electric Company), Heat Transfer and Pressure Drop Measurements for High Temperature Boiling Potassium in Forced Convection, USAEC Report ANL-7100, p. 53.
31. S. G. Sawochka (General Electric Company), Measurements of Forced Convection Condensing Potassium Heat Transfer, USAEC Report ANL-7100, p. 97.
32. H. Lurie (Atomics International), Sodium Boiling Heat Transfer and Hydrodynamics, USAEC Report ANL-7100, p. 549.
33. A. J. Sellers and M. K. Wong (Aerojet-General Corporation) and G. M. Thur (National Aeronautics and Space Administration), Recent Developments in Heat Transfer and Development of the Mercury Boiler for the SNAP-8 System, USAEC Report ANL-7100, p. 573.
34. R. J. Ziobro (TRW Equipment Laboratories), X-Ray Movie Film Report of Flow Patterns in a Once-Through Forced Circulation NaK Heated Mercury Boiler, USAEC Report ANL-7100, p. 633.

Digitized by Google

Advances in Materials for Organic-Cooled Reactors

By Edmund S. Sowa

Although organic coolants themselves cause no major corrosion problems in reactor systems, the successful development of organic-cooled reactors depends on understanding and solving problems related to (1) the most economically performing fuel elements and fuel-cladding and "pressure"-tube materials, (2) control of coolant impurities that cause fouling of heat-transfer surfaces, and (3) irradiation decomposition of the coolant. Recent engineering studies that indicate good progress toward the solution of these problems will be discussed in this article.

Background

Early efforts to capitalize on the advantages of organic coolants led to construction of reactors that used the organic as both coolant and moderator: the 6-Mw(t) Organic Moderated Reactor Experiment,[1-3] the 11.4-Mw(e) Piqua plant,[4] and the Russian 750-kw(e) ARBUS plant.[5] Numerous other organic-reactor designs have been reported—24 are listed in Ref. 6—and interest remains active in the United States, Europe,[7-9] and Canada.[10] However, the interest now is in reactors that are cooled by organics but moderated by heavy water. Such heavy-water organic-cooled reactors (HWOCR) combine the heat-transfer-system design advantages of organic coolants (low vapor pressure at high temperature) with the nuclear merits of heavy-water moderation.[11] The first such reactor is the 40- to 60-Mw(t) WR-1 at Whiteshell, Manitoba;[12] its principal functions are to test fuel, coolant, and other components for future power reactors.[13] Data from the WR-1 are expected to contribute greatly to the U. S. HWOCR program,[14,15] for which consideration is being given to construction of a prototype in the size range 350- to 750-Mw(e) to begin operation in the mid-1970s.

The prime interest in organic-cooled power reactors in the United States nowadays is for large advanced converters that can conserve fuel resources while producing power competitively; large dual-purpose power and desalting plants are one segment of this interest. In Europe and Canada the interest stems from a desire to operate power reactors with natural uranium, which, of course, is possible with a D_2O moderator. In either situation the incentive is economy. As compared with either H_2O-cooled and -moderated reactors or with reactors that are both cooled and moderated by an organic, heavy-water moderation gives better neutron economy, which leads to higher burnups for equivalent enrichments, and lower fuel costs. The organic coolant permits use of some higher density fuels (such as uranium carbide) that are not suitable for water-cooled reactors, and lower fuel costs help to compensate for the higher capital costs of the D_2O-moderated reactors.[16]

ADVANTAGES OF ORGANIC COOLANT

In a heavy-water reactor, replacement of D_2O coolant by organic coolant reduces the D_2O inventory by 5 to 20% (D_2O costs ~$20/lb, and the organics cost 12 to 40 cents/lb).[3,17,18] Organic coolants are compatible with mild-steel piping and vessels, an advantage that has promoted their use in the chemical industry. Other engineering advantages (Table 1) follow from the fact that the high temperature (600 to 800°F) achievable with low pressure (15 to 300 psi) in organic coolants simplifies reactor-vessel, piping-system design, and materials considerations.

Table 1 COMPARISON OF ORGANIC- AND D_2O-COOLED D_2O-MODERATED REACTORS[17]

Coolant	Coolant outlet temp., °F	Net overall efficiency, %	Design pressure, psi	Coolant-contained energy, rel.
D_2O	570	30.7	1560	8
Organic	760	34.2	300	1

Digitized by Google

As compared with water-cooled reactors, several advantages accrue from the favorable temperature–pressure relation in organic-cooled reactors: (1) the high temperature permits the generating plant to operate at a high thermal efficiency and (2) the moderate pressure permits savings in reactor-vessel and -system cost—and also allows construction of larger reactor vessels, including those of the modular pressure-tube type—as well as a reduction in D_2O leakage. Because organic coolants are compatible with sintered aluminum powder (SAP), which has a higher thermal conductivity than the zirconium used for cladding fuel in water reactors, finned SAP can be used to clad the fuel in organic reactors. The resulting higher power that can be obtained from each fuel channel means that reactor capital cost can be reduced.

Fuel Testing

Fuels of interest for organic reactors, UO_2 and UC, have been irradiated recently in the WR-1, NRX, and NRU. Uranium carbide is of major interest as a power-reactor fuel for the HWOCR concept because it offers higher power densities than UO_2; for the same reason, metallic uranium fuel also is of prospective interest.[16]

Uranium carbide fuels clad with SAP have been irradiated to burnups to a maximum of 11,100 Mwd per metric ton of uranium.[19] In elements fitted with internal thermocouples, the center temperature in one element was measured as 2948°F during the initial phase of the irradiation but fell to 1832°F at the end of the 3-month test period as fuel swelling improved the thermal contact between fuel and cladding. The density decreases for the two high-burnup cases are shown in Table 2, whose data are for

Table 2 IRRADIATION EFFECTS ON SAP-CLAD UC ELEMENTS[19]

Carbon content, wt.%	Average burnup, Mwd/metric ton of U	Density decrease, %
4.61	11,100	4.2–5.9
4.69–4.72	10,200	3.1–4.3

hypostoichiometric UC. The improvement in swelling characteristics with increasing carbon content is illustrated by these results. More recent experiments in an organic-cooled loop in the NRU reactor using hyperstoichiometric UC (~5 wt.% carbon), which is the fuel composition proposed for HWOCR, exhibit a density decrease as low as 2% per 10,000 Mwd per metric ton of uranium burnup.[20]

Uranium dioxide fuel clad with zirconium–2.5% niobium has been operated as the first fuel charge in the WR-1 (Ref. 12). Table 3 compares calculated and experimental data from fuel operated in organic coolant. The target burnups for these fuels are 7500 Mwd per metric ton of uranium.

Table 3 COMPARISON OF CALCULATED AND EXPERIMENTAL DATA FOR FUEL IRRADIATED UNDER WR-1 CONDITIONS[12]

Parameter	Calculated	Experimental
Cladding temperature	808°F	813–824°F
UO_2 maximum temperature	≈3270°F	≈3270°F
Fission-gas release in one experiment	18.8%	≈9%
Pressure drop across fuel rod	4.7 kg/cm²	4.4 kg/cm²

A multibundle fuel assembly is under irradiation in an NRU reactor organic loop to establish fuel characteristics for the HWOCR.[20,21] The fuel elements for the first irradiation were composed of SAP-clad UC and Zircaloy-clad UO_2 bundles. The peak fuel-centerline temperatures were 2000°F for the UC and 3000°F for the UO_2. Corresponding peak cladding temperatures were 850 and 860°F. The coolant used is Santowax OM at 570 to 650°F. By April 1966 some of the test fuel had reached peak burnups of 10,000 Mwd per metric ton of uranium for the UC and 8400 Mwd per metric ton of uranium for the UO_2, and the bundles were removed for hot-cell examination. The loop position now contains a multibundle assembly similar to the one removed and is being used to determine gross effects of coolant composition and purity on film formation.

Cladding and Pressure-Tube Materials

Two types of alloys that appear satisfactory for use in organic-reactor cores are SAP and the zirconium alloys.

SINTERED ALUMINUM POWDER

Sintered aluminum powder is the reference material selected for the fuel cladding and for pressure tubes.[3] Sintered aluminum powder exhibits low ductility at elevated temperature and low strain rate. Because the in-core behavior of fuel cladding is affected primarily by long-term effects such as creep, this property influences the design. Although zirconium alloys have greater ductility, this ductility can be lost if the alloy becomes hydrided at the approximately 800°F temperatures in the HWOCR.

The Al_2O_3 content in SAP adds high-temperature strength to the basic aluminum matrix. The fact that SAP has a much higher thermal conductivity than the zirconium alloys gives it excellent prospects; power densities achievable with UC fuel clad in finned SAP cladding can make this the most promising fuel for the HWOCR when manufacturing processes are developed for reliably producing high-quality SAP.[16] Although some irradiations of SAP-clad UO_2 at high linear heat rates (>15 kw/ft) have exhibited ratchetting effects, no chemical or mechanical incompatibility has been noted between UC and SAP.[23]

ZIRCONIUM ALLOYS

The zirconium alloys are generally satisfactory but are affected by hydriding, which causes embrittle-

Digitized by Google

ment. Chlorine impurities in the coolant disastrously increase hydriding of the zirconium alloys; tests in 752°F Santowax OM with 5 to 10 ppm chlorine resulted in hydriding rates up to 100 times greater than the normal 4×10^{-2} $\mu g/(cm^2)(hr)$ (which is 570 ppm/year for the cladding thickness in WR-1) found in clean (<2 ppm chlorine) coolant at 867°F (Ref. 22).

Two promising alloys that have shown hydriding rates (at 752°F) a half to a third of that of zirconium–2.5% niobium are zirconium–0.7% copper–0.2% iron and a Russian alloy called Ozhennite (zirconium–0.2% tin–0.1% iron–0.1% nickel–0.1% niobium). Because hydriding of pressure tubes may limit the life of zirconium–2.5% niobium, the performance of these alloys is very significant. Estimated operating times for pressure tubes of several alloys show the superiority of Ozhennite (Table 4). However, the creep behavior of these alloys is not known as yet. Nevertheless, pressure-tube life depends strongly on the design criteria and operating conditions. It might be possible to design for any tube life with any of these alloys by thickening the tube wall, although this involves a cost penalty because of increased parasitic absorption of neutrons.

Table 4 RELATIVE PERFORMANCE OF ZIRCONIUM ALLOYS IN ORGANIC* COOLANT[22]

Alloy	Operational life, years
Zircaloy-2	1–3
Zr–2.5% Nb	5
Ozhennite	~15

*Santowax OM or HB-40 at 687 to 752°F.

Coolant Performance

A summary of the chemical behavior of organic coolants was presented in a previous issue of *Power Reactor Technology*.[23] From the summary it can be seen that corrosion effects produced by high-purity coolant can be expected to be relatively small. However, breakdown of the coolant into lighter molecular-weight components and polymerization into high-boiling compositions can produce significant changes in coolant properties, and these, in turn, must be investigated to determine possible interference with reactor operation (although AECL calculations of fuel performance in a variety of coolant compositions, including up to 40% high-boiling compounds, indicate very little difference in heat-transfer behavior for any of the coolants).[16] The cost of organic-coolant makeup (12 to 40 cents/lb) to compensate for decomposition adds slightly to the cost of running a reactor. In a HWOCR system these costs amount to an additional 0.1 to 0.2 mill/kw-hr in operating costs and do not seriously affect the economic potential of these plants. Organic makeup costs can be reduced by up to an order of magnitude if the high-boiling compounds are reconstituted for reuse as coolant by hydrocracking. Such systems are being developed and are expected to reduce HWOCR operating costs by approximately 0.1 mill/kw-hr.[3]

Some proponents of organic reactors believe that changes in the coolant during use are not necessarily deleterious.[24] They emphasize the viewpoints that: (1) the coolant is not the feed material that one starts with but is the mixture obtained during steady operation of the reactor system; (2) the properties of the mixture generally are superior to those of the feed material; and (3) a range of properties is available from a given material, and reactor operating conditions will be chosen to take maximum advantage of these properties.

IN-REACTOR TESTS

Loop irradiations, important because organics decompose and polymerize when irradiated, have been performed under reactor conditions, and the physicochemical behavior of the coolants has been determined.[25] Major interest has centered on Santowax OM and HB-40 (Table 5).[26] The HB-40 coolant, a mixture of terphenyls reacted catalytically with hydrogen to form a 40%-saturated hydrocarbon, has the advantage of remaining liquid at room temperature, and thus offers greater handling convenience under operational conditions. Its major disadvantage lies in a lower autoignition temperature than that of Santowax OM (706 vs. 1072°F). However, the autoignition temperature is increased by irradiation, and so this disadvantage lessens during operation.

Table 5 PHYSICAL PROPERTIES OF TWO MAIN ORGANIC COOLANTS[26]

Temperature, °F	Density, g/cm³		Specific heat, Btu/(lb)(°F)		Viscosity, centipoise		Thermal conductivity, Btu/(hr)(ft)(°F)	
	Santowax OM	HB-40	Santowax OM	HB-40	Santowax OM	HB-40	Santowax OM	HB-40
400	0.950	0.866	0.492	0.45	0.85	0.82	0.071	0.065
500	0.904	0.828	0.531	0.49	0.47	0.53	0.069	0.065
600	0.859	0.788	0.568	0.53	0.31	0.36	0.066	0.065
700	0.813	0.737	0.604	0.57	0.23	0.26	0.064	0.065
800	0.765	0.682	0.640		0.17	0.16		

The NRX loop irradiations and WR-1 experience have shown that the performance of HB-40 is similar to Santowax OM.[25] Coolant decomposition results in a consumption rate of approximately 50 g/kw-hr absorbed, approximately equal for both compositions.

Digitized by Google

Decomposition of coolant from both pyrolytic and radiolytic processes produces high-boiling compounds and volatile products. In HB-40 at high temperatures, thermal degradation of high-boiling compounds partly offsets radiolytic production. The production of volatiles during HB-40 irradiation produced increased vapor pressure, which can be reduced by stripping out the volatiles (e.g., by helium purge) at the expense of a slight increase in coolant consumption. The increase in high-boiling compounds also increases the viscosity of the fluid (~0.4 raised to 0.5 centistokes at 662°F and 30% high boilers).[3] In these loop irradiations, composition was maintained by distillation purification and recovery, the technique to be employed also in a reactor system.

IMPURITY CONTROL

The most economical solution to the fouling and hydriding problems involves the control of impurities in the coolant, especially such impurities as chlorine and oxygen.[27] A fouling mass-transfer mechanism has been described in which an iron compound is formed and subsequently decomposes at the fuel-element surface to produce fouling.[23] Generally, fouling potentials are considered adequate if the chlorine-impurity content is kept at approximately 1 or 2 ppm and the water content is approximately 50 to 200 ppm[3,16,18] (water is added to the organic to impede polymerization). These conditions can be achieved with careful quality control—degassing and exclusion of air—in the initial charge of coolant followed by continuing control in subsequent makeup additions. Continuous side-stream purification through an absorbent such as Attapulgus clay is helpful in maintaining a low fouling potential.[16]

COKING

Another phenomenon that has been observed in organic reactors is coke formation caused by local overheating and irradiation of stagnant organic fluid. Such overheating has occurred in the Piqua reactor,[28] where a large mass of coke formed in the nearly stagnant organic fluid in the moderator region between fuel channels, not in the fuel channel itself. The stagnation caused continuous irradiation of a large quantity of organic material for an extended time. After the coke mass is removed from the Piqua reactor and the core is renovated, the core will be modified to prevent stagnation and excessive irradiation of the organic fluid.

Unlike the Piqua reactor, in an HWOCR the moderator would be heavy water and would not coke. The organic coolant would flow past the fuel at approximately 30 ft/sec, at which velocity there have been no instances of coking on heat-transfer surfaces[16] because the organic would be (1) irradiated for very short times and (2) continuously stripped of polymerized products by distillation during circulation through the primary coolant system.

* * *

I want particularly to acknowledge the contributions and comments extended by R. G. Hart (of Atomic Energy of Canada Ltd.) and B. L. Hoffman (of Atomics International) and their associates.

References

1. C. J. Raseman and L. Green, Commercial Power Reactors Cooled with Sodium, Heavy Water, or Organic Liquids, in *Reactor Technology, Selected Reviews — 1964*, L. E. Link (Ed.), USAEC Report TID-8540, pp. 111-129, 1964.
2. Reactor Table, *Nucleonics*, 19(11): 134-135 (November 1961).
3. B. L. Hoffman, Atomics International, personal communication.
4. Organic-Moderated Reactors: Piqua Auxiliary Systems, *Power Reactor Technol.*, 4(2): 82-88 (March 1961).
5. K. K. Polushkin et al., The ARBUS Organic Cooled and Moderated Nuclear Power Station, in *Proceedings of the Third United Nations International Conference on the Peaceful Uses of Atomic Energy, Geneva, 1964*, Vol. 5, pp. 487-495, United Nations, New York, 1965.
6. *Organic Coolants and Moderators*, Bibliographical Series No. 17, pp. 2-3, International Atomic Energy Agency, Vienna, 1965 (STI/PUB/21/17).
7. J. C. Leny, Towards an ORGEL Prototype, *Euratom*, 4(4): 122-126 (December 1965).
8. J. C. Leny and S. Orlowsk, The ORGEL Project, *Nucl. Eng.*, 10(106): 96-100 (March 1965).
9. H. W. Schleicher, Corrosion Studies in Organic Coolants for Nuclear Reactors, Report EUR-379 (CONF-28-6), European Atomic Energy Community, 1963.
10. WR-1: Unique Among Research Reactors, *Can. Nucl. Technol.*, 4(4): 30 (Fall 1965).
11. W. M. Campbell, A Current Assessment of the Organic-Cooled Heavy Water Moderated Reactor, in Papers Presented by AECL to the International Conference of the Canadian Nuclear Association, Ottawa, Ontario, May 28–30, 1962, Canadian Report AECL-1692, February 1963.
12. R. G. Hart et al., (AECL, Whiteshell), UO_2 Fuels in Organic Cooled Reactors, *Trans. Am. Nucl. Soc.*, 9(1): 47-48 (June 1966).
13. Canada and the Organic Reactor, *Can. Nucl. Technol.*, 5(4): 26-27 (July–August 1966).
14. *Nucleonics Week*, 7(25): 5 (June 23, 1966).
15. F. M. Stern, R. P. Varnes, and J. R. Hume, Design of the HWOCR Demonstration Plant, *Trans. Am. Nucl. Soc.*, 9(1): 213 (June 1966).
16. R. G. Hart, Atomic Energy of Canada Ltd., personal communication, Aug. 2, 1966.
17. K. H. Campbell, Evolution and Promises of Organic-Cooled Reactors, *Nucl. Eng.*, 11(117): 102-105 (February 1966).
18. A. N. Tardiff, U. S. Atomic Energy Commission, personal communication.
19. W. G. Mathers et al., UC Fuels in Organic Reactors, *Trans. Am. Nucl. Soc.*, 9(1): 46-47 (June 1966).
20. S. O. Arneson, R. H. Young, and W. P. Chernock, HWOCR Fuel-Irradiation Tests, *Trans. Am. Nucl. Soc.*, 9(1): 48-49 (June 1966).
21. Heavy Water Organic Cooled Reactor, Quarterly Technical Progress Report, July–September 1966, USAEC Report AI-CE-54, Atomics International and Combustion Engineering, Inc., Oct. 15, 1966.
22. J. Boulton, S. R. Hatcher, and R. E. Hollies (AECL, Whiteshell), The Use of Zirconium Alloys in Organic Coolants, *Trans. Am. Nucl. Soc.*, 9(1): 45-46 (June 1966).

Digitized by Google

23. J. E. Sawyers, Advancements in Organic Coolants, *Power Reactor Technol.*, 8(4): 290-295 (Winter 1965–1966).
24. M. Tomlinson, Atomic Energy of Canada Ltd., personal communication, Aug. 9, 1966.
25. M. C. Arneson et al., Some Characteristics of Irradiated HB-40, An Organic Liquid Coolant for Reactors, *Trans. Am. Nucl. Soc.*, 9(1): 44-45 (June 1966).
26. H. Mandel, Heavy Water Organic Cooled Reactor, USAEC Report AI-CE-15, p. 13, Atomics International and Combustion Engineering, Inc., Apr. 15, 1966.
27. B. A. Finlay, J. L. Smee, and S. R. Halcher (AECL, Whiteshell), Organic Coolant Performance in Reactor Loops, *Trans. Am. Nucl. Soc.*, 9(1): 44 (June 1966).
28. Piqua Nuclear Power Facility, Monthly Operating Report No. 37, USAEC Report COO-652-27, May 1966.

Digitized by Google

Two Advances in Reactor Neutron-Noise Analysis

By Charles E. Cohn

Measurement of the fluctuations in the neutron flux in chain-reacting systems and interpretation in terms of reactor kinetics and safety characteristics have been particularly useful for subcritical and critical assemblies and for training or research reactors. Although transfer functions, stabilities, and the ratio of delayed-neutron fraction to neutron lifetime have been measured in preoperational tests with a number of power reactors[1] (N.S. *Savannah*, Yankee, and Dresden, for instance), the numerous sources of noise in power reactors during operation have limited the usefulness of the technique. However, two relatively new developments, which permit faster measurements or lower detector efficiencies, have extended the usefulness of noise analysis and hold great promise for routine measurements on power reactors. These developments were described at the second symposium on Neutron Noise, Waves, and Pulse Propagation, which was held at the University of Florida.[2–4] The first symposium has been reported previously.[1,5]

Although the second symposium covered a broad field of work, both fundamental[6–24] and applied,[25–32] this article is restricted primarily to the experimental techniques of special interest to readers concerned with power reactors.

Pseudorandom Binary Inputs

The experimental technique of greatest interest for power-reactor applications, such as reliable and accurate measurements of shutdown reactivity, is the use of pseudorandom binary-input signals for measuring system transfer functions. Because the technique is compatible with typical reactor hardware (the control rod can be made to jump between two-position solenoids nearly instantaneously), and, although the statistical characteristics make the signal appear to be a random variable, the prescribed sequence of the binary signal means that the mathematical characteristics are known exactly. Thus techniques of random theory can be applied to yield measurements of increased precision.

The binary signal has an autocorrelation function (a measure of the degree of correlation in successive values of some signal, e.g., neutron level, coolant temperature, or fuel temperature) which approaches a delta function. Thus it contains components of all frequencies. The system transfer function is obtained by correlating this input signal and the resulting system output.

The two-valued nature of the input signal makes it easy to generate and also simplifies cross-correlation by eliminating the need for multipliers. The pseudorandom nature and small amplitude of the input signal assure minimum disturbance to the normal operation of the system being measured. Moreover, the technique frequently yields the same precision from measurements taken in 5 to 500% less time than with previous methods.

The method has been used for measuring transfer functions on critical reactors of the NERVA[33] and Phoebus[34] rocket types and others,[35] as well as on subcritical systems.[36] For the rocket reactors the input signals were superimposed on the reactor power demand (by oscillating the control drum) and in other cases on the hydrogen-turbopump speed demand, which varied between 21,000 and 23,000 rpm. For the subcritical reactor systems, the neutron source strength was varied in binary fashion by deflecting an accelerator beam on and off the target.

Two-Detector Cross-Correlation

Because it suppresses the effect of the unwanted background noise originating in the detector itself, the two-detector cross-correlation method allows measurement of reactor neutron noise with detector

Digitized by Google

efficiencies a hundred times lower than the 10^{-4} efficiency practicable with the conventional single-detector method. This gives the user more freedom in selecting detector location, size, and geometry. For instance, this is important for power reactors because the neutron detectors can be moved from the reactor vessel to shielded regions where the gamma background is lower.

The method was used originally in a pool type reactor in Japan[37] and in an Argonaut type reactor in Germany.[38] Stegemann[38] reports that the technique gives reliable measurements of prompt-neutron decay, absolute reactor power, and shutdown reactivity when the outputs from cross-correlated detectors have a ratio of correlated-to-uncorrelated noise of 0.1; in an equivalent single-detector experiment, this ratio would be approximately 2.

Lower detector efficiencies suffice because the correlation between the detection noise from two separate detectors has an expectation value of zero; thus only the correlated or reactor-noise component is seen. However, the detection-noise components introduce random error into the results. So a decrease in detection efficiency calls for longer measuring time to get statistical data for acceptable precision.

General Applications

Some power-reactor applications of more familiar noise-analysis techniques were also discussed at the meeting. These included measurements on the Molten Salt Reactor Experiment (MSRE) circulating-fuel reactor[39] which clearly showed the significant change in the transfer function produced by fuel circulation; rapid fuel flow reduces the effective delayed-neutron fraction in the core. Experiments have been made to detect the onset of nucleate boiling by analysis of neutron-flux noise[40] and of acoustical noise.[41] Low-frequency resonances have also been observed (Fig. 1) in a swimming-pool reactor with forced circulation and are believed to be caused by coolant-flow fluctuations that excite vibration of a control rod.[42]

MSRE DELAYED-NEUTRON FRACTIONS

Neutron fluctuation measurements were made at zero power to determine the difference in the effective delayed-neutron fraction β_e when fuel is, and is not, circulating in the primary loop.[39] When fuel is circulating, some precursors decay outside the core and lower β_e. Figure 2 shows power-density spectra that were analyzed with a point-reactor model assuming one average delayed group of neutrons. For a least-squares fit, β_e increased by a factor of 1.56 ± 0.21 when circulation ceased. For the same conditions, control-rod calibration measurements showed an increase by a factor of 1.47.

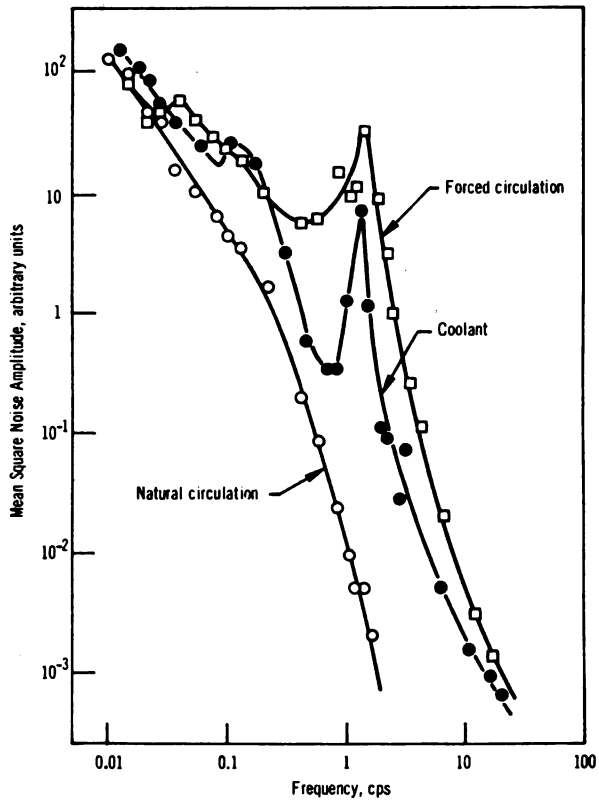

Fig. 1 Low-frequency resonances are induced by control-rod vibrations generated when coolant flow fluctuates in Hitachi Test Reactor at 80 kw (Ref. 42).

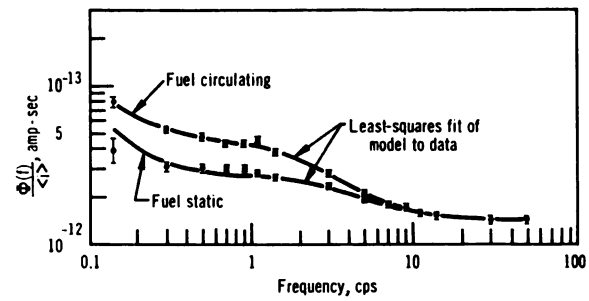

Fig. 2 Analysis of power-density spectra for the MSRE shows that the delayed-neutron fraction β_e decreases when fuel is circulated.[39]

References

Except for Refs. 1 and 3 to 5, all references are papers in Ref. 2.

1. M. F. Valerino, Conference on Noise Analysis in Nuclear Systems, *Power Reactor Technol.*, 7(3): 248-264 (Summer 1964).
2. Proceedings of the Symposium on Neutron Noise, Waves, and Pulse Propagation, held at University of Florida, Gainesville, Fla., February 14–16, 1966, USAEC Report CONF-660206, 1966.

Digitized by Google

3. D. N. Fry, Symposium on Neutron Noise, Waves, and Pulse Propagation, *Nucl. Safety*, 8(1): 37-40 (Fall 1966).
4. R. E. Uhrig, Neutron Noise, Waves, and Pulse Propagation, *Nucl. News*, 9(5): 32-33 (May 1966).
5. R. E. Uhrig (Coordinator), *Noise Analysis in Nuclear Systems*, AEC Symposium Series, No. 4 (TID-7679), University of Florida, Gainesville, Fla., June 1964.
6. R. B. Perez and R. E. Uhrig, Development of Neutron Waves and Pulse Propagation Techniques, Paper 1-1.
7. M. N. Moore, On the General Theory of Excitation Experiments in Space Dependent Kinetics, Paper 1-2.
8. A. Travelli, The Complex Relaxation Length of Neutron Waves in Multigroup Transport Theory, Paper 1-3.
9. R. L. Brehm, Analysis of Neutron Wave-Type Experiments, Paper 1-4.
10. M. J. Ohanian, R. B. Perez, and R. G. Cockrell, Propagation of Monochromatic Neutron Waves in Fast Nonmultiplying Media, Paper 1-5.
11. H. H. Kunaish, Consistent P-3 Theory of Neutron Wave Propagation, Paper 1-6.
12. G. H. Miley, Pulse Propagation Experiments Using a Reactor Source, Paper 2-1.
13. J. H. Dunlap and R. B. Perez, The Dispersion Law for a Natural Uranium, Heavy Water, Subcritical Assembly, Paper 2-2.
14. K. Sumita and A. Takahashi, A Simple Pulsed Neutron Source for Thermal Neutron Propagation Experiments and Its Application in Homogeneous and Heterogeneous Graphite Systems, Paper 2-3.
15. R. S. Booth and W. A. Frankhauser, Theoretical Justification for Neutron Pulse Propagation Experiments in Fast Nonmoderating Assemblies, Paper 2-4.
16. R. J. Johnson and R. N. Macdonald, Calculation of Space-Dependent Effects in Pile Oscillator and Reactor Noise Measurements, Paper 2-5.
17. J. R. Sheff, Space Dependent Cross-Spectral Density in a Bare Cube, Paper 2-6.
18. J. B. Dragt, Analysis of Reactor Noise Measured in a Zero Power Reactor and Calculations on Its Accuracy, Paper 3-3.
19. L. G. Kemeny, Fundamental Aspects of Stochastic Processes and Fluctuation Phenomena in Fission Reactors, Paper 5-1.
20. M. Natelson, R. K. Osborn, and F. Shure, Recent Developments in the Analysis of Neutron Noise Experiments, Paper 5-2.
21. R. J. Gelinas and R. K. Osborn, Reactor Noise Analysis from Observations on the High Energy Gamma Radiation from the Reactor Core, Paper 5-3.
22. R. J. Hooper and E. P. Gyftopoulos, On the Measurement of Characteristic Kernels of a Class of Nonlinear Systems, Paper 5-4.
23. A. Z. Akcasu, Angular Correlations in Neutron Density Fluctuations, Paper 5-5.
24. H. Borgwaldt and D. Sanitz, The Modal Synthesis of Rossi-Alpha Data for Moderator-Reflected Fast Assemblies, Paper 5-6.
25. M. A. Schultz, Measurement of Shutdown Reactivity in Large Gamma Fields, Paper 3-4.
26. E. S. Kenney, Noise Analysis of Nuclear Reactors Using Gamma Radiation, Paper 3-5.
27. H. Kataoka and M. Kubo, Identification of Transfer Function of Reactor Control System by Noise Analysis, Paper 3-6.
28. R. W. Albrecht and E. J. McGrath, Bias in Nuclear Reactor Power Spectral Density Estimates with Finite Record Lengths, Paper 3-7.
29. P. Meyer and E. Garelis, Impulse Response Measurements Using a Pseudorandom Source Input, Paper 4-3.
30. R. L. Randall and P. J. Pekrul, Applications of Analog Time and Frequency-Correlation Computers to Reactor System Analysis, Paper 6-3.
31. R. W. Albrecht and G. M. Hess, Reactor Noise Experiments in Reflected Plutonium Assemblies, Paper 6-4.
32. D. Babala et al., A Review of "NORA" Project Noise Experiments, Paper 6-7.
33. A. A. Wasserman et al., NERVA Reactor Transfer Function Measurements Using Cross-Correlation Techniques, Paper 4-2.
34. J. A. Johnson, Measurement of Pressure-to-Pressure Transfer Functions Through the Phoebus-1A Nuclear Reactor, Paper 6-5.
35. M. Hara and N. Suda, Some Investigations in the Application of Pseudorandom Binary Signals to Reactor Dynamics Measurements, Paper 4-1.
36. R. E. Uhrig and M. J. Ohanian, Pseudorandom Pulsing of Subcritical Systems, Paper 4-4.
37. T. Nomura, S. Gotoh, and K. Yamaki, Reactivity Measurements by Neutron Noise Analysis Using Two-Detector Correlation Method and Supercritical Reactor Noise Analysis, Paper 3-2.
38. W. Seifritz, D. Stegemann, and W. Vath, Two-Detector Cross-Correlation Experiments in the Fast-Thermal Argonaut Reactor "STARK" at Karlsruhe, Paper 3-1.
39. D. N. Fry et al., Neutron Fluctuation Measurements at Oak Ridge National Laboratory, Paper 6-1.
40. V. Rajagopal, Some Applications of Noise Measurements in Pressurized Water Reactors, Paper 6-2.
41. R. F. Saxe, Noise Analysis of the Oak Ridge Research Reactor, Paper 3-8.
42. S. Yamada and H. Kage, Reactor Noise Caused by Coolant Flow Fluctuations, Paper 6-6.

Digitized by Google

Water-Reactor Lattice Calculations and Measurements

By Edwin M. Pennington

Critical experiments—performed both to provide data that are used in power-reactor design and to test calculational methods—are the basis for many advances in water-reactor technology. Recent work encompasses heavy-water-moderated critical assemblies at Chalk River (where, for the first time, UC has been used with heavy water) and several light-water-moderated assemblies. The work with light-water lattices extends and interprets the data over a broader range of mixed-oxide fuel compositions.

Heavy-Water Lattices

Because not enough UC fuel was available to build critical lattices without a UO_2 driver zone, clusters of UC fuel were substituted into the central region of lattices containing UO_2 fuel. The validity of lattice parameters and analytical methods for these substitution experiments was studied in detail; the conclusion is that such substitution methods generally give results of adequate accuracy.

BUCKLING MEASUREMENTS FOR UC

Experiments have been carried out using seven-rod clusters of natural UC fuel in D_2O-moderated lattices in the ZED-2 critical facility at Chalk River.[1] The rods were of 2.52-cm-diameter UC clad in 1-mm-thick aluminum. The cluster arrangement was a central rod plus six rods on a 5.90-cm-diameter circle. Each cluster was contained in an aluminum pressure tube 9.1 cm in inside diameter with a 2-mm-thick wall and a calandria tube 10.1 cm in inside diameter with a 1.5-mm-thick wall.

Bucklings were determined by the substitution method in which up to 25 UC clusters successively replaced reference fuel at the core center. Nineteen-rod CANDU type bundles of UO_2 fuel were used as the reference. The difference in buckling between test and reference regions was derived from the changes in critical moderator level.

Measurements were made in square lattices at several pitches from 20 to 32 cm, with the UC clusters having four different coolants: D_2O, air, HB-40 ($C_{18}H_{22}$), and Dowtherm A. The reference fuel always had D_2O coolant.

Four methods were used in the analysis of the critical-height measurements. All methods gave reasonably good results except for the case of air-cooled clusters, where a problem with diffusion coefficients arose. To test the methods, substitution experiments were performed using fuel assemblies for which bucklings had been determined by flux-mapping experiments. The best agreement was given by a heterogeneous source-sink method, programmed under the name MICRETE.[2] It is believed that the bucklings for the seven-rod UC clusters determined by MICRETE, which range from about 1.9 m^{-2} to 5.0 m^{-2}, are accurate to less than or equal to 0.10 m^{-2}.

FINE STRUCTURE AND SPECTRUM PARAMETERS

Neutron-density fine structure and spectrum parameters were measured for the seven-rod UC clusters.[3] As is typical for D_2O-moderated lattices, the neutron-density fine structure is quite pronounced. The ratio of average neutron density in one of the six outer rods to that in the center rod varies from about 1.27 in a 20-cm-pitch lattice with air coolant to 1.61 in a 28-cm-pitch lattice with HB-40 coolant. Corresponding ratios of the moderator average neutron density to the average in the seven fuel rods are 2.063 and 3.257. These two values have since[27] been revised to 2.151 and 3.275.

The Westcott epithermal index r and the effective neutron temperature T_n were measured in the fuel, on the surface of the calandria tube, and at the cell boundary. These values were derived from the activity

Digitized by Google

ratios of indium to manganese and ^{177}Lu to manganese with a modification of the technique of Chidley et al.[4] The largest value of r was 0.0935 for the fuel of the 20-cm-pitch lattice with air coolant. The highest effective neutron temperature was about 100°C above the physical moderator temperature and occurred in the fuel of the 20-cm-pitch lattice with HB-40 coolant. For the loosest lattices the effective temperatures at the cell boundary differed little from the physical temperature.

VALIDITY

A study was made to determine whether lattice parameters can be obtained by using as few as seven test fuel rods at the center of a driver lattice.[5] Measurements were made both in the ZEEP reactor at 18- and 22-cm triangular lattice spacings and in the ZED-2 reactor at a 22-cm triangular lattice spacing. The ZEEP rods, which are 3.25-cm-diameter natural-uranium-metal rods, served as the driver fuel in the ZEEP reactor, and CANDU type 19-element natural-UO_2 fuel assemblies were the driver fuel in ZED-2. The natural-uranium test assemblies were 7-element UO_2, 19-element UO_2, and 19-element uranium-metal clusters, as well as ZEEP rods. The moderator was D_2O in all cases, and D_2O and HB-40 coolants were used.

If the neutron spectrum at the boundary of the center cell of the seven-element test region matches that in a full lattice of test fuel, then reaction-rate measurements in the central assembly of the test region should give the full-lattice values. Therefore Westcott's index r and the neutron temperature excess over the moderator temperature ΔT were measured at a central-cell boundary position midway between the central assembly and an assembly in the first ring of the test region. Comparisons with earlier values obtained using full lattices of test rods show that, for the 22-cm spacing, r and ΔT reached their equilibrium values at the central-cell boundary — whereas for the 18-cm spacing, ΔT but not r reached equilibrium.

Measurements of various lattice parameters were made in the fuel of the central 19-element UO_2 assembly containing D_2O coolant in the 18-cm ZEEP lattices. The results obtained agreed well with full-lattice results and indicate that, for natural-uranium D_2O-moderated lattices, lattice parameters can be measured using only seven test rods, even with the large mismatch of rod sizes in these experiments.

BUCKLINGS FROM SUBSTITUTION EXPERIMENTS

The MICRETE program,[2] which performs a two-group heterogeneous reactor calculation, has been used to determine the bucklings of natural-uranium D_2O-moderated lattices from measured changes in critical moderator height when 1 to 25 fuel assemblies are substituted into a reference core. In addition to the critical D_2O levels, the analysis requires calculated two-group parameters. However, the derived bucklings are insensitive to these, and they may be calculated by standard methods. First, a MICRETE calculation is performed for the reflected reference core using the observed height and calculated parameters. Then values of the resonance escape probability p and the effective outer radius of the D_2O reflector are adjusted until the reactor is critical and has a buckling, determined by the calculated flux shape near the core center, in agreement with the flux-mapping value. One or more test assemblies are then substituted in the calculation for reference assemblies, and their p value is adjusted until criticality is calculated to occur at the measured critical height. Then a MICRETE calculation is performed for a full lattice of test assemblies using the derived value of p and the other calculated parameters for the test lattice. After the dimensions of this core are altered until the system is critical, the buckling is determined from the flux shape near the center.

Application of MICRETE calculations to substitution experiments performed in the ZEEP and ZED-2 assemblies showed that values from MICRETE analysis with seven or more test rods and D_2O coolant are generally in good agreement with flux-mapping values. The largest buckling error for seven rods and D_2O coolant was 0.20 m^{-2}. Agreement is not as good for lattices with seven test rods and HB-40 or helium coolant, where the errors in bucklings were as large as 0.5 m^{-2} with the organic coolant and 0.7 m^{-2} with the helium.

Light-Water Lattices

Recent experiments have been performed with light-water lattices at Battelle–Northwest and at Argonne. At Battelle–Northwest the experiments used 2 wt.% PuO_2–UO_2 fuel with three different isotopic compositions of plutonium. These experiments supplemented previous ones at Battelle–Northwest performed with 1.5 wt.% PuO_2–UO_2 fuel. The Argonne experiments utilized 3.04% enriched UO_2 fuel and were done to extend the range of investigation of light-water lattices to highly undermoderated assemblies. Agreement between theory and experiment is usually satisfactory, although there are exceptions. Reference 6 comments on the state of the art of light-water criticals.

In connection with the analysis of light-water lattices, considerable work has been done in recent years on the behavior of the thermal disadvantage factor in tightly packed lattices and on the determination of bucklings by variable loading techniques. The main features of this work are also outlined here.

PuO_2–UO_2–H_2O LATTICES

Subcritical experiments and analytical correlations were performed for PuO_2–UO_2–H_2O lattices at Battelle–Northwest.[7] The fuel was 2 wt.% PuO_2–UO_2 (vibratory compacted) contained in 0.030-in.-thick

Digitized by Google

Zircaloy tubes 0.508 in. in inside diameter. The uranium in the UO_2 was of natural enrichment, whereas three compositions of plutonium were, by weight, (1) 91.62% ^{239}Pu, 7.65% ^{240}Pu, 0.70% ^{241}Pu, and 0.03% ^{242}Pu; (2) 81.11% ^{239}Pu, 16.54% ^{240}Pu, 2.15% ^{241}Pu, and 0.20% ^{242}Pu; and (3) 71.76% ^{239}Pu, 23.50% ^{240}Pu, 4.08% ^{241}Pu, and 0.66% ^{242}Pu. The rods were loaded in hexagonal lattices at spacings yielding moderator-to-PuO_2-UO_2 volume ratios of 0.61 to 9.7. All lattices were completely reflected with H_2O. The experimental procedures were the same as those used in determining critical masses and bucklings of 1.5 wt.% $PuO_2-UO_2-H_2O$ lattices.[8]

The calculations were performed using one-dimensional four-energy-group diffusion theory for a homogeneous core and H_2O reflector. Axial leakage effects were accounted for with transverse bucklings. Cross sections for the homogenized lattice were obtained using the HRG (Hanford-Revised GAM) code[9] for nonthermal events and the THERMOS code[10] with the Nelkin kernel for hydrogen in the thermal-energy range. Microscopic cross sections were taken from the Battelle–Northwest master library.[11]

The calculated multiplications, k_{eff}, for most of the lattices are somewhat low. Use of the more recently evaluated value of 2.115 for the thermal η of ^{239}Pu, rather than the older value of 2.093 which was used in the calculations, would increase the multiplications by about 1% and yield better agreement with experiment.

There are two main factors that make calculations for thermal plutonium lattices difficult. One is the fact that the plutonium cross sections are not, in general, as accurately known as those for uranium. The other is the presence of large low-lying resonances in ^{239}Pu, ^{240}Pu, and ^{241}Pu, which makes an accurate treatment of near-thermal events important. Uncertainties in resonance cross sections lead to larger uncertainties in multiplication values than do the uncertainties in thermal cross sections.[28]

UO_2-H_2O LATTICES

The High Conversion Critical Experiment (Hi-C) was initiated at Argonne to extend the range of investigation with light-water-moderated slightly enriched UO_2 cores to lower water-to-fuel ratios. Lattices were assembled with hydrogen-to-^{238}U atom ratios of from 4.16 to 0.50, which correspond to water-to-UO_2 volume ratios of from 1.37 to 0.17. The fuel consisted of 0.935-cm-diameter 3.04% enriched UO_2 pellets loaded in cladding tubes of either 0.048-cm-thick aluminum or 0.0496-cm-thick stainless steel. Both square and triangular lattice arrays were used.

Various cell parameters were measured in the full range of lattices; critical bucklings and reflector savings were measured in the looser assemblies. Calculations of critical bucklings and cell parameters were carried out in the framework of four-group diffusion theory. Cross sections for three fast groups were obtained using the GAM-I code,[12] whereas those for the thermal group were found using THERMOS[10] with the Nelkin kernel for hydrogen.

The critical bucklings, obtained by using the four-group constants in fundamental mode calculations, are in good agreement with experimental values.[13] Values of k_{eff} averaged about 0.5% too high when the P_1 approximation was used in GAM-I and about 1% too high when the B_1 approximation was used. Preliminary calculations yielded values much higher than experiment. The improvement resulted from replacing ^{238}U and ^{235}U cross sections in the original GAM-I library by values obtained from Hanford. Agreement between theory and experiment was reasonably good for reflector savings and various cell parameters, except for the case of the ^{238}U-to-^{235}U fission ratio δ^{28}, for which experimental values were much higher than calculated ones.

Improvements could be made in the theoretical methods used in the Hi-C program, although those used should be reasonably accurate. However, the extreme undermoderation of the lattices makes nonthermal events very important; thus inaccuracies in nonthermal cross sections can produce large uncertainties in the calculations. Figure 1 illustrates the

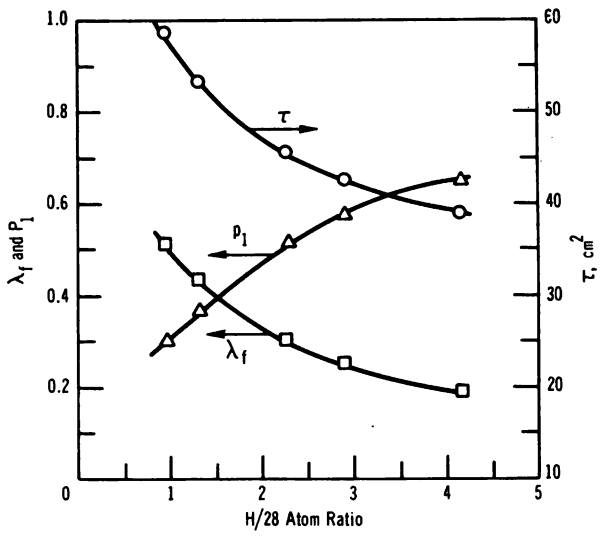

Fig. 1 Two-group parameters for Hi-C aluminum-clad lattices. The ordinate for p_1 and λ_f is dimensionless.[13]

large contribution of nonthermal events to criticality. The parameters plotted against the hydrogen-to-^{238}U atom ratio are p_1, λ_f, and τ of the two-group criticality equation used in the study of light-water lattices at Brookhaven.[14] This equation is

$$\frac{(1-p_1)(\eta f)_1}{1+\tau B^2}+\frac{p_1(\eta f)_2}{(1+\tau B^2)(1+L^2B^2)}=1 \qquad (1)$$

where the two terms on the left side are denoted by λ_f and λ_t and represent contributions from nonthermal and thermal neutrons, respectively.

Digitized by Google

DISADVANTAGE FACTORS IN TIGHTLY PACKED LATTICES

A problem that has received considerable attention in the last 2 or 3 years is that of disadvantage factors in tightly packed lattices of cylindrical fuel rods. Experimental evidence has been presented[15] that the cell disadvantage factor is not necessarily a monotonically decreasing function as the pitch decreases, although large error bars are associated with the results.

In Ref. 16, solutions of the P_3 approximation to the one-velocity Boltzmann equation for a two-region two-dimensional cell of cylindrical fuel rods in a moderator are obtained. It is found that the disadvantage factor δ has a minimum as the lattice pitch is decreased with the moderator cross section remaining constant. The breakdown of monotonic behavior of δ increases for cores where the optical thickness of the fuel is larger. Monte Carlo results for a few cases where the fuel rod has unit optical thickness show the same trend as the P_3 results. The two-dimensional P_1 approximation also yielded a minimum in the δ curve.

It has been shown that δ has a minimum as the moderator cross section is decreased at constant lattice pitch.[17] Both Brissenden's approximate collision-probability method[18] for a square cell and a cylindrical-cell approximation with the isotropic (white) boundary condition suggested by Honeck[19] were used.

Calculations corresponding to the experimental Hi-C lattices[15] using the THERMOS code[10] with 27 groups and the isotropic boundary condition, as well as in a cylindrical-cell collision-probability code with isotropic return and one-group cross sections from THERMOS, did not yield a minimum in δ. However, this lack of a minimum was the result of the progressive hardening of the cross sections as the pitch was decreased. When the one-group cylindrical-cell collision-probability calculations were repeated using constant cross sections, a minimum in δ was obtained.

Many of the results obtained for disadvantage factors in tightly packed lattices have been summarized.[20] Table 1, which is adapted from Ref. 20, presents trends of the disadvantage factor calculated by various methods. In the table an A-series lattice is one for which the moderator cross section is held constant and the moderator thickness decreased, whereas a B-series lattice has fixed-cell dimensions and the moderator cross section is decreased. The quantities Σ_1, a, and V are the moderator cross section, fuel radius, and moderator-to-fuel volume ratio, respectively.

Table 1 DISADVANTAGE-FACTOR TRENDS

Method	A-series lattice $\Sigma_1 a$ = 1 (constant)	B-series lattice V = 1 (constant)
P_1 approximation, cylindrical	Monotonic decrease	Monotonic decrease
P_1 Cohen,[24] square	Increases below V = 0.681	Monotonic decrease
P_3 Clendenin,[25] cylindrical		
(*a*) Boundary condition ψ_{33} = 0	Increases below a certain V	Monotonic decrease
(*b*) Boundary condition ψ_{31} = 0	Monotonic decrease	Monotonic decrease
Amouyal[26]	Monotonic decrease	Increases below a certain $\Sigma_1 a$
Collision probability, flat-flux approximation[20]		
(*a*) Cylindricized	Increases below a certain V	Increases below a certain $\Sigma_1 a$
(*b*) Exact square or hexagonal cell	Increases below a certain V	Increases below a certain $\Sigma_1 a$

Reference 20 also points out that the cylindrical-cell approximation with isotropic boundary condition breaks down somewhat for very tightly packed lattices — in that the disadvantage factor does not increase rapidly enough with decreasing pitch. Thus it is expected that, if an exact multigroup thermal calculation were carried out for the Hi-C lattices, rather than one using the isotropic boundary condition as in THERMOS, the disadvantage factor would show a minimum in spite of the tendency of the hardening of the cross sections to counteract the effect. This is in qualitative agreement with the results of 36-group Monte Carlo calculations[21] which treat the cell geometry exactly.

A significant effect has been discovered[22] in connection with the interpretation of thermal disadvantage-factor measurements. Three-dimensional Monte Carlo calculations explicitly including foils indicate that the flux in a foil is often considerably different from the flux in the medium in which it is placed, even for optically thin foils. The flux peaking or dipping depends strongly on the medium surrounding the foil.

Calculations were carried out using a 32-group thermal Monte Carlo code, DRAM, both for some lattices at Bettis Atomic Power Laboratory and for the Argonne Hi-C lattices. Thermal disadvantage factors were calculated both for the foil regions and for unperturbed regions in the rod and moderator. For all lattices the disadvantage factors for the unperturbed region were higher than those for the foil regions; disadvantage factors for the foil regions were in agreement with the experimental values. These results explain why calculated disadvantage factors tend to be larger than measured ones.

BUCKLINGS BY VARIABLE LOADING TECHNIQUES

In determining experimental bucklings from "variable-loading" techniques, to obtain accurate results it is necessary to allow for the variation in radial-reflector savings. The equation

$$\lambda r = \frac{\lambda_0}{(1 + M^2 B_z^2)^{1/2}} \frac{K_0\{[(1/M^2) + B_z^2]^{1/2} r\}}{K_1\{[(1/M^2) + B_z^2]^{1/2} r\}} + \Delta\lambda \qquad (2)$$

has been proposed[23] for the radial-reflector savings. In Eq. 2, B_z^2 is the axial buckling, λ_0 and M^2 are constants to be determined from the fit to a series of loadings, K_0 and K_1 are Bessel functions, and $\Delta\lambda$ is a correction for having assumed a linear extrapolation of the flux from its value at the core boundary to the radius at which it is zero.

Digitized by Google

Equation 2 was tested by using it in a variable-loading analysis of a series of theoretical four-group two-region cores. The variable-loading bucklings agreed with the infinite lattice values within 0.1 m^{-2}. Also both variable-loading and "flux-shape" techniques were applied to 32 experimental cores. The results were in good agreement for lattices where the radial buckling was less than 50 m^{-2}. For lattices with larger radial bucklings, the flux-shape values were systematically high. This illustrates the breakdown of the flux-shape technique for cores of small radius where radial energy transients are significant. For such cores the variable-loading method with variable-reflector savings is more suitable.

References

1. R. E. Green et al., Experimental Bucklings for Seven-Rod Clusters of Natural UC in Heavy Water Moderator, *Trans. Am. Nucl. Soc.*, 9(1): 123 (June 1966).
2. D. S. Craig et al., Bucklings from Substituion Experiments by Use of Source-Sink Calculation, *Trans. Am. Nucl. Soc.*, 9(1): 126 (June 1966).
3. R. E. Kay and R. E. Green, Experimental Neutron-Density Fine Structures and Spectrum Parameters for Natural-UC Clusters in Heavy-Water-Moderated Lattices with Air, Heavy Water, and Organic Coolants, *Trans. Am. Nucl. Soc.*, 9(1): 124 (June 1966).
4. B. G. Chidley et al., Neutron Temperatures in a CANDU-Type Power Reactor, *Nucl. Sci. Eng.*, 16(1): 39 (May 1963).
5. A. Okazaki and D. S. Craig, Measurement of Lattice Parameters in Natural-Uranium/Heavy-Water Lattices Using a Few Rods, *Trans. Am. Nucl. Soc.*, 9(1): 125 (June 1966).
6. C. N. Kelber, Water-Reactor Data Generally Verify Theory, *Power Reactor Technol.*, 8(4): 214-215 (Fall 1965).
7. R. C. Liikala and W. P. Stinson, Experimental and Analytical Results for $PuO_2-UO_2-H_2O$ Lattices, *Trans. Am. Nucl. Soc.*, 9(1): 127 (June 1966).
8. L. C. Schmid et al., Critical Masses and Bucklings of $PuO_2-UO_2-H_2O$ Systems, *Trans. Am. Nucl. Soc.*, 7(2): 216 (November 1964).
9. J. L. Carter, Jr., HRG-Hanford Revised GAM, Battelle-Northwest, unpublished.
10. H. C. Honeck, THERMOS, A Thermalization Transport Theory Code for Reactor Lattice Calculations, USAEC Report BNL-5826, Brookhaven National Laboratory, September 1961.
11. K. B. Stewart, BNW Master Library, USAEC Report BNWL-CC-325, Vols. I, II, and III, Battelle-Northwest, Sept. 1, 1965.
12. G. D. Joanou and J. S. Dudek, GAM-I: A Consistent P-1 Multigroup Code for the Calculation of Fast Neutron Spectra and Multigroup Constants, USAEC Report GA-1850, General Atomic Division, General Dynamics Corp., June 28, 1961.
13. A. R. Boynton and E. M. Pennington, Critical Experiments and Calculations in Some Very Undermoderated, Slightly Enriched, Uranium Oxide/Water Lattices, *Trans. Am. Nucl. Soc.*, 9(1): 129 (June 1966).
14. R. L. Hellens and H. C. Honeck, A Summary and Preliminary Analysis of the BNL Slightly Enriched Uranium, Water Moderated Lattice Measurements, in *Light Water Lattices*, pp. 27-71, Technical Report Series, No. 12, International Atomic Energy Agency, Vienna, 1962 (STI/DOC/10/12).
15. A. R. Boynton, Thermal Disadvantage Factors in Very Undermoderated Water-Uranium Oxide Lattices, *Nucl. Sci. Eng.*, 23(4): 393 (December 1965).
16. T. E. Dudley, Disadvantage Factors in Close-Packed Lattices, *Trans. Am. Nucl. Soc.*, 9(1): 130 (June 1966).
17. Z. Weiss and R. J. J. Stamm'ler, Calculation of Disadvantage Factors in Small Cells, *Nucl. Sci. Eng.*, 19(3): 374 (July 1964).
18. R. J. Brissenden, A Formula for the Escape Probability of a Rod in a Uniform Lattice, British Report AEEW-R-282, April 1963.
19. H. C. Honeck, Some Methods for Improving the Cylindrical Reflecting Boundary Condition in Cell Calculations of the Thermal Neutron Flux, *Trans. Am. Nucl. Soc.*, 5(2): 350 (November 1962).
20. Y. Fukai, On the Disadvantage Factor in a Closely Packed Cylindrical Lattice, *J. Nucl. Sci. Technol. (Tokyo)*, 3(4): 165 (April 1966).
21. J. Hardy et al., Thermal Neutron Spectral and Spatial Distributions in Light Water Moderated Uranium Lattices, USAEC Report WAPD-T-1594, Westinghouse Electric Corp., Bettis Atomic Power Laboratory, April 1963; also in *Exponential and Critical Experiments*, Symposium Proceedings, Amsterdam, 1963, Vol. II, pp. 339-359, International Atomic Energy Agency, Vienna, 1964 (STI/PUB/79).
22. F. E. Dunn, Flux Dipping and Peaking in Foils Used in Thermal Disadvantage-Factor Measurements, *Trans. Am. Nucl. Soc.*, 9(1): 189 (June 1966).
23. H. Windsor, The Effect of Radial-Energy Transients on Experimental Material-Buckling Measurements, *Trans. Am. Nucl. Soc.*, 9(1): 130 (June 1966).
24. E. R. Cohen, Thermal Neutron Flux in a Square Lattice Cell, *Nucl. Sci. Eng.*, 1(4): 268 (August 1956).
25. W. W. Clendenin, Effects of Zero Gradient Boundary Conditions on Cell Calculations in Cylindrical Geometry, *Nucl. Sci. Eng.*, 14(1): 103 (September 1962).
26. A. Amouyal, P. Benoist, and J. Horowitz, Nouvelle Methode de Determination du Facteur d'Utilisation Thermique d'une Cellule, *J. Nucl. Energy*, 6(1/2): 79-98 (1957-1958).
27. R. E. Kay and R. E. Green, Atomic Energy of Canada Ltd., personal communication, October 1966.
28. R. C. Liikala, W. L. Purcell, and J. R. Worden, Sensitivity of Reactor Multiplication Values to Cross Section Uncertainties for Thermal Systems, in Conference on Neutron Cross Section Technology, March 22-24, 1966, Washington, USAEC Report CONF-660303, Book 1, pp. 75-87, 1966.

Digitized by Google

Nuclear Power To Explore the Ocean Deeps

By Edward J. Croke

Nuclear power is ideally suited to opening the undersea environment to man's use.[1] One of the most immediate and potentially significant applications of nuclear power in the conquest of the oceans involves the use of deep-diving submersibles for undersea exploration. Although a number of conventionally powered research and exploration submersibles have been and are being built, and numerous studies have been made of nuclear propulsion for such vehicles, the U. S. Navy's *NR-1* is the only nuclear-powered deep-diving submarine actually being built. Because the design features of deep-diving research submersibles are sure to influence the course of man's use of the sea, it is interesting to consider what performance and design features are desirable.

Depth Incentive

Although continental shelves are relatively accessible for exploration and exploitation, Fig. 1 graphically illustrates why it is desirable that exploration vehicles be capable of penetrating well beyond the (by definition) 600-ft limit of the continental shelves. Figure 1 shows that a vehicle that can reach 12,000 to 15,000 ft could explore more than half the total sea floor; a 20,000-ft-depth capability would put nearly 98% of the sea bottom within range. The manifest advantages of extreme deep-submergence capability in terms of exploration range are more strikingly evident in Fig. 2, in which the attainable areas of the ocean floor are superimposed on a Mercator projection of the land masses of the globe to a depth of 12,000 ft.

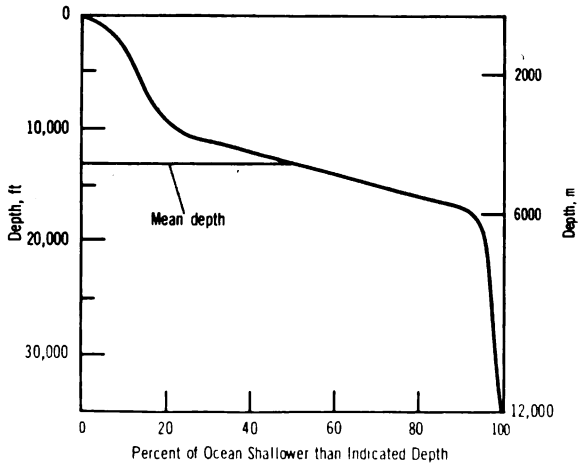

Fig. 1 Hypsographic curve of the oceans.[4]

Speed and Duration

Cruising speed need not be more than a few knots for an exploration vehicle (for fisheries research, speed might be somewhat greater); but if the submersible is to operate from a port, it would be desirable that speeds of tens of knots be maintained to minimize transit times between work sites. Submergence durations of several weeks at a time would be useful.

Configuration

For 12,000- to 20,000-ft depths, to minimize sealing problems associated with penetration of the hull by one or more rotating shafts, it would be appropriate to have a propulsion system whose electric propulsor motors are mounted in pods on the exterior of the hull. Hull construction might resemble a configuration proposed for the Deep Submergence Rescue Vehicle,[2] which consists of three interconnected pressure spheres surrounded by a hydrodynamic fairing. This arrangement lends itself to dividing the vehicle into separate dwelling, laboratory, and propulsion-system modules.

Digitized by Google

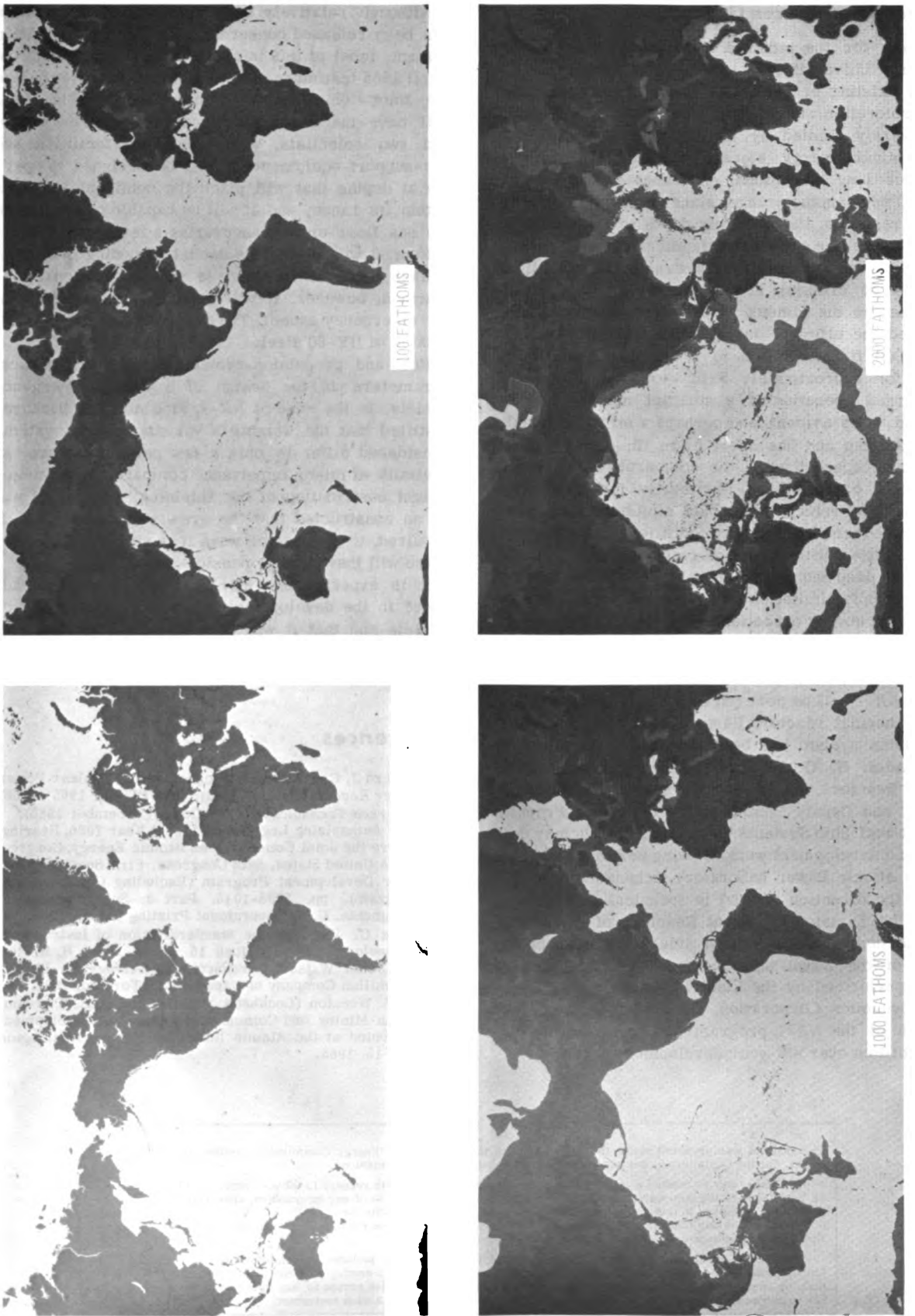

Fig. 2 The area of the sea floor that is attainable with vehicles capable of various operating depths.[5]

Digitized by Google

Conventional-Power Limitations

Except for the tethered *Kuroshio-II*, operated by Hokkaido University, Japan, the endurance of all 21 of the existing or projected "conventional" research and exploration submarines (see Table 2 of Ref. 1) is severely limited by the capacity of their electrochemical energy storage systems. *Kuroshio-II* achieves long operational endurance at the cost of limited performance range, since its umbilical power cable restricts its operating depth to about 600 ft. One of the best electrochemical-powered deep-submergence vessels, the *Aluminaut* (15,000 ft), is capable of cruising at 3 knots for only about 32 hr, whereas the famous *Trieste* bathyscaphe, which plumbed the ultimate deeps of the Philippine trench at 35,000 ft, is limited to a cruising speed of 1.5 knots for approximately 5 hr—or about 48 hr of submerged operation if significant maneuvering is avoided. It is evident, and perhaps a bit paradoxical, that man can and has spent more time and traveled farther in space than in the comparatively near and attainable ocean depths—primarily for want of a submersible vehicle that could simultaneously provide long-term life-support facilities and propulsive power. *NR-1*, with its reactor power supply, will be the first deep-submergence vehicle to overcome the power-supply limitation and open the ocean depth to long-term survey operations.

NR-1 Design Concept

The *NR-1* will be powered by a small, pressurized-water thermal reactor. Responsibility for the *NR-1* propulsion system has been assigned to the office of Vice Adm. H. G. Rickover, Director, Division of Naval Reactors, U. S. Atomic Energy Commission (AEC), and Deputy Commander for Nuclear Propulsion, Naval Ship Systems Command. The nuclear design and development work is being performed by the Knolls Atomic Power Laboratory, Schenectady, N.Y., under the direction of, and in technical cooperation with, the Division of Naval Reactors of AEC. The general design of the vehicle itself is the responsibility of the Naval Ship Systems Command and is being performed by the Electric Boat Division, General Dynamics Corporation, Groton, Conn. The AEC portion of the *NR-1* program was expected to cost $7.5 million over a 3-year development period.

Although relatively little unclassified information has been released concerning *NR-1* or its propulsion system, most of this information is derived from the April 1965 testimony of Vice Admiral Rickover before the Joint Committee on Atomic Energy.[3] The *NR-1* will have the capability of carrying a crew of five and two scientists, with laboratory facilities and life-support equipment. It will be designed to operate at depths that will place the continental shelves within its range, and it will be capable of settling on the sea floor or of maneuvering a few feet above the bottom. It will control its depth by flooding or blowing ballast tanks, as is the case with conventional submarines; however, it will be able to release weights for emergency ascent. The pressure hull will be fabricated of HY-80 steel.

Hull and propulsion-system weights are critical parameters in the design of a deep-submergence vehicle. In the case of *NR-1*, Vice Admiral Rickover testified that the weights of various reactor systems considered differ by only a few percent and are essentially of minor importance compared to the major weight contribution of the shielding. The vessel will be so constructed that the crew will have access, if required, to the reactor when it is shut down, and repairs will therefore be possible.

It is expected that the *NR-1* will be a major advance in the development of oceanographic research vessels and that it will provide the basic technology for the development of a generation of future nuclear-powered deep-submergence research vehicles.

References

1. Edward J. Croke, Ocean Technology and Nuclear Power, *Power Reactor Technol.*, 9(1): 1-18 (Winter 1965-1966).
2. *Undersea Technology*, 6(12): Cover (December 1965).
3. AEC Authorizing Legislation Fiscal Year 1966, Hearings Before the Joint Committee on Atomic Energy, Congress of the United States, 89th Congress, First Session on Reactor Development Program (Excluding Civilian Power Program), pp. 1038-1045, Part 2, Superintendent of Documents, U. S. Government Printing Office, 1965.
4. Allyn C. Vine, Depths Standardization of Instruments, *Oceanology*, 1(1): 12 (June 15, 1966). Also, H. H. Read and Janet Watson, *Introduction to Geology*, p. 11, The Macmillan Company of Canada Ltd., Toronto, 1962.
5. E. P. Wheaton (Lockheed Missiles and Space Division), Ocean Mining and Commercial Resources Development, presented at the Atomic Industrial Forum, Washington, Nov. 15, 1965.

LEGAL NOTICE

This journal was prepared under the sponsorship of the U. S. Atomic Energy Commission. Neither the United States, nor the Commission, nor any person acting on behalf of the Commission:

A. Makes any warranty or representation, expressed or implied, with respect to the accuracy, completeness, or usefulness of the information contained in this journal, or that the use of any information, apparatus, method, or process disclosed in this journal may not infringe privately owned rights; or

B. Assumes any liabilities with respect to the use of, or for damages resulting from the use of any information, apparatus, method, or process disclosed in this journal.

As used in the above, "person acting on behalf of the Commission" includes any employee or contractor of the Commission, or employee of such contractor, to the extent that such employee or contractor of the Commission, or employee of such contractor prepares, disseminates, or provides access to, any information pursuant to his employment or contract with the Commission, or his employment with such contractor.

Digitized by Google

Digitized by Google

640
GIFT
JAN 31 '67

Digitized by Google

NUCLEAR SCIENCE ABSTRACTS

The U. S. Atomic Energy Commission, Division of Technical Information, publishes *Nuclear Science Abstracts* (*NSA*), a semimonthly journal containing abstracts of the literature of nuclear science and engineering.

NSA covers (1) research reports of the U. S. Atomic Energy Commission and its contractors; (2) research reports of government agencies, universities, and industrial research organizations on a worldwide basis; and (3) translations, patents, books, and articles appearing in technical and scientific journals.

Complete indexes covering subject, author, source, and report number are included in each issue. These are cumulated quarterly, semiannually, and annually providing a detailed and convenient key to the literature.

Availability of *NSA*

SALE *NSA* is available on subscription from the Superintendent of Documents, U. S. Government Printing Office, Washington, D. C., 20402, at $30.00 per year for the semimonthly abstract issues and $22.00 per year for the four cumulated-index issues. Subscriptions are postpaid within the United States, Canada, Mexico, and all Central and South American countries, except Argentina, Brazil, Guyana, French Guiana, Surinam, and British Honduras. Subscribers in these Central and South American countries, and in all other countries throughout the world, should remit $37.00 per year for subscriptions to semimonthly abstract issues and $25.00 per year for the four cumulated-index issues.

EXCHANGE *NSA* is also available on an exchange basis to universities, research institutions, industrial firms, and publishers of scientific information. Inquiries should be directed to the Division of Technical Information Extension, U. S. Atomic Energy Commission, P. O. Box 62, Oak Ridge, Tennessee, 37830.

Digitized by Google

TECHNICAL PROGRESS REVIEWS may be purchased from Superintendent of Documents, U. S. Government Printing Office, Washington, D. C., 20402. *Nuclear Safety* at $3.00 per year for each subscription or $1.00 per issue; each of the other journals at $2.50 per year or $0.70 per issue. The use of the coupon below will facilitate the handling of your order.

POSTAGE AND REMITTANCE: Postpaid within the United States, Canada, Mexico, and all Central and South American countries except Argentina, Brazil, Guyana, French Guiana, Surinam, and British Honduras. For these Central and South American countries and all other countries, add $0.75 for each annual subscription or $0.20 for a single issue. Payment should be by check, money order, or document coupons, and MUST accompany order. Remittances from foreign countries should be made by international money order or draft on an American bank payable to the Superintendent of Documents or by UNESCO book coupons.

order form

SUPERINTENDENT OF DOCUMENTS
U. S. GOVERNMENT PRINTING OFFICE
WASHINGTON, D. C., 20402

Enclosed:
document coupons ☐ check ☐ money order ☐

Charge to Superintendent of Documents No. _____

Please send a one-year subscription to

☐ ISOTOPES AND RADIATION TECHNOLOGY

☐ POWER REACTOR TECHNOLOGY

☐ REACTOR MATERIALS

(Each subscription $2.50 per year; $0.70 per issue.)

☐ NUCLEAR SAFETY

(Each subscription $3.00 per year; $1.00 per issue.)

SUPERINTENDENT OF DOCUMENTS
U. S. GOVERNMENT PRINTING OFFICE
WASHINGTON, D. C., 20402

(Print clearly)

_____
Name

_____
Street

_____
City, State, ZIP Code

Digitized by Google

ENGINEERING
JUN 30 '67
LIBRARY

POWER REACTOR TECHNOLOGY

A Quarterly Technical Progress Review

Prepared for DIVISION OF TECHNICAL INFORMATION, USAEC, by
ARGONNE NATIONAL LABORATORY

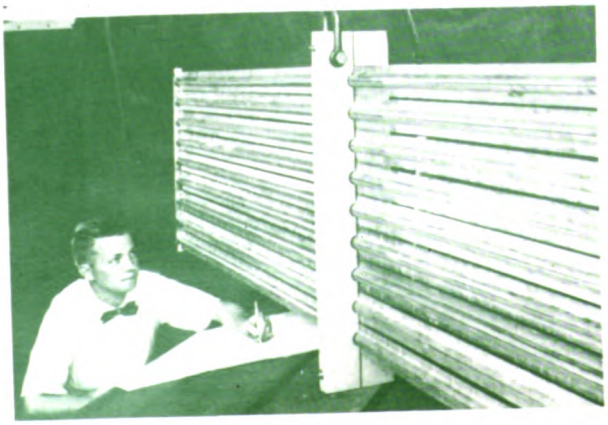

Rankine-cycle space power . . . page 194

Fall 1966

● VOLUME 9

● NUMBER 4

Digitized by Google

TECHNICAL PROGRESS REVIEWS

The United States Atomic Energy Commission publishes the Technical Progress Reviews to meet the needs of industry and government for concise summaries of current nuclear developments. Issued quarterly, each journal digests and evaluates the latest findings in a specific area of nuclear technology and science.

The journals are:

Isotopes and Radiation Technology
P. S. Baker, A. F. Rupp, and Associates
Oak Ridge National Laboratory

Nuclear Safety
Wm. B. Cottrell, W. H. Jordan, J. P. Blakely, and Associates
Nuclear Safety Information Center, Oak Ridge National Laboratory

Power Reactor Technology
Argonne National Laboratory

Reactor Materials
E. M. Simons and Associates
Battelle Memorial Institute

All are available from the U. S. Government Printing Office. See the back cover for ordering instructions.

The views expressed in this publication do not necessarily represent those of the United States Atomic Energy Commission, its divisions or offices, or of any Commission advisory committee or contractor.

Availability of Reports Cited in This Review

United States Atomic Energy Commission (USAEC) reports are available at USAEC depository libraries and are sold by the Clearinghouse for Federal Scientific and Technical Information (CFSTI), National Bureau of Standards, U. S. Department of Commerce, 5285 Port Royal Road, Springfield, Va. 22151. All reports sold by CFSTI are $3.00 for printed copy and $0.65 for microfiche. Each separately bound part of a report is priced as a separate report. Some reports may not be available because of their preliminary nature; however, the information contained in them will generally be found in later progress or topical reports on the subject.

Other U. S. Government agency reports identified in this journal generally are available from CFSTI.

Private-organization reports should be requested from the originator.

United Kingdom Atomic Energy Authority (UKAEA) and Atomic Energy of Canada Limited (AECL) reports are available at USAEC depository libraries. UKAEA reports are sold by Her Majesty's Stationery Office, London; AECL reports are sold by the Technical Information Officer, Atomic Energy of Canada Limited, Chalk River, Ontario, Canada. UKAEA and AECL reports issued after March 1, 1967, are sold by CFSTI to purchasers in the United States and its territories.

Digitized by Google

Contents

Power Reactor Technology

Vol. 9, No. 4

APPLICATIONS — New Departures in High-Flux Research Reactors . . . 153
Bernard I. Spinrad

PHYSICS — Zone-Loaded Critical Experiments for Fast Breeders . . . 162
George J. Fischer, Armando Travelli, and Daniel A. Meneley

CONTROL AND DYNAMICS — Let's Apply Optimal Control and Nonlinear Analysis . . . 169
Ronald R. Mohler

FLUID AND THERMAL TECHNOLOGY — Improved Design Predictions Through Liquid-Metal Heat-Transfer Research . . . 174
Ralph P. Stein

OPERATING EXPERIENCE — NPD Performance Indicates Merit of On-Power Refueling . . . 180
Karl K. Brown

ENERGY CONVERSION — Recent Developments in Liquid-Metal MHD Power Systems . . . 187
Michael Petrick

Component Development—Key to Rankine-Cycle Space Applications . . . 194
Edward J. Croke

INDEX — Volume 9 . . . 215

LIMITED COVERAGE OF FUEL PROCESSING

The Technical Progress Review *Reactor Fuel Processing* was terminated with the Vol. 9, No. 4, issue. Limited coverage of fuel processing will begin in this journal with the Winter issue, Vol. 10, No. 1.

Issued quarterly by the U. S. Atomic Energy Commission. Use of funds for printing this publication approved by the Director of the Bureau of the Budget on July 8, 1966.

Digitized by Google

Power Reactor Technology

is a quarterly review of developments in reactor technology — including new concepts and applications as well as research results, analysis, and experience with existing or new components and systems. Prepared by Argonne National Laboratory at the request of the Division of Technical Information of the U. S. Atomic Energy Commission, *Power Reactor Technology* is intended for reactor designers and other technical specialists concerned with the interplay among reactor development, design, construction, operation, and economics. Thus this quarterly journal reports and interprets progress in the power-reactor field in terms of its significance to the reactor designer. Its scope includes research and development in the various technical specialties in the field as well as design and construction practices, reactor concepts, applications, economics, and operating experience.

Some articles summarize and critically evaluate reported developments; others review a topic broadly so that designers can interpret new developments, experience, and trends. All, however, call the reader's attention to reports and publications that merit study. Because any appraisal involves the reviewer's opinion of the significance of the work reported, readers are urged to consult the references for additional information and the judgments of the original authors. If a reader has information that causes his evaluation to reinforce, modify, or contradict the opinions of our reviewers, he is encouraged to write to the Editor.

For reasonably timely coverage, articles often must be based on fragmentary information. Thus, whenever appropriate, continuity will be maintained from one issue to another by use of subject headings that reflect parts of the following scope of the journal:

> CONCEPTS and APPLICATIONS: Progress in evaluating the applicability and economics of various reactor types and systems (including unconventional approaches), as well as of fuel resources and cycles, for utility central-station generation of electricity, auxiliary power, process radiation and heat, desalting, and propulsion — and for terrestrial, undersea, aerospace, and other advanced uses.
>
> ANALYSIS and EXPERIMENTATION: Advancements in the techniques of reactor physics, fluid and thermal technology, power conversion, fuel elements, materials, mechanics, control and dynamics, and reactor safety.
>
> SYSTEMS and COMPONENTS: Experience as reflected in design and construction practice, components, systems technology, and operating performance of various specific types of reactors — including pressurized- and boiling-water reactors, molten-salt, organic-, gas-, and liquid-metal-cooled reactors, as well as generally applicable aspects of research and test reactors.

At Argonne National Laboratory, the Reactor Engineering Division (L. J. Koch, Director) has the principal responsibility for the preparation of *Power Reactor Technology*, with the regular assistance of the Reactor Physics Division (R. A. Avery, Director) and the occasional assistance of other Laboratory divisions (Metallurgy, Chemical Engineering, Chemistry, Reactor Operations, and Idaho). Thus, unless noted otherwise, the reviewers and authors of articles are Laboratory staff members. The editors will welcome interpretive review articles contributed by readers outside the Laboratory.

JAMES J. DUTTON, *Editor*
DAVID H. LENNOX, *Technical Editor;* KARL K. BROWN, *Managing Editor*
EDWARD J. CROKE and RAYMOND GOLD, *Associate Editors*
BARBARA A. SCHMEH, *Assistant Editor*

Argonne National Laboratory

Digitized by Google

New Departures in High-Flux Research Reactors

By Bernard I. Spinrad

The present generation of high-flux research reactors—heterogeneous, water cooled and moderated (light and heavy), with projected beam and irradiation fluxes of 1 to 5×10^{15} thermal neutrons/(cm^3)(sec)—represents the penultimate in research-reactor performance, according to their designers. That is, although they may be improved by design refinements as we learn more about actual system performance with regard to hot-channel factors, coolant flow patterns, burnout safety margins, and so on, it is unlikely that this improvement could lead to more than a factor of ~3 in available flux. (If this were not the case, these improvements would be the subject of vigorous research and development and would be incorporated in the most recent proposals.)

To go further in obtaining greater neutron fluxes for experimental purposes, it is necessary to overcome the limitations of present reactor types and to find new reactor concepts that are more amenable to very-high-flux design. After discussing methods by which present limitations can be overcome by relatively moderate design changes, this article considers a number of specific new concepts. Even though several of the new approaches might be able to deliver ~10^{17} neutrons/(cm^2)(sec), they, too, have foreseeable limits. It is likely that a flux greater than 2×10^{17} will never be achieved in a steady-state research reactor. However, if it were possible to "hire" the Jackass Flats hydrogen pumping capability for an occasional—and, indeed, very expensive—hour, fluxes up to 5×10^{17} might be contemplated with reactor designs appropriate for 50 Mw/liter operation. A similar complex (Fig. 1) that uses stored helium to cool a reactor (Fig. 2) might be more attractive from the standpoint of operating cost. Helium would be safer to handle than hydrogen, and there would be a greater variety of reactor materials that can tolerate it.

Overcoming Limitations

The major factor that limits the advance of fluxes in present types of research reactors is the power density, which is restricted by conflicting requirements of heat transfer, heat transport, and core materials. Designs now have coolant flows of 6 to 15 m/sec, core pressure drops of 5 to 10 atm, and core power densities of 1 to 3 Mw/liter. Typical heat-transfer rates are ~200 watts/cm^2, and system pressures are tens of atmospheres to suppress boiling. The materials and heat-transfer technologies do not permit much increase in power density with present reactor concepts. But, for experiment irradiation purposes, we can (1) alter the fissile material to obtain greater neutron-production rates, (2) take greater advantage of geometry, and (3) use the core flux more effectively. These steps lead to consideration of flux traps, core life, criticality, and power shape and their influence on reactor design and operation.

ALTERING THE FISSILE MATERIAL

Per fission yielding ν neutrons, the critical reactor core absorbs ν/k_∞ neutrons, where k_∞ is the infinite multiplication factor of the core. Therefore the excess neutrons produced per fission are $\nu(k_\infty - 1)/k_\infty$. Without parasitic absorption, the maximum value k_∞ can assume is η. Table 1 lists values of $\nu(\eta - 1)/\eta$, which represents the maximum number of neutrons that can be made available per fission, for three fissile isotopes. It is apparent that ^{239}Pu is a very superior fuel in the fast-energy range. Uranium-233 is the best fuel in the intermediate-energy range, and ^{239}Pu and ^{233}U are about equally good in thermal reactors.

Unfortunately, ^{235}U is the most available fuel and is used preferably. Its use in an intermediate-reactor core results in only half as many neutrons being

Digitized by Google

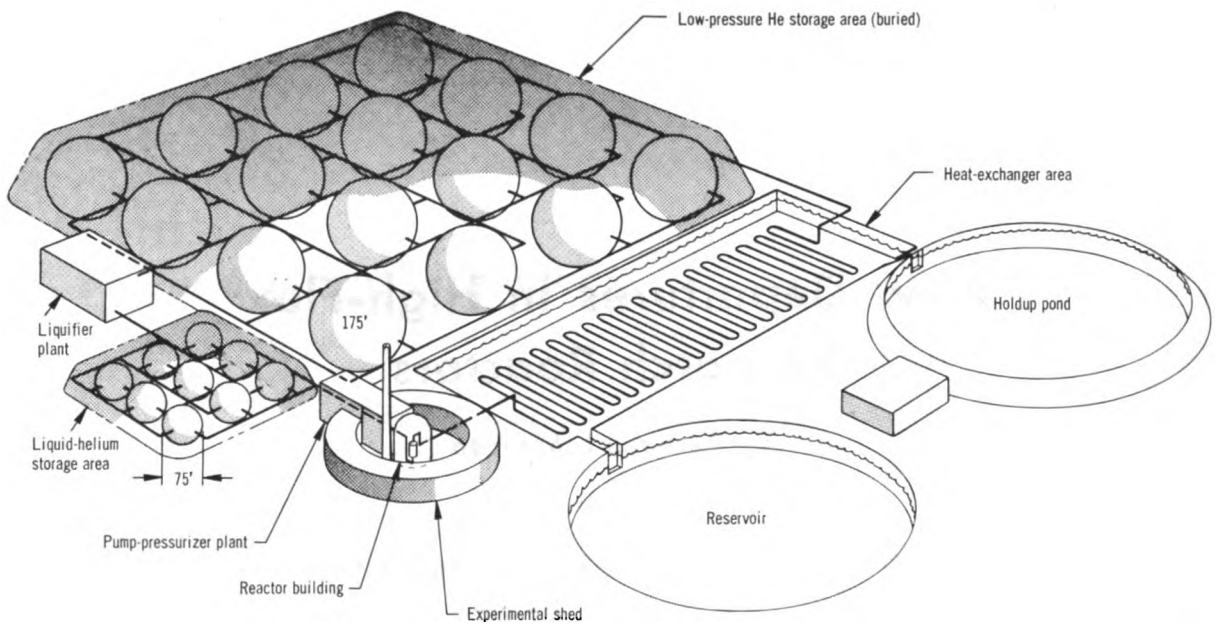

Fig. 1 Helium system for cooling reactor (Fig. 2) that might produce 5×10^{17} neutrons/(cm²)(sec). Coolant storage complex might be dubbed "Helium Hill."

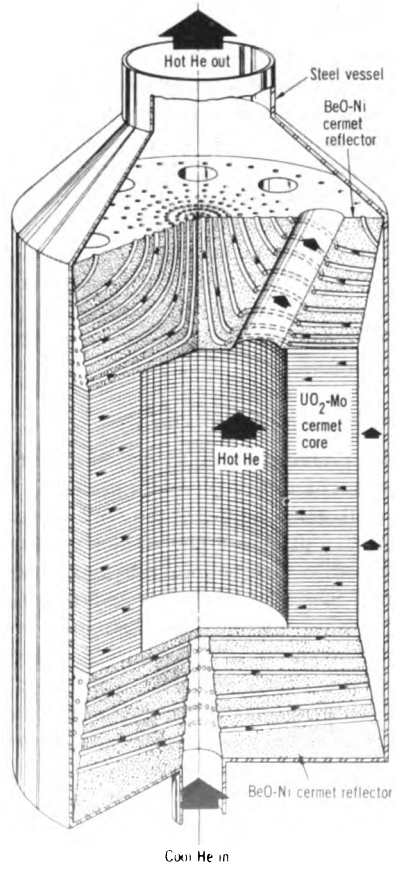

Fig. 2 Research-reactor concept capable of 50 Mw/liter operation to produce 5×10^{17} neutrons/(cm²)(sec).

available as in a plutonium-fueled fast core, and two-thirds as many as in a ^{233}U- or ^{239}Pu-fueled thermal reactor. Uranium-233 is the least available fuel. It would appear worthwhile, therefore, to explore the possibility of using ^{239}Pu, which is plentiful, to fuel research reactors. The desirability of ^{239}Pu is enhanced by its high neutron-absorption cross section at all energies, which makes it rather easy for the infinite multiplication factor to approach η.

Table 1 AVAILABLE NEUTRONS PER FISSION $[\nu(\eta-1)/\eta]$

Energy range	^{233}U	^{235}U	^{239}Pu
Thermal	1.41	1.26	1.43
Intermediate	1.39	0.96	1.28
Fast	1.50	1.41	1.90

TAKING ADVANTAGE OF GEOMETRY

Experiments are generally located in the reflector of the reactor system. To examine the geometrical factors, let us take the reactor as a sphere emitting Q neutrons, and let τ be the reflector age, a the core radius, L the reflector diffusion length, and D the diffusion coefficient for thermal neutrons. To enhance the ratio of thermal neutrons to high-energy neutrons, the experiment is usually located in the reflector at a distance of about $\sqrt{\tau}$ from the core edge. The unperturbed thermal flux is usually within a factor of 2 of $QL/(a+\sqrt{\tau})(a+L+\sqrt{\tau})D$.

The properties of moderators are such that the maximum flux is obtained in light water when $a \leq 15$

Digitized by Google

cm, in beryllium or BeO when 15 cm $\leq a \leq$ 30 cm, and in D_2O when $a \geq 30$ cm. More importantly, the flux increases for each moderator as a decreases—i.e., the diffusion processes merely serve to smear out the basic $1/r^2$ law. With moderator optimization taken into account, the unperturbed neutron flux follows a $1/r$ law up to about 1 m, whereas current (more appropriate for large beam setups) follows a $1/r^2$ law.

Thus it is obvious that the more the source can be compressed the more flux we will have—so the incentive is for high power density.

To some extent this argument may be slightly softened by the use of "external flux traps" or a "neutron hohlraum." External flux trapping, a means of leading more than the geometrical share of neutrons to an experiment, is usually done by putting some hydrogenous moderator around the experiment (when the reflecting material is beryllium or D_2O). In a neutron hohlraum the core and a small quantity of reflector are placed in a large cavity in a block of dense moderator. Even in these cases the advantages of high-power-density cores persist.

USING THE CORE FLUX

Under circumstances where the backgrounds can be made acceptable, it is desirable to get close to the source to obtain high flux for an experiment. In fact, in principle, it is possible to extract neutrons directly from the core. In this circumstance the previous arguments are not valid. Instead, one must examine core criticality and power density more closely.

If the core power density is PD (in megawatts per liter) and the macroscopic fission cross section is Σ_f, then the flux is

$$\phi = \frac{PD}{\Sigma_f} \times 3.25 \times 10^{13} \tag{1}$$

The macroscopic fission cross section is related to the critical mass and volume by

$$\Sigma_f = \left(\frac{N_0 \sigma_f}{A}\right)\left(\frac{M}{V}\right) \tag{2}$$

where N_0 = Avogadro's number
σ_f = the microscopic fission cross section
A = the molar mass
M = the critical mass
V = the core volume

Then

$$\phi = \frac{(3.25 \times 10^{13})\, A}{N_0 \sigma_f} PD \left(\frac{V}{M}\right) = \frac{(3.25 \times 10^{13})\, A}{N_0 \sigma_f} \left(\frac{P}{M}\right) \tag{3}$$

where P is total power.

Thus, to get high core flux, we attempt to attain a highly dilute core (small M/V) or a small critical mass, depending on whether power density or power is limiting. Additionally, we may get high epithermal fluxes by making the core undermoderated, and thereby achieving small values of σ_f. However, this factor is counterbalanced by the fact that critical masses of intermediate reactors tend to be large.

FLUX TRAPS

The ultimate in penetrating the core is to use the flux at its center. This poses no problem for lightly loaded reactors. However, heavily loaded small reactors immersed in a moderator have peak core flux at the outer edge and peak thermal flux in the moderating reflector at ~ 1 root age from the core.

This effect also can be observed in the center of the core. Geometrically, if one takes a slab core and deforms it into a cylindrical or spherical annulus, the thermal-neutron-flux peaks on both sides persist—and one of these peaks now can be at the center of the annulus. This peak is known as a flux trap and has been well investigated.[1–3] The most definitive study is that of Ergen.[4,5] However, it is now well known that the performance of a flux trap depends strongly on core configuration.

The following heuristic points have emerged as a result of the many investigations of moderator islands in research-reactor cores.[6]

- There is a limiting ratio of core-to-moderator blackness, below which no flux peak in a moderator island is possible. This does not mean that experimental fluxes in moderator islands embedded in cores of low absorption are necessarily low; such cores are characterized by already well-thermalized spectra. The flux trap in such cores has degenerated to a simple filter removing virgin-neutron background. Small quantities (dimensions small compared to thermal-neutron-diffusion length in the moderator) of materials such as D_2O or beryllium are optimal. In fact, maximum experimental flux per unit core power density can be obtained from such systems.
- The flux-trap principle peaks the thermal-neutron flux most dramatically when cores of high blackness to thermal neutrons are used, which means that, in the core, thermal-neutron flux is strongly depressed.

It follows from these two principles that the actual value of thermal-neutron flux in the center of a moderator island only mildly depends on core blackness and, in fact, is higher for cores of low blackness: the flux produced by thermalization of fast neutrons in the island is essentially additive to core flux.

The preceding argument assumes that "other things are equal." In practice, other things are not equal. For example, two idealizations of the moderator island assume that (1) the total source strength is constant (i.e., fast-neutron current at the edge of the island = $Q/4\pi a^2$, where Q is the available neutrons) and (2) fast current is constant at the edge. It turns out that geometrical factors prohibit flux peaking in

Digitized by Google

the former case, which is appropriate to large power-limited cores. Per unit source the maximum flux is attained with a vanishing island. However, the source entering a small island is more nearly described by a constant entering current from a power-density-limited reactor (Case 2). Nevertheless, this current may be made somewhat larger by maximizing the inward leakage to the flux trap relative to outward leakage. To do this:

- The core should be as thin as possible.
- The core should be externally reflected by a good fast-neutron reflector, particularly one with a high scattering cross section for epithermal neutrons. Beryllium and nickel are recommended.

These two arguments can also be arrived at by simply examining the contribution to fast-neutron current entering the island from fission sources originating at various points in the core. The contribution is greatest for sources close to the island and can be somewhat enhanced by a good external reflector. The two points of view are therefore functionally related.

So far, we have not commented on steps to maximize flux within the island. The following points should be considered:

- The "fast" neutrons leaking in should actually be as soft as possible.
- The neutron-absorption cross section of the flux-trap medium should be low, and the diffusion coefficient for thermal neutrons in it should also be low, to permit high flux buildup and to inhibit thermal-neutron migration from trap to core.

All these criteria are difficult to satisfy at once. For example, H_2O, D_2O, and beryllium can all function as flux-trap media of approximately equal efficiency, but the dimensions of the optimum trap vary greatly and the optima emphasize different properties of the media (the low age and thermal-neutron-diffusion coefficient of water, the low absorption by D_2O, and the intermediate properties of beryllium).

Although, ideally, the flux trap is completely surrounded by core, in practice not too much harm is done by penetrating the core with a beam tube. As with irradiation experiments, not too many neutrons must be extracted by means of a beam or the flux will be depressed. About half the neutrons in the trap may be used.

CORE LIFE AND REFUELING

Very-high-flux research reactors will operate at quite high power — 100 to 1000 Mw, and maybe even more. At these powers, fissile fuel is destroyed quite rapidly. At 100 Mw, about 1 kg is destroyed in 10 days, and at 1000 Mw, in 1 day.

For fluid-fuel reactors the problems of burnup are solvable by straightforward engineering.

For fixed-fuel reactors the rapid attrition of the fuel profoundly affects reactor design, both (1) because it is desirable to have operating time long compared to refueling time and (2) because of the changes in core characteristics due to having a time variation in fuel and poison concentrations. Conventional techniques [as used at the Materials Testing Reactor (MTR), the Engineering Test Reactor (ETR), and CP-5, for example] embody a refueling operation, performed after the reactor has been shut down and permitted to cool off, in which the fuel elements are replaced gradually and one at a time. The reloading shutdown takes 2 days to a week, depending on the cooling time adopted, the mechanisms available, and safety restrictions adopted. Thus cycle times of 20 to 70 days are necessary to achieve 90% operating time.

Even with a short time — 20 days — and a 100-Mw power, 2 kg of fuel is burned. Because thermal reactors are characterized by critical masses of 1 to 5 kg, this means that something of the order of an extra critical mass must be provided initially. (Actually, it is desirable economically to provide initially two or three extra critical masses so that core fabrication can be amortized over a longer period.)

Control System. The large overload of fuel requires that there be an elaborate control system. The fresh core must be held down, either by burnable or movable poison or by controlling leakage. Since leakage neutrons are what the experimenter wants, the latter method should be preferred, especially since core poisons additionally restrict neutron availability per unit power. Unfortunately, reactor designers have so far chosen the "conventional" approach of control rods rather than the "unconventional" one of reflector motion — to the experimenter's disadvantage.

To fulfill the requirements of core life, several expedients are, fortunately, available. In addition to the use of fluid fuel, which has several obvious advantages for the long run, two points may be capitalized:

1. Intermediate- and, particularly, fast-reactor cores show relatively less reactivity swing over a large fractional core burnup. This not only makes control generally easier but also makes it more feasible to adopt leakage control. Moreover, such reactors do not show large xenon-buildup effects when shut down briefly.

2. There is no physical reason for not having brief shutdowns for partial refueling, or, in the limit, designing for on-line refueling. The required engineering development to permit this, and to satisfy appropriate safety requirements, must ultimately be done.

CRITICALITY AND POWER SHAPE

Up to this point we have assumed that the high-flux reactor core can be made critical with an assumed volume, reflector material, configuration, and low parasitic core absorption. But this is not always the

Digitized by Google

case. Nearly all reactor types of potential utility can be made critical in volumes of 100 liters or more. However, attempts to capitalize on geometric factors by going to smaller cores require a progressive restriction of reactor type, and the smallest cores must be either proton-moderated or fast—a fact well illustrated in the choice of concepts for development as space nuclear power reactors.

Small cores pose another problem. They tend to be relatively black to low-energy neutrons. Therefore, when immersed in a pure moderator, they see a large reentrant low-energy flux, which creates a power spike at the interface. Although this is desirable experimentally—it produces neutrons close to the experiment—it is undesirable from the viewpoint of the core designer on three counts: (1) the power spike is a region of unusually high burnup and thus is not constant over life, (2) it limits total system power because the maximum power density is at the spike, and (3) the spike is likely to consist largely of epithermal fissions, the energy range least productive of experimental neutrons.

Consider New Concepts

The most compact reactor systems that can be made critical are the proton-moderated thermal reactors and fast reactors. In view of our familiarity through experience with them, water-moderated and -cooled reactors should be considered first.

SMALL-CORE H_2O REACTORS

There exists a body of information on the critical properties of these systems with H_2O reflectors (p. 182 ff in Ref. 7). As practical solutions, with fission products, ^{236}U, etc., water-reflected reactors can be made to go critical in a variety of sizes. Cores from 20 to 100 liters in volume all would require < 3 kg of ^{235}U and would be quite thermal in their power spectra. A small core might have a 20-liter volume, a k_∞ of 1.68, and a ^{235}U concentration of 100 g/liter; a middle-sized one would have $V = 50$ liters, $k_\infty = 1.40$, and $c = 36$ g/liter; a large one, $V = 100$ liters, $k_\infty = 1.25$, and $c = 25$ g/liter.

These cores would all be power-density limited. The "figure of merit," power times availability factor times geometry factor, could be approximated by $[\text{volume}/(r+6)^2]\,[(k_\infty - 1)/k_\infty]$. The results for the three sizes are almost identical.

Beryllium Reflector. The substitution of beryllium for H_2O as reflector would reduce critical-core radii by 6 to 7 cm. The result would be to permit a critical volume of ~20 liters at a k_∞ of ~1.39 and a volume of ~7 liters at k_∞ of ~1.7.

The smaller beryllium-reflected system may be profitably examined. For one thing, high power densities are more readily attained in small sizes than in large ones. Moreover, more concentrated systems can tolerate structural neutron poisons more readily than can dilute ones.

Although I have computed 7 liters as critical volume, reduced water density at power makes 10 liters a safer volume for a reactor of $k_\infty = 1.7$ and $c = 100$ g/liter. At 10 Mw/liter and a flow area of 50 cm^2 in the outlet pipe, this would have, as a homogeneous reactor with allowed temperature rise of 200°C, a coolant flow velocity of ~25 m/sec in the piping. The realization of such a reactor would probably be as an aqueous slurry.

Fluxes at beam locations would be several times 10^{15}. The major problems would be slurry circulation, radiolysis, and radiation damage to the container. It is probable that these could only be solved by using disposable (or, at least, dismountable) quick-connect primary components.

HEAVY-WATER REACTORS

A crucial difficulty with light-water reactors is that, unless they are quite small, the critical mass of fuel must compete with a significant quantity of water absorber for neutrons. Systems of more relaxed size—100 liters or more—have a low k_∞ and thus a small availability of excess neutrons per unit power. If one wants to keep the bulk of the fissions in the thermal range and yet have a large-volume core, the obvious step is to replace light water by very weakly absorbing heavy water.

A practical heavy-water core, with some fission products and xenon, could go critical at a 100-liter volume with a k_∞ of 1.88 and a ^{235}U concentration of about 6 g/liter. This is as estimated for a D_2O reflector, which is a convenient experimental medium. If, in some way, 1000 Mw could be extracted, the mean thermal flux would be greater than 4×10^{16}, and the peak would approach 10^{17}.

The core would, as a sphere, have a radius of slightly under 30 cm. At an experimental point 40 cm from the core center, the current would be about 1.8×10^{15} neutrons/(cm^2)(sec), and the small-beam flux would be close to 6×10^{16}.

The great improvement over the light-water system comes from several factors: (1) the artificial one of this article—had I chosen 200 Mw at 10 Mw/liter or 100 Mw at 5 Mw/liter, 20 liters would be the optimum-size core (although D_2O systems can be made critical at this size, their concentration approaches that of H_2O systems), (2) the higher k_∞ of D_2O cores makes them more productive of experimental neutrons for a given power, and (3) the higher flux/current ratio of D_2O reflectors, which again becomes apparent only in large sizes.

In summary to this point: D_2O systems with core sizes up to 100 liters have intrinsic neutronic advantages over H_2O reactors. If 10 Mw/liter core power can be attained, D_2O reactors are very attractive.

The low critical concentration—cited as 6 g/liter—makes it feasible to reconsider solution cores for this concept.

Digitized by Google

Central Zone. The very high core fluxes also make it attractive to consider locating experiments in an unfueled central zone. The peak core thermal flux for a constant-power reactor occurs with the core of minimum critical mass. According to my estimate this would occur with a core of ~120 liters—only slightly larger than the one just postulated—at which size the critical concentration would be 5 g/liter. A 10^{17} flux would be attainable in a central D_2O tube in such a reactor. (Not yet a flux trap; in D_2O it takes a very "gray" annular core and a large gap to develop maximum flux.)

The flux in a homogeneous reactor can of course be improved further by on-site fuel processing to remove fission products, with a consequent decrease in critical mass; this can be done for this reactor. There is only one other engineering problem that was not mentioned in the discussion of high power density from homogeneous reactors—the problem that all structural parts, including core pot and entrance pipes, must be very weak neutron absorbers. Otherwise, the virtues of the low absorption in D_2O would be seriously compromised. Materials such as beryllium, BeO, carbon, and magnesium, with zirconium as a possible cladding material, must be used.

As a possible alleviation of the high pipe flow rates, an "octopus" or "dodecapus," as sketched in Fig. 3, might be used. Such a reactor would have neutron production to some extent in the arms; and I can think of no easy way to figure out its real critical properties.

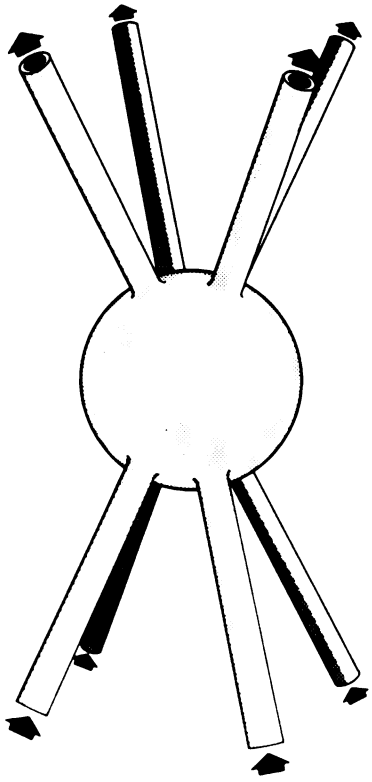

Fig. 3 Octopus-style homogeneous reactor would distribute out-of-core flow over four loops.

SMALL FAST REACTORS

Concentrated fast reactors are the smallest that can be made. For example, the critical mass of a ^{235}U sphere in a tub of H_2O is only about 23 kg (p. 582 of Ref. 7), corresponding to a core volume of 1.225 liters and a core radius of 6.64 cm. In D_2O the critical radius is ~5.6 cm. Even a bare sphere (such as Godiva) has a radius of only 8.4 cm. Plutonium spheres are even smaller; a high-density plutonium sphere in a thick beryllium reflector has a critical radius of < 3.2 cm.

These systems thus approach the "point source," and so the possibility of capitalizing on geometry must again be examined.

Selecting a point at radius 15 cm in a beryllium reflector as our experimental location, and assuming that a plutonium source has $\nu = 2.9$ and $k_\infty = 2$ (to account for the rather large fraction of epithermal fission), we have a net neutron availability of 4.7×10^{16} neutrons/Mw, a neutron current of 1.66×10^{13}/Mw at the experiment, and a thermal-neutron flux of almost 3×10^{14}/Mw.

A conservative example of the virtue of this system is illustrated below. It is conservative because performance could be markedly improved through use of plutonium and incorporation of very primitive internal cooling.

Let us consider a concentrated uranium sphere immersed in a 5-cm-thick sphere of H_2O. The critical radius would be under 7 cm, and the total assembly radius[7] would be 12 cm. The thermal conductivity of uranium is good enough that this assembly could operate at 8 kw for a uranium temperature rise of 200°C. At this power, given $k_\infty = 2.2$, the beam current from the water surface would be 1.9×10^{11} neutrons/(cm^2)(sec). In a graphite hohlraum this current may be somewhat intensified. This beam current is about what one would get from a 10^{12} flux research reactor—admittedly, not a high-flux system, but extremely good performance when compared with a 100-kw swimming pool! When such a reactor is opened for cooling, it can still be quite small. We consider now the next largest size, that of the Experimental Breeder Reactor I (EBR-I)[8] and Clementine.[9]

The EBR-I, as an example, has a core of a little over 6 liters, corresponding to a sphere of ~11-cm radius. With a most conservative cooling system, it produced 1 Mw of power. Its k_∞ was about 2.1.

Sodium Coolant. We now know how to achieve power densities of 1 Mw/liter in large sodium-cooled fast reactors, and so it would be straightforward engineering to do the same for a 6-liter fast reactor. The use of beryllium instead of uranium for the blanket would markedly increase reactivity, making it pos-

Digitized by Google

sible to use smaller rods and more sodium in the core. So a power density higher than 1 Mw/liter can be predicted for this type of system. Sodium coolant flow of 15 m/sec seems possible, and, at 30% core porosity and 10-cm core radius, this would amount to a mass flow rate of 115 kg/sec. Because heat capacity is ~1.25 joules/(g)(°C), a temperature rise of 400°C would permit a power of 57.5 Mw, or almost 10 Mw/liter.

Short Core-Residence Time. The key to this high power density is the small core size, which permits the coolant to have a very short core-residence time. Of course, all the numbers cited are advances over current practice (EBR-II, for example, has a core 2.5 times as long, sodium velocity ½ as great, and temperature rise ⅓ to ¼ as much, in achieving somewhat less than 1 Mw/liter). Nevertheless, the sodium route is one of the more straightforward ways of achieving high power density.

At 60 Mw in a 10-liter ^{235}U-fueled core with a beryllium reflector, we might achieve $k_\infty = 2.1$. With an experimental position at 24 cm, the experimental current would be 3.4×10^{14}, and the small-beam flux, around 7×10^{15}.

Hydrogen Coolant. A somewhat larger core could undoubtedly be built of refractory materials. We have investigated tungsten–UO_2 cermet fast-reactor systems for nuclear-rocket application. At about 50 liters and up, it becomes possible to extract 1000 Mw from them when the coolant is hydrogen, which can achieve high flow rates in small passages without unusual pressure drop and has a very high heat capacity per unit weight. The refractory core permits the heat source to sustain a high driving temperature difference for heat transfer to the bulk coolant.

Such a system — 1000 Mw, 20-cm radius, $k_\infty \sim 1.8$ — would yield the impressive flux of $\sim 1.6 \times 10^{17}$. Unfortunately, it is probably too costly to supply many cores of this type, and the cost of using hydrogen as a coolant is also extreme — as is likewise the hazard. Nevertheless, it indicates that technology in itself does not limit power density.

CAVITY AND THIN-SHELL REACTORS

It has been often observed, in this article and elsewhere, that a major limit to power density in heterogeneous reactors is a relatively long coolant-flow path through the core. Pressure drop increases with length, and temperature rise is constrained to some maximum. It is for these reasons that smaller cores may have higher power densities.

It is clear that shorter coolant path lengths can be achieved with radial coolant flow. For a more-or-less compact core, only a factor of 2 reduction in flow length is possible, and this is hardly worth the design difficulty. However, there are core types for which the fuel configuration can be a thin annular section. For such cores, quite short flow paths can be realized by radial flow.

The most intriguing of these systems are the D_2O flux-trap cores and their close relatives, D_2O cavity reactors. Several reactor systems of this general sort were investigated some years ago.[10] The basic observation is that, in a large body of moderator (D_2O being the best example), a spherical shell of fuel just thick enough to be black to thermal neutrons will be critical.[4,5] If the shell is made larger, its blackness can be reduced to some limiting value, which is that required for criticality in a thin slab. Moreover, if the interior of the shell is evacuated, only a slight increase in blackness keeps the system critical; and, if the contents of the shell are dispersed uniformly within the sphere (the cavity reactor), again only a little more fuel is required.

Cavity Reactor. The cavity reactor is often conceived in terms of a fissioning gas with temperatures approaching those of plasmas. It is a possible core for plasma-reactor schemes, such as those of Refs. 11 to 13. The cavity reactor may also be fueled with a suspension of fissioning "dust"; as such, it is effectively a gas-phase homogeneous reactor of potential quite similar to that of the large homogeneous heavy-water solution. Problems of corrosion and plateout are replaced by problems of erosion and adhesion.

Thin-Shell Reactor. The existence of thin-shell critical assemblies presents a more novel reactor concept. Figure 4 illustrates a possible configura-

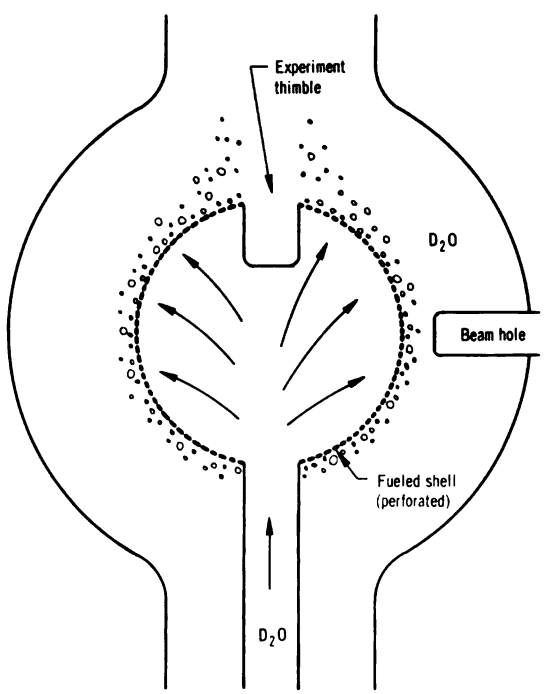

Fig. 4 Colander type D_2O thin-shell reactor.

Digitized by Google

tion: The core is a thin shell of a strong fueled material—such as a stainless-steel–urania cermet. This shell is perforated with a very large number of small holes, possibly drilled or punched at the time of fabrication, and probably clad by a chemical or electrochemical technique. The shell has at least one reentrant thimble for high-flux irradiations and a stem for coolant entry. Coolant is pumped in, forced through the holes of the colander, and dumped into the main moderator vessel.

Although the inlet pipe must contain the high flows characteristic of homogeneous reactors and the shell must support significant pressure, the high-temperature outlets of the homogeneous reactor have disappeared, and pressure drops do not approach those of parallel-flow heterogeneous systems. The D_2O may be permitted to evaporate and superheat in passing—it will recondense in the outer tank. (Not shown is the main cooling system, which withdraws warm moderator from the tank and returns part of the cold moderator by downward circulation around the outside of the shell.)

For those who are concerned with the strength of such a colander, an alternate scheme has been proposed.[14] The reactor shell is now solid (Fig. 5). The coolant is dispersed by flow through a nozzle head and impinges on the inner surface of the shell. The velocity of the coolant jets is high enough so that they can cut through the steam which comes off that surface, impinge on it, and be evaporated. The outer surface of the shell would be vapor bound in stable film boiling but not at a high enough temperature to burn out.

Finally, the scheme may be reduced to more conventional terms by reverting to parallel flow in small tubes of some appreciable length. Such a reactor looks like the colander of Fig. 4, with the thin shell replaced by a tubular fueled structure of 2 to 10 cm thickness (and flow length).[15]

The thin shell may also be used in reactors of more normal flow design. D_2O flux traps may be simulated by heterogeneous designs consisting of individual fuel elements spaced around a cylindrical annulus or a pseudospherical "basket." The large radius of optimal D_2O flux traps permits, in fact, enough space for a pressure-tube reactor design, which might make on-line reloading more feasible.

Another version of a thin-shell reactor is one computed by Ergen.[4,5] It seems possible to build a beryllium-moderated version in which the shell contains circulating molten salt. The excellent characteristics of molten salts as possible homogeneous reactor fuels (high permissible temperature rise and high gravimetric heat capacity) make a 100-Mw power for such a system credible. Ergen's calculation predicts a 7×10^{15} central-island flux for this case.

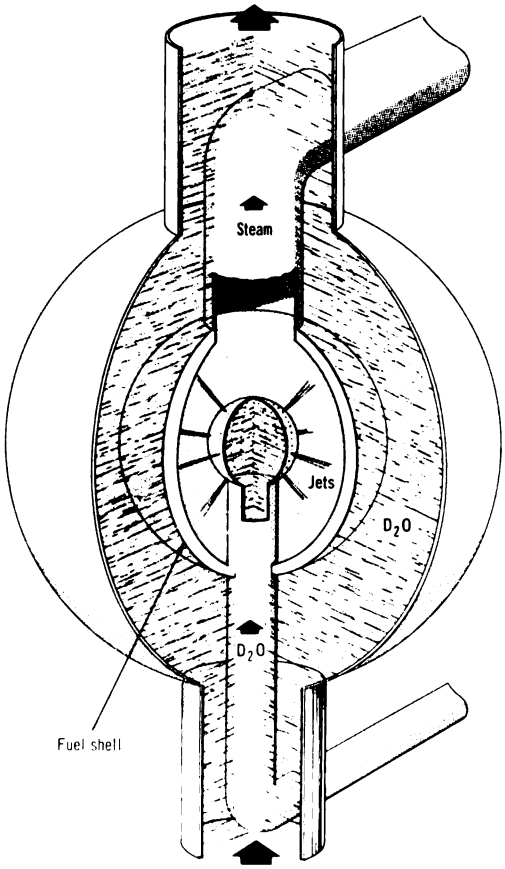

Fig. 5 Sprinkler type D_2O thin-shell reactor.

This article is based on a paper presented at the Symposium on Intense Neutron Sources,[16] Santa Fe, N. Mex., Sept. 19–23, 1966.

References

1. J. W. Webster, A Critical Assembly Having Maximum Sensitivity, USAEC Report IDO-16248, Phillips Petroleum Co., Aug. 31, 1953.
2. M. Osredkar and R. Stephenson, A Low Power, High Thermal-Flux Experimental Nuclear Reactor, *J. Nucl. Energy*, 5: 210 (1957).
3. M. Osredkar and R. Stephenson, Thermal Flux in the Central Moderator Zone of Thermal and Fast Reactors, in *Proceedings of the Second United Nations International Conference on the Peaceful Uses of Atomic Energy, Geneva, 1958*, Vol. 10, p. 174, United Nations, New York, 1958.
4. W. K. Ergen, Homogeneous High-Flux Reactor, USAEC Report CF-58-3-68, Oak Ridge National Laboratory, Mar. 31, 1958.
5. W. K. Ergen, The Highest Thermal Neutron Fluxes Obtainable from Fission Reactors, in *Proceedings of the Second United Nations International Conference on the Peaceful Uses of Atomic Energy, Geneva, 1958*, Vol. 10, p. 182, United Nations, New York, 1958.
6. C. N. Kelber, B. I. Spinrad and L. J. Templin, Advanced High-Flux Research Technology, *Trans. Amer. Nucl. Soc.*, 5(2): 425 (1962).
7. Argonne National Laboratory, Reactor Physics Constants, USAEC Report ANL-5800 (2nd ed.), July 1963.
8. H. V. Lichtenberger et al., Operating Experience and Experimental Results Obtained from a NaK-Cooled

Digitized by Google

Fast Reactor, in *Proceedings of the International Conference on the Peaceful Uses of Atomic Energy, Geneva, 1955*, Vol. 3, p. 345, United Nations, New York, 1956.
9. E. T. Jurney et al., The Los Alamos Fast Plutonium Reactor, USAEC Report LA-1679, Los Alamos Scientific Laboratory, May 1954.
10. G. Safonov, Externally Moderated Reactors, Report R-316, The Rand Corp., July 1957.
11. J. L. Kerrebrock and R. V. Meghreblian, Vortex Containment for the Gaseous Fission Rocket, Report JPL-TR-34-205, Jet Propulsion Laboratory, September 1961.
12. D. F. Spencer, Thermal and Criticality Analysis of the Plasma Core Reactor, Report JPL-TR-32-189, Jet Propulsion Laboratory, January 1962.
13. H. Weinstein and R. G. Ragsdale, A Coaxial Flow Reactor—A Gaseous Nuclear-Reactor Concept, *Amer. Rocket Soc.*, Preprint 1518-60, December 1960.
14. D. H. Lennox, Argonne National Laboratory, personal communication, 1961.
15. J. T. Weills, Conceptual Study of a Spherical Geometry Reactor with a High Flux Central Region, *Trans. Amer. Nucl. Soc.*, 5(2): 437 (November 1962).
16. Proceedings of the Symposium on Intense Neutron Sources, Santa Fe, N. Mex., Sept. 19–23, 1966 (to be published by the European Nuclear Energy Agency).

Digitized by Google

Zone-Loaded Critical Experiments for Fast Breeders

By George J. Fischer, Armando Travelli, and Daniel A. Meneley

Physics uncertainties—among others—limit the technology of the large fast power breeder, a reactor that might be fueled with 2000 kg of plutonium in a 6000-liter core and be capable of 1000 Mw(e). Some of these uncertainties influence safety analyses. Others relate to the behavior of the nuclear fuel over the fuel cycle and influence calculations of such parameters as doubling time and reactivity swing over core lifetime. These uncertainties force appropriate conservative design decisions that tend to lower the economic potential of the fast breeder.

Experiments on zero-power critical assemblies can effectively test the degree of uncertainty of many important calculations. They can also provide useful basic data to help reduce the uncertainties. There are some difficulties involved in straightforward mockup experiments, however. These difficulties will be discussed here; it is largely because of them that zone-loaded experiments are important.

A cross section of the material arrangement of a typical zone-loaded critical experiment is shown in Fig. 1. It is a zero-power critical assembly[1] and contains only a small fraction of the full core of interest. This fraction of the full $^{239}Pu-^{238}U$ fueled large breeder core is mounted as a center zone inside a "driver" region that supplies the additional reactivity needed to achieve criticality. A "buffer" or "filter" zone may be used between these two regions to improve such characteristics as the neutron-energy spectrum near the edge of the center zone. The driver is fueled with ^{235}U, which is more readily available than plutonium.

This article presents the reasons why zone-loaded experiments are important and describes a number of physics questions that can be answered through these experiments. It also discusses the limitations of the zone-loaded method, the safety aspects of this type of critical loading, and the major needs for further development of the concept. An example is given of a critical test of the ability of the analyst to predict full-core reactor properties on the basis of analysis of a zone-loaded critical experiment.

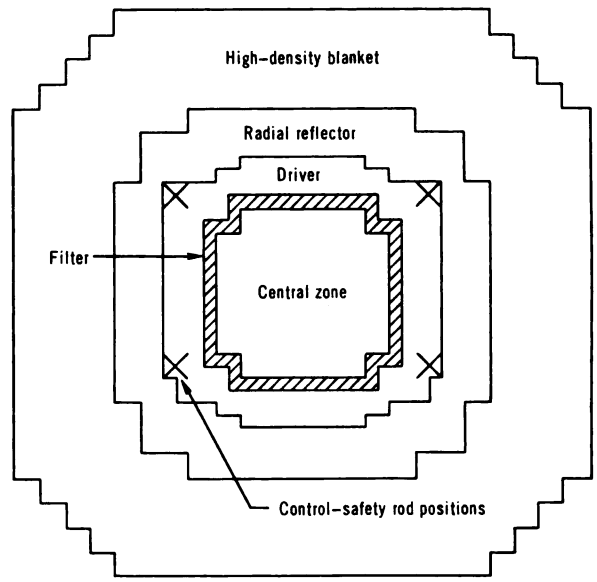

Fig. 1 Cross-section view of zone-loading assembly. Reactor materials are often loaded into matrix tubes of ~2-by 2-in. cross section, which gives the rectangular profile.[1]

Why Zone-Loaded Experiments?

Among the important advantages of zone-loaded experiments are:

- Smaller and presently available reactors such as ZPR-VI (Fig. 2) can be used effectively.
- Much smaller inventories of materials such as ^{239}Pu or ^{233}U fuels are needed in many cases.

Digitized by Google

- Cost of items directly related to reactor size is reduced.
- A program of survey type experiments on zone-loaded reactors could provide important basic data for a range of breeder-reactor compositions, possibly years sooner than these data might otherwise be obtained.
- There may be safety and health advantages to the use of zone-loaded mockups.

Difficulties involved in straightforward full-core mockups are numerous. The 6000-liter core, for example, would require a very large investment in fuel plates and other mockup materials — in amounts that usually are not obtainable at present. (Many nations will be forced into doing zone-loaded experiments because of limited availability of these materials.) Even when the materials are on hand, from 4 to 8 weeks would be needed just to assemble one full-core critical experiment. The radioactivity from ^{240}Pu, fission products, and possibly ^{233}U and its associated isotopes, all or some of which might need to be included, would be a hazard to operating personnel. Decay heat from these materials would induce reactor drift, which could limit the precision of reactivity measurements. Because of the high operating costs for facilities in which zero-power critical assemblies are built and because of the pressing need for experimental data, especially sodium-void and Doppler-effect measurements, it is essential that these facilities be employed with maximum effectiveness.

Physics Needs of the Fast Power-Breeder Reactor Program

Phenomena of particular concern in the difficult area of safety of the sodium-cooled large fast breeder — and comparatively difficult to calculate accurately — are the sodium-void effect and the Doppler effect. For some relatively simple and typical accident calculations that include both effects, sodium expulsion has been calculated to add reactivity at rates of 2 to 100 dollars per second. Addition of 1 dollar of reactivity to a reactor operating at a steady state (delayed critical) makes the reactor prompt critical — a dangerous condition in which the

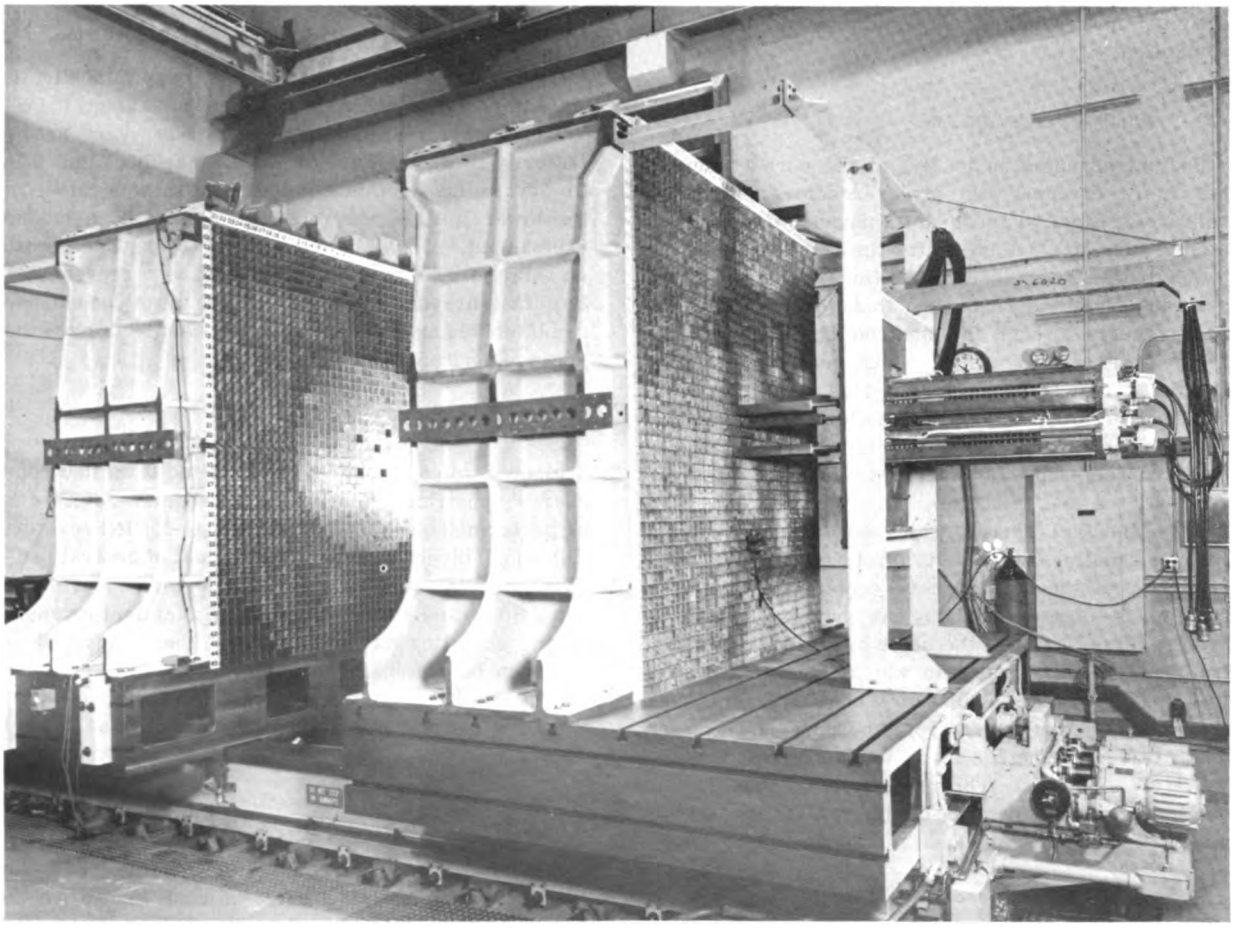

Fig. 2 Zero-power critical assembly ZPR-VI.

Digitized by Google

power doubles every few thousandths of a second. It is very important that careful experiments be performed to check the ability of the theoretician to calculate these two phenomena. In addition, since these effects have been calculated to be highly sensitive to the presence of higher plutonium isotopes, fission products, and the nature of the clad materials, the experiments must include these materials.

THE DOPPLER EFFECT

The Doppler effect is a prompt shutdown mechanism that operates primarily by absorbing neutrons in the energy range from about 1 to 15 kev, the low-energy tail of the neutron-energy spectrum of a fast reactor. This absorption takes place primarily in the fertile atoms, which exceed the fissile atoms by ratios of about 7:1 to 9:1, in the fissile isotopes, and, to a smaller extent, in structural materials. The effect occurs as a response to temperature changes, as in the heating of the fuel during a power surge. An objective of fast reactor designs is to achieve a Doppler-effect shutdown mechanism sufficiently strong that possible gains of positive reactivity upon voiding of sodium would be safely controlled.

THE SODIUM-VOID PROBLEM

Sodium occupies 50 to 70% of the core volume in the more common fast power-reactor designs. A relatively effective moderator because of its modest atomic weight, sodium shifts the neutron spectrum toward lower energies. In addition, sodium also has a large and broad resonance that peaks at 2.85 kev and strongly affects the neutron population in the 1- to 4-kev energy range, which contributes to the Doppler effect. Full or partial loss of sodium coolant, such as might follow pump failure or a transient, reverses these spectral effects. There is thus a spectral component of the reactivity change associated with the loss of sodium.

This spectral change which accompanies sodium voiding usually adds reactivity. Loss of sodium in a region about the reactor core center of some large fast power-breeder designs can increase reactivity by several dollars. On the other hand, loss of sodium from any reactor region in which there is a spatial flux gradient (as near the core boundary) increases the leakage of neutrons from the core and thereby tends to reduce the reactivity in competition with the spectral component. This reactivity change is the other component of the sodium-void effect and is called the leakage component.

OTHER NEEDS

In addition to the sodium-void and Doppler effects, there are many other uncertainties to be resolved. The theoretical physicist would like to check his cross-section choices for the materials in the reactor by means of material-worth measurements and of neutron-energy-spectrum measurements. He would like to check the reliability of some of his simplifying assumptions and procedures, such as the spatial dependence of his cross sections, heterogeneity corrections, choice of transport approximations, coupling between modules for a modular concept, and the change of this coupling with reactor operation. There are engineering problems that are sometimes difficult to calculate or important to verify. These include worths of partially inserted rods and effectiveness of shielding, for which additional approximations must be introduced and checked.

Plutonium became available for zero-power fast critical experimentation only a few years ago. Because physicists associated with the critical assemblies employing plutonium were required to devote a large part of the assembly availability time to mockup experiments, very little good basic experimental work on the reactor physics of plutonium–uranium fueled fast reactors exists.

Usefulness of Zone-Loaded Experiments

The central zone of the assembly[1] shown in Fig. 1, Assembly 45A of ZPR-III, mocked up a large ^{239}Pu–^{238}U monocarbide fast breeder reactor very satisfactorily with the use of only 51 kg of ^{239}Pu. The 21-cm radius of this central zone may be close to the lower limit of what is desirable on a zone-loaded experiment. A cylindrical geometry was used, with an axial core length of 91 cm chosen as a representative fast breeder core height. The zone-loaded assemblies discussed here will be assumed to have the arrangement of this assembly.

MEASURING NEUTRON-ENERGY SPECTRA

Many physics measurements related to the neutron-energy spectrum of large fast breeder reactors can be performed satisfactorily in a zone-loaded reactor. The most direct measurement is that of central neutron spectra. The experiments performed by Bennett, Gold, and Huber[2] provide an excellent example of the accuracy and resolution of the spectral data that can be obtained from a zone loading. Valuable energy-spectrum measurements in the direction of the axial blanket are equally possible in zone-loaded cores.

MEASURING SODIUM-VOID EFFECTS

Sodium-void measurements of several types can be performed satisfactorily on zone-loaded reactors.[1,3,4] The spectral component of the sodium-void effect is easily measured at the center of the zone loading, as are variations in the spectral effect due

Digitized by Google

to composition changes. Also straightforward are measurements of the important effects of channeled loss of sodium (related to the accidental voiding of a fuel subassembly). The leakage component of the sodium-void effect in the axial direction may also be measured. These experiments should be limited to one or more channels around the axis of the reactor. They frequently are sufficient to verify theoretical methods.

Care must be taken, of course, that the flux perturbations due to any measurement, especially if made at some radial distance away from the axis of the central zone, do not extend to a region where the neutron spectrum is affected by the buffer and driver zones. Although these effects might be compensated for to a considerable degree, it is always desirable to keep the measurement as free from uncertainties as possible.

As another precaution, the analyst must remain aware of the possibility that, in the approach of first-order perturbation theory, the denominator term

$$\int \left\{ \left(\sum_j \phi_j^\dagger \chi_j \right) \times \left(\sum_k (\nu \Sigma_f)_k \phi_k \right) \right\} dVol$$

may change upon removal of sodium over a significant region of the central zone.

MEASURING THE DOPPLER EFFECT

Doppler-effect measurements have been made at or near the center of the zone loadings of the ZPR-III reactor on Assemblies 43, 43A (Ref. 5), 45, and 45A (Ref. 1) and in zone-loaded Assembly 4Z of ZPR-VI at Argonne.[6] Atomics International has performed Doppler-effect measurements in zone-loaded assemblies that employed thermal drivers.[7] All these measurements used small samples, which allowed much freedom in such matters as the nature of materials that surrounded the samples to be heated.

Experimental difficulties in Doppler-effect measurements made thus far in zone-loaded assemblies are only in small part different from the difficulties that would be found in equivalent measurements on nonzoned assemblies. Particular care must be taken, however, in attempting to measure the change in Doppler reactivity effects when sodium is removed from the environment surrounding the heated sample. It is very easy for the domain in which the sodium is removed to become sufficiently large that the Doppler element "sees" the presence of the buffer zone.

With moderate care, multiple-sample and "pot" type Doppler-effect measurements should be successful in zone-loaded assemblies.

KINETICS STUDIES

Rossi-alpha type kinetics measurements can be performed in zone loadings and apparently can be interpreted to predict the full-core kinetic characteristics with considerable confidence.[8] This property was demonstrated first in ZPR-III experiments on a coupled fast thermal-reactor concept,[9] a form of zone loading.

EQUIVALENCE TO MODULAR FAST BREEDER SYSTEMS

The physics of the modular concepts can be related clearly to the physics of the zone-loaded concepts. The radius of the central zone can be increased so that its reactivity grows, and the nature of the buffer zone can be changed to approximate the blanket region between modules. By letting the driver region, now with perhaps the same fuel as the central zone, represent a simplification of the modules external to the central module, we achieve a "zone-loading" representation of the modular concept which is particularly amenable to analysis. Much of the statics and dynamics of the physics of interaction of the modules could be checked by this type of experiment. For instance, the change of the coupling between the modules with coolant loss or fissile isotope buildup in the blanket could be measured readily.

EQUIVALENCE TO FUEL-IRRADIATION FACILITIES

Some proposed fast reactor fuel-irradiation facilities are, in a sense, zone-loaded reactors. They frequently employ a central region containing fuel elements whose irradiation characteristics are to be learned, a buffer region to shape power distribution or neutron-energy spectrum, and a driver fuel chosen largely for its power density, burnup, and fabrication characteristics. Thus techniques learned during zone-loaded critical-assembly design can be useful to designers of fuel-irradiation facilities.

Limitations of Zone-Loading Procedures

A not unimportant difficulty of the zone-loading procedure as compared to the single-zone procedure is that the physicist must be more careful about the design and interpretation of some experiments. For example, the removal of sodium from a large portion of the central zone is an experimental variation that must be attempted only with caution. For such an experiment the best choice of buffer-zone composition becomes a matter of concern. For certain regions, transport-theory calculations may predict spectrum distributions significantly different from those predicted by diffusion-theory calculations. Greater care must be taken in the procedure for collapsing multigroup cross sections from ultrafine data because the spectrum over some of the groups may change considerably within short distances. However, awareness of these difficulties should assure satisfactory interpretation of zone-loaded experiments.

Digitized by Google

ESTIMATING REACTIVITY CHANGES

Another difficulty arises in trying to predict from the result of a reactivity measurement in a zone-loaded reactor the result that the same measurement would have yielded if it had been made in the full reactor that the center zone of the zone-loaded reactor represents. A simple example of this difficulty is found when a reactivity measurement is to be made at the center of the zone loading and when a perfect match of real and adjoint neutron-energy spectra with the corresponding spectra in the single-zone reactor has been achieved over the region of the reactor affected by the perturbation. A satisfactory approximation to this condition is achieved relatively easily with careful design of the zone loading.

If this measurement were to be interpreted by means of first-order perturbation theory, the expression for the perturbation of k would be

$$\frac{\Delta k}{k} = \frac{\sum_{i,j} \int_{\text{reactor}} \phi_j^+ \Delta[\chi_j \nu_i \Sigma_{f_i}/k + \Sigma_{i\to j} - \Sigma_{t_i} \delta_{i,j}] \phi_i \, dVol}{\sum_{i,j} \int_{\text{reactor}} \phi_j^+ [\chi_j \nu_i \Sigma_{f_i}/k] \phi_i \, dVol} \quad (1)$$

where all terms have their usual definitions. Both integrals extend over the entire reactor, but, of course, the terms in the numerator are nonzero only over the regions in which the perturbation is made. With the assumption that the real and adjoint fluxes in the zone loading match those of the full core over the region of the perturbation, the only difficulty in relating worth measurements made at the center of the two cores lies in the calculation of the denominator terms for the two reactors. For the full core this calculation is relatively straightforward. For the zone loading, each of the zones adds several sources of uncertainty. The results of an investigation of some of the more difficult calculational aspects of this problem are given in the subsection entitled "A Test of the Zone-Loading Method."

ESTIMATING CRITICAL MASS

The critical mass of a large fast power breeder cannot be directly determined by a zone-loading experiment. However, this is not necessarily a severe limitation. Many large power breeders will employ several zones of different enrichments to provide power flattening. Small changes in the location of the interfaces between the zones will result in criticality of the actual reactor. Many important indirect questions (e.g., material worth and detailed neutron-energy spectra at the core center and near the axial blanket) used to check the ability to calculate critical mass can be answered very well by a zone loading. Again, recent cross-section measurements and refinements in multigroup cross-section preparation procedures have improved the ability to estimate critical mass. Whereas errors in predicting critical mass were 30 to 40% for difficult cases a year or two ago, errors larger than 10% may be expected to be relatively unusual in the near future. The problem of predicting the critical mass of a large reactor by zone-loading procedures has been treated with some success recently in France.[10]

Safety Aspects of Zone-Loaded Critical Experiments

It would be thoroughly misleading to pretend that the issue of safety of zone-loaded critical experiments, even relative to that of full-core loaded reactors, can be adequately treated in a few sentences. The statements made here are intended only to point out important aspects of a complex problem.

A full-core (nonzone loaded) loading on a zero-power critical reactor can require from several hundred to several thousand kilograms of highly toxic plutonium fuel. If, in spite of the very considerable precautions taken in the design and operation of these reactors, a severe accident were to occur (definitely a highly improbable event), the containment of the reactor might be ruptured and very dangerous materials dispersed for several miles downwind. For this reason, operators of fast reactor critical experiments give much attention to safety.

An obvious aspect of the relative safety of the two types of experiments is that the zone-loaded reactor would contain 50 to 200 kg of ^{239}Pu in the central zone, approximately one-tenth as much as the full-core reactor mockup. The driver region of the zone-loaded core usually would be fueled with 200 to 300 kg of the far less toxic ^{235}U.

SHUTDOWN MECHANISMS

An important prompt shutdown mechanism of the critical assembly comes from the Doppler effect. This is achieved if the fertile ^{238}U is mixed with the ^{239}Pu in a ratio of about 3 : 1 when the fuel plates or rods are fabricated and if the assembly is composed of such other materials that the real and adjoint neutron-energy spectrum in the kiloelectron-volt region is sufficiently large. This second requirement may not be satisfied. It is especially difficult to provide an adequately soft spectrum in the driver region of a zone-loaded assembly. Furthermore, the driver fuel of older reactors may consist of ^{235}U separated from the ^{238}U. Under these conditions the ^{235}U will undergo many more fissions than the ^{238}U and therefore will heat more rapidly during an incident. Any Doppler effect in a driver of this type might add to the reactivity rather than subtract from it because of the generally positive nature of the ^{235}U Doppler effect.

Separated driver fuel, however, has better reactivity-loss characteristics through expansion on heating than does mixed driver fuel.

Digitized by Google

A Test of the Zone-Loading Method

How well can reactor analysts use data from a zone-loaded reactor experiment to predict the results for the same measurements in the full nonzoned core? We were recently given the opportunity, and challenge, to make such an analytical study and prediction. Although the success of the analytical prediction made for our test experiment does not assure the credibility of all analyses of zone-loading experiments, the study demonstrates that successful predictions of the properties of large fast breeder reactors can be based on zone-loaded experiments.

We were asked to analyze zone-loaded Assembly 4Z (in ZPR-VI) and to predict the results of the more crucial subsequent experiments on Assembly 5, a single-zone 2600-liter core of the same composition as the zone-loaded core. The assignment was resolved into several parts. One study was that of the deviation from the "correct" answer which results from the simplifying assumptions an analyst frequently makes in the course of his work. Examples of these approximations are the use of diffusion theory vs. transport theory and the use of one-dimensional calculations vs. the much more costly multidimensional calculations. A second study concentrated on the difficulties of evaluating the denominator terms of Eq. 1. Because of the nature of the construction of Assembly 4Z, it was evident that the accuracy of any prediction of Doppler, sodium-void, or other worth measurement would be sensitive to how well this term was calculated. The third objective was to predict the critical mass of Assembly 5. Much of the detail and physics of these studies has been published.[13] Only a summary of the results is given here.

A number of interesting results were obtained from the first study. It was shown that transport theory predicted very different behavior of the neutron flux, in certain energy intervals, near the edge of the central zone and through the filter and driver regions. The ^{238}U fission activity was significantly different, so that, if Assembly 4Z had been a fuel-irradiation facility, diffusion theory would have rather poorly predicted the power density due to ^{238}U fission. Other results showed cancellations of detail effects in Assembly 4Z, in some cases, which would help generate false confidence in the predictions of simpler methods.

In the important area of predicting analytically the worths of measurements of reactivity made at the center of the full core from those at the center of the zoned Assembly 4Z, it was predicted that the ratio of these worth measurements would be a constant and that the value of this constant would be 1.003. (Heterogeneity effects in the driver were not accounted for in the prediction because of the complexity of the geometry used.)

It was also predicted that the critical mass of the core of Assembly 5 would be 1664 kg of ^{235}U, with an uncertainty of ±150 kg mainly due to uncertainties in the cross sections used in the calculations.

These predictions were tested when Assembly 5 was built. It was found that the weighted average of the ratios of the reactivity worths of a large number of materials measured in the two assemblies was 1.003 ± 0.002, against the predicted value of 1.003. This agreement must be considered partly fortuitous. The experimental critical mass, corrected for edge effects, was close to 1580 kg of ^{235}U, 84 kg less than predicted but well within the estimated uncertainty of the calculation.

VIOLENT DISASSEMBLY

The most improbable but also the most severe accidents are those for which all other accident-termination mechanisms have failed and the accident is shut down by violent disassembly. The acceleration of material is caused by gradients in the hydraulic pressure generated by heating of reactor material, especially the fuel, which may melt or vaporize. The local pressure in a region is usually proportional to the power density there.

If a nonzoned large reactor is mocked up on the facility at the time of the accident, it may be the type that employs several regional fuel enrichments to obtain a flattened (economically desirable) power distribution. The flattened power distribution, however, leads to very small pressure gradients in a severe accident. Thus disassembly and shutdown of nuclear multiplication processes would be achieved only after large amounts of nuclear energy had been released.

A safety aspect of common zone-loading designs of the form represented by Fig. 1 is that they frequently are constructed, for practical reasons, with power densities in the driver zones which are from 1.5 to 3 times larger than those of the central zone. Thus, during a severe nuclear incident, very large pressures would occur, most probably, in the driver zone well before they would occur at other locations. Also, there usually is a large gradient in power density across the driver in the direction away from the reactor center, a very desirable safety characteristic. We have studied the neutronic and hydrodynamic behavior of several zone-loaded fast reactor experiments for severe accident conditions. The accident code Ax-1 (Ref. 11) and a more recent ANL code, PREAX,[12] able to handle meltdown histories as well as severe accidents were used. The calculations show that initial high pressures in the driver region begin to drive the inner boundary of the driver toward the center of the core (a reactivity-adding mechanism) and at the same time to drive most of the remainder of the driver outward (a reactivity-losing mechanism). A very short interval of time over which the reactor gains a very small amount of reactivity was seen, followed by a relatively rapid shutdown.

Because of the high power density of the driver, disassembly pressures in the driver region began early in the history of severe accidents calculated for zone-loaded reactors. Since small displacements of the driver produced rapid reactivity loss, nuclear-

Digitized by Google

energy release for accidents in zone-loaded reactors tended to be smaller than for comparable accidents in critical assemblies mounted with the equivalent full-core loadings.

Broad generalizations of this type, of course, must not be used to conclude that all zone-loaded experiments are inherently safe. This problem deserves much more careful attention than it has received.

Improvements Needed

Limited inventories of nuclear materials, especially isotopes of plutonium, make zone-loaded experiments the only available experimental means for many laboratories to study large fast power-breeder reactors. For others, the technique is an exceptionally useful research procedure. For these reasons, it is important to continue to extend the understanding and capabilities of the procedure.

Some rather basic practical questions have not yet been adequately resolved. An example is the question of what minimal amount of plutonium fuel, containing a varied enrichment of higher isotopes, should be purchased to study satisfactorily the physics of large power breeders having this fuel composition.

BETTER CROSS SECTIONS

Particularly needed for successful analysis of zone-loaded assemblies is an analytical tool which would produce spatially dependent multigroup cross sections from ultrafine cross sections and which would take into account the flux-perturbing presence of materials in adjacent regions. One such procedure is being developed by D. Meneghetti, A. Rago, and K. Phillips at Argonne.

HETEROGENEITY CORRECTIONS

The coarse plate structures used as mockup materials on zero-power critical experiments approximate only roughly the structures of power reactors, and they create a problem that has been recognized for some years. A satisfactory correction is especially needed for zone-loaded cores because driver regions are relatively thin and because they often include materials highly transparent to neutrons.

EXTENSIONS AND TESTS

There is a serious need to examine ways in which the zone-loading technique might be extended for even greater usefulness. There is also a need to identify clearly those cases in which zone-loading methods could lead to misinterpreted results. Finally, there is a need to specify a set of experiments that would most clearly test analytical procedures.

Further development of the zone-loaded reactor concept as an experimental research tool is important to fast breeder-reactor development and is also an intriguingly complex problem for the analyst.

References

1. G. J. Fischer et al., Doppler Effect Measurements in Plutonium-Fueled Fast Power Breeder Spectra, *Nucl. Sci. Eng.*, 25: 37-46 (1966).
2. E. F. Bennett, R. Gold, and R. J. Huber, Spectrum Measurements in a Large Plutonium-Fueled Fast Reactor, in Proceedings of the International Conference on Fast Critical Experiments and Their Analysis, October 10–13, 1966, USAEC Report ANL-7320, Argonne National Laboratory (to be published).
3. J. Gasidlo and P. Amundson, Reactor Development Program Progress Report, January 1965, USAEC Report ANL-7003, Argonne National Laboratory, Feb. 18, 1965.
4. R. A. Karam et al., Measured Physics Parameters in a Zoned Fast Uranium Carbide Core, Assembly 4Z, USAEC Report ANL-7281, Argonne National Laboratory, January 1967.
5. G. J. Fischer et al., Doppler Coefficient Measurements for U-238 in Fast Reactor Spectra, *Nucl. Sci. Eng.*, 18: 290 (1964).
6. C. E. Till, R. A. Lewis, and R. N. Hwang, Recent Doppler Effect Measurements in ZPR-6 and -9 and Comparisons with Theory, in Proceedings of the International Conference on Fast Critical Experiments and Their Analysis, October 10–13, 1966, USAEC Report ANL-7320, Argonne National Laboratory (to be published).
7. S. G. Carpenter et al., Dependence of the Doppler Coefficient of Reactivity for Heavy Elements on Chemical Form, Surface-to-Mass Ratio and Neutron Spectrum, in Proceedings of the International Conference on Fast Critical Experiments and Their Analysis, October 10–13, 1966, USAEC Report ANL-7320, Argonne National Laboratory (to be published).
8. G. S. Brunson et al., A Survey of Prompt Neutron Lifetimes in Fast Critical Systems, USAEC Report ANL-6681, Argonne National Laboratory, August 1963.
9. R. Avery et al., Coupled Fast-Thermal Critical Experiment, in *Proceedings of the Second United Nations International Conference on the Peaceful Uses of Atomic Energy, Geneva, 1958*, Vol. 12, p. 151, United Nations, New York, 1958.
10. F. Storrer and J. M. Chaumont, The Application of Space-Energy Synthesis to the Interpretation of Fast Multizone Critical Experiments, in Proceedings of the International Conference on Fast Critical Experiments and Their Analysis, October 10–13, 1966, USAEC Report ANL-7320, Argonne National Laboratory (to be published).
11. D. Okrent et al., Ax-1, A Computing Program for Coupled Neutronics–Hydrodynamics Calculations on the IBM-704, USAEC Report ANL-5977, Argonne National Laboratory, May 1959.
12. G. J. Fischer, D. A. Meneley, and L. Volodka, Argonne National Laboratory, personal communication, May 1966.
13. G. J. Fischer and A. Travelli, Zone Loading Studies, in Proceedings of the International Conference on Fast Critical Experiments and Their Analysis, October 10–13, 1966, USAEC Report ANL-7320, Argonne National Laboratory (to be published).

Digitized by Google

Let's Apply Optimal Control Theory and Nonlinear Analysis

By Ronald R. Mohler, University of New Mexico

Reactor-control problems traditionally have been solved—or at least satisfied—by trial-and-error techniques with digital- and analog-computer simulations based on classical linear-systems theory. With the aid of recently developed ["modern"] systems theory, i.e., optimal control and nonlinear stability analysis, we may achieve more precise solutions and gain the dual benefits of increased safety and economy.

Rather than the theoretical details of optimal control and nonlinear analysis, this article deals with results and their implications, constructively criticizes certain areas, and indicates some of the pitfalls into which researchers have stumbled.

Some of the easier reactor-control problems are discussed. You are most fortunate, though, if your reactor fits such cases. Tough practical problems unfortunately are the ones confronting reactor engineers. With the computations as involved as they are, it is no wonder the simplest possible problems are solved first. If the work is to be applied in everyday practice, however, systems people must dirty their sometimes sterile computations with practicality. Also, more cooperation is needed between the practical people and the theoretical people. Systems people must learn some practicality and reactor engineers must become knowledgeable in systems theory in order to break the communications barrier that often exists.

Optimal Reactor Control

The term optimum is by no means new to the practicing reactor engineer. The designer is continuously trying to optimize such things as flux distribution and fuel loading. Indeed the practicing reactor-controls engineer often arrives at an intuitive "optimum" design by eyeballing a response while tweaking a pot setting or by examining various root loci. In the selection of such an optimum controller, various indexes of performance, such as response time, overshoot, damping, bandwidth and peaking, might be considered.

The optimal control considered in this article, however, is one that results from a more precise (although not necessarily more meaningful) mathematical problem. For example, the problem might be to vary reactivity in such a manner that reactor power is increased while some performance index,

$$J = \int_{t_0}^{t_1} L \, dt$$

is held to a minimum. Here t_0 is an initial time, t_1 is a terminal time, and L is the cost, which might be a function of power, temperature, reactivity, and other state or control variables. (State variables and state-space analysis are treated for the uninitiated reader in Refs. 1 and 2.) For certain commercial reactors, L may be an economic cost in dollars per hour of operation. In general, such problems have not been studied. The physical system further implies certain constraints on the allowable optimal control.

Optimal control problems have been solved by the maximum principle,[3,4] dynamic programming,[5–7] and extensions of the classical calculus of variations.[5,7] The reader is referred to the indicated textbooks for excellent treatments of the theory along with examples.

Minimal-time control of nuclear reactors probably has been analyzed in more detail than any other optimal reactor-control problem.[8–11] Time-optimal control is a maximum allowable effort type of process (in the simplest form, a bang-bang control). Roughly this means that, to increase power level in minimum time, reactivity is added as rapidly as possible until some maximum allowable limit is reached—the whole process within values that guarantee safe operation. Since the control is not inertialess, reactivity must be decreased at some predetermined time so that the re-

Digitized by Google

quired reactivity is attained at the desired terminal power level. Further, precursor levels have not yet reached equilibrium, and the required terminal reactivity is time variant so as to maintain a constant power level.

All this looks good on paper, but it does not work in practice. First, the model used to describe the system and used to arrive at the optimal process is always erroneous. Second, the required terminal control requires a precise measurement–estimation of precursor levels. Fortunately there are various approximations to the time-optimal process which may be synthesized in practical ways. For example, when the appropriate time (or reactor power) is reached, a fast-correcting closed-loop process can be utilized to control the desired terminal value. Such a closed-loop process can itself be designed optimally with a cost that is a quadratic function of power error and control. Another effective technique utilizes a dither (multiple bang-bang) process with certain control rods jittering about their theoretically required positions. The switching is determined by a small allowable dead zone in reactor power.[8]

STATE-SPACE CONSTRAINTS AND PRACTICAL SUBOPTIMAL CONTROL

Complications in the optimal process also result from certain constraints in such state variables as power level (possibly reactor period) and temperature. Although the computation of optimal processes with state-variable constraints is complicated by the presence of more Lagrange multipliers, it can be carried through with computers (as discussed in Refs. 8 and 12). Again the exact process is not too practical because of a lack of knowledge of the precise system dynamics and state. As would be expected, approximations can be used to synthesize a near optimal or suboptimal control system for the entire portion of the trajectory. A fast-acting closed-loop control can be utilized. Also, state-variable constraints and control constraints can be handled by the proper power-demand limits (and any other control-loop inputs) as well as by the physical limits imposed on control variables (e.g., rod-position demand limited). Another way to manage these constraints is to optimize the loop design with a performance index that implicitly includes constraints (e.g., as a certain quadratic performance index). For the nuclear rocket engine, a simple suboptimal control synthesized by cut-and-try methods with the aid of a computer simulation gives nearly optimal performance.[8,12] A more exact optimal design is obtained in Ref. 13 by optimizing the closed-loop control with respect to a quadratic performance index. In any event the optimization analysis provides a yardstick and paves the way even if more classic control is desired. Further, the closed-loop optimization analysis indicates that all state variables should generally be used in the synthesis.

Another approach to the approximately time-optimal closed-loop control problem is presented in Ref. 14. This technique utilizes the Hamilton–Jacobi equation. Time-optimal reactor control is also utilized as the optimal control of a nuclear rocket engine if propellant consumption is minimized.[12] For such a system, specific impulse (propellant temperature) is increased to its rated value as fast as possible while propellant flow is kept as low as allowable. Near the terminal temperature, flow is increased rapidly to the level for design thrust. Many constraints such as those due to core support thermal stresses and turbopump performance (stall and cavitation) must be considered. Also, it is readily seen that a maximum allowable effort control is a candidate for the optimal reactor process as long as the cost function L is, at most, linear in the control.

The practicing engineer might suggest that the above controls could have been synthesized by physical arguments. Indeed, intuitive arguments were used to arrive at a practical suboptimal bang-bang reactivity process discussed in Ref. 15. Current optimal control theory puts this type of work on a firmer foundation and leads to a more thorough understanding of the optimal process.

Above all, it should be realized that the engineer cannot drop his physical reasoning and classical control theory to rely on mathematics alone to generate optimal solutions. All are necessary design ingredients.

QUADRATIC PERFORMANCE INDEXES

Zero-power reactor control that minimizes a quadratic performance index involving reactivity and power for some desired trajectory is analyzed by dynamic programming in Refs. 16 and 17. The optimal control is found by making a nonlinear transformation of the neutron kinetics to a linear system discussed in Ref. 16. Shen and Haag[16] applied dynamic programming to find a fairly complicated control process. A quadratic performance index involving a variation from a desired neutron level and from a desired rate of change of neutron level has been investigated;[17] the analysis utilizes the maximum principle to arrive at a fairly complicated optimal control. As in Ref. 16, the optimal feedback control involves time-variant gains (hyperbolic functions). Such solutions, although optimal with respect to a quadratic performance index, would be suboptimal relative to a minimal-time trajectory.

Optimal control of a two-energy group neutronic model has been analyzed in Ref. 18. Here it is suggested that the optimal control really involves spatial variations, as well as time variations, in reactivity. This presents a host of challenging design problems.

XENON POISON AND SINGULAR SOLUTIONS

Reactor shutdown to minimize xenon peak production has been analyzed by dynamic programming[19,20] and the maximum principle.[21] Power pulsing (a bang-bang process) was shown to produce the optimal shut-

Digitized by Google

down. Roberts and Smith[22] considered minimal-time reactor shutdown with xenon concentration constrained by some maximum allowable value. For such a process the optimal power variation usually includes a single power pulse but is complicated by a continuous power variation to maintain the maximum allowable xenon concentration if such a value is reached. Also, a singular solution — a state trajectory that causes the switching function to be zero — can be part of the optimal trajectory. In other words the ideal optimal power usually would be zero until the xenon constraint value is reached, and then power is varied to maintain constant maximum allowable xenon until a certain minimal-time full-power trajectory is intercepted. The latter trajectory is optimal until the zero-power trajectory tangent to the maximum xenon line (in xenon–iodine state space) is reached. This new portion is then optimal to the terminal end (no poison). If the initial poison buildup is small, the required shutdown is merely zero power to the end. Both cases assume the singular condition is never reached. If the singular condition arises, it replaces a portion of the above trajectories.

Singular solutions were analyzed in Ref. 8 but were not time optimal for such problems. In most studies, however, singular solutions have been neglected. Such neglect can lead to erroneous answers, as in the case of xenon-poison consideration for shutdown.

Nonlinear Analysis

Neutron kinetics ordinarily are defined by a bilinear system of ordinary differential equations. In other words the system includes a $\rho(t)n(t)$ term and is linear in state and input (reactivity ρ) but not jointly linear in both. If reactivity is a time function, the system is linear and time variant. Generally, however, reactivity is a function of neutron level (via temperature coefficients and control), and the system is nonlinear.

Although heat-exchange processes are nonlinear, distributed, and often time variant, it is almost always assumed in the papers discussed below that the feedback systems are lumped, linear, and time invariant. Such assumptions are not always valid, but still the results can be useful if one realizes the conditions.

In the following papers, classical topological techniques[23] are sometimes utilized, but most of the recent work leans heavily on Liapunov's second (or direct) method.[24] Although the second method is most powerful, it yields only sufficient conditions that frequently give conservative estimates of stability. The technique involves generation of a particular type of function called a Liapunov function. Fortunately some techniques have been devised to bypass the trial and error involved in the generation of Liapunov functions.

Normally it is required that the reactor be stable — at least to the desired terminal state. Over certain portions of optimal trajectories, however, divergent modes might be acceptable. Such is the case for minimal-time startups. Only the most recent work with which I am acquainted is presented here. But first it should be noted that significant spadework appeared earlier by Welton, Weinberg, Ergen, Smets, Gyftopoulos, Popov, Akcasu, and DeVooght,[25–33] to mention a few.

Two recent papers[34,35] show that reactor stability without delayed neutrons does not always imply stability with delayed neutrons. Although delayed neutrons usually have a stabilizing effect, reactor engineers should be aware of a destabilizing possibility. Furthermore, Smets[34] shows that, if reactor-feedback elements exhibit a phase-lag frequency response, delayed neutrons are stabilizing.

Because the second method of Liapunov yields sufficient but not necessary conditions, the conclusions are often so conservative as to have little practical value. This is the case despite the fact that researchers continuously are reporting the latest, most nonrestrictive criteria such as have been claimed justly in Refs. 35 and 36. Also, Schultz[37] has shown that Lure's method yields smaller stability regions for reactors (and is thus less useful) than does the variable-gradient method.[38] The second method does allow a start for detailed computer studies in the selection of certain control-system parameters.

A useful detailed comparison of the Lure–Welton criterion,[31,33] Popov's criterion,[39] Aizerman's method,[33,40] Rosen's method,[41] a topological scheme, and a direct application of Liapunov's second method is presented in Ref. 42. Although a combination of techniques should usually be considered in practice, for the typical case shown in Ref. 42, a Liapunov function can be found directly that ensures stability over a significantly larger region of operation than do the other methods.

In some cases, analyses have been too specific; erroneous conclusions have resulted. For example, the conclusions reached in Ref. 34 indicate that stability for small perturbations without delayed neutrons does not imply stability for small variations with delayed neutrons as previously indicated.[32] Also, it has been shown in Ref. 30 that results reached in Ref. 26 are erroneous. That is, a reactor can even be asymptotically stable without delayed neutrons and unstable with delayed neutrons.

Another interesting conclusion is formulated by Lellouche[43]: for systems with more than one reactivity coefficient and with a prompt negative coefficient, a delayed positive coefficient is more stabilizing than a delayed negative coefficient. Also, Akcasu and Noble[44] show that, if a prompt negative reactivity exists, the reactor is stable if total reactivity-feedback transfer function (with respect to neutron level) has no positive real zeros and if the time integration of the nonprompt feedback-impulse response is negative for all positive time.

Chernick[45] and Shotkin[46] have made worthy contributions to nonlinear reactor theory for some time. In fact, Chernick[47] was probably one of the first to indicate that delayed neutrons do not always provide

Digitized by Google

damping. In a more recent paper, Garabedian and Lynch[48] analyze a two-energy-group multiregion neutron-kinetics model. Also, stability of coupled-core reactors (which might be economically feasible for nuclear rocket propulsion) with delay times is analyzed by Liapunov's second method in Ref. 49. Such coupled systems seem to want to work together.

Conclusions

Classical assumptions that are usually made (sometimes erroneously) include one or more of the following: zero-power reactor model, prompt-neutron kinetics, single-precursor model, linear time-invariant heat exchange, infinitely fast actuators, constant inputs, and point (space) dynamics. In the optimal control papers, singular solutions have been neglected in most cases. Also, optimality is usually assumed when only extremal solutions have been derived. These assumptions are sometimes valid, but in most cases many of them are invalid.

Undoubtedly, trial-and-error techniques with digital- and analog-computer simulations and classical linear-systems theory will continue to be useful with increasing help from modern techniques. Although we cannot hope to find analytical solutions to most practical reactor-control problems, intuitive arguments would often bridge the gap between theory and practice. This has been especially useful in showing that extremal solutions are sometimes indeed optimal.[8]

Because of the urgency involved, many studies of modern reactor-control theory have involved aerospace or military applications. On the other hand, it should be realized that the same sort of analysis is feasible for commercial reactor systems. For example, minimal-time control and xenon-poison considerations are significant for commercial reactors if maximum operational time for a given cost is of interest. Similarly, it is important to understand the effect of certain design parameters on stability of the nonlinear reactor, for safety reasons if nothing else. Undoubtedly there is a need for studies of cost effectiveness and optimization on commercial reactors and nonlinear dynamical analyses of more realistic commercial reactor models.

* * *

The author is grateful to the Sandia Corporation for support of research in this area. Also, some of the ideas presented here are based on the author's previous work at the Los Alamos Scientific Laboratory.

References

1. L. A. Zadeh and C. A. Desoer, *Linear System Theory*, McGraw-Hill Book Company, Inc., New York, 1963.
2. P. M. DeRusso et al., *State Variables for Engineers*, John Wiley & Sons, Inc., New York, 1965.
3. M. Athans and P. Falb, *Optimal Control*, McGraw-Hill Book Company, Inc., New York, 1966.
4. L. S. Pontryagin et al., *The Mathematical Theory of Optimal Processes*, Interscience Publishers, a division of John Wiley & Sons, Inc., New York, 1962.
5. S. E. Dreyfus, *Dynamic Programming and the Calculus of Variations*, Academic Press Inc., New York, 1965.
6. R. E. Bellman, *Dynamic Programming*, Princeton University Press, Princeton, N. J., 1957.
7. C. W. Merriam, *Optimization Theory and the Design of Feedback Control Systems*, McGraw-Hill Book Company, Inc., New York, 1964.
8. R. R. Mohler, Optimal Control of Nuclear Reactor Processes, USAEC Report LA-3257, Los Alamos Scientific Laboratory, March 1965.
9. R. R. Mohler, Optimal Control of Nuclear Reactor Systems, *Trans. Amer. Nucl. Soc.*, 7(1): 58-59 (June 1964).
10. I. Kliger, An Adaptive Automatic Control of a Nuclear Reactor for a Minimal Time Response, *Trans. Amer. Nucl. Soc.*, 1(1): 59-60 (June 1964).
11. I. Kliger, An Automatic Control of a Nuclear Reactor for Minimal Time Control, in Proceedings of the Third International Federation of Automatic Control Congress, London, 1966.
12. R. R. Mohler, Optimal Nuclear Rocket Engine Control, in *Neutron Dynamics and Control*, AEC Symposium Series, No. 7 (CONF-650413), Tucson, Ariz., May 1966.
13. P. A. Secker, and L. E. Weaver, Synthesis of Optimal Feedback Control for Nuclear-Rocket-Engine Start-Up, in *Neutron Dynamics and Control*, AEC Symposium Series, No. 7 (CONF-650413), Tucson, Ariz., May 1966.
14. J. L. Melsa, A Closed-Loop Approximately Time-Optimal Control Method, in *Neutron Dynamics and Control*, AEC Symposium Series, No. 7 (CONF-650413), Tucson, Ariz., May 1966.
15. T. P. Mulcahey, Time-Optimum Control of Nuclear Reactors with Velocity-Limited Control Devices, in *Reactor Kinetics and Control*, AEC Symposium Series, No. 2 (TID-7662, pp. 278-298), Tucson, Ariz., April 1964. Also, T. P. Mulcahey, Time-Optimum Control of Nuclear Reactors with Velocity-Limited Control Devices, USAEC Report ANL-6695, Argonne National Laboratory, October 1963.
16. C. N. Shen and F. G. Haag, Application of Optimum Control to Nuclear Reactor Startup, *IEEE (Inst. Elec. Electron. Eng.), Trans. Nucl. Sci.*, NS-11(2): 1-9 (April 1964).
17. I. Kliger, Synthesis of an Optimal Nuclear Reactor Control System, in *Neutron Dynamics and Control*, AEC Symposium Series, No. 7 (CONF-650413), Tucson, Ariz., May 1966.
18. C. N. Shen and T. C. Liu, The Control of Absorption Cross Section for a Nuclear Rocket, in *Neutron Dynamics and Control*, AEC Symposium Series, No. 7 (CONF-650413), Tucson, Ariz., May 1966.
19. M. Ash, R. Bellman, and R. Kalaba, On Control of Reactor Shut-Down Involving Minimal Xenon Poisoning, *Nucl. Sci. Eng.*, 6(2): 152-156 (August 1959).
20. M. Ash, *Optimal Shutdown Control of Nuclear Reactors*, Academic Press Inc., New York, 1966.
21. Z. R. Rosztoczy and L. E. Weaver, Optimal Reactor Shutdown Program for Minimum Xenon Buildup, *Nucl. Sci. Eng.*, 20(3): 318-323 (November 1964).
22. J. J. Roberts and H. P. Smith, Equivalence of the Time Optimal and Minimax Solutions to the Xenon Shutdown Problem, *Nucl. Sci. Eng.*, 23(4): 397-399 (December 1965).
23. W. J. Cunningham, *Nonlinear Analysis*, McGraw-Hill Book Company, Inc., New York, 1958.
24. J. LaSalle and S. Lefschetz, *Stability by Liapunov's Direct Method*, Academic Press Inc., New York, 1961.
25. W. K. Ergen and A. M. Weinberg, Some Aspects of Nonlinear Reactor Dynamics, *Physica*, 20: 413-426 (1954).
26. V. M. Popov, Notes on the Inherent Stability of Nuclear Reactors, in *Proceedings of the Second International Conference on the Peaceful Uses of Atomic Energy, Geneva, 1958*, Vol. 11, pp. 245-250, United Nations, New York, 1958.

Digitized by Google

27. W. K. Ergen, H. J. Lipkin, and J. A. Nohel, Application of Liapunov's Second Method to Reactor Dynamics, *J. Math. Phys.*, 36: 36-48 (1957).
28. H. B. Smets and E. P. Gyftopoulos, The Application of Topological Methods to the Kinetics of Homogeneous Reactors, *Nucl. Sci. Eng.*, 6(4): 341-349 (October 1959).
29. E. P. Gyftopoulos and J. DeVooght, Boundedness and Stability in Nonlinear Reactor Dynamics, *Nucl. Sci. Eng.*, 7(6): 533-540 (June 1960).
30. A. Z. Akcasu and A. Dalfes, A Study of Nonlinear Dynamics, *Nucl. Sci. Eng.*, 8(2): 89-94 (August 1960).
31. T. A. Welton, Kinetics of Stationary Reactor Systems, in *Proceedings of the International Conference on the Peaceful Uses of Atomic Energy, Geneva, 1955*, Vol. 5, pp. 377-389, United Nations, New York, 1956.
32. E. P. Gyftopoulos, Application of Geometric Theory to Nonlinear Reactor Dynamics, *Nucl. Sci. Eng.*, 10(3): 254-268 (July 1961).
33. H. B. Smets, *Problems in Nuclear Power Reactor Dynamics*, Presses Universitaires de Bruxelles, Brussels, Belgium, 1962.
34. H. B. Smets, On the Effect of Delayed Neutrons in Reactor Dynamics, *Nucl. Sci. Eng.*, 25(3): 236-241 (July 1966).
35. W. Baran and K. Meyer, Effect of Delayed Neutrons on the Stability of a Nuclear Power Reactor, *Nucl. Sci. Eng.*, 24(4): 356-361 (April 1966).
36. E. P. Gyftopoulos, Some Applications of Mathematical Methods to Nuclear Engineering at the Massachusetts Institute of Technology, in *Neutron Dynamics and Control*, AEC Symposium Series, No. 7 (CONF-650413), Tucson, Ariz., May 1966.
37. D. G. Schultz, Semiannual Status Report No. 1 on Research in and Application of Modern Automatic Control Theory to Nuclear Rocket Dynamics and Control, University of Arizona, 1964.
38. D. G. Schultz and J. E. Gibson, The Variable Gradient Method for Generating Liapunov Functions, *Trans. Amer. Inst. Elec. Engrs.*, 81(Pt. II): 203-210 (1962).
39. V. M. Popov, Absolute Stability of Nonlinear Systems of Automatic Control, *Automat. Remote Contr. (Engl. Trans.)*, 22(8): 857 (1962).
40. M. A. Aizerman and F. R. Gantmacher, *Absolute Stability of Regulator Systems*, Holden-Day, Inc., San Francisco, 1964.
41. J. B. Rosen, Stability and Bounds for Nonlinear Systems of Difference and Differential Equations, *J. Math. Anal. Appl.*, 2: 370-393 (1961).
42. J. DeVooght and H. B. Smets, Determination of Stability Domains in Reactor Dynamics, presented at EAES Meeting on Reactor Theory, Karlsruhe, June 1966 (to be published).
43. G. S. Lellouche, Reactor Kinetics Stability Criteria, *Nucl. Sci. Eng.*, 24(1): 72-76 (January 1966).
44. A. Z. Akcasu and L. D. Noble, Lagrange Stability in Reactors with Linear Feedback, *Nucl. Sci. Eng.*, 25(4): 427-429 (August 1966).
45. J. Chernick, Evolution of the Finite-Escape-Time Concept in Reactor Kinetics, in *Neutron Dynamics and Control*, AEC Symposium Series, No. 7 (CONF-650413), Tuscon, Ariz., May 1966.
46. L. M. Shotkin, Centers and Limit Cycles in Reactor Kinetics, in *Neutron Dynamics and Control*, AEC Symposium Series, No. 7 (CONF-650413), Tucson, Ariz., May 1966.
47. J. Chernick, A Review of Nonlinear Reactor Dynamics Problems, USAEC Report BNL-774, Brookhaven National Laboratory, July 1962.
48. H. L. Garabedian and R. E. Lynch, Nonlinear Reactor Kinetics Analysis, *Nucl. Sci. Eng.*, 21(4): 550-564 (April 1965).
49. H. S. Murray and D. G. Schultz, Stability of Nonlinear Coupled-Core Reactors, in *Neutron Dynamics and Control*, AEC Symposium Series, No. 7 (CONF-650413), Tucson, Ariz., May 1966.

Digitized by Google

Improved Design Predictions Through Liquid-Metal Heat-Transfer Research

By Ralph P. Stein

One of the more frequently occurring objectives of basic research in heat transfer is to find prediction methods that will be useful for the design and analysis of systems in which there is technological interest. For convection heat transfer, the pertinent fundamentals are fairly well developed. These fundamentals include the familiar conservation laws related to mass, energy, and momentum together with relations describing their local rates of transport. Direct application of these fundamentals to specific situations usually results in complicated mathematical formulations that, for engineering purposes, would better be avoided if possible. As a result, research in this area has centered about application of these fundamentals to general situations so as to discover prediction methods that will be more convenient for engineering use.

To use a deceptively simple and certainly familiar example, consider the relation

$$q = h(t_s - t) \qquad (1)$$

where q is the local rate of heat flow per unit area of and from a surface at temperature t_s to a fluid with a suitably defined average temperature t. This equation defines the heat-transfer coefficient h. When h can be considered a constant, or treated as some appropriate average value, use of this equation is much simpler than the use of the mathematical formulation of fundamentals it replaces. Basic research studies discovered best definitions of t for several general classes of applications. The heat-transfer coefficient could then be considered independent of q and $(t_s - t)$ and easily related to other variables without destroying the simplicity of Eq. 1, thereby supporting its practical usefulness.

Similar potentially useful results of basic research pertaining to liquid-metal heat transfer will be reviewed here. These include improved methods for predicting surface temperatures in reactor coolant channels and heat-transfer rates in heat exchangers. They derive from applications of fundamentals to analytical investigations of liquid-metal forced-convection heat transfer.[1,2]

COEFFICIENTS FOR LIQUID METALS

With turbulent forced-convection heat transfer of nonmetallic fluids in ducts, the "heat-transfer-coefficient concept,"—namely, that it is possible and beneficial to consider q proportional to $(t_s - t)$—has proved to be both accurate and convenient in most situations of engineering interest. With liquid metals, however, the situation is more complicated because, unlike the situation with nonmetallic fluids, heat-transfer coefficients are affected significantly by the actual heat-transfer boundary conditions, such as heat-flux or temperature distributions at the duct surfaces.

Although the sensitivity of liquid-metal heat-transfer coefficients to boundary conditions is well known, satisfactory prediction methods that account for this sensitivity with engineering computations have not been firmly established. The implication of current practice is that Eq. 1 is still to be used, but with the complication that the heat-transfer coefficients must be appropriate to the specific boundary condition of the application. However, the many possible boundary conditions of interest cause much of the convenience and apparent simplicity of Eq. 1 to be lost. Further, in many cases determination of appropriate heat-transfer coefficients—for example, by application of fundamentals or experiment—is equivalent to "solving" the problem, after which application of Eq. 1 is no longer necessary. Thus basic research in liquid-metal convection heat transfer would search for prediction methods that can account for the effect of boundary conditions, as well as for other possible

Digitized by Google

effects, in more convenient forms than implied by a consistent use of Eq. 1.

HOW IMPORTANT?

How important is this type of basic research to current liquid-metal technology? In many design applications of Eq. 1 to systems involving liquid-metal heat transfer, the effects of boundary conditions on appropriate values of h are mostly ignored. This can be justified by expediency — why bother complicating a situation in which, when the entire system is considered, other aspects may be more important and cannot be accounted for accurately?

For example, because of the excellent thermal properties of liquid metals, predictions of temperatures and heat-transfer rates for most design problems in existing or proposed liquid-metal-cooled reactor systems are not greatly influenced by the accuracy with which liquid-metal heat transfer can be predicted. In typical liquid-metal-cooled reactors, because of the relatively poor thermal properties of present fuel materials, temperature differences between the surface of a coolant channel and the center of the fuel material are roughly an order of magnitude larger than temperature differences associated with convection of the coolant. Moreover, the pertinent physical properties of these fuel materials are not known very accurately. In current liquid-metal heat exchangers and liquid-metal-heated steam generators, structural and safety considerations usually result in large thermal resistance to heat transfer through the exchanger walls. As a result, inaccurate values of h for application of Eq. 1 have little effect on the overall design. Also, with steam generators, steam-side heat-transfer predictions are highly uncertain.

However, with the interest in liquid metals as industrial coolants[3] as well as working fluids in fast reactors and in space power plants, refinements in design soon may require improved accuracy in predicting liquid-metal heat transfer. How soon will depend on the future direction and interest of the related technology.

Improved Prediction Methods

Three examples of the results of basic research in liquid-metal heat transfer illustrate potentially useful design prediction methods. The first example is related to appropriate forms of Eq. 1 when applied to fuel-coolant channels idealized as annular spaces with unequal heat fluxes on opposite sides; it has its origins in a paper by Seban[4] in 1950. It was also discussed in the 1952 edition of the *Liquid Metals Handbook*[5] and reformulated in somewhat more generalized terms[6] in 1956. Even so, there are indications that communication of the results of basic research have not been effectively communicated for this particular example. This is evidenced by the contents of several recent surveys of liquid-metal heat transfer for design.

The second example suggests an extension of Eq. 1 that accounts for the effect of nonuniform axial heat-flux distributions. The third example refers to improvements in predictions of heat-transfer rates in liquid-metal-to-liquid-metal heat exchangers for which indiscriminate applications of Eq. 1 can lead to inaccurate designs.

UNIFORMLY HEATED ANNULAR SPACES

Let subscripts 1 and 2 identify quantities associated with the inner and outer walls of an annular space. Then Eq. 1 as applied to the inner wall can be written as

$$q_1 = h_1(t_{s,1} - t) \tag{2}$$

with t the bulk or heat-content mean temperature of the fluid. When q_1 and q_2 are known, the bulk temperature is computed easily by simple heat balance. But what is the proper value for the heat-transfer coefficient h_1 so that the surface temperature $t_{s,1}$ can be predicted? For liquid metals, h_1 is influenced[6] strongly by the ratio of the heat fluxes q_2/q_1. Let this ratio be represented by y, and consider the heat-transfer coefficient to be a function of y — that is, $h_1(y)$. Then Ref. 6 shows that

$$h_1(0)/h_1(y) = 1 = a_1 y \tag{3}$$

where a_1 is a positive number which depends on the Peclet and Prandtl numbers of the fluid, on the diameter ratio of the annular space, and, when the heat transfer is not "fully developed," on duct axial position also but which is independent of y. Using Eq. 3, we can rewrite Eq. 2 as

$$q_1 - a_1 q_2 = h_1(0)\ (t_{s,1} - t) \tag{4}$$

from which, with a_1 and $h_1(0)$ known, $t_{s,1}$ can be computed easily. For fully developed heat transfer, $h_1(0)$, the heat-transfer coefficient for an internally heated annulus can be obtained from existing correlations[7]; a_1 can be obtained from the detailed computations of Kays and Leung[8] over wide ranges of Peclet and Prandtl numbers and diameter ratios.[1] Alternately, a_1 can be obtained from existing correlations for fully developed heat-transfer coefficients in symmetrically heated annular spaces — that is, from $h_1(1)$ — since

$$a_1 = [h_1(1) - h_1(0)]/h_1(1) \tag{5}$$

from Eq. 3. By use of Eq. 5, another form of Eq. 4 can be written as

$$(q_1 - q_2)/h_1(0) + q_2/h_1(1) = t_{s,1} - t \tag{6}$$

Digitized by Google

which, with existing correlations for fully developed values of $h_1(0)$ and $h_2(1)$, may be the most convenient form for predicting $t_{s,1}$ for design purposes.

The appropriate form of Eq. 3 for the outer wall of the annular space is

$$h_2(0)/h_2(y) = 1 - a_2 y \tag{7}$$

where now $y = q_1/q_2$. Similar algebraic manipulation leads to

$$(q_2 - q_1)/h_2(0) + q_1/h_2(1) = t_{s,2} - t \tag{8}$$

for predicting the surface temperature of the outer wall of the annular space, $t_{s,2}$. Correlations of fully developed values for $h_2(0)$ and $h_2(1)$ are also available.[7,9] Note that Eqs. 6 and 8 give simple expressions for predicting $t_{s,1}$ when $q_1 = 0$ and for $t_{s,2}$ when $q_2 = 0$.

Relations similar to these are given in Refs. 5 and 10.

NONUNIFORM AXIAL HEAT FLUX

Equation 1—as applied to liquid-metal heat transfer with q a function of axial position l measured from the duct inlet—results in h being a function of the flux distribution and of the axial position (except for certain special cases). In fact, for simple "unchopped" cosine flux distributions, h—when defined by Eq. 1—will always be zero at the fuel-channel outlet. As a result the customary definition of h as given by Eq. 1, with t the usual bulk temperature, becomes cumbersome to use because then h must be determined in advance as a function of the flux distribution and of the axial position.

A recently suggested[1] extension of Eq. 1 avoids this difficulty but involves the use of higher ordered dimensionless thermal-resistance coefficients R_n, associated with successive derivatives of q with respect to l. The coefficients R_n are functions of Peclet (or Reynolds) and Prandtl numbers and duct shape but are independent of the flux distribution and, for sufficiently large l, are also independent of axial position. This extension of Eq. 1 for sufficiently large l can be written as

$$q + \sum_{n=1}^{\infty} R_n (d^n q/dx^n) = h(t_s - t) \tag{9}$$

where $x = l/D$ (D is the duct hydraulic equivalent diameter) and h is the fully developed heat-transfer coefficient for uniform heat-flux distribution for a circular tube, an internally or externally heated annular space, or an annular space with equal heat fluxes from both sides. Equation 9 is a dimensional form of Eq. 49 in Ref. 1. Note that when q is uniform—that is, independent of x—Eq. 9 reduces to Eq. 1.

The coefficients R_n decrease rapidly with increasing n, so that in most cases only a few terms of the infinite series need be retained. In other cases the higher order derivatives may be zero. For example, a reasonable approximation of $q(x)$ for many reactor applications is

$$q = (4q_{\max.})(D/L)^2(L/D - x)_x \tag{10}$$

where L is the fuel-coolant-channel length. Then Eq. 9 is simple to use to predict maximum fuel or channel surface temperatures because only the coefficients R_1 and R_2 are required.

For the coolant channel idealized as the space between infinitely wide parallel planes, the coefficients R_n can be computed from

$$R_n = (-1)^n\ (\mathrm{Nu}/2)\ (\mathrm{Pe}/4)^n \sum_{k=1}^{\infty} C_k/\lambda_k^{2n} \tag{11}$$

where Nu is the appropriate fully developed Nusselt number corresponding to the fully developed heat-transfer coefficient for uniform heat-flux distribution h used in Eq. 9 and Pe is the Peclet number. Representative values of C_k and λ_k^2 are given in Tables 1 and 2 as functions of Reynolds and Prandtl numbers. These values were computed from the "Fundamental Eigenvalues Problem"[1] related to liquid-metal heat transfer in heated parallel-plane ducts.[11] The computations were based on use of von Kármán's universal velocity profile with eddy diffusivities for

Table 1 VALUES OF C_k AS A FUNCTION OF REYNOLDS AND PRANDTL NUMBERS

Prandtl number	Reynolds number	C_k for Eq. 11				
		C_1	C_2	C_3	C_4	C_5
0.003	30,000	0.1798	0.0509	0.0232	0.0134	0.0086
	100,000	0.1619	0.0485	0.0219	0.0129	0.0082
	300,000	0.1280	0.0413	0.0183	0.0110	0.0070
	1,000,000	0.0802	0.0269	0.0119	0.0075	0.0049
0.01	30,000	0.1538	0.0463	0.0205	0.0117	0.0072
	100,000	0.1181	0.0388	0.0170	0.0102	0.0065
	300,000	0.0753	0.0255	0.0113	0.0072	0.0047
	1,000,000	0.0340	0.0199	0.0056	0.0038	0.0026
0.03	30,000	0.1127	0.0363	0.0149	0.0082	0.0045
	100,000	0.0694	0.0236	0.0103	0.0064	0.0040
	300,000	0.0336	0.0119	0.0055	0.0037	0.0025
	1,000,000	0.0120	0.0046	0.0023	0.0017	0.0012

Table 2 VALUES OF λ_k^2 AS A FUNCTION OF REYNOLDS AND PRANDTL NUMBERS

Prandtl number	Reynolds number	λ_k^2 for Eq. 11				
		λ_1^2	λ_2^2	λ_3^2	λ_4^2	λ_5^2
0.003	30,000	11.67	44.92	100.84	178.42	278.56
	100,000	13.16	51.24	116.08	206.54	322.96
	300,000	16.91	68.66	158.91	284.79	446.08
	1,000,000	26.63	121.16	290.52	523.80	819.36
0.01	30,000	13.87	53.84	121.96	216.96	339.36
	100,000	18.42	75.34	175.05	314.10	491.98
	300,000	28.18	129.58	311.83	562.13	879.13
	1,000,000	52.75	295.50	733.46	1320.98	2056.17
0.03	30,000	19.20	77.79	180.43	323.34	506.69
	100,000	30.38	140.43	338.16	609.74	953.43
	300,000	53.32	297.39	736.65	1327.76	2067.21
	1,000,000	116.24	785.12	1977.85	3551.05	5501.29

Digitized by Google

heat transfer taken equal to those for momentum transfer and assumed to be uniform and equal to their maximum values at the duct center. Computations by other methods will not give significantly different results, except possibly for large Peclet numbers where very accurate values of the coefficients R_n are not needed.

Reference 1 shows that, for cosine heat-flux distributions, when

$$(\pi/4)\ (\mathrm{Pe}D/L) \ll \lambda_1^2 \tag{12}$$

Eq. 9 reduces to the very simple form

$$q + R_1\ (dq/dx) = h(t_s - t) \tag{13}$$

Further computations[12] indicated that

$$(\pi/4)\ (\mathrm{Pe}D/L) \leq 0.05\lambda_1^2 \tag{14}$$

is usually sufficient to justify the use of Eq. 13. Applications of Eq. 13 to predict maximum fuel and surface temperatures for typical liquid-metal-cooled fast reactor designs revealed that neglecting the second term on the left side of Eq. 13 gave values that were less than 10°F too low. Thus, for practical design purposes, and with h taken equal to fully developed heat-transfer coefficients for uniform flux distributions, Eq. 13 will be sufficiently accurate for application to cosine heat-flux distributions when Eq. 14 is satisfied. Accurate predictions at the channel outlet, or in general with larger heat fluxes than those allowed in current designs, will require full use of Eq. 13.

Reference 1 also discusses the cosine heat-flux case when Eq. 14 is not satisfied, generalizations of Eqs. 6 and 8 for nonuniform heat-flux distributions, and cases for which the heat transfer is not fully developed. Tables 1 and 2 give the values of C_k and λ_k^2 (which were not available when Ref. 1 was written); they will be found useful for analyses of these special cases as applied to fuel-coolant channels idealized as the space between infinitely wide parallel planes.

PREDICTING RATES IN HEAT EXCHANGERS

The necessity of obtaining alternate or extended forms of Eq. 1 in the previous two examples is related to the sensitivity of liquid-metal heat-transfer coefficients—as defined by Eq. 1—to the duct heat-flux boundary conditions. With heat exchangers, these boundary conditions depend on the operating conditions of the exchanger and, except for special limiting cases, cannot be specified in advance. The situation is further complicated with liquid metals because a significant portion of the overall heat-transfer rate occurs along the entrance regions of the exchanger where heat-transfer coefficients are very large and vary with duct axial position—i.e., along regions where the heat transfer is not fully developed. These considerations suggest that the design of liquid-metal-to-liquid-metal heat exchangers based on the traditional applications of Eq. 1, as used for the turbulent flow of nonmetallic fluids, can lead to important inaccuracies.

Current basic research on simple double-pipe heat exchangers[1,2] has shown that traditional methods of heat-exchanger design, when applied to heat transfer between liquid metals, leads to inaccurate predictions in certain operating ranges—although in other ranges inaccuracies are not too important. When these inaccuracies are serious, oversized heat exchangers result.

The practical significance of this research is seen in Tables 3 and 4, which compare predictions of concentric-tube countercurrent-flow heat-exchanger lengths (or heat-transfer areas) required for various specified overall heat-transfer rates. Heat-exchanger

Table 3 ERRORS IN PREDICTING HEAT-EXCHANGER* LENGTHS

Specified efficiency	Error in predicted length, %		
	$H = 0.1$	$H = 0.5$	$H = 1.0$
0.3	202		56.9
0.4	178		39.2
0.5	167	65.0	27.3
0.6	154	55.4	16.9
0.7	143	46.0	11.4
0.8	136	36.9	8.0
0.9	122	30.9	2.6

*Countercurrent flow; $K = 0.1$, $K_w = 0.05$.

Table 4 ERRORS IN PREDICTING HEAT-EXCHANGER* LENGTHS

Specified efficiency	Errors in predicted length, %		
	$K_w = 0$	$K_w = 0.05$	$K_w = 0.1$
0.3	206		
0.4	155		
0.5	115	65	46
0.6	87	55.4	38.1
0.7	71.2	46.0	31.2
0.8	55.6	36.9	25.8
0.9	53.2	30.9	20.0

*Countercurrent flow; $K = 0.1$, $H = 0.5$.

lengths were computed by simple applications of Eq. 1, with h assumed to be independent of axial position and equal to values corresponding to the boundary condition of uniform heat flux; these are compared with accurate predictions by a detailed analysis based on fundamentals.[1,2] The detailed analyses show that the operating conditions of the exchanger are characterized by the three dimensionless parameters H, K, and K_w, so that these parameters must be defined before the comparisons can be understood.

The parameter H is the heat-capacity flow-rate ratio defined by

$$H = c_2 W_2 / c_1 W_1 \tag{15}$$

Digitized by Google

where c is the fluid specific heat, W is the mass rate of flow, and subscripts 1 and 2 refer to the tube and annulus sides of the exchanger. The parameter K is the relative thermal resistance of the fluid in the annular space and is defined as

$$K = (k_1 k_1^+ / k_2 k_2^+)(1 - R)/R \qquad (16)$$

where k is the fluid thermal conductivity, R is the diameter ratio of the annular space, and k^+ accounts for the contribution of turbulent flow to the heat transfer with satisfactory accuracy when Peclet numbers are less than 1000.[1] For the tube side of the exchanger

$$k_1 \approx 0.875 + 0.00312(\mathrm{Pe}_1)^{0.8} \qquad (17)$$

For the annulus side with R close to unity — that is, when the annular space is narrow,

$$k_2^+ \approx 0.965 + 0.00333(\mathrm{Pe}_2)^{0.8} \qquad (18)$$

The parameter K_w is the relative thermal resistance of the tube wall which, when the wall is thin, is defined by

$$K_w = (k_1 k_1^+ / k)(b/r_1) \qquad b/r_1 \ll 1 \qquad (19)$$

where k_w is the thermal conductivity of the wall material, b is the wall thickness, and r_1 is the tube radius. The computations assume R is close to unity, and thus K will be a very small number. The parameter K_w will usually be a small number also. A value of K of 0.1 and a range of values of K_w from 0 to 0.1 were chosen as reasonable representations of liquid-metal-to-liquid-metal concentric-tube exchangers with narrow annular spaces.

In Tables 3 and 4 the specified overall heat-transfer rate is shown as an "efficiency," defined as the ratio of the actual heat-transfer rate to the rate obtainable for an exchanger with infinite heat-transfer area at the same operating conditions. The length (or heat-transfer area) comparisons, shown as percent errors of the length predicted by use of Eq. 1 for three values of H, are always larger than the lengths computed by the accurate detailed analysis. The errors are extremely large for values of H of 0.1 but negligibly small for $H = 1$ with moderate to high efficiencies.

Errors in predicted lengths result from two effects: (1) the sensitivity of liquid-metal heat-transfer coefficients to heat-flux boundary conditions and (2) the high rates of heat transfer in the entrance regions of the exchanger. For the not unusual case of $H = 1$ and a sufficiently long exchanger (equivalent to a high efficiency), heat fluxes along the central regions of the exchanger become independent of axial position — so fully developed heat-transfer coefficients correspond to the boundary condition of uniform heat flux, as used when applying Eq. 1; thus errors are small. The increase in percent errors of predicted length with decreasing efficiency for the case of $H = 1$ reflects the importance of the entrance regions of the exchanger where heat fluxes are significantly higher than those in the central regions. For values of K_w significantly larger than 0.1, the wall thermal resistance begins to control the local heat-transfer rates; as a result the local heat-flux distributions and overall heat-transfer coefficient approach uniformity, so that the traditional applications of Eq. 1 become sufficiently accurate.

The computations of the detailed analysis based on fundamentals are complex and require the use of a large digital computer.[2] Simpler computational procedures are preferred for engineering applications, especially when heat-exchanger performance must be predicted over large ranges of conditions when the operation of a complete power-plant cycle is explored. Improved design and performance relations, based on extensions of the familiar effectiveness (or efficiency) vs. NTU types of equations,[13] have been suggested as part of the basic research investigations.[1,2] These extensions introduce two correction factors: η, which is the ratio of the actual fully developed overall heat-transfer coefficient to the fully developed overall heat-transfer coefficient based on uniform heat-flux boundary conditions, and ϕ, called the "effectiveness coefficient," which accounts for the high local heat-transfer rates in the entrance regions of the exchanger by multiplying the exponential terms in the usual effectiveness vs. NTU equations.

Both η and ϕ depend on H, K, and K_w, but ϕ also depends on the heat-exchanger length (or, equivalently, the heat-exchanger efficiency). However, for sufficiently large efficiencies, ϕ becomes independent of length and is called the "fully developed effectiveness coefficient." Table 5, an extension of a similar table in Ref. 2, shows typical values of these correction factors for the circular-tube countercurrent flow heat exchanger with a narrow annular space. The "fully developed effectiveness coefficient" is denoted by $\phi(\infty)$ and applies for values of the heat-exchanger

Table 5 CORRECTION FACTORS FOR THE CONCENTRIC-TUBE COUNTERCURRENT-FLOW HEAT EXCHANGER

		$K_w = 0$		$K_w = 0.05$		$K_w = 0.1$	
K	H	$\phi(\infty)$	η	$\phi(\infty)$	η	$\phi(\infty)$	η
0.01	0.1	0.6	4.74	0.8	2.39	0.8	1.851
	0.5	0.78	1.468	0.85	1.229	0.88	1.160
	0.9	0.966	1.037	0.976	1.025	0.982	1.018
	1.1	0.971	0.971	0.979	0.979	0.985	0.985
	2.0	0.85	0.851	0.881	0.890	0.91	0.916
0.05	0.1	0.63	3.50	0.8	2.18	0.82	1.767
	0.5	0.792	1.318	0.856	1.206	0.892	1.147
	0.9	0.968	1.033	0.978	1.023	0.983	1.017
	1.1	0.973	0.974	0.981	0.981	0.986	0.986
	2.0	0.86	0.863	0.888	0.898	0.914	0.922
	10.0	0.7	0.770	0.79	0.823	0.83	0.861
0.10	0.1	0.67	2.76	0.8	1.990	0.827	1.678
	0.5	0.811	1.269	0.867	1.181	0.899	1.133
	0.9	0.971	1.029	0.979	1.021	0.984	1.016
	1.1	0.975	0.977	0.982	0.983	0.986	0.987
	2.0	0.86	0.878	0.894	0.908	0.918	0.929
	10.0	0.75	0.795	0.79	0.842	0.83	0.876

Digitized by Google

efficiency larger than 0.7. The values of $\phi(\infty)$ may also apply for much smaller efficiencies, but further investigations are required to verify this possibility.[2] Most of the results shown in Tables 3 and 4 can be reproduced with satisfactory accuracy by the values of η and $\phi(\infty)$ in Table 5 and by noting that $\eta = 1$ and $\phi(\infty) = 1$ correspond to the traditional applications of Eq. 1 for heat-exchanger design as used with nonmetallic fluids in turbulent flow.

CONCLUDING REMARKS

These three examples of contributions of basic research to design are based on fundamental studies of relatively simple models. However, actual liquid-metal-cooled reactor fuel channels are not usually simple annular spaces or circular tubes — and actual heat exchangers rarely have simple double-pipe configurations. Even so, the research suggests general principles that often can be made applicable to more complex systems. For example, procedures for applying the results of basic research on simple annular spaces to fuel-element rod bundles or heat-exchanger tube-in-shell configurations have been suggested[14] and have been,[15] and continue to be, tested by experiment.

References

1. R. P. Stein, Liquid Metal Heat Transfer, in *Advances in Heat Transfer*, Vol. 3, pp. 101-174, Academic Press Inc., New York, 1966.
2. R. P. Stein, Mathematical and Practical Aspects of Heat Transfer in Double Pipe Heat Exchangers, in *Proceedings of the Third International Heat Transfer Conference*, Chicago, Ill., August 7–12, 1966, Vol. I. pp. 139-148, American Institute of Chemical Engineers, New York, 1966.
3. L. Rosenblum, Liquid Metal Technology, in Conference on New Technology, Lewis Research Center, Cleveland, Ohio, June 4–5, 1964, Report NASA-SP-5015 (CONF-640601), National Aeronautics and Space Administration, 1964.
4. R. A. Seban, Heat Transfer to a Fluid Flowing Turbulently Between Parallel Walls with Asymmetric Wall Temperatures, *Trans. ASME*, 72: 789 (1950).
5. R. N. Lyon, (Ed.), *Liquid-Metals Handbook*, 2nd ed., NAVEXOS P-733(Rev.), U. S. Atomic Energy Commission and Department of the Navy, Superintendent of Documents, U. S. Government Printing Office, Washington, June 1952.
6. R. P. Stein, The Dependence of Heat Transfer Coefficient on the Ratio of the Heat Fluxes from the Walls of Parallel Plane Channels, in Reactor Heat Transfer Conference of 1956, USAEC Report TID-7529(Pt.1)(Bk.2), November 1957.
7. O. E. Dwyer and P. S. Tu, Unilateral Heat Transfer to Liquid Metals Flowing in Annuli, *Nucl. Sci. Eng.*, 15(1): 58-68 (1963).
8. W. M. Kays and E. Y. Leung, Heat Transfer in Annular Passages — Hydrodynamically Developed Turbulent Flow with Arbitrary Prescribed Heat Flux, *Int. J. Mass Trans.*, 6(7): 537-557 (July 1963).
9. O. E. Dwyer, Heat Transfer to Liquid Metals Flowing Turbulently Between Parallel Plates, *Nucl. Sci. Eng.*, 21(1): 79-89 (1965).
10. C. F. Bonilla, Annuli and Parallel Plates, Sec. 2.1 of Chap. 2, Heat Transfer, in *Reactor Handbook*, 2nd ed., Vol. 4, *Engineering*, p. 49, S. McLain and J. H. Martens (Eds.), Interscience Publishers, New York, 1964.
11. J. M. Nichols, M. Chu, and R. N. Rice, The Fundamental Eigenvalue Problem Related to Liquid Metal Heat Transfer in Heated Ducts, AMU–ANL Summer Engineering Practice School Report, July 2, 1965.
12. J. S. Philbin, M. H. Richardson, and H. J. Weaver, Fuel Surface Temperatures in Liquid Metal Cooled Nuclear Reactors, AMU–ANL Summer Engineering Practice School Report, Sept. 3, 1965.
13. W. M. Kays and A. L. London, *Compact Heat Exchangers*, p. 11, The National Press, Palo Alto, Calif., 1955.
14. O. E. Dwyer and P. S. Tu, Analytical Study of Heat Transfer Rates for Parallel Flow of Liquid Metals Through Tube Bundles, in Chemical Engineering Progress Symposium Series, No. 30, pp. 183-193, American Institute of Chemical Engineers, New York, 1960.
15. A. J. Friedland et al., Heat Transfer to Mercury in Parallel Flow Through Bundles of Circular Rods, in *1961 International Heat Transfer Conference, International Developments in Heat Transfer*, Part 3, p. 526, American Society of Mechanical Engineers, New York, 1961.

Digitized by Google

NPD Performance Indicates Merit of On-Power Refueling

By Karl K. Brown

With enriched-uranium fuel, reactors can be designed to be refueled during plant shutdowns that coincide with annual turbine-generator overhauls. But when the fuel is natural uranium, power reactors must be refueled at least every 6 months to maintain reactivity. In Canada, where D_2O-moderated natural-uranium-fueled pressure-tube reactors[1] are favored, there is strong economic motivation to refuel while the reactor is operating at power so as to achieve high burnup and low fuel cost (Table 1). With successful on-line refueling comes the bonus of higher plant availability.

Canadian experience in refueling the 20-Mw(e) NPD plant (abridged in Ref. 2) is significant not only to their plants and to competing systems but also to related designs such as the U. S. Heavy Water Organic Cooled Reactor[3] (HWOCR) which also are to have on-line refueling. All committed Canadian nuclear power plants — the two 500-Mw(e) CANDU type units at Pickering, Ontario, scheduled for operation in 1970 and 1971, and the 250-Mw(e) CANDU-BLW, also scheduled for 1971 — will refuel at power.

On-power refueling machines are already installed in the new 200-Mw(e) CANDU reactor at Douglas Point, in the 20-Mw(e) NPD (Figs. 1 and 2), and also in a research reactor — the NRU. Operation of the NRU on-power refueling equipment began in 1957, although serious design consideration dates back to 1949. The more than 2 years of experience with on-power refueling machines on the NPD power reactor are statistically inadequate, but the prognosis is for high unit availability and low forced-outage rates. Plant unavailability resulting from refueling-machine problems at NPD amounted to only 2.44%

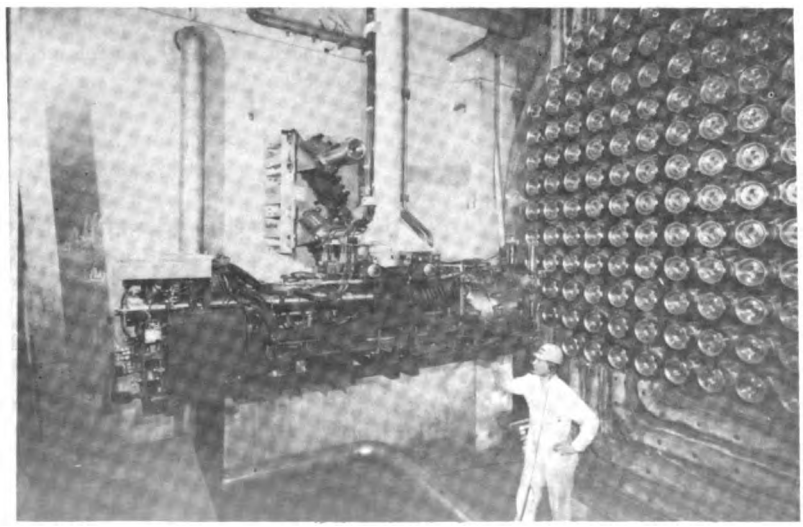

Fig. 1 NPD on-power refueling machine during commissioning in 1962.

Digitized by Google

Why Refuel at Power?

Natural uranium is an essential feature in the Canadian approach to nuclear power. In effect, they choose to enrich the moderator rather than the fuel.[4] With this choice, however, reactivity requirements commit them to refuel the reactor no less frequently than semiannually. Utility energy demands, the cost of shutdowns, and fueling costs make it desirable to refuel while the reactor continues producing power.

Table 1 shows comparative power costs for the first pair of 500-Mw(e) units in the Pickering generating station. These estimates are for conditions in Canada and are based on long-term Ontario Hydro finance criteria. Capital and operating costs of on-power refueling are included and are based on a burnup of 223 Mw-hr per kilogram of uranium, a net unit efficiency of 29.7%, and a unit fuel cost of (Canadian) $50 per kilogram of uranium. The low fuel cost of 0.75 mill/kw-hr can only be achieved with on-power refueling. In the Ontario Hydro power system, the difference in incremental operating costs between coal and nuclear generation is ~2 mills/kw-hr in favor of nuclear with on-power refueling.

Table 1 ESTIMATED POWER COST*
WITH REFUELING ON-POWER VS. OFF-POWER

Category	With on-power refueling	With off-power refueling		
		Two times per year	Three times per year	Four times per year
Capital charges	2.18	2.24	2.30	2.36
Operations and maintenance	0.42	0.43	0.44	0.45
Fuel	0.75	2.10	1.50	1.40
Total	3.35	4.77	4.24	4.21
Relative	100% (Reference)	143%	127%	126%

*Expressed as Canadian mills per kilowatt-hour and assuming 5.25% interest, 30-year life, 80% capacity factor, and 6.69% fixed charges for the Pickering generating station with two 500-Mw(e) net units.

If off-power refueling is employed, the reactivity-limited achievable burnup raises fuel cost and, thus, power cost. For instance, with semiannual off-power refueling, which is barely possible from a reactivity point of view, burnup is only 79 Mw-hr per kilogram of uranium and the complete core change triples the fuel cost from 0.75 mill/kw-hr to 2.1 mills/kw-hr. With off-power refueling three times annually, burnup can reach 110 Mw-hr per kilogram of uranium and the fuel cost is only approximately doubled to 1.5 mills/kw-hr. Quarterly refueling, which is unacceptable owing to seasonal peak-power requirements, would increase burnup to 120 Mw-hr/kg.

It can be assumed that one off-power refueling could coincide with an annual shutdown; others would cause shutdowns. The cost of unavailability is interdependent with the cost of fuel and also depends on both design concept and hardware. For infrequent off-power refueling, each additional shutdown reduces the annual availability by ~2% —which effectively increases the energy unit cost due to capital and operation (fixed charges) by 2% for each shutdown.

Cost of the entire on-power refueling system for a large station (e.g., Pickering) is estimated at <3% of total plant capital cost. It is unlikely that the cost of off-power refueling systems would be less. In fact, to secure high reactor availability, a faster machine would be desired; so machine cost might actually increase.

during the 26-month period ending Mar. 1, 1966. As refueling-machine performance improves, fuel-scheduling experience should also improve.

NPD Refueling Concept

The NPD overall refueling system is shown in Fig. 3. After an operator loads a new fuel bundle into the machine port and the machine automatically positions it in the machine "head," the machine traverses to the reactor, clamps (leaktight) onto the proper pressure-tube end fitting (Fig. 4), removes the seal plug (Fig. 5), and sets it aside within the head. Concurrently, a discharge machine similarly clamps onto the end fitting at the other end of the reactor pressure tube and removes the seal plug there.

Digitized by Google

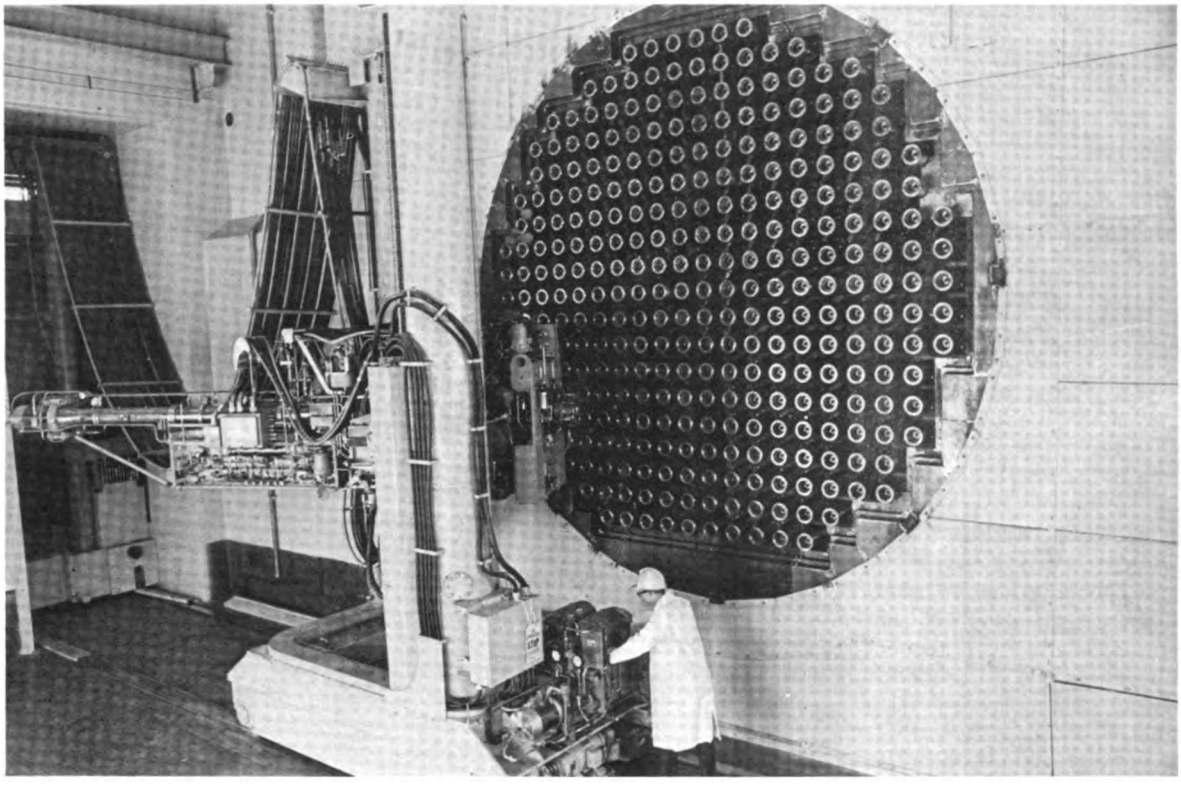

Fig. 2 Douglas Point on-power refueling machine during recent commissioning. This and later designs provide shutdown shielding between reactor and refueling machines.

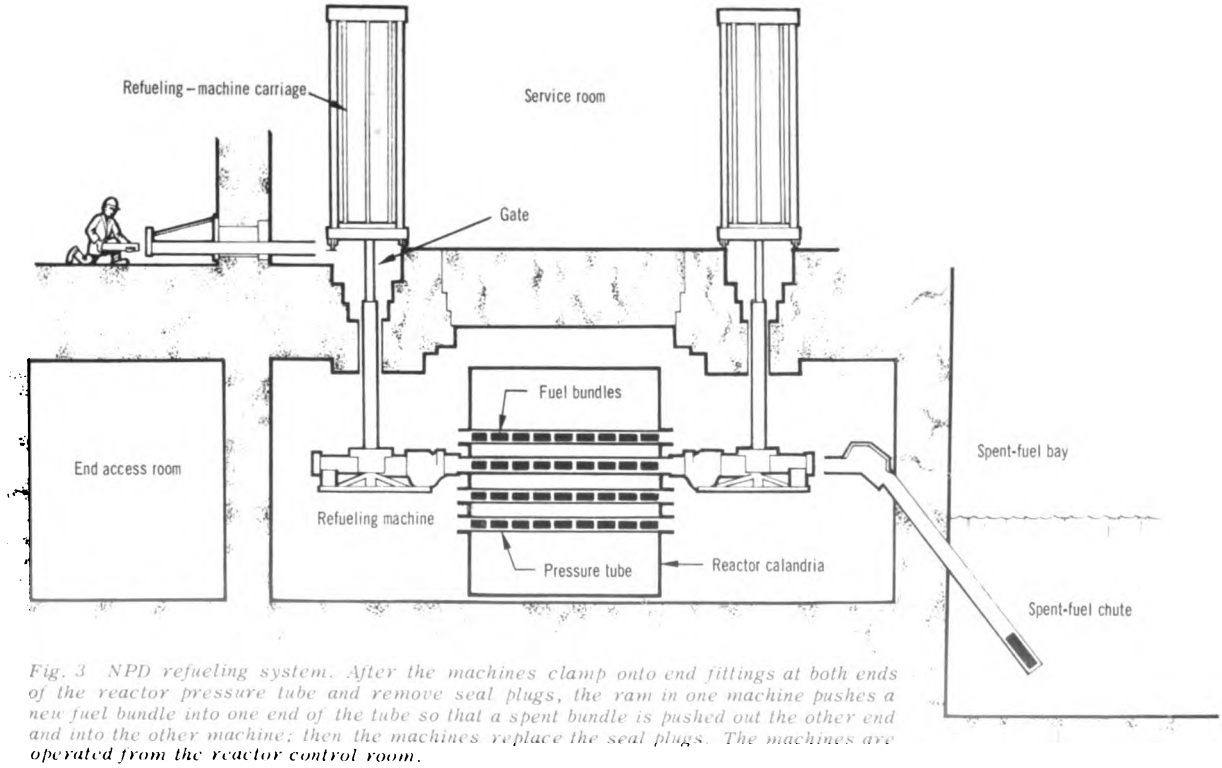

Fig. 3 NPD refueling system. After the machines clamp onto end fittings at both ends of the reactor pressure tube and remove seal plugs, the ram in one machine pushes a new fuel bundle into one end of the tube so that a spent bundle is pushed out the other end and into the other machine; then the machines replace the seal plugs. The machines are operated from the reactor control room.

Digitized by Google

Then the charging machine rams the new fuel into the pressure tube, pushing a spent-fuel bundle into the discharge machine, the machines replace the seal plugs in the end fittings, and the machines unclamp. Adjacent pressure tubes are refueled from opposite ends to balance power generation within the core.

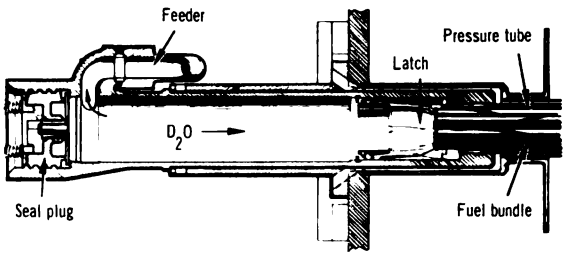

Fig. 4 End fitting of stainless steel on each end of Zircaloy-2 reactor pressure tube has seal plug that refueling machine removes for access to fuel bundles.

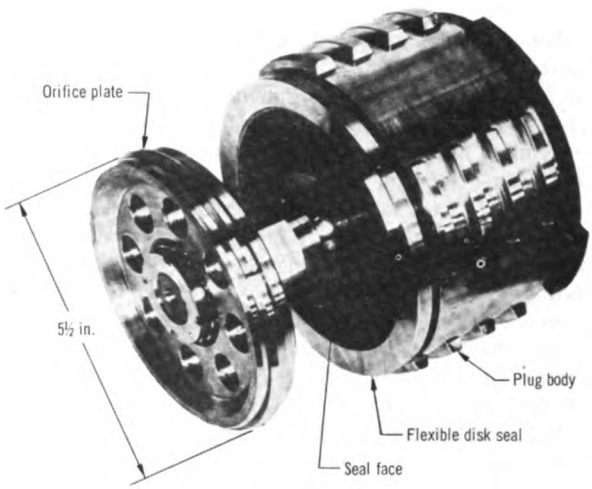

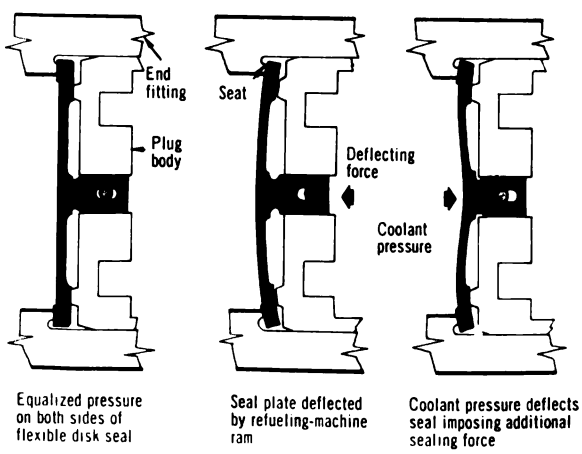
End fitting
Plug body
Seat
Deflecting force
Coolant pressure
Equalized pressure on both sides of flexible disk seal
Seal plate deflected by refueling-machine ram
Coolant pressure deflects seal imposing additional sealing force

Fig. 5 Seal plug has flexible-disk seal (stainless steel) on which reactor-coolant pressure acts to tighten disk against sealing faces.

Refueling-Machine Performance

When the refueling machines were first conceived, several obstacles were obvious: (1) leakage at the end fittings could cause high D_2O losses, (2) radioactivated equipment would complicate maintenance, and (3) sticking of fuel, seal plugs, and clamps could require plant shutdown for repairs. How well the design has overcome these obstacles can be seen from consideration of refueling-machine performance.

COMPONENTS

Figure 4 shows the NPD end fittings, which contain D_2O at 1050 psig, 530°F. Although several hundreds of tests were performed in the laboratory on the NPD design, a major leak occurred in the reactor in December 1962 when an elastomer seal extruded through a sealing face because of inadequate clamping forces. Since correction of this deficiency, 452 routine on-power fueling operations have been carried out (904 clampings) without further trouble (as of Mar. 1, 1966).

Seal plugs (Fig. 5) in the 264 end fittings in NPD must be routinely removed and replaced during refueling without serious chronic D_2O loss. This requirement is met in two ways: (1) development and use of a long-life self-energizing seal and (2) continued recovery of any escaped steam or liquid from the reactor-vault atmosphere or floor.

LEAKAGE

Low-leakage seal plugs are required whether fuel is changed under on-power or off-power conditions. To prove that each plug is leaktight, the machine automatically tests it before the machine seal is unclamped. Spare seal plugs are carried in the machine magazines and can be installed on the pressure tubes while the reactor is at power. There have been no outages or deratings due to seal-plug leakage.

The average chronic escape rate of heavy water into the reactor vault for all reasons during 1964 and 1965 was 280 g/hr. The average recovery rate was 262 g/hr during the same period, so the average loss rate was 18 g/hr, or ~1 lb/day.

RADIATION LEVELS

The refueling-machine heads and associated equipment in the reactor vault are subjected to high radiation levels. Although no outages or failures have resulted from radiation degradation, electrical wiring, hoses, and internal-machine elastomers have been replaced. Neoprene hoses lined with Buna-N rubber are now used to achieve good thermal stability.

MAINTENANCE

Maintenance of the refueling-machine heads results in personnel exposure to radiation produced by

Digitized by Google

direct neutron activation of surface contaminants as well as from corrosion products, fission products, and tritium. Although there has never been a case where a person has exceeded the allowable exposure of 5 rems/year, maintenance and modification of the refueling machines during 1964 and 1965 caused a total of 27 man-rems/year exposure. The present goal is <6 man-rems/year per unit (two machines).

Because the reactor vault is inaccessible to personnel and the machine could stick on an end fitting, the design permits manual emergency operations through openings in a rotating shield at the end of the reactor vault. Two machine outages have required the use of these openings at NPD. A special cone-shaped bung was inserted manually into the reactor pressure tube after the machine was detached. This has proved to be a relatively simple and straightforward operation.

In the Douglas Point and Pickering designs, this problem has been further reduced by placing shutdown shielding between the reactor and the refueling machine.

Emergency provisions were also made at NPD to permit a refueling-machine head containing jammed fuel to be transferred and immersed in the spent-fuel canal remotely. Although fuel has jammed in the head on two occasions, the emergency provisions proved unnecessary because radiation levels were much lower than indicated by the conservative calculations on which the design was based. Thus these events were handled with relative ease and caused no outages.

NPD Refueling-System Results

The NPD has operated with on-power refueling routinely since Jan. 1, 1964—the data presented here cover experience from then until March 1966. Clearly, 2 years of data for one unit during a period of plant immaturity are insufficient for firm conclusions. Early problems are still being identified, and development is in progress, so performance should improve.

STATION OPERATION

During the entire year 1964 and the first half of 1965, NPD was run to provide base load. From July to November 1965, numerous planned training and modification outages and some forced and maintenance outages occurred. During the 1965–1966 winter peak (December to February), the unit was base loaded with no planned outages.

No attempt is made here to discuss the overall unit statistics, nor have any attempts been made to adjust the records for tests, modifications, etc. The overall values are presented solely for the purpose of providing perspective for the refueling-machine statistics.

OUTAGES

Table 2 shows the unavailability of NPD for all reasons, together with unavailability caused by the refueling system. Although the refueling system caused three outages during 1964 and four during 1965, it caused no outages during January or February 1966. The average outage lasted 66 hr. Two limit-switch deficiencies on the refueling-machine heads accounted for 75% of the lost time.

Table 2 UNAVAILABILITY HISTORY FOR NPD STATION

Period	Station unavailability for all* reasons, %	Caused by refueling system	
		Unavailability, %	No. of outages
1964	14.14	0.63	3
1965	23.30	4.67	4
1966 (January and February)	0.06	0.00	0
Average per year	17.26	2.44	3.2

*All includes experiments, tests, modifications, maintenance, and all other events that caused NPD to be unable to produce electricity.

The forced-outage rate for the winter period is a vital statistic in the Ontario Hydro system and is particularly important in planning reserve capacity. The 1964–1965 2-month base-load run was during December and January; in the winter of 1965–1966, the base-load peak was during a 3-month run, December to February. During these two runs there were no outages caused by the refueling system. The perfect performance during this period is not statistically reliable, of course, and NPD will suffer forced outages caused by the refueling system in the future. However, by careful planning they expect to achieve a very low forced-outage rate during the system seasonal peaks.

The achievement of 2.44% refueling-machine unavailability might be interpreted as adequate or acceptable performance. However, the unavailability data can be, and in this case are, completely misleading. Unavailability cannot substitute for forced-outage rate in assessing system reserves and is a poor yardstick for economic evaluation. Perhaps its greatest virtue is the ease of measurement.

CAPABILITY

For economic purposes, unavailability is a poor yardstick because it does not include derating or energy consumed during outages and is too awkward for sophisticated treatment of coincident troubles. Accordingly, "capability" is defined as a measure of ability to produce net energy. Its complement, "incapability," is a measure of unit imperfection. Where availability uses a time base, capability uses an energy base.

Table 3 represents NPD capability data during the on-power experience period; it also shows the plant

Digitized by Google

Table 3 NPD STATION CAPABILITY STATISTICS

Period	Operating policy	Station factor, %		Station incapability, %						
				For all reasons			Caused by refueling system			
		Capacity*	Capability†	Outage	Derating	Total	Direct Outage	Indirect outage	Derating	Total
1964	Base load	82.6	82.9	14.93	2.14	17.07	0.8	2.5	0.2	3.5
1965	Modification and training	70.3	71.3	25.00	3.70	28.70	5.4	1.4	1.5	8.3
1966 (January and February)	Base load	99.9	99.9	00.07	0.00	0.07	0.0	0.0	0.0	0.0
Average annual		78.2	78.9	18.40	2.70	21.10	2.87	1.80	0.79	4.05

*Capacity factor = $\frac{\text{actual net energy produced} \times 100}{\text{net energy with perfect continuous operation at full capacity}}$.

†Capability factor = $\frac{\text{net energy unit capable of producing} \times 100}{\text{net energy with perfect continuous operation at full capacity}}$.

incapability caused by refueling-system troubles. For the latter the major difference between the average plant unavailability, 2.44%, and the average plant incapability, 4.05%, corresponds to energy consumed during shutdown, indirect outages, startup losses, derating during xenon buildup after outages, and derating as a result of refueling-machine trouble.

During 1965 the incapability rose to 8.3% for two reasons: (1) two limit-switch problems on the refueling machine increased direct-outage incapability to 5.4% (development work was required to correct the problems) and (2) equilibrium-fuel operation in 1965 was more representative of normal conditions and caused the derating incapability caused by refueling-system trouble to increase to 1.5%. Modifications made in late 1965 and improved maintenance were expected to yield a major improvement in refueling-system performance during 1966.

Table 4 gives present performance targets. Although these targets are not vital to the economics of this concept, they are desirable to minimize energy cost. The real balance is reached where increased performance is offset by increased capital and operating costs for each variable. McConnell concludes[2] that "although we are very pleased with the average fueling-system incapability experience of 4.05%, we are confident of achieving 1% in NPD."

Table 4 PERFORMANCE GOALS FOR MATURE STATIONS AND REFUELING SYSTEMS

Station	Station performance for all reasons					Station performance caused by refueling system			
	Lifetime capacity factor, %	Winter-peak forced-outage rate, %	Incapability, %			Winter-peak forced-outage rate, %	Incapability, %		
			Outage	Derating	Total		Outage	Derating	Total
NPD-2		1.50				0.33	0.85	0.15	1.00
Douglas Point-1	80	3.30	6.50	0.70	7.20	0.56	1.11	0.18	1.29
Pickering-1	80	4.70	9.00	1.00	10.00	0.55	1.06	0.25	1.31

Fuel-Scheduling Experience at NPD

The payoff for on-power refueling with the equipment described comes when it performs to help achieve design burnups on an equilibrium basis and to increase station availability. Fuel-scheduling experience so far, as reported by Fanjoy[5] and summarized here, covers the time from reactor startup to near-equilibrium burnup. (Equilibrium occurs when core-average burnup reaches a constant value with specified burnup profiles.) Figure 6, the actual core-average burnup, shows that NPD is approaching equilibrium — although the burnup profiles are not yet quite as had been specified. At equilibrium, twice the asymptotic value is the discharge burnup; thus the extrapolated value from this curve will be ~10% over the design discharge burnup (152 Mw-hr per kilogram of uranium).

In the ideal natural-fuel schedule, fuel is simply shifted from channel to channel until equilibrium (1200×10^3 Mw-hr) is reached. Then new fuel is added at the equilibrium rate (Fig. 7), and there is no further shifting of bundles among channels. However, the ideal schedule cannot be achieved in practice because of physical limitations of the system — mainly fuel movement, maximum burnup, and flux distribution. Furthermore, NPD scheduling was also complicated by our use of depleted fuel in the core center to compensate for the excess reactivity caused by the new fuel in the initial loading. Thus Fig. 7 also shows the schedule calculated[6] for adding new fuel bundles on the basis of the depleted-fuel effect and practical shift rules. (Fuel bundles are kept within the design burnup by shifting the bundles removed with low burnups to alternate channels and discharging the others.)

THE ACTUAL SCHEDULE

Figure 7 also shows the actual numbers of bundles shifted between channels and the number replaced by new bundles. Decisions on whether and where to move

Digitized by Google

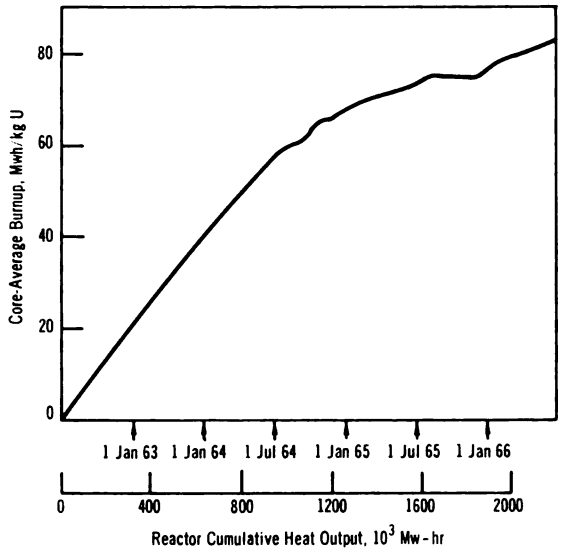

Fig. 6 Actual core-average burnup is approaching equilibrium value; discharge burnup is twice the asymptotic value.

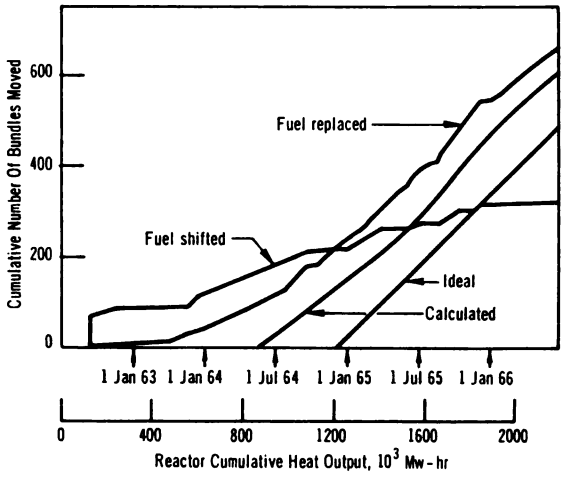

Fig. 7 Refueling schedules—theoretical ideal, calculated,[6] and actual—during the time from reactor startup with all-new fuel to the achievement of near-equilibrium burnup. Note actual refueling upsurge to prepare for winter 1965–1966 peak-demand period.

fuel were made in the following order: (1) fuel was moved only when the reactor needed reactivity, (2) channels with the highest burnup were refueled first, (3) problems unrelated directly to the fuel were considered, and (4) flux profile was checked. The flux profile did not cause much difficulty because the conservativeness of the reactor design allowed sufficient maneuvering room.

There are not yet quantitative data to explain the difference between the calculated and the actual schedules in Fig. 7; however, the difference is caused by (1) optimistic refueling rules in the calculated case; (2) imperfect refueling-maching operation [resulting in increased use of enriched booster (93% enriched UAl), more shutdown fueling than desired, premature discharge of fuel, and some preferential fueling of the core center to maximize reactivity gain]; (3) the experimental program resulting in more discharge than demanded by the schedule; (4) mechanical difficulties requiring that specific channels be left untouched; and (5) one accidental addition of light water—approximately 1000 gal—that reduced moderator purity from 99.8 to 99.1% D_2O. Continued refueling-machine development may eliminate most of these difficulties.

FOR THE FUTURE

Experience with NPD indicates that, during the period before equilibrium, on-power refueling of a large power reactor must be scheduled with the aid of a sophisticated computer program that calculates the flux profile and the burnup in individual channels. But after equilibrium is achieved, much of the computer work can be eliminated because the flux profile will be relatively static. Then refueling can be decided on the basis of (1) bundle burnups calculated with static flux profiles or (2) decreased coolant temperature at a pressure-tube outlet as an indication of burnup of fuel bundles in that tube.

* * *

This article has been prepared with the cooperation and assistance of Messrs. McConnell, Fanjoy, and Elston of the Hydro-Electric Power Commission of Ontario.

References

1. Heavy-Water-Moderated Pressure Tube Reactors, *Power Reactor Technol.*, 8(1): 35-46 (Winter 1964–1965).
2. L. G. McConnell, Canadian On-Power Fueling Experience, *Trans. Amer. Nucl. Soc.*, 9(1): 220 (June 1966).
3. W. B. Murray, Availability Assurance for the Heavy-Water Organic Cooled Reactor (HWOCR), *Trans. Amer. Nucl. Soc.*, 9(1): 219 (June 1966).
4. J. O. Holt, Canadian HWR Economic Assessment, *Nucl. Eng.*, 11(121): 461-463 (June 1966).
5. G. R. Fanjoy, Fuel Scheduling Experience at NPD, *Trans. Amer. Nucl. Soc.*, 9(2): 535 (October–November 1966).
6. W. M. Barss, A Computer Study of Reactor Fueling, Canadian Report AECL-1528, May 1962.

Digitized by Google

Recent Developments in Liquid-Metal MHD Power Systems

By Michael Petrick

The growing interest in magnetohydrodynamic (MHD) generation of electric power stems from the potential 15 to 25% increase in power-station overall efficiency possible with an MHD generator in a topping cycle on a steam plant.[1] However, the modest temperatures achievable with economic central-station reactors likely to be available in the relatively near future make MHD generators of earlier interest for space applications. Recent developments in magnetohydrodynamic technology, as described in the more than 200 papers presented in the third International Symposium on Magnetohydrodynamic Electrical Power Generation,[2-4] focus attention on defining both the promise and the specific problems of the various types of MHD systems. This article summarizes recent significant advances in liquid-metal MHD cycles, which were discussed in detail for the first time at the third symposium.

Future articles will similarly review other closed-cycle MHD systems and open-cycle MHD systems. Closed-cycle developments involved system experiments, nonequilibrium theory and measurements, conformal mapping of the potential field and electrical leakage between electrodes. Discussions of open-cycle MHD concentrated on magnet and materials problems, striated flows, and combustion plasma physics. General MHD problems, such as diagnostics, shock tubes, flow and field distributions, auxiliary ionization, and relaxation, were also discussed at the symposium.

ROLE OF REACTORS

The future of MHD power generation is very closely related to the direction and rate of development of nuclear power reactors.

Closed-cycle MHD systems can become successful only if high-temperature reactors or equivalent heat sources can be developed. Reactors for closed-cycle gas plasma systems must operate at ~3000°F, whereas liquid-metal cycles require reactor temperatures 1000 to 1500°F less. For either system the temperature imposes specialized requirements on reactor design and development.

On the other hand, and perhaps most important, the economic justification for MHD will be affected by the impact nuclear power is having on power costs. If nuclear fuel costs continue to decline as they are now doing, then the incentive for improving power-plant efficiency by means of MHD or other topping cycles will diminish.

Status of Liquid-Metal MHD

The feasibility of liquid-metal MHD conversion systems has been demonstrated. On the basis of the indicated performance of known fluid-flow devices (nozzles, separators, etc.), practical cycle efficiency of ~60% can be achieved. Such efficiency appears adequate for space power—and the general consensus is that liquid-metal MHD will probably be used initially in various space applications. In fact, liquid-metal MHD power cycles could be available for use in space before turboelectric systems.

There is considerable doubt, however, concerning the adaptability of liquid-metal MHD power cycles to commercial power systems. Minimum MHD topping-cycle efficiencies of 12 to 15% will be required to gain an economic incentive. It is not clear that such efficiencies can, in fact, be realized because of extensive friction losses in various system components—especially in the 1100 to 1600°F range, which appears to be a reasonable extrapolation of today's state of the art in reactor and materials technology.

The most crucial area where additional work is necessary in liquid-metal MHD is in the development of efficient liquid accelerators for converting the thermal energy of the fluid emerging from the heat source to kinetic energy (or stagnation head) of the

Digitized by Google

fluid before it enters the MHD generator. The basic MHD cycles differ essentially in the method chosen for accomplishing this transformation. Generator development has proceeded more rapidly and is closer to resolution. There is little fundamentally new or different in liquid-metal MHD generators; the problem is to tailor the generator to the cycle and achieve acceptable performance. As with the cycle, generator performance is also friction limited. A complete small-scale liquid-metal MHD power cycle could be operating at temperature within the next 5 years.

Progress in liquid-metal MHD during the past 2 years has been very substantial. The symposium called attention to the fact that liquid-metal MHD has emerged from its embryonic stage of development and is now a bona fide area of magnetohydrodynamics which is sparking considerable and increasing interest.

The major areas of liquid-metal MHD which have received and are continuing to receive the most intensive study are: (1) generator performance, (2) methods for liquid acceleration, and (3) cycles.

Generators

Impressive progress has been made toward the development of liquid-metal MHD generators. Most of this has concerned either the induction generator operating with single-phase flow or the conduction generator operating with two-phase flow.

A-C INDUCTION GENERATORS

Progress has perhaps been greatest with induction-generator development. An induction generator, such as is shown in Fig. 1, is a linear version of the conventional induction machine.[5] A traveling magnetic field is produced by polyphase windings, and, for the machine to run as a generator, the fluid velocity v must exceed the wave velocity v_s, or the slip, defined as $s = (v_s - v)/v_s$, must be negative. Two phases are shown in Fig. 1, but a three-phase winding would probably be used, as in conventional machines.

Sequence. Significant events in the development of induction generators occurred in the following sequence. In the spring of 1964 the first induction generator was tested at the Massachusetts Institute of Technology (MIT) by Jackson, Pierson, and Porter.[6] In August of 1965 a 350-cps 10-pole-pair flat-channel constant-fluid-velocity induction generator was tested by Prem of Atomics International on a NaK blowdown facility at Jet Propulsion Laboratory.[7] Net power of 1840 watts at 215 volts was generated with an electrical efficiency of 36%. Because operation was on a blowdown facility, the experiment ran for less than a minute. Evaluation of these tests shows that a sinusoidal magnetic field and induced current and voltage can be produced. Extrapolation of these data to a large-scale generator led the author to conclude that efficiencies as high as 70% could be obtained.

The next induction generator was run in early 1966 by Radebold and coworkers[8] at the Technical University of Berlin. This generator produced a net power of 1 kw at 50 cps and 210 volts; the excitation power required was 9.5 kva. This generator, which ran for $\sim\frac{1}{2}$ hr under steady-state conditions, was designed primarily to produce basic data that could be compared to theory, not to demonstrate high efficiency.

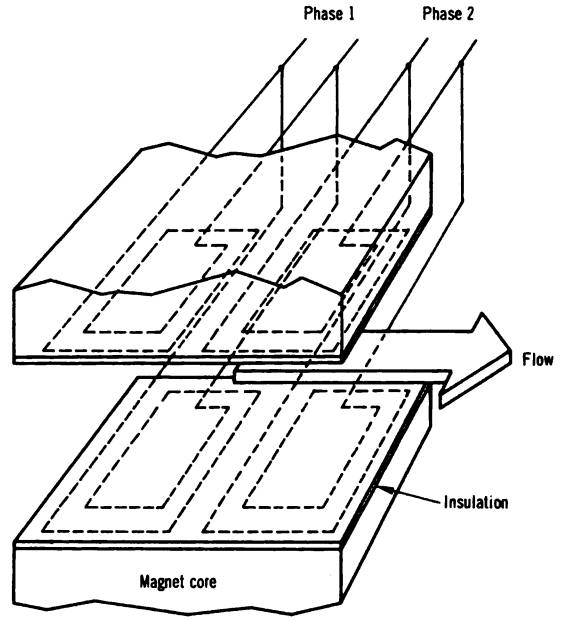

Fig. 1 Linear a-c induction MHD generator.[5]

Immediately preceding the symposium another significant development occurred which was not reported in a symposium paper. The author had the opportunity of witnessing the startup of a generator from a capacitor bank at the Technical University of Berlin. This successful experiment was also carried out by the AEG (Allgemeine Elektricitäts-Gesellschaft) group in collaboration with W. D. Jackson.

Perhaps the most significant development in regard to induction generators was reported by Elliott and coworkers[9]—the development of a short (1 to 2) wavelength machine with compensation poles at the generator entrance and exit to reduce end losses. Generator development in the past progressed toward long-, many-wavelength machines to eliminate end effects. However, performance suffered because of extreme friction losses. The solution to the problem as proposed in Ref. 9 is to try to make an electrically short generator appear like a 1-wavelength section of an infinite generator. Analyses indicate that, with compensation poles, efficiencies up to 70% are attainable if the generator has a length/gap ratio of no

Digitized by Google

more than 70 (for low friction loss) and an electrical length of no more than 1 or 2 wavelengths (for low winding loss). A 1-wavelength generator has been built (Fig. 2) and is being tested at Jet Propulsion Laboratory.[9]

Increasing Current Density. A way is being investigated to overcome the potentially serious problem of generator performance being limited by the current density in the generator windings.[10] In MHD-generator configurations the windings system consists of a conventional multiphase system like that used for the conventional asynchronous machine. But, unlike these, the gap between iron cores is increased to a channel height generally 20 to 30 times greater. Therefore the reactance of the machine and the inductive component of the current become large, which in turn give the machine a small power factor. Compensation is made by an increase in the current density of the primary windings to about 20 to 30 times that in the conventional asynchronous machine. This is only possible by use of a cryogenically cooled primary winding system. An MHD converter utilizing windings cryogenically cooled with liquid nitrogen and employing mercury as the working fluid is now being run to study the predicted performance and the technological problems involved.

Materials Considerations. The generator channel must be able to withstand >1100 to 1600°F liquid metals flowing at several hundred feet per second with negligible corrosion or erosion.[11] Refractory metals such as niobium and its alloys, which are good electrical and thermal conductors, are envisioned as candidates. The protection of the magnetic core and windings from excessive temperatures would require thermal insulation between the hot liquid metal and the field structure. Even so, to minimize insulation thickness and refrigeration power required for space applications, the magnetic core should be operated at the highest temperature consistent with high permeability and low loss. Thus the authors discussed feasible operating temperatures for magnetic and excitation-winding materials, as well as cooling methods for the field structure.

In considering design-engineering aspects, the authors extended MHD induction-generator theory to include both the conducting channel walls and the thermal insulation. Although the thermal insulation would have only a small effect on machine electrical

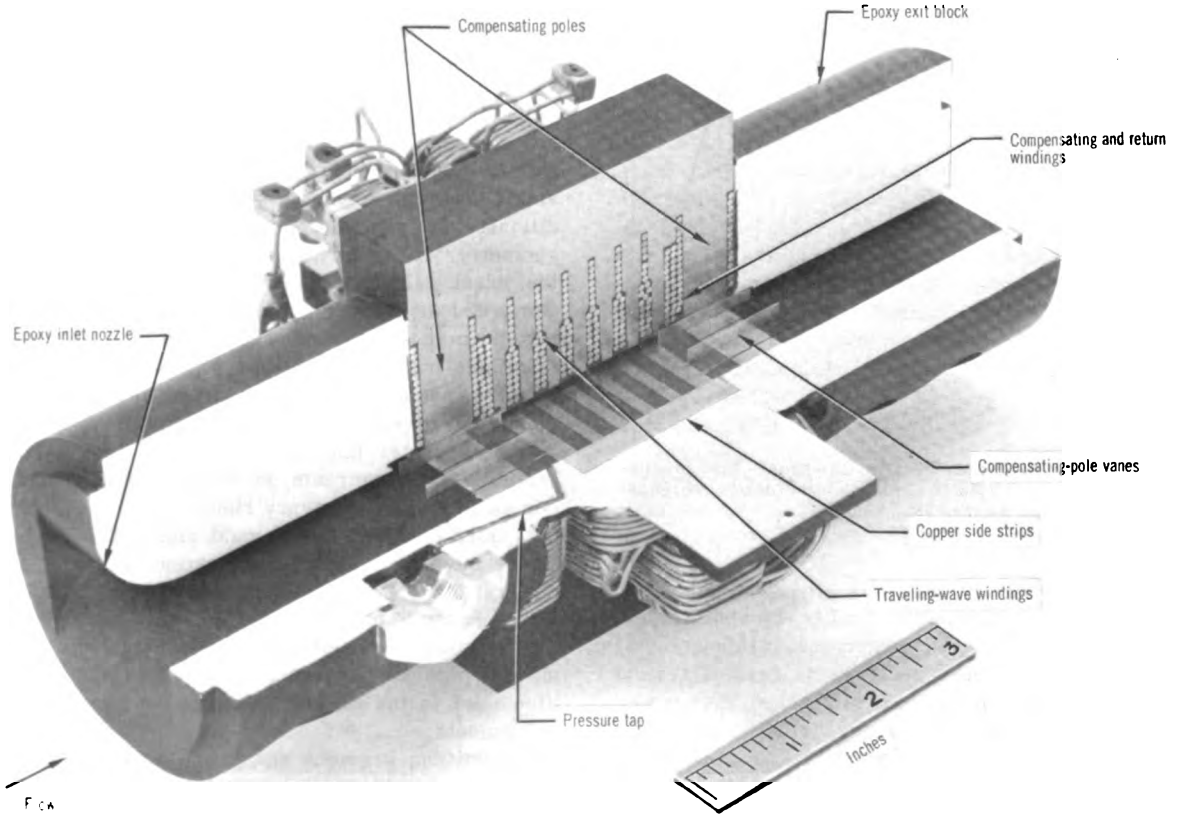

Fig. 2 Experimental 1-wavelength generator is being tested at Jet Propulsion Laboratory.[9]

Digitized by Google

performance, the channel wall thickness required (on the basis of pressure-vessel codes) to contain pressures of several hundred pounds per square inch would cause excessive electrical losses if conventional construction methods were employed. Thus novel construction schemes are suggested along with practical materials questions. (Some cycles do not involve generator-channel pressures requiring thick walls; for instance, the concept being pursued at Atomics International has 1- to 5-psi channel pressure.)

D-C CONDUCTION GENERATORS

The possibility of operating conduction generators on two-phase mixtures was discussed in Refs. 12 and 13. Initial performance data on both a film-flow and a two-phase-flow conduction generator indicate that there are limited parameter areas of operation which are feasible.[12] As shown in Fig. 3, data obtained from a two-phase ($NaK-N_2$)-flow generator indicate that, as the mixture quality and void-volume fraction are increased, generator efficiency decreases. The efficiency decrease is gradual until a mixture void fraction of ~0.85 is reached, then power and efficiency suddenly drop to virtually zero. The performance drop-off was attributed to rapidly decreasing electrical conductivity of the two-phase mixture with increasing void fraction.

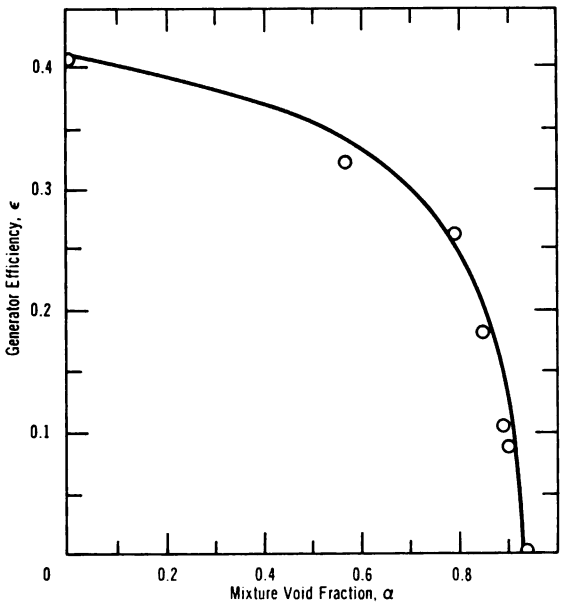

Fig. 3 Efficiency decreases in a two-phase-flow generator as mixture quality and void-volume fraction increase. Magnetic field was 4900 to 5500 gauss.[15]

The problem of defining the conductivity of two-phase mixtures remains unsettled, as evidenced by newly reported data for potassium mixtures at elevated temperatures.[13] Experiments carried out with potassium mixtures (vapor content varied from 2 to 95%) at 1100°F indicated substantial electrical conductivity. The authors hypothesize that the emission of electrons from the surface of the liquid droplets — and not the influence of the liquid film — is the cause of the enhanced electrical conductivity.

Preliminary film-flow-generator data were taken on a small-scale generator;[12] the maximum measured power achieved was 237 watts. Performance was poor at very low liquid flow rates and magnetic fields but increased with increasing values of these parameters. The limited data presented indicate that a film-flow generator apparently is feasible and stable in operation. However, many unanswered questions remain in regard to efficiency, range of stability, etc.

REDUCING END LOSSES

The end-loss problem has been analyzed for both a-c induction generators[9,14] and d-c conduction generators.[15] End losses in a generator usually arise from the large gradients of magnetic field at the inlet and outlet of the generator channel.

Methods were investigated for reducing the end losses in conduction generators, in both constant- and variable-area channels, by employing insulating vanes parallel to the flow.[15] In an initial attempt to determine optimum vane configuration, considering both electrical and viscous losses, a number of channel vane configurations were studied. The author was also able to extend the method of Sutton, Hurwitz, and Poritsky[16] to channels of linearly variable area with the assumption of large Reynolds number and small magnetic Reynolds number. Under those conditions, and with the use of an "equivalent channel geometry," a conformal-mapping technique permits the exact calculation of the net electrode current. For a 2:1 aspect-ratio channel with which no attempt has been made to use vanes to reduce end losses, maximum possible generator efficiency is 40.4%. If simple vanes are used, they must be very long, which means large viscous losses. Thus, with long vanes down the center line of the previous duct (both upstream and downstream so that the aspect ratio becomes 4:1), top efficiency rises to only 52.1%. Short but more complex vanes could yield 66% efficiency in the most promising configuration with a 2:1 aspect ratio or 74% in a 4:1 channel.

The scheme[9] proposed for resolving the a-c induction generator end-effect problem by using compensating poles at the generator entrance and exit was discussed in the section on induction-generator developments.

In addition, previous analyses[17,18] of end losses in linear induction generators have been extended to include circle diagrams depicting real and reactive currents.[14] The two-dimensional induction MHD generator of finite length is treated as a boundary-value problem by a two-sided Laplace transform.

Digitized by Google

MHD Cycles and Acceleration Methods

Because of detailed analyses by numerous investigators, there is more general agreement on the predicted efficiencies of the various proposed cycles than has ever existed in the past. All the papers on this topic dealt with three basic cycles, namely, the separator cycle, condensing injector cycle, and the two-phase generator cycle. The first two have been discussed and described in detail in the literature,[19] whereas the latter was discussed in detail for the first time at this symposium.[20,21] The two-phase generator cycle was discussed initially in a preliminary manner at a previous symposium[19] and in Ref. 22.

TWO-PHASE GENERATOR CYCLE

This cycle can operate with either one- or two-component fluids (Fig. 4). In the one-component fluid cycle, the two-phase mixture generated in the heat source passes directly through the MHD generator to a condenser–diffuser and back to the heat source. In the two-component flow cycle, additional components needed are the mixer and separator.

If the fluid is expanded through the MHD generator directly, the separate nozzle or stagnation head generator can be eliminated. In a sense, the MHD generator behaves as an expansion engine and produces electrical energy as the expanding conductive fluid interacts with the magnetic field. The two-phase flow generator behaves in a manner analogous to that of the plasma flow generator.

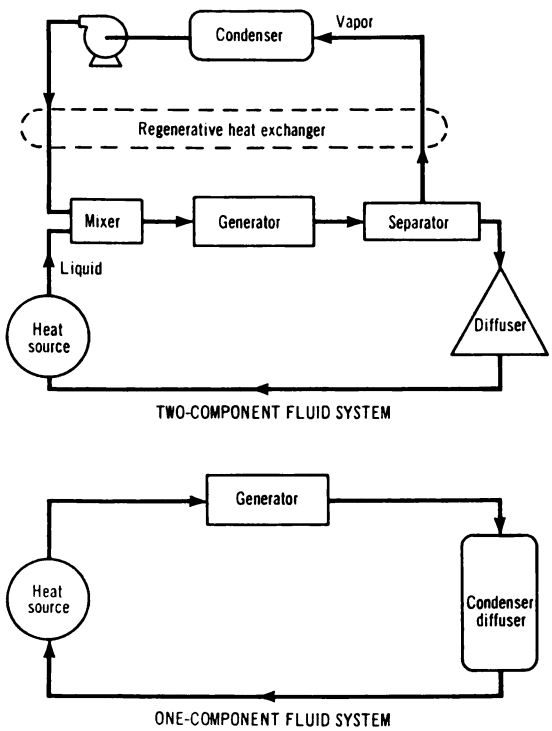

Fig. 4 Two-phase generator cycle variations can be either two-component system (above) or one-component system (below).

The efficiency of a two-phase generator cycle is potentially higher because power can be extracted under controlled velocity conditions to minimize friction—and the two-component mixture then can be separated at a lower energy and with lower losses. The potentially attractive performance of the cycle was discussed by Hammitt.[20] He showed that higher cycle efficiencies are obtainable if a high gas-to-liquid volume flow ratio can be tolerated in the generator without undue loss in efficiency; under this condition, cycles that can use successfully a high volume flow ratio appear best. However, if the generator efficiency decreases seriously with volume flow ratios, this conclusion is reversed.

A novel two-phase generator cycle was also proposed by Bidard and Sterlini.[21] The cycle features an MHD pump instead of a diffuser to return the fluid to the high-pressure end of the cycle. Another unique feature of this proposed cycle is that the entire apparatus would be enclosed within a magnet so that end effects in the pump and generator could be eliminated.

CONDENSING-INJECTOR CYCLE

Several new variations of the condensing-injector cycle were also proposed. Both Prem[7] and Radebold[8] stress the possibility of minimizing the losses associated with mixing fluids of different velocities by the use of a multistage concept in which the injected-fluid velocity would be matched stepwise with the flow velocity in the nozzle. The theoretical thermodynamic efficiency of such a cycle was reported to be 60% of the Carnot efficiency,[7] although no numerical analysis was presented to corroborate quantitatively the improved performance claimed. Present and planned studies will determine the conversion of a liquid into a foglike two-phase flow in the heat source, dispersion of the liquid injected in the different steps of the transformation, and condensation of the fog flow.

Because of the potential for considerably higher internal efficiency, the two-component cycle was perhaps the most important variation of the condensing injector analyzed.[23,24] With lithium as the subcooled injection stream and cesium or potassium as the vaporized stream, the losses due to the acceleration of the injection stream would be reduced because of the high heat-sink capacity (and thus lower injection flow rate) of lithium. For a cycle with lithium–cesium as the two-component working fluid, vapor–liquid internal efficiency may approach 80% and cycle thermal efficiency could reach 30% with a 1200°K maximum cycle temperature. There is an optimum vapor quality that gives maximum injector and cycle performance; lower mixing-chamber pressure reduces injector efficiency but raises overall efficiency; increased inlet liquid velocity diminishes

Digitized by Google

performance. Because the results presented in both studies are based solely on thermodynamic considerations and no losses are accounted for, the results represent the maximum thermodynamic performance that can be achieved. Although the results are comparable to those presented previously for other fluids and cycles,[25–27] these studies underscore the possible gains that might be obtained through the use of two fluids in the cycle.

Additional experimental data[28] on the performance of the condensing injector for space power show exit pressures greater than both liquid and vapor inlet pressures. The data, which are encouraging in terms of predictability and efficiency performance, also indicate that detailed knowledge of the mixing process is needed to design high-performance condensing injectors. The highest efficiencies occur when the velocity ratio between vapor and liquid is maximum and the flow ratio of liquid to vapor is minimized.

Progress Expected in Next 2 Years

The greatest effort in the next 2 years will probably be directed toward building and testing an efficient induction generator. As rapporteur, W. D. Jackson stated in his analysis of the state of the art of generator development, "A quick calculation of the relevant magnetic Reynolds number and a comparison of it with what rotating machine designers call the reactance to the distance ratio allowable in solid rotor induction machines shows that the results presented for the operation of these generators, their self-excitation, their steady running, and so on, was never really seriously in doubt. The basic issue remains one of realizing an induction generator of acceptable real efficiency within the limitations imposed by systems and materials considerations."

Another major question that is expected to be resolved in this time period will be the feasibility and performance of the condensing-injector cycle. The geometries, fluids, and parameters of interest to liquid-metal power cycles have not been studied experimentally thus far. However, studies under way at MIT and Argonne National Laboratory and elsewhere will remove the uncertainty concerning injector performance.

References

Except for Refs. 1 to 6, 16 to 19, 22, and 25 to 27, all references are papers presented at the Symposium on Magnetohydrodynamic Electrical Power Generation, jointly sponsored by the International Atomic Energy Agency and the European Nuclear Energy Agency, (OECD), held in Salzburg, Austria, July 4–8, 1966. Volume 1 of the proceedings, *Electricity from MHD*, is now available in the United States through the National Agency for International Publications, Inc., 319 E. 34th Street, New York, N. Y. 10016.

1. M. Petrick, Liquid-Metal MHD Topping Cycles, *Power Reactor Technol.*, 8(4): 199-209 (Fall 1965).
2. Proceedings of Third Symposium on Magnetohydrodynamic Electrical Power Generation, Salzburg, Austria, July 4–8, 1966, to be published.
3. *Magnetohydrodynamic Electrical Power Generation*, Symposium Proceedings, Paris, July 1964, Vols. 1 to 4, European Nuclear Energy Agency, Organization for Economic Cooperation and Development, 1964.
4. *Magnetoplasmadynamic Electrical Power Generation*, Symposium Proceedings, Newcastle-on-Tyne, England, 1962, The Institution of Electrical Engineers, London, 1963.
5. W. D. Jackson, Magnetohydrodynamic Power Generation—A Status Report, *Electron. Power*, 10: 258-263 (August 1964).
6. W. D. Jackson, E. S. Pierson, and R. P. Porter, Design Considerations for MHD Induction Generators, in *Magnetohydrodynamic Electrical Power Generation*, Symposium Proceedings, Paris, July 1964, Paper 61, European Nuclear Energy Agency, Organization for Economic Cooperation and Development, 1964.
7. L. L. Prem, Analytical and Experimental Results of the Fluid Metal MHD Power Conversion Programme, Paper SM-74/184.
8. R. Radebold, H. Lang, T. Schultz, H. Weh, E. Klein, and K. H. Wagner, Energy Conversion with Liquid Metal Working Fluids in MHD-Staustrahlrohr, Paper SM-74/30.
9. D. G. Elliott, D. J. Cerini, L. G. Hays, and E. Weinberg, Theoretical and Experimental Investigation of Liquid-Metal MHD Power Generation, Paper SM-74/177.
10. W. Peschka, C. Carpetis, A. Gann, and B. Tries, Some Aspects of the Use of a Cryogenically-Cooled Primary Windings System for an A.C. MHD Generator, Paper SM-74/196.
11. W. D. Jackson and E. S. Pierson, Material Limitations in the MHD Induction Generator, Paper SM-74/161.
12. M. Petrick, MHD Generators Operating with Two-Phase Liquid Metal Flows, Paper SM-74/196.
13. P. L. Kirillov, V. I. Subbotin, I. P. Stakhanov, and N. M. Turchin, Measuring the Electrical Conductivity of a Liquid-Vapour Potassium Mixture, Paper SM-74/106.
14. F. Engeln and W. Peschka, End Effects on the Linear Induction MHD Generator Calculated by Two-Sided Laplace Transform, Paper SM-74/93.
15. J. R. Moszynski, End Losses in MHD Channels of Variable Cross-Section and Their Reduction, Paper SM-74/194.
16. G. W. Sutton, H. Hurwitz, Jr., and H. Poritsky, Electrical and Pressure Losses in a Magnetohydrodynamic Channel Due to End Current Loops, *IEEE (Inst. Elec. Electron. Eng.) Trans. Commun. Electron.*, 80(58): 687-695 (1961).
17. R. N. Sudan, Interaction of a Conducting Fluid Stream with a Traveling Wave of Magnetic Field of Finite Extension, *J. Appl. Phys.*, 34: 641-650 (1963).
18. E. S. Pierson, The MHD Induction Machine, Sc. D. Thesis, Massachusetts Institute of Technology, September 1964; also Report AFAPL-TR-65-107, Chap. 6, August 1965.
19. M. Petrick, Performance Characteristics of a Liquid Metal MHD Generator, in *Magnetohydrodynamic Electrical Power Generation*, Symposium Proceedings, Paris, July 1964, Paper 62, European Nuclear Energy Agency, Organization for Economic Cooperation and Development, 1964.
20. A. G. Hammitt, Magnetohydrodynamic Liquid Metal Power Conversion Systems, Paper SM-74/193.
21. R. Bidard and J. Sterlini, MHD Generator Using an Emulsion, Paper SM-74/108.
22. W. F. Wade and M. B. Moffett, The Bubble-Flow Magnetofluid-Mechanical Energy Conversion System for Space Power, Report ER-5978, Thompson Ramo Wooldridge Inc., May 18, 1964.

Digitized by Google

23. S. N. Basov, P. L. Kirillov, V. I. Subbotin, and N. M. Turchin, Injection of Liquid Metals in MHD Converters, Paper SM-74/107.
24. K. A. Yakimovich, E. E. Shpilrain, and Yu. M. Syaskin, Thermodynamics of a Two-Component Liquid-Metal Power MHD Assembly with Injector, Paper SM-74/218.
25. K. S. Lee, Analysis of an MHD Power Generation System for Liquid Metals, S.M. Thesis, Massachusetts Institute of Technology, January 1964.
26. G. A. Brown and K. S. Lee, A Liquid Metal MHD Power Generation Cycle Using a Condensing Ejector, in *Magnetohydrodynamic Electrical Power Generation*, Symposium Proceedings, Paris, July 1964, Paper 60, European Nuclear Energy Agency, Organization for Economic Cooperation and Development, 1964.
27. M. Petrick and K. Y. Lee, Liquid MHD Power Cycle Studies, USAEC Report ANL-6954, Argonne National Laboratory, June 1965.
28. G. A. Brown and E. K. Levy, Liquid-Metal Magnetohydrodynamic Power Generation with Condensing Ejector Cycles, Paper SM-74/171.
29. K. I. Dmitriev, Yu. M. Mikhailov, and V. S. Presnyakov, Experimental Investigation of the Magnetohydrodynamic Flow of a Liquid Metal in a Rectangular Duct with Conducting Walls, Paper SM-74/93.
30. I. B. Stechkina and F. R. Ulinich, Hydrodynamics of Flow Two-Component Mixtures in Nozzles, Paper SM-74/100.
31. T. Sekiguchi, M. Katsurai, and K. Yokoyama, An MHD Rotating Machine — A New Type of A.C. Magnetohydrodynamic Power Generator and Turbine, Paper SM-74/137.
32. R. R. Barthelemy and C. E. Oberly, Optimum Magnets for MHD Generators, Paper SM-74/167.
33. L. D. Nichols, Criteria for Use of Rankine–MHD Systems in Space, Paper SM-74/190.
34. A. Maciulaitis, A. L. Loeffler, Jr., and P. J. Calcanes, Experimental Investigation of MHD Flows Through Circular Pipes at High Hartmann and Reynolds Numbers, Paper SM-74/195.
35. Ya. Ya. Lielpeter, Applicability of the Electrodynamic Approximation in the Theory of Liquid-Metal Induction MHD Converters, Paper SM-74/240.
36. L. A. Vulis and V. T. Yaglenko, Observations of Mercury Flowing Along a Trough in a Transverse Magnetic Field, Paper SM-74/249.

Digitized by Google

Component Development: Key to Rankine-Cycle Space Applications

By Edward J. Croke

The development of reactor and isotope heat sources, combined with projected requirements for compact, lightweight electric-power generators for space and undersea application, has given rise to extensive turboelectric-power development programs intended to exploit the potentially high efficiency of the Rankine cycle. Experience in these system development programs has spotlighted the importance of improving the technology of high-performance components capable of long-time unattended operation.

In terms of practical engineering, a great deal of Rankine-cycle component development has taken place in recent years. Much of it has been based on very pragmatic developmental methods. At present, bearing wear, boiler conditioning, and turbine erosion are the most significant problems in achieving reliable Rankine cycles. Fabrication techniques for longer life bearings and higher temperature turbines, more efficient pumps, and less vulnerable radiators are being developed. Heat-transfer properties of useful liquid metals are being investigated in several research facilities. Nevertheless, for the long term, the work done so far indicates that additional basic research is needed in the areas of heat transfer, materials, and structural mechanics. The situation is illustrated by consideration of the status of the four major Rankine-cycle programs and the component experience discussed in this article.

Rankine-System Development Programs

The four major Rankine-system development programs include the mercury Rankine program sponsored by the U. S. Atomic Energy Commission (AEC),[1] the SNAP-8 Program of the AEC and the National Aeronautics and Space Administration (NASA),[2] the SNAP-50/SPUR Program of the AEC and the U. S. Air Force,[3] and the Organic Working Fluid Rankine Cycle Programs of the U. S. Navy, Air Force, and AEC.[4] There also have been associated component studies and development efforts at various government and industrial facilities.

The early history of Rankine-system development parallels the growth of the national space program. Initially, mission requirements were not well defined, and, with a premature sense of optimism, full-scale systems were projected before the problems of building a component technology were fully evident. When experience spotlighted the component problems, and as mission requirements were seen to change rapidly, most of the systems programs evolved into component and technology programs that will permit development of a range of Rankine systems that can supply power for a variety of anticipated space missions.

MERCURY RANKINE PROGRAM

Development of the AEC's SNAP-2 system began in 1957 with the objective of producing a flyable 3-kw(e) reactor-powered mercury Rankine system (Fig. 1) capable of operating for 1 year (Ref. 5). With changes in mission requirements, the SNAP-2 program evolved into the mercury Rankine program—whose initial objectives were to develop system technology and qualify components (exclusive of the reactor or isotope heat source) for a space power plant with 3- to 5-kw(e) power-conversion modules so that the plant could be adapted to supply 3 to 25 kw(e) for 2500 hr of operation in space.[1] The ultimate goal was to achieve reliable performance for 10,000 hr. The mercury Rankine program is now in the process of being phased out, with only two combined-rotating-unit turbomachinery tests to be completed.

Component Tests. Development tests of the components at Atomics International, the prime contractor, indicated that the required operating life

Digitized by Google

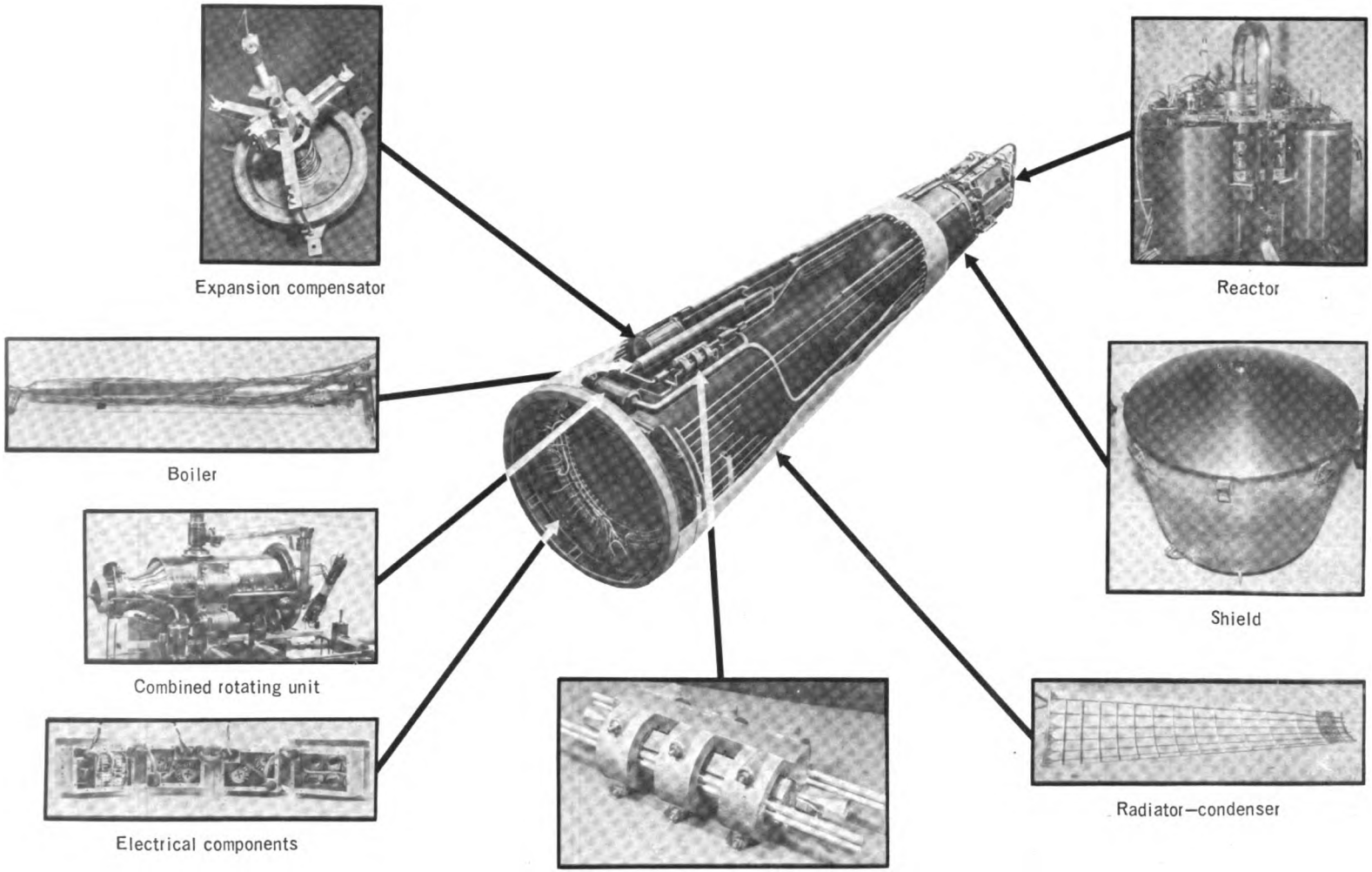

Fig. 1 Mercury Rankine-cycle turboelectric system, as envisioned by Atomics International, would develop 3 to 5 kw(e) at 120 volts and 1800 cycles/sec. Compact reactor heats NaK in primary loop, which circulates NaK into a boiler, where it evaporates and superheats mercury. Mercury vapor drives a turbine that powers a permanent-magnet alternator and a mercury pump, all three of which are mounted on a single mercury-lubricated shaft to form a combined rotating unit. From the turbine the mercury passes through a radiator–condenser and then is pumped back to the boiler to complete the cycle. The NaK is pumped by a thermoelectric direct-current conduction pump that uses the NaK as the hot junction and the mercury as the cold junction for the thermoelements.[1]

Digitized by Google

could be achieved. System performance, orbital start-up capability, and structural integrity have been verified in system-test facilities.[1] Although one combined rotating unit was tested for 7000 hr without major damage, the major developmental problem has been journal-bearing erosion, which could limit the life of the mercury rotating machinery.

The previously experienced bearing erosion–cavitation has been decreased by almost an order of magnitude by reducing loads and increasing bearing pressure. Life capabilities well beyond 10,000 hr now seem feasible.

Other components demonstrated satisfactory performance. The model-5C boiler, which was tested for 38,000 hr, has proved to be structurally and thermally acceptable for long-life operation if protected from exposure to air and contaminants such as trace quantities of oil. The adequacy of the thermoelectric pump was demonstrated by many hours of testing. Several pumps have operated for >20,000 hr. Both the honeycomb and aluminum-fin radiator–condensers have demonstrated good structural and operational characteristics, although the process for bonding aluminum radiator fins to the Haynes 25 condenser tubes caused some developmental problems. The startup components (pressure regulator and injection tanks) posed no problems more serious than the fabrication of the metal starting bellows.

System Startup. Orbital (zero-gravity) transient characteristics of the integrated Rankine system have been simulated successfully, and automatic startup has been accomplished with a nonnuclear installation. Although the simulated system achieved stable operation, long operating lifetimes remain to be demonstrated—and performance degradation, control interactions, mercury corrosion, metallurgical-processing effectiveness, and long-term exposure to vacuum must be evaluated to qualify the system for flight operation. Multiple-restart capability has also been demonstrated.

SNAP-8 SYSTEM

The NASA Lewis Research Center has project-management responsibility for the development of SNAP-8 power-conversion equipment, and the AEC Space Nuclear Systems Division is charged with nuclear-systems development.

The mercury Rankine turboelectric-power system (Fig. 2) for the SNAP-8 Program, which was based considerably on technology developed under the SNAP-2 program, has had a history somewhat similar to that of the SNAP-2 Program and the mercury Rankine program. The initial objective of developing a 35-kw(e) reactor-powered system for 10,000 hr of operation in space after a remote-controlled startup has remained more or less intact from program inception in 1960 to the present. However, limitations of the state of the art of liquid-metal-systems technology in 1962 resulted in a major redesign of the prototype system. With system-level development curtailment in 1965, actual development was limited

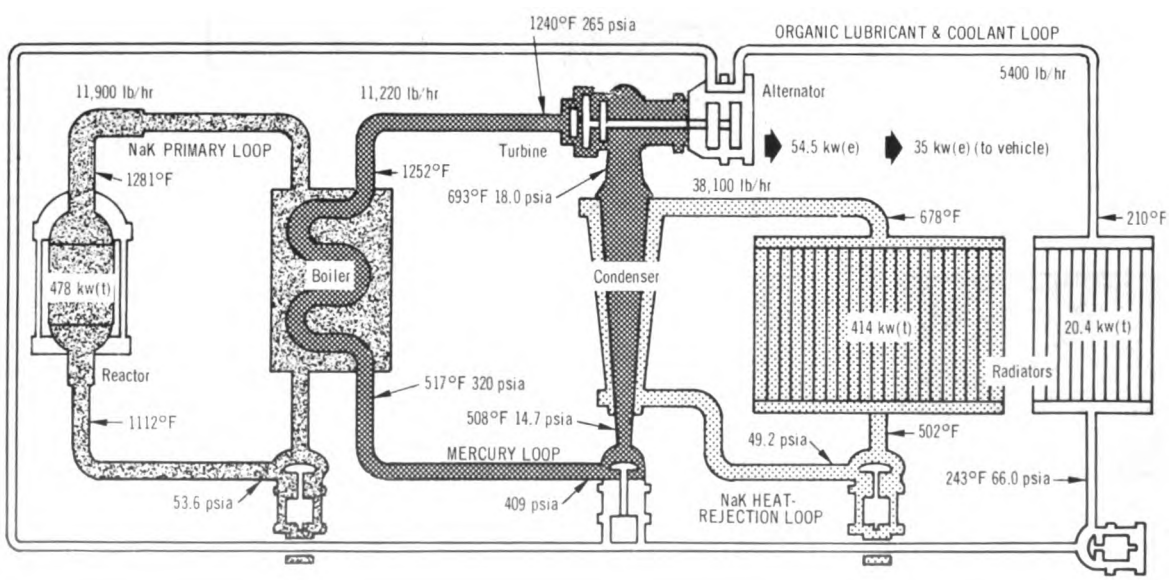

Fig. 2 The SNAP-8 mercury Rankine-cycle system, developed for NASA Lewis Research Center by Aerojet-General Corporation, consists of a compact uranium–zirconium fueled-and-moderated reactor (developed by Atomics International), a boiler, condenser, turboalternator, radiator–condenser, mercury and NaK pumps, and a control system. These are arranged in three liquid-metal circulating loops: A NaK primary loop cools the reactor and powers the mercury Rankine-cycle secondary loop; the tertiary NaK loop transfers heat from the mercury condenser to the radiator–condenser, where the heat is rejected to space. In a fourth loop an organic fluid circulates to lubricate bearings and to cool the alternator, electric motors, and controls.[2]

Digitized by Google

to an attempt to qualify the first power-conversion test system for 10,000 hr of operation.

Reactor Tests. The SNAP-8 test reactor went critical in June 1963 and later demonstrated sustained power operation and static and dynamic stability. The longest continuous test run was 5000 hr; the reactor and test facility were shut down as planned in April 1965 after accumulating a total of 12,000 test hours that included 100 days of operation at 600 kw(t) with a NaK exit temperature of 1300°F. Design has been completed, and fabrication is under way for the second SNAP-8DR reactor test.

Component Tests. Although the boiler designed for SNAP-8 proved generally satisfactory, it was plagued with inconsistent boiler conditioning (scouring of scale oxides and contaminants from the heat-transfer surface). The mercury condenser performed generally well in preliminary tests. The 51.6-kw(e) turboalternator performed satisfactorily in more than 830 hr of tests at approximately design conditions. The NaK pump-motor assemblies accumulated more than 1000 hr of operation in >1100°F NaK; the mercury pump-motor assemblies completed >120 hr of operation at an inlet temperature of 500°F; a Thompson Ramo Wooldridge Inc. lubricant–coolant pump-motor assembly achieved >1000 hr of operation at rated conditions without performance degradation (seven of these units accumulated a total of more than 4300 hr of operation). The start system, voltage regulator, speed controller, and related electrical subsystems demonstrated satisfactory performance.

Although the mercury boiler, turbine, condenser, and pump demonstrated satisfactory combined performance for 837 hr in a multiple-component test loop, the entire nonnuclear four-loop system has not yet been operated as an integral unit. Such a test of the first power-conversion system is scheduled for early 1967 as part of the component qualification program.

SNAP-50/SPUR SYSTEM

Little information is available on this program, but AiResearch Mfg. Co. (a division of the Garrett Corp.) indicates that turbine-rotor bearing materials, lubrication, and stability may be among the foremost problems.[6] Blade erosion and associated turbine-life limitations are no longer expected to loom large among development difficulties. Experience with these components will be considered in greater detail in the Rankine Component Technology subsection of this article.

ORGANIC RANKINE-CYCLE SYSTEM

This 1.5-kw(e) Rankine system, whose combined rotating unit was being developed by Sundstrand Corp. for the U. S. Air Force, would have been heated either by a ^{210}Po source or by solar energy concentrated by a mirror. The Dowtherm A working fluid reaches a maximum temperature of ~700°F, and so the high-temperature problems of the liquid-metal Rankine systems are avoided. The organic Rankine system (Fig. 3) consists of a boiler, a combined rotating unit (including turboalternator and Pitot pump), a radiator–condenser, a regenerator, and the control system. The thermodynamic cycle is shown in Fig. 4.

The combined rotating unit accumulated more than 2000 hr of successful tests; a single set of bearings has served for more than 600 hr of cumulative running time with more than 100 restarts. Although these tests have shown good performance, long-endurance

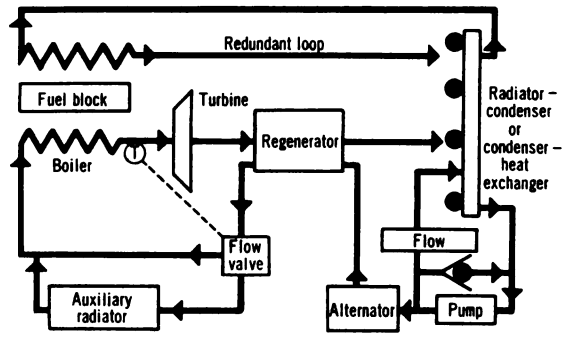

Fig. 3 Organic Rankine-cycle turboelectric system for Apollo type mission would have a 17.5% overall cycle efficiency (including losses and control power) with 750°F 157-psia Dowtherm A working fluid and ^{210}Po as fuel. The system would provide 1.5 kw(e) for a 14-day mission plus a 30-day hold. Fuel block and shielding would weigh 250 lb, and redundant conversion equipment would weigh 280 lb (Ref. 4).

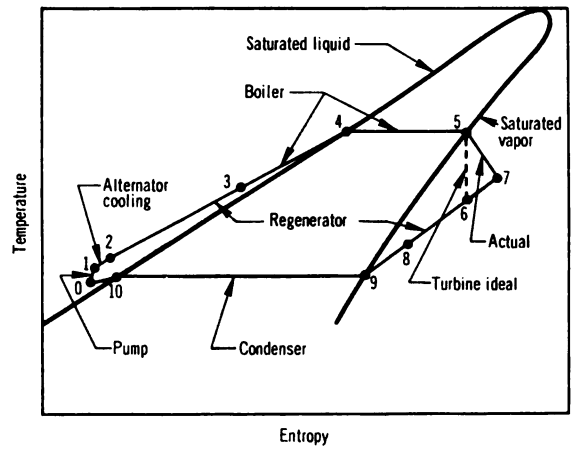

Fig. 4 Temperature–entropy diagram for Dowtherm A Rankine cycle. Dowtherm A has a composition of 26.5% by weight $(C_6H_5)_2$ and 73.5% $(C_6H_5)_2O$, molecular weight of 165.65, freezing point of 53.6°F, and vapor pressure of 0.63 psia at 300°F and 106.81 at 700°F. Corresponding characteristics of biphenyl, another organic fluid, are $(C_6H_5)_2$ composition, 154.20 molecular weight, 158°F freezing point, and vapor pressure of 0.68 psia at 300°F and 109.0 psia at 700°F (Ref. 4).

Digitized by Google

system capability equivalent to 10,000 hr of unattended operation in space remains to be demonstrated. Because the thermal stability of the working fluid may limit system life, AEC programs are evaluating this uncertainty.

Rankine Component Technology

Each major component of a high-temperature Rankine system has its own developmental and operational problems. Thus it is worthwhile to consider and compare components developed in the various Rankine programs. In general, parallel and essentially independent solutions seem characteristic of Rankine technology.

PUMPS

Notable among the pumps under development are the mercury and NaK pumps for SNAP-8, the NaK pumps for the mercury Rankine program, the potassium pumps operated at Oak Ridge National Laboratory (ORNL), and those being developed by General Electric Company for NASA.

Mercury Pumps for SNAP-8. The duty cycle of the mercury pump in SNAP-8 includes 10,000 hr of unattended operation in a radiation environment of 10^{13} neutrons/cm^2 at a speed of 8000 rpm and with an inlet suction temperature of 405°F. Pump flow rate is 1.775 gal/min at a nominal head of 10.5 psi (Ref. 2).

A jet pump at the inlet of the main pump housing overcomes potential cavitation difficulties at the rather low specified pump suction head. The mercury pump is a single-shaft overhung system with an impeller at one extremity (upstream of the jet pump) and a drive motor at the other. The semiopen-vane centrifugal impeller is ball-bearing mounted in a housing that has been designed to minimize bearing loads. The bearing lubricant, organic 4P3E (polyphenyl ether), is separated from the mercury flow by a dynamic seal system consisting of a viscopump that maintains a stable liquid–vapor interface in the fluid. Leakage of the fluid to space is minimized by a helical thread molecular pump that has a 3-mil rotating clearance.

On the bearing side of the rotating system, a similar dynamic seal is used; however, additional low-speed (6000 rpm) and stationary sealing is provided by stationary carbon face seals; a bellows arrangement lifts the carbon face seals off the bearing surface at rotational speeds > 6000 rpm. The central housing of the pump supports two angular contact end bearings of M-50 tool steel. Between these end bearings is a rotating "slinger" seal and a molecular pump. The pump motor has silicon-steel laminae and is a 400-cycle induction unit cooled with 4P3E. At the ends of the motor, the terminals are hermetically sealed. Between the motor and one end bearing is a scavenging seal; at the other end of the pump, there is a face seal. The prospect of running the pump flooded was considered, but the system temperature rise caused by viscous effects proved to be excessive, and hence the end scavenger was provided.

The test pump weighs ~186 lb in the fully instrumented state. Much of this weight is in the 9% chronium–1% molybdenum steel housings hogged from solid forgings. A realistic flight weight for the system would be ~110 lb.

Tests have been conducted on both the subassembly and system levels. The cavitation performance of the jet pump has been tested with mercury, and the sealing system has been tested for 1000 hr in vacuum. Extrapolation of the results of these tests shows that the mercury loss to space will be ~1.75 lb per 10,000 hr and that 0.1 lb of 4P3E will be lost in this same time. The motor has been tested for over 20,000 hr immersed in 4P3E, and, although the coolant temperature reached 350°F during the tests, no compatibility problems were evident.

Three pump assemblies were built. Two were retained at Aerojet-General Nucleonics and one was sent to NASA Lewis Research Center for testing. More than 140 starts were accumulated on these units, of which 72 starts were on one pump. Except for two failures of the space-seal lift-off bellows, all tests were successful. However, some degree of cavitation was detected near the end of the tests.

The cavitation limit of the assembly was imposed by the centrifugal impeller, which is provided with a 2-ft head by the jet pump. The minimum net positive suction head ranged from 0.1 ft at 0.5 gal/min to 0.75 ft at 2.25 gal/min. Overall efficiency of the pump was found to be ~13%.

NaK Pumps for SNAP-8. In the primary and tertiary NaK loops of the SNAP-8 system, each pump is a self-contained hermetically sealed unit with a single-shaft connecting motor (208-volt induction, rated at 1530 rpm) and an impeller. The type 410 stainless-steel impeller, a semiopen-vane unit with 90° backvanes, has a rated specific speed of 1600 rpm and is enclosed in a double volute housing of type 304 stainless steel. It is designed for use with 1170°F fluid.[7]

The pump has been tested in a loop containing a heat-exchanger cold trap, an economizer, and a 5-μ NaK filter. The fluid discharged at 350°F into the economizer, where it was cooled to 320°F and sent to the heat-exchanger cold trap and cooled to 290°F. It then entered a canister containing stainless-steel wire mesh (to trap oxides) and returned to the economizer, where it was heated to 300°F and filtered. (Reheating prevents the filter from becoming an oxide trap since it is not permitted to become the coldest part of the system.)

Considerable testing of this design also has been done on the subassembly level. The motor has been dynamometer checked in air, and the bearings have

Digitized by Google

been run in both oil and NaK to determine the minimum allowable bearing thickness as a function of bearing load. The capability of the cold trap to keep the oxide level below 20 ppm was tested and verified, and water tests have determined the heat-exchanger heat-transfer characteristics.

A major development problem was NaK leakage (at temperatures above 500°F) through inclusions in the original type 347 stainless-steel pump housing. This design was successfully fabricated in type 304 stainless steel. Another problem was rotor sticking, caused by flat bearing pads; this situation was corrected by grinding a radial taper on the bearings to obtain a line contact.

Eight pumps were built and tested at fluid temperatures up to 1200°F. One unit was run for 2040 hr. The design is reported to have met or exceeded all requirements with a demonstrated efficiency of 35 to 40%. (The significant NaK pump losses are frictional.)

Thermoelectric-Powered NaK Pump. The Atomics International electromagnetic pump (Fig. 5) is an unusual device in that the 3.5 kw(e) required for its operation is generated thermoelectrically from the waste heat of the primary loop.[8] Rated for a flow of 12 gal/min at 1200°F, the pump has a pressure head of 1 psi. The design has been optimized in terms of weight vs. thermoelectric thickness, weight vs. throat height, and weight vs. magnetic-field strength.

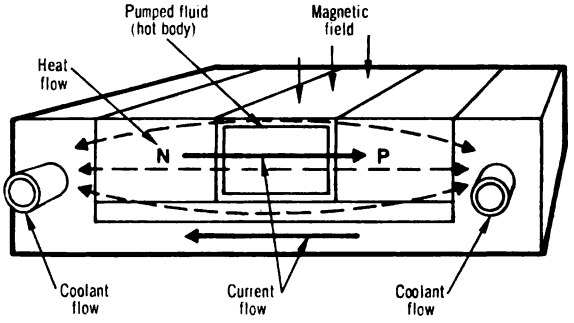

Fig. 5 Schematic of SNAP-2 thermoelectric-powered electromagnetic NaK pump.[8]

An electrically heated test loop was constructed for this direct-current induction pump. Four test series were devised: (1) flight-operation duty cycle, (2) startup transient tests, (3) steady-state performance evaluation, and (4) endurance testing. Of the 12 pumps built, 10 have been tested at rated conditions. About 20,000 hr have been accumulated on each of three units; two tests were terminated after 5000 hr of operation each.

The maximum temperature transient encountered was 363°F/sec — well above the specification limit of 50°F/sec — but no adverse results were reported. Maximum observed degradation in performance was associated with a 16% flow decrease after 5000 hr of operation on one unit and a 10% flow decrease after 5000 hr on another. Two units, tested in a vacuum environment for 800 to 1000 hr, showed no significant performance degradation; test units subjected to thermal cycling evidenced leakage only after 3000 to 5000 hr. Magnet degradation caused by nuclear radiation at operating levels appeared negligible over the time considered.

Potassium Pumps with Turbine Drives. A program was established at ORNL to accumulate experience with liquid-metal turbopumps by fabricating and testing several machines of typical performance and behavior.[9] High reliability was found to depend on bearing design and materials, minimization of turbine-bucket damage, and minimization of pump cavitation.

The turbopump developed at ORNL (Fig. 6) used bearings of tungsten carbide with 12% cobalt binder. Because the coefficient of thermal expansion of this material differs significantly from that of the austenitic steel casing, TZM bearing housings were chosen. Radial thermal expansion was accommodated by cantilever-mounting the bearings to obtain radially soft but axially stiff behavior. Journal bearings were lubricated with potassium. Axial loads were carried by two flat-plate thrust bearings.

The turbine shown in Fig. 6 is 2.75 in. in diameter, and the impeller is 1.0 in. in diameter. Turbine speed is 24,000 rpm, and the design inlet temperature is 1540°F. Eight of these units were fabricated, and seven were successfully tested to failure for periods ranging from 0.5 to 327 hr. One continuous run was 140 hr, and total accumulated operating time was >540 hr. More than 125 starts were recorded. In these tests, termination was caused by such failures as bearing-sleeve fractures, seizing of the journal bearings of the turbine or impeller, impeller rubbing against the pump housing, or filter clogging. Figure 7 shows pump performance.

Fabrication of two larger pumps was contracted to Aeronutronic/Philco. The first of these, Mark I (Fig. 8), had a 6-in.-diameter turbine wheel and a 2.75-in.-diameter impeller; the second model, Mark II, was similar but was rated for a higher flow and had a more massive casing. Other improvements in the Mark II included (1) carburizing all TZM surfaces to eliminate galling, (2) nitriding all stainless-steel surfaces to reduce corrosion, (3) mounting the WC bearing housings on conical surfaces to compensate partially for differential thermal expansion, and (4) lengthening certain bearings. The Mark I turbine used convergent–divergent nozzles, but the Mark II turbine used only convergent nozzles.

Characteristics and performance of three turbopumps are shown in Table 1. Although one of these pumps was run to 75% of theoretical cavitation conditions, cavitation damage was not found. The low

Digitized by Google

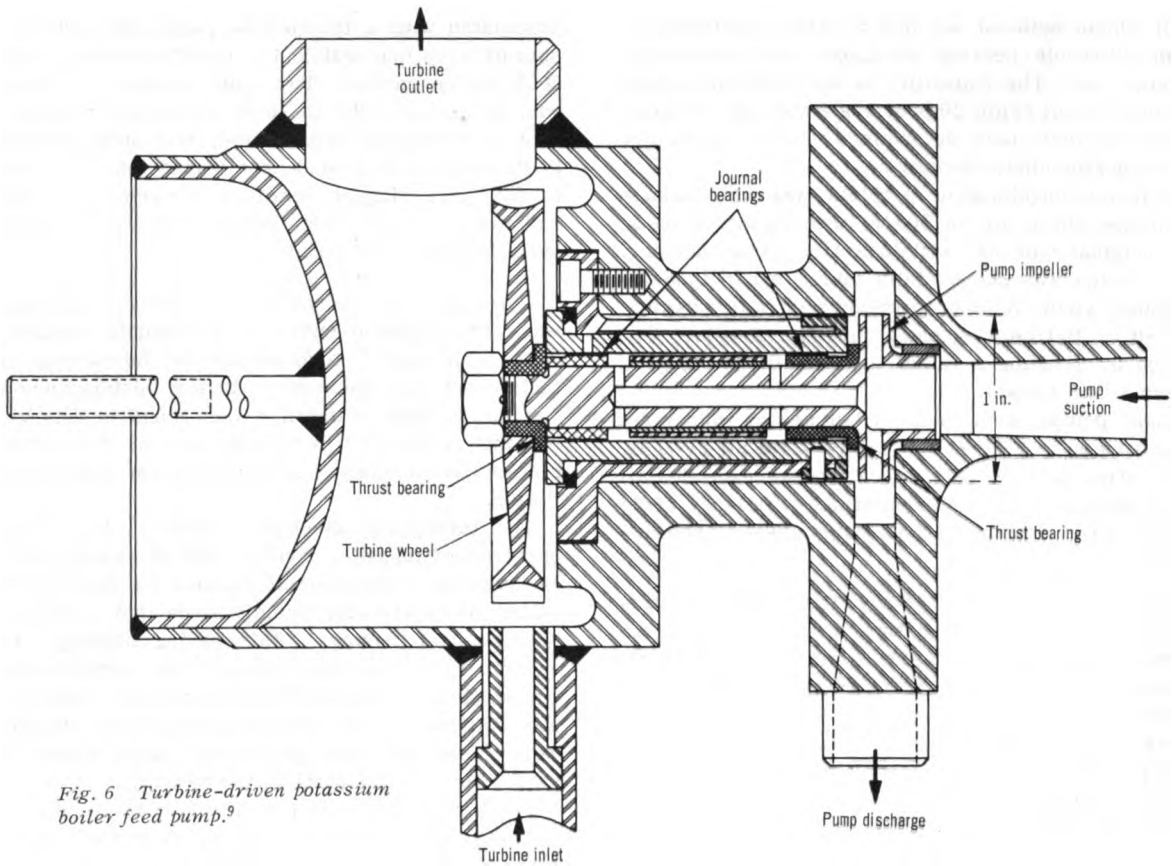

Fig. 6 Turbine-driven potassium boiler feed pump.[9]

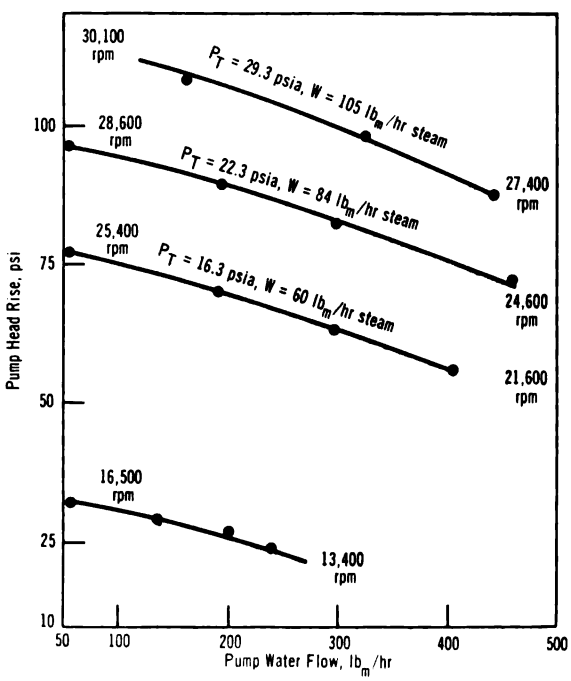

Fig. 7 Turbine-driven-pump performance characteristics on steam and water. P_T is turbine inlet pressure, W is turbine vapor flow; turbine outlet pressure is ~2 psia for all runs.[9]

velocities and short runs may have prevented damage, but there is reason to believe that extreme cavitation need be no more damaging to a machine than mild cavitation—depending upon the properties of the fluid and the degree of subcooling involved. The quality of the turbine exhaust was ~ 95% for these units. Little erosion was detected under these conditions, in which the condensated consisted of very finely divided particles.

BOILERS

A principal factor limiting Rankine-system boiler design has been a lack of precise liquid-metal heat-transfer data. A better design basis has been established by studies with mercury, potassium, and sodium.

MRP Mercury Boiler. Considerable test experience has been achieved with the mercury Rankine program compact boiler; three design models have accumulated a total of 38,000 hr. Major problems have been with the mercury corrosion and boiling heat-transfer conditioning of the Haynes 25 tubing. The mercury corrosion rate is diffusion controlled, decaying with time such that the generated "crud" products can be adequately trapped or filtered to assure at least 1 year of operation. The boiler deconditioning appears to be controllable if precautions

Digitized by Google

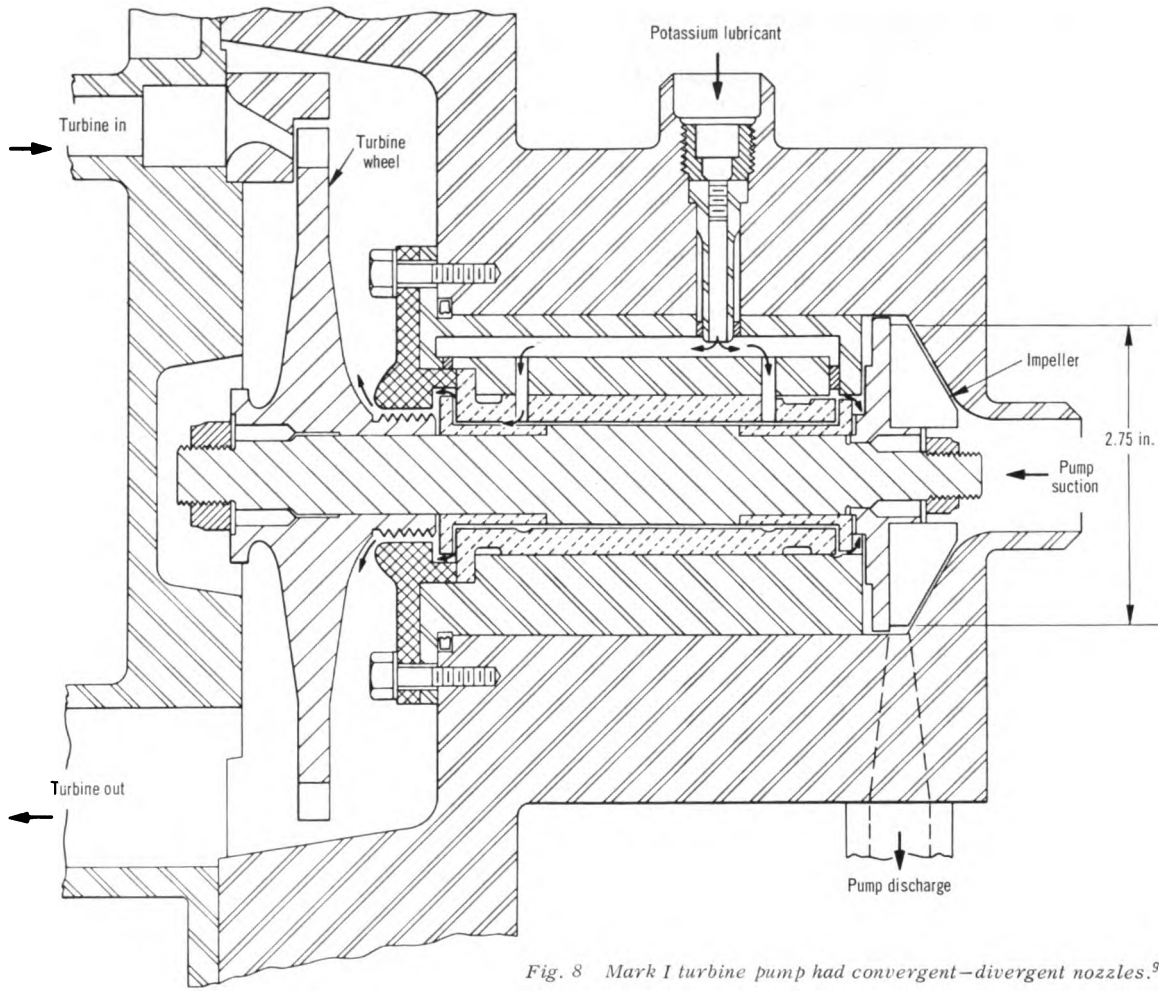

Fig. 8 Mark I turbine pump had convergent–divergent nozzles.[9]

are taken with respect to cleanliness, air inclusion, and surface treatment. Even with some degree of boiler deconditioning, the power from the model-V combined rotating unit was generally adequate. The endurance experience of various boiler tests indicates generally that conditioning characteristics improve with time with a leaktight system.

Mercury Boiler for SNAP-8. Considerable boiler test experience was accumulated during the SNAP-8 development effort.[10] A 480-kw(t) forced-convection one-pass mercury boiler heated by NaK (with a gas-fired heater) was extensively tested. The NaK enters this tube-in-shell boiler at 1280 to 1330°F. Mercury enters (0.3 ft/sec) the double spiral helical coils surrounding the NaK shell at 320 psia and 517°F, and, at rated operation, exits at 1252°F. The helical tubes are 9% chromium–1% molybdenum steel, chosen for its corrosion resistance, and the NaK shell is of type 315 stainless steel. Over 1600 test hours were accumulated on this configuration—1400 hr were on a single unit.

Table 1 TURBINE-DRIVEN POTASSIUM BOILER FEED PUMPS[9]

	Pump		
	ORNL	Mark I	Mark II
Speed, rpm	25,000	8,000	8,400
Inlet temp., °F	1,540	1,540	1,540
Turbine inlet pressure, psi	30	30	30
Turbine exhaust temp., °F	1,050	1,050	1,140
Turbine exhaust pressure, psi	1.5	1.5	3.0
Flow, gal/min	1.5	1.5	3.0
Suction temp., °F	1,050	1,050	1,050
Suction pressure, psi	1.5	1–4	1–4
Pump discharge pressure, psi	70	50	60
Accumulated run time, hr	327	1,500	

These boilers are rated for 11,000 lb/hr flow and have mass velocities of 200 lb/(sec)(sq ft). Instability was 4 to 6 cycles/min or ~200 psi. Predictions of pressure drops and heat transfer were made with the Martinelli correlation.

Boiler conditioning proved to have a major influence on performance. The first unit tested required ~100 hr of operation to become wetted and to achieve rated performance. When conditioning was complete, the pressure drop and the exit temperature stabilized near the predicted values for a wetted system. A second boiler operated for ~20 hr in a

Digitized by Google

derated condition with an exit temperature of ~900°F rather than the rated 1252°F. Exit quality was only ~70%, and the pressure drop was correspondingly low. After 20 hr the exit temperature stabilized at 1200°F, and near rated performance was achieved.

Later tests revealed that the addition of ~20 ppm liquid rubidium (to serve as a wetting agent) rapidly raised the exit temperature of an unconditioned boiler from 800 to 1200°F with a corresponding increase of pressure drop. After boiler shutdown and restart, further rubidium injection was required—probably because of consumption as oxides during the shutdown period. Because rubidium does form oxides that cause unpredictable alteration of the heat-transfer properties of the mercury, this conditioning technique was not favored for the SNAP-8 system. After 200 hr of operation with rubidium, the boiler was shut down, cleaned out, and restarted; rated performance was attained immediately. Rubidium appears to have promoted the cleaning of scale from the boiler-tube surfaces.

Heat Transfer in Mercury Boilers. Four basic modes of heat transfer in mercury flow have been defined: (1) contact boiling in the liquid regime, (2) slug flow, (3) intermediate contact (semiboiling), and (4) film boiling. The first, third, and fourth of these flow regimes are fairly well understood, but the second, slug flow, is neither well known nor easy to investigate. Liquid slugs form at low flow velocities (~0.5 ft/sec) and tend to use up considerable boiling length without significant heat transfer. High flow velocities are required to avoid slug flow in a heat exchanger; however, the associated pressure drops are frequently prohibitive. To achieve a high pressure drop and flow velocity in a test boiler at Aerojet-General Nucleonics, workers fabricated several inlet plugs that would provide high flow velocities.[11] These were constructed in two sections, a high-velocity section that gave 0.9 to 6 ft/sec with some preheating of the fluid and a two-phase section with a swirl inducer. Each plug consisted of a cylindrical core spirally wrapped with wire. The amount of flow constriction was such as to initiate boiling at the exit of the first section of the plug since, if boiling were not in progress at the plug exit, the high velocities achieved would not be maintained downstream of the plug, and slug flow might ensue.

A plug designed for an exit velocity of 0.9 ft/sec was installed in a helically wound NaK–mercury boiler fabricated from type 315 stainless-steel tubing. Tests with this plug indicated that the boiler remained unconditioned over most of its length even after extended operation. With a 6 ft/sec plug, significant conditioning was observed after 4 hr and nearly complete conditioning was observed after 20 hr of operation. Subsequent tests with a 4.5 ft/sec plug and with a 0.9 ft/sec plug indicated full conditioning. From these tests was drawn the rather obvious conclusion that a fully conditioned boiler is free of slug flow and needs no inlet plug.

Contaminated fluid tests run with the same set of plugs, but with the addition of oil (contaminant) to the fluid, proved more interesting. When the conditioned boiler with the 0.9 ft/sec plug was contaminated with oil, no deconditioning was observed until the system was shut down. When restart was attempted, the boiler was found to be deconditioned; no amount of running would recondition it.

A conditioned boiler was then fitted with the 4.5 ft/sec plug. The addition of oil caused deconditioning, but reconditioning began after continued operation. Regression was observed after shutdown, but full reconditioning was achieved after restart and 75 hr of operation. In the next test the boiler was fitted with the 6.5 ft/sec plug, and oil was added. Deconditioning occurred, but reconditioning was complete in only 25 hr. Higher plug velocities promoted corrosion and erosion in the systems. (Each of the test plugs was designed for 30% exit quality.)

Deconditioning inevitably occurred after boiler shutdown in these tests. Thompson Ramo Wooldridge reported that hydrogen bright annealing of boilers tends to minimize or to eliminate this effect.

Potassium Boiler for SNAP-50/SPUR. A multitube potassium boiler, designed to test overall heat-transfer performance against theoretical predictions and to verify the results of Freon tests, was fabricated at AiResearch Mfg. Co.[3] The unit, a 19-tube Haynes 25 tube-in-shell boiler, is counterflow heated by sodium in the primary loop. The outer shell is semicircular; the inner 0.25-in.-OD tubes contain twisted tape inserts diffusion bonded to the tube walls. Potassium is circulated by an induction pump; an auxiliary heater at the boiler inlet assures the desired fluid inlet temperature.

The design flow was 5 to 15 lb/min at a mass velocity of 10 to 30 lb/(sec)(sq ft). Exit conditions of up to 150°F superheat were anticipated. Tests indicated that system performance was correlated well by means of the Martinelli equation incremented by 30% to correct for the twisted tape inserts. For fluid exit qualities as low as 40%, the overall measured heat-transfer coefficient was lower than the predicted value, as for low flow rates (~5 lb/sec), where data scatter was considerable.

Operation of the boiler was stable at all times, and boiling was easily initiated by providing sodium at only ~10°F above the potassium saturation temperature. Superheating up to 150°F was readily attained. The achievement of a pressure drop sufficient to ensure two-phase flow was achieved with inlet orificing.

High-Performance Potassium Boiling. A 300-kw Haynes 25 potassium boiler was fabricated by General Electric Company in Evendale, Ohio. This unit employs a gas-fired sodium loop as the heat source and features an air-cooled condenser. The test sec-

Digitized by Google

tion is illustrated in Fig. 9. A series of tests measured local heat-transfer coefficients over the entire series of flow regimes from the subcooled liquid to the superheated vapor states. Local heat-transfer data were evaluated in the nucleate-boiling, critical-heat-flux, transition-boiling, and superheated vapor phases. The tests also produced average heat-transfer data and pressure-drop measurements.[12]

Data runs included tests in which subcooled heating, nucleate boiling, transition-zone boiling, and superheating occurred simultaneously in the flow channel. Local heat fluxes and heat-transfer coefficients were measured in each zone. Figures 10 to 12 are typical of the results obtained. This information should be useful in the design of potassium boilers over a wide range of operating conditions.

Additional nucleate-boiling data were taken at a power level of 100 kw. The effect of vapor quality on heat transfer was not observed to be significant, but the magnitude of the total heat flux did influence the heat-transfer coefficient.

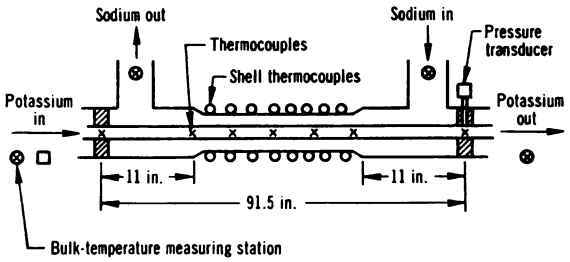

Fig. 9 Instrumentation of 300-kw test facility that includes Haynes 25 potassium boiler.[12]

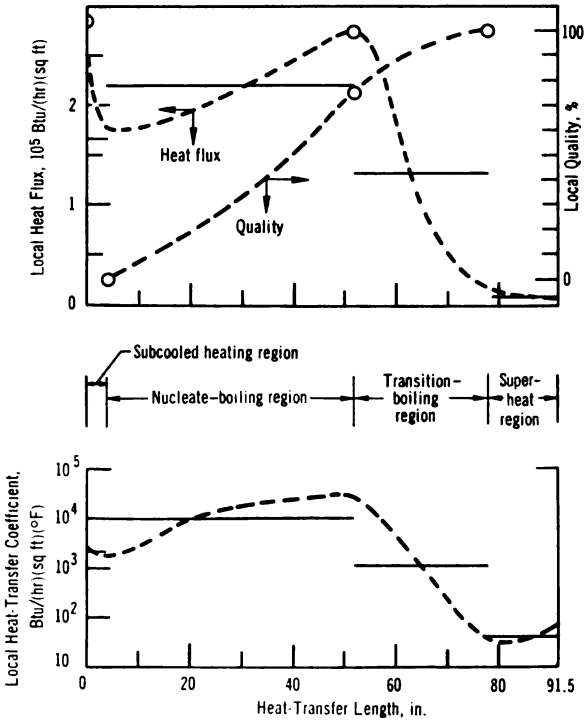

Fig. 10 Results of a typical once-through boiling run with P/D = 6 insert in the 300-kw facility shown in Fig. 9. Data points show calculated or known values; solid lines show average values; dashed lines show estimated values.[12]

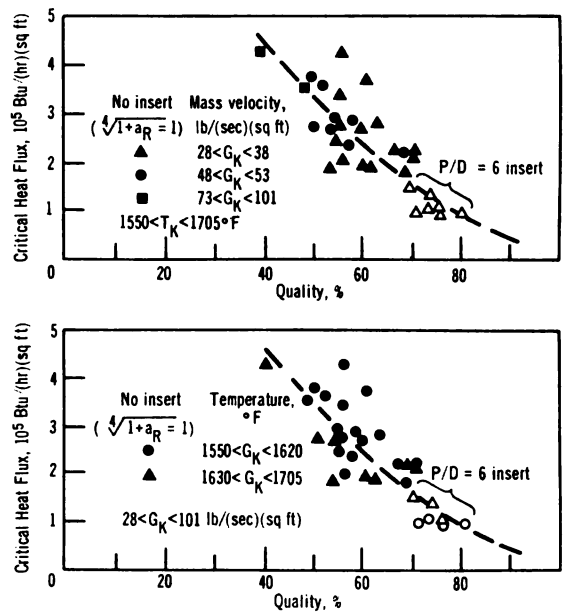

Fig. 11 Critical-heat-flux results for a 0.67-in.-ID boiler tube, showing (top) the effect of mass velocity and (bottom) the effect of temperature.[12]

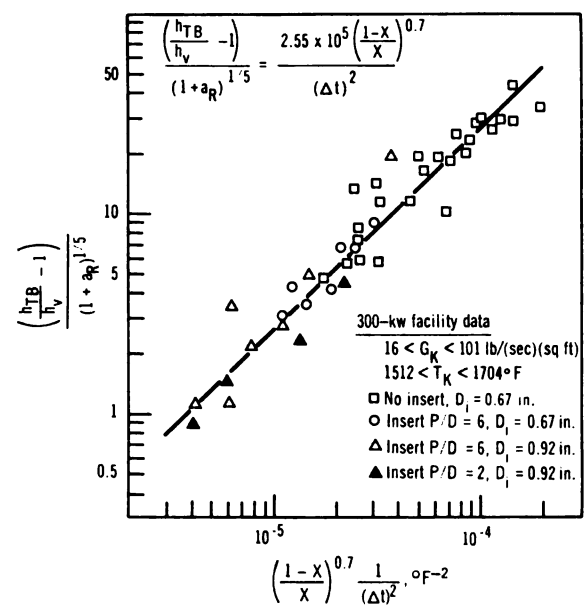
300-kw facility data
16 < G_K < 101 lb/(sec)(sq ft)
1512 < T_K < 1704°F
No insert, D_i = 0.67 in.
Insert P/D = 6, D_i = 0.67 in.
Insert P/D = 6, D_i = 0.92 in.
Insert P/D = 2, D_i = 0.92 in.

Fig. 12 Potassium transition-boiling data plotted in terms of the empirical correlation given.[12]

Digitized by Google

Pressure-drop data for boiling potassium were taken at 300 kw (Fig. 13); fairly good agreement was established with the Martinelli correlation. It appeared that the variation of the overall heat-transfer coefficient could be predicted with reasonable accuracy for flow conditions which were not very different from those set up for the tests, but, for flow conditions which differ significantly from those tested, local heat-transfer coefficients must be employed. A homogeneous flow model usually predicts a lower heat-transfer coefficient than is actually the case.

Forced-Flow Boiling of Sodium. A high-temperature test loop was assembled at NASA Lewis Research Center to study the heat-transfer characteristics of boiling sodium.[13] All components, including the 4-ft-long single-pass tube-in-shell heat exchanger, which were expected to operate above 1500°F, were constructed of niobium–1% zirconium alloy. The primary fluid, sodium or potassium, was electrically heated. Maximum oxygen partial pressure of $\sim 10^{-8}$ torr was maintained by baking out the system at 1400 to 2000°F with temperature cycling and by exposing the system to vacuum to ensure that all niobium components had completely outgassed.

Boiling was difficult to achieve with this apparatus, and, when obtained, was unstable. Two distinct boiling regimes were observed: (1) a low-heat-flux mode with relatively large oscillations in flow, pressure drop, and fluid temperature with low (<10%) quality and considerable superheating; (2) a high-heat-flux [$\sim 10^6$ Btu/(hr)(sq ft)] mode that was associated with relatively high quality (>35%) and little superheating. Although these two conditions were repeatable over a series of tests, no explanation of the reason for two coexistent flow regimes was evident. Apparently some source cavities for boiling that were dormant in the low-heat-flux regime were activated at elevated temperatures.

The test series was conducted with shell Peclet numbers ranging from 50 to 350, and the overall heat-transfer coefficients for the boiler were found to be between those predicted for constant-temperature and constant-heat-flux surfaces. The heat-transfer coefficient and vapor quality were obtained as functions of flow rate, and pressure-drop data were taken. Temperatures >1920°F were attained, and over 400 hr of running time at >1500°F were accumulated. Flow rates were ~1000 lb/hr, and the temperature differential across the heat exchanger was ~250°F. Flow oscillations up to 50% were observed in the first boiling mode (probably amplified by the condenser).

TURBOELECTRIC COMPONENTS

Turboelectric design involves the development of lightweight machinery, usually turboalternators, operable at rotational speeds from 12,000 to 36,000 rpm and at turbine inlet temperatures from 650 to 1800°F. Temperature gradients of 600 to 700°F across a few inches are encountered, and close

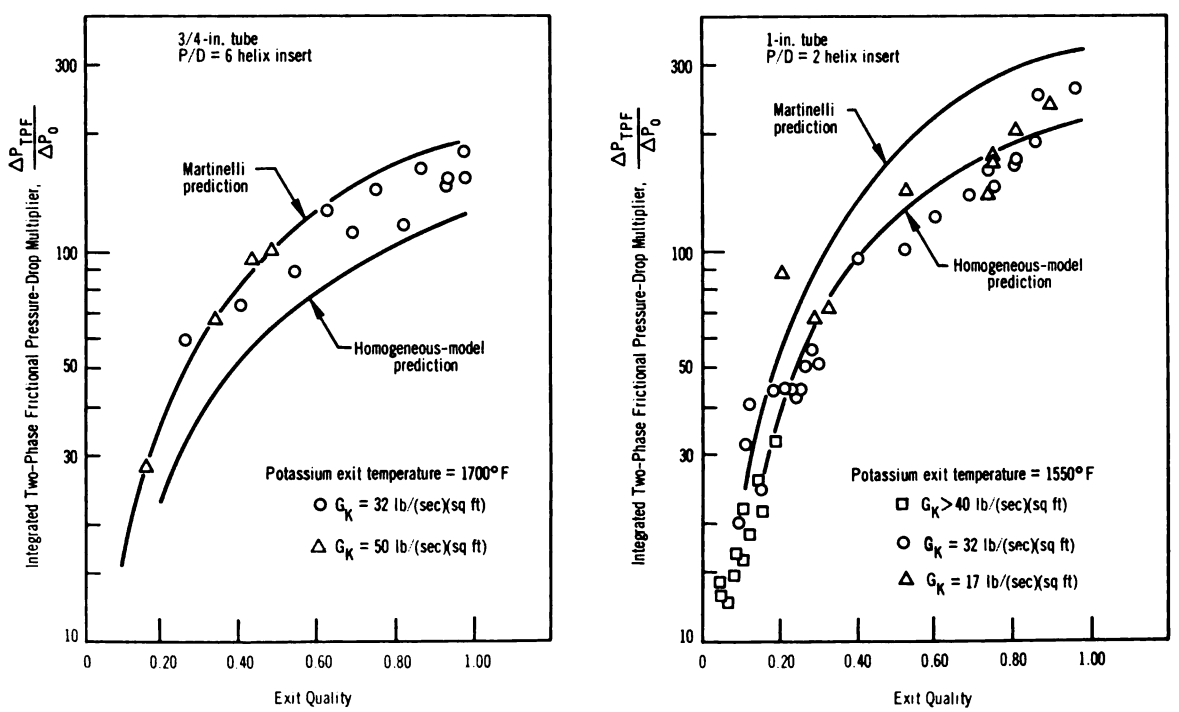
3/4-in. tube
P/D = 6 helix insert
Martinelli prediction
Homogeneous-model prediction
Potassium exit temperature = 1700°F
G_K = 32 lb/(sec)(sq ft)
G_K = 50 lb/(sec)(sq ft)
Integrated Two-Phase Frictional Pressure-Drop Multiplier, $\frac{\Delta P_{TPF}}{\Delta P_0}$
Exit Quality
1-in. tube
P/D = 2 helix insert
Martinelli prediction
Homogeneous-model prediction
Potassium exit temperature = 1550°F
G_K > 40 lb/(sec)(sq ft)
G_K = 32 lb/(sec)(sq ft)
G_K = 17 lb/(sec)(sq ft)
Integrated Two-Phase Frictional Pressure-Drop Multiplier, $\frac{\Delta P_{TPF}}{\Delta P_0}$
Exit Quality

Fig. 13 Typical two-phase boiling-potassium pressure-drop data.[12]

Digitized by Google

clearances and manufacturing tolerances are mandatory. Material creep and coefficient-of-expansion data for liquid-metal turbine operation up to and beyond 10,000 hr at high temperatures are not abundant for the materials of interest; turbine design technique is pressing the limits of metallurgical technology.

Turboalternator for SNAP-2. The model-V combined rotating unit (Table 2) developed by Thompson Ramo Wooldridge for the SNAP-2 system (Fig. 14) and the Mercury Rankine Power Conversion Program has a mercury-vapor-driven turbine, a pump, and an alternator on a common shaft.[5] These rotating components of the mercury loop are also lubricated by mercury. Figure 15 shows the bearings for possible use in this system.

The 4.1-kw alternator is an 1800-cycle unit with a design efficiency of 87%. This three-phase device has a four-wire Y-connected circuit that is externally grounded neutral.

The two-stage turbine consists of a subsonic impulse type first stage with 30% admission and a transonic impulse-reaction second stage with full admission.

Two sets of impellers were tested for the centrifugal mercury pump. The first set has five vanes with a 10° inlet angle and a 31° discharge angle, and the second set has six vanes with a 45° discharge angle. Pump efficiency of 30% was obtained in tests at 45 lb/min flow.

Table 2 SPECIFICATIONS FOR THE COMBINED ROTATING UNIT IN SNAP-2 (REF. 5)

Speed, rpm	36,000
Turbine	
Inlet pressure, psia	115
Inlet temperature, °F	1150
Discharge pressure, psia	9
Discharge temperature, °F	628
Efficiency, % (min)	55
Flow rate, lb/min	20
Alternator	
Frequency, cycles/sec	1800
Voltage, volts	
Line-to-neutral	63 ± 9.5
Line-to-line	110 ± 16.5
Output power, kw	4.1
Power factor	1.0 to 0.8
Duty cycle	Continuous
Efficiency at gross power, %	87
Mercury pump	
Inlet pressure to jets, psia (min)	5.9
Inlet temperature, °F (max.)	443
Discharge pressure, psia	525 ± 25
Flow, lb/min	50 ± 5
Efficiency (with dynamic seal), %	41
Bearings	Three-pad
Power consumption, watts	
Alternator	210
Turbine	210
Thrust	100
Flow rate, lb/min	
Alternator	8–10
Turbine	8–10
Thrust	7–8

The combined rotating units have been subjected to design-verification tests, including endurance, shock, and vibration testing. Five units have accumulated a total of >30,000 hr of running time with more than 100 starts. Unit endurance-run times were 6637, 2558, 2049, 861, 3159, 1277, 760, 863,

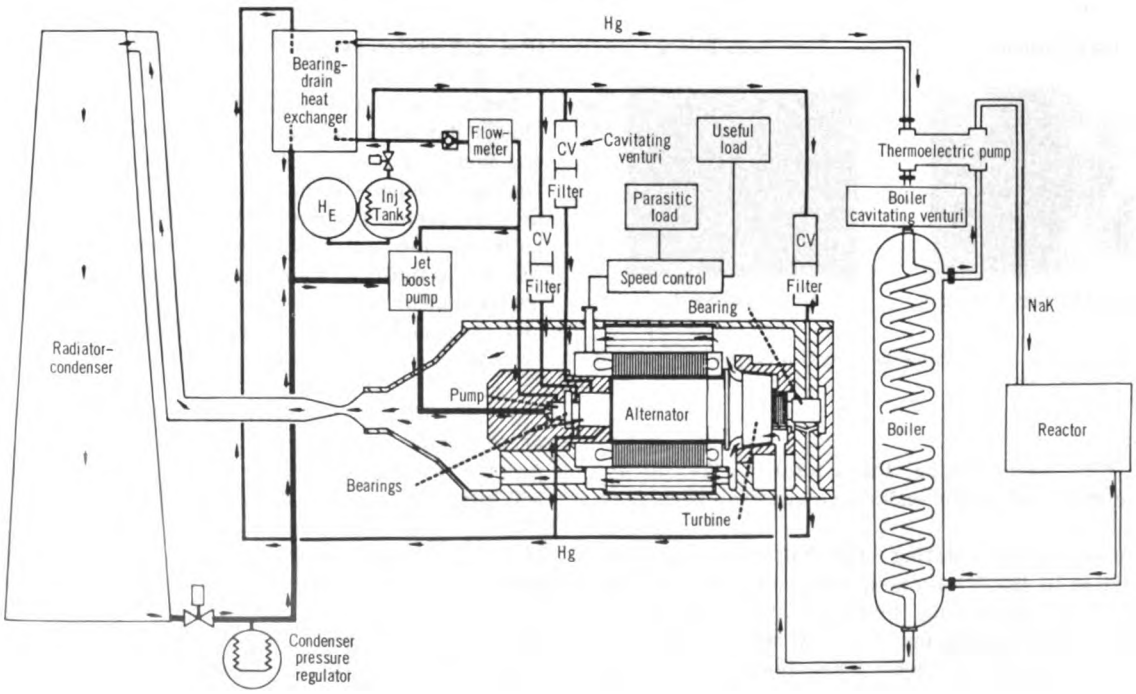

Fig. 14 Combined rotating unit in SNAP-2 (Ref. 5).

Digitized by Google

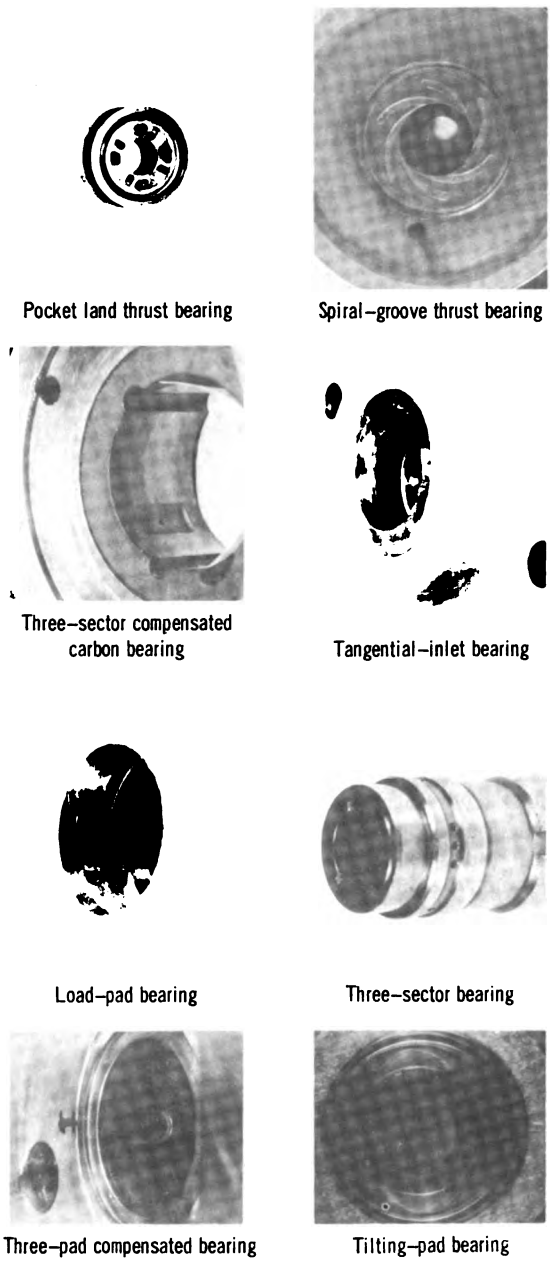

Fig. 15 Mercury-lubricated bearings for the SNAP-2 combined rotating unit.[5]

2500, 4767, and > 900 hr, for a total of ~25,000 hr. Degradation during the endurance runs has been very slight.

The combined rotating unit has been run with preheating to 400°F with no detrimental effects noted; however, a preheating level of 200°F apparently resulted in some bearing wear. At near rated conditions, 4.2 kw(e) has been generated at a maximum mercury temperature of 1150°F. The unit has demonstrated its capability of operating for 2500 hr and has passed all dynamic and performance tests, except that zero-gravity operation has not been verified.

Turboalternator for SNAP-8. The SNAP-8 turbine is a four-stage axial-flow impulse machine with a rotational speed of 12,000 rpm. The first two stages have 38% admission, whereas the latter two stages have full admission. The turbine wheels are of Haynes Stellite 6B, and the inner housing is type 316 stainless steel. Inlet temperature and pressure are 1260°F and 265 psi; exit conditions are 265°F and 16.5 psia. Turbine measured efficiency is 54% (the dry-gas efficiency is 58%). The turbine and alternator operate with separate but connected shafts. Overall efficiency is ~49.4% (Ref. 14).

The turbine bearings are angle-contact preloaded units of iron–silicon–bronze, mounted in a back-to-back configuration. They are lubricated with 4P3E and include dynamic slingers so that flooded operation is avoided. A portion of the turbine shaft is vented to space to prevent bearing lubricant from leaking into the mercury working fluid.

The alternator is a one-piece straddle-mounted rotor with angle contact bearings lubricated with 4P3E, which also cools the windings. This unit has been operated successfully up to a power level of 53 kw(e) and has an efficiency of 87%. In testing, the turboalternator has run 830 hr and had 45 starts prior to the failure of a spiral-wound snap ring in one of the turbine-shaft labyrinth seals. The Stellite 6B in the nozzle diaphragm and turbine wheel proved to be notch sensitive, and cracks were observed in these components. During operation the grain structure of the Stellite 6B changed. Redesign eliminated all sharp corners and the separate blade shroud. A type 316 stainless-steel nozzle block was used, and Stellite 6B blades were inserted in the wheel.

During test runs totaling 830 hr, the Stellite 6B blades did not erode, but performance for 10,000 hr has not been verified. Bearing-wear and space-sealing problems remain to be solved for the 10,000-hr duty cycle. Turbine critical speed is 20,000 rpm; however, the unit has been operated at 19,000 rpm with no significant increase in vibration. In general, performance requirements for this unit have been met, but endurance and reliability have yet to be achieved.

Turbogenerator for SNAP-50/SPUR. The turbogenerator under development by AiResearch Mfg. Co. for the SNAP-50 system was intended to produce 350 kw(e). The turbine design, Fig. 16, was for a six-stage 50% reaction device with a final stage diameter of 8.5 in. and a speed of 24,000 rpm. The final stage has an exit quality of 86% (Ref. 6). A single journal bearing is provided at each end of the turbine, and a thrust bearing is installed at the discharge end.

A problem is the development of suitable bearings (Fig. 17). A single-stage Inconel X impulse turbine with supersonic nozzles and an efficiency of 50% was

Digitized by Google

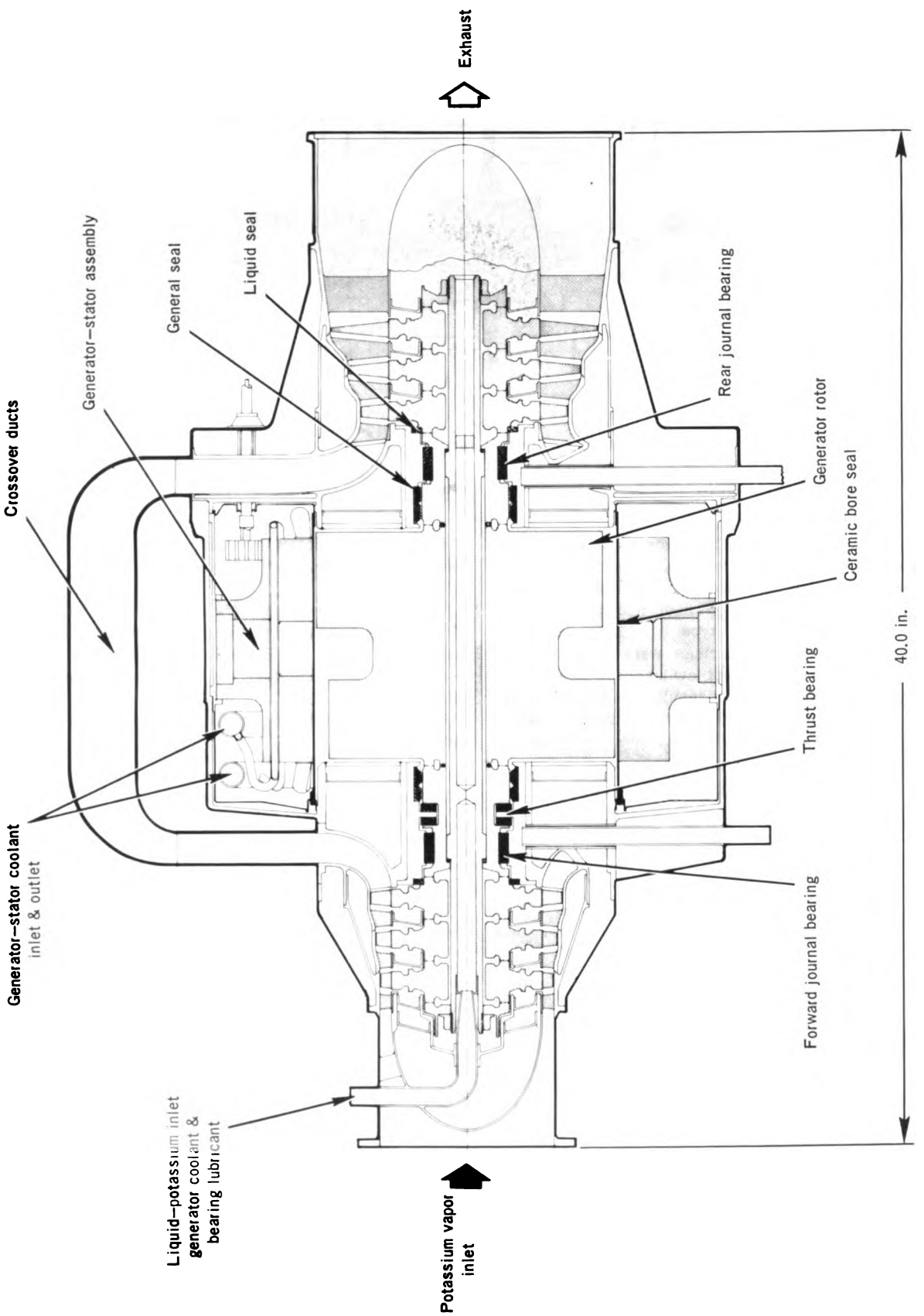

Fig. 16 Potassium turbogenerator for SNAP-50/SPUR (Ref. 6).

Digitized by Google

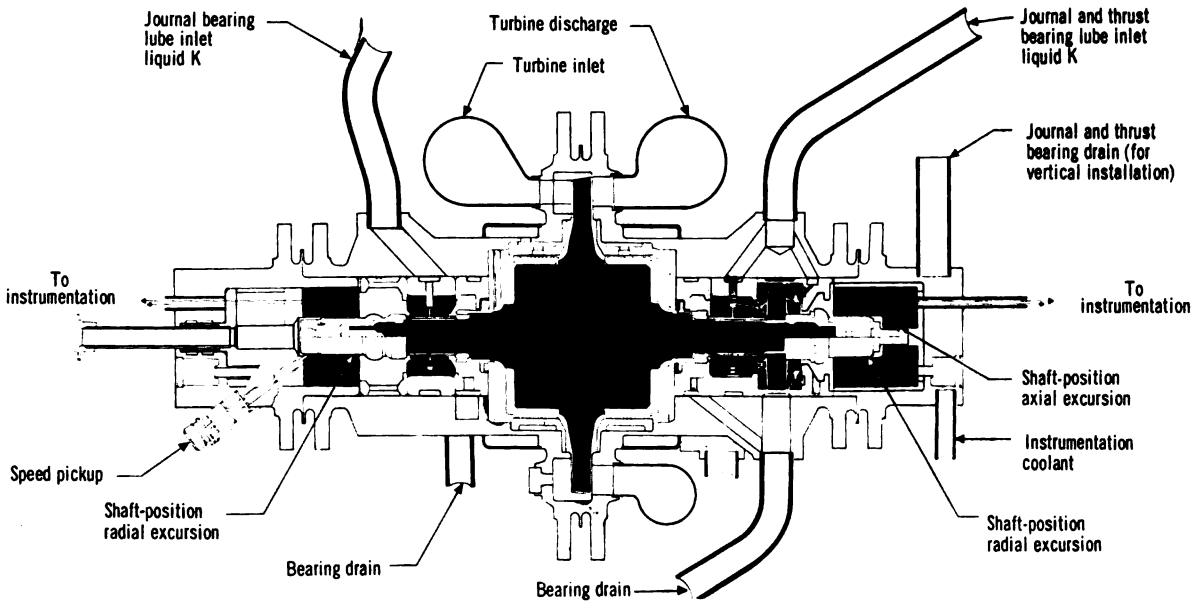

Fig. 17 Dynamic bearing test rig uses a single-stage Inconel X impulse turbine.[6]

employed in bearing tests. This wheel was lubricated by 550°F potassium, which was supplied through grooves in the bearing sleeves. Excellent bearing-test results were obtained with tungsten carbide tilting-pad bearings in a type 316 stainless-steel housing. The tungsten bearings were run for over 1000 hr continuously without evidence of wear, and, although subsequent restarts resulted in journal wear (as a result of retaining-ring movement), the lubricated bearings continued to operate smoothly at 24,000 rpm. Table 3 summarizes the bearing-wear-test experience.

A 200-Hp Two-Stage Potassium-Vapor Turbine. Under a NASA contract General Electric Company developed a 200-hp potassium turbine that represented the third and fourth stages of a Rankine-cycle turbogenerator (Fig. 18) (Ref. 15). Turbine speed was 19,200 rpm, and it operated with a pressure ratio of 2.95.

Table 3 FRICTION AND WEAR* OF BEARING MATERIALS IN 500°F POTASSIUM

Materials,† rotor/shoe	Starting torque, in.-lb	Running torque, av. in.-lb	Calculated coefficient of friction	Weight change, mg	Remarks‡
K94/Mo−0.5 Ti	18.3	13.1	0.266/0.190	+0.6/−4.0	Poor
K601/Mo−0.5 Ti	17.4	10.9	0.253/0.159	−1.1/−3.7	Poor
TZM/K94	>26	Shutdown	0.380/	−40.0/−9.2	Very poor
K94/TZM	17.0	10.9	0.247/0.159	+1.0/−5.0	Poor
K601/TZM	28.4	Fractured	0.410/		
TZM/K94	26.2	14.0	0.381/0.204	−59.0/−0.5	Poor
Mo−0.5 Ti/K94	24.0	17.4	0.350/0.253	−69.8/+0.2	Poor
K601/TZM	28.4	Fractured	0.410/		
TZM/W	>35.0	Shutdown	0.510/	−108.4/−14.0	Very poor
W/TZM	22.7	17.4	0.333/0.253	−15.4/−0.5	Poor
K94/K94	15.3	13.0	0.222/0.189	−0.2/−0.4	Excellent
K94/W	26.2	19.6	0.381/0.285	−666.3/−288.6	Poor
W/TZM	4.3	4.0	0.062/0.058	−5.5/−0.7	Poor
Mo−0.5 Ti/W	2.1		0.03/	−50.0/+5.0	Poor
K96/K96	8.3	1.75	0.121/0.025	−1.1/−0.1	Excellent
K11/K11	4.36	2.18	0.063/0.052	−0.8/−0.3	Excellent
K94/K94	4.36	4.36	0.063/0.063	+0.2/+0.2	Excellent
K701/K701	2.18	3.9	0.032/0.057	−0.6/−0.2	Excellent
K701/K11	3.06	2.62	0.045/0.039	−0.5/−0.2	Excellent
K11/K701	4.36	3.92	0.063/0.057	−0.9/−0.1	Excellent

*50 in./sec; O_2 - 50 ppm.

†TZM: Mo−0.5% Ti−0.1% Zr−0.027 C; Mo−0.5 Ti: Mo−0.5 Ti−0.02 C; W: pure arc-cast W; K11: WC−3 Co−0.1 TiC; K94: WC−12 Co−2(Ta, Cb)C; K96: WC−12 Co−2(Ta, Cb)C; K701: WC−9.5 Co−0.1 TiC−4.0 Cr_3C_2; and K601: 84.5 W−10 Ta−5.5 C, no limit.

‡Excellent: Negligible wear, no material transfer, and polish both specimens. Poor: Excessive wear, surface roughened, material transfer, and high friction. Very poor: Test not completed due to excessive wear, friction, material roughening, and transfer.

Digitized by Google

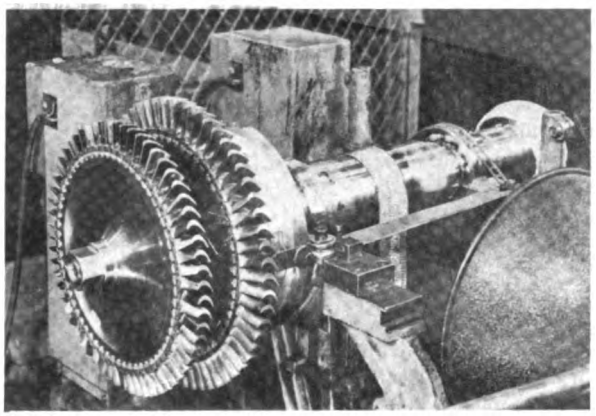

Fig. 18 Saturated-vapor test turbine designed for 1600°F potassium at 92% inlet quality.[15]

One attempt was made to simulate the wet conditions of the latter turbine stages by spraying liquid into the inlet stream. This was not successful because of the inability to obtain the fine droplets that would be present in an actual machine.

Oil-lubricated bearings were employed during the tests to separate blade-erosion investigation from the equally important problem of bearing wear. Heat was supplied by a gas-fired boiler. Test conditions are shown in Table 4.

Table 4 POTASSIUM-TURBINE TEST CONDITIONS[15]

Inlet temperature, °F	1450–1580
Turbine speed, rpm	15,400–21,000
Pressure ratio	1.4–4.4
Flow rate, lb/sec	1.6–2.1
Efficiency, %	40–70
Inlet quality, %	99

Subsequent to the successful completion of performance tests, an endurance run was begun, and a total of 5000 hr (two runs) was logged.

There was no visible second-stage blade erosion. A three-stage machine is being built for tests at higher last-stage moistures.

Organic Working-Fluid System. A relatively low temperature Rankine turbine developed by Sundstrand uses Dowtherm as the working fluid.[4] This system consists of a boiler, turboalternator, regenerator, condenser, and pump in which the maximum fluid temperature attained is 653°F. The working-fluid serves as the lubricant for all rotating components.

The shrouded, single-stage, Inconel X, radial-impulse turbine (Fig. 19) has a wheel radius of 3 in. and rotates at 24,000 rpm. It uses four supersonic (Mach 3) nozzles with a pressure ratio of 100 at an inlet pressure and temperature of 75 psi and ~650°F. Turbine efficiency of 54 to 61% has been attained. Because the expansion of the Dowtherm through the turbine is a superheated process, no condensation problems are encountered. The turbine nozzles are set at a fixed tangential angle of 17°; power output is varied by changing nozzle size.

A Pitot pump was employed since a minimum-leakage design was required for the very low (0.06 lb/sec) flows associated with this system. At 24,000 rpm the pump exit pressure is 95 psi. Only partially successful, this design attained the specified pressure ratio but not the specified flow rate, a deficiency attributed to inlet cavitation effects. Net pump efficiency achieved was ~26%.

The homopolar alternator consists of a main alternator and a parasitic unit that provides for load variation with constant turbine output. This 120- to 280-volt three-phase 3200-cycle unit was initially intended to produce 1.5 kw(e) but later was redesigned to yield 4 kw(e). Design efficiency of the alternator is 85%.

The bearings of the combined rotating unit, which consists of turbine, pump, and alternator, were tested with dry-start spin-ups to 24,000 rpm. Over 137 starts and 905 hr of operation were accumulated on one set of bearings, and the feasibility of startup with dry bearings was verified. The turbine and alternator employed in these tests accumulated > 2200 hr of operation.

The system was designed for flight use with a solar heat source. Therefore component weights are

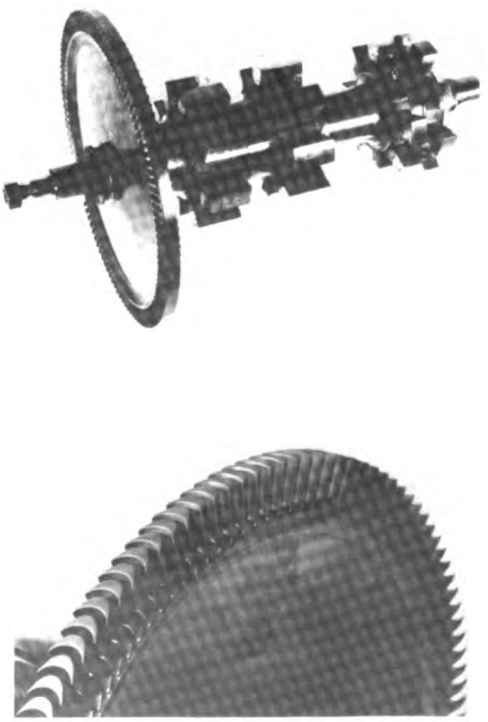

Fig. 19 Organic Rankine-cycle impulse turbine wheel uses 115 electrochemically machined Inconel X blades.[4]

Digitized by Google

minimal (Table 5). Further testing and modification of this system are in progress at Sundstrand.

Follow-on programs have been initiated. One of the key problems in the long-term operation of an organic system is the stability of the working fluid with time and temperature. The AEC-sponsored programs at Sundstrand, Philco, and the National Bureau of Standards are investigating the long-term behavior of several candidate working fluids in simulated power-conversion loops. Under Air Force sponsorship, Sundstrand is investigating the feasibility of a 2- to 10-kw(e) combined rotating unit.

Table 5 DOWTHERM RANKINE-CYCLE COMPONENT WEIGHTS[4]

Component	Weight, lb
Alternator housing and windings	32
Alternator rotor	6.5
Nozzle housing	7.5
Pump housing	1.75
Rear bearing housing	2.25
Pump and bearings	1.25
Total	51.25

RADIATOR–CONDENSERS

A number of designs have been tested and appear to be satisfactory. As with boilers, the limiting factor is precise heat-transfer data. Radiator-tube vulnerability to meteors has also been studied briefly.

Condensing Mercury in Low-Gravity Environments. Two mercury-vapor-condensation test systems have been set up at the NASA Lewis Research Center. The first of these (Fig. 20) was a nitrogen-cooled tapered-glass-tube apparatus that was tested in both 0- and 1-*g* environments. Glass tubes were selected to permit photography and to promote nonwetting flow for the tests. Test results included 4000 frame/sec records of the condensing flow pattern.[16]

Pressure drops were correlated with the Martinelli parameter over flow rates from 0.028 to 0.049 lb/sec. The Martinelli correlation proved effective for high-quality flow (a low value of the two-phase flow modulus) but gave results significantly lower than the measured value for low-quality flow. The presence or absence of gravity had little effect on the measured pressure drops.

Tests were made with both wetting and nonwetting flow conditions (Fig. 21), and it was found that, at the lower flow rates, the pressure drop was only slightly affected by wetting. At higher flow rates the nonwetting pressure drop was lower than the wetted-tube pressure drop.

A second series of tests was conducted with a NaK-cooled counterflow tapered-tube mercury system. As predicted, it was found that the mercury inlet static pressure initially dropped off rapidly with increasing condensing length but eventually leveled out.

Mercury Rankine Radiator–Condenser. Atomics International conducted a series of mercury-radiator development tests for a 3- to 5-kw(e) Rankine system with 19.8 lb/min flow. Quality of the 625°F mercury entering the prototype radiator was 97%. An exit temperature of 371°F was required with a flow-passage pressure drop of 2.5 psi against a 9-psi backpressure.[17]

The test radiator is an array of tapered Haynes 25 steel tubes with aluminum cooling fins. Versions with 24 and 36 tubes were tested (preheat, operate, drain, and shutdown). The condensing length of the array was ~120 in. Although the radiator temperature during operational tests was nearly constant at 625°F over the initial 100 in. of tube length, a very rapid drop to the rated exit temperature occurred in the last 10 to 20 in. of tubing. The configuration tested appeared to be successful, but experiments with other configurations were planned.

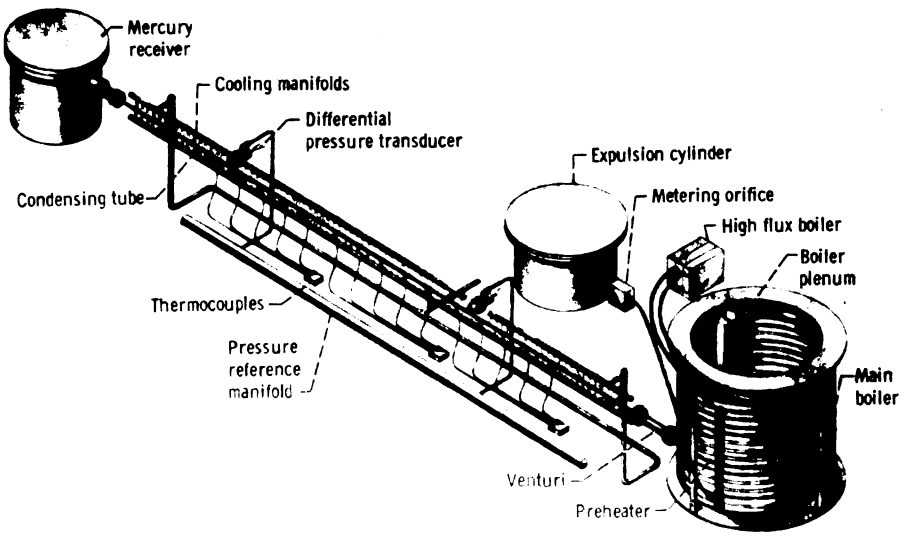

Fig. 20 Condensing mercury-vapor test rig.[16]

Digitized by Google

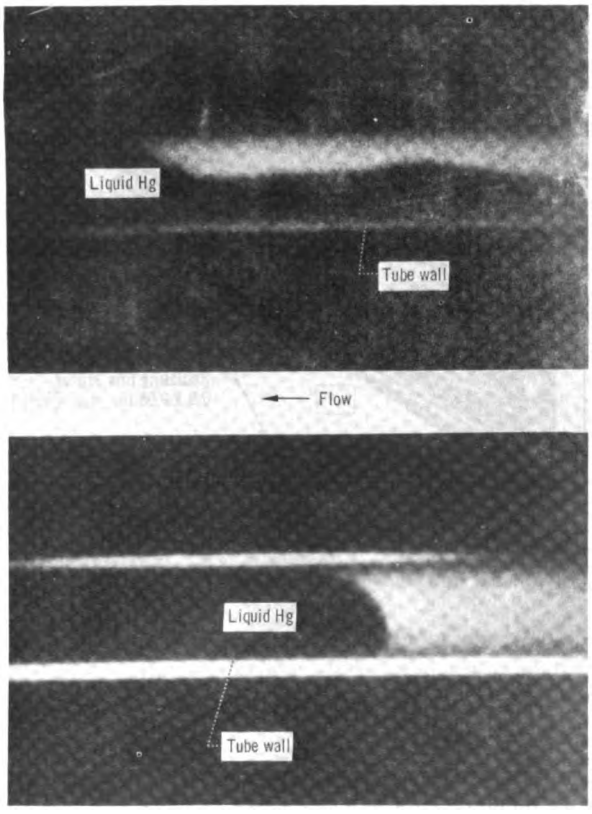

Fig. 21 Flow configurations at interface locations for wetting mercury condensation in copper tube (upper) and nonwetting condensation in stainless-steel tube.[16]

Two full-scale horizontal radiator–condensers simulating zero-gravity operation were tested. Over a range of conditions, no instabilities were noted. Satisfactory operation was also achieved against gravity by tilting the installation slightly.

Multitube Condenser for SNAP-8. Aerojet-General Nucleonics has tested a single-phase counterflow tube-in-shell NaK–mercury device containing 73 tapered 9% chromium–1% molybdenum steel tubes in a type 410 stainless-steel shell.[18] The 40-in.-long tubes are 0.25 in. in diameter at the inlet end and 0.20 in. at the exit. The total flow in the condenser is 11,500 lb/hr, and the variation in fluid quality is about linear with the tube length. The condenser pressure drop was successfully correlated with a modified Martinelli equation.

The only significant fabrication problem encountered in the assembly of the condenser was the welding of the 4° tapered tubes to the tube header support plate. A tapered-backbraze technique proved to be successful.

Tests showed that 420 kw(t) could be transferred, of which 15% was caused by subcooling of the condensate. Multitube-array performance differed little from results obtained earlier with a single-tube apparatus. This condenser appears to have satisfied all design requirements.

Direct-Condensing Potassium Radiators. A potassium, single-fluid, radiator–condenser for a space power system was tested at ORNL.[19] Each tube has copper radiator fins and is partially enclosed by a back reflector. A set of shutters attached to the reflector can be employed to open or completely enclose each condenser tube. These shutters, closed for launching, can be kept shut for low-power operation to control tube temperature and limit condensation. For operation at rated power, the shutters are opened and form part of the reflector.

Operational tests indicated satisfactory performance; no maldistribution or instability was observed. Data-gathering equipment included infrared films of the 800°F radiator surface.

Potassium-Condensing Tests. A 50-kw(t) condensing heat-transfer loop (Fig. 22) has been operated at the General Electric facility in Evendale, Ohio.[20] Single tubes $\frac{3}{8}$ and $\frac{5}{8}$ in. in inside diameter were flow tested with and without tapered-pin and helical inserts.

Potassium temperatures ranged from 1100 to 1400°F, and heat fluxes from 3×10^4 to 3×10^5 Btu/(hr)(sq ft) were obtained. Flow velocities of 100 to 1700 ft/sec were produced.

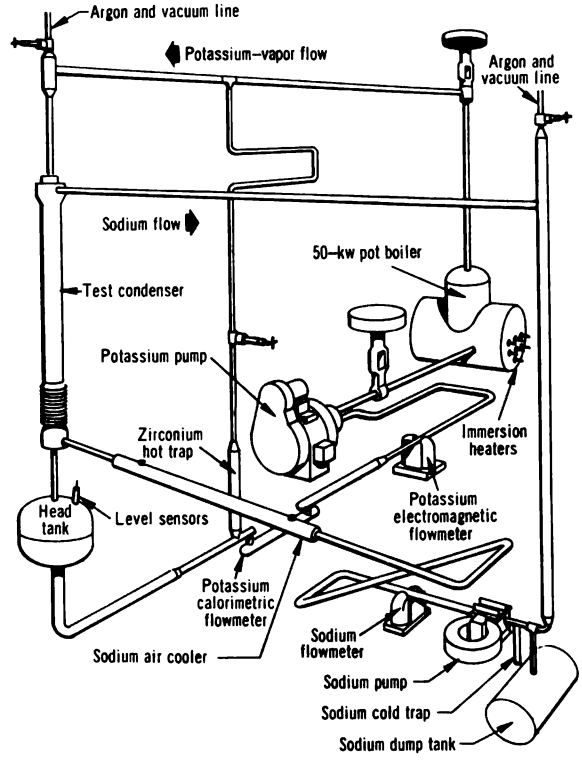

Fig. 22 Condensing potassium has been studied in this 50-kw(t) loop[20] *at heat fluxes up to 3×10^5 Btu/(hr)(sq ft).*

Digitized by Google

The Martinelli correlation successfully predicted pressure variations, and no evidence of flow instability was encountered. The data taken (Fig. 23 is typical) included the axial temperature distribution, heat-transfer coefficients vs. temperature, the variation of the Martinelli parameter with temperature, and the radial temperature variation in the condensing-tube walls.

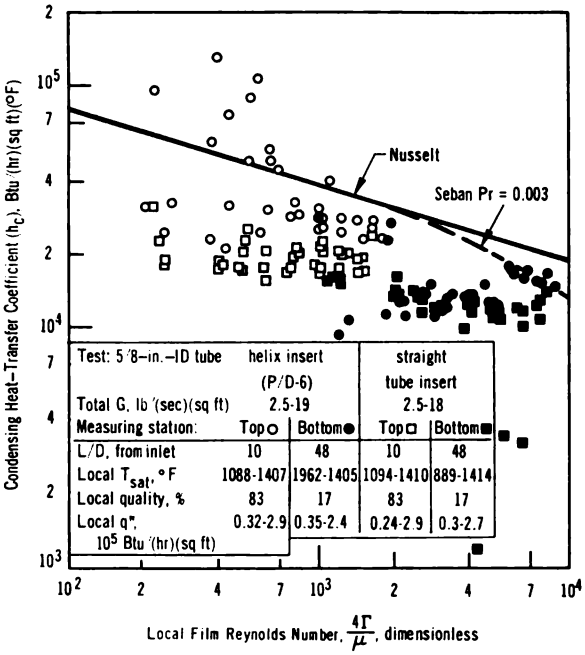
Condensing Heat-Transfer Coefficient (h_c), Btu/(hr)(sq ft)(°F)
Nusselt
Seban Pr = 0.003
Test: 5/8-in.-ID tube
helix insert (P/D-6)
straight tube insert
Total G, lb/(sec)(sq ft) 2.5-19 2.5-18
Measuring station: Top○ Bottom● Top□ Bottom■
L/D, from inlet 10 48 10 48
Local T_{sat}, °F 1088-1407 1962-1405 1094-1410 889-1414
Local quality, % 83 17 83 17
Local q", 10^5 Btu/(hr)(sq ft) 0.32-2.9 0.35-2.4 0.24-2.9 0.3-2.7
Local Film Reynolds Number, $\frac{4\Gamma}{\mu}$, dimensionless

Fig. 23 Potassium-condensing data obtained with the test loop shown in Fig. 22 (Ref. 20).

A three-loop potassium-condensing system was assembled at NASA Lewis Research Center.[21] This system consisted of a NaK primary loop, a two-phase potassium secondary loop, and a NaK cooling loop. Each NaK loop flowed 35,000 lb/hr, whereas the two-phase potassium loop design flow rate was 600 lb/hr.

The potassium condenser was a type 316 stainless-steel tube-in-shell assembly 16 ft long. The tubes had an outside diameter of 0.5 in. and a wall thickness of 0.03 in. The inside diameter of the shell was 2.0 in. Actual test conditions involved 1400°F potassium flow at 300 to 500 lb/hr with an inlet quality of 88%. Heat fluxes as high as 450,000 Btu/(hr)(sq ft) were observed.

A 14- by 3-ft radiator–condenser was also tested during this study. The radiator, ~ 10 ft long, consisted of an array of nine parallel, finned tubes with a wall thickness of 0.042 in. and an inside diameter of 0.5 in. (Fig. 24). The radiator was mounted in a cooled vacuum chamber to provide an environmental pressure of 10^{-5} mm Hg. Heat fluxes ranging from 23,000 to 49,000 Btu/(hr)(sq ft) were obtained.

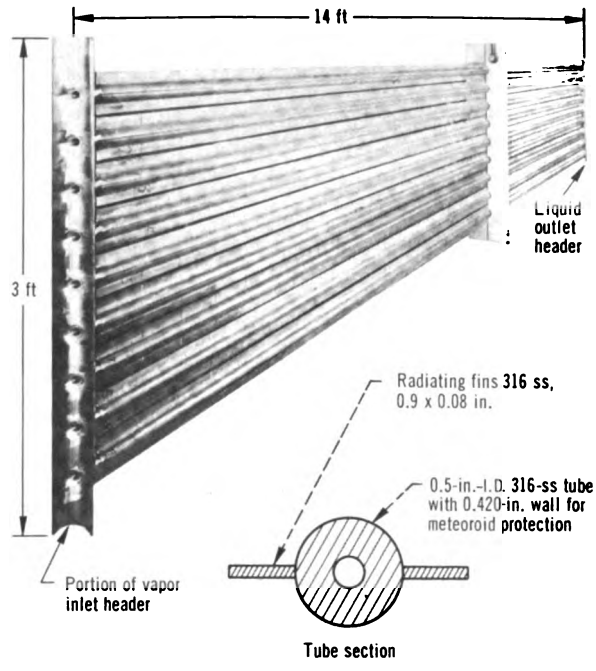
14 ft
3 ft
Liquid outlet header
Radiating fins 316 ss, 0.9 x 0.08 in.
0.5-in.-I.D. 316-ss tube with 0.420-in. wall for meteoroid protection
Portion of vapor inlet header
Tube section

Fig. 24 Potassium radiator–condenser with nine finned tubes.[21]

A typical condensing radiator wall-temperature profile was obtained in these tests over most of the length of the assembly; subcooling occurred near the radiator exit. With a vapor inlet temperature of 1426°F and inlet quality of 83%, a flow of 569 lb/hr was obtained. Pressure drop, temperature, and heat flux were measured. Satisfactory operation of the radiator–condenser was obtained over a range of pressures that included test conditions with a near-zero pressure drop.

Radiator Meteor Vulnerability. A program conducted by the NASA Lewis Research Center has attempted to provide some basic empirical data that would permit predicting how deeply a high-velocity particle would penetrate the wall of a radiator tube.[22]

Pyrex projectiles were fired into flat-plate targets of aluminum, type 316 stainless steel, niobium, nickel, and cobalt and into tubes of 2024T6 aluminum and type 316 stainless steel. Penetrations were correlated by an empirical relation. The flat-plate data were not, in most cases, very different from corresponding tube data. However, no general pattern of penetration was evident in tests that covered a range of penetrations from mild dimpling through severe spalling and perforation. These modes of damage are illustrated in Fig. 25.

In a series of impacts performed with lined tubes, spalling occurred with thick liners, but thin liners either dimpled or were penetrated. If mild dimpling could be tolerated, tube and liner weight could be reduced by about 45%.

Digitized by Google

A series of tests with beryllium armor over type 315 stainless-steel tubes revealed that damage could be expected consistently with unreinforced beryllium. A reinforcing scheme wherein kinked wire or steel screening was embedded in the beryllium considerably increased the efficacy of the armor. For a 500-day mission in which dimpled but not spalled radiator tubes would be tolerated, the minimum radiator specific weight [lb/kw(e)] would be obtained with lined beryllium tubes. In order of increasing weight, ATJ graphite, vanadium, and molybdenum follow beryllium.

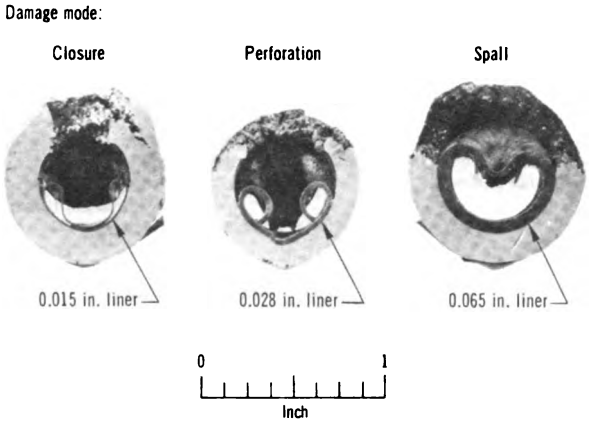

Fig. 25 Limiting damage modes in type 316 stainless-steel tubes armored with cast aluminum. Tubes were at room temperature and were impacted by $^3/_{32}$-in.-diameter pyrex projectiles at 25,000 ft/sec (Ref. 22).

Conclusions

Most of the current work in the field is directed toward building a backlog of component experience. Because of the complexity and cost of this kind of power system, development must proceed along a rather narrow front and in a somewhat piecemeal fashion. The total effort reported in this article was under the aegis of only four government and seven commercial organizations.

The prediction of heat-transfer coefficients in two-phase flow, wherein semiwetting conditions prevail, and the development of high-temperature turbines (1200 to 1800°F) and high-speed high-temperature bearings constitute the foremost technical problems. These represent a very straightforward projection of conventional rotating-machinery problems into a more severe and stringent environment. There is also the reliability problem—these Rankine systems must operate for relatively long periods without maintenance. At present an engineering approach to the solution of these problems is, for better or worse, being followed. Perhaps the seeming underemphasis on basic heat-transfer and dynamics research is only an apparent one, and fundamental design principles as well as practical techniques may emerge from current Rankine-cycle work.

References

All references are papers presented at the American Institute of Aeronautics and Astronautics Specialists Conference on Rankine Space Power Systems, in Cleveland, Ohio, October 26, 1965, USAEC Report CONF-651026, Vol. I.

1. R. Wallerstedt and D. Miller, Mercury Rankine Program Development Status and Multiple System Application.
2. E. S. Chalpin, J. R. Pope, and C. L. Foss, Development of the SNAP 8 Pump for Mercury Service.
3. J. A. Boppart, K. O. Parker, and P. J. Berenson, Multiple-Tube Potassium Boiler Development.
4. J. Malohn, Organic Working Fluid Cycle: Development Status.
5. R. C. Biering and Otto Decker, MRPC (SNAP 2) Turboalternator.
6. J. H. Dannan and L. E. Chadbourne, Potassium Turbine-Generator Development.
7. E. S. Chalpin, C. P. Colker, and C. L. Foss, Design and Development of Pumps for High Temperature NaK Service.
8. M. A. Perlow, H. H. Hanlin, and J. M. Hochman, Development of the MRP Thermoelectric NaK Pump.
9. L. V. Wilson, H. C. Young, and A. M. Smith, Experience with Turbine Driven Potassium Boiler Feed Pumps at ORNL.
10. A. H. Kreeger, A. J. Sellers, and J. N. Hodgson, Design and Development of the Mercury Boiler for the SNAP 8 System.
11. R. S. Carey and B. Farwell, Effects of Oil Contamination on Heat Transfer Performance.
12. J. R. Peterson, High Performance Once-Through Boiling of Potassium.
13. J. P. Lewis, Experimental Investigation of Forced Flow Boiling of Sodium.
14. M. G. Cherry and G. Oiye, Design and Development of a Turbine Alternator Assembly for the SNAP 8 System.
15. R. J. Rossback et al., Performance Test of Two-Stage 200-Hp Turbine in Wet Potassium Vapor.
16. D. Namkoong and J. Albers, An Experimental Study of the Condensing Characteristics of Mercury Vapor Flowing in Single Tubes.
17. D. H. Heiskala et al., Mercury Rankine Radiator Condenser Development Experience.
18. A. J. Kreeger and J. N. Hodgson, Design and Development of the SNAP 8 Multi-Tube Condenser.
19. A. P. Fraas, Design and Development Tests of Direct-Condensing Potassium Radiators.
20. S. C. Sawochka, Thermal and Fluid Dynamic Performance of Potassium During Condensing Inside a Tube.
21. Q. A. Gutierrez et al., Potassium Condensing Tests of Horizontal Multi-Tube Convective and Radiative Condensers Operating at Vapor Temperatures of 1250°F to 1500°F.
22. N. Clough and J. H. Diederich, Results of Hypervelocity Impacts into Space Radiator Materials.

Digitized by Google

Digitized by Google

Index

Power Reactor Technology

Volume 9

Note: The page range for each of the four issues of Vol. 9 is as follows:

No. 1, pages 1 to 63
No. 2, pages 65 to 100
No. 3, pages 101 to 152
No. 4, pages 153 to 213

A

Accidents
  loss-of-coolant, studies in fast breeder reactors by zone-loading experiments, 164-65
Aeroball system
  neutron-flux distribution measurement by, 28
Aluminum (SAP)
  use as fuel cladding in organic-cooled reactors, 138-39
Argon isotopes (^{40}Ar)
  use in neutron-flux distribution measurements, 28-29

B

Beacons
  lighting on offshore platforms, SNAP-7F power source for, 3
Bearings (liquid-metal)
  film-thickness measurement techniques, 125-26
Boilers
  development for Rankine-cycle power systems, 132-34, 200-04

C

Cavitation
  damage studies of metals in liquid alkali metals, instrument for, 128
Cobalt isotopes (^{60}Co)
  use as heat source in turbine-Rankine-cycle engine, 12-13
Computer programs
  development for loss-of-coolant accident, 47
  development for shielding analysis, 19-23
Condensers
  development for Rankine-cycle power systems, 210-13
  meteor vulnerability, 212-13
Conferences and meetings
  high-temperature instrumentation in liquid-metal experiments, 123-35
  two-phase fluid flow, 35-44
Copper alloys
  Cu–Fe–Zr, use as fuel cladding in organic-cooled reactors, 139
Critical experiments
  zone-loading for fast breeder reactors, 162-68
Critical mass
  estimating in fast breeders by zone-loading experiments, 166

D

Deep-submergence vehicles
  list, 7
  NR-1, 14-15
  nuclear powered for fisheries research, 4-8
  nuclear propulsion systems, 13-15
  SWR, 14
Density probes
  design of nuclear for measuring deep-sea sediments, 4
Divers
  scuba-suit heating by isotopic power, 6
Doppler effect
  measurement in zone-loaded fast breeder experiments, 164-65
Dowtherm A
  use as working fluid for turbine-Rankine-cycle engine, 13, 197-98
Drilling
  nuclear power sources for offshore, 2-3

E

Economics
  neutron-flux distribution measurements as aid in power increase, 25
  on-power refueling systems, 181
  organic coolants, 137-40
Engines (steam)
  radioisotope powered for oceanography applications, 12-13

F

Fishing industry
  nuclear power applications in, 4-8
Flowmeters
  for liquid-metal systems, 124-25
Fluid flow (two-phase)
  compressibility, effects on stability and burnout, 65-68
  inverse temperature profiles in boiling K, 129-30
  symposium on, review, 35-44
  volume-fraction measurements in liquid metals, 124-25
Foghorns
  on offshore platforms, SNAP-7A power source for, 3
Food
  harvesting from the ocean, nuclear power for, 4-8
Foils
  use in neutron-flux distribution measurements, 26, 86-94
France
  liquid-metal steam-generator program, 69-73

G

Gamma-adsorption analysis
  use in measuring volume fraction in two-phase flows, 124
Gases
  monitoring of inert in liquid metals, instrument for, 128
  use in neutron-flux distribution measurement, 28-29
Generators
  liquid-metal MHD, review, 188-92

H

Haynes 25 alloy
  performance as Hg boiler material, 134-35
HB-40
  properties as organic coolant, 137-40
Heat exchangers
  design for liquid metals, 177-79
Heat sources
  development of isotopic for oceanography applications, 9-10
Heat transfer
  coefficients for liquid metals, 174-79
  heat transfer in double-pipe liquid metal, method for determination of, 129
  inverse temperature profile in boiling two-phase flow of K, 129-30
Heaters
  for liquid-metal experiments, 123

Digitized by Google

I

Instruments
for high-temperature liquid-metal experiments, 123-35
Ion chambers
use in neutron-flux distribution measurement, 29-31
Iron alloys
Cu–Fe–Zr, use as fuel cladding in organic-cooled reactors, 139
Fe–Ni–Nb–Sb–Zr, use as fuel cladding in organic-cooled reactors, 139
Isotopic engines
development of steam piston, 13
development of turbine-Rankine-cycle system, 12-13
Isotopic thermal power systems
application in oceanography, 9-10
Isotopic thermoelectric systems
application in oceanography, 10-12

L

Liquid-metal steam generators
U. S. and French programs, 69-73

M

Magnetohydrodynamic power systems
review of technology, 187-92
Mercury
boiler development for Rankine-cycle power systems, 132-34, 200-02
condenser development for Rankine-cycle power systems, 210-11
pump development for Rankine-cycle power systems, 198
Metals (liquid)
cavitation damage studies, instrument for, 128
flowmeters, 124-25
heat-transfer coefficients, 174-79
heat transfer in double-pipe heat exchangers, method for determination of, 129
high-temperature instrumentation in experiments, 123-35
level measurement techniques, 126
monitoring for dissolved oxygen, instrument for, 128
monitoring for inert gases, instrument for, 128
pressure measurement, instrument for, 123-24
use in MHD power systems, 187-92
use in steam-generating systems, review of French program, 69-73
volume-fraction measurement in two-phase flow, 124-25
Minerals
exploration and production from the ocean floor, nuclear power for, 3-4
Mining
of minerals from the ocean floor, nuclear power for, 3-4

N

Neutron sources
design of high-flux research reactors for, 153-60
Neutron spectra
measurement in fast breeders by zone-loading experiments, 164
measurement in operating reactors, 25-33
measurement by two-detector cross-correlation, 142-43
measurement by pseudorandom binary inputs, 142-43
measurement of thermal and epithermal, 80-94
Nickel alloys
Fe–Ni–Nb–Sb–Zr, use as fuel cladding in organic-cooled reactors, 139
Niobium alloys
Fe–Ni–Nb–Sb–Zr, use as fuel cladding in organic-cooled reactors, 139
Nb–Zr, use as fuel cladding in organic-cooled reactors, 138-39
NR-1 deep-submergence vehicle
development, 7, 14
Nuclear ships
(see Ships (nuclear))

O

Oceanography
nuclear power applications, 1-17, 150-52
Ores
(see Minerals)
Organic materials
use as reactor coolants, 137-40
Organic Rankine-cycle power-system development, 197-98, 209-10
Oxygen
monitoring in liquid metals, instrument for, 126
Ozhennite
use as cladding in organic-cooled reactors, 139

P

Petroleum
offshore exploration and production, nuclear power for, 1-3
Potassium (liquid)
boiler development for Rankine-cycle power systems, 202-04
condenser development for Rankine-cycle power systems, 211-12
inverse temperature profiles in boiling two-phase flow of, 129-30
pump development for Rankine-cycle power systems, 199-200
Pressure
measurement in liquid-metal systems, devices for, 123-24
Pressure vessels
cladding failure in water reactors, 101-109
cladding with stainless steel, 102-104
Propulsion
nuclear power systems for deep-submergence vehicles, 6-9, 12-17, 150-52
Prospecting
for minerals on the ocean floor, nuclear power for, 4
Protein
harvesting from the ocean, nuclear power for, 4-5
Pumps
development for Rankine-cycle power systems, 198-200

R

Radiators
development for Rankine-cycle power systems, 210-13
meteor vulnerability, 212-13
Radioisotope Submersible Engine (RISE)
development, 12-13
Rankine-cycle power systems
component development, 194-213
use in RISE, 12-13
Reactor control systems
optimal theory, 169-71
Reactor coolants
dynamics in fast reactors, effects on safety, 46-49
loss in fast breeders, analysis by zone-loading experiments, 164-65
materials for organic, technology advances, 137-40
Reactor fuels
uniform burnup, neutron-flux distribution measurements as aid in, 25-26
Reactor safety
neutron-flux distribution measurements in, 26
Reactors
core design, use of neutron-spectra measurements in, 80-94
kinetics, measurement in fast breeders by zone-loading experiments, 165
kinetics, nonlinear analysis, 171-72
neutron-flux distribution measurement in operating, 25-33
neutron-noise analysis, 142-43
neutron-spectra measurement by differential techniques, 80-86
neutron-spectra measurement by integral techniques, 86-94
power rating increase, use of neutron-flux distribution measurement in, 25
on-power refueling systems, merits of, 180-86
role in magnetohydrodynamic power systems, 187-92
shielding analysis, advance methods in, 19-23
Reactors (Big Rock Point)
modifications, description and procedures, 76-78
operating experience, outages, 112, 120-21
neutron-flux distribution measurement system, 25
Reactors (cavity)
design concepts for high-flux research, 159
Reactors (Connecticut Yankee)
neutron-flux distribution measurement system, 25
Reactors (Dresden)
neutron-flux distribution measurement system, 25-26
operating experience, outages, 112, 119
Reactors (EBR-II)
neutron-flux distribution measurement systems, 26
Reactors (EBWR)
modifications, description and procedures, 78
neutron-flux distribution measurement system, 28
pressure-vessel cladding failure, 102-06
pressure-vessel cladding with stainless steel, 102
Reactors (Elk River)
pressure-vessel cladding failure, 107-09
Reactors (fast)
power excursions, effect of coolant dynamics on events, 46-49
Reactors (fast breeder)
zone-loaded critical experiments, 162-68

Digitized by Google

Reactors (gas-cooled)
applications for undersea power plants, 15
Reactors (HBWR)
neutron-flux distribution measurement system, 26
Reactors (Heavy Water Components Test) (HWCTR)
modifications, description and procedures, 78
Reactors (heavy-water moderated)
lattice calculations and measurements, 145-46
Reactors (high-flux research)
design concepts, 153-60
Reactors (Humboldt Bay)
neutron-flux distribution measurement system, 25
operating experience, outages, 112, 121-22
Reactors (Indian Point)
operating experience, outages, 119-120
Reactors (liquid-metal-cooled)
steam generators, U. S. and French programs, 69-73
Reactors (MH-1A)
development for floating power source, 15-16
Reactors (NPD)
on-power refueling system, 180-86
Reactors (NR-1)
design concept, 152
Reactors (NRU)
on-power refueling systems, 180
Reactors (Oak Ridge Graphite)
neutron-flux distribution measurement system, 26
Reactors (Plutonium Recycle Test)
neutron-flux distribution measurement system, 28
Reactors (San Onofre)
neutron-flux distribution measurement system, 25, 28
Reactors (Saxton)
neutron-flux distribution measurement system, 25
Reactors (SELNI)
neutron-flux distribution measurement system, 28
Reactors (Shippingport)
operating experience, outages, 112, 117-19
Reactors (SNAP-8A)
development for deep-submergence vehicle propulsion, 13-14
Reactors (SNAP-10A)
design, 2
power source for offshore oil and gas platforms, 3
use as undersea power units, 13-14
158-59
Reactors (Sodium Experiment) (SRE)
modifications, description and procedures, 74-76
Reactors (supercritical-water)
development for deep-submergence vehicle propulsion, 14-15
Reactors (thin shell)
design concepts for high-flux research, 159-60
Reactors (TURPS)
applications for surface and undersea power plants, 15, 17
Reactors (UHTREX)
design and projected operating characteristics, 51-62
Reactors (water-moderated)
lattice calculations and measurements, 146-49
Reactors (Yankee)
neutron-flux distribution measurement system, 25, 26-28
operating experience, outages, 112, 115-17
power-rating increase, 25
pressure-vessel cladding failure, 106-07
RISE
[see Radioisotope Submersible Engine (RISE)]

S

Safety
zone-loaded critical experiments, 166-68
Santowax OM
properties as organic coolant, 137-40
Shielding
analysis, advance methods in, 19-23
Ships (nuclear)
development for fishing industry, 4-5
Sodium
boiler development for Rankine-cycle power systems, 204
two-phase flow of boiling, properties of, 131-32
Sodium-potassium alloys (liquid)
pump development for Rankine-cycle power systems, 198-99
reaction with water, 72-73
Spheres
use in neutron-flux distribution measurements, 27-28
Stainless steel
crack analysis in pressure-vessel cladding, 101-109
Steam generators
liquid metal, U. S. and French programs, 69-73
Submarines
(see also Deep-submergence vehicles)
development for deep-sea research, 6-9
Systems for Nuclear Auxiliary Power (SNAP-2)
component development for Rankine-cycle power system, 194-96, 199, 205-6
Systems for Nuclear Auxiliary Power (SNAP-7A)
use in navigational buoy, 10
Systems for Nuclear Auxiliary Power (SNAP-7B)
use in lighthouses, 10-11
Systems for Nuclear Auxiliary Power (SNAP-7C)
use in Antarctic weather station, 11
Systems for Nuclear Auxiliary Power (SNAP-7D)
use in Gulf of Mexico weather station, 11
Systems for Nuclear Auxiliary Power (SNAP-7E)
use in sonobuoy near Bermuda, 11-12
Systems for Nuclear Auxiliary Power (SNAP-7F)
use for beacons and foghorns on offshore oil platforms, 3
Systems for Nuclear Auxiliary Power (SNAP-8)
component development for Rankine-cycle power systems, 132-33, 194, 196-99, 201-02, 206, 211
development for deep-submergence vehicle propulsion, 13-14
Systems for Nuclear Auxiliary Power (SNAP-10A)
design, 2
use for offshore platform power units, 3
use for undersea power units, 13-14
Systems for Nuclear Auxiliary Power (SNAP-15)
development for undersea power sources, 11-12
Systems for Nuclear Auxiliary Power (SNAP-21)
development for undersea power sources, 12
Systems for Nuclear Auxiliary Power (SNAP-50/SPUR)
component development for Rankine-cycle power system, 194, 197, 206-08
Symposia
(see Conferences and meetings)

T

Terphenyls
(see Santowax OM and HB-40)
Thermometers
use in neutron-flux distribution measurements, 31
Tin alloys
Fe–Ni–Nb–Sb–Zr, use as fuel cladding in organic-cooled reactors, 139
Turbines (potassium vapor)
pressure measurement, devices for, 123-24
Turbogenerators
development for Rankine-cycle power systems, 204-10

U

Uranium carbides
UC–D_2O, critical masses and neutron buckling in lattices of, 145
Uranium oxides
PuO_2–UO_2–H_2O, critical masses and neutron buckling in lattices of, 146-47
UO_2, testing of Zr–Nb alloy-clad, in organic-cooled reactors, 138
UO_2–H_2O, critical masses and neutron buckling in lattices of, 147

W

Welding
stainless-steel cladding to pressure vessels, 101-02
Wires
use in neutron-flux distribution measurements, 26

Z

Zircaloy-2
use as fuel cladding in organic-cooled reactors, 139
Zirconium alloys
Cu–Fe–Zr, use as fuel cladding in organic-cooled reactors, 139
Fe–Ni–Nb–Sb–Zr, use as fuel cladding in organic-cooled reactors, 139
Nb–Zr, use as fuel cladding in organic-cooled reactors, 138-39

U. S. GOVERNMENT PRINTING OFFICE: 1967—252338/2

Digitized by Google

LEGAL NOTICE

This journal was prepared under the sponsorship of the U. S. Atomic Energy Commission. Neither the United States, nor the Commission, nor any person acting on behalf of the Commission:

A. Makes any warranty or representation, expressed or implied, with respect to the accuracy, completeness, or usefulness of the information contained in this journal, or that the use of any information, apparatus, method, or process disclosed in this journal may not infringe privately owned rights; or

B. Assumes any liabilities with respect to the use of, or for damages resulting from the use of any information, apparatus, method, or process disclosed in this journal.

As used in the above, "person acting on behalf of the Commission" includes any employee or contractor of the Commission, or employee of such contractor, to the extent that such employee or contractor of the Commission, or employee of such contractor prepares, disseminates, or provides access to, any information pursuant to his employment or contract with the Commission, or his employment with such contractor.

Digitized by Google

NUCLEAR SCIENCE ABSTRACTS

The U. S. Atomic Energy Commission, Division of Technical Information, publishes *Nuclear Science Abstracts* (*NSA*), a semimonthly journal containing abstracts of the literature of nuclear science and engineering.

NSA covers (1) research reports of the U. S. Atomic Energy Commission and its contractors; (2) research reports of government agencies, universities, and industrial research organizations on a worldwide basis; and (3) translations, patents, books, and articles appearing in technical and scientific journals.

Complete indexes covering subject, author, source, and report number are included in each issue. These are cumulated quarterly, semiannually, and annually providing a detailed and convenient key to the literature.

Availability of *NSA*

SALE *NSA* is available on subscription from the Superintendent of Documents, U. S. Government Printing Office, Washington, D. C., 20402, at $30.00 per year for the semimonthly abstract issues and $22.00 per year for the four cumulated-index issues. Subscriptions are postpaid within the United States, Canada, Mexico, and all Central and South American countries, except Argentina, Brazil, Guyana, French Guiana, Surinam, and British Honduras. Subscribers in these Central and South American countries, and in all other countries throughout the world, should remit $37.00 per year for subscriptions to semimonthly abstract issues and $25.00 per year for the four cumulated-index issues.

EXCHANGE *NSA* is also available on an exchange basis to universities, research institutions, industrial firms, and publishers of scientific information. Inquiries should be directed to the Division of Technical Information Extension, U. S. Atomic Energy Commission, P. O. Box 62, Oak Ridge, Tennessee, 37830.

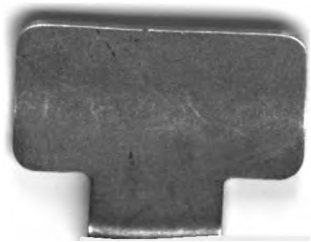

Digitized by Google

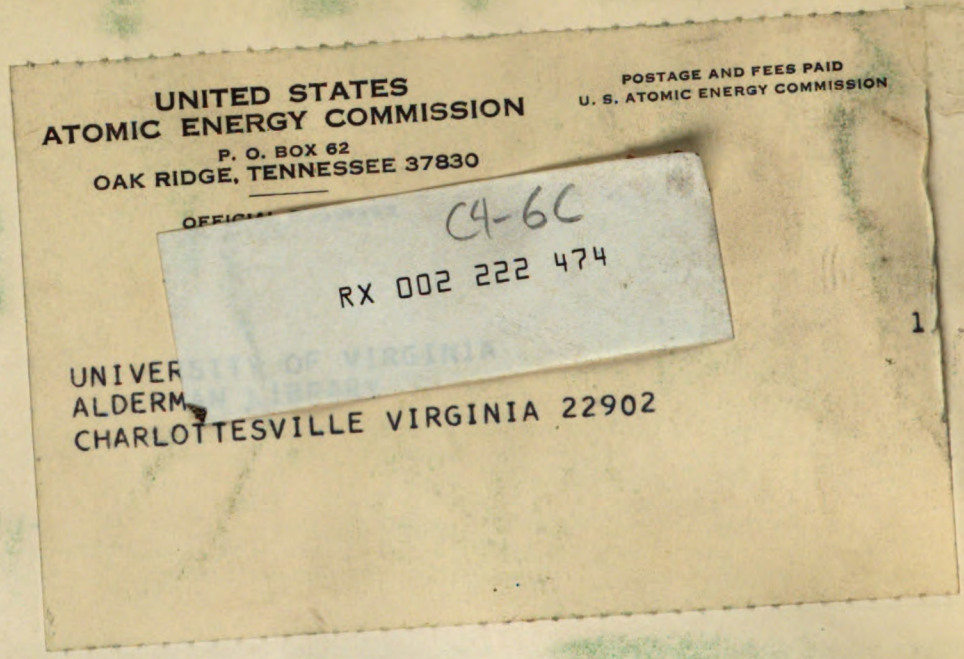

TECHNICAL PROGRESS REVIEWS may be purchased from Superintendent of Documents, U. S. Government Printing Office, Washington, D. C., 20402. *Nuclear Safety* at $3.00 per year for each subscription or $1.00 per issue; each of the other journals at $2.50 per year or $0.70 per issue. The use of the coupon below will facilitate the handling of your order.

POSTAGE AND REMITTANCE: Postpaid within the United States, Canada, Mexico, and all Central and South American countries except Argentina, Brazil, Guyana, French Guiana, Surinam, and British Honduras. For these Central and South American countries and all other countries, add $0.75 for each annual subscription or $0.20 for a single issue. Payment should be by check, money order, or document coupons, and MUST accompany order. Remittances from foreign countries should be made by international money order or draft on an American bank payable to the Superintendent of Documents or by UNESCO book coupons.

order form

SUPERINTENDENT OF DOCUMENTS
U. S. GOVERNMENT PRINTING OFFICE
WASHINGTON, D. C., 20402

Enclosed:
document coupons ☐ check ☐ money order ☐

Charge to Superintendent of Documents No. _____

Please send a one-year subscription to

☐ ISOTOPES AND RADIATION TECHNOLOGY
☐ POWER REACTOR TECHNOLOGY
☐ REACTOR MATERIALS

(Each subscription $2.50 per year; $0.70 per issue.)

☐ NUCLEAR SAFETY

SUPERINTENDENT OF DOCUMENTS
U. S. GOVERNMENT PRINTING OFFICE
WASHINGTON, D. C., 20402

(Print clearly)

_____
Name

_____
Street

_____

Digitized by Google